U.PORTO

FEUP FACULDADE DE ENGENHARIA
UNIVERSIDADE DO PORTO

Characterization of marine biofilms formed by filamentous cyanobacteria

A Dissertation presented to the

University of Porto, Faculty of Engineering, for the degree of

Doctor in Chemical and Biological Engineering

by

Maria João Leal Romeu

Supervisor: Professor Filipe Mergulhão

Co-supervisor: Professor Vítor Vasconcelos

Porto, 2023

ALiCE ASSOCIATE LABORATORY IN CHEMICAL ENGINEERING

Lepabe Laboratory for Process Engineering, Environment, Biotechnology and Energy

This work was funded by i) UID/EQU/00511/2019, UIDB/00511/2020 and UIDP/00511/2020 of the Laboratory for Process Engineering, Environment, Biotechnology and Energy – LEPABE – , and LA/P/0045/2020 of the ALiCE funded by national funds through FCT/MCTES (PIDDAC); ii) CVMAR+i – Industrial Innovation and Marine Biotechnology Valorisation, funded by INTERREG V A Espanha Portugal (POCTEP) [0302_CVMAR_I_1_P]; iii) Strategic Funding UIDB/04423/2020 and UIDP/04423/2020 through national funds provided by the Foundation for Science and Technology (FCT) and the European Regional Development Fund (ERDF) in the framework of the program PT2020; iv) project SurfSAFE supported by the European Union's Horizon 2020 Research and Innovation Programme under grant agreement no. 952471; v) project HealthyWaters (NORTE-01-0145-FEDER-000069), supported by Norte Portugal Regional Operational Programme (NORTE 2020), under the PORTUGAL 2020 Partnership Agreement, through the European Regional Development Fund (ERDF); vi) FCT project NanoCAT (PTDC/CTM-COM/4844/2020), funded by national funds through FCT/MCTES (PIDDAC); vii) Ph.D. Grant from the Portuguese Foundation from Science and Technology (FCT) (SFRH/BD/140080/2018).

"Para ser grande, sê inteiro: nada
Teu exagera ou exclui.

Sê todo em cada coisa. Põe quanto és
No mínimo que fazes.

Assim em cada lago a lua toda
Brilha, porque alta vive.

Ricardo Reis, in "Odes"
Heterónimo de Fernando Pessoa

Acknowledgments

This PhD was a memorable journey of life-changing experiences that would not be possible without the guidance, support, and friendship that I received from a lot of people.

I would like to express my personal appreciation to my supervisor, Professor Filipe Mergulhão, for all the guidance, advice, encouragement, enthusiasm, scientific discussions, and opportunities over this PhD, which allowed me to grow as a researcher. I would also like to thank my co-supervisor Professor Vítor Vasconcelos, for all the helpfulness and guidance during this thesis.
Your scientific knowledge and experience were essential in the progress of this work.

I am grateful to Dr. João Miranda from the *Centro de Estudos de Fenómenos de Transporte* (CEFT) group for the support in the work developed in this PhD.

I am also grateful to all my colleagues from CIIMAR, especially to João and Dany, for providing the cyanobacterial suspensions, and for proteomic analyses. It was an honor working with you, thank you for your availability and insightful comments.

I would like to thank all the professional collaborations throughout my PhD: the support from the EU COST Actions European Network of multidisciplinary research to Improve the Urinary Stents (ENIUS), the European Network of Bioadhesion Expertise (ENBA) and SurfSAFE Project for all the meetings, training schools and short-term scientific missions that allowed me to grow personally and professionally during this PhD.

I would like to thank Jelmer for welcoming me to his lab at University Medical Center Groningen (UMCG), as well as Ed and Prashant for all the suggestions and sharing knowledge. You were so welcoming, and I learned so much with you! I would also like to express my gratitude to Mette, for having me in her lab at Copenhagen University and

to her gentleness. To all wonderful people I was lucky to meet at UMCG and Copenhagen University, as well as in other scientific missions during this PhD, thank you!

To all those in DEQ and LEPABE, to technical and administrative staff, special to Carla, Sílvia, Paula and Joana, thank you for providing good working facilities and for your support.

To all my colleagues from the BEL group, with special thanks to Marta for the good times in the Netherlands, and to Luciana for all the support during this PhD.

To my friends, a special appreciation to Inês, Marta, Sara, Alexandra, Patrícia, Joana, Rita, and Andreia for all the moments that we had together and for your friendship.
A special gratitude to Marta(s), Márcia, and Rosa, thank you for always being there.
João, thank you for your patience, encouraging words and for always being around.
To all, thanks for all the laughs and sweet memories throughout time!

My deepest appreciation to my family, who were always encouraging and motivating me. Thank you for always taking care of me and the endless support, and sorry for all moments of physical distance. I will be forever grateful for all your confidence, dedication, and love.

Thank you all!

Abstract

Marine biofouling is a global concern in aquatic environments, with several economic, environmental, and ecological impacts. Despite significant breakthroughs aimed at controlling the undesirable adhesion and growth of marine fouling organisms on submerged surfaces, biofouling remains a persistent challenge. Biofilm development is the initial step in the marine fouling process, and cyanobacteria are considered common microfouler organisms responsible for their formation.

The main aims of this work comprised the study of an *in vitro* platform that mimics the hydrodynamics of marine environments, the analysis of the effect of hydrodynamic conditions and surface properties on protein expression of filamentous cyanobacterial biofilm cells, and the structure analysis of filamentous cyanobacterial biofilms developed on several surfaces using different imaging techniques.

The potential of agitated 12-well microtiter plates to mimic marine environments was assessed by Computational Fluid Dynamics (CFD), and it was shown that the bottom of the wells is subjected to a shear rate range comprising the value obtained for a ship hull in a harbour (50 s^{-1}). After the *in vitro* operational conditions were defined, qualitative and quantitative proteomic analyses were performed to characterize protein expression of cyanobacterial biofilms formed under two different hydrodynamic conditions on glass and perspex surfaces. In general, biofilms formed at different hydrodynamic conditions (4 s^{-1} *vs.* 40 s^{-1}) demonstrated higher variations in the proteomic profile when compared with those obtained from distinct surfaces. The structure of filamentous cyanobacterial biofilms formed on different surfaces, and under controlled hydrodynamic conditions was also evaluated by several imaging techniques. Most of the quantitative results showed no significant differences in biofilms developed on glass and perspex. In turn, the impact of carbon composite surfaces on filamentous cyanobacterial biofilm development, namely carbon nanotubes (CNTs)- and pristine graphene nanoplatelet (GNP)-modified surfaces, showed a significant antifouling/antimicrobial effect at the maturation stage of biofilm development, indicating their potential to be used as long-term

antifouling/antimicrobial materials in marine applications. Moreover, a structural rearrangement of biofilms developed on these surfaces was observed over time.

In all of the studies performed in this work, biofilm development was higher under low shear conditions (4 s^{-1} *vs.* 40 s^{-1}), and the cyanobacterial biofilm architecture was distinct between the two hydrodynamics. Indeed, compact biofilms were formed at higher shear values (40 s^{-1}), whereas streamer structures were more evident in cyanobacterial biofilms developed at lower shear values (4 s^{-1}). The influence of the increased shear was more evident during cyanobacterial biofilm maturation.

During this work, proteomic protocols and novel quantitative biofilm parameters (obtained from Optical Coherence Tomography) were optimized and developed, which may be of great interest for the development of novel antifouling strategies. The biofilm formation capacity of several filamentous cyanobacterial strains was evaluated in controlled hydrodynamic conditions using different surfaces and organisms isolated from the Portuguese coast and beyond. Given the inherent technical difficulties in studying this type of organisms, this work also contributed to the development of standardizable protocols for biofilm formation and analysis in different research contexts.

Keywords: marine biofouling, filamentous cyanobacterial biofilms, hydrodynamic conditions, surface effect, proteomic analysis, optical coherence tomography, marine coatings, carbon composite surfaces

Resumo

A bioincrustação marinha é uma preocupação global em ambientes marinhos, apresentando diversos impactos económicos, ambientais e ecológicos. Apesar dos avanços significativos no controlo da adesão e do crescimento indesejado de organismos bioincrustantes marinhos em superfícies submersas, a bioincrustação continua a ser um desafio constante. O desenvolvimento de biofilmes é o passo inicial no processo de incrustação marinha, e as cianobactérias são consideradas organismos microincrustantes comuns responsáveis pela sua formação.

Os principais objetivos deste trabalho incluíram o estudo de uma plataforma *in vitro* que mimetiza a hidrodinâmica de ambientes marinhos, a análise do efeito das condições hidrodinâmicas e propriedades de superfície na expressão de proteínas de células de biofilme de cianobactérias filamentosas e a análise da estrutura de biofilmes formados por cianobactérias filamentosas desenvolvidos em diversas superfícies usando diferentes técnicas de imagem.

O potencial uso de placas de microtitulação de 12 poços em agitação de modo a mimetizar ambientes marinhos foi analisado por Dinâmica de Fluídos Computacional (DFC), tendo sido demonstrado que o fundo dos poços está sujeito a uma gama de taxa de cisalhamento que compreende o valor obtido para um casco de navio no porto (50 s^{-1}). Após as condições operacionais *in vitro* terem sido definidas, análises proteómicas qualitativa e quantitativa foram realizadas de modo a caracterizar a expressão proteómica de biofilmes de cianobactérias formados sob duas condições hidrodinâmicas diferentes e em superfícies de vidro e perspex. Em geral, os biofilmes formados em diferentes condições hidrodinâmicas (4 s^{-1} *vs.* 40 s^{-1}) apresentaram variações mais significativas no perfil proteómico quando comparados aos obtidos em diferentes superfícies. A estrutura de biofilmes de cianobactérias filamentosas formados em diferentes superfícies, e sob condições hidrodinâmicas controladas, também foi avaliada por diversas técnicas de imagem. A maioria dos resultados quantitativos não demonstraram diferenças significativas em biofilmes desenvolvidos em vidro e perspex. No entanto, o impacto das superfícies de compósitos de carbono no desenvolvimento de biofilmes de cianobactérias

filamentosas, nomeadamente superfícies modificadas com nanotubos de carbono (NTC) e nanoagregados de grafeno (NPG), revelou um significativo efeito anti-incrustante/antimicrobiano na fase de maturação de desenvolvimento do biofilme, indicando potencial para serem usadas como materiais anti-incrustante/antimicrobiano em aplicações marinhas a longo prazo. Além disso, foi observado um rearranjo estrutural dos biofilmes desenvolvidos nestas superfícies ao longo do tempo.

Em todos os estudos realizados neste trabalho, o desenvolvimento do biofilme foi maior em condições de baixo cisalhamento (4 s^{-1} *vs.* 40 s^{-1}), e a arquitetura do biofilme cianobacteriano foi distinta entre as duas hidrodinâmicas. De facto, biofilmes compactos foram formados a valores de cisalhamento mais altos (40 s^{-1}), enquanto estruturas em apêndice ("streamers") foram mais evidentes em biofilmes de cianobactérias desenvolvidos a valores de cisalhamento mais baixos (4 s^{-1}). A influência do aumento de cisalhamento foi mais evidente durante a maturação dos biofilmes cianobacterianos.

Durante este trabalho foram otimizados e desenvolvidos protocolos de proteómica, assim como novos parâmetros quantitativos de biofilme (obtidos através de Tomografia de Coerência Óptica), os quais podem ser relevantes para o desenvolvimento de novas estratégias anti-incrustantes. A capacidade de formação de biofilme de várias estirpes de cianobactérias filamentosas foi avaliada em condições hidrodinâmicas controladas, usando diferentes superfícies e organismos isolados da costa portuguesa e também de outros locais. Dadas as dificuldades técnicas inerentes ao estudo deste tipo de organismos, este trabalho também contribuiu para o desenvolvimento de protocolos padronizáveis para formação e análise de biofilmes em diferentes contextos de pesquisa.

Palavras-chave: bioincrustação marinha, biofilmes de cianobactérias filamentosas, condições hidrodinâmicas, efeito da superfície, análise proteómica, tomografia de coerência óptica, revestimentos marinhos, superfícies de compósitos de carbono

Table of contents

Acknowledgments ..... *vii*

Abstract ..... *ix*

Resumo ..... *xi*

Table of contents ..... *xiii*

List of figures ..... *xvii*

List of tables ..... *xxx*

Nomenclature ..... *xxxii*

1 General overview *1*

1.1 Relevance and motivation **1**

1.2 Objectives and outline of the thesis **3**

1.3 Scientific outputs **6**

2 Literature review *11*

2.1 Introduction: biofilms overview **11**

2.2 Importance of marine biofouling **14**

2.3 Role of cyanobacteria in biofouling **16**

2.4 Main factors affecting biofouling **23**

2.4.1 Hydrodynamic conditions 26

2.4.2 Surface properties 31

2.5 Proteomic analysis of cyanobacteria **54**

2.6 Marine antifouling strategies **68**

3 Biofilm formation behaviour of marine filamentous cyanobacterial strains in controlled hydrodynamic conditions *71*

Abstract **71**

3.1 Introduction **72**

3.2 Materials and Methods **74**

3.2.1 CFD analysis 74

3.2.2 Organisms and inocula preparation 75

3.2.3 Surface analysis 76

3.2.4 Biofilm formation 76

3.2.5 Biofilm analysis 77

3.2.6 Statistical analysis 79

3.3 Results and Discussion **79**

3.3.1 CFD analysis 79

3.3.2 Surface analysis 83

3.3.3 Biofilm analysis 84

3.4 Conclusions **92**

3.5 Supplementary Material 94

4 Characterization of planktonic and biofilm cells from two filamentous cyanobacteria using a shotgun proteomic approach 101

Abstract 101

4.1 Introduction 102

4.2 Materials and Methods 105
4.2.1 Organism and inocula preparation 105
4.2.2 Biofilm formation 105
4.2.3 Biofilm analysis 107
4.2.4 Proteomic analysis 109
4.2.5 Statistical analysis 111

4.3 Results and Discussion 111
4.3.1 Biofilm development analysis 111
4.3.2 Proteomic analysis 117

4.4 Conclusions 124

4.5 Supplementary Material 126

5 Quantitative proteomic analysis of marine biofilms formed by filamentous cyanobacterium 139

Abstract 139

5.1 Introduction 140

5.2 Material and Methods 143
5.2.1 Organisms and inocula preparation 143
5.2.2 Biofilm formation 143
5.2.3 Biofilm analysis 145
5.2.4 Proteomics analysis 147

5.3 Results and Discussion 152
5.3.1 Biofilm development analysis 152
5.3.2 Proteomic analysis 156

5.4 Conclusions 167

5.5 Supplementary Material 169

6 Hydrodynamic conditions affect the proteomic profile of marine biofilms formed by filamentous cyanobacterium 177

Abstract 177

6.1 Introduction 178

6.2 Material and Methods 181
6.2.1 DNA extraction, amplification (PCR) and sequencing 181
6.2.2 Phylogenetic analysis 182
6.2.3 Organism and inoculum preparation 183
6.2.4 Biofilm formation 183
6.2.5 Biofilm analysis 185
6.2.6 Proteomic analysis 186

6.3 Results and Discussion 189
6.3.1 Phylogenetic analysis 189

6.3.2 Biofilm development analysis 191
6.3.3 Proteomic analysis 194

6.4 Conclusions 207

6.5 Supplementary Material 208

7 Characterization and biofouling potential analysis of two cyanobacterial strains isolated from Cape Verde and Morocco 211

Abstract 211

7.1 Introduction 212

7.2 Material and Methods 216
7.2.1 Sampling and isolation 216
7.2.2 DNA extraction, 16S rRNA gene amplification (PCR), and sequencing 217
7.2.3 Phylogenetic analysis 218
7.2.4 Light microscopy and morphological characterization 219
7.2.5 Biofilm formation assay 219
7.2.6 Biofilm analysis 220
7.2.7 Statistical analysis 223

7.3 Results and Discussion 223
7.3.1 Phylogenetic analysis 223
7.3.2 Morphological description 225
7.3.3 Biofilm development 226

7.4 Conclusions 232

7.5 Supplementary Material 234

8 The use of 3D Optical Coherence Tomography to analyze the architecture of cyanobacterial biofilms formed on a carbon nanotube composite 237

Abstract 237

8.1 Introduction 238

8.2 Material and Methods 242
8.2.1 Surface preparation 242
8.2.2 Surface characterization 243
8.2.3 Organism and inoculum preparation 244
8.2.4 Biofilm formation 244
8.2.5 Biofilm analysis 245
8.2.6 Statistical analysis 250

8.3 Results and Discussion 250
8.3.1 Surface characterization 250
8.3.2 Biofilm formation 252

8.4 Conclusions 262

8.5 Supplementary Material 263

9 How do graphene composite surfaces affect the development and structure of marine cyanobacterial biofilms? 265

Abstract 265

9.1 Introduction 266

9.2 Material and Methods 268
9.2.1 Surface preparation 269
9.2.2 Surface characterization 270
9.2.3 Organism and inoculum preparation 271
9.2.4 Biofilm formation 271
9.2.5 Biofilm analysis 273
9.2.6 Statistical analysis 274

9.3 Results and Discussion 275
9.3.1 Surface analysis 275
9.3.2 Biofilm development 278

9.4 Conclusions 285

9.5 Supplementary Material 287

10 Concluding remarks and future perspectives 289

10.1 Concluding remarks 289

10.2 Future perspectives 293

References 297

Annex A. Overview of filamentous cyanobacterial strains characteristics 331

Annex B. Composition of Z8 medium supplemented with 25 g.L^{-1} of synthetic sea salts (Tropic Marin) and B$_{12}$ vitamin. 335

Annex C. Publications from this PhD. 337

List of figures

Figure 2.1. Temporal representation of marine biofouling process and involved organisms. This image was created with BioRender (https://biorender.com/). 17

Figure 2.2.. Cell-surface interactions, EPS production, and QS phenomena involved in the initial steps of marine biofouling - adhesion and biofilm development. This image was created with BioRender (https://biorender.com/). 18

Figure 2.3. Cyanobacterial forms and cell envelopes composition: (A) coccoid unicellular, (B) colonial, (C) filamentous, (D) unsheathed trichome, (E) sheathed trichome, (F) different cell types in filamentous cyanobacteria, (G) cyanobacterial cell envelopes composition (mucilaginous sheath can be present in some taxa). This image was created with BioRender (https://biorender.com/). Adapted from Allaf, 2022. 20

Figure 2.4. Structural model of cyanobacterial phycobilisome. This image was created with BioRender (https://biorender.com/). 22

Figure 2.5. Main factors affecting marine biofouling. This image was created with BioRender (https://biorender.com/). 24

Figure 2.6. Representation of some marine equipment and devices, such as partially submerged underwater cameras, flotation spheres, sensors, and transparent hulls of boats or their windows, that are likely to be subjected to average shear rate values of 50 s^{-1}. This image was created with BioRender (https://biorender.com/). 30

Figure 2.7. Representative 3D OCT images of *S. salina* LEGE 00041 and *Cyanobium* sp. LEGE 10375 biofilms formed on epoxy-coated glass and silicone hydrogel coatings after 7 weeks of *in vitro* incubation. The color scale shows the range of biofilm thickness. Adapted from Faria, Teixeira-Santos, Romeu, *et al.*, 2021. 37

Figure 3.1. CFD simulation of the free liquid surface at 40 and 185 rpm. 80

Figure 3.2. Wall shear rate at the bottom wall (at 40 and 185 rpm). 81

Figure 3.3. Representation of shear strain rate variation over a complete cycle. A normalized time scale was used since the period is different for each shaking frequency. The dashed line represents the shear strain rate reported for a ship in a harbour (50 s^{-1}). The area represented by light and dark

grey (both delimited by average and maximum values) indicates the shear strain rate achieved at 40 and 185 rpm respectively. 82

Figure 3.4. Evaluation of *Nodosilinea* sp. LEGE 06020 biofilm development. The parameters analysed refer to wet weight (A, C), chlorophyll *a* (B, D). Biofilms were formed in glass (A, B) or perspex (C, D), at two average shear rates, 4 s^{-1} (closed circles) and 40 s^{-1} (open circles) during 49 days. Standard deviations from three replicates are represented. Symbols * and ** indicate statistically different values for $P < 0.1$ and $P < 0.05$ (respectively) at each incubation time. 85

Figure 3.5. Evaluation of unidentified filamentous Synechococcales LEGE 07185 biofilm development. The parameters analysed refer to wet weight (A, C), chlorophyll *a* (B, D). Biofilms were formed in glass (A, B) or perspex (C, D), at two average shear rates, 4 s^{-1} (closed circles) and 40 s^{-1} (open circles) during 49 days. Standard deviations from three replicates are represented. Symbols * and ** indicate statistically different values for $P < 0.1$ and $P < 0.05$ (respectively) at each incubation time**.** 86

Figure 3.6. Evaluation of *Nodosilinea* sp. LEGE 06022 biofilm development. The parameters analysed refer to wet weight (A, C), chlorophyll *a* (B, D). Biofilms were formed in glass (A, B) or perspex (C, D), at two average shear rates, 4 s^{-1} (closed circles) and 40 s^{-1} (open circles) during 49 days. Standard deviations from three replicates are represented. Symbols * and ** indicate statistically different values for $P < 0.1$ and $P < 0.05$ (respectively) at each incubation time. 87

Figure 3.7. Evaluation of cyanobacterial biofilm thickness (left; A - C) and roughness coefficient (right; D - F) in both surfaces and different shear rates (A, D - *Nodosilinea* sp. LEGE 06020; B, E - unidentified filamentous Synechococcales LEGE 07185; C, F - *Nodosilinea* sp. LEGE 06022). Mean values ± SD from three replicates for each sampling day are represented. For each condition, different lowercase letters indicate significant differences between incubation times (28 days – very light grey bars; 35 days – light grey bars; 42 days – dark grey bars; 49 days – black bars; $P \leq 0.05$; unpaired *t*-test). 88

Figure 3.8. Representative images obtained by OCT of *Nodosilinea* sp. LEGE 06020 biofilms formed after 49 days on glass and perspex. A-D: 2D cross-sectional OCT images (scale bar = 200 μm); E – H: 3D OCT images, top view projection (the color scale shows the range of biofilm thickness). Biofilms were formed at two different shear rates, 4 s^{-1} (A, C, E ,G) and 40 s^{-1} (B, D, F, H). 90

Figure 3.9. Representative images obtained by OCT of unidentified filamentous Synechococcales LEGE 07185 biofilms formed after 49 days on glass and perspex. A-D: 2D cross-sectional OCT images (scale bar = 200 μm); E – H: 3D OCT images, top view projection (the color scale shows the

range of biofilm thickness). Biofilms were formed at two different shear rates, 4 s^{-1} (A, C, E, G) and 40 s^{-1} (B, D, F, H). 91

Figure 3.10. Representative images obtained by OCT of *Nodosilinea* sp. LEGE 06022 biofilms formed after 49 days on glass and perspex. A-D: 2D cross-sectional OCT images (scale bar = 200 μm); E – H: 3D OCT images, top view projection (the color scale shows the range of biofilm thickness). Biofilms were formed at two different shear rates, 4 s^{-1} (A, C, E, G) and 40 s^{-1} (B, D, F, H). 92

Figure 4.1. Evaluation of *Nodosilinea* sp. LEGE 06145 biofilm development. The parameters analyzed refer to wet weight (A, B), chlorophyll *a* (C, D) and biofilm thickness (E, F). Biofilms were formed in glass (A, C, E) or perspex (B, D, F), at two average shear rates, 4 s^{-1} (closed circles) and 40 s^{-1} (open circles) for 49 days. SDs from two biological assays with three replicates each are represented. Symbols * and ** indicate statistically different values for $p < 0.1$ and $p < 0.05$ (respectively) at each incubation time. 114

Figure 4.2. Evaluation of *Nodosilinea* sp. LEGE 06119 biofilm development. The parameters analysed refer to wet weight (A, B), chlorophyll a (C, D) and biofilm thickness (E,F). Biofilms were formed in glass (A, C, E) or perspex (B, D, F), at two average shear rates, 4 s^{-1} (closed circles) and 40 s^{-1} (open circles) for 49 days. SDs from two biological assays with three replicates each are represented. Symbols * and ** indicate statistically different values for $p < 0.1$ and $p < 0.05$ (respectively) at each incubation time. 115

Figure 4.3. 2D cross-sectional OCT images of *Nodosilinea* sp. LEGE 06145 biofilms formed after 49 days on glass and perspex at two different shear rates, 4 s^{-1} (A, C) and 40 s^{-1} (B, D). Scale bar = 200 μm. 116

Figure 4.4. 2D cross-sectional OCT images of *Nodosilinea* sp. LEGE 06119 biofilms formed after 49 days on glass and perspex at two different shear rates, 4 s^{-1} (A, C) and 40 s^{-1} (B, D). Scale bar = 200 μm. 117

Figure 4.5. Venn diagrams obtained from the distribution of proteins identified among different conditions for the two cyanobacterial strains. The total of proteins for each condition is represented by (N=). The composite figure shows the unique and common proteins identified in both cyanobacterial strains of each condition represented from each Venn diagram: A – total proteins identified on *Nodosilinea* sp. LEGE 06145 cells *vs* proteins identified on *Nodosilinea* sp. LEGE 06119 cells; B – proteins identified on planktonic *Nodosilinea* sp. LEGE 06145 cells *vs* proteins identified on planktonic *Nodosilinea* sp. LEGE 06119 cells; C – proteins identified on *Nodosilinea* sp. LEGE 06145

cells *vs* proteins identified on *Nodosilinea* sp. LEGE 06119 cells derived from biofilms formed on glass at 4 s^{-1}; D – proteins identified on *Nodosilinea* sp. LEGE 06145 cells *vs* proteins identified on *Nodosilinea* sp. LEGE 06119 cells derived from biofilms formed on perspex at 4 s^{-1}; E – proteins identified on *Nodosilinea* sp. LEGE 06145 cells *vs* proteins identified on *Nodosilinea* sp. LEGE 06119 cells derived from biofilms formed on glass at 40 s^{-1}; F – proteins identified on *Nodosilinea* sp. LEGE 06145 cells *vs* proteins identified on *Nodosilinea* sp. LEGE 06119 cells derived from biofilms formed on perspex at 4 s^{-1}. 119

Figure 5.1. Evaluation of unidentified filamentous cyanobacterium LEGE 06007 biofilm development. The parameters analysed refer to wet weight (A, B), chlorophyll *a* quantification (C, D), total biomass quantification by CV assay (E, F) and biofilm thickness (G, H). Biofilms were formed in glass (A, C, E, G) or perspex (B, D, F, H), at two average shear rates, 4 s^{-1} (closed circles, orange) and 40 s^{-1} (open circles, green) for 49 days. Standard deviations from two biological assays with three replicates each are represented. Symbol ** indicate statistically different values for $P < 0.05$ at each incubation time. 154

Figure 5.2. 2D cross-sectional OCT images of unidentified filamentous cyanobacterium LEGE 06007 biofilms formed after 49 days on glass and perspex at two different shear rates, 4 s^{-1} (A, C) and 40 s^{-1} (B, D). Scale bar = 200 μm. 156

Figure 5.3. Volcano plot of the differentially expressed proteins (DEPs) among the 4 biofilm conditions studied. Black points represent the DEPs showing the corresponding gene symbol, or the protein accession number when lacking the corresponding gene annotation. The axis depicts the *P* values ($-\log_{10}$) plotted against the fold changes ($\log_2$) between each paired-comparison. A) glass *vs* perspex at 4 s^{-1} (down and up-regulated proteins on glass at 4 s^{-1} when compared with perspex at 4 s^{-1}); B) 4 s^{-1} *vs* 40 s^{-1} on glass (down and up-regulated proteins at 4 s^{-1} on glass when compared with 40 s^{-1} on glass); C) 4 s^{-1} *vs* 40 s^{-1} on perspex (down and up-regulated proteins at 4 s^{-1} on perspex when compared with 40 s^{-1} on perspex); D) glass *vs* perspex at 40 s^{-1} (down and up-regulated proteins on glass at 40 s^{-1} when compared with perspex at 40 s^{-1}). 158

Figure 5.4. Venn diagram displaying the unique and shared DEPs found between 4 s^{-1} glass *vs* 4 s^{-1} perpex and 4 s^{-1} glass *vs* 40 s^{-1} glass. 161

Figure 5.5. Functional annotation of the three major GO Categories: Biological Process (BP), Molecular Function (MF) and Cellular Components (CC) according to the GO Distribution by Level (4). The figure shows the number of sequences (number of proteins) in a descendent manner matching GO-terms of the unique up-regulated DEPs (19 proteins) and the eight shared DEPs (8

proteins), overlapped between the comparison glass *vs* perspex at 4 s^{-1} and 4 s^{-1} *vs* 40 s^{-1} on glass. More details about GO annotation can be found in Supplementary Material, Table S 5.2. 162

Figure 5.6. Enrichment of DEPs revealed by the hypergeometric distribution significance test. The enriched GO terms (Fisher's exact test, $P < 0.05$) are represented by a stacked bar (in green) as the percentage of the GO terms found in the References Set (in red, represent all 546 identified). Each panel displays the set of 27 up-regulated and seven down-regulated DEPs found in the comparison glass *vs* perspex at 4 s^{-1}. More details about GO annotation can be found in the Supplementary Material, Table S 5.2. 166

Figure 6.1. Maximum likelihood (ML) phylogenetic tree based on 61 partial 16S rRNA gene sequences of cyanobacteria strains belonging to the orders Pseudanabaenales and Synechococcales. *Gloeobacter violaceus* PCC 7421 and *Gloeobacter violaceus* PCC 8105 were used as outgroup. Phylogenetic position of *Toxifilum* sp. LEGE 06021 is indicated in bold. Bootstrap values over 50% are indicated at the nodes. Black stars represent the strains whose sequences were obtained in this work. Strains labeled with quotes indicate that names correspond to Genbank labels. 190

Figure 6.2. Evaluation of *Toxifilum* sp. LEGE 06021 biofilm development. The parameters analysed refer to wet weight (A, B), chlorophyll *a* quantification (C, D) and biofilm thickness (E, F). Biofilms were formed in glass (A, C, E) or perspex (B, D, F), at two average shear rates, 4 s^{-1} (closed circles) and 40 s^{-1} (open circles) for 49 days. Standard deviations from two biological assays with three replicates each are represented. Symbol * indicate statistically different values for $P < 0.05$ (unpaired *t*-tests) at each incubation time. 193

Figure 6.3. 2D cross-sectional OCT images of *Toxifilum* sp. LEGE 06021 biofilms. The representative images show biofilms formed on glass and perspex at two different shear rates, 4 s^{-1} (A-D) and 40 s^{-1} (E-H), and the biofilm structure evolution from days 28 to 49. Scale bar = 200 μm. 194

Figure 6.4. Principal Component Analysis (PCA) of the proteins identified from marine biofilms formed by filamentous cyanobacteria under four different biofilm growing conditions. The PCA plot displays a grouping pattern among the six replicates studied from each biofilm condition formed on glass and perspex, but some differences were observed between the two hydrodynamic conditions studied (4 s^{-1} and 40 s^{-1}). The two principal components extracted (PC1 and PC2) can explain the 48% total variability revealed among the proteins analysed. PCA was performed with the respective function provided within the "DEP" R package (Zhang *et al.*, 2018), used for the downstream proteomic analyses. 196

Figure 6.5. Heatmaps of the Differentially Expressed Proteins (DEPs) identified between comparisons of the same surface studied at different hydrodynamics conditions. The figures display the DEPs resulting from the comparisons between the conditions A) 4 s^{-1} *vs.* 40 s^{-1} on glass clustered in six groups by k-means clustering, and B) 4 s^{-1} *vs.* 40 s^{-1} on perspex clustered in four groups. The rows show the corresponding UniProt accession of DEPs with their corresponding expression in the columns as the log_2 fold-change (red: enriched; blue: depleted) of the intensity from each replicate. 197

Figure 6.6. Volcano plot of the differentially expressed proteins (DEPs) identified between comparisons of the same surface studied at different hydrodynamics conditions. The figure displays the DEPs (black dots) and their corresponding accession/gene names, as the resulting *P* values (− log_{10}) in the y-axis, plotted against the fold changes (log_2) in the x-axis, obtained between the comparisons 4 s^{-1} *vs.* 40 s^{-1} on glass (A) and on perspex (B). 198

Figure 6.7. Gene Ontology (GO) distribution and GO enrichment of Differentially Expressed Proteins (DEPs). In the left panel is shown the GO distribution by level 4 of the DEPs, whereas the right panel displays the corresponding enriched GO terms. The divergent stacked bars (negative and positive) represent the percentage of DEPs (x-axis) matching each GO Category (y-axis), relative to the number of DEPs found at both sides (up/down) of the tested conditions (DEPs Conditions). The total number of DEPs obtained from each comparison were 11-up/4-down (from glass 4 s^{-1} *vs.* 40 s^{-1}) and 2-up/3-down (from perspex 4 s^{-1} *vs.* 40 s^{-1}). The GO annotation was performed with the OmicsBox software version 1.4.11, as well as the enrichment analyses (Fisher's exact test, $P < 0.05$). 199

Figure 7.1. Sampling locations: A) dried soil crust near Mrizika Beach, Morocco; B) green mat on ramp port for boats at Calhau, São Vicente Island, Cape Verde. 216

Figure 7.2. Maximum likelihood (ML) phylogenetic tree based on 58 partial 16S rRNA gene sequences of cyanobacterial strains belonging to the orders Pseudanabaenales and Synechococcales. *Gloeobacter violaceus* PCC 7421 and *Gloeobacter violaceus* PCC 8105 were used as outgroups. Phylogenetic positions of *Leptothoe* sp. LEGE 181153 and *Jaaginema* sp. LEGE 191154 are indicated in bold and with a black star. Bootstrap values over 50% are indicated at the nodes. Strains labelled with quotes indicate that names correspond to Genbank labels. 224

Figure 7.3. Light microscopy of A) *Leptothoe* sp. LEGE 181153 (400x); B) *Jaaginema* sp. LEGE 191154 (400x); C) *Leptothoe* sp. LEGE 181153 (1000x); D) *Jaaginema* sp. LEGE 191154 (1000x). Scale bars = 10 μm. 225

Figure 7.4. Evaluation of cyanobacterial biofilm development. The parameters analysed refer to wet weight (A, B), chlorophyll *a* (C, D), and biofilm thickness (E, F). Biofilms of *Jaaginema* sp. LEGE 191154 (closed circles) and *Leptothoe* sp. LEGE 181153 (open circles) were formed on glass or perspex at an average shear rate of 40 s^{-1} for 49 days. Symbols * and ** indicate statistically different values for $P < 0.1$ and $P < 0.05$ on each incubation time, respectively. 229

Figure 7.5. 2D cross-sectional OCT images of cyanobacterial biofilms formed at 35 and 49 days on glass and perspex. Scale bars = 200 μm. 230

Figure 7.6. CLSM images of cyanobacterial biofilms formed after 49 days on glass and perspex. Scale bars = 50 μm. 232

Figure 7.7. Biovolume obtained from CLSM *z*-stacks of *Jaaginema* sp. LEGE 191154 (green bars) and *Leptothoe* sp. LEGE 181153 (red bars) biofilms formed after 49 days on glass and perspex. Symbols * and ** indicate statistically different values for $P < 0.1$ and $P < 0.05$ between both cyanobacterial strains on the same surface, respectively. 232

Figure 8.1. 2D and 3D coordinate systems for 2D and 3D OCT analyses, respectively. *X* represents the width, *Y* is the height, and *Z* refers to the depth. 247

Figure 8.2. Two-dimensional AFM (A–C) and SEM (D–F) images of glass, epoxy resin, and CNT composite. The vertical color bars in the AFM images correspond to the *z*-range (surface height range) of the respective image. The SEM images have a magnification of 100× and the scale bar is equivalent to 100 μm. 252

Figure 8.3. *Nodosilinea* cf. *nodulosa* LEGE 10377 biofilm development on different surfaces (glass—black, epoxy resin—grey, CNT composite—white). The parameters analyzed refer to biofilm wet weight (A), thickness (B), contour coefficient (C), biovolume (D), porosity (E), and average size of non-connected pores (F). Mean values and SD from two biological assays with two technical replicates each are represented. For each sampling day, different lowercase letters indicate significant differences between surfaces ($P \leq 0.05$; one-way ANOVA with Tukey's multiple comparisons test. 254

Figure 8.4. Representative 2D cross-sectional OCT images of *Nodosilinea* cf. *nodulosa* LEGE 10377 257

Figure 8.5. Representative 3D OCT images of *Nodosilinea* cf. *nodulosa* LEGE 10377 biofilms formed on glass (A), epoxy resin (C), and CNT composite (E) after 49 days. The spatial distribution of non-connected pores on the biofilm is also shown (B, D, F). The color scale shows the distance from the substrate surface. 257

Figure 8.6. Representative 3D OCT images of the distribution of non-connected pores by size from *Nodosilinea* cf. *nodulosa* LEGE 10377 biofilms formed on glass (A), epoxy resin (B) and CNT composite (C) after 49 days. The color scale shows the range of the size of non-connected pores. 258

Figure 8.7. SEM images of *Nodosilinea* cf. *nodulosa* LEGE 10377 biofilms formed on glass (A), epoxy resin (B), and CNT composite (C) after 49 days of incubation. The red arrows in (C) indicate clusters of CNTs. Magnification = 1000×; scale bar = 10 μm. 260

Figure 9.1. Scheme of the experimental steps of the present work. 269

Figure 9.2. Water contact angles (A) and average roughness (Sa) (B) of the tested surfaces. The means ± SD are shown. 276

Figure 9.3. 3D profilometer images of glass (A), epoxy resin (B), and GNP composite (C). 277

Figure 9.4. SEM images of glass (A), epoxy resin (B), GNP composite (C), and magnified GNP composite (D). The micrographs have a magnification of 500×, except for (D), which corresponds to a higher magnification image (10,000×) of the surface area marked in red in (C). 277

Figure 9.5. *Lusitaniella coriacea* LEGE 07157 biofilm development on different surfaces: glass (black), epoxy resin (grey), GNP composite (white). The parameters analyzed refer to biofilm wet weight (A), biofilm thickness (B), average percentage of empty spaces (C), and their respective average size (D) on biofilm structure. Mean values and SD from two biological assays with two technical replicates each are represented. For each sampling day, different lowercase letters (a, b, and c) indicate significant differences between surfaces ($P < 0.05$). 280

Figure 9.6. Representative 2D cross-sectional OCT images obtained for *Lusitaniella coriacea* LEGE 07157 biofilms on glass (A), epoxy resin (B), and GNP composite (C) after 49 days. The empty spaces on the biofilm structure are indicated in blue (scale bar = 100 μm). 281

Figure 9.7. Three-dimensional confocal reconstructions of *Lusitaniella coriacea* LEGE 07157 biofilms grown on (A) glass, (B) epoxy resin, and (C) GNP composite after 49 days of incubation (white scale bars = 50 μm). These images show the biofilm aerial view, with the virtual shadow projection on the right (representative of biofilm thickness). Biovolume (D) and surface coverage (E) values of cyanobacterial biofilms were extracted from confocal files with the COMSTAT program. The means ± SD are presented. Different letters in the graphs (a, b, and c) indicate a significant difference among surfaces ($P < 0.05$). 283

Figure 9.8. SEM micrographs of *Lusitaniella coriacea* LEGE 07157 biofilms grown on glass (A), epoxy resin (B), and GNP composite (C) after 49 days of incubation. Magnification = 2500×; scale bar = 10 μm. 284

Supplementary Figures

Figure S 3.1. Velocity profiles obtained at both shaking frequencies: 40 rpm and 185 rpm. 94

Figure S 3.2. Correlation between wet weight and chlorophyll *a* on *Nodosilinea* sp. LEGE 06020. Biofilm development in glass (A, B) and perspex (C, D), at two different shear rates, 4 s^{-1} (A, C) and 40 s^{-1} (B, D). Full line represents the linear regression whereas the dashed line represents the confidence limits (95%). Closed symbols refer to data points that were considered for the regression (all except one) and the single open symbol refers to a data point that was excluded from the regression. 95

Figure S 3.3. Correlation between wet weight and chlorophyll *a* on unidentified filamentous Synechococcales LEGE 07185. Biofilm development in glass (A, B) and perspex (C, D), at two different shear rates, 4 s^{-1} (A, C) and 40 s^{-1} (B, D). Full line represents the linear regression whereas the dashed line represents the confidence limits (95%). Closed symbols refer to data points that were considered for the regression (all except three) and the open symbols refer to a data points that were excluded from the regression. 96

Figure S 3.4. Correlation between wet weight and chlorophyll *a* on *Nodosilinea* sp. LEGE 06022. Biofilm development in glass (A, B) and perspex (C, D), at two different shear rates, 4 s^{-1} (A, C) and 40 s^{-1} (B, D). Full line represents the linear regression whereas the dashed line represents the confidence limits (95%). Closed symbols refer to data points that were considered for the regression (all except five) and the open symbols refer to a data points that were excluded from the regression. 97

Figure S 3.5. Evaluation of *Nodosilinea* sp. LEGE 06020 biofilm development under the same hydrodynamic condition on different surfaces. The parameters analyzed refer to wet weight (A, C), chlorophyll *a* (B, D). Biofilms were formed at 4 s^{-1} (A, B) or 40 s^{-1} (C, D), on two different surfaces, glass (closed circles) and perspex (open circles) during 49 days. Standard deviations from 3 replicates are represented. Symbols *; ** indicate statistically different values for $P < 0.1$ and $P < 0.05$ (respectively) at each incubation time. 98

Figure S 3.6. Evaluation of unidentified filamentous Synechococcales LEGE 07185 biofilm development under the same hydrodynamic condition on different surfaces. The parameters

analysed refer to wet weight (A, C), chlorophyll *a* (B, D). Biofilms were formed at 4 s^{-1} (A, B) or 40 s^{-1} (C, D), on two different surfaces, glass (closed circles) and perspex (open circles) during 49 days. Standard deviations from 3 replicates are represented. Symbols *; ** indicate statistically different values for $P < 0.1$ and $P < 0.05$ (respectively) at each incubation time. 99

Figure S 3.7. Evaluation of *Nodosilinea* sp. LEGE 06022 biofilm development under the same hydrodynamic condition on different surfaces. The parameters analysed refer to wet weight (A, C), chlorophyll *a* (B, D). Biofilms were formed at 4 s^{-1} (A, B) or 40 s^{-1} (C, D), on two different surfaces, glass (closed circles) and perspex (open circles) during 49 days. Standard deviations from 3 replicates are represented. Symbols *; ** indicate statistically different values for $P < 0.1$ and $P < 0.05$ (respectively) at each incubation time. 100

Figure S 4.1. Correlation between wet weight and chlorophyll *a* on *Nodosilinea* sp. LEGE 06145. Biofilm development in glass (A, C) and perspex (B, D) at two different shear rates, 4 s^{-1} (A, B) and 40 s^{-1} (C, D). Full line represents the linear regression, and the dashed line represents the confidence limits (95%). Closed symbols refer to data points that were considered for the regression (all except three) and the single open symbol refers to a data point that was excluded from the regression. 126

Figure S 4.2. Correlation between wet weight and chlorophyll *a* on *Nodosilinea* sp. LEGE 06119. Biofilm development in glass (A, C) and perspex (B, D) at two different shear rates, 4 s^{-1} (A, B) and 40 s^{-1} (C, D). Full line represents the linear regression, and the dashed line represents the confidence limits (95%). Closed symbols refer to data points that were considered for the regression (all except four) and open symbols refer to a data points that were excluded from the regression. 127

Figure S 4.3. Evaluation of biofilm development under 4 s^{-1}. The parameters analysed refer to wet weight (A, B), chlorophyll *a* (C, D) and biofilm thickness (E, F). Biofilms were formed on two different surfaces, glass (A, C, E) and perspex (B, D, F) for 49 days. Closed and open circles refer to *Nodosilinea* sp. LEGE 06145 and *Nodosilinea* sp. LEGE 06119 biofilm development, respectively. Standard deviations from two biological assays with three replicates each, are represented. Symbols *; ** indicate statistically different values for $P < 0.1$ and $P < 0.05$ (respectively) at each incubation time. 128

Figure S 4.4. Evaluation of biofilm development under 40 s^{-1}. The parameters analysed refer to wet weight (A, B), chlorophyll *a* (C, D) and biofilm thickness (E, F). Biofilms were formed on two different surfaces, glass (A, C, E) and perspex (B, D, F) for 49 days. Closed and open circles refer to *Nodosilinea* sp. LEGE 06145 and *Nodosilinea* sp. LEGE 06119 biofilm development, respectively. Standard deviations from two biological assays with three replicates each, are represented.

Symbols *; ** indicate statistically different values for $P < 0.1$ and $P < 0.05$ (respectively) at each incubation time. 129

Figure S 4.5. Evaluation of N*odosilinea* sp. LEGE 06145 biofilm development under the same hydrodynamic on different surfaces. The parameters analysed refer to wet weight (A, B), chlorophyll a (C, D) and biofilm thickness (E, F). Biofilms were formed at 4 s^{-1} (A, C, E) or 40 s^{-1} (B, D, F), on two different surfaces, glass (closed circles) and perspex (open circles) for 49 days. Standard deviations from two biological assays with three replicates each, are represented. Symbols *; ** indicate statistically different values for $P < 0.1$ and $P < 0.05$ (respectively) at each incubation time. 130

Figure S 4.6. Evaluation of *Nodosilinea* sp. LEGE 06119 biofilm development under the same hydrodynamic on different surfaces. The parameters analysed refer to wet weight (A, B), chlorophyll *a* (C, D) and biofilm thickness (E, F). Biofilms were formed at 4 s^{-1} (A, C, E) or 40 s^{-1} (B, D, F), on two different surfaces, glass (closed circles) and perspex (open circles) for 49 days. Standard deviations from two biological assays with three replicates each, are represented. Symbols *; ** indicate statistically different values for $P < 0.1$ and $P < 0.05$ (respectively) at each incubation time. 131

Figure S 5.1. Correlation between wet weight and chlorophyll *a* content on biofilm development from unidentified filamentous cyanobacterium LEGE 06007. Biofilm development in glass (A, C) and perspex (B, D) at two different shear rates, 4 s^{-1} (A, B) and 40 s^{-1} (C, D). Full line represents the linear regression, and the dashed line represents the confidence limits (95%). Closed symbols refer to data points that were considered for the regression (all except one) and open symbols refer to data points that were excluded from the regression. 170

Figure S 5.2. Correlation between crystal violet and biofilm thickness on biofilm development from unidentified filamentous cyanobacterium LEGE 06007. Biofilm development in glass (A, C) and perspex (B, D) at two different shear rates, 4 s^{-1} (A, B) and 40 s^{-1} (C, D). Full line represents the linear regression, and the dashed line represents the confidence limits (95%). Closed symbols refer to data points that were considered for the regression (all except two) and open symbols refer to data points that were excluded from the regression. 171

Figure S 5.3. Correlation between crystal violet and wet weight on biofilm development from unidentified filamentous cyanobacterium LEGE 06007. Biofilm development in glass (A, C) and perspex (B, D) at two different shear rates, 4 s^{-1} (A, B) and 40 s^{-1} (C, D). Full line represents the linear regression, and the dashed line represents the confidence limits (95%). Closed symbols refer to

data points that were considered for the regression (all except two) and open symbols refer to data points that were excluded from the regression. 172

Figure S 5.4. Evaluation of unidentified filamentous cyanobacterium LEGE 06007 biofilm development under the same hydrodynamic condition on different surfaces. The parameters analysed refer to wet weight (A, B), chlorophyll *a* quantification (C, D), total biomass quantification by CV assay (E, F) and biofilm thickness (G, H). Biofilms were formed at 4 s^{-1} (A, C, E, G) or 40 s^{-1} (B, D, F, H) on two different surfaces, glass (closed circles) and perspex (open circles) for 49 days. Standard deviations from two biological assays with three replicates each, are represented. Symbols *; ** indicate statistically different values for $P < 0.1$ and $P < 0.05$ (respectively) at each incubation time. 173

Figure S 5.5. Evaluation of roughness coefficient of unidentified filamentous cyanobacterium LEGE 06007 biofilm development on glass (A) and perspex (B) at 4 s^{-1} (closed circles) and 40 s^{-1} (open circles) between day 35 and day 49. 174

Figure S 5.6. Distribution of total proteins identified according to biological process (54% of proteins identified without associated biological process are not shown in this graph). 174

Figure S 5.7. Bar plots depicting the content of the superoxide dismutase (SOD) throughout the experiment. The fold changes of SOD content of all replicates from each condition studied (40 s^{-1} glass, 40 s^{-1} perspex, 4 s^{-1} glass and 4 s^{-1} perspex) are depicted as centered log_2 intensities. Error bars represent the 95% confidence intervals 175

Figure S 6.1. Evaluation of unidentified filamentous Synechococcales LEGE 06021 biofilm development under the same hydrodynamic condition on different surfaces. The parameters analysed refer to wet weight (A, B), chlorophyll *a* quantification (C, D) and biofilm thickness (E, F). Biofilms were formed at 4 s^{-1} (A, C, E) or 40 s^{-1} (B, D, F) on two different surfaces, glass (closed circles) and perspex (open circles) for 49 days. Standard deviations from two biological assays with three replicates each are represented. Symbol * indicates statistically different values for $P < 0.05$ (unpaired t-tests) at each incubation time. 208

Figure S 6.2. Correlation between wet weight and chlorophyll *a* content on biofilm development from unidentified filamentous Synechococcales LEGE 06021. Biofilm development in glass (A, C) and perspex (B, D) at two different shear rates, 4 s^{-1} (A, B) and 40 s^{-1} (C, D). The full line represents the linear regression, and the dashed line represents the confidence limits (95%). Closed symbols refer to data points that were considered for the regression (all except two), and open symbols refer to data points that were excluded from the regression. 209

Figure S 6.3. Distribution of total proteins identified according to the biological process (34.8% of proteins identified without an associated biological process are not shown in this graph). 210

Figure S 7.1. Evaluation of biofilm empty spaces. The parameter analysed refers to the percentage of empty spaces on *Leptothoe* sp. LEGE 181153 biofilms formed on glass for 49 days. The empty spaces on cyanobacterial biofilm structures were determined as described in Faria *et al.* 2021 and represented in blue **(**scale bars = 200 μm). The values regarding the percentage of empty spaces are indicated from day 21 since the biofilm thickness was below the OCT range on the first two sampling days. 234

Figure S 7.2. Evaluation of biofilm development on different surfaces. The parameters analysed refer to wet weight, chlorophyll *a* quantification, and biofilm thickness. Biofilms of *Jaaginema* sp. LEGE 191154 and *Leptothoe* sp. LEGE 181153 were formed on glass (closed circles) or perspex (open circles) at an average shear rate of 40 s^{-1} for 49 days. Symbols * and ** indicate statistically different values for $P < 0.1$ and $P < 0.05$ on each incubation time, respectively. 235

Figure S 8.1. Representative SEM image of an agglomerate of CNTs on the CNT composite surface. Magnification = 10,000×; scale bar = 1 μm. 263

Figure S 9.1. Representative 2D cross-sectional OCT images obtained for *Lusitaniella coriacea* LEGE 07157 biofilms on glass (A), epoxy resin (B), and GNP composite (C) after 28 days. The empty spaces on the biofilm structure are indicated in blue (scale bar = 100 μm). 287

Figure S 9.2. Roughness coefficient[1] values of *Lusitaniella coriacea* LEGE 07157 biofilms on different surfaces: glass (black), epoxy resin (grey), and GNP composite (white). Mean values and SD from two biological assays with two technical replicates each are represented. For each surface, different lowercase letters indicate significant differences between the sampling day (day 28 *vs*. day 49; $p < 0.05$; unpaired t-test). The *p* value obtained for glass and epoxy resin was < 0.0001, and for GNP composite was 0.0104. 287

List of tables

Table 2.1. Main consequences of marine biofouling in industrial and environmental sectors. 15

Table 2.2. Main relevant characteristics of cyanobacteria for marine biofouling. 23

Table 2.3. Commonly used materials in marine equipment, their applications, main benefits, and disadvantages. 32

Table 2.4. Studies focused on different surface/coatings used in marine environments in the last ten years (studies performed exclusively on macrofouler organisms were not included in this table). 40

Table 2.5. Cyanobacterial proteome studies in response to various environmental stresses. 57

Table 2.6. Proteins/factors related to cyanobacterial adhesion and biofilm development. 64

Table 4.1. Enumeration of proteins obtained from different biofilm samples in both cyanobacterial strains. For each protein, the frequency of appearance among the four biofilms conditions (glass, perspex, 4 s^{-1} and 40 s^{-1}) is indicated by different shaded colors (black – appearance in all four conditions; dark grey - appearance in three of four conditions; light grey - appearance in two of four conditions; without shading – appearance in only one of the four conditions). 121

Table 5.1. List of the 41 DEPs and their corresponding accession number (Protein IDs), gene names, description and the log_2 fold-changes obtained from each comparison. 159

Table 6.1. List of the DEPs found between comparisons of the same surface studied at different hydrodynamics conditions. The corresponding UniProt accession of DEPs is provided with their corresponding gene and a brief description, as well as the log 2-fold-changes (LFC) and the resulting and adjusted *P*-values (p.adj) for each comparison (4 s^{-1} *vs.* 40 s^{-1} on glass, and 4 s^{-1} *vs.* 40 s^{-1} on perspex). 200

Table 7.1. Oligonucleotide primers used for 16s rRNA amplification. 218

Table 8.1. Variable definition. 247

Table 8.2. Water contact angle measurements (θ_w) and roughness (Ra) determined for the tested surfaces. 251

Supplementary Tables

Table S 4.1. Number of proteins identified from planktonic and different biofilm samples. 132

Table S 4.2. Number and identification of common proteins found under the different biofilm conditions. This table lists the proteins that were detected in more than 1 of the 8 experimental conditions. The frequency of appearance (from 2 to 8) is indicated in bold on the left column. For each subgroup (proteins that appear in 7 of the 8 conditions and so forth) the condition with the highest frequency of appearance is shaded (only frequencies of appearance higher than 55% were shaded. 132

Table S 5.1. Summary of proteomic analysis. 174

Table S 5.2. DEPs description and GO annotation. 175

Table S 6.1. Summary of proteomic analysis. 209

Table S 6.2. DEPs description and GO annotation. 210

Nomenclature

Abbreviations

2D	Two-dimensional
2D-GE	Two-Dimensional polyacrylamide Gel Electrophoresis
3D	Three-dimensional
ABC	ATP-Binding Cassette
ACN	Acetonitrile
AFM	Atomic Force Microscopy
AIC	Akaike Information Criterion
ATP	Adenosine Triphosphate
BIC	Bayesian Information Criterion
BLAST	Basic Local Alignment Search Tool
BM	Ball Milling
BP	Biological Process
CC	Cellular Components
CCM	CO_2 Concentrating Mechanism
c-di-GMP	cyclic dimeric GMP
CFD	Computational Fluid Dynamics
CFU	Colony Forming Unit
CIIMAR	Interdisciplinary Centre of Marine and Environmental Research
CNT	Carbon Nanotubes
CO_2	Carbon dioxide
Cph2	Cyanobacterial phytochrome2
CS	Chitosan
CSLM	Confocal Laser Scanning Microscopy
Cu_2O	Copper oxide
CuPy	Copper pyrithione
CuSCN	Copper thiocyanate
CV	Crystal Violet
DEPs	Differentially Expressed Proteins
DIGE	Differential In Gel Electrophoresis
DNA	Deoxyribonucleic Acid
EbfG1-4	Enabling biofilm formation with a double-glycine-motif
EPS	Extracellular Polymeric Substances
FA	Formic Acid
FASP	Filter Aided Sample Preparation
FDR	False Discovery Rates
FOV	Field Of View
FRC	Fouling Release Coatings
GNP	Graphene Nanoplatelet
GO	Gene Ontology
GSH	Glutathione
GTP	Guanosine Triphosphate
Hik	Histidine kinase
ICAT	Isotope-Coded Affinity Tag
iTOL	Interactive Tree of Life
iTRAQ	Isobaric Tags for Relative and Absolute Quantitation

LC	Liquid Chromatography
LC-MS/MS	Liquid Chromatography tandem Mass Spectrometry
LEGE-CC	Blue Biotechnology and Ecotoxicology Culture Collection
LFC	Log 2-fold-changes
MF	Molecular Function
MIC	Minimal Inhibitory Concentration
ML	Maximum Likelihood
MrpC	Microcystin-related Protein C
MS/MS	tandem Mass Spectrometry
MWCNTs	Multi-Walled Carbon Nanotubes
NaCl	Sodium Chloride
NADPH	Nicotinamide Adenine Dinucleotide Phosphate
NMWL	Nominal Molecular Weight Limit
OCT	Optical Coherence Tomography
OD	Optical Density
OMV	Outer Membrane Vesicles
p.adj	Adjusted *P*-values
PCA	Principal Component Analysis
PDMS	Polydimethylsiloxane
PLA	Poly(lactic acid)
PMMA	Poly(methyl methacrylate)
PS I	Photosystem I
PS II	Photosystem II
PVC	Polyvinyl chloride
QS	Quorum sensing
ROI	Region Of Interest
ROS	Reactive Oxygen Species
RPM	Revolutions Per Minute
Rre	Response regulator
SD	Standard Deviation
SDS-PAGE	Sodium Dodecyl Sulfate-Polyacrylamide Gel Electrophoresis
SDT	Sodium Dithionite
SEM	Scanning Electron Microscopy
SILAC	Stable Isotope Labeling
SLH	S-layer Homology
SOD	Superoxide Dismutase
SP3	Single-pot Solid-phase-enhanced Sample-preparation
SPC	Self-Polishing Copolymers
SWCNTs	Single-Walled Carbon Nanotubes
TBT	Tributyl Tin
TES-KOH	N-[Tris(hydroxymethyl)-methyl]-2-aminoethanesulfonic acid - potassium hydroxide
TFA	Trifluoracetic Acid
TiO_2	Titanium Dioxide
UV	Ultraviolet
VBNC	Viable But Non-Culturable
VNSS	Våatanen Nine Salt Solution
ZnO	Zinc oxide
ZnPy	Zinc pyrithione

Symbols

A_{ROI}	total area of the ROI (mm^2)
$Acon_{x,z}$	number of connected voxels identified as belonging to biofilm matrix/bacteria in the biofilm (biovolume) in a horizontal plane at position y
$Ancp_{x,z}$	number of non-biofilm-connected voxels without an open connection to the environment (biofilm holes) in a horizontal plane at position y
Chla a	Chlorophyll *a* concentration ($\mu g.mL^{-1}$)
$C_{F,i}$	number of voxels identified as belonging to biofilm matrix/bacteria in the biofilm (biovolume) in column i (vertical line of voxels at position i) and connected to the environment (including corner voxels)
$L_{(F,i)}$	biofilm thickness at a given position i (μm; from OCT analysis)
$\bar{L}_F$	average biofilm thickness (μm; from OCT analysis)
$R^*_\propto$	relative roughness coefficient (adimensional; from OCT analysis)
R_a	average roughness (nm; from AFM analysis)
S_a	average roughness (nm; from optical profilometry)
S_{BET}	specific surface area ($m^2.g^{-1}$)
S_{meso}	external surface área ($m^2.g^{-1}$)
V_{micro}	micropore volume ($cm^3.g^{-1}$)
V_p	total pore volume ($cm^3.g^{-1}$)
V_{vox}	volume of a voxel (μm^3)
i	index of x,z position in the horizontal plane
x	pixel position on the horizontal axis (width)
y	pixel position on the vertical axis (height)
z	pixel position on the perpendicular axis (depth)
θ_w	contact angles with water (°)
λ	wavelength (nm)

1.

1 General overview

1.1 Relevance and motivation

Biofilms are complex microenvironments formed by single or multiple species in which microorganisms are involved in a gelatinous polymeric matrix consisting mainly of water and extracellular polymeric substances (EPS) (Flemming *et al.*, 2016). They are the most common form of microbial organization, mainly due to the set of advantages that this lifestyle features compared to planktonic cells, contributing to successful microbial survival in hostile environments (Verderosa *et al.*, 2019). Biofilms are ubiquitous in natural environments and on man-made surfaces. In aquatic environments, all immersed surfaces are rapidly colonized by organisms (Dang and Lovell, 2016), contributing to the biofouling process, which includes both micro and macrofouling events. Marine biofouling creates extensive challenges for marine industries worldwide, with environmental consequences and harmful effects on public health.

The complexity of marine environments due to variations in temperature, microbial population, seawater composition, light propagation, hydrodynamics, etc., is such that laboratory analysis of marine biofilms is challenging. Although several factors affect biofilm development in marine ecosystems, hydrodynamic conditions (Fanesi *et al.*, 2021; Chun *et al.*, 2022) and surface properties (von Ammon *et al.*, 2018; Cai *et al.*, 2019) assume particular relevance. Although laboratory tests cannot fully capture the complexity of the marine environment, they are amenable to standardization, which is

crucial when comparing datasets from different experiments. Even though the biofilm formation process is difficult to reproduce in independent experiments, standardization of operation conditions enables the researcher to draw meaningful conclusions given the controlled (and simplified) laboratory setup.

Although *in vitro* studies of marine biofilms are relatively common, laboratory studies with detailed hydrodynamic characterization in marine biofilm reactors are scarce (Dimartino *et al.*, 2014; Chun *et al.*, 2022). Therefore, it is crucial to perform biofilm formation studies in controlled hydrodynamic conditions so that *in vitro* experiments can better mimic natural aquatic environments. Likewise, most *in vitro* studies are usually performed for short periods of time. Studies based on surface characterization and their influence on biofilm formation are also needed for the development of novel surfaces that may reduce biofouling. Indeed, advances in nanotechnology have prompted the progress of novel marine antifouling coatings. A promising approach to delay macrofouling is to prevent the initial adhesion and biofilm development by microorganisms such as cyanobacteria since they are responsible for initiating biofilm formation, excreting large amounts of EPS (Rossi and De Philippis, 2015). Although useful for understanding which parameters drive marine biofilm development, few studies focus on multiple factors evaluation, especially using filamentous cyanobacterial biofilms due to the difficulty of studying these organisms. Multidisciplinary biofilm analyses are thus required to evaluate the complex phenomenon of filamentous cyanobacterial biofilm development.
Currently, the available information regarding the composition and function of the components in biofilms represents a significant gap in scientific research. The importance of proteins in biofilm composition, structure, and resistance has been featured in many publications that have improved our fundamental understanding of the biofilm development process (Rani and Babu, 2018). As more proteins and their roles in biofilm development are uncovered, new potential targets for the mitigation of biofilms and their control may be considered. Therefore, proteomic approaches in marine biofouling are an important research field, but few studies on filamentous cyanobacteria have been available until now due to the challenging tasks in cyanobacterial proteomic experiments (Babele *et al.*, 2019). Additionally, since we are experiencing exciting developments in advanced imaging techniques that widen our understanding of the structure and function

of biofilms, it seems essential to explore these novel approaches in filamentous cyanobacteria biofilms developed under different hydrodynamic conditions and surfaces.

This work benefits from a collaboration between FEUP and CIIMAR, where expertise in biological/chemical engineering and marine sciences can be found. Furthermore, it takes advantage of the biodiversity that exists on the Portuguese coast (and other selected locations), which is accessible through the Blue Biotechnology and Ecotoxicology Culture Collection (LEGE-CC) from CIIMAR[1] (Ramos *et al.*, 2018). Therefore, this work comprises different filamentous cyanobacterial genera (Annex A) that can be found in different ecosystems around the world, and it becomes even more significant due to the cosmopolitan distribution of these organisms.

To perform a multidisciplinary analysis of filamentous cyanobacterial biofilms, different tools, including Computational fluid dynamics (CFD), proteomic approaches, surface analysis and different imaging techniques were used.

[1] https://lege.ciimar.up.pt/

1.2 Objectives and outline of the thesis

One of the main goals of this work was to develop a laboratory platform for marine biofilm formation under controlled hydrodynamic conditions. The second goal was to analyse the effect of hydrodynamic conditions and surface properties on protein expression of cyanobacterial biofilm cells and also assess differences regarding their planktonic counterparts. A third objective was to evaluate the effect of different surfaces (including surface modifications) on biofilm formation by filamentous cyanobacterial biofilms using advanced imaging techniques.

The work is presented in this thesis in three different parts:

(1) development of an *in vitro* platform that mimics the hydrodynamics of marine environments (Chapter 3),

(2) characterization of filamentous cyanobacterial biofilms formed in controlled hydrodynamic conditions using proteomic approaches (Chapters 4 - 6),
(3) structure and architecture analysis of filamentous cyanobacterial biofilms development using different imaging techniques (Chapters 7 - 9).

For that, this thesis is divided into ten main chapters that are summarized below.

The present chapter, **Chapter 1**, includes the motivation for the research and the main objectives of this work.

Chapter 2 provides a literature review on marine biofouling. The main consequences, as well as the importance of cyanobacteria in this complex process, are discussed. The main factors that affect marine biofouling are reviewed, and the impact of hydrodynamics and surface properties are highlighted. Subsequently, a description of current proteomic analysis of cyanobacteria is also presented, and particular emphasis is given to factors that are related to cyanobacterial biofilm development. Finally, an overview of marine antifouling strategies is presented.

In order to determine if *in vitro* hydrodynamic conditions are similar to those prevailing in relevant marine environments, a CFD analysis was performed on the proposed reactor (agitated microtiter plate) used for *in vitro* cyanobacterial biofilm assays. **Chapter 3** presents the study for the validation of this marine biofilm reactor, which is used throughout this work. Moreover, three filamentous cyanobacterial strains isolated from the Portuguese coast, two different hydrodynamic conditions and two different surfaces (glass and perspex) were used**.** The chosen surfaces represent commonly found materials in submerged marine artificial devices and equipment. Moreover, to complement biofilm characterization, a three-dimensional (3D) Optical Coherence Tomography (OCT) analysis was performed using an image analysis software developed in partnership with Jelmer Sjollema's group from the University Medical Center Groningen (the Netherlands) during this PhD thesis.

Following the definition of the operational conditions that enable mimicking relevant aquatic environments, proteomic tools were used to characterize protein expression of cyanobacterial biofilms formed under two different hydrodynamic conditions on glass and perspex surfaces **(Chapters 4 - 6),** together with a simplified analysis by two-dimensional (2D) OCT and standard methodologies commonly used to evaluate these biofilms. **Chapter 4** includes an initial qualitative proteomic study, where planktonic cells and cells from biofilms formed under different conditions were analyzed. Since quantitative approaches provide a deeper insight into how biofilm development is affected by different parameters, **Chapters 5** and **6** describe quantitative studies in biofilm cyanobacterial cells. Furthermore, **Chapter 6** includes improvements in the sample preparation and peptide identification protocol to enhance data quality. Four different cyanobacterial strains isolated from the Portuguese coast were used in these proteomic studies.

Following the proteomic evaluation, the architecture of biofilms formed under different different surfaces was analyzed (**Chapters 7 - 9**). Since proteomic studies showed a highly variable profile between cyanobacterial strains and also to include isolates from more geographically distinct areas, in **Chapter 7,** the characterization and biofilm development of two cyanobacterial strains isolated from Morocco and Cape Verde is presented. Biofilm development also occurred under hydrodynamic conditions that mimic real marine environments and using glass and perspex as the substratum for biofilm formation.

Due to the pressing need to develop novel antifouling surfaces, the impact of carbon composite surfaces on filamentous cyanobacterial biofilm development is presented in **Chapters 8** and **9**. In these chapters, two different control surfaces are used (glass and commercial epoxy resin), as well as two different filamentous cyanobacterial strains isolated from the Portuguese coast. These studies are important to understand the interactions between polymer surface properties and cyanobacterial biofilm development and architecture over time.

Therefore, **Chapter 8** assesses the effect of carbon nanotubes (CNTs)-modified surfaces on cyanobacterial biofilm development. Moreover, improvements in the 3D OCT technique were developed to enable the architectural analysis of these biofilms. A set of novel parameters was obtained, including the contour coefficient, total biofilm volume, biovolume, volume of non-connected pores and the average size of non-connected pores. Since OCT is a promising technique that can be applied to different fields, the analysis of novel biofilm properties obtained by this imaging technique in this chapter is extremely important for a deeper understanding of the biofilm development process.

Additionally, in **Chapter 9** the effect of pristine graphene nanoplatelet (GNP)-modified surfaces on cyanobacterial biofilm formation is evaluated. After surface characterization, cyanobacterial biofilm development and architecture were evaluated by several imaging techniques, including OCT, Confocal Laser Scanning Microscopy (CLSM), and Scanning Electron Microscopy (SEM).

Finally, **Chapter 10** presents the main conclusions of the work developed and suggestions for future research to improve knowledge in this field.

1.3 Scientific outputs

The results presented in this thesis are included in the following publications:

Papers in peer-reviewed journals

Romeu M.J., Alves P., Morais J., Miranda J.M., Jong E.D., Sjollema J., Ramos V., Vasconcelos V., Mergulhão F.J.M. (2019) Biofilm formation behaviour of marine filamentous cyanobacterial strains in controlled hydrodynamic conditions". *Environmental Microbiology* **21**: 4411-4424. https://doi.org/10.1111/1462-2920.14807 **(Chapter 3)**

Romeu M.J., Domínguez-Pérez D., Almeida D., Morais J., Campos A., Vasconcelos V., Mergulhão F. (2020) Characterization of planktonic and biofilm cells from two filamentous cyanobacteria using a shotgun proteomic approach. *Biofouling* **36**: 631-645. http://dx.doi.org/10.1080/08927014.2020.1795141 **(Chapter 4)**

Romeu M.J., Domínguez-Pérez D., Almeida D., Morais J., Araújo M.J., Osório H., Campos A., Vasconcelos V., Mergulhão F.J. (2021) Quantitative proteomic analysis of marine biofilms formed by filamentous cyanobacterium. *Environmental Research* **201**: 111566-111566. https://doi.org/10.1016/j.envres.2021.111566 **(Chapter 5)**

Romeu M.J., Domínguez-Pérez D., Almeida D., Morais J., Araújo M.J., Osório H., Campos A., Vasconcelos V., and Mergulhão F.J. (2022) Hydrodynamic conditions affect the proteomic profile of marine biofilms formed by filamentous cyanobacterium. *npj Biofilms Microbiomes* **8**: 80. https://doi.org/10.1038/s41522-022-00340-w **(Chapter 6)**

Romeu M.J., Lima M., Gomes L.C., Jong E.D. De, Morais J., Vasconcelos V., Pereira M.F.R., Soares O.S.G.P., Sjollema J., Mergulhão F. (2022) The Use of 3D Optical Coherence Tomography to Analyze the Architecture of Cyanobacterial Biofilms Formed on a Carbon Nanotube Composite. *Polymers (Basel)* **14**: 4410. https://doi.org/10.3390/polym14204410 **(Chapter 8)**

Romeu M.J., Gomes L.C., Sousa-Cardoso F., Morais J., Vasconcelos V., Whitehead K.A., Pereira M.F.R., Soares O.S.G.P., Mergulhão F. (2022) How do Graphene Composite Surfaces Affect the Development and Structure of Marine Cyanobacterial Biofilms? *Coatings* **12**: 1775. https://doi.org/10.3390/coatings12111775 **(Chapter 9)**

Romeu M.J., Morais J., Gomes L.C., Silva R., Vasconcelos V., Mergulhão F. (2023) Characterization and biofouling potentital analysis of two cyanobacterial strains isolated from Cape Verde and Morocco. *FEMS Microbiology Ecology* **99***:* fiad004. https://doi.org/10.1093/femsec/fiad004 **(Chapter 7)**

Book chapters

Romeu M.J., Gomes L.C., Teixeira-Santos R., Mergulhão F. (2022) Cyanobacteria in Marine Biofilms: Hydrodynamic and Surface Effects. In *Cyanobacteria and Their Importance.* Sinha, R. P. (eds). New York: Nova Science Publishers Inc., pp. 297–332. https://doi.org/10.52305/ONRA2232 **(Chapter 2)**

Communications at scientific meetings

Oral communications:

Romeu M.J., Faria S., Mergulhão F. Biofilm formation by filamentous cyanobacteria isolated from the Portuguese Coast. *BEL Workshop.* Porto, Portugal, 2018.

Romeu M.J., Faria S., Mergulhão F. Characterization of marine biofilms formed by filamentous cyanobacteria. *BEL Workshop.* Porto, Portugal, 2019.

Romeu M.J., Morais J., Miranda J.M., De Jong E.D., Sjollema J., Vasconcelos V, Mergulhão F. Marine biofilms development: the importance of hydrodynamic conditions and their impacts. *International Conference on Environmental Science and Technology.* Atenas, Greece (hybrid conference), 2021.

Romeu M.J., Faria S., Mergulhão F. Characterization of cyanobacterial biofilms formed under different conditions. *SURFSAFE Workshop (online)* 2021.

Romeu M.J., Domínguez-Pérez D., Almeida D., Morais J., Araújo M.J., Osório H., Campos A., Vasconcelos V., Mergulhão F. Proteomic analysis of marine cyanobacterial biofilms developed at different surfaces. *SURFSAFE Workshop.* Groningen, The Netherlands, 2021.

Poster communications:

Romeu Maria. Qualitative proteomic study on cyanobacteria: from planktonic to biofilm lifestyle. *4th Doctoral Congress in Engineering.* Porto, Portugal, 2021.

Other publications

Papers in peer-reviewed journal

Faria S.I., Teixeira-Santos R., **Romeu M.J.,** Morais J., Vasconcelos V., Mergulhão F.J. (2020) The Relative Importance of Shear Forces and Surface Hydrophobicity on Biofilm Formation by Coccoid Cyanobacteria. *Polymers (Basel)* **12**: 653. https://doi.org/10.3390/polym12030653

Faria S., Teixeira-Santos R., **Romeu M.J.,** Morais J., de Jong E.D., Sjollema, J., Vasconcelos, V., Mergulhão, F. (2021) Unveiling the antifouling performance of different

marine surfaces and their effect on the development and structure of cyanobacterial biofilms. *Microorganisms* **9**: 1102. http://dx.doi.org/10.3390/microorganisms9051102

Lima M., Gomes L.C., Teixeira-Santos R., **Romeu M.J.,** Valcárcel J., Vázquez J.A., Cerqueira M.A., Pastrana L., Bourbon A.I., de Jong E.D., Sjollema J., Mergulhão F. (2022) Assessment of the Antibiofilm Performance of Chitosan-Based Surfaces in Marine Environments. *Int J Mol Sci* **23**: 14647. https://doi.org/10.3390/ijms232314647

Book chapters

Romeu M., Alves P., Morais, J., Ramos V., Vasconcelos V., Mergulhão, F. (2016) Biofilm Formation by a Cyanobacterium Strain Belonging to a Distinct Leptolyngbya phylotype: Surface Effect. In *Biofilms: Characterization, Applications and Recent Advances*. Henderson, J. (eds). New York: Nova Science Publishers Inc., pp. 153-174.

Poster communications:

Romeu M., Alves P., Morais J., Vasconcelos V., Mergulhão F.J.M. Biofilm formation by *Leptolyngbya mycoidea* LEGE 06118: surface effect (Microbial Works of Art. No. P1: 26). *Biofilms 7*, Porto, Portugal, 2016.

Romeu M.J., Mergulhão F. Novel marine compounds for the control of CAUTIs. *ENIUS COST ACTION Training School: Ureteral stents: from modelling to commercialization.* Bern, Switzerland, 2019.

Faria S., Teixeira-Santos R., **Romeu M**., Morais J., Vasconcelos V., Mergulhão F. The Impact of Shear Forces and Surface Hydrophobicity on Coccoid Cyanobacterial Biofilm Development. *Biofilms 9*, online conference, 2020.

Lima M., Gomes L.C., Teixeira-Santos R., **Romeu M.J.,** Valcárcel J., Vázquez J.A., Cerqueira M.A., Pastrana L., Bourbon A.I., de Jong E.D., Sjollema J., Mergulhão F. Assessment of the Antibiofilm Performance of Chitosan-Based Surfaces in Marine Environments. *Euro-MIC COST ACTION Conference: Microbiologically influenced Corrosion.* Berlin, Germany, 2022.

2.

2 Literature review

Part of this chapter was adapted from the following publication:

Romeu, M.J., Gomes, L.C., Teixeira-Santos, R., Mergulhão, F. (2022) Cyanobacteria in Marine Biofilms: Hydrodynamic and Surface Effects. In *Cyanobacteria and Their Importance.* Sinha, R. P. (eds). New York: Nova Science Publishers Inc., pp. 297–332.

2.1 Introduction: biofilms overview

Biofilms were first described after observations of attached bacteria on glass slides inoculated with sea water (Zobell, 1943). However, the first definition of biofilms was proposed by Bill Costerton and coworkers in 1978 (Costerton *et al.*, 1978). The developed biofilm concept was that microorganisms are mainly found in the attached sessile state on wetted surfaces rather than as the free-floating planktonic cells and that the cells that develop within the biofilm are phenotypically distinct from planktonic cells (Lappin-scott *et al.*, 2014). Thereafter, a multistage approach has been described for biofilm development, including five main stages: reversible attachment of planktonic cells, irreversible attachment, biofilm maturation by development of microcolonies and high EPS production, maturation of the biofilm, and dispersal/detachment, which can involve erosion and sloughing events (Stoodley *et al.*, 2002). While erosion is defined as the

removal of single cells or small particles from the biofilm, sloughing implies the detachment of relatively large portions of the biofilm. Therefore, the forces around the biofilm are crucial to provide a balance between growth and detachment over biofilm development since they can promote cell attachment but also cell dispersion, leading to the migration of these cells to colonize new areas. Biofilm development is a complex and dynamic process that can be affected by different factors, from surface properties to environmental parameters and microbial content. Although the schematic conceptual biofilm developmental model based on five stages has been widely generalized to describe all biofilms, this model does not necessarily describe the complexity of biofilms in the real world as in industrial, natural, and clinical settings. Indeed, this model, which typically describes biofilms as a classic mushroom-shaped structure, was recently reviewed by the scientific community, which proposed a most inclusive model involving three major events: aggregation, growth, and disaggregation (Sauer *et al.*, 2022).

Although no developmental model accurately represents biofilm formation for all microorganisms, numerous *in vitro* systems have been designed to study biofilm formation to better mimic real development conditions. These platforms can include microtiter plates, Calgary device, flow chambers and flow cells, Robbins device, rotary biofilm reactors and microfluids devices (I. B. Gomes *et al.*, 2018; Gomes and Mergulhão, 2021). Advantages and limitations of these devices, as well as the application aim must be considered when choosing the most appropriate platform.

Biofilm science has changed considerably during the last decades due to technological progress, including new imaging technologies, biochemical methods, and molecular biology tools (Azeredo *et al.*, 2017). Different microbiological, physical, chemical, microscopy and molecular methods are now available to study biofilm formation, development, and behavior. Among microscopic techniques, several imaging systems have been used to detect biofilm biomass, structure, and cell viability, including CLSM, SEM and Atomic Force Microscopy (AFM). CLSM allows the reconstruction of 3D architecture of the biofilm, as well as extracting quantitative structural parameters such as biovolume, thickness, and roughness of the biofilm (L. C. Gomes *et al.*, 2018). In turn, SEM is based on surface scattering and absorption of electrons (Azeredo *et al.*, 2017), and it can reveal the morphology of bacteria adhered to a surface and the surface topography

(Gomes and Mergulhão, 2017). Since SEM can detect the presence of EPS, it has been a useful method for visualizing biofilms (Hung *et al.*, 2013). However, most imaging methods to analyze biofilms are *ex situ* and destructive (Azeredo *et al.*, 2017). OCT is a non-destructive, fast, and real-time approach, allowing biofilm *in situ* imaging (Wagner and Horn, 2017). Moreover, although staining is not required for OCT analysis, 3D biofilm images and the measurement of different parameters, such as biofilm thickness and roughness, can be obtained.

A deeper knowledge of the biofilm requires a multidisciplinary approach since distinct techniques provide valuable and complementary information about different aspects of the biofilm's complex structure. Moreover, it is also relevant to understand how biofilms interplay with the surrounding environment, either structurally or morphologically.

Although beneficial biofilms can be found for wastewater treatment, production of value-added compounds, and bioremediation processes, biofilms are commonly associated with negative impacts (Muhammad *et al.*, 2020). This microbial lifestyle can contribute to the contamination of food processing areas and drinking water distribution systems, chronic infections associated with medical devices, and cause negative impacts in different industries (Fitridge *et al.*, 2012; Abdallah *et al.*, 2014). In aquatic environments, biofilms are a common feature on all submerged surfaces, contributing to marine biofouling, which is responsible for several detrimental impacts on the efficiency of shipping, aquaculture industries, equipment corrosion and maintenance, as well as disturbances in ecosystems.

This literature review aims to collect evidence on the consequences of marine biofouling, as well as the relevance of cyanobacteria on marine biofilms. The impact of different parameters on marine biofilm development is addressed, focusing mainly on the effect of hydrodynamic conditions and surface properties. A brief description on the proteomic analysis of cyanobacteria is also presented, as well as the current factors that have been related to cyanobacterial biofilm development are also discussed. Finally, a brief overview of current marine antifouling strategies is introduced.

2.2 Importance of marine biofouling

Biofouling is a massive problem in marine environments leading to industrial, economic, environmental, and health-related problems (Table 2.1). Estimated costs due to biofilm development in industrial activities, such as in heat exchangers and aquaculture and water desalination stations, are relatively high. In the oil and gas industry, about 20-30% are material deterioration and corrosion-related costs (Skovhus *et al.*, 2017), while in marine transport, around 35-50% of costs are related to increased fuel consumption (Schultz *et al.*, 2011). Indeed, fuel consumption increases of about 40% have been observed due to biofouling (Champ, 2000); for example, the cost of one trip from San Francisco to Yokohama has increased about 77% due to vessel's hull fouling (Abbott *et al.*, 2000). Besides the increased fuel consumption, marine biofouling also leads to costs related to hull cleaning, paint removal, and repainting. The direct economic costs of managing marine biofouling in the aquaculture industry are estimated to be around 10% of production costs (Lane and Willemsen, 2004). The impacts on aquaculture infrastructures include the increased disease risk due to biofoulers and associated pathogens, modified hydrodynamics in and around the cage affecting oxygen levels, water quality, and the cage's volume and stability, increased weight, and physical damage, that culminate in substantially reduced productivity (Bannister *et al.*, 2019). Additional problems related to biofouling in marine environments are found in partially submerged or even moored equipment such as underwater cameras, flotation spheres, measuring devices, transparent hulls of boats, or their windows and sensors. On this equipment, the most obvious problems are related to optical and electrochemical sensors, which are used for on-site monitoring with weekly, monthly, or continuous measuring because even a thin biofilm on the optics can give rise to incorrect measurements (Delauney *et al.*, 2010).

Table 2.1. Main consequences of marine biofouling in industrial and environmental sectors.

Sector	Consequences
Industry	Increase of hydrodynamic drag and frictional in vessels and ships
	Decrease in operational efficiency of propulsion, navigation, and water intake equipment
	Increase in fuel consumption
	Material corrosion of different facilities, infrastructures, and submerged equipment
	Increase in management intervention time
	Cleaning, paint removal, and repainting related costs
	Decrease of heat transfer
	Incorrect measurements in submerged sensors
Environmental and health-related problems	Marine species invasion
	Establishment of exotic biofouling species in ports
	Air pollution and an increase in greenhouse gas emissions
	Contamination of aquaculture facilities, such as fish cages and shellfish sites
	Cyanobacterial blooms from benthic mat proliferations
	Water contamination by toxin accumulation

Compiled from Minchin and Gollasch, 2003; Visser *et al.*, 2005; Myers *et al.*, 2007; Delauney *et al.*, 2010; Schultz *et al.*, 2011; Fitridge *et al.*, 2012; Aldred and Clare, 2014; Davidson *et al.*, 2016; Fernandes *et al.*, 2016; Skovhus *et al.*, 2017; Demirel *et al.*, 2017; Maddah and Chogle, 2017; Bannister *et al.*, 2019; Giakoumi *et al.*, 2019.

Marine biofouling might also impact the dynamic of marine ecosystems. Biofouling on ship hulls or in submerged structures that provide a variety of niches favorable to biofilm formation, such as propellers and pipe systems, can also act as a pathway for marine species invasion. Non-native fouling species might attach directly to these structures and be transported over great distances (Godwin, 2003; Minchin and Gollasch, 2003; Davidson *et al.*, 2009), affecting the marine ecology of new areas through predation and competition events with native species, or even become a significant fouling pest (Aldred and Anthony S Clare, 2014). Several frameworks focus on marine invasive species management (Giakoumi *et al.*, 2019), presenting specific policies for their control on islands (IUCN, 2018) or in marine protected areas (Keith *et al.*, 2016). Additionally, at the environmental level, the increased frictional drag in vessels caused by marine biofouling may contribute to air pollution and greenhouse gas emissions (Hunsucker *et al.*, 2018).

Biofilms in aquatic environments can also impact public health, as biofilms are considered a temporary or permanent refuge for bacterial pathogens in shellfish, finfish, and seaweed aquaculture facilities contributing to the persistence of harmful microorganisms and transmission of their genetic determinants (Wietz *et al.*, 2009; Bannister *et al.*, 2019). Particularly, cyanobacteria can threaten animal and human health through their ability to produce cyanotoxins (Miller *et al.*, 2010; Gibble *et al.*, 2016; Regueiras *et al.*, 2018; Breinlinger *et al.*, 2021). These toxins, which can be retained on biofilm structure, degrade water quality and may cause additional consequences by their ingestion through contaminated food or even by drinking water during recreational activities (Buratti *et al.*, 2017; Huisman *et al.*, 2018).

2.3 Role of cyanobacteria in biofouling

Marine biofouling is a highly complex and dynamic process in which different agents and their interactions are involved at different stages. It has been considered that marine biofouling development comprises both micro and macrofouling events. Microfouling encompasses the adhesion of cells and biofilm formation, while macrofouling involves the settlement of invertebrate organisms (Figure 2.1). Although various stages can overlap or occur in parallel, it is often observed that microbial biofilm formation is a primordial step to marine biofouling (Salta, Wharton, *et al.*, 2013; Anderson, 2016). Briefly, a conditioning film comprised of organic molecules from the surrounding environment is formed on the submerged surface within the first minutes of immersion. Consequently, the physicochemical properties of the surfaces can be modified, affecting the adhesion and biofilm formation (Renner and Weibel, 2011). Diatoms (unicellular algae), cyanobacteria, and additional marine bacteria adhere to this conditioning layer within minutes or hours by a reversible process caused by diffusion, gravitation, Brownian motion, electrostatic (repulsion and attraction), hydrophobic and van der Waals interactions (Marshall *et al.*, 1970). Additionally, bacteria use a variety of organelles to attach to surfaces, including pili, flagella, and outer membrane proteins (Tuson and Weibel, 2013). Although Gram-negative cyanobacteria do not contain genes encoding flagella components, the extracellular non-flagellar appendages, called pili or fimbriae,

are widespread in these organisms (Schuergers and Wilde, 2015). After this initial step, the irreversible adhesion of cells occurs through interactions as dipole-dipole forces, hydrogen bonds, and secretion of EPS from cells (Renner and Weibel, 2011).

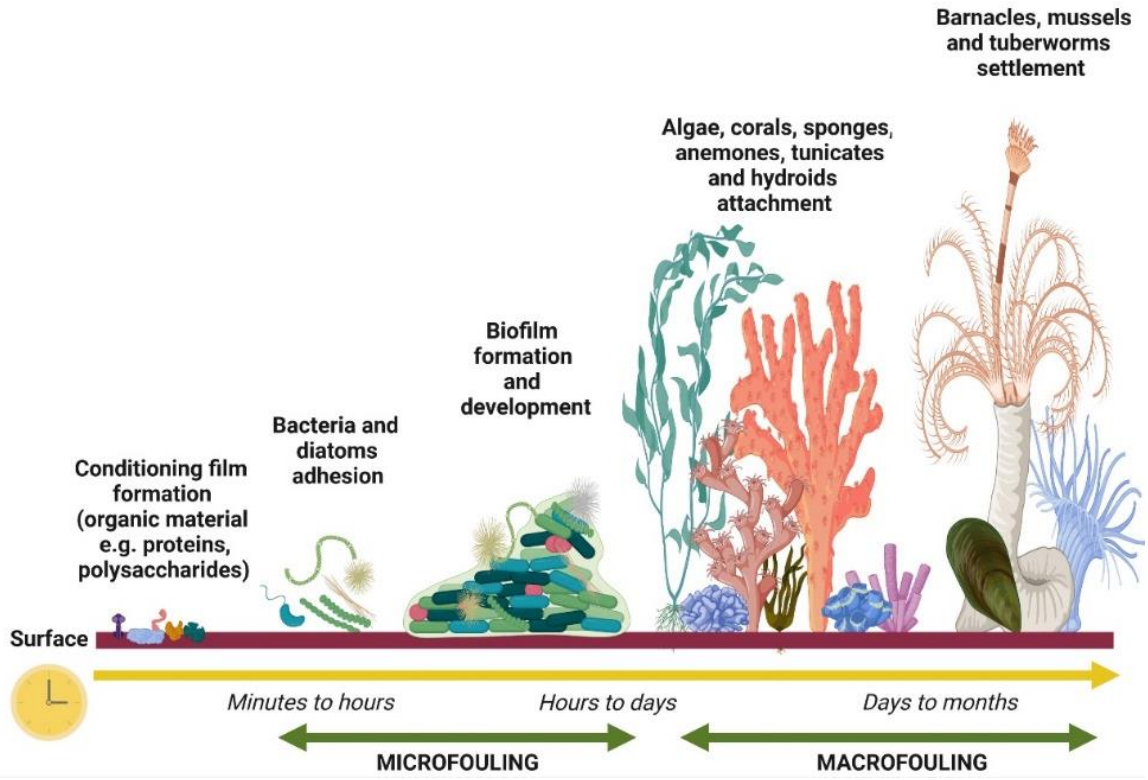

Figure 2.1. Temporal representation of marine biofouling process and involved organisms. This image was created with BioRender (https://biorender.com/).

The change from planktonic to biofilm state is thought to be dependent on quorum sensing (QS) phenomena, a process of cell-to-cell communication by which bacteria sense and respond to their own density or changes in their environment (Dobretsov *et al.*, 2009; Di Donato *et al.*, 2016). These steps are followed by biofilm formation and development, in which a continuous production of EPS is achieved (Figure 2.2). This is mainly regulated by external conditions (Nichols *et al.*, 2005) and QS signals (Hammer and Bassler, 2003). In fact, QS may be necessary for EPS synthesis and biofilm growth, or it can induce motility and biofilm dispersal (Hoang *et al.*, 2008; McDougald *et al.*, 2011). After a few days, macrofoulers organisms may attach to this initial biofilm formed by microfoulers. The macrofouling community consists of algae, corals, sponges, anemones, tunicates and hydroids (soft fouling organisms), and barnacles, mussels and tubeworms as hard fouling

organisms (Mieszkin *et al.*, 2013). One of the most promising approaches for biofouling mitigation is to interfere with the initial adhesion since if microfouling is delayed, macrofouling can be managed more effectively (Cao *et al.*, 2011; Telegdi *et al.*, 2016).

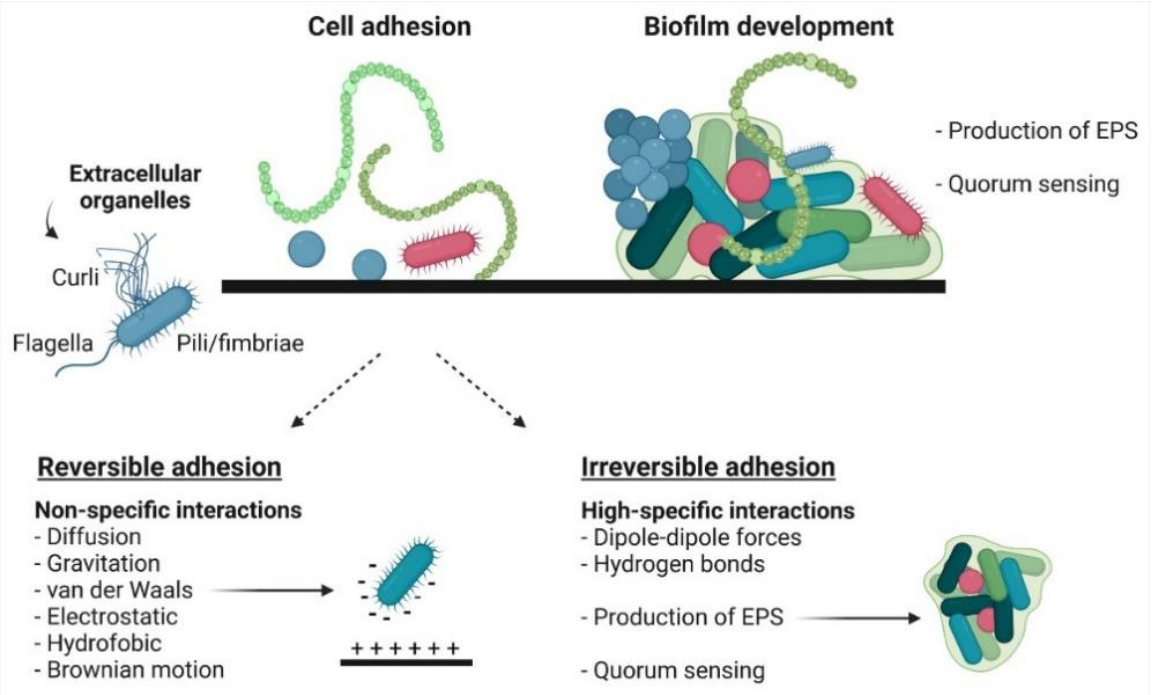

Figure 2.2.. Cell-surface interactions, EPS production, and QS phenomena involved in the initial steps of marine biofouling - adhesion and biofilm development. This image was created with BioRender (https://biorender.com/).

Cyanobacteria are a widespread group of photosynthetic prokaryotes that assumes a particular relevance on marine biofouling (Table 2.2). Cyanobacteria present a significant morphological diversity, comprising coccoid and filamentous forms with different degrees of complexity. Indeed, cyanobacteria can be categorized as unicellular, colonial (bound together by the mucilaginous sheath), or multicellular filamentous (Figure 2.3 A-C), and their cell size varies from 1 µm in diameter up to 100 µm (Whitton, 1992; Schulz-Vogt *et al.*, 2007; Humbert and Fastner, 2017). A mutation during cell division of ancestral coccoid cyanobacteria could have led to the origin of a primordial filament that would have represented the evolution for multicellular forms (Schirrmeister *et al.*, 2011). Although filamentous phenotype can be disadvantageous due to impaired motility or reduced buoyancy in aquatic environments, the stress and predation resistance, as well as the improved resource acquisition may be beneficial (Claessen *et al.*, 2014). In

filamentous cyanobacteria, after cell division, the cells remain adhered to each other and form a trichome, which can be enveloped in a mucous sheath (Figure 2.3 D, E) (Uyeda *et al.*, 2016; Vidal *et al.*, 2021). Hormogonia (filaments of cells with gliding motility), heterocysts (nitrogen-fixing cell type), and akinetes (spore-like cells) are distinct cell types that can differentiate from filamentous cyanobacteria cells (Figure 2.3F) (Singh and Montgomery, 2011; Dvořák *et al.*, 2015). Although the major role of hormogonia is the movement and the symbiotic colonization of hosts (Meeks and Elhai, 2002; Wong and Meeks, 2002; Adams and Duggan, 2008; Uyeda *et al.*, 2016), some of these cells can comprise gas vacuoles to regulate buoyancy (Meeks and Elhai, 2002). In turn, heterocysts and akinetes present a thicker envelope in comparison with vegetative cells (Meeks and Elhai, 2002; Uyeda *et al.*, 2016). While heterocysts are large round-shaped cells present in many multicellular cyanobacteria (e.g., Anabaena and Nostoc), and they are specialized for fixing nitrogen (Meeks and Elhai, 2002; Kumar *et al.*, 2010), akinetes are perennating spore-like cells that can be developed under adverse growth conditions such as drought or cold (Kumar *et al.*, 2010). Additionally, the cyanobacterial cell wall belongs to a specific group of Gram-negative bacteria (Figure 2.3G), since it comprises a lipopolysaccharide outer membrane (Durai *et al.*, 2015) and a thicker peptidoglycan layer (10 – 700 nm) compared to most Gram-negative bacteria (2 – 6 nm) (Hoiczyk and Hansel, 2000). Indeed, while a thin peptidoglycan layer was reported in unicellular cyanobacteria (~15 nm) (Samuel *et al.*, 2001), in filamentous forms the values can reach more than 700 nm (Hoiczyk and Baumeister, 1995).

Under Phylum Cyanobacteria (or Cyanophyta), and according to molecular and morphological analysis, different cyanobacterial orders are categorized (Allaf, 2022). Chroococcales, which includes the freshwater bloom-forming species *Microcystis aeruginosa*, comprises coccoid unicellular and colonial cyanobacteria inside a mucilaginous envelope (Komárek, 2003). In turn, Spirulinales species have screw-like coiled filaments and Gloeobacterales are unicellular or rod-shaped freshwater cyanobacteria that lack thylakoids (Guiry and Guiry, 2015). Nostocales include some species that are able to fix nitrogen and comprise the greatest number of the identified filamentous species (Vidal *et al.*, 2021). However, the highest number of benthic filamentous species are associated with Oscillatoriales (Vidal *et al.*, 2021) and

Pleurocapsales, which can be coccoid or resemble filaments, and form complex colony formations (Vincent, 2009; Dvořák *et al.*, 2017). Synechococcales order involves the oldest, ecologically significant, and most abundant cyanobacteria, and it contains unicellular, such as *Synechocystis* sp., colonial and filamentous cyanobacteria (Komárek *et al.*, 2014; Dvořák *et al.*, 2017).

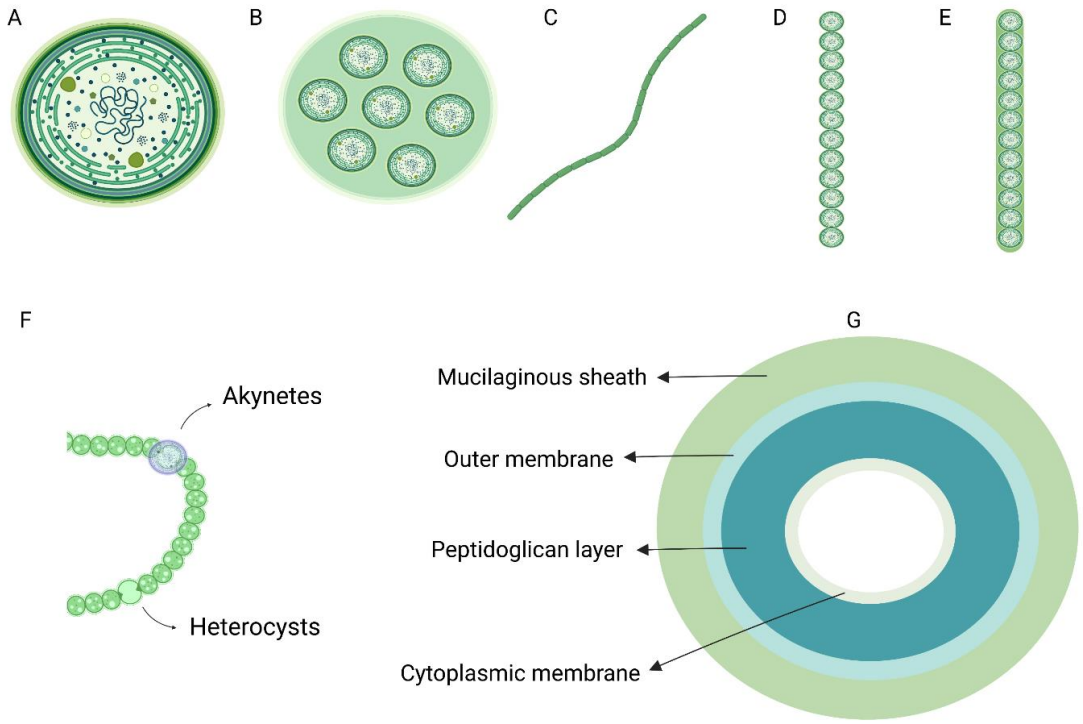

Figure 2.3. Cyanobacterial forms and cell envelopes composition: (A) coccoid unicellular, (B) colonial, (C) filamentous, (D) unsheathed trichome, (E) sheathed trichome, (F) different cell types in filamentous cyanobacteria, (G) cyanobacterial cell envelopes composition (mucilaginous sheath can be present in some taxa). This image was created with BioRender (https://biorender.com/). Adapted from Allaf, 2022.

Likewise, cyanobacteria had a large impact on the evolution of life since they were responsible for the production and accumulation of oxygen, which started to change the Earth's environment and challenged the existent forms of life (Lyons *et al.*, 2014), as well as for the evolution of eukaryotic organisms from ancient cyanobacteria (Ku *et al.*, 2015). Cyanobacteria contribute to the oxygen, carbon and nitrogen biogeochemical cycles, are involved in the primary production of trophic chains, and can persist in harsh conditions due to their high adaptability (Berg and Sutula 2015; Anderson 2016). Cyanobacteria produce green pigment chlorophyll *a*, but also additional photosynthetic blue and red

pigments known as phycobilin (phycocyanin and phycoerythrin, respectively), which enable them to grow under low-light conditions, as well as carotenoids, as protectors against oxidative stress (Melnicki *et al.*, 2016). Therefore, the cyanobacterial photosynthetic system comprises several units that absorb light energy and produce chemical bond energy, such as reduced nicotinamide adenine dinucleotide phosphate (NADPH) and adenosine triphosphate (ATP) (Grossman *et al.*, 1995). Photosystem I (PS I, plastocyaninferredoxin oxidoreductase) and photosystem II (PS II, waterplastoquinone oxidoreductase) are multisubunit protein complexes located in the thylakoid membranes (Nelson and Yocum, 2006). However, phycobilisome is the major light-harvesting complex associated with the blue-pigmented phycocyanin (A_{max} 620 nm, which absorbs photons in the orange-red part of the light spectrum), and the red-pigmented phycoerythrin (A_{max} 560 nm, which absorbs photons in the green-yellow part of the light spectrum, in combination with the phycobilisome core of allophycocyanin (A_{max} 650 nm) (Figure 2.4) (Grossman *et al.*, 1995; Stomp *et al.*, 2004; Sonani *et al.*, 2015). In most cyanobacteria, while the cytoplasmatic membrane system is involved in respiration but not photosynthesis, thylakoid membranes catalyze both photosynthetic and respiratory electron transport (Vermaas, 2001). These features, largely due to the metabolic flexibility to perform oxygen photosynthesis and respiration simultaneously (Vermaas, 2001; Mullineaux, 2014), allow cyanobacteria to resist the heterogeneous marine environment, which can be challenging for bacterial survival. These microorganisms are common in many habitats such as lakes, ponds, springs, wetlands, streams, rivers, soil crust, microbial mats, sands, and rocks (Ramos *et al.*, 2018; De Oliveira *et al.*, 2019; Cordeiro *et al.*, 2020). For instance, cyanobacteria are the primary colonizers of ice sheets by forming and surviving in pigmented mats, making these ecosystems productive (Vincent, 2000), and their association with heterotrophic organisms in the desert facilitates the productivity of soil crust (Pointing and Belnap, 2012). Moreover, as early colonizers of submerged surfaces, these microorganisms may determine the structure and function of the mature biofilm (Mitbavkar *et al.*, 2012; Dang and Lovell, 2016). Cyanobacteria species also produce large amounts of EPS (Rossi and De Philippis, 2015; Anderson, 2016), which represent the major and an essential component of biofilms communities. EPS include polysaccharides, proteins, lipids, and extracellular DNA as a result of metabolism and cell

death (Sutherland, 2001). These substances are responsible not only for biofilm structure, stability, and cohesion but also provide anchoring sites for extracellular enzymes, which may degrade toxic compounds (Limoli *et al.*, 2015). Moreover, EPS maintains a highly hydrated microenvironment due to water retention ability, thus promoting nutrients' entrapment (Flemming and Wingender, 2010). Advantages of EPS for embedded microorganisms on biofilms also include establishing an ideal microenvironment for the exchange of genetic information and protection from predation (Decho and Gutierrez, 2017).

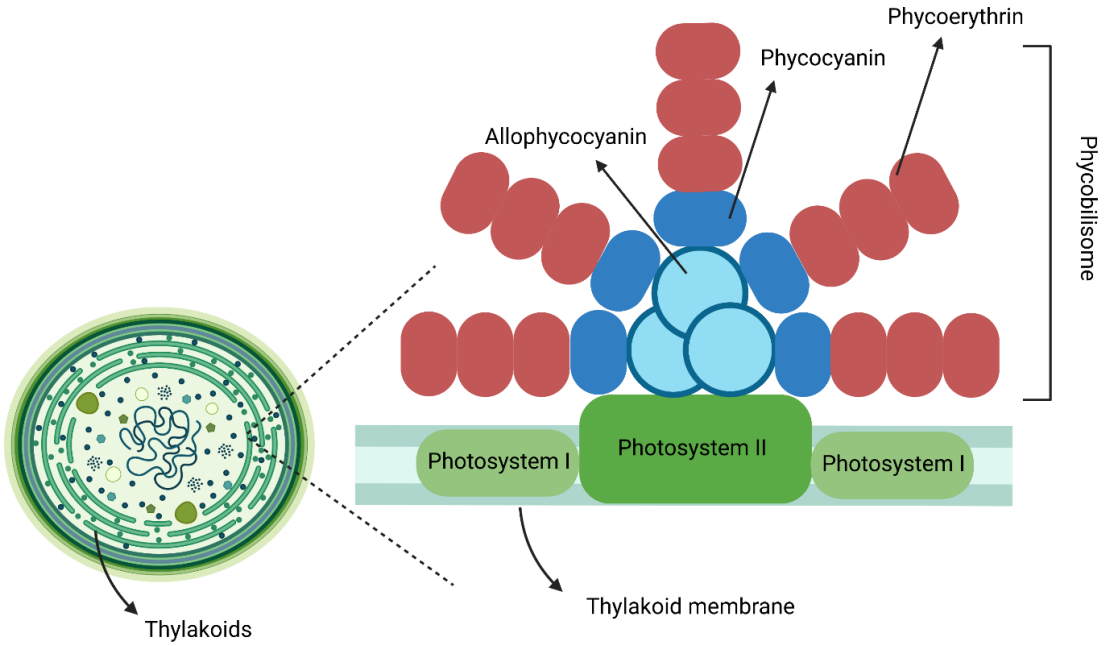

Figure 2.4. Structural model of cyanobacterial phycobilisome. This image was created with BioRender (https://biorender.com/).

Although their prevalence depends on geographical area and season, together with diatoms, cyanobacteria constitute the major components of marine biofilms (Narváez-Zapata *et al.*, 2005; Salta, Wharton, *et al.*, 2013; Bharti *et al.*, 2017). It is noteworthy that the ratio of bacteria:diatoms:flagellates observed in biofilms in the White Sea was 640:4:1 (Railkin, 2003). Moreover, symbiotic relations between cyanobacteria and diatoms can occur on marine biofilms (Amin *et al.*, 2012) since nitrogen-fixing cyanobacteria supply fixed nitrogen to diatoms, likely in the form of ammonia or dissolved organic nitrogen (Foster *et al.*, 2011). Despite several studies that focus on the interaction of microfoulers

and the attachment of macrofouler organisms showed contradictory results, most of them presented a positive correlation between biofilm formation and macrofouling attachment and development (Mieszkin *et al.*, 2013; Salta, Wharton, *et al.*, 2013). It has been considered that biofilm formation by bacteria and algae is important to the subsequent settlement of macrofouler organisms. Nevertheless, this process can be influenced by many factors such as biofilm age (Chung *et al.*, 2010; Campbell *et al.*, 2011), density, the presence of single or mixed species, and the surface material (Mieszkin *et al.*, 2012).

Table 2.2. Main relevant characteristics of cyanobacteria for marine biofouling.

Characteristics	Reference
High adaptation ability to harsh conditions	Berg and Sutula, 2015; Bharti *et al.*, 2017
Early marine surface colonizers Major components of marine biofilms	Nagarkar *et al.*, 2004; Narváez-Zapata *et al.*, 2005; Nayar *et al.*, 2005; Mitbavkar *et al.*, 2012; Salta *et al.*, 2013; Oberbeckmann *et al.*, 2014; Bharti *et al.*, 2017; Jiang *et al.*, 2018; Azevedo *et al.*, 2020
Produce large amounts of EPS	Abed *et al.*, 2009; Rossi and De Philippis, 2015; Di Donato *et al.*, 2016(Abed *et al.*, 2009; Rossi and De Philippis, 2015; Di Donato *et al.*, 2016)
Promote the settlement and metamorphosis of macrofouler organisms	Chung *et al.*, 2010; Campbell *et al.*, 2011; Toupoint *et al.*, 2012; Wang *et al.*, 2012

2.4 Main factors affecting biofouling

In marine environments, different environmental, physical, chemical, and biological parameters affect biofouling development (Figure 2.5). Environmental factors such as radiation (Behrendt *et al.*, 2012), water dynamic flux, pH (Brown *et al.*, 2018), salinity, temperature (Lau *et al.*, 2005), dissolved oxygen (Lagos *et al.*, 2016), CO_2 (Brown *et al.*, 2018), and nutrient availability (Briand *et al.*, 2012) can influence biofilm community dynamics. In fact, unlike in dark environments, photosynthetic conditions promote the production of EPS and proteins involved in micronutrient transport (Stuart *et al.*, 2016). Surface energy, colour, topography, wettability, roughness, electrostatic charge, and hydrophobicity are some properties that may affect the first steps of biofouling, from cell

adhesion to biofilm growth, and their characteristics (Dang and Lovell, 2000; Hodson *et al.*, 2000; Jones *et al.*, 2007; Palmer *et al.*, 2007; Lee *et al.*, 2008; Chung *et al.*, 2010; Gambino *et al.*, 2019). Moreover, bacterial community variability has been reported on different marine biofilms (Catão *et al.*, 2019; Caruso, 2020).

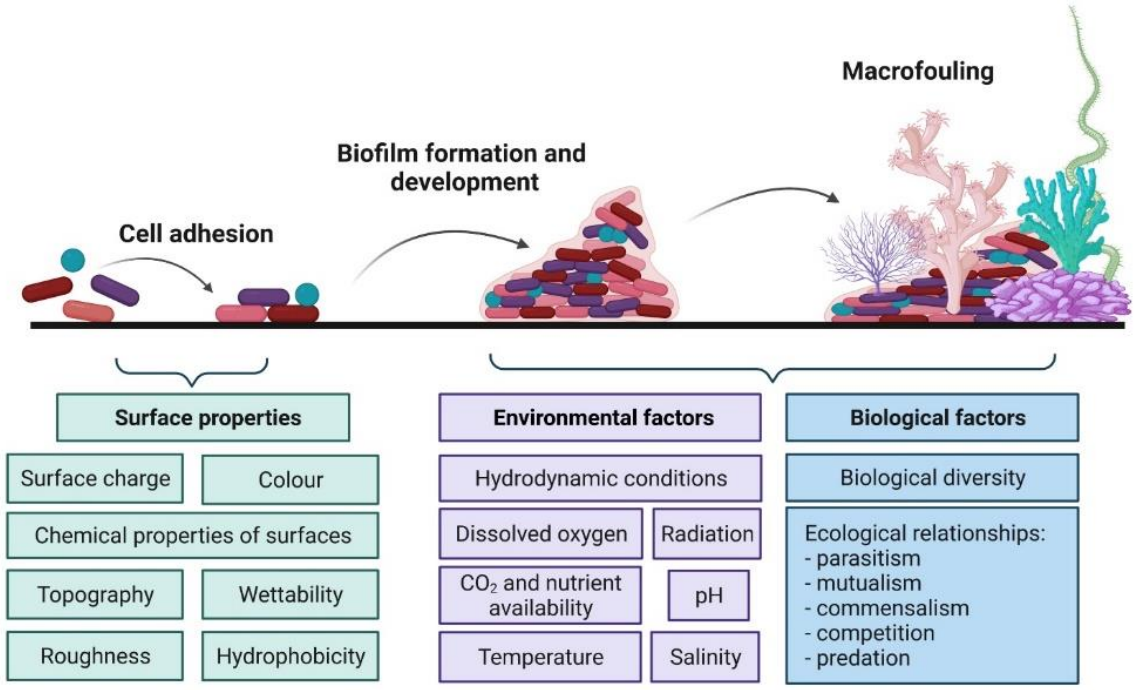

Figure 2.5. Main factors affecting marine biofouling. This image was created with BioRender (https://biorender.com/).

More than 4,000 biofouling species have been identified in marine environments (Yebra *et al.*, 2004). The composition of biofouling communities changes significantly with the geographical location, season, and local depths, and is affected by several abiotic and biotic factors, as discussed before. Among biotic factors, the biology of the different organisms dictates how likely a settlement occurs on a submerged substratum (Vinagre *et al.*, 2020). After the initial attachment of bacteria, surfaces get colonized by cyanobacteria, fungi, unicellular algae, and bacteria-eating protozoa. In the absence of high hydrodynamic forces, such biofilm communities can grow extensive mats or slimes (Matz, 2011). The close spatial proximity of these microorganisms at surfaces is responsible for specific interspecies interactions (competition or cooperation) and

generates complex and highly differentiated microbial communities (Guillonneau *et al.*, 2018).

In the case of cyanobacteria, they are usually found in biofilms from a particular tidal level (Qian *et al.*, 2007) and such specificity may be associated with the differential larval settlement observed by some authors (Morse *et al.*, 1984; Lee *et al.*, 2014). It has been reported that cyanobacteria induce larval settlement of molluscs (Morse *et al.*, 1984); however, their ability to induce or inhibit the larval settlement of barnacles has not been studied in detail (Morse *et al.*, 1984). Therefore, certain microorganisms in marine biofilms, such as cyanobacteria and proteobacteria, might have an essential role in larval settlement preference (Lee *et al.*, 2014), and further studies focusing on these candidates would definitely be valuable.

As most biofilm communities are composed of multiple different organisms living in close proximity, it is intuitive that the microbial composition plays a major role in surface colonization and should probably be considered when evaluating the performance of novel antifouling surfaces. Nevertheless, numerous difficulties exist in studying mixed biofilms at a laboratory scale: (i) the lack of knowledge regarding the identity and abundance of each biofilm resident, which makes it difficult to select the organisms and their initial concentration for the *in vitro* assays, (ii) labeling the different populations, in particular when they are not amenable to genetic manipulations, (iii) identifying which metabolites can be produced and by who, interpreting why one strain is more fit than another, and (iv) some technical limitations associated with biofilm reactors (Guillonneau *et al.*, 2018; Faria, Gomes, *et al.*, 2021). As a result, very limited information is available on multispecies biofilms and their microhabitats in aquatic scenarios (Rao *et al.*, 2005; Burmølle *et al.*, 2006; Guillonneau *et al.*, 2018). A recent work from our research group (Faria, Gomes, *et al.*, 2021) discusses exactly the relevance of using mixed populations instead of single cultures for *in vitro* screening assays of marine antifouling materials. Single and dual-species biofilms of a marine bacterium (*Pseudoalteromonas tunicata*) and a coccoid cyanobacterium (*Cyanobium* sp. LEGE 10375) were grown for 49 days on an epoxy resin with known antifouling activity (Faria, Teixeira-Santos, Romeu, *et al.*, 2020). Whereas *P. tunicata* alone showed a biofilm growth kinetics similar to mixed biofilms, cyanobacterial biofilms presented a higher number of cells, wet weight, thickness, and

biovolume when compared to dual-species biofilms (Faria, Gomes, *et al.*, 2021). Indeed, *Cyanobium* sp. LEGE 10375 biofilms corresponded to the worst-case scenario, i.e., the conditions that originated higher biofilm amounts on the tested surface (Faria, Gomes, *et al.*, 2021). These results suggest that for initial screening, starting with a single representative organism like a cyanobacterium is a good compromise between the high complexity of *in vivo* marine ecosystems and the ease of *in vitro* testing.

2.4.1 Hydrodynamic conditions

Hydrodynamic conditions may affect all stages of biofilm development. While higher flow velocities improve molecular transport by convection, the higher density of biofilms decreases the diffusivity of the molecules inside them (Stewart, 2003). Furthermore, stronger shear forces are responsible for higher biofilm sloughing or detachment (Liu and Tay, 2002). There is evidence that hydrodynamics affects not only the biofilm structure and architecture but also plays a crucial role in mass transfer, EPS production, energy metabolism, and can induce genetic or molecular changes (Horn *et al.*, 2003; Rochex *et al.*, 2008; Graba *et al.*, 2013; Gloag *et al.*, 2020). Previous studies concluded that shear forces also affects biofilm diversity since biofilm species composition changed with increasing shear stress (Rochex *et al.*, 2008; Catão *et al.*, 2019). Indeed, a study that aimed to evaluate the settlement of diatoms to different antifouling coating revealed that biofilm adhesion, diatom abundance and diversity were found to be significantly different between static and dynamic treatments (Zargiel and Swain, 2014). Therefore, when the performance of antifouling surfaces is assessed *in vitro*, it is crucial that experiments are performed in controlled hydrodynamic conditions, where the shear stress or shear rate are well defined (Gomes *et al.*, 2019; Alves, Gomes, Vorobii, *et al.*, 2020) in order to bring the *in vitro* operational conditions closer to the natural aquatic environments. Due to the effect of reactor geometry on the flow, these two parameters should be considered to characterize shear effects/hydrodynamic conditions. The shear rate is the derivative of the velocity in the perpendicular direction from the wall system (Munson *et al.*, 2002), quantifying the frequency at which cells contact the surface. The shear stress in Newtonian fluids is proportional to the shear rate, where the fluid viscosity

is the constant of proportionality (Munson *et al.*, 2002), translating the friction from the fluid acting on the adhered cells/biofilm. CFD is a commonly used approach to model biofilm reactors since it enables the estimation of the fluid flow parameters of these systems faster and at a relatively low cost in comparison to experimental techniques (Werner *et al.*, 2014). Moreover, CFD provides much more detailed information about the flow field since the results are obtained for a larger number of points in the flow than in a regular experiment (Alexandrou, 2001). The geometry of the reactor is divided into a finite set of volumes - the cells, forming a computational grid - the mesh. Fluid flows are described by differential equations, and CFD replaces these equations with algebraic equations, which can be numerically solved for each cell, resulting in a flow field (Sharma *et al.*, 2011). Through the standardization of biofilm reactors and operation conditions, the comparison of hydrodynamics data obtained from different laboratories is possible. However, few experimental setups have been used to study the effect of hydrodynamics in marine biofilms; most of them are microfluidic devices (Salta, Capretto, *et al.*, 2013; Alles and Rosenhahn, 2015; Nolte *et al.*, 2017; Chun *et al.*, 2022), or platforms that specifically evaluate macrofouling development (Qian *et al.*, 1999, 2000; Dimartino *et al.*, 2014). Microfluidic devices have demonstrated high potential and versatility for the study of biofilm formation under different growth conditions. These platforms allow the testing of different types of materials at highly controlled hydrodynamic conditions through a precise, non-invasive, and real-time analysis (De Grazia *et al.*, 2020). In fact, a microfluidic assay used to quantify how easily diatoms can be removed from several surfaces through shear forces application showed that, while the number of adhered cells was barely affected by the different coatings, the critical shear stress required for their removal varied significantly (Alles and Rosenhahn, 2015). Although these devices require small volumes to operate and can be custom-made for specific purposes, they require special equipment for manufacturing and operation. Moreover, clogging events can occur due to the small dimensions, air bubbles can have a very significant effect, and viscosity effects are also critical (Gomes and Mergulhão, 2021).

It was also demonstrated that biofilms grown at lower velocities exhibit lower cell density and higher effective diffusivity, whereas biofilms grown at higher flow velocities have higher cell density and lower effective diffusion (Horn *et al.*, 2003). Since it has been

reported that the slow flow of water (0.2 $m.s^{-1}$) promotes the growth of filamentous green algae and cyanobacteria (Flemming *et al.*, 2009), biofouling can be favoured at these low fluid velocities that can be found in harbours and dockyards (when ships are anchored, berthed or moored), and by slow-moving vessels such as oil platforms, oceanic barges, tugs, dredges, fishing vessels, and recreational crafts (Minchin and Gollasch, 2003; Hewitt *et al.*, 2009). In addition, long stays at harbours also increase the opportunities for marine fouling species to attach to immersed surfaces and accumulate (Davidson *et al.*, 2009; Hewitt *et al.*, 2009). Indeed, containerships that travel at relatively high speeds and remain in ports for short periods seem to be less colonized than other types of vessels (Davidson *et al.*, 2009). However, the impact of hydrodynamic conditions in the marine environment is a considerable challenge since the fouling organisms have evolved the ability to attach and proliferate on a range of surfaces, not only when subjected to lower water velocities but even under high turbulent conditions, like at 125,000 s^{-1}, the reported shear rate value for a navigating ship (Alexandrou, 2001; Bakker *et al.*, 2003).

In marine environments, although a shear rate of 50 s^{-1} has been reported for a ship in a harbour (Alexandrou, 2001; Bakker *et al.*, 2003), equipment and devices which are in similar environments, such as partially submerged or moored equipment as underwater cameras, flotation spheres, sensors, and even transparent hulls of boats or their windows, are likely to be subjected to similar shear values (Figure 2.6). Few studies have focused on the impact of hydrodynamic conditions on marine biofilms. To study how microalgae biofilms respond to different hydrodynamic conditions, the architecture and cohesion of *Chlorella vulgaris* biofilms were investigated in flow-cells at three different shear stress: 1, 6.5 and 11 mPa. Biofilms cohesion was heterogeneous at low shear stress, resulting in a strong layer, close to the substrate, and in more loose superficial ones. In turn, higher shear stress increased the cohesion of the biofilms allowing them to grow thicker and produce more biomass (Fanesi *et al.*, 2021). Using a microfluidic flow cell, the impact of shear stress on *Cobetia marina* and *Pseudomonas aeruginosa* biofilm formation was also evaluated (Chun *et al.*, 2022). The results indicated that hydrodynamics affect biomass, maximum thickness, and surface area of biofilms, with the higher shear stress (5.6 Pa) promoting thinner biofilms than lower shear stress (0.2 Pa). Particularly on cyanobacterial biofilms, studies performed by our group on coccoid cyanobacteria (Faria, Teixeira-

Santos, Romeu, *et al.*, 2020; Faria, Teixeira-Santos, Morais, *et al.*, 2021) at controlled hydrodynamic conditions (values of shear rate of 4 s^{-1} and 40 s^{-1}) showed a higher biofilm development at the lower shear rate. In fact, a study performed on *Synechocystis salina* LEGE 00041, *Synechocystis salina* LEGE 06155 and *Cyanobium* sp. LEGE 06097 revealed that the number of adhered cells was higher at 4 s^{-1} than 40 s^{-1} for both adhesion (7.5 h) and biofilm development (6 weeks) assays (Faria, Teixeira-Santos, Morais, *et al.*, 2021), suggesting that shear forces have an influence not only on the early stages of adhesion and biofilm formation but also during maturation. Indeed, higher shear forces may hamper initial cell adhesion and facilitate the detachment of adhered microorganisms during irreversible steps of biofilm formation, whereas at later stages of biofilm development, erosion and sloughing events can be promoted by the increased shear forces. A study performed by David *et al.* (2015) also showed significant differences in biofilm development of *Synechocystis* sp. PCC 6803 in a capillary microreactor depending on the hydrodynamic conditions applied. Two different flow patterns were applied: a single-phase flow (after the cell attachment phase, the flow was set to 100 $\mu L.min^{-1}$, and it was kept constant during the whole cultivation time), and a segmented flow (after the cell attachment phase, the flow was set to 100 $\mu L.min^{-1}$, kept constant for 2 days and subsequently, segmented flow was established, and air segments were introduced). While under single-phase flow, clogging of the capillary occurred due to uncontrolled biomass formation, the application of segmented flow prevented clogging by changing the structure of the cyanobacterial biofilm. A photosynthetically active, compact, and flat biofilm was formed upon the introduction of an air segment into the system without any cell detachment events (David *et al.*, 2015). Heuschkel *et al.*, (2020) also observed that the change in flow conditions from single to aqueous-air segmented flow resulted in faster growth, improved surface coverage, and enhanced biomass formation. In this study, the growth and catalytic performance of mixed-species biofilms comprising *Synechocystis* sp. PCC 6803 and *Pseudomonas* sp. VLB120 was investigated under biofilm cultivation in capillary glass reactors at different flow regimes. Four phases could be observed for mixed-species biofilm growth in the glass-capillaries, which include biofilm growth in the single-phase flow condition, a rapid increase in biofilm spatial coverage after the start of

air-segments, biofilm sloughing and detachment, and the final stage consisted of biofilm regrowth (Heuschkel *et al.*, 2020).

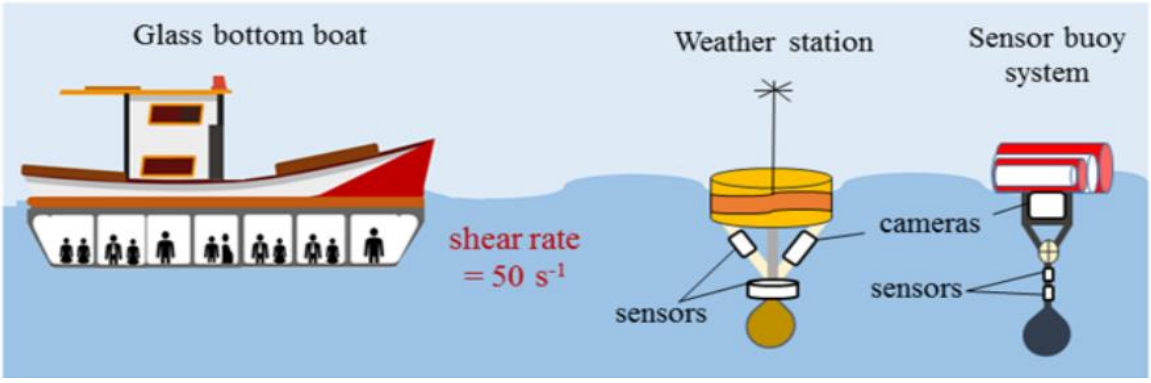

Figure 2.6. Representation of some marine equipment and devices, such as partially submerged underwater cameras, flotation spheres, sensors, and transparent hulls of boats or their windows, that are likely to be subjected to average shear rate values of 50 s^{-1}. This image was created with BioRender (https://biorender.com/).

When external shear forces become more substantial than the biofilm adhesive forces, sloughing and detachment events occur (Horn *et al.*, 2003; Paul *et al.*, 2012), which are phenomena considered to be an integral part of biofilm development (Rumbaugh and Sauer, 2020). Viscoelasticity can promote biofilm resistance when subjected to higher shear forces (Gloag *et al.*, 2020), and this property is largely governed by EPS from the biofilm matrix (Peterson *et al.*, 2021). Moreover, in photosynthetic organisms, the shear sensitivity is determined by cell morphology, the presence of flagella, and cell wall, which in cyanobacteria are mainly composed of peptidoglycan (Stanier and Cohen-Bazire, 1977).

Due to the importance of hydrodynamic conditions on biofilm development, *in vitro* studies should consider and mimic the conditions that typically prevail in marine environments. Consequently, novel marine reactors should be developed and/or characterized, based on the study goals, the balance between the pros and cons associated with their use, and the operational conditions that should enable them to mimic, as closely as possible, the marine environment.

2.4.2 Surface properties

The first step in the biofouling process consists of finding a suitable surface, which for cyanobacteria in an aquatic environment is essential to form a biofilm and gain access to light and nutrients (Wetherbee *et al.*, 1998; Rossi and De Philippis, 2015). Surface association is considered a survival mechanism for microorganisms since it enhances organism interactions, access to nutritional resources, and environmental stability, which is of particular importance in natural ecosystems where conditions are highly dynamic and nutrients are growth limiting (Dang and Lovell, 2016).

Numerous types of surfaces with distinct physicochemical properties exist in marine environments (Caruso, 2020). These surfaces include living animals and plants or abiotic surfaces such as mineral substrata or submerged constructions. Different materials are used in marine submerged man-made equipment, like aquaculture facilities, underwater windows, sensors and measuring devices, protective equipment, swim platforms, ship and boat structures, and anchors, which are susceptible to biofouling. Common materials include glass, plastic, thermoplastics (e.g., acrylic, polyvinyl chloride, polystyrene, nylon, polypropylene), metallic materials (e.g., copper, steel, stainless steel, aluminum, titanium), foams (e.g., epoxy syntactic foam), and polymeric composite materials (e.g., fiber-reinforced plastics, wood, metal) (Table 2.3). It has already been reported that the nature and characteristics of the surface where a biofilm develops have a strong influence on biofilm structure, differentiation, and function (von Ammon *et al.*, 2018; Cai *et al.*, 2019). Erosion and sloughing mechanisms in cyanobacterial biofilms can also be affected by the surface (Hoschek *et al.*, 2019; Heuschkel *et al.*, 2020). Indeed, sloughing events that occurred on glass (Heuschkel *et al.*, 2020) were more significant than those that occurred on polystyrene (Hoschek *et al.*, 2019). This finding could be related to the fact that biofilm cells were weakly adhered to glass compared to polystyrene, or glass biofilms became weaker with growth due to nutrient starvation, oxidative stress, or a different stress response (Heuschkel *et al.*, 2020).

Table 2.3. Commonly used materials in marine equipment, their applications, main benefits, and disadvantages.

Material		Marine equipment/devices	Advantages	Drawbacks
Plastics		Boats windows Floating or submersible cages Hydrographic sensors / measuring devices (lenses, housings, underwater cameras) Protective equipment, deck components and dock fender facings Structural components in the oil drilling and exploration industry Swim platforms Underwater seismology industry	UV, saltwater, chemical, and corrosion resistance. Insulating properties.	Unsuitable for high temperatures. Marine exposure may cause some swelling.
Thermo-plastics	**Poly(methyl methacrylate) (e.g., commercial perspex)**	Hydrographic sensors / measuring devices (lenses, housings, underwater cameras) Underwater windows for swimming pools	UV, and chemical resistance. Greater clarity than glass. Lightweight. Easy to shape and repair.	More expensive than glass. Sensitive to strong acids and bases.
	Polyvinyl chloride (PVC)	Recirculating aquaculture systems and aquaculture facilities (fish cages) Sensor mounting blocks, housings Pipes and tanks	Generally, it shows good resistance to the marine environment. Resistant to alcohols, aliphatic hydrocarbons, oils, bases, and weak acids. Easy to shape.	Absorbs some moisture with time. Often broken by shock. Sensitive to strong acids, ketones, esters, and aromatic hydrocarbons.
	Polystyrene	Small boats Hydrographic sensors / measuring devices Floating docks, pontoons, buoys, net and fishing floats	Cost-effective. Good floatation properties. Easy to cut.	Poor UV resistance.
	Nylon	Small boats Aquaculture facilities Bearings, gears, bushings, housings, rods, ropes, coatings for saltwater pipes	Chemical resistance. Strong and stretchy. Resistant to bases, weak acids, and to the most common solvents. Moderate price.	Embrittled by prolonged exposure to sunlight. Sensitive to strong acids, phenols, and formic acid. Water absorption and swelling may alter dimensions and mechanical properties. Performance weakens after wetting.

Material		Marine equipment/devices	Advantages	Drawbacks
	Polypropylene	Small boats Wire and cable coatings, ropes, and packaging.	Floating and elastic material. Oil, grease, abrasion, chemical resistance. Excellent resistance to the marine environment. Low price. No water absorption.	Sensitive to strong acids. Poor UV resistance. Low stretchability (not as good as nylon).
Metallic materials	**Titanium**	Ship structures (pumps, impellers, structural members), submarine hulls Offshore industry	Corrosion resistance.	Expensive. Harder to get material configured.
	Copper	Hydrographic sensors / measuring devices Aquaculture facilities (fish cages)	Antimicrobial properties. Corrosion resistance.	Expensive.
	Stainless steel	Hydrographic sensors / measuring devices (underwater cameras) Recirculating aquaculture systems Cargo tanks, boating applications and oil rigs	Corrosion resistance. Good stability, appearance, durability, strength, and stiffness.	High fabrication costs.
	Steel	Boats, commercial ships, large tankers, container ships, and ship hulls Navigation buoys, anchors Offshore platforms	Low price. Amenable to molding, rolling, forging, spinning, and stamping.	Weight of steel in ship constructions.
	Aluminum/ aluminum alloys	Superstructures of large ships Floating buoys Hull structure of some ferries and small boats	Very flexible and easy to solder (available in most shapes) and sizes. Lighter than steel. Corrosion and chemical resistance. Non-magnetic properties. Low-cost maintenance.	High initial and fabrication costs.
Glass		Flotation spheres Recirculating aquaculture systems Hydrographic sensors / measuring devices (lenses, housings) Underwater windows for swimming pools	Costs less than plastics. More scratch resistant than plastic. Resistance to the marine environment.	Easily broken. Repairs are time-consuming. Does not insulate as well as plastics. Sensitive to hydrofluoric acid and sodium hydroxide.
Polymeric composite materials (e.g. fiber-reinforced plastics, metals, or combinations of fiber-reinforced plastics, wood, metal)		Recirculating aquaculture systems Offshore and dock infrastructures Boats, canoes, small harbour craft, fishing trawlers, yachts, lifeboats	Low maintenance cost. High specific strength. Corrosion and thermal resistance. Low weight.	High material cost.

Material	Marine equipment/devices	Advantages	Drawbacks
	Marine renewable energy devices		
Foams (e.g. commercial Surlyn foam and epoxy syntactic foam)	Floating buoys or on dock Marine coatings, adhesives, patching compounds	Easy to shape. Resistant to organic solvents and weak acids and bases.	Expensive. Sensitive to sulfuric and acetic acid.

Compiled from Roy, 1994; Taylor, 1996; King *et al.*, 2006; Mansour and Liu, 2008; Mohan, 2008; Molland, 2008; Davies and Rajapakse, 2013; Harper *et al.*, 2016; Cai and Arias, 2017; Dong and Le, 2018.

Different approaches have been used to correlate bacterial adhesion with the physicochemical properties of surfaces. However, a detailed understanding of the mechanisms underlying cell-surface interactions is still not available. Although recent studies have attempted to replace macroscopic measurements for methods that directly measure cell-surface interaction forces by using, for example, atomic force microscopy, total internal reflection microscopy, quartz crystal microbalance, microbial adhesion to hydrocarbons (Bos *et al.*, 1999; Li and Logan, 2004; Tuson and Weibel, 2013), contact angle measurements remain a commonly used, fast and economic method to determine the surface energy in the laboratory (Soon *et al.*, 2013). Electrostatic, Lifshitz–van der Waals and Lewis acid-base interactions are usually considered responsible for the interactions at the surface interface. The thermodynamic approach refers to bacteria/surface interaction as an equilibrium process (Flemming *et al.*, 2009). The ratio between Lifshitz-van der Waals apolar component and the electron donor component (γ^{LW}/γ^{-}) was shown to correlate with bacterial adhesion to the surfaces of ship hulls and heat exchangers (Liu and Zhao, 2011). In a study performed by Liu and Zhao (2011), coatings with the lowest γ^{LW}/γ^{-} ratio had the lowest bacterial adhesion values. Understanding the thermodynamics of microbial adhesion is important since it helps to predict whether the adhesion of a given bacterium is favorable or not on different surfaces (Moreira, Simões, *et al.*, 2015). Moreover, knowing the physicochemical parameters of the surface, it is possible to develop new strategies that make the surface less prone to microbial adhesion. Antifouling coatings can be divided into chemically bioactive coatings and biocide-free coatings. The chemically active antifouling technologies, which act through the controlled release of bioactive molecules, most recently of booster biocides, can be subdivided into three main categories: contact leaching coatings, controlled-depletion paints and self-polishing copolymers (SPC), and a few combinations thereof. All these technologies control the release of bioactive molecules via various chemical mechanisms, many of which remain partially understood (Bressy *et al.*, 2009). From those, SPC coatings are the most successful antifouling coating technology in terms of long-term efficiency in service life, and where the biocidal compound is chemically bonded to the binder, which gradually hydrolysed and dissolved in water to release the antifouling bioactive agent. On the other hand, among the biocide-free coatings technologies, the fouling release coatings (FRC) are the most acceptable and

implemented in the marine industry, mostly allied to its eco-friendly biocide-free antifouling strategy, acting through physical-chemical and mechanical mechanisms, and long-term efficiency, particularly for dynamic systems (e.g., ships) (Camps *et al.*, 2014). Several studies have also described the influence of surface roughness in biofilm formation (Whitehead *et al.*, 2010; Skovager *et al.*, 2012). Since surface roughness increases the surface area available for bacterial adhesion, it serves as a scaffold for attachment, as well as a protection for bacteria against hydrodynamic forces (Scardino *et al.*, 2008; Yandi *et al.*, 2014). Therefore, the consensus is that bacterial adhesion and biofilm development increase as surface roughness increases (Zheng *et al.*, 2021). Several methodologies have been used to extract topographical data from a surface, such as surface roughness, which includes AFM (Alves, Gomes, Vorobii, *et al.*, 2020) and Optical Profilometry (Skovager *et al.*, 2012).

Fouling organisms have mechanisms that allow them to colonize different surfaces, and studies relating to surface properties and marine fouling have been performed (Table 2.4). Epoxy-coated glass and silicone hydrogel coating were effective in inhibiting coccoid cyanobacterial biofilm formation, also affecting its architecture (Faria, Teixeira-Santos, Gomes, *et al.*, 2020; Faria, Teixeira-Santos, Romeu, *et al.*, 2020, 2021; Faria, Teixeira-Santos, Morais, *et al.*, 2021). 2D OCT analyses performed on biofilms developed on the silicone hydrogel coating revealed that these biofilms had a lower percentage and size of empty spaces when compared to perspex, polystyrene, glass, and epoxy-coated glass (Faria, Teixeira-Santos, Romeu, *et al.*, 2021). Additionally, biofilm structure was strongly affected by the cyanobacterial strain, regardless of the surface (Faria, Teixeira-Santos, Romeu, *et al.*, 2021). For example, a homogeneous arrangement and uniform layer closer to the surface were observed for *Synechocystis salina* LEGE 00041, while for *Cyanobium* sp. LEGE 10375 the biofilm structure was more heterogeneous and the presence of 3D streamers on the biofilm top was observed for the same surface material (Figure 2.7). Epoxy and silicone hydrogel are two commercially available marine coatings for ship hulls, marine water inlet piping, and grids in power stations (Taylor, 1996; Blain *et al.*, 2004). Epoxy-coated glass surfaces were effective in inhibiting biofilm formation at the initial stages, while the silicone hydrogel coating showed high antibiofilm efficacy during biofilm maturation (Faria, Teixeira-Santos, Gomes, *et al.*, 2020). Silicone hydrogel surfaces used in that work are a third-generation

hydrogel-based FRC that acquires a more hydrophilic behavior upon contact with water (Xie *et al.*, 2011; Tulcidas *et al.*, 2015). They are among the most successful marine antifouling coatings due to their high elasticity properties, along with the prevention of either hydrophobic or hydrophilic interactions, which delay the adsorption of proteins, bacteria, and subsequent fouling (Selim *et al.*, 2017; Hu *et al.*, 2020). Additionally, it has been evident that sequential biofilm dynamics should be carefully considered since initial processes of formation differ from the long-term ones (Faria, Teixeira-Santos, Gomes, *et al.*, 2020; Briand *et al.*, 2022).

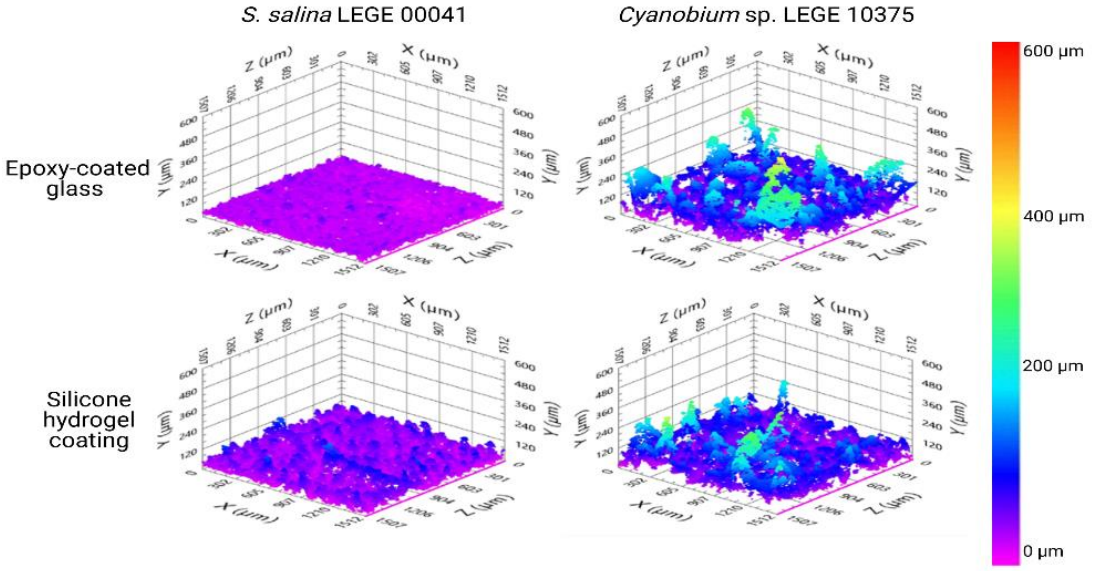

Figure 2.7. Representative 3D OCT images of *S. salina* LEGE 00041 and *Cyanobium* sp. LEGE 10375 biofilms formed on epoxy-coated glass and silicone hydrogel coatings after 7 weeks of *in vitro* incubation. The color scale shows the range of biofilm thickness. Adapted from Faria, Teixeira-Santos, Romeu, *et al.*, 2021.

Advances in novel and effective environmentally friendly coatings are needed to control marine fouling. The use of natural compounds with antifouling activity such as QS inhibitors, phytochemicals, antimicrobial peptides, bacteriophages, or specific enzymes which degrade adhesives used for settlement, disrupt the biofilm matrix, or interfere with intercellular communication, are under investigation and some of them can be incorporated on surfaces (Dobretsov *et al.*, 2007, 2013; Kristensen *et al.*, 2008; Fusetani, 2011; Carvalho, 2012; Almeida and Vasconcelos, 2015; Michailidis *et al.*, 2020). Although some of these compounds can be obtained

from marine organisms, including cyanobacteria (Almeida *et al.*, 2015; Antunes, Pereira, *et al.*, 2019), they need to be produced in significant amounts to be incorporated into surface materials, which carries technical and economic challenges. Modifications of surface charge potential, hydrophobicity, and surface topography (Scardino *et al.*, 2008; Schumacher *et al.*, 2008) are also promising strategies. Recently, biomimetic antifouling surfaces have also been explored, and they have produced promising results (Scardino and de Nys, 2011; Brzozowska *et al.*, 2014, 2017). Nanostructured surface-based approaches could open new perspectives for developing antibiofilm surface materials, however nanoscience-based surface modifications are still at an early stage of research. Therefore, further investigation related to nanoscience-based technologies is required for these to become promising candidates for the development of novel materials for biofilm inhibition (Zheng *et al.*, 2021). For example, graphene-coated materials can affect the surface energy and electrostatic interactions between material and bacteria (Parra, Dorta, *et al.*, 2015; Jin, Bing, *et al.*, 2019; Jin *et al.*, 2021; Zhang and Mikkelsen, 2021). Superhydrophobic surfaces, which present a high water contact angle, typically > 150°, have also been tested as improvements for marine surfaces (Scardino *et al.*, 2009; Ferrari *et al.*, 2015; Selim, Elmarakbi, *et al.*, 2018). A study performed by Scardino et al. (2009) reported three superhydrophobic coatings that inhibited the attachment of spores of algae and larvae of several invertebrates. Furthermore, studies performed by Ellinas *et al.* (2017) and Kefallinou *et al.* (2020) described "hybrid" metal-sputtered superhydrophobic surfaces demonstrating both bacterial repulsion and long-term killing efficacy against the cyanobacteria *Synechococcus* sp. PCC7942. Among the two low surface energy hydrophobic coatings used, a chlorosilane and a fluorocarbon coating, the fluorocarbon layer managed to better secure the superhydrophobicity and anti-adhesiveness of the surface when enriched with an adequate amount of copper (Kefallinou *et al.*, 2020). These bifunctional surfaces with both antifouling and bactericidal action can be a promising strategy to manage marine biofouling.

Overall, to manage environmental concerns associated with marine fouling and comply with the increasingly strict and demanding legislation in this area, solutions to the development of a new generation of environmentally friendly marine coatings are required. Improvements in

nanotechnology, polymer science, and the development of innovative surface models inspired by nature, are expected to have a significant impact on the progress of antifouling methodologies.

Table 2.4. Studies focused on different surface/coatings used in marine environments in the last ten years (studies performed exclusively on macrofouler organisms were not included in this table).

Surface/coatings	Organism	Experimental setup	Major findings	Reference
Titanium Aluminum Limestone Shale Glass	Deep-sea bacterial communities	*In situ* study Ionian Sea, Greece Sea (1500, 2500, 3500 and 4500 m below the water level, and surfaces were deployed in vertical and horizontal positions) 155 days, 14 °C	Depth played an important role in the composition of deep-sea biofouling communities, while substratum type and orientation of substrata throughout the water column were less important.	Bellou *et al.*, 2012
Polystyrene Teflon® Sea Quantum Classic® antifouling commercial coating (Cu_2O-CuPy (copper(I) oxide-copper pyrithione)) Intersmooth® 360 antifouling commercial coating (Cu_2O-ZnPy (copper(I) oxide-zinc pyrithione) 2 antifouling coatings synthesized at the laboratory (Cu_2O(copper(I) oxide)-A4S ® -Sea Nine ® -Zineb ® and Cu_2O(copper(I) oxide)-Zineb ®)	Microfoulers	*In situ* study French Mediterranean coast (Toulon military harbour and the natural protected area of Porquerolles Island) 2 weeks	Pioneer microalgal communities on all surfaces were dominated by the same two diatom species: *Licmophora gracilis* and *Cylindrotheca Closterium*. A low diatom abundance was observed on antifouling coatings when compared to polystyrene and Teflon®.	Briand *et al.*, 2012
Glass Smooth and patterned PDMS samples (biomimicking	*Amphora coffeaeformis* (diatom)	*In vitro* study Filtered seawater	The results showed a significant reduction in settlement on the micropatterned surfaces, as well as a synergistic effect when the microtopographies are combined with a zwitterionic	Brzozowska *et al.*, 2014

Surface/coatings	Organism	Experimental setup	Major findings	Reference
micropatterned surfaces inspired by the marine decapod crab *Myomenippe hardwickii*) coated with 1H,1H,2H,2H-perfluorododecyltrichlorosilane, zwitterionic polymer brush, which consists of sulfobetaine, and with layer-by-layer assembly of polyelectrolytes	*Amphibalanus amphitrite* (barnacle) Micro and macrofoulers	Diatom adhesion (24 h, 24 °C) Barnacle settlement (48 h) *In situ* Natural seawater (0.5 m below of the water level) 7 weeks	polymer brush and with the assembly of polyelectrolyte coatings.	
PVC Intersleek 757 (biocide-free commercial coating) 5 self-polishing copolymer coatings (Cu_2O-CuPy (ZnO)*, Cu_2O-ZnPy, Econea-Sea Nine, Cu_2O-A4S-Sea Nine-Zineb (ZnO)* and Cu_2O-CuSCN-ZnPy)	Microfoulers	*In situ* study Toulon Bay, Northwestern Mediterranean Sea, France (1 m below the water level) 30 days	Biocide-free coatings showed higher densities than all other coatings, except for one biocidal coating, whatever the group of microorganisms. Heterotrophic bacteria showed the highest densities, and diatoms showed the lowest, but the relative abundances of these groups varied depending on the coating. In particular, the copper-free self-polishing copolymer coatings failed to prevent diatom settlement.	Camps *et al.*, 2014
Graphene oxide in alkyd resin surface	*Escherichia coli* *Staphylococcus aureus* *Pseudomonas aeruginosa* (bacteria) Micro and macrofoulers	*In vitro* study Static assay Nutrient medium 24 and 48 h Room temperature *In situ* study Jeju Sea, South Korea 3 weeks	Graphene oxide-coated surfaces greatly reduced bacterial growth (up to 94% loss of cell viability) *in vitro* and biofouling *in situ*. These antifouling surfaces showed good corrosion-resistance behavior in both acidic and high-salt-content solutions.	Krishnamoorthy *et al.*, 2014

Surface/coatings	Organism	Experimental setup	Major findings	Reference
Graphene-coated silica	*Halomonas* spp. (bacterium)	*In vitro* study Static assay Saline solution (0.5 wt%), 72 h, 20 °C	Graphene coatings were effective in reducing the adhesion and expression levels of adhesion genes of biofilm-producing bacteria *Halomonas* spp. The effect on biofilm formation is localized right at the coated surface, and no bactericide effect of graphene coatings was observed.	Parra, Dorta, *et al.*, 2015
Cationic polymer brush (PDMAEMA) Anionic polymer brush (PSPMA) Neutral polymer brush (PHEMA-co-PEG10MA) Zwitterionic polymer brush (PSBMA)	*Cobetia marina* (bacterium) *Ulva linza* (green alga) *Balanus amphitrite* *Balanus improvises* (barnacles) Micro and macrofoulers	*In vitro* study Static/dynamic assays Tropic Marin artificial seawater Attachment of *Cobetia marina* (50 rpm, 1 h, room temperature) Settlement (static, 45 min) and adhesion strength of *Ulva linza* zoospores (shear stress of 52 Pa, 5 min) Settlement of barnacles (24 h and 48 h, 28 °C) *In situ* study Hartlepool Marina, County Durham, UK (50 cm below the water level) 2 months, 12 – 15 °C	PSPMA showed good resistance towards attachment of *Cobetia marina*, low settlement, and adhesion of *Ulva linza* zoospores, and lower biofouling than on PHEMA-co-PEG10MA or PSBMA after a field test for one week. PDMAEMA revealed potential as a contact-active anti-algal coating due to its capacity to damage attached spores. After field testing for eight weeks no significant differences in biofouling coverage were observed among the surfaces.	Yandi *et al.*, 2016
Glass Polydimethylsiloxane (PDMS) Multi-Walled Carbon Nanotubes (MWCNTs)-PDMS surfaces	Bacteria and diatoms *Mytilus*	*In situ* study Natural seawater, Zhoushan, China (0.5 – 1 m below water level) 28 days	MWCNTs- and titanium dioxide-PDMS surfaces improved bacterial density, but MWCNTs-PDMS surfaces decreased diatom density in biofilms after 28 days.	Yang *et al.*, 2016

Surface/coatings	Organism	Experimental setup	Major findings	Reference
Titanium dioxide-PDMS surfaces	*coruscus* (mussel)	*In vitro* study Static assay Autoclaved filtered seawater, 12 h, 18 °C	The maximum decreased settlement rate in 28-day-old biofilms on MWCNTs- and titanium dioxide-PDMS surfaces was > 50% in comparison to those on glass and PDMS. MWCNTs- and titanium dioxide-PDMS surfaces changed the biomass and community composition of biofilms, and decreased mussel settlement.	
Graphene-silver nanocomposites	*Halomonas pacifica* (bacterium) *Dunaliella tertiolecta* *Isochrysis* sp. (microalgae)	*In vitro* study Static assay Marine broth, 24 h, 26 °C *In vitro* study Static assay Provasoli medium 4 days	The nanocomposite displayed significant bacterial biofilm inhibition (99.6% reduction) and antiproliferative effects on marine microalgae (growth inhibition greater than 80%).	Yee *et al.*, 2016
Cupreous coatings Primocon ™ (commercially available paint)	Micro and macrofoulers	*In situ* study Auckland Westhaven Marina, New Zealand 3 months	Bacterial and eukaryotic biofouling communities responded significantly to cupreous coatings, but in opposite directions. With increasing copper concentration, bacterial diversity decreased while eukaryotic diversity increased. The highest copper concentration promoted a less taxonomically diverse micro-community, which maintained strong positive interactions between bacterial and eukaryotic species.	von Ammon *et al.*, 2018
Carboxyl and hydroxyl-modified MWCNTs-PDMS nanocomposites	Micro- and macrofoulers	*In situ* study Weihai Western Port, China (1.5 m below the water level) 56 days, 11 °C	Most nanocomposites showed weak modulating effects on pioneer biofilm communities.	Ji *et al.*, 2018

Surface/coatings	Organism	Experimental setup	Major findings	Reference
			Carboxyl-modified MWCNTs-PDMS nanocomposite with lower carboxyl content % (*w*/*w*) demonstrated a strong perturbation effect on pioneer prokaryotic colonization.	
Graphene oxide-alumina nanorods – PDMS nanocomposites	*Micrococcus* sp. *Pseudomonas putida* (bacteria) *Aspergillus niger* (fungus) Micro and macrofoulers	*In vitro* study Nutrient-infused medium 28 days, 35 °C *In situ* study Natural seawater 3 months pH of 7.6 – 8.3, salinity of 37%, 23 – 28 °C	The nanocomposite showed high adhesion resistance (up to around 95% reduction in the number of bacterial cells). The field trial revealed no fouling or surface deterioration for the nano-filled sample, as opposed to pristine PDMS.	Selim, El-Safty, *et al.*, 2018
Hydroxyl-modified MWCNTs-silicone oil-infused PDMS coatings	Marine bacteria Micro and macrofoulers	*In vitro* study Fresh seawater 10 days, 28 °C *In situ* study (1 – 2 m below the water level) Yellow Sea, China 8 months	Anti-adhesion and antifouling properties were enhanced, mainly when higher volume ratios of hydroxylated MWCNTs were used.	Ba *et al.*, 2019
Polyethylene Polypropylene Polyethylene terephthalate PVC	*Escherichia coli* *Bacillus subtilis* *Bacillus pumilus* (bacteria)	*In vitro* study Static assay 10 min of post-incubation for all bacteria (short-term attachment) 4 h post-incubation for *Escherichia coli* and *Bacillus pumilus* and 16 h for *Bacillus subtilis* (long-term attachment)	The number of bacteria that adhered to polyethylene and PVC surfaces was much greater than that attached to polypropylene and polyethylene terephthalate. A similar adhesion behavior of bacteria was found in both short-term and long-term assays. After analysis of the physicochemical factors, the surface hardness of the plastics was found to be the key factor dominating the adhesion of bacteria onto plastic.	Cai *et al.*, 2019

Surface/coatings	Organism	Experimental setup	Major findings	Reference
		30 / 37 °C		
Graphene oxide-cuprous oxide nanoparticles-coated acrylic resin surfaces	Micro and macrofoulers	*In situ* study (0.2 – 2.0 m below the water level, weak water currents, less than 2 $m.s^{-1}$) South China Sea 90 and 365 days	Bare panels showed an abundant growth of marine organisms within 90 days, while coated surfaces were hardly fouled by marine organisms after 365 days.	Gu *et al.*, 2019
Graphene oxide-polymeric membrane calcium ion selective electrode sensor	Marine bacteria	*In vitro* study Luria-Bertani medium 1 h and 5 h Room temperature	Compared to the non-coated sensor, the graphene oxide-coated sensor presented significantly improved antifouling properties, inhibiting the formation of biofilms.	Jiang *et al.*, 2019
Graphene-silicone rubber composite surfaces	*Paracoccus pantotrophus* (bacterium)	*In vitro* study Artificial seawater Quasi-static assay (7 days) Dynamic assay (7 days, from 0.2 to 0.5 $m.s^{-1}$)	Under quasi-static conditions, the graphene-silicone surfaces showed similar antifouling performance to that of the control surface (rigid polystyrene sheet). However, under dynamic conditions, the graphene-based surfaces showed better antifouling performance (around 40% reduction in colony-forming units (CFUs)).	Jin, Zhang, *et al.*, 2019
Graphene oxide-silicone rubber composite surfaces	*Triceratium* sp. (diatom)	*In vitro* study Static assay (8 days) Dynamic assay (10 days, 3.4 $m.s^{-1}$) Algal broth medium	Under static conditions no color effect on antifouling behavior was observed, while the studies under hydrodynamic conditions revealed that the combined effects of color and elastic modulus determine the antifouling performance (lighter colors and low Young's moduli provided enhanced performance). Surfaces with 0.36 wt% of graphene oxide showed excellent antifouling performance.	Jin, Bing, *et al.*, 2019
Irgarol® 1051** and Econea® biocide *** immobilized to polyurethane and foul-release PDMS surfaces	*Pseudoalteromonas tunicate* (bacterium)	*In vitro* study Våatanen Nine Salt Solution 24 h	The best performance in ship trial tests was found for the foul-release PDMS based coatings containing immobilized Econea®.	Silva *et al.*, 2019

Surface/coatings	Organism	Experimental setup	Major findings	Reference
	Micro and macrofoulers	*In situ* study Estaleiros Navais de Peniche dock, Portugal (3 m below the water level, pH of 8.3, 14 – 22 °C) Raft in Singapore (3 m below the water level, and temperature ranged between 32 – 35 °C) 9 months	The field tests reflected the previous *in situ* results, corroborating the biofilm adhesion performances, which enables a powerful tool for the prediction of antifouling behavior.	
Epoxy-coated glass Silicone hydrogel coating	*Cyanobium* sp. LEGE 10375 (unicellular cyanobacterium) *Pseudoalteromonas tunicata* (bacterium)	*In vitro* study Dynamic assay (shear rate 40 s^{-1}) Z8 medium 7 weeks, 25 °C	Epoxy-coated glass surfaces were effective in inhibiting biofilm formation at the initial stages, while silicone hydrogel coating showed high antibiofilm efficacy during biofilm maturation. Biofilm wet weight, thickness, and CLSM analysis revealed that silicone hydrogel was less prone to biofilm formation. Efficacy of silicone hydrogel surfaces may be dependent on the fouling microorganism, while the performance of epoxy-coated glass was strongly influenced by a combined effect of surface and microorganism.	Faria, Teixeira-Santos, Gomes, *et al.*, 2020
Glass Epoxy-coated glass	*Synechocystis salina* LEGE 00041 *Cyanobium sp.* LEGE 06097 (unicellular cyanobacteria)	*In vitro* study Dynamic assay (shear rate 40 s^{-1}) Z8 medium 24 h and 6 weeks 25° C	Higher biofilm development was observed on glass. The antibiofilm performance of the epoxy-coated glass was confirmed at the hydrodynamic conditions prevailing in ports.	Faria, Teixeira-Santos, Romeu, *et al.*, 2020
Graphene oxide-silver nanoparticles- PDMS-silica coatings	*Escherichia coli* (bacterium) *Phaeodactylum*	*In vitro* study Saline solution (0.9 wt%), 24 h, 37 °C	The coating containing silver nanoparticles showed improved antibacterial (60% greater inactivation rate) and antialgal (up to 17% reduction in surface coverage) properties, in comparison to pristine graphene oxide.	Liu *et al.*, 2020

Surface/coatings	Organism	Experimental setup	Major findings	Reference
	tricornutum *Navicula torguatum* (diatoms) *Chlorella* sp. (algae)	*In vitro* study Artificial seawater 24 h		
PMMA Glass	*Phormidium* AP3 *Phormidium* AP9F (filamentous cyanobacteria)	*In vitro* study ASN-III medium 30 days	Higher biofilm development was observed in PMMA than in glass flasks.	Maruthanayagam *et al.*, 2020
Carboxyl and hydroxyl-modified MWCNTs, graphitized MWCNTs and Carboxyl-modified Single-Walled Carbon Nanotubes (SWCNTs)-PDMS surfaces	Pioneer biofilm bacteria	*In situ* study Xiaoshi Island, China (1.5 m below the water level) 24 days, 10 - 17 °C	All carbon nanotubes (CNT)-PDMS surfaces reduced Proteobacteria biofilm formation, but increased cyanobacteria biofilm development.	Sun, Yanhe Lang, *et al.*, 2020
Graphene oxide-silica nanoparticles- PDMS composite coatings on carbon steel surfaces	*Pseudomonas* sp. *Bacillus* sp. (bacteria) Freshwater bacterial culture	*In vitro* study Nutrient broth 72 h	The efficiency of the coated surfaces was 99.9% against *Bacillus* sp. and freshwater culture, and it was 89.6% against *Pseudomonas* sp.	Balakrishnan *et al.*, 2021
Copper-based self-polishing-based fiberglass antifouling coatings Uncoated fiberglass Nylon ropes	Marine filamentous fungi	*In situ* study Marina Bandar Rowdha, Sea of Oman (1 m below the water level) 6 months, 24 – 30 °C, pH of 8.2	Six fungal isolates were obtained from the antifouling coating, while just four isolates were isolated from uncoated fiberglass and nylon ropes. Fungi isolated from the antifouling coating were highly resistant to copper, which suggests that filamentous fungi can grow on marine antifouling coatings.	Dobretsov *et al.*, 2021

Surface/coatings	Organism	Experimental setup	Major findings	Reference
Nano-magnetite-hydroxyl-modified MWCNTs-silicone oil-infused PDMS coating	Marine bacteria	*In vitro* study Fresh seawater 24 h and 30 days, 28 °C	The novel coating presented extraordinary antibiofilm adhesion performance with up to 98% removal rate compared with PDMS.	Fan *et al.*, 2021
Glass Perspex Polystyrene Epoxy-coated glass Silicone hydrogel coating	*Synechocystis salina* LEGE 00041 *Cyanobium* sp. LEGE 06098 *Cyanobium* sp. LEGE 10375 (unicellular cyanobacteria)	*In vitro* study Dynamic assay (shear rate 40 s^{-1}) Z8 medium 7 weeks, 25 °C	Silicone hydrogel coating was effective in inhibiting cyanobacterial biofilm formation. Cyanobacterial biofilms formed on silicone hydrogel coating showed a lower percentage and size of empty spaces among all tested surfaces.	Faria, Teixeira-Santos, Romeu, *et al.*, 2021
Glass Epoxy-coated glass	*Synechocystis salina* LEGE 00041 *Synechocystis salina* LEGE 06155 *Cyanobium* sp. LEGE 06097 (unicellular cyanobacteria)	*In vitro* study Dynamic assay (shear rate 40 s^{-1}) Z8 medium 7.5 h and 6 weeks, 25 °C	For both adhesion and biofilm assays, the number of adhered cells was higher on glass than on epoxy-coated glass. Higher biofilm development on glass was confirmed by chlorophyll *a* content and biofilm wet weight and thickness values. Initial adhesion assays can be used to estimate marine biofilm development on different surfaces.	Faria, Teixeira-Santos, Morais, *et al.*, 2021
Epoxy-matrix polyaniline/*p*-phenylenediamine functionalized graphene oxide coatings	Organisms in simulated marine environment (including guppy fish, algae and dwarf hair grass)	*In vitro* study Simulated marine environment 3 months, 25 – 27 °C	The anticorrosion and antifouling properties of commercialized epoxy coatings were enhanced by the addition of the functionalized graphene oxide composite.	Fazli-Shokouhi *et al.*, 2021

Surface/coatings	Organism	Experimental setup	Major findings	Reference
Elasnin-based coatings	Micro and macrofoulers	*In situ* study Fish farm at Yung Shue O, Hong Kong 4 weeks	Elasnin-based coatings inhibited the formation of multi-species biofilms and the attachment of large biofouling organisms in the marine environment. However, coatings began to lose their effectiveness after the third week in the field.	Long *et al.*, 2021
Laser-induced graphene coatings	*Cobetia marina* (bacterium)	*In vitro* study Dynamic assay (65 rpm) Artificial seawater 1 and 36 h	Compared with negative control surfaces, laser-induced graphene coatings showed greater initial bacterial attachment but up to 80% less bacterial coverage after 36 h. Initial attachment rates were reduced by the application of negative or positive potential.	Manderfeld *et al.*, 2021
PDMS-based marine coating containing grafted Econea® biocide***	*Pseudoalteromonas tunicate* (bacterium)	*In vitro* study Dynamic assay (shear rate 40 s^{-1}) Väätänen Nine-Salt Solution medium 7 weeks, 25 °C *In situ* study Estaleiros Navais de Peniche dock, Portugal (3 m below the water level, pH of 8.3, 13 – 22 °C) 30 months	The multifunctional coating showed auspicious antifouling effects after 30 months at a real immersion scenario on the Portuguese shore of the Atlantic Ocean. These field results corroborated the antibiofilm performance evaluated with *Pseudoalteromonas tunicata* at simulated dynamic marine conditions after seven-week assays.	Silva *et al.*, 2021
Graphene hydroxide/ silver composite, bare graphene oxide and MWCNTs incorporated into PDMS-based coatings	Micro and macrofoulers	*In situ* study Persian Gulf, Iran (1 m below the water level, 23 – 32 °C, pH of 8, salinity of 38 ppm, oxygen of 6 $mg.L^{-1}$) 60 days	Field assessments showed that 0.5 wt% graphene hydroxide/ silver composite coating showed better performance in preventing biofilm formation and the attachment of fouling organisms.	Soleimani *et al.*, 2021
Pristine silicon rubber, graphene added silicon	*Paracoccus pantotrophus*	*In vitro* study Static conditions	Results showed that the bactericidal graphene added silicon rubber filled with quaternary ammonium salt coating showed	Tian *et al.*, 2021

Surface/coatings	Organism	Experimental setup	Major findings	Reference
rubber, and graphene added silicon rubber filled with quaternary ammonium salt coatings	(bacterium) *Chlorella pyrenoidosa* (algae) Micro and macrofoulers	24 and 48 h, 37 °C (bacterium) 2 and 4 days, 25 °C (algae) *In situ* study East China Sea 9 months	anti-adhesion effect under laboratory conditions, but the antiadhesion effect was not durable, since it lost antifouling effects completely in real marine conditions. In turn, the non-bactericidal film of graphene added silicon rubber coating exhibited stronger antifouling ability when immersed in the marine environment for 9 months.	
Silicone oil-infused CNTs/epoxy resin coating	*Chlorella* sp. *Phaeodactylum tricornutum* (algae)	*In vitro* study Artificial seawater 21 days, 22 °C	Silicone oil-infused CNTs/epoxy resin coating demonstrated a greater inhibition of algae biofilm formation (up to 90% cell reduction).	Xie *et al.*, 2021
Graphene oxide/silver nanoparticles-polypropylene sensor	*Halomonas pacifica* (bacteria) Marine microalgae	*In vitro* study Static assay Marine broth 24 h, 26 °C *In vitro* study Adam medium (artificial freshwater) 1 week	Graphene oxide/silver nanocomposites showed more than 80% biofilm inhibition, as well as no visible fouling by microalgae. The antifouling property has been proven to be closely related to the dispersibility of silver nanoparticles.	Zhang and Mikkelsen, 2021
Guanidine-functionalized graphene/boron acrylate polymer composite	*Escherichia coli* *Staphylococcus aureus* (bacteria) *Phaeodactylum tricornutum* *Nitzschia closterium f.*	*In vitro* study Luria-Bertani medium 12 h, 37 °C *In vitro* study F/2 medium 14 days, 21 °C *In situ* study	The coatings presented excellent antibacterial properties (up to 94.2% and 95% of reduction for *Escherichia coli* and *Staphylococcus aureus*, respectively) and diatom anti-adhesion rates (up to 99.2%). The field trial revealed no fouling adhesion or surface deterioration.	Z. Zhang *et al.*, 2021

Surface/coatings	Organism	Experimental setup	Major findings	Reference
	minutíssima *Halamphora* sp. (diatoms) Micro and macrofoulers	Yellow Sea, China 2 months		
Fluorinated MWCNTs-coated silicon surfaces	*Escherichia coli* (bacterium)	*In vitro* study Phosphate-buffered saline, 6 h, 37 °C	The incorporation of fluorinated MWCNTs showed a decrease of about 98% on CFUs when compared with bare silicon surfaces.	D. Zhang *et al.*, 2021
PVC Copper-releasing coating PDMS-based elastomer FRC	Heterotrophic prokaryotes	*In situ* study Toulon bay and Banyuls-sur Mer bay (lower nutrients and stronger currents than Toulon bay), Mediterranean coast, France 75 days	PVC (control surface) showed higher biofilm development than antifouling coatings. A remarkably low and unique diversity was found in copper-releasing coating. Clear differences were found between the two locations, since biofilm developed in Banyuls bay was less dense compared to those formed in Toulon and presented a slower dynamic of biofilm formation.	Briand *et al.*, 2022
PVC coated with 3 different environmentally friendly alkaloids (5-chlorosclerotiamide, circumdatin F and notoamide C)	Micro and macrofoulers	*In situ* study Fish farm in Daya Bay, China (1 m below the water level) 30 days	The three alkaloids affected the composition and diversity of marine fouling microbial communities. Moreover, 5-chlorosclerotiamide and notoamide C coated PVC completely inhibited many macrofouler-inductive-bacteria, such as *Pseudoalteromonas* and *Pseudomonas*.	Gao *et al.*, 2022
Acrylic acid-modified graphene oxide / acrylate composites	Micro and macrofoulers	*In situ* study Zhoushan Sea, China 6 months	The composites exhibited self-polishing antifouling performance in natural seawater and high corrosion resistance and mechanical strength.	Li *et al.*, 2022
Poly(lactic acid) (PLA)-chitosan (CS) surfaces	*Cobetia marina* (bacterium)	*In vitro* study Dynamic assay (shear rate 40 s^{-1}) Väätänen Nine-Salt Solution medium	Although the activity of PLA-CS surfaces was dependent of CS molecular weight, these surfaces were able to reduce the number of culturable cells up to 68% compared to the control, and the biofilm thickness by up to 36%.	Lima *et al.*, 2022

Surface/coatings	Organism	Experimental setup	Major findings	Reference
		7 weeks, 25 °C		
GBA26 **** (synthetic gallic acid derivative) incorporated in a polyurethane-based coating	*Pseudoalteromonas tunicate* (bacterium)	*In vitro* study Dynamic assay (shear rate 40 s^{-1}) Våatanen Nine Salt Solution 7 weeks, 25 °C	Polyurethane-based coating containing 2 wt.% GBA26 and the trimethylolpropane triaziridine propionate crosslinker provided the best long-term performance, indicating that the service life of the generated matrix, were improved due to the crosslinks with trimethylolpropane triaziridine propionate.	Neves *et al.*, 2022
CNT CNT coated with cyanoacrylate (polymer coating)	Micro and macrofoulers	*In situ* study Atlantic Ocean, off the eastern coast of Florida 12 months	Cyanoacrylate coatings increase durability and reduce the colonization of biofouling compared to CNTs. Diatoms were most species identified by scanning electron microscopy on surfaces.	Rossi *et al.*, 2022
Reduced graphene oxide/PDMS Graphene oxide-boehmite nanorods/PDMS composites	*Staphylococcus aureus* *Kocuria rhizophila* *Pseudomonas fluorescens* *Pseudomonas aeruginosa* (bacteria) *Candida albicans* (yeast) *Aspergillus brasiliensis* (fungus) Micro and macrofoulers	*In vitro* study Nutrient-infused medium 28 days, 25 °C *In situ* study 45 days, 23 – 28 °C	*In vitro* study revealed that boehmite nanorod composite coating showed higher antibacterial activity in comparison with bare PDMS and reduced graphene oxide/PDMS. The higher self-cleaning and foul-release performance of the boehmite nanorod composite coating was confirmed by the *in situ* study.	Selim *et al.*, 2022

Abbreviations: CFUs – Colony Forming Units, CLSM – confocal laser scanning microscopy, CNTs – Carbon Nanotubes, CS – chitosan, Cu_2O – copper oxide, CuPy – copper pyrithione, CuSCN – copper thiocyanate, FRC – fouling release coatings, MWCNTs – Multi-Walled Carbon Nanotubes, PDMAEMA – Cationic polymer brush, PDMS – Polydimethylsiloxane, PHEMA-co-PEG10MA – Neutral polymer brush, PLA – Poly(lactic acid), PMMA – poly(methyl methacrylate), PSBMA – Zwitterionic polymer brush, PSPMA – Anionic polymer brush, PVC – Polyvinyl chloride, SWCNTs – Single-Walled Carbon Nanotubes, ZnO – zinc oxide, ZnPy – zinc pyrithione.

* Zinc oxide (ZnO) is not considered a biocide by regulations but was added in the formulation.
** Irgarol® 1051 (N'-tert-butyl-N-cyclopropyl-6-(methylthio)-1,3,5-triazine-2,4-diamine).
*** Econea® biocide (4-bromo-2-(4-chlorophenyl)-5-(trifluoromethyl)-1H-pyrrole-3 carbonitrile).
**** GBA26 (N-(2-aminoethyl)-3,4,5-trihydroxybenzamide hydrobromide).

2.5 Proteomic analysis of cyanobacteria

Advancements in high-throughput omics approaches like genomics, transcriptomics, proteomics, and metabolomics are constantly improving our capacity to understand biofilm-related phenomena (Krohn-Molt *et al.*, 2017; Misra *et al.*, 2019). These technologies have revolutionized analyses through systems biology and have been commonly employed to advance the knowledge of biological processes, namely describing the occurrence of bacterial virulence factors under different conditions (Leary *et al.*, 2014; D'Agostino *et al.*, 2016; Babele *et al.*, 2019; Ding *et al.*, 2019; Pjeta *et al.*, 2020; Yan *et al.*, 2020). Upon adaptation to a specific stress condition, cellular mechanisms are activated, stress response pathways are triggered, thus affecting protein synthesis (Hernández-Prieto *et al.*, 2014; Muthusamy *et al.*, 2017; Battchikova *et al.*, 2018). The proteomics research field complements genome sequencing, which alone is of limited value in obtaining a complete understanding of gene function. As proteins are the final products of gene expression, qualitative and quantitative proteomics has become an indispensable tool in biological research. Additionally, physiological, and metabolic rearrangements at the genotype level during stress adaptation and tolerance lead to modification in the proteome (D. Z. Wang *et al.*, 2016; Babele *et al.*, 2019). Through qualitative approaches, the identification of these stress-responsive proteins can be performed, providing a general overview of the proteins that are translated under different circumstances. However, as is critical to understand the expression level of the identified proteins, quantitative approaches are required. Quantitative proteomic analysis includes an appropriate sample collection, protein extraction, digestion of proteins into peptides, separation by liquid chromatography methods followed by mass spectrometry, identification, quantification and additionally, the use of supplementary bioinformatics approaches to evaluate differential protein expression and functional classification.

The development and application of molecular biology tools in cyanobacteria seem more limited when compared with those widely applied for heterotrophic organisms (Alvarenga *et al.*, 2017; Sun *et al.*, 2018). Over the years, proteomic studies on cyanobacteria have been dealing with several issues and the standardization of the proteomic protocol

in these organisms remains a challenge (Barrios-Llerena *et al.*, 2006; Pandhal *et al.*, 2009). The limiting factors are related to the efficacy of protein extraction, separation, and recovery of low abundant proteins (Ow *et al.*, 2011; D'Agostino *et al.*, 2016). Indeed, cyanobacteria contain several proteases, oxidative enzymes, phycobiliproteins, cellulose-rich pigments and other pigments, which hinder different steps in the proteomic analysis workflow. Nevertheless, novel protein extraction and separation protocols have arisen (Gundry *et al.*, 2010; Araújo *et al.*, 2021; Mikulášek *et al.*, 2021). Likewise, technology optimization and advancement contribute to the development of alternatives to gel-based methods (Ow and Wright, 2009). Although these electrophoresis tools, which include sodium dodecyl sulfate-polyacrylamide gel electrophoresis (SDS-PAGE), two-dimensional polyacrylamide gel electrophoresis (2D-GE), and differential in gel electrophoresis (DIGE), were quite popular in the early period of proteomic analysis, they are time-consuming and lack throughput and quantitative ability (Ramos *et al.*, 2017; V. Anand *et al.*, 2017). Highly sensitive mass spectrometry labeling technologies, e.g., stable isotope labeling (SILAC), isotope-coded affinity tag (ICAT), and isobaric tags for relative and absolute quantitation (iTRAQ) have become popular to reliable protein analysis (Ow *et al.*, 2008; Khemiri *et al.*, 2016). Indeed, mass spectrometry is now an indispensable and well-established tool, which employs both label-based and label-free quantitative strategies (S. Anand *et al.*, 2017). Recently, the progress of protein separation by high-resolution liquid chromatography (LC) and analysis by advanced tandem mass spectrometry (MS/MS) enhanced the reliable identification of cyanobacterial proteins by shotgun proteomics (Babele *et al.*, 2019; Kwon *et al.*, 2020). Although each of these technologies has its own limitations, a high throughput analysis can be obtained by LC–MS/MS since this methodology requires low amount of sample, the data acquisition is almost fully automated, providing low variations, increasing the sensitivity, and allowing the detection of minimal differences in protein abundances (Aebersold and Mann, 2016; Gamage *et al.*, 2022).

Although only a small number of proteomic studies has been performed in cyanobacteria compared to heterotrophic organisms (Babele *et al.*, 2019), most of these studies are restricted to the well-studied model unicellular cyanobacterium *Synechocystis* sp. PCC 6803 (Jahn *et al.*, 2018), and only a few comprise analysis from filamentous cyanobacteria,

such as *Anabaena* and *Spirulina* cyanobacterial genus. Table 2.5 describes the current major findings of cyanobacterial proteome research under several environmental stresses. Different filamentous cyanobacterial strains should be considered, since its morphology may be related with ecological benefits (Schirrmeister *et al.*, 2011; Claessen *et al.*, 2014). Additionally, these studies only analyzed the impact of limited and specific parameters on protein expression (Castielli *et al.*, 2009; Giner-Lamia *et al.*, 2016; Rachedi *et al.*, 2020).

Table 2.5. Cyanobacterial proteome studies in response to various environmental stresses.

Cyanobacterial morphology	Strains	Stress	Major findings	Reference
Unicellular	*Synechocystis* sp. PCC 6803	pH	From cytoplasmatic fraction, only 4 proteins showed significant changes in their abundance. Either heat shock family proteins or chaperonins, did not show perceptible fold changes in response to acidity. However, the periplasmic proteome showed remarkable changes as a function of external pH.	Kurian *et al.*, 2006
		Temperature	Heat shock promoted change in about 65 proteins, including the classical heat shock proteins, proteins related with biosynthetic machinery, amino acid biosynthetic enzymes, photosynthesis, and energy metabolism.	Slabas *et al.*, 2006
		Salt	During salt stress, 5 proteins were expressed in lower amounts and the expression of 20 proteins was up-regulated. Up-regulated proteins included binding proteins of ABC transporters, proteins involved in protection of PS II under iron deficiency as well as in thylakoid membrane formation.	Huang *et al.*, 2006
		Salt	By salt shock and/or after long-term salt acclimation, 55 proteins were up-regulated, including heat-shock and ROS scavenging proteins. Changes in enzymes involved in basic carbohydrate metabolism were also detected.	Fulda *et al.*, 2006
		UV-B light exposure	Different expression levels of proteins related to amino acid biosynthesis, photosynthesis and respiration, energy metabolism, protein biosynthesis and cell defense were found. Moreover, 30 novel proteins not previously found related to UV-B stress were identified.	Gao *et al.*, 2009
	Synechocystis sp. PCC 6803 and *Euhalothece* sp. BAA001	Salt	In 0% salt, *Euhalothece (*extremely halotolerant cyanobacterium) displayed higher abundance of stress associated proteins, including a putative DNA binding stress protein and antioxidative enzymes. In turn, *Synechocystis* (moderately halotolerant) expressed a greater number of stress proteins in 3% and 6% salt.	Pandhal *et al.*, 2009
	Synechocystis sp. PCC 6803	pH	At high pH (11.0), the expression of 25 proteins was induced and 14 were expressed at lower levels. Although most proteins were classified as transport and binding proteins of ABC transporters, additional proteins involved in cell division, signaling, photosynthesis and respiration were also identified.	Zhang *et al.*, 2009
		Salt	The histidine kinase mutation significantly changed substrate-binding proteins of ABC transporters and regulatory proteins. A total of 26 differentially expressed proteins was identified.	Li *et al.*, 2012

Cyanobacterial morphology	Strains	Stress	Major findings	Reference
Unicellular	*Synechocystis* sp. PCC 6803	Hexane	Among 1492 proteins identified, 77 and 164 were down- and up-regulated, respectively. A high number of transporters and membrane-bound proteins, proteins against oxidative stress related to sulfur relay system and photosynthesis were induced.	Liu *et al.*, 2012
		Ethanol	A total of 135 and 293 proteins with differential abundance levels were identified between control and ethanol-treated samples at 24 and 48 h, respectively. Proteins related to photosynthesis were up-regulated in the ethanol-treated cells. Modifications of cell membrane and envelope, and induction of multiple transporters, cell mobility-related proteins and common stress response proteins were related as protection mechanisms against ethanol toxicity.	Qiao *et al.*, 2012
		Butanol	A total of 303 differentially regulated proteins by butanol were identified. The major protection mechanisms against butanol were related with heat-shock protein, transporters, as well as modifications of cell membrane and envelope proteins.	Tian *et al.*, 2013
		Cadmium, nickel and cobalt	Photosynthesis and carbon metabolism were the main processes affected by the metals. In turn, chaperones were specifically induced by each metal.	Mehta *et al.*, 2014
	Tropical *Synechococcus* strain WH8102 and temperate strain BL107	Temperature	While at low temperature, growth, and photosynthesis of strain WH8102 was significantly decreased, strain BL107 presented better survival ability under these conditions due to the maintenance of the membrane fluidity, photosynthesis efficiency, and expression of protein biosynthesis machinery.	Varkey *et al.*, 2016
	Synechocystis sp. PCC 6803	3-hydroxypropionic acid	Proteins related to oxidative phosphorylation, photosynthesis, ribosome, central carbon metabolism and ABC-type transporters were up-regulated.	Y. Wang *et al.*, 2016
		Nitrogen starvation	After nitrogen starvation, by cultivation with a fluctuating and limiting nitrogen supplementation and/or day/night cycles, cells accumulated cyanophycin during the night and used it as an internal nitrogen source during the day. This study demonstrates that cyanophycin can be used as temporary nitrogen storage to uncouple nitrogen assimilation from photosynthesis.	Watzer and Forchhammer, 2018
		Nutrient starvation	The FtsH1/3 complex (one of membrane embedded FtsH proteases homolog localized to cytoplasmic membranes and essential for cell viability complex) was of	Krynická *et al.*, 2019

Cyanobacterial morphology	Strains	Stress	Major findings	Reference
			critical importance for acclimation to iron, phosphate, carbon, and nitrogen starvation.	
		Salt	A total of 190 proteins were up-regulated and 189 protein down-regulated among the 1805 quantified proteins after 7 days of salt shock (4% NaCl).	Klähn *et al.*, 2021
Multicellular filamentous	*Spirulina platensis*	Salt	Salt stress displayed several effects on photosynthetic electron transport activities due to the significant variations in the composition of thylakoid membrane proteins.	Sudhir *et al.*, 2005
		Temperature	Expression of chlorophyll biosynthetic proteins immediately decreased during the first 45 min of low temperature exposure. In contrast, their expression levels significantly increased after low-temperature exposure, indicating the relevance of the chlorophyll biosynthesis in response to low-temperature stress.	Hongsthong *et al.*, 2008
	Anabaena sp. PCC 7120	N_2-fixing and non-N_2-fixing conditions	A total of 506 proteins were successfully identified, and among them about 400 shown confident quantifications.	Ow *et al.*, 2008
	Spirulina platensis	Temperature	Low-temperature stress was closely linked with oxidative stress and photosynthesis. In turn, no specific mechanism was revealed in the case of the high temperature stress response. Proteins linked to nitrogen and ammonia assimilation were identified as common between the two temperature stresses.	Kurdrid *et al.*, 2011
	Anabaena sp. PCC 7120	Arsenic	Up-regulation of catalase, peroxiredoxin, thioredoxin and oxidoreductase protected the cells from oxidative stress.	Pandey *et al.*, 2012
	Arthrospira (Spirulina) plantensis-YZ	Salt	Among 141 differentially expressed proteins identified. These proteins are involved in photosynthesis, glucose metabolism, cysteine and methionine metabolism, lysine synthesis, fatty acid metabolism, glutathione metabolism. The group also included some heat shock and ABC transporter proteins.	Wang *et al.*, 2013
	Anabaena sp. strain PCC 7120	Methyl viologen	Levels of proteins involved in ROS detoxification and chaperoning activities were enhanced, while proteins involved in light and dark reactions of photosynthesis were declined. Since the abundance of proteins involved in carbon and energy biogenesis were also altered, these mechanisms are the possible major targets of methyl viologen sensitivity.	Panda *et al.*, 2014

Cyanobacterial morphology	Strains	Stress	Major findings	Reference
Multicellular filamentous	*Anabaena* sp. PCC 7120, *Anabaena* L31 and *Anabaena doliolum*	Methyl viologen	While proteins involved in oxidative stress alleviation and protein homeostasis were up-regulated, proteins associated to photosynthesis and carbon metabolism related enzymes were down-regulated.	Panda *et al.*, 2015
	Anabaena L31, *Anabaena* sp. PCC 7120 and *Anabaena doliolum*	UV-B light exposure	An early accumulation of glutamate ammonia ligase, transketolase, inorganic pyrophosphatase and trigger protein could be used as a stress biomarker of UV stress.	Shrivastava *et al.*, 2015
	Anabaena sp. strain 90	Inorganic phosphorus	A total of 43 proteins were differentially expressed after prolonged phosphorus stress.	Teikari *et al.*, 2015
	Arthrospira sp. PCC 8005	Gamma rays	Reduction of carbon fixation, and reduced pigment, lipid, and secondary metabolite synthesis was observed. However, cells did not induce the classical antioxidant such SOD enzyme.	Badri *et al.*, 2015
	Arthrospira sp. strain L31	UV-B light exposure	Proteins involved in carbon, amino acid biosynthesis and energy metabolism, translation, cellular processes, and reductases were identified.	Babele *et al.*, 2015
	Anabaena sp. strain PCC 7120 and *Anabaena* sp. strain L-31	Uranium	Significant differences in proteins related to photosynthesis, carbon metabolism, and oxidative stress were observed.	Panda *et al.*, 2017
	Halomicronema hongdechloris	Light (far-red light (~ 730 nm) illumination *vs* fluorescent white light illumination at a light intensity of 20 μmol	Under different light conditions, the proteomic data showed that essential cellular metabolic reactions remained constant, including most of the enzymes related to chlorophyll biosynthesis and photosynthetic carbon fixation. Moreover, an increase in the concentration of allophycocyanin subunits and increased levels of alternative subunits in photosystem reaction centers, including the core proteins for PSI and PSII under far-red light were observed.	Chen *et al.*, 2019

Cyanobacterial morphology	Strains	Stress	Major findings	Reference
		photons m^{-2} s^{-1})		

Abbreviations: ABC transporters – ATP-binding cassette transporters, DNA – deoxyribonucleic acid, NaCl – sodium chloride, PS I – Photosystem, PS II – Photosystem II, ROS – reactive oxygen species, SOD superoxide dismutase, UV – ultraviolet.

Proteomic studies are also extremely valuable approaches to understand biofilm formation, regulation, and phenotype (Leary *et al.*, 2014; Rani and Babu, 2018). In addition to providing information about essential cell processes such as cell division, motility, and metabolism (Parnasa *et al.*, 2016), proteomic approaches offer advanced clues about the influence of physiological and environmental parameters (Chen *et al.*, 2019), as well as interspecies interactions on biofilms (Herschend *et al.*, 2017). Although proteomic studies on marine biofilms are not abundant, these analyses can contribute to the identification of pathways involved in the adhesion and the attachment of micro- and macrofoulers (Domínguez-Pérez *et al.*, 2019, 2020; Pjeta *et al.*, 2020; Yan *et al.*, 2020; Davey *et al.*, 2021; Liu, 2022). Cyanobacterial events such as motility, aggregation, and flocculation, are clearly related to cell-cell and cell-surface adhesion, and biofilm development stages. The RNA chaperone homolog Hfq was shown to be involved in the regulation of motility in *Synechocystis* sp. PCC 6803 (Schuergers *et al.*, 2014). Additional studies have been highlighting the involvement of pili structures in cyanobacterial mechanisms. In addition to driving surface motility, pili facilitate the phototaxis and the establishment of nitrogen-fixing symbioses with eukaryotes and influence cell sedimentation and dispersal (R. Allen *et al.*, 2018). Recent studies have shown that *Synechocystis* sp. PCC 6803 possesses pili structures that mediate cell motility required for locomotion, adhesion, and biofilm formation (Chen *et al.*, 2020), as well as the loss of pili promoted cyanobacterial sedimentation and biofilm formation in the same unicellular cyanobacterium (Conradi *et al.*, 2019). Although type IV pili has been shown to be dispensable for biofilm development in the unicellular cyanobacterium *Synechococcus elongatus* PCC 7942 (Nagar *et al.*, 2017), modified type IV pilus-like system was shown to be involved in gliding motility of filamentous *Nostoc punctiforme* (Khayatan *et al.*, 2015). In turn, an exoprotein of *Anabaena* sp. PCC7120 was required for filament adhesion and aggregation (Oliveira *et al.*, 2015). A surface exposed glycoprotein, MrpC - microcystin-related protein C, also showed to contribute to cell-cell interaction in microcystin-producing strains of *Microcystis aeruginosa* PCC 7806 (Zilliges *et al.*, 2008). Likewise, a different surface-exposed protein, the lectin microvirin, was involved in cell-cell recognition and cell-cell attachment of the same toxin-producing cyanobacterium (Kehr *et al.*, 2006). Involvement of the signaling molecule cyclic dimeric GMP (c-di-GMP) in biofilm formation was also

observed for *Thermosynechococcus elongatus.* Indeed, blue light irradiation, acting through the cyanobacteriochrome SesA, improved c-di-GMP levels and triggered a sessile phenotype at 31 °C, which is a relatively low temperature for this thermophilic unicellular cyanobacterium (Enomoto *et al.*, 2014). Despite different proteins and factors have been reported on cyanobacterial adhesion and biofilm development, most of them are related to unicellular cyanobacteria, and disregard the application of hydrodynamic conditions that prevail in aquatic environments, not mimicking the real biofouling conditions (Table 2.6). Therefore, it is even more relevant to improve filamentous cyanobacterial proteomic approaches to be able to characterize stress-responsive proteins related to virulence factors and cellular processes involved in biofilm regulation. Moreover, the discovery of these proteins using high-throughput proteomic tools can also lead to the discovery of novel targets for the improvement of antifouling strategies for marine purposes. Likewise, these analyses can also provide useful insights for additional research fields (Gamage *et al.*, 2022), due to the wide range of promising secondary metabolites produced by cyanobacteria (Lau *et al.*, 2015), which can be applied in medical applications (Pagels *et al.*, 2019; Ding *et al.*, 2021), biotechnological processes (Chakdar *et al.*, 2022), as well as in the food and cosmetic industries (Manirafasha *et al.*, 2016).

The integration between omics datasets is paramount for a complete knowledge of the adaptive mechanisms that allow the survival of organisms under different environments, such as marine biofilm communities (Pathania *et al.*, 2022). Consequently, as experimental design largely influences high-quality proteomic data, cyanobacterial molecular biology is an emergent topic for further investigations and improvements (Sun *et al.*, 2018; Santos-Merino *et al.*, 2019).

Table 2.6. Proteins/factors related to cyanobacterial adhesion and biofilm development.

Cyanobacterial morphology	Strains	Hydrodynamic conditions	Surface	Experimental setup	Major findings	Reference
Unicellular	*Synechocystis* sp. PCC 6803	Static conditions	Glass Plastic	Adhesion assay occurred over 4 days in BG11 medium, under light (40 μmol photons m^{-1} s^{-1}) at 30 °C. Note: EPS extraction and analysis were performed from suspension cultures.	Mutant strains with gene deletions were predicted to encode a permease component of an ABC transporter, an ATP binding component of an ABC transporter and a methyltransferase demonstrated increased adherence to glass. Instead of a 3D architecture, a monolayer of cells adhered to glass was observed. EPS purified from mutants also showed altered composition when compared to wild-type strain. Mutant strains grown on plastic did not demonstrate increased adherence relative to wild-type strains.	Fisher *et al.*, 2013
	Synechocystis sp. PCC 6803	Static conditions	24-well microtiter plates (material *n.a.*)	Biofilm was developed over 4 days, under light-activated heterotrophic growth (cells were incubated in the dark with 15 min of light (30 μmol m^{-2} s^{-1}) per day) in BG11 medium supplemented with 10mM TES-KOH (pH 8.0) and 10mM glucose at 30 °C.	The cyanobacterial phytochrome2 (Cph2) presented as regulator of key metabolic enzymes to support the heterotrophic metabolism during biofilm formation.	Schwarzkopf *et al.*, 2014

Cyanobacterial morphology	Strains	Hydrodynamic conditions	Surface	Experimental setup	Major findings	Reference
Unicellular	*Synechococcus elongatus* PCC 7942	*n.a.*	Glass	Biofilm formation occurred for 6-7 days in BG11 medium supplemented with 0.0226 mM ferric ammonium citrate and 0.0312 mM citric acid, under incandescent light (20–30 μ mol photons m^{-2} sec^{-1}) and continuous bubbling (3% CO_2 in air), at 30 °C.	An efficient secretion of EbfG1-4 (enabling biofilm formation with a double-glycine (GG)-motif) proteins by a transport system, in which the cysteine peptidase takes part, was required for biofilm formation.	Parnasa *et al.*, 2016
	Synechococcus elongatus PCC 7942	Adhesion and sedimentation assays were performed in a flow cell system (flow rate of 0.2 $mL.min^{-1}$). Hydrodynamic conditions to biofilm assays *n.a.*	Glass	Adhesion occurred after 5, 15 and 30 min of bacterial injection in the flow cell. The sedimentation assays were carried out in the following series of injection stages: cell culture for 5 min, washing solution for 3 min, and images of deposited cells were acquired after 10 min. Further injection of a cell culture for 10 and 15 min were performed. Biofilm formation occurred with continuous bubbling (3% CO_2 in air), at 30 °C. All assays were	The presence of pili interfered with adhesion, decreased sedimentation, and slowed down the kinetics of biofilm formation. Type IV pili were dispensable for biofilm development in this cyanobacterial strain.	Nagar *et al.*, 2017

Cyanobacterial morphology	Strains	Hydrodynamic conditions	Surface	Experimental setup	Major findings	Reference
				performed in BG11 medium.		
	Synechocystis sp. PCC 6803	72 rpm	Glass	Biofilm was formed over 3 days in BG11 medium under light (40 μmol photons m^{-2} s^{-1}) at 30 °C.	Cell surface structures as Type IV pili and S-layer were essential for biofilm formation by *Synechocystis*.	R. Allen *et al.*, 2018
	Synechocystis sp. PCC 6803	Static conditions	Polystyrene	Biofilm was developed over 3 days in BG11 medium, without and with 500 mM NaCl, at 29 °C.	A two-component regulatory system, which consists of a sensor histidine kinase (Hik) and a response regulator (Rre) (Hik36-Hik43 and Rre6), exhibited an important role in the prevention of auto aggregation under normal condition, and in the promotion of adhesion and biofilm formation under salt stress.	Kera *et al.*, 2020
Unicellular and multicellular filamentous	*Synechocystis* sp. PCC 6803 (unicellular cyanobacterium, which displays lower levels of c-di-GMP) and *Fremyella Diplosiphon* (filamentous cyanobacterium, which displays higher	Static conditions	Glass	Biofilm was developed over 14 days, in BG11 medium supplemented with 20Mm HEPES buffer under fluorescent white light (35 μmol photons m^{-2} s^{-1}), at 28 °C. Biofilms were also grown under red (λmax at 660 nm), green (λmax at 530 nm), and blue light (λmax at 452 nm).	Involvement of the signaling molecule cyclic dimeric GMP (c-di-GMP) in biofilm formation, cellular aggregation, flocculation, and cellular buoyancy was shown for both strains. Expression of the c-di-GMP producing enzyme, diguanylate cylase, in *Synechocystis* sp. PCC 6803 results in biofilm formation, whereas expression of phosphodiesterase to reduce c-di-GMP promoted enhanced cellular buoyancy in both cyanobacterial strains.	Agostoni *et al.*, 2016

Cyanobacterial morphology	Strains	Hydrodynamic conditions	Surface	Experimental setup	Major findings	Reference
	intracellular c-di-GMP levels)					

Abbreviations: λ – wavelength, 3D – three-dimensional, ABC transporters – ATP-binding cassette transporters, ATP – adenosine triphosphate, c-di-GMP – cyclic dimeric GMP, CO_2 – carbon dioxide, Cph2 – cyanobacterial phytochrome2, EbfG1-4 – enable biofilm formation with a double-glycine (GG)-motif**,** EPS - extracellular polymeric substances, Hik – histidine kinase, *n.a.* – not available, NaCl – sodium chloride, rpm – revolutions per minute, Rre – response regulator, TES-KOH – N-[Tris(hydroxymethyl)-methyl]-2-aminoethanesulfonic acid - potassium hydroxide.

2.6 **Marine antifouling strategies**

Marine biofouling has been an emerging issue and several strategies have been used to deal with this serious concern. These approaches can prevent and/or delay biofilm development and the attachment of macrofoulers, comprising both antimicrobial and antifouling surfaces (Silva *et al.*, 2019), or control already established biofilms and fouling communities. Control methodologies involve the use of bacteriophages, QS inhibitors, disruption of the biofilm matrix, disinfectants, as well additional treatments methods and cleaning technologies (Kristensen *et al.*, 2008; Cahill *et al.*, 2019; Bradbeer *et al.*, 2020; Arndt *et al.*, 2021; Delgado *et al.*, 2021).

Antifouling paints were the initial strategy used to manage the impact of marine biofouling (Bosselmann, 1996; Evans, 1999). Copper, arsenic, zinc, tin, and mercury coatings were commonly used until their toxicity on the surrounding marine environment was demonstrated (Callow and Callow, 2002; Sonak, 2009; Sonak *et al.*, 2009). Indeed, in the 1960s, coatings incorporating a tributyl tin (TBT)-based biocide were the first to present a robust effectiveness with relatively low cost of production to tackle marine biofouling. However, ten years later, several findings indicated negative impacts of TBT-based compounds related to their persistence and toxicity, showing adverse effects on non-target marine organisms. Several governments restricted its use, and the International Maritime Organization decided to ban the use of this type of biocides in the manufacturing of antifouling paints from 2003, and the presence of these paints on ship surfaces from 2008 (Bressy and Lejars, 2014). Therefore, numerous strategies to prevent biofilm formation or control established biofilms have been developed (Nurioglu *et al.*, 2015; Silva *et al.*, 2019; Mishra *et al.*, 2020). A broad-spectrum of aquatic disinfectants has been demonstrated to effectively control biofouling, being one of the most widespread treatments for cleaning and disinfecting marine equipment and devices (Stout *et al.*, 2016; Bradbeer *et al.*, 2020; Zhou *et al.*, 2020). They can be applied through immersion of the equipment into disinfectant solutions or spray applications since these disinfectants are available in powder and/or tablet form. TermoRens® Liquid 104 cleansing fluid (5–15% citric acid and < 10% phosphoric acid) was formulated to remove mussels, barnacles, and additional marine growth, and is marketed as environmentally friendly. Likewise,

Barnacle Buster® (85% phosphoric acid) promoted as a safe, non-toxic, and biodegradable marine growth removal (Cahill *et al.*, 2019). In the peroxygen family, Virkon® Aquatic is 99.9% biodegradable and breaks down to water and oxygen (Stockton-Fiti and Moffitt, 2017). It is one of very few US Environmental Protection Agency-registered disinfectants labeled specifically for use in aquaculture facilities on aquatic bacterial, fungal, and viral pathogens available through aquaculture suppliers such as Syndel in North America (Mainous *et al.*, 2012; Moffitt *et al.*, 2015). In turn, in the European Community, Antec International Limited indicates that the compound is registered as a disinfectant only for professional users. Due to the restrictive legislation, which requires several risk studies before registration and marketing authorization, the global costs of development of new biocides or new antifouling coatings incorporating biocides have increased (Bressy and Lejars, 2014). These costs reactivated the development of non-toxic approaches, including novel antifouling surfaces, as already discussed in the previous chapter. Although the choice of the correct strategy depends on the cost and application possibilities, antifouling coatings are probably the most cost-effective method for boats and other submerged devices and equipment (Parra, Dorta, *et al.*, 2015).

Additional biofouling treatments include thermal stress, osmotic shock, deoxygenation, UV, laser and/or ultrasonic irradiation, and hydrodynamic cavitation (Department of Agriculture Fisheries and Forestry, 2008; Cahill *et al.*, 2019; Arndt *et al.*, 2021; Delgado *et al.*, 2021). The most commonly available cleaning technologies are brushing, scraping, pressure cleaning with water/air jetting or mechanical cleaning using wipers (Granhag *et al.*, 2004; Department of Agriculture Fisheries and Forestry, 2008; Aldred and Anthony S. Clare, 2014; Cahill *et al.*, 2019; Arndt *et al.*, 2021; Delgado *et al.*, 2021). These mitigation strategies vary in their effectiveness in removing biofouling organisms, as well as in their suitability for use on different marine coating surfaces. For instance, although the intensity of cavitation erosion of submerged surfaces depends on the strength characteristics of the surface, liquid temperature, the distance from the edge of the working tool to the fouling which should be removed, cavitation technology allows lower surface damage compared to brush-based technologies (Akinfiev *et al.*, 2007).

Nowadays, cleaning of boats, ships and additional moveable marine equipment like cages and nets can be done in dry-dock or by in-water cleaning technologies (Akinfiev *et*

al., 2007; Arndt *et al.*, 2021). Although in-water biofouling approaches are cheaper than onshore activities, they present higher chemical contamination and biosecurity risks, e.g., the application of underwater technology may increase recolonization of surrounding surfaces (Paetzold and Davidson, 2010). It is important to invest in research and development of innovative technology that can provide practical and feasible tools to control biofouling while protecting the marine environment from harmful chemical and/or biological waste. Therefore, economic factors and biosecurity risk management decisions should be taken into consideration to contemplate the practicality, feasibility, and environmental impact of biofouling management options.

Since biofouling is the major factor affecting the operation, maintenance, and data quality of submerged marine devices and large equipment such as boats and ships, antifouling strategies play a critical role in the present and future of the marine industry. The ideal antifouling strategy should be low-cost, robust and highly efficient to allow long-term continuous monitoring. However, to date, there is no available universal approach that is effective, and a combination of different strategies should be considered. Further fundamental research is required to advance the knowledge of the underlying biofouling mechanisms, such as biofilm development by common microfoulers. The application of "omics" technologies to marine biofilm studies is an emerging approach that can help to identify pathways evolved on adhesion, attachment, and biofilm formation, and consequently, contribute to novel improvements in marine antifouling strategies. However, genetic and "omic" studies in microfouler organisms such as cyanobacteria and their processes are still limited. Also, not all novel antifouling strategies are technically and/or economically feasible at a large scale.

Although biofouling is an ongoing concern for the marine industry, environmental managers and marine scientists, their motivations and approaches to tackling it are very diverse among sectors (Davidson *et al.*, 2016).

3.

3 Biofilm formation behaviour of marine filamentous cyanobacterial strains in controlled hydrodynamic conditions

The contents of this chapter as published as:

Romeu M.J., Alves P., Morais J., Miranda J.M., Jong E.D., Sjollema J., Ramos V., Vasconcelos V., Mergulhão F.J.M. (2019) Biofilm formation behaviour of marine filamentous cyanobacterial strains in controlled hydrodynamic conditions". *Environmental Microbiology* **21**: 4411-4424.

Abstract

Marine biofouling has severe economic impacts and cyanobacteria play a significant role as early surface colonizers. Despite this fact, cyanobacterial biofilm formation studies in controlled hydrodynamic conditions are scarce. In this work, computational fluid dynamics was used to determine the shear rate field on coupons that were placed inside the wells of agitated 12-well microtiter plates. Biofilm formation by three different cyanobacterial strains was assessed at two different shear rates (4 and 40 s^{-1}) which can be found in natural ecosystems and using different surfaces (glass and perspex). Biofilm formation was higher under low shear conditions, and differences obtained between

surfaces were not always statistically significant. The hydrodynamic effect was more noticeable during the biofilm maturation phase rather than during initial cell adhesion and optical coherence tomography showed that different shear rates can affect biofilm architecture. This study is particularly relevant given the cosmopolitan distribution of these cyanobacterial strains and the biofouling potential of these organisms.

Keywords: marine biofouling, cyanobacterial biofilms, computational fluid dynamics, hydrodynamic conditions, optical coherence tomography, shear rate

3.1 Introduction

Biofouling is an ongoing concern in aquatic environments and marine applications, leading to material deterioration, surface corrosion, decrease of hydrodynamic performance and significant economic losses (Salta, Wharton, *et al.*, 2013). Moreover, biofilms are recognised as a permanent or temporary refuge for bacterial pathogens in aquaculture facilities (King *et al.*, 2006). Additional problems related to biofouling on marine environments are present in marine underwater support structures, sensors and housings, which are used for on-site monitoring with weekly, monthly, or continuous measuring. On these devices, the most obvious problems are related to optical and electrochemical sensors, because even a thin biofilm on the optics can give rise to incorrect measurements (Delauney *et al.*, 2010). Although marine biofouling is a dynamic process encompassing different agents and their interactions, it has been considered that biofilm formation by bacteria and algae is a primordial step that occurs prior to the adhesion of macrofouler organisms such as invertebrate larvae, mussels, seaweeds and barnacles (Mieszkin *et al.*, 2013). Cyanobacteria are a widespread group of photosynthetic prokaryotes which, together with diatoms, constitute the major components of marine biofilms (Salta, Wharton, *et al.*, 2013; Bharti *et al.*, 2017; Di Pippo and Congestri, 2017). Moreover, cyanobacteria produce large amounts of extracellular polymeric substances (EPS), which increase biofilm cohesion (Rossi and De Philippis, 2015). This is particularly

important because it has been shown that the main challenge in marine biofouling control is associated with microorganisms which are also responsible for the initiation of biofilm formation and those which are also able to excrete large amounts of EPS (Mieszkin *et al.*, 2013; Salta, Wharton, *et al.*, 2013; Telegdi *et al.*, 2016). Thus, a promising approach to delay macrofouling is to prevent the adhesion and biofilm formation by cyanobacteria.
In this work, two strains from the *Nodosilinea* genus, collected from the same site in the Portuguese coast, and a Synechococcales strain from a different location were studied. To the best of our knowledge, no studies about the biofilm formation behaviour of these commonly occurring cyanobacterial strains have been published so far.

Amongst the parameters that affect biofilm development, physicochemical factors related with the surface (Crawford *et al.*, 2012) and flow velocity and shear rate (A. A. Allen *et al.*, 2018) are some of the most important. There is evidence that shear forces affect not only biofilm structure but also composition, mass transfer, exopolysaccharides production, energy metabolism and can also induce genetic or molecular changes in biofilms (Moreira, Gomes, *et al.*, 2015). It has been reported that a slow flow of water (0.2 $m.s^{-1}$) promotes the growth of filamentous green algae and cyanobacteria (Minchin and Gollasch, 2003; Flemming *et al.*, 2009) and that biofouling can be favoured at low fluid velocities. These lower flow velocity values can be found in harbours and when underwater devices and sensors are moored or floating in their vicinity (Minchin and Gollasch, 2003). Therefore, it is important to perform biofilm formation studies in controlled hydrodynamic conditions where the shear rate is well defined. Although the effects of hydrodynamic conditions on the architecture of some bacterial biofilms have been described (Teodósio *et al.*, 2011) there is a comparatively low information regarding the effects of hydrodynamics in filamentous cyanobacterial biofilms. Moreover, some filamentous cyanobacteria species produce cyanotoxins, which pose a particular risk to aquatic organisms and to human health (Frazão *et al.*, 2010; Regueiras *et al.*, 2018). Poisoning and additional chronic effects might be caused by the ingestion of contaminated food or even by drinking water during recreational activities (Martins *et al.*, 2005; Buratti *et al.*, 2017).

In order to analyse and predict flow conditions in an easy to handle biofilm reactor assay like a 12-well microtiter plate, flow simulation and modelling are highly useful.

Computational fluid dynamics (CFD) is a numerical simulation technique that involves the solution of fluid flow and/or heat/mass transfer problems and provides a detailed understanding of flow phenomena that are difficult to analyse experimentally. Although CFD applications in biotechnological and biological processes are common (Dean *et al.*, 2016), this technique is not commonly used to predict the shear rate occurring inside reactors that are used in marine biofilm research. A detailed hydrodynamic analysis of these biofilm reactors is useful, and CFD is a powerful tool used to model flow situations to assess if the hydrodynamic conditions *in vitro* are similar to those prevailing in some marine systems *in situ.* In order to define the operational conditions that can be used *in vitro* to simulate the hydrodynamics prevailing in natural aquatic environments, the first goal of this research was to predict the shear rate occurring in a marine biofilm reactor (agitated 12-well microtiter plates). The second goal was to evaluate the effects of different shear rates and surface properties on the biofilm formation behaviour of different marine cyanobacteria. The chosen surfaces, glass and perspex, represent commonly submerged artificial surfaces found on different equipment in aquatic and marine environments such as underwater windows of boats, aquaculture equipment, flotation spheres, moored buoys, underwater cameras, measuring devices or sensors (Blain *et al.*, 2004; King *et al.*, 2006; Roy, 1983; Taylor, 1996).

3.2 Materials and Methods

3.2.1 CFD analysis

For the flow simulation inside a 12-well microtiter plate, a cylindrical well (diameter of 22 mm and height of 18 mm) containing liquid (3 mL of water) and gas (air, filling the remaining volume), at 25 °C, was simulated using Ansys Fluent CFD package (version 14.5). The domain was built in Design Modeller 14.5 and discretized into a grid of 40,441 hexahedral cells by Meshing 14.5.

The two phase flow in the vessel was simulated by the VOF methodology (Hirt and Nichols, 1981). The air/water interface was determined by the Geo-Reconstruct method (Youngs, 1982). The PISO algorithm was used to solve the velocity-pressure coupled

equations, the QUICK scheme for the discretization of the momentum equations and the PRESTO! scheme for pressure discretization. The surface tension effects were modelled by the continuum surface force (Brackbill *et al.*, 1992), which was introduced through a source term in the momentum equation. An accelerating reference frame was adopted, and the effect of the circular orbital motion on the fluid was modeled by a source term. The no-slip boundary condition and a contact angle of 83° were considered for all the walls (Gomes *et al.*, 2014).

Simulations were made for rotation frequencies of 40 and 185 rpm and an orbital diameter of 25 mm. For each case, 8 s of physical time were simulated with a fixed time step of 2.5×10^{-4} s. The primary numerical results obtained, for each time step, were the velocity components, the pressure and the liquid or gas phase volume fractions. For each simulation, after the stabilization of the flow, the average instantaneous shear rate was obtained by integrating an instantaneous solution over the bottom surface of the well (corresponding to the coupon surface). The time-averaged shear rate was calculated by averaging the instantaneous shear rate throughout a complete rotation cycle.

3.2.2 Organisms and inocula preparation

In order to evaluate the behaviour of different filamentous cyanobacteria from different marine environments, three cyanobacterial strains were used in this study. All strains were obtained from the Blue Biotechnology and Ecotoxicology Culture Collection (LEGE-CC) located at CIIMAR, Portugal (Ramos *et al.*, 2018). *Nodosilinea* sp. LEGE 06020 and *Nodosilinea* sp. LEGE 06022 (order Synechococcales) were isolated from a seawater sample collected in the surf zone and from a sample scraped from a wave-sheltered rock in the intertidal zone, respectively (Ramos *et al.*, 2018). Both strains were originally collected at Coxos beach, Portugal (39°00'16.4"N 9°25'33.0"W). The unidentified filamentous Synechococcales LEGE 07185 was isolated from a submerged stone collected in a tide pool, at Lavadores beach, Portugal (41°07'45.1"N 8°40'06.9"W) (Ramos *et al.*, 2018). Cells were grown in 750 mL culture in Z8 medium (Kotai, 1972) supplemented with 25 $g.L^{-1}$ of synthetic sea salts (Tropic Marin) and B_{12} vitamin. Cultures were performed under 14 h light (10–30 μmol photons m^{-2} s^{-1})/10 h dark cycles, at 25°C. Cyanobacterial

strains from unidentified filamentous Synechococcales and *Nodosilinea* genus are present in dissimilar geographies, including different continents (Europe, Africa, America and Antarctica). Specimens can be found in different environments and ecologies such as brackish water, freshwater, hypersaline, marine and even terrestrial (Ramos *et al*., 2018). This cosmopolitan distribution highlights the importance of studying biofilm formation by these organisms.

3.2.3 Surface analysis

In order to assess the biofilm behaviour of the cyanobacterial strains, two artificial surfaces commonly placed in aquatic environments, glass and perspex, were tested. Surface analysis was performed by measuring the contact angles with water (θ_w) as reference liquid. This determination was performed in three independent experiments at 25 °C ± 2 °C, by the sessile drop method using a contact angle meter (Dataphysics OCA 15 Plus, Filderstadt, Germany), as described in Gomes *et al*. 2015. On each experiment, at least 25 determinations for each material were made.

3.2.4 Biofilm formation

Glass (Vidraria Lousada, Lda, Portugal) and perspex (Neves & Neves, Lda, Portugal) coupons (1 cm^2) were immersed in a solution of 2% (v/v) TEGO 2000® industrial detergent (JohnsonDiversey, Northampton, United Kingdom) (Meireles *et al*., 2017) and sterile distilled water for 20 min under agitation (150 rpm). In order to remove any remaining disinfectant, coupons were rinsed in sterile distilled water and air-dried. Additionally, glass coupons were autoclaved (121 °C, 15 min) (Azevedo *et al*., 2006). After drying, all coupons were aseptically pre-weighted. Biofilm formation was assessed on 12-well microtiter plates (VWR International, Carnaxide, Portugal) under optimized conditions for cyanobacterial growth. Transparent double-sided adhesive tape was used to fix the coupons, and once the tape was placed in the wells, all coupons and the plates were subjected to UV sterilization for 30 min after which the sterile coupons were fixed. A volume of 3 mL of each cyanobacterial suspension in Z8 medium (prepared as described above) supplemented with nutritional factors, which support the growth and

cyanobacteria maintenance (Kotai, 1972), was inoculated in each well. For control, Z8 medium without cyanobacterial cells was introduced on the wells. Observations demonstrated that the applied methodology was efficient for surface sterilization since no bacterial growth was observed. Microtiter plates were incubated at 25 °C in an orbital shaker with a 25 mm orbital diameter (Agitorb 200ICP, Norconcessus, Portugal) at 40 rpm and 185 rpm. Biofilm development of the three cyanobacterial strains was followed for 7 weeks (49 days), because it is accepted that a two-month interval for maintenance is the minimum duration for economically viable underwater monitoring systems (Blain *et al.*, 2004). During this incubation time, the medium was replaced twice a week. In order to mimic real light exposure periods, a photoperiod of 14 h light (8-10 μmol photons m^{-2} s^{-1})/10 h dark cycles) was applied.

3.2.5 Biofilm analysis

3.2.5.1 Optical Coherence Tomography

Biofilm development was primarily assessed by determination of biofilm structure, thickness and roughness through OCT (Thorlabs Ganymede Spectral Domain Optical Coherence Tomography system with a central wavelength of 930 nm, Thorlabs GmbH, Dachau, Germany). Sampling was performed every 7 days, and at each sampling day, 3 coupons for each surface and hydrodynamic condition for all strains were analysed. Culture medium was carefully removed, and the wells were filled with 3 mL of sterile sodium chloride solution (8.5 $g.L^{-1}$). The solution was carefully removed to eliminate loosely attached cyanobacteria. Subsequently, the wells were filled again with 3 mL of sterile sodium chloride solution and imaged. The captured volume was ~ 4 x 4 x 3 mm^3 (509 x 313 x 1024 $pixels^3$). Since biofilms are mainly composed (90%) of water (Bakke *et al.*, 2001), the refractive index was set to 1.40, close to the refractive index of water (1.33). 2D and 3D imaging were performed, and for each coupon, a minimum of three fields of view were analysed to ensure accuracy and reliability of the results obtained. Image analysis was performed as previously described (Gusnaniar *et al.*, 2017). First, the bottom of the biofilm was determined as the best fitting parabole (or hyperboloid when imaged in 3D) that connects the white pixels resulting from light reflection on the substratum

surface. Subsequently, a grey-value threshold that separates the biofilm from the background was calculated on the basis of the grey-value histogram of the entire image (Otsu, 1979). The upper contour line of the biofilm was defined as those pixels in the image that have a grey value just higher than the grey-value threshold and are connected to the bottom of the biofilm by pixels with grey values higher than the grey-value threshold. The image was then converted to a binary black and white image and objects not connected to the bottom were rejected from the biofilm structure. Finally, the mean biofilm thickness was calculated based on the number of pixels between the bottom of the biofilm and the upper contour line for each vertical line in the image. Biofilm roughness was analysed by determination of roughness coefficient, because this parameter allows comparing the structure of different biofilms, across different studies as well as across scales, once this value is normalized to mean biofilm thickness. The relative roughness coefficient (R_{α}^{*}) was calculated using the following equation (3.1), according Wagner & Horn 2017:

$$R_{\alpha}^{*} = \frac{1}{N} \sum_{i=1}^{N} \frac{|L_{F,i} - \bar{L}_F|}{\bar{L}_F} \quad (3.1)$$

where $L_{F,i}$ is a local biofilm thickness measurements at location *i* and *N* equals the number of thickness measurements and $\bar{L}_F$ is the mean biofilm thickness.

3.2.5.2 Wet weight determination and chlorophyll *a* quantification

In order to complement the characterization of cyanobacterial biofilms, the determination of their wet weight and chlorophyll *a* content was performed. To determine the wet weight, coupons were detached from the wells with the aid of sterile tweezers and weighted. Biofilm wet weight was obtained by the difference to the initial coupon weight (determined prior to inoculation).

Chlorophyll *a* is the predominant and the unique pigment present in all groups of alga and cyanobacteria, and it is commonly used as biomass indicator in aquatic environments. Cyanobacterial cells were detached from the coupons by immersing each coupon in 2 mL of 8.5 $g.L^{-1}$ sodium chloride solution and vortexing (VV3,VWR) for 2 min

at maximum rotational speed (2500 rpm). Coupons were then removed from the liquid and observed under the microscope to confirm complete cell detachment. Detached cells were harvested by centrifugation (3202*g*, for 5 min at room temperature) and the supernatant discarded. Since chlorophyll pigments are light sensitive, the following chlorophyll extraction procedures were performed in the dark using a protocol adapted from Henriques *et al*. 2007. A volume of 2 mL of 99.8% methanol (Methanol ACS Basic, Scharlau Basic, Barcelona) was added for chlorophyll extraction, and suspensions were incubated at 4 °C for a period of 24 h for maximal chlorophyll *a* extraction. Samples were then centrifuged at 3202*g*, for 5 min at room temperature, and the supernatant was transferred to a glass cuvette. The absorbance at 750 nm (turbidity), 665 nm (chlorophyll *a*) and 652 nm (chlorophyll *b*) was determined using a V-1200 spectrophotometer (VWR International China Co., Ltd, Shanghai, China). The chlorophyll *a* concentration was calculated through the following equation (3.2) (Porra *et al.*, 1989):

$$\text{Chl } a \ (\mu g.mL^{-1}) = 16.29 \times A^{665} - 8.54 \times A^{652} \quad (3.2)$$

where A^{665} and A^{652} are the absorbances at 665 nm and 652 nm, respectively.

3.2.6 Statistical analysis

All experiments were performed in triplicate. Data analysis was performed using the statistical program GraphPad Prism® for Windows, version 6.01 (GraphPad Software, Inc., San Diego, CA, USA) and results were compared using unpaired *t*-tests with a confidence level of 95% (**; $P < 0.05$) and 90% (*; $P < 0.1$).

3.3 Results and Discussion

3.3.1 CFD analysis

The first goal of this study was the determination of the shear rate field in the bottom of an agitated 12-well microtiter plate and to assess its similarity to published shear rate values occurring in some marine systems. Secondly, the effects of shear rate

and surface properties on the biofilm formation behaviour of different cyanobacterial strains were also evaluated.

Flow simulation on the 12-well microtiter plates was performed by CFD. Figure 3.1 shows the free liquid surface at a given instant upon agitation of the microtiter plate at two shaking frequencies. The liquid surface is not flat in either condition, and the surface inclination is higher at the highest shaking frequency. The velocity profiles were also determined for both shaking frequencies (Supplementary Material, Figure S 3.1). With a higher fluid velocity (obtained at the higher shaking frequency), a decreased liquid depth (associated to the surface inclination) was obtained. As previously suggested, the increased fluid velocity may facilitate mass transfer of nutrients from the bulk liquid to the biofilm and also access to oxygen and light may be promoted in this condition (Gomes *et al.*, 2014).

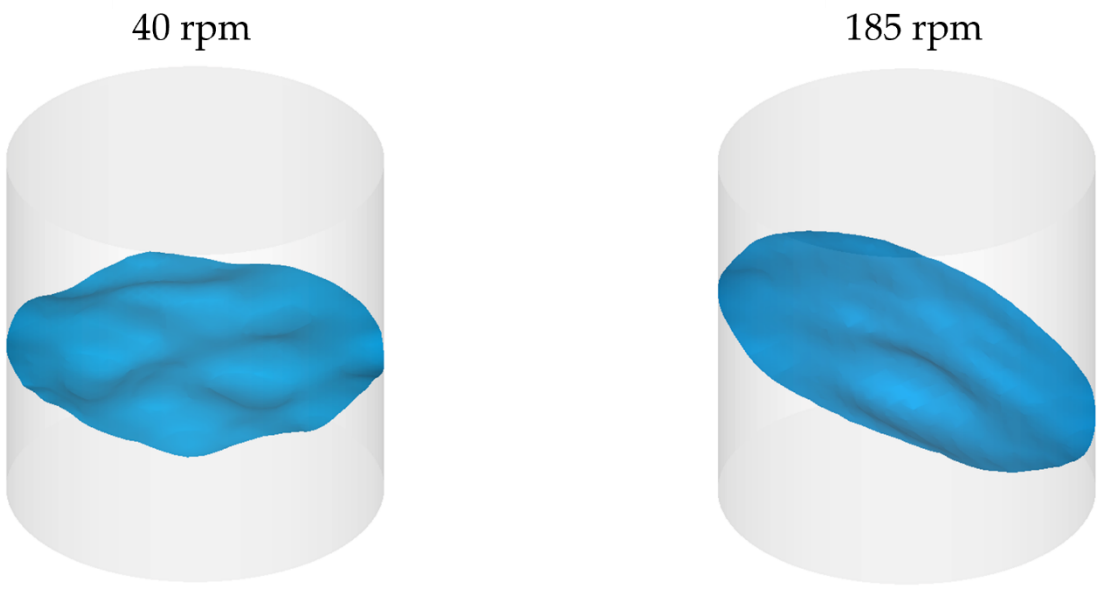

Figure 3.1. CFD simulation of the free liquid surface at 40 and 185 rpm.

The shear rate distribution on the surface at different degrees of a full rotation is shown in Figure 3.2, where it can be seen that higher shear rate values were obtained at the highest shaking frequency. In a full rotation (360°) of the orbital platform, the instant maximum and minimum wall shear rate values at any given point on the coupon surface are compensated over time. Therefore, the representative wall shear rate was obtained by averaging the results throughout a complete rotation cycle over the coupon surface.

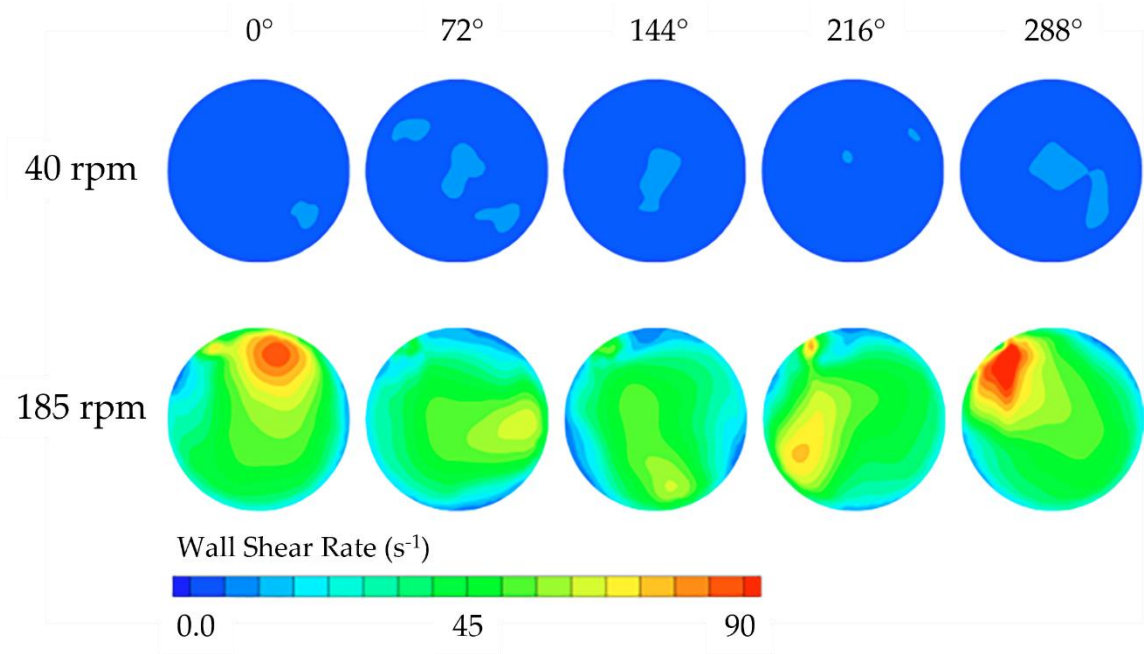

Figure 3.2. Wall shear rate at the bottom wall (at 40 and 185 rpm).

Figure 3.3 shows the shear strain rate variation over time. An average shear rate value of 40 s^{-1} was obtained for 185 rpm, reaching a maximum value of 120 s^{-1}, whereas an average value of 4 s^{-1} was calculated for 40 rpm, reaching a maximum value of 11 s^{-1}. At the shaking frequency of 185 rpm, the range of shear rates that can be reached includes different values that can be found in marine environments. Although a shear rate of 50 s^{-1} has been reported for a ship in a harbor (Bakker *et al.*, 2003), equipment and devices which are in similar environments (partially submerged or even moored equipment such as underwater cameras, flotation spheres and sensors) and even transparent hulls of boats or their windows are likely to be subjected to similar shear values. Moreover, this marine reactor also allows the biofilm development at lower shear rate conditions (at 4 s^{-1}), which is important because lower fluid velocities promote marine biofouling (Minchin and Gollasch, 2003; Flemming *et al.*, 2009).

Although different experimental setups have been used to study the effect of hydrodynamics particularly at later stages of marine biofilm development, including larval settlement (Qian *et al.*, 1999; 2000), the use of agitated microtiter plates in the

laboratory can be very convenient since it is an affordable and inexpensive platform. Microtiter plates present several advantages such as low volume requirements (reduced operational costs), are easy to handle and enable the control of different parameters like temperature and shear rate. Also, in the real scenario of a ship in a harbour, the shear rate field will oscillate due to tidal currents and because of the wakes caused by passing ships. Since the agitated microtiter plate induces a wave-like shear, it generates a flow topology that is more similar to marine systems than most flow systems.

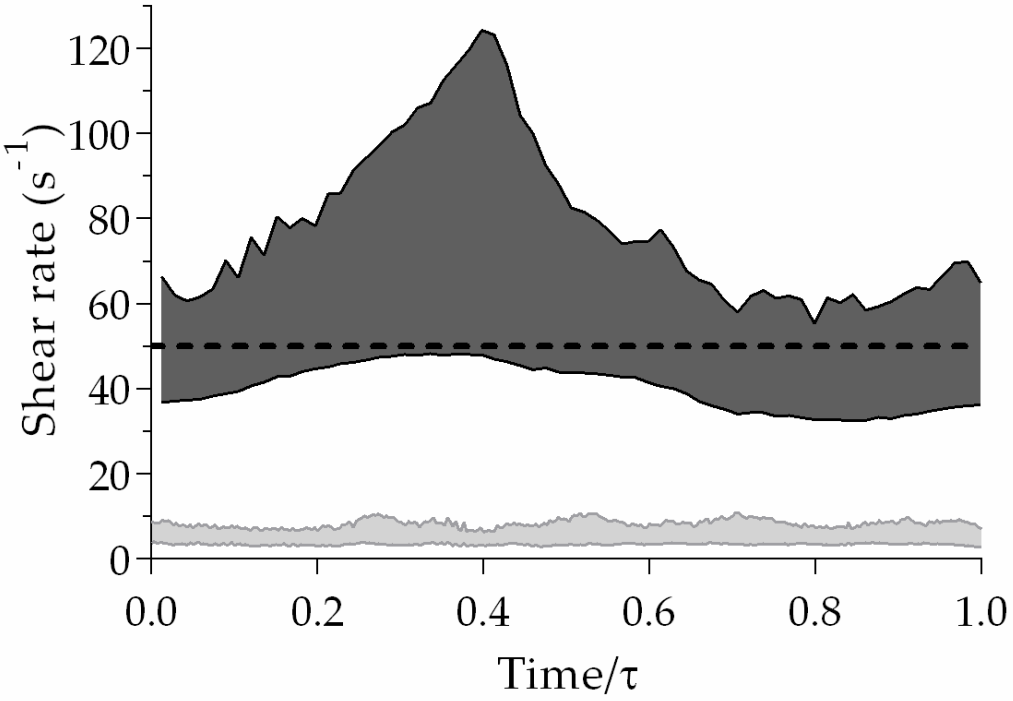

Figure 3.3. Representation of shear strain rate variation over a complete cycle. A normalized time scale was used since the period is different for each shaking frequency. The dashed line represents the shear strain rate reported for a ship in a harbour (50 s^{-1}). The area represented by light and dark grey (both delimited by average and maximum values) indicates the shear strain rate achieved at 40 and 185 rpm respectively.

Although CFD studies have already been performed on our group for 96-well plates (Gomes *et al.*, 2014), the present study focuses on 12-well microtiter plates, which enable a higher shear rate range (as can be found in marine environments) and the use of coupons to test different surfaces. A previous study using micro- and macro-flow systems to test *Escherichia coli* adhesion (Moreira, Ponmozhi, *et al.*, 2015) has shown that when the shear

forces are kept constant between these platforms, the obtained results were similar despite the large differences in size. Edge effects were also not shown to be important given the relative dimensions of the system and of the bacteria. Since in the present study, the shear rate range achieved (Figure 3.3) comprises the values found on real aquatic environments (50 s^{-1}; Bakker *et al.*, 2003), 12-well microtiter plates may be used as marine biofilm reactor to mimic these environments.

3.3.2 Surface analysis

Surface hydrophobicity was assessed by contact angle measurement with water (θ_w). Contact angle determination provides information about the interaction of the fluid with a solid material through the determination of the wettability and hydrophobicity of the surface. While wettability refers to the tendency of fluid spreading on a surface, hydrophobicity describes the tendency of non-polar molecular aggregation and consequently water molecule repulsion (Yuan and Lee, 2013). By definition, surfaces can be classified into hydrophilic or hydrophobic if the contact angle of water with the surfaces is lower or higher than 90° respectively (Sedlmeier *et al.*, 2008). Thus, low contact angle values indicate liquid spreading along the surface, which is associated with high wettability and hydrophilic properties. In turn, low wettability is associated with hydrophobicity. Since the contact angle of water on glass was θ_w = 48.55° ± 2.41° and in perspex θ_w = 73.05° ± 3.42°, perspex is relatively hydrophobic compared to glass, exhibiting a lower wettability. Although lower values for glass have been reported, some studies performed with glass surfaces, also shown values in the 40° range (Sener *et al.*, 2013; Thukkaram *et al.*, 2014; Gomes *et al.*, 2015; Moreira, Gomes, *et al.*, 2015). This slightly increased value may be related to the composition of this specific glass although other glass surfaces that can be used to construct submerged devices (underwater cameras, measuring devices or sensors) can have different hydrophobicities.

3.3.3 Biofilm analysis

Cyanobacterial biofilm formation was monitored for 49 days, and the evolution of wet weight and chlorophyll *a* content is shown in Figures 3.4 - 3.6. For all cyanobacterial strains, biofilm mass was in general higher at the lowest shear rate on both surfaces although statistically significant differences were mostly found on glass. Biofilm mass obtained on glass under low agitation was on average 22.4% higher for *Nodosilinea* sp. LEGE 06020 (Figure 3.4A), 58% higher for the unidentified filamentous Synechococcales LEGE 07185 (Figure 3.5A) and 32% higher for *Nodosilinea* sp. LEGE 06022 (Figure 3.6A) when compared to those obtained at higher shear conditions. Likewise, chlorophyll *a* was 29.5%, 93.9% and 62.7% higher in these conditions for each of the strains respectively (Figure 3.4B, 3.5B, 3.6B). On perspex, the biofilm wet weight was on average 17.6%, 37.2%, 26.9% higher at 4 s^{-1} (Figure 3.4C, 3.5C, 3.6C), whereas chlorophyll *a* was 31.5%, 91.9%, 70.8% higher at this shear rate (Figure 3.4D, 3.5D, 3.6D). Analysis of the biofilm wet weight and chlorophyll *a* suggests that, despite the tenfold difference on average shear rate, biofilm development was similar in both hydrodynamic conditions for the first two weeks. This suggests that shear rate had a lower impact on initial cell adhesion and a more noticeable effect during biofilm maturation, which in turn may be the result of two opposing effects caused by higher flow velocities (Supplementary Material, Figure S 3.1). Although nutrient mass transfer from the bulk liquid and oxygen transfer are facilitated at higher flow velocities, which may promote the biofilm development, the increased shear rate may hamper cell adhesion and may be more challenging for biofilm cohesion (erosion and sloughing events may be promoted). It is likely that the relative importance of these effects varies along the biofilm development stages. Since the effect of fluid velocity was more noticeable during biofilm maturation rather than during cell adhesion, it seems that the increased shear stress was not a significant obstacle to attachment whereas biofilm erosion may be the cause for a lower biofilm accumulation at the higher shear rate (Duddu *et al.*, 2009). It has been suggested that monitoring the chlorophyll *a* production can be a good way to follow cyanobacterial growth (Chorus and Cavalieri 2000; Lawton *et al.*, 1999). A correlation between chlorophyll *a* production and biofilm wet weight was observed in some cases (Supplementary Material, Figure S 3.2, 3.3, 3.4). This

correlation was more noticeable at the lowest shear rate (4 s^{-1}) for all cyanobacterial strains (Supplementary Material, Figure S 3.2A, C, 3.3A, C, 3.4A, C).

In this study, the effect of surface hydrophobicity was probably less important than the hydrodynamic effect, because similar values of wet weight and chlorophyll *a* were obtained for biofilms developed under different surfaces at the same hydrodynamic conditions (Supplementary Material, Figure S 3.5, 3.6). The fact that the hydrodynamic conditions may be more important than surface properties during initial biofilm development has already been shown during *E. coli* adhesion to glass and PDMS (Moreira *et al.*, 2014) where the effects of the surface properties were modulated by the shear forces. However, biofilm development of *Nodosilinea* sp. LEGE 06022 has also shown significant differences between glass and perspex surfaces (Supplementary Material, Figure S 3.7), with greater biofilm development on perspex, the most hydrophobic surface.

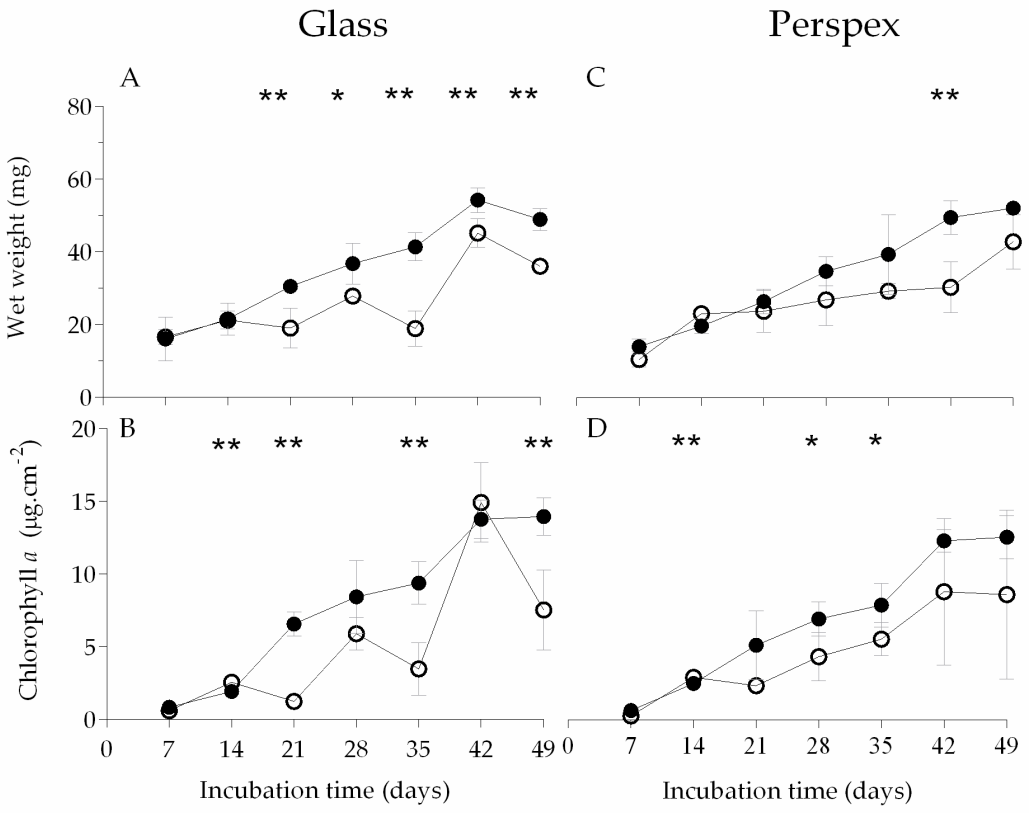

Figure 3.4. Evaluation of *Nodosilinea* sp. LEGE 06020 biofilm development. The parameters analysed refer to wet weight (A, C), chlorophyll *a* (B, D). Biofilms were formed in glass (A, B) or perspex (C, D), at two average shear rates, 4 s^{-1} (closed circles) and 40 s^{-1} (open circles) during 49

days. Standard deviations from three replicates are represented. Symbols * and ** indicate statistically different values for $P < 0.1$ and $P < 0.05$ (respectively) at each incubation time.

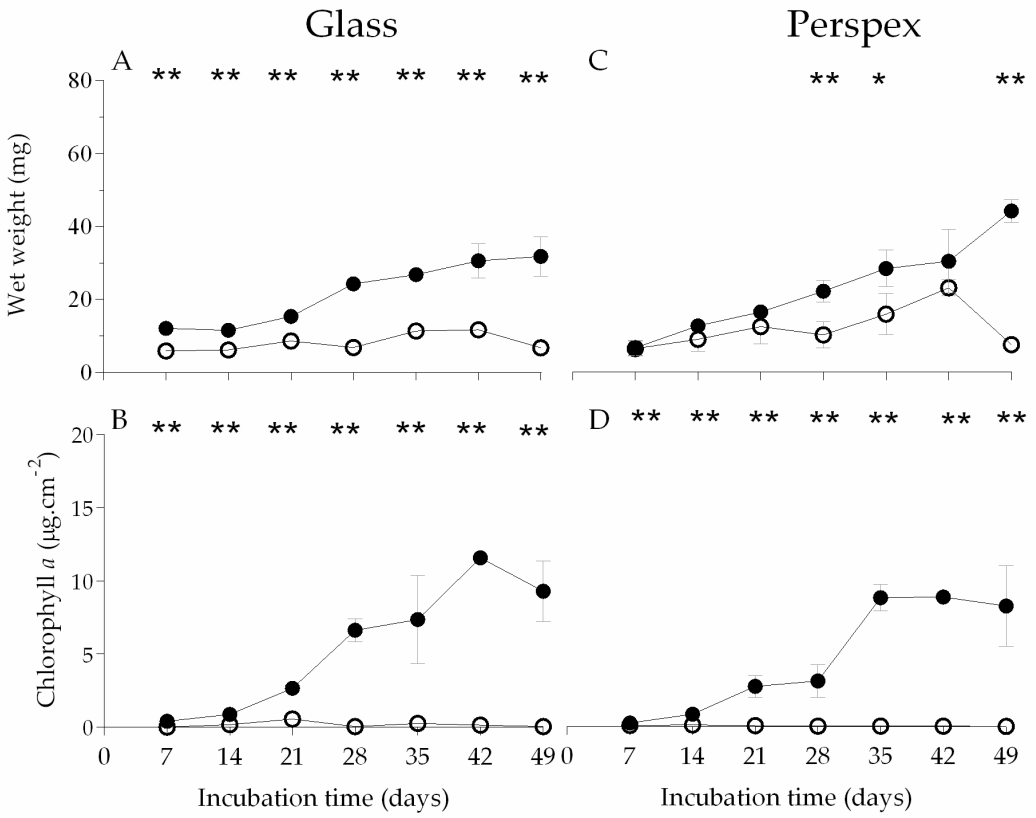

Figure 3.5. Evaluation of unidentified filamentous Synechococcales LEGE 07185 biofilm development. The parameters analysed refer to wet weight (A, C), chlorophyll *a* (B, D). Biofilms were formed in glass (A, B) or perspex (C, D), at two average shear rates, 4 s^{-1} (closed circles) and 40 s^{-1} (open circles) during 49 days. Standard deviations from three replicates are represented. Symbols * and ** indicate statistically different values for $P < 0.1$ and $P < 0.05$ (respectively) at each incubation time.

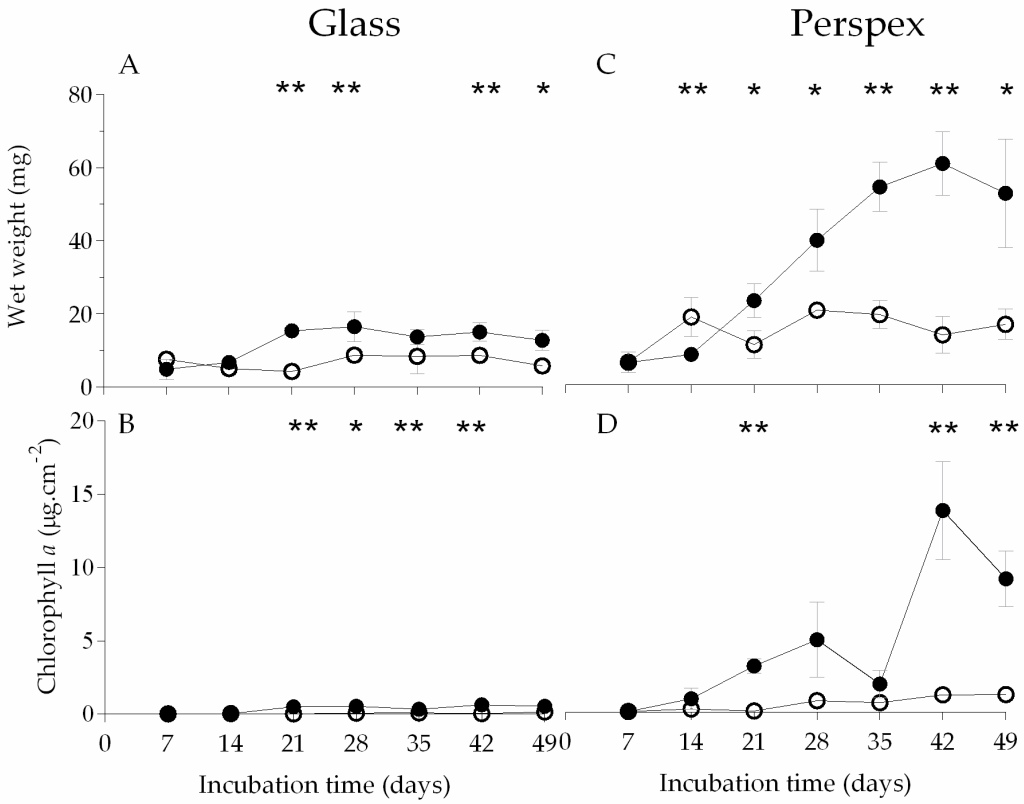

Figure 3.6. Evaluation of *Nodosilinea* sp. LEGE 06022 biofilm development. The parameters analysed refer to wet weight (A, C), chlorophyll *a* (B, D). Biofilms were formed in glass (A, B) or perspex (C, D), at two average shear rates, 4 s^{-1} (closed circles) and 40 s^{-1} (open circles) during 49 days. Standard deviations from three replicates are represented. Symbols * and ** indicate statistically different values for $P < 0.1$ and $P < 0.05$ (respectively) at each incubation time.

Since most commonly applied imaging methods to analyse biofilms are *ex-situ* and destructive (Azeredo *et al.*, 2017), Optical Coherence Tomography (OCT) is an interesting technique enabling *in situ*, non-invasive and real-time imaging without affecting biofilm structure (Wagner and Horn, 2017). Moreover, as biofilm thickness has a strong effect on the performance of underwater devices (Delauney *et al.*, 2010), the knowledge of this biofouling parameter is essential for the design and maintenance of marine equipment. Therefore, biofilm thickness, roughness and structure analyses were performed by OCT from day 28, because the shear rate effect became more pronounced from day 21 (Figures 3.4 – 3.6). Figure 3.7 shows the biofilm thickness and roughness coefficient evolution and Figures 3.8 – 3.10 shows representative images obtained at the end of the experiment.

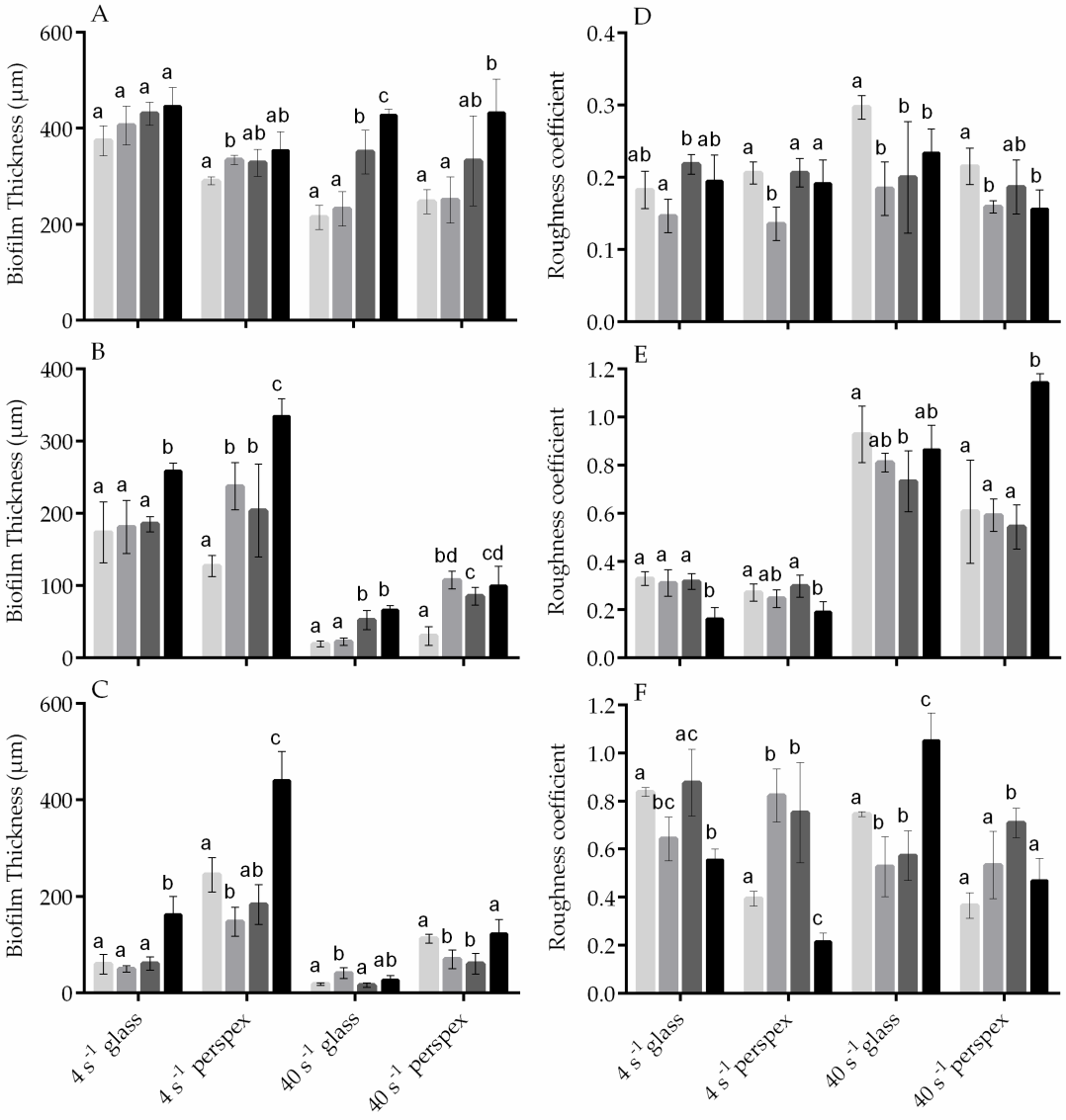

Figure 3.7. Evaluation of cyanobacterial biofilm thickness (left; A - C) and roughness coefficient (right; D - F) in both surfaces and different shear rates (A, D - *Nodosilinea* sp. LEGE 06020; B, E - unidentified filamentous Synechococcales LEGE 07185; C, F - *Nodosilinea* sp. LEGE 06022). Mean values ± SD from three replicates for each sampling day are represented. For each condition, different lowercase letters indicate significant differences between incubation times (28 days – very light grey bars; 35 days – light grey bars; 42 days – dark grey bars; 49 days – black bars; $P \leq 0.05$; unpaired *t*-test).

The biofilm thickness values obtained for the highest shear rate (40 s^{-1}) were lower than for the lowest shear rate (4 s^{-1}; Figure 3.7A, B, C). This was more noticeable for biofilm development of the unidentified filamentous Synechococcales LEGE 07185 (Figure 3.7B) and *Nodosilinea* sp. LEGE 06022 (Figure 3.7C) strains. For all cases except for *Nodosilinea* sp. LEGE 06020 at 4 s^{-1} and *Nodosilinea* sp. LEGE 06022 at 40 s^{-1}, (in which similar values were achieved, Figure 3.7A and 3.7C respectively), biofilm thickness increased from day 28 to the end of the experiment. The highest values of biofilm thickness were observed for *Nodosilinea* sp. LEGE 06020 at 4 s^{-1} on glass (around 446 μm; Figure 3.7A, 49 days) and the lowest for *Nodosilinea* sp. LEGE 06022 at 40 s^{-1} on glass (around 16 μm; Figure 3.7C, 42 days). Differences on biofilm thickness between the surfaces were more evident on *Nodosilinea* sp. LEGE 06022 (Figure 3.7C), with higher biofilm development on perspex, as previously reported for wet weight and chlorophyll *a* quantification (Supplementary Material, Figure S 3.7). Large variations on biofilm roughness under different shear rate were only observed for the unidentified filamentous Synechococcales LEGE 07185 (Figure 3.7E), in which lower values of the roughness coefficient were obtained for the lowest shear rate. In general, no significant differences between glass and perspex were observed for biofilm roughness coefficient (P = 0.20 for *Nodosilinea* sp. LEGE 06020, Figure 3.7D; P = 0.66 for the unidentified filamentous Synechococcales LEGE 07185, Figure 3.7E and P = 0.07 for *Nodosilinea* sp. LEGE 06022; Figure 3.7F). The highest (about 1.14) and the lowest (0.14) values of biofilm roughness coefficient were obtained for the unidentified filamentous Synechococcales LEGE 07185 at 40 s^{-1} on perspex (Figure 3.7E, 49 days) and *Nodosilinea* sp. LEGE 06020 at 4 s^{-1} on perspex (Figure 3.7D, 35 days) respectively. Biofilm of *Nodosilinea* sp. LEGE 06020 obtained at a higher shear rate (Figures 3.8B, D) seemed more compact than those obtained at low shear (Figures 3.8A, C). This effect was not observed for the unidentified filamentous Synechococcales LEGE 07185 and *Nodosilinea* sp. LEGE 06022 possibly because a lower biofilm biomass was obtained at a higher shear rate (40 s^{-1}) for both strains. A compact architecture probably increases biofilm cohesion and may therefore be an adaptation to the environmental shear forces (Teodósio *et al.*, 2011; Graba *et al.*, 2013). The formation of a less compact structure at lower shear may enhance mass transfer of nutrients to the inner layers of the biofilm (Teodósio *et al.*, 2011).

For most cases, except for biofilms obtained at 40 s^{-1} on glass (Figures 3.8, 3.9, 3.10B, F) and for *Nodosilinea* sp. LEGE 06020 on perspex at 4 s^{-1} (Figure 3.8C, G), the presence of three-dimensional streamers on the biofilm surface could be observed (Figures 3.8A, E, D, H, 3.9A, E, C, G, D, H; 3.10A, E, C, G, D, H). However, these structures were more noticeable for *Nodosilinea* sp. LEGE 06022 on perspex at lower shear rate (4 s^{-1}; Figure 3.10C, G). The formation of these streamers may contribute to the formation of "sieve-like" networks that can capture cells and other biomass (Drescher *et al*. 2013), therefore, contributing to the biofilm growth.

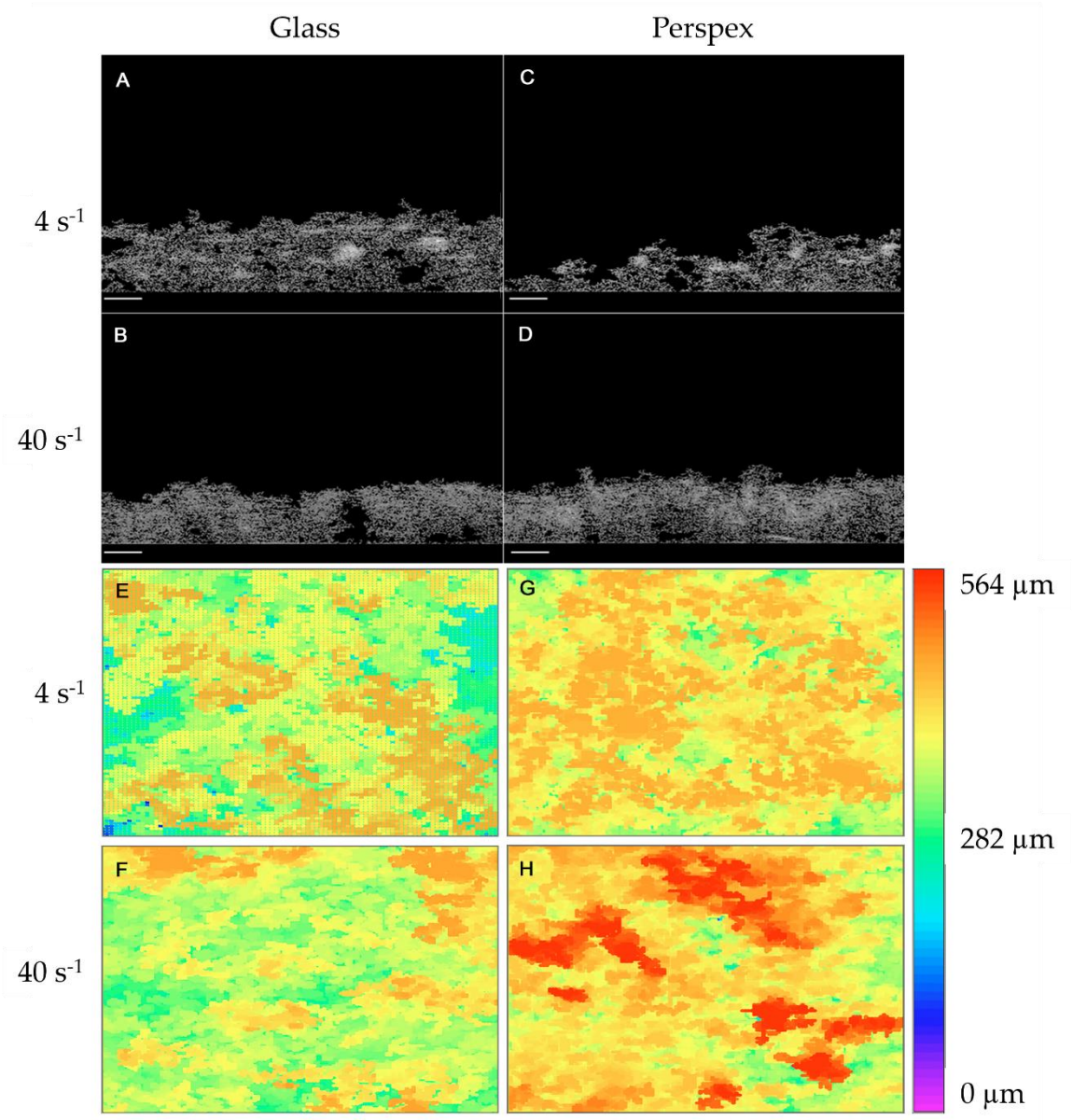

Figure 3.8. Representative images obtained by OCT of *Nodosilinea* sp. LEGE 06020 biofilms formed after 49 days on glass and perspex. A-D: 2D cross-sectional OCT images (scale bar = 200 µm); E –

H: 3D OCT images, top view projection (the color scale shows the range of biofilm thickness). Biofilms were formed at two different shear rates, 4 s^{-1} (A, C, E ,G) and 40 s^{-1} (B, D, F, H).

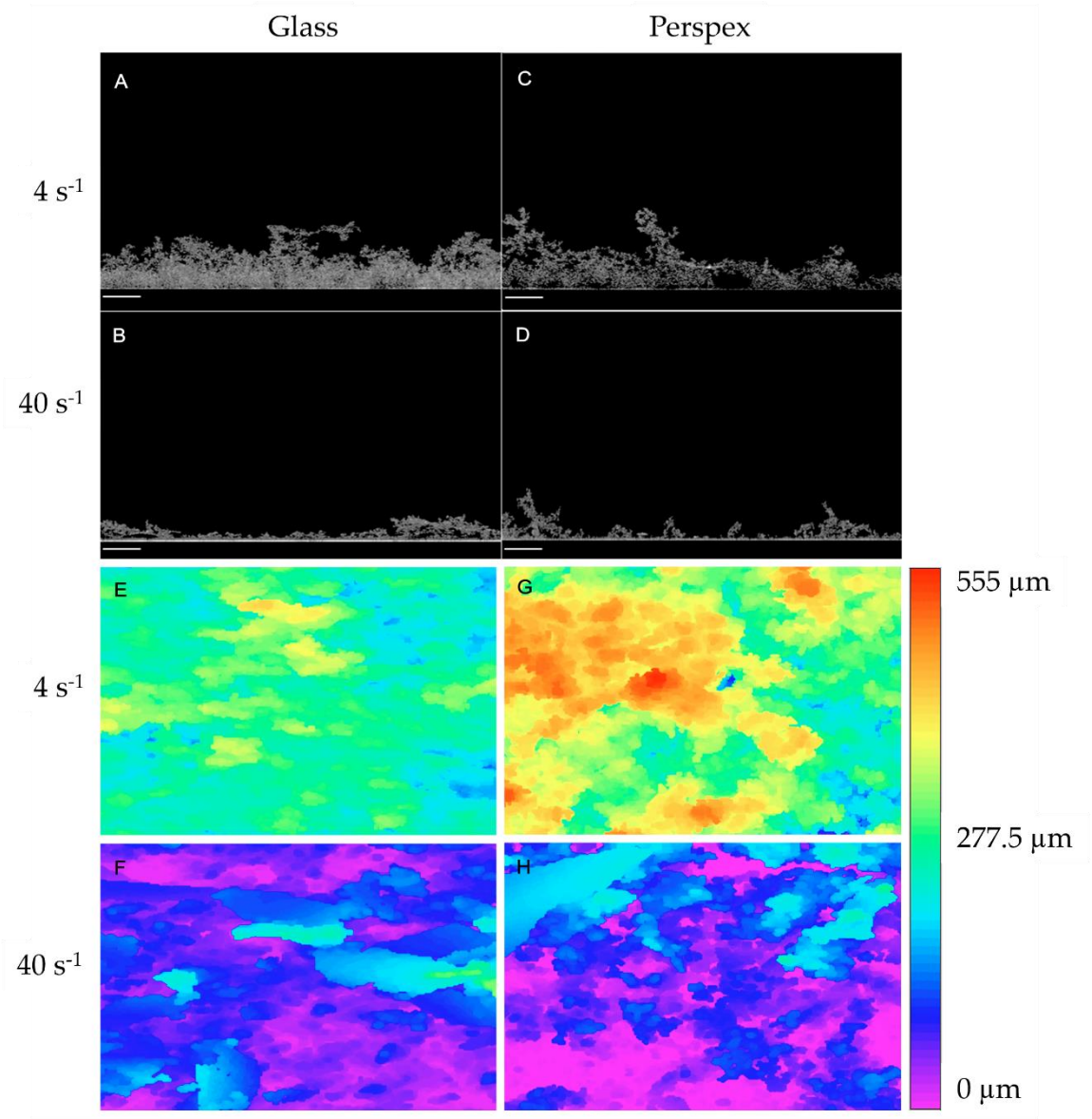

Figure 3.9. Representative images obtained by OCT of unidentified filamentous Synechococcales LEGE 07185 biofilms formed after 49 days on glass and perspex. A-D: 2D cross-sectional OCT images (scale bar = 200 µm); E – H: 3D OCT images, top view projection (the color scale shows the range of biofilm thickness). Biofilms were formed at two different shear rates, 4 s^{-1} (A, C, E, G) and 40 s^{-1} (B, D, F, H).

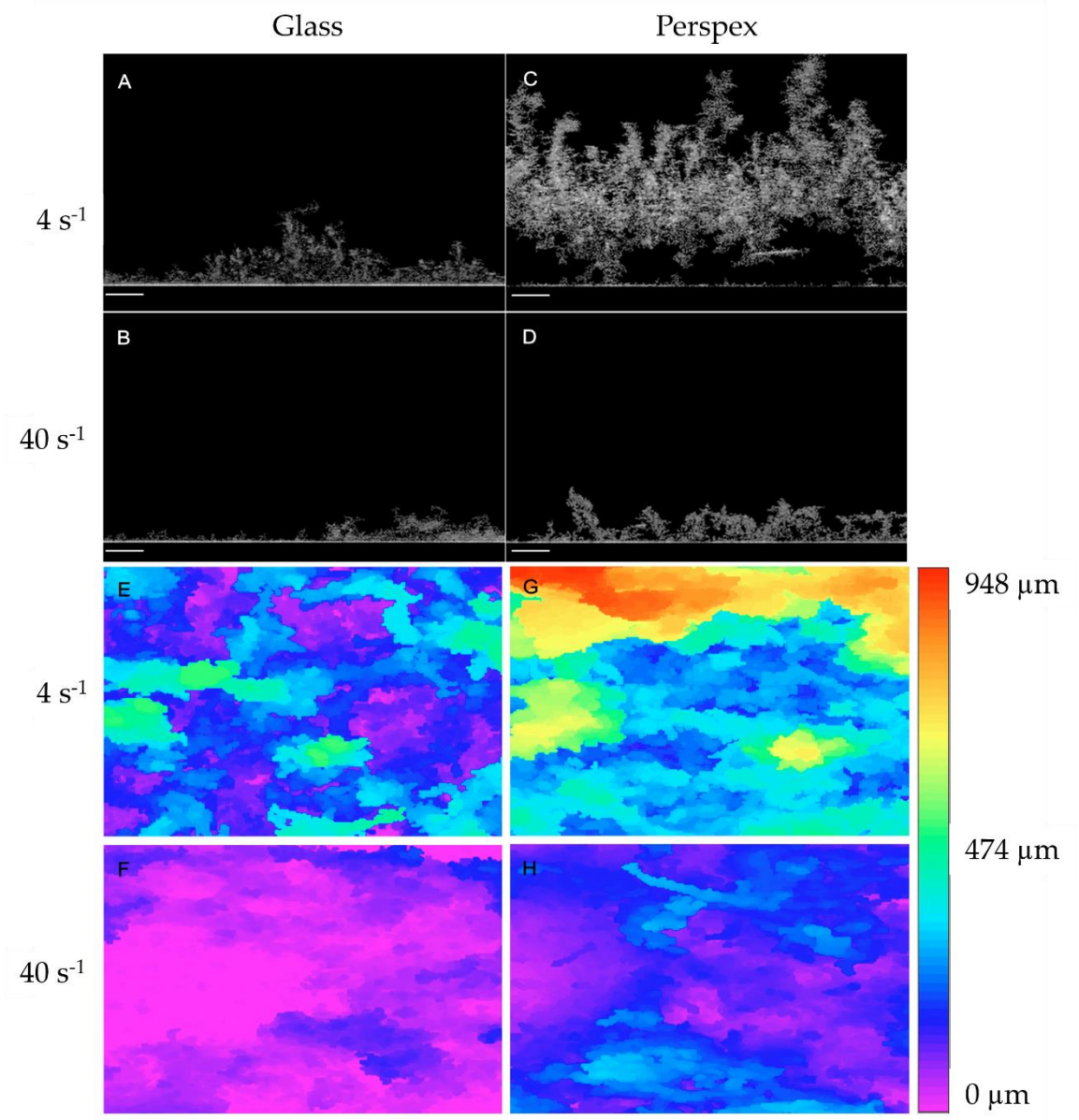

Figure 3.10. Representative images obtained by OCT of *Nodosilinea* sp. LEGE 06022 biofilms formed after 49 days on glass and perspex. A-D: 2D cross-sectional OCT images (scale bar = 200 µm); E – H: 3D OCT images, top view projection (the color scale shows the range of biofilm thickness). Biofilms were formed at two different shear rates, 4 s^{-1} (A, C, E, G) and 40 s^{-1} (B, D, F, H).

3.4 Conclusions

The CFD analysis in this work shows that the agitated 12-well microtiter plates can be used to attain shear rate values that can mimic aquatic environments. It was demonstrated that OCT analysis can be a valuable tool to analyze the architecture of marine biofilms and to further understand the biofilm formation dynamics. It was shown

that hydrodynamics plays a crucial role in the development of these biofilms and that these effects are likely to be more important during biofilm maturation rather than during the initial adhesion phase. Cyanobacterial biofilm formation studies performed in controlled hydrodynamic conditions are scarce, but the importance of studying filamentous cyanobacterial strains with such a cosmopolitan distribution is even more relevant given the biofouling potential of these organisms in different ecosystems around the globe

3.5 **Supplementary Material**

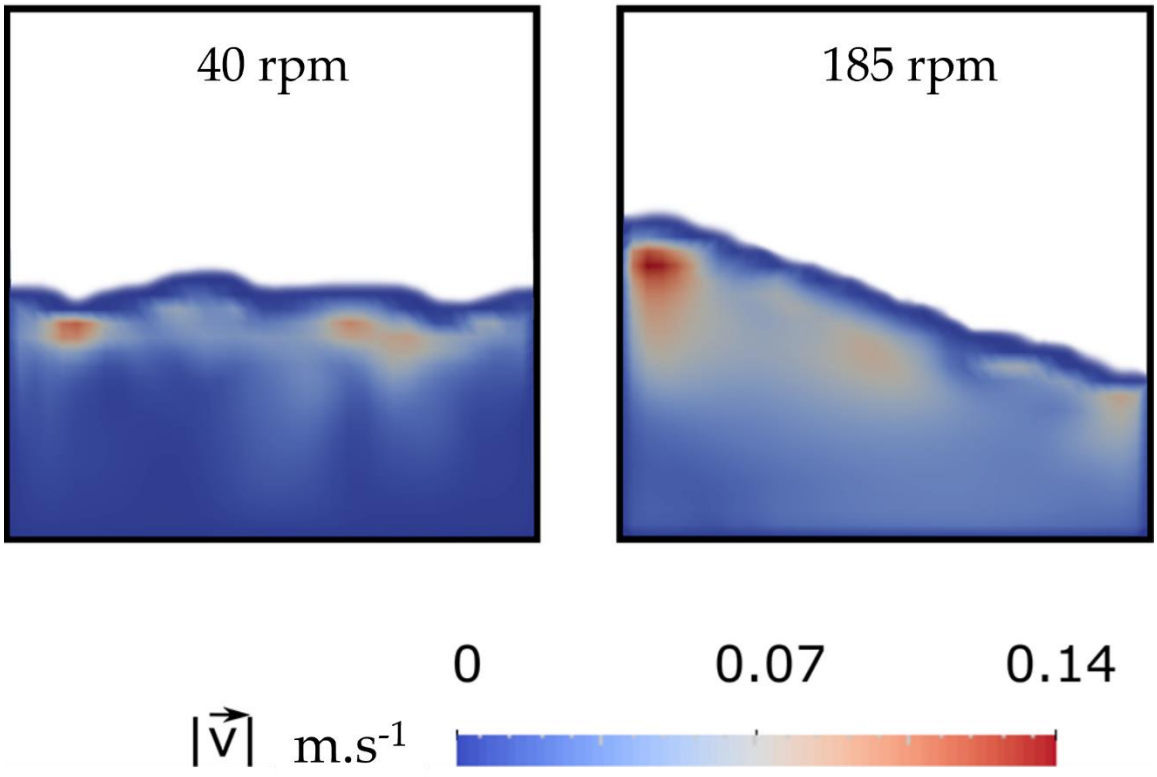

Figure S 3.1. Velocity profiles obtained at both shaking frequencies: 40 rpm and 185 rpm.

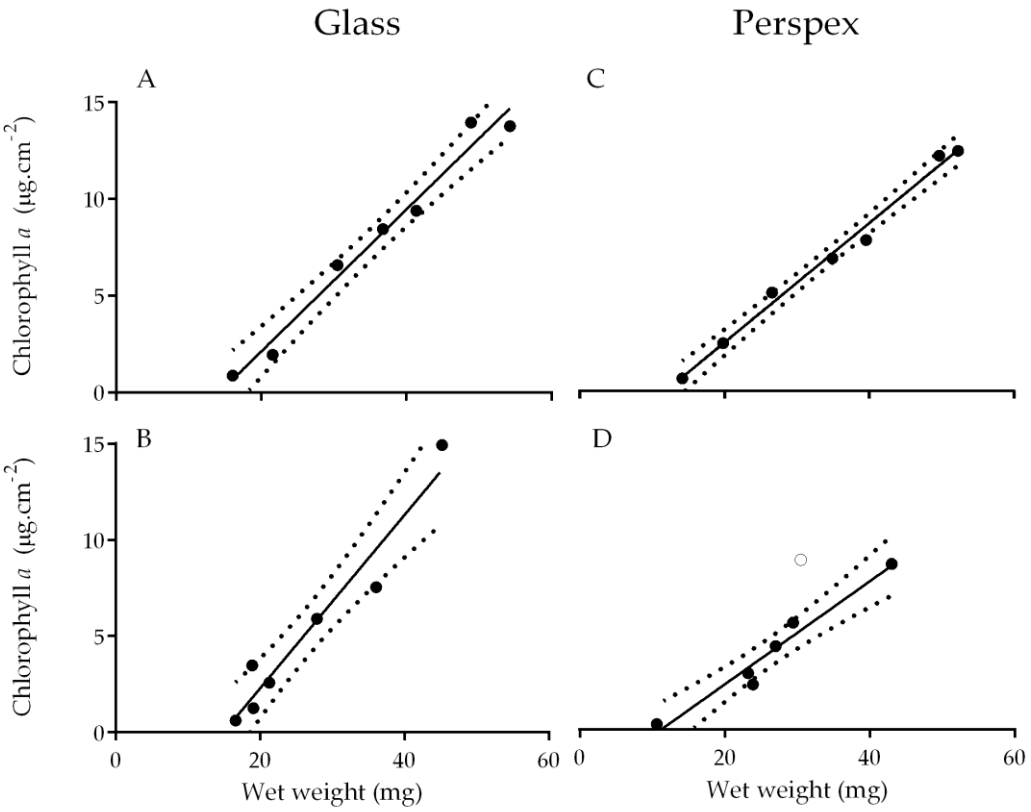

Figure S 3.2. Correlation between wet weight and chlorophyll *a* on *Nodosilinea* sp. LEGE 06020. Biofilm development in glass (A, B) and perspex (C, D), at two different shear rates, 4 s^{-1} (A, C) and 40 s^{-1} (B, D). Full line represents the linear regression whereas the dashed line represents the confidence limits (95%). Closed symbols refer to data points that were considered for the regression (all except one) and the single open symbol refers to a data point that was excluded from the regression.

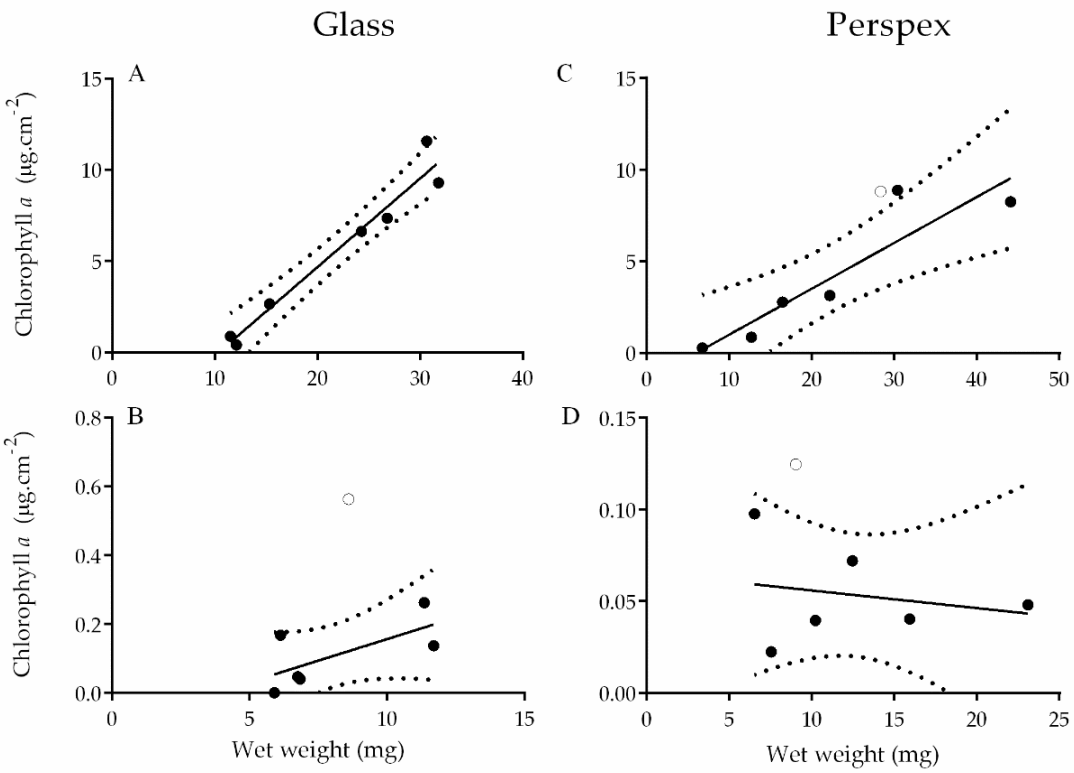

Figure S 3.3. Correlation between wet weight and chlorophyll *a* on unidentified filamentous Synechococcales LEGE 07185. Biofilm development in glass (A, B) and perspex (C, D), at two different shear rates, 4 s^{-1} (A, C) and 40 s^{-1} (B, D). Full line represents the linear regression whereas the dashed line represents the confidence limits (95%). Closed symbols refer to data points that were considered for the regression (all except three) and the open symbols refer to a data points that were excluded from the regression.

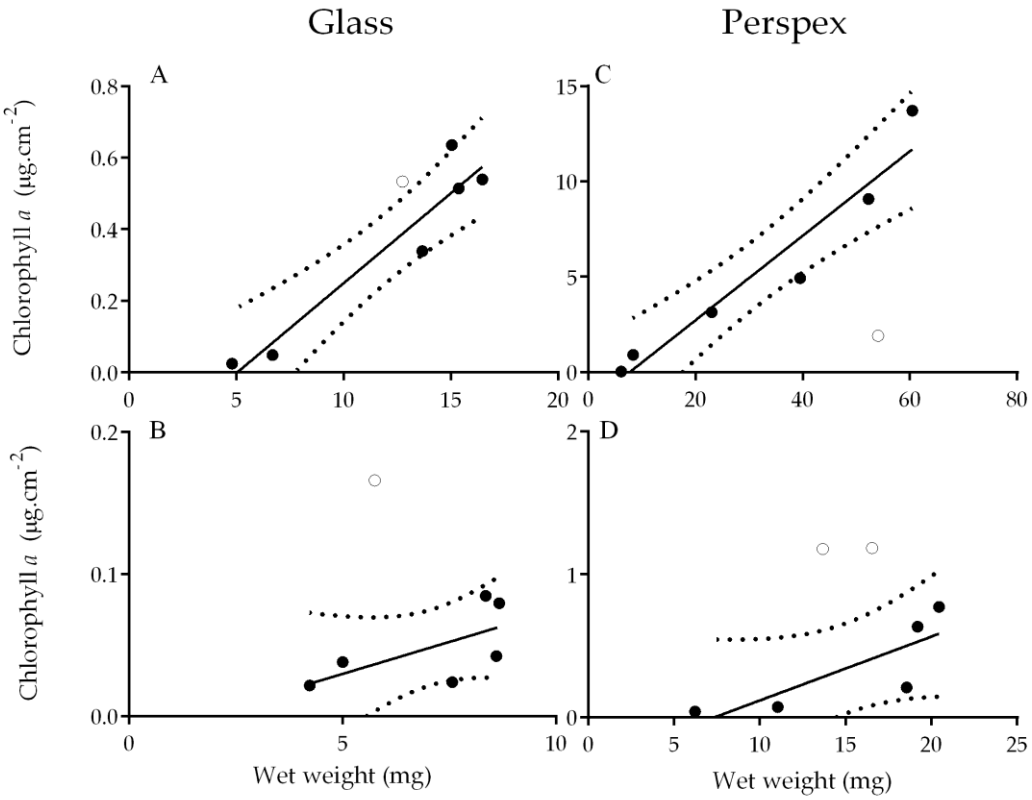

Figure S 3.4. Correlation between wet weight and chlorophyll *a* on *Nodosilinea* sp. LEGE 06022. Biofilm development in glass (A, B) and perspex (C, D), at two different shear rates, 4 s^{-1} (A, C) and 40 s^{-1} (B, D). Full line represents the linear regression whereas the dashed line represents the confidence limits (95%). Closed symbols refer to data points that were considered for the regression (all except five) and the open symbols refer to a data points that were excluded from the regression.

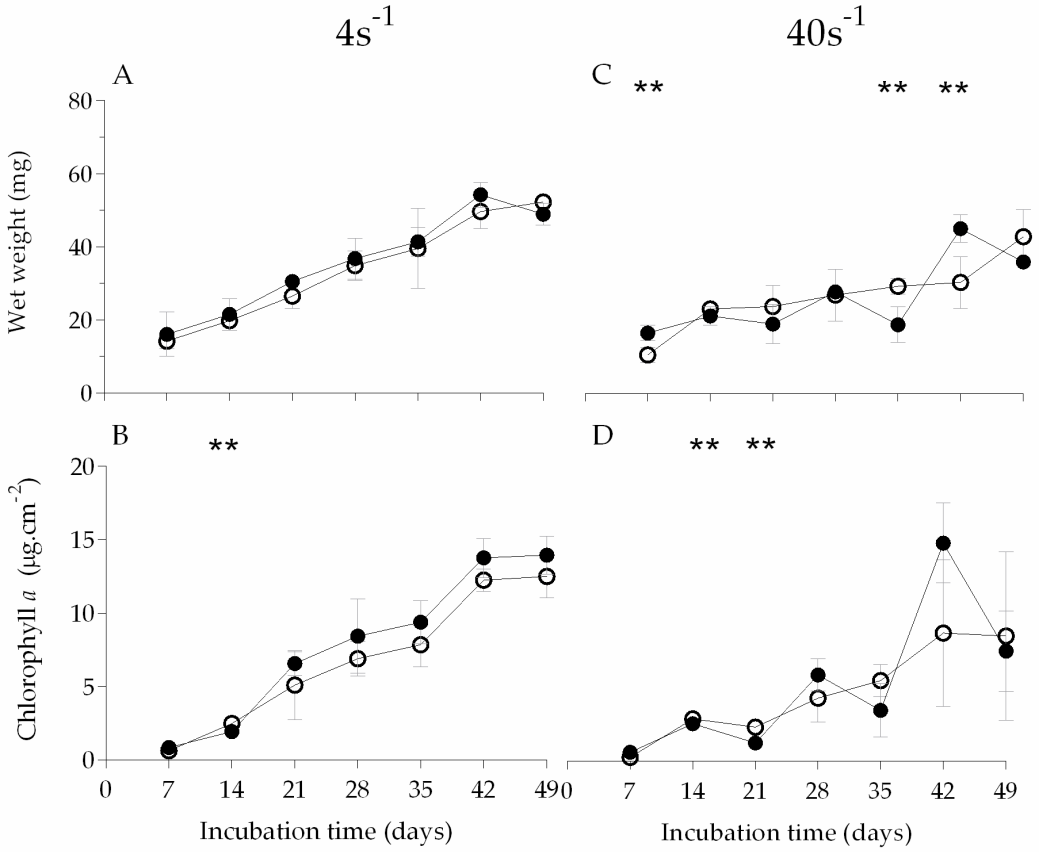

Figure S 3.5. Evaluation of *Nodosilinea* sp. LEGE 06020 biofilm development under the same hydrodynamic condition on different surfaces. The parameters analyzed refer to wet weight (A, C), chlorophyll *a* (B, D). Biofilms were formed at 4 s^{-1} (A, B) or 40 s^{-1} (C, D), on two different surfaces, glass (closed circles) and perspex (open circles) during 49 days. Standard deviations from 3 replicates are represented. Symbols *; ** indicate statistically different values for $P < 0.1$ and $P < 0.05$ (respectively) at each incubation time.

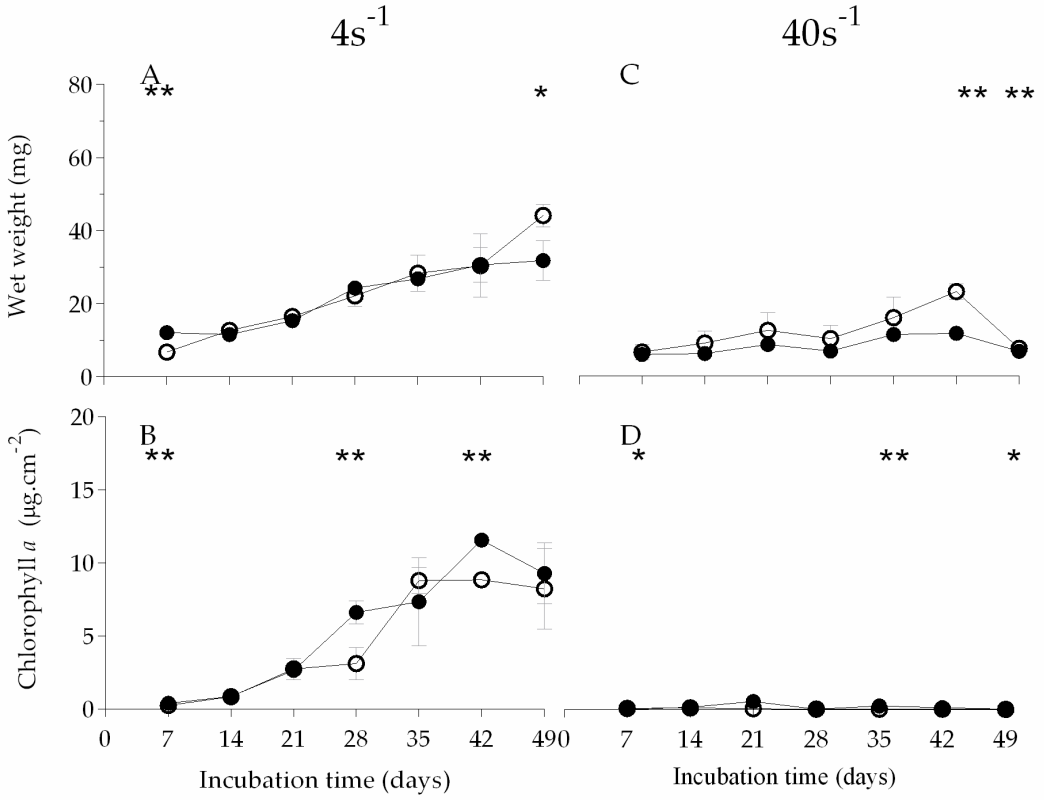

Figure S 3.6. Evaluation of unidentified filamentous Synechococcales LEGE 07185 biofilm development under the same hydrodynamic condition on different surfaces. The parameters analysed refer to wet weight (A, C), chlorophyll *a* (B, D). Biofilms were formed at 4 s^{-1} (A, B) or 40 s^{-1} (C, D), on two different surfaces, glass (closed circles) and perspex (open circles) during 49 days. Standard deviations from 3 replicates are represented. Symbols *; ** indicate statistically different values for $P < 0.1$ and $P < 0.05$ (respectively) at each incubation time.

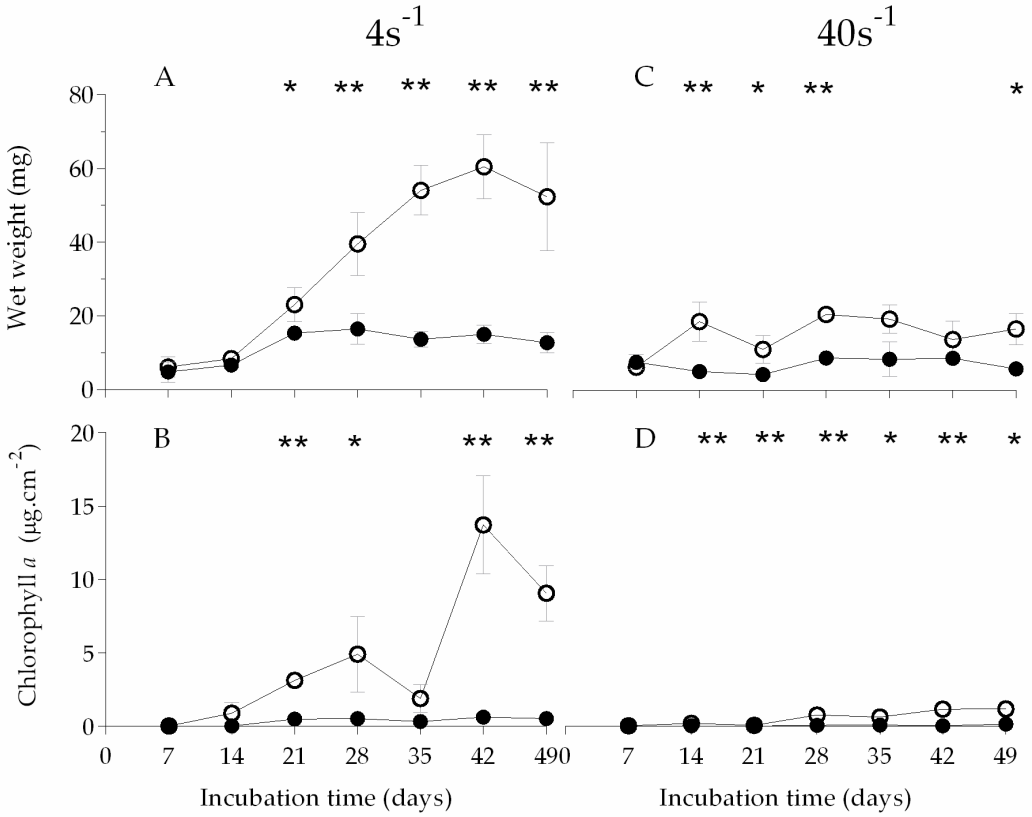

Figure S 3.7. Evaluation of *Nodosilinea* sp. LEGE 06022 biofilm development under the same hydrodynamic condition on different surfaces. The parameters analysed refer to wet weight (A, C), chlorophyll *a* (B, D). Biofilms were formed at 4 s^{-1} (A, B) or 40 s^{-1} (C, D), on two different surfaces, glass (closed circles) and perspex (open circles) during 49 days. Standard deviations from 3 replicates are represented. Symbols *; ** indicate statistically different values for $P < 0.1$ and $P < 0.05$ (respectively) at each incubation time.

4.

4 Characterization of planktonic and biofilm cells from two filamentous cyanobacteria using a shotgun proteomic approach

The contents of this chapter as published as:

Romeu M.J., Domínguez-Pérez D., Almeida D., Morais J., Campos A., Vasconcelos V., Mergulhão F. (2020) Characterization of planktonic and biofilm cells from two filamentous cyanobacteria using a shotgun proteomic approach. *Biofouling* **36**: 631-645.

Abstract

Cyanobacteria promote marine biofouling with significant impacts. A qualitative proteomic analysis, by LC-MS/MS, of planktonic and biofilm cells from two cyanobacteria was performed. Biofilms were formed on glass and perspex at two relevant hydrodynamic conditions for marine environments (average shear rates of 4 s^{-1} and 40 s^{-1}). For both strains and surfaces, biofilm development was higher at 4 s^{-1}. Biofilm development of *Nodosilinea* sp. LEGE 06145 was substantially higher than *Nodosilinea* sp. LEGE 06119, but no significant differences were found between surfaces. Overall, 377 and 301 different proteins were identified for *Nodosilinea* sp. LEGE 06145 and *Nodosilinea* sp. LEGE 06119. Differences in protein composition were more noticeable in biofilms formed

under different hydrodynamic conditions than those formed on different surfaces. Ribosomal and photosynthetic proteins were identified in most conditions. The characterization performed gives new insights into how shear rate and surface affect the planktonic to biofilm transition, from a structural and proteomics perspective.

Keywords: marine biofouling, cyanobacterial biofilms, shotgun proteomics, LC-MS/MS, hydrodynamic conditions, real-time imaging, Optical Coherence Tomography

4.1 Introduction

Marine biofouling causes several ecological problems and severe economic impacts on aquatic environments and marine industries (Carvalho, 2018). Biofilm formation on submerged equipment containing optical and electrochemical sensors (which are used for on-site monitoring with continuous measuring) can affect readings and lead to incorrect measurements (Delauney *et al.*, 2010). Cyanobacteria and diatoms are responsible for the initiation of biofilm formation by the production of large amounts of extracellular polymeric substances (EPS), and they also represent the major components of marine biofilms (Bharti *et al.*, 2017). Additionally, these microfouler organisms can promote the adhesion of macrofouler organisms such as invertebrate larvae, mussels, seaweeds and barnacles (Mieszkin *et al.*, 2013).

Physico-chemical factors related to the surface being colonized (Crawford *et al.*, 2012) and flow velocity and shear rate (R. Allen *et al.*, 2018) are some of the most critical parameters that affect biofilm composition, structure and development. Moreover, these factors can also impact the EPS production, energy metabolism and induce molecular changes in biofilms (Moreira, Gomes, *et al.*, 2015). The development of novel antifouling strategies for marine applications is of paramount importance (Telegdi *et al.*, 2016). Therefore, molecular studies capable of identifying the agents and pathways affecting the settlement of biofouling organisms are necessary to obtain new targets and develop more effective biofilm mitigation strategies.

Omics approaches such as genomics, transcriptomics, proteomics and metabolomics have been widely used to characterize bacterial virulence factors (Alexova *et al.*, 2011; Babele *et al.*, 2019) and provide new information about biofilm development and regulation (Leary *et al.*, 2014; Parnasa *et al.*, 2016). Specifically, proteomics studies have also been used to understand the molecular mechanisms involved in important cellular processes such as cell division, metabolism, transport, stress response and motility in these microbial communities (Parnasa *et al.*, 2016; Wang *et al.*, 2020). Furthermore, proteomic analysis allows the study of interspecies interactions on biofilms (Herschend *et al.*, 2017) and how biofilm development is affected by physiological and environmental factors (Chen *et al.*, 2019). In a stressful condition, the long-term adaptation is governed by mechanisms of cellular regulation as the synthesis and/or modified expression of proteins. The identification of these proteins using high throughput proteomic tools has provided new insights into the cellular response to a defined stress condition and also regarding the cell signaling and stress response pathways that are activated under different conditions (Muthusamy *et al.*, 2017; Battchikova *et al.*, 2018). Since modifications in the proteome are associated with physiological and metabolic rearrangements at the genotype level during stress adaptation and tolerance, qualitative proteomics studies lead to the identification and characterization of these stress-responsive proteins (Babele *et al.*, 2019). Therefore, qualitative proteomic experiments can provide a general picture of the physiological state of a given organism through the identification of proteins which are translated under different conditions.

The isolation and purification of stable and high-quality proteins is the most challenging task in cyanobacterial proteomic experiments (Pandhal *et al.*, 2009), since cyanobacteria contain several proteases, oxidative enzymes, phycobiliproteins and other pigments which hinder the effective extraction, purification and recovery of less abundant proteins (Ow *et al.*, 2011). In this context, novel extraction protocols have been developed and were a major step for today's high throughput proteomic workflows (Anderson *et al.*, 2006). The development of high-resolution liquid chromatography (LC) and more advanced tandem mass spectrometry (MS/MS) enabled the development of shotgun proteomics (Babele *et al.*, 2019). Since proteomes are directly digested and analyzed *in situ* by a combination of liquid chromatographic separation and analysis using high-speed

tandem mass spectrometry, shotgun proteomics opened up opportunities to perform fast and reliable identification of cyanobacterial proteins (Anderson *et al.*, 2006). Furthermore, LC–MS/MS data acquisition is nearly fully automated, which enables analysis in a high throughput mode leading to low variations, thus, improving the confidence of the results.

Although several studies investigated the proteome of planktonic and sessile forms, only a few address marine biofilms (Leary *et al.*, 2014). The data available on cyanobacteria are sparse (Babele *et al.*, 2019) and focus on well-studied model cyanobacteria, such as the unicellular cyanobacterium *Synechocystis* sp. PCC 6803 (Jahn *et al.*, 2018). Moreover, the small number of proteomic studies performed on filamentous cyanobacteria is rather old and restricted to the cyanobacterial genera *Nostoc, Anabaena,* and *Spirulina* (Anderson *et al.*, 2006; Kurdrid *et al.*, 2011).

The main aim of this study was to perform a qualitative proteomic analysis on filamentous cyanobacteria under planktonic and different conditions of biofilm development. To the best of the authors' knowledge, there are no proteomic studies evaluating the impact of different surfaces and different hydrodynamic conditions on cyanobacterial biofilm behavior. Since no proteomic analysis of the genus *Nodosilinea* is available, this represents the first work that investigated the proteome obtained from different conditions of biofilm development of this ubiquitous cyanobacterial genus. Cyanobacterial strains from the genus *Nodosilinea* are present in dissimilar geographies, including different continents (Europe, Antarctica, Asia and America), and specimens can also be found in different ecologies, such as brackish water, freshwater, marine and even terrestrial environments (Heidari *et al.*, 2018; Ramos *et al.*, 2018; Vázquez-Martínez *et al.*, 2018; Radzi *et al.*, 2019). This cosmopolitan distribution highlights the importance of studying biofilm formation by these organisms. Moreover, the relevance of studying these filamentous cyanobacterial strains is even more critical given the biofouling potential of these organisms. Indeed, some studies showed the high biofouling potential of the genus *Nodosilinea* on different surfaces. Additionally, cyanobacterial strains from this genus were recovered from biofilms on a house wall (Perkerson III *et al.*, 2011), from a benthic mat in a thermal spring with very high natural radioactivity (Heidari *et al.*, 2018) and even from mats collected in Antarctica (Radzi *et al.*, 2019). *Nodosilinea* strains were also found on subaerial biofilms, which develop on mineral surfaces and on archaeological stone

monuments experiencing extended periods of heat, insolation and dehydration (Vázquez-Martínez *et al.*, 2018). These biofilms have been widely studied due to their impact on deterioration of cultural heritage.

4.2 Materials and Methods

4.2.1 Organism and inocula preparation

Two cyanobacterial strains were used in this study, and both were obtained from the Blue Biotechnology and Ecotoxicology Culture Collection (LEGE-CC) located at CIIMAR, Portugal (Ramos *et al.*, 2018). *Nodosilinea* sp. LEGE 06145 was isolated from a sample scraped from a wave-exposed rock in the tide puddle collected at Moledo beach, Portugal (41.84963 N 8.866717 W). *Nodosilinea* sp. LEGE 06119 was isolated from a seawater sample collected in the surf zone at Burgau beach, Portugal (37.07156 N 8.774722 W) (Ramos *et al.*, 2018). Cells from an initial 50 mL culture were grown for 30 days in 750 mL culture in Z8 medium (Kotai, 1972) supplemented with 25 $g.L^{-1}$ of synthetic sea salts (Tropic Marin) and vitamin B_{12} (Sigma Aldrich, Merck, Saint Louis, MO, USA). Cultures were performed under 14 h light (10–30 μmol photons m^{-2} s^{-1})/10 h dark cycles, at 25 °C.

4.2.2 Biofilm formation

Biofilm formation was assessed on agitated 12-well microtiter plates (VWR International, Carnaxide, Portugal), since this platform was shown to mimic the hydrodynamic conditions found on marine environments (Romeu *et al.*, 2019). In order to assess the effect of the surface on protein expression, biofilms were developed on glass (Vidraria Lousada, Lda, Portugal) and perspex (Neves & Neves, Lda, Portugal) coupons (1 cm^2). These represent commonly submerged artificial surfaces found on different equipment in aquatic and marine environments (Taylor, 1996; King *et al.*, 2006). Moreover, these surfaces present different hydrophobicity (perspex is relatively hydrophobic compared to glass) (Romeu *et al.*, 2019). Surface preparation was performed as described in Romeu et al., 2019. All coupons were aseptically pre-weighted. Transparent double-sided adhesive tape was used to fix the coupons and once the tape was placed in the wells,

all coupons and the plates were subjected to UV sterilization for 30 min after which the sterile coupons were fixed. Since chlorophyll *a* concentration is commonly used as biomass indicator in aquatic environments, prior to inoculation each cyanobacterial suspension was adjusted to a chlorophyll *a* concentration of 1.5 $\mu g.mL^{-1}$. Briefly, 2 mL of each suspension were incubated for 24 h at 4 °C in the dark for a maximal chlorophyll *a* extraction. The samples were then centrifuged at 3202*g*, for 5 min at room temperature, and the supernatant was transferred to a glass cuvette. The absorbance at 750 nm (turbidity), 665 nm (chlorophyll *a*) and 652 nm (chlorophyll *b*) was determined using a V-1200 spectrophotometer (VWR International China Co., Ltd, Shanghai, China). The chlorophyll *a* concentration was calculated through the following equation (4.1) (Porra *et al.*, 1989):

$$\text{Chl } a \ (\mu g.mL^{-1}) = 16.29 \times A^{665} - 8.54 \times A^{652} \quad (4.1)$$

where A^{665} and A^{652} are the absorbances at 665 nm and 652 nm, respectively.

These measurements were performed in triplicate and the dilutions were performed using Z8 medium supplemented with 25 $g.L^{-1}$ of synthetic sea salts and B_{12} vitamin. After cyanobacterial suspension adjustment, planktonic samples for proteomic analysis were collected and kept at -80 °C.

A volume of 3 mL of adjusted cyanobacterial suspension in Z8 medium (prepared as described above) supplemented with nutritional factors, which support the growth and cyanobacteria maintenance (Kotai, 1972), was inoculated in each well. In order to assess the hydrodynamic effect on protein expression, cyanobacterial biofilm formation at different shear rates was tested. In order to attain the shear rate values that can mimic aquatic environments, such as those found in a ship hull in a harbour and in partially submerged or even moored equipment and devices (as underwater cameras, flotation spheres, sensors and even transparent hulls of boats or their windows), microtiter plates were incubated at 25 °C in an orbital shaker with a 25 mm orbital diameter (Agitorb 200ICP, Norconcessus, Portugal) at 185 rpm (achieving the average shear rate of 40 s^{-1}, Romeu *et al.*, 2019). Moreover, since lower fluid velocities can promote marine biofouling

(Flemming *et al.*, 2009), biofilm development was also assessed at lower shear rate conditions (average shear rate of 4 s^{-1}, achieved at 40 rpm). Biofilm development was followed for seven weeks (49 days) since it is accepted that a two-month interval for maintenance is the minimum duration for economically viable underwater monitoring systems, as previously reported (Romeu *et al.*, 2019). During this incubation time, the medium was replaced twice a week. In order to mimic real light exposure periods, a photoperiod of 14 h light (8-10 μmol photons m^{-2} s^{-1})/10 h dark cycles) was applied.

4.2.3 Biofilm analysis

Sampling was performed every seven days and at each sampling day, three coupons for each surface and hydrodynamic condition were analysed for both cyanobacteria. The culture medium was carefully removed and the wells were filled with 3 mL of sterile sodium chloride solution (8.5 $g.L^{-1}$) to evaluate the cyanobacterial biofilm structure and thickness by Optical Coherence Tomography (OCT). In order to complement the characterization of cyanobacterial biofilms, the determination of their wet weight and chlorophyll *a* content was performed.

4.2.3.1 Optical Coherence Tomography

Images from cyanobacterial biofilms developed on both surfaces and under different hydrodynamic conditions were captured as reported in Romeu *et al.*, (2019). Briefly, the captured volume was ~ 4 x 4 x 3 mm^3 (509 x 313 x 1024 $pixels^3$) and since biofilms are mainly composed (90%) of water (Bakke *et al.*, 2001), the refractive index was set to 1.40. For each coupon, 2D imaging was performed with a minimum of three fields of view, to ensure the accuracy and reliability of the results obtained. Image analysis was performed using a routine developed in the Image Processing Toolbox from MATLAB 8.0 and Statistics Toolbox 8.1 (The MathWorks, Inc., Natick, Massachusetts, USA). The processing steps include image denoising, detection of the surface layer/biofilm bottom and segmentation of the biofilm structure by the upper contour line of the biofilm. The acquired image is denoised using Haar wavelets (Mayer *et al.*, 2012). The method used for the detection of the biofilm bottom consists of edge detection, using the Canny edge filter

(Canny, 1986) and straight-line detection, using the Hough line transform (Duda and Hart, 1972). The highest peak in Hough space corresponds to the surface layer and biofilm bottom. For the segmentation of the biofilm structure, a Sobel operator is applied, and the result is thresholded. Then, the resulting binary image is dilated, using a vertical structuring element and a horizontal structuring element and the holes inside the biofilm are filled in. Finally, the contours of the resulting binary image are smoothed, by eroding the image with a diamond structuring element. In this way, a binary "mask" that covers the biofilm region is obtained. The biofilm is delimited by the upper boundary of this "mask" and by the surface layer/biofilm bottom. The mean of biofilm thickness was calculated based in the distance between the biofilm bottom and the upper contour line according to the following equation (4.2):

$$\bar{L}_F = \frac{1}{N}\sum_{i=1}^{N} L_{F,i} \qquad (4.2)$$

where $L_{F,i}$ is a local biofilm thickness measurements at location *i* and *N* equals the number of thickness measurements and $\bar{L}_{F,i}$ is the mean biofilm thickness.

4.2.3.2 Wet weight determination and chlorophyll *a* quantification

The determination of cyanobacterial biofilms wet weight and chlorophyll *a* content was performed as reported in Romeu *et al.*, 2019. Briefly, to determine the wet weight, coupons were detached from the wells and weighted. Biofilm wet weight was obtained by the difference to the initial coupon weight (determined prior to inoculation). Afterward, cyanobacterial cells were detached from the coupons by immersing each coupon in 2 mL of 8.5 $g.L^{-1}$ sodium chloride solution and vortexing, and the suspensions were incubated for 24 h at 4 °C in the dark for a maximal chlorophyll *a* extraction, as previously described through the equation 4.1.

4.2.4 Proteomic analysis

4.2.4.1 Protein extraction and sample preparation

Biomass of 40 biofilm samples comprising four replicates from each biofilm condition of *Nodosilinea* sp. LEGE 06145 and *Nodosilinea* sp. LEGE 06119 and four samples consisting of two replicates from planktonic samples of both cyanobacterial strains were kept at -80 °C until protein extraction. Biomass for biofilm samples was obtained as previously described. Briefly, cyanobacterial biofilms were detached from the coupons by immersing each coupon in 2 mL of 8.5 $g.L^{-1}$ sodium chloride solution and vortexing. The total protein extraction was performed into sodium dithionite (SDT) buffer (2% SDS, 100 mM Tris/HCl pH 7.6, 0.1 M DTT) + Protease inhibitors (PIs, Roche, 11697498001), as a variant of the method carried out by Campos *et al.* (2016). Briefly, the biomass from each replicate was weighted and a proper volume of SDT buffer was added to the samples (0.5 $g.mL^{-1}$ SDT), sonicated 5 x 4 sec and 23 kHz – 105 μm (amplitude) and incubated at room temperature overnight. Afterward, samples were sonicated 5 x 4 sec and 23 kHz – 105 μm (amplitude); heated for 3 min at 95 °C and subsequently centrifuged at 16000*g* for 20 min. Finally, the supernatant was collected, and total protein concentration was measured indirectly by optical density (OD) at 280 nm using a microplate reader (PowerWave; Biotek, VT, USA). Samples containing the extracted protein were stored for 24 h at -20 °C. The extracted proteins were processed using the Filter Aided Sample Preparation (FASP) protocol described by Wiśniewski *et al.*, 2009. In summary, this approach comprised the alkylation and digestion of 30 μg of the extracted proteins with trypsin (recombinant, proteomics grade, Roche, Basel, Switzerland) at an enzyme to protein ratio of 1:100 (w/w) for 16 h at 37 °C using centrifugal filter units with nominal molecular weight limit (NMWL) of 30 kDa (MRCPRT030, Millipore, Billerica, MA, USA). Through centrifugal filtration, peptides were recovered and acidified with Trifluoracetic acid (TFA) (10% $v.v^{-1}$). Samples were desalted and concentrated by reversed-phase extractions (C18 Tips, 100 μL, Thermo Scientific, 87784) with acetonitrile (ACN) (50% $v.v^{-1}$) and TFA (0.1% $v.v^{-1}$) for peptide elution. Before LC-MS/MS analysis, samples were dried in the speed-vac and resuspended in formic acid (FA) (0.1% $v.v^{-1}$) to a final concentration of 0.04–0.06 $\mu g.\mu L^{-1}$.

4.2.4.2 LC-MS/MS analysis

FASP protein digests were processed using a nano LC-MS/MS, composed by an Ultimate 3000 liquid chromatography system coupled to a Q-Exactive Hybrid Quadrupole – Orbitrap mass spectrometer (Thermo Scientific, Bremen, Germany). Samples were loaded onto a trapping cartridge (Acclaim PepMap C18 100Å, 5 mm x 300 μm i.d., 160454, Thermo Scientific) in a mobile phase of 2% ACN, 0.1% FA at 10 $\mu L.min^{-1}$. After 3 min loading, the trap column was switched in-line to a 15 cm by 75 μm inner diameter EASY-Spray column (ES800, PepMap RSLC, C18, 3 μm, Thermo Scientific, Bremen, Germany) at 300 $mL.min^{-1}$. Separation was generated by mixing A: 0.1% FA and B: 80% ACN, with the following gradient: 5 min (2.5% B to 10% B), 60 min (10% B to 35% B), 5 min (35% B to 99% B) and 5 min (hold 99% B). Subsequently, the column was equilibrated with 2.5% B for 12 min. Data acquisition was controlled by Xcalibur 4.0 and Tune 2.8 software (Thermo Scientific, Bremen, Germany). The mass spectrometer was operated in data-dependent (dd) positive acquisition mode alternating between a full scan (m/z 380-1580) and subsequent HCD MS/MS of the 10 most intense peaks from full scan (normalized collision energy of 27%). ESI spray voltage was 1.9 kV and capillary temperature was 275 °C. Global settings: use lock masses best (m/z 445.12003), lock mass injection Full MS, chrom. peak width (FWHM) 15 s. Full scan settings: 70k resolution (m/z 200), AGC target 3e6, maximum injection time 50 ms. dd settings: minimum AGC target 8e3, intensity threshold 7.3e4, charge exclusion: unassigned, 1, 8, >8, peptide match preferred, exclude isotopes on, dynamic exclusion 20 s. MS2 settings: microscans 1, resolution 35k (m/z 200), AGC target 2e5, maximum injection time 110 ms, isolation window 2.0 m/z, isolation offset 0.0 m/z, spectrum data type profile.

4.2.4.3 Protein identification

The raw data was analysed and processed using the Proteome Discoverer 2.2.0.388 software (Thermo Scientific) and searched against the UniProt database for Bacteria taxonomic selection (2018_07 release). The Sequest HT search engine was used for protein identification. The ion mass tolerance was 10 ppm for precursor ions and 0.02 Da for-fragment ions. The maximum allowed missing cleavage sites was set to 2. Cysteine carbamidomethylation was defined as a constant modification. Methionine oxidation and

protein N-terminus acetylation were defined as variable modifications. Peptide confidence was set to high. The processing node Percolator was enabled with the following settings: maximum delta Cn 0.05; decoy database search target FDR 1%, validation was based on q-value.

4.2.4.4 Protein distribution among different conditions of biofilm development

The distribution of protein identified among replicates and among the different conditions was analyzed by Venn diagram using an online free tool, available at the webserver of the Bioinformatics and Evolutionary Genomics Center (BEG/Van de Peer Lab site), Ghent University, Belgium, http://bioinformatics.psb.ugent.be/webtools/Venn/. For comparison purposes, the identified proteins from all replicates of each treatment were merged into a single file and duplicates removed. Finally, the corresponding distribution of unique and shared proteins among different conditions were reported.

4.2.5 Statistical analysis

All experiments were performed in triplicate. Data analysis was performed using the statistical program GraphPad Prism® for Windows, version 6.01 (GraphPad Software, Inc., San Diego, CA, USA) and results were compared using unpaired *t*-tests with a confidence level of 95% (**; $p < 0.05$) and 90% (*; $p < 0.1$).

4.3 Results and Discussion

4.3.1 Biofilm development analysis

Monitoring of cyanobacterial biofilm development was done for 49 days (progress of wet weight, chlorophyll *a* and biofilm thickness), as shown in Figures 4.1 and 4.2. For both cyanobacterial strains and both surfaces, biofilm development was higher at the lowest shear rate. Compared to the values obtained at higher shear rate (40 s^{-1}), the biofilm

mass obtained on glass surface under lower shear conditions (4 s^{-1}) was on average 63.9% and 48% higher for *Nodosilinea* sp. LEGE 06145 (Figure 4.1A) and *Nodosilinea* sp. LEGE 06119 (Figure 4.2A), respectively. Likewise, on perspex, biofilm wet weight was on average 40.6% higher for *Nodosilinea* sp. LEGE 06145 (Figure 4.1B) and 29.6% for *Nodosilinea* sp. LEGE 06119 (Figure 4.2B). the chlorophyll *a* content at 4 s^{-1} and on glass was, on average 64.6% and 98.8% higher for *Nodosilinea* sp. LEGE 06145 (Figure 4.1C) and *Nodosilinea* sp. LEGE 06119 (Figure 4.2C), respectively, whereas on perspex it was, on average, 35.7% higher for *Nodosilinea* sp. LEGE 06145 (Figure 4.1D) and 97.4% for *Nodosilinea* sp. LEGE 06119 (Figure 4.2D) compared with higher shear conditions. Since a correlation between chlorophyll *a* production and biofilm wet weight was observed (Supplementary Material, Figure S 4.1, 4.2), chlorophyll *a* content monitorization demonstrated to be a useful tool to follow cyanobacterial biofilm growth, as previously reported (Romeu *et al.*, 2019).

Although some differences in biofilm development at different shear conditions were noticed in the early stages, major differences were found in the maturation phase of biofilm development (on general from day 28 and mainly in wet weight quantification), which corroborates previous results obtained with different cyanobacterial strains (Romeu *et al.*, 2019). The increased shear rate during biofilm development may promote sloughing events and erosion, affecting the biofilm cohesion. Moreover, this difference in biofilm development between the two hydrodynamic conditions was more noticeable for *Nodosilinea* sp. LEGE 06119 (Figure 4.2 A-D).

The biofilm thickness obtained on the glass surface under lower shear conditions was on average 54.5% and 64.2% higher for *Nodosilinea* sp. LEGE 06145 (Figure 4.1E) and *Nodosilinea* sp. LEGE 06119 (Figure 4.2E), respectively, when compared to those obtained at 40 s^{-1}. On perspex, the biofilm thickness was, on average 42.9% higher for *Nodosilinea* sp. LEGE 06145 (Figure 4.1F) and 54.3% for *Nodosilinea* sp. LEGE 06119 (Figure 4.2F). The highest value of biofilm thickness was observed at 4 s^{-1} on glass for *Nodosilinea* sp. LEGE 06145 (~ 800 μm; Figure 4.1E, 49 days). Values of biofilm thickness obtained for *Nodosilinea* sp. LEGE 06119 were significantly lower, achieving a maximum of 120 μm at 4 s^{-1} on glass (Figure 4.2E). Indeed, all parameters analysed showed that biofilm development by

Nodosilinea sp. LEGE 06145 was substantially higher than by *Nodosilinea* sp. LEGE 06119 (Supplementary Material, Figure S 4.3, 4.4).

Despite the different properties of glass and perspex, the latter of which is the most hydrophobic surface (Romeu *et al.*, 2019), similar values of wet weight, chlorophyll *a* content and biofilm thickness were obtained for biofilms developed on different surfaces at the same hydrodynamic conditions (Supplementary Material, Figure S 4.5, 4.6). These findings, which show that the effect of surface hydrophobicity was less important than the hydrodynamic effect on cyanobacterial biofilm development, had already been shown for other cyanobacterial strains (Romeu *et al.*, 2019; Faria, Teixeira-Santos, Romeu, *et al.*, 2020).

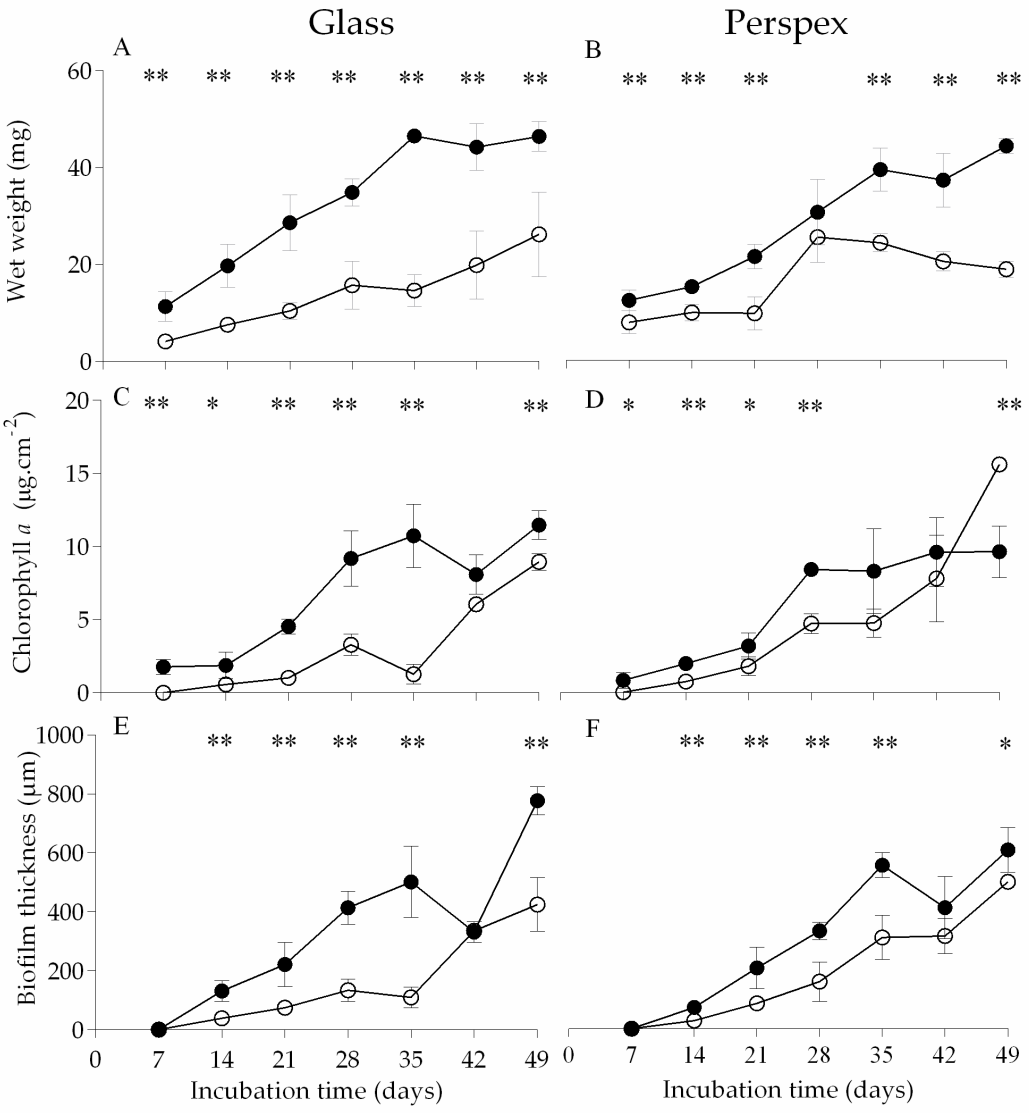

Figure 4.1. Evaluation of *Nodosilinea* sp. LEGE 06145 biofilm development. The parameters analyzed refer to wet weight (A, B), chlorophyll *a* (C, D) and biofilm thickness (E, F). Biofilms were formed in glass (A, C, E) or perspex (B, D, F), at two average shear rates, 4 s^{-1} (closed circles) and 40 s^{-1} (open circles) for 49 days. SDs from two biological assays with three replicates each are represented. Symbols * and ** indicate statistically different values for $p < 0.1$ and $p < 0.05$ (respectively) at each incubation time.

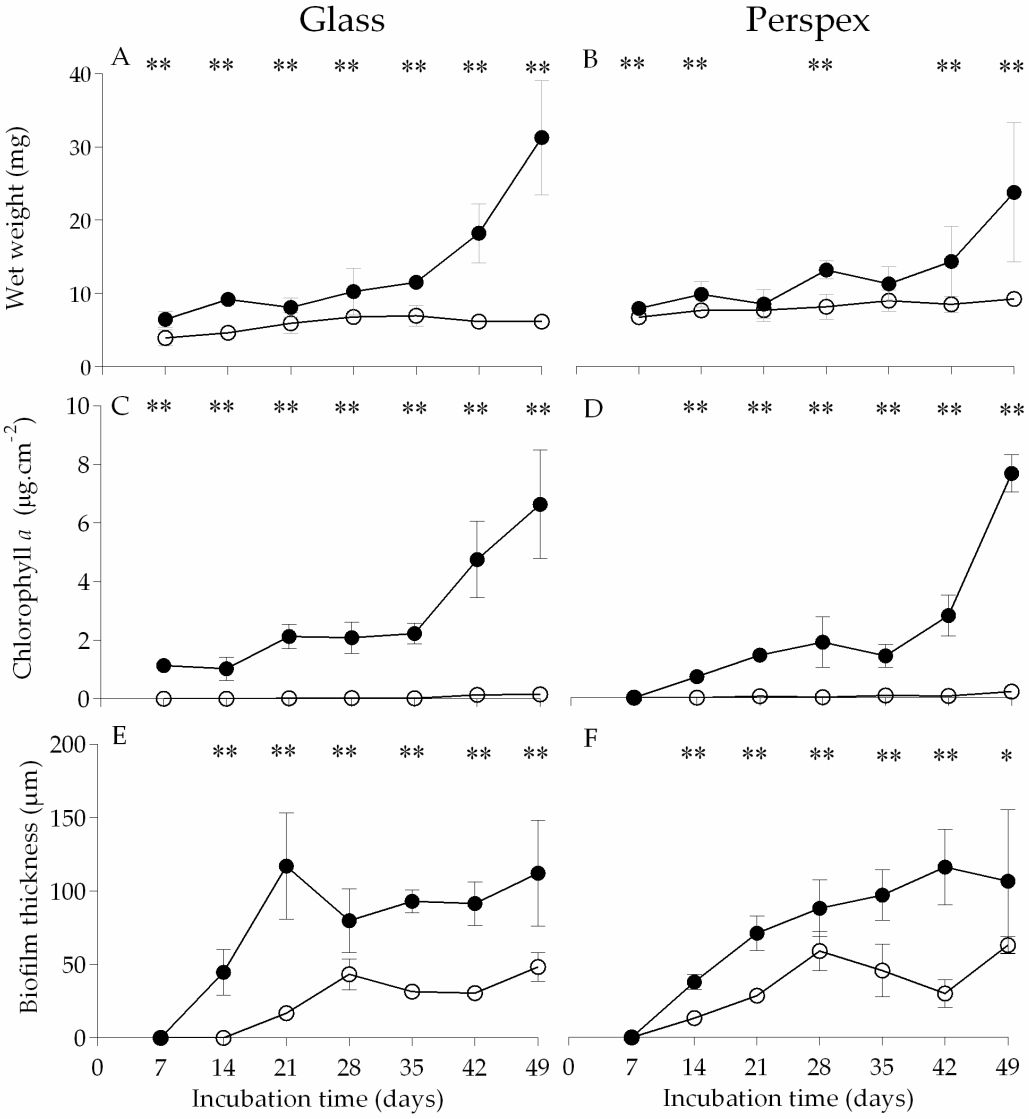

Figure 4.2. Evaluation of *Nodosilinea* sp. LEGE 06119 biofilm development. The parameters analysed refer to wet weight (A, B), chlorophyll a (C, D) and biofilm thickness (E,F). Biofilms were formed in glass (A, C, E) or perspex (B, D, F), at two average shear rates, 4 s^{-1} (closed circles) and 40 s^{-1} (open circles) for 49 days. SDs from two biological assays with three replicates each are represented. Symbols * and ** indicate statistically different values for $p < 0.1$ and $p < 0.05$ (respectively) at each incubation time.

Figures 4.3 and 4.4 show representative 2D cross-sectional images of *Nodosilinea* sp. LEGE 06145 and *Nodosilinea* sp. LEGE 06119, respectively, obtained from OCT at the end of the experiment (49 days). From these OCT images, the difference in biofilm development between the cyanobacterial strains is clear. Again, the differences in biofilm structure between hydrodynamic conditions were also more noticeable than between the

two surfaces. Despite the lower biofilm biomass obtained at a higher shear rate (40 s^{-1}) for *Nodosilinea* sp. LEGE 06119 (Figure 4.4 B, D), it is possible to observe that cyanobacterial biofilms obtained at 4 s^{-1} were less homogeneous in their structure, presenting three-dimensional streamers on the biofilm surface. The appearance of these structures was previously reported for other cyanobacterial biofilm formed under different hydrodynamic conditions (Romeu *et al.*, 2019). Instead, biofilms formed under the higher shear rate presented a more compact structure. While a compacted structure may be relevant in biofilms formed under higher shear conditions to increase the biofilm cohesion and avoid biofilm sloughing and erosion, a lower degree of compaction in biofilms formed under lower shear rates is an appropriate adaptation to improve the mass transfer to the inner layers of the biofilm (Teodósio *et al.*, 2011).

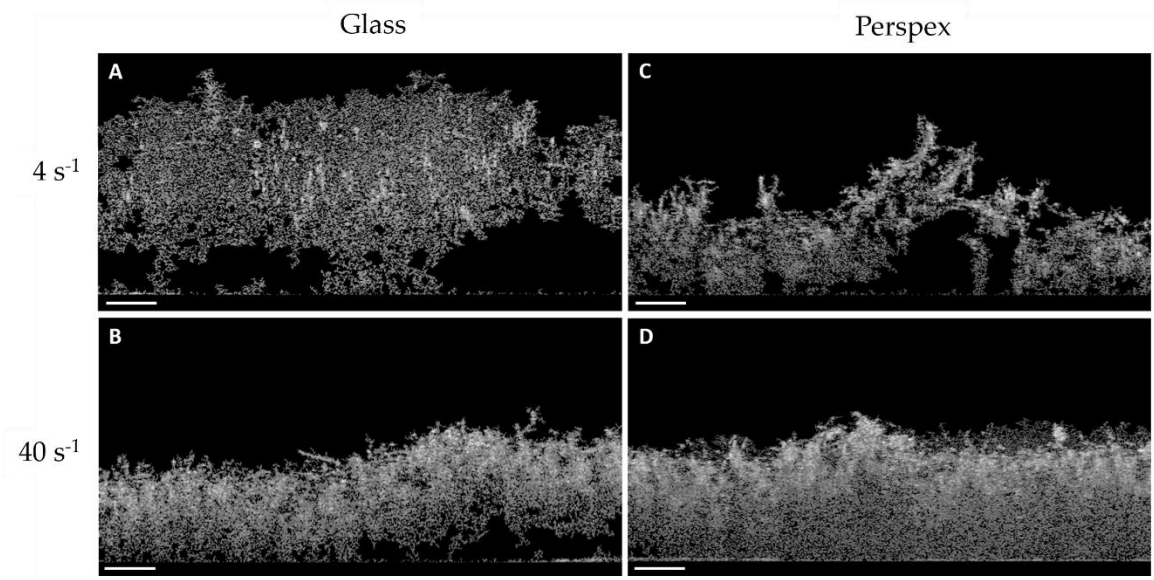

Figure 4.3. 2D cross-sectional OCT images of *Nodosilinea* sp. LEGE 06145 biofilms formed after 49 days on glass and perspex at two different shear rates, 4 s^{-1} (A, C) and 40 s^{-1} (B, D). Scale bar = 200 μm.

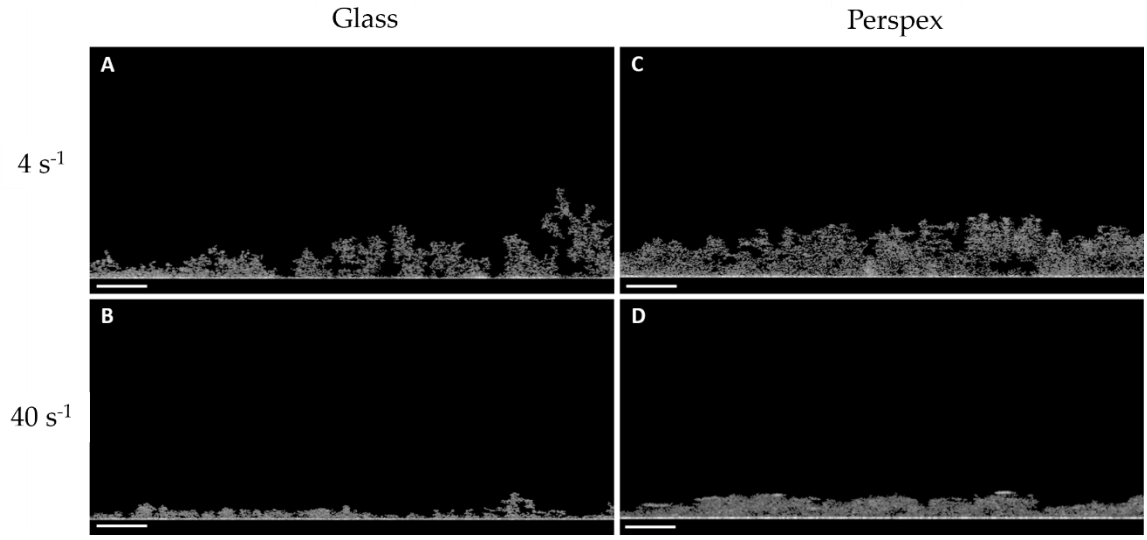

Figure 4.4. 2D cross-sectional OCT images of *Nodosilinea* sp. LEGE 06119 biofilms formed after 49 days on glass and perspex at two different shear rates, 4 s^{-1} (A, C) and 40 s^{-1} (B, D). Scale bar = 200 μm.

4.3.2 Proteomic analysis

A qualitative proteomic analysis by LC-MS/MS was performed, and the number and the distribution of proteins found for both cyanobacterial strains in different conditions is shown in Figure 4.5. The number of cyanobacterial proteins identified from all planktonic and biofilm samples is available in Supplementary Material, Table S 4.1. A total of 377 and 301 different proteins were identified for *Nodosilinea* sp. LEGE 06145 and *Nodosilinea* sp. LEGE 06119, respectively, of which 108 were found on both cyanobacterial strains (Figure 4.5A). Among the 16 common proteins identified on cyanobacterial planktonic samples (Figure 4.5B), none of them is exclusive of planktonic form because they were identified in an additional biofilm condition. A previous quantitative proteomic study performed in the marine bacterium *Pseudoalteromonas lipolytica* TC8 also aimed at highlighting specific metabolic shifts between planktonic and biofilm cultures. This study showed that 90% of proteins were present in the proteomes of both planktonic and biofilm samples (Favre *et al.*, 2018). Moreover, the percentage of proteins found in the four different biofilm conditions and which were identified in both cyanobacterial strains was similar and below 22%. Amongst the four possibilities tested for biofilm development, biofilms that were formed on perspex and at 40 s^{-1} showed a higher

percentage of common proteins between the two cyanobacterial strains (21.1%, Figure 4.5F). Conversely, biofilms that were formed on perspex but at 4 s^{-1} showed a lower number of common proteins between the two cyanobacterial strains (7.8%, Figure 4.5D). A broad diversity in the protein expression profiles of each strain was observed. Similarly, substantial differences in protein expression among cyanobacterial strains at the same conditions were also observed in a study of *Microcystis aeruginosa* (Alexova *et al.*, 2011) and only 29 - 43% of the identified proteins were found to be expressed in all six strains analyzed in this study. Moreover, a study performed with the marine cyanobacterium *Prochlorococcus* spp. showed that the elemental composition of their proteomes was strongly influenced by their site of isolation and the nutritional availability at that site (Lv *et al.*, 2008). Since *Nodosilinea* sp. LEGE 06145 was isolated from a sample scraped from a wave-exposed rock in the tide puddle collected at Moledo beach and *Nodosilinea* sp. LEGE 06119 was isolated from a seawater sample collected in the surf zone collected at Burgau beach, the observed proteome diversity supports the view that strains should be considered as ecotypes adapted to survival in a particular environmental niche (Otsuka *et al.*, 2001). For the same cyanobacterial strain, a higher number of proteins was identified on glass rather than on perspex, and comparing the two hydrodynamic conditions, a higher number of proteins was obtained at 4 s^{-1} for both cyanobacteria (Figura 4.5C - F). This lower shear condition corresponds to the scenario in which a higher amount of biofilm formation was observed (Figures 4.1 - 4.4). For both cyanobacterial strains, differences between the number of proteins identified from biofilms formed under different hydrodynamic conditions were more noticeable than those obtained for different surfaces (77.8% and 48.5% higher at 4 s^{-1} than 40 s^{-1} for *Nodosilinea* sp. LEGE 06145 and *Nodosilinea* sp. LEGE 06119, 28.1% and 33.4% higher on glass than perspex, for *Nodosilinea* sp. LEGE 06145 and *Nodosilinea* sp. LEGE 06119, respectively (Supplementary Material, Table S 4.1). Except for the on biofilms at 40 s^{-1} in which the number of proteins found in *Nodosilinea* sp. LEGE 06119 was 41.2% higher compared with *Nodosilinea* sp. LEGE 06145, in all biofilm samples, a higher number of proteins were identified in *Nodosilinea* sp. LEGE 06145. The complete list of identified proteins and their frequencies in different biofilm conditions is available in Supplementary Material, Table S 4.2.

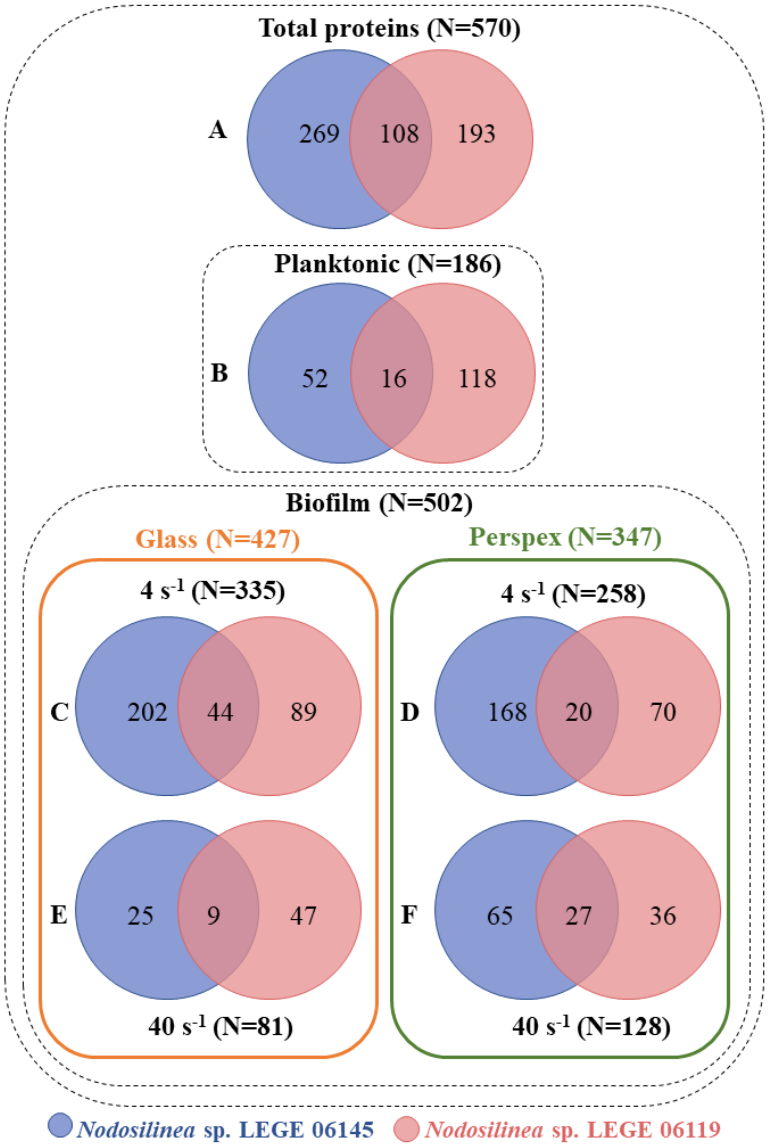

Figure 4.5. Venn diagrams obtained from the distribution of proteins identified among different conditions for the two cyanobacterial strains. The total of proteins for each condition is represented by (N=). The composite figure shows the unique and common proteins identified in both cyanobacterial strains of each condition represented from each Venn diagram: A – total proteins identified on *Nodosilinea* sp. LEGE 06145 cells *vs* proteins identified on *Nodosilinea* sp. LEGE 06119 cells; B – proteins identified on planktonic *Nodosilinea* sp. LEGE 06145 cells *vs* proteins identified on planktonic *Nodosilinea* sp. LEGE 06119 cells; C – proteins identified on *Nodosilinea* sp. LEGE 06145 cells *vs* proteins identified on *Nodosilinea* sp. LEGE 06119 cells derived from biofilms formed on glass at 4 s^{-1}; D – proteins identified on *Nodosilinea* sp. LEGE 06145 cells *vs* proteins identified on *Nodosilinea* sp. LEGE 06119 cells derived from biofilms formed on perspex at 4 s^{-1}; E – proteins identified on *Nodosilinea* sp. LEGE 06145 cells *vs* proteins identified on *Nodosilinea* sp. LEGE 06119 cells derived from biofilms formed on glass at 40 s^{-1}; F – proteins identified on *Nodosilinea* sp. LEGE 06145 cells *vs* proteins identified on *Nodosilinea* sp. LEGE 06119 cells derived from biofilms formed on perspex at 4 s^{-1}.

The identification and description of common proteins obtained from biofilm samples and for both cyanobacterial strains are represented in Table 4.1. While from biofilms formed on glass only one protein was identified on both cyanobacterial strains, 10 common proteins were identified from biofilms on the perspex surface. Additionally, 12 and 10 proteins for both cyanobacterial strains were identified in biofilm samples formed at 4 s^{-1} and 40 s^{-1}, respectively. It should be noted that despite biofilm development being substantially lower in *Nodosilinea* sp. LEGE 06119 than *Nodosilinea* sp. LEGE 06145 (Supplementary Material, Figure S 4.3, S 4.4), these proteins were also found in this strain. The 50S ribosomal protein L7/L12 was identified in all biofilm conditions of the two cyanobacterial strains. This protein forms part of the ribosomal stalk, which helps the ribosome interact with guanosine triphosphate (GTP)-bound translation factors and it is responsible for accurate translation (Diaconu *et al.*, 2005). This is an essential protein in the core metabolic functions and it was identified in all biofilm samples (Table 4.1 and Supplementary Material, Table S 4.2). This result demonstrates the relevance and validity of the proteomic analysis performed in the present work. Additional cyanobacterial proteomic studies have revealed that 50% of proteins found could be assigned to core metabolic and transport functions (Anderson *et al.*, 2006). However, a proteomic study performed with *Halorubrum lacusprofundi,* an extreme halophile archaeon, showed a decrease in the proteins involved in protein synthesis and folding in biofilms when comparing with planktonic cells, including a large number of ribosomal proteins (Liao *et al.*, 2016).

Proteins related to photosystems I and II and with allophycocyanin were found in three of the four biofilm conditions groups (Table 4.1 in dark grey shading). The specific conditions in which these proteins were identified can be found in the Supplementary Material, Table S 4.2. Photosystem I (PS I, plastocyaninferredoxin oxidoreductase) and photosystem II (PS II, waterplastoquinone oxidoreductase) are multisubunit protein complexes located in the thylakoid membranes of cyanobacteria, algae and higher plants (Nelson and Yocum, 2006). Although in the present study the PsaF protein was only identified in biofilms of both the cyanobacterial strains formed at 40 s^{-1} (Table 4.1), this protein is also related to photosystems (Photosystem I subunit III). A study performed by Huang *et al.*, (2002) also identified proteins related to photosystems in the plasma

membrane of *Synechocystis* PCC 6803. A proteomic study with different strains of *M. aeruginosa*, showed that the majority of proteins shared among all strains were involved in photosynthesis and respiration (Alexova *et al.*, 2011). Thus, the distribution of protein identification obtained in the present study is typical for cyanobacteria.

Table 4.1. Enumeration of proteins obtained from different biofilm samples in both cyanobacterial strains. For each protein, the frequency of appearance among the four biofilms conditions (glass, perspex, 4 s^{-1} and 40 s^{-1}) is indicated by different shaded colors (black – appearance in all four conditions; dark grey - appearance in three of four conditions; light grey - appearance in two of four conditions; without shading – appearance in only one of the four conditions).

Biofilm development condition	Number of proteins found on both cyanobacterial strains	Accession number	Description
Glass	1	A0A1Z3HSI0	50S ribosomal protein L7/L12
Perspex	10	A0A077JIC2	Elongation factor Tu
		A0A0N7LBT2	Alkyl hydroperoxide reductase/ Thiol specific ant ioxidant/ Mal allergen
		A0A1U7J348	Photosystem II CP43 reaction center protein
		A0A1U7J7J4	Allophycocyanin subunit beta
		A0A1U7JAP1	Allophycocyanin subunit beta
		A0A1U7JAR5	Photosystem I reaction center subunit X
		A0A1U7JAT3	Allophycocyanin
		A0A1Z3HSI0	50S ribosomal protein L7/L12
		A0A2P8ZU54	Photosystem I P700 chlorophyll a apoprotein A2
		I4HUB3	Carbon dioxide-concentrating mechanism protein CcmK
4 s^{-1}	12	A0A073CH81	Photosystem I reaction center subunit XI
		A0A0N7LBT2	Alkyl hydroperoxide reductase/ Thiol specific ant ioxidant/ Mal allergen
		A0A120MWU4	Transketolase
		A0A1U7J348	Photosystem II CP43 reaction center protein
		A0A1U7J7J4	Allophycocyanin subunit beta
		A0A1U7J8S7	Photosystem I reaction center subunit II
		A0A1Z3HSI0	50S ribosomal protein L7/L12
		A0A2P8VVE3	Allophycocyanin subunit beta
		A0A2P8W6V3	Amino acid ABC transporter substrate-binding protein
		A0A2P8ZWG1	HU family DNA-binding protein

Biofilm development condition	Number of proteins found on both cyanobacterial strains	Accession number	Description
		A0A2P8ZXU5	Phycobilisome rod-core linker polypeptide CpcG
		I4HUB3	Carbon dioxide-concentrating mechanism protein CcmK
40 s^{-1}	7	A0A073CM30	PsaF
		A0A0U1Z975	Phycocyanin beta chain (Fragment)
		A0A1U7JAP1	Allophycocyanin subunit beta
		A0A1U7JAT3	Allophycocyanin
		A0A1Z3HSI0	50S ribosomal protein L7/L12
		A0A2P8ZU54	Photosystem I P700 chlorophyll a apoprotein A2
		K9F192	Phycobilisome protein

Allophycocyanin is a protein from the light-harvesting phycobiliprotein family, along with phycocyanin, phycoerythrin and phycoerythrocyanin, which may be found in the phycobilisome core complex (Sonani *et al.*, 2015). Although proteins related to allophycocyanin were found in three of the four biofilm conditions, a protein fragment of phycocyanin beta chain and an additional non-specific phycobilisome protein were identified on both cyanobacterial strains for biofilms formed at 40 s^{-1}. Phycobilisomes are present in cyanobacteria and red algae and are formed by phycobiliproteins and also linker proteins (MacColl, 1998). Allophycocyanin is considered an accessory pigment to chlorophyll and exhibits unique absorbance and fluorescence characteristics due to a lack of susceptibility to internal and external fluorescence quenching. Due to these features, allophycocyanin is ideal for highly sensitive studies as flow cytometry and immunoassays (Manirafasha *et al.*, 2016). Indeed, phycobiliproteins are regularly found in high abundance and they may constitute up to 50% of the total cellular protein of a cyanobacterium (Anderson *et al.*, 2006). Previous proteomics studies with other cyanobacterial strains (*Synechocystis* PCC 6803) also identified proteins related to this phycobiliprotein family in their plasma membrane (Huang *et al.*, 2002; Pisareva *et al.*, 2007). In another study, which aimed to evaluate proteomic changes after heat shock in *Synechocystis* PCC 6803, a decreased expression level for phycobilisome was observed (Slabas *et al.*, 2006).

For both cyanobacterial strains, in biofilms formed on perspex and also at 4 s^{-1} a protein from the peroxiredoxin superfamily was identified (alkyl hydroperoxide

reductase/thiol specific antioxidant/Mal allergen). This protein protects cells against membrane oxidation through glutathione (GSH)-dependent reduction of phospholipid hydroperoxides to corresponding alcohols (Wood *et al.*, 2003). A study performed with *Spirulina platensis*, which focused on comparative proteome analyses at low- and high-temperature stresses, indicated that low-temperature stress is tightly linked to oxidative stress as well as photosynthesis (Kurdrid *et al.*, 2011). A quantitative proteomic study to define pathways and cellular processes involved in forming biofilms of *H. lacusprofundi* showed that these proteins associated with responses to oxidative stress are also related to biofilm forming ability (Liao *et al.*, 2016). Although in the present study this protein was only found on perspex and also at 4 s^{-1}, this hydrodynamic condition resulted in greater biofilm development, which may have facilitated its detection.

Moreover, for both cyanobacterial strains, in biofilms formed on perspex and at 4 s^{-1} a protein involved in the formation of the carboxysome (carbon dioxide-concentrating mechanism protein CcmK) was also found. Carboxysomes are polyhedral inclusion where the ribulose-1,5-bisphosphate carboxylase/oxygenase (Rubisco; the central enzyme in photosynthetic carbon assimilation) is sequestered. The CO_2 concentrating mechanism (CCM) is an adaptive and effective strategy evolved in cyanobacteria and also in eukaryotic microalgae for carbon acquisition, and it enables these organisms to survive when the CO_2 concentration limits the photosynthesis (Wang *et al.*, 2015). Baba et al., (2011) also studied this mechanism in the unicellular green alga *Chlamydomonas reinhardtii*. When the CO_2 concentration was elevated from the ambient air level to 3%, the algal growth rate increased 1.5-fold, and the amount and composition of extracellular proteins clearly changed. However, significant changes were not found in intracellular proteins (Baba *et al.*, 2011). In a study performed by Slabas *et al.* (2006) a decrease in Rubisco proteins was observed after heat shock in *Synechocystis* PCC 6803. Moreover, the CCM is a fundamental aspect of photosynthesis, metabolism, growth and biomass production in photosynthetic organisms and understanding this process provides guidance for potential molecular manipulation to improve biomass yield for commercial applications (Badger and Price, 2003).

Despite the fact that in the present study, the elongation factor Tu and the amino acid ABC transporter substrate-binding protein were only identified for both

cyanobacterial strains on biofilms formed on perspex and at 4 s^{-1}, respectively (Table 4.1), these proteins were found in other cyanobacteria studies, such as in the plasma membrane of *Synechocystis* PCC 6803 (Huang *et al.*, 2002). Moreover, a higher abundance of elongation factors and ABC transporters in *Enterococcus faecalis* (Qayyum *et al.*, 2016) and *H. lacusprofundi* (Liao *et al.*, 2016) biofilms, respectively, was observed when compared with those obtained in planktonic cells.

4.4 Conclusions

In this study, standard methodologies for following cyanobacterial biofilm development were complemented with a qualitative proteomics approach. The results showed greater biofilm development at a lower shear rate (4 s^{-1}) and it was also shown that hydrodynamic effects may be more important than surface properties in the formation of cyanobacterial biofilms. Moreover, the analysis of cyanobacterial biofilms by OCT is a useful methodology for understanding biofilm structure and dynamics under different conditions.

Cyanobacterial proteome analysis revealed that the strains under study had highly variable protein expression profiles, which may be a result of the adaptation of these organisms to the specific environmental niche that they occupy. Although this proteomic analysis was performed using a widely employed methodology and the proteome reported was biased on proteins expressed at higher levels, it is well known that there are limitations in the present technology for resolution and identification of proteins. Since none of the proteins identified on planktonic samples were exclusive to this form, that is, they were identified in an additional biofilm condition, the majority of the proteins were detected in both physiological states. The qualitative proteomic analysis investigated in this work was extremely relevant, given the few studies performed in this research field on filamentous cyanobacteria. Analyses of protein expression could provide an essential understanding of how cyanobacteria adapt to different environmental settings. However, in addition to studying which proteins were synthesized in the different conditions, it would be crucial to study the expression level of these proteins, since biofilm development in these different conditions may be associated with quantitative differences

in their proteome. Therefore, future work should focus on quantitative proteomic studies in order to allow the establishment of a relationship between the relative expression level of the identified proteins under different conditions. Moreover, due to their particular characteristics, cyanobacteria are promising organisms to be used in biotechnological processes. Vitamins, amino acids, fatty acids, lipopeptides and pigments belong to a broad spectrum of secondary metabolites and added-value compounds produced by cyanobacterial strains (Lau *et al.*, 2015). For example, the allophycocyanin identified in two biofilm conditions of the present work is a valuable molecule to be applied in several biotechnological applications as fluorescent probes in flow cytometry and microarray assays, but also in cosmetic, feed and food industries (Manirafasha *et al.*, 2016). Moreover, as phycobiliproteins have been associated with antioxidant, anticancer and anti-inflammatory capacities, these compounds can also be used for medical purposes (Pagels *et al.*, 2019). Improvements in cyanobacterial molecular biology are urgently required, since the omics tools available for these organisms are limited compared with heterotrophic model organisms (Sun *et al.*, 2018).

4.5 **Supplementary Material**

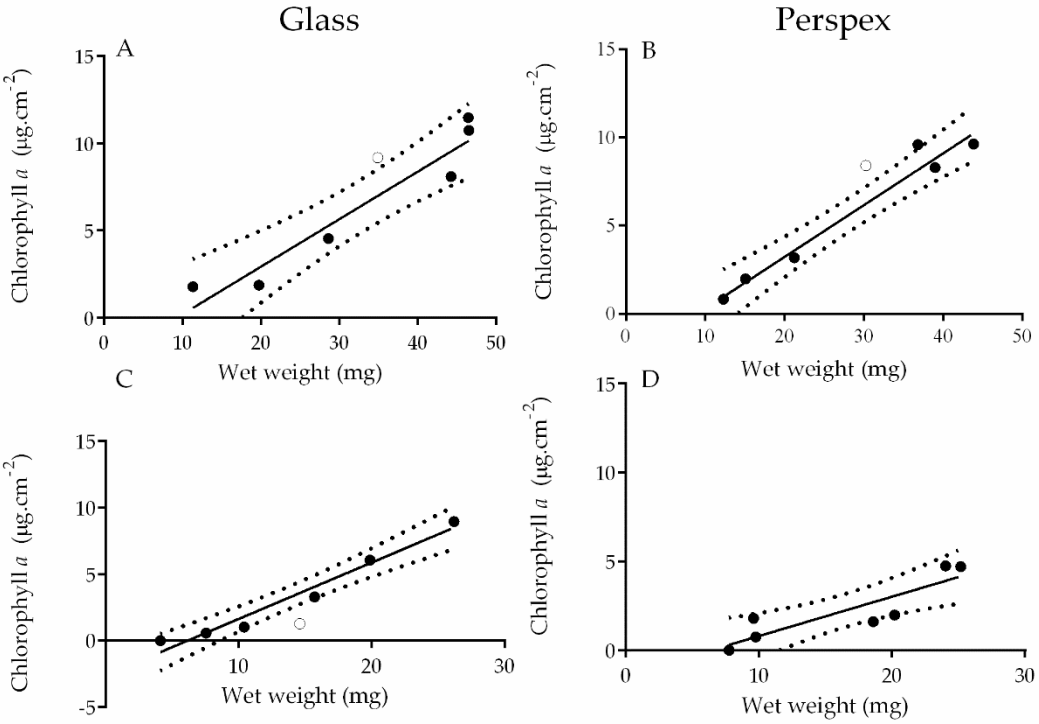

Figure S 4.1. Correlation between wet weight and chlorophyll *a* on *Nodosilinea* sp. LEGE 06145. Biofilm development in glass (A, C) and perspex (B, D) at two different shear rates, 4 s^{-1} (A, B) and 40 s^{-1} (C, D). Full line represents the linear regression, and the dashed line represents the confidence limits (95%). Closed symbols refer to data points that were considered for the regression (all except three) and the single open symbol refers to a data point that was excluded from the regression.

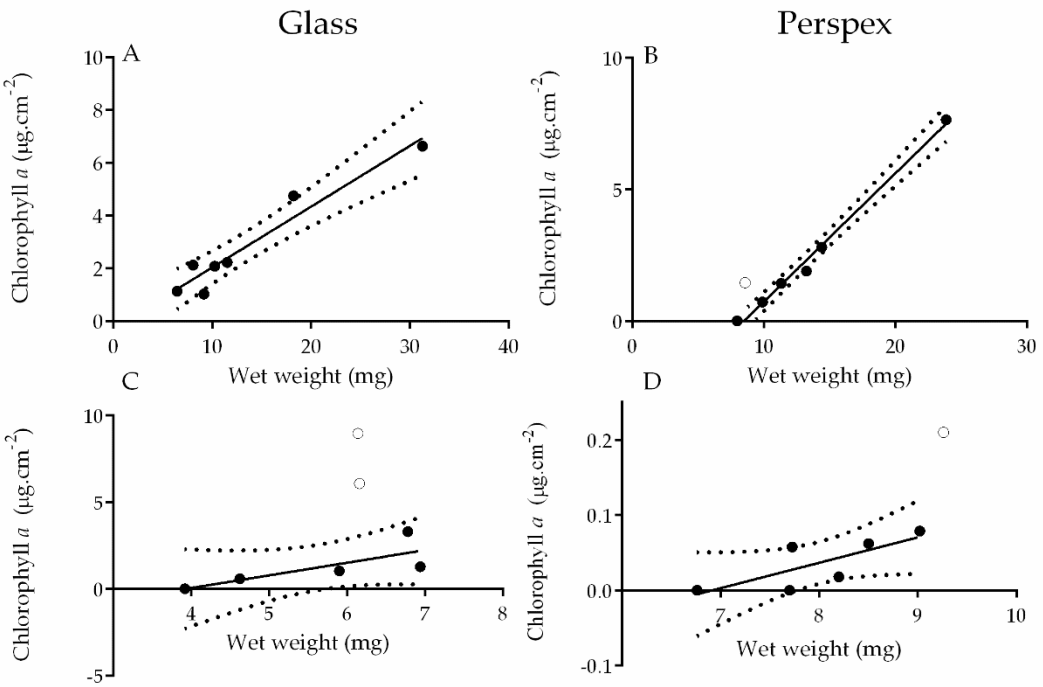

Figure S 4.2. Correlation between wet weight and chlorophyll *a* on *Nodosilinea* sp. LEGE 06119. Biofilm development in glass (A, C) and perspex (B, D) at two different shear rates, 4 s^{-1} (A, B) and 40 s^{-1} (C, D). Full line represents the linear regression, and the dashed line represents the confidence limits (95%). Closed symbols refer to data points that were considered for the regression (all except four) and open symbols refer to a data points that were excluded from the regression.

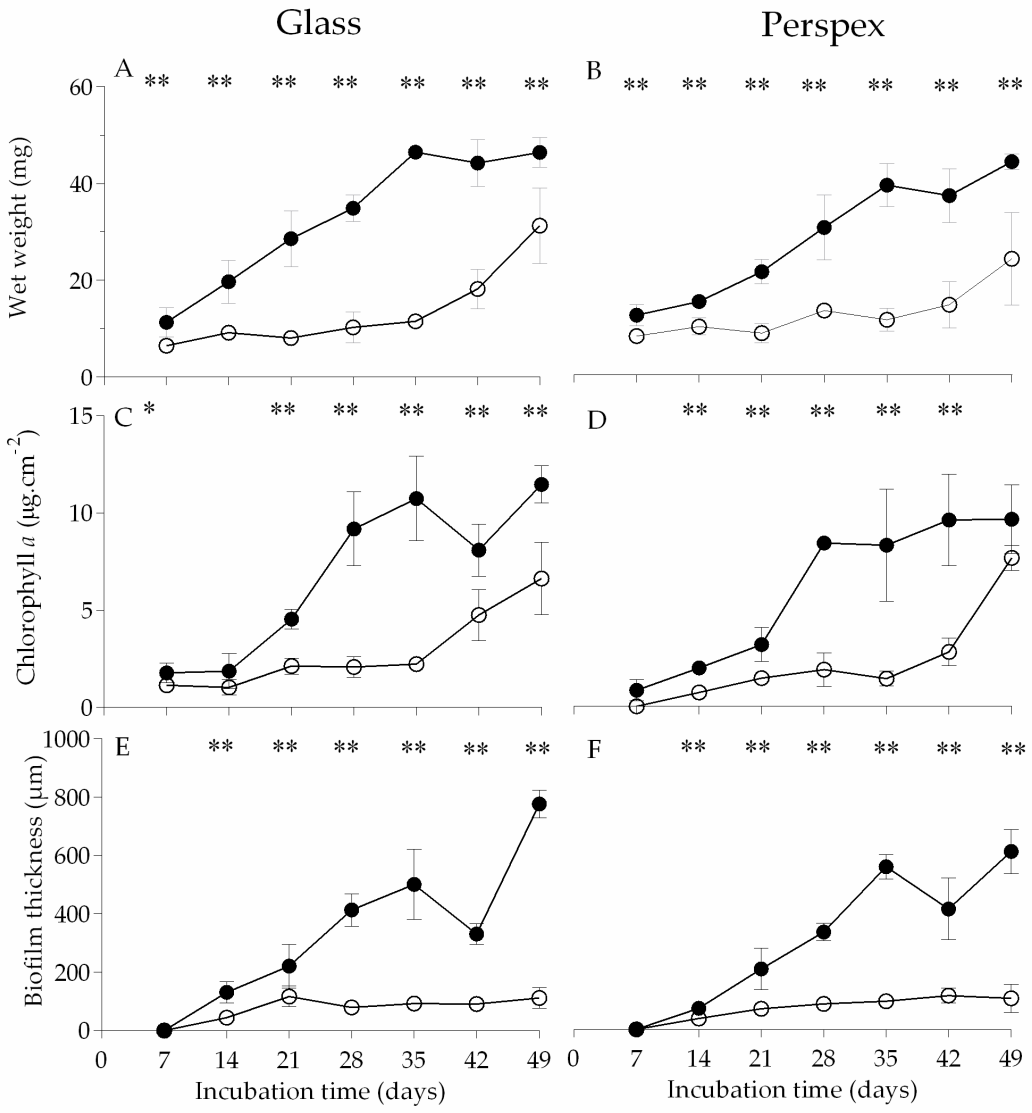

Figure S 4.3. Evaluation of biofilm development under 4 s^{-1}. The parameters analysed refer to wet weight (A, B), chlorophyll *a* (C, D) and biofilm thickness (E, F). Biofilms were formed on two different surfaces, glass (A, C, E) and perspex (B, D, F) for 49 days. Closed and open circles refer to *Nodosilinea* sp. LEGE 06145 and *Nodosilinea* sp. LEGE 06119 biofilm development, respectively. Standard deviations from two biological assays with three replicates each, are represented. Symbols *; ** indicate statistically different values for $P < 0.1$ and $P < 0.05$ (respectively) at each incubation time.

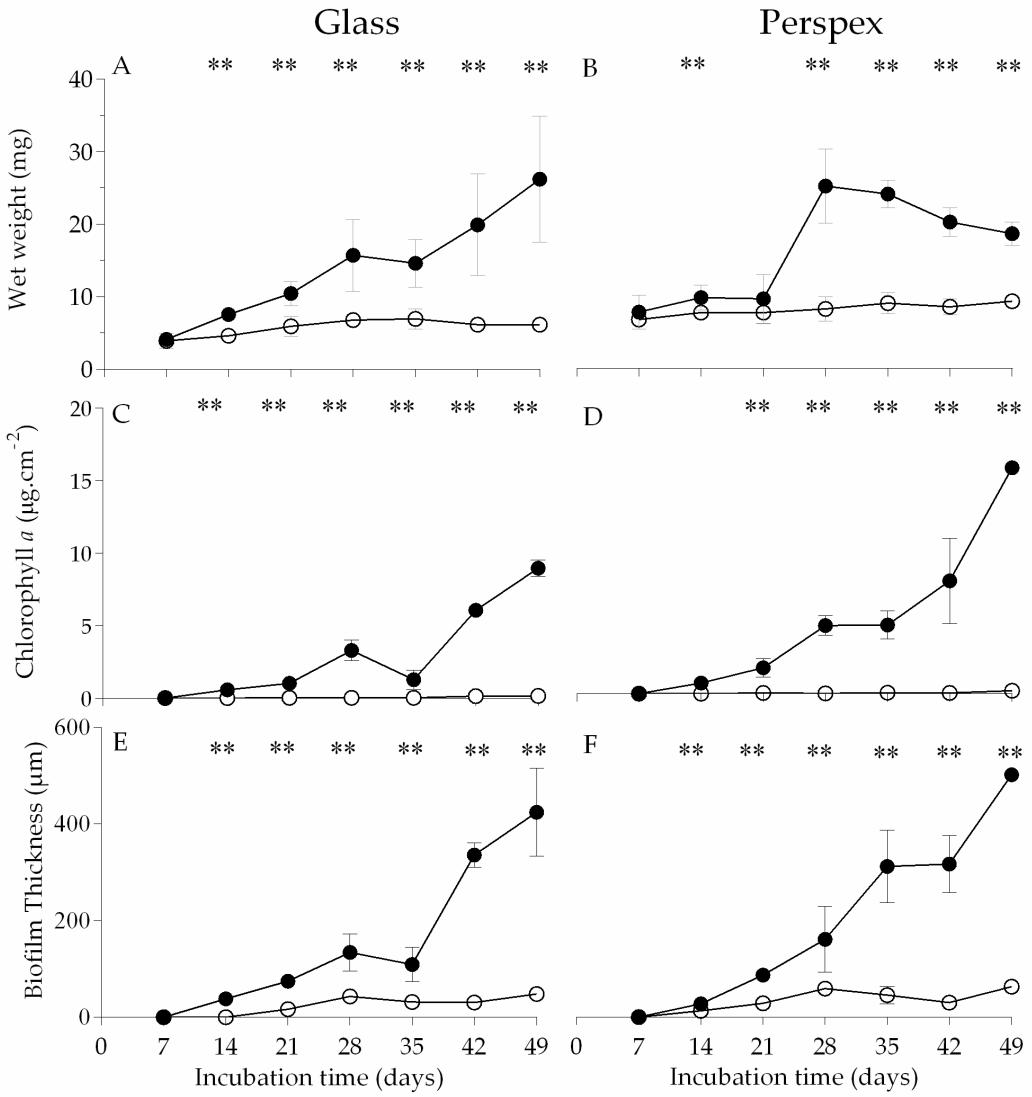

Figure S 4.4. Evaluation of biofilm development under 40 s^{-1}. The parameters analysed refer to wet weight (A, B), chlorophyll *a* (C, D) and biofilm thickness (E, F). Biofilms were formed on two different surfaces, glass (A, C, E) and perspex (B, D, F) for 49 days. Closed and open circles refer to *Nodosilinea* sp. LEGE 06145 and *Nodosilinea* sp. LEGE 06119 biofilm development, respectively. Standard deviations from two biological assays with three replicates each, are represented. Symbols *; ** indicate statistically different values for $P < 0.1$ and $P < 0.05$ (respectively) at each incubation time.

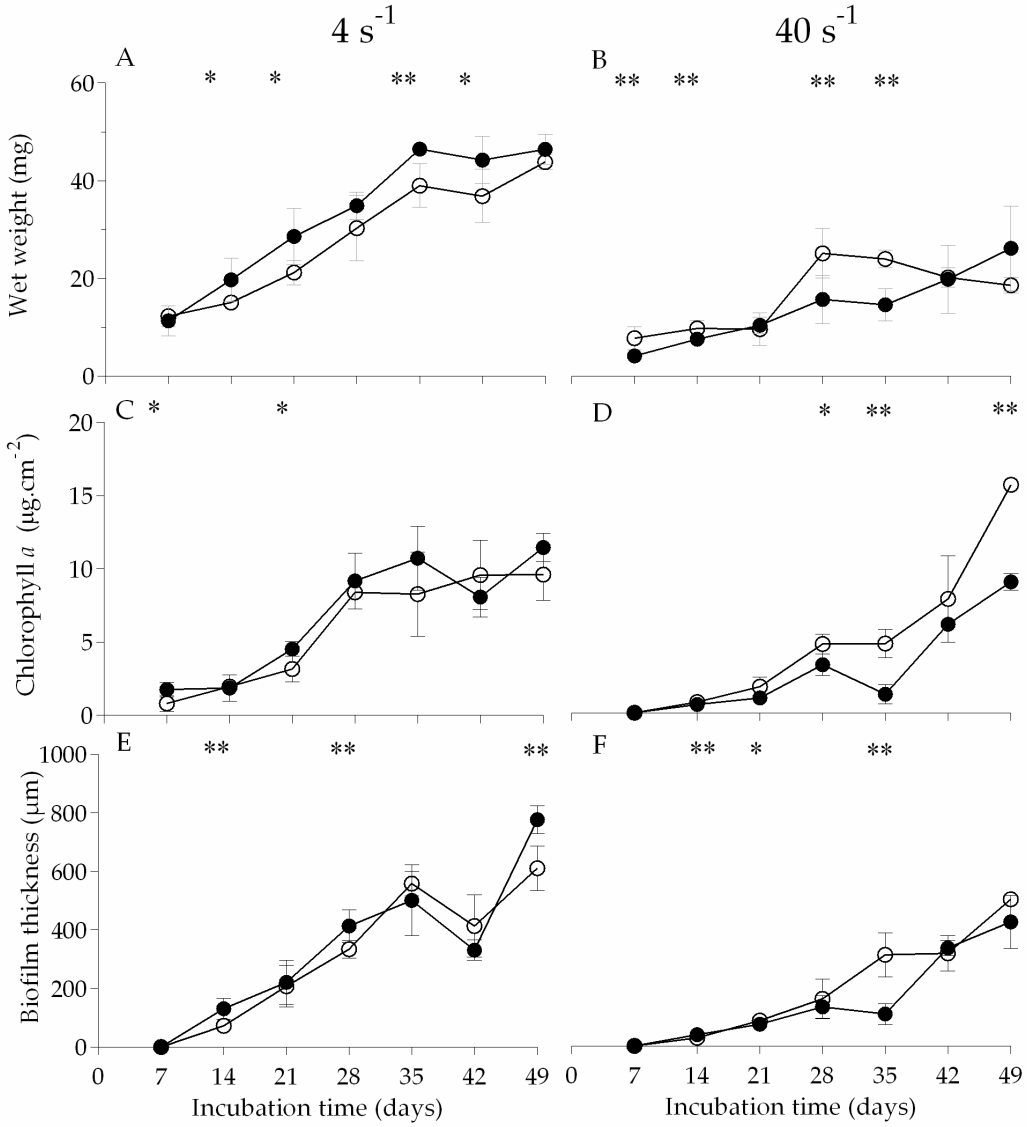

Figure S 4.5. Evaluation of N*odosilinea* sp. LEGE 06145 biofilm development under the same hydrodynamic on different surfaces. The parameters analysed refer to wet weight (A, B), chlorophyll a (C, D) and biofilm thickness (E, F). Biofilms were formed at 4 s^{-1} (A, C, E) or 40 s^{-1} (B, D, F), on two different surfaces, glass (closed circles) and perspex (open circles) for 49 days. Standard deviations from two biological assays with three replicates each, are represented. Symbols *; ** indicate statistically different values for $P < 0.1$ and $P < 0.05$ (respectively) at each incubation time.

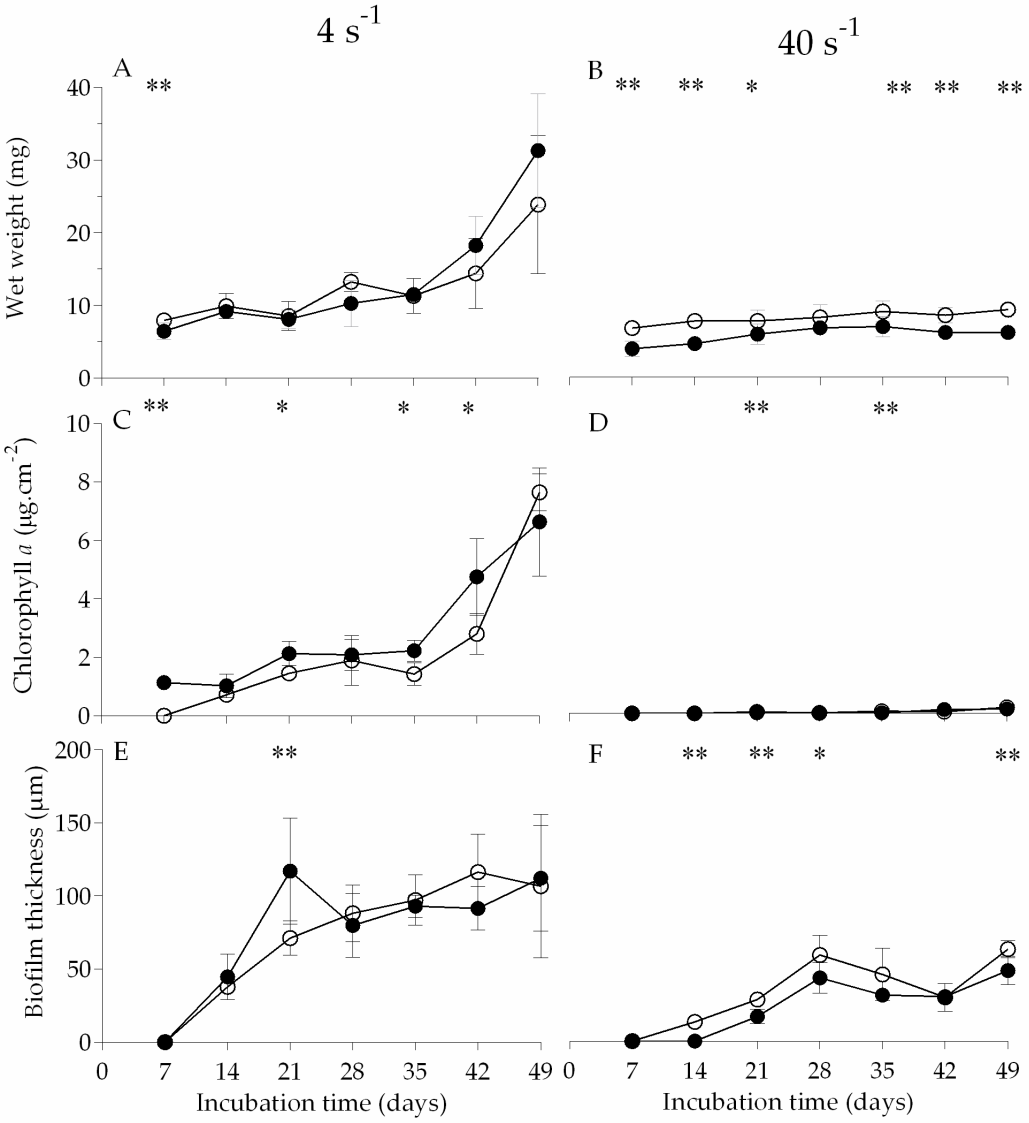

Figure S 4.6. Evaluation of *Nodosilinea* sp. LEGE 06119 biofilm development under the same hydrodynamic on different surfaces. The parameters analysed refer to wet weight (A, B), chlorophyll *a* (C, D) and biofilm thickness (E, F). Biofilms were formed at 4 s^{-1} (A, C, E) or 40 s^{-1} (B, D, F), on two different surfaces, glass (closed circles) and perspex (open circles) for 49 days. Standard deviations from two biological assays with three replicates each, are represented. Symbols *; ** indicate statistically different values for $P < 0.1$ and $P < 0.05$ (respectively) at each incubation time.

Table S 4.1. Number of proteins identified from planktonic and different biofilm samples.

		Cyanobacterial strains	
		***Nodosilinea* sp. LEGE 06145**	***Nodosilinea* sp. LEGE 06119**
Total protein identified		377	301
	Planktonic samples	68	134
	Biofilm samples	357	229
	Glass	261	167
	Perspex	232	125
	4 s^{-1}	311	192
	40 s^{-1}	100	99
	Glass 4 s^{-1}	246	133
	Perspex 4 s^{-1}	188	90
	Glass 40 s^{-1}	34	56
	Perspex 40 s^{-1}	92	63

Table S 4.2. Number and identification of common proteins found under the different biofilm conditions. This table lists the proteins that were detected in more than 1 of the 8 experimental conditions. The frequency of appearance (from 2 to 8) is indicated in bold on the left column. For each subgroup (proteins that appear in 7 of the 8 conditions and so forth) the condition with the highest frequency of appearance is shaded (only frequencies of appearance higher than 55% were shaded.

Number of common proteins under the different biofilm conditions / Protein identification		*Nodosilinea* sp. LEGE 06119				*Nodosilinea* sp. LEGE 06145			
		4 s $^{-1}$		40 s $^{-1}$		4 s $^{-1}$		40 s $^{-1}$	
		glass	perspex	glass	perspex	glass	perspex	glass	perspex
8	A0A1Z3HSI0	x	x	x	x	x	x	x	x
7	A0A1U7J348	x	x	x	x	x	x		x
	A0A1U7J7J4	x	x	x	x	x	x		x
	A0A1U7JAP1		x	x	x	x	x	x	x
	A0A1U7JAT3		x	x	x	x	x	x	x
	A0A2P8ZU54		x	x	x	x	x	x	x
	I4HUB3	x	x	x	x	x	x		x
6*	A0A0N7LBT2	**x**	x		x	x	x		x
	A0A0U1Z975			x	x	x	x	x	x
	A0A162C5Y8	**x**			x	x	x	x	x
	A0A1U7J8S7	**x**	x	x		x	x		x
	A0A261KIT4		x	x		x	x	x	x
	A0A2P9A1R4	**x**			x	x	x	x	x
	A0A2P9A1T2	x			x	x	x	x	x
	F5UHJ9	x	x		x	x		x	x
5	A0A073CH81	x	x		x	x	x		
	A0A073CM30		x	x	x			x	x
	A0A077JIC2		x	x	x		x		x
	A0A1U7J0Z8	x			x	x	x	x	
	A0A1U7J9U5	x			x	x	x		x
	A0A1U7JAR5		x		x	x	x		x
	A0A2P8VVE3	x	x			x	x		x
	A0A2P8W059	x			x	x	x		x
	A0A2P8W6V3	x	x		x	x	x		
	A0A2P8ZWG1	x	x			x	x		x
	A0A2P8ZXU5	x	x			x	x		x
	A0A2P9A6M6	x			x	x	x		x
4	A0A0M2PWT4	x			x	x	x		
	A0A120MWU4	x	x			x	x		
	A0A165B204					x	x	x	x
	A0A1D8TY51	x	x	x	x				
	A0A1E5QVW6	x				x	x		x
	A0A1L9QY46	x	x	x	x				
	A0A1U7HVH4		x	x				x	x
	A0A1U7J679					x	x	x	x
	A0A1U7JB89	x	x		x				x
	A0A1U7JBA1	x	x	x	x				
	A0A1U7JBE0	x	x	x	x				
	A0A1Z4PQ70	x	x	x	x				

	A0A251ZAG5		x	x		x				x
	A0A2L2NU31					x		x	x	x
	A0A2P8W0E5					x	x	x		x
	A0A2P8W8A0		x				x	x		x
	A0A2P8ZU31						x	x	x	x
	A0A2P9A1V4						x	x	x	x
	A0A2P9A6M4		x			x	x	x		
	B0B2A7						x	x	x	x
	B4WMS8		x	x		x	x			
	B4WS90						x	x	x	x
	K9F192				x	x			x	x
	K9X5E3		x	x		x		x		
		A0A073CCC2					x	x		x
		A0A0C1UTD1	x				x	x		
		A0A0C1V458			x			x		x
		A0A0C1WHE0	x				x	x		
		A0A0P8C657					x	x		x
		A0A0P8CDR3					x	x		x
		A0A0T7BR98		x					x	x
		A0A1J0ABC8	x				x	x		
		A0A1J0PBA6		x	x	x				
		A0A1Q1EWS3	x	x	x					
		A0A1U7J0C2	x				x	x		
		A0A1U7J0I0					x	x		x
		A0A1U7J341	x					x		x
		A0A1U7J6Z9					x	x		x
		A0A1U7JBJ8	x		x	x				
	3	A0A1U7JBL0					x	x		x
		A0A1V8NDW1	x	x				x		
		A0A1Z3HRF8	x				x	x		
		A0A254VXE7					x		x	x
		A0A2E2G8H3				x	x	x		
		A0A2G4EW90					x	x		x
		A0A2P8VV58	x	x			x			
		A0A2P8VWZ0	x				x	x		
		A0A2P8W0U6	x		x	x				
		A0A2P8W6L9	x				x	x		
		A0A2P8W9Q5	x				x	x		
		A0A2P8WAN6					x	x		x
		A0A2P8WJE4	x	x	x					
		A0A2P8ZZK3	x				x	x		
		A0A2P9A1T6					x	x		x
		A0A2P9A5K6					x	x		x

	A0A2P9A6P1	x				x	x		
	A8ZQJ6	x		x	x				
	B2J5T3	x	x		x				
	B4VID1			x		x			x
	H9LIQ2					x	x		x
	I1YDD3	x				x	x		
	K9EH21					x		x	x
	K9VBM2		x		x	x			
	L8LZA3	x				x	x		
	Q7NL78		x					x	x
	Q7NMS0			x			x		x
	A0A0A1VZG0				x				x
	A0A0C1T9B4		x			x			
	A0A0C1WGB5					x	x		
	A0A0C1XWD0	x	x						
	A0A0D6AJ93					x	x		
	A0A0D6KIM4	x		x					
	A0A0D8ZR23	x				x			
	A0A0M1JQN5					x	x		
	A0A0N8KMT9	x			x				
	A0A0N8KPW9	x							x
	A0A0P4UWU7	x		x					
	A0A0P7ZJ21					x	x		
	A0A0P8A1K4				x				x
	A0A0S3TRY9							x	x
	A0A0V7ZNE4					x	x		
	A0A0X8WZ15					x	x		
	A0A120MWD1					x	x		
	A0A168V9D7		x						x
	A0A182ANB3					x	x		
	A0A1E5QRX1					x	x		
2	A0A1J0AB12		x		x				
	A0A1J1JI14				x	x			
	A0A1J1KAB3					x	x		
	A0A1J1KU37					x	x		
	A0A1L9QVX3	x	x						
	A0A1Q4R6N6	x				x			
	A0A1Q6DDY3	x		x					
	A0A1Q8ZE73		x	x					
	A0A1Q8ZG15				x			x	
	A0A1U7HUT8	x		x					
	A0A1U7IYB9						x		x
	A0A1U7J140		x						x

	A0A1U7J1A8					x	x		
	A0A1U7J2Q3					x	x		
	A0A1U7J2S0					x	x		
	A0A1U7J2T9					x	x		
	A0A1U7J2U2					x	x		
	A0A1U7J304					x	x		
	A0A1U7J3G7					x	x		
	A0A1U7J3I5					x	x		
	A0A1U7J481	x				x			
	A0A1U7J4J2	x				x			
	A0A1U7J4J9					x	x		
	A0A1U7J5R6					x	x		
	A0A1U7J6L3					x	x		
	A0A1U7J7B7					x	x		
	A0A1U7J8E3					x	x		
	A0A1U7J9P1					x	x		
	A0A1U7J9U4					x	x		
	A0A1U7JA40					x	x		
	A0A1U7JAE4					x	x		
	A0A1U7JAG3					x	x		
	A0A1U7JAN0					x	x		
	A0A1U7JB19					x	x		
	A0A1U7JB82						x		x
	A0A1Z3HIM7				x				x
	A0A1Z3HIN6					x	x		
	A0A1Z3HPV6	x			x				
	A0A1Z3HSH6					x	x		
	A0A1Z4GXM5					x	x		
	A0A1Z4NKK4					x	x		
	A0A1Z4QPV0		x	x					
	A0A1Z4UGX5	x			x				
2	A0A1Z8NBM9	x			x				
	A0A218N0M0					x	x		
	A0A218QHQ5	x					x		
	A0A251WGJ8	x					x		
	A0A254WT29		x	x					
	A0A2E1IMA9	x					x		
	A0A2K2ZSH6	x		x					
	A0A2N5JPX1					x	x		
	A0A2N6L6G2		x						x
	A0A2N6MRK8		x	x					
	A0A2P8VR06					x	x		
	A0A2P8VRH1					x	x		

A0A2P8VRR4	x				x			
A0A2P8VTT8					x	x		
A0A2P8VU31					x			x
A0A2P8W6J2					x	x		
A0A2P8W8E1					x	x		
A0A2P8W8P0					x	x		
A0A2P8W8U3					x	x		
A0A2P8W8Y6					x	x		
A0A2P8W907					x	x		
A0A2P8WDG7	x		x					
A0A2P8WID7					x	x		
A0A2P8ZR41					x	x		
A0A2P8ZSC4					x	x		
A0A2P8ZTP8					x	x		
A0A2P8ZWB0					x	x		
A0A2P8ZXT6					x	x		
A0A2P8ZZL1					x	x		
A0A2P9A1S7					x	x		
A0A2P9A525					x	x		
A0A2P9A675					x	x		
A0A2P9A6S9					x	x		
B4W482			x					x
B4WFP8	x			x				
D5A4Y5		x						x
K0J955					x	x		
K9FMV2					x	x		
K9PC88		x	x					
K9PUV5					x	x		
K9PW98	x		x					
K9SVF4	x					x		
K9UQL4					x	x		
K9XAV9					x	x		
L0L519							x	x
Q7NFT5	x	x						
T2IZZ1					x	x		
U9VTX8	x				x			
U9VXF7	x	x						
U9VXT1		x		x				

** As the distribution of these seven proteins among the 4 conditions (4 s^{-1}, 40 s^{-1}, glass and perspex) was similar (52%, 48%, 48% and 52%, respectively), there was not experimental condition in which the frequency of appearance was highlighted.*

5.

5 Quantitative proteomic analysis of marine biofilms formed by filamentous cyanobacterium

The contents of this chapter as published as:

Romeu M.J., Domínguez-Pérez D., Almeida D., Morais J., Araújo M.J., Osório H., Campos A., Vasconcelos V., Mergulhão F.J. (2021) Quantitative proteomic analysis of marine biofilms formed by filamentous cyanobacterium. *Environmental Research* **201**: 111566-111566.

Abstract

Cyanobacterial molecular biology can identify pathways that affect the adhesion and settlement of biofouling organisms and, consequently, obtain novel antifouling strategies for marine applications. Proteomic analyses can provide an essential understanding of how cyanobacteria adapt to different environmental settings. However, only a few qualitative studies have been performed in some cyanobacterial strains. Considering the limited knowledge about protein expression in cyanobacteria in different growing conditions, a quantitative proteomic analysis by LC-MS/MS of biofilm cells from a filamentous strain was performed. Biofilms were also analysed through standard

methodologies for following cyanobacterial biofilm development. Biofilms were formed on glass and perspex at two relevant hydrodynamic conditions for marine environments (average shear rates of 4 s^{-1} and 40 s^{-1}). Biofilm development was higher at 4 s^{-1} and no significant differences were found between surfaces. Proteomic analysis identified 546 proteins and 41 were differentially expressed. Differences in protein expression were more noticeable between biofilms formed on glass and perspex at 4 s^{-1}. When comparing biofilms formed on different surfaces, results suggest that biofilm development may be related to the expression of several proteins like a beta-propeller domain-containing protein, chaperone DnaK, SLH domain-containing proteins, an OMF family outer membrane protein, and/or additional uncharacterized proteins. Regarding the hydrodynamic effect, biofilm development can be related to SOD enzyme expression, to proteins related to photosynthetic processes and to a set of uncharacterized proteins with calcium binding domains, disordered proteins, and others involved in electron transfer activity. Studies that combine distinct approaches are essential for finding new targets for antibiofilm agents. The characterisation performed in this work provides new insights into how shear rate and surface affect cyanobacterial biofilm development and how cyanobacteria adapt to these different environmental settings from a macroscopic standpoint to a proteomics context.

Keywords: marine biofouling, cyanobacterial biofilms, shotgun proteomic, LC-MS/MS, hydrodynamics, fouling surfaces

5.1 Introduction

Marine biofouling has several economic, environmental, and ecological impacts (Bharti *et al.*, 2017; Carvalho, 2018). Biofilms are a particular concern in aquaculture, heat exchangers, maritime transport, water desalination and the oil and gas industry. In biofilms, organisms cooperate and improve their chances of survival when subjected to harsh environmental conditions. Indeed, in marine environments, several parameters can

affect the development of these biofilms, such as salt, nutrient and organic matter concentration, light access, pH, temperature, hydrodynamic conditions, as well as the abiotic or biotic surface in which biofilm formation occurs (Carvalho, 2018). Cyanobacteria dominate marine and phototrophic biofilms and they have cosmopolitan distribution due to their inherent capacity to withstand various biotic and abiotic stresses. These microfouler organisms can also promote the adhesion of macrofouler organisms such barnacles, mussels, algae and seaweeds in aquatic environments (Mieszkin *et al.*, 2013). Integration among several disciplines, such as genetics, biology, and chemistry, is essential for progress in marine biofilm research. Therefore, cyanobacterial molecular biology is an emerging field for further developments and improvements (Sun *et al.*, 2018; Santos-Merino *et al.*, 2019). Analyses of protein expression can provide an essential understanding of how cyanobacteria adapt to different environmental settings. It is crucial to study the protein expression level in different conditions, particularly in biofilms, since biofilm development under altered conditions may be associated with quantitative differences in their proteome. Therefore, quantitative proteomics studies allow establishing a relationship between the relative expression level of the identified proteins under different conditions. However, few proteomics studies address marine biofilms (Leary *et al.*, 2014), and cyanobacteria data is scarce (Babele *et al.*, 2019). Moreover, the small number of quantitative proteomic studies performed with filamentous cyanobacterium is restricted to *Anabaena, Nostoc,* and *Spirulina* cyanobacterial genus. These studies only analysed the impact of limited and specific parameters on protein expression, such as temperature (Kurdrid *et al.*, 2011), salt (Wang *et al.*, 2013) and arsenic stress (Pandey *et al.*, 2012), ultraviolet-B light exposure (Babele *et al.*, 2015), uranium tolerance (Panda *et al.*, 2017) or N_2-fixing and non-N_2-fixing conditions (Ow *et al.*, 2008). Different factors have been reported on cyanobacterial biofilm development, such as the involvement of the signaling molecule cyclic dimeric GMP (Enomoto *et al.*, 2014; Agostoni *et al.*, 2016), extracellular proteins (Zilliges *et al.*, 2008; Oliveira *et al.*, 2015; Parnasa *et al.*, 2016) or type IV pili (R. Allen *et al.*, 2018).

Identifying proteins expressed in a defined condition is a useful tool to understand the cellular response and to identify pathways that are activated or down-regulated under different circumstances to which cells were subjected (Muthusamy *et al.*, 2017;

Battchikova *et al.*, 2018). Knowledge about protein expression under different biofilm development conditions is essential to clarify their role on biofilm phenotypes. These studies can help to identify pathways affecting adhesion and settlement of biofouling organisms and can lead to new targets for the development of novel antifouling strategies for marine applications.

The Blue Biotechnology and Ecotoxicology Culture Collection (LEGE-CC) is a biological resource center that comprises more than 1000 different cyanobacterial and microalgae strains (Ramos *et al.*, 2018). The unidentified filamentous cyanobacterium LEGE 06007 strain was used in this study, given the relevance of cyanobacteria on marine biofouling. This strain has also shown good biofilm formation behavior during pre-screening of the collection. Although several biological and physico-chemical parameters have been identified as modulators of biofilm development, the fouling surface properties and flow velocity/shear rate have a critical impact on marine biofilms (Faria, Teixeira-Santos, Gomes, *et al.*, 2020; Faria, Teixeira-Santos, Romeu, *et al.*, 2020; Faria, Teixeira-Santos, Morais, *et al.*, 2021). Hence, the first goal of this study was to perform a biofouling potential evaluation of this marine cyanobacterium, which has recently been restructured on taxonomic level (Ramos *et al.*, 2018). Previously included on *Phormidium* genus, after a revaluation of taxonomic assignments based on approaches that combine morphological and phylogenetic data, evaluation of its characteristics did not allow an unequivocal identification at the genus or order level. The second aim of this study was to perform a quantitative proteomics analysis of this cyanobacterium under different biofilm development conditions to establish a relationship between the relative expression level of the identified proteins under different settings (different hydrodynamic conditions and surfaces) and biofilm development. For this purpose, we performed a shotgun proteomic analysis of the digested peptides obtained from two distinct sample preparation methods – the Filter Aided Sample Preparation (FASP) (Wiśniewski *et al.*, 2009), and the single-pot solid-phase-enhanced sample-preparation (SP3) protocol (Hughes *et al.*, 2019). To the best of our knowledge, there are no quantitative proteomics studies evaluating the impact of different surfaces and different hydrodynamic conditions on cyanobacterial biofilm behavior. Therefore, this is the first work investigating the biofouling potential of this cyanobacterial strain and its proteome profile obtained from different biofilm

development conditions by applying standard methodologies for biofilm development and a quantitative proteomics approach. Since the information on the molecular basis of these processes in cyanobacteria is scarce, the quantitative proteomic analysis carried out in this work is extremely relevant. Moreover, few studies have been performed in this research field addressing filamentous cyanobacterial biofilms.

5.2 Material and Methods

5.2.1 Organisms and inocula preparation

Unidentified filamentous cyanobacterium LEGE 06007 was isolated from a wave-exposed rock in the intertidal zone at São Martinho do Porto beach, Portugal (39.50694 N 9.136311 W), and it was obtained from the LEGE-CC located at CIIMAR, Matosinhos, Portugal (Ramos *et al.*, 2018). Cells were grown in 750 mL culture in Z8 medium (Kotai, 1972) supplemented with 25 $g.L^{-1}$ of synthetic sea salts (Tropic Marin) and B_{12} vitamin (Sigma Aldrich, Merck, Saint Louis, MO, USA), which supports the growth and cyanobacteria maintenance. The culture was performed under 14 h light (10–30 μmol photons m^{-2} s^{-1})/10 h dark cycles, at 25 °C.

5.2.2 Biofilm formation

Biofilm development was evaluated on agitated 12-well microtiter plates (VWR International, Carnaxide, Portugal), since this platform was shown to mimic the hydrodynamic conditions found in marine environments (Romeu *et al.*, 2019). To assess the surface effect on protein expression, biofilms were developed on glass (Vidraria Lousada, Lda, Portugal) and perspex (Neves & Neves, Lda, Portugal) coupons (1 cm^2). These substrates have different hydrophobicity (Romeu *et al.*, 2019) and they also represent commonly submerged artificial surfaces found on different equipment in aquatic and marine environments such as underwater windows of boats, aquaculture equipment, flotation spheres, moored buoys, underwater cameras, measuring devices or sensors (Taylor, 1996; Blain *et al.*, 2004; King *et al.*, 2006). Surface preparation and sterilisation was performed as previously described (Romeu *et al.*, 2019). Before

inoculation, the cyanobacterial suspension was adjusted to a chlorophyll *a* concentration of 1.5 μg.mL^{-1}, since chlorophyll *a* concentration is commonly used as biomass indicator in aquatic environments. After 2 mL of cyanobacterial suspension were incubated for 24 h at 4 °C in the dark for a maximal chlorophyll *a* extraction, the samples were centrifuged at 3202*g*, for 5 min at room temperature and the supernatant was transferred to a glass cuvette. The absorbance at 750 nm (turbidity), 665 nm (chlorophyll *a*) and 652 nm (chlorophyll *b*) was determined using a V-1200 spectrophotometer (VWR International China Co., Ltd, Shanghai, China). The chlorophyll *a* concentration was calculated through the following equation (5.1) (Porra *et al.*, 1989):

$$\text{Chl } a \text{ } (\mu g.mL^{-1}) = 16.29 \times A^{665} - 8.54 \times A^{652} \quad (5.1)$$

where A^{665} and A^{652} are the absorbances at 665 nm and 652 nm, respectively.

These measurements were assessed in triplicate and dilutions were performed using Z8 medium supplemented with 25 g.L^{-1} of synthetic sea salts and vitamin B_{12}. Thus, a volume of 3 mL of adjusted cyanobacterial suspension was inoculated in each well, in which coupons of each surface were previously fixed with transparent double-sided adhesive tape. To assess the effect of hydrodynamics on protein expression, cyanobacterial biofilm formation at different shear rates was tested. Although a shear rate of 50 s^{-1} has been reported for a ship in a harbour (Bakker *et al.*, 2003), equipment and devices which are in similar environments such as partially submerged or even moored equipment, as underwater cameras, flotation spheres, sensors, and even transparent hulls of boats or their windows are likely to be subjected to similar shear values (Romeu *et al.*, 2019). Microtiter plates were incubated at 25 °C in an orbital shaker with a 25 mm orbital diameter (Agitorb 200ICP, Norconcessus, Portugal) at 185 rpm, yielding average and maximum shear rates of 40 and 120 s^{-1}, respectively (Romeu *et al.*, 2019). Moreover, it has been reported that lower fluid velocities (0.2 m s^{-1}) promote the growth of filamentous green algae and cyanobacteria (Minchin and Gollasch, 2003; Flemming *et al.*, 2009) and that marine biofouling can be favoured at low shear rates (Faria, Teixeira-Santos, Romeu, *et al.*, 2020). Therefore, biofilm development was also assessed at lower shear rate

conditions (average shear rate of 4 s^{-1}, reaching a maximum value of 11 s^{-1}, which are obtained in the same incubator at a shaking frequency of 40 rpm). Overall, these values of shear rate include different ranges that can be found in marine environments, and which are important for marine biofouling. Biofilm development was followed for seven weeks (49 days) since it is accepted that a two-month interval for maintenance is the minimum duration for economically viable underwater monitoring systems, as previously reported (Blain *et al.*, 2004; Romeu *et al.*, 2019). During this incubation time, the medium was replaced twice a week. In order to mimic real light exposure periods, a photoperiod of 14 h light (8-10 μmol photons m^{-2} s^{-1})/10 h dark cycles) was applied (Romeu *et al.*, 2019). This methodology, which has been used to assess the antifouling performance of different surfaces, was further validated by field tests as previously described (Silva *et al.*, 2021).

5.2.3 Biofilm analysis

Although the initial stages of biofilm formation could be assessed by counting the number of adhered cells if a coccoid cyanobacterium was used (Faria, Teixeira-Santos, Morais, *et al.*, 2021), this study uses a filamentous cyanobacterial strain which precludes reliable determination of adhered cell numbers. Since preliminary studies have shown that seven days was the minimum time to obtain reliable and quantifiable results through the methods used in this work, biofilm analysis was performed every seven days, at which three coupons for each surface and hydrodynamic condition were analysed. To eliminate loosely attached cyanobacteria, the culture medium was carefully removed, and the wells were filled with 3 mL of sterile sodium chloride solution (8.5 $g.L^{-1}$) (Romeu *et al.*, 2019) to evaluate the cyanobacterial biofilms structure by Optical Coherence Tomography (OCT). In order to complement the characterization of cyanobacterial biofilms, the determination of their wet weight and chlorophyll *a* content was performed. Additionally, the crystal violet assay was performed to total biomass quantification.

5.2.3.1 Optical Coherence Tomography

Images from cyanobacterial biofilms developed on both surfaces and under the different hydrodynamic conditions were captured as reported in Romeu *et al*. (2019.) For each coupon, 2-D imaging was performed with a minimum of three fields of view, to ensure the accuracy and reliability of the results obtained. Image analysis was performed using a routine developed in the Image Processing Toolbox from MATLAB 8.0 and Statistics Toolbox 8.1 (The MathWorks, Inc., Natick, Massachusetts, USA) as reported in Romeu *et al.* (2020). The mean biofilm thickness was calculated according to the following equation (5.2):

$$\bar{L}_F = \frac{1}{N} \sum_{i=1}^{N} L_{F,i} \quad (5.2)$$

where $L_{F,i}$ is a local biofilm thickness measurement at location i, N equals the number of thickness measurements and $\bar{L}_F$ is the mean biofilm thickness.

Biofilm roughness was analysed by determining the roughness coefficient because this parameter allows comparing the structure of different biofilms, across different studies and across scales once this value is normalized to the mean biofilm thickness (Romeu *et al.*, 2019). The relative roughness coefficient (R_α^*) was calculated using the following equation (5.3), according to Wagner and Horn, 2017:

$$R_\alpha^* = \frac{1}{N} \sum_{i=1}^{N} \frac{|L_{F,i} - \bar{L}_F|}{\bar{L}_F} \quad (5.3)$$

5.2.3.2 Wet weight determination and chlorophyll *a* quantification

The determination of cyanobacterial biofilms wet weight and chlorophyll *a* content was performed as reported in Romeu *et al*., 2019. In order to determine the wet weight, coupons were detached from the wells and weighed. Biofilm wet weight was obtained as the difference from the initial coupon weight (determined prior to inoculation). Afterwards, cyanobacterial cells were detached from the coupons by immersing each coupon in 2 mL of 8.5 $g.L^{-1}$ sodium chloride solution and vortexing. The suspensions were

incubated for 24 h at 4 °C in the dark and chlorophyll *a* determination was performed as previously described through Equation 5.1.

5.2.3.3 Crystal violet assay

Additional coupons, representative of all conditions, were transferred to sterile 24-well plates at each sampling day. Crystal violet assay was adapted from a previously described protocol (Moreira *et al.*, 2017). Briefly, to fix the cyanobacterial biofilms, 1 mL of 100% (v/v) ethanol was added to each well for 15 min. Afterwards, culture plates were allowed to air dry at room temperature. The fixed biofilms were stained with 1 mL of 1% (v/v) crystal violet solution (Merck KGaA, Germany) for 5 min and to solubilize the crystal violet (CV), 1 mL of 33% (v/v) acetic acid (VWR, Portugal) was added to each well. Then, 200 µl of this solution was transferred to sterile 96-well plates, and the optical density was measured at 570 nm in a plate reader (SpectroStar Nano, BMG LABTECH).

5.2.3.4 Statistical analysis of biofilm development

A total of six replicates (two biological assays with three technical replicates each) were analyzed. Data analysis was performed using the statistical program GraphPad Prism® for Windows, version 6.01 (GraphPad Software, Inc., San Diego, CA, USA) and results were compared using unpaired *t*-tests with a confidence level of 95% (**; $P < 0.05$) and 90% (*; $P < 0.1$).

5.2.4 Proteomics analysis

5.2.4.1 Protein extraction and sample preparation

At the last sampling time (49 days), biofilm samples of unidentified filamentous cyanobacterium LEGE 06007 strain from each condition were recovered for proteomic analysis and processed as previously described (Romeu *et al.*, 2020) with some modifications. Briefly, cyanobacterial biofilms were detached from the surface by immersing each coupon in 2 mL of 8.5 $g.L^{-1}$ sodium chloride solution and vortexing. To maximise the biomass yield, suspensions obtained from four coupons of the same condition were pooled. The samples were centrifuged at 3202*g* for 10 min at room

temperature and the pellets of biomass originating from 24 biofilm samples comprising six independent-replicates from four different growing conditions were kept at -20 °C for further processing. Following previously described protocols (Campos *et al.*, 2016), the amount of sample was calculated, and an appropriate volume of SDT buffer (0.5 g FW/mL SDT) + Protease inhibitors (PIs, Roche, 11697498001, Basel, Switzerland) was added to the samples. These were sonicated 10 x 3 sec and 23 kHz – 105 μm (amplitude) and incubated for 4 h at room temperature. Then, samples were heated for 3 min at 95 °C and subsequently centrifuged at 16000*g* for 20 min. Finally, the supernatant was collected, and total protein concentration was measured indirectly by optical density (OD) at 280 nm using a DeNovix DS-11 Spectrophotometer (DeNovix Technologies, Wilmington, Delaware, USA). Samples containing the extracted protein were stored for 24 hours at -20 °C. The extracted proteins were processed using two distinct protocols based on FASP protocol described by (Wiśniewski *et al.*, 2009) and the SP3 (Hughes *et al.*, 2019) technology.

FASP

Similar to previous works, the samples containing the extracted proteins stored at -20 °C were defrosted in ice for further processing using the FASP protocol as previously described (Almeida *et al.*, 2020; Martins *et al.*, 2020; Matos *et al.*, 2020; Romeu *et al.*, 2020). This approach comprised the alkylation with iodoacetamide and digestion of 40 μg of the extracted proteins with trypsin (recombinant, proteomics grade, Roche, Basel, Switzerland) at an enzyme to protein ratio of 1:100 (w/w) for 16 h at 37 °C using centrifugal filter units with nominal molecular weight limit (NMWL) of 30 kDa (MRCPRT030, Millipore, Billerica, MA, USA). Through centrifugal filtration, peptides were recovered and acidified with Trifluoracetic acid (TFA: 10% v/v). Samples were desalted and concentrated by reversed-phase extractions (C18 Tips, 100 μL, Thermo Scientific, Thermo Fisher Scientific, Wilmington, DE, USA) with acetonitrile (CAN: 50% v/v) and TFA (0.1% v/v) for peptide elution. Before LC-MS/MS analysis, samples were dried in a Concentrator Plus vacuum rotator (Eppendorf, Hamburg, Germany) and resuspended in 25 μL formic acid (FA: 0.1% v/v). The final concentration was determined with 2 μL of digested peptides, measured indirectly by optical density (OD) at 280 nm using a DeNovix DS-11 Spectrophotometer (DeNovix Technologies, Wilmington, Delaware, USA).

SP3

Prior to digestion, 100 μg of extracted proteins in approximately 5 μL were reduced in 45 μL SDT in new 1.5 mL Eppendorf tubes. Then, alkylation of samples was performed with 10 μL of 0.1 M iodoacetamide (AppliChem) in 8 M Urea, 0.1 M Tris/HCl pH 8.5 for 30 min. in the dark at room temperature.

Digestion followed Hughes *et al.*, (2019) SP3 for proteomics experiments with some modifications. New magnetized beads (Sera Mag SP3 beads, CAT#45152105050250 and CAT#65152105050250, GE Healthcare) were initially washed and reconstituted in water (HPLC grade, VWR) at a final concentration of 10 $\mu g.\mu L^{-1}$ (from an initial stock concentration of 50 $mg.mL^{-1}$), using a magnetic rack (MagnaRack, Invitrogen) for 1 min, and the protein digestion was conducted according to specifications of the manufacturer. Then, after removing the supernatant, 100 μL ammonium bicarbonate (Fluka) 0.05 M was added to the tubes and incubated for 5 min at 1000 rpm. After bead spin and magnetizing, the supernatant containing the tryptic peptides was transferred to clean 1.5 mL Eppendorf tubes. The peptide concentration was estimated using the DeNovix (A280 application). Acidification was performed by adding 20 μL of formic acid 5% v/v (Optima LC/MS grade, Fisher Chemical) to the samples. Afterwards, tryptic peptides were dried in a Concentrator Plus vacuum rotator (Eppendorf, Hamburg, Germany) and resuspended in 25 μL formic acid (FA: 0.1% v/v). The final concentration was determined with 2 μL of digested peptides, measured indirectly by optical density (OD) at 280 nm using a DeNovix DS-11 Spectrophotometer (DeNovix Technologies, Wilmington, Delaware, USA). A detailed description of the SP3 protocol can be found in Supplementary Material, Detailed Protocol S 5.1.

5.2.4.2 LC-MS/MS analysis

Considering that both sample preparation methods are complementary, tryptic peptides from both methods were mixed in the same tube to a final concentration of 0.1 μg and 0.5 μg from FASP and SP3, respectively. Then, protein digests from both protocols were analysed in the same run with a nano LC-MS/MS, composed by an Ultimate 3000 liquid chromatography system coupled to a Q-Exactive Hybrid Quadrupole – Orbitrap mass spectrometer (Thermo Scientific, Bremen, Germany), as previously described (Osório

et al., 2021). Separation was performed in a 15 cm by 75μm inner diameter EASY-Spray column (ES800, PepMap RSLC, C18, 3 μm, Thermo Scientific, Bremen, Germany) at 300 $nL.min^{-1}$ using a gradient generated by mixing A: 0.1% FA and B: 80% ACN, in the following quantities: 5 min (2.5% B to 10% B), 60 min (10% B to 35% B), 5 min (35% B to 99% B) and 5 min (hold 99% B). Subsequently, the column was equilibrated with 2.5% B for 12 min. Data acquisition was controlled by Xcalibur 4.0 and Tune 2.8 software (Thermo Scientific, Bremen, Germany). The specific LC-MS parameters were full scan settings: 70k resolution (m/z 200), AGC target 3e6, maximum injection time 50 ms. dd settings: minimum AGC target 8e3, intensity threshold 7.3e4, charge exclusion: unassigned, 1, 8, >8, peptide match preferred, exclude isotopes on, dynamic exclusion 20s. MS2 settings: microscans 1, resolution 35k (m/z 200), AGC target 2e5, maximum injection time 110 ms, isolation window 2.0 m/z, isolation offset 0.0 m/z, spectrum data type profile.

5.2.4.3 Protein identification

The raw data was analysed and processed using the Proteome Discoverer 2.2.0.388 software (Thermo Scientific) and searched against the UniProt database for Cyanobacteria taxonomic selection (2018_07 release). The Sequest HT search engine was used for protein identification. The ion mass tolerance was 10 ppm for precursor ions and 0.02 Da for-fragment ions. Maximum allowed missing cleavage sites was set to 2. Cysteine carbamidomethylation was defined as a constant modification. Methionine oxidation and protein N-terminus acetylation were defined as variable modifications. Peptide confidence was set to high. The processing node Percolator was enabled with the following settings: maximum delta Cn 0.05; decoy database search target false discovery rates (FDR) 1%, validation was based on q-value. Protein label-free quantitation was performed with the Minora feature detector node at the processing step. Precursor ion quantification was performed at the processing step with the following parameters: unique plus razor peptides were considered for quantification and precursor abundance was based on intensity.

5.2.4.4 Differential protein expression and enrichment

Statistical analyses applied to the proteomic data were performed using R software version 4.0.0. (Dessau and Pipper, 2008). The Differentially Expressed Proteins (DEPs) and/or gene enrichment were assessed using the "DEP" R package (Zhang *et al.*, 2018), based on the *limma* algorithm (Ritchie *et al.*, 2015). Missing values were filtered according to the fraction of protein found in each paired comparison with a cut-off of 0.33%, considering the possibility of having a minimum of 4 out of 6 replicates of at least one condition. Imputation of missing values was performed considering a non-random distribution (MNAR) using "MinProb" as an imputation function. Significant differences between conditions for each condition were paired tested by protein-wise linear models and empirical Bayes statistics. Finally, adjusted P-value (alpha = 0.05), and the $\log_2$ fold change (lfc = $\log_2(1.5)$, $\log_2$ fold change >0.6) were used as a filter threshold to classify them as DEPs or enriched genes. For comparison purposes, the distribution of DEPs among conditions was analysed by Venn diagrams using an online free tool, available at the webserver of the Bioinformatics and Evolutionary Genomics Center (BEG/Van de Peer Lab site), Ghent University, Belgium, http://bioinformatics.psb.ugent.be/webtools/Venn/.

5.2.4.5 Functional annotation

Functional classification (gene ontology) was carried out using the OmicsBox software version 1.4.11 (https://www.biobam.com/omicsbox/). Protein signatures were also obtained from the InterPro member databases (*e.g.* Pfam, PROSITE, PRINTS, ProDom, SMART, TIGRFAMs, PIRSF, SUPERFAMILY, Gene3D, and PANTHER) using the InterProScan software (Mitchell *et al.*, 2019) integrated into the OmicsBox tool. All annotation and the corresponding gene ontology (GO) terms were then transferred to the sequences and eventually merged with existing GO terms resulting from blast search. Additional functional analyses to determine over/underexpressed pathways were performed to the categorical GO terms corresponding to DEPs, using the hypergeometric distribution significance test (Fisher's exact test, $P < 0.05$).

5.3 Results and Discussion

5.3.1 Biofilm development analysis

Cyanobacterial biofilm development was assessed for 49 days, and the wet weight, chlorophyll *a* content, total biomass and thickness evolution is shown in Figure 5.1. Biofilm biomass was higher at the lowest shear rate for both surfaces, as it is particularly noticeable in the biofilm thickness obtained on glass (Figure 5.1G). Previous studies performed with different filamentous cyanobacterial strains have shown that despite the tenfold difference in average shear rate, cyanobacterial biofilm behaviour was similar in both hydrodynamic conditions for the first weeks of biofilm development (Romeu *et al*., 2019, 2020). In the present study, differences in biofilm development at different shear conditions were noticed in the early stages, but major differences were also found in the maturation phase of biofilm development. It is possible that sloughing and erosion events related to the shear rate also assume particular significance at later stages of biofilm development. Similar results were also obtained with coccoid cyanobacteria, *Synechocystis salina* and *Cyanobium* sp. strains, when glass and a polymeric epoxy coating were used (Faria, Teixeira-Santos, Romeu, *et al*., 2020). The major differences between the two hydrodynamic conditions were observed from data obtained from thickness quantification (Figure 5.1G, H) but also from biofilm wet weight (Figure 5.1A, B). Biofilm mass obtained on glass under lower shear conditions (4 s^{-1}) was on average 71.5% higher when compared to the values obtained at a higher shear rate (40 s^{-1}; Figure 5.1A). On perspex, biofilm wet weight at 4 s^{-1} was on average 53.9% higher (Figure 5.1B). Whereas chlorophyll *a* content at 4 s^{-1} on glass and perspex was on average 75% higher (Figures 5.1C, D) than at higher shear conditions. As previously reported (Chorus and Cavalieri, 2000; Romeu *et al*., 2019, 2020), chlorophyll *a* content monitorisation demonstrated to be a useful tool to follow cyanobacterial biofilm growth since a correlation between chlorophyll *a* production and biofilm wet weight was observed (Supplementary Material, Figure S 5.1). Due to the complexity of filamentous cyanobacteria, there is a need to develop novel methodologies to study these organisms. To evaluate if the crystal violet assay (CV) can be a suitable approach for cyanobacterial biofilms analysis, quantification of total biomass was performed by CV. On glass, the total biomass quantified by this

method was on average 28.1% higher at lower shear when compared to the values obtained at a higher shear rate (40 s^{-1}; Figure 5.1E), whereas on perspex the average value obtained was about 33.2% higher at 4 s^{-1} (Figure 5.1F). Data obtained from this parameter corroborates observations from additional parameters, since higher biofilm biomass was obtained at the lowest shear rate for both surfaces. A correlation between data obtained from total biomass quantification by CV and biofilm thickness and from wet weight was observed (Supplementary Material, Figures S 5.2 and 5.3, respectively). Therefore, based on the results obtained for this strain, the quantification of total biomass from CV demonstrated to be useful tool to follow cyanobacterial biofilm growth.

Similar values of wet weight, chlorophyll *a* content, total biomass quantification and biofilm thickness were obtained for biofilms developed on different surfaces at the same hydrodynamic conditions (Supplementary Material, Figure S 5.4), showing that the effect of surface properties was less important than the hydrodynamic effect on cyanobacterial biofilm development in a macroscopic biofilm evaluation. Despite the different hydrophobicity of glass and perspex (Romeu *et al.*, 2019), these findings had already been shown for other coccoid (Faria, Teixeira-Santos, Romeu, *et al.*, 2020) and filamentous cyanobacterial strains (Romeu *et al.*, 2019, 2020).

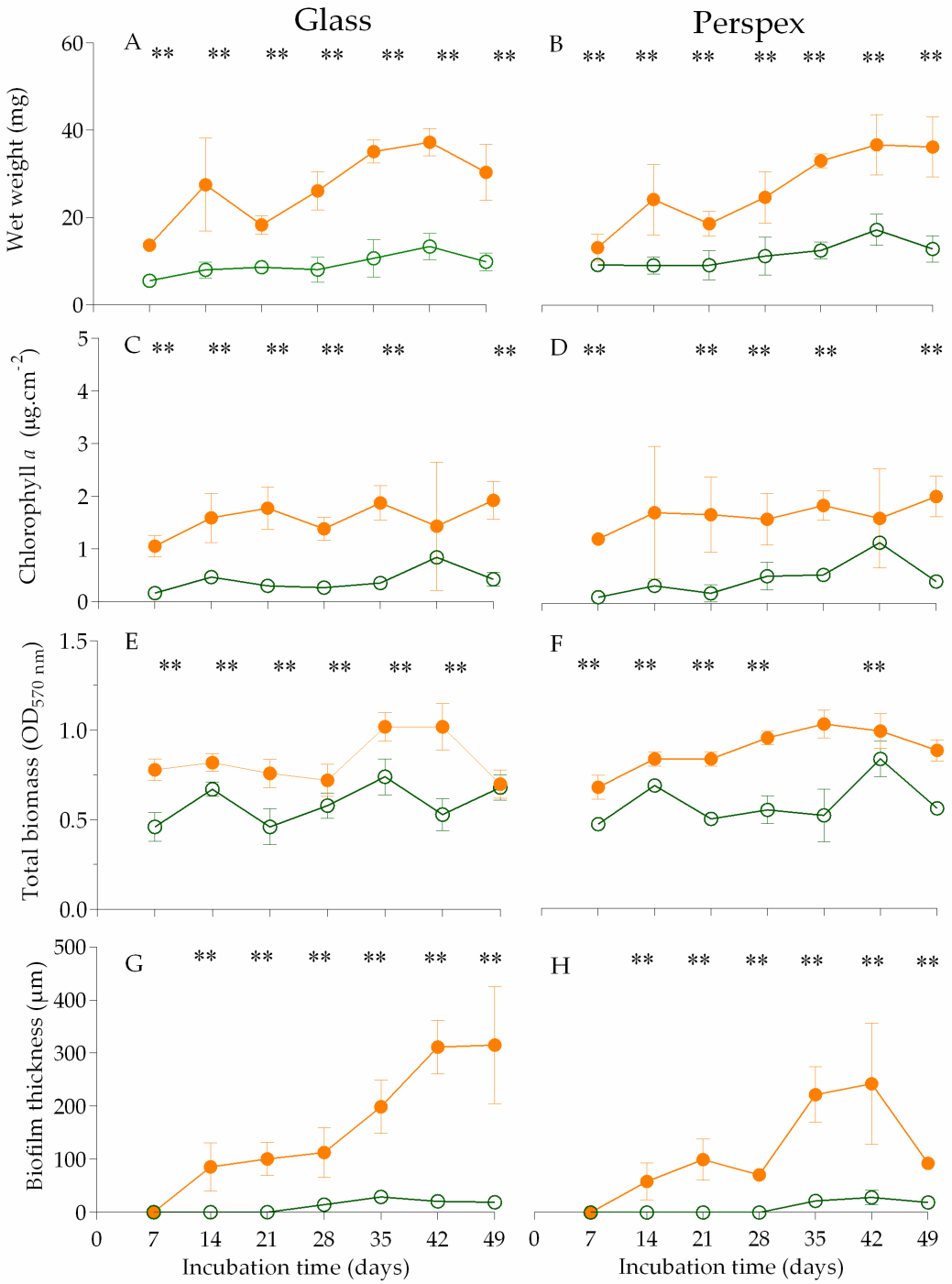

Figure 5.1. Evaluation of unidentified filamentous cyanobacterium LEGE 06007 biofilm development. The parameters analysed refer to wet weight (A, B), chlorophyll *a* quantification (C, D), total biomass quantification by CV assay (E, F) and biofilm thickness (G, H). Biofilms were formed in glass (A, C, E, G) or perspex (B, D, F, H), at two average shear rates, 4 s^{-1} (closed circles, orange) and 40 s^{-1} (open circles, green) for 49 days. Standard deviations from two biological assays with three replicates each are represented. Symbol ** indicate statistically different values for $P < 0.05$ at each incubation time.

OCT analysis was used to analyse biofilm roughness and structure at different conditions. Biofilm roughness was only evaluated in the maturation phase of biofilm development, in which differences in biofilm thickness were more evident (from day 35). The analysis revealed that biofilms formed under the lower shear rate showed lower roughness coefficient values than those formed at higher shear on both surfaces (Supplementary Material, Figure S 5.5). Once again, the values obtained from biofilms developed under the same hydrodynamic condition at different surfaces were very similar. Figure 5.2 shows representative 2D cross-sectional images obtained from OCT at the end of the experiment (49 days). These figures highlight the importance of the hydrodynamic effect when compared to the surface effect. Previous studies showed that cyanobacterial biofilms developed under higher shear rates present a more compact structure (Romeu *et al.*, 2019, 2020), which probably increases biofilm cohesion (Teodósio *et al.*, 2011). In this study, the low biofilm biomass obtained under a higher shear rate (40 s^{-1}) on both surfaces (Figure 5.2 B, D) did not enable a comprehensive interpretation of biofilm structure and compaction.

Excessive shear stress can cause increased cell mortality, decreased growth rate and cell viability, or even cell lysis. Different organisms have different tolerances for the damage caused by hydrodynamic forces (Sobczuk *et al.*, 2006). Among photosynthetic organisms, green algae have the greatest tolerance to shear stress, followed by cyanobacteria, red algae and diatoms, with dinoflagellates comprising the most shear-sensitive species (Wang and Lan, 2018). In these organisms, the shear-sensitivity is determined primarily by cell wall strength, cell morphology and the presence of flagella. Cyanobacterial cell walls are mainly composed by peptidoglycan (Gumbo *et al.*, 2008), they comprise three to four layers and range from 10 to 20 nm in thickness and an envelope may also surround the cell to form a sheath (Stanier and Cohen-Bazire, 1977). On biofilms, as cells are embedded in a matrix mainly composed by extracellular polymeric substances (EPS), the interaction between EPS components promotes biofilm cohesion, with stronger EPS interactions preventing biofilm mechanical failure (Cense *et al.*, 2006). Moreover, it has been recognized that biofilms are viscoelastic materials (Gloag *et al.*, 2020). Viscoelasticity allows biofilm survival, promoting the formation of stronger biofilms when exposed to higher shear forces. Therefore, viscoelasticity emerged as a

general survival adaptation for biofilms in the surrounding environment, such as shear stresses. Several studies showed that viscoelasticity is an emergent behavior of bacteria when they form biofilms, and that these properties are largely governed by EPS (Peterson *et al.*, 2013). In our study, if some cells rupture, the impact of organic matter release from the cells may not have a significant impact on biofilm development since the surrounding environment is constantly renewed.

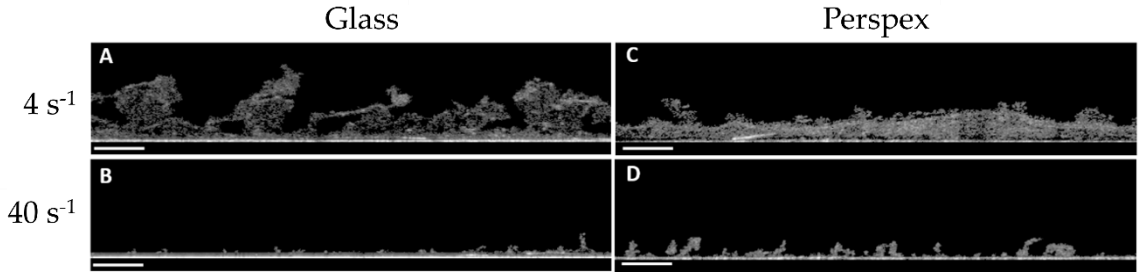

Figure 5.2. 2D cross-sectional OCT images of unidentified filamentous cyanobacterium LEGE 06007 biofilms formed after 49 days on glass and perspex at two different shear rates, 4 s^{-1} (A, C) and 40 s^{-1} (B, D). Scale bar = 200 μm.

5.3.2 Proteomic analysis

This work revealed for the first time the differential proteome expression of cyanobacterial biofilm cells developed in different conditions. Overall, 546 proteins were identified through the shotgun proteomics analysis from 24 biofilm samples of four different conditions (Supplementary Material, Table S 5.1). Herein, the total number of protein identified was relatively higher than a previous qualitative proteomic study performed on two different cyanobacterial strains at the same biofilm conditions (Romeu *et al.*, 2020). Similar to the aforementioned study, most of the proteins identified in this work corresponded to intracellular proteins since the surrounding environment, supernatant and exudate were not analysed. However, excreted proteins may have also been identified since they may have been retained in the biofilm matrix.

5.3.2.1 Enrichment and distribution of DEPs among conditions

The quantitative proteomic analysis was performed with the "DEP" R package (Zhang *et al.*, 2018), revealing a total of 41 DEPs (Figure 5.3, Table 5.1). Some of these DEPs

were also previously identified in the qualitative approach from different cyanobacterial strains (Romeu *et al.*, 2020). Among these proteins, ribosomal proteins were found, and others involved in photosynthesis and respiration, which are essential in primary metabolic functions, as well as proteins associated with phycobilisomes and elongation factors. Although a macroscopic evaluation of biofilm revealed a greater difference between the two hydrodynamic conditions, the proteomic analysis showed a higher difference in protein expression between the biofilms formed on glass and perspex at 4 s^{-1}, followed by the biofilms formed on glass at 4 s^{-1} and 40 s^{-1}, which demonstrated the importance of studies addressing different approaches. Indeed, among the four comparisons performed, most of the proteomic variations corresponded to the paired-comparison between samples from glass *vs* perspex at 4 s^{-1} (Figure 5.3A). In this comparison, 34 DEPs were found, where 27 DEPs were up-regulated and seven down-regulated in the glass surface relatively to perspex (Figure 5.3A). 10 DEPs were identified in the comparison between at 4 s^{-1} *vs* 40 s^{-1} on glass (Figure 5.3B), whereas two DEPs were found between samples from biofilms developed at 4 s^{-1} *vs* 40 s^{-1} on perspex (Figure 5.3C). Finally, four up-regulated DEPs were revealed in the glass surface relatively to perspex in comparing between biofilms developed on glass *vs* perspex at 40 s^{-1}, (Figure 5.3D).

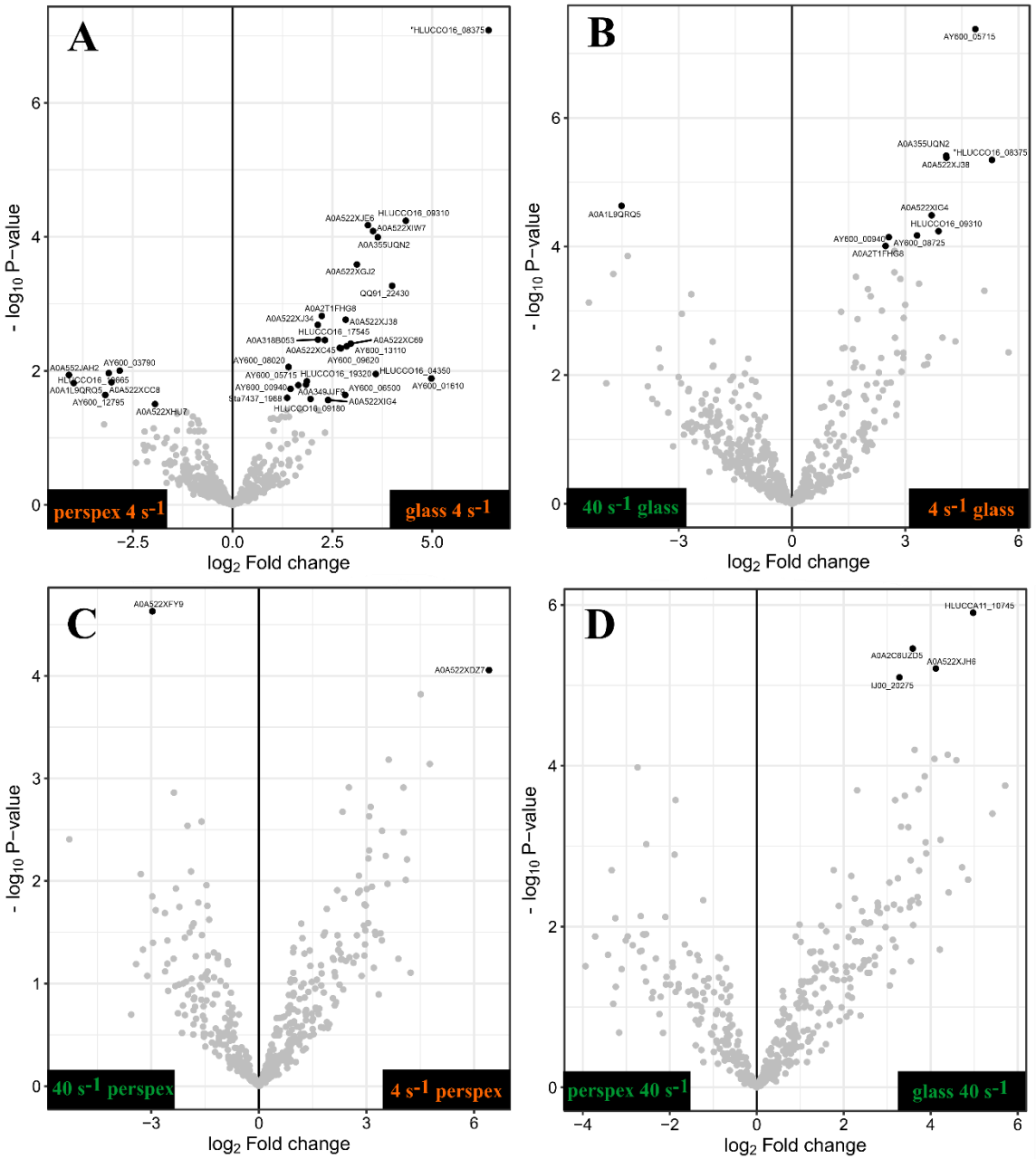

Figure 5.3. Volcano plot of the differentially expressed proteins (DEPs) among the 4 biofilm conditions studied. Black points represent the DEPs showing the corresponding gene symbol, or the protein accession number when lacking the corresponding gene annotation. The axis depicts the *P* values ($-\log_{10}$) plotted against the fold changes ($\log_2$) between each paired-comparison. A) glass *vs* perspex at 4 s^{-1} (down and up-regulated proteins on glass at 4 s^{-1} when compared with perspex at 4 s^{-1}); B) 4 s^{-1} *vs* 40 s^{-1} on glass (down and up-regulated proteins at 4 s^{-1} on glass when compared with 40 s^{-1} on glass); C) 4 s^{-1} *vs* 40 s^{-1} on perspex (down and up-regulated proteins at 4 s^{-1} on perspex when compared with 40 s^{-1} on perspex); D) glass *vs* perspex at 40 s^{-1} (down and up-regulated proteins on glass at 40 s^{-1} when compared with perspex at 40 s^{-1}).

Table 5.1. List of the 41 DEPs and their corresponding accession number (Protein IDs), gene names, description and the log_2 fold-changes obtained from each comparison.

UniProt accession number	Gene Names	Description	glass *vs* perspex at 4 s^{-1}	4 s^{-1} *vs* 40 s^{-1} on glass	4 s^{-1} *vs* 40 s^{-1} on perspex	glass *vs* perspex at 40 s^{-1}
A0A0P8BXS9	HLUCCO16_08375	Uncharacterized protein (Fragment)	6.41	5.30		
A0A1L9QRQ5		Allophycocyanin	-3.98	-4.51		
A0A2T1FHG8		Elongation factor Tu	2.23	2.48		
A0A318B053		Aldehyde dehydrogenase	2.14			
A0A349JJF9		SLH domain-containing protein (Fragment)	1.84			
A0A355UQN2		50S ribosomal protein L5	3.64	4.09		
A0A522XC45		Photosystem II CP43 reaction center protein	2.68			
A0A522XC69		Alpha/beta hydrolase	2.96			
A0A522XCC8		Isoleucine--tRNA ligase (Fragment)	-3.03			
A0A522XGJ2		SLH domain-containing protein	3.11			
A0A522XHU7		60 kDa chaperonin	-1.94			
A0A522XIG4		30S ribosomal protein S8	2.39	3.70		
A0A522XIW7		O-acetylhomoserine aminocarboxypropyltransferase/cysteine synthase	3.52			
A0A522XJ34		50S ribosomal protein L1	2.13			
A0A522XJ38		Phycobilisome rod-core linker polypeptide CpcG	2.83	4.09		
A0A522XJE6		Gfo/Idh/MocA family oxidoreductase	3.39			
A0A552JAH2		Chaperone protein DnaK	-4.10			
A0A168VPC8	AY600_00940	Uncharacterized protein	1.45	2.56		
A0A168UQZ4	AY600_01610	Cytochrome c-550	4.98			
A0A168SDR0	AY600_03790	Ferredoxin--NADP reductase	-2.83			
A0A168SSA6	AY600_05715	Cytochrome c6	1.65	4.86		
A0A168VLH9	AY600_06500	Uncharacterized protein	2.82			
A0A168WPD9	AY600_08020	Uncharacterized protein	1.40			
A0A168VRY4	AY600_09620	Beta-propeller domain-containing protein, methanol dehydrogenase	2.71			
A0A168UP82	AY600_12795	Elongation factor P	-3.19			
A0A168VMU3	AY600_13110	Ferredoxin	2.86			
A0A0P7Z9L3	HLUCCO16_04350	Photosystem I reaction center subunit XI	3.59			

UniProt accession number	Gene Names	Description	glass *vs* perspex at 4 s^{-1}	4 s^{-1} *vs* 40 s^{-1} on glass	4 s^{-1} *vs* 40 s^{-1} on perspex	glass *vs* perspex at 40 s^{-1}
A0A0P8DQC9	HLUCCO16_09180	Uncharacterized protein	1.95			
A0A0N8KPF0	HLUCCO16_09310	ATP synthase subunit delta	4.34	3.88		
A0A0P7ZV78	HLUCCO16_17545	OMF family outer membrane protein	2.31			
A0A0P8BGT0	HLUCCO16_19320	Phosphomannomutase	1.86			
A0A0P8BV27	HLUCCO16_19665	Uncharacterized protein	-3.10			
A0A0C1UQ05	QQ91_22430	Aconitate hydratase	4,00			
K9XV32	Sta7437_1968	Polyribonucleotide nucleotidyltransferase	1.37			
A0A168SH97	AY600_08725	Uncharacterized protein		3.31		
A0A522XDZ7		Superoxide dismutase			6.42	
A0A522XFY9		Uncharacterized protein			-2.97	
A0A2C6UZD5		Aldehyde dehydrogenase (Fragment)				3.59
A0A522XJH6		DUF2862 domain-containing protein				4.12
A0A0P8BNN3	HLUCCA11_10745	Phycocyanin, beta subunit				4.98
A0A0T7BVN2	IJ00_20275	Elongation factor Tu				3.28

5.3.2.2 Linking DEPs to the functional categories involved

Around 39.6% of the DEPs were related to metabolic processes and 11% with transport (Supplementary Material, Figure S 5.6). Additionally, 4.9% and 3.3% were associated with the regulation of biological processes and response to a stimulus, respectively. Among the 34 DEPs identified on the glass surface relatively to perspex (Figure 5.3A), nine of them overlapped with results from biofilm cells formed on glass at 4 s^{-1} vs 40 s^{-1} (Figure 5.3B, Figure 5.4). It is noteworthy that among these nine DEPs, a protein related to allophycocyanin was down-regulated in both comparisons, which suggests that compared to perspex at 40 s^{-1}, the expression of this phycobiliprotein was decreased on glass (Figure 5.3A) and at 4 s^{-1}, respectively (Figure 5.3B, Table 5.1).

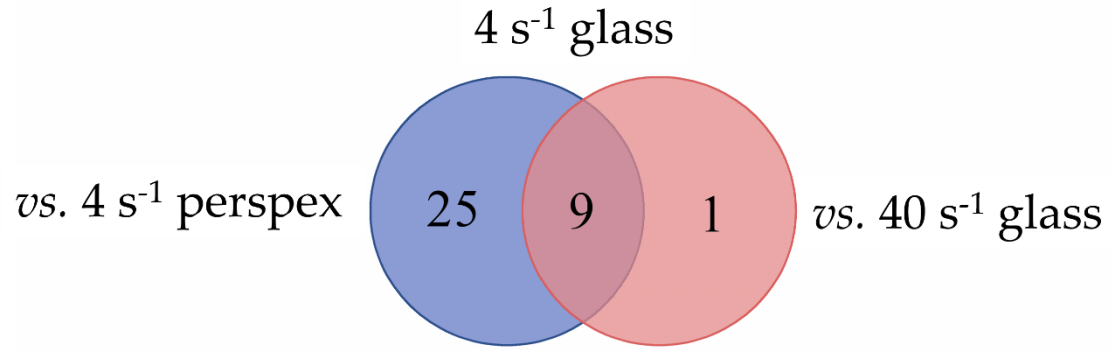

Figure 5.4. Venn diagram displaying the unique and shared DEPs found between 4 s^{-1} glass *vs* 4 s^{-1} perpex and 4 s^{-1} glass *vs* 40 s^{-1} glass.

The same 8 up-regulated proteins were identified when comparing biofilms formed on glass and perspex at 4 s^{-1} (Figure 5.3A) and when comparing biofilms formed on glass at both shear rates (Figure 5.3B, Table 5.1). These proteins are mainly involved in metabolic process, photosynthetic activity, binding and transport, similarly to the unique 19 up-regulated sequences found in the biofilms developed on glass at 4 s^{-1} in comparison to perspex (Figure 5.5). Among the eight shared proteins, a protein related to elongation factor Tu was identified (A0A2T1FHG8, Figure 5.3A, B, Table 5.1). Indeed, elongation factors have already been described as virulence factors and associated with filament formation (López-Ochoa *et al.*, 2017) and biofilm formation (Qayyum *et al.*, 2016) in different organisms (Harvey *et al.*, 2019). However, from the data obtained in the present study, it is possible to consider that this may not be the major factor for increased biofilm development. In fact, the up-regulation of an additional elongation factor Tu was also observed on biofilm cells developed at 40 s^{-1} in glass compared to perspex (A0A0T7BVN2; Table 5.1), and no considerable biofilm increase was observed in that case (Supplementary Material, Figure S 5.4B, D, F, H). Moreover, an elongation factor P (AY600_12795) was down-regulated on glass when compared to biofilms formed on perspex at 4 s^{-1} (Figure 5.3A, Table 5.1). Therefore, additional pathways and/or factors must have contributed to cyanobacterial biofilm development in these conditions. Additional up-regulated proteins shared between biofilms formed on glass and perspex at 4 s^{-1} (Figure 5.3A) and biofilms developed at 4 s^{-1} and 40 s^{-1} on glass (Figure 5.3B) include ribosomal proteins, proteins related to phycobilisome rod-core linker polypeptide CpcG, cytochrome c6, ATP

synthase and two uncharacterized proteins (Table 5.1). It is noteworthy that both ribosomal proteins and those related to photosynthesis, as well as phycobilisome rod-core linker polypeptide CpcG have already been found in a previous qualitative proteomic study performed on biofilm cells from two different cyanobacterial species (Romeu et al., 2020). Since the same surfaces and hydrodynamic conditions were used in both studies, this suggests the relevance of this set of proteins in the cyanobacterial biofilm development in these conditions.

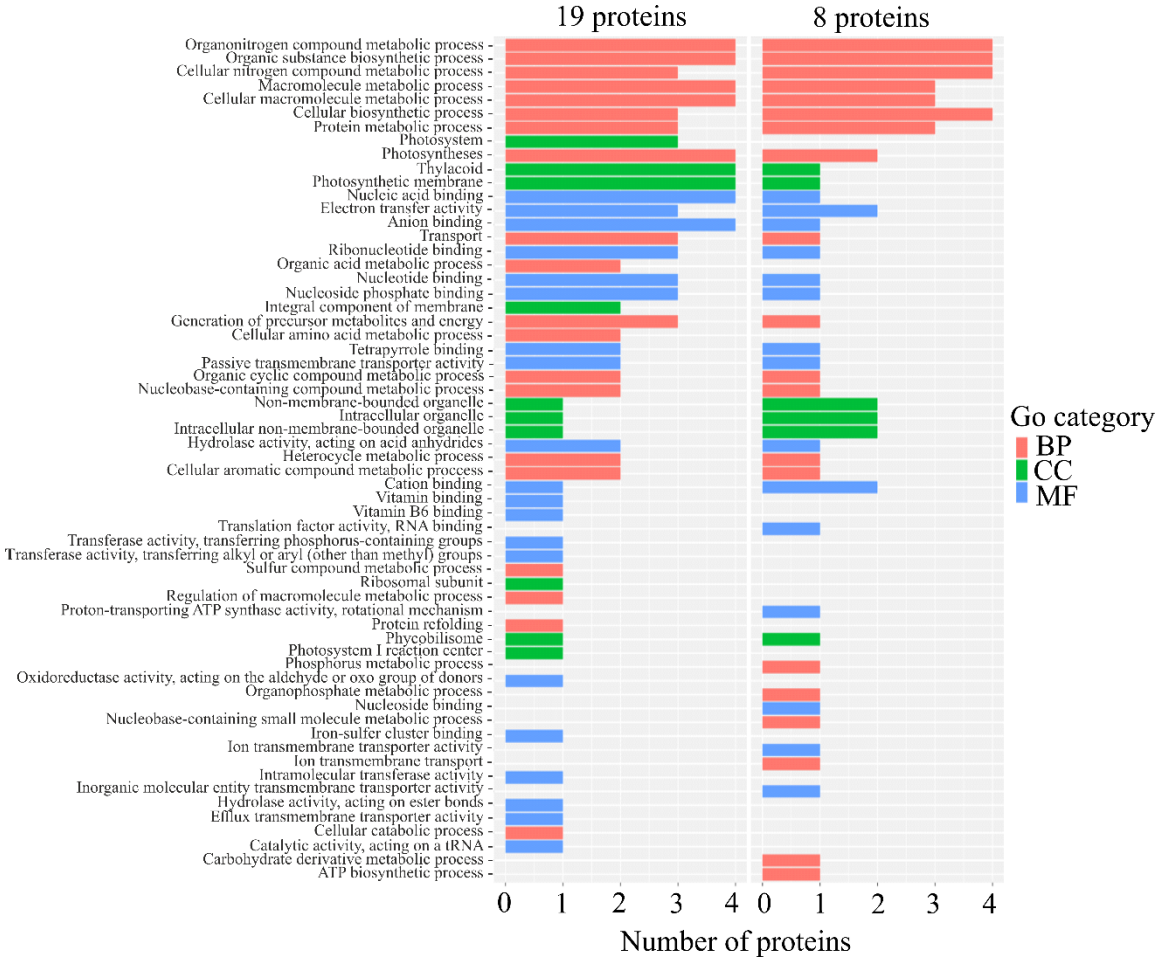

Figure 5.5. Functional annotation of the three major GO Categories: Biological Process (BP), Molecular Function (MF) and Cellular Components (CC) according to the GO Distribution by Level (4). The figure shows the number of sequences (number of proteins) in a descendent manner matching GO-terms of the unique up-regulated DEPs (19 proteins) and the eight shared DEPs (8 proteins), overlapped between the comparison glass *vs* perspex at 4 s^{-1} and 4 s^{-1} *vs* 40 s^{-1} on glass. More details about GO annotation can be found in Supplementary Material, Table S 5.2.

Among the two uncharacterized proteins shared between these two paired-comparison, proteins involved in the electron transport pathway of photosynthesis

activity (A0A0P8BXS9) and related with calcium ion binding (A0A168VPC8) were identified. In addition, the unique protein not shared between glass *vs* perspex at 4 s^{-1} and 4 s^{-1} *vs* 40 s^{-1} on glass conditions was also an uncharacterized protein related to calcium ion binding (A0A168SH97, Figure 5.4, Table 5.1), suggesting that calcium may play an important role in these cyanobacterial biofilms. Moreover, these two uncharacterized proteins related to calcium ion binding are disordered proteins. Although disordered proteins do not have unique structures, they possess biological functions. It is expected that disordered proteins possess some advantages over ordered proteins due their exceptional spatio-temporal heterogeneity and high conformational flexibility (Uversky, 2019). Indeed, they are more likely to maintain stability under extreme conditions due to the lack of structural conservation (Liu and Huang, 2014). In a real scenario, these proteins can perform their functions in complex environments, which can be affected by various factors such as hydrodynamic conditions or surface properties. Several proteins with disordered domains were identified in the cement-multicomplex adhesive-system from goose barnacles, applying a similar proteogenomic approach (Domínguez-Pérez *et al.*, 2020; Romeu *et al.*, 2021). Moreover, additional studies described surface-coupling proteins as structurally disordered, which confers them elasticity (Cheng *et al.*, 2010; X. Wang *et al.*, 2018).

Between the unique 19 up-regulated sequences found in the biofilms developed on glass at 4 s^{-1} when compared to perspex (Figure 5.3A, 5.5, Table 5.1), uncharacterized proteins were also differentially expressed including one disordered protein (A0A168VLH9). In addition, proteins like a beta-propeller domain-containing protein, a methanol dehydrogenase (AY600_09620), the chaperone protein DnaK (A0A552JAH2), SLH domain-containing proteins (A0A349JJF9 and A0A522XGJ2) and OMF family outer membrane protein (HLUCCO16_17545) were also identified as DEPs. Although secreted beta-propeller proteins are largely unexplored in bacteria and even more in cyanobacteria, some studies suggest that they may be involved in the maintenance of the cell envelope, secretion, adhesion, and host immune responses (Fu *et al.*, 2018; Kim *et al.*, 2018). A study on *Vibrio cholerae* biofilms showed that the beta-propeller domains might form interactions with proteins or other substrates (including polysaccharides) within the biofilm matrix (Kaus *et al.*, 2019). In a study on *Acinetobacter baumannii* cells it was

observed that the expression of a chaperone-usher secretion system is required for pili formation and the concomitant attachment to plastic surfaces and biofilm formation (Tomaras *et al.*, 2003). DnaJ2 and DnaK2 together behave as an RNA chaperone shielding the psbAII transcript from RNaseE-intervened degradation, in this way helping to prevent the inhibition of photosynthesis under conditions of stress (Ehrnsperger *et al.*, 1997). Although cyanobacteria have many dnaK genes in their genome (Haslbeck *et al.*, 2005), there is no knowledge regarding their relation to biofilm development. S-layer homology (SLH) domains are cell wall-targeting modules employed by various Gram-positive and -negative bacteria to display extracellular proteins such as enzymes and outer membrane proteins on the bacterial cell surface (Engelhardt and Peters, 1998). A study performed by Janesh *et al.* (2013), demonstrated the involvement of the SLH domain-containing protein SlhA in swarming and biofilm formation of *Paenibacillus alvei* (Janesch *et al.*, 2013). Outer membrane proteins and outer membrane vesicles (OMV) have been relevant in biofilm studies. It was demonstrated that *Helicobacter pylori* TK1402 exhibited a strong ability for biofilm formation, and its OMVs play an important role in the formation of their extracellular matrix (Yonezawa *et al.*, 2011). A proteomic study of *Burkholderia multivorans* C1576 revealed that OMVs production is the most important source of proteins for the biofilm matrix (Terán *et al.*, 2020). OMVs are highly enriched in outer membrane proteins and siderophores. Of note, some of the identified proteins were proteins involved in reactive oxygen species (ROS) scavenging. Therefore, proteins responsible for detoxification of ROS are also a relevant fraction of both matrix- and OMVs-associated proteins. Accordingly, the data obtained in this study showed the possible role of a beta-propeller domain-containing protein, chaperone DnaK, SLH domain-containing proteins and an OMF family outer membrane protein on biofilm developed on glass at 4 s^{-1} in comparison to perspex for this cyanobacterial strain (Figure 5.3A, 5.5, Table 5.1).

Additionally, biofilm development on perspex at 4 s^{-1} was higher than at 40 s^{-1} (Figure 5.1B, D, F). The proteomic analysis only revealed the underexpression of an uncharacterized protein (A0A522XFY9) and overexpression of an enzyme, superoxide dismutase (SOD) at 4 s^{-1} (A0A522XDZ7, Figure 5.3C, Table 5.1) when compared with biofilm formed at 40 s^{-1}. Similar to previous uncharacterized proteins, the down-regulated

protein identified in this paired comparison presented a disordered domain. SOD are ubiquitous enzymes that scavenge superoxide radicals to peroxide and molecular oxygen through alternate oxidation and reduction of their metal ions. Since cyanobacteria produce ROS that can damage cellular components leading to cell death, the co-evolution of an antioxidant system was necessary for their survival and SOD is the initial enzyme evolved to alleviate this toxic effect (Priya *et al.*, 2007). Several SOD genes were found on cyanobacteria strains (Kaneko *et al.*, 1996; Shirkey *et al.*, 2000; Zhao *et al.*, 2007), even on filamentous strains (Campbell and Laudenbach, 1995; Priya *et al.*, 2007). Besides their role in oxidative stress and resistance, the relevance of SOD has already been reported in several studies from other bacteria than cyanobacteria on adhesion, biofilm formation and invasion of epithelial cells (Trémoulet *et al.*, 2002; Bink *et al.*, 2011; Suo *et al.*, 2012; Y. Wang *et al.*, 2018; Najmuldeen *et al.*, 2019). Therefore, the higher biofilm development observed on perspex at 4 s^{-1} can also be related to the up-regulation of this enzyme in this filamentous cyanobacterial strain.

Moreover, with a higher biofilm development at 4 s^{-1}, the production of ROS may have increased along with respiration and photosynthesis, which may have prompted an increased activity of this enzyme to prevent damage caused by oxidative stress. A study on *Klebsiella pneumoniae* also shows the role of SOD in biofilm architecture and cell morphology (Najmuldeen *et al.*, 2019). Although the detailed mechanisms of alterations in biofilm architecture are unclear, it could be speculated that *Klebsiella pneumoniae* biofilm architecture is significantly influenced by oxygen and by the activity of SOD. Therefore, alteration in biofilm architecture might occur in response to redox balance, which is essential for cellular function and survival. In the present study, a different structure was also observed for biofilms developed on perspex at 4 s^{-1} and 40 s^{-1} (Figure 5.3C, D). Once again, SOD can present an active role in the biofilm architecture of this cyanobacterial strain between biofilms developed on perspex at 4 s^{-1} and 40 s^{-1}. The proteomic changes of SOD on all replicates from each condition throughout the experiment can be found in Supplementary Material, Figure S 5.7.

Finally, the total of 27 up-regulated DEPs found on biofilm cells from glass at 4 s^{-1} compared to perspex, shows a different enrichment pattern than the seven down-regulated DEPs at the same condition when compared to the ones encoded in the whole

proteome (Figure 5.6). In the 27 up-regulated DEPs, the GO terms "electron transfer activity" and "electron transport chain", processes related to electron chain and actively involved in photosynthesis, were found as enriched categories (Figure 5.6, Supplementary Material, Table S 5.2). On the other hand, in the seven down-regulated DEPs, GO terms related to enzyme binding and activity were found as an enriched category when compared with the total of proteins identified (Figure 5.6, Supplementary Material, Table S 5.2). These findings confirm that cyanobacterial biofilm development is closely associated with the up-regulation of the photosynthesis process.

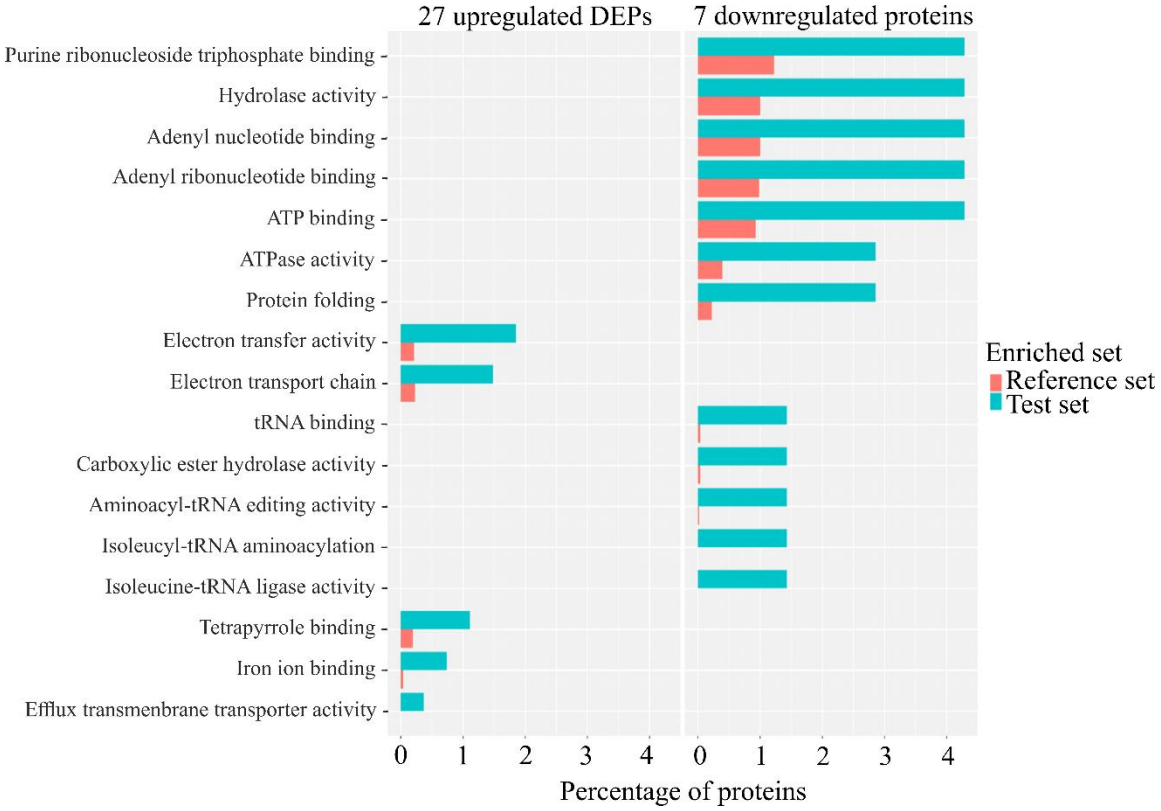

Figure 5.6. Enrichment of DEPs revealed by the hypergeometric distribution significance test. The enriched GO terms (Fisher's exact test, $P < 0.05$) are represented by a stacked bar (in green) as the percentage of the GO terms found in the References Set (in red, represent all 546 identified). Each panel displays the set of 27 up-regulated and seven down-regulated DEPs found in the comparison glass *vs* perspex at 4 s^{-1}. More details about GO annotation can be found in the Supplementary Material, Table S 5.2.

The analysis of 41 DEPs found in this study is extremely important. Indeed, combining macroscopic evaluation of biofilm development with information about DEPs from proteomic analysis may provide new clues for mitigating marine biofouling. Since

this study identified which proteins were down and up-regulated under different biofilms conditions, novel antifouling strategies which target these proteins can potentially be developed.

5.4 Conclusions

The present study, which presented several analyses, from the molecular to the macroscopic level, revealed the importance of combining different approaches to evaluate a complex phenomenon like biofilm formation. Based on macroscopic evaluation (biofilm biomass, thickness, and chlorophyll *a* quantification), the results showed that hydrodynamic effects might be more important than surface properties in the development of cyanobacterial biofilms. However, on the proteomic approach, a large differential protein expression was found between biofilms formed on glass and perspex at 4 s^{-1}. New quantitative clues were provided to understand the diversity and function of proteins in cyanobacterial biofilm development. Combining all approaches applied in this study, the higher biofilm development at 4 s^{-1} may be related to up-regulation of SOD and differential expression of some uncharacterized proteins and proteins related to the photosynthetic process. On the other hand, the differential biofilm development observed on different surfaces is probably associated with different expression of a beta-propeller domain-containing protein, chaperone DnaK, SLH domain-containg proteins and/or an OMF family outer membrane protein and the differential expression of some uncharacterized proteins on this cyanobacterial strain. Indeed, the fact that 50% of uncharacterized proteins found as DEPs in this study presented a disordered domain was a significant finding for cyanobacterial biofilm studies as these proteins represent complex systems that are specifically regulated by various means. Some of those uncharacterized proteins could be considered as a new relevant group of biofilm adaptation proteins since structural disorder can be beneficial for their resistance to environmental perturbations.

Advances in "omics" technologies are constantly evolving and their application to marine biofilm studies is an emerging approach that can lead to new improvements in antifouling strategies. Future studies should focus on different cyanobacterial strains, as

well as evaluation of EPS secretion on these different biofilm conditions. Proteomic analysis should also be performed at different biofilm stages to evaluate differences in proteomic profile along biofilm formation and maturation. Moreover, different omics approaches, such as metabolomic studies, may be useful to identify additional pathways that can be involved in these biofilm development conditions. These further studies should also focus on cyanobacterial gene modifications or deletions, which encode relevant proteins reported in the present study as crucial for biofilm development to clarify their role on biofilm phenotypes.

5.5 Supplementary Material

Detailed protocol S 5.1. Detailed description of the single-pot solid-phase-enhanced sample-preparation (SP3) protocol adapted from Hughes *et al.*, (2019).

Prior to the digestion, 100 µg of extracted proteins in approximately 5 µL were reduced in 45 µL SDT in new 1.5 mL Eppendorf tubes. Then, alkylation of samples was performed with 10 µL of 0.1 M iodoacetamide (AppliChem) in 8 M Urea, 0.1 M Tris/HCl pH 8.5 for 30 min. in the dark at room temperature.
Digestion followed Hughes *et al.*, 2019 SP3 for proteomics experiments with some modifications. New magnetized beads (Sera Mag SP3 beads, CAT#45152105050250 and CAT#65152105050250, GE Healthcare) were initially washed and reconstituted in water (HPLC grade, VWR) at a final concentration of 10 $\mu g.\mu L^{-1}$ (from an initial stock concentration of 50 $mg.mL^{-1}$), using a magnetic rack (MagnaRack, Invitrogen) for 1 min. A 10:1 ratio (beads:proteins) was reached by adding 100 µL of beads to each tube followed by pipette mixing. Then, 160 µL of absolute ethanol (molecular biology grade, Fisher) was added to achieve 50% v/v, also followed by pipette mixing. Incubation was performed in an Eppendorf Thermomixer with shaking (1000 rpm) for 10 min at room temperature. Then, tubes with samples were placed in the magnetic rack and the supernatant was removed. Beads were gently reconstituted in 180 µL of 80% ethanol. Tubes were placed again in a magnetic rack and the supernatant was discarded. This cleaning step was performed three times. Extraction was then performed gently by adding 100 µL of ammonium bicarbonate (0.1 M pH 8) containing 0.04 $\mu g.\mu L^{-1}$ Trypsin/rLysC Mix (MS grade, Promega) to each tube at a 1:50 ratio (enzyme:protein) followed by an incubation period of 14 h at 37 °C with mixing at 1000 rpm. Then, 1.300 mL of 100% acetonitrile (HPLC grade, Chem-Lab NV) was added and incubated for 18 min at 1000 rpm. Beads were spun down, and tubes placed in the magnetic rack. The supernatant was discarded, and beads were washed twice with 180 µL acetonitrile 100%. After removing the supernatant, 100 µL ammonium bicarbonate (Fluka) 0.05 M was added to the tubes and incubated for 5 min at 1000 rpm. After bead spin and magnetising, the supernatant containing the tryptic peptides was transferred to clean 1.5 mL Eppendorf tubes. The peptide concentration was estimated using the DeNovix (A280 application). Acidification was performed by adding 20 µL of formic acid 5% v/v (Optima LC/MS grade, Fisher Chemical) to the samples. Afterwards, tryptic peptides were dried in a Concentrator Plus vacuum rotator (Eppendorf, Hamburg, Germany) and resuspended in 25 µL formic acid (FA: 0.1% v/v). The final concentration was determined with 2 µL of digested peptides, measured indirectly by optical density (OD) at 280 nm using a DeNovix DS-11 Spectrophotometer (DeNovix Technologies, Wilmington, Delaware, USA).

Reference:

Hughes, C.S., Moggridge, S., Müller, T., Sorensen, P.H., Morin, G.B., Krijgsveld, J., 2019. Single-pot, solid-phase-enhanced sample preparation for proteomics experiments. Nat. Protoc. 14, 68–85. https://doi.org/10.1038/s41596-018-0082-x

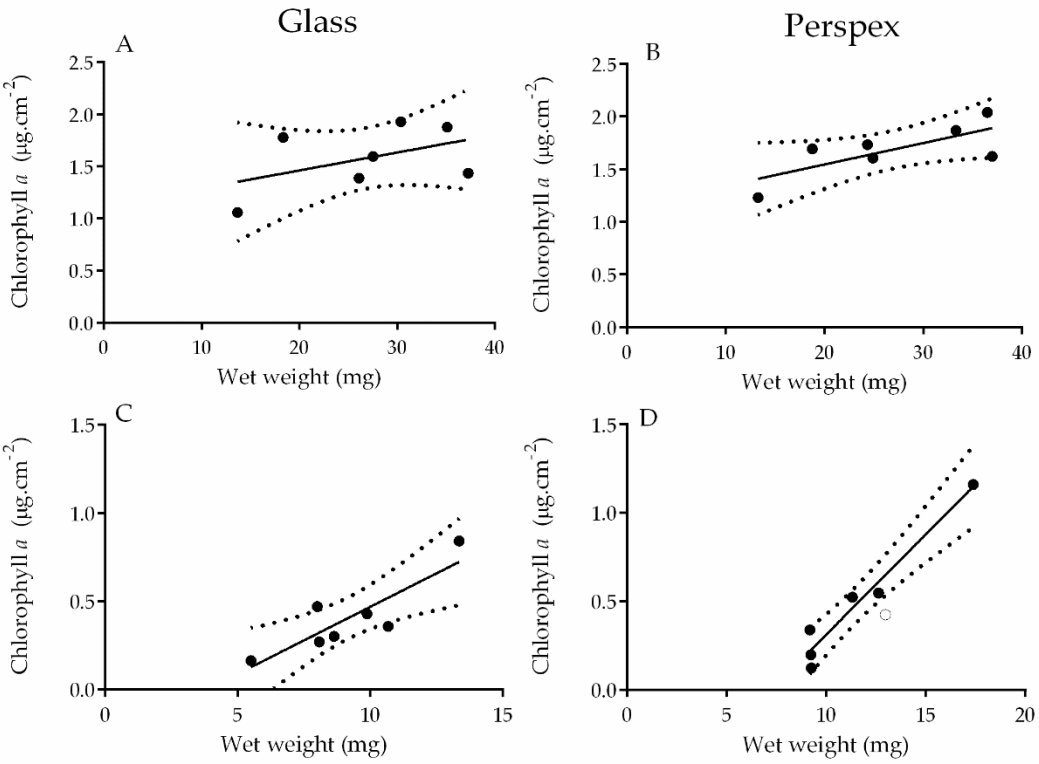

Figure S 5.1. Correlation between wet weight and chlorophyll *a* content on biofilm development from unidentified filamentous cyanobacterium LEGE 06007. Biofilm development in glass (A, C) and perspex (B, D) at two different shear rates, 4 s^{-1} (A, B) and 40 s^{-1} (C, D). Full line represents the linear regression, and the dashed line represents the confidence limits (95%). Closed symbols refer to data points that were considered for the regression (all except one) and open symbols refer to data points that were excluded from the regression.

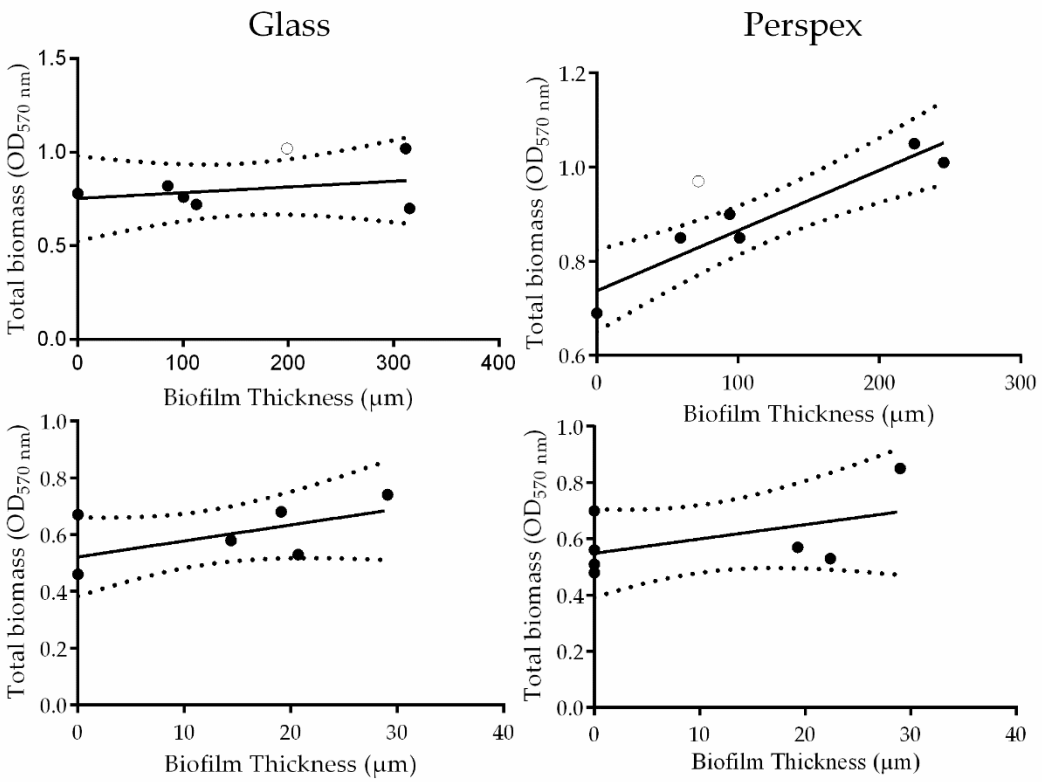

Figure S 5.2. Correlation between crystal violet and biofilm thickness on biofilm development from unidentified filamentous cyanobacterium LEGE 06007. Biofilm development in glass (A, C) and perspex (B, D) at two different shear rates, 4 s^{-1} (A, B) and 40 s^{-1} (C, D). Full line represents the linear regression, and the dashed line represents the confidence limits (95%). Closed symbols refer to data points that were considered for the regression (all except two) and open symbols refer to data points that were excluded from the regression.

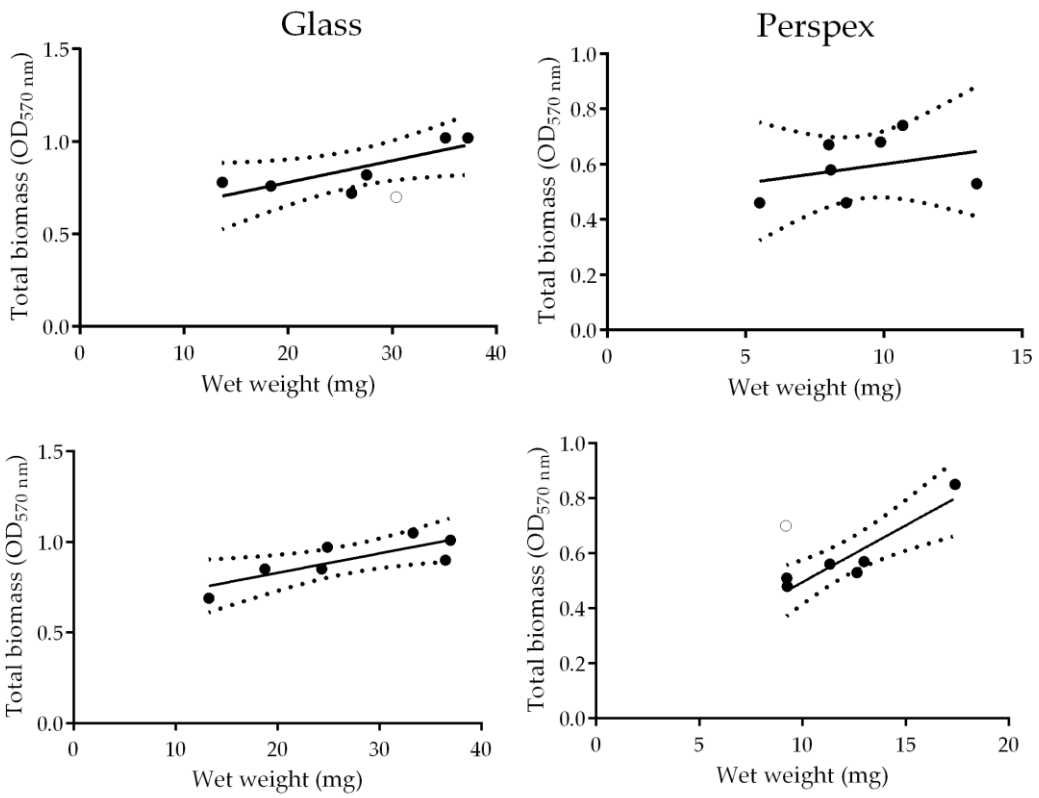

Figure S 5.3. Correlation between crystal violet and wet weight on biofilm development from unidentified filamentous cyanobacterium LEGE 06007. Biofilm development in glass (A, C) and perspex (B, D) at two different shear rates, 4 s^{-1} (A, B) and 40 s^{-1} (C, D). Full line represents the linear regression, and the dashed line represents the confidence limits (95%). Closed symbols refer to data points that were considered for the regression (all except two) and open symbols refer to data points that were excluded from the regression.

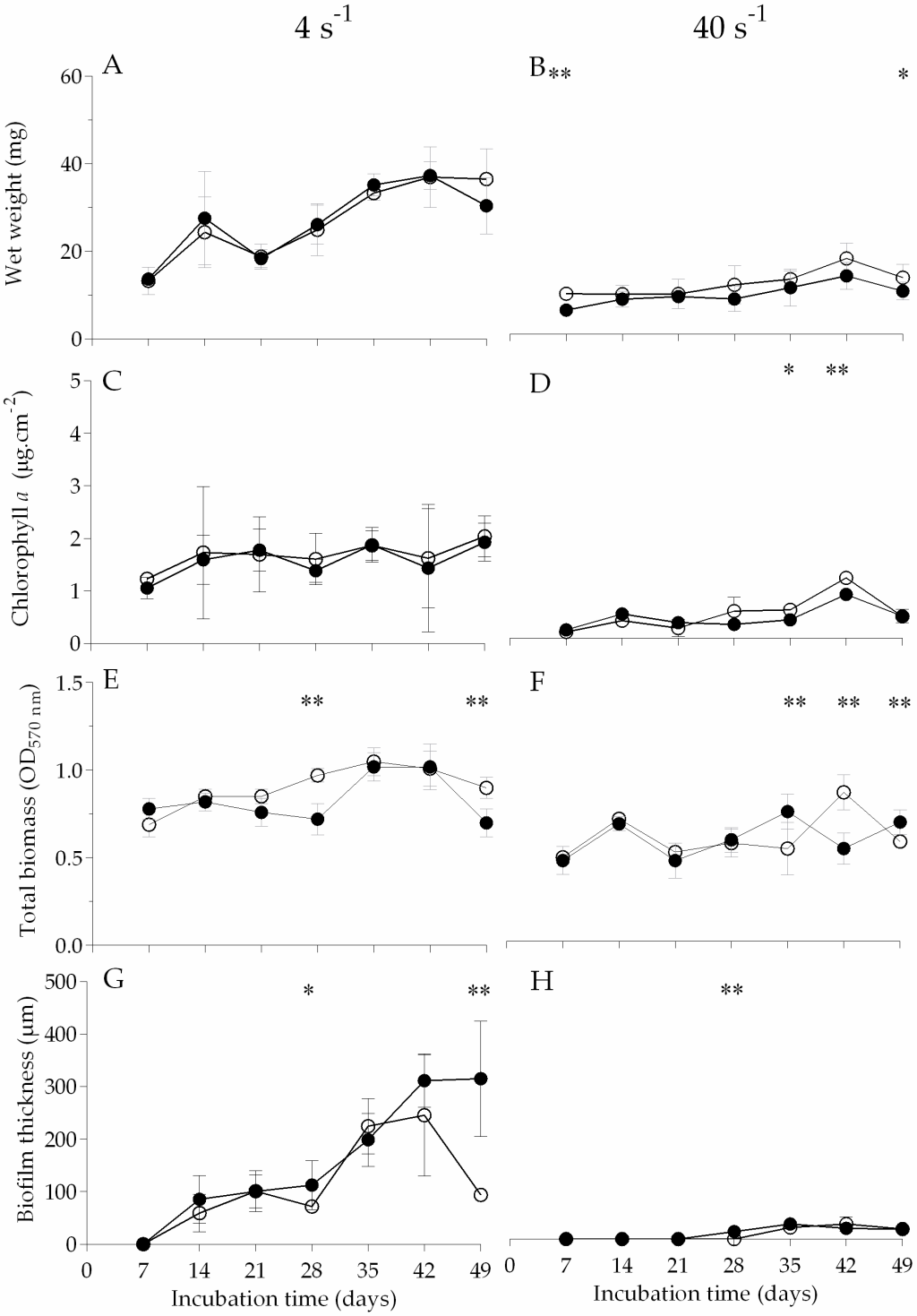

Figure S 5.4. Evaluation of unidentified filamentous cyanobacterium LEGE 06007 biofilm development under the same hydrodynamic condition on different surfaces. The parameters analysed refer to wet weight (A, B), chlorophyll *a* quantification (C, D), total biomass quantification by CV assay (E, F) and biofilm thickness (G, H). Biofilms were formed at 4 s^{-1} (A, C, E, G) or 40 s^{-1} (B, D, F, H) on two different surfaces, glass (closed circles) and perspex (open circles) for 49 days. Standard deviations from two biological assays with three replicates each, are represented.

Symbols *; ** indicate statistically different values for $P < 0.1$ and $P < 0.05$ (respectively) at each incubation time.

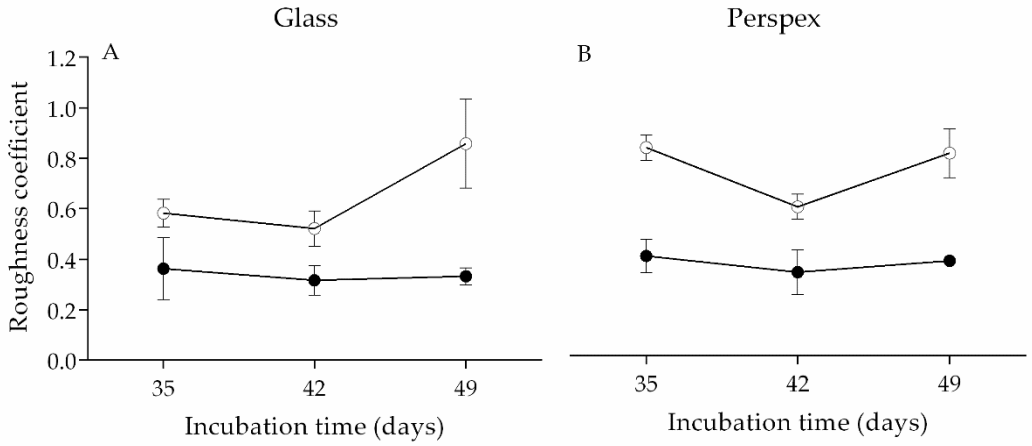

Figure S 5.5. Evaluation of roughness coefficient of unidentified filamentous cyanobacterium LEGE 06007 biofilm development on glass (A) and perspex (B) at 4 s^{-1} (closed circles) and 40 s^{-1} (open circles) between day 35 and day 49.

Table S 5.1. Summary of proteomic analysis.

Available at https://doi.org/10.1016/j.envres.2021.111566

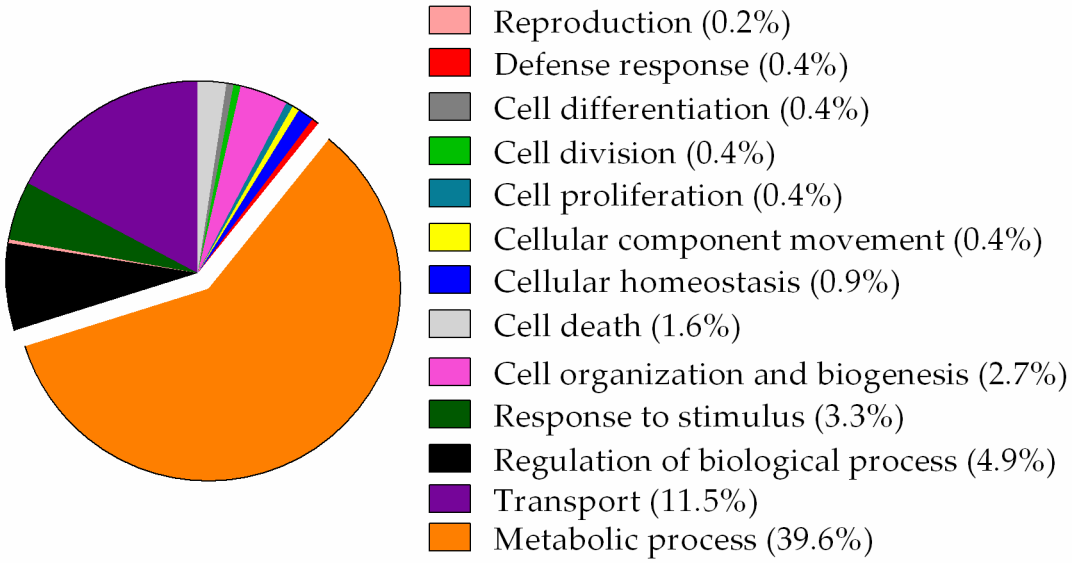

Figure S 5.6. Distribution of total proteins identified according to biological process (54% of proteins identified without associated biological process are not shown in this graph).

Table S 5.2. DEPs description and GO annotation.

Available at https://doi.org/10.1016/j.envres.2021.111566

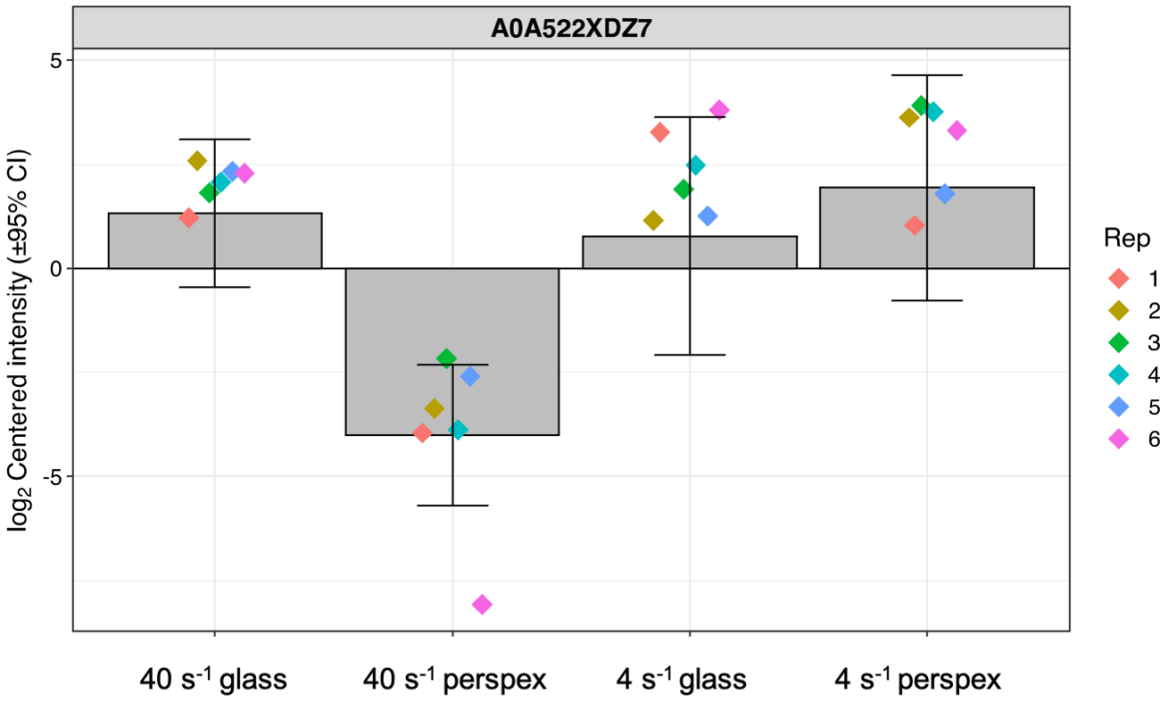

Figure S 5.7. Bar plots depicting the content of the superoxide dismutase (SOD) throughout the experiment. The fold changes of SOD content of all replicates from each condition studied (40 s^{-1} glass, 40 s^{-1} perspex, 4 s^{-1} glass and 4 s^{-1} perspex) are depicted as centered log_2 intensities. Error bars represent the 95% confidence intervals

6.

6 Hydrodynamic conditions affect the proteomic profile of marine biofilms formed by filamentous cyanobacterium

The contents of this chapter as published as:

Romeu M.J., Domínguez-Pérez, D., Almeida, D., Morais, J., Araújo, M.J., Osório, H., Campos, A., Vasconcelos, V., and Mergulhão, F.J. (2022) Hydrodynamic conditions affect the proteomic profile of marine biofilms formed by filamentous cyanobacterium. *npj Biofilms Microbiomes* **8**: 80.

Abstract

Proteomic studies on cyanobacterial biofilms can be an effective approach to unravel metabolic pathways involved in biofilm formation and, consequently, obtain more efficient biofouling control strategies. Biofilm development by the filamentous cyanobacterium *Toxifilum* sp. LEGE 06021 was evaluated on different surfaces, glass and perspex, and at two significant shear rates for marine environments (4 s^{-1} and 40 s^{-1}). Higher biofilm development was observed at 4 s^{-1}. Overall, about 1,877 proteins were identified, and differences in proteome were more noticeable between hydrodynamic conditions than those found between surfaces. Twenty Differentially Expressed Proteins (DEPs) were found between 4 s^{-1} *vs.* 40 s^{-1}. On glass, some of these DEPs include phage tail proteins, a carotenoid protein, cyanophynase glutathione-dependent formaldehyde

dehydrogenase, and the MoaD/ThiS family protein, while on perspex, DEPs include transketolase, dihydroxy-acid dehydratase, iron ABC transporter substrate-binding protein and protein NusG. This study contributes to developing a standardized protocol for proteomic analysis of filamentous cyanobacterial biofilms. This kind of proteomic analysis can also be useful for different research fields, given the broad spectrum of promising secondary metabolites and added-value compounds produced by cyanobacteria as well as for the development of new antibiofilm strategies.

Keywords: marine biofouling, cyanobacterial biofilms, shotgun proteomics, hydrodynamics, shear rates, fouling surfaces

6.1 Introduction

Over the past years, eutrophication and climate changes have been promoting cyanobacterial blooms in aquatic environments (Gaget *et al.*, 2017). In addition to threatening the ecosystem, this phenomenon also degrades water quality for fisheries and public health (Huisman *et al.*, 2018). Cyanobacteria can also affect animal and human health through their ability to produce cyanotoxins (Miller *et al.*, 2010; Gibble *et al.*, 2016; Regueiras *et al.*, 2018; Breinlinger *et al.*, 2021). These toxins can also have detrimental effects through ingestion of contaminated food or even by drinking water during recreational activities (Buratti *et al.*, 2017). Moreover, cyanobacteria blooms from benthic mat proliferations have increased worldwide (Gaget *et al.*, 2017). Indeed, cyanobacteria are the major constituents of marine biofilms, and they respond quickly to environmental pattern changes, which allows them to have a diverse distribution. Besides the contamination of aquaculture facilities (King *et al.*, 2006), marine biofilms cause problems related to the corrosion of different facilities and submerged equipment (Delauney *et al.*, 2010). Marine biofouling can also lead to increased fuel consumption in ships and associated pollution (Schultz *et al.*, 2011; Davidson *et al.*, 2016), as well as the spread of invasive non-indigenous species on marine vessels between different ecosystems (Mineur

et al., 2007). Overall, marine biofouling challenges include environmental, as well as economic and health concerns (Caruso, 2020).

Several cues have been identified regarding cyanobacterial adhesion and biofilm formation, particularly for *Synechocystis* (Duggan *et al.*, 2007; Schatz *et al.*, 2013; Agostoni *et al.*, 2016; R. Allen *et al.*, 2018), *Thermosynechococcus elongatus* (Enomoto *et al.*, 2014), *Microcystis aeruginosa* (Zilliges *et al.*, 2008), *Anabaena* sp. PCC 7120 (Oliveira *et al.*, 2015), *Synechococcus elongatus* PCC 7942 (Parnasa *et al.*, 2016) and *Nostoc punctiforme* (Duggan *et al.*, 2007).

Advancements in omics technologies are continuously progressing. Although cyanobacteria proteomics has dealt with many technical challenges (Pandhal *et al.*, 2009), cyanobacteria molecular biology is a promising field for further advancements (Sun *et al.*, 2018; Santos-Merino *et al.*, 2019). The fouling surface properties and shear rate are two parameters that have a critical impact on marine biofilms (Faria, Teixeira-Santos, Romeu, *et al.*, 2020, 2021). In a previous qualitative proteomic study, the proteomic profile of biofilm cells from two cyanobacterial strains developed on glass and perspex, and at different shear forces was analysed (Romeu *et al.*, 2020). The results revealed that variances in protein composition were more noticeable in biofilms formed under different hydrodynamic conditions than in those formed on different surfaces (Romeu *et al.*, 2020). However, to identify pathways that are triggered under different circumstances to which cells were subjected, quantitative proteomic analyses are the most relevant tool (Battchikova *et al.*, 2015; Muthusamy *et al.*, 2017). A recent quantitative study performed with the unidentified filamentous cyanobacterium LEGE 06007 revealed 41 Differentially Expressed Proteins (DEPs) (Romeu *et al.*, 2021). The proteomic profile can help in the characterization of virulence factors and cellular processes involved in biofilm regulation. Besides improving the fundamental understanding of biofilm development and behavior, the identification of these proteins using high throughput proteomic tools provides new insights into the response to stress conditions, including cell signaling and stress response pathways that are activated under different conditions. Therefore, as more proteins and their roles in biofilm development are explored, novel potential targets for biofilm control may be discovered. Moreover, by knowing which proteins are produced under stress conditions and which metabolic pathways are activated, it may be possible that new

metabolites can be identified with antibiofilm properties. Cyanobacteria are known to produce nearly 800 bioactive secondary metabolites, and it is known that cyanobacteria are able to interfere with other organisms in their communities through the release of compounds into the surrounding medium (Leão *et al.*, 2010). The isolation of these metabolites led to the discovery of a strong inhibitory activity against other marine organisms and is currently being explored for the production of antifouling coatings (Antunes, Pereira, *et al.*, 2019). However, data available on cyanobacterial proteomic are still scarce (Babele *et al.*, 2019) and most of the studies focus on well-studied model cyanobacteria, such as the unicellular cyanobacterium *Synechocystis* sp. PCC 6803 (Jahn *et al.*, 2018). Different cyanobacterial strains should be considered, and this is of particular importance for filamentous cyanobacterial strains, in which the stress and predation resistance, as well as the improved resource acquisition, may be beneficial (Claessen *et al.*, 2014). However, the standardization of the proteomic protocol in these organisms is a hard task, and the knowledge needs to be increased incrementally. This work mainly focuses on the improvement of proteomic methodology as well as on the significance of the results obtained and the raw data availability. Due to the high production of cellulose-rich pigments by cyanobacteria, all sample preparation, protein extraction and accurate quantification is a difficult endeavor and hinder the standardization of the proteomic protocol for these organisms. This study contributes to the development of a standardized protocol for proteomic analysis of filamentous cyanobacterial biofilms, enabling other groups to advance their research in this field and facilitating inter-lab comparisons. Moreover, this kind of proteomic analyses can also be useful for different research fields given the broad spectrum of promising secondary metabolites and added-value compounds produced by cyanobacteria (Lau *et al.*, 2015) that can be used in biotechnological applications, cosmetic, feed and food industries (Manirafasha *et al.*, 2016) and medical purposes (Pagels *et al.*, 2019). Synechococcales order includes both filamentous and single-celled types and involves several cyanobacteria genera, among which the ubiquitous *Nodosilinea, Synechococcus, Cyanobium* and *Leptolyngbya* genus. Unidentified Synechococcales include about 32 different strains, and some of them are able to produce common cyanotoxins such as β-methylamino-L-alanine (Mai *et al.*, 2018; Ramos *et al.*, 2018). These strains can be found in different ecosystems like brackish water,

freshwater, marine, and even hypersaline environments. Moreover, cyanobacterial strains from Synechococcales are present in distinct geographies around the world, including Portugal, Chile, Mexico, and Morocco (Ramos *et al.*, 2018). The Blue Biotechnology and Ecotoxicology Culture Collection (LEGE-CC) is a biological resource center, which among several additional organisms, maintains different cyanobacterial strains (Mai *et al.*, 2018; Ramos *et al.*, 2018). The unidentified filamentous Synechococcales LEGE 06021 strain was used in this study, given the relevance of cyanobacteria on marine biofouling. To complete the current study, a genus identification of this cyanobacterial strain was performed. This study addresses biofilm development of this filamentous cyanobacterial strain, as well as its proteomic profile when subjected to different conditions of shear and surfaces. Therefore, this study aims to characterise the biofouling potential of this filamentous cyanobacteria, on a long-term assay, under two different hydrodynamic conditions and with two surfaces, as well as to explore the quantitative proteomic profile under these different biofilm development conditions.

6.2 Material and Methods

6.2.1 DNA extraction, amplification (PCR) and sequencing

A 50 mL culture of a cyanobacterium previously classified as unidentified filamentous Synechococcales LEGE 06021 (Ramos *et al.*, 2018) was grown and cells were harvested after 2 - 3 weeks. Total genomic DNA was extracted using the commercial PureLink Genomic DNA Mini Kit (Invitrogen, USA), according to the manufacturer's instructions provided for Gram-negative bacteria. To obtain the sequence of 16S rRNA gene, PCR amplification was performed using the 27F (Lane, 1991), CYA359F, CYA781R (Nübel *et al.*, 1997) and 1494R (Lane, 1991) oligonucleotide primers. PCR reactions were performed in a final volume of 20 μL containing 1x Green GoTaq Flexi Buffer, 2.5 mM of $MgCl_2$, 125.0 mM of each deoxynucleotide triphosphate, 1.0 μM of each primer, 0.5 U of GoTaq Flexi DNA Polymerase (Promega, Madison, WI, USA), 10 $mg.mL^{-1}$ of bovine serum albumin (BSA), and 10–30 ng of template DNA, on a Veriti™ 96-Well Thermal Cycler. The PCR conditions were as follows: initial denaturation at 95 °C for 2 min,

followed by 35 cycles of denaturation at 95 °C for 1 min, annealing at 50 °C for 45 s, and extension at 72 °C for 1 min, with a final extension step at 72 °C for 5 min. The PCR reactions were performed in duplicate. PCR products were separated by 1.5% agarose gel stained with SYBR® safe (Invitrogen,Waltham, MA, USA) and DNA fragments with the expected size were excised and purified using NZYGelpure (NzyTech, Genes and Enzymes, Lisbon, Portugal) according to the manufacturer's instructions. Sequencing was performed at GATC Biotech (Ebersberg, Germany) and the nucleotide sequence obtained was manually inspected for quality and assembled using the Geneious 11.1.5 software (Biomatters Ltd., Auckland, New Zealand). Possible chimera formation during the sequences was checked using the software DECIPHER (Wright *et al.*, 2012). The sequence obtained was inserted in the BLASTn (Basic Local Alignment and Search Tool for Nucleotides) database and the results were analysed. The sequence associated with this study was deposited in the GenBank database under the accession number ON258650.

6.2.2 Phylogenetic analysis

A total of 61 sequences were used in the final analysis, including 2 strains of *Gloeobacter violaceus* as outgroup, 58 sequences of cyanobacteria, including type, reference and related strains belonging to the orders Pseudanabaenales and Synechococcales were retrieved from GenBank (National Center for Biotechnology Information, NCBI, Bethesda, MD, USA), and 1 sequence of unidentified filamentous Synechococcales LEGE 06021 obtained in this work. Multiple sequence alignment was carried out using ClustalW in MEGA7 (Thompson *et al.*, 1994; Kumar *et al.*, 2016), and sequences were manually proofread and edited. The best fit model was assessed using jModelTest 2.1.10 (Darriba *et al.*, 2012) according to the Bayesian information criterion (BIC) and Akaike information criterion (AIC) scores. Maximum likelihood (ML) analysis was carried out using substitution model GTR+G+I with 1000 bootstrap resampling replicates using the MEGA7 software (Kumar *et al.*, 2016). The final phylogenetic tree was visualized and edited on iTOL (Interactive Tree of Life) (Letunic and Bork, 2021).

6.2.3 Organism and inoculum preparation

The cyanobacterium previously identified as unidentified filamentous Synechococcales LEGE 06021 was obtained from the Blue Biotechnology and Ecotoxicology Culture Collection (LEGE-CC) located at CIIMAR, Portugal(Ramos *et al.*, 2018). This cyanobacterial strain was firstly isolated from a sample scraped from a wave-exposed rock in the intertidal zone at Coxos beach, Santo Isidoro, Portugal (39.00455 N 9.425842 W). Cells were grown in 750 mL culture in Z8 medium(Kotai, 1972) supplemented with 25 $g.L^{-1}$ of synthetic sea salts (Tropic Marin) and B_{12} vitamin (Sigma Aldrich, Merck, Saint Louis, MO, USA). Cultures were performed under 14 h light (10–30 μmol photons m^{-2} s^{-1})/10 h dark cycles, at 25 °C.

6.2.4 Biofilm formation

In order to assess the biofouling potential on different surfaces, as well as to evaluate their protein expression profiles, biofilms were developed on glass (Vidraria Lousada, Lda, Portugal) and perspex (Neves & Neves, Lda, Portugal) coupons (1 cm^2). These represent typically submerged artificial surfaces found on different apparatus in aquatic environments such as aquaculture equipment, measuring devices and sensors, flotation spheres, moored buoys, underwater cameras, or even in underwater windows of boats (Taylor, 1996; Blain *et al.*, 2004; King *et al.*, 2006) that can be affected by biofouling. Moreover, a previous study shows that these surfaces present different properties since perspex is relatively hydrophobic compared to glass (Romeu *et al.*, 2019). Surface sterilization and preparation were performed as follows. Glass and perspex coupons were immersed in a solution of 2% (v/v) TEGO 2000® industrial detergent (Johnson Diversey, Northampton, United Kingdom) (Meireles *et al.*, 2017) and sterile distilled water for 20 min under agitation (150 rpm). In order to remove any remaining disinfectant, coupons were rinsed in sterile distilled water and air-dried. Additionally, glass coupons were autoclaved (121 °C, 15 min) (Azevedo *et al.*, 2006). After drying, all coupons were aseptically pre-weighted. Biofilm formation was evaluated on agitated 12-well microtiter plates (VWR International, Carnaxide, Portugal), since this platform was shown to mimic the hydrodynamic conditions found in marine environments (Romeu *et al.*, 2019).

Transparent double-sided adhesive tape was used to fix the coupons, and once the tape was placed in the wells, all coupons plates were subjected to UV sterilization for 30 min after which the sterile coupons were fixed. Moreover, to assess the hydrodynamic effect on protein expression, cyanobacterial biofilm formation at different shear rates was also tested. Briefly, to attain the shear rate values that can mimic aquatic environments, such as those found in a ship hull in a harbor and in partially submerged or even moored equipment and devices, microtiter plates were incubated at 25 °C in an orbital shaker with a 25 mm orbital diameter (Agitorb 200ICP, Norconcessus, Portugal) at 185 rpm (achieving the average shear rate of 40 s^{-1}) (Romeu *et al.*, 2019). Biofilm development was also assessed at lower shear rate conditions (average shear rate of 4 s^{-1}, achieved at 40 rpm) since lower fluid velocities can promote marine biofouling (Minchin and Gollasch, 2003; Flemming *et al.*, 2009). As chlorophyll *a* concentration is commonly used as biomass indicator in aquatic environments, the cyanobacterial suspension was adjusted to a chlorophyll *a* concentration of 1.5 $\mu g.mL^{-1}$ to inoculation. Briefly, 2 mL of cyanobacterial suspension were incubated at 4 °C in the dark for a maximal chlorophyll *a* extraction. After 24 h, the samples were centrifuged at 3,202*g* for 5 min at room temperature, and the supernatant was transferred to a glass cuvette. The absorbance at 750 nm (turbidity), 665 nm (chlorophyll *a*), and 652 nm (chlorophyll *b*) was determined using a V-1200 spectrophotometer (VWR International China Co., Ltd, Shanghai, China). The chlorophyll *a* concentration was calculated through the following equation (6.1) (Porra *et al.*, 1989):

$$\text{Chl } a \ (\mu g.mL^{-1}) = 16.29 \times A^{665} - 8.54 \times A^{652} \quad (6.1)$$

where A^{665} and A^{652} are the absorbances at 665 nm and 652 nm, respectively.

These measurements were assessed in triplicate, and dilutions were performed using Z8 medium supplemented with 25 $g.L^{-1}$ of synthetic sea salts and vitamin B_{12}. Thus, a volume of 3 mL of adjusted cyanobacterial suspension was inoculated in each well, in which coupons of each surface were previously fixed with transparent double-sided adhesive tape. Biofilm development was followed for 49 days (seven weeks) since it is accepted

that a two-month interval for maintenance is the minimum duration for economically viable underwater monitoring systems(Blain *et al.*, 2004; Romeu *et al.*, 2019). During this incubation time, the medium was replaced twice a week. Moreover, to mimic real light exposure periods, a photoperiod of 14 h light (8-10 μmol photons m^{-2} s^{-1})/10 h dark cycles) was applied.

6.2.5 Biofilm analysis

Every seven days, biofilm analysis was performed and three coupons for each surface and hydrodynamic condition were analysed. The culture medium was carefully removed, and the wells were filled with 3 mL of sterile sodium chloride solution (8.5 $g.L^{-1}$) (Romeu *et al.*, 2019). The solution was carefully removed to eliminate loosely attached cyanobacteria and subsequently, the wells were filled again with 3 mL of sterile sodium chloride solution to evaluate the cyanobacterial biofilms thickness and structure by OCT. In order to complement the characterization of cyanobacterial biofilms, the determination of their wet weight and chlorophyll *a* content was also performed.

6.2.5.1 Optical Coherence Tomography

Images from cyanobacterial biofilms developed on both surfaces and under the different hydrodynamic conditions were captured. For each coupon, 2D imaging was performed with a minimum of 3 fields of view to ensure the accuracy and reliability of the results obtained (Romeu *et al.*, 2019). Image analysis was performed using a routine developed in the Image Processing Toolbox from MATLAB 8.0 and Statistics Toolbox 8.1 (The MathWorks, Inc., Natick, Massachusetts, USA) (Romeu *et al.*, 2020). The mean of biofilm thickness was calculated based on the distance between the biofilm bottom and the upper contour line according to the following equation (6.2):

$$\bar{L}_F = \frac{1}{N}\sum_{i=1}^{N} L_{F,i} \qquad (6.2)$$

where $L_{F,i}$ is a local biofilm thickness measurement at location i, N equals the number of thickness measurements, and $\bar{L}_F$ is the mean biofilm thickness.

6.2.5.2 Wet weight determination and chlorophyll *a* quantification

To determine the wet weight, coupons were detached from the wells, weighed, and the biofilm wet weight was obtained as the difference from the initial coupon weight (determined prior to inoculation) (Romeu *et al.*, 2021). Subsequently, cyanobacterial cells were detached from the coupons by immersing each coupon in 2 mL of 8.5 $g.L^{-1}$ sodium chloride solution and vortexing. The suspensions were incubated for 24 h at 4 °C in the dark, and chlorophyll *a* determination was performed as previously described through Equation 6.1.

6.2.5.3 Statistical analysis of biofilm development

A total of six replicates (two biological assays with three technical replicates each) were analysed. Data analysis was performed using the statistical program GraphPad Prism® for Windows, version 6.01 (GraphPad Software, Inc., San Diego, CA, USA), and results were compared using unpaired *t*-tests with a confidence level of 95% (*; $P < 0.05$).

6.2.6 Proteomic analysis

6.2.6.1 Protein extraction and sample preparation for proteomic analysis

At the last sampling time (49 days), biofilm samples of unidentified filamentous Synechococcales LEGE 06021 were recovered for proteomic analysis (Romeu *et al.*, 2021). Cyanobacterial biofilms were detached from the coupons by immersing each coupon in 2 mL of 8.5 $g.L^{-1}$ sodium chloride solution and vortexing. The pooled samples from four coupons of the same condition were centrifuged at 3202*g* for 10 min at room temperature, and the pellet of biomass from 24 biofilm samples comprising six independent-replicates from four different growing conditions were kept at -80 °C for further processing. The amount of sample was calculated, and an appropriate volume of SDT buffer (0.5 g FW/mL

SDT) + Protease inhibitors (PIs, Roche, 11697498001, Basel, Switzerland) was added to the samples, sonicated 10 x 3 s and 23 kHz – 105 μm (amplitude) and incubated for 4 h at room temperature. Afterward, samples were heated for 3 min at 95 °C and subsequently centrifuged at 16000*g* for 20 min. Finally, the supernatant was collected, and total protein concentration was measured indirectly by optical density (OD) at 280 nm using a DeNovix DS-11 Spectrophotometer (DeNovix Technologies, Wilmington, Delaware, USA). Samples containing the extracted protein were stored for 24 h at -20 °C.

The extracted proteins were processed according to Romeu et al. (Romeu *et al.*, 2021), which used a modified version of two distinct protocols based on FASP protocol described by (Wiśniewski *et al.*, 2009) and the SP3 technology(Hughes *et al.*, 2019). Herein, the samples containing 40 μg of the extracted proteins were processed by the FASP using centrifugal filter units with nominal molecular weight limit (NMWL) of 30 kDa (MRCPRT030, Millipore, Billerica, MA, USA), whereas 200 μg of the extracted proteins were reduced prior the digestion with trypsin in the SP3 protocol (Romeu *et al.*, 2021).

6.2.6.2 LC-MS/MS analysis

Considering both sample preparation methods are complementary, tryptic peptides from both methods were mixture in the same tube to a final concentration of 0.1 μg and 0.5 μg from FASP and SP3, respectively. Then, protein digests from both protocols were analysed in the same run with a nano LC-MS/MS, composed by an Ultimate 3000 liquid chromatography system coupled to a Q-Exactive Hybrid Quadrupole – Orbitrap mass spectrometer (Thermo Scientific, Bremen, Germany) (Osório *et al.*, 2021). Separation was performed in a 15 cm by 75 μm inner diameter EASY-Spray column (ES800, PepMap RSLC, C18, 3 μm, Thermo Scientific, Bremen, Germany) at 300 nl min^{-1} by generated by mixing A: 0.1% FA and B: 80% ACN, with the following gradient: 5 min (2.5% B to 10% B), 60 min (10% B to 35% B), 5 min (35% B to 99% B) and 5 min (hold 99% B). Subsequently, the column was equilibrated with 2.5% B for 12 min. Data acquisition was controlled by Xcalibur 4.0 and Tune 2.8 software (Thermo Scientific, Bremen, Germany). The specific LC-MS parameters were full scan settings: 70k resolution (m/z 200), AGC target 3e6, maximum injection time 50 ms. dd settings: minimum AGC target 8e3, intensity threshold 7.3e4,

charge exclusion: unassigned, 1, 8, >8, peptide match preferred, exclude isotopes on, dynamic exclusion 20 s. MS2 settings: microscans 1, resolution 35k (m/z 200), AGC target 2e5, maximum injection time 110 ms, isolation window 2.0 m/z, isolation offset 0.0 m/z, spectrum data type profile. The mass spectrometry proteomics data have been deposited to the ProteomeXchange Consortium via the PRIDE (Vizcaíno *et al.*, 2016) partner repository with the data set identifier PXD029048.

6.2.6.3 Protein identification

The raw data were analysed and processed using the Proteome Discoverer 2.2.0.388 software (Thermo Scientific) and searched against the UniProt database for Cyanobacteria taxonomic selection (2018_07 release). The Sequest HT search engine was used for protein identification. The ion mass tolerance was 10 ppm for precursor ions and 0.02 Da for-fragment ions. Maximum allowed missing cleavage sites was set to 2. Cysteine carbamidomethylation was defined as a constant modification. Methionine oxidation and protein N-terminus acetylation were defined as variable modifications. Peptide confidence was set to high. The processing node Percolator was enabled with the following settings: maximum delta Cn 0.05; decoy database search target false discovery rates (FDR) 1%, validation was based on q-value. Protein label-free quantitation was performed with the Minora feature detector node at the processing step. Precursor ions quantification was performed at the processing step with the following parameters: unique plus razor peptides were considered for quantification, and precursor abundance was based on intensity.

6.2.6.4 Differential protein expression and enrichment

Statistical analyses applied to the proteomic data were performed using R software version 4.0.0. (Dessau and Pipper, 2008). The Differentially Expressed Proteins (DEPs) and/or gene enrichment was assessed using the "DEP" R package (Zhang *et al.*, 2018), based on the *limma* algorithm (Ritchie *et al.*, 2015). Similar to previous work (Romeu *et al.*, 2021), the missing values were filtered according to the fraction of protein found in each paired comparison with a cut-off of 0.33%, considering the possibility to have a minimum of 4 out of 6 replicates at least one condition. Imputation of missing values was performed

considering a non-random distribution (MNAR) using "MinProb" as an imputation function. Significant differences between conditions for each condition were paired tested by protein-wise linear models and empirical Bayes statistics. Finally, adjusted *P*-value (alpha = 0.05) and the log2 fold change (lfc = log2(1.5), log2 fold change >0.6) were used as a filter threshold to classify them as DEPs or enriched genes.

Functional classification (gene ontology) was carried out using the OmicsBox software version 1.4.11 (https://www.biobam.com/omicsbox/). Additional functional analyses to determine over/under-expressed pathways were performed to the categorical GO terms corresponding to DEPs, using the hypergeometric distribution significance test (Fisher's exact test, $P < 0.05$).

6.3 Results and Discussion

6.3.1 Phylogenetic analysis

Phylogenetic relationships of unidentified filamentous Synechococcales LEGE 06021 and other relatives were investigated by using a maximum likelihood phylogenetic tree constructed from their partial 16S rRNA gene sequences (Figure 6.1). Our phylogenetic results confirmed that this strain belongs to the *Toxifilum* genus (related to the type species *Toxifilum mysidocida)* (Zimba *et al.*, 2017).

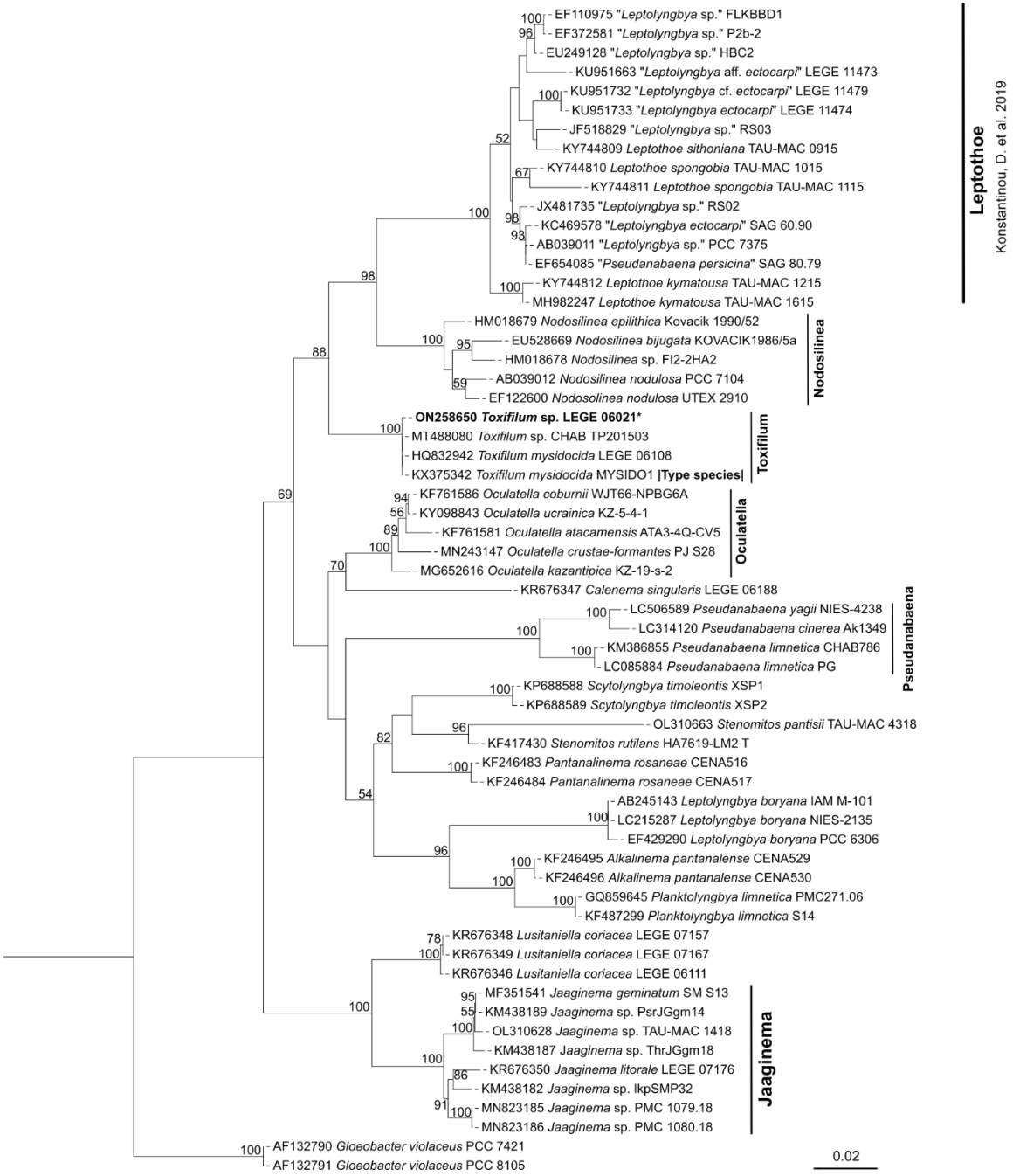

Figure 6.1. Maximum likelihood (ML) phylogenetic tree based on 61 partial 16S rRNA gene sequences of cyanobacteria strains belonging to the orders Pseudanabaenales and Synechococcales. *Gloeobacter violaceus* PCC 7421 and *Gloeobacter violaceus* PCC 8105 were used as outgroup. Phylogenetic position of *Toxifilum* sp. LEGE 06021 is indicated in bold. Bootstrap values over 50% are indicated at the nodes. Black stars represent the strains whose sequences were obtained in this work. Strains labeled with quotes indicate that names correspond to Genbank labels.

6.3.2 Biofilm development analysis

Wet weight, chlorophyll *a* content and biofilm thickness evolution from cyanobacterial biofilm under different conditions were assessed for 49 days (Figure 6.2). Biofilm biomass was higher at the lowest shear rate on both surfaces. However, this tendency was more evident for biofilm thickness values obtained from perspex (Figure 6.2F). Biofilm mass obtained on the glass surface under lower shear conditions (4 s^{-1}) was on average 70.5% higher (Figure 6.2A) when compared to the values obtained at a higher shear rate (40 s^{-1}), whereas on perspex, biofilm wet weight was on average 57.3% higher (Figure 6.2B). The chlorophyll *a* content at 4 s^{-1} on glass was on average 87.5% higher (Figure 6.2C) than at 40 s^{-1}, on perspex, it was, on average 83.9% higher (Figure 6.2D). Regarding biofilm thickness, values obtained on glass under lower shear conditions were on average 87.0% higher (Figure 6.2E), whereas on perspex, they were on average 93.3% higher (Figure 6.2F). Moreover, the highest value of biofilm thickness was observed at 4 s^{-1} on perspex (around 955.9 μm; Figure 6.2F, 49 days). When biofilms developed under different surfaces at the same hydrodynamic conditions were compared, similar values from these four parameters were obtained (Supplementary Material, Figure S 6.1). Figure 6.3 shows representative 2D cross-sectional images obtained by Optical Coherence Tomography (OCT) at 28 days and at the end of the experiment (49 days). This period corresponds to a maturation phase of biofilm development and the time at which major differences between the two hydrodynamics conditions were observed (Figure 6.2).

Chlorophyll *a* content monitorization proved to be a useful tool for following cyanobacterial biofilm growth since a correlation between chlorophyll *a* production and biofilm wet weight was observed (Supplementary Material, Figure S 6.2) as already reported for different filamentous cyanobacterial strains (Romeu *et al.*, 2019, 2020, 2021). In the present study, differences in biofilm development at different shear conditions were noticed in the early stages of biofilm development, but major differences were found in the maturation phase of biofilm development, as previously observed for filamentous (Romeu *et al.*, 2019, 2020, 2021) and coccoid cyanobacteria (Faria, Teixeira-Santos, Romeu, *et al.*, 2020). Probably, the increased shear rate has a weaker impact during adhesion and initial biofilm formation, but later on, it may promote sloughing and erosion events,

affecting biofilm cohesion and structure. At lower fluid velocities, external mass transfer of nutrients to the top layers of the biofilm is reduced and this may reduce diffusion to the inner layers of the biofilm (Moreira *et al.*, 2013). It is therefore possible that the biofilm adapts its architecture to facilitate this nutrient transfer as previously shown for other bacterial biofilms produced under flow conditions (Teodósio *et al.*, 2011). Moreover, the lower biofilm biomass obtained under a higher shear rate (Figure 6.3E-H) does not allow a detailed analysis of the biofilm structure. However, given the results obtained from biofilm thickness (Figure 6.2E, F), in which the effect of fluid velocity was more noticeable during biofilm maturation rather than during cell adhesion, it seems that the increased shear stress was a significant obstacle to biofilm development at 40 s^{-1} most likely due to erosion/sloughing effects. Despite the different properties of glass and perspex, which is the most hydrophobic surface (Romeu *et al.*, 2019), the finding that the effect of surface hydrophobicity was less important than the hydrodynamic effect on cyanobacteria biofilm development had already been shown for other cyanobacterial strains (Romeu *et al.*, 2019, 2020; Faria, Teixeira-Santos, Romeu, *et al.*, 2020).

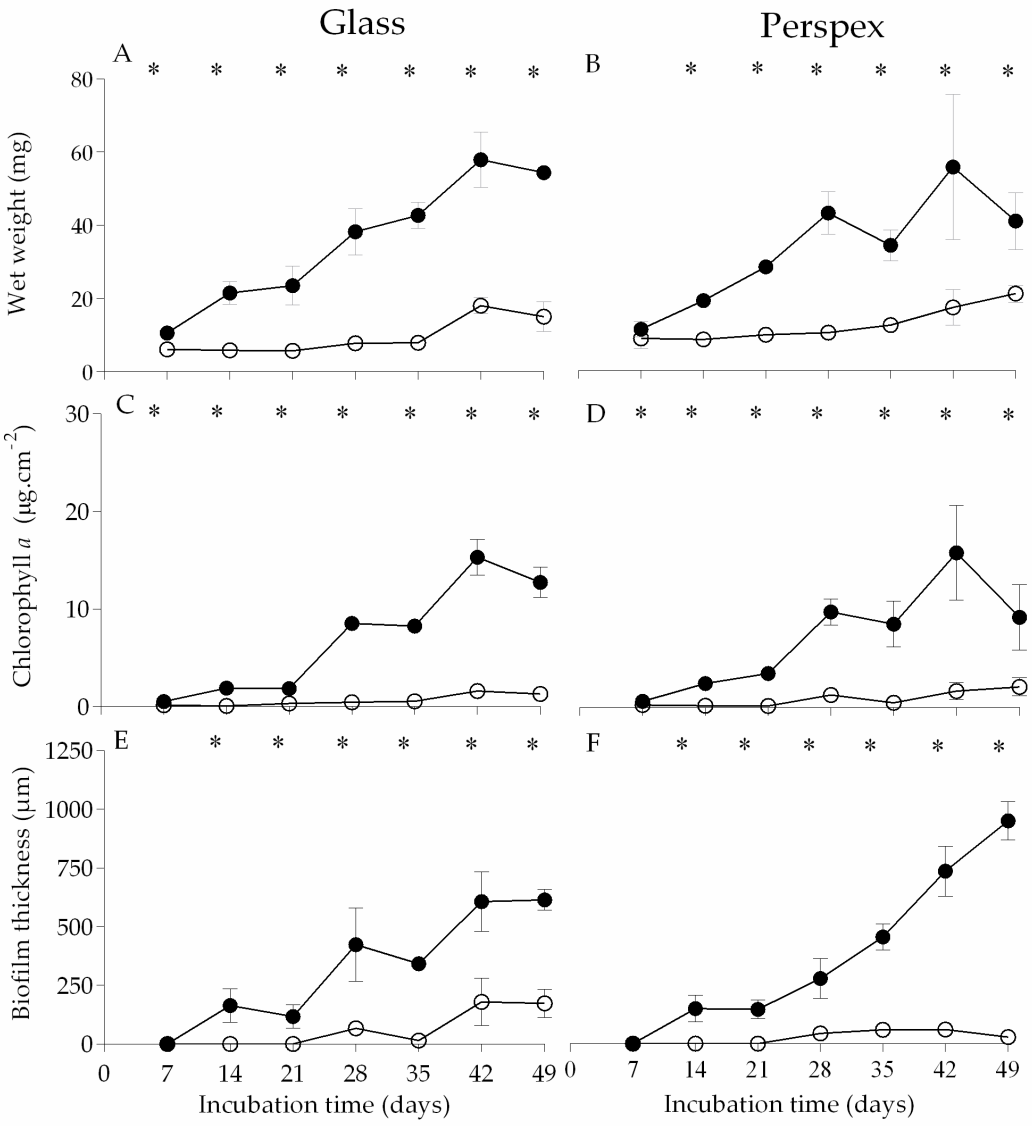

Figure 6.2. Evaluation of *Toxifilum* sp. LEGE 06021 biofilm development. The parameters analysed refer to wet weight (A, B), chlorophyll *a* quantification (C, D) and biofilm thickness (E, F). Biofilms were formed in glass (A, C, E) or perspex (B, D, F), at two average shear rates, 4 s^{-1} (closed circles) and 40 s^{-1} (open circles) for 49 days. Standard deviations from two biological assays with three replicates each are represented. Symbol * indicate statistically different values for $P < 0.05$ (unpaired *t*-tests) at each incubation time.

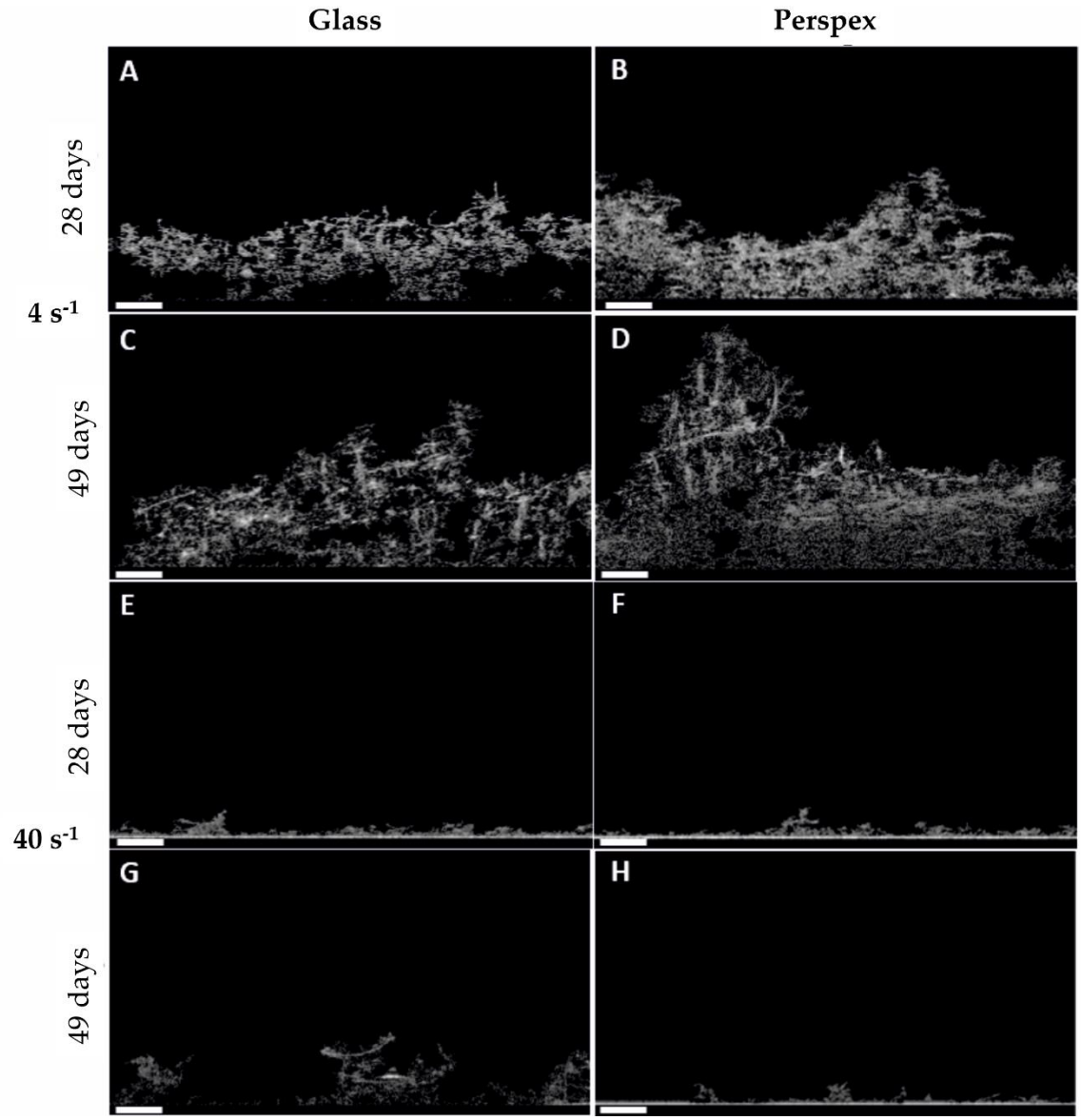

Figure 6.3. 2D cross-sectional OCT images of *Toxifilum* sp. LEGE 06021 biofilms. The representative images show biofilms formed on glass and perspex at two different shear rates, 4 s^{-1} (A-D) and 40 s^{-1} (E-H), and the biofilm structure evolution from days 28 to 49. Scale bar = 200 μm.

6.3.3 Proteomic analysis

At the last sampling time, biofilm samples of *Toxifilum* LEGE 06021 were recovered for proteomic analysis. Altogether, 1877 proteins were identified from 24 biofilm samples of four different biofilm conditions using a shotgun proteomics approach (Supplementary Material, Table S 6.1). Among these proteins, 54.2% are related to metabolic processes, and 23.5% to proteomic metabolism (Supplementary Material, Figure S 6.3).

The Principal Component Analysis (PCA) plot revealed a similar pattern among replicates of the same conditions, whereas some differences were visualized between the different shear rates for the same surface used (Figure 6.4). As revealed by the macroscopic evaluation of cyanobacterial biofilm, the proteomic analysis also showed a higher difference in protein expression between the two hydrodynamic conditions than those found between the two surfaces. Indeed, these differences between different hydrodynamic conditions were quantitatively significant, resulting in 20 DEPs, of which 15 DEPs were found between the comparison at 4 s^{-1} *vs.* 40 s^{-1} on glass (Figure 6.5A, 6.6A), whereas five DEPs were found between samples from biofilms developed at 4 s^{-1} *vs.* 40 s^{-1} on perspex (Figure 6.5B, 6.6B). Most of these DEPs (around 50%) were found as up-regulated at 4 s^{-1} *vs.* 40 s^{-1} on glass (Figure 6.6A). Like the GOs Categories of the two up-regulated DEPs found in 4 s^{-1} *vs.* 40 s^{-1} on perspex, these 11 up-regulated DEPs found in 4 s^{-1} *vs.* 40 s^{-1} on glass are related to cellular components (intracellular organelle, plastid, thylakoid, membrane-bounded organelle), cation binding and oxidoreductase activity (Figure 6.7).

From all of DEPs found on glass, a fragment of condensation protein, uncharacterized proteins, PRC domain-containing proteins, one orange carotenoid protein, and enzymes like cyanophynase and glutathione-dependent formaldehyde dehydrogenase were identified as up-regulated at 4 s^{-1} (Table 6.1). Among these uncharacterized proteins, two disordered proteins (A0A2T2W171 and A0A522XHL7), which are more likely to perform their function under extreme conditions(Liu and Huang, 2014), were also identified. Glutathione-dependent formaldehyde dehydrogenase seems to have a strong impact on biofilm development at this condition since this subset of 11 DEPs contained three enriched GO terms related to S-(hydroxymethyl) glutathione dehydrogenase NAD/NADP activity (Figure 6.7). Overall, all these up-regulated proteins found at 4 s^{-1} on glass are related to the photosynthetic process (Figure 6.6). On the other hand, two phage tail proteins, a MoaD/ThiS family protein and an uncharacterized protein with a disordered domain, were found as down-regulated proteins on glass at 4 s^{-1} when compared with biofilm cells from 40 s^{-1} (Table 6.1).

On perspex, DEPs include iron ABC transporter substrate-binding protein and transketolase, as up-regulated proteins, and transcription termination/antitermination

protein NusG, dihydroxy-acid dehydratase, and 30S ribosomal protein S16 as down-regulated proteins at 4 s^{-1} (Table 6.1). More details about DEPs description and their GO annotation can be found in Supplementary Material, Table S 6.2.

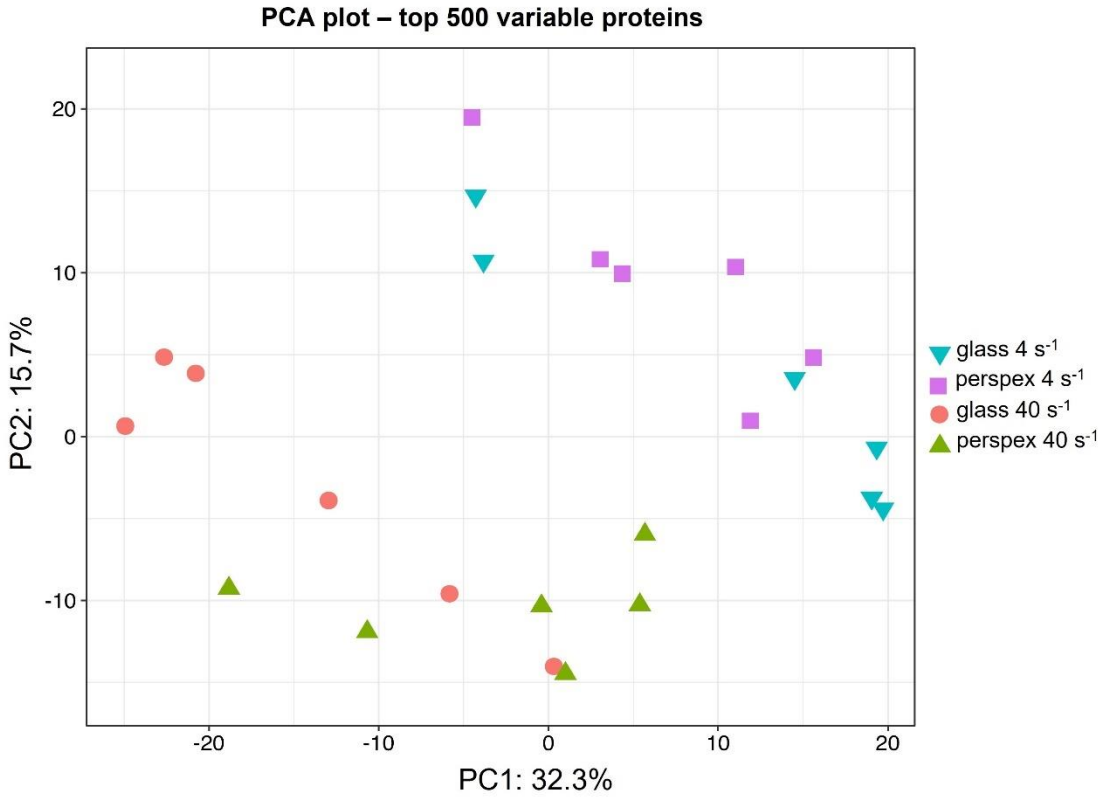

Figure 6.4. Principal Component Analysis (PCA) of the proteins identified from marine biofilms formed by filamentous cyanobacteria under four different biofilm growing conditions. The PCA plot displays a grouping pattern among the six replicates studied from each biofilm condition formed on glass and perspex, but some differences were observed between the two hydrodynamic conditions studied (4 s^{-1} and 40 s^{-1}). The two principal components extracted (PC1 and PC2) can explain the 48% total variability revealed among the proteins analysed. PCA was performed with the respective function provided within the "DEP" R package (Zhang *et al.*, 2018), used for the downstream proteomic analyses.

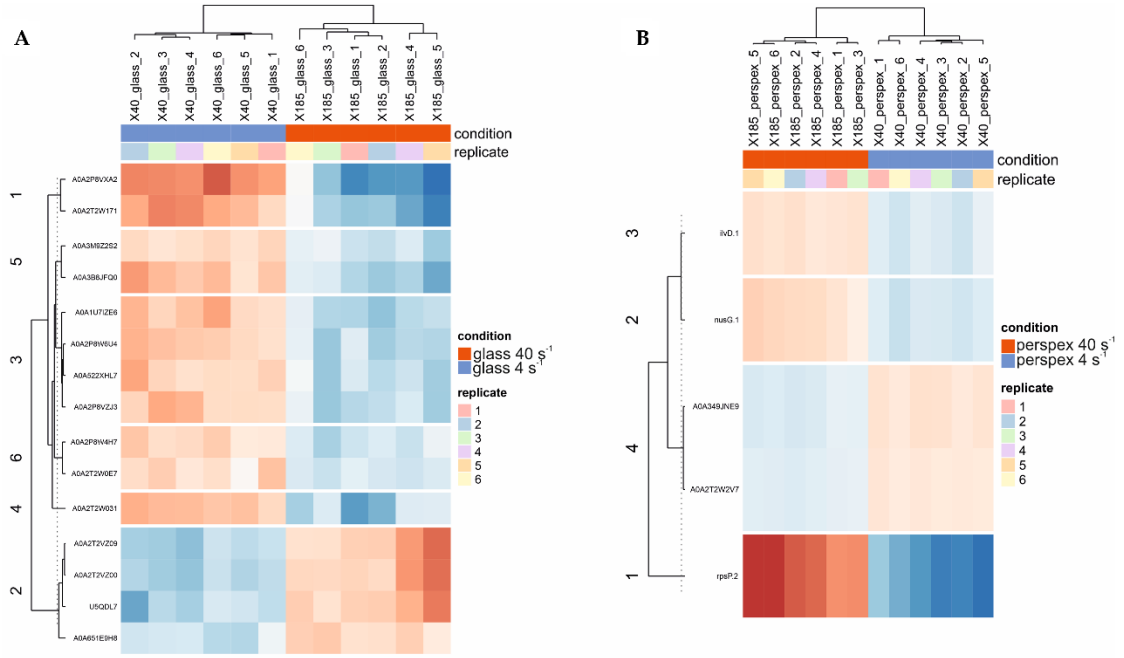

Figure 6.5. Heatmaps of the Differentially Expressed Proteins (DEPs) identified between comparisons of the same surface studied at different hydrodynamics conditions. The figures display the DEPs resulting from the comparisons between the conditions A) 4 s^{-1} *vs.* 40 s^{-1} on glass clustered in six groups by k-means clustering, and B) 4 s^{-1} *vs.* 40 s^{-1} on perspex clustered in four groups. The rows show the corresponding UniProt accession of DEPs with their corresponding expression in the columns as the log_2 fold-change (red: enriched; blue: depleted) of the intensity from each replicate.

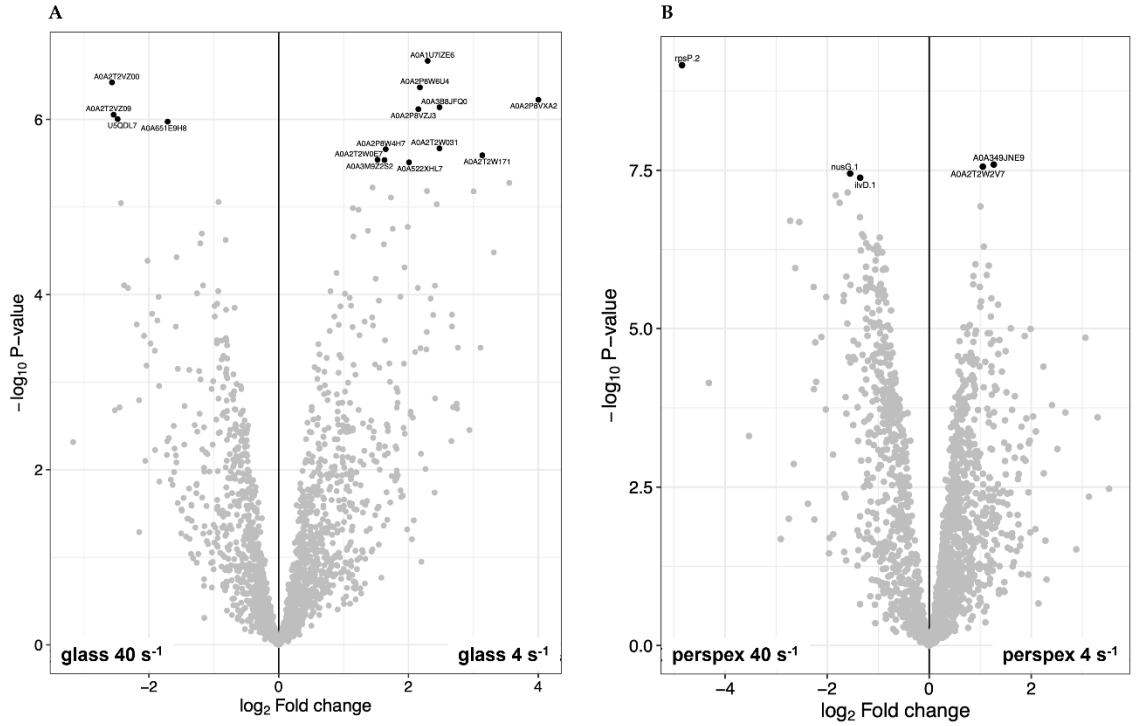

Figure 6.6. Volcano plot of the differentially expressed proteins (DEPs) identified between comparisons of the same surface studied at different hydrodynamics conditions. The figure displays the DEPs (black dots) and their corresponding accession/gene names, as the resulting *P* values (− $\log_{10}$) in the y-axis, plotted against the fold changes ($\log_2$) in the x-axis, obtained between the comparisons 4 s^{-1} *vs.* 40 s^{-1} on glass (A) and on perspex (B).

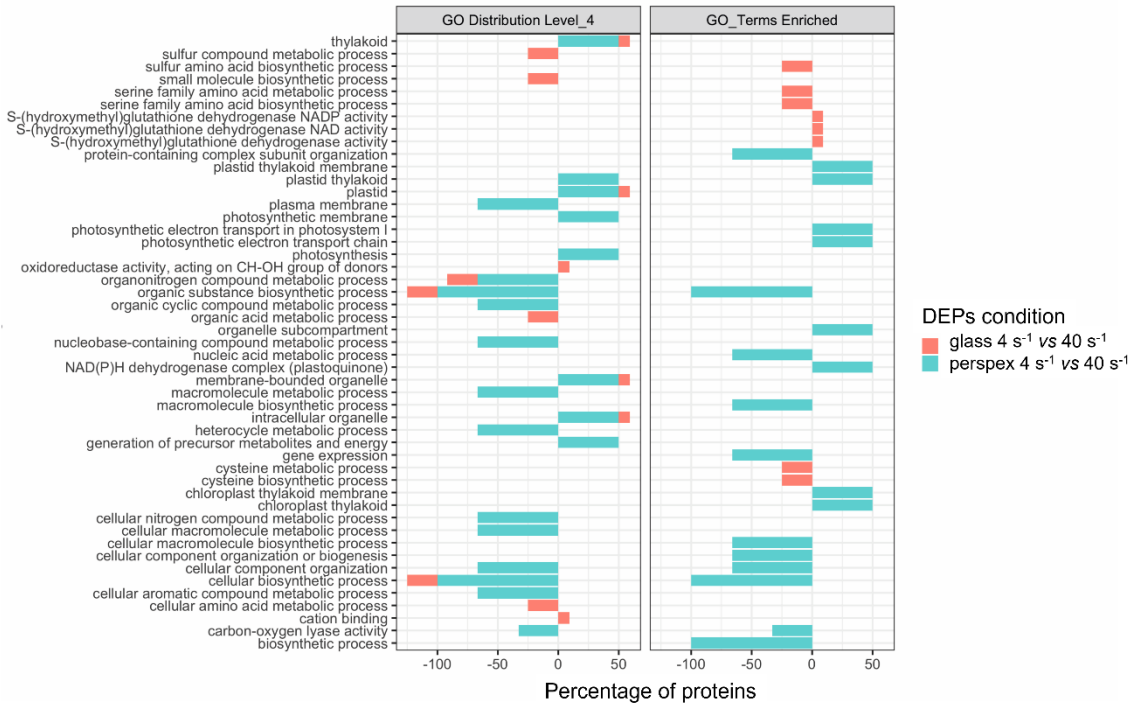

Figure 6.7. Gene Ontology (GO) distribution and GO enrichment of Differentially Expressed Proteins (DEPs). In the left panel is shown the GO distribution by level 4 of the DEPs, whereas the right panel displays the corresponding enriched GO terms. The divergent stacked bars (negative and positive) represent the percentage of DEPs (x-axis) matching each GO Category (y-axis), relative to the number of DEPs found at both sides (up/down) of the tested conditions (DEPs Conditions). The total number of DEPs obtained from each comparison were 11-up/4-down (from glass 4 s^{-1} *vs.* 40 s^{-1}) and 2-up/3-down (from perspex 4 s^{-1} *vs.* 40 s^{-1}). The GO annotation was performed with the OmicsBox software version 1.4.11, as well as the enrichment analyses (Fisher's exact test, $P < 0.05$).

Table 6.1. List of the DEPs found between comparisons of the same surface studied at different hydrodynamics conditions. The corresponding UniProt accession of DEPs is provided with their corresponding gene and a brief description, as well as the log 2-fold-changes (LFC) and the resulting and adjusted *P*-values (p.adj) for each comparison (4 s^{-1} *vs.* 40 s^{-1} on glass, and 4 s^{-1} *vs.* 40 s^{-1} on perspex).

UniProt accession	Description	Glass 4 s^{-1} *vs.* 40 s^{-1} (LFC)	Glass 4 s^{-1} *vs.* 40 s^{-1} (p.adj)	Perspex 4 s^{-1} *vs.* 40 s^{-1} (LFC)	Perspex 4 s^{-1} *vs.* 40 s^{-1} (p.adj)
A0A1U7IZE6	Orange carotenoid protein	2.3	0.01		
A0A2P8VXA2	Glutathione-dependent formaldehyde dehydrogenase	4	0.01		
A0A2P8VZJ3	Uncharacterized protein	2.15	0.01		
A0A2P8W4H7	Uncharacterized protein	1.65	0.03		
A0A2P8W6U4	PRC domain-containing protein	2.18	0.01		
A0A2T2VZ00	Phage tail protein	-2.57	0.01		
A0A2T2VZ09	Phage tail protein	-2.55	0.01		
A0A2T2W031	PRC domain-containing protein	2.48	0.03		
A0A2T2W0E7	Uncharacterized protein	1.52	0.04		
A0A2T2W171	Uncharacterized protein	3.14	0.03		
A0A3B8JFQ0	Condensation protein (Fragment)	2.48	0.01		
A0A3M9Z2S2	Cyanophycinase	1.63	0.04		
A0A522XHL7	Uncharacterized protein	2.01	0.04		
A0A651E9H8	MoaD/ThiS family protein	-1.71	0.01		
U5QDL7	Uncharacterized protein	-2.48	0.01		
A0A2T2W2V7	Transketolase			1.05	0.04
A0A349JNE9	Iron ABC transporter substrate-binding protein			1.27	0.04
A0A6G3Z7U9 [1]	Dihydroxy-acid dehydratase			-1.35	0.05
A0A651DR21 [2]	Transcription termination/antitermination protein NusG			-1.55	0.05
A0A651DTD2 [3]	30S ribosomal protein S16			-4.84	0

Gene names: [1] ilvD; [2] nusG; [3] rpsP.

Similar to a previous quantitative study, the majority of identified proteins were related to metabolic processes (Romeu *et al.*, 2021). Due to optimizations performed in the experimental protocol, the total number of proteins identified in the present study was much higher (1877 vs 546), a 3.5-fold increase compared with our last publication using the FASP + SP3 protocol (Romeu *et al.*, 2021). These results highly improved the quality of data (e.g., more peptides identified, fewer gaps in the proteomic profile comprising six replicates per condition tested). We were now able to identify several ribosomal proteins

and others involved in photosynthesis and respiration, which are essential in primary metabolic functions, as well as proteins associated with phycobilisomes, elongation factors, and transporter proteins.

Previous studies performed on the proteome analysis of the adhesion and biofilm formation of other species also identified the presence of several proteins with disordered domains as DEPs (Domínguez-Pérez *et al.*, 2020; Romeu *et al.*, 2021). Moreover, one of them is related to protein secretion (A0A522XHL7). PRC domain-containing proteins are involved in photosynthesis activity mainly by transferring electrons within the cyclic electron transport pathway. Produced by all photosynthetic organisms, carotenoids act as light-harvesting pigments and as protectors against oxidative stress (Melnicki *et al.*, 2016). Indeed, the photoactivation of the soluble orange carotenoid protein is the initial step for photoprotective mechanisms, which decrease the excitation energy that arrives at the photochemical centers by increasing thermal dissipation (Lu *et al.*, 2017). Cyanophycin is a water-insoluble peptide and a valuable exogenous substrate, which enables cyanobacteria to store nitrogen in environments subjected to fluctuating nitrogen supply (Watzer and Forchhammer, 2018). A previous proteomic study performed on *Microcoleus* cyanobacteria also showed cyanophycinase expression throughout biofilm growth, suggesting active utilization of cyanophycin granules to cope with fluctuations in nutrient supply (Tee *et al.*, 2020). Glutathione-dependent formaldehyde dehydrogenase is one of the three pathways for the detoxification of formaldehyde widely distributed in biological processes (Chen *et al.*, 2016). Formaldehyde can be generated endogenously during redox processes, including during the enzymatic demethylation of methylated nucleic acids and proteins, leading to cellular dysfunction (Denby *et al.*, 2016). A study on *Acinetobacter baumannii 8399* showed the induction of *adhC1* gene, which encodes for a glutathione-dependent formaldehyde dehydrogenase, under iron limitation and its repression when the cells are cultured in the presence of free inorganic iron (Echenique *et al.*, 2001). Moreover, in *Paracoccus denitrificans*, the expression of the gene encoding this enzyme is increased when either formaldehyde or metabolic sources of this compound, such as methanol, are present (Harms *et al.*, 2001). Likewise, in *Saccharomyces cerevisiae* the glutathione-dependent formaldehyde dehydrogenase expression level is increased by the presence of methylated compounds like methyl methanesulphonate or formaldehyde

(Weimer *et al.*, 1993). An additional study (Chen *et al.*, 2013) demonstrated that a glutathione-dependent detoxification system was required for formaldehyde resistance and optimal survival of *Neisseria meningitidis* in biofilms, suggesting the role of this enzyme in this complex lifestyle.

Cyanobacterial development on glass at 40 s^{-1} promoted the up-regulation of two phage tail proteins, a MoaD/ThiS family protein and an uncharacterized protein with a disordered domain, when compared to 4 s^{-1}. Bacteriophage tail core is important for phage adsorption to the bacterial cell wall and host infection (Brzozowska *et al.*, 2018). Although cyanophages have been barely investigated, they play an important role in regulating the dynamics of cyanobacterial communities in aquatic environments (Xiong *et al.*, 2019). Cyanophages may introduce genes involved in photosynthesis, carbon metabolism, and nutrient acquisition into host cells during lysogeny, thereby modifying the metabolism of cyanobacteria and providing a vehicle for horizontal transfer of genetic material and evolution and diversity of marine cyanobacteria (Williamson *et al.*, 2008; Zborowsky and Lindell, 2019). Moreover, they also impact globally in the marine biogeochemical cycles (Williamson *et al.*, 2008; Bischoff *et al.*, 2021). Cyanophages can play an essential role in the control of cyanobacterial blooms (Mühling *et al.*, 2005; Bischoff *et al.*, 2021). For example, phage lysis of *Nodularia* leads to the release of nitrogen and stimulates the growth of *Synechococcus* (Bischoff *et al.*, 2021). Therefore, it is noteworthy the identification of two phage tail proteins in this biofilm development condition due to their critical role in marine environments. Receptor-binding proteins could be used in genetic engineering to alter host ranges of cyanophages for biocontrol or to develop bacteriophage-based genetic tools for cyanobacteria (Xiong *et al.*, 2019). Furthermore, cyanophages could potentially be used to control biofilms, opening up new developments in antifouling solutions. A recent study showed that phage protein reduces biofilm and improves antibiotic action (Brzozowska *et al.*, 2018). MoaD and ThiS are sulfur carrier proteins required for the synthesis of cofactors of molybdenum and thiamin. Additionally, sulfur is one of the essential elements which is incorporated in proteins as thiol groups of cysteine residues (Kotera *et al.*, 2010). Unlike in the previous works (Romeu *et al.*, 2020, 2021), the hydrodynamic effect was clearly revealed through PCA analyses, allowing us to consolidate that hydrodynamics may have a more significant effect than surface

properties on biofilm formation (Figure 6.4). The differential biofilm development observed on glass at 4 s^{-1} and 40 s^{-1} (Figure 6.2) can be related to the differential expression of these proteins in this filamentous cyanobacterial strain. Indeed, GO distribution and GO enrichment of DEPs analysis (Figure 6.7) revealed two enriched GO terms related to cysteine (cysteine metabolic process and cysteine biosynthetic process) and two additional GO terms related to sulfur metabolic pathways (sulfur compound metabolic process and sulfur amino acid biosynthetic process).

Iron ABC transporter substrate-binding protein, transketolase, transcription termination/antitermination protein NusG, dihydroxy-acid dehydratase, and 30S ribosomal protein S16 were identified as DEPs on biofilm cells developed on perspex. ABC transporters are vital in the transport of essential substrates across the cytoplasmic membrane (Delepelaire, 2019). In the case of iron, which is not always readily available from the environment, this metal is a relevant component of key molecules such as cytochromes, and its deficiency can impact ATP production, nucleotide synthesis, and the activity of numerous critical enzymes. Some studies emphasize the role of iron ABC transporters in stress response and virulence (Nagayama *et al.*, 2014; Tanaka *et al.*, 2018). In fact, since at 4 s^{-1} the mass transfer of oxygen and nutrients to the inner layers of the biofilm may be reduced, the up-regulation of this protein can be considered as a virulence factor in biofilms. Moreover, a study performed in the anaerobic hyperthermophilic bacterium *Thermotoga maritima* also revealed the up-regulation of an iron ABC transporter on biofilm when compared with planktonic cells (Pysz *et al.*, 2004). Therefore, they can also be considered as promising targets for antimicrobial strategies. Transketolase is one of the Calvin cycle enzymes involved in biosynthesis, metal ion binding, carbon metabolism, providing a link between glycolysis and the pentose-phosphate pathway (Liang and Lindblad, 2016). Differential regulation of transketolase has been reported on adhesion, biofilm, and persistence studies. Indeed, a study on *Shewanella oneidensis* showed that transketolase was slightly up-regulated in *luxS* mutant, which developed an undifferentiated, loosely connected biofilm that covered the glass surface more homogenously than the wild type (Bodor *et al.*, 2011). A proteomic analysis of the biofilm extracellular matrix of *Haemophilus influenzae* biofilms was compared with proteomic analysis of total proteins taken from planktonic bacteria, revealing that transketolase was

associated only with the 96 h biofilms (Wu *et al.*, 2014). A study performed on *S. aureus* showed that inactivation of a gene that encodes a transketolase leads to a significant decrease in intracellular bacteria proliferation and survival in endothelial cells, associated with a non-persister-like phenotype, suggesting that transketolase is required for bacterial persistence (X. Tan *et al.*, 2019).

All down-regulated proteins found at 4 s^{-1}, or up-regulated at 40 s^{-1}, on perspex are relevant to critical cyanobacterial processes. Indeed, NusG is an important transcription factor that modulates the initiation, elongation, and termination steps of bacterial transcription by RNA polymerase. Dihydroxy-acid dehydratase is related to amino acid synthesis and acquisition, whereas the ribosomal protein S16 is one of the 21 proteins which belong to the 30S small subunit of the bacterial ribosome involved in translation and protein synthesis. A study that evaluated the whole-transcriptome shotgun sequencing to compare the *S. pneumoniae* transcriptome in biofilms and dispersed conditions showed down-regulation of dihydroxy-acid dehydratases and 30S ribosomal protein S16 and up-regulation of ABC transporter proteins under actively dispersed cells (Pettigrew *et al.*, 2014). This finding suggests that the behavior of these proteins is susceptible not only to different hydrodynamic conditions of biofilm development but also to different lifestyles (planktonic and biofilm). Interestingly, cyanobacterial dihydroxy-acid dehydratases have also been considered a promising growth inhibition target (Zhang *et al.*, 2020). GO distribution and enrichment analysis (Figure 6.7) also confirmed the involvement of these proteins in essential processes since GO terms as "protein-containing complex subunit organization, macromolecule biosynthetic process, cellular macromolecule biosynthetic process, cellular component organization or biogenesis, cellular component organization, cellular biosynthetic process, biosynthetic process" were identified for this biofilm condition.

Proteomic analyses performed on filamentous cyanobacteria demonstrated different mechanisms for biofilm regulation, which are strongly dependent on cyanobacterial species, as well as on their isolation sites (Romeu *et al.*, 2020, 2021). Although ribosomal proteins, proteins involved in photosynthesis and respiration, as well as proteins associated with phycobilisomes, elongation factors, and proteins with transporter activity were found in all these studies, a broad diversity in the DEP's profile

of each strain was observed. Therefore, future studies should focus on different cyanobacterial strains to determine a proteomic profile according to the isolation site and/or the cyanobacterial genus.

The effective management of cyanobacterial growth is vital to restore ecosystem function, as well as to mitigate the biofouling effects. This work demonstrates how hydrodynamic conditions and surface properties affect biofilm development and the protein expression on biofilms cells. Macroscopic biofilm analysis revealed a higher biofilm development at the lowest shear rate, while surface effects were less pronounced. The quantitative proteomic analysis also revealed higher variations between biofilm formed at different shear rates when compared with protein profiles obtained from distinct surfaces. Among all DEPs found between 4 s^{-1} and 40 s^{-1}, up-regulated proteins associated with the photosynthesis process and related pathways were identified on both surfaces. However, it is important to highlight the influence of the glutathione-dependent formaldehyde dehydrogenase found on glass. While down-regulated proteins related to essential processes such as transcription and translation were found at 4 s^{-1} on perspex, on glass, these down-regulated proteins were linked to metabolic processes. Interestingly, phage tail proteins, which presented a significant effect on cyanobacteria blooms and aquatic environments, were also identified on glass.

The possible proteomic functions reported in this study were verified by their quantitative and relative expression in all biofilm conditions and supported by statistical analysis. Considering the lack of biomarkers identified in previous works using a similar approach, the role of the different DEPs can only be discussed by their biological signatures, such as protein domains, annotations, and their relationship in enriched pathways.

Further studies should include gene silencing or knockout strains to establish a stronger link between differential expression levels of a given protein and the impact on biofilm development and behavior. However, the methodologies required for performing this work in this type of organisms are still under development. Nevertheless, and even considering the low availability of data, this study demonstrates with statistical significance that some proteins are differentially expressed under the different conditions and these experimental variations induce changes in biofilm development. Although this

is a limitation of our work, to the best of our knowledge, it reflects the state of the art of the research in this field. Additionally, two relevant and clear conclusions were achieved. Regarding the proteomic protocol improvement, the sample preparation, including ultrasounds treatment of the biomass in SDT buffer for cell rupture and protein extraction, followed by a combination of FASP and SP3 protocol, notably improves the peptide and protein identification by shotgun proteomics. Moreover, related to the SP3, in this study we demonstrated its suitability to capture and retain a higher number of peptides originating from complex samples. Regarding the effect of surface properties and hydrodynamic conditions on cyanobacterial biofilm development, it was shown that hydrodynamics had a stronger effect causing the up-regulation of 13 proteins and the down-regulation of 7 proteins when biofilms developed at a shear rate value of $4s^{-1}$ with 40 s^{-1} are compared (Figure 6.6).

Moreover, the isolation of marine organisms (namely marine bacteria) from fouled submerged surfaces (for instance ship hulls and pontoons) and the determination of their proteomic profile can provide information about the metabolic pathways that are activated during biofilm formation under these conditions. Since it is known that cyanobacteria interfere with other organisms in their communities through the release of compounds into the surrounding medium (Leão *et al.*, 2010), the identification and *in vitro* production of these compounds can be exploited towards the development of marine antifouling strategies where the growth of different fouling organisms can be inhibited (Gademann, 2007; Ma *et al.*, 2015; Antunes, Pereira, *et al.*, 2019; K. Tan *et al.*, 2019). This concept has been applied in the use of nostocarboline, a carboline alkaloid from *Nostoc* 78-12A, as an environmentally friendly candidate for antifouling coating against both prokaryotic and eukaryotic photosynthetic organisms (Becher *et al.*, 2005; Blom *et al.*, 2006). Additionally, other metabolites derived from cyanobacteria have been explored as new candidates for antifouling coatings, such as the diterpenoid comnostin B, isolated from *Nostoc commune*, which shown a molluscicidal effect (Jaki *et al.*, 2000), or the *epi*-hapalindole E from *Fischerella* sp., which exhibited antibacterial, antifungal, antialgal and activities against mammalian cells (Thanh Doan *et al.*, 2000). Previous studies with portoamides, cyclic dodecapeptides isolated from the cyanobacterium *Phormidium* sp. LEGE 05292, also reveal a broad-spectrum bioactivity towards diverse biofouling species,

given their allelopathic effect on the microalga *Chlorella vulgaris* (Leão *et al.*, 2010) and the high effectiveness in the prevention of the attachment of mussel larvae, (Antunes, Pereira, *et al.*, 2019) showing potential to be incorporated as an active ingredient in antifouling coatings.

6.4 Conclusions

This study is particularly important given the reduced number of studies addressing filamentous cyanobacterial biofilm development in conditions that mimic the natural environment and that are able to integrate macroscopic biofilm techniques and proteomic approaches. The relatively high number of uncharacterized proteins that were identified in this study is further proof that this area requires further interdisciplinary work so that new insights on biofilm formation and mitigation in marine environments can be obtained.

6.5 Supplementary Material

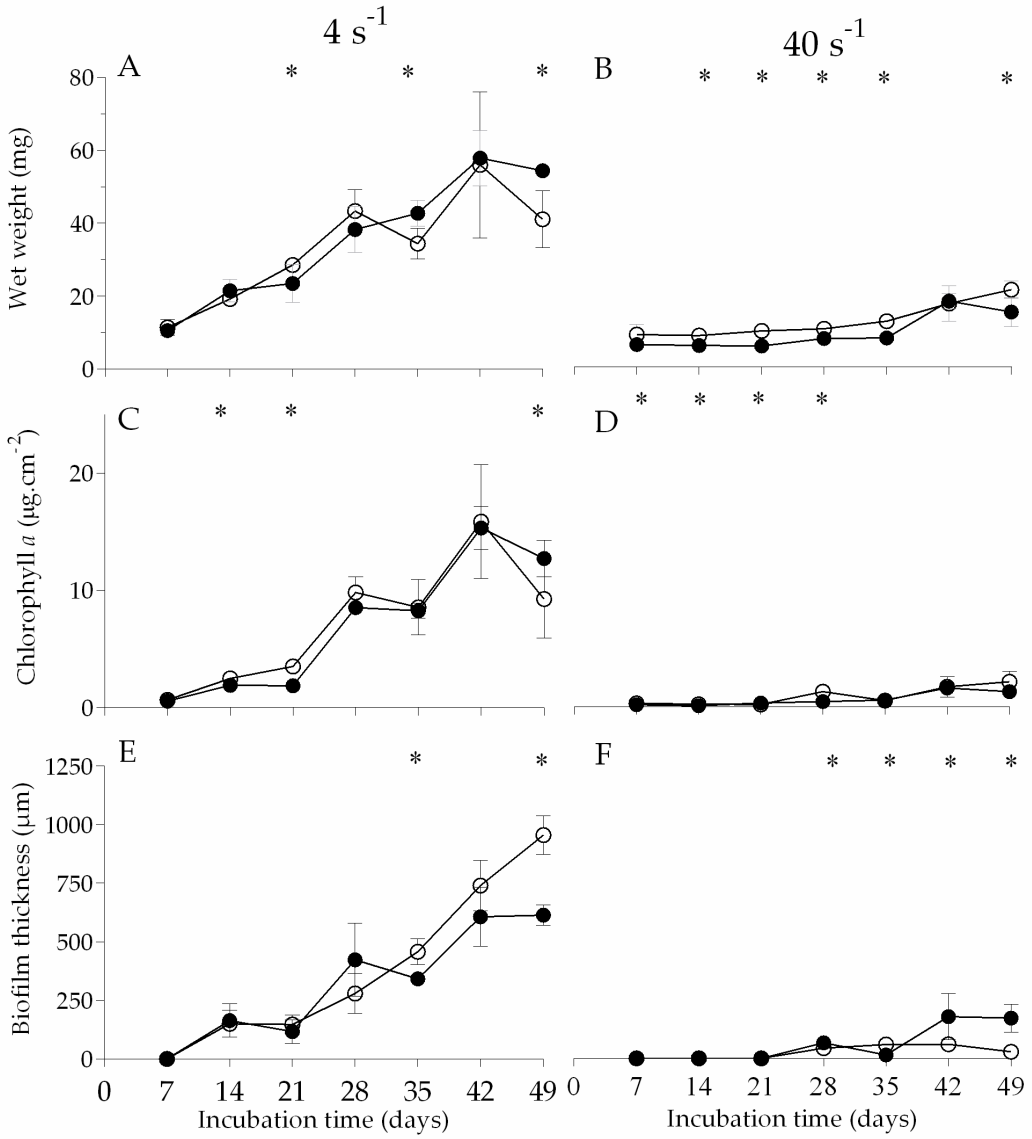

Figure S 6.1. Evaluation of unidentified filamentous Synechococcales LEGE 06021 biofilm development under the same hydrodynamic condition on different surfaces. The parameters analysed refer to wet weight (A, B), chlorophyll *a* quantification (C, D) and biofilm thickness (E, F). Biofilms were formed at 4 s^{-1} (A, C, E) or 40 s^{-1} (B, D, F) on two different surfaces, glass (closed circles) and perspex (open circles) for 49 days. Standard deviations from two biological assays with three replicates each are represented. Symbol * indicates statistically different values for $P < 0.05$ (unpaired t-tests) at each incubation time.

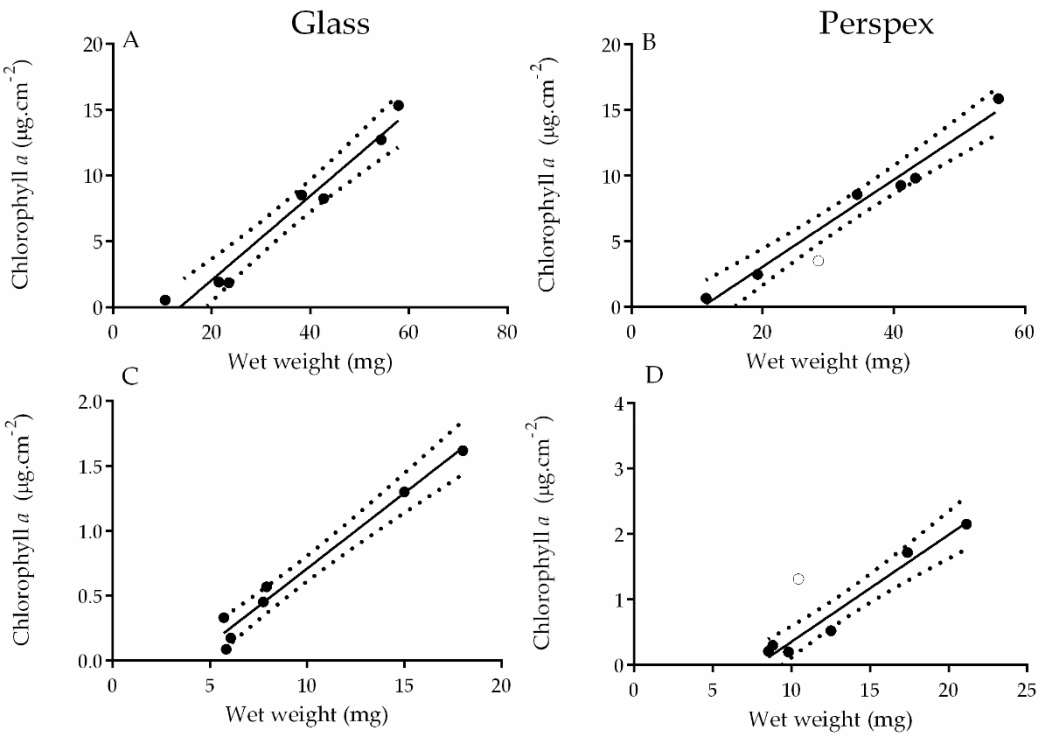

Figure S 6.2. Correlation between wet weight and chlorophyll *a* content on biofilm development from unidentified filamentous Synechococcales LEGE 06021. Biofilm development in glass (A, C) and perspex (B, D) at two different shear rates, 4 s^{-1} (A, B) and 40 s^{-1} (C, D). The full line represents the linear regression, and the dashed line represents the confidence limits (95%). Closed symbols refer to data points that were considered for the regression (all except two), and open symbols refer to data points that were excluded from the regression.

Table S 6.1. Summary of proteomic analysis.

Available at https://www.nature.com/articles/s41522-022-00340-w

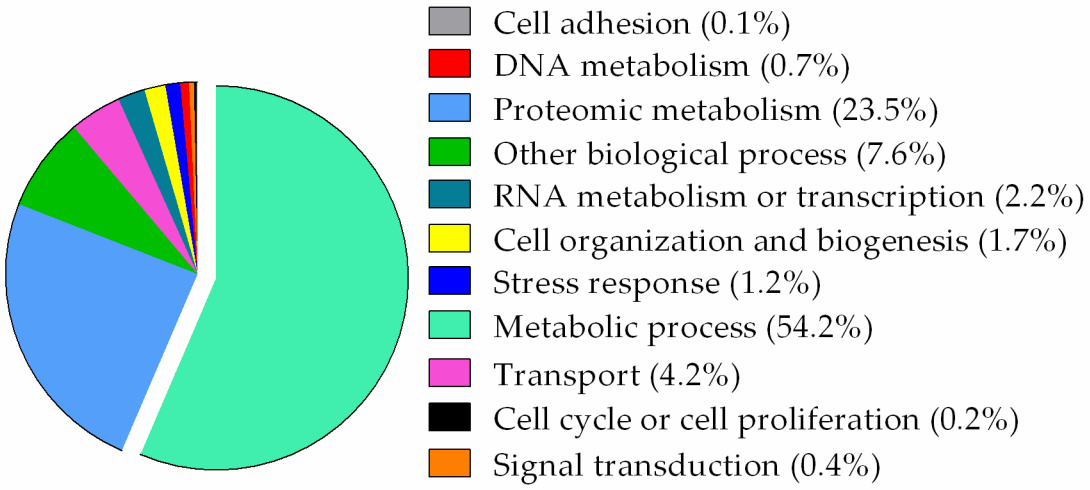

Figure S 6.3. Distribution of total proteins identified according to the biological process (34.8% of proteins identified without an associated biological process are not shown in this graph).

Table S 6.2. DEPs description and GO annotation.

Available at https://www.nature.com/articles/s41522-022-00340-w

7.

7 Characterization and biofouling potential analysis of two cyanobacterial strains isolated from Cape Verde and Morocco

The contents of this chapter as published as:

Romeu, M.J., Morais, J., Gomes, L.C.; Silva, R., Vasconcelos, V., Mergulhão, F. (2023) Characterization and biofouling potentital analysis of two cyanobacterial strains isolated from Cape Verde and Morocco. *FEMS Microbiology Ecology* **99:** fiad004.

Abstract

Cyanobacteria are new sources of value-added compounds but also ubiquitous and harmful microfoulers on marine biofouling. In this work, the isolation and identification of two cyanobacterial strains isolated from Cape Verde and Morocco, as well as their biofilm-forming ability on glass and perspex under controlled hydrodynamic conditions, were performed. Phylogenetic analysis revealed that cyanobacterial strains isolated belong to *Leptothoe* and *Jaaginema* clades (*Leptothoe* sp. LEGE 181153 and *Jaaginema* sp. LEGE 191154). From quantitative and qualitative data of wet weight, chlorophyll *a* content and biofilm thickness obtained by Optical Coherence Tomography, no significant differences were found in biofilms developed by the same cyanobacterial strain on different surfaces (glass and perspex). However, the biofilm-forming potential of

Leptothoe sp. LEGE 181153 proved to be higher when compared to *Jaaginema* sp. LEGE 191154, particularly at the maturation stage of biofilm development. Three-dimensional biofilm images obtained from Confocal Laser Scanning Microscopy showed different patterns between both cyanobacterial strains and also among the two surfaces. Because standard methodologies to evaluate cyanobacterial biofilms formation, as well as two different optical imaging techniques were used, this work also highlights the possibility to integrating different techniques to evaluate a complex phenomenon like cyanobacterial biofilm development.

Keywords: cyanobacteria characterization, cyanobacteria isolation, cyanobacterial biofilms, filamentous cyanobacteria, marine biofouling, surface effect

7.1 Introduction

Cyanobacteria are a widespread and significant group of photosynthetic prokaryotes responsible for the accumulation of oxygen in the Earth's environment (Lyons *et al.*, 2014) and the evolution of eukaryotic organisms, according to the widely accepted endosymbiotic theory (Ku *et al.*, 2015). They contribute to the nitrogen and carbon biogeochemical cycles, and can persist in harsh conditions due to their high adaptability (Berg and Sutula, 2015; Anderson, 2016). The metabolic flexibility between oxygen photosynthesis and respiration (Vermaas, 2001; Mullineaux, 2014) allows them to thrive in diverse environments. While some cyanobacteria can be associated with heterotrophic organisms in the desert to facilitate the productivity of soil crust (Pointing and Belnap, 2012), some of them are the primary colonizers of ice sheets (Vincent, 2000). Therefore, these particular bacteria are common in many habitats such as lakes, ponds, springs, wetlands, streams, rivers, soil crust, microbial mats, sands and rocks (Ramos *et al.*, 2018). Cyanobacteria strains present a considerable morphological diversity, comprising distinct degrees of complexity (Schirrmeister *et al.*, 2011). When compared with unicellular coccoid morphology, the filamentous phenotype can be beneficial

because it has a higher resistance to stress and predation, as well as improved resource acquisition (Claessen *et al.*, 2014).

Cyanobacteria have been considered promising organisms for biotechnological processes due to the broad spectrum of secondary metabolites produced by some strains (Lau *et al.*, 2015; Manirafasha *et al.*, 2016). These added-value compounds can be applied to enhance the sustainable production of food and green energy sources (Singh *et al.*, 2017), and they can also be used for medical purposes due to their antioxidant, anticancer, and anti-inflammatory properties (Pagels *et al.*, 2019). However, cyanobacteria can also have a detrimental impact on human purposes due to their ability to produce toxins (Breinlinger *et al.*, 2021), promote cyanobacterial blooms (Huisman *et al.*, 2018) and participate in the biofouling processes (Carvalho, 2018). Marine biofouling consequences include environmental, economic, ecological, and health concerns (Caruso, 2020). The corrosion of different facilities and fouling in equipment may lead to incorrect measurements of submerged sensors and measuring devices, and high costs related to cleaning and/or repainting (Delauney *et al.*, 2010), contributing to the industrial and economic consequences associated with biofouling. Moreover, the introduction and spread of invasive non-indigenous pathogens on marine vessels between different ecosystems (Davidson *et al.*, 2009; Georgiades *et al.*, 2021) and the contamination of aquaculture facilities (Bannister *et al.*, 2019) may impact the ecology and global health. In the environmental field, marine biofouling can lead to increased fuel consumption by ships and, consequently, enhanced air pollution and greenhouse gas emissions (Hunsucker *et al.*, 2018).

Marine biofouling is a complex process and it has been suggested that the adhesion and biofilm development by microfouler organisms may affect the continuous biofouling process, particularly for larval recruitment and settlement of macrofouler organisms (Antunes, Leão, *et al.*, 2019; Dobretsov and Rittschof, 2020). Although their prevalence depends on the surface, geographical area and environmental settings, cyanobacteria are microfoulers and the major constituents of marine biofilms together with diatoms (Bharti *et al.*, 2017; Antunes *et al.*, 2020; Papadatou *et al.*, 2021). These organisms produce extracellular polymeric substances (EPS), which are essential compounds of biofilm

communities for maintaining their cohesion, structure and stability (Limoli *et al.*, 2015; Rossi and De Philippis, 2015; Anderson, 2016).

Marine biofilms are affected by several factors, including physical, chemical, and biological drivers (Caruso, 2020; Faria, Teixeira-Santos, Romeu, *et al.*, 2020; Faria, Teixeira-Santos, Morais, *et al.*, 2021). After the formation of the conditioning film comprising the adsorption of molecules (proteins, carbohydrates, etc.) from the surrounding environment, the second step in the biofouling process involves cell adhesion. Surface binding is considered a critical survival mechanism for enhancing organism interactions and accessing nutritional resources (Dang and Lovell 2016). Different materials are used in marine submerged man-made equipment, like aquaculture facilities (King *et al.*, 2006; Cai and Arias, 2017), underwater windows, sensors and measuring devices (Roy, 1994; Taylor, 1996; Davies and Rajapakse, 2013), protective equipment, swim platforms, ship and boat structures, and anchors (Taylor, 1996; Mansour and Liu, 2008; Molland, 2008; Davies and Rajapakse, 2013), which are susceptible to biofouling. Therefore, studies focused on the effects of substrate properties and organisms' variability in the growth stages of biofilms, and their composition, structure and behavior, are of great importance (Faria et al., 2021a, 2021c; Faria et al., 2020a). Indeed, previous studies showed a broad diversity in the protein expression profiles of cyanobacterial biofilms isolated from different sites (Romeu *et al.*, 2020), which may be a result of the adaptation of these organisms to the specific environmental niche that they occupy, such as their site of isolation and the nutritional availability at that site (Bragg *et al.*, 2006; Lv *et al.*, 2008). Through the simultaneous analysis of physiological characteristics, the distribution in the environment, and the genome and/or proteomic profiles, it is possible to identify the environmental factors that are most important to drive evolution and shape populations. For instance, greater depths are associated with lower light intensity and temperature, but also with higher content of phosphorus (Coleman and Chisholm, 2007). For instance, to cyanobacterium *Prochlorococcus*, phosphorus availability is a key ecological factor and a potential driver of evolution (Lv *et al.*, 2008). Different *Prochlorococcus* strains possess distinct physiological adaptations for dealing with the low phosphorus availability, including the replacement of phospholipids with sulfolipids (Van Mooy *et al.*, 2006), growth in a more limited range of phosphorus sources (Moore *et al.*, 2005), and the

upregulation of known phosphorus-assimilation genes and novel genes, which may enable them to tolerate phosphorus starvation periods (Martiny *et al.*, 2006). Moreover, recent metagenomic studies showed that the abundance of phosphate transport genes is also correlated with phosphorus availability (Rusch *et al.*, 2007). In the low-phosphorus waters of the Caribbean, the gene encoding a phosphate-binding protein is more abundant compared with the higher-phosphorus waters of the Pacific.

The main novelty of this study is the isolation, identification (morphological characterization), and assessment of the biofilm-formation potential of cyanobacterial strains isolated from underexplored marine environments and locations along the coast of Cape Verde and Morocco. These are locations with unknown biodiversity that will provide new knowledge and tools to understand the impact of global changes in temperate areas. Cyanobacterial strains from these genera seem to be quite frequent, at least in the Atlantic Ocean, North Aegean Sea, and Mediterranean Sea (Foster *et al.*, 2009; Konstantinou *et al.*, 2018, 2019; Ramos *et al.*, 2018). As they are distributed around dissimilar geographies, including different continents and port areas, this cosmopolitan distribution highlights the importance of studying biofilm formation by these organisms, which, in turn, present a significant concern to public health, environment, and aquatic ecology. Given the relevance of cyanobacteria to marine biofouling, their biofilm-forming ability was assessed for the first time in a long-term assay under controlled hydrodynamic conditions that mimics marine environments (Romeu *et al.*, 2019), and using two different surfaces as the substratum for biofilm formation (glass and perspex). These materials represent submerged artificial surfaces typically found on different aquatic apparatus such as sensors, flotation spheres, moored buoys, underwater cameras, aquaculture equipment, measuring devices, or even in underwater windows of boats (Taylor, 1996; Blain *et al.*, 2004; King *et al.*, 2006) that can be affected by biofouling. Additionally, given the broad spectrum of promising secondary metabolites and value-added compounds produced by cyanobacteria (Lau *et al.*, 2015) that can be used in biotechnological applications, cosmetics, feed, and food industries (Manirafasha *et al.*, 2016), and for medical purposes (Pagels *et al.*, 2019), this kind of study can also be useful in different research fields.

7.2 Material and Methods

7.2.1 Sampling and isolation

Environmental samples were collected on July 11, 2019, near Mrizika Beach, Morroco (32°57'31.3"N 8°46'34.1"W) from a dried soil crust, and on April 24, 2019, at Calhau, Cape Verde (São Vicente Island - 16°51'07.6"N 24°51'58.8"W), scraping from a port boat ramp with the help of a previously cleaned knife (Figure 7.1). Samples were transferred to 15 mL tubes with Z8 medium (Kotai, 1972) supplemented with 25 $g.L^{-1}$ of synthetic sea salts (Tropic Marin) and B_{12} vitamin (Sigma Aldrich, Merck, Saint Louis, MO, USA) (Croft *et al.*, 2006; Helliwell *et al.*, 2016) until further analysis. Isolation of cyanobacterial isolates was performed using the streak plate method (Rippka, 1988). Briefly, using a sterile plastic Pasteur pipette, a homogeneous drop from each environmental sample was inoculated in different agar plates with Z8 medium, and with a loop, each sample was spread, making successive smears in the different quadrants of the plate. After approximately 1 month of growth under 14 h light (10–30 μmol photons m^{-2} s^{-1})/10 h dark cycles, at 25 °C, isolated cells or filaments were picked up using a sterile surgical blade and transferred to 50 mL culture flasks with a liquid medium, growing in the previously described conditions. After 2-3 weeks of growth, isolation was confirmed by checking samples under the microscope.

Figure 7.1. Sampling locations: A) dried soil crust near Mrizika Beach, Morocco; B) green mat on ramp port for boats at Calhau, São Vicente Island, Cape Verde.

7.2.2 DNA extraction, 16S rRNA gene amplification (PCR), and sequencing

The two filamentous cyanobacterial isolates obtained in this work were grown in 50 mL flasks in the conditions previously described and harvested by centrifugation (5000*g* for 5 min at 4° C) after 2-3 weeks. Total genomic DNA was extracted using the commercial PureLink Genomic DNA Mini Kit (Invitrogen, USA), according to the manufacturer's instructions provided for Gram-negative bacteria. To obtain the 16S rRNA gene sequence, PCR amplification was performed using the oligonucleotide primers set 27F and 23S30R (Table 7.1). PCR reactions were performed in a final volume of 20 µl containing 1× Green GoTaq Flexi Buffer, 2.5 mM of $MgCl_2$, 125.0 mM of each deoxynucleotide triphosphate, 1.0 µM of each primer, 0.5 U of GoTaq Flexi DNA Polymerase (Promega, Madison, WI, USA), 10 $mg.mL^{-1}$ of bovine serum albumin (BSA), and 10–30 ng of template DNA, on a Veriti™ 96-Well Thermal Cycler (Applied Biosystems™, USA). The PCR conditions were as follows: initial denaturation at 94 °C for 5 min, followed by 10 cycles of denaturation at 94 °C for 45 s, annealing at 57 °C for 45 s, and extension at 72 °C for 2 min, followed by 25 cycles of denaturation at 92 °C for 45 s, annealing at 54 °C for 45 s, and extension at 72 °C for 2 min with a final elongation step at 72 °C for 7 min. The PCR reactions were performed in duplicate. PCR products were separated by 1.5% agarose gel stained with SYBR® safe (Invitrogen, Waltham, MA, USA), and DNA fragments with the expected size were excised and purified using NZYGelpure (NzyTech, Genes and Enzymes, Lisbon, Portugal) according to the manufacturer's instructions. Because the sequences were obtained by direct sequencing of purified amplicons, CYA359F, CYA781R, and 1494R internal primers (Table 7.1) were used to improve the quality of the sequences. Sequencing was performed at GATC Biotech (Ebersberg, Germany) and the nucleotide sequences obtained were manually inspected for quality and assembled using the Geneious 11.1.5 software (Biomatters Ltd., Auckland, New Zealand). Possible chimera formation during the sequences was checked using the software DECIPHER (Wright *et al.*, 2012). The sequences obtained were inserted in the BLASTn (Basic Local Alignment and Search Tool for Nucleotides) database and the

results were analysed. The sequences associated with this study were deposited in the GenBank database under the accession numbers ON311284 and ON311285.

Table 7.1. Oligonucleotide primers used for 16s rRNA amplification.

Primer	Sequence 5′-3′	Reference
27F	AGAGTTTGATCCTGGCTCAG	(Lane, 1991)
359F	GGGGAATYTTCCGCAATGGG	(Nübel *et al.*, 1997)
781R	GACTACWGGGGTATCTAATCCCWTT	(Nübel *et al.*, 1997)
1494R	TACGGCTACCTTGTTACGAC	(Lane, 1991)
23S30R	CTTCGCCTCTGTGTGCCTAGGT	(Lepère *et al.*, 2000)

7.2.3 Phylogenetic analysis

A total of 58 sequences were used in the final analysis, including two strains of *Gloeobacter violaceus* as an outgroup, 56 sequences of cyanobacteria, including type, reference and related strains belonging to the orders Pseudanabaenales and Synechococcales were retrieved from GenBank (National Center for Biotechnology Information, NCBI, Bethesda, MD, USA), and two sequences of isolates obtained in this work. Multiple sequence alignment was carried out using ClustalW in MEGA7 (Thompson *et al.*, 1994; Kumar *et al.*, 2016), and sequences were manually proofread and edited. The best fit model was assessed using jModelTest 2.1.10 (Darriba *et al.*, 2012) according to the Bayesian information criterion (BIC) and Akaike information criterion (AIC) scores. Maximum likelihood (ML) analysis was carried out using substitution model GTR+G+I with 1000 bootstrap resampling replicates using the MEGA7 software (Kumar *et al.*, 2016). The final phylogenetic tree was visualized and edited on Interactive Tree of Life (Letunic and Bork, 2021).

7.2.4 Light microscopy and morphological characterization

Morphological features (e.g. cell dimensions, shape, color, sheath, constriction at cross walls, specialized cells or shape of apical cells) of cyanobacterial strains isolated in this work were examined and imaged using a Leica DMLB light microscope coupled to a Leica ICC50 HD digital camera (Leica Microsystems, Germany). For each strain, microphotographs were taken using 400x and 1000x magnifications. Morphometric measurements were then performed using the image analysis software Leica Application Suite version 4.2.0 (Leica Microsystems). Cell dimensions were determined by measuring at least 20-30 cells for each strain along different positions of the slide preparation.

7.2.5 Biofilm formation assay

Cyanobacterial isolates were grown in 750 mL of Z8 medium (Kotai, 1972) supplemented with 25 $g.L^{-1}$ of synthetic sea salts (Tropic Marin) and B_{12} vitamin (Sigma Aldrich, Merck, Saint Louis, MO, USA), under 14 h light (10–30 μmol photons m^{-2} s^{-1})/10 h dark cycles at 25 °C. To assess the biofilm-forming ability of both strains on different surfaces, biofilms were developed on commercial perspex (poly(methyl methacrylate)) surfaces (Neves & Neves, Lda, Portugal) and glass (Vidraria Lousada, Lda, Portugal) coupons (1 cm^2). Surface sterilization and preparation were performed as previously described (Romeu *et al.*, 2019). Biofilms were formed on agitated 12-well microtiter plates (VWR International, Carnaxide, Portugal) because this platform was shown to mimic the hydrodynamic conditions found in marine environments (Romeu *et al.*, 2019). To attain the shear rate values of aquatic environments, such as those found in a ship hull in a harbor (Bakker *et al.*, 2003) and in partially submerged or even moored equipment and devices (average shear rate of 40 s^{-1}), microtiter plates were incubated at 25 °C in an orbital shaker with a 25 mm orbital diameter (Agitorb 200ICP, Norconcessus, Portugal) at 185 rpm (Romeu *et al.*, 2019). Biofilm formation in this system was shown to predict the biofouling behavior observed upon immersion in the sea for prolonged periods (Silva *et al.*, 2021). Prior to inoculation, the cyanobacterial suspensions were adjusted to a chlorophyll *a* concentration of 1.5 $\mu g.mL^{-1}$ since chlorophyll *a* is commonly used as a biomass indicator in aquatic environments (Romeu *et al.*, 2019, 2021). Briefly, 2

mL of cyanobacterial suspension were incubated at 4 °C in the dark for maximal chlorophyll *a* extraction. After 24 h, the samples were centrifuged at 3202*g* (Eppendorf Centrifuge 5810R, Hamburg, Germany) for 5 min at room temperature, and the supernatant was transferred to a glass cuvette. The absorbance at 750 nm (turbidity), 665 nm (chlorophyll *a*), and 652 nm (chlorophyll *b*) were determined using a V-1200 spectrophotometer (VWR International China Co., Ltd, Shanghai, China). The chlorophyll *a* concentration was calculated through the following equation (7.1) (Porra *et al.*, 1989):

$$\text{Chl } a \text{ } (\mu g.mL^{-1}) = 16.29 \times A^{665} - 8.54 \times A^{652} \quad (7.1)$$

where A^{665} and A^{652} are the absorbances at 665 nm and 652 nm, respectively.

These measurements were assessed in triplicate, and dilutions were performed using Z8 medium supplemented with 25 $g.L^{-1}$ of synthetic sea salts and vitamin B_{12} (Sigma Aldrich, Merck, Saint Louis, MO, USA). Then a volume of 3 mL of each cyanobacterial suspension (previously adjusted to chlorophyll *a* concentration of 1.5 $\mu g.mL^{-1}$) was inoculated in each well, in which coupons of each surface were previously fixed with transparent double-sided adhesive tape. Biofilm development was followed for 49 days (7 weeks) because it is accepted that a 2-month interval is the minimum duration for economically viable underwater monitoring systems (Blain *et al.*, 2004; Romeu *et al.*, 2019). During this incubation time, the medium was replaced twice a week. Moreover, to mimic real light exposure periods, a photoperiod of 14 h light (8-10 μmol photons m^{-2} s^{-1})/10 h dark cycles was applied.

7.2.6 Biofilm analysis

Biofilm analysis was performed every 7 days, in which two coupons of each surface were analysed. The culture medium was carefully removed by gentle pipetting, and the wells were filled with 3 mL of sterile sodium chloride solution (8.5 $g.L^{-1}$) (Romeu *et al.*, 2019). The solution was carefully removed to eliminate loosely attached cyanobacteria and, subsequently, the wells were filled again with 3 mL of sterile sodium chloride

solution to evaluate the thickness and structure of the cyanobacterial biofilms by Optical Coherence Tomography (OCT). To complement the characterization of cyanobacterial biofilms, the determination of their wet weight and chlorophyll *a* content was also performed over the 7 weeks. At the last sampling point (49 days), cyanobacterial biofilms of both strains formed on both surfaces were also analysed by Confocal Laser Scanning Microscopy (CLSM).

7.2.6.1 Optical Coherence Tomography

Images from cyanobacterial biofilms developed on both surfaces were captured as reported in Romeu et al. (2019). For each coupon, 2D imaging was performed with a minimum of three fields of view to ensure the reliability and accuracy of the results obtained. Image analysis was performed using a routine developed in the Image Processing Toolbox from MATLAB 8.0 and Statistics Toolbox 8.1 (The MathWorks, Inc., Natick, Massachusetts, USA) as described in Romeu et al. (2020). The mean of biofilm thickness was calculated based on the distance between the biofilm bottom and the upper contour line according to the following equation (7.2):

$$\bar{L}_F = \frac{1}{N}\sum_{i=1}^{N} L_{F,i} \qquad (7.2)$$

where $L_{F,i}$ is a local biofilm thickness measurement at location i, N equals the number of thickness measurements, and $\bar{L}_F$ is the mean biofilm thickness.

7.2.6.2 Wet weight determination and chlorophyll *a* quantification

After OCT analysis, the determination of the biofilm wet weight and chlorophyll *a* content was performed as previously reported (Romeu *et al.*, 2021). To determine the wet weight, sterile sodium chloride solution (8.5 $g.L^{-1}$) was carefully removed from the wells, and coupons were detached and weighed. The biofilm wet weight was obtained as the difference from the initial coupon weight, which was determined prior to inoculation. Subsequently, cyanobacterial cells were detached from the coupons by immersing each coupon in 2 mL of 8.5 $g.L^{-1}$ sodium chloride solution and vortexing (Romeu *et al.*, 2019).

The suspensions were incubated for 24 h at 4 °C in the dark, and chlorophyll *a* determination was performed through Equation 7.1.

7.2.6.3 Confocal Laser Scanning Microscopy

At the last sampling point (day 49), additional coupons were removed from the microplates, washed with saline solution, and the biofilms were stained for 10 min with 6 μM cell-permeant nucleic acid markers: biofilms formed by the cyanobacterial strain isolated from Morocco (*Jaaginema* sp. LEGE 191154) were stained with SYTO®9 (a green fluorescent stain; Thermo Fisher Scientific, Waltham, Massachusetts, USA), whereas biofilms formed by the cyanobacterial strain isolated from Cape Verde (*Leptothoe* sp. LEGE 181153) were marked with SYTO®61 (a red fluorescent stain; Thermo Fisher Scientific, Waltham, Massachusetts, USA). Both stains were chosen to match the colors of cyanobacteria pigments visible by optical microscopy, as well as to have minimal interference. Each stained biofilm was mounted on a microscopic slide and image acquisition was performed using a Leica TCS SP5 II Confocal Laser Scanning Microscope (Leica Microsystems, Wetzlar, Germany). All biofilms were scanned using a 40× water objective lens (LEICA HCX PL APO CS 40.0x/1.10WATER UV) using a protocol previously described (Faria et al., 2021a; Faria et al., 2020a) with some modifications. Given the used stains, *Jaaginema* sp. LEGE 191154 biofilms were observed with a 488 nm argon laser, whereas *Leptothoe* sp. LEGE 181153 biofilms were imaged with a 633 nm helium-neon laser. A minimum of five stacks of horizontal-plane images (512 x 512 pixels, corresponding to 387.5 μm x 387.5 μm) with a *z*-step of 1 μm were acquired per sample.

3D projections of the biofilms were constructed from the CLSM acquisitions using the "Easy 3D" function of the IMARIS 9.1 software (Bitplane, Zurich, Switzerland). Biovolume ($\mu m^3.\mu m^{-2}$) was extracted from confocal image series with the plug-in COMSTAT2 (Heydorn *et al.*, 2000) run in ImageJ 1.48v software (National Institutes of Health, Bethesda, Maryland, USA).

7.2.7 Statistical analysis

A total of four replicates (two biological assays with two technical replicates each) were analyzed. Data analysis was performed using the statistical program GraphPad Prism® for Windows, version 6.01 (GraphPad Software, Inc., San Diego, California, USA). The D'Agostino-Pearson and Shapiro-Wilk normality tests were performed to check if the data distribution presented a normal distribution. Differences between biofilm wet weight, chlorophyll *a* quantification, biofilm thickness obtained by OCT and biovolume obtained by CLSM were evaluated using the unpaired, non-parametric Mann-Whitney test because the variables were not normally distributed. The error bars shown in the graphs correspond to the standard deviation of the mean. Statistically significant differences were considered for P values < 0.05 (corresponding to a confidence level greater than 95%; and asterisks * and ** denote significance where $P < 0.1$ and $P < 0.05$, respectively).

7.3 Results and Discussion

7.3.1 Phylogenetic analysis

The phylogenetic analysis of the 16S rRNA gene (Figure 7.2) showed that the sequence from the cyanobacterium isolated from Cape Verde (*Leptothoe* sp. LEGE 181153) belongs to the *Leptothoe* clade, a recent genus described by Konstantinou et al. (2019), a clade with previous *Leptolyngbya* members but not related to the true (sensu stricto) *Leptolyngbya* clade. Sequence from the cyanobacterium isolated from Morocco (*Jaaginema* sp. LEGE 191154) fits in the *Jaaginema* clade, which consists of *Jaaginema litorale* LEGE 07176, a strain isolated from a wave-exposed rock on the Portuguese Coast (Ramos *et al*., 2018), *Jaaginema geminatum* SM S13 isolated from a hot spring in Iran (Heidari *et al*., 2018), *Jaaginema* sp. PsrJGgm14, from Psoroneria, a hot spring in Greece, *Jaaginema* sp. PMC 1079.18 and *Jaaginema* sp. PMC 1080.18, isolated from a dense periphytic biofilm covering immersed branch fragment, Guadeloupe (Duperron *et al*., 2019), *Jaaginema* sp. TAU-MAC 1418 (Panou and Gkelis, 2022), *Jaaginema* sp. ThrJGgm18 from Thermopyles Thermal

Springs in Greece and *Jaaginema* sp. IkpSMP32 isolated from Apolon hot spring, also in Greece. The two cyanobacterial isolates obtained in this work were deposited at the Blue Biotechnology and Ecotoxicology Culture Collection (LEGE-CC) located at CIIMAR, Portugal (Ramos *et al.*, 2018), under the names of *Leptothoe* sp. LEGE 181153 (cyanobacterial strain isolated from Cape Verde) and *Jaaginema* sp. LEGE 191154 (cyanobacterial strain isolated from Morocco).

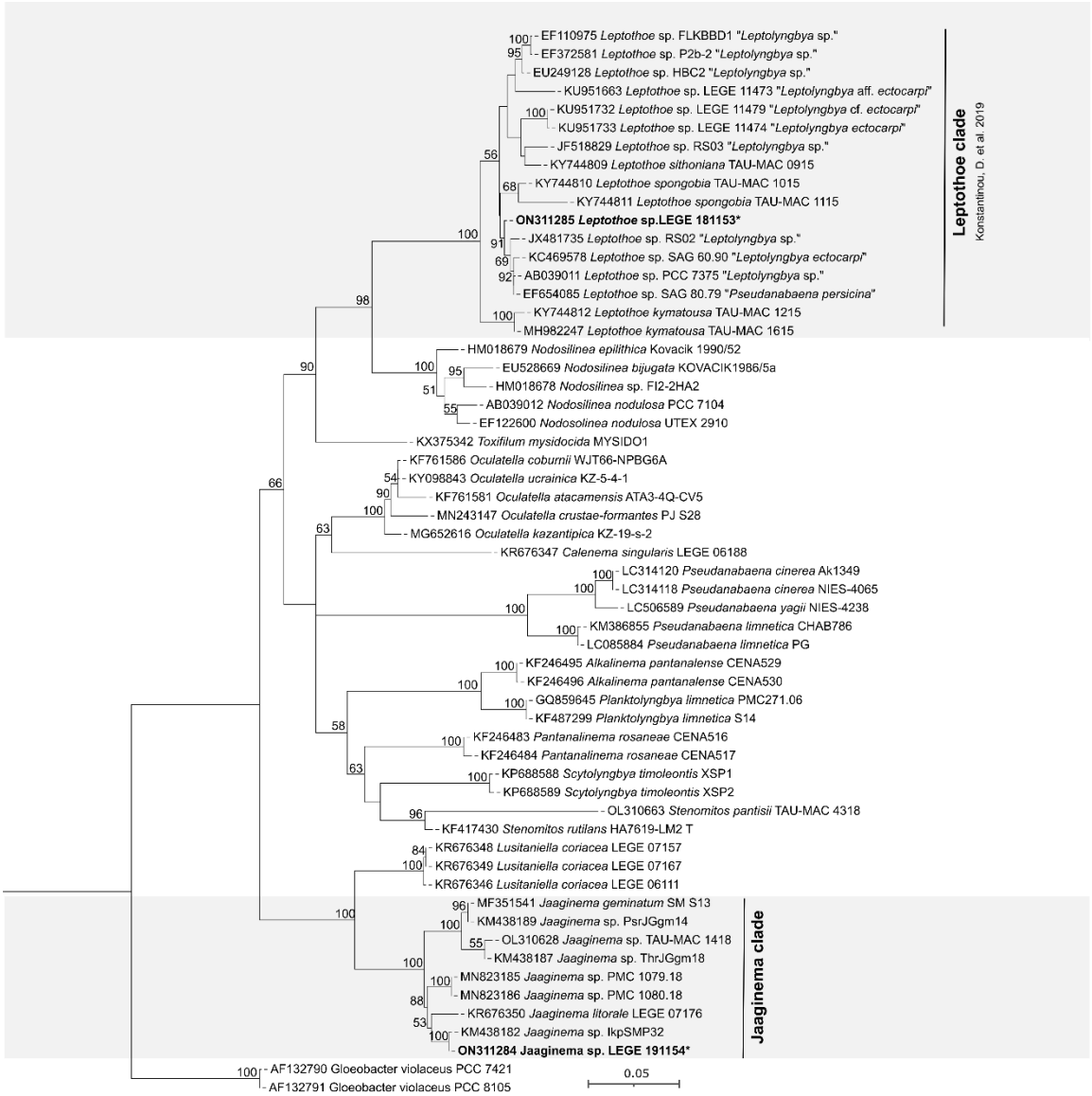

Figure 7.2. Maximum likelihood (ML) phylogenetic tree based on 58 partial 16S rRNA gene sequences of cyanobacterial strains belonging to the orders Pseudanabaenales and Synechococcales. *Gloeobacter violaceus* PCC 7421 and *Gloeobacter violaceus* PCC 8105 were used as outgroups. Phylogenetic positions of *Leptothoe* sp. LEGE 181153 and *Jaaginema* sp. LEGE 191154 are indicated in bold and with a black star. Bootstrap values over 50% are indicated at the nodes. Strains labelled with quotes indicate that names correspond to Genbank labels.

7.3.2 Morphological description

Leptothoe sp. LEGE 181153 filaments present a single trichome per sheath, unbranched, straight to curved, occasionally wavy, densely and irregularly entangled. Sheaths are colourless, thin, and slightly distinct. Trichomes are cylindrical, slightly constricted at the cross walls, and pinkish. Cells are typically barrel-shaped, isodiametric to longer than wide, 2.0 ± 0.3 μm in length and 1.5 ± 0-2 μm in width. Cell content is homogeneous. Apical cells are rounded (Figures 7.3A and 7.3C).

Jaaginema sp. LEGE 191154 presents blue-green filaments, unbranched, straight to curved, and entangled in cluster and without sheaths (sometimes with a fine mucilaginous layer around the trichomes). Trichomes can vary from not constricted to slightly constricted at the cross walls. Cells are cylindrical, longer than wide, 4.6 ± 1.1 μm in length and 2.7 ± 0.3 μm in width. Cell content is homogeneous. Apical cells are narrowed or rounded, without calyptra (Figures 7.3B and 7.3D).

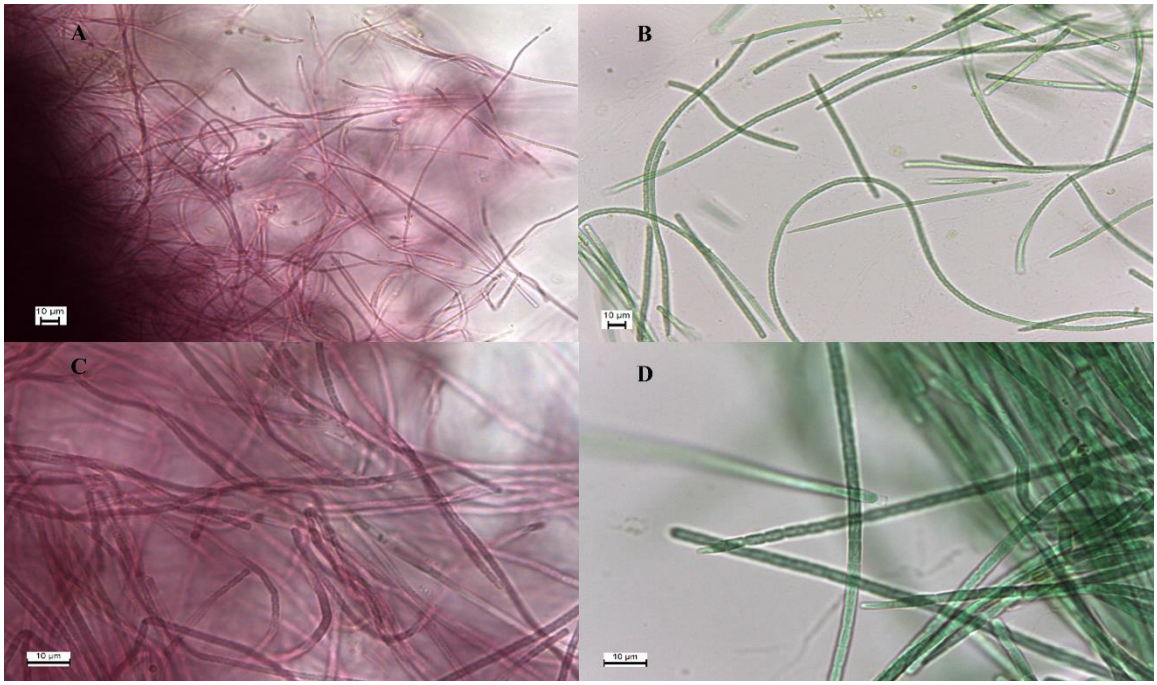

Figure 7.3. Light microscopy of A) *Leptothoe* sp. LEGE 181153 (400x); B) *Jaaginema* sp. LEGE 191154 (400x); C) *Leptothoe* sp. LEGE 181153 (1000x); D) *Jaaginema* sp. LEGE 191154 (1000x). Scale bars = 10 μm.

7.3.3 Biofilm development

The biofilm-forming capacity of the *Jaaginema* sp. LEGE 191154 and *Leptothoe* sp. LEGE 181153 strains on two different surfaces (glass and perspex) was assessed. Results obtained for wet weight, chlorophyll *a* content, and biofilm thickness for both cyanobacterial strains over 49 days are presented in Figure 7.4. The values regarding the biofilm thickness (Figures 7.4E, F) are indicated from day 21 since the biofilm thickness was below the OCT range on the first two sampling days. Biofilm development was similar for both cyanobacteria, regardless of the surface material, and the major differences between the strains were observed for the biofilm thickness parameter (Figures 7.4E, F). This tendency was more evident in biofilm thickness values obtained for glass (Figure 7.4E) from 35 to 49 days, which corresponds to a maturation stage of biofilm development. Interestingly, previous studies performed with filamentous (Romeu *et al.*, 2019, 2020, 2021) and coccoid cyanobacteria (Faria, Teixeira-Santos, Romeu, *et al.*, 2020) also showed major differences in biofilm development in their maturation phase. The effects of different conditions may be less noticeable in the initial steps of biofilm formation, while the maturation stage promotes significant variances in biofilm composition and structure.

Also noteworthy is the behaviour of both cyanobacterial biofilms developed on glass (Figures 7.4A, C, E). While for wet weight and biofilm thickness, the values were similar up to 28 days and increased on *Leptothoe* sp. LEGE 181153 biofilms from 35 to 49 days, for chlorophyll *a* quantification, a different trend between cyanobacterial strains was observed over the 49 days. Indeed, biofilm mass and thickness obtained from 35 to 49 days for *Jaaginema* sp. LEGE 191154 was on average 29% and 54% lower, respectively, compared to the values obtained for *Leptothoe* sp. LEGE 181153 strain on the same period (Figures 7.4A, E). In turn, chlorophyll *a* quantification obtained from 7 to 28 days for *Leptothoe* sp. LEGE 181153 was on average 77% lower compared to the values obtained for *Jaaginema* sp. LEGE 191154 (Figure 7.4B), but from 35 to 49 days, the chlorophyll *a* amount of *Jaaginema* sp. LEGE 191154 biofilms was on average 58% lower compared with the values obtained for *Leptothoe* sp. LEGE 181153 (Figure 7.4B), which supports the results obtained for wet weight and biofilm thickness on the same days (Figures 7.4A, E).

Chlorophyll *a* monitorization has been used to follow cyanobacterial biofilm growth (Romeu *et al.*, 2019, 2020, 2021). Considering the similarity of values obtained for wet weight and biofilm thickness up to 28 days, and the opposite trend of chlorophyll *a* quantification during this period, two hypotheses arise. First, *Leptothoe* sp. LEGE 181153 biofilms developed from 7 to 28 days may contain a higher percentage of EPS and/or of void spaces/porous structure filled with water, which can contribute to the higher values of biofilm biomass and thickness, having no impact on chlorophyll *a* level. In turn, cyanobacterial cells in these initial stages of biofilm development may be metabolically less active, contributing to the low chlorophyll *a* amount detected. Additional analysis of empty spaces from 2D cross-sectional OCT images obtained for *Leptothoe* sp. LEGE 181153 biofilms formed on glass (Supplementary Material, Figure S 7.1) revealed that the percentage of empty spaces in biofilms developed in the initial stage (21 and 28 days) was similar to the values obtained for the later stages of biofilm development (35 and 42 days), and even lower than those obtained for the last day (49 days). Hence, a porous architecture was not detected in the early biofilm growth stage. Moreover, previous studies on filamentous (Romeu *et al.*, 2019, 2020; Romeu, Domínguez-Pérez, *et al.*, 2022) and coccoid (Faria, Teixeira-Santos, Romeu, *et al.*, 2020) cyanobacterial biofilms also showed that in the initial stages of biofilm development, the chlorophyll *a* amount is lower than those detected in the later stages of biofilm development. Therefore, it is more reasonable that *Leptothoe* sp. LEGE 181153 biofilms developed from 7 to 28 days presented metabolically less active cells and consequently low chlorophyll *a* production.

For both cyanobacterial strains, the biofouling potential on the two surfaces (glass and perspex) was similar (Supplementary Material, Figure S 7.2). The major difference was observed for biofilm thickness obtained for the *Leptothoe* sp. LEGE 181153 strain at day 42 (Supplementary Material, Figure S 7.2E). On this day, a 69% decrease in biofilm thickness was achieved on perspex in comparison with biofilms developed on glass. Although perspex is relatively more hydrophobic than glass (Romeu *et al.*, 2019), previous studies which comprise different genera of cyanobacteria and cyanobacteria isolated from different locations also showed that surface hydrophobicity on its own may not have a significant impact on cyanobacterial biofilm development (Romeu *et al.*, 2019, 2020; Faria, Teixeira-Santos, Romeu, *et al.*, 2020).

Comparing the behavior of the cyanobacterial strains used in this study with strains isolated from the Portuguese coast (through laboratory experiments performed under the same conditions), it was possible to observe that the present cyanobacterial strains revealed higher biofilm development potential (Romeu *et al.*, 2019, 2020, 2021). Indeed, based on the results obtained for wet weight, chlorophyll *a* quantification, and biofilm thickness, among the six filamentous cyanobacterial strains isolated from the Portuguese coast, only two, *Nodosilinea* sp. LEGE 06020 (Romeu *et al.*, 2019) and *Nodosilinea* sp. LEGE 06145 (Romeu *et al.*, 2020), showed enhanced biofilm development ability. While both cyanobacterial strains used in this study presented biofilm wet weight, chlorophyll *a* content, and biofilm thickness values between 5 - 40 mg, 0 - 6 $\mu g.cm^{-2}$ and up to 150 μm, respectively, over the 49 days, the values achieved by *Nodosilinea* sp. LEGE 06020 (Romeu et al. 2019) and *Nodosilinea* sp. LEGE 06145 (Romeu et al. 2020) were between 5 – 50 mg, 0 – 15 $\mu g.cm^{-2}$ and up to 600 μm.

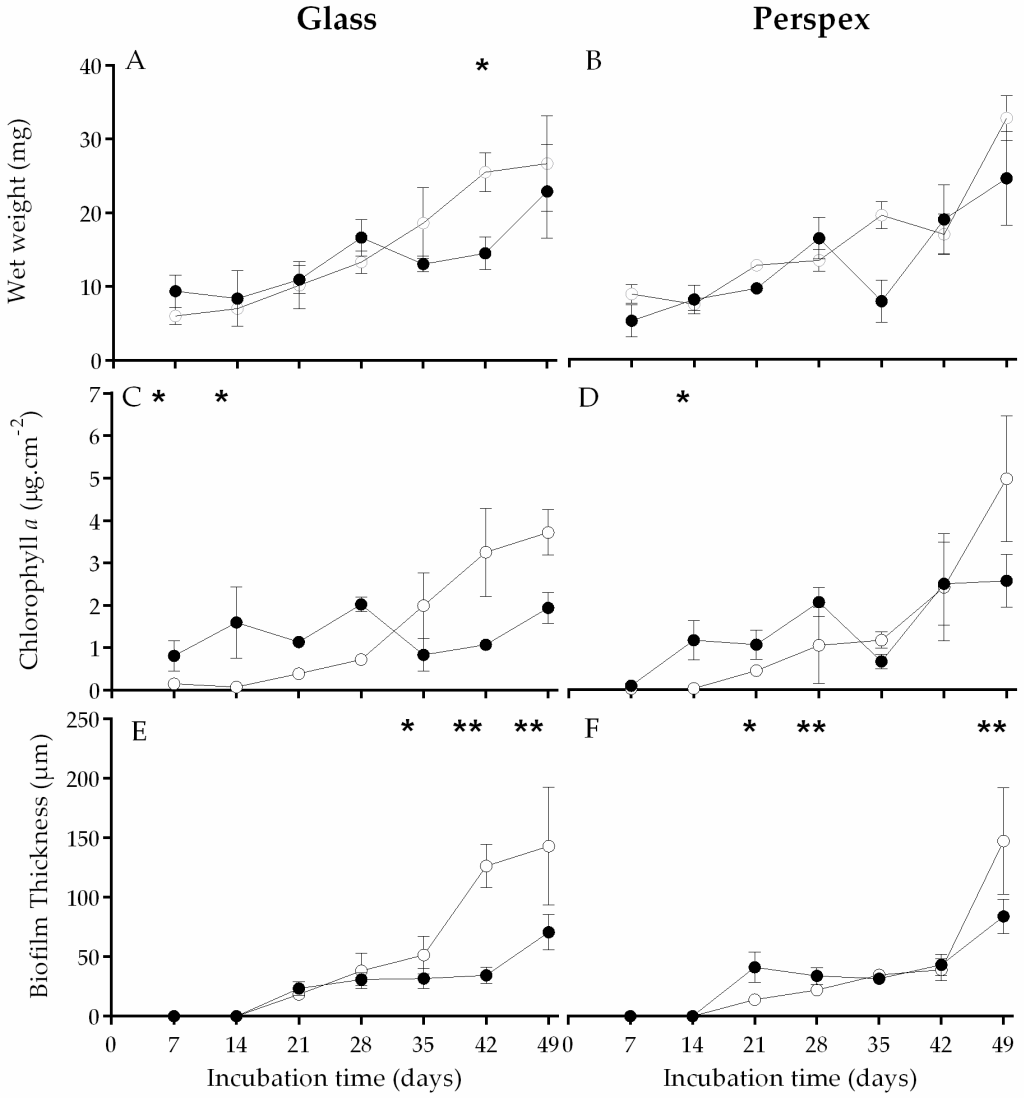

Figure 7.4. Evaluation of cyanobacterial biofilm development. The parameters analysed refer to wet weight (A, B), chlorophyll *a* (C, D), and biofilm thickness (E, F). Biofilms of *Jaaginema* sp. LEGE 191154 (closed circles) and *Leptothoe* sp. LEGE 181153 (open circles) were formed on glass or perspex at an average shear rate of 40 s^{-1} for 49 days. Symbols * and ** indicate statistically different values for $P < 0.1$ and $P < 0.05$ on each incubation time, respectively.

Figure 7.5 shows representative 2D cross-sectional images obtained by OCT at 35 and 49 days. This period corresponds to a maturation phase of biofilm development and the time at which major differences in biofilm thickness between the two cyanobacterial strains were observed (Figures 7.4E, F). The representative 2D cross-sectional images obtained by OCT confirmed the quantitative results obtained from wet weight, chlorophyll *a* quantification and biofilm thickness over these days (Figure 7.4). Indeed, thicker biofilms were formed by *Leptothoe* sp. LEGE 181153 and the major difference

between both cyanobacterial strains was observed for the last day of the experiment (49 days). Alterations in biofilm structure along this maturation stage can also be noted through a qualitative analysis. For instance, biofilms at 35 days appear to be denser than biofilms developed after 49 days, in which some void spaces are visible (Figure 7.5). Moreover, this finding is more evident for *Leptothoe* sp. LEGE 181153 biofilms, in which a denser structure can be noted at the biofilm bottom and streamers structures are shown at the biofilm top. An adjustment of biofilm structure may be required over time because, with the gradual biofilm growth, the inner layers of biofilms can have limited access to nutrients, oxygen and light (Teodósio *et al.*, 2011; Najmuldeen *et al.*, 2019; Gloag *et al.*, 2020; Peterson *et al.*, 2021). Therefore, this can be a vital adaptation strategy to ensure continuous cyanobacterial biofilm development.

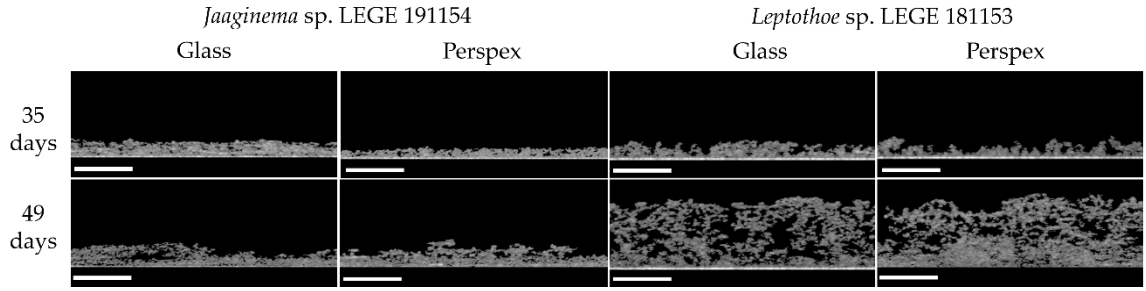

Figure 7.5. 2D cross-sectional OCT images of cyanobacterial biofilms formed at 35 and 49 days on glass and perspex. Scale bars = 200 μm.

At the end of the experiment, the structural differences between the two cyanobacterial biofilms developed on glass and perspex were also evaluated using CLSM. Examples of 3D biofilm images are presented in Figure 7.6 and biovolume values, which provide an estimate of the biomass in the biofilm ($\mu m^3.\mu m^{-2}$), are shown in Figure 7.7. Once again, it is possible to observe that denser and thicker biofilms were formed by *Leptothoe* sp. LEGE 181153, regardless of the surface used. Indeed, biovolume obtained for *Jaaginema* sp. LEGE 191154 was on average 71% and 58% lower, respectively, compared to the values obtained for *Leptothoe* sp. LEGE 181153 strain on glass and perspex, respectively. These results corroborate the quantitative values obtained from biofilm wet weight, chlorophyll *a* concentration and biofilm thickness (Figure 7.4), as well as the qualitative 2D images obtained from OCT on day 49 (Figure 7.5). Moreover, 3D biofilm

images obtained from CLSM showed different patterns between cyanobacterial strains but also among the two surfaces. While on biofilms formed by *Jaaginema* sp. LEGE 191154 extended and oriented filaments were detected, tangled and contracted filaments were formed by *Leptothoe* sp. LEGE 181153 (Figure 7.6). In turn, filaments of biofilms formed on glass appeared individualized and distanced from each other, while on perspex the filaments have a cohesive architecture (Figure 7.6). Moreover, biovolume values obtained on glass range from 23 to 80 $\mu m^3.\mu m^{-2}$, and on perspex from 47 to 112 $\mu m^3.\mu m^{-2}$ (Figure 7.7). Unlike the porous structure of the biofilms developed on glass, the biofilms of both strains formed on the perspex seem to have some organic matter such as EPS filling the voids (Figure 7.7). Previous studies showed that the EPS abundance is more dependent on the environmental conditions (Mota *et al.*, 2015) or the intrinsic characteristics of the organisms rather than on the physical and chemical features of the substratum (Del Mondo *et al.*, 2018). However, a recent paper revealed that EPS amount can also be related to biofilm production on different surfaces (Maruthanayagam *et al.*, 2020). Indeed, Maruthanayagam and his coworkers showed that cyanobacteria produced higher amounts of EPS on hydrophobic polymethyl methacrylate than on the hydrophilic glass surface.

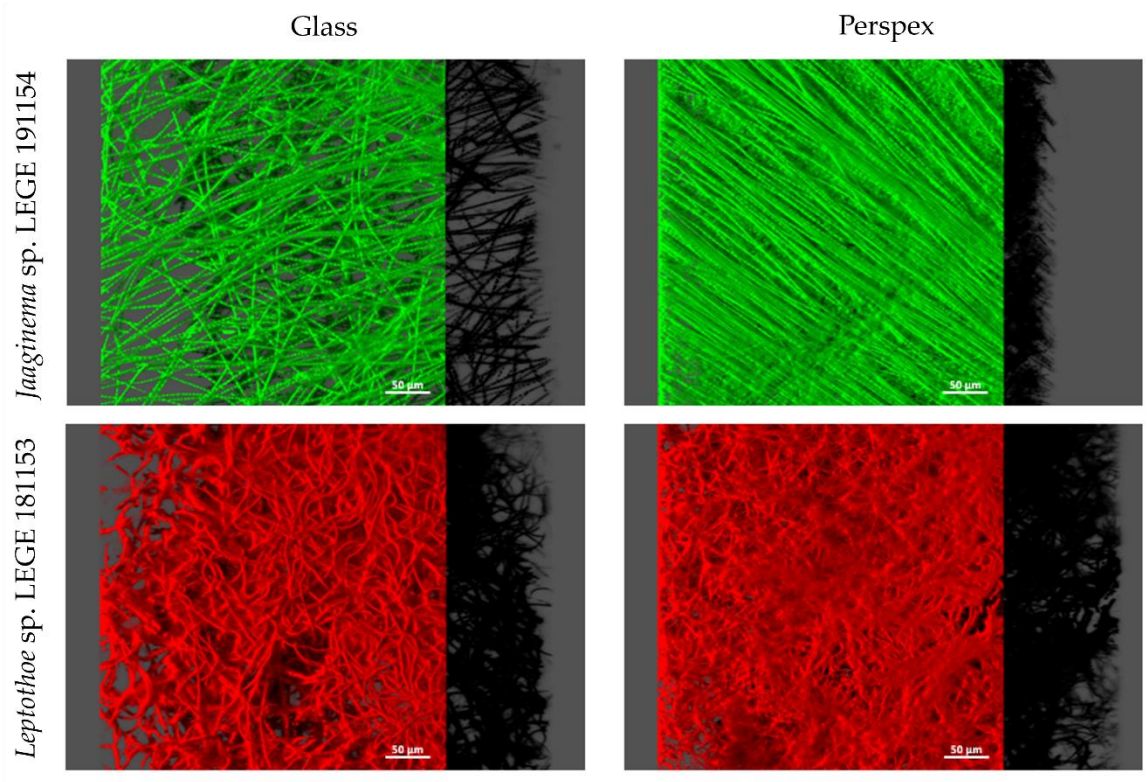

Figure 7.6. CLSM images of cyanobacterial biofilms formed after 49 days on glass and perspex. Scale bars = 50 μm.

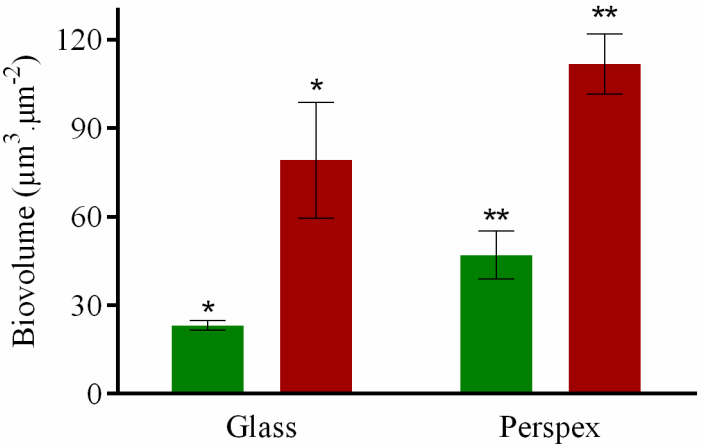

Figure 7.7. Biovolume obtained from CLSM *z*-stacks of *Jaaginema* sp. LEGE 191154 (green bars) and *Leptothoe* sp. LEGE 181153 (red bars) biofilms formed after 49 days on glass and perspex. Symbols * and ** indicate statistically different values for $P < 0.1$ and $P < 0.05$ between both cyanobacterial strains on the same surface, respectively.

7.4 Conclusions

The isolation and characterization of cyanobacterial strains are an important endeavor, due to their potential as new sources of added-value compounds, as well as their adverse and harmful impact on marine biofouling. In this work, two different cyanobacterial strains from underexplored locations in Morocco and Cape Verde were isolated and identified. Both strains showed the capacity to form biofilms, but *Leptothoe* sp. LEGE 181153 proved to be a better biofilm former than *Jaaginema* sp. LEGE 191154 under the hydrodynamic and nutritional conditions tested. Although no significant differences were found in biofilms developed by the same cyanobacterial strain on different surfaces, images obtained by CLSM denoted that biofilms formed on perspex were denser. Thus, the biofilms of *Leptothoe* sp. LEGE 181153 may be more harmful in marine environments where this surface material is present. Additional assays may evaluate the expression of virulence, adhesion and biofilm development factors by the use of omics approaches to complement the present study (Babele *et al.*, 2019; Romeu,

Domínguez-Pérez, *et al.*, 2022). Additionally, to consider the biofilm forming potential of these cyanobacterial strains in real marine environments, it would be interesting to immerse these surfaces in the sea water for prolonged periods, as already performed by the group for other promising coatings against marine biofouling (Silva *et al.*, 2021).

7.5 Supplementary Material

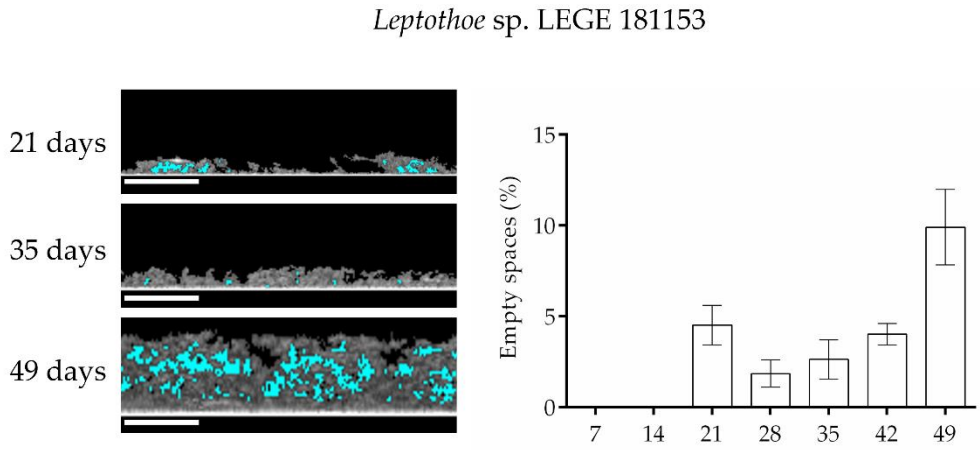

Figure S 7.1. Evaluation of biofilm empty spaces. The parameter analysed refers to the percentage of empty spaces on *Leptothoe* sp. LEGE 181153 biofilms formed on glass for 49 days. The empty spaces on cyanobacterial biofilm structures were determined as described in Faria *et al.* 2021 and represented in blue **(**scale bars = 200 μm). The values regarding the percentage of empty spaces are indicated from day 21 since the biofilm thickness was below the OCT range on the first two sampling days.

Reference:

Faria S, Teixeira-Santos R, Romeu MJ *et al.* Unveiling the antifouling performance of different marine surfaces and their effect on the development and structure of cyanobacterial biofilms. *Microorganisms* 2021;**9**:1102.

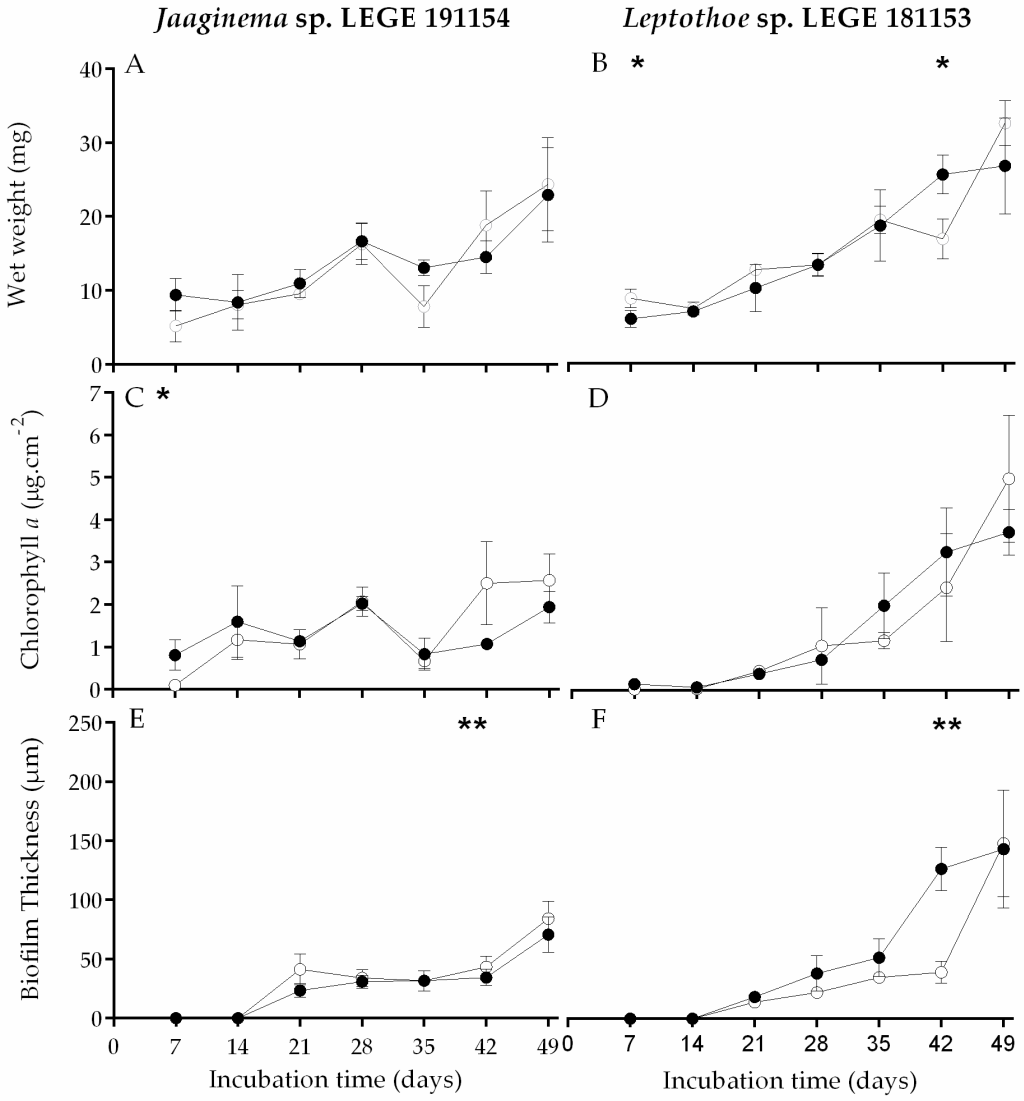

Figure S 7.2. Evaluation of biofilm development on different surfaces. The parameters analysed refer to wet weight, chlorophyll *a* quantification, and biofilm thickness. Biofilms of *Jaaginema* sp. LEGE 191154 and *Leptothoe* sp. LEGE 181153 were formed on glass (closed circles) or perspex (open circles) at an average shear rate of 40 s^{-1} for 49 days. Symbols * and ** indicate statistically different values for $P < 0.1$ and $P < 0.05$ on each incubation time, respectively.

8.

8 The use of 3D Optical Coherence Tomography to analyze the architecture of cyanobacterial biofilms formed on a carbon nanotube composite

The contents of this chapter as published as:

Romeu, M.J., Lima, M., Gomes, L.C., Jong, E.D. De, Morais, J., Vasconcelos, V., Pereira, M.F.R., Soares, O.S.G.P., Sjollema, J., Mergulhão, F. (2022) The Use of 3D Optical Coherence Tomography to Analyze the Architecture of Cyanobacterial Biofilms Formed on a Carbon Nanotube Composite. *Polymers (Basel)* **14**: 4410.

Abstract

The development of environmentally friendly antifouling strategies for marine applications is of paramount importance, and the fabrication of innovative nanocomposite coatings is a promising approach. Moreover, since Optical Coherence Tomography (OCT) is a powerful imaging technique in biofilm science, the improvement of its analytical power is required to better evaluate the biofilm structure under different scenarios. In this study, the effect of carbon nanotube (CNT)-modified surfaces in cyanobacterial biofilm development was assessed over a long-term assay under controlled hydrodynamic conditions. Their impact on the cyanobacterial biofilm

architecture was evaluated by novel parameters obtained from 3D OCT analysis, such as the contour coefficient, total biofilm volume, biovolume, volume of non-connected pores, and the average size of non-connected pores. The results showed that CNTs incorporated into a commercially used epoxy resin (CNT composite) had a higher antifouling effect at the biofilm maturation stage compared to pristine epoxy resin. Along with a delay in biofilm development, a decrease in biofilm wet weight, thickness, and biovolume was also achieved with the CNT composite compared to epoxy resin and glass (control surfaces). Additionally, biofilms developed on the CNT composite were smoother and presented a lower porosity and a strictly packed structure when compared with those formed on the control surfaces. The novel biofilm parameters obtained from 3D OCT imaging are extremely important when evaluating the biofilm architecture and behavior under different scenarios beyond marine applications.

Keywords: marine biofouling, cyanobacterial biofilms, antifouling surfaces, carbon nanotubes, Optical Coherence Tomography

8.1 Introduction

Marine biofouling causes severe economic and energetic losses, along with critical environmental and ecological consequences. Carbon nanomaterials, including carbon nanotubes (CNTs), graphene, fullerenes, and diamond-like carbon, have been recognized for their antimicrobial and anti-adhesive properties (Al-Jumaili *et al.*, 2017). Due to their remarkable mechanical strength, high thermal conductivity, and structural stability, CNTs are promising nanomaterials for several applications, namely in the industrial, environmental, and medical fields (Venkataraman *et al.*, 2019; Teixeira-Santos *et al.*, 2021). CNTs have already been tested in antifouling formulations to prevent biofouling, mainly to protect ship hulls, as well as in composite materials that come into contact with seawater. Likewise, CNTs have been reported to impact the composition of marine biofilms, as well as the settlement of macrofouling organisms (Ji *et al.*, 2018; Ba *et al.*, 2019). CNTs can be represented as a single rolled-up graphene sheet (single-walled carbon

nanotubes, SWCNTs) or a series of concentric graphene sheets (multi-walled carbon nanotubes, MWCNTs) (Lukowiak *et al.*, 2016). These carbon nanomaterials exhibit a concentric cylindrical structure with a diameter in the order of nanometers, varying according to the number of walls, and a length of several microns that is extendable by up to a few millimeters (around 4 mm). CNTs are generally incorporated into a polymeric matrix for application in protective coatings, such as polydimethylsiloxane (PDMS) (Lejars *et al.*, 2012), to improve their mechanical strength (Dustebek *et al.*, 2016). The main antibacterial and antifouling mechanisms of CNTs include the disruption of membrane integrity by electrostatic forces between the microbial outer surface and CNTs, leading to membrane oxidation. Moreover, reactive oxygen species generation may directly harm biological molecules of bacteria and/or indirectly prompt DNA destruction (Smith and Callow, 2006; Kang *et al.*, 2008; Al-Jumaili *et al.*, 2017). Although the mechanism behind the antifouling properties of CNTs is still not clear, their length, diameter, surface area, concentration, and treatment time play a significant role in their antifouling and antimicrobial activity (Smith and Callow, 2006; Kang *et al.*, 2008; Gomes *et al.*, 2021). Regarding CNT concentration, a loss of cell viability was shown to be correlated with increasing SWCNT loading. Remarkably, 5% SWCNTs may reduce biofilm development from *Bacillus anthracis* spores by 81%, while SWCNT concentrations ≥ 20% can inhibit biofilm formation (Dong and Yang, 2014). Likewise, 0.1 wt% SWCNTs can decrease *Escherichia coli* biofilms by 18%, while, with 1 wt% SWCNTs, the biofilm reduction may reach 76% (Schiffman and Elimelech, 2011). On the other hand, a study in which different CNT concentrations (0.1, 1, 2, 3, 4, and 5 wt%) were tested to inhibit *E. coli* biofilm development reported an increase in *E. coli* culturability for surfaces with CNT concentrations between 0.1 and 2 wt% compared to bare surfaces, while a decrease was observed for the remaining CNT concentrations (Gomes *et al.*, 2021).

Among these higher CNT concentrations, 3 wt% was the most promising surface for the inhibition of *E. coli* biofilms. Since CNTs' antimicrobial activity also depends on their dispersion state (Saleemi *et al.*, 2020), a lower dispersion may occur at higher loadings (4 and 5 wt%), leading to a lower antimicrobial effect on CNT-based surfaces (Gomes *et al.*, 2021). Moreover, it has also been reported that introducing small quantities of CNTs into a polymer network can result in a considerable increase in the antibacterial performance

of that polymeric matrix (Schiffman and Elimelech, 2011). In fact, polyvinyl-N-carbazole (97 wt%) with 3% of SWCNTs demonstrated similar or stronger bactericidal performance than the surfaces consisting of 100% SWCNTs (Ahmed *et al.*, 2012).

The attachment by macrofoulers, such as calcareous hard-fouling organisms (barnacles, mussels, and tubeworms) and soft-fouling organisms (non-calcareous algae, sponges, anemones, tunicates, and hydroids), is responsible for the main consequences of marine biofouling. However, the prevention of adhesion and biofilm development by microfoulers such as bacteria, cyanobacteria, and diatoms reduces the progression of biofouling to the next stages. A deeper knowledge of biofilm behavior and how it interplays with the surrounding environment will enable the development of efficient methodologies to control biofouling and mitigate its negative impacts. New imaging technologies, biochemical methods, and molecular biology tools have contributed to the technological development of biofilm science. Optical Coherence Tomography (OCT) is an exciting modality that overcomes the time-consuming and destructive methodologies of biofilm analysis, such as some microscopic techniques. In addition to the tedious sample preparation, most of the relevant microscopic techniques applied to the study of biofilms require the staining of the sample or the use of fluorochromes, which are expensive and can interfere with the local properties of the biofilm (Azeredo *et al.*, 2017). Moreover, some of them provide low-resolution images only covering a small field of view (FOV). OCT presents several advantages over the common microscopic methods since it is a simple and inexpensive technique, does not require sample preparation and/or staining procedures, and allows for the reconstruction of 3D images by *in situ*, non-invasive, and real-time imaging without affecting the biofilm structure (Wagner and Horn, 2017). Moreover, OCT can provide images at the mesoscale relatively quickly, and it allows for a great penetration depth, revealing several details of the biofilm structure (Hou *et al.*, 2019). Despite all of the advantages of this optical technique, only a limited set of image processing scripts have been specifically developed for processing OCT biofilm images. Furthermore, the analysis of structural parameters obtained from OCT is not advanced when compared, for instance, to microscopy techniques such as CLSM. Indeed, there are several software tools and libraries for biofilm image processing from microscopy, including Image Structure Analyzer (ISA) (Yang *et al.*, 2000), COMSTAT

(Heydorn *et al.*, 2000), PHobia Laser scanning microscopy Imaging Processor (PHLIP) (Mueller *et al.*, 2006), *bio*Image_L (Chávez de Paz, 2009), and DAIME (Daims *et al.*, 2006).

Studies focused on assessing the marine biofouling mitigation effect of CNT coatings can greatly contribute to improving the knowledge regarding the antifouling properties of these promising materials. Moreover, most marine studies focus on unicellular bacteria, and it is pertinent to address additional microfouler organisms such as filamentous cyanobacteria due to their improved stress and predation resistance (Claessen *et al.*, 2014). Therefore, the main goal of this study was to analyze the potential of CNT-modified surfaces to delay cyanobacterial biofilms, as well as to evaluate their impact on biofilm architecture using an in-depth OCT analysis. CNTs were incorporated in a commercially available polymer, epoxy resin, since it is commonly used to coat the hulls of small recreational vessels (Chambers *et al.*, 2006; Palmer *et al.*, 2007) due to its unique physical, chemical, and mechanical properties, no safety issues, and low cost (Mostafaei and Nasirpouri, 2013). Additionally, epoxy composites have demonstrated high durability and resistance to fatigue and UV irradiation (Hoge and Leach, 2016). CNT loading (3 wt%) was chosen according to results obtained in previous studies, in which these carbon-based surfaces were tested to inhibit *E. coli* biofilm development in the medical field (Gomes *et al.*, 2021). Additionally, textural modifications of CNTs were performed by ball milling (BM) treatment over 4 h to enhance its antimicrobial performance (Vagos *et al.*, 2020) by adjusting the CNT length and opening their closed ends to increase the specific surface area (Soares *et al.*, 2015). The textural modifications induced by ball-milling treatment proved to be effective in the inhibition of biofilm formation, reducing the amount of biofilm per surface area, biofilm thickness and surface coverage by 31, 47 and 27%, respectively, when compared to surfaces where CNTs were not ball-milled (Gomes *et al.*, 2021).

The specific aim of this study comprises the development of novel analysis parameters obtained from 3D OCT imaging to evaluate the biofilm structure. Since OCT is an *in situ*, non-destructive technique that can be applied to different fields (e.g., marine, medical, and industrial), and the knowledge of biofilm architecture is important to understand all phenomena related to this complex lifestyle, the analysis carried out in this

work is extremely relevant. To the best of our knowledge, this is the first study evaluating the impact of CNT-modified surfaces on cyanobacterial biofilm behavior using an *in vitro* platform that mimics the hydrodynamic conditions prevailing in real marine environments.

8.2 Material and Methods

8.2.1 Surface preparation

To assess the surface antifouling performance on cyanobacterial biofilm development, two control surfaces (glass, a commonly submerged artificial surface found on different equipment in aquatic and marine environments, and epoxy resin, a commercially available coating) and a CNT composite were used. The epoxy resin-coated glass was prepared following the protocol described by Faria et al. (Faria, Teixeira-Santos, Gomes, *et al.*, 2020). Briefly, the epoxy resin was produced by HB Química (Matosinhos, Porto, Portugal) and consisted of a mixture of HB Eposurf 2 resin and HB Eposurf hardener in a ratio of 10:3 (v/v). To produce the epoxy resin-coated surfaces, 70 µL of epoxy resin was deposited on the top of glass coupons using spin coating (Spin150 PolosTM, Paralab, Porto, Portugal) at 6000 rpm, with increments of 1000 rpm, for 40 s. The surfaces were dried for over 12 h at room temperature and then for 3 h at 60 °C, according to the instructions of the manufacturer.

The methodology for the preparation of the CNT composite surface was adapted from Gomes et al. (Gomes *et al.*, 2021), in which the PDMS matrix was replaced by epoxy resin. Briefly, commercially available pristine MWCNTs (NanocylTM NC3100, Sambreville, Belgium), produced by catalytic chemical vapor deposition with an average length and diameter of 1.5 µm and 9.5 nm, respectively, were used. CNTs were physically modified by BM treatment (Retsch MM200, Haan, Germany) at 15 vibrations s^{-1} for 4 h. After mixing the two epoxy resin portions, 3 wt% of CNTs was incorporated into the epoxy resin mixture since it was shown to be the most effective CNT load to reduce bacterial biofilm formation in previous studies (Gomes *et al.*, 2021). After that, 70 µL of the composite (3 wt% CNT-BM/epoxy resin) was deposited on the top of the glass

coupons using spin coating, as reported above. In previous work (Gomes *et al.*, 2021), our research group showed that bare PDMS surfaces and CNT composites had a similar film thickness (about 30 µm).

8.2.2 Surface characterization

8.2.2.1 Water contact angle measuremnts

The wettability of glass, epoxy resin, and CNT composite surfaces was assessed by measuring the contact angles with water (θ_w). This determination was performed using the sessile drop method on an SL200C optical contact angle meter (Solon Information Technology Co., Ltd., Shanghai, China) at room temperature (25 °C), as previously described (Luan *et al.*, 2020). At least 25 determinations for each material were made.

8.2.2.2 Atomic Force Microscopy (AFM)

AFM studies were performed using a Bruker Catalyst microscope in contact mode by a DNP-D cantilever with a spring constant of 0.06 N/m (Bruker, Billerica, MA, USA). The surface roughness was determined from random areas (75 × 75 or 100 × 100 µm^2) on two coupons of each material at room temperature. Surface roughness calculations and 2D images were made using the NanoScope Analysis software from Bruker. The roughness height parameter determined was the average roughness (R_a), which gives the average absolute deviation of the roughness irregularities from the mean line over one sampling length (Alves, Gomes, Vorobii, *et al.*, 2020).

8.2.2.3 Scanning Electron Microscopy (SEM)

The surface morphology at nanometer resolution was assessed by SEM. All tested surfaces were fixed to SEM stubs using carbon pads (Agar Scientific, UK) and sputter-coated with gold in an SEM coating system (Polaron CVT Ltd., Milton Keynes, UK). The sputter coating conditions were: 5 mA (plasma current), pressure < 0.1 mbar, 800 V, and argon gas for 30 s. The secondary electron detector of a Supra 40VP scanning electron microscope (Carl Zeiss Ltd., Cambridge, UK) was used to obtain the images at an

accelerating voltage of 2 kV under different magnifications. Three regions of three different coupons of each material were analyzed.

8.2.3 Organism and inoculum preparation

A filamentous cyanobacterial strain, *Nodosilinea* cf. *nodulosa* LEGE 10377, was obtained from the Blue Biotechnology and Ecotoxicology Culture Collection (LEGE-CC) located at the Interdisciplinary Centre of Marine and Environmental Research (CIIMAR), Matosinhos, Portugal (Ramos *et al.*, 2018). This cyanobacterial strain was previously isolated from a marine sponge at an intertidal zone of Aguda Beach, Arcozelo, Portugal (41.04954N8.655339 W). Cyanobacterial cells were grown in 750 mL of Z8 medium (Kotai, 1972), supplemented with 25 $g.L^{-1}$ of synthetic sea salts (Tropic Marin) and vitamin B_{12} (Sigma Aldrich, Merck, Saint Louis, MO, USA). Cultures were grown under 14 h light (10–30 µmol photons m^{-2} s^{-1}, λ = 380–700 nm)/10 h dark cycles at 25 °C.

8.2.4 Biofilm formation

To mimic the hydrodynamic conditions found in marine environments, biofilm formation was evaluated on agitated 12-well microtiter plates (VWR International, Carnaxide, Portugal) under previously optimized conditions for cyanobacterial biofilm development (Romeu *et al.*, 2019). Firstly, transparent double-sided adhesive tape was placed in the wells to fix the coupons. All coupons and plates were then subjected to UV sterilization, after which the sterile coupons were fixed as previously described (Romeu *et al.*, 2019; Gomes *et al.*, 2021).

Prior to inoculation, the cyanobacterial suspensions were adjusted to a chlorophyll *a* concentration of 0.77 ± 0.03 $µg.mL^{-1}$, since chlorophyll *a* quantification is a common method to estimate the biomass in marine environments, and this pigment is unique and predominant in all groups of cyanobacteria (Boyer *et al.*, 2009; Romeu *et al.*, 2019). Briefly, cells were harvested by centrifugation (3202*g*, for 5 min at room temperature), the supernatant was discarded and a volume of 2 mL of 99.8% methanol (Methanol ACS Basic, Scharlau Basic, Barcelona, Spain) was added. Then, the cyanobacterial suspension

was incubated for 24 h at 4 °C in the dark for maximal chlorophyll *a* extraction, the samples were centrifuged at 3202 *g* for 5 min at room temperature and the supernatant was transferred to a glass cuvette. Absorbance measurements were performed at 750 nm (turbidity), 665 nm (chlorophyll *a*), and 652 nm (chlorophyll *b*) using a V-1200 spectrophotometer (VWR International China Co., Ltd., Shanghai, China). The values obtained were used to calculate the chlorophyll *a* concentration (μg.mL^{-1}) through Equation (8.1) (Porra *et al.*, 1989):

$$Chl\ a\ (\mu g.\mathrm{mL}^{-1}) = 16.29 \times A^{665} - 8.54 \times A^{652} \quad (8.1)$$

where A^{665} and A^{652} are the absorbances at 665 nm and 652 nm, respectively.

These measurements were assessed in triplicate and dilutions were performed using Z8 medium supplemented with 25 g.L^{-1} of synthetic sea salts and vitamin B_{12}. A volume of 3 mL of the respective adjusted cyanobacterial suspension was inoculated in each well. Microtiter plates were then incubated at 25 °C in an orbital shaker with a 25 mm orbital diameter (Agitorb 200ICP, Norconcessus, Ermesinde, Portugal) at 185 rpm, resulting in an average and maximum shear rate of 40 and 120 s^{-1}, respectively (Romeu *et al.*, 2019). Biofilm formation in this system includes the shear rate estimated for a ship in a harbor, 50 s^{-1} (Bakker *et al.*, 2003), and it was shown to predict the biofouling behavior observed upon immersion in the sea for prolonged periods (Silva *et al.*, 2021). In order to mimic real light exposure periods, microtiter plates were kept under 14 h light (8–10 μmol photons m^{-2} s^{-1})/10 h dark cycles (Romeu *et al.*, 2019). Biofilm development was followed for seven weeks (49 days) since a two-month interval for maintenance is the minimum duration for economically viable underwater monitoring systems (Romeu *et al.*, 2019). During this incubation time, the medium was replaced twice a week.

8.2.5 Biofilm analysis

Biofilm analysis was performed every seven days, in which two coupons of each surface were analyzed. The culture medium was carefully removed, and the wells were

filled with 3 mL of sterile sodium chloride solution (8.5 $g.L^{-1}$) (Romeu *et al.*, 2019). The solution was carefully removed to eliminate loosely attached cyanobacteria. Subsequently, the wells were filled again with 3 mL of sterile sodium chloride solution to evaluate the structure of the cyanobacterial biofilms by OCT. To complement the characterization of cyanobacterial biofilms, the determination of their wet weight was also performed over the seven weeks, and at the end of the experiment, the morphology of cyanobacterial biofilms was evaluated by SEM.

8.2.5.1 Optical Coherence Tomography (OCT)

Images from cyanobacterial biofilms were captured and analyzed as previously described (Romeu *et al.*, 2019; Faria, Teixeira-Santos, Romeu, *et al.*, 2021). For each coupon, 2D and 3D imaging were performed with a minimum of two FOVs to ensure the accuracy and reliability of the obtained results. The 2D and 3D coordinate systems used in this work are shown in Figure 8.1. For image analysis, the bottom of the biofilm was determined as the best-fitting parabole and hyperboloid, in 2D and 3D images, respectively, that connected the white pixels resulting from light reflection on the substratum surface. A gray-value threshold that separates the biofilm from the background was calculated based on the gray-value histogram of the entire ROI (region of interest) selected (Otsu, 1979). The upper contour line of the biofilm was defined as the pixels with the highest distance to the bottom that had a gray value higher than the gray-value threshold and which were connected to the bottom of the biofilm. Objects not connected to the bottom were rejected from the biofilm structure, and the average biofilm thickness ($\bar{L}_F$) was calculated as a function of the number of pixels (or voxels) between the bottom of the biofilm and the upper contour line for each vertical line in the image ($\bar{L}_F$ is the mean of $L_{F,i}$ along the area described as $A_{x,z}$ where $L_{F,i}$ is the local biofilm thickness (μm) connected to the bottom at location i for each vertical x,z column (line of voxels)). In addition to biofilm thickness, novel parameters were analyzed from 3D analysis obtained by OCT, such as the contour coefficient, total biofilm volume, biovolume, volume of non-connected pores and the average size of non-connected pores. For this analysis, the voxel volume of a non-connected pore was defined as about 117 μm^3, and the standard

minimum non-connected pore size in the analysis was 1000 μm^3. The values of the total biofilm volume, biovolume, and volume of non-connected pores were used as cumulative values along the $L_{F,i}$ to the maximum biofilm thickness obtained for each FOV. Consequently, the final values from these parameters were represented as the values achieved at the maximum biofilm thickness. A summary of all variables used in this section is presented in Table 8.1.

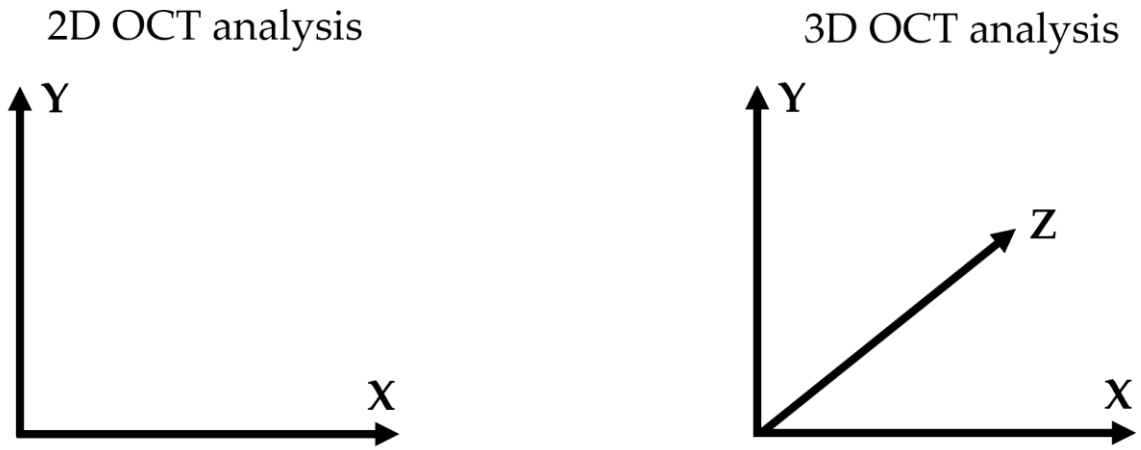

Figure 8.1. 2D and 3D coordinate systems for 2D and 3D OCT analyses, respectively. *X* represents the width, *Y* is the height, and *Z* refers to the depth.

Table 8.1. Variable definition.

Symbol	Description
x	Pixel position on the horizontal axis (width)
y	Pixel position on the vertical axis (height)
z	Pixel position on the perpendicular axis (depth)
i	Index of *x*,*z* position in the horizontal plane
N	Number of voxels in the horizontal plane of the region of interest (ROI)
V_{vox}	Volume of a voxel (μm^3)
$L_{F,i}$	Biofilm thickness at a given position *i* (μm)
$\bar{L}_F$	Average biofilm thickness (μm)
A_{ROI}	Total area of the ROI (mm^2)
$Acon_{x,z}$	Number of connected voxels identified as belonging to biofilm matrix / bacteria in the biofilm (biovolume) in a horizontal plane at position y
$Ancp_{x,z}$	Number of non-biofilm-connected voxels without an open connection to the environment (biofilm holes) in a horizontal plane at position y
$C_{F,i}$	Number of voxels identified as belonging to biofilm matrix/bacteria in the biofilm (biovolume) in column *i* (vertical line of voxels at position *i*) and connected to the environment (including corner voxels)

Contour Coefficient

The biofilm structure was analyzed by a novel structural parameter—the *contour coefficient*—defined as the number of voxels connected to the background divided by the number of voxels of a horizontal plane, $A_{x,z}$, according to Equation (8.2):

$$Contour\ coefficient = \frac{1}{N}\sum_{i=1}^{N}\frac{C_{F,i}}{A_{x,z}} \quad (8.2)$$

This parameter enables the analysis of the fraction of the biofilm that is exposed to the surrounding medium. Therefore, values close to 1 reflect a homogeneous and flat biofilm, while in biofilms with heterogeneous structures (e.g., biofilms with streamers), the values are higher than 1.

Total Biofilm Volume

The *total biofilm volume* is defined as the number of all connected voxels and nonconnected voxels in all images of a horizontal plane multiplied by the voxel size, and it provides an estimate of the total volume of the biofilm (μm^3) per area of the ROI. The *total biofilm volume* is determined according to Equation (8.3):

$$Total\ biofilm\ volume\ (\mu m^3/mm^2) = \frac{\sum_{all\ planes}[(Acon_{x,z}+Ancp_{x,z})\times V_{vox}]}{A_{ROI}} \quad (8.3)$$

Biovolume

The *biovolume* is defined by the number of all connected voxels in all images of a horizontal plane multiplied by the voxel size, and it provides an estimate of the biomass in the biofilm (μm^3) per area of the ROI. Biovolume is determined according to Equation (8.4):

$$Biovolume\ (\mu m^3/mm^2) = \frac{\sum_{all\ planes}[(Acon_{x,z})\times V_{vox}]}{A_{ROI}} \quad (8.4)$$

Porosity

The percentage of biofilm *porosity* was quantified from data obtained from the *volume of non-connected pores* and the *total biofilm volume*, according to Equation (8.5):

$$Porosity\ (\%) = \frac{Volume\ of\ non{-}connected\ pores}{Total\ biofilm\ volume} \times 100 \quad (8.5)$$

The *volume of non-connected pores* (μm³) per area of the ROI is defined as the number of non-connected voxels in all images of a stack multiplied by the voxel size and normalized by area, and it is determined according to Equation (8.6):

$$Volume\ of\ non-connected\ pores_{x,z}\ (\mu m^3/mm^2) = \frac{\sum_{all\ planes}[Ancp_{x,z} \times V_{vox}]}{A_{ROI}} \quad (8.6)$$

Average Size of Non-Connected Pores

The determination of the average size of *non-connected pores* inside the biofilm structure was quantified, assuming a minimum size of *non-connected pores* equal to 1000 μm³ and defining a voxel size of 1 as corresponding to 117 μm³, as reported above.

8.2.5.2 Wet weight determination

The determination of the biofilm wet weight was performed as previously reported (Romeu *et al.*, 2021). Briefly, a sterile sodium chloride solution (8.5 $g.L^{-1}$) was carefully removed from the wells, coupons were detached, weighed, and the biofilm wet weight was obtained as the difference from the initial coupon weight determined prior to inoculation.

8.2.5.3 Scanning Electron Microscopy (SEM)

After 49 days of incubation, the morphology of cyanobacterial biofilms formed on the three surface materials was analyzed by SEM. Coupons were removed from the microtiter plates, dehydrated in aqueous solutions of increasing ethanol concentrations (10, 25, 40, 50, 70, 80, 90, and 100% (v/v)) and left in a desiccator until SEM analysis (Alves,

Gomes, Rodríguez-Emmenegger, *et al.*, 2020). The samples were then sputter-coated using the equipment and conditions described in Section 8.2.2.3 and observed in a Supra 40 VP scanning electron microscope (Carl Zeiss Ltd., Cambridge, UK) at a 2 kV accelerating voltage and a magnification of 1000×.

8.2.6 Statistical analysis

A total of four replicates (two biological assays with two technical replicates each) were analyzed. Data analysis was performed using the statistical program GraphPad Prism® for Windows, version 6.01 (GraphPad Software, Inc., San Diego, CA, USA). Differences between biofilm wet weight, biofilm thickness, total biofilm volume, biovolume, porosity, and the average size of non-connected pores from data obtained by OCT were evaluated using one-way ANOVA with Tukey's multiple comparisons test. The error bars shown in the graphs correspond to the standard deviation (SD) of the mean. Statistically significant differences between the different surfaces for the same sampling day were considered for P values < 0.05 (corresponding to a confidence level greater than 95%).

8.3 Results and Discussion

8.3.1 Surface characterization

It is recognized that surface properties such as topography and physicochemistry affect their antiadhesive and/or antimicrobial behavior (Selim, El-Safty, *et al.*, 2018; Fan *et al.*, 2021). Thus, all tested surfaces were first investigated regarding (i) wettability by water contact angle measurements, (ii) topography and roughness by Atomic Force Microscopy (AFM), and (iii) morphology and structure by Scanning Electron Microscopy (SEM). The results obtained from the water contact angle measurements and roughness analysis are shown in Table 8.2. Given that substrates with a water contact angle (θ_w) of < 90° are considered to be hydrophilic (Mahltig, 2016), glass is the most hydrophilic surface (θ_w = 40.9° ± 7.4°), followed by the CNT composite (θ_w = 68.9° ± 4.9°), and the epoxy resin-coated glass (θ_w = 76.3° ± 2.5°), which is significantly more hydrophobic (P < 0.05) than the resin

composite. Lower hydrophobic properties caused by the incorporation of 3 wt% ball-milled CNTs were also observed in previous work in another polymeric matrix (PDMS) (Gomes *et al.*, 2021). Regarding the average roughness (R_a) value determined by AFM (Table 8.2), glass and epoxy resin appeared to be smoother surfaces (R_a of 6.3 and 13 nm, respectively) than the CNT composite, which registered a R_a value of about 70 times higher than the remaining surfaces.

Table 8.2. Water contact angle measurements (θ_w) and roughness (R_a) determined for the tested surfaces.

Surface	**Water contact angle** θ_w (°)	**Roughness** R_a (nm)
Glass	40.9 ± 7.4	6.3
Epoxy resin	76.3 ± 2.5	13.1
CNT composite	68.9 ± 4.9	644

Figure 8.2 reveals the topography and morphology of the tested surfaces obtained from AFM and SEM imaging, respectively. Glass and epoxy resin-coated glass were the most homogeneous and smooth materials (Figure 8.2A, B, D, E). In opposition, the CNT composite (Figure 8.2C, F) was the roughest surface, presenting CNT agglomerates that form small elevations on the material (Figure 8.2F).

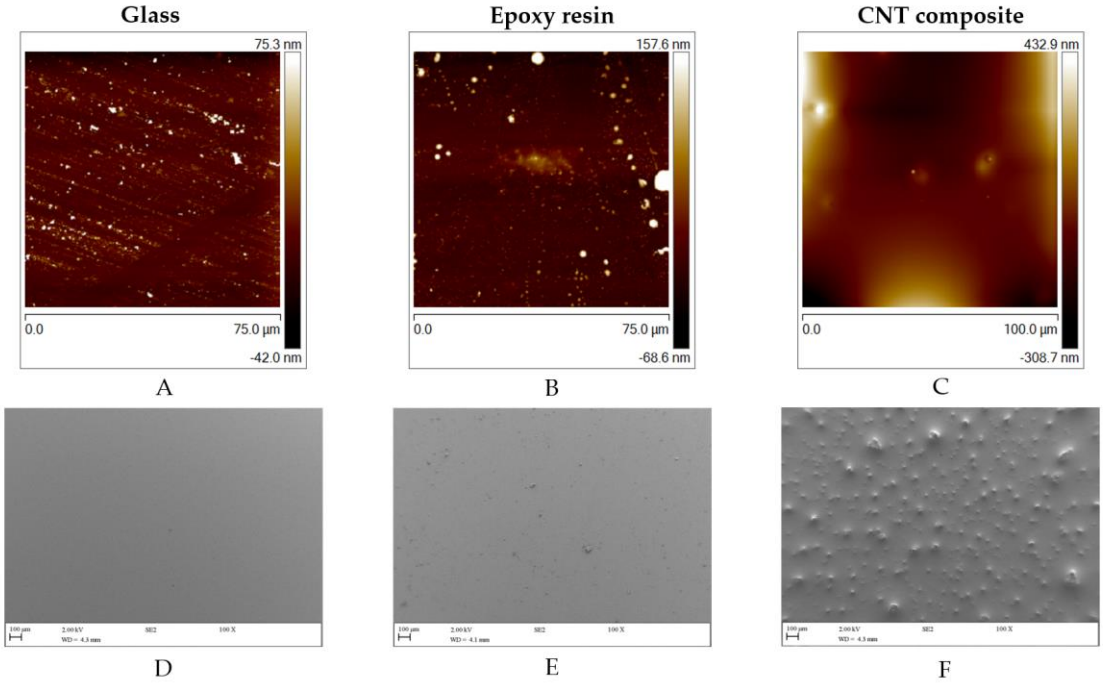

Figure 8.2. Two-dimensional AFM (A–C) and SEM (D–F) images of glass, epoxy resin, and CNT composite. The vertical color bars in the AFM images correspond to the *z*-range (surface height range) of the respective image. The SEM images have a magnification of 100× and the scale bar is equivalent to 100 µm.

8.3.2 Biofilm formation

The structure of biofilms can be numerically quantified with imaging tools to investigate and monitor the effect of different compounds, surfaces and/or environmental factors on biofilm architecture. In the present work, cyanobacterial biofilm development on different surfaces was monitored over 7 weeks and the quantitative results obtained from 3D OCT analysis are shown in Figure 8.3. The values indicated in Figure 8.3B–F are only presented from day 14 since, for the first sampling day (day 7), the biofilm thickness was below the OCT range. In general, a gradual temporal increase in biofilm wet weight (Figure 8.3A), thickness (Figure 8.3B), and biovolume (Figure 8.3D) were observed, showing that this filamentous cyanobacterium is a good biofilm former. However, growth was more evident on glass and epoxy resin than on the CNT composite. In fact, for biofilm wet weight (Figure 8.3A), from day 7 to day 49, increases of 71%, 64%, and 49% were observed for glass, epoxy resin, and the CNT composite, respectively, and for biofilm thickness (Figure 8.3B), increases of 87%, 82%, and 72% were registered over time for the same surfaces. Regarding biovolume, increases of 77%, 64%, and 64% were observed for

glass, epoxy resin and the CNT composite, which indicates that these CNT-modified surfaces can delay biofilm development when compared to pristine epoxy resin and glass. Moreover, on days 42 and 49, a reduction in cyanobacterial biofilm development was observed on the CNT composite surface. Regarding the biofilm thickness, on day 42, the values obtained on glass and epoxy surfaces were 58% and 47% higher than those obtained on the CNT composite surface, respectively, while on day 49, the biofilm thickness was 58% and 23% higher than those attained on the composite (Figure 8.3B). Additionally, the biovolume obtained on the glass and epoxy surface was 45% and 43% higher when compared to the values obtained on the CNT composite surface, respectively. Moreover, on day 49, these values were 46% and 6% higher as compared to the modified epoxy resin (Figure 8.3B). Since, in the early stages of biofilm formation (days 7, 14, and 21), all parameters were similar between the surfaces, the results suggest that the CNT composite surface may have a greater antifouling effect on the maturation stage of these cyanobacterial biofilms as compared to the other two types of substrates.

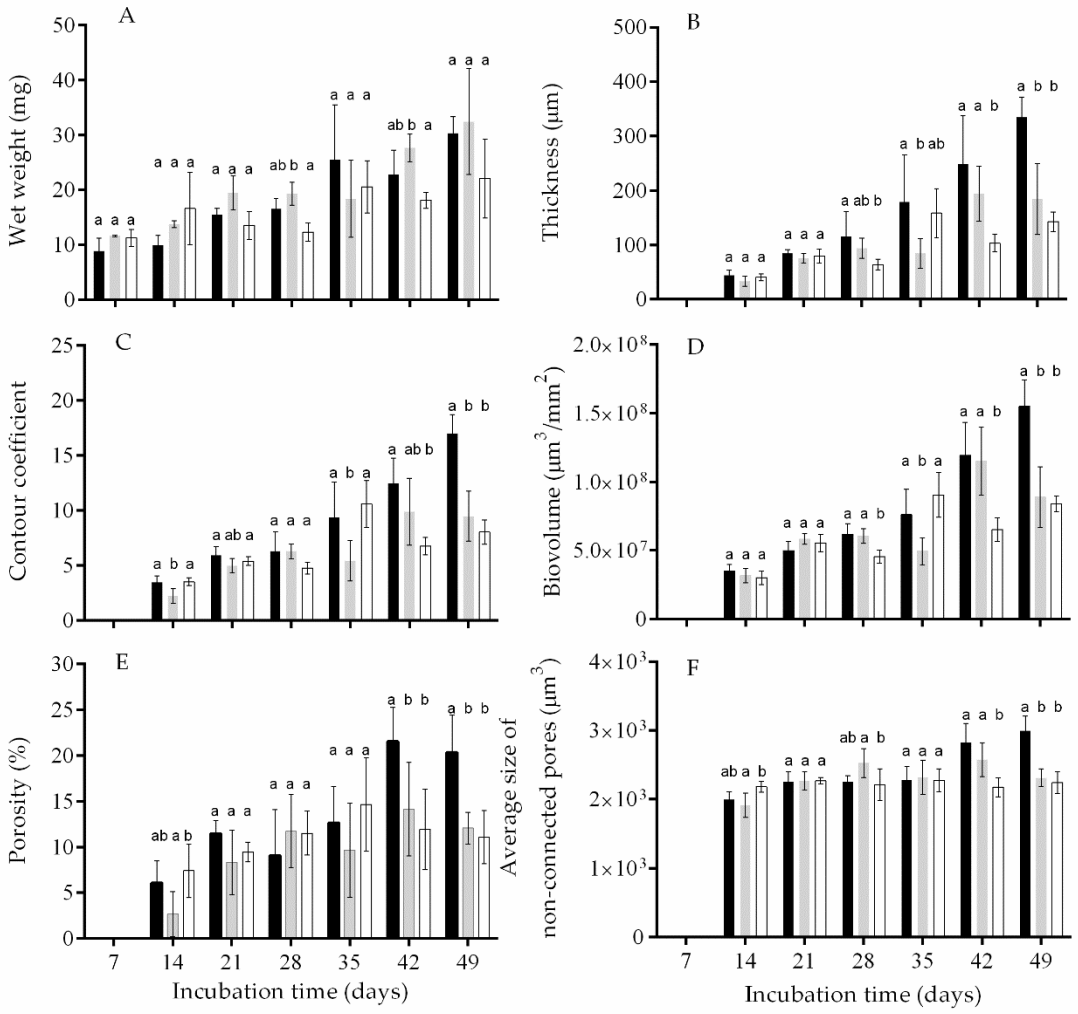

Figure 8.3. *Nodosilinea* cf. *nodulosa* LEGE 10377 biofilm development on different surfaces (glass—black, epoxy resin—grey, CNT composite—white). The parameters analyzed refer to biofilm wet weight (A), thickness (B), contour coefficient (C), biovolume (D), porosity (E), and average size of non-connected pores (F). Mean values and SD from two biological assays with two technical replicates each are represented. For each sampling day, different lowercase letters indicate significant differences between surfaces ($P \leq 0.05$; one-way ANOVA with Tukey's multiple comparisons test.

Surface topography plays a considerable role in the way in which marine fouling organisms adhere to surfaces, settle on them, and interact with them (Leonardi and Ober, 2019). In the nanoregime, the topography can have a robust impact on the wettability of the surface, as well as a direct effect on the contact area available for fouler adhesion. Once more surface contact area is available, more settlement may take place and, consequently, the organisms may be more difficult to remove (Schumacher *et al.*, 2007). Moreover, the

surface roughness may also promote an increase in the settlement and adhesion strength of biomolecules, including the proteinaceous adhesives used by many marine organisms (Yandi *et al.*, 2014). Therefore, rough surfaces present an opportunity for fouling organisms to settle within and between the topographic features, protecting them from hydrodynamic forces (Scardino *et al.*, 2008). Highly textured surfaces also provide greater surface area for adhesive cements to adhere (Brady and Singer, 2000). Even though topography does not act as a unique mechanism, it is still a key feature that must be considered in the design of new materials. Since, in the early stages of biofilm formation, the values attained were similar between the surfaces (Figure 8.3), it appears that differences in surface properties, namely in average roughness (Table 8.2, Figure 8.2), may have been responsible for the differences registered in the later stages of biofilm development. Therefore, an antimicrobial effect rather than an anti-adhesive effect may explain the impact of CNT-modified surfaces in long-term cyanobacterial biofilm development. CNT composite may lead to unstable and weak biofilm development due to the piercing effect in the cell's membrane of the first biofilm layers (Gomes *et al.*, 2021). However, this viability effect may be reflected only in the subsequent biofilm layers, as cell-to-cell adhesion will be hampered if cells in the initial layers are damaged (Moreira *et al.*, 2017). Moreover, biological processes such as cell reproduction and EPS production by these first-adhered impaired cells may affect biofilm development.

Biofilms formed on the CNT composite were also more homogenous on days 42 and 49 than those developed on glass and epoxy resin (Figure 8.3C), since the values of the contour coefficients were closer to 1, which reflects a homogeneous and flatter biofilm. Indeed, on day 42, the contour coefficient was around 46% and 32% lower for the CNT composite surface when compared to glass and epoxy resin, respectively. On the other hand, on day 49, these differences reached 53% and 15% when compared to the values obtained on glass and epoxy resin. Since the top of the biofilm grown on the carbon-based surface became flattened, without heterogeneous top structures (such as streamer structures), the superficial area in contact with the surrounding environment decreased, as well as the ability of nutrients and oxygen to penetrate within the biofilm. Likewise, in the maturation stage of biofilm development, a lower percentage of porosity (Figure 8.3E)

and a smaller average size of non-connected pores (Figure 8.3F) were determined for biofilms formed on the CNT composite surface when compared with control surfaces.

The lower porosity and average size of non-connected pores may contribute to the lower viability of the cells located on the deepest biofilm layers since the internal mass transfer of nutrients to the inner layers of the biofilm may be hindered, contributing to the antimicrobial effect of these surfaces.

Figures 8.4 – 8.6 show representative 2D cross-sectional and 3D OCT images of *Nodosilinea* cf. *nodulosa* LEGE 10377 biofilms on glass, epoxy resin, and CNT composite after 49 days. Both 2D and 3D OCT images illustrate quantitative data on biofilm biomass and porosity (Figure 8.3). In fact, on the last day of the experiment, a higher percentage of biofilm biomass and porosity was observed on the glass surface when compared with the epoxy resin and the CNT composite surface. The biofilm top structure can also be observed as flatter for biofilms formed on the CNT composite than biofilms developed on glass and epoxy resin (Figures 8.4 and 8.5), as it was also indicated by quantitative data (Figure 8.3C). Moreover, in the biofilm formed on the glass, it was possible to observe long streamers, which can reach around 500 μm (Figure 8.4). On the other hand, according to representative 3D OCT images, biofilms developed on the CNT composite only present structures that reach around 250 μm. Through representative images of the size of non-connected pores, it was also possible to observe that these values can reach around 98,000 μm^3 in biofilms developed on glass, while values around 35,000 μm^3 and 19,000 μm^3 were achieved on epoxy resin and the CNT composite, respectively.

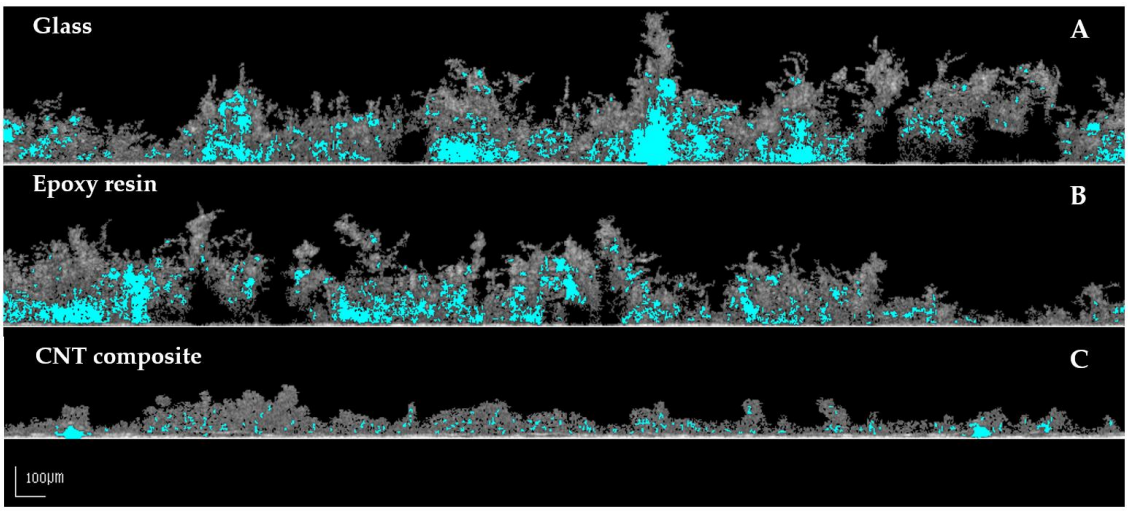

Figure 8.4. Representative 2D cross-sectional OCT images of *Nodosilinea* cf. *nodulosa* LEGE 10377 biofilms developed on glass (A), epoxy resin (B), and CNT composite (C) after 49 days. The empty spaces in the biofilm structure are filled in blue (scale bar = 100 µm).

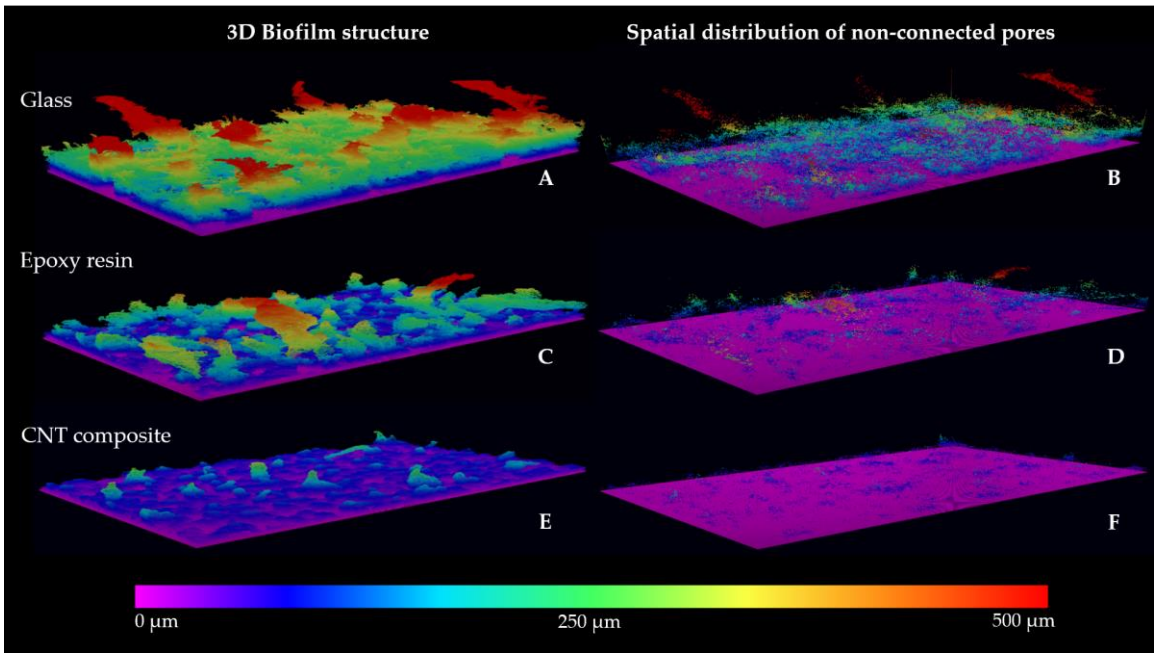

Figure 8.5. Representative 3D OCT images of *Nodosilinea* cf. *nodulosa* LEGE 10377 biofilms formed on glass (A), epoxy resin (C), and CNT composite (E) after 49 days. The spatial distribution of non-connected pores on the biofilm is also shown (B, D, F). The color scale shows the distance from the substrate surface.

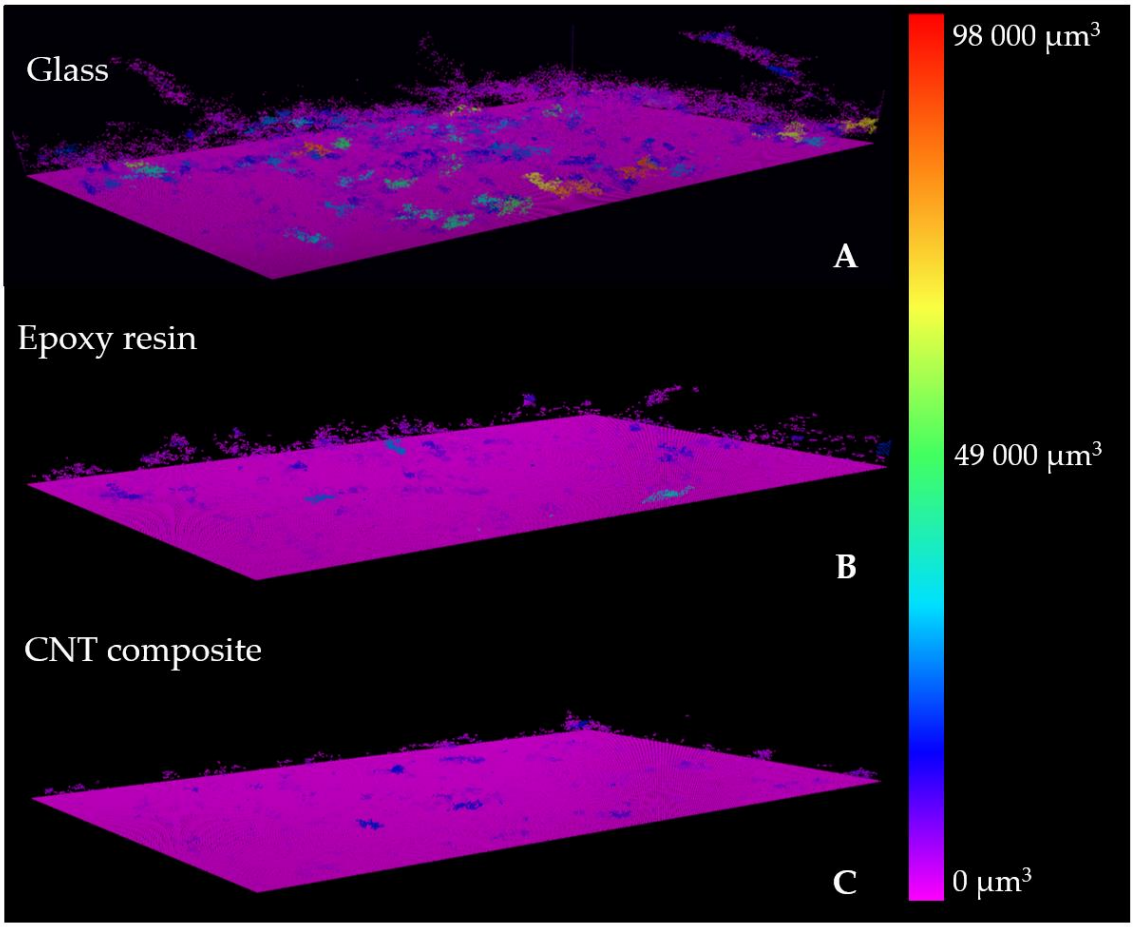

Figure 8.6. Representative 3D OCT images of the distribution of non-connected pores by size from *Nodosilinea* cf. *nodulosa* LEGE 10377 biofilms formed on glass (A), epoxy resin (B) and CNT composite (C) after 49 days. The color scale shows the range of the size of non-connected pores.

Mature biofilms consist of multidimensional heterogeneous structures with interstitial pores, which ensure the water and nutrient flow and that influence their resistance to mechanical or chemical challenges (Laspidou and Aravas, 2007; Peterson *et al.*, 2015, 2021; Bas *et al.*, 2017). Biofilm biomass, thickness, and structure have a strong effect on the performance of underwater marine devices (Delauney *et al.*, 2010). Consequently, the knowledge of these biofouling parameters is essential for the design and maintenance of submerged marine equipment. In this work, CNT composite surfaces were tested for the prevention of cyanobacterial biofilms. Biofilms formed on this carbon-modified surface were more homogeneous, flatter, less porous, and had a tightly packed structure compared with the control surfaces, as it can be proved by the quantitative (Figure 8.3C, E, F) and qualitative (Figures 8.4 – 8.6) data. Although biofilm growth is reduced on these

surfaces, which may be beneficial for the performance of nautical equipment, it may have an impact on the efficacy of methods to eradicate the biofilms formed on this surface material. Firstly, due to their lower porosity and a smaller average size of non-connected pores (Figure 8.3E, F), the internal mass transfer may be hampered, and chemical compounds used for biofouling control may not reach the inner layers of the biofilm (Sjollema *et al.*, 2011). Moreover, a homogeneous structure (Figure 8.3C) can be associated with greater cohesion across the whole biofilm structure. In this scenario, the detachment of biofilm components either by increasing hydrodynamic forces or by applying mechanical cleaning methods would be facilitated if a heterogeneous structure was present (such as the presence of some streamers). As a flatter biofilm was present, the detachment or removal phenomena may be hindered. Although there are several biofilm structural parameters described in the literature (Milferstedt *et al.*, 2009; Pons *et al.*, 2009), there has been a tendency to use only a limited number of them (Rodríguez and Bishop, 2006; de Carvalho and da Fonseca, 2007; Luef *et al.*, 2009). This evidence makes cross-comparisons difficult and can be justified by the fact that only some of these parameters computed from biofilm images can be intuitively associated with identifiable biological processes. The analysis of biofilms based on biofilm weight, thickness, and biovolume alone, which are typically used for the description of biofilm structure, does not provide complete information on biofilm development. Only the combination of all evaluated structural parameters leads to a complete overview of biofilm behavior on the different surfaces. Moreover, the contour coefficient reported in this work may be a relevant parameter to replace or complement the analysis of biofilm roughness since more reliable structural biofilm information is provided by this novel parameter.

Analysis by SEM was also performed to assess the morphological differences shown by the cyanobacterial biofilms grown on the distinct surfaces (Figure 8.7). As observed by OCT (Figures 8.3 – 8.5), the SEM analysis reveals differences in the cyanobacterial biofilm growth patterns on different surfaces. The highest and lowest cyanobacterial biofilm amounts were observed on glass and the CNT composite surfaces, respectively. Indeed, SEM observations showed that while the biofilm formed on the control surfaces (glass and epoxy resin) looks like a dense filamentous network that

covers practically the entire surface area, the biofilm grown on the composite surface presented lower-density cell aggregates.

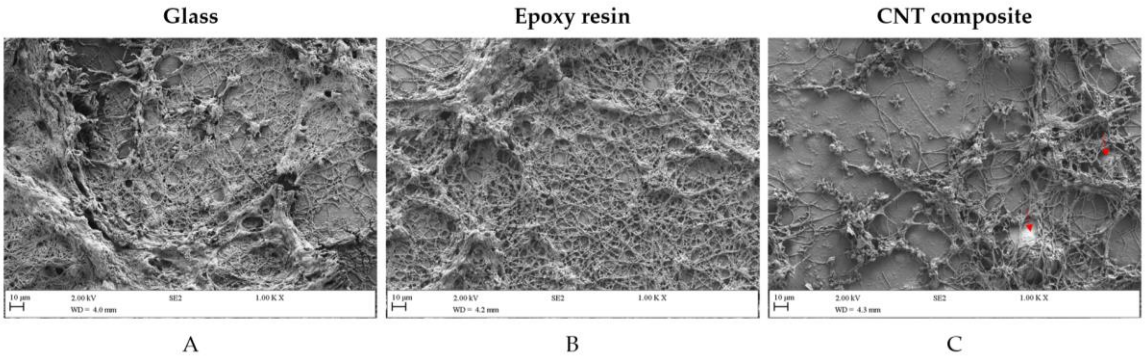

Figure 8.7. SEM images of *Nodosilinea* cf. *nodulosa* LEGE 10377 biofilms formed on glass (A), epoxy resin (B), and CNT composite (C) after 49 days of incubation. The red arrows in (C) indicate clusters of CNTs. Magnification = 1000×; scale bar = 10 μm.

OCT is a relevant tool for assessing the spatial organization and heterogeneity of biofilm since 2D and 3D datasets contain a representative description of the overall biofilm structure at the mesoscale with μm-resolution (Wagner and Horn, 2017). Moreover, by OCT analysis, the laborious nature, as well as the costs entailed with microscopic techniques, can be reduced.

Few studies focus on longer assays for the assessment of CNTs on marine biofilm formation (Sousa-Cardoso *et al.*, 2022). In fact, some *in vitro* studies have been performed between 6 (Martinelli *et al.*, 2011) and 10 days (Ba *et al.*, 2019), but only a study performed by Xie et al. (Xie *et al.*, 2021) achieved the 20 days necessary to evaluate the antifouling effect of CNT-based antifouling coatings. Moreover, these studies focus on other marine bacteria, diatoms, algae, and macrofoulers (Martinelli *et al.*, 2011; Ba *et al.*, 2019; Xie *et al.*, 2021). For instance, an *in situ* study performed by Sun et al. (Sun, Yanhe Lang, *et al.*, 2020) with pioneer biofilm bacteria over 24 days showed that all CNT/PDMS composites decreased Proteobacteria biofilm formation but increased cyanobacterial biofilm development. Other studies showed a promising reduction in biofilms formed by different microfoulers at different times on distinct CNT-based antifouling coatings (Sun and Zhang, 2016; Yang *et al.*, 2016; Ji *et al.*, 2018; Sun, Yanghe Lang, *et al.*, 2020; D. Zhang *et al.*, 2021; Fan *et al.*, 2021; Xie *et al.*, 2021).

In this study, biofilm was evaluated as a whole structure, including cells, water, and the compounds excreted by the cyanobacterial cells. Considering that a greater number of active cells in a biofilm can lead to greater surface colonization and biofilm development potential, future studies should include complementary techniques to assess the viability and/or the metabolic state of biofilm cyanobacterial cells (Van den Driessche *et al.*, 2014; Mountcastle *et al.*, 2021). Since the mechanisms behind the antifouling properties of CNTs are still not clear (Teixeira-Santos *et al.*, 2021), it is relevant to conduct further assays in marine conditions with CNT-/epoxy resin surfaces, incorporating different CNT concentrations, lengths, diameters, and surface areas, as well as functionalized CNTs, with different polymeric matrices and different fouling organisms (Smith and Callow, 2006; Kang *et al.*, 2008; Gomes *et al.*, 2021; Teixeira-Santos *et al.*, 2021). The generation of oxidative stress and mechanical damage through the direct perforation of the microorganisms' outer membranes and the release of intracellular content are some of the mechanisms that may be involved in CNT action (Kang *et al.*, 2008). Indeed, the representative SEM images of the morphology and structure of CNTs in the composite reveal the presence of CNT agglomerates (Figure 8.2F; Supplementary Material, Figure S 8.1), which can interact with the membrane of cyanobacterial cells by the known piercing phenomenon and be one of the strategies associated with the antifouling properties of these surfaces. *In situ* assays are also particularly recommended to assess the impact of these surfaces on the adhesion and biofilm formation of multiple microfouling organisms, as well as on the subsequent attachment of macrofoulers. Moreover, additional concerns with these nanostructured surfaces may be related to the fact that they may be damaged in harsh marine environments, leading to a reduction in their antifouling ability and lifespan. Hence, the development of robust and mechanically stabilized surfaces is critical (Jin *et al.*, 2022).

Different biofilm techniques provide valuable and complementary information about different aspects of the complex biofilm structure. Therefore, a multidisciplinary approach that integrates different methodologies is recommended to obtain a more realistic biofilm representation and to better understand the complex phenomenon of marine biofilm development.

8.4 Conclusions

A set of novel structural parameters obtained from OCT imaging was developed to quantify the marine biofilm structure over time and on three different surface materials, one of them with recognized antifouling activity. CNT-modified surfaces delayed cyanobacterial biofilm development in the maturation stage of the biofilm. Biofilms developed on the composite had reduced wet weight, thickness, and biovolume and were smoother and less porous than those formed on epoxy resin and glass (control surfaces). Analysis of novel parameters obtained by OCT imaging enables a deeper understanding of the biofilm development process in different settings, including the marine environment.

8.5 Supplementary Material

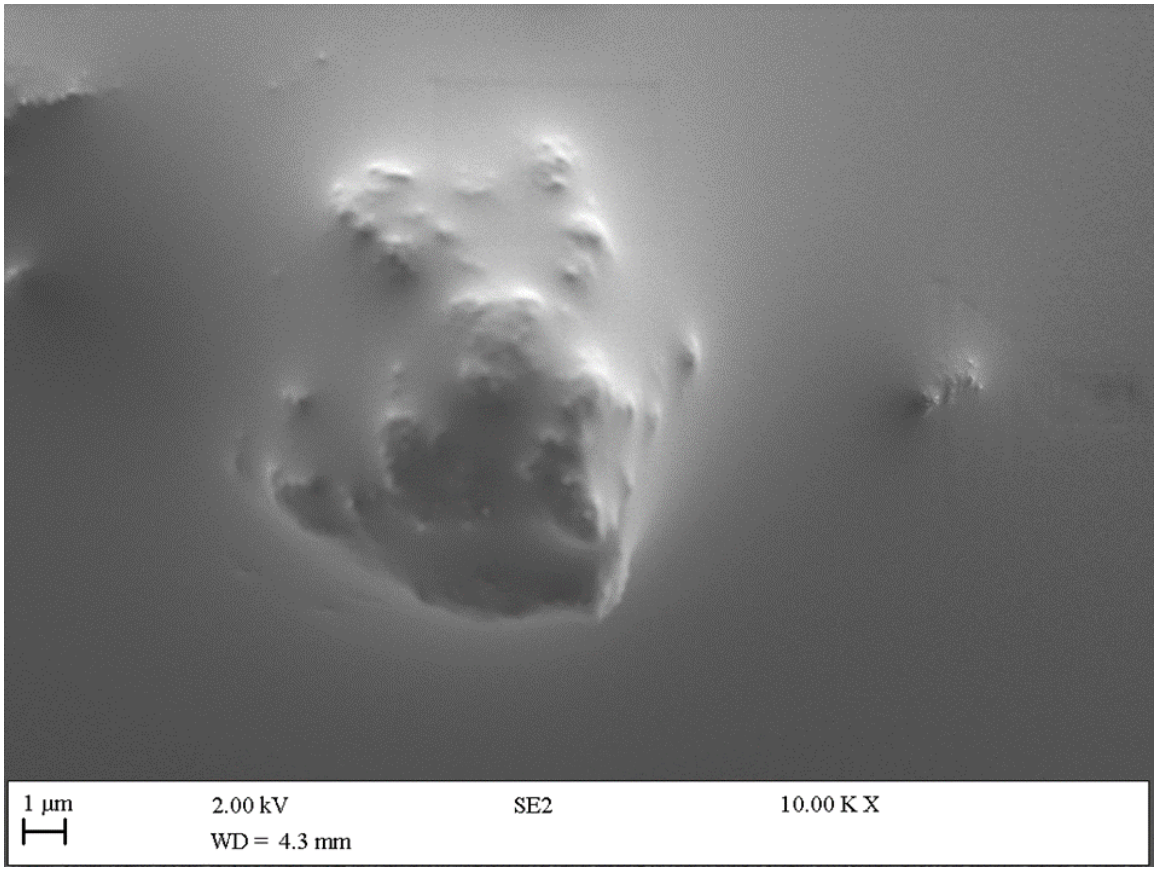

Figure S 8.1. Representative SEM image of an agglomerate of CNTs on the CNT composite surface. Magnification = 10,000×; scale bar = 1 µm.

9.

9 How do graphene composite surfaces affect the development and structure of marine cyanobacterial biofilms?

The contents of this chapter as published as:

Romeu, M.J., Gomes, L.C., Sousa-Cardoso, F., Morais, J., Vasconcelos, V., Whitehead, K.A., Pereira, M.F.R., Soares, O.S.G.P., Mergulhão, F. (2022) How do Graphene Composite Surfaces Affect the Development and Structure of Marine Cyanobacterial Biofilms? *Coatings* **12**: 1775.

Abstract

The progress of nanotechnology has prompted the development of novel marine antifouling coatings. In this study, the influence of a pristine graphene nanoplatelet (GNP)-modified surface in cyanobacterial biofilm formation was evaluated over a long-term assay using an *in vitro* platform which mimics the hydrodynamic conditions that prevail in real marine environments. Surface characterization by Optical Profilometry and Scanning Electron Microscopy has shown that the main difference between GNP incorporated into a commercially used epoxy resin (GNP composite) and both control surfaces (glass and epoxy resin) was related to roughness and topography, where the GNP composite had a roughness value about 1000 times higher than control surfaces. The

results showed that, after 7 weeks, the GNP composite reduced the biofilm wet weight (by 44%), biofilm thickness (by 54%), biovolume (by 82%), and surface coverage (by 64%) of cyanobacterial biofilms compared to the epoxy resin. Likewise, the GNP-modified surface delayed cyanobacterial biofilm development, modulated biofilm structure to a less porous arrangement over time, and showed a higher antifouling effect at the biofilm maturation stage. Overall, this nanocomposite seems to have the potential to be used as a long-term antifouling material in marine applications. Moreover, this multifactorial study was crucial to understanding the interactions between surface properties and cyanobacterial biofilm development and architecture over time.

Keywords: antifouling surface, biofilm architecture, cyanobacterial biofilm, graphene, marine biofouling

9.1 Introduction

The oil, gas, and maritime industry are significantly impacted by biofouling, either through the costs related to the increased fuel consumption, hull cleaning, material deterioration, repainting, and corrosion (Schultz *et al.*, 2011), or even by the management intervention time and incorrect measurements in the submerged and moored sensors (Delauney *et al.*, 2010). Ecologically, fouling events in marine environments promote species invasion and the establishment of exotic biofouling species in ports (Giakoumi *et al.*, 2019). Moreover, biofouling can be a major concern in health-related problems since contamination of aquaculture facilities, such as fish cages, can occur by toxin accumulation, and air pollution may be increased through greenhouse gas emissions (Bannister *et al.*, 2019).

The non-toxic marine antifouling approaches available in the market are often expensive and not as effective as conventional biocides, which can accumulate in the marine environment and affect non-target aquatic organisms. Inorganic ingredient-based coatings have been used for biofouling prevention, including silver nanoparticles (Kumar *et al.*, 2017), carbon nanotubes (CNTs) (D. Zhang *et al.*, 2021), graphene (Jin, Zhang, *et al.*,

2019), and metal oxides semiconductors such as zinc oxide (ZnO) (Kumar *et al.*, 2019) and titanium dioxide (TiO_2) (Kim *et al.*, 2016). Overall, antifouling marine paints containing nanomaterials have been reported to offer superhydrophobicity, microbial resistance, high durability, water repellency, anti-sticking, and anti-corrosive properties (Callow and Callow, 2011), being novel solutions for the sustainable development of the maritime industry. Advancements in materials technology have introduced carbon nanomaterials such as CNTs and graphene as a powerful approach for various applications in the marine and shipping industries (Al-Jumaili *et al.*, 2017). Graphene consists of a single layer of carbon atoms arranged in a sp^2-bonded hexagonal pattern. It is considered one of the strongest and thinnest materials available, which shows high specific surface area, electrical conductivity, and thermal stability, making it appealing for different applications (Parra, Montero-Silva, *et al.*, 2015; Xu *et al.*, 2018). Moreover, due to its high strength level (Naddaf *et al.*, 2019), this material is a breakthrough alternative in the naval industry. All these features make the application of graphene in technical processes of maritime industries attractive, such as in water management systems, desalination, removing toxic pollutants and filtering gasses, and as a coating material (Pan *et al.*, 2018; Hu *et al.*, 2019; Smaradhana *et al.*, 2021). As a coating on marine structures, besides the anti-corrosive properties, graphene can also be used in de-icing surfaces for ship operations in extremely low-temperature regions, such as the Arctic and Antarctica, due to its electrical conductivity (Smaradhana *et al.*, 2021).

Nanotechnology-based technologies can be of great interest in creating novel low-toxic antifouling coatings (Balaure, 2022). However, analysis of the literature indicates that there is little information about the use of pristine graphene. Indeed, most *in situ* studies on graphene-based surfaces were performed with functionalized graphene and graphene oxide coatings (Selim, El-Safty, *et al.*, 2018; Gu *et al.*, 2019; Z. Zhang *et al.*, 2021; Li *et al.*, 2022; Selim *et al.*, 2022). Diatom adhesion was completely inhibited after 10 days by surfaces containing 0.36 wt% graphene oxide (Jin, Bing, *et al.*, 2019). In turn, graphene oxide-silver nanoparticle coatings improved antibacterial and anti-algal properties (Liu *et al.*, 2020), and showed more than 80% *Halomonas pacifica* biofilm inhibition (Zhang and Mikkelsen, 2021). Since the current trend is to study the potential of modified and functionalized graphene, the antibiofilm performance of graphene alone is poorly

understood. Moreover, most *in vitro* studies are usually performed for short periods and under hydrodynamic conditions that do not mimic the real marine environment (Sousa-Cardoso *et al.*, 2022). In fact, some of the *in vitro* studies have been performed until 24 h (Yee *et al.*, 2016; Jiang *et al.*, 2019; Liu *et al.*, 2020; D. Zhang *et al.*, 2021; Z. Zhang *et al.*, 2021), most of them between days and weeks (Krishnamoorthy *et al.*, 2014; Parra, Dorta, *et al.*, 2015; Selim, El-Safty, *et al.*, 2018; Jin, Bing, *et al.*, 2019; Jin, Zhang, *et al.*, 2019; Balakrishnan *et al.*, 2021; Manderfeld *et al.*, 2021; Selim *et al.*, 2022), but only a study performed by Fazli-Shokouhi *et al.* 2021 extended the assay period for 3 months to evaluate the antifouling potential of graphene-based coatings. Moreover, these studies focus on organisms other than cyanobacteria, namely diatoms, algae, and macrofoulers. Therefore, the main goal of this work was to evaluate the potential of a graphene composite surface to prevent and control the development of biofilms by marine microfoulers over a long-term assay and using an *in vitro* platform that mimics the hydrodynamic conditions found in real marine scenarios. Cyanobacterial biofilm architecture was evaluated by three different imaging techniques: Optical Coherence Tomography (OCT), Confocal Laser Scanning Microscopy (CLSM), and Scanning Electron Microscopy (SEM). Since the epoxy resin is a commercially available coating generally used to coat the hulls of small recreational vessels (Chambers *et al.*, 2006; Palmer *et al.*, 2007) due to its exceptional physical, chemical, and mechanical properties, no safety issues, and low cost (Mostafaei and Nasirpouri, 2013), pristine graphene nanoplatelets (GNP) were incorporated into this polymer matrix. Furthermore, epoxy composites exhibited high durability and resistance to fatigue and UV irradiation (Hoge and Leach, 2016). Surface characterization was also performed by water contact angle measurements, Optical Profilometry, and SEM.

9.2 Material and Methods

Figure 9.1 presents the flowchart of the experimental work fully described in the upcoming sections.

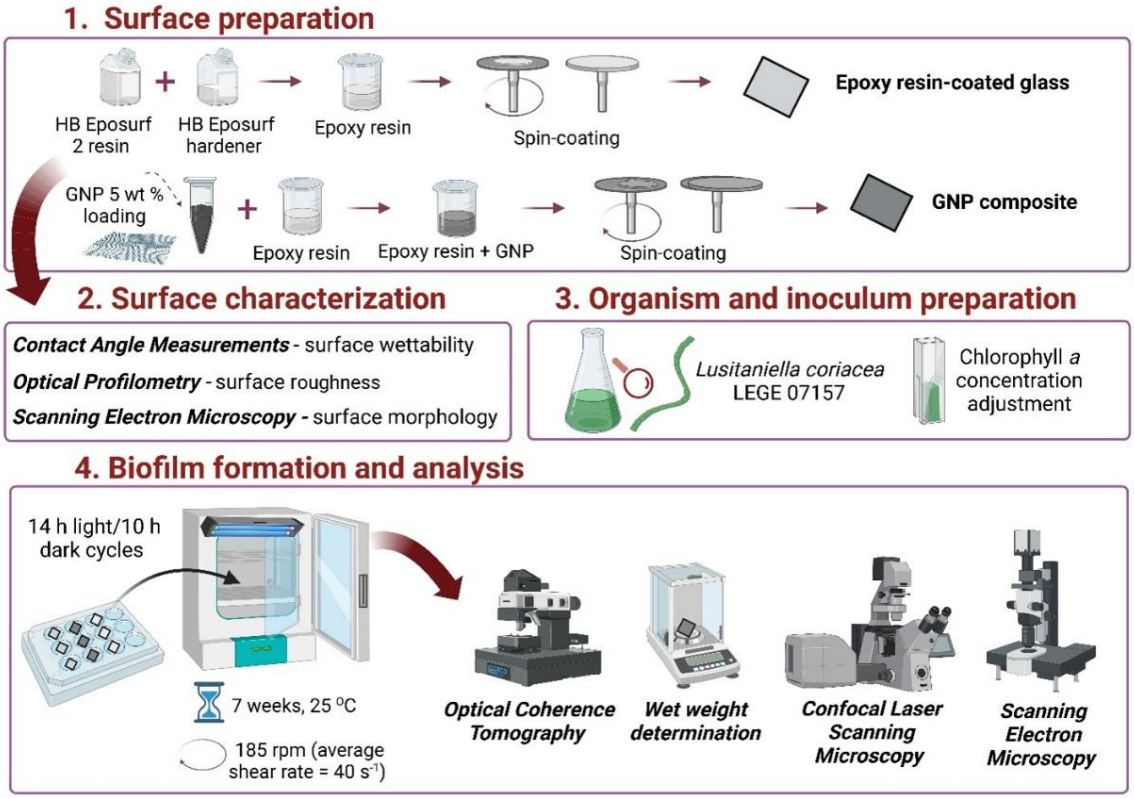

Figure 9.1. Scheme of the experimental steps of the present work.

9.2.1 Surface preparation

Two control surfaces (glass, a commonly submerged artificial surface found on diverse equipment in aquatic environments, and epoxy resin, a commercially available marine coating) and a GNP composite were tested to determine their performance against cyanobacterial biofilm development. The epoxy resin-coated glass was prepared following the protocol described by Faria, Teixeira-Santos, Gomes, *et al.* 2020. Briefly, HB Eposurf 2 resin and HB Eposurf hardener, both from HB Química (Matosinhos, Portugal), were mixed in a ratio of 10:3 (v/v). To produce the epoxy resin-coated surfaces, 70 µL of the above mixture was placed on top of 1 cm × 1 cm glass coupons (Vidraria Lousada, Lda, Lousada, Portugal) using a spin coater (Spin150 PolosTM, Paralab, Porto, Portugal) at 6000 rpm for 40 s. After 12 h at room temperature, the surfaces were dried for 3 h at 60 °C.

The methodology for the preparation of the GNP composite was adapted from Oliveira *et al.* 2022, in which the polydimethylsiloxane (PDMS) matrix was replaced by the epoxy resin. Briefly, after mixing the two epoxy resin components, 5 wt% of GNPs

aggregates (Alfa Aesar, Thermo Fisher Scientific, Erlenbachweg, Germany) were incorporated into the epoxy resin mixture. The specific surface area (S_{BET}), external surface area (S_{meso}), micropore volume (V_{micro}), and total pore volume (V_p) of these GNPs are 464 $m^2\ g^{-1}$, 363 $m^2\ g^{-1}$, 0.045 $cm^3\ g^{-1}$, and 0.535 $cm^3\ g^{-1}$, respectively (Oliveira *et al.*, 2022). In the same study (Oliveira *et al.*, 2022), 5 wt% was demonstrated to be an effective load in reducing single- and mixed-species biofilms of *Pseudomonas aeruginosa* and *Staphylococcus aureus* formation after 24 h. After the incorporation step, 70 μL of the composite (5 wt% GNP/epoxy resin) was deposited on glass squares by spin coating.

9.2.2 Surface characterization

9.2.2.1 Wettability

The measurement of water contact angles (θ_w) was performed through the sessile drop method using an SL200C optical contact angle meter (Solon Information Technology Co., Ltd., Shanghai, China) as previously described (Faria, Teixeira-Santos, Romeu, *et al.*, 2020; Lima *et al.*, 2022; Romeu, Lima, *et al.*, 2022). At least 25 determinations for each material at room temperature were performed.

9.2.2.2 Optical Profilometry

Optical profilometry was used to determine the average roughness (S_a) of the glass, epoxy resin, and GNP composite surfaces, as previously performed (Whitehead *et al.*, 2010; Skovager *et al.*, 2012). A MicroXAM surface mapping microscope (ADE Corporation, XYZ model 4400 mL system, *Tucson*, AZ, USA), with an objective of 50× and connected to an AD phase shift controller (Omniscan, Wrexham, UK), was used to image five areas (167 μm × 167 μm) of at least four different coupons. The MapView AE 2.17 software (Omniscan, Wrexham, UK) was chosen to determine the (S_a) values through extended range vertical scanning interferometry, and the 3D images were extracted by SPIP™ 6.7.9 software (Image Metrology A/S, Hørsholm, Denmark).

9.2.2.3 Scanning Electron Microscopy (SEM)

The surface morphology of the three surfaces used in this study was investigated using SEM. The surfaces were placed on SEM stubs (Agar Scientific, Stansted, UK) and sputter-coated with gold for 30 s in an SEM coating system (Polaron, London, UK). The secondary electron detector of a Supra 40VP scanning electron microscope (Carl Zeiss Ltd., Cambridge, UK) was used to obtain images of at least three coupons for each surface at an accelerating voltage of 2 kV.

9.2.3 Organism and inoculum preparation

A filamentous cyanobacterial strain *Lusitaniella coriacea* LEGE 07157 was obtained from the Interdisciplinary Centre of Marine and Environmental Research (CIIMAR), Matosinhos, Portugal (Ramos *et al.*, 2018). *Lusitaniella coriacea* LEGE 07157 was isolated by rock surface scraping from a zone tide pool at Lavadores beach, Porto, Portugal (41.12919 N 8.668578 W). It was grown in Z8 medium (Kotai, 1972) enhanced with 25 $g.L^{-1}$ of synthetic sea salts (Tropic Marin) and vitamin B_{12} (Sigma Aldrich, Merck, Saint Louis, MO, USA), and at 25 °C under 14 h light (10–30 μmol photons m^{-2} s^{-1}, λ = 380–700 nm)/10 h dark cycles, as recommended by Ramos *et al.*, 2018.

9.2.4 Biofilm formation

Cyanobacterial suspensions were adjusted to a chlorophyll *a* concentration of 1.22 ± 0.09 $\mu g.mL^{-1}$ since this pigment is unique and predominant in all groups of cyanobacteria and its quantification is a standard methodology to estimate the biomass in marine environments (Boyer *et al.*, 2009; Romeu *et al.*, 2019). Briefly, cyanobacterial cells were collected by centrifugation (3202*g* for 5 min) and a volume of 2 mL of 99.8% methanol (Methanol ACS Basic, Scharlau Basic, Barcelona, Spain) was added. After 24 h of dark incubation at 4 °C, cyanobacterial suspensions were centrifuged and absorbance measurements of the supernatant were performed at 750 nm (turbidity), 665 nm (chlorophyll *a*), and 652 nm (chlorophyll *b*) (V-1200 spectrophotometer, VWR

International China Co., Ltd., Shanghai, China). The values obtained were used to calculate chlorophyll a concentration (μg.mL^{-1}) through Equation (9.1) (Porra *et al.*, 1989):

$$Chl\ a\ (\mu g \cdot mL^{-1}) = 16.29 \times A^{665} - 8.54 \times A^{652} \quad (9.1)$$

where A^{665} and A^{652} are the absorbances at 665 nm and 652 nm, respectively.

Biofilm formation was tested on agitated 12-well plates (VWR International, Carnaxide, Portugal) under previously optimized conditions for cyanobacterial biofilm development (Romeu *et al.*, 2019). All coupons and plates were subjected to UV sterilization, after which the coupons were fixed on double-sided adhesive tape (Romeu *et al.*, 2019; Oliveira *et al.*, 2022). A volume of 3 mL of the adjusted cyanobacterial suspension was added to each well. To mimic the hydrodynamic conditions found in marine environments, microplates were then incubated at 25 °C in a shaker with a 25 mm orbital diameter (Agitorb 200ICP, Norconcessus, Ermesinde, Portugal) at 185 rpm, resulting in an average shear rate of 40 s^{-1} (Romeu *et al.*, 2019). Biofilm formation in this platform includes the shear rate valued for a ship in a harbor, 50 s^{-1} (Bakker *et al.*, 2003), and it was shown to predict the biofouling behavior observed upon immersion in the sea for prolonged periods (Silva *et al.*, 2021). Moreover, to simulate marine biofilm formation on submerged surfaces, microtiter plates were kept under 14 h light (8–10 μmol photons m^{-2} s^{-1})/10 h dark cycles (Romeu *et al.*, 2019; Faria, Gomes, *et al.*, 2021; Romeu, Domínguez-Pérez, *et al.*, 2022). The light intensity was decreased from 10–30 μmol photons m^{-2} s^{-1} to 8–10 μmol photons m^{-2} s^{-1} because biofouling organisms have reduced access to light when in immersion (either by the effect of the marine equipment/device/ship to which they are attached, or by the influence of the biofilm structure in which the accumulation of different organisms occurs, and some of them are located in the inners layers of biofilm). Since a 2-month interval for maintenance is the minimum time for economically viable underwater monitoring systems (Romeu *et al.*, 2019), biofilm development was followed for 7 weeks (49 days), and during this incubation time, the medium was changed twice a week in the sample and control wells.

9.2.5 Biofilm analysis

Two coupons of each surface were analyzed every 7 days. For that, the culture medium was removed, and the wells were filled with 3 mL of sodium chloride solution (8.5 $g.L^{-1}$) (Romeu *et al.*, 2019). The solution was carefully removed, and the wells were filled again with 3 mL of sodium chloride to assess the cyanobacterial biofilm structure through OCT. The determination of biofilm wet weight was also performed over 7 weeks, and at the end of the experiment (49 days), cyanobacterial biofilm architecture and morphology were analyzed by CLSM and SEM, respectively.

9.2.5.1 Optical Coherence Tomography (OCT)

Images from cyanobacterial biofilms were captured as reported by Romeu *et al.*, 2019, through OCT (Thorlabs Ganymede Spectral Domain Optical Coherence Tomography system with a central wavelength of 930 nm, Thorlabs GmbH, Dachau, Germany). Briefly, for each coupon, 2D imaging was performed (with a minimum of 2 fields of view) and evaluated through a routine developed in the Image Processing Toolbox from MATLAB 8.0 and Statistics Toolbox 8.1 (The MathWorks, Inc., Natick, MA, USA) (Romeu *et al.*, 2020). The mean of biofilm thickness was calculated according to Equation (9.2):

$$\bar{L}_F = \frac{1}{N}\sum_{i=1}^{N} L_{F,i} \qquad (9.2)$$

where $L_{(F,i)}$ is a local biofilm thickness measurement at location i, N equals the number of thickness measurements, and $\bar{L}_F$ is the mean biofilm thickness. The percentage of empty spaces in the biofilm structure, as well as their average size, was also assessed (Faria, Teixeira-Santos, Romeu, *et al.*, 2021).

9.2.5.2 Wet weight determination

The determination of the biofilm wet weight was performed as previously reported (Romeu *et al.*, 2021) and considered as the difference from the initial coupon weight determined before inoculation.

9.2.5.3 Confocal Laser Scanning Microscopy (CLSM)

Biofilms with 49 days were stained with 6 μM SYTO®61 (Thermo Fisher Scientific, Waltham, MA, USA), mounted on a microscopic slide, and observed in a Leica TCS SP5 II Confocal Laser Scanning Microscope (Leica Microsystems, Wetzlar, Germany) with a 40× water objective lens (Leica HCX PL APO CS 40.0x/1.10WATER UV) and 633-nm helium-neon laser. Image stacking was acquired with a z-step of 1 μm for each sample at a minimum of five random fields of 387.5 μm × 387.5 μm (equivalent to 512 pixels × 512 pixels. The "Easy 3D" tool of the IMARIS 9.1 software (Bitplane, Zurich, Switzerland) was used to create 3D projections of the biofilms. Additionally, biofilm architectural parameters such as biovolume ($\mu m^3.\mu m^{-2}$) and surface coverage (%) were determined using the COMSTAT image-analysis software (Heydorn *et al.*, 2000).

9.2.5.4 SEM

After 49 days of incubation, *Lusitaniella coriacea* LEGE 07157 biofilms grown on the three tested surfaces were observed by SEM. Samples were taken from the microplates, dehydrated with increasing ethanol concentrations (10, 25, 40, 50, 70, 80, 90, and 100% (v/v)), and left in a desiccator until microscopic analysis (Alves, Gomes, Rodríguez-Emmenegger, *et al.*, 2020). Then, they were sputter-coated using the equipment and conditions described before and imaged in the Supra 40VP scanning electron microscope.

9.2.6 Statistical analysis

Two biological experiments with two technical replicates each were analyzed. Quantitative parameters obtained from biofilm wet weight, OCT, and CLSM were compared using one-way ANOVA with Tukey's multiple comparisons test (GraphPad

Prism® version 6.01, GraphPad Software, Inc., San Diego, CA, USA). Statistically significant differences between the different surfaces for the same sampling day were considered for P values < 0.05 (corresponding to a confidence level greater than 95%). The error bars represent the standard deviation (SD) of the mean.

9.3 Results and Discussion

9.3.1 Surface analysis

It is known that surface properties, including wettability, roughness, and morphology, are important factors governing initial bacterial adhesion to surfaces and consequently affect the development of mature biofilms (Zheng *et al.*, 2021). Therefore, the three tested surfaces (glass, epoxy resin, and GNP composite) were evaluated regarding (i) wettability by water contact angle measurements, (ii) topography and roughness by Optical Profilometry, and (iii) morphology by SEM.

Results obtained from water contact angle measurements are shown in Figure 9.2A. Contact angle determination provides information about the wettability of the surface, i.e., the tendency of the fluid to spread on a surface, and the hydrophobicity of the surface, which describes the tendency of non-polar molecular aggregation and, consequently, water molecule repulsion (Yuan and Lee, 2013). Surfaces can be classified as superhydrophilic, hydrophilic, hydrophobic, or superhydrophobic, if the contact angle of water with the surfaces is lower than 10°, between 10° and 90°, between 90° and 150°, or over 150°, respectively (Doshi *et al.*, 2018). While glass is considered hydrophilic (θ_w = 40.9° ± 7.4°), the GNP composite (θ_w = 68.6° ± 2.4°) and epoxy-coated surfaces (θ_w = 76.3° ± 2.5°) are slightly more hydrophobic than glass. The wettability of the epoxy resin was weakly affected by the incorporation of graphene on the coating; the GNP composite is slightly more hydrophilic than the resin. Similar results were observed in previous studies (Rafiee *et al.*, 2012; Oliveira *et al.*, 2022). In fact, in a study performed by (Rafiee *et al.*, 2012), the water contact angle of a copper substrate coated with graphene was up to 90.6°, while that of the pure copper substrate was about 85.9°. Oliveira and her coworkers (Oliveira *et al.*, 2022) also verified that 5 wt% GNP/PDMS and PDMS surfaces presented similar water

contact angles, 121.8° and 110.2°, respectively. Since the wetting properties at the water–graphene interface had little effect on the water–substrate interaction, this peculiar wettability of graphene has been described by the term ''wetting transparency of graphene'' (Rafiee *et al.*, 2012). In the present study, as dispersed GNPs were used instead of graphene layers, it is conceivable to assume that the wettability of the substrate may be even less affected by the presence of graphene.

Results obtained from roughness analysis are shown in Figures 9.2B and 9.3. The GNP composite was the roughest surface (S_a = 1351 nm), followed by the epoxy resin (S_a = 13 nm) and glass (S_a = 10 nm). Therefore, the average roughness values of both control surfaces are on the nanometric scale, being about 1000 times lower than the roughness value determined for the GNP composite (Figure 9.2B). The difference in roughness and topography between the graphene composite and both control surfaces (glass and epoxy resin) is particularly evident in the 3D images of the surfaces given by profilometry (Figure 9.3). While glass and resin without incorporated carbon material were homogeneous and smooth surfaces (Figure 9.3A, B, respectively), the nanocomposite presented some irregularities distributed along the analyzed surface area (Figure 9.3C). Looking at the SEM images (Figure 9.4C, D), it was possible to confirm that these surface elevations correspond to agglomerated graphene nanoplatelets in the polymer matrix. Some of the larger agglomerates had sizes ranging from 7–30 μm.

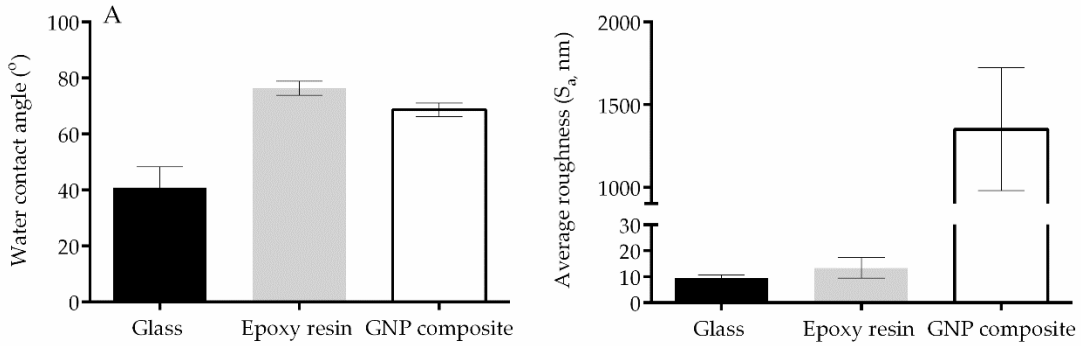

Figure 9.2. Water contact angles (A) and average roughness (S_a) (B) of the tested surfaces. The means ± SD are shown.

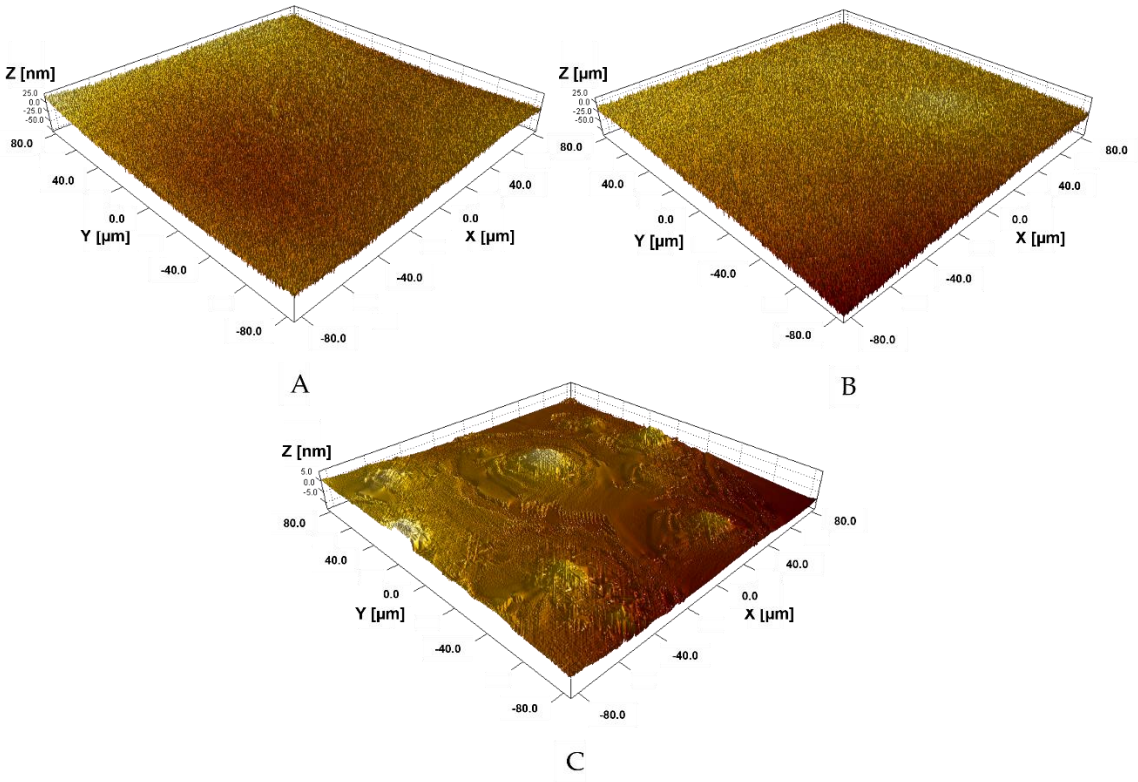

Figure 9.3. 3D profilometer images of glass (A), epoxy resin (B), and GNP composite (C).

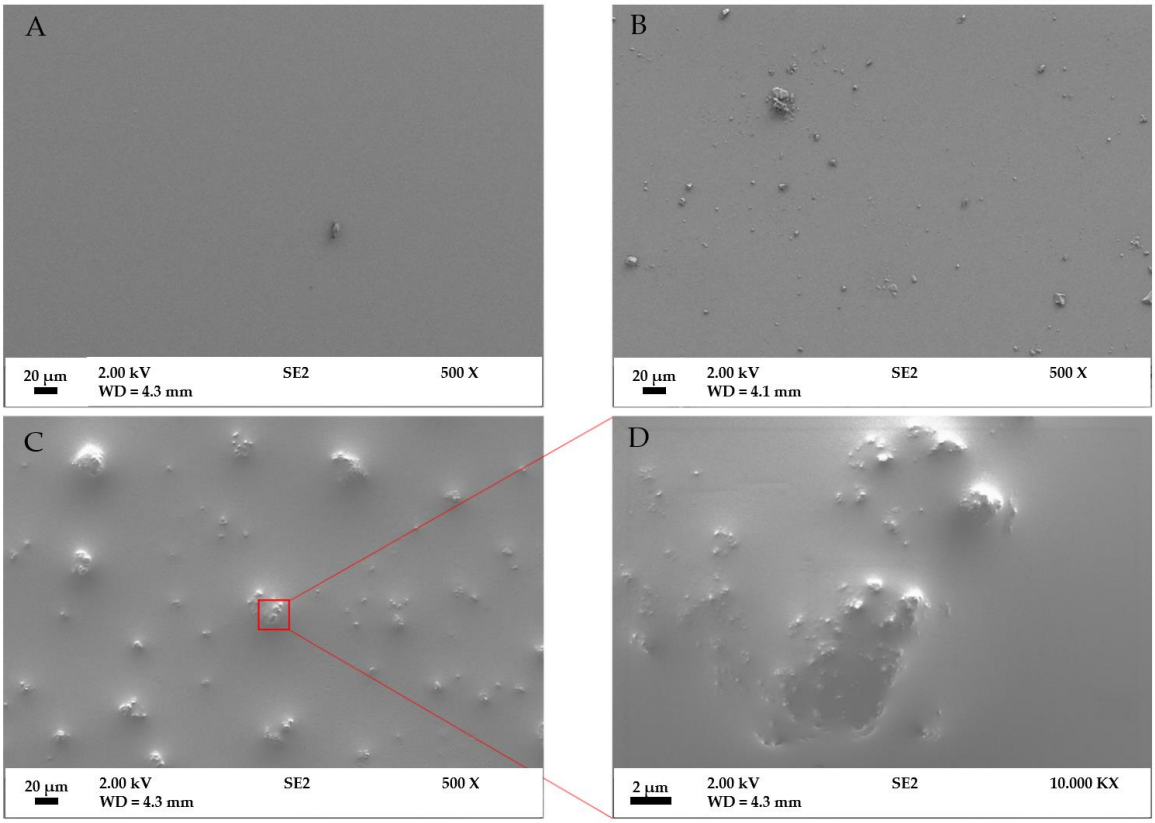

Figure 9.4. SEM images of glass (A), epoxy resin (B), GNP composite (C), and magnified GNP composite (D). The micrographs have a magnification of 500×, except for (D), which corresponds to a higher magnification image (10,000×) of the surface area marked in red in (C).

It is a challenge to disperse GNPs, especially compared to other carbon materials such as CNTs, due to the van der Waals forces and a strong π–π interaction between the individual GNP sheets, which are responsible for their layer-stacked compact structure (Chatterjee *et al.*, 2011; Oliveira *et al.*, 2022). Their incorporation in the polymeric resin may facilitate graphene dispersion, thus reducing the tendency to aggregate (Santos *et al.*, 2012). In the higher magnification image of the GNP composite (Figure 9.4D), it was interesting to detect some areas on top of the embedded GNP clusters where this carbon material was more exposed. It is described that one of the factors directing the antimicrobial activity of graphene is the agglomeration tendency, which causes a reduced surface area and shape alteration (Zou *et al.*, 2016; Mohammed *et al.*, 2020). However, the presence of more exposed GNPs in the epoxy resin may facilitate their interaction with the microorganisms that come in contact with the surface, triggering the predominant antimicrobial mechanisms of this carbon nanomaterial—oxidative stress, mechanical damage of cell membrane/wall by nanoknives, and wrapping/trapping (Mohammed *et al.*, 2020; Staneva *et al.*, 2021).

In vitro assays showed that no detectable leaching occured under the conditions used in this work as assessed by UV-Vis spectroscopy (data not shown).

9.3.2 Biofilm development

As there are several mechanisms affecting the microbial response and the disruption of biofilm architecture, the long-term antifouling properties of a given surface for marine applications should be extensively studied. Although the Minimal Inhibitory Concentration (MIC) of the studied GNPs could not be determined for *Lusitaniella coriacea* LEGE 07167 (it is a filamentous cyanobacterium and therefore cell numbers cannot be accurately determined), it was found to be higher than 5% (w/v, in a VNSS suspension assay) for a model marine bacterium (*Cobetia marina*). Cyanobacterial biofilm development was monitored over 7 weeks (49 days) and the quantitative results obtained from wet weight determination and 2D OCT analysis are shown in Figure 9.5. The values regarding the biofilm thickness, the percentage of empty spaces, and the average size of empty spaces on biofilm structure (Figure 9.5B–D) are indicated from day 14 since the biofilm thickness was below the OCT range on the first sampling day. Although a

progressive increase in biofilm development was observed from the results of wet weight (Figure 9.5A) and biofilm thickness (Figure 9.5B), this evolution over the 7 weeks was more noticeable on glass and epoxy resin than on the GNP composite. Indeed, for biofilm wet weight (Figure 9.5A), from day 7 to day 49, an increase of 84%, 77%, and 67% was observed for glass, epoxy resin, and GNP composite, respectively, while for biofilm thickness (Figure 9.5B), from day 14 to day 49, an increase of 85%, 86%, and 58% was observed for the same surfaces. This behavior was also seen regarding biofilm architecture (Figure 9.5C) given that an increase of 92%, 98%, and just 28% for the percentage of empty spaces was observed on glass, epoxy resin, and GNP composite. This suggests that graphene-modified surfaces may delay biofilm development (Figure 9.5A, B) and change its structure to a less porous arrangement (Figure 9.5C). Additionally, on days 35, 42, and 49, a reduction of biofilm wet weight and thickness was observed on the GNP composite surface when compared to the epoxy resin itself. In fact, on days 35, 42 and 49, the wet weight values obtained for the GNP composite were 46%, 47%, and 44% lower than those obtained on the epoxy resin surface, respectively (Figure 9.5A). For biofilm thickness on the same days, the values obtained on the GNP composite were 46%, 42%, and 54% lower than those obtained on the epoxy resin surface, respectively (Figure 9.5B). The delay effect caused by this carbon nanomaterial on cyanobacterial biofilm development, as well as the greater antifouling effect on the maturation stage of biofilm development, was also observed in previous work where CNT-modified surfaces were used as potential antifouling surfaces (Romeu, Lima, *et al.*, 2022). In addition, in the maturation stage of biofilm development (days 42 and 49), a lower percentage of empty spaces (Figure 9.5C) and an average size of empty spaces on biofilm structure (Figure 9.5D) were detected for biofilms formed on the GNP composite when compared with control surfaces (glass and epoxy resin).

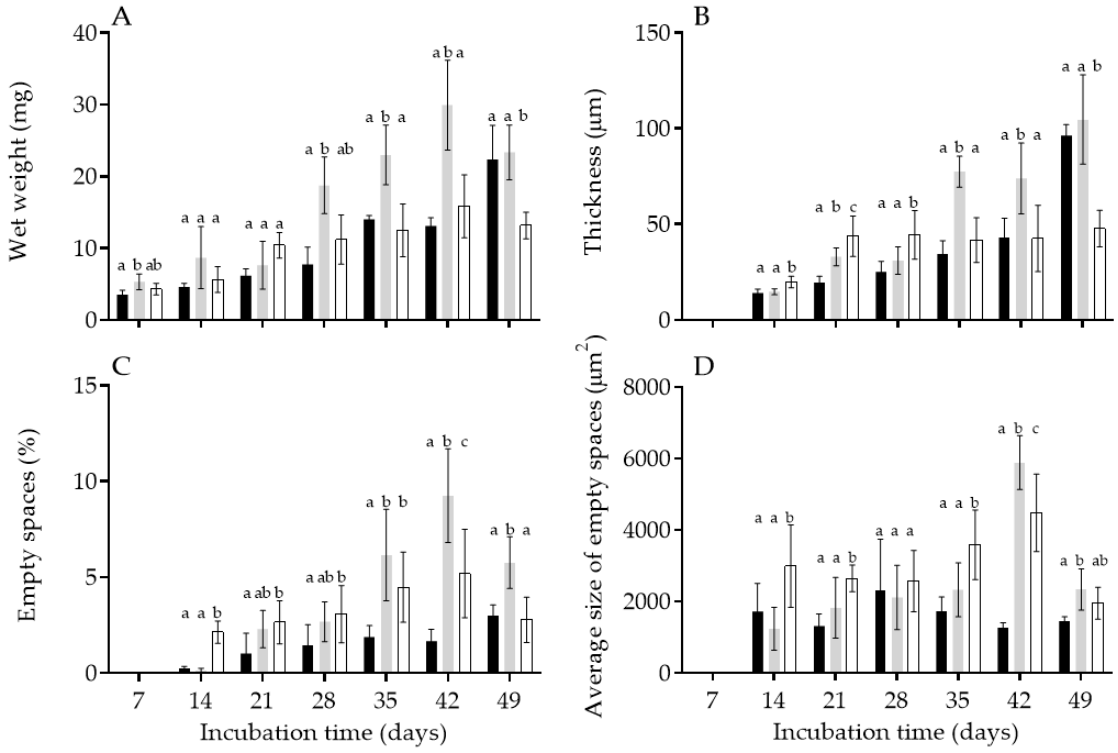

Figure 9.5. *Lusitaniella coriacea* LEGE 07157 biofilm development on different surfaces: glass (black), epoxy resin (grey), GNP composite (white). The parameters analyzed refer to biofilm wet weight (A), biofilm thickness (B), average percentage of empty spaces (C), and their respective average size (D) on biofilm structure. Mean values and SD from two biological assays with two technical replicates each are represented. For each sampling day, different lowercase letters (a, b, and c) indicate significant differences between surfaces ($P < 0.05$).

Figure 9.6 shows representative 2D cross-sectional images of *Lusitaniella coriacea* LEGE 07157 biofilm development on glass, epoxy resin, and GNP composite after 49 days. These images corroborate the quantitative data obtained from biofilm biomass (Figure 9.5A, B) and empty spaces on biofilm architecture (Figure 9.5C, D) since a lower amount of biofilm mass and percentage of empty spaces and its average size were observed on the GNP composite compared to the control epoxy resin. Although the reduced biofilm development on the GNP-based coating may be beneficial for the performance of marine devices and/or equipment, the efficacy of chemical methods to eradicate biofilms formed on this surface material may be hampered. Given the lower percentage of empty spaces and their smaller average size shown in biofilms formed on the GNP composite, the diffusion of chemical compounds typically used for biofouling control through the inner layers of the biofilm may be hindered (Sjollema *et al.*, 2011). The biofilm structure could also be compared between the three surfaces. While a flatter and homogeneous biofilm

was observed on glass (Figure 9.6A), biofilms formed on the epoxy resin (Figure 9.6B) and GNP composite (Figure 9.6C) had heterogeneous shapes. Additionally, more streamers could be observed on top of the biofilm developed on the epoxy resin surface (Figure 9.6B), which probably contributed to the higher thickness of biofilms developed on this surface compared to the GNP composite (Figure 9.5B). Opposing results were obtained in a previous study focused on CNT-based surfaces (Romeu, Lima, *et al.*, 2022), in which a flatter and homogeneous cyanobacterial biofilm was observed on the CNT composite. However, this divergent finding may be related to the use of a different cyanobacterial strain and carbon-based surface.

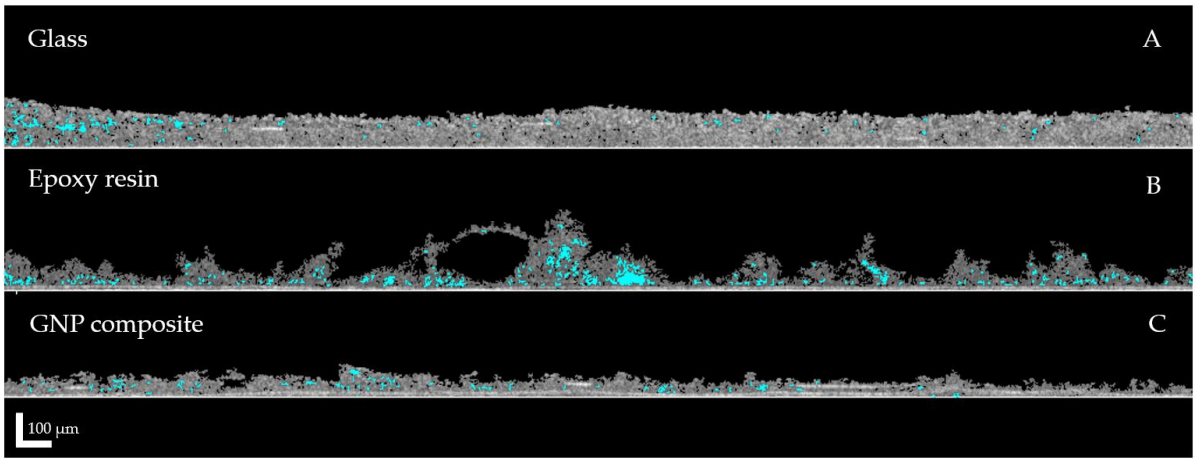

Figure 9.6. Representative 2D cross-sectional OCT images obtained for *Lusitaniella coriacea* LEGE 07157 biofilms on glass (A), epoxy resin (B), and GNP composite (C) after 49 days. The empty spaces on the biofilm structure are indicated in blue (scale bar = 100 µm).

Comparing the biofilm structure over the 49 days (Figure 9.5B, C), it was possible to observe different patterns between biofilms formed on the epoxy resin without and with embedded GNPs. In the early stages of biofilm formation (days 14 to 28), biofilms formed on the GNP composite were thicker and presented a higher percentage of empty spaces when compared to the epoxy resin surface, while in the maturation phase (days 35 to 49) these parameters became lower. These findings suggest that the higher roughness of the GNP composite may initially promote the development of a porous and thicker biofilm, and at the maturation stage, a biofilm structural arrangement may occur. In fact, 2D cross-sectional OCT images obtained for *Lusitaniella coriacea* LEGE 07157 biofilms after 28 days (Supplementary Material, Figure S 9.1) revealed that biofilms formed on the GNP

composite presented a higher number of streamers than the older biofilm (Figure 9.6C). Initially, to avoid the direct contact with GNP present on epoxy resin, cyanobacterial cells may have adapted their adhesion for vertical biofilm growth rather than a homogeneous development along the surface, contributing to the higher values of thickness between days 14 and 28. Although some previous studies revealed that the first dead cells could prevent the direct contact of live cells with graphene oxide surfaces, serving as a nutrient for live cells and consequently enhancing biofilm formation (Song *et al.*, 2018), the differences in architectural adaptation observed over time may provide an additional explanation for the antibiofilm mechanisms of the GNP composite. Indeed, values obtained from the biofilm roughness coefficient (Supplementary Material, Figure S 9.2) showed that all biofilms formed on day 28 presented a higher roughness compared with biofilms developed on day 49 ($P < 0.05$), including biofilms formed on the GNP composite.

Moreover, it was also hypothesized that the inability of *Lusitaniella coriacea* LEGE 07157 to form a dense and robust biofilm on the GNP composite was related to the damaging effect of graphene in the first cells adhered to the surface. These bacterial cells could be affected by the higher roughness of the graphene-based nanocomposite since the surface peaks corresponding to GNP clusters may directly affect bacterial viability by increasing the surface contact area and, consequently, the piercing action of exposed graphene particles. These initial adhered cells would become more fragile, probably leading to the improper adherence of the following layers of cells and hindering long-term biofilm formation. In previous work, Oliveira et al. showed that 5 wt% GNP/PDMS surfaces reduced the number of total (57%), viable (69%), culturable (55%), and VBNC cells (85%) of 24 h *S. aureus* biofilms compared to PDMS (Oliveira *et al.*, 2022). Besides cell death, the increased permeability of cell membranes caused by nanoparticles may affect EPS production, resulting in a disrupted 3D structure of biofilm.

The CLSM analysis was performed to analyze structural differences between the biofilms formed on the three tested surface materials (glass, epoxy resin, and GNP composite; Figure 9.7). While the 49-day-old biofilm developed on glass was dense, preventing the observation of individual filaments on the cyanobacterial cells in the top view (Figure 9.7A), the biofilms formed on epoxy resin surfaces without and with GNPs (Figures 9.7B, C, respectively) displayed randomly distributed filaments. Furthermore, a

drastic reduction in total biofilm amount was observed on the GNP composite when compared to both glass and epoxy resin surfaces. This was corroborated by the quantitative data extracted from the confocal stacks (Figure 9.7D, E), in which a decrease in biovolume (on average 86%, $P < 0.05$; Figure 9.7D) and surface coverage (on average 65%, $P < 0.05$; Figure 9.7E) was observed on the graphene-based surface compared to control surfaces.

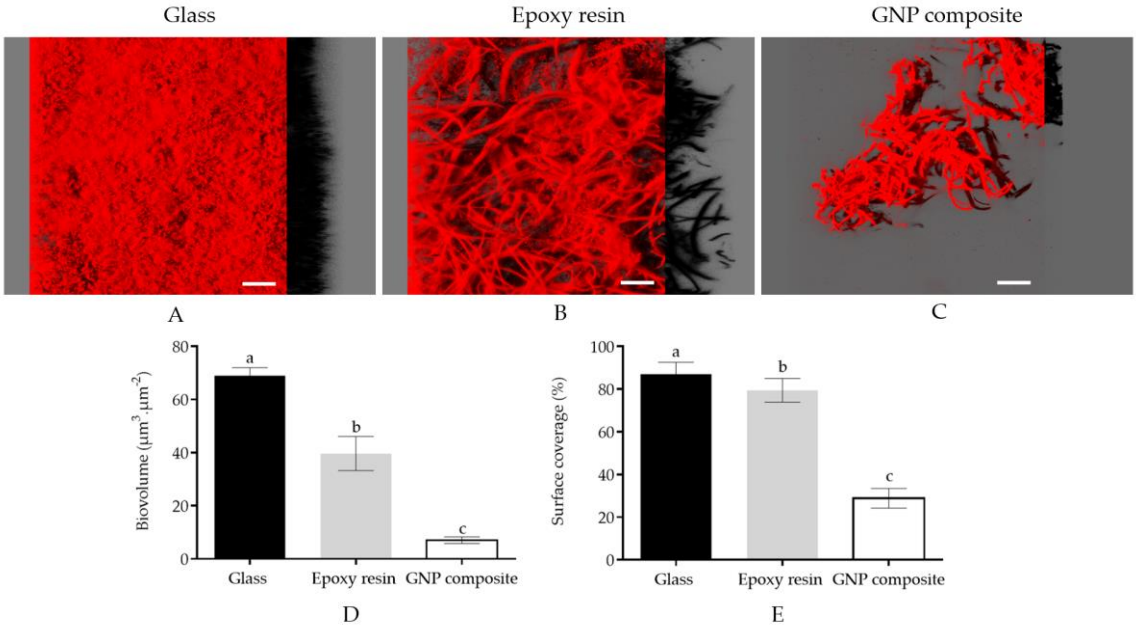

Figure 9.7. Three-dimensional confocal reconstructions of *Lusitaniella coriacea* LEGE 07157 biofilms grown on (A) glass, (B) epoxy resin, and (C) GNP composite after 49 days of incubation (white scale bars = 50 μm). These images show the biofilm aerial view, with the virtual shadow projection on the right (representative of biofilm thickness). Biovolume (D) and surface coverage (E) values of cyanobacterial biofilms were extracted from confocal files with the COMSTAT program. The means ± SD are presented. Different letters in the graphs (a, b, and c) indicate a significant difference among surfaces ($P < 0.05$).

The morphology of 49-day-old *Lusitaniella coriacea* LEGE 07157 biofilms on glass, epoxy resin, and GNP composite surfaces was also studied by SEM (Figure 9.8). The appearance of the biofilm developed on each surface was different, particularly when comparing the biofilm formed on glass (Figure 9.8A) with that formed on the epoxy resin without and with GNPs (Figures 9.8B and 9.8C, respectively). Indeed, the biofilm formed on the glass surface was very dense, and filamentous cyanobacteria were completely embedded in a complex matrix, which is a crucial feature of biofilm formation, making it

impossible to distinguish the morphology of the individual *Lusitaniella coriacea* cells. Contrariwise, the electron micrograph of the epoxy resin surface (Figure 9.8B) displayed mesh-like structures around the *Lusitaniella* cells (possibly resulting from exopolysaccharide secretion), and filaments made of chains of cells that covered the entire surface and which were arranged in random directions. The cyanobacterial filaments were even more visible in the biofilm formed on the GNP composite, where the amount of extracellular material seemed to be lower and where uncovered areas of surface areas could be seen (Figure 9.8C). Therefore, SEM observations corroborated the results of the biofilm wet weight (Figure 9.5A), and those obtained by OCT (Figure 9.6) and CLSM (Figure 9.7), indicating that the graphene composite surface had a lower biofilm amount than the control surfaces after 49 days. Likewise, SEM micrographs also supported the finding that GNP-modified surfaces may decrease EPS production, resulting in a disrupted 3D structure of biofilm at the maturation stage. Similar results were obtained on CNT-based surfaces compared to the control surfaces (glass and epoxy resin) since SEM images of cyanobacterial biofilm grown on the CNT composite presented lower-density cell aggregates (Romeu, Lima, *et al.*, 2022).

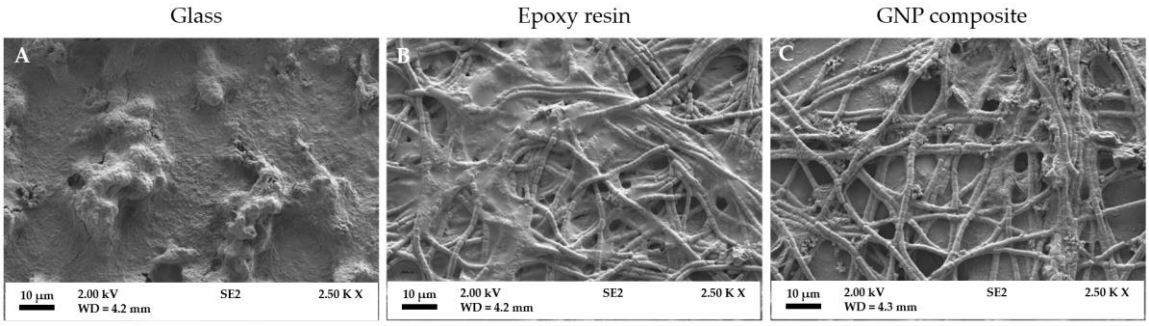

Figure 9.8. SEM micrographs of *Lusitaniella coriacea* LEGE 07157 biofilms grown on glass (A), epoxy resin (B), and GNP composite (C) after 49 days of incubation. Magnification = 2500×; scale bar = 10 µm.

This work may be limited by the use of cyanobacterial monocultures, the lack of field tests, and the absence of surface tribological characterization for long periods of immersion. Taking into account that the most studied forms of graphene within the marine context are graphene oxide and graphene oxide functionalized with metal nanoparticles (Sousa-Cardoso *et al.*, 2022), further experimental assays with other

graphene-based surfaces for the marine environment should be performed. These assays can comprise different physical and chemical properties (e.g., dimension, number of layers, and functionalization), but also focus on factors related to the production of the surface (e.g., graphene loading, nanoparticle dispersion, and aggregation) (Azizi-Lalabadi *et al.*, 2020; Fatima *et al.*, 2021; Radhi *et al.*, 2021). Future *in situ* studies should also include other foulers, as well as being performed for a longer period since, in the present study, a distinct effect was observed over time. In fact, few studies on graphene-based surfaces were performed over one (Selim, El-Safty, *et al.*, 2018; Selim *et al.*, 2022) or more months (Fazli-Shokouhi *et al.*, 2021). Although different optical techniques have been used in this study, further work should assess the metabolic state and the viability of biofilm cyanobacterial cells (Van den Driessche *et al.*, 2014; Mountcastle *et al.*, 2021). Omics approaches such as transcriptomic analysis to consider the expression of virulence factors and adhesion genes related to biofilm development (Parra, Dorta, *et al.*, 2015), and proteomic analysis to elucidate cyanobacterial defense mechanisms to graphene toxicity, should also be considered (Romeu *et al.*, 2020, 2021; Romeu, Domínguez-Pérez, *et al.*, 2022). Moreover, computational simulation approaches have been widely used for the characterization of novel materials (Ammarullah *et al.*, 2022). Strong coupling between experimental data and numerical simulation is required for predicting macroscopic behavior with a fine description of local fields. By combining modeling approaches and corresponding experiments, the studies take advantage of the simplicity, efficiency, and mechanistic insight gained from the models, and the physicality, meaningful reproducibility, and reality check provided by the experiments (Dingreville *et al.*, 2016). Thus, future studies should include computational simulations to evaluate the potential use of GNP composites as a marine coatings.

9.4 Conclusions

Biofilms developed on the GNP composite had reduced wet weight, thickness, biovolume, and surface coverage in the maturation stage when compared to the control surfaces (glass and epoxy resin). Moreover, the GNP composite delayed cyanobacterial biofilm development and promoted the development of a less porous biofilm. As the

graphene coating should serve as a long-term antifouling material for marine applications, the analysis of cyanobacterial biofilm behavior over time performed in this study is particularly relevant. The analysis of these GNP-based surfaces *in vitro* to assess their performance against mixed-species biofilms, and *in situ* to assess their effect on biofilm formation by additional microfoulers or to evaluate the potentially damaging effect of harsh marine environments on these nanostructured surfaces, will be performed in future studies. Therefore, upcoming tests should focus on tribological parameters such as the friction coefficient, wear, temperature, and durability related to the application, and surface characterization for long-term assays.

9.5 Supplementary Material

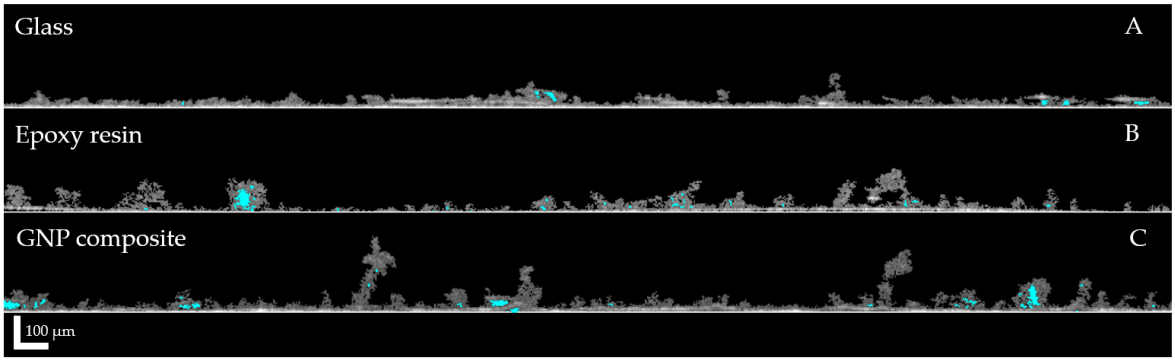

Figure S 9.1. Representative 2D cross-sectional OCT images obtained for *Lusitaniella coriacea* LEGE 07157 biofilms on glass (A), epoxy resin (B), and GNP composite (C) after 28 days. The empty spaces on the biofilm structure are indicated in blue (scale bar = 100 µm).

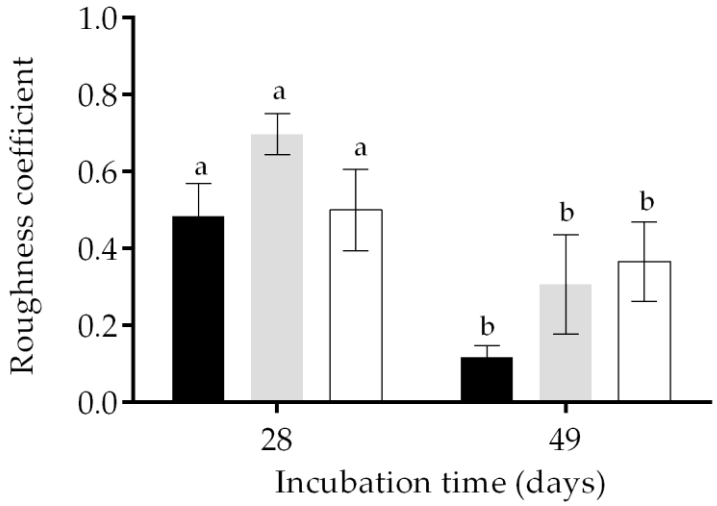

Figure S 9.2. Roughness coefficient[1] values of *Lusitaniella coriacea* LEGE 07157 biofilms on different surfaces: glass (black), epoxy resin (grey), and GNP composite (white). Mean values and SD from two biological assays with two technical replicates each are represented. For each surface, different lowercase letters indicate significant differences between the sampling day (day 28 *vs*. day 49; $p < 0.05$; unpaired t-test). The p value obtained for glass and epoxy resin was < 0.0001, and for GNP composite was 0.0104.

[1]The relative roughness coefficient (R_{α}^{*}) was calculated as previously reported (Romeu et al., 2019) using the following equation:

$$R_{\alpha}^{*} = \frac{1}{N}\sum_{i=1}^{N}\frac{\left|L_{F,i} - \bar{L}_{F}\right|}{\bar{L}_{F}}$$

where $L_{F,i}$ is a local biofilm thickness measurement at location i, N equals the number of thickness measurements and $\bar{L}_F$ is the mean biofilm thickness.

References

Romeu, M.J.; Alves, P.; Morais, J.; Miranda, J.M.; de Jong, E.D.; Sjollema, J.; Ramos, V.; Vasconcelos, V.; Mergulhão, F.J.M. Biofilm Formation Behaviour of Marine Filamentous Cyanobacterial Strains in Controlled Hydrodynamic Conditions. *Environ. Microbiol.* **2019**, *21*, 4411–4424.

10.

10 Concluding remarks and future perspectives

10.1 Concluding remarks

The adhesion and settlement of marine organisms is an ongoing concern in aquatic environments as marine biofouling causes several economic, environmental, and ecological problems, and cyanobacteria play a significant role (Bannister *et al.*, 2019; Giakoumi *et al.*, 2019). Several biological, environmental, physical and chemical parameters have been identified as modulators of biofilm development affecting its composition and structure. Among these, the fouling surface properties (von Ammon *et al.*, 2018; Cai *et al.*, 2019) and hydrodynamic conditions (Fanesi *et al.*, 2021; Chun *et al.*, 2022) have a critical impact on marine biofilms. Therefore, studies based on the influence of surface parameters and those performed under controlled hydrodynamic conditions are essential for developing effective antifouling strategies for marine applications. The main goals of this study included (1) the development and characterization of a laboratory platform for marine biofilm formation under controlled hydrodynamic conditions; (2) the analysis of the effect of hydrodynamic conditions and surface properties on protein expression of cyanobacterial biofilm cells, and (3) the characterization of the structure and architecture analysis of filamentous cyanobacterial biofilms development under different surfaces using several imaging techniques. Therefore, the characterization performed in this work provided new insights into how shear rate and surface affect cyanobacterial

biofilm development and how cyanobacteria adapt to these different settings from a proteomics perspective to a macroscopic point of view.

Despite the importance of shear forces on biofilm behavior in all stages of the biofouling process, marine biofilm formation studies performed in controlled hydrodynamic conditions are scarce (Dimartino *et al.*, 2014; Chun *et al.*, 2022). Consequently, it was critical to perform biofilm formation studies in controlled hydrodynamic conditions, which mimic real aquatic environments. The CFD analysis performed in this work **(Chapter 3)** showed that the agitated 12-well microtiter plates can be used as a marine biofilm reactor to mimic these environments since the shear rate range achieved comprises the values found on real aquatic environments (50 s^{-1}; Alexandrou, 2001; Bakker *et al.*, 2003). Indeed, the use of agitated microtiter plates at defined hydrodynamic conditions can be a very convenient and affordable approach since this platform requires low volumes (and consequently has reduced costs) and is easy to handle. Furthermore, it enables the control of different parameters and the use of coupons from various materials to test the impact of different surfaces in marine biofouling in a high throughput modality (often required for studies performed during long time intervals with sampling on different days). Moreover, the first attempt to use 3D OCT to evaluate the structure of filamentous cyanobacterial biofilms was successful, allowing an *in situ*, non-destructive and real-time analysis and providing quantitative values for biofilm thickness and roughness.

After describing the *in vitro* operational conditions, proteomic approaches were used to characterize protein expression of cyanobacterial biofilms formed under two different hydrodynamic conditions on glass and perspex surfaces. From the qualitative proteomic study **(Chapter 4)** about 300 - 400 proteins were identified, and the differences in protein composition were more noticeable in biofilms formed under different hydrodynamic conditions than in those formed on different surfaces. Remarkably, none of the proteins identified in planktonic samples was exclusive to this form since they were also identified in at least one biofilm condition. Furthermore, cyanobacterial proteome analysis revealed that the two strains had highly variable protein expression profiles. In the first quantitative study **(Chapter 5)**, about 500 proteins and 41 DEPs were identified. Although results obtained from the macroscopic evaluation (biofilm biomass, thickness,

and chlorophyll *a* quantification) revealed that hydrodynamic effects might be more important than surface properties in the development of cyanobacterial biofilms, a large differential protein expression was found between biofilms formed on glass and perspex at 4 s^{-1}. After improvements in the sample preparation and peptide identification protocols, in the second proteomic study (**Chapter 6**), about 1800 proteins were identified, and both macroscopic and proteomic analysis revealed higher variations between biofilm formed at different hydrodynamic conditions when compared with protein profiles obtained from distinct surfaces. In both quantitative studies, several proteins with disordered domains were found. Once again, in all these proteomic studies, 2D OCT analysis was also demonstrated to be a valuable tool for understanding the structure of filamentous cyanobacterial biofilms. The proteomic profile can help in the characterization of virulence factors and cellular processes involved in biofilm regulation. As more proteins and their roles in biofilm development are explored, novel potential targets for biofilm control may be discovered. Additionally, the qualitative proteomic study (**Chapter 4**) contributed to the identification of a broad spectrum of secondary metabolites and added-value compounds produced by cyanobacterial strains under the conditions tested that currently are, or can be used, on biotechnological and medical applications. Although we could not definitively show that the expression of a determined protein was responsible for increased or decreased biofilm development, it was possible to associate the over or underexpressed proteins with a lower or a higher biofilm development, possibly contributing to the development of novel antibiofilm strategies.

Finally, the architecture of filamentous cyanobacterial biofilms formed on different surfaces was analyzed through several imaging techniques, including a novel 3D OCT approach, SEM and CLSM, and under hydrodynamic conditions that mimic real marine environments (**Chapters 7 - 9**). Although cyanobacterial isolates from geographically distinct areas (Cape Verde and Morocco) had been used in the **Chapter 7**, the majority of the quantitative results obtained showed that no significant differences were found in biofilms developed by the same cyanobacterial strain on the different surfaces (glass and perspex), as already observed in the previous studies performed in this work. In turn, the

biofilm-forming potential among different cyanobacteria was distinct, particularly at the maturation stage of biofilm development.

Since the development of innovative nanocomposite coatings is a promising approach to tackling marine biofouling (Zhang and Mikkelsen, 2021; Rossi *et al.*, 2022), subsequently, the impact of carbon composite surfaces on filamentous cyanobacterial biofilm development was assessed by using CNTs- (**Chapter 8**) and GNP-modified surfaces (**Chapter 9**). CNT and GNP composites showed a higher antifouling/antimicrobial effect at the biofilm maturation stage of biofilm development, indicating their potential to be used as long-term antifouling/antimicrobial material in marine applications. Likewise, along with a delay in biofilm development, a decrease in biofilm wet weight, thickness, and biovolume was also achieved with both carbon composite surfaces compared to control surfaces. A biofilm structural rearrangement was observed over time as CNT and GNP composites originated a less porous biofilm arrangement over time, which can hamper the efficacy of chemical treatment. Additionally, the novel biofilm parameters obtained from 3D OCT imaging in the study performed in **Chapter 8** enabled a deeper understanding of the biofilm structure.

In all of the studies performed in this work, biofilm development was higher under low shear conditions (4 s^{-1} *vs.* 40 s^{-1}), and overall, cyanobacterial biofilm architecture using 2D and 3D OCT revealed that more compact biofilm structures were formed at higher shear values (40 s^{-1}). On the contrary, the presence of biofilm streamers, which contribute to biofilm development (Drescher *et al.*, 2013), was more evident in cyanobacterial biofilms developed at lower shear values (4 s^{-1}). Therefore, the increased shear stress was not a considerable obstacle to cyanobacterial adhesion and biofilm formation, but its effect was more noticeable during biofilm maturation, probably due to erosion and sloughing events that may occur at higher shear values. These studies also show that the effect of hydrodynamic conditions is more significant in the maturation stage of cyanobacterial biofilm development.

Multifactorial studies performed along all this work were important to understanding the interactions between hydrodynamics, surface properties and cyanobacterial biofilm development and its architecture over time. This enabled the development of novel protocols and techniques to study these complex organisms, as well

as biofilms in distinct areas. Moreover, this work can also be useful for different research fields, given the broad spectrum of promising secondary metabolites and added-value compounds produced by cyanobacteria, as well as for the development of new anti-biofilm strategies.

10.2 **Future perspectives**

In order to improve the understanding of the impact of hydrodynamic conditions and surface properties on filamentous cyanobacterial biofilm development, several aspects require further research.

Future studies should include complementary techniques to assess cyanobacterial biofilm cells' viability and metabolic state since active cells can promote biofilm development. Due to the relevance of EPS on biofilm development, the secretion of these biofilm components should also be considered in upcoming studies. Future studies should also compare the biofilm forming potential of filamentous *vs.* coccoid cyanobacteria using results already obtained by the group through multivariable regression and principal component analysis. Likewise, mixed-species biofilms and additional marine foulers should be considered in future studies.

The advancement of computational simulation techniques enables the application of mathematical models in the biofilm field, allowing *in silico* estimation of biofilm behavior under a wide range of conditions. CFD analysis may be applied to characterize biofilm reactors with productive purposes (Gomes and Mergulhão, 2021), and it may also be used to describe fluid-structure interactions in cell adhesion and biofilm processes, such as bacterial twitching (Jayathilake *et al.*, 2019) and oscillations of biofilm streamers (Taherzadeh *et al.*, 2010; Xia *et al.*, 2021). Furthermore, regarding marine environments, CFD approaches have developed significantly as a tool to predict the effect of biofouling on the drag on ships and the performance of marine vehicles (Baital and Pria Utama, 2017; Farkas *et al.*, 2018, 2021). As the combination of biofilm modeling and *in situ* experimental measurements of biofilm parameters is a valuable approach to studying biofilms in the

laboratory, the potential of CFD for predicting biofilm-flow interactions under different hydrodynamic conditions should be explored in future studies.

Considering proteomic studies, a proteomic analysis should be performed at different biofilm stages to evaluate differences in proteomic profile over biofilm development. Moreover, the supernatant recovered from biofilm assays should also be analysed to provide new information since some proteins may have been released from the biofilm structure. Different omics approaches, such as metabolomic studies, will be valuable to complement the results obtained in this work, allowing the identification of pathways triggered under the different biofilm formation conditions and novel virulence, adhesion and biofilm development factors. Further studies should also focus on cyanobacterial gene modifications and deletions, which encode relevant proteins reported in the present studies as crucial for biofilm development. This would clarify their role in biofilm phenotypes and establish a relation between differential expression levels of a given protein and the effect on biofilm development. Additionally, the analysis of the proteomic profile of marine organisms isolated from fouled submerged surfaces may suggest novel evidence or confirm the results obtained in this work about the metabolic pathways that are up-regulated during biofilm development.

Regarding the CNT and GNP-modified surfaces tested in this work, it would be interesting to immerse them in real marine environments for long periods to evaluate micro and macrofouling. Additionally, transcriptomic, proteomic and metabolic studies should be applied to biofilm cells recovered from different surfaces to evaluate the impact of surface properties on metabolic pathways and biofilm composition. Long i*n situ* assays with modified surfaces are of paramount importance since these materials can be damaged in harsh marine environments, reducing their antifouling/antimicrobial ability and lifespan. Therefore, surface tribological characterization and ecotoxicity testing of these surfaces to marine organisms is also relevant.

Currently, as we are experiencing exciting improvements in techniques that will widen our understanding of the structure and function of microbial communities, a deeper knowledge of the impact of hydrodynamic and surface properties could be obtained by the characterization of specific cell clusters from the biofilm structure. For instance, evaluating the metabolic state of cyanobacterial cells from the inner layers to

biofilm streamers could provide novel insights into the impact of hydrodynamic and surface properties on biofilm development.

References

References

Abbott, A., Abel, P.D., Arnold, D.W., and Milne, A. (2000) Cost–benefit analysis of the use of TBT: the case for a treatment approach. *Sci Total Environ* **258**: 5–19.

Abdallah, M., Benoliel, C., Drider, D., Dhulster, P., and Chihib, N.E. (2014) Biofilm formation and persistence on abiotic surfaces in the context of food and medical environments. *Arch Microbiol* **196**: 453–472.

Abed, R.M.M., Dobretsov, S., and Sudesh, K. (2009) Applications of cyanobacteria in biotechnology. *J Appl Microbiol* **106**: 1–12.

Adams, D.G. and Duggan, P.S. (2008) Cyanobacteria-bryophyte symbioses. *J Exp Bot* **59**: 1047–1058.

Aebersold, R. and Mann, M. (2016) Mass-spectrometric exploration of proteome structure and function. *Nature* **537**: 347–355.

Agostoni, M., Waters, C.M., and Montgomery, B.L. (2016) Regulation of biofilm formation and cellular buoyancy through modulating intracellular cyclic di-GMP levels in engineered cyanobacteria. *Biotechnol Bioeng* **113**: 311–319.

Ahmed, F., Santos, C.M., Vergara, R.A.M. V, Tria, M.C.R., Advincula, R., and Rodrigues, D.F. (2012) Antimicrobial Applications of Electroactive PVK-SWNT Nanocomposites. *Environ Sci Technol* **46**: 1804–1810.

Akinfiev, T., Janushevskis, A., and Lavendelis, E. (2007) A Brief Survey of Ship Hull Cleaning Devices. *Transp Eng* 133–146.

Al-Jumaili, A., Alancherry, S., Bazaka, K., and Jacob, M. V (2017) Review on the Antimicrobial Properties of Carbon Nanostructures. *Mater (Basel)* **10**: 1066.

Aldred, N. and Clare, Anthony S (2014) Mini-review: impact and dynamics of surface fouling by solitary and compound ascidians. *Biofouling* **30**: 259–270.

Alexandrou, A. (2001) Principles of fluid mechanics, Upper Saddle River, N.J.: Prentice Hall.

Alexova, R., Haynes, P.A., Ferrari, B.C., and Neilan, B.A. (2011) Comparative protein expression in different strains of the bloom-forming cyanobacterium *Microcystis aeruginosa*. *Mol Cell Proteomics* **10**: 1–16.

Allaf, M.M. (2022) Cyanobacteria : Model Microorganisms and Beyond. *Microorganisms* 2022, **10:** 696.

Allen, A.A., Habimana, O., and Casey, E. (2018) The effects of extrinsic factors on the structural and mechanical properties of *Pseudomonas fluorescens* biofilms: a combined study of nutrient concentrations and shear conditions. *Colloids Surfaces B Biointerfaces* **165**: 127–134.

Allen, R., Rittmann, B.E., and Curtiss, R. (2018) Axenic Biofilm Formation and Aggregation by *Synechocystis* PCC 6803 is Induced by Changes in Nutrient Concentration, and Requires Cell Surface Structures. *bioRxiv* 1–33.

Alles, M. and Rosenhahn, A. (2015) Microfluidic detachment assay to probe the adhesion strength of diatoms. *Biofouling* **31**: 469–480.

References

Almeida, D., Domínguez-Pérez, D., Matos, A., Agüero-Chapin, G., Osório, H., Vasconcelos, V., et al. (2020) Putative antimicrobial peptides of the posterior salivary glands from the cephalopod octopus vulgaris revealed by exploring a composite protein database. *Antibiotics* **9**: 1–20.

Almeida, J.R., Freitas, M., Cruz, S., Leão, P.N., Vasconcelos, V., and Cunha, I. (2015) Acetylcholinesterase in biofouling species: Characterization and mode of action of cyanobacteria-derived antifouling agents. *Toxins (Basel)* **7**: 2739–2756.

Almeida, J.R. and Vasconcelos, V. (2015) Natural antifouling compounds: Effectiveness in preventing invertebrate settlement and adhesion. *Biotechnol Adv* **33**: 343–357.

Alvarenga, D.O., Fiore, M.F., and Varani, A.M. (2017) A metagenomic approach to cyanobacterial genomics. *Front Microbiol* **8**: 1–16.

Alves, P., Gomes, L.C., Rodríguez-Emmenegger, C., and Mergulhão, F.J. (2020) Efficacy of A Poly(MeOEGMA) Brush on the Prevention of *Escherichia coli* Biofilm Formation and Susceptibility. *Antibiotics* **9**: 216.

Alves, P., Gomes, L.C., Vorobii, M., Rodriguez-Emmenegger, C., and Mergulhão, F.J. (2020) The potential advantages of using a poly(HPMA) brush in urinary catheters: effects on biofilm cells and architecture. *Colloids Surfaces B Biointerfaces* **191**: 110976.

Amin, S.A., Parker, M.S., and Armbrust, E.V. (2012) Interactions between Diatoms and Bacteria. *Microbiol Mol Biol Rev* **76**: 667–684.

Ammarullah, M.I., Santoso, G., Sugiharto, S., Supriyono, T., Wibowo, D.B., Kurdi, O., et al. (2022) Minimizing Risk of Failure from Ceramic-on-Ceramic Total Hip Prosthesis by Selecting Ceramic Materials Based on Tresca Stress. *Sustainability* **14**: 13413.

von Ammon, U., Wood, S.A., Laroche, O., Zaiko, A., Tait, L., Lavery, S., et al. (2018) The impact of artificial surfaces on marine bacterial and eukaryotic biofouling assemblages: A high-throughput sequencing analysis. *Mar Environ Res* **133**: 57–66.

Anand, S., Samuel, M., Ang, C.-S., Keerthikumar, S., and S, M. (2017) Label-Based and Label-Free Strategies for Protein Quantitation. In *Proteome Bioinformatics, Methods in Molecular Biology Molecular Biology*. KeerthikumaR, S. and Mathivanan, S. (eds). New York, USA: Humana Press, pp. 56–74.

Anand, V., Singh, P.K., Banerjee, C., and Shukla, P. (2017) Proteomic approaches in microalgae: perspectives and applications. *3 Biotech* **7**: 1–10.

Anderson, D.C., Campbell, E.L., and Meeks, J.C. (2006) A soluble 3D LC/MS/MS proteome of the filamentous cyanobacterium *Nostoc punctiforme*. *J Proteome Res* **5**: 3096–3104.

Anderson, O. (2016) Marine and estuarine natural microbial biofilms: ecological and biogeochemical dimensions. *AIMS Microbiol* **2**: 304–331.

Antunes, J., Leão, P., and Vasconcelos, V. (2019) Marine biofilms: diversity of communities and of chemical cues. *Environ Microbiol Rep* **11**: 287–305.

Antunes, J., Pereira, S., Ribeiro, T., Plowman, J.E., Thomas, A., Clerens, S., et al. (2019) A multi-bioassay integrated approach to assess the antifouling potential of the cyanobacterial metabolites portoamides. *Mar Drugs* **17**: 1–19.

Antunes, J.T., Sousa, A.G.G., Azevedo, J., Rego, A., Leão, P.N., and Vasconcelos, V. (2020) Distinct Temporal Succession of Bacterial Communities in Early Marine Biofilms in a Portuguese Atlantic Port. *Front Microbiol* **11**: 1–17.

Araújo, M.J., Sousa, M.L., Felpeto, A.B., Turkina, M. V., Fonseca, E., Martins, J.C., et al. (2021) Comparison of sample preparation methods for shotgun proteomic studies in aquaculture species. *Proteomes* **9**: 1–19.

Arndt, E., Robinson, A., and Hester, S. (2021) Factors that influence vessel biofouling and its prevention and management. *Final Report for CEBRA Project 190803.* Melbourne, VIC: Centre of Excellence for Biosecurity Risk Analysis (CEBRA), vii + 98.

Azeredo, J., Azevedo, N.F., Briandet, R., Cerca, N., Coenye, T., Costa, A.R., et al. (2017) Critical review on biofilm methods. *Crit Rev Microbiol* **43**: 313–351.

Azevedo, J., Antunes, J.T., Machado, A.M., Vasconcelos, V., Leão, P.N., and Froufe, E. (2020) Monitoring of biofouling communities in a Portuguese port using a combined morphological and metabarcoding approach. *Sci Rep* **10**: 13461.

Azevedo, N.F., Pacheco, A.P., Keevil, C.W., and Vieira, M.J. (2006) Adhesion of water stressed *Helicobacter pylori* to abiotic surfaces. *J Appl Microbiol* **101**: 718–724.

Azizi-Lalabadi, M., Hashemi, H., Feng, J., and Jafari, S.M. (2020) Carbon nanomaterials against pathogens; the antimicrobial activity of carbon nanotubes, graphene/graphene oxide, fullerenes, and their nanocomposites. *Adv Colloid Interface Sci* **284**: 102250.

Ba, M., Zhang, Z., and Qi, Y. (2019) The influence of MWCNTs-OH on the properties of the fouling release coatings based on polydimethylsiloxane with the incorporation of phenylmethylsilicone oil. *Prog Org Coatings* **130**: 132–143.

Baba, M., Suzuki, I., and Shiraiwa, Y. (2011) Proteomic analysis of high-CO 2-inducible extracellular proteins in the unicellular Green Alga, *Chlamydomonas reinhardtii*. *Plant Cell Physiol* **52**: 1302–1314.

Babele, P.K., Kumar, J., and Chaturvedi, V. (2019) Proteomic De-regulation in cyanobacteria in response to abiotic stresses. *Front Microbiol* **10**: 1–22.

Babele, P.K., Singh, G., Kumar, A., and Tyagi, M.B. (2015) Induction and differential expression of certain novel proteins in Anabaena L31 under UV-B radiation stress. *Front Microbiol* **6**: 1–14.

Badger, M.R. and Price, G.D. (2003) CO_2 concentrating mechanisms in cyanobacteria: Molecular components, their diversity and evolution. *J Exp Bot* **54**: 609–622.

Badri, H., Monsieurs, P., Coninx, I., Wattiez, R., and Leys, N. (2015) Molecular investigation of the radiation resistance of edible cyanobacterium *Arthrospira* sp. PCC 8005. *Microbiologyopen* **4**: 187–207.

Baital, M.S. and Pria Utama, I.K.A. (2017) CFD Analysis into the Drag Estimation of Smooth and Roughened Surface Due to Marine Biofouling. *IPTEK J Technol Sci* **28**: 90–97.

Bakke, R., Kommedal, R., and Kalvenes, S. (2001) Quantification of biofilm accumulation by an optical approach. *J Microbiol Methods* **44**: 13–26.

Bakker, D.P., Plaats, A. Van Der, Verkerke, G.J., Busscher, H.J., and Mei, H.C. Van Der (2003) Comparison of velocity profiles for different flow chamber designs used in studies of microbial adhesion to surfaces. *Appl Environ Microbiol* **69**: 6280–6287.

Balakrishnan, A., Jena, G., Pongachira George, R., and Philip, J. (2021) Polydimethylsiloxane–graphene oxide nanocomposite coatings with improved anti-corrosion and anti-biofouling properties. *Environ Sci Pollut Res* **28**: 7404–7422.

Balaure, P.C. (2022) Special Issue: Advances in Engineered Nanostructured Antibacterial Surfaces and Coatings. *Coatings* **12**: 1041.

Bannister, J., Sievers, M., Bush, F., and Bloecher, N. (2019) Biofouling in marine aquaculture: a review of recent research and developments. *Biofouling* **35**: 631–648.

Barrios-Llerena, M.E., Chong, P.K., Gan, C.S., Snijders, A.P.L., Reardon, K.F., and Wright, P.C. (2006) Shotgun proteomics of cyanobacteria - Applications of experimental and data-mining techniques. *Briefings Funct Genomics Proteomics* **5**: 121–132.

Bas, S., Kramer, M., and Stopar, D. (2017) Biofilm surface density determines biocide effectiveness. *Front Microbiol* **8**: 1–9.

Battchikova, N., Angeleri, M., and Aro, E.M. (2015) Proteomic approaches in research of cyanobacterial photosynthesis. *Photosynth Res* **126**: 47–70.

Battchikova, N., Muth-Pawlak, D., and Aro, E.M. (2018) Proteomics of cyanobacteria: current horizons. *Curr Opin Biotechnol* **54**: 65–71.

Becher, P.G., Beuchat, J., Gademann, K., and Jüttner, F. (2005) Nostocarboline: isolation and synthesis of a new cholinesterase inhibitor from Nostoc 78-12A. *J Nat Prod* **68**: 1793–1795.

Behrendt, L., Schrameyer, V., Qvortrup, K., Lundin, L., Sørensen, S.J., Larkum, A.W.D., and Kühl, M. (2012) Biofilm growth and near-infrared radiation-driven photosynthesis of the chlorophyll d-containing cyanobacterium *Acaryochloris marina*. *Appl Environ Microbiol* **78**:

3896–3904.

Bellou, N., Papathanassiou, E., Dobretsov, S., Lykousis, V., and Colijn, F. (2012) The effect of substratum type, orientation and depth on the development of bacterial deep-sea biofilm communities grown on artificial substrata deployed in the Eastern Mediterranean. *Biofouling* **28**: 199–213.

Berg, M. and Sutula, M. (2015) Factors affecting the growth of cyanobacteria with special emphasis on the Sacramento-San Joaquin Delta. *Technical Report 869. Southern California Coastal Water Research Project Authority.* Costa Mesa (CA).

Bharti, A., Velmourougane, K., and Prasanna, R. (2017) Phototrophic biofilms: diversity, ecology and applications. *J Appl Phycol* **29**: 2729–2744.

Bink, A., Vandenbosch, D., Coenye, T., Nelis, H., Cammue, B.P.A., and Thevissen, K. (2011) Superoxide dismutases are involved in *Candida albicans* biofilm persistence against miconazole. *Antimicrob Agents Chemother* **55**: 4033–4037.

Bischoff, V., Zucker, F., and Moraru, C. (2021) Marine Bacteriophages. In *Encyclopedia of virology, 4th ed*. Bamford DH, Zuckerman M (eds). Oxford, United Kingdom: Academic Press pp. 322–341.

Blain, S., Guillou, J., Tréguer, P.J., Woerther, P., Delauney, L., Follenfant, E., et al. (2004) High frequency monitoring of the coastal marine environment using the MAREL buoy. *J Environ Monit* **6**: 569–575.

Blom, J.F., Brütsch, T., Barbaras, D., Bethuel, Y., Locher, H.H., Hubschwerlen, C., and Gademann, K. (2006) Potent Algicides Based on the Cyanobacterial Alkaloid Nostocarboline. *Org Lett* **8**: 737–740.

Bodor, A.M., Jänsch, L., Wissing, J., and Wagner-Döbler, I. (2011) The luxS mutation causes loosely-bound biofilms in *Shewanella oneidensis*. *BMC Res Notes* **4**: 1–11.

Bos, R., van der Mei, H.C., and Busscher, H.J. (1999) Physico-chemistry of initial microbial adhesive interactions – its mechanisms and methods for study. *FEMS Microbiol Rev* **23**: 179–230.

Bosselmann, K. (1996) Environmental law and tributyltin in the environment. In *Tributyltin: Case study of an environmental contaminant*. de Mora, S. (ed). Cambridge, UK: Cambridge University Press, pp. 237–263.

Bourne, D.G., Høj, L., Webster, N.S., Swan, J., and Hall, M.R. (2006) Biofilm development within a larval rearing tank of the tropical rock lobster, *Panulirus ornatus*. *Aquaculture* **260**: 27–38.

Boyer, J.N., Kelble, C.R., Ortner, P.B., and Rudnick, D.T. (2009) Phytoplankton bloom status: Chlorophyll a biomass as an indicator of water quality condition in the southern estuaries of Florida, USA. *Ecol Indic* **9**: 56–67.

Brackbill, J.U., Kothe, D.B., and Zemach, C. (1992) A continuum method for modeling surface tension. *J Comput Phys* **100**: 335–354.

Bradbeer, S.J., Coughlan, N.E., Cuthbert, R.N., Crane, K., Dick, J.T.A., Caffrey, J.M., et al. (2020) The effectiveness of disinfectant and steam exposure treatments to prevent the spread of the highly invasive killer shrimp, *Dikerogammarus villosus*. *Sci Rep* **10**: 1–7.

Brady, R.F. and Singer, I.L. (2000) Mechanical factors favoring release from fouling release coatings. *Biofouling* **15**: 73–81.

Bragg, J.G., Thomas, D., and Baudouin-Cornu, P. (2006) Variation among species in proteomic sulphur content is related to environmental conditions. *Proceedings Biol Sci* **273**: 1293–1300.

Breinlinger, S., Phillips, T.J., Haram, B.N., Mareš, J., Martínez Yerena, J.A., Hrouzek, P., et al. (2021) Hunting the eagle killer: A cyanobacterial neurotoxin causes vacuolar myelinopathy. *Science (80)* **371**: eaax9050.

Bressy, C. and Lejars, M. (2014) Marine fouling : An overview marine fouling. *J Ocean Technol* **9**: 19–28.

Bressy, C., Margaillan, A., Faÿ, F., Linossier, I., and Réhel, K. (2009) Tin-free self-polishing marine antifouling coatings. In *Woodhead Publishing Series in Metals and Surface Engineering*. Hellio, C. and Yebra, D.B.T.-A. in M.A.C. and T. (eds). Woodhead Publishing, pp. 445–491.

Briand, J.-F., Djeridi, I., Jamet, D., Coupé, S., Bressy, C., Molmeret, M., et al. (2012) Pioneer marine biofilms on artificial surfaces including antifouling coatings immersed in two contrasting French Mediterranean coast sites. *Biofouling* **28**: 453–463.

Briand, J.F., Pollet, T., Misson, B., Garnier, C., Lejars, M., Maintenay, M., et al. (2022) Surface Characteristics Together With Environmental Conditions Shape Marine Biofilm Dynamics in Coastal NW Mediterranean Locations. *Front Mar Sci* **8**.

Brown, N.E.M., Milazzo, M., Rastrick, S.P.S., Hall-Spencer, J.M., Therriault, T.W., and Harley, C.D.G. (2018) Natural acidification changes the timing and rate of succession, alters community structure, and increases homogeneity in marine biofouling communities. *Glob Chang Biol* **24**: e112–e127.

Brzozowska, A.M., Maassen, S., Goh Zhi Rong, R., Benke, P.I., Lim, C.S., Marzinelli, E.M., et al. (2017) Effect of Variations in Micropatterns and Surface Modulus on Marine Fouling of Engineering Polymers. *ACS Appl Mater Interfaces* **9**: 17508–17516.

Brzozowska, A.M., Parra-Velandia, F.J., Quintana, R., Xiaoying, Z., Lee, S.S.C., Chin-Sing, L., et al. (2014) Biomimicking micropatterned surfaces and their effect on marine biofouling. *Langmuir* **30**: 9165–9175.

Brzozowska, E., Pyra, A., Pawlik, K., and Gamian, A. (2018) The antibiofilm activity of dual-function tail tubular protein B from KP32 phage. *Preprints* **2018030075**.

Buratti, F.M., Manganelli, M., Vichi, S., Stefanelli, M., Scardala, S., Testai, E., and Funari, E. (2017) Cyanotoxins: producing organisms, occurrence, toxicity, mechanism of action and human health toxicological risk evaluation. *Arch Toxicol* **91**: 1049–1130.

Burmølle, M., Webb, J.S., Rao, D., Hansen, L.H., Sørensen, S.J., and Kjelleberg, S. (2006) Enhanced biofilm formation and increased resistance to antimicrobial agents and bacterial invasion are caused by synergistic interactions in multispecies biofilms. *Appl Environ Microbiol* **72**: 3916–3923.

Cahill, P.L., Lewis, P.N., Solutions, B., Tait, L., and Floerl, O. (2019) Treatment agents for biofouling in internal pipework of recreational vessels: A review of pipework configurations, biofouling risk, and operational considerations. *MPI Technical Paper No: 2019/03*. New Zealand.

Cai, L., Wu, D., Xia, J., Shi, H., and Kim, H. (2019) Influence of physicochemical surface properties on the adhesion of bacteria onto four types of plastics. *Sci Total Environ* **671**: 1101–1107.

Cai, W. and Arias, C.R. (2017) Biofilm Formation on Aquaculture Substrates by Selected Bacterial Fish Pathogens. *J Aquat Anim Heal* **29**: 95–104.

Callow, J.A. and Callow, M.E. (2011) Trends in the development of environmentally friendly fouling-resistant marine coatings. *Nat Commun* **2**: 244.

Callow, M.E. and Callow, J.A. (2002) Marine biofouling: A sticky problem. *Biologist* **49**: 10–14.

Campbell, A.H., Meritt, D.W., Franklin, R.B., Boone, E.L., Nicely, C.T., and Brown, B.L. (2011) Effects of age and composition of field-produced biofilms on oyster larval setting. *Biofouling* **27**: 255–265.

Campbell, W.S. and Laudenbach, D.E. (1995) Characterization of four superoxide dismutase genes from a filamentous cyanobacterium. *J Bacteriol* **177**: 964–972.

Campos, A., Danielsson, G., Farinha, A.P., Kuruvilla, J., Warholm, P., and Cristobal, S. (2016) Shotgun proteomics to unravel marine mussel (*Mytilus edulis*) response to long-term exposure to low salinity and propranolol in a Baltic Sea microcosm. *J Proteomics* **137**: 97–106.

Camps, M., Barani, A., Gregori, G., Bouchez, A., le Berre, B., Bressy, C., et al. (2014) Antifouling coatings influence both abundance and community structure of colonizing biofilms: A case study in the Northwestern Mediterranean Sea. *Appl Environ Microbiol* **80**: 4821–4831.

Canny, J. (1986) A Computational Approach to Edge Detection. *IEEE Trans Pattern Anal Mach Intell* **8**: 679–698.

Cao, S., Wang, J., Chen, H., and Chen, D. (2011) Progress of marine biofouling and antifouling technologies. *Chinese Sci Bull* **56**: 598–612.

Caruso, G. (2020) Microbial colonization in marine environments: Overview of current knowledge

and emerging research topics. *J Mar Sci Eng* **8**: 1–22.

Carvalho, C.C.C.R. (2018) Marine biofilms: A successful microbial strategy with economic implications. *Front Mar Sci* **5**: 1–11.

Carvalho, C.C.C.R. de (2012) Biofilms: New Ideas for An Old Problem. *Recent Pat Biotechnol* **6**: 13–22.

de Carvalho, C.C.C.R. and da Fonseca, M.M.R. (2007) Assessment of three-dimensional biofilm structure using an optical microscope. *Biotechniques* **42**: 616,618-620.

Castielli, O., De la Cerda, B., Navarro, J.A., Hervás, M., and De la Rosa, M.A. (2009) Proteomic analyses of the response of cyanobacteria to different stress conditions. *FEBS Lett* **583**: 1753–1758.

Catão, E.C.P., Pollet, T., Misson, B., Garnier, C., Ghiglione, J.-F., Barry-Martinet, R., et al. (2019) Shear Stress as a Major Driver of Marine Biofilm Communities in the NW Mediterranean Sea. *Front Microbiol* **10**: 1–16.

Cense, A.W., Peeters, E.A., Gottenbos, B., Baaijens, F.P., Nuijs, A.M., and van Dongen, M.E. (2006) Mechanical properties and failure of *Streptococcus mutans* biofilms, studied using amicroindentation device. *J Microbiol Methods* **67**: 463–472.

Chakdar, H., Thapa, S., Srivastava, A., and Shukla, P. (2022) Genomic and proteomic insights into the heavy metal bioremediation by cyanobacteria. *J Hazard Mater* **424**: 127609.

Chambers, L.D., Stokes, K.R., Walsh, F.C., and Wood, R.J.K. (2006) Modern approaches to marine antifouling coatings. *Surf Coatings Technol* **201**: 3642–3652.

Champ, M.A. (2000) A review of organotin regulatory strategies, pending actions, related costs and benefits. *Sci Total Environ* **258**: 21–71.

Chatterjee, S., Nüesch, F.A., and Chu, B.T.T. (2011) Comparing carbon nanotubes and graphene nanoplatelets as reinforcements in polyamide 12 composites. *Nanotechnology* **22**: 275714.

Chávez de Paz, L.E. (2009) Image analysis software based on color segmentation for characterization of viability and physiological activity of biofilms. *Appl Environ Microbiol* **75**: 1734–1739.

Chen, M., Hernandez-Prieto, M.A., Loughlin, P.C., Li, Y., and Willows, R.D. (2019) Genome and proteome of the chlorophyll f-producing cyanobacterium *Halomicronema hongdechloris*: Adaptative proteomic shifts under different light conditions. *BMC Genomics* **20**: 1–15.

Chen, N.H., Couñago, R.M., Djoko, K.Y., Jennings, M.P., Apicella, M.A., Kobe, B., and McEwan, A.G. (2013) A glutathione-dependent detoxification system is required for formaldehyde resistance and optimal survival of neisseria meningitidis in biofilms. *Antioxidants Redox Signal* **18**: 743–755.

Chen, N.H., Djoko, K.Y., Veyrier, F.J., and McEwan, A.G. (2016) Formaldehyde Stress Responses in Bacterial Pathogens. *Front Microbiol* **7**: 257.

Chen, Z., Li, X., Tan, X., Zhang, Y., and Wang, B. (2020) Recent Advances in Biological Functions of Thick Pili in the Cyanobacterium *Synechocystis* sp. PCC 6803. *Front Plant Sci* **11**: 1–10.

Cheng, S., Cetinkaya, M., and Gräter, F. (2010) How Sequence Determines Elasticity of Disordered Proteins. *Biophys J* **99**: 3863–3869.

Chun, A.L.M., Salta, M., Mosayyebi, A., Butt, A., and Carugo, D. (2022) Early biofilm and streamer formation is mediated by wall shear stress and surface wettability: A multifactorial microfluidic study.

Chung, H.C., Lee, O.O., Huang, Y.-L., Mok, S.Y., Kolter, R., and Qian, P.-Y. (2010) Bacterial community succession and chemical profiles of subtidal biofilms in relation to larval settlement of the polychaete Hydroides elegans. *ISME J* **4**: 817–828.

Claessen, D., Rozen, D.E., Kuipers, O.P., Søgaard-Andersen, L., and van Wezel, G.P. (2014) Bacterial solutions to multicellularity: a tale of biofilms, filaments and fruiting bodies. *Nat Rev Microbiol* **12**: 115–124.

Coleman, M.L. and Chisholm, S.W. (2007) Code and context: *Prochlorococcus* as a model for cross-scale biology. *Trends Microbiol* **15**: 398–407.

Conradi, F., Zhou, R.-Q., Oeser, S., Schuergers, N., Wilde, A., and Mullineaux, C. (2019) Factors Controlling Floc Formation and Structure in the Cyanobacterium *Synechocystis* sp. Strain PCC 6803. *J Bacteriol* **201:** e00344-19.

Cordeiro, R., Luz, R., Vilaverde, J., Vasconcelos, V., Fonseca, A., and Gonçalves, V. (2020) Distribution of toxic cyanobacteria in volcanic lakes of the azores islands. *Water (Switzerland)* **12**: 1–19.

Costerton, J.W., Geesey, G.G., and Cheng, K.J. (1978) How bacteria stick. *Sci Am* **238**: 86–95.

Crawford, R.J., Webb, H.K., Truong, V.K., Hasan, J., and Ivanova, E.P. (2012) Surface topographical factors influencing bacterial attachment. *Adv Colloid Interface Sci* **179–182**: 142–149.

Croft, M.T., Warren, M.J., and Smith, A.G. (2006) Algae need their vitamins. *Eukaryot Cell* **5**: 1175–1183.

D'Agostino, P.M., Woodhouse, J.N., Makower, A.K., Yeung, A.C.Y., Ongley, S.E., Micallef, M.L., et al. (2016) Advances in genomics, transcriptomics and proteomics of toxin-producing cyanobacteria. *Environ Microbiol Rep* **8**: 3–13.

Daims, H., Lücker, S., and Wagner, M. (2006) Daime, a novel image analysis program for microbial ecology and biofilm research. *Environ Microbiol* **8**: 200–213.

Dang, H. and Lovell, C.R. (2000) Bacterial Primary Colonization and Early Succession on Surfaces in Marine Waters as Determined by Amplified rRNA Gene Restriction Analysis and Sequence Analysis of 16S rRNA Genes. *Appl Environ Microbiol* **66**: 467–475.

Dang, H. and Lovell, C.R. (2016) Microbial Surface Colonization and Biofilm Development in Marine Environments. *Microbiol Mol Biol Rev* **80**: 91–138.

Darriba, D., Taboada, G.L., Doallo, R., and Posada, D. (2012) jModelTest 2: more models, new heuristics and parallel computing. *Nat Methods* **9**: 772.

Davey, P.A., Power, A.M., Santos, R., Bertemes, P., Ladurner, P., Palmowski, P., et al. (2021) Omics-based molecular analyses of adhesion by aquatic invertebrates. *Biol Rev* **96**: 1051–1075.

David, C., Bühler, K., and Schmid, A. (2015) Stabilization of single species *Synechocystis* biofilms by cultivation under segmented flow. *J Ind Microbiol Biotechnol* **42**: 1083–1089.

Davidson, I., Scianni, C., Hewitt, C., Everett, R., Holm, E., Tamburri, M., and Ruiz, G. (2016) Mini-review: Assessing the drivers of ship biofouling management – aligning industry and biosecurity goals. *Biofouling* **32**: 411–428.

Davidson, I.C., Brown, C.W., Sytsma, M.D., and Ruiz, G.M. (2009) The role of containerships as transfer mechanisms of marine biofouling species. *Biofouling J Bioadhesion Biofilm Res* **25**: 645–655.

Davies, P. and Rajapakse, Y.D.S. (2013) Durability of Composites in a Marine Environment, Netherlands: Springer.

Dean, C., Soloviev, A., Hirons, A., Frank, T., and Wood, J. (2016) Biomixing due to diel vertical migrations of zooplankton: comparison of computational fluid dynamics model with observations. *Ocean Model* **98**: 51–64.

Decho, A.W. and Gutierrez, T. (2017) Microbial extracellular polymeric substances (EPSs) in ocean systems. *Front Microbiol* **8**: 1–28.

Delauney, L., Compare, C., and Lehaitre, M. (2010) Biofouling protection for marine environmental sensors. *Ocean Sci* **6**: 503–511.

Delepelaire, P. (2019) Bacterial ABC transporters of iron containing compounds. *Res Microbiol* **170**: 345–357.

Delgado, A., Briciu-Burghina, C., and Regan, F. (2021) Antifouling strategies for sensors used in water monitoring: Review and future perspectives. *Sensors (Switzerland)* **21**: 1–25.

Demirel, Y.K., Uzun, D., Zhang, Y., Fang, H.C., Day, A.H., and Turan, O. (2017) Effect of barnacle fouling on ship resistance and powering. *Biofouling* **33**: 819–834.

Denby, K.J., Iwig, J., Bisson, C., Westwood, J., Rolfe, M.D., Sedelnikova, S.E., et al. (2016) The mechanism of a formaldehyde-sensing transcriptional regulator. *Sci Rep* **6**: 38879.

Department of Agriculture Fisheries and Forestry (2008) Operational Procedures Manual —

Decontamination (Version 1.0). Australian Aquatic Veterinary Emergency Plan (AQUAVETPLAN), Canberra.

Dessau, R.B. and Pipper, C.B. (2008) [''R"--project for statistical computing]. *Ugeskr Laeger* **170**: 328—330.

Diaconu, M., Kothe, U., Schlünzen, F., Fischer, N., Harms, J.M., Tonevitsky, A.G., et al. (2005) Structural basis for the function of the ribosomal L7/12 stalk in factor binding and GTpase activation. *Cell* **121**: 991–1004.

Dimartino, S., Mather, A. V, Alestra, T., Nawada, S., and Haber, M. (2014) Experimental and computational analysis of a novel flow channel to assess the adhesion strength of sessile marine organisms. Interface Focus 5: 20140059.

Ding, L., Bar-Shalom, R., Aharonovich, D., Kurisawa, N., Patial, G., Li, S., et al. (2021) Metabolomic characterization of a cf. *Neolyngbya* cyanobacterium from the south china sea reveals wenchangamide a, a lipopeptide with in vitro apoptotic potential in colon cancer cells. *Mar Drugs* **19**: 1–18.

Ding, W., Zhang, W., Alikunhi, N.M., Batang, Z., Pei, B., Wang, R., et al. (2019) Metagenomic Analysis of Zinc Surface–Associated Marine Biofilms. *Microb Ecol* **77**: 406–416.

Dingreville, R., Karnesky, R.A., Puel, G., and Schmitt, J.H. (2016) Synergies between computational modeling and experimental characterization of materials across length scales. *J Mater Sci* **51**: 1176–1177.

Dobretsov, S., Abed, R.M.M., and Teplitski, M. (2013) Mini-review: Inhibition of biofouling by marine microorganisms. *Biofouling* **29**: 423–41.

Dobretsov, S., Al-Shibli, H., Maharachchikumbura, S.S.N., and Al-Sadi, A.M. (2021) The presence of marine filamentous fungi on a copper-based antifouling paint. *Appl Sci* **11**: 8277.

Dobretsov, S. and Rittschof, D. (2020) Love at first taste: Induction of larval settlement by marine microbes. *Int J Mol Sci* **21**: 731.

Dobretsov, S., Teplitski, M., and Paul, V. (2009) Mini-review: quorum sensing in the marine environment and its relationship to biofouling. *Biofouling* **25**: 413–27.

Dobretsov, S., Xiong, H., Xu, Y., Levin, L.A., and Qian, P.Y. (2007) Novel antifoulants: Inhibition of larval attachment by proteases. *Mar Biotechnol* **9**: 388–397.

Domínguez-Pérez, D., Almeida, D., Wissing, J., Machado, A.M., Jänsch, L., Castro, L.F., et al. (2020) The Quantitative Proteome of the Cement and Adhesive Gland of the Pedunculate Barnacle, Pollicipes pollicipes. *Int J Mol Sci* **21**: 2524.

Domínguez-Pérez, D., Lippolis, J., Dennis, M., Miller, B., Tiley, K., Vasconcelos, V., et al. (2019) The Queen Conch (*Lobatus gigas*) Proteome: A Valuable Tool for Biological Studies in Marine Gastropods. *Protein J* **38**: 628–639.

Di Donato, P., Poli, A., Taurisano, V., Abbamondi, G.R., Nicolaus, B., and Tommonaro, G. (2016) Recent advances in the study of marine microbial biofilm: From the involvement of quorum sensing in its production up to biotechnological application of the polysaccharide fractions. *J Mar Sci Eng* **4**:.

Dong, T.M.H. and Le, V.V. (2018) As-Used Materials for Marine Industry. *Eur J Eng Res Sci* **3**: 111–116.

Dong, X. and Yang, L. (2014) Inhibitory effects of single-walled carbon nanotubes on biofilm formation from *Bacillus anthracis* spores. *Biofouling* **30**: 1165–1174.

Doshi, B., Sillanpää, M., and Kalliola, S. (2018) A review of bio-based materials for oil spill treatment. *Water Res* **135**: 262–277.

Drescher, K., Shen, Y., Bassler, B.L., and Stone, H.A. (2013) Biofilm streamers cause catastrophic disruption of flow with consequences for environmental and medical systems. *Proc Natl Acad Sci* **110**: 4345–50.

Van den Driessche, F., Rigole, P., Brackman, G., and Coenye, T. (2014) Optimization of resazurin-based viability staining for quantification of microbial biofilms. *J Microbiol Methods* **98**: 31–34.

Duda, R.O. and Hart, P.E. (1972) Use of the Hough Transformation to Detect Lines and Curves in

Pictures. *Commun ACM* **15**: 11–15.

Duddu, R., Chopp, D.L., and Moran, B. (2009) A two-dimensional continuum model of biofilm growth incorporating fluid flow and shear stress based detachment. *Biotechnol Bioeng* **103**: 92–104.

Duggan, P.S., Gottardello, P., and Adams, D.G. (2007) Molecular analysis of genes in *Nostoc punctiforme* involved in pilus biogenesis and plant infection. *J Bacteriol* **189**: 4547–4551.

Duperron, S., Beniddir, M.A., Durand, S., Longeon, A., Duval, C., Gros, O., et al. (2019) New Benthic Cyanobacteria from Guadeloupe Mangroves as Producers of Antimicrobials. *Mar Drugs* **18**: 16.

Durai, P., Batool, M., and Choi, S. (2015) Structure and Effects of Cyanobacterial Lipopolysaccharides. *Mar Drugs* **13**: 4217–4230.

Dustebek, J., Kandemir-Cavas, C., Nitodas, S.F., and Cavas, L. (2016) Effects of carbon nanotubes on the mechanical strength of self-polishing antifouling paints. *Prog Org Coatings* **98**: 18–27.

Dvořák, P., Casamatta, D.A., Hašler, P., Jahodářová, E., Norwich, A.R., and Poulíčková, A. (2017) Diversity of the cyanobacteria. In *Modern topics in the phototrophic prokaryotes*. Hallenbeck, P. (ed). Cham, Switzerland: Springer, pp. 3–46.

Dvořák, P., Poulíčková, A., Hašler, P., Belli, M., Casamatta, D.A., and Papini, A. (2015) Species concepts and speciation factors in cyanobacteria, with connection to the problems of diversity and classification. *Biodivers Conserv* **24**: 739–757.

Echenique, J.R., Dorsey, C.W., Patrito, L.C., Petroni, A., Tolmasky, M.E., and Actis, L.A. (2001) *Acinetobacter baumannii* has two genes encoding glutathione-dependent formaldehyde dehydrogenase: Evidence for differential regulation in response to iron. *Microbiology* **147**: 2805–2815.

Ehrnsperger, M., Gräber, S., Gaestel, M., and Buchner, J. (1997) Binding of non-native protein to Hsp25 during heat shock creates a reservoir of folding intermediates for reactivation. *EMBO J* **16**: 221–229.

Ellinas, K., Kefallinou, D., Stamatakis, K., Gogolides, E., and Tserepi, A. (2017) Is There a Threshold in the Antibacterial Action of Superhydrophobic Surfaces? *ACS Appl Mater Interfaces* **9**: 39781–39789.

Engelhardt, H. and Peters, J. (1998) Structural research on surface layers: A focus on stability, surface layer homology domains, and surface layer-cell wall interactions. *J Struct Biol* **124**: 276–302.

Enomoto, G., Nomura, R., Shimada, T., Win, N.N., Narikawa, R., and Ikeuchi, M. (2014) Cyanobacteriochrome SesA is a diguanylate cyclase that induces cell aggregation in *Thermosynechococcus*. *J Biol Chem* **289**: 24801–24809.

Evans, S.M. (1999) TBT or not TBT?: That is the question. *Biofouling* **14**: 117–129.

Fan, F. Xin, Zheng, Y. Ming, Ba, M., Wang, Y. Feng, Kong, J. Jun, Liu, J. Hao, and Wu, Q. (2021) Long time super-hydrophobic fouling release coating with the incorporation of lubricant. *Prog Org Coatings* **152**: 106136.

Fanesi, A., Lavayssière, M., Breton, C., Bernard, O., Briandet, R., and Lopes, F. (2021) Shear stress affects the architecture and cohesion of *Chlorella vulgaris* biofilms. *Sci Rep* **11**: 1–11.

Faria, S., Gomes, L.C., Teixeira-Santos, R., Morais, J., Vasconcelos, V., and Mergulhão, F.J.M. (2021) Developing new marine antifouling surfaces: Learning from single-strain laboratory tests. *Coatings* **11**: 1–11.

Faria, S., Teixeira-Santos, R., Morais, J., Vasconcelos, V., and Mergulhão, F.J. (2021) The association between initial adhesion and cyanobacterial biofilm development. *FEMS Microbiol Ecol* **97**: fiab052.

Faria, S., Teixeira-Santos, R., Romeu, M.J., Morais, J., Jong, E. de, Sjollema, J., et al. (2021) Unveiling the antifouling performance of different marine surfaces and their effect on the development and structure of cyanobacterial biofilms. *Microorganisms* **9**: 1102.

Faria, S.I., Teixeira-Santos, R., Gomes, L.C., Silva, E.R., Morais, J., Vasconcelos, V., and Mergulhão,

F.J.M. (2020) Experimental assessment of the performance of two marine coatings to curb biofilm formation of microfoulers. *Coatings* **10**: 893.

Faria, S.I., Teixeira-Santos, R., Romeu, M.J., Morais, J., Vasconcelos, V., and Mergulhão, F.J. (2020) The Relative Importance of Shear Forces and Surface Hydrophobicity on Biofilm Formation by Coccoid Cyanobacteria. *Polymers (Basel)* **12**: 653.

Farkas, A., Degiuli, N., and Martić, I. (2021) Assessment of the effect of biofilm on the ship hydrodynamic performance by performance prediction method. *Int J Nav Archit Ocean Eng* **13**: 102–114.

Farkas, A., Degiuli, N., and Martić, I. (2018) Towards the prediction of the effect of biofilm on the ship resistance using CFD. *Ocean Eng* **167**: 169–186.

Fatima, N., Qazi, U.Y., Mansha, A., Bhatti, I.A., Javaid, R., Abbas, Q., et al. (2021) Recent developments for antimicrobial applications of graphene-based polymeric composites: A review. *J Ind Eng Chem* **100**: 40–58.

Favre, L., Ortalo-Magné, A., Pichereaux, C., Gargaros, A., Burlet-Schiltz, O., Cotelle, V., and Culioli, G. (2018) Metabolome and proteome changes between biofilm and planktonic phenotypes of the marine bacterium Pseudoalteromonas lipolytica TC8. *Biofouling* **34**: 132–148.

Fazli-Shokouhi, S., Nasirpouri, F., and Khatamian, M. (2021) Epoxy-matrix polyaniline/p-phenylenediamine-functionalised graphene oxide coatings with dual anti-corrosion and anti-fouling performance. *RSC Adv* **11**: 11627–11641.

Fernandes, J.A., Santos, L., Vance, T., Fileman, T., Smith, D., Bishop, J.D.D., et al. (2016) Costs and benefits to European shipping of ballast-water and hull-fouling treatment: Impacts of native and non-indigenous species. *Mar Policy* **64**: 148–155.

Ferrari, M., Benedetti, A., Santini, E., Ravera, F., Liggieri, L., Guzman, E., and Cirisano, F. (2015) Biofouling control by superhydrophobic surfaces in shallow euphotic seawater. *Colloids Surfaces A Physicochem Eng Asp* **480**: 369–375.

Fisher, M.L., Allen, R., Luo, Y., and Curtiss, R. (2013) Export of Extracellular Polysaccharides Modulates Adherence of the Cyanobacterium *Synechocystis*. *PLoS One* **8**: e74514.

Fitridge, I., Dempster, T., Guenther, J., and de Nys, R. (2012) The impact and control of biofouling in marine aquaculture: a review. *Biofouling* **28**: 649–69.

Flemming, H.-C., Murthy, P.S., Venkatesan, R., and Cooksey, K. (2009) Marine and Industrial Biofouling, Costerton, J.W. (ed) Los Angeles, USA: Springer Berlin Heidelberg.

Flemming, H. and Wingender, J. (2010) The biofilm matrix. *Nat Rev Microbiol* **8**: 623–33.

Flemming, H.C., Wingender, J., Szewzyk, U., Steinberg, P., Rice, S.A., and Kjelleberg, S. (2016) Biofilms: An emergent form of bacterial life. *Nat Rev Microbiol* **14**: 563–575.

Foster, J.S., Green, S.J., Ahrendt, S.R., Golubic, S., Reid, R.P., Hetherington, K.L., and Bebout, L. (2009) Molecular and morphological characterization of cyanobacterial diversity in the stromatolites of highborne cay, bahamas. *ISME J* **3**: 573–587.

Foster, R.A., Kuypers, M.M.M., Vagner, T., Paerl, R.W., Musat, N., and Zehr, J.P. (2011) Nitrogen fixation and transfer in open ocean diatom-cyanobacterial symbioses. *ISME J* **5**: 1484–1493.

Frazão, B., Martins, R., and Vasconcelos, V. (2010) Are known cyanotoxins involved in the toxicity of picoplanktonic and filamentous north atlantic marine cyanobacteria? *Mar Drugs* **8**: 1908–1919.

Fu, J., Zong, G., Zhang, P., Gu, Y., and Cao, G. (2018) Deletion of the β-Propeller Protein Gene Rv1057 Reduces ESAT-6 Secretion and Intracellular Growth of *Mycobacterium tuberculosis*. *Curr Microbiol* **75**: 401–409.

Fulda, S., Mikkat, S., Huang, F., Huckauf, J., Marin, K., Norling, B., and Hagemann, M. (2006) Proteome analysis of salt stress response in the cyanobacterium *Synechocystis* sp. strain PCC 6803. *Proteomics* **6**: 2733–2745.

Fusetani, N. (2011) Antifouling marine natural products. *Nat Prod Rep* **28**: 400–410.

Gademann, K. (2007) Cyanobacterial natural products for the inhibition of biofilm formation and

biofouling. *Chimia (Aarau)* **61**: 373–377.

Gaget, V., Humpage, A.R., Huang, Q., Monis, P., and Brookes, J.D. (2017) Benthic cyanobacteria: A source of cylindrospermopsin and microcystin in Australian drinking water reservoirs. *Water Res* **124**: 454–464.

Gamage, N.T.G., Miyashita, R., Takahashi, K., Asakawa, S., and Senevirathna, J.D.M. (2022) Proteomic Applications in Aquatic Environment Studies. *Proteomes* **10**: 32.

Gambino, M., Sanmartín, P., Longoni, M., Villa, F., Mitchell, R., and Cappitelli, F. (2019) Surface colour: An overlooked aspect in the study of cyanobacterial biofilm formation. *Sci Total Environ* **659**: 342–353.

Gao, Y., Meng, Q., Zhou, X., Luo, X., Su, Z., Chen, Z., et al. (2022) How do environmentally friendly antifouling alkaloids affect marine fouling microbial communities? *Sci Total Environ* **820**: 152910.

Gao, Y., Xiong, W., Li, X.B., Gao, C.F., Zhang, Y.L., Li, H., and Wu, Q.Y. (2009) Identification of the proteomic changes in *Synechocystis* sp. PCC 6803 following prolonged UV-B irradiation. *J Exp Bot* **60**: 1141–1154.

Georgiades, E., Scianni, C., Davidson, I., Tamburri, M.N., First, M.R., Ruiz, G., et al. (2021) The Role of Vessel Biofouling in the Translocation of Marine Pathogens: Management Considerations and Challenges. *Front Mar Sci* **8**: 1–20.

Giakoumi, S., Katsanevakis, S., Albano, P.G., Azzurro, E., Cardoso, A.C., Cebrian, E., et al. (2019) Management priorities for marine invasive species. *Sci Total Environ* **688**: 976–982.

Gibble, C.M., Peacock, M.B., and Kudela, R.M. (2016) Evidence of freshwater algal toxins in marine shellfish: Implications for human and aquatic health. *Harmful Algae* **59**: 59–66.

Giner-Lamia, J., Pereira, S.B., Bovea-Marco, M., Futschik, M.E., Tamagnini, P., and Oliveira, P. (2016) Extracellular proteins: Novel key components of metal resistance in cyanobacteria? *Front Microbiol* **7**: 1–8.

Gloag, E.S., Fabbri, S., Wozniak, D.J., and Stoodley, P. (2020) Biofilm mechanics: Implications in infection and survival. *Biofilm* **2**: 100017.

Godwin, L.S. (2003) Hull fouling of maritime vessels as a pathway for marine species invasions to the Hawaiian Islands. *Biofouling* **19**: 123–132.

Gomes, I.B., Meireles, A., Gonçalves, A.L., Goeres, D.M., Sjollema, J., Simões, L.C., and Simões, M. (2018) Standardized reactors for the study of medical biofilms: a review of the principles and latest modifications. *Crit Rev Biotechnol* **38**: 657–670.

Gomes, L., Miranda, J., and Mergulhão, F. (2019) Operation of biofilm reactors for the food industry using CFD. In *Computational fluid dynamics in food processing.* Sun, D. (ed). New York: CRC PRESS, pp. 561–590.

Gomes, L.C., Deschamps, J., Briandet, R., and Mergulhão, F.J. (2018) Impact of modified diamond-like carbon coatings on the spatial organization and disinfection of mixed-biofilms composed of *Escherichia coli* and *Pantoea agglomerans* industrial isolates. *Int J Food Microbiol* **277**: 74–82.

Gomes, L.C. and Mergulhão, F.J. (2017) SEM Analysis of Surface Impact on Biofilm Antibiotic Treatment. *Scanning* **2017**: 2960194.

Gomes, L.C. and Mergulhão, F.J.M. (2021) A selection of platforms to evaluate surface adhesion and biofilm formation in controlled hydrodynamic conditions. *Microorganisms* **9**: 1993.

Gomes, L.C., Moreira, J.M.R., Teodósio, J.S., Araújo, J.D.P., Miranda, J.M., Simões, M., et al. (2014) 96-well microtiter plates for biofouling simulation in biomedical settings. *Biofouling* **30**: 535–546.

Gomes, L.C., Silva, L.N., Simões, M., Melo, L.F., and Mergulhão, F.J. (2015) *Escherichia coli* adhesion, biofilm development and antibiotic susceptibility on biomedical materials. *J Biomed Mater Res - Part A* **103**: 1414–1423.

Gomes, M., Gomes, L.C., Teixeira-Santos, R., Pereira, M.F.R., Soares, O.S.G.P., and Mergulhão, F.J. (2021) Optimizing CNT loading in antimicrobial composites for urinary tract application. *Appl Sci* **11**: 4038.

Graba, M., Sauvage, S., Moulin, F.Y., Urrea, G., Sabater, S., and Sanchez-Pérez, J.M. (2013) Interaction between local hydrodynamics and algal community in epilithic biofilm. *Water Res* **47**: 2153–2163.

Granhag, L.M., Finlay, J.A., Jonsson, P.R., Callow, J.A., and Callow, M.E. (2004) Roughness-dependent removal of settled spores of the green alga *Ulva* (syn. Enteromorpha) exposed to hydrodynamic forces from a water jet. *Biofouling* **20**: 117–122.

De Grazia, A., LuTheryn, G., Meghdadi, A., Mosayyebi, A., Espinosa-Ortiz, E.J., Gerlach, R., and Carugo, D. (2020) A Microfluidic-Based Investigation of Bacterial Attachment in Ureteral Stents. *Micromachines* **11**: 408.

Grossman, A.R., Bhaya, D., Apt, K.E., and Kehoe, D.M. (1995) Light-harvesting complexes in oxygenic photosynthesis: diversity, control, and evolution. *Annu Rev Genet* **29**: 231–288.

Gu, J., Li, L., Huang, D., Jiang, L., Liu, L., Li, F., et al. (2019) *In Situ* Synthesis of Graphene@cuprous Oxide Nanocomposite Incorporated Marine Antifouling Coating with Elevated Antifouling Performance. *Open J Org Polym Mater* **9**: 47–62.

Guillonneau, R., Baraquet, C., Bazire, A., and Molmeret, M. (2018) Multispecies Biofilm Development of Marine Bacteria Implies Complex Relationships Through Competition and Synergy and Modification of Matrix Components. *Front Microbiol* **9**: 1960.

Guiry, M.D. and Guiry, G.. (2015) AlgaeBase. *World-Wide Electron Publ Natl Univ Ireland, Galw*.

Gumbo, R.J., Ross, G., and Cloete, E.T. (2008) Biological control of *Microcystis* dominated harmful algal blooms. *African J Biotechnol* **7**: 4765–4773.

Gundry, R.L., White, M.Y., Murray, C.I., Kane, L.A., Fu, Q., Stanley, B.A., and Van Eyk, J.E. (2010) Preparation of Proteins and Peptides for Mass Spectrometry Analysis in a bottom-up proteomics workflow. *Curr Protoc Mol Biol* **77**: 342–355.

Gusnaniar, N., Sjollema, J., Nuryastuti, T., Peterson, B.W., van de Belt-Gritter, B., de Jong, E.D., et al. (2017) Structural changes in *S. epidermidis* biofilms after transmission between stainless steel surfaces. *Biofouling* **33**: 712–721.

Hammer, B.K. and Bassler, B.L. (2003) Quorum sensing controls biofilm formation in *Vibrio cholerae*. *Mol Microbiol* **50**: 101–104.

Harms, N., Reijnders, W.N.M., Koning, S., and van Spanning, R.J.M. (2001) Two-Component System That Regulates Methanol and Formaldehyde Oxidation in *Paracoccus denitrificans*. *J Bacteriol* **183**: 664–670.

Harper, P., Hallett, S., Fleming, A., and Dawson, M. (2016) Advanced fibre-reinforced composites for marine renewable energy devices. In *Woodhead Publishing Series in Composites Science and Engineering*. Graham-Jones, J. and Summerscales, J.B.T.-M.A. of A.F.-R.C. (eds). Woodhead Publishing, pp. 217–232.

Harvey, K.L., Jarocki, V.M., Charles, I.G., and Djordjevic, S.P. (2019) The diverse functional roles of elongation factor tu (Ef-tu) in microbial pathogenesis. *Front Microbiol* **10**: 1–19.

Haslbeck, M., Franzmann, T., Weinfurtner, D., and Buchner, J. (2005) Some like it hot: The structure and function of small heat-shock proteins. *Nat Struct Mol Biol* **12**: 842–846.

Heidari, F., Zima, J., Riahi, H., and Hauer, T. (2018) New simple trichal cyanobacterial taxa isolated from radioactive thermal springs. *Fottea* **18**: 137–149.

Helliwell, K.E., Lawrence, A.D., Holzer, A., Kudahl, U.J., Sasso, S., Kräutler, B., et al. (2016) Cyanobacteria and Eukaryotic Algae Use Different Chemical Variants of Vitamin B12. *Curr Biol* **26**: 999–1008.

Henriques, M., Silva, A., and Rocha, J. (2007) Extraction and quantification of pigments from a marine microalga : a simple and reproducible method. *Commun Curr Res Educ Top Trends Appl Microbiol* 586–593.

Hernández-Prieto, M.A., Semeniuk, T.A., and Futschik, M.E. (2014) Toward a systems-level understanding of gene regulatory, protein interaction, and metabolic networks in cyanobacteria. *Front Genet* **5**: 1–18.

Herschend, J., Damholt, Z.B.V., Marquard, A.M., Svensson, B., Sørensen, S.J., Hägglund, P., and

Burmølle, M. (2017) A meta-proteomics approach to study the interspecies interactions affecting microbial biofilm development in a model community. *Sci Rep* **7**: 1–13.

Heuschkel, I., Dagini, R., Karande, R., and Bühler, K. (2020) The Impact of Glass Material on Growth and Biocatalytic Performance of Mixed-Species Biofilms in Capillary Reactors for Continuous Cyclohexanol Production. *Front Bioeng Biotechnol* **8**: 588729.

Hewitt, C.L., Gollasch, S., and Minchin, D. (2009) The Vessel as a Vector – Biofouling, Ballast Water and Sediments. In *Biological Invasions in Marine Ecosystems: Ecological, Management, and Geographic Perspectives*. Rilov, G. and Crooks, J.A. (eds). Heidelberg: Springer-Verlag, pp. 117–131.

Heydorn, A., Nielsen, A.T., Hentzer, M., Sternberg, C., Givskov, M., Ersboll, B.K., and Molin, S. (2000) Quantification of biofilm structures by the novel computer program COMSTAT. *Microbiology* **146**: 2395–2407.

Hirt, C.W. and Nichols, B.D. (1981) Volume of fluid (VOF) method for the dynamics of free boundaries. *J Comput Phys* **39**: 201–225.

Hoang, H., Gurich, N., and González, J.E. (2008) Regulation of Motility by the ExpR/Sin Quorum-Sensing System in Sinorhizobium meliloti. *J Bacteriol* **190**: 861–871.

Hodson, S.L., Burke, C.M., and Bissett, A.P. (2000) Biofouling of fish-cage netting: The efficacy of a silicone coating and the effect of netting colour. *Aquaculture* **184**: 277–290.

Hoge, J. and Leach, C. (2016) Epoxy resin infused boat hulls. *Reinf Plast* **60**: 221–223.

Hoiczyk, E. and Baumeister, W. (1995) Envelope structure of four gliding filamentous cyanobacteria. *J Bacteriol* **177**: 2387–2395.

Hoiczyk, E. and Hansel, A. (2000) Cyanobacterial cell walls: news from an unusual prokaryotic envelope. *J Bacteriol* **182**: 1191–1199.

Hongsthong, A., Sirijuntarut, M., Prommeenate, P., Lertladaluck, K., Porkaew, K., Cheevadhanarak, S., and Tanticharoen, M. (2008) Proteome analysis at the subcellular level of the cyanobacterium *Spirulina platensis* in response to low-temperature stress conditions. *FEMS Microbiol Lett* **288**: 92–101.

Horn, H., Reiff, H., and Morgenroth, E. (2003) Simulation of growth and detachment in biofilm systems under defined hydrodynamic conditions. *Biotechnol Bioeng* **81**: 607–617.

Hoschek, A., Heuschkel, I., Schmid, A., Bühler, B., Karande, R., and Bühler, K. (2019) Mixed-species biofilms for high-cell-density application of *Synechocystis* sp. PCC 6803 in capillary reactors for continuous cyclohexane oxidation to cyclohexanol. *Bioresour Technol* **282**: 171–178.

Hou, J., Wang, C., Rozenbaum, R.T., Gusnaniar, N., de Jong, E.D., Woudstra, W., et al. (2019) Bacterial Density and Biofilm Structure Determined by Optical Coherence Tomography. *Sci Rep* **9**: 1–12.

Hu, M., Cui, Z., Li, Jian, Zhang, L., Mo, Y., Dlamini, D.S., et al. (2019) Ultra-low graphene oxide loading for water permeability, antifouling and antibacterial improvement of polyethersulfone/sulfonated polysulfone ultrafiltration membranes. *J Colloid Interface Sci* **552**: 319–331.

Hu, P., Xie, Q., Ma, C., and Zhang, G. (2020) Silicone-Based Fouling-Release Coatings for Marine Antifouling. *Langmuir* **36**: 2170–2183.

Huang, F., Fulda, S., Hagemann, M., and Norling, B. (2006) Proteomic screening of salt-stress-induced changes in plasma membranes of *Synechocystis* sp. strain PCC 6803. *Proteomics* **6**: 910–920.

Huang, F., Parmryd, I., Nilsson, F., Persson, A.L., Pakrasi, H.B., Andersson, B., and Norling, B. (2002) Proteomics of *Synechocystis* sp. strain PCC 6803: identification of plasma membrane proteins. *Mol Cell Proteomics* **1**: 956–966.

Hughes, C.S., Moggridge, S., Müller, T., Sorensen, P.H., Morin, G.B., and Krijgsveld, J. (2019) Single-pot, solid-phase-enhanced sample preparation for proteomics experiments. *Nat Protoc* **14**: 68–85.

Huisman, J., Codd, G.A., Paerl, H.W., Ibelings, B.W., Verspagen, J.M.H., and Visser, P.M. (2018)

Cyanobacterial blooms. *Nat Rev Microbiol* **16**: 471–483.

Humbert, J.F. and Fastner, J. (2017) Ecology of cyanobacteria. In *Handbook of Cyanobacterial Monitoring and Cyanotoxin Analysis*. Meriluoto, J., Spoof, L., and Codd, G.. (eds). Chichester, UK: JohnWiley & Sons, Ltd., pp. 11–18.

Hung, C., Zhou, Y., Pinkner, J.S., Dodson, K.W., Crowley, J.R., Heuser, J., et al. (2013) *Escherichia coli* biofilms have an organized and complex extracellular matrix structure. *MBio* **4**: e00645-13.

Hunsucker, K.Z., Vora, G.J., Hunsucker, J.T., Gardner, H., Leary, D.H., Kim, S., et al. (2018) Biofilm community structure and the associated drag penalties of a groomed fouling release ship hull coating. *Biofouling* **34**: 162–172.

IUCN (2018) *Guidelines for invasive species planning and management on islands*. Cambridge, UK and Gland, Switzerland: IUCN. viii + 40pp.

Jahn, M., Vialas, V., Karlsen, J., Maddalo, G., Edfors, F., Forsström, B., et al. (2018) Growth of Cyanobacteria Is Constrained by the Abundance of Light and Carbon Assimilation Proteins. *Cell Rep* **25**: 478-486.e8.

Jaki, B., Orjala, J., Heilmann, J., Linden, A., Vogler, B., and Sticher, O. (2000) Novel extracellular diterpenoids with biological activity from the cyanobacterium *Nostoc commune*. *J Nat Prod* **63**: 339–343.

Janesch, B., Koerdt, A., Messner, P., and Schäffer, C. (2013) The S-Layer Homology Domain-Containing Protein SlhA from *Paenibacillus alvei* CCM 2051T Is Important for Swarming and Biofilm Formation. *PLoS One* **8**: 1–17.

Jayathilake, P.G., Li, B., Zuliani, P., Curtis, T., and Chen, J. (2019) Modelling bacterial twitching in fluid flows: a CFD-DEM approach. *Sci Rep* **9**: 1–10.

Ji, Y., Sun, Y., Lang, Y., Wang, L., Liu, B., and Zhang, Z. (2018) Effect of CNT/PDMS Nanocomposites on the Dynamics of Pioneer Bacterial Communities in the Natural Biofilms of Seawater. *Mater (Basel, Sw)* **11**: 902.

Jiang, P., Zhao, S., Zhu, L., and Li, D. (2018) Microplastic-associated bacterial assemblages in the intertidal zone of the Yangtze Estuary. *Sci Total Environ* **624**: 48–54.

Jiang, T., Qi, L., and Qin, W. (2019) Improving the Environmental Compatibility of Marine Sensors by Surface Functionalization with Graphene Oxide. *Anal Chem* **91**: 13268–13274.

Jin, H., Bing, W., Tian, L., Wang, P., and Zhao, J. (2019) Combined effects of color and elastic modulus on antifouling performance: A study of graphene oxide/silicone rubber composite membranes. *Materials (Basel)* **12**: 2608.

Jin, H., Tian, L., Bing, W., Zhao, J., and Ren, L. (2022) Bioinspired marine antifouling coatings: Status, prospects, and future. *Prog Mater Sci* **124**: 100889.

Jin, H., Tian, L., Bing, W., Zhao, J., and Ren, L. (2021) Toward the application of graphene for combating marine biofouling. *Adv Sustain Syst* **5**: 2000076.

Jin, H., Zhang, T., Bing, W., Dong, S., and Tian, L. (2019) Antifouling performance and mechanism of elastic graphene-silicone rubber composite membranes. *J Mater Chem B* **7**: 488–497.

Jones, P.R., Cottrell, M.T., Kirchman, D.L., and Dexter, S.C. (2007) Bacterial community structure of biofilms on artificial surfaces in an estuary. *Microb Ecol* **53**: 153–162.

Kaneko, T., Sato, S., Kotani, H., Tanaka, A., Asamizu, E., Nakamura, Y., et al. (1996) Sequence analysis of the genome of the unicellular cyanobacterium *Synechocystis* sp. strain PCC6803. II. Sequence determination of the entire genome and assignment of potential protein-coding regions (supplement). *DNA Res* **3**: 185–209.

Kang, S., Herzberg, M., Rodrigues, D.F., and Elimelech, M. (2008) Antibacterial effects of carbon nanotubes: size does matter! *Langmuir* **24**: 6409–6413.

Kaus, K., Biester, A., Chupp, E., Lu, J., Visudharomn, C., and Olson, R. (2019) The 1.9 Acrystal structure of the extracellular matrix protein Bap1 from *Vibrio cholerae* provides insights into bacterial biofilm adhesion. *J Biol Chem* **294**: 14499–14511.

Kefallinou, D., Ellinas, K., Speliotis, T., Stamatakis, K., Gogolides, E., and Tserepi, A. (2020)

Optimization of Antibacterial Properties of "Hybrid" Metal-Sputtered Superhydrophobic Surfaces. *Coatings* **10**: 25.

Kehr, J.C., Zilliges, Y., Springer, A., Disney, M.D., Ratner, D.D., Bouchier, C., et al. (2006) A mannan binding lectin is involved in cell-cell attachment in a toxic strain of *Microcystis aeruginosa*. *Mol Microbiol* **59**: 893–906.

Keith, I., Foundation, C.D., Dawson, T.P., Collins, K.J., and Campbell, M.L. (2016) Marine invasive species : Establishing pathways , their presence and potential threats in the Galapagos Marine Reserve. *Pacific Conserv Biol* **22**: 377–385.

Kera, K., Yoshizawa, Y., Shigehara, T., Nagayama, T., Tsujii, M., Tochigi, S., and Uozumi, N. (2020) Hik36–Hik43 and Rre6 act as a two-component regulatory system to control cell aggregation in *Synechocystis* sp. PCC6803. *Sci Rep* **10**: 1–9.

Khayatan, B., Meeks, J.C., and Risser, D.D. (2015) Evidence that a modified type IV pilus-like system powers gliding motility and polysaccharide secretion in filamentous cyanobacteria. *Mol Microbiol* **98**: 1021–1036.

Khemiri, A., Jouenne, T., and Cosette, P. (2016) Proteomics dedicated to biofilmology: What have we learned from a decade of research? *Med Microbiol Immunol* **205**: 1–19.

Kim, Jungchan, Baek, Y., Hong, S.P., Yoon, H., Kim, S., Kim, C., et al. (2016) Evaluation of thin-film nanocomposite RO membranes using TiO_2 nanotubes and TiO_2 nanoparticles: a comparative study. *Desalin Water Treat* **57**: 24674–24681.

Kim, Y.H., Choi, Y., Oh, Y.Y., Ha, N.C., and Song, J. (2018) Plant growth-promoting activity of beta-propeller protein YxaL secreted from *Bacillus velezensis* strain GH1-13. *bioRxiv* 1–29.

King, R.K., Flick, G.J., Pierson, M.D., Smith, S. a, Boardman, G.D., and Coale, C.W. (2004) Identification of bacterial pathogens in biofilms of recirculating aquaculture systems. *J Aquat Food Prod Technol* **13**: 125–133.

King, R.K., Flick, G.J., Smith, S.A., Pierson, M.D., Boardman, G.D., and Coale, C.W. (2006) Comparison of bacterial presence in biofilms on different materials commonly found in recirculating aquaculture systems. *J Appl Aquac* **18**: 79–88.

Klähn, S., Mikkat, S., Riediger, M., Georg, J., Hess, W.R., and Hagemann, M. (2021) Integrative analysis of the salt stress response in cyanobacteria. *Biol Direct* **16**: 1–23.

Komárek, J. (2003) Coccoid and colonial cyanobacteria. In *Freshwater Algae of North America, Ecology and Classification*. Wehr, J.D. and Sheath, R.G. (eds). San Diego, CA, USA: Academic Press, pp. 59–116.

Komárek, J., Kaštovský, J., Mareš, J., and Johansen, J.R. (2014) Taxonomic classification of cyanoprokaryotes (cyanobacterial genera) 2014, using a polyphasic approach. *Preslia* **86**: 295–335.

Konstantinou, D., Gerovasileiou, V., Voultsiadou, E., and Gkelis, S. (2018) Sponges-cyanobacteria associations: Global diversity overview and new data from the Eastern Mediterranean. *PLoS One* **13**: 1–22.

Konstantinou, D., Voultsiadou, E., Panteris, E., Zervou, S.-K., Hiskia, A., and Gkelis, S. (2019) *Leptothoe*, a new genus of marine cyanobacteria (Synechococcales) and three new species associated with sponges from the Aegean Sea. *J Phycol* **55**: 882–897.

Kotai, J. (1972) *Instructions for the Preparation of Modified Nutrient Solution Z8 for Algae*. Norwegian Institute for Water Research: Blindern, Norway, 1972; p.5.

Kotera, M., Bayashi, T., Hattori, M., Tokimatsu, T., Goto, S., Mihara, H., and Kanehisa, M. (2010) Comprehensive genomic analysis of sulfur-relay pathway genes. *Genome Informatics* **24**: 104–115.

Krishnamoorthy, K., Jeyasubramanian, K., Premanathan, M., Subbiah, G., Shin, H.S., and Kim, S.J. (2014) Graphene oxide nanopaint. *Carbon NY* **72**: 328–337.

Kristensen, J.B., Meyer, R.L., Laursen, B.S., Shipovskov, S., Besenbacher, F., and Poulsen, C.H. (2008) Antifouling enzymes and the biochemistry of marine settlement. *Biotechnol Adv* **26**: 471–481.

Krohn-Molt, I., Alawi, M., Förstner, K.U., Wiegandt, A., Burkhardt, L., Indenbirken, D., et al. (2017) Insights into Microalga and bacteria interactions of selected phycosphere biofilms using metagenomic, transcriptomic, and proteomic approaches. *Front Microbiol* **8**: 1–14.

Krynická, V., Georg, J., Jackson, P.J., Dickman, M.J., Hunter, C.N., Futschik, M.E., et al. (2019) Depletion of the FtsH1/3 Proteolytic Complex Suppresses the Nutrient Stress Response in the Cyanobacterium *Synechocystis* sp strain PCC 6803. *Plant Cell* **31**: 2912–2928.

Ku, C., Nelson-Sathi, S., Roettger, M., Sousa, F.L., Lockhart, P.J., Bryant, D., et al. (2015) Endosymbiotic origin and differential loss of eukaryotic genes. *Nature* **524**: 427–432.

Kumar, K., Mella-Herrera, R.A., and Golden, J.W. (2010) Cyanobacterial heterocysts. *Cold Spring Harb Perspect Biol* **2**: a000315.

Kumar, S., Bhattacharya, W., Singh, M., Halder, D., and Mitra, A. (2017) Plant latex capped colloidal silver nanoparticles: A potent anti-biofilm and fungicidal formulation. *J Mol Liq* **230**: 705–713.

Kumar, S., Boro, J.C., Ray, D., Mukherjee, A., and Dutta, J. (2019) Bionanocomposite films of agar incorporated with ZnO nanoparticles as an active packaging material for shelf life extension of green grape. *Heliyon* **5**: e01867.

Kumar, S., Stecher, G., and Tamura, K. (2016) MEGA7: Molecular Evolutionary Genetics Analysis version 7.0 for bigger datasets. *Mol Biol Evol* msw054.

Kurdrid, P., Senachak, J., Sirijuntarut, M., Yutthanasirikul, R., Phuengcharoen, P., Jeamton, W., et al. (2011) Comparative analysis of the *Spirulina platensis* subcellular proteome in response to low- and high-temperature stresses: Uncovering cross-talk of signaling components. *Proteome Sci* **9**: 39.

Kurian, D., Phadwal, K., and Mäenpää, P. (2006) Proteomic characterization of acid stress response in *Synechocystis* sp. PCC 6803. *Proteomics* **6**: 3614–3624.

Kwon, D., Park, J.M., Duong, V.A., Hong, S.J., Cho, B.K., Lee, C.G., et al. (2020) Comparative proteomic profiling of marine and freshwater *Synechocystis* strains using liquid chromatography-tandem mass spectrometry. *J Mar Sci Eng* **8**: 1–16.

Lagos, M.E., White, C.R., and Marshall, D.J. (2016) Biofilm history and oxygen availability interact to affect habitat selection in a marine invertebrate. *Biofouling* **32**: 645–655.

Lane, A. and Willemsen, P. (2004) Collaborative effort looks into biofouling. *Fish Farming Int* **44**: 34–35.

Lane, D.J. (1991) 16S/23S rRNA sequencing. In *Nucleic Acid Techniques in Bacterial Systematics*. Chichester, UK: JohnWiley and Sons, pp. 115–175.

Lappin-scott, H., Burton, S., and Stoodley, P. (2014) Revealing a world of biofilms — the pioneering research of Bill Costerton. *Nat Publ Gr* 1–7.

Laspidou, C.S. and Aravas, N. (2007) Variation in the mechanical properties of a porous multi-phase biofilm under compression due to void closure. *Water Sci Technol* **55**: 447–453.

Lau, N.S., Matsui, M., and Abdullah, A.A.A. (2015) Cyanobacteria: Photoautotrophic Microbial Factories for the Sustainable Synthesis of Industrial Products. *Biomed Res Int* **2015**: 754934.

Lau, S.C.K., Thiyagarajan, V., Cheung, S.C.K., and Qian, P. (2005) Roles of bacterial community composition in biofilms as a mediator for larval settlement of three marine invertebrates. *Aquat Microb Ecol* **38**: 41–51.

Leão, P.N., Pereira, A.R., Liu, W.T., Ng, J., Pevzner, P.A., Dorrestein, P.C., et al. (2010) Synergistic allelochemicals from a freshwater cyanobacterium. *Proc Natl Acad Sci USA* **107**: 11183–11188.

Leary, D.H., Li, R.W., Hamdan, L.J., Hervey, W.J., Lebedev, N., Wang, Z., et al. (2014) Integrated metagenomic and metaproteomic analyses of marine biofilm communities. *Biofouling* **30**: 1211–1223.

Lee, J.-W., Nam, J.-H., Kim, Y.-H., Lee, K.-H., and Lee, D.-H. (2008) Bacterial communities in the initial stage of marine biofilm formation on artificial surfaces. *J Microbiol* **46**: 174–182.

Lee, O.O., Chung, H.C., Yang, J., Wang, Y., Dash, S., Wang, H., and Qian, P.-Y. (2014) Molecular techniques revealed highly diverse microbial communities in natural marine biofilms on

polystyrene dishes for invertebrate larval settlement. *Microb Ecol* **68**: 81–93.
Lejars, M., Margaillan, A., and Bressy, C. (2012) Fouling release coatings: a nontoxic alternative to biocidal antifouling coatings. *Chem Rev* **112**: 4347–4390.
Leonardi, A.K. and Ober, C.K. (2019) Polymer-based marine antifouling and fouling release surfaces: Strategies for synthesis and modification. *Annu Rev Chem Biomol Eng* **10**: 241–264.
Lepère, C., Wilmotte, A., and Meyer, B. (2000) Molecular Diversity of *Microcystis* Strains (Cyanophyceae, Chroococcales) Based on 16S rDNA Sequences. *Syst Geogr Plants* **70**: 275–283.
Letunic, I. and Bork, P. (2021) Interactive Tree Of Life (iTOL) v5: an online tool for phylogenetic tree display and annotation. *Nucleic Acids Res* **49**: W293–W296.
Li, T., Yang, H.M., Cui, S.X., Suzuki, I., Zhang, L.F., Li, L., et al. (2012) Proteomic study of the impact of Hik33 mutation in *Synechocystis* sp. PCC 6803 under normal and salt stress conditions. *J Proteome Res* **11**: 502–514.
Li, X. and Logan, B.E. (2004) Analysis of bacterial adhesion using a gradient force analysis method and colloid probe atomic force microscopy. *Langmuir* **20**: 8817–8822.
Li, Y., Huang, Y., Wang, F., Liang, W., Yang, H., and Wu, D. (2022) Fabrication of acrylic acid modified graphene oxide (AGO)/acrylate composites and their synergistic mechanisms of anticorrosion and antifouling properties. *Prog Org Coatings* **168**: 106910.
Liang, F. and Lindblad, P. (2016) Effects of overexpressing photosynthetic carbon flux control enzymes in the cyanobacterium *Synechocystis* PCC 6803. *Metab Eng* **38**: 56–64.
Liao, Y., Williams, T.J., Ye, J., Charlesworth, J., Burns, B.P., Poljak, A., et al. (2016) Morphological and proteomic analysis of biofilms from the Antarctic archaeon, *Halorubrum lacusprofundi*. *Sci Rep* **6**: 1–17.
Lima, M., Gomes, L.C., Teixeira-santos, R., Romeu, M.J., Valcárcel, J., Vázquez, J.A., et al. (2022) Assessment of the Antibiofilm Performance of Chitosan-Based Surfaces in Marine Environments. *Int J Mol Sci* **23**: 14647.
Limoli, D.H., Jones, C.J., and Wozniak, D.J. (2015) Bacterial Extracellular Polysaccharides in Biofilm Formation and Function. *Microbiol Spectr* **3**: 223–247.
Liu, C. (2022) Comparative proteomics for an in-depth understanding of bioadhesion mechanisms and evolution across metazoans. *J Proteomics* **256**: 104506.
Liu, C. and Zhao, Q. (2011) Influence of surface-energy components of Ni-P-TiO2-PTFE nanocomposite coatings on bacterial adhesion. *Langmuir* **27**: 9512–9519.
Liu, J., Chen, L., Wang, J., Qiao, J., and Zhang, W. (2012) Proteomic analysis reveals resistance mechanism against biofuel hexane in *Synechocystis* sp. PCC 6803. *Biotechnol Biofuels* **5**: 68.
Liu, Y. and Tay, J. (2002) The essential role of hydrodynamic shear force in the formation of biofilm and granular sludge. *Water Res* **36**: 1653–1665.
Liu, Z. and Huang, Y. (2014) Advantages of proteins being disordered. *Protein Sci* **23**: 539–550.
Liu, Z., Tian, S., Li, Q., Wang, J., Pu, J., Wang, G., et al. (2020) Integrated Dual-Functional ORMOSIL Coatings with AgNPs@rGO Nanocomposite for Corrosion Resistance and Antifouling Applications. *ACS Sustain Chem Eng* **8**: 6786–6797.
Long, L., Wang, R., Chiang, H.Y., Ding, W., Li, Y.X., Chen, F., and Qian, P.Y. (2021) Discovery of Antibiofilm Activity of Elasnin against Marine Biofilms and Its Application in the Marine Antifouling Coatings. *Mar Drugs* **19**: 19.
López-Ochoa, J., Montes-García, J.F., Vázquez, C., Sánchez-Alonso, P., Pérez-Márquez, V.M., Blackall, P.J., et al. (2017) *Gallibacterium* elongation factor-Tu possesses amyloid-like protein characteristics, participates in cell adhesion, and is present in biofilms. *J Microbiol* **55**: 745–752.
Lu, Y., Liu, H., Saer, R.G., Zhang, H., Meyer, C.M., Li, V.L., et al. (2017) Native mass spectrometry analysis of oligomerization states of fluorescence recovery protein and orange carotenoid protein: Two proteins involved in the cyanobacterial photoprotection cycle. *Biochemistry* **56**: 160–166.
Luan, Y., Van Der Mei, H.C., Dijk, M., Geertsema-Doornbusch, G.I., Atema-Smit, J., Ren, Y., et al. (2020) Polarization of Macrophages, Cellular Adhesion, and Spreading on Bacterially

Contaminated Gold Nanoparticle-Coatings *in Vitro*. *ACS Biomater Sci Eng* **6**: 933–945.

Luef, B., Neu, T.R., Zweimüller, I., and Peduzzi, P. (2009) Structure and composition of aggregates in two large European rivers, based on confocal laser scanning microscopy and image and statistical analyses. *Appl Environ Microbiol* **75**: 5952–5962.

Lukowiak, A., Kedziora, A., and Strek, W. (2016) Antimicrobial graphene family materials: Progress, advances, hopes and fears. *Adv Colloid Interface Sci* **236**: 101–112.

Lv, J., Li, N., and Niu, D.K. (2008) Association between the availability of environmental resources and the atomic composition of organismal proteomes: Evidence from *Prochlorococcus* strains living at different depths. *Biochem Biophys Res Commun* **375**: 241–246.

Lyons, T.W., Reinhard, C.T., and Planavsky, N.J. (2014) The rise of oxygen in Earth's early ocean and atmosphere. *Nature* **506**: 307–315.

Ma, H., Wu, Y., Gan, N., Zheng, L., Li, T., and Song, L. (2015) Growth inhibitory effect of *Microcystis* on Aphanizomenon flos-aquae isolated from cyanobacteria bloom in Lake Dianchi, China. *Harmful Algae* **42**: 43–51.

MacColl, R. (1998) Cyanobacterial phycobilisomes. *J Struct Biol* **124**: 311–334.

Maddah, H. and Chogle, A. (2017) Biofouling in reverse osmosis: phenomena, monitoring, controlling and remediation. *Appl Water Sci* **7**: 2637–2651.

Mahltig, B. (2016) 10 - Smart hydrophobic and soil-repellent protective composite coatings for textiles and leather. In *Woodhead Publishing Series in Composites Science and Engineering*. Montemor, M.F.B.T.-S.C.C. and M. (ed). Woodhead Publishing, pp. 261–292.

Mai, T., Johansen, J.R., Pietrasiak, N., Bohunicka, M., and Martin, M.P. (2018) Revision of the Synechococcales (Cyanobacteria) through recognition of four families including Oculatellaceae fam. nov. and Trichocoleaceae fam. nov. and six new genera containing 14 species. *Phytotaxa* **365**: 1–59.

Mainous, M.E., Kuhn, D.D., and Smith, S.A. (2012) Efficacy of Common Aquaculture Compounds for Disinfection of *Flavobacterium columnare* and *F. psychrophilum*. *J Appl Aquac* **24**: 262–270.

Manderfeld, E., Kleinberg, M.N., Thamaraiselvan, C., Koschitzki, F., Gnutt, P., Plumere, N., et al. (2021) Electrochemically activated laser-induced graphene coatings against marine biofouling. *Appl Surf Sci* **569**: 150853.

Manirafasha, E., Ndikubwimana, T., Zeng, X., Lu, Y., and Jing, K. (2016) Phycobiliprotein: Potential microalgae derived pharmaceutical and biological reagent. *Biochem Eng J* **109**: 282–296.

Mansour, A. and Liu, D. (2008) The Principles of Naval Architecture Series: Strength of Ships and Ocean Structures, Paulling, J.R. (ed) Jersey City, NJ: The Society of Naval Architects and Marine Engineers.

Marshall, K.C., Stout, R., and Mitchell, R. (1970) Mechanism of the Initial Events in the Sorption of Marine Bacteria to Surfaces. *Microbiology* **68**: 337–348.

Martinelli, E., Suffredini, M., Galli, G., Glisenti, A., Pettitt, M.E., Callow, M.E., et al. (2011) Amphiphilic block copolymer/poly(dimethylsiloxane) (PDMS) blends and nanocomposites for improved fouling-release. *Biofouling* **27**: 529–541.

Martins, J.C., Domínguez-Pérez, D., Azevedo, C., Braga, A.C., Costa, P.R., Osório, H., et al. (2020) Molecular Responses of Mussel *Mytilus galloprovincialis* Associated to Accumulation and Depuration of Marine Biotoxins Okadaic Acid and Dinophysistoxin-1 Revealed by Shotgun Proteomics. *Front Mar Sci* **7**: 1–15.

Martins, R., Pereira, P., Welker, M., Fastner, J., and Vasconcelos, V.M. (2005) Toxicity of culturable cyanobacteria strains isolated from the Portuguese coast. *Toxicon* **46**: 454–464.

Martiny, A.C., Coleman, M.L., and Chisholm, S.W. (2006) Phosphate acquisition genes in *Prochlorococcus* ecotypes: Evidence for genome-wide adaptation. *Proc Natl Acad Sci USA* **103**: 12552–12557.

Maruthanayagam, V., Basu, S., Bhattacharya, D., and Mukherjee, J. (2020) Effects of surface material on growth pattern and bioactive exopolymers production of intertidal cyanobacteria *Phormidium* sp. *Indian J Geo-Marine Sci* **49**: 1669–1677.

Matos, A., Domínguez-Pérez, D., Almeida, D., Aguëro-Chapin, G., Campos, A., Osório, H., et al. (2020) Shotgun Proteomics of Ascidians Tunic Gives New Insights on Host-Microbe Interactions by Revealing Diverse Antimicrobial Peptides. *Mar Drugs* **18**: 362.

Matz, C. (2011) Competition, communication, cooperation: molecular crosstalk in multi-species biofilms. In *Biofilm Highlights*. HC, F., J, W., and U, S. (eds). Berlin, Heidelberg: Springer Series on Biofilms.

Mayer, M.A., Borsdorf, A., Wagner, M., Hornegger, J., Mardin, C.Y., and Tornow, R.P. (2012) Wavelet denoising of multiframe optical coherence tomography data. *Biomed Opt Express* **3**: 572.

McDougald, D., Rice, S.A., Barraud, N., Steinberg, P.D., and Kjelleberg, S. (2011) Should we stay or should we go: mechanisms and ecological consequences for biofilm dispersal. *Nat Rev Microbiol* **10**: 39–50.

Meeks, J.C. and Elhai, J. (2002) Regulation of Cellular Differentiation in Filamentous Cyanobacteria in Free-Living and Plant-Associated Symbiotic Growth States. *Microbiol Mol Biol Rev* **66**: 94–121.

Mehta, A., López-Maury, L., and Florencio, F.J. (2014) Proteomic pattern alterations of the cyanobacterium *Synechocystis* sp. PCC 6803 in response to cadmium, nickel and cobalt. *J Proteomics* **102**: 98–112.

Meireles, A., Fulgêncio, R., Machado, I., Mergulhão, F., Melo, L., and Simões, M. (2017) Characterization of the heterotrophic bacteria from a minimally processed vegetables plant. *LWT - Food Sci Technol* **85**: 293-300.

Melnicki, M.R., Leverenz, R.L., Sutter, M., López-Igual, R., Wilson, A., Pawlowski, E.G., et al. (2016) Structure, Diversity, and Evolution of a New Family of Soluble Carotenoid-Binding Proteins in Cyanobacteria. *Mol Plant* **9**: 1379–1394.

Michailidis, M., Gutner-Hoch, E., Wengier, R., Onderwater, R., D'Sa, R.A., Benayahu, Y., et al. (2020) Highly Effective Functionalized Coatings with Antibacterial and Antifouling Properties. *ACS Sustain Chem Eng* **8**: 8928–8937.

Mieszkin, S., Callow, M.E., and Callow, J.A. (2013) Interactions between microbial biofilms and marine fouling algae: a mini review. *Biofouling* **29**: 1097–113.

Mieszkin, S., Martin-Tanchereau, P., Callow, M.E., and Callow, J.A. (2012) Effect of bacterial biofilms formed on fouling-release coatings from natural seawater and *Cobetia marina*, on the adhesion of two marine algae. *Biofouling* **28**: 953–68.

Mikulášek, K., Konečná, H., Potěšil, D., Holánková, R., Havliš, J., and Zdráhal, Z. (2021) SP3 Protocol for Proteomic Plant Sample Preparation Prior LC-MS/MS. *Front Plant Sci* **12**: 635550.

Milferstedt, K., Pons, M.-N., and Morgenroth, E. (2009) Analyzing characteristic length scales in biofilm structures. *Biotechnol Bioeng* **102**: 368–379.

Miller, M.A., Kudela, R.M., Mekebri, A., Crane, D., Oates, S.C., Tinker, M.T., et al. (2010) Evidence for a novel marine harmful algal bloom: Cyanotoxin (microcystin) transfer from land to sea otters. *PLoS One* **5**: 1–11.

Minchin, D. and Gollasch, S. (2003) Fouling and ships' hulls : How changing circumstances and spawning events may result in the spread of exotic species. *Biofouling* **19**: 111–122.

Mineur, F., Johnson, M.P., Maggs, C.A., and Stegenga, H. (2007) Hull fouling on commercial ships as a vector of macroalgal introduction. *Mar Biol* **151**: 1299–1307.

Mishra, R., Panda, A.K., De Mandal, S., Shakeel, M., Bisht, S.S., and Khan, J. (2020) Natural Anti-biofilm Agents: Strategies to Control Biofilm-Forming Pathogens. *Front Microbiol* **11**: 2640.

Misra, B.B., Langefeld, C., Olivier, M., and Cox, L.A. (2019) Integrated omics: Tools, advances and future approaches. *J Mol Endocrinol* **62**: R21–R45.

Mitbavkar, S., C., R., K.M., R., and D., P. (2012) Picophytoplankton community from tropical marine biofilms. *J Exp Mar Bio Ecol* **426–427**: 88–96.

Mitchell, A.L., Attwood, T.K., Babbitt, P.C., Blum, M., Bork, P., Bridge, A., et al. (2019) InterPro in 2019: Improving coverage, classification and access to protein sequence annotations. *Nucleic*

Acids Res **47**: D351–D360.

Moffitt, C.M., Barenberg, A., Stockton, K.A., and Watten, B.J. (2015) Efficacy of two approaches for disinfecting surfaces and water infested with quagga mussel veligers. In *Biology and Management of Invasive Quagga and Zebra Mussels in the Western United States.* Wong, W.H. and Gerstenberger, S. (eds). Boca Raton, FL, USA: CRC PRESS, pp. 467–477.

Mohammed, H., Kumar, A., Bekyarova, E., Al-Hadeethi, Y., Zhang, X., Chen, M., et al. (2020) Antimicrobial Mechanisms and Effectiveness of Graphene and Graphene-Functionalized Biomaterials. A Scope Review. *Front Bioeng Biotechnol* **8**: 465.

Mohan, M. (2008) The advantages of composite material in marine renewable energy devices. The Royal Institution of Naval Architects Conference on marine renewable energy, London, UK.

Molland, A.F. (2008) Ship design, construction and operation. In *The Maritime Engineering Reference Book: A Guide to Ship Design, Construction and Operation*. United Kingdom: Butterworth-Heinemann.

Del Mondo, A., Pinto, G., Carbone, D.A., Pollio, A., and De Natale, A. (2018) Biofilm architecture on different substrates of an *Oculatella subterranea* (Cyanobacteria) strain isolated from Pompeii archaeological site (Italy). *Environ Sci Pollut Res* **25**: 26079–26089.

Moore, L.R., Ostrowski, M., Scanlan, D.J., Feren, K., and Sweetsir, T. (2005) Ecotypic variation in phosphorus-acquisition mechanisms within marine picocyanobacteria. *Aquat Microb Ecol* **39**: 257–269.

Van Mooy, B.A.S., Rocap, G., Fredricks, H.F., Evans, C.T., and Devol, A.H. (2006) Sulfolipids dramatically decrease phosphorus demand by picocyanobacteria in oligotrophic marine environments. *Proc Natl Acad Sci USA* **103**: 8607–8612.

Moreira, J., Araújo, J.D.P., Miranda, J.M., Simões, M., Melo, L.F., and Mergulhão, F.J. (2014) The effects of surface properties on *Escherichia coli* adhesion are modulated by shear stress. *Colloids Surfaces B Biointerfaces* **123**: 1–7.

Moreira, J., Teodósio, J.S., Silva, F.C., Simões, M., Melo, L.F., and Mergulhão, F.J. (2013) Influence of flow rate variation on the development of *Escherichia coli* biofilms. *Bioprocess Biosyst Eng* **36**: 1787–1796.

Moreira, J.M.R., Gomes, L.C., Simões, M., Melo, L.F., and Mergulhão, F.J. (2015) The impact of material properties, nutrient load and shear stress on biofouling in food industries. *Food Bioprod Process* **95**: 228–236.

Moreira, J.M.R., Gomes, L.C., Whitehead, K.A., Lynch, S., Tetlow, L.A., and Mergulhão, F.J. (2017) Effect of surface conditioning with cellular extracts on *Escherichia coli* adhesion and initial biofilm formation. *Food Bioprod Process* **104**: 1–12.

Moreira, J.M.R., Ponmozhi, J., Campos, J.B.L.M., Miranda, J.M., and Mergulhão, F.J. (2015) Micro- and macro-flow systems to study *Escherichia coli* adhesion to biomedical materials. *Chem Eng Sci* **126**: 440–445.

Moreira, J.M.R., Simões, M., Melo, L., and Mergulhão, F. (2015) *Escherichia coli* adhesion to surfaces – a thermodynamic assessment. *Colloid Polym Sci* **293**: 177–185.

Morse, A.N.C., Froyd, C.A., and Morse, D.E. (1984) Molecules from cyanobacteria and red algae that induce larval settlement and metamorphosis in the mollusc *Haliotis rufescens*. *Mar Biol* **81**: 293–298.

Mostafaei, A. and Nasirpouri, F. (2013) Preparation and characterization of a novel conducting nanocomposite blended with epoxy coating for antifouling and antibacterial applications. *J coatings Technol Res* **10**: 679–694.

Mota, R., Pereira, S.B., Meazzini, M., Fernandes, R., Santos, A., Evans, C.A., et al. (2015) Effects of heavy metals on *Cyanothece* sp. CCY 0110 growth, extracellular polymeric substances (EPS) production, ultrastructure and protein profiles. *J Proteomics* **120**: 75–94.

Mountcastle, S.E., Vyas, N., Villapun, V.M., Cox, S.C., Jabbari, S., Sammons, R.L., et al. (2021) Biofilm viability checker: An open-source tool for automated biofilm viability analysis from confocal microscopy images. *npj Biofilms Microbiomes* **7**: 44.

Mueller, L.N., de Brouwer, J.F.C., Almeida, J.S., Stal, L.J., and Xavier, J.B. (2006) Analysis of a marine phototrophic biofilm by confocal laser scanning microscopy using the new image quantification software PHLIP. *BMC Ecol* **6**: 1.

Muhammad, M.H., Idris, A.L., Fan, X., Guo, Y., Yu, Y., Jin, X., et al. (2020) Beyond Risk: Bacterial Biofilms and Their Regulating Approaches. *Front Microbiol* **11**: 1–20.

Mühling, M., Fuller, N.J., Millard, A., Somerfield, P.J., Marie, D., Wilson, W.H., et al. (2005) Genetic diversity of marine Synechococcus and co-occurring cyanophage communities: Evidence for viral control of phytoplankton. *Environ Microbiol* **7**: 499–508.

Mullineaux, C.W. (2014) Co-existence of photosynthetic and respiratory activities in cyanobacterial thylakoid membranes. *Biochim Biophys Acta* **1837**: 503–511.

Munson, B.R., Young, D.F., and Okiishi, T.H. (2002) Fundamentals of Fluid Mechanics, 4th ed., Chicago, IL, USA: John Wiley & Sons, Inc.

Muthusamy, S., Lundin, D., Mamede Branca, R.M., Baltar, F., González, J.M., Lehtiö, J., and Pinhassi, J. (2017) Comparative proteomics reveals signature metabolisms of exponentially growing and stationary phase marine bacteria. *Environ Microbiol* **19**: 2301–2319.

Myers, J.L., Sekar, R., and Richardson, L.L. (2007) Molecular Detection and Ecological Significance of the Cyanobacterial Genera *Geitlerinema* and *Leptolyngbya* in Black Band Disease of Corals. *Appl Environ Microbiol* **73**: 5173–5182.

Naddaf, A., Zeinali Heris, S., and Pouladi, B. (2019) An experimental study on heat transfer performance and pressure drop of nanofluids using graphene and multi-walled carbon nanotubes based on diesel oil. *Powder Technol* **352**: 369–380.

Nagar, E., Zilberman, S., Sendersky, E., Simkovsky, R., Shimoni, E., Gershtein, D., et al. (2017) Type 4 pili are dispensable for biofilm development in the cyanobacterium *Synechococcus elongatus*. *Environ Microbiol* **19**: 2862–2872.

Nagarkar, S., Williams, G.A., Subramanian, G., and Saha, S.K. (2004) Cyanobacteria-dominated biofilms: a high quality food resource for intertidal grazers. *Asian Pacific Phycol 21st Century Prospect Challenges* 89–95.

Nagayama, K., Fujita, K., Takashima, Y., Ardin, A.C., Ooshima, T., and Matsumoto-Nakano, M. (2014) Role of ABC transporter proteins in stress responses of *Streptococcus mutans*. *Oral Health Dent Manag* **13**: 359–65.

Najmuldeen, H., Alghamdi, R., Alghofaili, F., and Yesilkaya, H. (2019) Functional assessment of microbial superoxide dismutase isozymes suggests a differential role for each isozyme. *Free Radic Biol Med* **134**: 215–228.

Narváez-Zapata, J., Tebbe, C.C., and Ortega-Morales, B.O. (2005) Molecular diversity and biomass of epilithic biofilms from intertidal rocky shores in the Gulf of Mexico. *Biofilms* **2**: 93–103.

Nayar, S., Goh, B.P.L., and Chou, L.M. (2005) Settlement of marine periphytic algae in a tropical estuary. *Estuar Coast Shelf Sci* **64**: 241–248.

Nelson, N. and Yocum, C.F. (2006) Structure and Function of Photosystems I and II. *Annu Rev Plant Biol* **57**: 521–565.

Neves, A.R., Gomes, L.C., Faria, S.I., Sousa, J., Ruivo, R., Páscoa, I., et al. (2022) Antifouling Marine Coatings with a Potentially Safer and Sustainable Synthetic Polyphenolic Derivative. *Mar Drugs* **20**: 507.

Nichols, C.A., Guezennec, J., and Bowman, J.P. (2005) Bacterial exopolysaccharides from extreme marine environments with special consideration of the Southern Ocean, sea ice, and deep-sea hydrothermal vents: A review. *Mar Biotechnol* **7**: 253–271.

Nolte, K.A., Schwarze, J., and Rosenhahn, A. (2017) Microfluidic accumulation assay probes attachment of biofilm forming diatom cells. *Biofouling* **33**: 531–543.

Nübel, U., Garcia-Pichel, F., and Muyzer, G. (1997) PCR primers to amplify 16S rRNA genes from cyanobacteria. *Appl Environ Microbiol* **63**: 3327–3332.

Nurioglu, A.G., Esteves, A.C.C., and De With, G. (2015) Non-toxic, non-biocide-release antifouling coatings based on molecular structure design for marine applications. *J Mater Chem B* **3**: 6547–

6570.
Oberbeckmann, S., Loeder, M.G.J., Gerdts, G., and Osborn, M.A. (2014) Spatial and seasonal variation in diversity and structure of microbial biofilms on marine plastics in Northern European waters. *FEMS Microbiol Ecol* **90**: 478–492.
De Oliveira, E.D.C., Da Cunha, A.C., Da Silva, N.B., Castelo-Branco, R., Morais, J., Schneider, M.P.C., et al. (2019) Morphological and molecular characterization of cyanobacterial isolates from the mouth of the amazon river. *Phytotaxa* **387**: 269–288.
Oliveira, I.M., Gomes, M., Gomes, L.C., Pereira, M.F.R., Soares, O.S.G.P., and Mergulhão, F.J. (2022) Performance of Graphene/Polydimethylsiloxane Surfaces against *S. aureus* and *P. aeruginosa* Single-and Dual-Species Biofilms. *Nanomaterials* **12**: 355.
Oliveira, P., Pinto, F., Pacheco, C.C., Mota, R., and Tamagnini, P. (2015) HesF, an exoprotein required for filament adhesion and aggregation in *Anabaena* sp. PCC 7120. *Environ Microbiol* **17**: 1631–1648.
Osório, H., Silva, C., Ferreira, M., Gullo, I., Máximo, V., Barros, R., et al. (2021) Proteomics Analysis of Gastric Cancer Patients with Diabetes Mellitus. *J Clin Med* **10**: 407.
Otsu, N. (1979) A threshold selection method from gray-level histograms. *IEEE Trans Syst Man Cybern* **9**: 62–66.
Otsuka, S., Suda, S., Oyaizu, H., Matsumoto, S., and Watanabe, M.M. (2001) A proposal for the unification of five species of the cyanobacterial genus Microcystis Kützing ex Lemmermann 1907 under the rules of the Bacteriological Code. *Int J Syst Evol Microbiol.* **51**: 873–879.
Ow, S.Y., Cardona, T., Taton, A., Magnuson, A., Lindblad, P., Stensjö, K., and Wright, P.C. (2008) Quantitative shotgun proteomics of enriched heterocysts from *Nostoc* sp. PCC 7120 using 8-plex isobaric peptide tags. *J Proteome Res* **7**: 1615–1628.
Ow, S.Y., Salim, M., Noirel, J., Evans, C., and Wright, P.C. (2011) Minimising iTRAQ ratio compression through understanding LC-MS elution dependence and high-resolution HILIC fractionation. *Proteomics* **11**: 2341–2346.
Ow, S.Y. and Wright, P.C. (2009) Current trends in high throughput proteomics in cyanobacteria. *FEBS Lett* **583**: 1744–1752.
Paetzold, S.C. and Davidson, J. (2010) Viability of golden star tunicate fragments after high-pressure water treatment. *Aquaculture* **303**: 105–107.
Pagels, F., Guedes, A.C., Amaro, H.M., Kijjoa, A., and Vasconcelos, V. (2019) Phycobiliproteins from cyanobacteria: Chemistry and biotechnological applications. *Biotechnol Adv* **37**: 422–443.
Palmer, J., Flint, S., and Brooks, J. (2007) Bacterial cell attachment, the beginning of a biofilm. *J Ind Microbiol Biotechnol* **34**: 577–588.
Pan, L., Liu, S., Oderinde, O., Li, K., Yao, F., and Fu, G. (2018) Facile fabrication of graphene-based aerogel with rare earth metal oxide for water purification. *Appl Surf Sci* **427**: 779–786.
Panda, B., Basu, B., Acharya, C., Rajaram, H., and Apte, S.K. (2017) Proteomic analysis reveals contrasting stress response to uranium in two nitrogen-fixing *Anabaena* strains, differentially tolerant to uranium. *Aquat Toxicol* **182**: 205–213.
Panda, B., Basu, B., Rajaram, H., and Apte, S.K. (2015) Comparative proteomics of oxidative stress response in three cyanobacterial strains native to Indian paddy fields. *J Proteomics* **127**: 152–160.
Panda, B., Basu, B., Rajaram, H., and Kumar Apte, S. (2014) Methyl viologen responsive proteome dynamics of *Anabaena* sp. strain PCC7120. *Proteomics* **14**: 1895–1904.
Pandey, S., Rai, R., and Rai, L.C. (2012) Proteomics combines morphological, physiological and biochemical attributes to unravel the survival strategy of *Anabaena* sp. PCC7120 under arsenic stress. *J Proteomics* **75**: 921–937.
Pandhal, J., Ow, S.Y., Wright, P.C., and Biggs, C.A. (2009) Comparative proteomics study of salt tolerance between a nonsequenced extremely halotolerant cyanobacterium and its mildly halotolerant relative using in vivo metabolic labeling and in vitro isobaric labeling. *J Proteome Res* **8**: 818–828.

Panou, M. and Gkelis, S. (2022) Unravelling unknown cyanobacteria diversity linked with HCN production. *Mol Phylogenet Evol* **166**: 107322.

Papadatou, M., Robson, S.C., Dobretsov, S., Watts, J.E.M., Longyear, J., and Salta, M. (2021) Marine biofilms on different fouling control coating types reveal differences in microbial community composition and abundance. *Microbiologyopen* **10**: 1–17.

Parnasa, R., Nagar, E., Sendersky, E., Reich, Z., Simkovsky, R., Golden, S., and Schwarz, R. (2016) Small secreted proteins enable biofilm development in the cyanobacterium *Synechococcus elongatus*. *Sci Rep* **6**: 1–10.

Parra, C., Dorta, F., Jimenez, E., Henríquez, R., Ramírez, C., Rojas, R., and Villalobos, P. (2015) A nanomolecular approach to decrease adhesion of biofouling-producing bacteria to graphene-coated material. *J Nanobiotechnology* **13**: 82.

Parra, C., Montero-Silva, F., Henríquez, R., Flores, M., Garín, C., Ramírez, C., et al. (2015) Suppressing Bacterial Interaction with Copper Surfaces through Graphene and Hexagonal-Boron Nitride Coatings. *ACS Appl Mater Interfaces* **7**: 6430–6437.

Pathania, R., Srivastava, A., Srivastava, S., and Shukla, P. (2022) Metabolic systems biology and multi-omics of cyanobacteria: Perspectives and future directions. *Bioresour Technol* **343**: 126007.

Paul, E., Ochoa, J.C., Pechaud, Y., Liu, Y., and Liné, A. (2012) Effect of shear stress and growth conditions on detachment and physical properties of biofilms. *Water Res* **46**: 5499–5508.

Perkerson III, R.B., Johansen, J.R., Kovácik, L., Brand, J., Kaštovský, J., and Casamatta, D.A. (2011) A unique pseudanabaenalean (cyanobacteria) genus *Nodosilinea* gen. nov. based on morphological and molecular data. *J Phycol* **47**: 1397–1412.

Peterson, B.W., He, Y., Ren, Y., Zerdoum, A., Libera, M.R., Sharma, P.K., et al. (2015) Viscoelasticity of biofilms and their recalcitrance to mechanical and chemical challenges. *FEMS Microbiol Rev* **39**: 234–245.

Peterson, B.W., van der Mei, H.C., Sjollema, J., Busscher, H.J., and Sharma, P.K. (2013) A Distinguishable Role of eDNA in the Viscoelastic Relaxation of Biofilms. *MBio* **4**: e00497-13.

Peterson, B.W., van der Mei, H.C., Sjollema, J., Busscher, H.J., Sharma, P.K., Chapman, M., and Hultgren, S.J. (2021) A Distinguishable Role of eDNA in the Viscoelastic Relaxation of Biofilms. *MBio* **4**: e00497-13.

Pettigrew, M.M., Marks, L.R., Kong, Y., Gent, J.F., Roche-Hakansson, H., and Hakansson, A.P. (2014) Dynamic changes in the *Streptococcus pneumoniae* transcriptome during transition from biofilm formation to invasive disease upon influenza A virus infection. *Infect Immun* **82**: 4607–4619.

Di Pippo, F. and Congestri, R. (2017) Culturing Toxic Benthic Blooms: The Fate of Natural Biofilms in a Microcosm System. *Microorganisms* **5**: 46.

Pisareva, T., Shumskaya, M., Maddalo, G., Ilag, L., and Norling, B. (2007) Proteomics of *Synechocystis* sp. PCC 6803: Identification of novel integral plasma membrane proteins. *FEBS J* **274**: 791–804.

Pjeta, R., Lindner, H., Kremser, L., Salvenmoser, W., Sobral, D., Ladurner, P., and Santos, R. (2020) Integrative transcriptome and proteome analysis of the tube foot and adhesive secretions of the sea urchin paracentrotus lividus. *Int J Mol Sci* **21**:.

Pointing, S.B. and Belnap, J. (2012) Microbial colonization and controls in dryland systems. *Nat Rev Microbiol* **10**: 551–562.

Pons, M.-N., Milferstedt, K., and Morgenroth, E. (2009) Biofilm monitoring on rotating discs by image analysis. *Biotechnol Bioeng* **103**: 105–116.

Porra, R., Thompson, W., and Kriedemann, P. (1989) Determination of accurate extinction coefficients and simultaneous equations for assaying chlorophylls a and b extracted with four different solvents: verification of the concentration of chlorophyll standards by atomic absorption spectroscopy. *Biochim Biophys Acta* **975**: 384–394.

Priya, B., Premanandh, J., Dhanalakshmi, R.T., Seethalakshmi, T., Uma, L., Prabaharan, D., and

Subramanian, G. (2007) Comparative analysis of cyanobacterial superoxide dismutases to discriminate canonical forms. *BMC Genomics* **8**: 1–10.

Pysz, M.A., Conners, S.B., Montero, C.I., Shockley, K.R., Johnson, M.R., Ward, D.E., and Kelly, R.M. (2004) Transcriptional analysis of biofilm formation processes in the anaerobic, hyperthermophilic bacterium *Thermotoga maritima*. *Appl Environ Microbiol* **70**: 6098–6112.

Qayyum, S., Sharma, D., Bisht, D., and Khan, A.U. (2016) Protein translation machinery holds a key for transition of planktonic cells to biofilm state in *Enterococcus faecalis*: A proteomic approach. *Biochem Biophys Res Commun* **474**: 652–659.

Qian, P.-Y., Rittschof, D., and Sreedhar, B. (2000) Macrofouling in unidirectional flow: Miniature pipes as experimental models for studying the interaction of flow and surface characteristics on the attachment of barnacle, bryozoan and polychaete larvae. *Mar Ecol Ser* **207**: 109–121.

Qian, P.-Y., Rittschof, D., Sreedhar, B., and Chia, F.S. (1999) Macrofouling in unidirectional flow: Miniature pipes as experimental models for studying the effects of hydrodynamics on invertebrate larval settlement. *Mar Ecol Ser* **191**: 141–151.

Qian, P.Y., Lau, S.C.K., Dahms, H.U., Dobretsov, S., and Harder, T. (2007) Marine biofilms as mediators of colonization by marine macroorganisms: Implications for antifouling and aquaculture. *Mar Biotechnol* **9**: 399–410.

Qiao, J., Wang, J., Chen, L., Tian, X., Huang, S., Ren, X., and Zhang, W. (2012) Quantitative iTRAQ LC-MS/MS proteomics reveals metabolic responses to biofuel ethanol in cyanobacterial *Synechocystis* sp. PCC 6803. *J Proteome Res* **11**: 5286–5300.

Rachedi, R., Foglino, M., and Latifi, A. (2020) Stress signaling in cyanobacteria: A mechanistic overview. *Life* **10**: 1–24.

Radhi, A., Mohamad, D., Abdul Rahman, F.S., Abdullah, A.M., and Hasan, H. (2021) Mechanism and factors influence of graphene-based nanomaterials antimicrobial activities and application in dentistry. *J Mater Res Technol* **11**: 1290–1307.

Radzi, R., Muangmai, N., Broady, P., Wan Omar, W.M., Lavoue, S., Convey, P., and Merican, F. (2019) *Nodosilinea signiensis* sp. nov. (Leptolyngbyaceae, Synechococcales), a new terrestrial cyanobacterium isolated from mats collected on Signy Island, South Orkney Islands, Antarctica. *PLoS One* **14**: e0224395.

Rafiee, J., Mi, X., Gullapalli, H., Thomas, A. V, Yavari, F., Shi, Y., et al. (2012) Wetting transparency of graphene. *Nat Mater* **11**: 217–222.

Railkin, A.I. (2003) Marine biofouling: Colonization processes and defenses, Boca Raton: CRC PRESS.

Ramos, V., Morais, J., Castelo-Branco, R., Pinheiro, Â., Martins, J., Regueiras, A., et al. (2018) Cyanobacterial diversity held in microbial biological resource centers as a biotechnological asset: the case study of the newly established LEGE culture collection. *J Appl Phycol* **30**: 1437–1451.

Ramos, V.M.C., Castelo-Branco, R., Leão, P.N., Martins, J., Carvalhal-Gomes, S., da Silva, F.S., et al. (2017) Cyanobacterial diversity in microbial mats from the hypersaline lagoon system of Araruama, Brazil: An in-depth polyphasic study. *Front Microbiol* **8**: 1–16.

Rani, A. and Babu, S. (2018) Environmental proteomic studies: closer step to understand bacterial biofilms. *World J Microbiol Biotechnol* **34**: 120.

Rao, D., Webb, J.S., and Kjelleberg, S. (2005) Competitive interactions in mixed-species biofilms containing the marine bacterium *Pseudoalteromonas tunicata*. *Appl Environ Microbiol* **71**: 1729–1736.

Regueiras, A., Pereira, S., Costa, M.S., and Vasconcelos, V. (2018) Differential toxicity of cyanobacteria isolated from marine sponges towards echinoderms and crustaceans. *Toxins (Basel)* **10**: 1–12.

Renner, L.D. and Weibel, D.B. (2011) Physicochemical regulation of biofilm formation. *MRS Bull* **36**: 347–355.

Rippka, R. (1988) Isolation and purification of cyanobacteria. *Methods Enzymol* **167**: 3–27.

Ritchie, M.E., Phipson, B., Wu, D., Hu, Y., Law, C.W., Shi, W., and Smyth, G.K. (2015) Limma powers differential expression analyses for RNA-sequencing and microarray studies. *Nucleic Acids Res* **43**: e47.

Rochex, A., Godon, J.J., Bernet, N., and Escudié, R. (2008) Role of shear stress on composition, diversity and dynamics of biofilm bacterial communities. *Water Res* **42**: 4915–4922.

Rodríguez, S.J. and Bishop, P.L. (2006) Three-Dimensional Quantification of Soil Biofilms Using Image Analysis. *Environ Eng Sci* **24**: 96–103.

Romeu, M.J., Alves, P., Morais, J., Miranda, J.M., de Jong, E.D., Sjollema, J., et al. (2019) Biofilm formation behaviour of marine filamentous cyanobacterial strains in controlled hydrodynamic conditions. *Environ Microbiol* **21**: 4411–4424.

Romeu, M.J., Domínguez-Pérez, D., Almeida, D., Morais, J., Araújo, M.J., Osório, H., et al. (2022) Hydrodynamic conditions affect the proteomic profile of marine biofilms formed by filamentous cyanobacterium. *npj Biofilms Microbiomes* **8**: 80.

Romeu, M.J., Domínguez-Pérez, D., Almeida, D., Morais, J., Araújo, M.J., Osório, H., et al. (2021) Quantitative proteomic analysis of marine biofilms formed by filamentous cyanobacterium. *Environ Res* 111566.

Romeu, M.J., Domínguez-Pérez, D., Almeida, D., Morais, J., Campos, A., Vasconcelos, V., and Mergulhão, F.J.M. (2020) Characterization of planktonic and biofilm cells from two filamentous cyanobacteria using a shotgun proteomic approach. *Biofouling* **36**: 631–645.

Romeu, M.J., Lima, M., Gomes, L.C., Jong, E.D. De, Morais, J., Vasconcelos, V., et al. (2022) The Use of 3D Optical Coherence Tomography to Analyze the Architecture of Cyanobacterial Biofilms Formed on a Carbon Nanotube Composite. *Polymers (Basel)* **14**: 4410.

Rossi, F. and De Philippis, R. (2015) Role of cyanobacterial exopolysaccharides in phototrophic biofilms and in complex microbial mats. *Life* **5**: 1218–1238.

Rossi, J.E., Schauerman, C.M., Lawlor, C.C., Cress, C.D., Ganter, M.J., Bucossi, A.R., and Landi, B.J. (2022) Carbon nanotube survivability in marine environments and method for biofouling removal. *Biofouling* **38**: 593–604.

Roy, G.J. (1994) Notes on Instrumentation and Control (Marine engineering), Oxford, Boston: Newnes.

Rumbaugh, K.P. and Sauer, K. (2020) Biofilm dispersion. *Nat Rev Microbiol* **18**: 571–586.

Rusch, D.B., Halpern, A.L., Sutton, G., Heidelberg, K.B., Williamson, S., Yooseph, S., et al. (2007) The Sorcerer II Global Ocean Sampling expedition: Northwest Atlantic through eastern tropical Pacific. *PLoS Biol* **5**: 0398–0431.

Saleemi, M.A., Fouladi, M.H., Yong, P. V, and Wong, E.H. (2020) Elucidation of Antimicrobial Activity of Non-Covalently Dispersed Carbon Nanotubes. *Materials (Basel)* **13**: 1676.

Salta, M., Capretto, L., Carugo, D., Wharton, J.A., and Stokes, K.R. (2013) Life under flow: A novel microfluidic device for the assessment of anti-biofilm technologies. *Biomicrofluidics* **7**: 1–16.

Salta, M., Wharton, J.A., Blache, Y., Stokes, K.R., and Briand, J.F. (2013) Marine biofilms on artificial surfaces: structure and dynamics. *Environ Microbiol* **15**: 2879–2893.

Samuel, A.D.T., Petersen, J.D., and Reese, T.S. (2001) Envelope structure of *Synechococcus* sp. WH8113, a nonflagellated swimming cyanobacterium. *BMC Microbiol* **1**: 4.

Santos-Merino, M., Singh, A.K., and Ducat, D.C. (2019) New applications of synthetic biology tools for cyanobacterial metabolic engineering. *Front Bioeng Biotechnol* **7**: 1–24.

Santos, C.M., Mangadlao, J., Ahmed, F., Leon, A., Advincula, R.C., and Rodrigues, D.F. (2012) Graphene nanocomposite for biomedical applications: fabrication, antimicrobial and cytotoxic investigations. *Nanotechnology* **23**: 395101.

Sauer, K., Stoodley, P., Goeres, D.M., Hall-Stoodley, L., Burmølle, M., Stewart, P.S., and Bjarnsholt, T. (2022) The biofilm life cycle: expanding the conceptual model of biofilm formation. *Nat Rev Microbiol* **20**: 608–620.

Scardino, A.J., Guenther, J., and de Nys, R. (2008) Attachment point theory revisited: the fouling response to a microtextured matrix. *Biofouling* **24**: 45–53.

Scardino, A.J. and de Nys, R. (2011) Mini review: Biomimetic models and bioinspired surfaces for fouling control. *Biofouling* **27**: 73–86.

Scardino, A.J., Zhang, H., Cookson, D.J., Lamb, R.N., and de Nys, R. (2009) The role of nano-roughness in antifouling. *Biofouling* **25**: 757–767.

Schatz, D., Nagar, E., Sendersky, E., Parnasa, R., Zilberman, S., Carmeli, S., et al. (2013) Self-suppression of biofilm formation in the cyanobacterium *Synechococcus elongatus*. *Environ Microbiol* **15**: 1786–1794.

Schiffman, J.D. and Elimelech, M. (2011) Antibacterial Activity of Electrospun Polymer Mats with Incorporated Narrow Diameter Single-Walled Carbon Nanotubes. *ACS Appl Mater Interfaces* **3**: 462–468.

Schirrmeister, B.E., Antonelli, A., and Bagheri, H.C. (2011) The origin of multicellularity in cyanobacteria. *BMC Evol Biol* **11**: 45.

Schuergers, N., Ruppert, U., Watanabe, S., Nürnberg, D.J., Lochnit, G., Dienst, D., et al. (2014) Binding of the RNA chaperone Hfq to the type IV pilus base is crucial for its function in *Synechocystis* sp. PCC 6803. *Mol Microbiol* **92**: 840–852.

Schuergers, N. and Wilde, A. (2015) Appendages of the Cyanobacterial Cell. *Life* **5**: 700–715.

Schultz, M.P., Bendick, J.A., Holm, E.R., and Hertel, W.M. (2011) Economic impact of biofouling on a naval surface ship. *Biofouling* **27**: 87–98.

Schulz-Vogt, H.N., Angert, E.R., and Garcia-Pichel, F. (2007) Giant bacteria. *eLS* 1–7.

Schumacher, J.F., Aldred, N., Callow, M.E., Finlay, J.A., Callow, J.A., Clare, A.S., and Brennan, A.B. (2007) Species-specific engineered antifouling topographies: correlations between the settlement of algal zoospores and barnacle cyprids. *Biofouling* **23**: 307–317.

Schumacher, J.F., Long, C.J., Callow, M.E., Finlay, J.A., Callow, J.A., and Brennan, A.B. (2008) Engineered nanoforce gradients for inhibition of settlement (attachment) of swimming algal spores. *Langmuir* **24**: 4931–4937.

Schwarzkopf, M., Yoo, Y.C., Hückelhoven, R., Park, Y.M., and Proels, R.K. (2014) Cyanobacterial phytochrome2 regulates the heterotrophic metabolism and has a function in the heat and high-light stress response. *Plant Physiol* **164**: 2157–2166.

Sedlmeier, F., Janecek, J., Sendner, C., Bocquet, L., Netz, R.R., and Horinek, D. (2008) Water at polar and nonpolar solid walls (Review). *Biointerphases* **3**: FC23–FC39.

Selim, M.S., El-Safty, S.A., Fatthallah, N.A., and Shenashen, M.A. (2018) Silicone/graphene oxide sheet-alumina nanorod ternary composite for superhydrophobic antifouling coating. *Prog Org Coatings* **121**: 160–172.

Selim, M.S., Elmarakbi, A., Azzam, A.M., Shenashen, M.A., EL-Saeed, A.M., and El-Safty, S.A. (2018) Eco-friendly design of superhydrophobic nano-magnetite/silicone composites for marine foul-release paints. *Prog Org Coatings* **116**: 21–34.

Selim, M.S., Fatthallah, N.A., Higazy, S.A., Hao, Z., and Jing Mo, P. (2022) A comparative study between two novel silicone/graphene-based nanostructured surfaces for maritime antifouling. *J Colloid Interface Sci* **606**: 367–383.

Selim, M.S., Shenashen, M.A., El-Safty, S.A., Higazy, S.A., Selim, M.M., Isago, H., and Elmarakbi, A. (2017) Recent progress in marine foul-release polymeric nanocomposite coatings. *Prog Mater Sci* **87**: 1–32.

Sener, G., Ozgur, E., Rad, A.Y., Uzun, L., Say, R., and Denizli, A. (2013) Rapid real-time detection of procalcitonin using a microcontact imprinted surface plasmon resonance biosensor. *Analyst* **138**: 6422–6428.

Sharma, C., Malhotra, D., and Rathore, A.S. (2011) Review of Computational fluid dynamics applications in biotechnology processes. *Biotechnol Prog* **27**: 1497–1510.

Shirkey, B., Kovarcik, D.P., Wright, D.J., Wilmoth, G., Prickett, T.F., Helm, R.F., et al. (2000) Active Fe-containing superoxide dismutase and abundant sodF mRNA in *Nostoc commune* (cyanobacteria) after years of desiccation. *J Bacteriol* **182**: 189–197.

Shrivastava, A.K., Chatterjee, A., Yadav, S., Singh, P.K., Singh, S., and Rai, L.C. (2015) UV-B stress

induced metabolic rearrangements explored with comparative proteomics in three *Anabaena* species. *J Proteomics* **127**: 122–133.

Silva, E.R., Ferreira, O., Ramalho, P.A., Azevedo, N.F., Bayón, R., Igartua, A., et al. (2019) Eco-friendly non-biocide-release coatings for marine biofouling prevention. *Sci Total Environ* **650**: 2499–2511.

Silva, E.R., Tulcidas, A. V, Ferreira, O., Bayón, R., Igartua, A., Mendoza, G., et al. (2021) Assessment of the environmental compatibility and antifouling performance of an innovative biocidal and foul-release multifunctional marine coating. *Environ Res* **198**: 111219.

Singh, R., Parihar, P., Singh, M., Bajguz, A., Kumar, J., Singh, S., et al. (2017) Uncovering potential applications of cyanobacteria and algal metabolites in biology, agriculture and medicine: Current status and future prospects. *Front Microbiol* **8**: 1–37.

Singh, S.P. and Montgomery, B.L. (2011) Determining cell shape: adaptive regulation of cyanobacterial cellular differentiation and morphology. *Trends Microbiol* **19**: 278–285.

Sjollema, J., Rustema-Abbing, M., van der Mei, H.C., and Busscher, H.J. (2011) Generalized relationship between numbers of bacteria and their viability in biofilms. *Appl Environ Microbiol* **77**: 5027–5029.

Skovager, A., Whitehead, K., Siegumfeldt, H., Ingmer, H., Verran, J., and Arneborg, N. (2012) Influence of flow direction and flow rate on the initial adhesion of seven *Listeria monocytogenes* strains to fine polished stainless steel. *Int J Food Microbiol* **157**: 174–181.

Skovhus, T.L., Enning, D., and Lee, J. eds. (2017) Microbiologically Influenced Corrosion in the Upstream Oil and Gas Industry (1st ed.), Boca Raton: CRC PRESS.

Slabas, A.R., Suzuki, I., Murata, N., Simon, W.J., and Hall, J.J. (2006) Proteomic analysis of the heat shock response in Synechocystis PCC6803 and a thermally tolerant knockout strain lacking the histidine kinase 34 gene. *Proteomics* **6**: 845–864.

Smaradhana, D.F., Prabowo, A.R., and Ganda, A.N.F. (2021) Exploring the potential of graphene materials in marine and shipping industries – A technical review for prospective application on ship operation and material-structure aspects. *J Ocean Eng Sci* **6**: 299–316.

Smith, A.M. and Callow, J.A. (2006) Biological adhesives, Springer.

Soares, O., Gonçalves, A.G., Delgado, J.J., Órfão, J.J.M., and Pereira, M.F.R. (2015) Modification of carbon nanotubes by ball-milling to be used as ozonation catalysts. *Catal Today* **249**: 199–203.

Sobczuk, T.M., Camacho, F.G., Grima, E.M., and Chisti, Y. (2006) Effects of agitation on the microalgae *Phaeodactylum tricornutum* and *Porphyridium cruentum*. *Bioprocess Biosyst Eng* **28**: 243–250.

Soleimani, S., Jannesari, A., Yousefzadi, M., Ghaderi, A., and Shahdadi, A. (2021) Eco-friendly foul release coatings based on a novel reduced graphene oxide/Ag nanocomposite prepared by a green synthesis approach. *Prog Org Coatings* **151**: 106107.

Sonak, S. (2009) Implications of organotins in the marine environment and their prohibition. *J Environ Manage* **90**: 1–3.

Sonak, S., Pangam, P., Giriyan, A., and Hawaldar, K. (2009) Implications of the ban on organotins for protection of global coastal and marine ecology. *J Environ Manage* **90**: 96–108.

Sonani, R.R., Gupta, G.D., Madamwar, D., and Kumar, V. (2015) Crystal structure of allophycocyanin from marine cyanobacterium *Phormidium* sp. A09DM. *PLoS One* **10**: 1–16.

Song, C., Yang, C.-M., Sun, X.-F., Xia, P.-F., Qin, J., Guo, B.-B., and Wang, S.-G. (2018) Influences of graphene oxide on biofilm formation of gram-negative and gram-positive bacteria. *Environ Sci Pollut Res* **25**: 2853–2860.

Soon, C.F., Omar, W.I.W., Nayan, N., Basri, H., Narawi, M.B., and Tee, K.S. (2013) A Bespoke Contact Angle Measurement Software and Experimental Setup for Determination of Surface Tension. *Procedia Technol* **11**: 487–494.

Sousa-Cardoso, F., Teixeira-Santos, R., and Mergulhão, F.J.M. (2022) Antifouling Performance of Carbon-Based Coatings for Marine Applications: A Systematic Review. *Antibiotics* **11**: 1102.

Staneva, A.D., Dimitrov, D.K., Gospodinova, D.N., and Vladkova, T.G. (2021) Antibiofouling

activity of graphene materials and graphene-based antimicrobial coatings. *Microorganisms* **9**: 1–20.

Stanier, R.Y. and Cohen-Bazire, G. (1977) Phototrophic prokaryotes: the cyanobacteria. *Annu Rev Microbiol* **31**: 225–274.

Stewart, P.S. (2003) Diffusion in Biofilms. *J Bacteriol* **185**: 1485–1491.

Stockton-Fiti, K.A. and Moffitt, C.M. (2017) Safety and efficacy of Virkon® aquatic as a control tool for invasive Molluscs in aquaculture. *Aquaculture* **480**: 71–76.

Stomp, M., Huisman, J., De Jongh, F., Veraart, A.J., Gerla, D., Rijkeboer, M., et al. (2004) Adaptive divergence in pigment composition promotes phytoplankton biodiversity. *Nature* **432**: 104–107.

Stoodley, P., Sauer, K., Davies, D.G., and Costerton, J.W. (2002) Biofilms as complex differentiated communities. *Annu Rev Microbiol* **56**: 187–209.

Stout, J.B., Avila, B.W., and Fetherman, E.R. (2016) Efficacy of Commercially Available Quaternary Ammonium Compounds for Controlling New Zealand Mudsnails *Potamopyrgus antipodarum*. *North Am J Fish Manag* **36**: 277–284.

Strunecký, O., Ivanova, A.P., and Mareš, J. (2022) An updated classification of cyanobacterial orders and families based on phylogenomic and polyphasic analysis. *J Phycol* 59: 120–2.

Stuart, R.K., Mayali, X., Lee, J.Z., Craig Everroad, R., Hwang, M., Bebout, B.M., et al. (2016) Cyanobacterial reuse of extracellular organic carbon in microbial mats. *ISME J* **10**: 1240–1251.

Sudhir, P.R., Pogoryelov, D., Kovács, L., Garab, G., and Murthy, S.D.S. (2005) The effects of salt stress on photosynthetic electron transport and thylakoid membrane proteins in the cyanobacterium *Spirulina platensis*. *J Biochem Mol Biol* **38**: 481–485.

Sun, T., Li, S., Song, X., Diao, J., Chen, L., and Zhang, W. (2018) Toolboxes for cyanobacteria: Recent advances and future direction. *Biotechnol Adv* **36**: 1293–1307.

Sun, Y., Lang, Yanghe, Sun, T., Liu, Q., Pan, Y., Qi, Z., et al. (2020) Antifouling potential of multi-walled carbon nanotubes-modified chlorinated rubber-based composites on the colonization dynamics of pioneer biofilm-forming eukaryotic microbes. *Int Biodeterior Biodegradation* **149**: 104921.

Sun, Y., Lang, Yanhe, Yan, Z., Wang, L., and Zhang, Z. (2020) High-throughput sequencing analysis of marine pioneer surface-biofilm bacteria communities on different PDMS-based coatings. *Colloids Surfaces B Biointerfaces* **185**: 110538.

Sun, Y. and Zhang, Z. (2016) New anti-biofouling carbon nanotubes-filled polydimethylsiloxane composites against colonization by pioneer eukaryotic microbes. *Int Biodeterior Biodegradation* **110**: 147–154.

Suo, Y., Huang, Y., Liu, Y., Shi, C., and Shi, X. (2012) The Expression of Superoxide Dismutase (SOD) and a Putative ABC Transporter Permease Is Inversely Correlated during Biofilm Formation in *Listeria monocytogenes* 4b G. *PLoS One* **7**: 1–9.

Sutherland, I.W. (2001) The biofilm matrix--an immobilized but dynamic microbial environment. *Trends Microbiol* **9**: 222–7.

Taherzadeh, D., Picioreanu, C., Küttler, U., Simone, A., Wall, W.A., and Horn, H. (2010) Computational study of the drag and oscillatory movement of biofilm streamers in fast flows. *Biotechnol Bioeng* **105**: 600–610.

Tan, K., Huang, Z., Ji, R., Qiu, Y., Wang, Z., and Liu, J. (2019) A review of allelopathy on microalgae. *Microbiol* **165**: 587–592.

Tan, X., Ramond, E., Jamet, A., Decaux-Tramoni, B., Dupuis, M., Euphrasie, D., et al. (2019) Transketolase is involved in the control of Sigma B during chronic infection by *Staphylococcus aureus*. *bioRxiv* 538900.

Tanaka, K.J., Song, S., Mason, K., and Pinkett, H.W. (2018) Selective substrate uptake: The role of ATP-binding cassette (ABC) importers in pathogenesis. *Biochim Biophys Acta - Biomembr* **1860**: 868–877.

Taylor, D.A. (1996) Introduction to Marine Engineering, United Kingdom: Butterworth-

Heinemann.

Tee, H.S., Waite, D., Payne, L., Middleditch, M., Wood, S., and Handley, K.M. (2020) Tools for successful proliferation: diverse strategies of nutrient acquisition by a benthic cyanobacterium. *ISME J* **14**: 2164–2178.

Teikari, J., Österholm, J., Kopf, M., Battchikova, N., Wahlsten, M., Aro, E.M., et al. (2015) Transcriptomic and proteomic profiling of *Anabaena* sp. strain 90 under inorganic phosphorus stress. *Appl Environ Microbiol* **81**: 5212–5222.

Teixeira-Santos, R., Gomes, M., Gomes, L.C., and Mergulhão, F.J. (2021) Antimicrobial and anti-adhesive properties of carbon nanotube-based surfaces for medical applications: a systematic review. *iScience* **24**: 102001.

Telegdi, J., Trif, L., and Románszki, L. (2016) Smart anti-biofouling composite coatings for naval applications. In *Smart composite coatings and membranes: transport, structural, environmental and energy applications*. Montemor, M.F. (ed). Cambridge, UK, pp. 123–155.

Teodósio, J.S., Simões, M., Melo, L.F., and Mergulhão, F.J. (2011) Flow cell hydrodynamics and their effects on *E. coli* biofilm formation under different nutrient conditions and turbulent flow. *Biofouling* **27**: 1–11.

Terán, L.C., Distefano, M., Bellich, B., Petrosino, S., Bertoncin, P., Cescutti, P., and Sblattero, D. (2020) Proteomic studies of the biofilm matrix including outer membrane vesicles of burkholderia multivorans c1576, a strain of clinical importance for cystic fibrosis. *Microorganisms* **8**: 1–18.

Thanh Doan, N., Rickards, R.W., Rothschild, J.M., and Smith, G.D. (2000) Allelopathic actions of the alkaloid 12-epi-hapalindole E isonitrile and calothrixin A from cyanobacteria of the genera *Fischerella* and *Calothrix*. *J Appl Phycol* **12**: 409–416.

Thompson, J.D., Higgins, D.G., and Gibson, T.J. (1994) CLUSTAL W: improving the sensitivity of progressive multiple sequence alignment through sequence weighting, position-specific gap penalties and weight matrix choice. *Nucleic Acids Res* **22**: 4673–4680.

Thukkaram, M., Sitaram, S., Kannaiyan, S.K., and Subbiahdoss, G. (2014) Antibacterial efficacy of iron-oxide nanoparticles against biofilms on different biomaterial surfaces. *Int J Biomater* **2014**:.

Tian, L., Wang, H., Bing, W., Jin, H., Shang, Y., Dong, S., et al. (2021) Exploring the antifouling performance of non-bactericidal and bactericidal film for combating marine biofouling. *J Taiwan Inst Chem Eng* **126**: 270–277.

Tian, X., Chen, L., Wang, J., Qiao, J., and Zhang, W. (2013) Quantitative proteomics reveals dynamic responses of *Synechocystis* sp. PCC 6803 to next-generation biofuel butanol. *J Proteomics* **78**: 326–345.

Tomaras, A.P., Dorsey, C.W., Edelmann, R.E., and Actis, L.A. (2003) Attachment to and biofilm formation on abiotic surfaces by *Acinetobacter baumannii*: Involvement of a novel chaperone-usher pili assembly system. *Microbiology* **149**: 3473–3484.

Toupoint, N., Mohit, V., Linossier, I., Bourgougnon, N., Myrand, B., Olivier, F., et al. (2012) Effect of biofilm age on settlement of Mytilus edulis. *Biofouling* **28**: 985–1001.

Trémoulet, F., Duché, O., Namane, A., Martinie, B., and Labadie, J.C. (2002) Comparison of protein patterns of *Listeria monocytogenes* grown in biofilm or in planktonic mode by proteomic analysis. *FEMS Microbiol Lett* **210**: 25–31.

Tulcidas, A. V, Bayón, R., Igartua, A., Bordado, J.C.M., and Silva, E.R. (2015) Friction reduction on recent non-releasing biocidal coatings by a newly designed friction test rig. *Tribol Int* **91**: 140–150.

Tuson, H.H. and Weibel, D.B. (2013) Bacteria-surface interactions. *Soft Matter* **9**: 4368–4380.

Uversky, V.N. (2019) Intrinsically disordered proteins and their "Mysterious" (meta)physics. *Front Phys* **7**: 8–23.

Uyeda, J.C., Harmon, L.J., and Blank, C.E. (2016) A Comprehensive Study of Cyanobacterial Morphological and Ecological Evolutionary Dynamics through Deep Geologic Time. *PLoS*

One **11**: e0162539.

Vagos, M.R., Gomes, M., Moreira, J.M.R., Soares, O.S.G.P., Pereira, M.F.R., and Mergulhão, F.J. (2020) Carbon Nanotube/Poly(dimethylsiloxane) Composite Materials to Reduce Bacterial Adhesion. *Antibiotics* **9**: 434.

Varkey, D., Mazard, S., Ostrowski, M., Tetu, S.G., Haynes, P., and Paulsen, I.T. (2016) Effects of low temperature on tropical and temperate isolates of marine *Synechococcus*. *ISME J* **10**: 1252–1263.

Vázquez-Martínez, J., Guitierrez-Villagomez, J.M., Fonseca-García, C., Ramírez-Chávez, E., Mondragón-Sánchez, M.L., Partida-Martínez, L., et al. (2018) *Nodosilinea chupicuarensis* sp. nov. *Phytotaxa* **334**: 167–182.

Venkataraman, A., Amadi, E.V., Chen, Y., and Papadopoulos, C. (2019) Carbon nanotube assembly and integration for applications. *Nanoscale Res Lett* **14**: 1–47.

Verderosa, A.D., Totsika, M., and Fairfull-Smith, K.E. (2019) Bacterial Biofilm Eradication Agents: A Current Review. *Front Chem* **7**: 1–17.

Vermaas, W.F.J. (2001) Photosynthesis and Respiration in Cyanobacteria, New York: Macmillan Publishers Ltd, Nature Publishing Group.

Vidal, L., Ballot, A., Azevedo, S.M.F.O., Padisák, J., and Welker, M. (2021) Introduction to cyanobacteria. In *Toxic Cyanobacteria in Water, 2nd ed.* Chorus, I. and Welker, M. (eds). Boca Raton, FL, USA: CRC PRESS, pp. 163–211.

Vinagre, P.A., Simas, T., Cruz, E., Pinori, E., and Svenson, J. (2020) Marine biofouling: A European database for the marine renewable energy sector. *J Mar Sci Eng* **8**: 495.

Vincent, W.F. (2009) Cyanobacteria. In *Plankton of Inland Waters*. Liknes, G.E. (ed). San Diego, CA, USA: Academic Press, pp. 142–148.

Vincent, W.F. (2000) Cyanobacterial Dominance in the Polar Regions. In *The Ecology of Cyanobacteria*. Whitton, B.A. and Potts, M. (eds). Dordrecht: Springer Netherlands, pp. 321–340.

Visser, P., Ibelings, B., R. Mur, L., and E. Walsby, A. (2005) The ecophysiology of the harmful cyanobacterium *Microcystis*. In *Harmful Cyanobacteria*. Huisman, J., Matthijs, H.C.P., and Visser, P.M. (eds). Dordrecht: Springer, pp. 109–142.

Vizcaíno, J.A., Csordas, A., del-Toro, N., Dianes, J.A., Griss, J., Lavidas, I., et al. (2016) 2016 update of the PRIDE database and its related tools. *Nucleic Acids Res* **44**: D447–D456.

Wagner, M. and Horn, H. (2017) Optical coherence tomography in biofilm research: A comprehensive review. *Biotechnol Bioeng* **114**: 1386–1402.

Wang, C., Bao, W.-Y., Gu, Z.-Q., Li, Y.-F., Liang, X., Ling, Y., et al. (2012) Larval settlement and metamorphosis of the mussel *Mytilus coruscus* in response to natural biofilms. *Biofouling* **28**: 249–256.

Wang, C. and Lan, C.Q. (2018) Effects of shear stress on microalgae – A review. *Biotechnol Adv* **36**: 986–1002.

Wang, D.Z., Kong, L.F., Li, Y.Y., and Xie, Z.X. (2016) Environmental microbial community proteomics: Status, challenges and perspectives. *Int J Mol Sci* **17**: 1–20.

Wang, H., Yang, Y., Chen, W., Ding, L., Li, P., Zhao, X., et al. (2013) Identification of differentially expressed proteins of Arthrospira (Spirulina) plantensis-YZ under salt-stress conditions by proteomics and qRT-PCR analysis. *Proteome Sci* **11**: 1.

Wang, N., Sadiq, F.A., Li, S., He, G., and Yuan, L. (2020) Tandem mass tag-based quantitative proteomics reveals the regulators in biofilm formation and biofilm control of *Bacillus licheniformis*. *Food Control* **110**: 107029.

Wang, X., Wang, C., Xu, B., Wei, J., Xiao, Y., and Huang, F. (2018) Adsorption of intrinsically disordered barnacle adhesive proteins on silica surface. *Appl Surf Sci* **427**: 942–949.

Wang, Y., Chen, L., and Zhang, W. (2016) Proteomic and metabolomic analyses reveal metabolic responses to 3-hydroxypropionic acid synthesized internally in cyanobacterium *Synechocystis* sp. PCC 6803. *Biotechnol Biofuels* **9**: 1–15.

Wang, Y., Stessman, D.J., and Spalding, M.H. (2015) The CO_2 concentrating mechanism and photosynthetic carbon assimilation in limiting CO_2: How *Chlamydomonas* works against the gradient. *Plant J* **82**: 429–448.

Wang, Y., Yi, L., Zhang, J., Sun, L., Wen, W., Zhang, C., and Wang, S. (2018) Functional analysis of superoxide dismutase of *Salmonella typhimurium* in serum resistance and biofilm formation. *J Appl Microbiol* **125**: 1526–1533.

Watzer, B. and Forchhammer, K. (2018) Cyanophycin Synthesis Optimizes Nitrogen Utilization in the Unicellular Cyanobacterium *Synechocystis* sp. Strain PCC 6803. *Appl Environ Microbiol* **84**: e01298-18.

Weimer, E.P., Rao, E., and Brendel, M. (1993) Molecular structure and genetic regulation of SFA, a gene responsible for resistance to formaldehyde in *Saccharomyces cerevisiae*, and characterization of its protein product. *Mol Gen Genet MGG* **237**: 351–358.

Werner, S., Kaiser, S.C., Kraume, M., and Eibl, D. (2014) Computational fluid dynamics as a modern tool for engineering characterization of bioreactors. *Pharm Bioprocess* **2**: 85–99.

Wetherbee, R., Lind, J.L., Burke, J., and Quatrano, R.S. (1998) Minireview—the First Kiss: Establishment and Control of Initial Adhesion By Raphid Diatoms. *J Phycol* **34**: 9–15.

Whitehead, K., Kelly, P., Li, H., and Verran, J. (2010) Surface topography and physicochemistry of silver containing titanium nitride nanocomposite coatings. *J Vac Sci Technol B* **28**: 180–187.

Whitton, B.A. (1992) Diversity, ecology, and taxonomy of the cyanobacteria. In *Photosynthetic Prokaryotes*. Mann, N.H. and Carr, N.G. (eds). New York, USA: Plenum Press, pp. 1–51.

Wietz, M., Hall, M.R., and Høj, L. (2009) Effects of seawater ozonation on biofilm development in aquaculture tanks. *Syst Appl Microbiol* **32**: 266–277.

Williamson, S.J., Rusch, D.B., Yooseph, S., Halpern, A.L., Heidelberg, K.B., Glass, J.I., et al. (2008) The sorcerer II global ocean sampling expedition: Metagenomic characterization of viruses within aquatic microbial samples. *PLoS One* **5**: e77.

Wiśniewski, J.R., Zougman, A., Nagaraj, N., and Mann, M. (2009) Universal sample preparation method for proteome analysis. *Nat Methods* **6**: 359–362.

Wong, F.C.Y. and Meeks, J.C. (2002) Establishment of a functional symbiosis between the cyanobacterium *Nostoc punctiforme* and the bryophyte *Anthoceros punctatus* requires genes involved in nitrogen control and initiation of heterocyst differentiation. *Microbiology* **148**: 315–323.

Wood, Z.A., Schröder, E., Harris, J.R., and Poole, L.B. (2003) Structure, mechanism and regulation of peroxiredoxins. *Trends Biochem Sci* **28**: 32–40.

Wright, E.S., Yilmaz, L.S., and Noguera, D.R. (2012) DECIPHER, a search-based approach to chimera identification for 16S rRNA sequences. *Appl Environ Microbiol* **78**: 717–725.

Wu, S., Baum, M.M., Kerwin, J., Guerrero, D., Webster, S., Schaudinn, C., et al. (2014) Biofilm-specific extracellular matrix proteins of nontypeable Haemophilus influenzae. *Pathog Dis* **72**: 143–160.

Xia, Y., Jayathilake, P.G., Li, B., Zuliani, P., and Chen, J. (2021) CFD–DEM modelling of biofilm streamer oscillations and their cohesive failure in fluid flow. *Biotechnol Bioeng* **118**: 918–929.

Xie, L., Hong, F., He, C., Ma, C., Liu, J., Zhang, G., and Wu, C. (2011) Coatings with a self-generating hydrogel surface for antifouling. *Polymer (Guildf)* **52**: 3738–3744.

Xie, M., Zhao, W., and Wu, Y. (2021) Preventing algae biofilm formation via designing long-term oil storage surfaces for excellent antifouling performance. *Appl Surf Sci* **554**: 149612.

Xiong, Z., Wang, Y., Dong, Y., Zhang, Q., and Xua, X. (2019) Cyanophage A-1(L) Adsorbs to Lipopolysaccharides of *Anabaena* sp. Strain PCC 7120 via the Tail Protein Lipopolysaccharide-Interacting Protein (ORF36). **201**: 1–11.

Xu, H., Ma, L., and Jin, Z. (2018) Nitrogen-doped graphene: Synthesis, characterizations and energy applications. *J Energy Chem* **27**: 146–160.

Yan, G., Sun, J., Wang, Z., Qian, P.Y., and He, L. (2020) Insights into the synthesis, secretion and curing of barnacle cyprid adhesive via transcriptomic and proteomic analyses of the cement

gland. *Mar Drugs* **18**:.

Yandi, W., Mieszkin, S., di Fino, A., Martin-Tanchereau, P., Callow, M.E., Callow, J.A., et al. (2016) Charged hydrophilic polymer brushes and their relevance for understanding marine biofouling. *Biofouling* **32**: 609–625.

Yandi, W., Mieszkin, S., Martin-Tanchereau, P., Callow, M.E., Callow, J.A., Tyson, L., et al. (2014) Hydration and Chain Entanglement Determines the Optimum Thickness of Poly(HEMA-co-PEG10MA) Brushes for Effective Resistance to Settlement and Adhesion of Marine Fouling Organisms. *ACS Appl Mater Interfaces* **6**: 11448–11458.

Yang, J.L., Li, Y.F., Guo, X.P., Liang, X., Xu, Y.F., Ding, D.W., et al. (2016) The effect of carbon nanotubes and titanium dioxide incorporated in PDMS on biofilm community composition and subsequent mussel plantigrade settlement. *Biofouling* **32**: 763–777.

Yang, X., Beyenal, H., Harkin, G., and Lewandowski, Z. (2000) Quantifying biofilm structure using image analysis. *J Microbiol Methods* **39**: 109–119.

Yebra, D.M., Kiil, S., and Dam-Johansen, K. (2004) Antifouling technology - Past, present and future steps towards efficient and environmentally friendly antifouling coatings. *Prog Org Coatings* **50**: 75–104.

Yee, M.S.L., Khiew, P.S., Chiu, W.S., Tan, Y.F., Kok, Y.Y., and Leong, C.O. (2016) Green synthesis of graphene-silver nanocomposites and its application as a potent marine antifouling agent. *Colloids Surfaces B Biointerfaces* **148**: 392–401.

Yonezawa, H., Osaki, T., Woo, T., Kurata, S., Zaman, C., Hojo, F., et al. (2011) Analysis of outer membrane vesicle protein involved in biofilm formation of Helicobacter pylori. *Anaerobe* **17**: 388–390.

Youngs, D. (1982) Time-Dependent Multi- material Flow with Large Fluid Distortion. In *Numerical Methods for Fluid Dynamics*. Morton, K. and Baibnes, M. (eds). New York: Academic Press, pp. 273–285.

Yuan, Y. and Lee, T.R. (2013) Contact angle and wetting properties. In *Surface science techniques. Springer Series in surface sciences 51*. Bracco, G. and Holst, B. (eds). Heidelberg: Springer-Verlag, pp. 3–34.

Zargiel, K.A. and Swain, G.W. (2014) Static vs dynamic settlement and adhesion of diatoms to ship hull coatings. *Biofouling* **30**: 115–129.

Zborowsky, S. and Lindell, D. (2019) Resistance in marine cyanobacteria differs against specialist and generalist cyanophages. *Proc Natl Acad Sci U S A* **116**: 16899–16908.

Zhang, D., Liu, Z., Wu, G., Yang, Z., Cui, Y., Li, H., and Zhang, Y. (2021) Fluorinated Carbon Nanotube Superamphiphobic Coating for High-Efficiency and Long-Lasting Underwater Antibiofouling Surfaces. *ACS Appl Bio Mater* **4**: 6351–6360.

Zhang, L.F., Yang, H.M., Cui, S.X., Hu, J., Wang, J., Kuang, T.Y., et al. (2009) Proteomic analysis of plasma membranes of cyanobacterium *Synechocystis* sp. strain PCC 6803 in response to high pH stress. *J Proteome Res* **8**: 2892–2902.

Zhang, P., MacTavish, B.S., Yang, G., Chen, M., Roh, J., Newsome, K.R., et al. (2020) Cyanobacterial Dihydroxyacid Dehydratases Are a Promising Growth Inhibition Target. *ACS Chem Biol* **15**: 2281–2288.

Zhang, X. and Mikkelsen, Ø. (2021) Graphene Oxide/Silver Nanocomposites as Antifouling Coating on Sensor Housing Materials. *J Clust Sci* **33**: 627–635.

Zhang, X., Smits, A.H., Van Tilburg, G.B.A., Ovaa, H., Huber, W., and Vermeulen, M. (2018) Proteome-wide identification of ubiquitin interactions using UbIA-MS. *Nat Protoc* **13**: 530–550.

Zhang, Z., Chen, R., Song, D., Yu, J., Sun, G., Liu, Q., et al. (2021) Guanidine-functionalized graphene to improve the antifouling performance of boron acrylate polymer. *Prog Org Coatings* **159**: 106396.

Zhao, W., Guo, Q., and Zhao, J. (2007) A membrane-associated Mn-superoxide dismutase protects the photosynthetic apparatus and nitrogenase from oxidative damage in the cyanobacterium

Anabaena sp. PCC 7120. *Plant Cell Physiol* **48**: 563–572.

Zheng, S., Bawazir, M., Dhall, A., Kim, H.E., He, L., Heo, J., and Hwang, G. (2021) Implication of Surface Properties, Bacterial Motility, and Hydrodynamic Conditions on Bacterial Surface Sensing and Their Initial Adhesion. *Front Bioeng Biotechnol* **9**: 1–22.

Zhou, T., Cao, H., Zheng, J., Teng, F., Wang, X., Lou, K., et al. (2020) Suppression of water-bloom cyanobacterium *Microcystis aeruginosa* by algaecide hydrogen peroxide maximized through programmed cell death. *J Hazard Mater* **393**: 122394.

Zilliges, Y., Kehr, J.C., Mikkat, S., Bouchier, C., De Marsac, N.T., Börner, T., and Dittmann, E. (2008) An extracellular glycoprotein is implicated in cell-cell contacts in the toxic cyanobacterium *Microcystis aeruginosa* PCC 7806. *J Bacteriol* **190**: 2871–2879.

Zimba, P. V, Huang, I.-S., Foley, J.E., and Linton, E.W. (2017) Identification of a new-to-science cyanobacterium, *Toxifilum mysidocida* gen. nov. & sp. nov. (Cyanobacteria, Cyanophyceae). *J Phycol* **53**: 188–197.

Zobell, C.E. (1943) The Effect of Solid Surfaces upon Bacterial Activity. *J Bacteriol* **46**: 39–56.

Zou, X., Zhang, L., Wang, Z., and Luo, Y. (2016) Mechanisms of the Antimicrobial Activities of Graphene Materials. *J Am Chem Soc* **138**: 2064–2077.

Annex A.

Annex A. Overview of filamentous cyanobacterial strains characteristics

Table A. Characteristics of filamentous cyanobacterial strains, which were previously collected from marine environments, used in this work.
All filamentous cyanobacterial strains were obtained from the Blue Biotechnology and Ecotoxicology Culture Collection (LEGE-CC) located at CIIMAR, Portugal. https://lege.ciimar.up.pt/wp-content/uploads/2018/01/LEGE-CC-Catalog.pdf

Strain	**Order classification 2014** (Komárek *et al.*, 2014)	**Order classification 2022** (Strunecký *et al.*, 2022)	**Location of isolation**	**Morphometrics (Width × Length or Diameter) (µm)**	**Taxonomic notes/diacritical features**	**Macroscopic growth features**	**Habitat Sample Description**
Nodosilinea sp. LEGE 06020	Synechococcales	Nodosilineales	Coxos beach, Portugal	1,2 ± 0,1 × 1,6 ± 0,6	-	color: cyano; forming a smooth biofilm and aggregates	sea water sample, coastal, surf zone
Nodosilinea sp. LEGE 06022	Synechococcales	Nodosilineales	Coxos beach, Portugal	1,5 ± 0,1 × 2,3 ± 0,4	-	color: cyano; forming a smooth biofilm	intertidal zone, wave-sheltered rock

Strain	**Order classification 2014** (Komárek *et al.*, 2014)	**Order classification 2022** (Strunecký *et al.*, 2022)	**Location of isolation**	**Morphometrics (Width × Length or Diameter) (µm)**	**Taxonomic notes/diacritical features**	**Macroscopic growth features**	**Habitat Sample Description**
unidentified filamentous Synechococcales LEGE 07185	Synechococcales	Synechococcales	Lavadores beach, Portugal	1,3 ± 0,2 × 1,4 ± 0,3	filaments constricted at cross-walls, distinguishable centro- and chromatoplasm	color: olive green; forming a firm biofilm and also aggregates	tide pool, on a submerged stone
Nodosilinea sp. LEGE 06145	Synechococcales	Nodosilineales	Moledo beach, Portugal	1,2 ± 0,1 × 1,2 ± 0,2	-	color: cyano; forming a smooth biofilm	wave-exposed tide puddle, rock surface scraping
Nodosilinea sp. LEGE 06119	Synechococcales	Nodosilineales	Burgau beach, Portugal	1,2 ± 0,2 × 1,3 ± 0,3	-	color: cyano; growing homogeneously, mucilaginous	sea water sample, coastal, surf zone
Unidentified filamentous cyanobacterium LEGE 06007	undefined	undefined	São Martinho do Porto beach, Portugal	2,2 ± 0,3 × 2,5 ± 0,4	with hormogonia and narrow sheath	color: cyano; forming a smooth biofilm	intertidal zone, wave-exposed rock
Toxifilum sp. LEGE 06021	Synechococcales	Oculatellales	Coxos beach, Santo Isidoro, Portugal	1,4 ± 0,1 × 2,1 ± 0,4	-	color: cyano; forming a smooth biofilm; mucilaginous	intertidal zone, wave-exposed rock
Jaaginema sp. LEGE 191154	Synechococcales	Leptolyngbyales	Mrizika Beach, Morroco	2.7 ± 0.3 × 4.6 ± 1.1	filaments unbranched, straight to curved, without sheaths (sometimes with a fine mucilaginous layer around the trichomes)	Color: cyano; forming a biofilm	dried soil crust
Leptothoe sp. LEGE 181153	Synechococcales	Nodosilineales	Calhau, Cape Verde	1.5 ± 0-2 × 2.0 ± 0.3	single trichome per sheath, unbranched, straight to curved,	Color: reddish; forming a biofilm	port boat ramp

Strain	Order classification 2014 (Komárek *et al.*, 2014)	Order classification 2022 (Strunecký *et al.*, 2022)	Location of isolation	Morphometrics (Width × Length or Diameter) (µm)	Taxonomic notes/diacritical features	Macroscopic growth features	Habitat Sample Description
					occasionally wavy, densely, and irregularly entangled. Sheaths are colourless, thin, and slightly distinct		
Nodosilinea cf. *nodulosa* LEGE 10377	Synechococcales	Nodosilineales	Aguda Beach, Arcozelo, Portugal	1,3 ± 0,1 × 1,6 ± 0,4	-	color: cyano; forming a smooth biofilm	intertidal zone, on a marine sponge
Lusitaniella coriacea LEGE 07157	undefined	Spirulinales	Lavadores beach, Porto, Portugal	1,6 ± 0,2 × 3, 2 ± 0,4	-	color: olive green; forming a leather-like biofilm	tide pool, rock surface scraping

Annex B.

Annex B. Composition of Z8 medium supplemented with 25 g.L^{-1} of synthetic sea salts (Tropic Marin) and B_{12} vitamin.

Z8 medium is composed of A, B, Fe-EDTA and micronutrients solutions, which should be autoclaved separately. The medium should be prepared in the flow chamber under aseptic conditions. Solutions should be added at room temperature to prevent precipitation, and in the end stock solutions should be stored in the refrigerator.

1. Add the solutions to water according to the following concentrations:

Solution A	10 mL.L^{-1}
Solution B	10 mL.L^{-1}
Fe-EDTA Solution	10 mL.L^{-1}
Micronutrients Solution	1 mL.L^{-1}

Composition of stock solutions:

Solution A

Reagent	Name	Concentration (g.L^{-1})
$NaNO_3$	Sodium nitrate	46.7
$Ca(NO_3)_2.4H_2O$	Calcium nitrate tetrahydrate	5.9
$MgSO_4.7H_2O$	Magnesium sulphate heptahydrate	2.5

Solution B

Reagent	Name	Concentration (g.L^{-1})
K_2HPO_4	Potassium phosphate dibasic	3.1
Na_2CO_3	Sodium carbonate	2.1

Fe-EDTA solution

FeCl3 solution *10 mL.L^{-1}

EDTA-Na ** 9.5 mL.L^{-1}

Composition of FeCl3 solution

Reagent	Name	Concentration (100 mL)
$FeCl_3.6H_2O$	Ferric chloride	2.8 g
HCl (0.1 N)	Hydrochloric Acid	100 mL

Composition of EDTA-Na solution

Reagent	Name	Concentration (100 mL)
EDTA	Ethylenediamine tetraacetic acid	3.9 g
NaOH (0.1 N)	Sodium hydroxide solution	100 mL

Micronutrients solution

Micronutrients 1 to 12 10 $mL.L^{-1}$

Micronutrients 13 and 14 100 $mL.L^{-1}$

Micronutrients	Reagents	Name	Concentration ($g.L^{-1}$)
1	$Na_2WO_4 \cdot 2H_2O$	Sodium tungstate	0.33
2	$(NH_4)_6Mo_7O_{24} \cdot 2H_2O$	Ammonium heptamolybdate	0.88
3	KBr	Potassium bromide	1.2
4	KI	Potassium iodide	0.83
5	$ZnSO_4.7H_2O$	Zinc sulphate	2.87
6	$Cd(NO_3).4H_2O$	Cadmium nitrate	1.55
7	$Co(NO_3)_2.6H_2O$	Cobalt(II) nitrate	1.46
8	$CuSO_4.5H_2O$	Cupric sulphate	1.25
9	$NiSO_4(NH_4)_2SO_4 \cdot 6H_2O$	Ammonium nickel sulphate	1.98
10	$Cr(NO_3)_3.9H_2O$	Chromium(III) nitrate	0.41
11	V_2O_5	Vanadium(V) oxide	0.089
12	$AlK(SO_4)_2SO_4.12H_2O$	Potassium aluminium sulphate	9.48
13	H_3BO_3	Boric Acid	3.1
14	$MnSO_4.4H_2O$	Manganese Sulphate	2.23

To supplement Z8 medium, autoclave deonized water with 25 $g.L^{-1}$ of salt. After cooling, vitamin B_{12} is added in the flow chamber (final concentration in the medium 10 $\mu g.L^{-1}$). After defrosting the stock solution (1000x concentrated), a 0,2 µm syringe filter should be used to add the vitamin to the medium.

Annex C.

Annex C. Publications from this PhD.

C.1 – Cyanobacteria in Marine Biofilms: Hydrodynamic and Surface Effects (2022) https://doi.org/10.52305/ONRA2232 (Chapter 2)

C.2 – Biofilm formation behaviour of marine filamentous cyanobacterial strains in controlled hydrodynamic conditions (2019) https://doi.org/10.1111/1462-2920.14807 (Chapter 3)

C.3 – Characterization of planktonic and biofilm cells from two filamentous cyanobacteria using a shotgun proteomic approach (2020) http://dx.doi.org/10.1080/08927014.2020.1795141 (Chapter 4)

C.4 – Quantitative proteomic analysis of marine biofilms formed by filamentous cyanobacterium (2021) https://doi.org/10.1016/j.envres.2021.111566 (Chapter 5)

C.5 – Hydrodynamic conditions affect the proteomic profile of marine biofilms formed by filamentous cyanobacterium (2022) https://doi.org/10.1038/s41522-022-00340-w (Chapter 6)

C.6 – Characterization and biofouling potentital analysis of two cyanobacterial strains isolated from Cape Verde and Morocco (2023) https://doi.org/10.1093/femsec/fiad004 *(2023)* (Chapter 7)

C.7 – The Use of 3D Optical Coherence Tomography to Analyze the Architecture of Cyanobacterial Biofilms Formed on a Carbon Nanotube Composite (2022) https://doi.org/10.3390/polym14204410 (Chapter 8)

C.8 – How do Graphene Composite Surfaces Affect the Development and Structure of Marine Cyanobacterial Biofilms? (2022) https://doi.org/10.3390/coatings12111775 (Chapter 9)

Chapter 8

Cyanobacteria in Marine Biofilms: Hydrodynamic and Surface Effects

M. J. Romeu, L. C. Gomes, R. Teixeira-Santos and F. J. Mergulhão*

LEPABE - Laboratory for Process Engineering,
Environment, Biotechnology and Energy,
Faculty of Engineering, University of Porto,
Rua Dr. Roberto Frias, Porto, Portugal, and
ALiCE - Associate Laboratory in Chemical Engineering,
Faculty of Engineering, University of Porto,
Rua Dr. Roberto Frias, Porto, Portugal

Abstract

The adhesion and settlement of biofouling organisms is an ongoing concern in aquatic environments as marine biofouling causes several economic, environmental and ecological problems. Coccoid and filamentous cyanobacteria play a significant role in marine biofouling development. Several biological, physical and chemical parameters have been identified as modulators of biofilm development affecting its composition and structure. Among these, the fouling surface properties and flow velocity/shear rate have a critical impact on marine biofilms. Therefore, studies based on the influence of surface parameters and those performed under controlled hydrodynamic conditions are essential for developing effective antifouling strategies for marine application. This chapter reviews the major impacts of marine biofouling and the role of cyanobacteria on biofilm development. Moreover, the effects of

* Corresponding Author's Email: filipem@fe.up.pt.

In: Cyanobacteria and Their Importance
Editor: Rajeshwar P. Sinha
ISBN: 978-1-68507-934-5
© 2022 Nova Science Publishers, Inc.

COMPLIMENTARY COPY

hydrodynamic conditions, surface properties, and microbial content on cyanobacterial biofilm development are highlighted.

Keywords: marine biofouling, cyanobacterial biofilms, hydrodynamics, surface properties

Introduction

Biofilms are complex microenvironments formed by single or multiple species, in which microorganisms are involved in a gelatinous polymeric matrix consisting mainly of water and extracellular polymeric substances (EPS) (Flemming et al. 2016). They are the most common form of microbial organization, mainly due to the set of advantages that this lifestyle features compared to planktonic cells, contributing to successful microbial survival in hostile environments (Verderosa et al. 2019). Biofilms are ubiquitous in natural environments and on man-made surfaces. Although beneficial biofilms can be found for wastewater treatment, production of value-added compounds, and bioremediation processes, biofilms are commonly associated with negative impacts (Muhammad et al. 2020). This microbial lifestyle can contribute to contamination of food processing areas and drinking water distribution systems, chronic infections associated with medical devices, as well as present detrimental impacts in different industries (Fitridge et al. 2012; Abdallah et al. 2014). In aquatic environments, all immersed surfaces are rapidly colonized by organisms (Dang and Lovell 2016), and here cyanobacteria can promote marine biofouling with significant impacts (Faria et al. 2020a; Romeu et al. 2020). Although several environmental, physical, and chemical factors affect biofilm development in marine ecosystems, hydrodynamic conditions and surface properties assume particular relevance (Romeu et al. 2019; Faria et al. 2020a). Moreover, few studies address the influence of these particular parameters on cyanobacterial biofilm growth. Therefore, in this chapter, the consequences of marine biofouling, as well as the relevance of cyanobacteria on marine biofilms, will be addressed. The impact of hydrodynamic conditions, surface properties and microbial content on marine biofilm development by cyanobacteria will also be discussed, and current antibiofouling strategies will be introduced.

COMPLIMENTARY COPY

Importance of Marine Biofouling

Table 1. Main consequences of marine biofouling in industrial and environmental sectors

Sector	Consequences
Industry	Increase of hydrodynamic drag and frictional in vessels and ships
	Decrease in operational efficiency of propulsion, navigation, and water intake equipment
	Increase in fuel consumption
	Material corrosion of different facilities, infrastructures, and submerged equipment
	Increase in management intervention time
	Cleaning, paint removal, and repainting related costs
	Decrease of heat transfer
	Incorrect measurements in submerged sensors
Environmental and health-related problems	Marine species invasion
	Establishment of exotic biofouling species in ports
	Air pollution and an increase in greenhouse gas emissions
	Contamination of aquaculture facilities, such as fish cages and shellfish sites
	Cyanobacterial blooms from benthic mat proliferations
	Water contamination by toxin accumulation

Compiled from Minchin and Gollasch 2003, Visser et al. 2005, Myers et al. 2007, Delauney et al. 2010; Schultz et al. 2011, Fitridge et al. 2012, Aldred and Clare 2014, Davidson et al. 2016, Fernandes et al. 2016, Demirel et al. 2017, Maddah and Chogle 2017, Skovhus et al. 2017, Bannister et al. 2019, Giakoumi et al. 2019.

Biofouling is a massive problem in marine environments leading to industrial, economic, environmental, and health-related problems (Table 1). Estimated costs due to biofilm development in industrial activities, such as in heat exchangers and aquaculture and water desalination stations, are relatively high. In the oil and gas industry, about 20-30% are material deterioration and corrosion-related costs (Skovhus et al. 2017), while in marine transport, around 35-50% of costs are related to increased fuel consumption (Schultz et al. 2011). Indeed, fuel consumption increases of about 40% have been observed due to biofouling (Champ 2000); for example, the cost of one trip from San Francisco to Yokohama has increased about 77% due to vessel's hull fouling (Abbott et al. 2000). Besides the increased fuel consumption, marine biofouling also leads to costs related to hull cleaning, paint removal, and repainting. Additional problems related to biofouling in marine environments are found in partially submerged or even moored equipment such as underwater cameras, flotation spheres, measuring devices, transparent hulls of boats, or their windows and sensors. On this equipment, the most obvious

COMPLIMENTARY COPY

problems are related to optical and electrochemical sensors, which are used for on-site monitoring with weekly, monthly, or continuous measuring because even a thin biofilm on the optics can give rise to incorrect measurements (Delauney et al. 2010).

Marine biofouling might also impact the dynamic of marine ecosystems. Biofouling on ship hulls or in submerged structures that provide a variety of niches favorable to biofilm formation, such as propellers and pipe systems, can also act as a pathway for marine species invasion. Non-native fouling species might attach directly to these structures and be transported over great distances (Godwin 2003; Minchin and Gollasch 2003; Davidson et al. 2009), affecting the marine ecology of new areas through predation and competition events with native species, or even become a significant fouling pest (Aldred and Clare 2014). Several frameworks focus on marine invasive species management (Giakoumi et al. 2019), presenting specific policies for their control on islands (IUCN, 2018) or in marine protected areas (Keith et al. 2016). Additionally, at the environmental level, the increased frictional drag in vessels caused by marine biofouling may contribute to air pollution and greenhouse gas emissions (Hunsucker et al. 2018).

Biofilms in aquatic environments can also impact public health, as biofilms are considered a temporary or permanent refuge for bacterial pathogens in aquaculture facilities, contributing to the persistence of harmful microorganisms and transmission of their genetic determinants (Wietz et al. 2009; Bannister et al. 2019). Particularly, cyanobacteria can threaten animal and human health through their ability to produce cyanotoxins (Miller et al. 2010; Gibble et al. 2016; Regueiras et al. 2018; Breinlinger et al. 2021). These toxins, which can be retained on biofilm structure, degrade water quality and may cause additional consequences by their ingestion through contaminated food or even by drinking water during recreational activities (Buratti et al. 2017; Huisman et al. 2018).

The Role of Cyanobacteria (Filamentous and Coccoid) in Marine Biofouling

Marine biofouling is a highly complex and dynamic process in which different agents and their interactions are involved at different stages. It has been considered that marine biofouling development comprises both micro and macrofouling events. Microfouling encompasses the adhesion of cells and

COMPLIMENTARY COPY

biofilm formation, while macrofouling involves the settlement of invertebrate organisms (Figure 1).

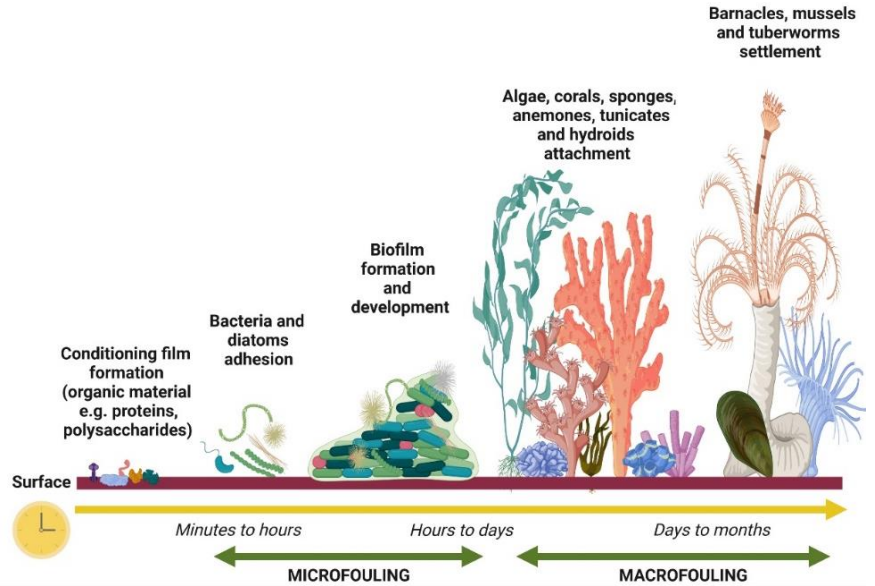

Figure 1. Temporal representation of marine biofouling process and involved organisms.

Although various stages can overlap or occur in parallel, it is often observed that microbial biofilm formation is a primordial step to marine biofouling (Salta et al. 2013a; Anderson 2016). Briefly, a conditioning film comprised of organic molecules from the surrounding environment is formed on the submerged surface within the first minutes of immersion. Consequently, the physicochemical properties of the surfaces can be modified, affecting the adhesion and biofilm formation (Renner and Weibel 2011). Diatoms (unicellular algae), cyanobacteria, and additional marine bacteria adhere to this conditioning layer within minutes or hours by a reversible process caused by diffusion, gravitation, Brownian motion, electrostatic (repulsion and attraction), hydrophobic and van der Waals interactions (Marshall et al. 1971). Additionally, bacteria use a variety of organelles to attach to surfaces, including pili, flagella, and outer membrane proteins (Tuson and Weibel 2013). Although Gram-negative cyanobacteria do not contain genes encoding flagella components, the extracellular non-flagellar appendages, called pili or fimbriae, are widespread in these organisms

COMPLIMENTARY COPY

(Schuergers and Wilde 2015). After this initial step, the irreversible adhesion of cells occurs through interactions as dipole-dipole forces, hydrogen bonds, and secretion of EPS from cells (Renner and Weibel 2011). The change from planktonic to biofilm state is thought to be dependent on quorum sensing (QS) phenomena, a process of cell-to-cell communication by which bacteria sense and respond to their own density or changes in their environment (Dobretsov et al. 2009; Di Donato et al. 2016). These steps are followed by biofilm formation and development, in which a continuous production of EPS is achieved (Figure 2).

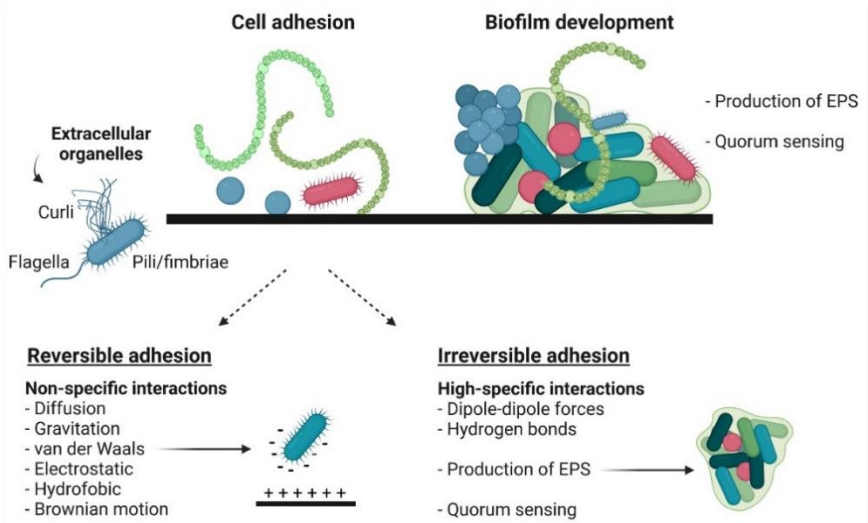

Figure 2. Cell-surface interactions, EPS production, and QS phenomena involved in the initial steps of marine biofouling - adhesion and biofilm development.

This is mainly regulated by external conditions (Nichols et al. 2005) and QS signals (Hammer and Bassler 2003). In fact, QS may be necessary for EPS synthesis and biofilm growth, or it can induce motility and biofilm dispersal (Hoang et al. 2008; McDougald et al. 2012). After a few days, macrofoulers organisms may attach to this initial biofilm formed by microfoulers. The macrofouling community consists of algae, corals, sponges, anemones, tunicates and hydroids (soft fouling organisms), and barnacles, mussels and tubeworms as hard fouling organisms (Mieszkin et al. 2013). One of the most promising approaches for biofouling mitigation is to interfere with the initial adhesion since if microfouling is delayed, macrofouling can be managed more effectively (Cao et al. 2011; Telegdi et al. 2016).

COMPLIMENTARY COPY

Cyanobacteria are a widespread group of photosynthetic prokaryotes that assumes a particular relevance on marine biofouling (Table 2). Cyanobacteria present a significant morphological diversity, comprising coccoid and filamentous forms with different degrees of complexity. A mutation during cell division of ancestral coccoid cyanobacteria could have led to the origin of a primordial filament that would have represented the evolution for multicellular forms (Schirrmeister et al. 2011). Although filamentous phenotype can be disadvantageous due to impaired motility or reduced buoyancy in aquatic environments, the stress and predation resistance, as well as the improved resource acquisition may be beneficial (Claessen et al. 2014). Likewise, cyanobacteria had a large impact on the evolution of life since they were responsible for the accumulation of oxygen, which started to change the Earth's environment and challenged the existent forms of life (Lyons et al. 2014), as well as for the evolution of eukaryotic organisms from ancient cyanobacteria (Ku et al. 2015). Cyanobacteria contribute to the oxygen, carbon and nitrogen biogeochemical cycles, are involved in the primary production of trophic chains, and can persist in harsh conditions due to their high adaptability (Berg and Sutula 2015; Anderson 2016). These features, largely due to the metabolic flexibility to perform oxygen photosynthesis and respiration simultaneously (Vermaas 2001; Mullineaux 2014), allow them to resist the heterogeneous marine environment, which can be challenging for bacterial survival. These microorganisms are common in many habitats such as lakes, ponds, springs, wetlands, streams, rivers, soil crust, microbial mats, sands, and rocks (Ramos et al. 2018). For instance, cyanobacteria are the primary colonizers of ice sheets by forming and surviving in pigmented mats, making these ecosystems productive (Vincent 2000), and their association with heterotrophic organisms in the desert facilitates the productivity of soil crust (Pointing and Belnap 2012). Moreover, as early colonizers of submerged surfaces, these microorganisms may determine the structure and function of the mature biofilm (Mitbavkar et al. 2012; Dang and Lovell 2016). Cyanobacteria species also produce large amounts of EPS (Rossi and De Philippis 2015; Anderson 2016), which represent the major and an essential component of biofilms communities. EPS include polysaccharides, proteins, lipids, and extracellular DNA as a result of metabolism and cell death (Sutherland 2001). These substances are responsible not only for biofilm structure, stability, and cohesion but also provide anchoring sites for extracellular enzymes, which may degrade toxic compounds (Limoli et al. 2015). Moreover, EPS maintains a highly hydrated microenvironment due to water retention ability, thus promoting nutrients' entrapment (Flemming and

COMPLIMENTARY COPY

Wingender 2010). Advantages of EPS for embedded microorganisms on biofilms also include establishing an ideal microenvironment for the exchange of genetic information and protection from predation (Decho and Gutierrez 2017).

Although their prevalence depends on geographical area and season, together with diatoms, cyanobacteria constitute the major components of marine biofilms (Narváez-Zapata et al. 2005; Salta et al. 2013a; Bharti et al. 2017). It is noteworthy that the ratio of bacteria:diatoms:flagellates observed in biofilms in the White Sea was 640:4:1 (Railkin 2003). Moreover, symbiotic relations between cyanobacteria and diatoms can occur on marine biofilms (Amin et al. 2012) since nitrogen-fixing cyanobacteria supply fixed nitrogen to diatoms, likely in the form of ammonia or dissolved organic nitrogen (Foster et al. 2011). Despite several studies that focus on the interaction of microfoulers and the attachment of macrofouler organisms showed contradictory results, most of them presented a positive correlation between biofilm formation and macrofouling attachment and development (Mieszkin et al. 2013; Salta et al. 2013a). It has been considered that biofilm formation by bacteria and algae is important to the subsequent settlement of macrofouler organisms. Nevertheless, this process can be influenced by many factors such as biofilm age (Chung et al. 2010; Campbell et al. 2011), density, the presence of single or mixed species, and the surface material (Mieszkin et al. 2012).

Table 2. Main relevant characteristics of cyanobacteria for marine biofouling

Characteristics	Reference
High adaptation ability to harsh conditions	Berg and Sutula 2015 Bharti et al. 2017
Early marine surface colonizers Major components of marine biofilms	Nagarkar et al. 2004 Narváez-Zapata et al. 2005 Nayar et al. 2005 Mitbavkar et al. 2012 Salta et al. 2013a Oberbeckmann et al. 2014 Bharti et al. 2017 Jiang et al. 2018 Azevedo et al. 2020
Produce large amounts of extracellular polymeric substances (EPS)	Abed et al. 2009 Rossi and De Philippis 2015 Di Donato et al. 2016
Promote the settlement and metamorphosis of macrofouler organisms	Chung et al. 2010 Campbell et al. 2011 Wang et al. 2012 Toupoint et al. 2012

COMPLIMENTARY COPY

Main Factors Affecting Marine Biofouling

In marine environments, different environmental, physical, chemical, and biological parameters affect biofouling development (Figure 3). Environmental factors such as radiation (Behrendt et al. 2012), water dynamic flux, pH (Brown et al. 2018), salinity, temperature (Lau et al. 2005), dissolved oxygen (Lagos et al. 2016), CO_2 (Brown et al. 2018), and nutrient availability (Briand et al. 2012) can influence biofilm community dynamics. In fact, unlike in dark environments, photosynthetic conditions promote the production of EPS and proteins involved in micronutrient transport (Stuart et al. 2016). Surface energy, colour, topography, wettability, roughness, electrostatic charge, and hydrophobicity are some properties that may affect the first steps of biofouling, from cell adhesion to biofilm growth, and their characteristics (Dang and Lovell 2000; Hodson et al. 2000; Jones et al. 2007; Palmer et al. 2007; Lee et al. 2008; Chung et al. 2010; Gambino et al. 2019). Moreover, bacterial community variability has been reported on different marine biofilms (Catão et al. 2019; Caruso 2020).

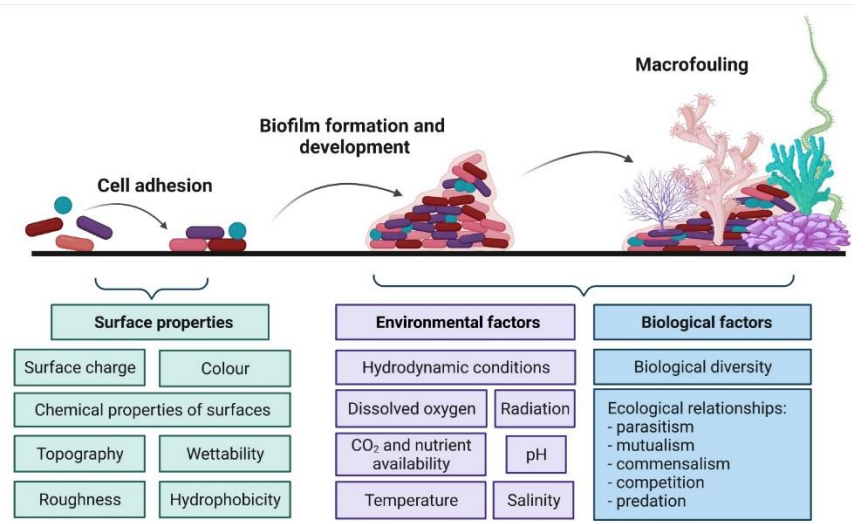

Figure 3. Main factors affecting marine biofouling.

COMPLIMENTARY COPY

Hydrodynamics

Hydrodynamic conditions may affect all stages of biofilm development. Indeed, there is evidence that hydrodynamics affects not only the biofilm structure and architecture but also plays a crucial role in mass transfer, EPS production, energy metabolism, and can induce genetic or molecular changes (Horn et al. 2003; Rochex et al. 2008; Gloag et al. 2020; Romeu et al. 2021). Previous studies concluded that shear stress also affects biofilm diversity since biofilm species composition changed with increasing shear stress (Rochex et al. 2008; Catão et al. 2019). Therefore, when the performance of antifouling surfaces is assessed *in vitro*, it is crucial that experiments are performed in controlled hydrodynamic conditions, where the shear stress or shear rate are well defined (Gomes et al. 2019; Alves et al. 2020), in order to bring the *in vitro* operational conditions closer to the natural aquatic environments. However, few experimental setups have been used to study the effect of hydrodynamics in marine biofilms; most of them are microfluidic devices (Salta et al. 2013b; Alles and Rosenhahn 2015; Nolte et al. 2017) or platforms that specifically evaluate macrofouling development (Qian et al. 1999; Qian et al. 2000). The use of agitated microtiter plates at defined hydrodynamic conditions, which achieved the shear stress or shear rate values described for real aquatic and marine environments, can be a very convenient and affordable approach (Romeu et al. 2019). Moreover, microtiter plates enable the use of coupons from different materials to test the impact of different surfaces in marine biofouling. A previous study to compare *Escherichia coli* biofilm development by using microtiter plates and a parallel plate flow chamber as micro and macro-flow systems, respectively, has shown that when the shear forces are kept constant between these platforms, the obtained results were similar despite the large differences in size (Gomes et al. 2017). It was also demonstrated that biofilms grown at lower velocities exhibit lower cell density and higher effective diffusivity, whereas biofilms grown at higher flow velocities have higher cell density and lower effective diffusion (Horn et al. 2003). Since it has been reported that the slow flow of water (0.2 m s^{-1}) promotes the growth of filamentous green algae and cyanobacteria (Flemming et al. 2009), biofouling can be favoured at these low fluid velocities that can be found in harbours and dockyards (when ships are anchored, berthed or moored), and by slow-moving vessels such as oil platforms, oceanic barges, tugs, dredges, fishing vessels, and recreational crafts (Minchin and Gollasch 2003; Hewitt et al. 2009). In addition, long stays at harbours also increase the opportunities for marine fouling species to attach to immersed surfaces and

COMPLIMENTARY COPY

accumulate (Davidson et al. 2009; Hewitt et al. 2009). Indeed, containerships that travel at relatively high speeds and remain in ports for short periods seem to be less colonized than other types of vessels (Davidson et al. 2009). However, the impact of hydrodynamic conditions in the marine environment is a considerable challenge since the fouling organisms have evolved the ability to attach and proliferate on a range of surfaces, not only when subjected to lower water velocities but even under high turbulent conditions.

In marine environments, although a shear rate of 50 s^{-1} has been reported for a ship in a harbour (Bakker et al. 2003), equipment and devices which are in similar environments, such as partially submerged or moored equipment as underwater cameras, flotation spheres, sensors, and even transparent hulls of boats or their windows, are likely to be subjected to similar shear values (Figure 4). Few studies have focused on the impact of hydrodynamic conditions on marine biofilms, particularly on cyanobacterial biofilms (Table 3). Overall, studies performed on coccoid (Faria et al. 2020a; 2021a) and filamentous cyanobacterial biofilms (Romeu et al. 2019; 2020; 2021) at controlled hydrodynamic conditions (values of shear rate of 4 s^{-1} and 40 s^{-1}) showed a higher biofilm development at the lower shear rate. In fact, a study performed on coccoid cyanobacteria revealed that the number of adhered cells was higher at 4 s^{-1} than 40 s^{-1} for both adhesion and biofilm development assays (Faria et al. 2021a), suggesting that shear forces have an influence not only on the early stages of adhesion and biofilm formation but also during maturation. Indeed, higher shear forces may hamper initial cell adhesion and facilitate the detachment of adhered microorganisms during irreversible steps of biofilm formation, whereas at later stages of biofilm development, erosion and sloughing events can be promoted by the increased shear forces.

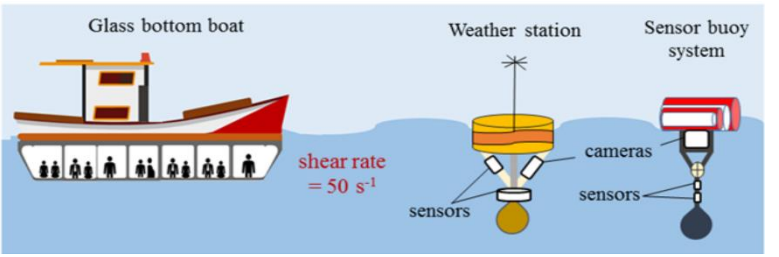

Figure 4. Representation of some marine equipment and devices, such as partially submerged underwater cameras, flotation spheres, sensors, and transparent hulls of boats or their windows, that are likely to be subjected to average shear rate values of 50 s^{-1}.

COMPLIMENTARY COPY

COMPLIMENTARY COPY

Table 3. Cyanobacterial biofilm studies to evaluate the effect of different hydrodynamic conditions

Cyanobacteria form	Strains	Shear rate	Biofilm development time	Study aim	Main conclusions	Reference
Coccoid	*Synechocystis salina* LEGE 00041 *Cyanobium sp.* LEGE 06097	4 and 40 s^{-1}	6 weeks	Effect of different shear rates on adhesion and biofilm development from 24 h to 6 weeks	- Higher biofilm development was observed at 4 s^{-1} - The presence of streamers was more noticeable in biofilms formed at 4 s^{-1} - Shear forces were shown to have a profound impact on biofilm development, regardless of the fouling capacity of cyanobacterial strains and the surface hydrophobicity	Faria et al. 2020a
	Synechocystis salina LEGE 00041 *Synechocystis salina* LEGE 06155 *Cyanobium* sp. LEGE 06097	4 and 40 s^{-1}	Adhesion assays: 7.5 h Biofilm assays: 6 weeks	Potential of short-time adhesion assays on the estimation of biofilm development at different hydrodynamic conditions	- For both adhesion and biofilm assays, the number of adhered cells was higher at 4 s^{-1} than 40 s^{-1} - Higher biofilm development at 4 s^{-1} was confirmed by biofilm wet weight, thickness, and chlorophyll *a* content values - Initial adhesion assays can be used to estimate marine biofilm development under different hydrodynamic conditions	Faria et al. 2021a
Filamentous	*Nodosilinea* sp. LEGE 06020 *Nodosilinea* sp. LEGE 06022 Unidentified filamentous	4 and 40 s^{-1}	7 weeks	Impact of different shear rates on biofilm development over 7 weeks	- Higher biofilm development was observed at 4 s^{-1} - The hydrodynamic effect was more noticeable during biofilm maturation - Shear rates affected biofilm architecture since biofilm streamers were more notorious at 4 s^{-1}	Romeu et al. 2019

Cyanobacteria form	Strains	Shear rate	Biofilm development time	Study aim	Main conclusions	Reference
	Synechococcales LEGE 07185					
Cyanobac-teria form	Strains	Shear rate	Biofilm development time	Study aim	Main conclusions	Reference
	Nodosilinea sp. LEGE 06145 *Nodosilinea* sp. LEGE 0611	4 and 40 s^{-1}	7 weeks	Qualitative proteomic analyses of biofilms formed under different shear rates after 7 weeks	- Higher biofilm development was observed at 4 s^{-1}, as well as the presence of streamers - Qualitative proteomic analysis revealed that biofilms developed at different shear rates show differences in protein composition - Highly variable protein expression profile was observed between cyanobacterial strains	Romeu et al. 2020
	Unidentified filamentous cyanobacterium LEGE 06007	4 and 40 s^{-1}	7 weeks	Quantitative proteomic analyses of biofilms formed under different shear rates after 7 weeks	- Higher biofilm development was observed at 4 s^{-1} - Quantitative proteomic analysis revealed differentially expressed proteins between shear rates (related to superoxide dismutase expression, photosynthetic processes, and a set of uncharacterized proteins with calcium-binding domains, disordered proteins, and other proteins involved in electron transfer activity	Romeu et al. 2021

COMPLIMENTARY COPY

A study performed by David et al. (2015) also showed significant differences in biofilm development of *Synechocystis* sp. PCC 6803 in a capillary microreactor depending on the hydrodynamic conditions applied. Two different flow patterns were applied: a single-phase flow (after the cell attachment phase, the flow was set to 100 µL min^{-1}, and it was kept constant during the whole cultivation time), and a segmented flow (after the cell attachment phase, the flow was set to 100 µL min^{-1}, kept constant for 2 days and subsequently, segmented flow was established and air segments were introduced). While under single-phase flow, clogging of the capillary occurred due to uncontrolled biomass formation, the application of segmented flow prevented clogging by changing the structure of the cyanobacterial biofilm. A photosynthetically active, compact, and flat biofilm was formed upon the introduction of air segment into the system without any cell detachment events (David et al. 2015). Heuschkel et al. (2020) also observed that the change in flow conditions from single to aqueous-air segmented flow resulted in faster growth, improved surface coverage, and enhanced biomass formation. In this study, the growth and catalytic performance of mixed-species biofilms comprising *Synechocystis* sp. PCC 6803 and *Pseudomonas* sp. VLB120 was investigated under biofilm cultivation in capillary glass reactors at different flow regimes. Four phases could be observed for mixed-species biofilm growth in the glass-capillaries, which include biofilm growth in the single-phase flow condition, a rapid increase in biofilm spatial coverage after the start of air-segments, biofilm sloughing and detachment, and the final stage consisted of biofilm regrowth (Heuschkel et al. 2020).

When external shear forces become more substantial than the biofilm adhesive forces, sloughing and detachment events occur (Horn et al. 2003; Paul et al. 2012), which are phenomena considered to be an integral part of biofilm development (Rumbaugh and Sauer, 2020). Viscoelasticity can promote biofilm resistance when subjected to higher shear forces (Gloag et al. 2020), and this property is largely governed by EPS from the biofilm matrix (Peterson et al. 2021). Moreover, in photosynthetic organisms, the shear sensitivity is determined by cell morphology, the presence of flagella, and cell wall, which in cyanobacteria are mainly composed of peptidoglycan (Stanier and Cohen-Bazire 1977).

Our research group analyzed cyanobacterial biofilm architecture using two-dimensional (2D) and three-dimensional (3D) Optical Coherence Tomography (OCT) and revealed that more compact biofilm structures were formed at higher shear values (Romeu et al. 2019; 2020; 2021). On the contrary, the presence of 3D biofilm streamers, which contribute to the

COMPLIMENTARY COPY

formation of "sieve-like" networks that can capture cells and other biomass, contributing to biofilm development (Drescher et al. 2013), are more evident in cyanobacterial biofilms developed at lower shear values (Romeu et al. 2019; 2020; Faria et al. 2020a).

Surface

The first step in the biofouling process consists of finding a suitable surface, which for cyanobacteria in an aquatic environment is essential to form a biofilm and gain access to light and nutrients (Wetherbee et al. 1998; Rossi and De Philippis 2015). Surface association is considered a survival mechanism for microorganisms since it enhances organism interactions, access to nutritional resources, and environmental stability, which is of particular importance in natural ecosystems where conditions are highly dynamic and nutrients are growth limiting (Dang and Lovell 2016).

Numerous types of surfaces with distinct physicochemical properties exist in marine environments (Caruso 2020). These surfaces include living animals and plants or abiotic surfaces such as mineral substrata or submerged constructions. Different materials are used in marine submerged man-made equipment, like aquaculture facilities, underwater windows, sensors and measuring devices, protective equipment, swim platforms, ship and boat structures, and anchors, which are susceptible to biofouling. Common materials include glass, plastic, thermoplastics (e.g., acrylic, polyvinyl chloride, polystyrene, nylon, polypropylene), metallic materials (e.g., copper, steel, stainless steel, aluminum, titanium), foams (e.g., epoxy syntactic foam), and polymeric composite materials (e.g., fiber-reinforced plastics, wood, metal) (Roy 1994; Taylor 1996; King et al. 2006; Mansour and Liu 2008; Mohan 2008; Molland 2008; Summerscales 2014; Harper et al. 2015; Cai and Arias 2017). It has already been reported that the nature and characteristics of the surface where a biofilm develops have a strong influence on biofilm structure, differentiation, and function (von Ammon et al. 2018; Cai et al. 2019). Erosion and sloughing mechanisms in cyanobacterial biofilms can also be affected by the surface (Hoschek et al. 2019; Heuschkel et al. 2020). Indeed, sloughing events that occurred on glass (Heuschkel et al. 2020) were more significant than those that occurred on polystyrene (Hoschek et al. 2019). This finding could be related to the fact that biofilm cells were weakly adhered to glass compared to polystyrene, or glass biofilms became weaker with growth

COMPLIMENTARY COPY

due to nutrient starvation, oxidative stress, or a different stress response (Heuschkel et al. 2020).

Different approaches have been used to correlate bacterial adhesion with the physicochemical properties of surfaces. However, a detailed understanding of the mechanisms underlying cell-surface interactions is still not available. Although recent studies have attempted to replace macroscopic measurements for methods that directly measure cell-surface interaction forces by using, for example, atomic force microscopy, total internal reflection microscopy, quartz crystal microbalance, microbial adhesion to hydrocarbons (Bos et al. 1999; Li and Logan 2004; Tuson and Weibel 2013), contact angle measurements remain a commonly used, fast and economic method to determine the surface energy in the laboratory (Soon et al. 2013). Electrostatic, Lifshitz–van der Waals and Lewis acid-base interactions are usually considered responsible for the interactions at the surface interface. The thermodynamic approach refers to bacteria/surface interaction as an equilibrium process (Flemming et al. 2009). The ratio between Lifshitz-van der Waals apolar component and the electron donor component (γ^{LW}/γ^{-}) was shown to correlate with bacterial adhesion to the surfaces of ship hulls and heat exchangers (Liu and Zhao 2011). In a study performed by Liu and Zhao (2011), coatings with the lowest γ^{LW}/γ^{-} ratio had the lowest bacterial adhesion values. Understanding the thermodynamics of microbial adhesion is important since it helps to predict whether the adhesion of a given bacterium is favorable or not on different surfaces (Moreira et al. 2015). Moreover, knowing the physicochemical parameters of the surface, it is possible to develop new strategies that make the surface less prone to microbial adhesion.

Fouling organisms have mechanisms that allow them to colonize different surfaces, and studies relating to surface properties and marine fouling have been performed (von Ammon et al. 2018; Cai et al. 2019). The cyanobacterial biofilm studies performed under controlled hydrodynamic conditions and which evaluated the impact of different surfaces are shown in Table 4. Epoxy-coated glass and silicone hydrogel coating were effective in inhibiting coccoid cyanobacterial biofilm formation, also affecting its architecture (Faria et al. 2020a; 2020b; 2021a; 2021b). 2D OCT analyses performed on biofilms developed on the silicone hydrogel coating revealed that these biofilms had a lower percentage and size of empty spaces when compared to Perspex, polystyrene, glass, and epoxy-coated glass (Faria et al. 2021b). Additionally, biofilm structure was strongly affected by the cyanobacterial strain, regardless of the surface (Faria et al. 2021b). For example, a homogeneous arrangement and uniform layer closer to the surface were observed for *Synechocystis salina*

COMPLIMENTARY COPY

LEGE 00041, while for *Cyanobium* sp. LEGE 10375 the biofilm structure was more heterogeneous and the presence of 3D streamers on the biofilm top was observed for the same surface material (Figure 5). Epoxy and silicone hydrogel are two commercially available marine coatings for ship hulls, marine water inlet piping, and grids in power stations (Taylor 1996; Blain et al. 2004). Epoxy-coated glass surfaces were effective in inhibiting biofilm formation at the initial stages, while the silicone hydrogel coating showed high antibiofilm efficacy during biofilm maturation (Faria et al. 2020b). Silicone hydrogel surfaces used in that work are a third-generation hydrogel-based fouling-release coating that acquires a more hydrophilic behavior upon contact with water (Xie et al. 2011; Tulcidas et al. 2015). They are among the most successful marine antifouling coatings due to their high elasticity properties, along with the prevention of either hydrophobic or hydrophilic interactions, which delay the adsorption of proteins, bacteria, and subsequent fouling (Selim et al. 2017; Hu et al. 2020).

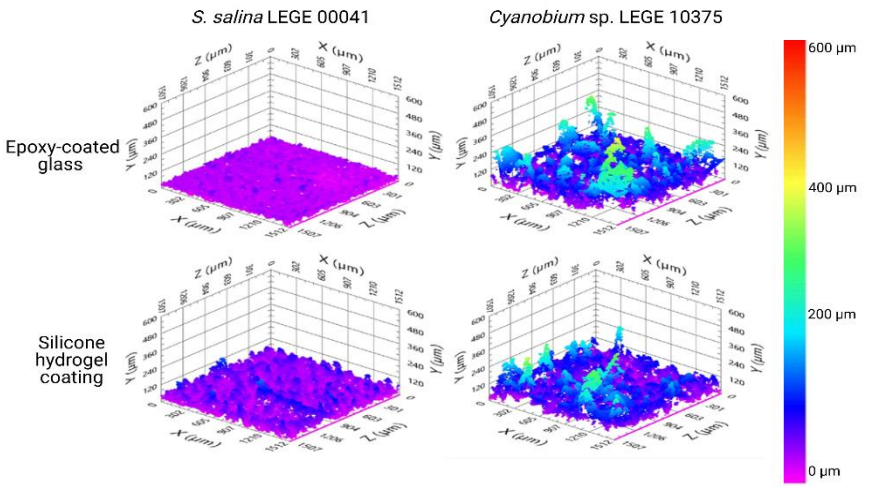

Figure 5. Representative 3D OCT images of *S. salina* LEGE 00041 and *Cyanobium* sp. LEGE 10375 biofilms formed on epoxy-coated glass and silicone hydrogel coatings after 7 weeks of *in vitro* incubation. The color scale shows the range of biofilm thickness. Adapted from Faria et al. 2021b.

COMPLIMENTARY COPY

Table 4. Cyanobacterial biofilm studies to evaluate the effect of different surfaces

Cyanobacterial form	Strains	Surface	Biofilm development time	Study aim	Main conclusions	Reference
Coccoid	*Cyanobium* sp. LEGE 10375 *Pseudoalteromonas tunicata* (marine bacterium)	Epoxy-coated glass Silicone hydrogel coating	7 weeks	Performance of different surfaces in inhibiting biofilm formation and their impact on biofilm structure	- Epoxy-coated glass surfaces were effective in inhibiting biofilm formation at the initial stages, while silicone hydrogel coating showed high antibiofilm efficacy during biofilm maturation - Biofilm wet weight, thickness, and CLSM analysis revealed that silicone hydrogel was less prone to biofilm formation - Efficacy of silicone hydrogel surfaces may be dependent on the fouling microorganism, while the performance of epoxy-coated glass was strongly influenced by a combined effect of surface and microorganism	Faria et al. 2020b
	Synechocystis salina LEGE 00041 *Cyanobium sp.* LEGE 06097	Glass Epoxy-coated glass	6 weeks	Analysis of different surfaces on adhesion and biofilm development from 24 h to 6 weeks	- Higher biofilm development was observed on glass - The antibiofilm performance of the epoxy-coated glass was confirmed at the hydrodynamic conditions prevailing in ports	Faria et al. 2020a
	Synechocystis salina LEGE 00041 *Cyanobium* sp. LEGE 06098 *Cyanobium* sp. LEGE 10375	Glass Perspex Polystyrene Epoxy-coated glass Silicone hydrogel coating	7 weeks	Performance of different surfaces in inhibiting biofilm formation and their impact on biofilm structure	- Silicone hydrogel coating was effective in inhibiting cyanobacterial biofilm formation - Cyanobacterial biofilms formed on silicone hydrogel coating showed a lower percentage and size of empty spaces among all tested surfaces	Faria et al. 2021b

COMPLIMENTARY COPY

COMPLIMENTARY COPY

Cyanobacterial form	Strains	Surface	Biofilm development time	Study aim	Main conclusions	Reference
Coccoid (cont.)	*Synechocystis salina* LEGE 00041 *Synechocystis salina* LEGE 06155 *Cyanobium* sp. LEGE 06097	Glass Epoxy-coated glass	Adhesion assays: 7.5 h Biofilm assays: 6 weeks	Potential of short-time adhesion assays on the estimation of biofilm development on different surfaces	- For both adhesion and biofilm assays, the number of adhered cells was higher on glass than on epoxy-coated glass - Higher biofilm development on glass was confirmed by biofilm wet weight, thickness, and chlorophyll *a* content values - Initial adhesion assays can be used to estimate marine biofilm development on different surfaces	Faria et al. 2021a
Filamentous	*Nodosilinea* sp. LEGE 06020 *Nodosilinea* sp. LEGE 06022 Unidentified filamentous Synechococcales LEGE 07185	Glass Perspex	7 weeks	Analysis of different surfaces on biofilm development over 7 weeks	- *Nodosilinea* sp. LEGE 06022 formed a higher amount of biofilm on Perspex. - In biofilms formed by *Nodosilinea* sp. LEGE 06020 or unidentified filamentous Synechococcales LEGE 07185, no significant differences were found between surfaces	Romeu et al. 2019
	Nodosilinea sp. LEGE 06145 *Nodosilinea* sp. LEGE 0611	Glass Perspex	7 weeks	Qualitative proteomic analyses of biofilms formed on different surfaces after 7 weeks	- In general, slight differences were found in biofilm development between surfaces - Higher biofilm formation was observed on glass when biofilms were formed at 4 s^{-1}, whereas at 40 s^{-1} higher biofilm formation was observed on Perspex - Qualitative proteomic analysis revealed that biofilms developed on different surfaces show differences in protein composition - Highly variable protein expression profile between cyanobacterial strains was observed	Romeu et al. 2020

COMPLIMENTARY COPY

Table 4. (Continued)

Cyanobacterial form	Strains	Surface	Biofilm development time	Study aim	Main conclusions	Reference
Filamentous (cont.)	Unidentified filamentous cyanobacterium LEGE 06007	Glass Perspex	7 weeks	Quantitative proteomic analyses of biofilms formed on different surfaces after 7 weeks	- In general, no significant differences were found in biofilm development between surfaces over 7 weeks - After 7 weeks, high biofilm thickness was observed in biofilms formed at 4 s^{-1} on glass when compared with those formed on Perspex - Differences in protein expression were more noticeable between biofilms formed on glass and Perspex at 4 s^{-1} than at 40 s^{-1} - Quantitative proteomic analysis revealed differentially expressed proteins between surfaces related to a beta-propeller domain-containing protein, chaperone DnaK, SLH domain-containing proteins, an OMF family outer membrane protein, and/or additional uncharacterized proteins	Romeu et al. 2021
	Leptolyngbya mycoidea LEGE 06118	Glass Perspex	3 weeks	Analysis of different surfaces on cyanobacterial biofilm development over 3 weeks	- Higher biofilm development was observed on Perspex - Biofilm wet weight on perspex was on average 50% higher than in glass	Romeu et al. 2016

Abbreviations: CLSM - confocal laser scanning microscopy, OMF - outer membrane factor, SLH – S-layer homology.

Laboratory studies performed on glass and perspex have shown quantitative differences between filamentous cyanobacterial biofilms developed on the two surfaces during 21 days (Romeu et al. 2016). However, when longer studies were carried out, the differences between surfaces were not so noticeable (Romeu et al. 2019; 2020; 2021). Indeed, when artificial substrates are compared, the effect of the material can be more relevant in the early stages of biofilm development (Zhang et al. 2014). In advanced stages of biofilm growth, differences appear to be more dependent on additional parameters such as hydrodynamic conditions (Catão et al. 2019; Romeu et al. 2019; 2020; 2021). Over a long period, the physicochemical properties of the surface can be modified due to exposure to seawater or microorganisms activity (Urbanek et al. 2018). Moreover, since the conditioning film formed on the fouling surface has a greater impact on initial bacterial adhesion and biofilm development, studies on new antifouling surfaces should take its influence into account.

Microbial Content

More than 4,000 biofouling species have been identified in marine environments (Yebra et al. 2004). The composition of biofouling communities changes significantly with the geographical location, season, and local depths, and is affected by several abiotic and biotic factors, as discussed before. Among biotic factors, the biology of the different organisms dictates how likely a settlement occurs on a submerged substratum (Vinagre et al. 2020). After the initial attachment of bacteria, surfaces get colonized by cyanobacteria, fungi, unicellular algae, and bacteria-eating protozoa. In the absence of high shear forces, such biofilm communities can grow extensive mats or slimes (Matz 2011). The close spatial proximity of these microorganisms at surfaces is responsible for specific interspecies interactions (competition or cooperation) and generates complex and highly differentiated microbial communities (Guillonneau et al. 2018).

In the case of cyanobacteria, they are usually found in biofilms from a particular tidal level (Qian et al. 2007) and such specificity may be associated with the differential larval settlement observed by some authors (Morse et al. 1984; Lee et al. 2014). It has been reported that cyanobacteria induce larval settlement of molluscs (Morse et al. 1984); however, their ability to induce or inhibit the larval settlement of barnacles has not been studied in detail (Morse et al. 1984). Therefore, certain microorganisms in marine biofilms, such as

COMPLIMENTARY COPY

cyanobacteria and proteobacteria, might have an essential role in larval settlement preference (Lee et al. 2014), and further studies focusing on these candidates would definitely be valuable.

As most biofilm communities are composed of multiple different organisms living in close proximity, it is intuitive that the microbial composition plays a major role in surface colonization and should probably be considered when evaluating the performance of novel antifouling surfaces. Nevertheless, numerous difficulties exist in studying mixed biofilms at a laboratory scale: (i) the lack of knowledge regarding the identity and abundance of each biofilm resident, which makes it difficult to select the organisms and their initial concentration for the *in vitro* assays, (ii) labeling the different populations, in particular when they are not amenable to genetic manipulations, (iii) identifying which metabolites can be produced and by who, interpreting why one strain is more fit than another, and (iv) some technical limitations associated with biofilm reactors (Guillonneau et al. 2018; Faria et al. 2021c). As a result, very limited information is available on multispecies biofilms and their microhabitats in aquatic scenarios (Rao et al. 2005; Burmølle et al. 2006, Guillonneau et al. 2018). To the best of our knowledge, only two studies dealt with marine bacterial isolates (Burmølle et al. 2006, Guillonneau et al. 2018). A recent work from our research group (Faria et al. 2021c) discusses exactly the relevance of using mixed populations instead of single cultures for *in vitro* screening assays of marine antifouling materials. Single and dual-species biofilms of a marine bacterium (*Pseudoalteromonas tunicata*) and a coccoid cyanobacterium (*Cyanobium* sp. LEGE 10375) were grown for 49 days on an epoxy resin with known antifouling activity (Faria et al. 2020a). Whereas *P. tunicata* alone showed a biofilm growth kinetics similar to mixed biofilms, cyanobacterial biofilms presented a higher number of cells, wet weight, thickness, and biovolume when compared to dual-species biofilms (Faria et al. 2021c). Indeed, *Cyanobium* sp. LEGE 10375 biofilms corresponded to the worst-case scenario, i.e., the conditions that originated higher biofilm amounts on the tested surface (Faria et al. 2021c). These results suggest that for initial screening, starting with a single representative organism like a cyanobacterium is a good compromise between the high complexity of *in vivo* marine ecosystems and the ease of *in vitro* testing.

COMPLIMENTARY COPY

Marine Antifouling Strategies

Marine biofouling has been an emerging issue and several approaches have been used to deal with this serious concern. Antifouling paints were the initial strategy used to manage the impact of marine biofouling (Bosselmann 1996; Evans 1999). Copper, arsenic, zinc, tin, and mercury coatings were commonly used until their toxicity on the surrounding marine environment was demonstrated (Callow and Callow 2002; Sonak et al. 2009; Sonak 2009). Advances in novel and effective environmentally friendly coatings are needed to control marine fouling. Numerous strategies to prevent biofilm formation or control established biofilms have been developed (Nurioglu et al. 2015; Silva et al. 2019; Mishra et al. 2020). The use of natural compounds with antifouling activity such as quorum sensing inhibitors, phytochemicals, antimicrobial peptides, bacteriophages, or specific enzymes which degrade adhesives used for settlement, disrupt the biofilm matrix, or interfere with intercellular communication, are under investigation and some of them can be incorporated on surfaces (Dobretsov et al. 2007; Kristensen et al. 2008; Fusetani 2011; Carvalho 2012; Dobretsov et al. 2013; Almeida and Vasconcelos 2015; Michailidis et al. 2020). Although some of these compounds can be obtained from marine organisms, including cyanobacteria (Almeida et al. 2015; Antunes et al. 2019), they need to be produced in significant amounts to be incorporated into surface materials, which carries technical and economic challenges.

Modifications of surface charge potential, hydrophobicity, and surface topography (Scardino et al. 2008; Schumacher et al. 2008) are also promising strategies. For example, graphene-coated materials can affect the surface energy and electrostatic interactions between material and bacteria (Parra et al. 2015; Jin et al. 2019; 2021; Zhang et al. 2021). Superhydrophobic surfaces, which present a high water contact angle, typically > 150°, have also been tested as improvements for marine surfaces (Scardino et al. 2009; Ferrari et al. 2015; Selim et al. 2018). A study performed by Scardino et al. (2009) reported three superhydrophobic coatings that inhibited the attachment of spores of algae and larvae of several invertebrates. Furthermore, studies performed by Ellinas et al. (2017) and Kefallinou et al. (2020) described “hybrid” metal-sputtered superhydrophobic surfaces demonstrating both bacterial repulsion and long-term killing efficacy against the cyanobacteria *Synechococcus* sp. PCC7942. Among the two low surface energy hydrophobic coatings used, a chlorosilane and a fluorocarbon coating, the fluorocarbon layer managed to better secure the superhydrophobicity and anti-adhesiveness of the surface

COMPLIMENTARY COPY

when enriched with an adequate amount of copper (Kefallinou et al. 2020). These bifunctional surfaces with both antifouling and bactericidal action can be a promising strategy to manage marine biofouling.

Overall, to manage environmental concerns associated with marine fouling and comply with the increasingly strict and demanding legislation in this area, solutions to the development of a new generation of environmentally friendly marine coatings are required. Improvements in nanotechnology, polymer science, and the development of innovative surface models inspired by nature, are expected to have a significant impact on the progress of antifouling methodologies. Moreover, the application of "omics" technologies to marine biofilm studies is an emerging approach that can help to identify pathways evolved on adhesion, attachment, and biofilm formation, and consequently, contribute to novel improvements in marine antifouling strategies (Romeu et al. 2020; 2021). However, genetic and "omic" studies in cyanobacteria and their processes are still limited. Also, not all novel antifouling strategies are technically and/or economically feasible at a large scale. Although biofouling is an ongoing concern for the marine industry, environmental managers and marine scientists, their motivations and approaches to tackling it are very diverse among sectors (Davidson et al. 2016).

Conclusion

The complexity of marine environments due to temperature and population variation, seawater composition, light propagation, and dynamic flux is such that laboratory analysis of marine biofouling is challenging. A promising approach to delay macrofouling is to prevent the adhesion and biofilm development by cyanobacteria since they are responsible for the initiation of biofilm formation and excrete large amounts of EPS. Although useful for understanding which parameters drive marine biofilm development, few studies focus on multiple factors evaluation, especially using coccoid and filamentous cyanobacterial biofilms. Analyses on the influence of hydrodynamics, surface, and microbial content on cyanobacterial biofilms showed that the impact of hydrodynamics on biofilm development is generally stronger than the impact of surface hydrophobicity. Furthermore, a combined effect of these two parameters strongly depends on biofilm-producing organisms. Multidisciplinary biofilm analyses are required to evaluate the complex phenomenon of marine biofilm development.

COMPLIMENTARY COPY

Acknowledgments

This work was financially supported by: LA/P/0045/2020 (ALiCE), UIDB/00511/2020, and UIDP/00511/2020 (LEPABE), funded by national funds through the FCT/MCTES (PIDDAC), project HealthyWaters (NORTE-01-0145-FEDER-000069), supported by Norte Portugal Regional Operational Programme (NORTE 2020), under the PORTUGAL 2020 Partnership Agreement, through the European Regional Development Fund (ERDF). M.J.R. acknowledges a PhD grant from FCT (SFRH/BD/140080/2018). L.C.G. thanks FCT for the financial support of her work contract through the Scientific Employment Stimulus—Individual Call—[CEECIND/01700/2017]. R.T.-S. acknowledges the receipt of a junior researcher fellowship from the Project PTDC/BII-BIO/29589/2017—POCI-01-0145-FEDER-029589—funded by FEDER funds through COMPETE2020—Programa Operacional Competitividade e Internacionalização (POCI) and by national funds (PIDDAC) through FCT/MCTES.

References

Abbott A, Abel PD, Arnold DW, Milne A (2000) Cost–benefit analysis of the use of TBT: the case for a treatment approach. *Sci Total Environ* 258(1): 5–19.

Abdallah M, Benoliel C, Drider D, Dhulster P, Chihib NE (2014) Biofilm formation and persistence on abiotic surfaces in the context of food and medical environments. *Arch Microbiol* 196(7): 453–472.

Abed RMM, Dobretsov S, Sudesh K (2009) Applications of cyanobacteria in biotechnology. *J Appl Microbiol* 106(1): 1–12.

Aldred N, Clare AS (2014) Mini-review: impact and dynamics of surface fouling by solitary and compound ascidians. *Biofouling* 30(3): 259–270.

Alles M, Rosenhahn A (2015) Microfluidic detachment assay to probe the adhesion strength of diatoms. *Biofouling* 31(5): 469-480.

Almeida JR, Freitas M, Cruz S, Leão PN, Vasconcelos V, Cunha I (2015) Acetylcholinesterase in biofouling species: characterization and mode of action of cyanobacteria-derived antifouling agents. *Toxins* 7(8): 2739–2756.

Almeida JR, Vasconcelos V (2015) Natural antifouling compounds: effectiveness in preventing invertebrate settlement and adhesion. *Biotechnol Adv* 33(3–4): 343–357.

Alves P, Gomes LC, Vorobii M, Rodriguez-Emmenegger C, Mergulhao FJ (2020) The potential advantages of using a poly(HPMA) brush in urinary catheters: effects on biofilm cells and architecture. *Colloid Surface B* 191: 110976.

Amin SA, Parker MS, Armbrust EV (2012) Interactions between diatoms and bacteria. *Microbiol Mol Biol Rev* 76(3): 667–684.

COMPLIMENTARY COPY

Anderson O (2016) Marine and estuarine natural microbial biofilms: ecological and biogeochemical dimensions. *AIMS Microbiol* 2(3): 304–331.

Antunes J, Pereira S, Ribeiro T, Plowman JE, Thomas A, Clerens S, Campos A, Vasconcelos V, Almeida JR (2019) A multi-bioassay integrated approach to assess the antifouling potential of the cyanobacterial metabolites portoamides. *Mar Drugs* 17(2): 1–19.

Azevedo J, Antunes JT, Machado AM, Vasconcelos V, Leão PN, Froufe E (2020) Monitoring of biofouling communities in a Portuguese port using a combined morphological and metabarcoding approach. *Sci Rep*10:13461.

Bakker DP, Plaats A Van Der, Verkerke GJ, Busscher HJ, Mei HC Van Der (2003) Comparison of velocity profiles for different flow chamber designs used in studies of microbial adhesion to surfaces. *Appl Environ Microbiol* 69(10): 6280–6287.

Bannister J, Sievers M, Bush F, Bloecher N (2019) Biofouling in marine aquaculture: a review of recent research and developments. *Biofouling* 35(6): 631–648.

Behrendt L, Schrameyer V, Qvortrup K, Lundin L, Sørensen SJ, Larkum AWD, Kühl M (2012) Biofilm growth and near-infrared radiation-driven photosynthesis of the chlorophyll d-containing cyanobacterium *Acaryochloris marina*. *Appl Environ Microbiol* 78(11): 3896–3904.

Berg M, Sutula M (2015) Factors affecting the growth of cyanobacteria with special emphasis on the Sacramento-San Joaquin Delta. Southern California Coastal Water Research Project, Technical Report 869 August 2015.

Bharti A, Velmourougane K, Prasanna R (2017) Phototrophic biofilms: diversity, ecology and applications. *J Appl Phycol* 29(6): 2729–2744.

Blain S, Guillou J, Tréguer P, Woerther P, Delauney L, Follenfant E, Gontier O, Hamon M, Leildé B, Masson A, et al. (2004) High frequency monitoring of the coastal marine environment using the MAREL buoy. *J Environ Monit* 6: 569–575.

Bos R, van der Mei HC, Busscher HJ (1999) Physico-chemistry of initial microbial adhesive interactions – its mechanisms and methods for study. *FEMS Microbiol Rev* 23(2): 179–230.

Bosselmann K (1996) Environmental law and tributyltin in the environment. In: de Mora SJ editor. Tributyltin: Case study of an environmental contaminant: Cambridge University Press, Cambridge, pp. 237–263.

Breinlinger S, Phillips TJ, Haram BN, Mareš J, Martínez Yerena JA, Hrouzek P, Sobotka R, Henderson WM, Schmieder P, Williams SM, et al. (2021) Hunting the eagle killer: A cyanobacterial neurotoxin causes vacuolar myelinopathy. *Science* (80): 371(6536).

Briand J-F, Djeridi I, Jamet D, Coupé S, Bressy C, Molmeret M, Le Berre B, Rimet F, Bouchez A, Blache Y (2012) Pioneer marine biofilms on artificial surfaces including antifouling coatings immersed in two contrasting French Mediterranean coast sites. *Biofouling* 28(5): 453–463.

Brown NEM, Milazzo M, Rastrick SPS, Hall-Spencer JM, Therriault TW, Harley CDG (2018) Natural acidification changes the timing and rate of succession, alters community structure, and increases homogeneity in marine biofouling communities. *Glob Chang Biol.* 24(1): e112–e127.

COMPLIMENTARY COPY

Buratti FM, Manganelli M, Vichi S, Stefanelli M, Scardala S, Testai E, Funari E (2017) Cyanotoxins: producing organisms, occurrence, toxicity, mechanism of action and human health toxicological risk evaluation. *Arch Toxicol* 91(3): 1049–1130.

Burmølle M, Webb JS, Rao D, Hansen LH, Sørensen SJ, Kjelleberg S (2006) Enhanced biofilm formation and increased resistance to antimicrobial agents and bacterial invasion are caused by synergistic interactions in multispecies biofilms. *Appl Environ Microbiol* 72(6): 3916-3923.

Cai L, Wu D, Xia J, Shi H, Kim H (2019) Influence of physicochemical surface properties on the adhesion of bacteria onto four types of plastics. *Sci Total Environ* 671: 1101-1107.

Cai W, Arias CR (2017) Biofilm formation on aquaculture substrates by selected bacterial fish pathogens. *J Aquat Anim Heal* 29: 95–104.

Callow ME, Callow JA (2002) Marine biofouling: A sticky problem. *Biologist* 49(1): 10–14.

Campbell AH, Meritt DW, Franklin RB, Boone EL, Nicely CT, Brown BL (2011) Effects of age and composition of field-produced biofilms on oyster larval setting. *Biofouling* 27(3): 255–265.

Cao S, Wang J, Chen H, Chen D (2011) Progress of marine biofouling and antifouling technologies. *Chinese Sci Bull* 56(7): 598–612.

Caruso G (2020) Microbial colonization in marine environments: Overview of current knowledge and emerging research topics. *J Mar Sci Eng* 8(2): 1–22.

Carvalho CCCR de (2012) Biofilms: New ideas for an old problem. *Recent Pat Biotechnol* 6(1): 13–22.

Catão ECP, Pollet T, Misson B, Garnier C, Ghiglione J-F, Barry-Martinet R, Maintenay M, Bressy C, Briand J-F (2019) Shear stress as a major driver of marine biofilm communities in the NW Mediterranean Sea. *Front Microbiol* 10(7): 1–16.

Champ MA (2000) A review of organotin regulatory strategies, pending actions, related costs and benefits. *Sci Total Environ* 258(1): 21–71.

Chung HC, Lee OO, Huang Y-L, Mok SY, Kolter R, Qian P-Y (2010) Bacterial community succession and chemical profiles of subtidal biofilms in relation to larval settlement of the polychaete *Hydroides elegans*. *ISME J* 4(6): 817–828.

Claessen D, Rozen DE, Kuipers OP, Søgaard-Andersen L, van Wezel GP (2014) Bacterial solutions to multicellularity: a tale of biofilms, filaments and fruiting bodies. *Nat Rev Microbiol.* 12(2): 115–124.

Dang H, Lovell CR (2000) Bacterial primary colonization and early succession on surfaces in marine waters as determined by amplified rRNA gene restriction analysis and sequence analysis of 16S rRNA genes. *Appl Environ Microbiol* 66(2): 467–475.

Dang H, Lovell CR (2016) Microbial surface colonization and biofilm development in marine environments. *Microbiol Mol Biol Rev* 80(1): 91–138.

David C, Bühler K, Schmid A (2015) Stabilization of single species *Synechocystis* biofilms by cultivation under segmented flow. *J Ind Microbiol Biotechnol* 42(7): 1083-9.

Davidson I, Scianni C, Hewitt C, Everett R, Holm E, Tamburri M, Ruiz G (2016) Mini-review: Assessing the drivers of ship biofouling management – aligning industry and biosecurity goals. *Biofouling* 32(4): 411–428.

COMPLIMENTARY COPY

Davidson IC, Brown CW, Sytsma MD, Ruiz GM (2009) The role of containerships as transfer mechanisms of marine biofouling species. *Biofouling* 25(7): 645–655.

Decho AW, Gutierrez T (2017) Microbial extracellular polymeric substances (EPSs) in ocean systems. *Front Microbiol* 8(5): 1–28.

Delauney L, Compare C, Lehaitre M (2010) Biofouling protection for marine environmental sensors. *Ocean Sci* 6(2): 503–511.

Demirel YK, Uzun D, Zhang Y, Fang HC, Day AH, Turan O (2017) Effect of barnacle fouling on ship resistance and powering. *Biofouling* 33(10): 819–834.

Dobretsov S, Abed RMM, Teplitski M (2013) Mini-review: Inhibition of biofouling by marine microorganisms. *Biofouling* 29(4): 423–41.

Dobretsov S, Teplitski M, Paul V (2009) Mini-review: quorum sensing in the marine environment and its relationship to biofouling. *Biofouling* 25(5): 413–27.

Dobretsov S, Xiong H, Xu Y, Levin LA, Qian PY (2007) Novel antifoulants: inhibition of larval attachment by proteases. *Mar Biotechnol* 9(3): 388–397.

Di Donato P, Poli A, Taurisano V, Abbamondi GR, Nicolaus B, Tommonaro G (2016) Recent advances in the study of marine microbial biofilm: From the involvement of quorum sensing in its production up to biotechnological application of the polysaccharide fractions. *J Mar Sci Eng* 4(2).

Drescher K, Shen Y, Bassler BL, Stone HA (2013) Biofilm streamers cause catastrophic disruption of flow with consequences for environmental and medical systems. *Proc Natl Acad Sci USA* 110(11): 4345–50.

Ellinas K, Kefallinou D, Stamatakis K, Gogolides E, Tserepi A (2017) Is there a threshold in the antibacterial action of superhydrophobic surfaces? *ACS Appl Mater Interfaces* 9: 39781–39789.

Evans SM (1999) TBT or not TBT? That is the question. *Biofouling* 14(2): 117–129.

Faria SI, Teixeira-Santos R, Gomes LC, Silva ER, Morais J, Vasconcelos V, Mergulhão FJM (2020b) Experimental assessment of the performance of two marine coatings to curb biofilm formation of microfoulers. *Coatings* 10(9).

Faria SI, Teixeira-Santos R, Morais J, Vasconcelos V, Mergulhão FJ (2021a) The association between initial adhesion and cyanobacterial biofilm development. *FEMS Microbiol Ecol* 97: 5.

Faria SI, Teixeira-Santos R, Romeu MJ, Morais J, Jong E de, Sjollema J, Vasconcelos V, Mergulhão FJ (2021b) Unveiling the antifouling performance of different marine surfaces and their effect on the development and structure of cyanobacterial biofilms. *Microorganisms* 9(5).

Faria SI, Teixeira-Santos R, Romeu MJ, Morais J, Vasconcelos V, Mergulhão FJ (2020a) The relative importance of shear forces and surface hydrophobicity on biofilm formation by coccoid cyanobacteria. *Polymers* 12(3): 653.

Faria SI, Gomes LC, Teixeira-Santos R, Morais J, Vasconcelos V, Mergulhão FJM (2021c) Developing new marine antifouling surfaces: learning from single-strain laboratory tests. *Coatings* 11(1): 1–11.

Fernandes JA, Santos L, Vance T, Fileman T, Smith D, Bishop JDD, Viard F, Queirós AM, Merino G, Buisman E, Austen MC (2016) Costs and benefits to European shipping of ballast-water and hull-fouling treatment: impacts of native and non-indigenous species. *Mar Polic*64: 148–155.

COMPLIMENTARY COPY

Ferrari M, Benedetti A, Santini E, Ravera F, Liggieri L, Guzman E, Cirisano F (2015) Biofouling control by superhydrophobic surfaces in shallow euphotic seawater. *Colloids Surfaces A Physicochem Eng Asp* 480:369–375.

Fitridge I, Dempster T, Guenther J, de Nys R (2012) The impact and control of biofouling in marine aquaculture: a review. *Biofouling* 28(7): 649–69.

Flemming HC, Murthy PS, Venkatesan R, Cooksey K (2009) *Marine and Industrial Biofouling*. Costerton JW, editor. Springer Berlin Heidelberg, Los Angeles, USA.

Flemming HC, Wingender J (2010) The biofilm matrix. *Nat Rev Microbiol* 8(9): 623–33.

Flemming HC, Wingender J, Szewzyk U, Steinberg P, Rice SA, Kjelleberg S (2016) Biofilms: An emergent form of bacterial life. *Nat Rev Microbiol* 14(9): 563–575.

Foster RA, Kuypers MMM, Vagner T, Paerl RW, Musat N, Zehr JP (2011) Nitrogen fixation and transfer in open ocean diatom-cyanobacterial symbioses. *ISME J* 5(9): 1484–1493.

Fusetani N (2011) Antifouling marine natural products. *Nat Prod Rep* 28(2): 400–410.

Gambino M, Sanmartín P, Longoni M, Villa F, Mitchell R, Cappitelli F (2019) Surface colour: An overlooked aspect in the study of cyanobacterial biofilm formation. *Sci Total Environ* 659: 342–353.

Giakoumi S, Katsanevakis S, Albano PG, Azzurro E, Cardoso AC, Cebrian E, Deidun A, Edelist D, Francour P, Jimenez C, Mačić V, Occhipinti-Ambrogi A, Rilov G, Sghaier YR (2019) Management priorities for marine invasive species. *Sci Total Environ* 20: 976-982.

Gibble CM, Peacock MB, Kudela RM (2016) Evidence of freshwater algal toxins in marine shellfish: Implications for human and aquatic health. *Harmful Algae* 59: 59–66.

Gloag ES, Fabbri S, Wozniak DJ, Stoodley P (2020) Biofilm mechanics: implications in infection and survival. *Biofilm* 2:100017.

Godwin LS (2003) Hull fouling of maritime vessels as a pathway for marine species invasions to the Hawaiian Islands. *Biofouling* 19: 123–132.

Gomes LC, Miranda J, Mergulhão FJ (2019) Operation of biofilm reactors for the food industry using CFD. In: Sun DW editor. Computational fluid dynamics in food processing: CRC Press, New York, pp. 561-590.

Gomes LC, Moreira JMR, Araújo JDP, Mergulhão FJ (2017) Surface conditioning with *Escherichia coli* cell wall components can reduce biofilm formation by decreasing initial adhesion. *AIMS Microbiol* 18(3): 613-6280.

Guillonneau R, Baraquet C, Bazire A, Molmeret M (2018) Multispecies biofilm development of marine bacteria implies complex relationships through competition and synergy and modification of matrix components. *Front Microbiol* 9: 1960.

Hammer BK, Bassler BL (2003) Quorum sensing controls biofilm formation in *Vibrio cholerae*. *Mol Microbiol* 50: 101–104.

Harper P, Hallett S, Fleming A, Dawson M (2016) Advanced fibre-reinforced composites for marine renewable energy device. In: Graham-Jones J, Summerscales J, Editors. *Marine Applications of Advanced Fibre-Reinforced Composites*: Woodhead Publishing, pp. 217-232.

Hewitt CL, Gollasch S, Minchin D (2009) The vessel as a vector – Biofouling, ballast water and sediments. In: Rilov G, Crooks JA, Editors. *Biological Invasions in Marine Ecosystems, Ecological Studies:* Springer-Verlag, Heidelberg, pp. 117–131.

COMPLIMENTARY COPY

Heuschkel I, Dagini R, Karande R, Bühler K (2020) The impact of glass material on growth and biocatalytic performance of mixed-species biofilms in capillary reactors for continuous cyclohexanol production. *Front Bioeng Biotechnol* 15(8): 588729.

Hoang H, Gurich N, González J (2008) Regulation of motility by the ExpR/Sin quorum-sensing system in *Sinorhizobium meliloti. J Bacteriol* 190(3): 861–871.

Hodson SL, Burke CM, Bissett AP (2000) Biofouling of fish-cage netting: The efficacy of a silicone coating and the effect of netting colour. *Aquaculture* 184(3–4): 277–290.

Horn H, Reiff H, Morgenroth E (2003) Simulation of growth and detachment in biofilm systems under defined hydrodynamic conditions. *Biotechnol Bioeng* 81(5): 607–617.

Hoschek A, Heuschkel I, Schmid A, Bühler B, Karande R, Bühler K (2019) Mixed-species biofilms for high-cell-density application of *Synechocystis* sp. PCC 6803 in capillary reactors for continuous cyclohexane oxidation to cyclohexanol. *Bioresour Technol* 282: 171–178.

Hu P, Xie Q, Ma C, Zhang, G (2020) Silicone-based fouling-release coatings for marine antifouling. *Langmuir* 36: 2170–2183.

Huisman J, Codd GA, Paerl HW, Ibelings BW, Verspagen JMH, Visser PM (2018) Cyanobacterial blooms. *Nat Rev Microbiol* 16(8): 471–483.

Hunsucker KZ, Vora GJ, Hunsucker JT, Gardner H, Leary DH, Kim S, Lin B, Swain G (2018) Biofilm community structure and the associated drag penalties of a groomed fouling release ship hull coating. *Biofouling* 34(2): 162–172.

IUCN (2018) *Guidelines for Invasive Species Planning and Management on Islands*. Cambridge, UK and Gland, Switzerland: IUCN. viii + 40pp.

Jiang P, Zhao S, Zhu L, Li D (2018) Microplastic-associated bacterial assemblages in the intertidal zone of the Yangtze Estuary. *Sci Total Environ* 624: 48–54.

Jin H, Bing W, Tian L, Wang P, Zhao J (2019) Combined effects of color and elastic modulus on antifouling performance: A study of graphene oxide/silicone rubber composite membranes. *Materials* 12(16): 2608.

Jin H, Tian L, Bing W, Zhao J, Ren L (2021) Toward the application of graphene for combating marine biofouling. *Adv Sustainable Syst* 5: 2000076.

Jones PR, Cottrell MT, Kirchman DL, Dexter SC (2007) Bacterial community structure of biofilms on artificial surfaces in an estuary. *Microb Ecol* 53(1): 153–162.

Kefallinou D. Ellinas K, Speliotis T, Stamatakis K, Gogolides E, Tserepi A (2020) Optimization of antibacterial properties of "hybrid" metal-sputtered superhydrophobic surfaces. *Coatings* 10: 25.

Keith I, Dawson TP, KJ Collins, KJ, Campbell ML (2016) Marine invasive 3 species: establishing pathways, their presence and potential threats in the 4 Galapagos Marine Reserve. *Pac Conserv Biol* 22(4): 377-385.

King RK, Flick GJ, Smith SA, Pierson MD, Boardman, GD, Coale CW (2006) Comparison of bacterial presence in biofilms on different materials commonly found in recirculating aquaculture systems. *J Appl Aquaculture* 18: 79–88.

Kristensen JB, Meyer RL, Laursen BS, Shipovskov S, Besenbacher F, Poulsen CH (2008) Antifouling enzymes and the biochemistry of marine settlement. *Biotechnol Adv* 26(5): 471–481.

COMPLIMENTARY COPY

Ku C, Nelson-Sathi S, Roettger M, Sousa FL, Lockhart PJ, Bryant D, Hazkani-Covo E, McInerney JO, Landan G, Martin WF (2015) Endosymbiotic origin and differential loss of eukaryotic genes. *Nature* 524(7566): 427–432.

Lagos ME, White CR, Marshall DJ (2016) Biofilm history and oxygen availability interact to affect habitat selection in a marine invertebrate. *Biofouling* 32(6): 645–655.

Lau SCK, Thiyagarajan V, Cheung SCK, Qian P (2005) Roles of bacterial community composition in biofilms as a mediator for larval settlement of three marine invertebrates. *Aquat Microb Ecol* 38: 41–51.

Lee J-W, Nam J-H, Kim Y-H, Lee K-H, Lee D-H (2008) Bacterial communities in the initial stage of marine biofilm formation on artificial surfaces. *J Microbiol* 46(2): 174–182.

Lee OO, Chung HC, Yang J, Wang Y, Dash S, Wang H, Qian P-Y (2014) Molecular techniques revealed highly diverse microbial communities in natural marine biofilms on polystyrene dishes for invertebrate larval settlement. *Microb Ecol* 68: 81–93.

Li X, Logan BE (2004) Analysis of bacterial adhesion using a gradient force analysis method and colloid probe atomic force microscopy. *Langmuir* 20(20): 8817–8822.

Limoli DH, Jones CJ, Wozniak DJ (2015) Bacterial extracellular polysaccharides in biofilm formation and function. *Microbiol Spectrum* 3(3): MB-0011-2014.

Liu C, Zhao Q (2011) Influence of surface-energy components of Ni-P-TiO2-PTFE nanocomposite coatings on bacterial adhesion. *Langmuir* 27(15): 9512–9519.

Lyons TW, Reinhard CT, Planavsky NJ (2014) The rise of oxygen in Earth's early ocean and atmosphere. *Nature* 506(7488): 307–315.

Maddah H, Chogle A (2017) Biofouling in reverse osmosis: phenomena, monitoring, controlling and remediation. *Appl Water Sci* 7(6): 2637–2651.

Mansour AE, Liu J, Paulling R (2008) Strength of ships and ocean structures. Society of Naval Architects and Marine Engineers: Jersey City, NJ.

Marshall KC, Stout R, Mitchell R (1971) Mechanism of the initial events in the sorption of marine bacteria to surfaces. *J Gen Microbiol* 68: 337–348.

Matz C (2011) Competition, communication, cooperation: molecular crosstalk in multispecies biofilms. In: Flemming HC, Wingender J, Szewzyk U, editors. *Biofilm Highlights*: Springer Series on Biofilms, Berlin, Heidelberg.

McDougald D, Rice S, Barraud N, Steinberg PD, Kjelleberg S (2012) Should we stay or should we go: mechanisms and ecological consequences for biofilm dispersal. *Nat Rev Microbiol* 10: 39–50.

Michailidis M, Gutner-Hoch E, Wengier R, Onderwater R, D'Sa RA, Benayahu Y, Semenov A, Vinokurov V, Shchukin DG (2020) Highly effective functionalized coatings with antibacterial and antifouling properties. *ACS Sustain Chem Eng* 8(24): 8928–8937.

Mieszkin S, Callow ME, Callow JA (2013) Interactions between microbial biofilms and marine fouling algae: a mini review. *Biofouling* 29(9): 1097–113.

Mieszkin S, Martin-Tanchereau P, Callow ME, Callow JA (2012) Effect of bacterial biofilms formed on fouling-release coatings from natural seawater and *Cobetia marina*, on the adhesion of two marine algae. *Biofouling* 28(9): 953–68.

COMPLIMENTARY COPY

Miller MA, Kudela RM, Mekebri A, Crane D, Oates SC, Tinker MT, Staedler M, Miller WA, Toy-Choutka S, Dominik C, et al. (2010) Evidence for a novel marine harmful algal bloom: Cyanotoxin (microcystin) transfer from land to sea otters. *PLoS One* 5(9): 1–11.

Minchin D, Gollasch S (2003) Fouling and ships' hulls: How changing circumstances and spawning events may result in the spread of exotic species. *Biofouling* 19(4): 111–122.

Mishra R, Panda AK, De Mandal S, Shakeel M, Bisht SS, Khan J (2020) Natural anti-biofilm agents: strategies to control biofilm-forming pathogens. *Front Microbiol* 11: 2640.

Mitbavkar S, Raghu C, Rajaneesh KM, Pavan D (2012) Picophytoplankton community from tropical marine biofilms. *J Exp Mar Bio Ecol* 426–427: 88–96.

Mohan M (2008) The advantages of composite material in marine renewable energy devices, Marine Renewable Energy Conference, RINA.

Molland AF (2008) The maritime engineering reference book: a guide to ship design, construction and operation. Butterworth-Heinemann, Amsterdam.

Moreira JMR, Simões M, Melo LF, Mergulhão FJ (2015) *Escherichia coli* adhesion to surfaces – a thermodynamic assessment. *Colloid Polym Sci* 293: 177–185.

Morse A, Froyd C, Morse D (1984) Molecules from cyanobacteria and red algae that induce larval settlement and metamorphosis in the mollusc *Haliotis rufescens. Mar Biol* 81:293–298.

Muhammad MH, Idris AL, Fan X, Guo Y, Yu Y, Jin X, Qiu J, Guan X, Huang T (2020) Beyond risk: bacterial biofilms and their regulating approaches. *Front Microbiol* 11(5): 1–20.

Mullineaux CW (2014) Co-existence of photosynthetic and respiratory activities in cyanobacterial thylakoid membranes. *Biochim Biophys Acta* 1837(4): 503–511.

Myers JL, Sekar R, Richardson LL (2007) Molecular detection and ecological significance of the cyanobacterial genera *Geitlerinema* and *Leptolyngbya* in Black Band Disease of corals. *Appl Environ Microbiol* 73(16): 5173–5182.

Nagarkar S, Williams GA, Subramanian G, Saha SK (2004) Cyanobacteria-dominated biofilms: a high quality food resource for intertidal grazers. In: Ang PO, Editor. *Asian Pacific phycology in the 21st century: prospects and challenges*. Developments in Hydrobiology: Springer, Dordrecht, pp. 89-95.

Narváez-Zapata J, Tebbe CC, Ortega-Morales BO (2005) Molecular diversity and biomass of epilithic biofilms from intertidal rocky shores in the Gulf of Mexico. *Biofilms* 2(2): 93–103.

Nayar S, Goh BPL, Chou LM (2005) Settlement of marine periphytic algae in a tropical estuary. *Estuar Coast Shelf Sci* 64(2–3): 241–248.

Nichols CM, Guezennec J, Bowman J (2005) Bacterial exopolysaccharides from extreme marine environments with special consideration of the Southern Ocean, Sea Ice, and Deep-Sea Hydrothermal Vents: a review. *Mar Biotechnol* 7: 253–271.

Nolte KA, Schwarze J, Rosenhahn A. Microfluidic accumulation assay probes attachment of biofilm forming diatom cells (2017) *Biofouling* 33(7): 531-543.

COMPLIMENTARY COPY

Nurioglu AG, Esteves ACC, De With G (2015) Non-toxic, non-biocide-release antifouling coatings based on molecular structure design for marine applications. *J Mater Chem B* 3(32): 6547–6570.

Oberbeckmann S, Loeder MGJ, Gerdts G, Osborn MA (2014) Spatial and seasonal variation in diversity and structure of microbial biofilms on marine plastics in Northern European waters. *FEMS Microbiol Ecol* 90(2): 478–492.

Palmer J, Flint S, Brooks J (2007) Bacterial cell attachment, the beginning of a biofilm. *J Ind Microbiol Biotechnol* 34(9): 577–588.

Parra C, Dorta F, Jimenez E, Henríquez R, Ramírez C, Rojas R, Villalobos P (2015) A nanomolecular approach to decrease adhesion of biofouling-producing bacteria to graphene-coated material. *J Nanobiotechnology* 13(1): 82.

Paul E, Ochoa JC, Pechaud Y, Liu Y, Line A (2012) Effect of shear stress and growth conditions on detachment and physical properties of biofilms. *Water Res* 46: 5499–5508.

Peterson BW, van der Mei HC, Sjollema J, Busscher HJ, Sharma PK, Chapman M, Hultgren SJ (2021) A distinguishable role of eDNA in the viscoelastic relaxation of biofilms. *MBio* 4(5): e00497-13.

Pointing SB, Belnap J (2012) Microbial colonization and controls in dryland systems. *Nat Rev Microbiol* 10(8):551–562.

Qian P-Y, Lau SCK, Dahms HU, Dobretsov S, Harder T. (2007) Marine biofilms as mediators of colonization by marine macroorganisms: implications for antifouling and aquaculture. *Mar Biotechnol* 9: 399-410.

Qian P-Y, Rittschof D, Sreedhar B (2000) Macrofouling in unidirectional flow: Miniature pipes as experimental models for studying the interaction of flow and surface characteristics on the attachment of barnacle, bryozoan and polychaete larvae. *Mar Ecol Ser* 207: 109–121.

Qian P-Y, Rittschof D, Sreedhar B, Chia FS (1999) Macrofouling in unidirectional flow: Miniature pipes as experimental models for studying the effects of hydrodynamics on invertebrate larval settlement. *Mar Ecol Ser* 191: 141–151.

Railkin AI (2003) *Marine Biofouling: Colonization Processes and Defenses*. CRC Press, Boca Raton.

Ramos V, Morais J, Castelo-Branco R, Pinheiro Â, Martins J, Regueiras A, Pereira AL, Lopes VR, Frazão B, Gomes D, et al. (2018) Cyanobacterial diversity held in microbial biological resource centers as a biotechnological asset: the case study of the newly established LEGE culture collection. *J Appl Phycol* 30(3): 1437–1451.

Rao D, Webb JS, Kjelleberg S (2005) Competitive interactions in mixed-species biofilms containing the marine bacterium *Pseudoalteromonas tunicata*. *Appl Environ Microbiol* 71(4): 1729-36.

Regueiras A, Pereira S, Costa MS, Vasconcelos V (2018) Differential toxicity of cyanobacteria isolated from marine sponges towards echinoderms and crustaceans. *Toxins* 10(7): 1–12.

Renner LD, Weibel DB (2011) Physicochemical regulation of biofilm formation. *MRS Bull.* 36(5): 347-355.

COMPLIMENTARY COPY

Rochex A, Godon JJ, Bernet N, Escudié R (2008) Role of shear stress on composition, diversity and dynamics of biofilm bacterial communities. *Water Res* 42(20): 4915–4922.

Romeu MJ, Alves P, Morais J, Miranda JM, de Jong ED, Sjollema J, Ramos V, Vasconcelos V, Mergulhão FJM (2019) Biofilm formation behaviour of marine filamentous cyanobacterial strains in controlled hydrodynamic conditions. *Environ Microbiol* 21(11): 4411–4424.

Romeu MJ, Alves P, Morais J, Ramos V, Vasconcelos V, Mergulhão FJ (2016) Biofilm formation by a cyanobacterial strain belonging to a distinct *Leptolyngbya* phylotype: surface effect. In: Judith Henderson, Editor. *Biofilms: Characterization, Applications and Recent Advances*: Nova Science Publishers, pp. 153–174.

Romeu MJ, Domínguez-Pérez D, Almeida D, Morais J, Araújo MJ, Osório H, Campos A, Vasconcelos V, Mergulhão FJ (2021) Quantitative proteomic analysis of marine biofilms formed by filamentous cyanobacterium. *Environ Res*: 111566.

Romeu MJ, Domínguez-Pérez D, Almeida D, Morais J, Campos A, Vasconcelos V, Mergulhão FJM (2020) Characterization of planktonic and biofilm cells from two filamentous cyanobacteria using a shotgun proteomic approach. *Biofouling* 36(6): 631–645.

Rossi F, De Philippis R (2015) Role of cyanobacterial exopolysaccharides in phototrophic biofilms and in complex microbial mats. *Life* 5(2): 1218–1238.

Roy GJ (1994) Notes on instrumentation and control. MA: Newnes, Oxford, UK and Boston.

Rumbaugh KP, Sauer K (2020) Biofilm dispersion. *Nat Rev Microbiol.* 18(10):571-586.

Salta M, Capretto L, Carugo D, Wharton JA, Stokes KR (2013b) Life under flow: A novel microfluidic device for the assessment of anti-biofilm technologies. *Biomicrofluidics* 7(6): 1–16.

Salta M, Wharton JA, Blache Y, Stokes KR, Briand JF (2013a) Marine biofilms on artificial surfaces: structure and dynamics. *Environ Microbiol* 15(11): 2879–2893.

Scardino AJ, Guenther J, de Nys R (2008) Attachment point theory revisited: the fouling response to a microtextured matrix. *Biofouling* 24(1): 45–53.

Scardino AJ, Zhang H, Cookson DJ, Lamb RN, de Nys R (2009) The role of nano-roughness in antifouling. *Biofouling* 25(8): 757–767.

Schirrmeister BE, Antonelli A, Bagheri HC (2011) The origin of multicellularity in cyanobacteria. *BMC Evol Biol* 11(1): 45.

Schuergers N, Wilde A (2015) Appendages of the cyanobacterial cell. *Life* 5(1): 700-715.

Schultz MP, Bendick JA, Holm ER, Hertel WM (2011) Economic impact of biofouling on a naval surface ship. *Biofouling* 27(1): 87–98.

Schumacher JF, Long CJ, Callow ME, Finlay JA, Callow JA, Brennan AB (2008) Engineered nanoforce gradients for inhibition of settlement (attachment) of swimming algal spores. *Langmuir* 24(9): 4931–4937.

Selim MS, Elmarakbi A, Azzam AM, Shenashen MA, EL-Saeed AM, El-Safty SA (2018) Eco-friendly design of superhydrophobic nano-magnetite/silicone composites for marine foul-release paints. *Prog Org Coat* 116: 21-34.

COMPLIMENTARY COPY

Selim MS, Shenashen MA, El-Safty SA, Higazy SA, Selim MM, Isago H, Elmarakbi A (2017) Recent progress in marine foul-release polymeric nanocomposite coatings. *Prog Mater Sci* 87:1–32.

Silva ER, Ferreira O, Ramalho PA, Azevedo NF, Bayón R, Igartua A, Bordado JC, Calhorda MJ (2019) Eco-friendly non-biocide-release coatings for marine biofouling prevention. *Sci Total Environ* 650: 2499–2511.

Skovhus TL, Enning D, Lee JS (2017) *Microbiologically Influenced Corrosion in the Upstream Oil and Gas Industry*: CRC Press, Boca Raton.

Sonak S (2009) Implications of organotins in the marine environment and their prohibition. *J Environ Manage* 90: 1–3.

Sonak S, Pangam P, Giriyan A, Hawaldar K (2009) Implications of the ban on organotins for protection of global coastal and marine ecology. *J Environ Manage* 90: 96–108.

Soon CF, Omar WIW, Nayan N, Basri H, Narawi MB, Tee KS (2013) A Bespoke contact angle measurement software and experimental setup for determination of surface tension. *Procedia Technol* 11: 487–494.

Stanier RY, Cohen-Bazire G (1977) Phototrophic prokaryotes: The cyanobacteria. *Annual Rev Microbiol* 31: 225-274.

Stuart RK, Mayali X, Lee JZ, Craig Everroad R, Hwang M, Bebout BM, Weber PK, Pett-Ridge J, Thelen MP (2016) Cyanobacterial reuse of extracellular organic carbon in microbial mats. *ISME J* 10(5): 1240–1251.

Summerscales J (2014) Durability of composites in the marine environment. *Solid Mech Appl* 208: 1-14.

Sutherland IW (2001) The biofilm matrix - an immobilized but dynamic microbial environment. *Trends Microbiol* 9(5): 222-7.

Taylor DA (1996) Instrumentation and control. In: Introduction to Marine Engineering: Butterworth-Heinemann, Oxford, pp. 279–325.

Telegdi J, Trif L, Románszki L (2016) Smart anti-biofouling composite coatings for naval applications. In: Montemor MF, editor. *Smart Composite Coatings and Membranes*. *Transport, Structural, Environmental and Energy Applications*: Woodhead P. Cambridge, UK. pp.123–155.

Toupoint N, Mohit V, Linossier I, Bourgougnon N, Myrand B, Olivier F, Lovejoy C, Tremblay R. (2012) Effect of biofilm age on settlement of *Mytilus edulis*. *Biofouling* 28(9): 985–1001.

Tulcidas AV, Bayón R, Igartua A, Bordado JCM, Silva ER (2015) Friction reduction on recent non-releasing biocidal coatings by a newly designed friction test rig. *Tribol Int* 91: 140–150.

Tuson HH, Weibel DB (2013) Bacteria-surface interactions. *Soft Matter* 9(18): 4368-4380.

Urbanek AK, Rymowicz W, Mirończuk AM (2018) Degradation of plastics and plastic-degrading bacteria in cold marine habitats. *Appl Microbiol Biotechnol* 102(18): 7669–7678.

Verderosa AD, Totsika M, Fairfull-Smith KE (2019) Bacterial biofilm eradication agents: A current review. *Front Chem* 7(11): 1–17.

Vermaas WFJ (2001) Photosynthesis and respiration in cyanobacteria. In: eLS editor.

Vinagre PA, Simas T, Cruz E, Pinori E, Svenson J (2020) Marine biofouling: A european database for the marine renewable energy sector. *J Mar Sci Eng* 8(7): 495.

COMPLIMENTARY COPY

Vincent WF (2000) Cyanobacterial dominance in the polar regions. In: Whitton BA, Potts M, editors. *The Ecology of Cyanobacteria*: Springer Netherlands, Dordrecht, pp. 321–340.

Visser P, Ibelings B, R. Mur L, E. Walsby A (2005) The ecophysiology of the harmful cyanobacterium *Microcystis*. In: Huisman J, Matthijs HCP, Visser PM, Editors. *Harmful Cyanobacteria*. Springer, Dordrecht, pp.109–142.

von Ammon U, Wood SA, Laroche O, Zaiko A, Tait L, Lavery S, Inglis G, Pochon X (2018) The impact of artificial surfaces on marine bacterial and eukaryotic biofouling assemblages: A high-throughput sequencing analysis. *Mar Environ Res* 133: 57-66.

Wang C, Bao W-Y, Gu Z-Q, Li Y-F, Liang X, Ling Y, Cai S-L, Shen H-D, Yang J-L (2012) Larval settlement and metamorphosis of the mussel *Mytilus coruscus* in response to natural biofilms. *Biofouling* 28(3): 249–256.

Wetherbee R, Lind JL, Burke J, Quatrano RS (1998) Minireview—the first kiss: establishment and control of initial adhesion by raphid diatoms. *J Phycol* 34(1): 9–15.

Wietz M, Hall MR, Høj L (2009) Effects of seawater ozonation on biofilm development in aquaculture tanks. *Syst Appl Microbiol* 32(4): 266–277.

Xie L, Hong F, He C, Ma C, Liu J, Zhang G, Wu C (2011) Coatings with a self-generating hydrogel surface for antifouling. *Polymer* 52: 3738–3744.

Yebra DM, Kiil S, Dam-Johansen K (2004) Antifouling technology - Past, present and future steps towards efficient and environmentally friendly antifouling coatings. *Prog Org Coatings* 50(2): 75–104.

Zhang WP, Wang Y, Tian RM, Bougouffa S, Yang B, Cao HL, Zhang G, Wong YH, Xu W, Batang Z, et al. (2014) Species sorting during biofilm assembly by artificial substrates deployed in a cold seep system. *Sci Rep* 4(1):6647.

Zhang X, Mikkelsen Ø (2021) Graphene oxide/silver nanocomposites as antifouling coating on sensor housing materials. *J Clust Sci* 4.

COMPLIMENTARY COPY

environmental microbiology

Environmental Microbiology (2019) **21**(11), 4411–4424 doi:10.1111/1462-2920.14807

Biofilm formation behaviour of marine filamentous cyanobacterial strains in controlled hydrodynamic conditions

Maria J. Romeu,[1] Patrícia Alves,[1] João Morais,[2] João M. Miranda,[3] Ed.D. de Jong,[4] Jelmer Sjollema,[4] Vítor Ramos,[2] Vitor Vasconcelos[2,5] and Filipe J. M. Mergulhão[1*]

[1]*LEPABE—Department of Chemical Engineering, Faculty of Engineering, University of Porto, Porto, Portugal.*

[2]*CIIMAR—Interdisciplinary Centre of Marine and Environmental Research, University of Porto, Terminal de Cruzeiros do Porto de Leixões, Matosinhos, Portugal.*

[3]*CEFT—Department of Chemical Engineering, Faculty of Engineering, University of Porto, Porto, Portugal.*

[4]*Department of Biomedical Engineering, University of Groningen, University Medical Center Groningen, Groningen, The Netherlands.*

[5]*Department of Biology, Faculty of Sciences, University of Porto, Porto, Portugal.*

Summary

Marine biofouling has severe economic impacts and cyanobacteria play a significant role as early surface colonizers. Despite this fact, cyanobacterial biofilm formation studies in controlled hydrodynamic conditions are scarce. In this work, computational fluid dynamics was used to determine the shear rate field on coupons that were placed inside the wells of agitated 12-well microtiter plates. Biofilm formation by three different cyanobacterial strains was assessed at two different shear rates (4 and 40 s^{-1}) which can be found in natural ecosystems and using different surfaces (glass and perspex). Biofilm formation was higher under low shear conditions, and differences obtained between surfaces were not always statistically significant. The hydrodynamic effect was more noticeable during the biofilm maturation phase rather than during initial cell adhesion and optical coherence tomography showed that different shear rates can affect biofilm architecture. This study is particularly relevant given the cosmopolitan distribution of these cyanobacterial strains and the biofouling potential of these organisms.

Received 7 March, 2019; revised 16 July, 2019; accepted 14 September, 2019. *For correspondence. E-mail filipem@fe.up.pt; Tel. (+351) 225081668; Fax (+351) 5081449.

© 2019 Society for Applied Microbiology and John Wiley & Sons Ltd.

Introduction

Biofouling is an ongoing concern in aquatic environments and marine applications, leading to material deterioration, surface corrosion, decrease of hydrodynamic performance and significant economic losses (Salta *et al*., 2013). Moreover, biofilms are recognized as a permanent or temporary refuge for bacterial pathogens in aquaculture facilities (King *et al*., 2006). Additional problems related to biofouling on marine environments are present in marine underwater support structures, sensors and housings, which are used for on-site monitoring with weekly, monthly or continuous measuring. On these devices, the most obvious problems are related to optical and electrochemical sensors, because even a thin biofilm on the optics can give rise to incorrect measurements (Delauney *et al*., 2010). Although marine biofouling is a dynamic process encompassing different agents and their interactions, it has been considered that biofilm formation by bacteria and algae is a primordial step that occurs prior to the adhesion of macrofouler organisms such as invertebrate larvae, mussels, seaweeds and barnacles (Mieszkin *et al*., 2013). Cyanobacteria are a widespread group of photosynthetic prokaryotes which, together with diatoms, constitute the major components of marine biofilms (Salta *et al*., 2013; Bharti *et al*., 2017; Di Pippo and Congestri, 2017). Moreover, cyanobacteria produce large amounts of extracellular polymeric substances (EPS), which increase biofilm cohesion (Rossi and De Philippis, 2015). This is particularly important because it has been shown that the main challenge in marine biofouling control is associated with microorganisms which are also responsible for the initiation of biofilm formation and those which are also able to excrete large amounts of EPS (Mieszkin *et al*., 2013; Salta *et al*., 2013; Telegdi *et al*., 2016). Thus, a promising approach to delay macrofouling is to prevent the adhesion and biofilm formation by cyanobacteria.

14622920, 2019, 11, Downloaded from https://ami-journals.onlinelibrary.wiley.com/doi/10.1111/1462-2920.14807 by Cochrane Portugal, Wiley Online Library on [20/01/2023]. See the Terms and Conditions (https://onlinelibrary.wiley.com/terms-and-conditions) on Wiley Online Library for rules of use; OA articles are governed by the applicable Creative Commons License

In this work, two strains from the *Nodosilinea* genus, collected from the same site in the Portuguese coast, and a Synechococcales strain from a different location were studied. To the best of our knowledge, no studies about the biofilm formation behaviour of these commonly occurring cyanobacterial strains have been published so far.

Amongst the parameters that affect biofilm development, physicochemical factors related with the surface (Crawford *et al*., 2012) and flow velocity and shear rate (Allen *et al*., 2018) are some of the most important. There is evidence that shear forces affect not only biofilm structure but also composition, mass transfer, exopolysaccharides production, energy metabolism and can also induce genetic or molecular changes in biofilms (Moreira *et al*., 2015a). It has been reported that a slow flow of water (0.2 $m{\cdot}s^{-1}$) promotes the growth of filamentous green algae and cyanobacteria (Minchin and Gollasch, 2003; Flemming *et al*., 2009) and that biofouling can be favoured at low fluid velocities. These lower flow velocity values can be found in harbours and when underwater devices and sensors are moored or floating in their vicinity (Minchin and Gollasch, 2003). Therefore, it is important to perform biofilm formation studies in controlled hydrodynamic conditions where the shear rate is well defined. Although the effects of hydrodynamic conditions on the architecture of some bacterial biofilms have been described (Teodósio *et al*., 2011), there is a comparatively low information regarding the effects of hydrodynamics in filamentous cyanobacterial biofilms. Moreover, some filamentous cyanobacteria species produce cyanotoxins, which pose a particular risk to aquatic organisms and to human health (Frazão *et al*., 2010; Regueiras *et al*., 2018). Poisoning and additional chronic effects might be caused by the ingestion of contaminated food or even by drinking water during recreational activities (Martins *et al*., 2005; Buratti *et al*., 2017).

In order to analyse and predict flow conditions in an easy to handle biofilm reactor assay like a 12-well microtiter plate, flow simulation and modelling are highly useful. Computational fluid dynamics (CFD) is a numerical simulation technique that involves the solution of fluid flow and/or heat/mass transfer problems and provides a detailed understanding of flow phenomena that are difficult to analyse experimentally. Although CFD applications in biotechnological and biological processes are common (Dean *et al*., 2016), this technique is not commonly used to predict the shear rate occurring inside reactors that are used in marine biofilm research. A detailed hydrodynamic analysis of these biofilm reactors is useful, and CFD is a powerful tool used to model flow situations to assess if the hydrodynamic conditions *in vitro* are similar to those prevailing in some marine systems *in situ*. In order to define the operational conditions that can be used *in vitro* to simulate the hydrodynamics prevailing in natural aquatic environments, the first goal of this research was to predict the shear rate occurring in a marine biofilm reactor (agitated 12-well microtiter plates). The second goal was to evaluate the effects of different shear rates and surface properties on the biofilm formation behaviour of different marine cyanobacteria. The chosen surfaces, glass and perspex, represent commonly submerged artificial surfaces found on different equipment in aquatic and marine environments such as underwater windows of boats, aquaculture equipment, flotation spheres, moored buoys, underwater cameras, measuring devices or sensors (Roy, 1983; Taylor, 1996; Blain *et al*., 2004; King *et al*., 2006).

Results and discussion

The first goal of this study was the determination of the shear rate field in the bottom of an agitated 12-well microtiter plate and to assess its similarity to published shear rate values occurring in some marine systems. Secondly, the effects of shear rate and surface properties on the biofilm formation behaviour of different cyanobacterial strains were also evaluated.

Flow simulation on the 12-well microtiter plates was performed by CFD. Figure 1 shows the free liquid surface at a given instant upon agitation of the microtiter plate at two shaking frequencies. The liquid surface is not flat in either condition, and the surface inclination is higher at the highest shaking frequency. The velocity profiles were also determined for both shaking frequencies (Supporting Information, S1—Velocity profiles). With a higher fluid velocity (obtained at the higher shaking frequency), a decreased liquid depth (associated to the surface inclination) was obtained. As previously suggested, the increased fluid velocity may facilitate mass transfer of

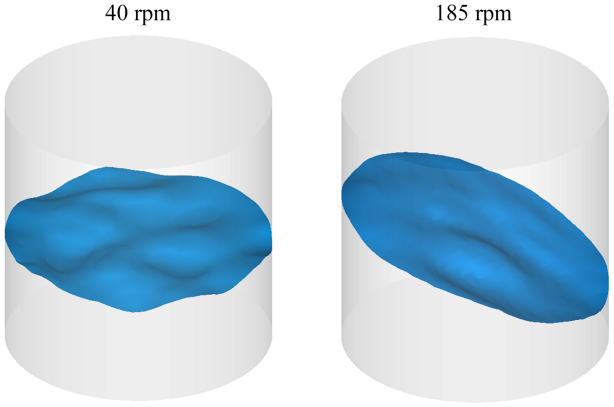

Fig. 1. CFD simulation of the free liquid surface at 40 and 185 rpm. [Color figure can be viewed at wileyonlinelibrary.com]

14622920, 2019, 11, Downloaded from https://ami-journals.onlinelibrary.wiley.com/doi/10.1111/1462-2920.14807 by Cochrane Portugal, Wiley Online Library on [20/01/2023]. See the Terms and Conditions (https://onlinelibrary.wiley.com/terms-and-conditions) on Wiley Online Library for rules of use; OA articles are governed by the applicable Creative Commons License

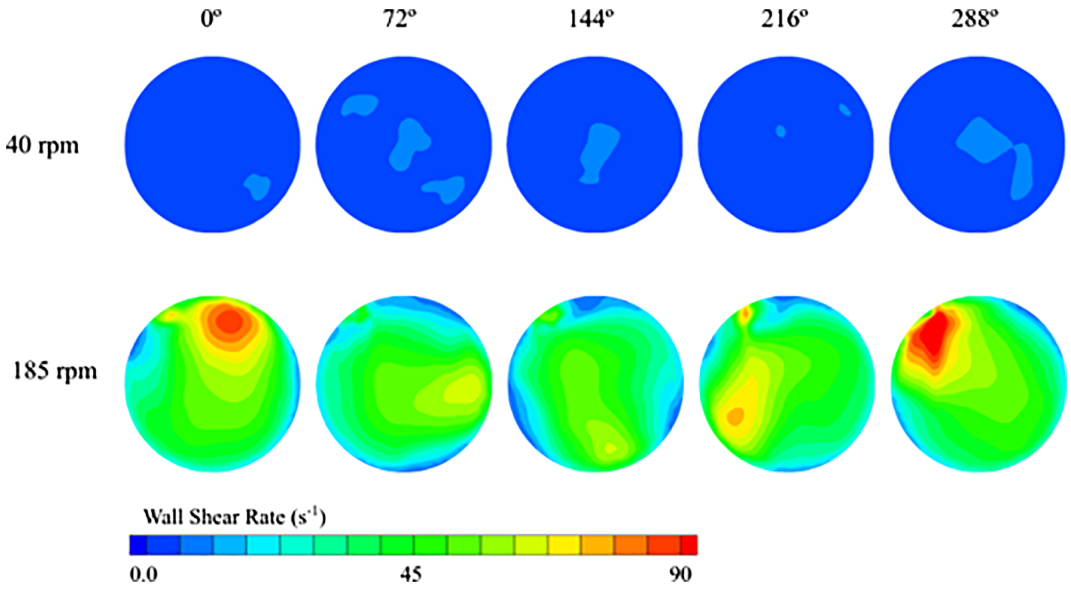

Fig. 2. Wall shear rate at the bottom wall (at 40 and 185 rpm). [Color figure can be viewed at wileyonlinelibrary.com]

nutrients from the bulk liquid to the biofilm and also access to oxygen and light may be promoted in this condition (Gomes *et al*., 2014).

The shear rate distribution on the surface at different degrees of a full rotation is shown in Fig. 2, where it can be seen that higher shear rate values were obtained at the highest shaking frequency. In a full rotation (360°) of the orbital platform, the instant maximum and minimum wall shear rate values at any given point on the coupon surface are compensated over time. Therefore, the representative wall shear rate was obtained by averaging the results throughout a complete rotation cycle over the coupon surface.

Figure 3 shows the shear strain rate variation over time. An average shear rate value of 40 s^{-1} was obtained for 185 rpm, reaching a maximum value of 120 s^{-1}, whereas an average value of 4 s^{-1} was calculated for 40 rpm, reaching a maximum value of 11 s^{-1}. At the shaking frequency of 185 rpm, the range of shear rates that can be reached includes different values that can be found in marine environments. Although a shear rate of 50 s^{-1} has been reported for a ship in a harbour (Bakker *et al*., 2003), equipment and devices which are in similar environments (partially submerged or even moored equipment such as underwater cameras, flotation spheres and sensors) and even transparent hulls of boats or their windows are likely to be subjected to similar shear values. Moreover, this marine reactor also allows the biofilm development at lower shear rate conditions (at 4 s^{-1}), which is important because lower fluid velocities promote marine biofouling (Minchin and Gollasch, 2003; Flemming *et al*., 2009).

Although different experimental setups have been used to study the effect of hydrodynamics particularly at later stages of marine biofilm development, including larval settlement (Qian *et al*., 1999, 2000), the use of agitated microtiter plates in the laboratory can be very convenient because it is an affordable and inexpensive platform. Microtiter plates present several advantages such as low volume requirements (reduced operational costs) are easy to handle and enable the control of different parameters like temperature and shear rate. Also, in the real scenario of a ship in a harbour, the shear rate field will oscillate due to tidal currents and because of the wakes

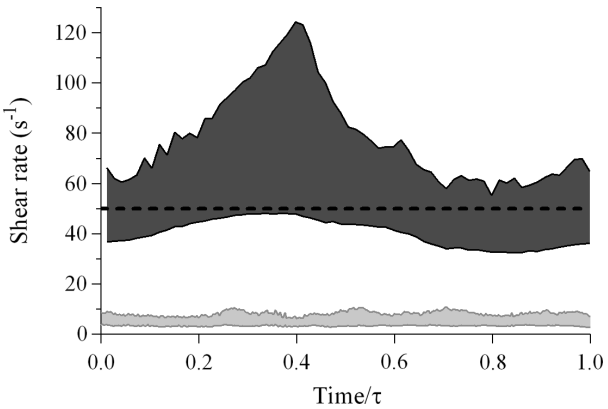

Fig. 3. Representation of shear strain rate variation over a complete cycle. A normalized time scale was used since the period is different for each shaking frequency. The dashed line represents the shear strain rate reported for a ship in a harbour (50 s^{-1}). The area represented by light and dark grey (both delimited by average and maximum values) indicates the shear strain rate achieved at 40 and 185 rpm respectively.

14622920, 2019, 11, Downloaded from https://ami-journals.onlinelibrary.wiley.com/doi/10.1111/1462-2920.14807 by Cochrane Portugal, Wiley Online Library on [20/01/2023]. See the Terms and Conditions (https://onlinelibrary.wiley.com/terms-and-conditions) on Wiley Online Library for rules of use; OA articles are governed by the applicable Creative Commons License

caused by passing ships. Since the agitated microtiter plate induces a wave-like shear, it generates a flow topology that is more similar to marine systems than most flow systems.

Although CFD studies have already been performed on our group for 96-well plates (Gomes *et al*., 2014), the present study focuses on 12-well microtiter plates, which enable a higher shear rate range (as can be found in marine environments) and the use of coupons to test different surfaces. A previous study using micro- and macro-flow systems to test *Escherichia coli* adhesion (Moreira *et al*., 2015b) has shown that when the shear forces are kept constant between these platforms, the obtained results were similar despite the large differences in size. Edge effects were also not shown to be important given the relative dimensions of the system and of the bacteria. Since in the present study, the shear rate range achieved (Fig. 3) comprises the values found on real aquatic environments (50 s^{-1}; Bakker *et al*., 2003), 12-well microtiter plates may be used as a marine biofilm reactor to mimic these environments.

Surface hydrophobicity was assessed by contact angle measurement with water (θ_w). Contact angle determination provides information about the interaction of the fluid with a solid material through the determination of the wettability and hydrophobicity of the surface. While wettability refers to the tendency of fluid spreading on a surface, hydrophobicity describes the tendency of non-polar molecular aggregation and consequently water molecule repulsion (Yuan and Lee, 2013). By definition, surfaces can be classified into hydrophilic or hydrophobic if the contact angle of water with the surfaces is lower or higher than 90° respectively (Sedlmeier *et al*., 2008). Thus, low contact angle values indicate liquid spreading along the surface, which is associated with high wettability and hydrophilic properties. In turn, low wettability is associated with hydrophobicity. Since the contact angle of water on glass was $\theta_w = 48.55 \pm 2.41$ and in perspex $\theta_w = 73.05 \pm 3.42$, perspex is relatively hydrophobic compared to glass, exhibiting a lower wettability. Although lower values for glass have been reported, some studies performed with glass surfaces, also showed values in the 40° range (Sener *et al*., 2013; Thukkaram *et al*., 2014; Gomes *et al*., 2015; Moreira *et al*., 2015a). This slightly increased value may be related to the composition of this specific glass although other glass surfaces that can be used to construct submerged devices (underwater cameras, measuring devices or sensors) can have different hydrophobicities.

Cyanobacterial biofilm formation was monitored for 49 days, and the evolution of wet weight and chlorophyll *a* content is shown in Figs 4–6. For all cyanobacterial strains, biofilm mass was in general higher at the lowest shear rate on both surfaces although statistically significant differences were mostly found on glass. Biofilm mass obtained on glass under low agitation was on average 22.4% higher for *Nodosilinea* sp. LEGE 06020 (Fig. 4A), 58% higher for the unidentified filamentous Synechococcales LEGE 07185 (Fig. 5A) and 32% higher for *Nodosilinea* sp. LEGE 06022 (Fig. 6A) when compared to those obtained at higher shear conditions. Likewise, chlorophyll *a* was 29.5%, 93.9% and 62.7% higher in these conditions for each of the strains respectively (Fig. 4B, 5B, 6B). On perspex, the biofilm wet weight was on average 17.6%, 37.2%, 26.9% higher at 4 s^{-1} (Fig. 4C, 5C, 6C), whereas chlorophyll *a* was 31.5%, 91.9%, 70.8% higher at this shear rate (Fig. 4D, 5D, 6D). Analysis of the biofilm wet weight and chlorophyll *a* suggests that, despite the tenfold difference on average shear rate, biofilm development was similar in both hydrodynamic conditions for the first two weeks. This suggests that shear rate had a lower impact on initial cell adhesion and a more noticeable effect during biofilm maturation, which in turn may be the result of two opposing effects caused by higher flow velocities (Supporting Information S1 – Velocity profiles). Although nutrient mass transfer from the bulk liquid and oxygen transfer are facilitated at higher flow velocities, which may promote the biofilm development, the increased shear rate may hamper cell adhesion and may be more challenging for biofilm cohesion (erosion and sloughing events may be promoted). It is likely that the relative importance of these effects varies along the biofilm development stages. Since the effect of fluid velocity was more noticeable during biofilm maturation rather than during cell adhesion, it seems that the increased shear stress was not a significant obstacle to attachment whereas biofilm erosion may be the cause for a lower biofilm accumulation at the higher shear rate (Duddu *et al*., 2009). It has been suggested that monitoring the chlorophyll *a* production can be a good way to follow cyanobacterial growth (Lawton *et al*., 1999; Chorus and Cavalieri, 2000). A correlation between chlorophyll *a* production and biofilm wet weight was observed in some cases (Supporting Information, S2 – Correlation between wet weight and chlorophyll *a*). This correlation was more noticeable at the lowest shear rate (4 s^{-1}) for all cyanobacterial strains (Supporting Information, S2 – Correlation between wet weight and chlorophyll *a*; Fig. S2.1 A,C; S2.2 A,C; S2.3 A,C).

In this study, the effect of surface hydrophobicity was probably less important than the hydrodynamic effect, because similar values of wet weight and chlorophyll *a* were obtained for biofilms developed under different surfaces at the same hydrodynamic conditions (Supporting Information, S3 – Evaluation of cyanobacterial biofilm development under the same hydrodynamic condition on different surfaces; Fig. S3.1; Fig. 3.2). The fact that the

14622920, 2019, 11, Downloaded from https://ami-journals.onlinelibrary.wiley.com/doi/10.1111/1462-2920.14807 by Cochrane Portugal, Wiley Online Library on [20/01/2023]. See the Terms and Conditions (https://onlinelibrary.wiley.com/terms-and-conditions) on Wiley Online Library for rules of use; OA articles are governed by the applicable Creative Commons License

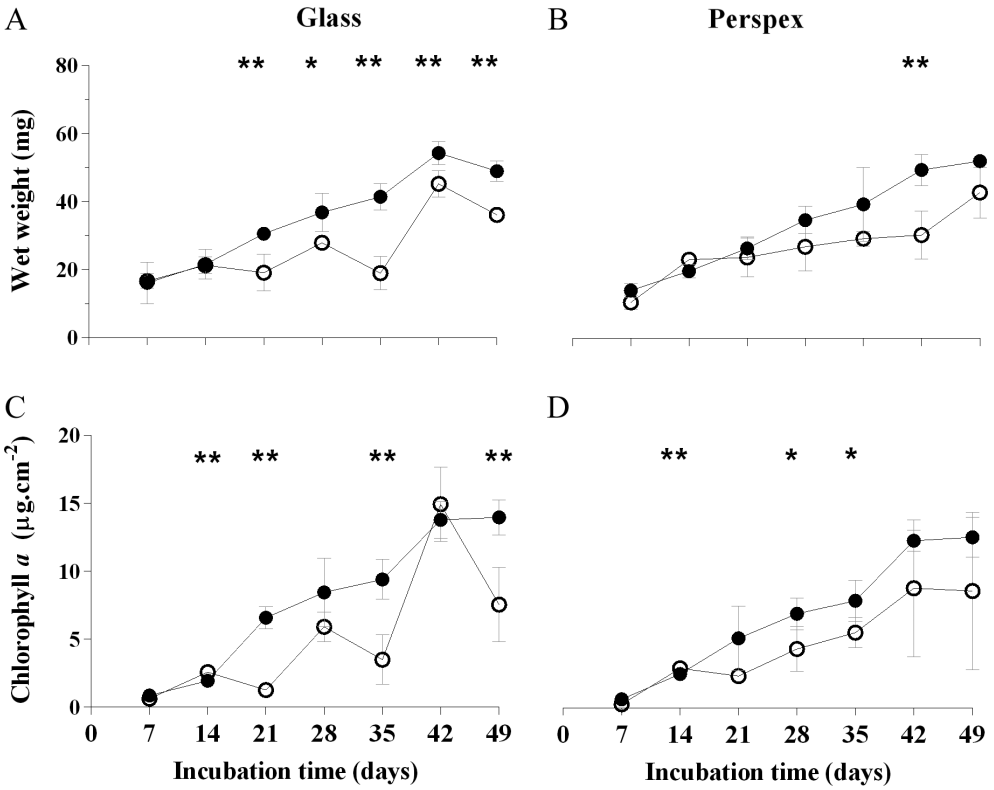

Fig. 4. Evaluation of *Nodosilinea* sp. LEGE 06020 biofilm development. The parameters analysed refer to wet weight (A, C), chlorophyll *a* (B, D). Biofilms were formed in glass (A, B) or perspex (C, D), at two average shear rates, 4 s^{-1} (closed circles) and 40 s^{-1} (open circles) during 49 days. Standard deviations from three replicates are represented. Symbols * and ** indicate statistically different values for $P < 0.1$ and $P < 0.05$ (respectively) at each incubation time.

hydrodynamic conditions may be more important than surface properties during initial biofilm development has already been shown during *E. coli* adhesion to glass and PDMS (Moreira *et al*., 2014) where the effects of the surface properties were modulated by the shear forces. However, biofilm development of *Nodosilinea* sp. LEGE 06022 has also shown significant differences between glass and perspex surfaces (Supporting Information, S3 – Evaluation of cyanobacterial biofilm development under the same hydrodynamic condition on different surfaces; Fig. S3.3), with greater biofilm development on perspex, the most hydrophobic surface.

Since most commonly applied imaging methods to analyse biofilms are *ex situ* and destructive (Azeredo *et al*., 2017), optical coherence tomography (OCT) is an interesting technique enabling *in situ*, non-invasive and real-time imaging without affecting biofilm structure (Wagner and Horn, 2017). Moreover, as biofilm thickness has a strong effect on the performance of underwater devices (Delauney *et al*., 2010), the knowledge of this biofouling parameter is essential for the design and maintenance of marine equipment. Therefore, biofilm thickness, roughness and structure analyses were performed by OCT from day 28, because the shear rate effect became more pronounced from day 21 (Figs 4–6). Figure 7 shows the biofilm thickness and roughness coefficient evolution and Figs 8–10 shows representative images obtained at the end of the experiment.

The biofilm thickness values obtained for the highest shear rate (40 s^{-1}) were lower than for the lowest shear rate (4 s^{-1}; Fig. 7A–C). This was more noticeable for biofilm development of the unidentified filamentous Synechococcales LEGE 07185 (Fig. 7B) and *Nodosilinea* sp. LEGE 06022 (Fig. 7C) strains. For all cases except for *Nodosilinea* sp. LEGE 06020 at 4 s^{-1} and *Nodosilinea* sp. LEGE 06022 at 40 s^{-1}, (in which similar values were achieved, Fig. 7A and C respectively), biofilm thickness increased from day 28 to the end of the experiment. The highest values of biofilm thickness were observed for *Nodosilinea* sp. LEGE 06020 at 4 s^{-1} on glass (around 446 μm; Fig. 7A, 49 days) and the lowest for *Nodosilinea* sp. LEGE 06022 at 40 s^{-1} on glass (around 16 μm; Fig. 7C, 42 days). Differences on biofilm thickness between the surfaces were more evident on *Nodosilinea* sp. LEGE 06022 (Fig. 7C), with higher biofilm development on perspex, as previously reported for wet weight and chlorophyll *a* quantification (Supporting Information, S3 – Evaluation of cyanobacterial biofilm

14622920, 2019, 11, Downloaded from https://ami-journals.onlinelibrary.wiley.com/doi/10.1111/1462-2920.14807 by Cochrane Portugal, Wiley Online Library on [20/01/2023]. See the Terms and Conditions (https://onlinelibrary.wiley.com/terms-and-conditions) on Wiley Online Library for rules of use; OA articles are governed by the applicable Creative Commons License

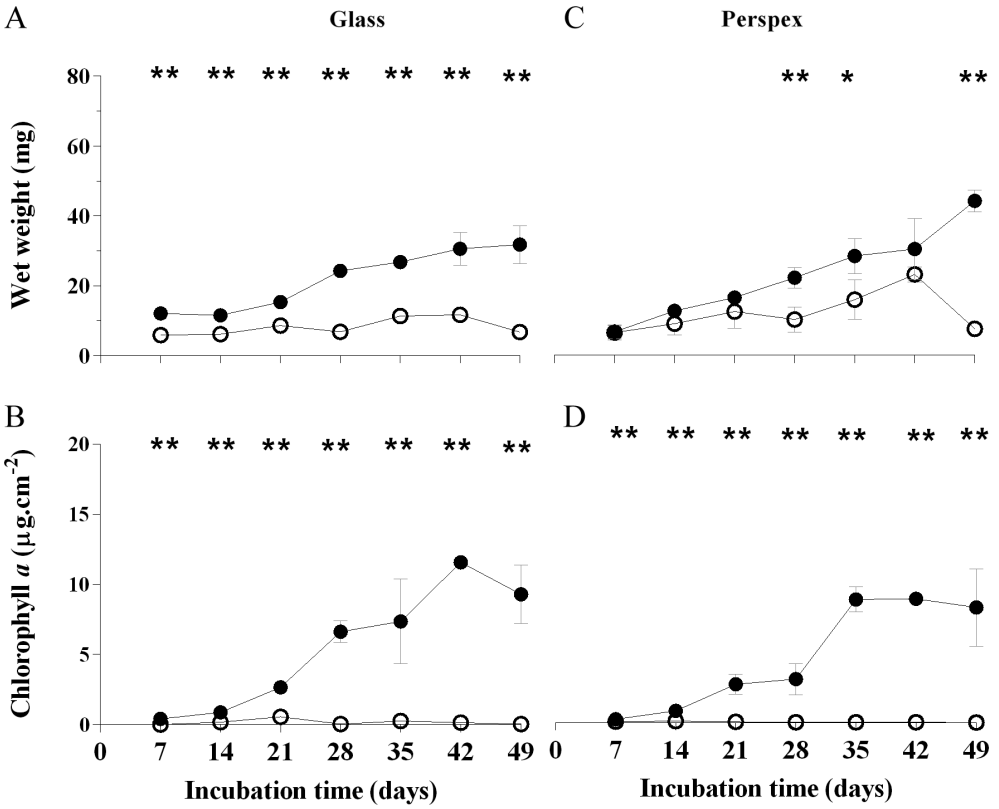

Fig. 5. Evaluation of unidentified filamentous Synechococcales LEGE 07185 biofilm development. The parameters analysed refer to wet weight (A, C), chlorophyll *a* (B, D). Biofilms were formed in glass (A, B) or perspex (C, D), at two average shear rates, 4 s^{-1} (closed circles) and 40 s^{-1} (open circles) during 49 days. Standard deviations from three replicates are represented. Symbols * and ** indicate statistically different values for $P < 0.1$ and $P < 0.05$ (respectively) at each incubation time.

development under the same hydrodynamic condition on different surfaces; Fig. S3.3). Large variations on biofilm roughness under different shear rate were only observed for the unidentified filamentous Synechococcales LEGE 07185 (Fig. 7E), in which lower values of the roughness coefficient were obtained for the lowest shear rate. In general, no significant differences between glass and perspex were observed for biofilm roughness coefficient ($P = 0.20$ for *Nodosilinea* sp. LEGE 06020, Fig. 7D; $P = 0.66$ for the unidentified filamentous Synechococcales LEGE 07185, Fig. 7E and $P = 0.07$ for *Nodosilinea* sp. LEGE 06022; Fig. 7F). The highest (about 1.14) and the lowest (0.14) values of biofilm roughness coefficient were obtained for the unidentified filamentous Synechococcales LEGE 07185 at 40 s^{-1} on perspex (Fig. 7E, 49 days) and *Nodosilinea* sp. LEGE 06020 at 4 s^{-1} on perspex (Fig. 7D, 35 days) respectively. Biofilm of *Nodosilinea* sp. LEGE 06020 obtained at a higher shear rate (Figs 8B,D) seemed more compact than those obtained at low shear (Fig 8A,C). This effect was not observed for the unidentified filamentous Synechococcales LEGE 07185 and *Nodosilinea* sp. LEGE 06022 possibly because a lower biofilm biomass was obtained at a higher shear rate (40 s^{-1}) for both strains. A compact architecture probably increases biofilm cohesion and may therefore be an adaptation to the environmental shear forces (Teodósio *et al*., 2011; Graba *et al*., 2013). The formation of a less compact structure at lower shear may enhance mass transfer of nutrients to the inner layers of the biofilm (Teodósio *et al*., 2011).

For most cases, except for biofilms obtained at 40 s^{-1} on glass (Figs 8, 9 and 10B,F) and for *Nodosilinea* sp. LEGE 06020 on perspex at 4 s^{-1} (Fig. 8C,G), the presence of three-dimensional streamers on the biofilm surface could be observed (Figs 8A,E,D,H; 9A,E,C,G,D, H; 10A,E,C,G,D,H). However, these structures were more noticeable for *Nodosilinea* sp. LEGE 06022 on perspex at lower shear rate (4 s^{-1}; Fig. 10C,G). The formation of these streamers may contribute to the formation of 'sieve-like' networks that can capture cells and other biomass (Drescher *et al*., 2013), therefore, contributing to the biofilm growth.

Concluding remarks

The CFD analysis in this work shows that the agitated 12-well microtiter plates can be used to attain shear rate values that can mimic aquatic environments. It was

14622920, 2019, 11, Downloaded from https://ami-journals.onlinelibrary.wiley.com/doi/10.1111/1462-2920.14807 by Cochrane Portugal, Wiley Online Library on [20/01/2023]. See the Terms and Conditions (https://onlinelibrary.wiley.com/terms-and-conditions) on Wiley Online Library for rules of use; OA articles are governed by the applicable Creative Commons License

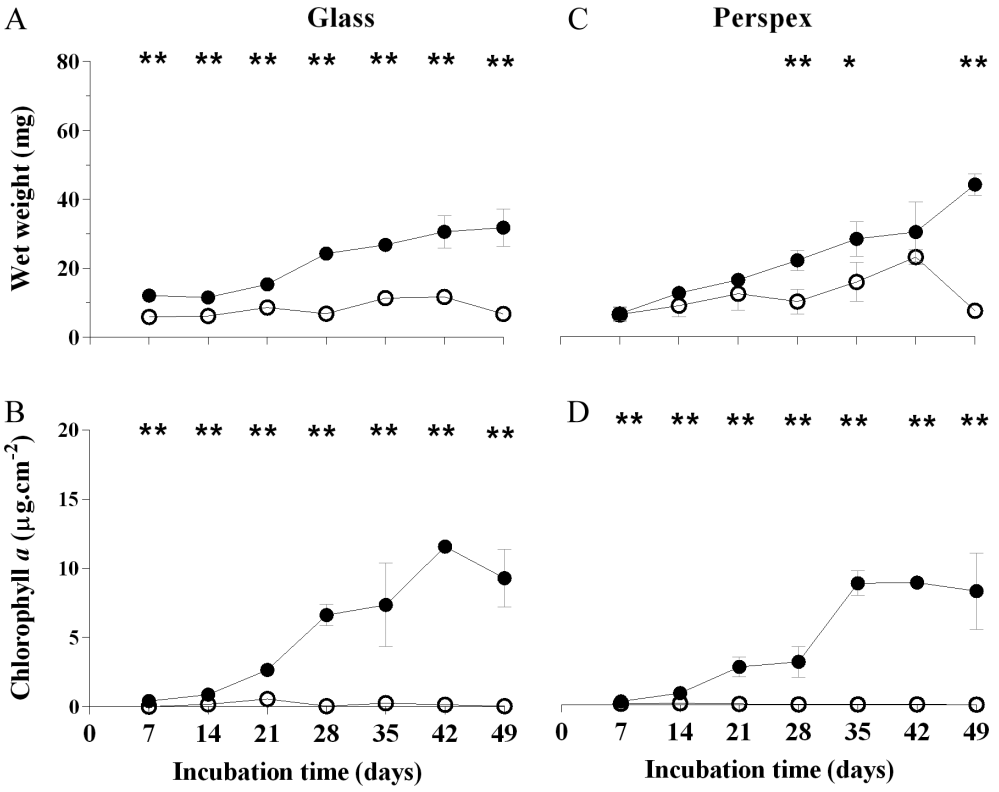

Fig. 6. Evaluation of *Nodosilinea* sp. LEGE 06022 biofilm development. The parameters analysed refer to wet weight (A, C), chlorophyll a (B, D). Biofilms were formed in glass (A, B) or perspex (C, D), at two average shear rates, 4 s^{-1} (closed circles) and 40 s^{-1} (open circles) during 49 days. Standard deviations from three replicates are represented. Symbols * and ** indicate statistically different values for $P < 0.1$ and $P < 0.05$ (respectively) at each incubation time.

demonstrated that OCT analysis can be a valuable tool to analyse the architecture of marine biofilms and to further understand the biofilm formation dynamics. It was shown that hydrodynamics play a crucial role in the development of these biofilms and that these effects are likely to be more important during biofilm maturation rather than during the initial adhesion phase. Cyanobacterial biofilm formation studies performed in controlled hydrodynamic conditions are scarce, but the importance of studying filamentous cyanobacterial strains with such a cosmopolitan distribution is even more relevant given the biofouling potential of these organisms in different ecosystems around the globe.

Experimental procedures

CFD analysis

For the flow simulation inside a 12-well microtiter plate, a cylindrical well (diameter of 22 mm and height of 18 mm) containing liquid (3 ml of water) and gas (air, filling the remaining volume), at 25°C, was simulated using Ansys Fluent CFD package (version 14.5). The domain was built in Design Modeller 14.5 and discretized into a grid of 40,441 hexahedral cells by Meshing 14.5.

The two-phase flow in the vessel was simulated by the VOF methodology (Hirt and Nichols, 1981). The air/water interface was determined by the Geo-Reconstruct method (Youngs, 1982). The PISO algorithm was used to solve the velocity–pressure coupled equations, the QUICK scheme for the discretization of the momentum equations and the PRESTO! scheme for pressure discretization. The surface tension effects were modelled by the continuum surface force (Brackbill *et al*., 1992), which was introduced through a source term in the momentum equation. An accelerating reference frame was adopted, and the effect of the circular orbital motion on the fluid was modelled by a source term. The no-slip boundary condition and a contact angle of 83° were considered for all the walls (Gomes *et al*., 2014).

Simulations were made for rotation frequencies of 40 and 185 rpm and an orbital diameter of 25 mm. For each case, 8 s of physical time were simulated with a fixed time step of 2.5×10^{-4} s. The primary numerical results obtained, for each time step, were the velocity components, the pressure and the liquid or gas phase volume fractions. For each simulation, after the stabilization of the flow, the average instantaneous shear rate was obtained by integrating an instantaneous solution over the bottom surface of the well (corresponding to the

14622920, 2019, 11, Downloaded from https://ami-journals.onlinelibrary.wiley.com/doi/10.1111/1462-2920.14807 by Cochrane Portugal, Wiley Online Library on [20/01/2023]. See the Terms and Conditions (https://onlinelibrary.wiley.com/terms-and-conditions) on Wiley Online Library for rules of use; OA articles are governed by the applicable Creative Commons License

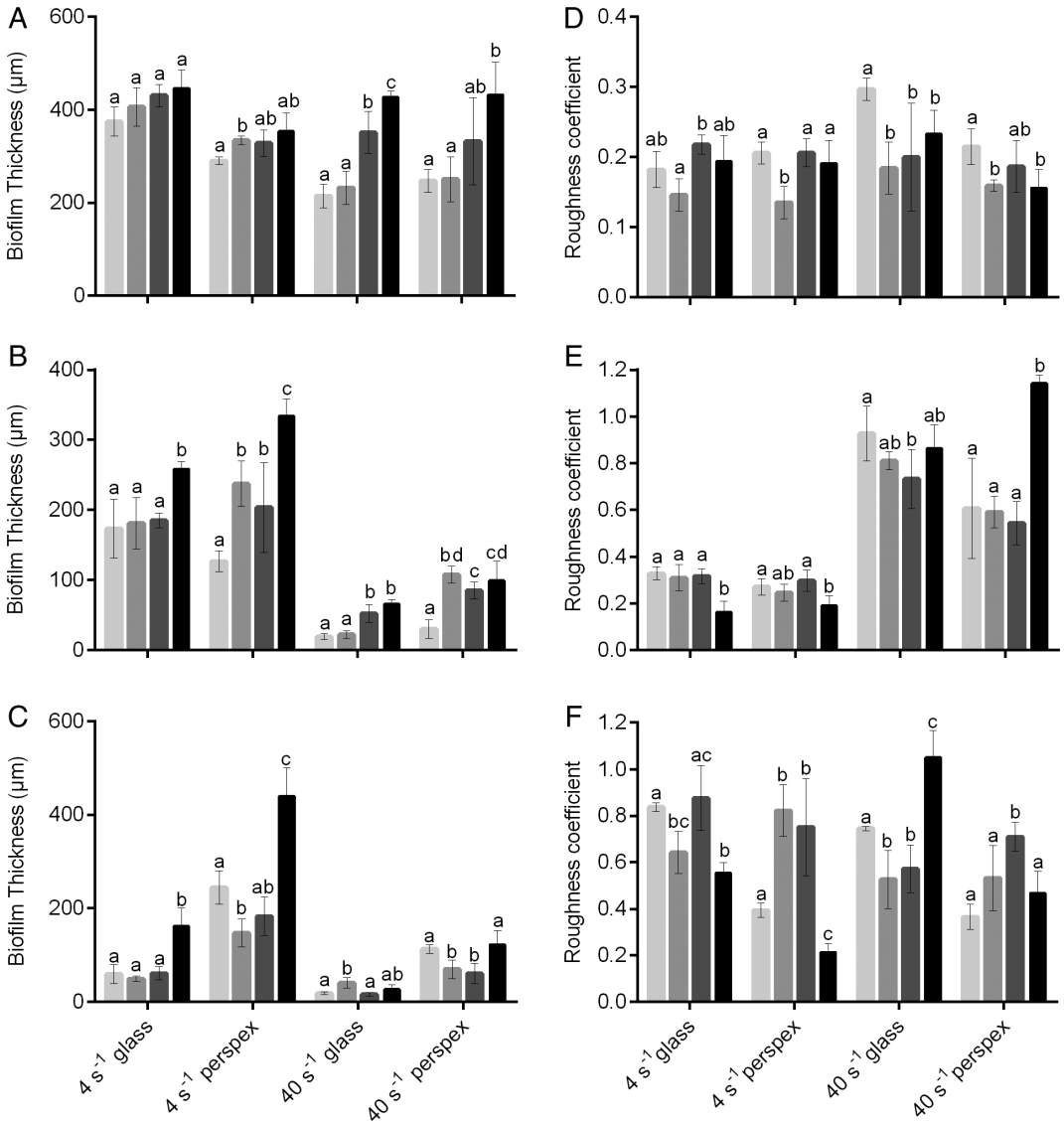

Fig. 7. Evaluation of cyanobacterial biofilm thickness (left; A–C) and roughness coefficient (right; D–F) in both surfaces and different shear rates (A, D – *Nodosilinea* sp. LEGE 06020; B, E – unidentified filamentous Synechococcales LEGE 07185; C, F – *Nodosilinea* sp. LEGE 06022). Mean values ± SD from three replicates for each sampling day are represented. For each condition, different lowercase letters indicate significant differences between incubation times (28 days - very light grey bars; 35 days - light grey bars; 42 days – dark grey bars; 49 days – black bars; $P \leq 0.05$; unpaired t-test).

coupon surface). The time-averaged shear rate was calculated by averaging the instantaneous shear rate throughout a complete rotation cycle.

Organisms and inocula preparation

In order to evaluate the behaviour of different filamentous cyanobacteria from different marine environments, three cyanobacterial strains were used in this study. All strains were obtained from the Blue Biotechnology and Ecotoxicology Culture Collection (LEGE-CC) located at CIIMAR, Portugal (Ramos *et al*., 2018). *Nodosilinea* sp. LEGE 06020 and *Nodosilinea* sp. LEGE 06022 (order Synechococcales) were isolated from a seawater sample collected in the surf zone and from a sample scraped from a wave-sheltered rock in the intertidal zone respectively (Ramos *et al*., 2018). Both strains were originally collected at Coxos beach, Portugal (39°00′16.4"N 9°25′33.0"W). The unidentified filamentous Synechococcales LEGE 07185 was isolated from a submerged stone collected in a tide pool, at Lavadores beach, Portugal (41°07′45.1"N 8°40′06.9"W; Ramos *et al*., 2018). Cells were grown in 750 ml culture in Z8 medium (Kotai, 1972) supplemented with 25 $g \cdot L^{-1}$ of synthetic sea salts (Tropic Marin) and B_{12} vitamin. Cultures were performed under 14 h light (10–30 µmol photons m^{-2} s^{-1})/10 h dark cycles, at 25°C. Cyanobacterial strains from

14622920, 2019, 11, Downloaded from https://ami-journals.onlinelibrary.wiley.com/doi/10.1111/1462-2920.14807 by Cochrane Portugal, Wiley Online Library on [20/01/2023]. See the Terms and Conditions (https://onlinelibrary.wiley.com/terms-and-conditions) on Wiley Online Library for rules of use; OA articles are governed by the applicable Creative Commons License

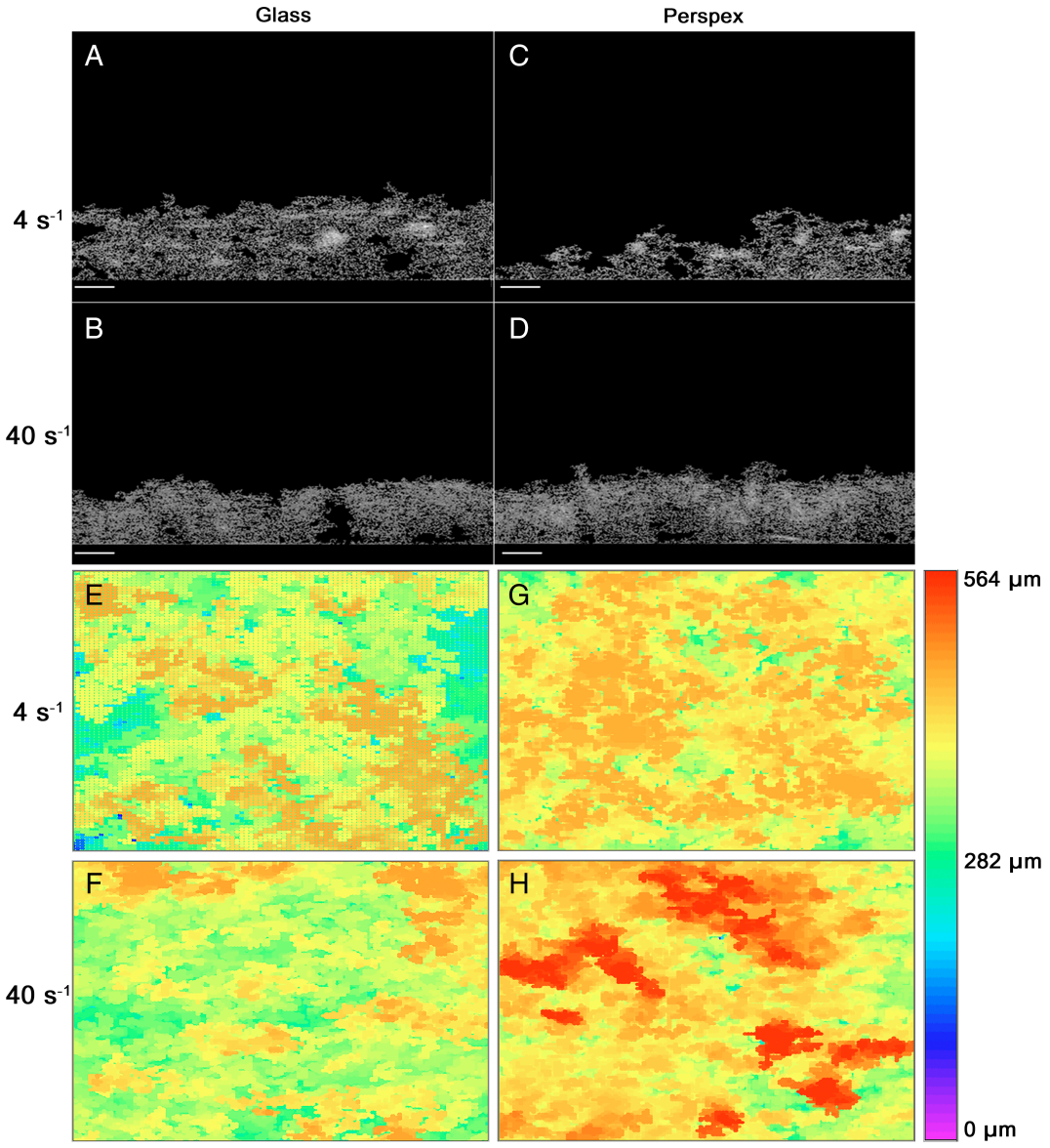

Fig. 8. Representative images obtained by OCT of *Nodosilinea* sp. LEGE 06020 biofilms formed after 49 days on glass and perspex. A–D. 2D cross-sectional OCT images (scale bar = 200 µm). E–H. 3D OCT images, top view projection (the colour scale shows the range of biofilm thickness). Biofilms were formed at two different shear rates, 4 s^{-1} (A, C, E, G) and 40 s^{-1} (B, D, F, H). [Color figure can be viewed at wileyonlinelibrary.com]

unidentified filamentous Synechococcales and *Nodosilinea* genus are present in dissimilar geographies, including different continents (Europe, Africa, America and Antarctica). Specimens can be found in different environments and ecologies such as brackish water, freshwater, hypersaline, marine and even terrestrial (Ramos *et al*., 2018). This cosmopolitan distribution highlights the importance of studying biofilm formation by these organisms.

Surface analysis

In order to assess the biofilm behaviour of the cyanobacterial strains, two artificial surfaces commonly placed in aquatic environments, glass and perspex, were tested. Surface analysis was performed by measuring the contact angles with water (θ_w) as reference liquid. This determination was performed in three independent experiments at 25°C ± 2°C, by the sessile drop method using a contact angle meter (Dataphysics OCA 15 Plus, Filderstadt, Germany), as described in Gomes *et al*., 2015. On each experiment, at least 25 determinations for each material were made.

Biofilm formation

Glass (Vidraria Lousada, Lda, Portugal) and perspex (Neves & Neves, Lda, Portugal) coupons (1 cm^2) were immersed in a solution of 2% (vol/vol) TEGO 2000®

14622920, 2019, 11, Downloaded from https://ami-journals.onlinelibrary.wiley.com/doi/10.1111/1462-2920.14807 by Cochrane Portugal, Wiley Online Library on [20/01/2023]. See the Terms and Conditions (https://onlinelibrary.wiley.com/terms-and-conditions) on Wiley Online Library for rules of use; OA articles are governed by the applicable Creative Commons License

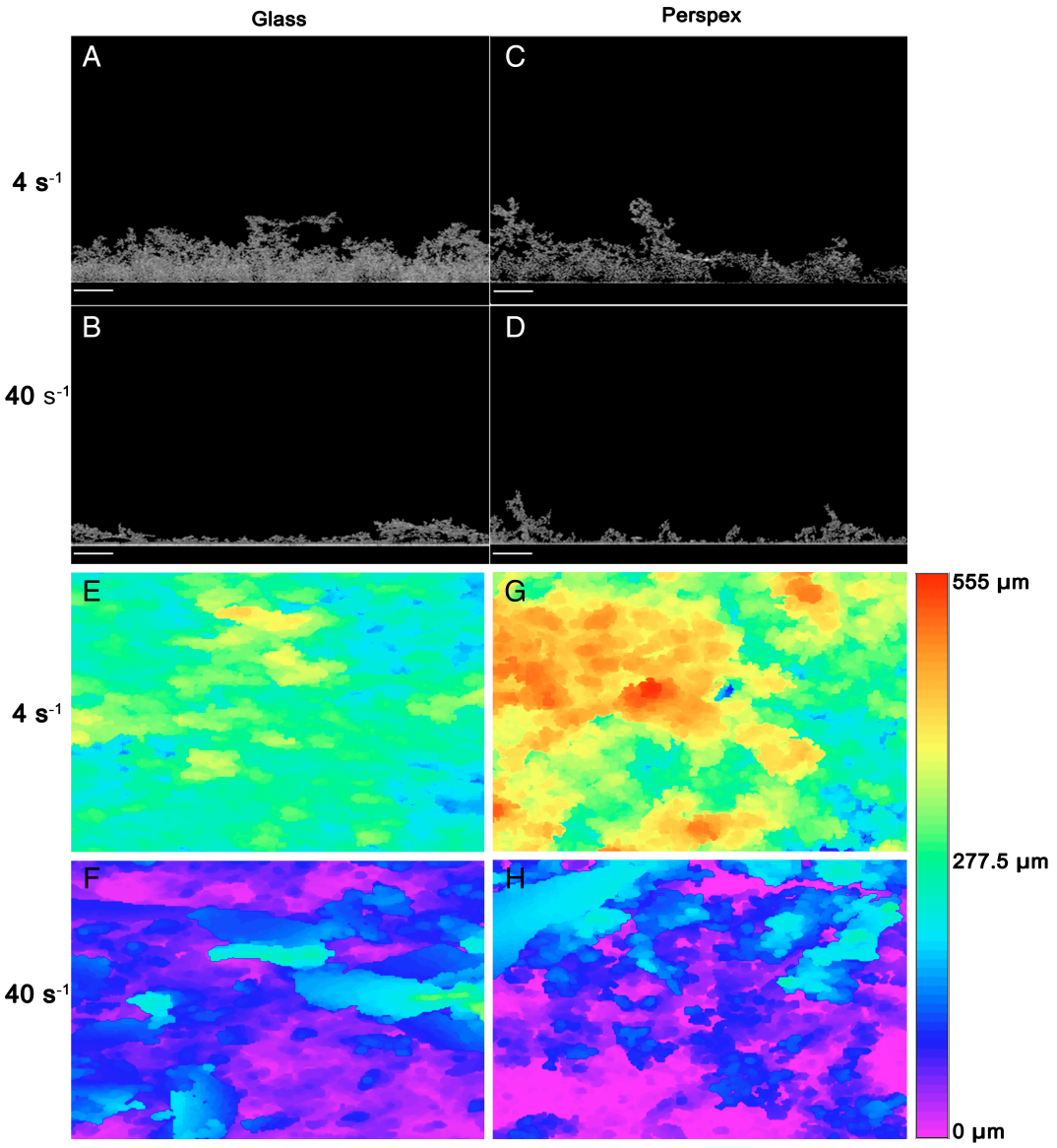

Fig. 9. Representative images obtained by OCT of unidentified filamentous Synechococcales LEGE 07185 biofilms formed after 49 days on glass and perspex. A–D. 2D cross-sectional OCT images (scale bar = 200 µm). E–H. 3D OCT images, top view projection (the colour scale shows the range of biofilm thickness). Biofilms were formed at two different shear rates, 4 s^{-1} (A, C, E, G) and 40 s^{-1} (B, D, F, H). [Color figure can be viewed at wileyonlinelibrary.com]

industrial detergent (Johnson Diversey, Northampton, United Kingdom; Meireles *et al*., 2017) and sterile distilled water for 20 min under agitation (150 rpm). In order to remove any remaining disinfectant, coupons were rinsed in sterile distilled water and air-dried. Additionally, glass coupons were autoclaved (121°C, 15 min; Azevedo *et al*., 2006). After drying, all coupons were aseptically preweighted. Biofilm formation was assessed on 12-well microtiter plates (VWR International, Carnaxide, Portugal) under optimized conditions for cyanobacterial growth. Transparent double-sided adhesive tape was used to fix the coupons, and once the tape was placed in the wells, all coupons and the plates were subjected to UV sterilization for 30 min after which the sterile coupons were fixed. A volume of 3 ml of each cyanobacterial suspension in Z8 medium (prepared as described above) supplemented with nutritional factors, which support the growth and cyanobacteria maintenance (Kotai, 1972), was inoculated in each well. For control, Z8 medium without cyanobacterial cells was introduced on the wells. Observations demonstrated that the applied methodology was efficient for surface sterilization because no bacterial growth was observed. Microtiter plates were incubated at 25°C in an orbital shaker with a 25 mm orbital radius (Agitorb 200ICP, Norconcessus, Portugal) at 40 and 185 rpm. Biofilm development of the three cyanobacterial strains was followed for 7 weeks (49 days), because it is

14622920, 2019, 11, Downloaded from https://ami-journals.onlinelibrary.wiley.com/doi/10.1111/1462-2920.14807 by Cochrane Portugal, Wiley Online Library on [20/01/2023]. See the Terms and Conditions (https://onlinelibrary.wiley.com/terms-and-conditions) on Wiley Online Library for rules of use; OA articles are governed by the applicable Creative Commons License

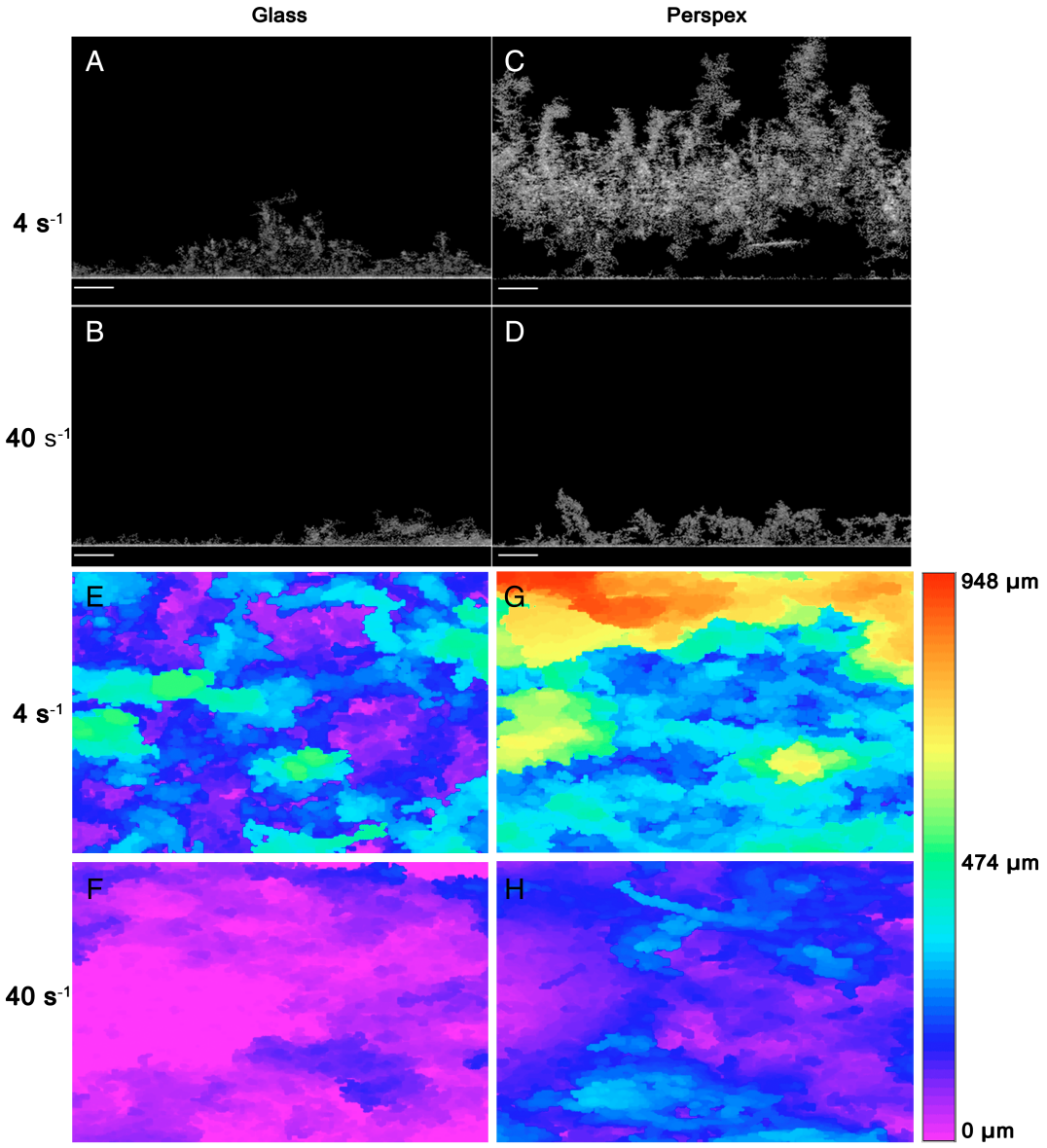

Fig. 10. Representative images obtained by OCT of *Nodosilinea* sp. LEGE 06022 biofilms formed after 49 days on glass and perspex. A–D. 2D cross-sectional OCT images (scale bar = 200 µm). E–H. 3D OCT images, top view projection (the colour scale shows the range of biofilm thickness). Biofilms were formed at two different shear rates, 4 s^{-1} (A, C, E, G) and 40 s^{-1} (B, D, F, H). [Color figure can be viewed at wileyonlinelibrary.com]

accepted that a two-month interval for maintenance is the minimum duration for economically viable underwater monitoring systems (Blain *et al*., 2004). During this incubation time, the medium was replaced twice a week. In order to mimic real light exposure periods, a photoperiod of 14 h light (8–10 µmol photons m^{-2} s^{-1})/10 h dark cycles) was applied.

Biofilm analysis

Optical coherence tomography. Biofilm development was primarily assessed by determination of biofilm structure, thickness and roughness through OCT (Thorlabs Ganymede Spectral Domain Optical Coherence Tomography system with a central wavelength of 930 nm, Thorlabs GmbH, Dachau, Germany). Sampling was performed every 7 days, and at each sampling day, 3 coupons for each surface and hydrodynamic condition for all strains were analysed. Culture medium was carefully removed, and the wells were filled with 3 ml of sterile sodium chloride solution (8.5 $g{\cdot}L^{-1}$). The solution was carefully removed to eliminate loosely attached cyanobacteria. Subsequently, the wells were filled again with 3 ml of sterile sodium chloride solution and imaged. The captured volume was ~ 4 × 4 × 3 mm^3 (509 × 313 × 1024 $pixels^3$). Since biofilms are mainly composed

14622920, 2019, 11, Downloaded from https://ami-journals.onlinelibrary.wiley.com/doi/10.1111/1462-2920.14807 by Cochrane Portugal, Wiley Online Library on [20/01/2023]. See the Terms and Conditions (https://onlinelibrary.wiley.com/terms-and-conditions) on Wiley Online Library for rules of use; OA articles are governed by the applicable Creative Commons License

(90%) of water (Bakke *et al*., 2001), the refractive index was set to 1.40, close to the refractive index of water (1.33). 2D and 3D imaging were performed, and for each coupon, a minimum of three fields of view were analysed to ensure accuracy and reliability of the results obtained. Image analysis was performed as previously described (Gusnaniar *et al*., 2017). First, the bottom of the biofilm was determined as the best fitting parabole (or hyperboloid when imaged in 3D) that connects the white pixels resulting from light reflection on the substratum surface. Subsequently, a grey-value threshold that separates the biofilm from the background was calculated on the basis of the grey-value histogram of the entire image (Otsu, 1979). The upper contour line of the biofilm was defined as those pixels in the image that have a grey value just higher than the grey-value threshold and are connected to the bottom of the biofilm by pixels with grey values higher than the grey-value threshold. The image was then converted to a binary black and white image, and objects not connected to the bottom were rejected from the biofilm structure. Finally, the mean biofilm thickness was calculated based on the number of pixels between the bottom of the biofilm and the upper contour line for each vertical line in the image. Biofilm roughness was analysed by determination of the roughness coefficient, because this parameter allows comparing the structure of different biofilms, across different studies as well as across scales, once this value is normalized to mean biofilm thickness. The relative roughness coefficient ($R^*_\propto$) was calculated using the following Eq. 1, according Wagner and Horn, 2017:

$$R^*_\propto = \frac{1}{N}\sum_{i=1}^{N}\frac{|L_{F,i}-\overline{L}_F|}{\overline{L}_F}, \quad (1)$$

where $L_{F,\,i}$ is a local biofilm thickness measurements at location i and N equals the number of thickness measurements and $\overline{L}_F$ is the mean biofilm thickness.

Wet weight determination and chlorophyll a quantification. In order to complement the characterization of cyanobacterial biofilms, the determination of their wet weight and chlorophyll *a* content was performed. To determine the wet weight, coupons were detached from the wells with the aid of sterile tweezers and weighted. Biofilm wet weight was obtained by the difference to the initial coupon weight (determined prior to inoculation).

Chlorophyll *a* is the predominant and the unique pigment present in all groups of alga and cyanobacteria, and it is commonly used as biomass indicator in aquatic environments. Cyanobacterial cells were detached from the coupons by immersing each coupon in 2 ml of 8.5 $g{\cdot}L^{-1}$ sodium chloride solution and vortexing (VV3, VWR) for 2 min at maximum rotational speed (2500 rpm). Coupons were then removed from the liquid and observed under the microscope to confirm complete cell detachment. Detached cells were harvested by centrifugation (3202*g*, for 5 min at room temperature) and the supernatant discarded. Since chlorophyll pigments are light sensitive, the following chlorophyll extraction procedures were performed in the dark using a protocol adapted from Henriques *et al*., 2007. A volume of 2 ml of 99.8% methanol (Methanol ACS Basic, Scharlau Basic, Barcelona) was added for chlorophyll extraction, and suspensions were incubated at 4°C for a period of 24 h for maximal chlorophyll *a* extraction. Samples were then centrifuged at 3202*g*, for 5 min at room temperature, and the supernatant was transferred to a glass cuvette. The absorbance at 750 nm (turbidity), 665 nm (chlorophyll *a*) and 652 nm (chlorophyll *b*) was determined using a V-1200 spectrophotometer (VWR International China Co., Ltd, Shanghai, China). The chlorophyll *a* concentration ($\mu g{\cdot}cm^{-2}$) was calculated through the following Eq. 2 (Porra *et al*., 1989):

$$\text{Chl}\,a\,(\mu g\cdot mL^{-1}) = 16.29\times A^{665} - 8.54\times A^{652}. \quad (2)$$

Statistical analysis

All experiments were performed in triplicate. Data analysis was performed using the statistical program GraphPad Prism® for Windows, version 6.01 (GraphPad Software, Inc, San Diego, CA, USA), and results were compared using unpaired *t*-tests with a confidence level of 95% (**P < 0.05) and 90% (*P < 0.1).

Acknowledgements

This work was financially supported by project UID/EQU/00511/2019 – Laboratory for Process Engineering, Environment, Biotechnology and Energy – LEPABE funded by national funds through FCT/MCTES (PIDDAC) and by the CVMAR+i – Industrial Innovation and Marine Biotechnology Valorisation, funded by INTERREG V A Espanha Portugal (POCTEP) [0302_CVMAR_I_1_P]. The authors also acknowledge support from the EU COST Actions iPROMEDAI (TD1305) and ENBA (CA15216), and M.J.R. acknowledges a PhD grant from FCT (SFRH/BD/140080/2018).

References

Allen, A.A., Habimana, O., and Casey, E. (2018) The effects of extrinsic factors on the structural and mechanical properties of *Pseudomonas fluorescens* biofilms: a combined study of nutrient concentrations and shear conditions. *Colloids Surf B Biointerfaces* **165**: 127–134.

14622920, 2019, 11, Downloaded from https://ami-journals.onlinelibrary.wiley.com/doi/10.1111/1462-2920.14807 by Cochrane Portugal, Wiley Online Library on [20/01/2023]. See the Terms and Conditions (https://onlinelibrary.wiley.com/terms-and-conditions) on Wiley Online Library for rules of use; OA articles are governed by the applicable Creative Commons License

Azeredo, J., Azevedo, N.F., Briandet, R., Cerca, N., Coenye, T., Costa, A.R., *et al*. (2017) Critical review on biofilm methods. *Crit Rev Microbiol* **43**: 313–351.

Azevedo, N.F., Pacheco, A.P., Keevil, C.W., and Vieira, M.J. (2006) Adhesion of water stressed *Helicobacter pylori* to abiotic surfaces. *J Appl Microbiol* **101**: 718–724.

Bakke, R., Kommedal, R., and Kalvenes, S. (2001) Quantification of biofilm accumulation by an optical approach. *J Microbiol Methods* **44**: 13–26.

Bakker, D.P., Van Der Plaats, A., Verkerke, G.J., Busscher, H.J., and Van Der Mei, H.C. (2003) Comparison of velocity profiles for different flow chamber designs used in studies of microbial adhesion to surfaces. *Appl Environ Microbiol* **69**: 6280–6287.

Bharti, A., Velmourougane, K., and Prasanna, R. (2017) Phototrophic biofilms: diversity, ecology and applications. *J. Appl. Phycol.* **29**: 2729–2744.

Blain, S., Guillou, J., Tréguer, P.J., Woerther, P., Delauney, L., Follenfant, E., *et al*. (2004) High frequency monitoring of the coastal marine environment using the MAREL buoy. *J Environ Monit* **6**: 569–575.

Brackbill, J.U., Kothe, D.B., and Zemach, C. (1992) A continuum method for modeling surface tension. *J Comput Phys* **100**: 335–354.

Buratti, F.M., Manganelli, M., Vichi, S., Stefanelli, M., Scardala, S., Testai, E., and Funari, E. (2017) Cyanotoxins: producing organisms, occurrence, toxicity, mechanism of action and human health toxicological risk evaluation. *Arch Toxicol* **91**: 1049–1130.

Chorus, I., and Cavalieri, M. (2000) Cyanobacteria and algae. In *Monitoring Bathing Waters: A Practical Guide to the Design and Implementation of Assessments and Monitoring Programmes*, Bartram, J., and Rees, G. (eds). London and New York: World Health Organization Report. E & FN Spon, pp. 219–271.

Crawford, R.J., Webb, H.K., Truong, V.K., Hasan, J., and Ivanova, E.P. (2012) Surface topographical factors influencing bacterial attachment. *Adv Colloid Interface Sci* **179–182**: 142–149.

Dean, C., Soloviev, A., Hirons, A., Frank, T., and Wood, J. (2016) Biomixing due to diel vertical migrations of zooplankton: comparison of computational fluid dynamics model with observations. *Ocean Model* **98**: 51–64.

Delauney, L., Compare, C., and Lehaitre, M. (2010) Biofouling protection for marine environmental sensors. *Ocean Sci* **6**: 503–511.

Di Pippo, F., and Congestri, R. (2017) Culturing toxic benthic blooms: the fate of natural biofilms in a microcosm system. *Microorganisms* **5**: 46.

Drescher, K., Shen, Y., Bassler, B.L., and Stone, H.A. (2013) Biofilm streamers cause catastrophic disruption of flow with consequences for environmental and medical systems. *Proc Natl Acad Sci U S A* **110**: 4345–4350.

Duddu, R., Chopp, D.L., and Moran, B. (2009) A two-dimensional continuum model of biofilm growth incorporating fluid flow and shear stress based detachment. *Biotechnol Bioeng* **103**: 92–104.

Flemming, H.-C., Murthy, P.S., Venkatesan, R., and Cooksey, K. (2009). In *Marine and Industrial Biofouling*, Costerton, J.W. (ed). Los Angeles, CA: Springer Berlin Heidelberg.

Frazão, B., Martins, R., and Vasconcelos, V. (2010) Are known cyanotoxins involved in the toxicity of picoplanktonic and filamentous North Atlantic marine cyanobacteria? *Mar. Drugs* **8**: 1908–1919.

Gomes, L.C., Moreira, J.M.R., Teodósio, J.S., Araújo, J.D.P., Miranda, J.M., Simões, M., *et al*. (2014) 96-well microtiter plates for biofouling simulation in biomedical settings. *Biofouling* **30**Placeholder Text: 535–546.

Gomes, L.C., Silva, L.N., Simões, M., Melo, L.F., and Mergulhão, F.J. (2015) *Escherichia coli* adhesion, biofilm development and antibiotic susceptibility on biomedical materials. *J Biomed Mater Res Part A* **103**: 1414–1423.

Graba, M., Sauvage, S., Moulin, F.Y., Urrea, G., Sabater, S., and Sanchez-Pérez, J.M. (2013) Interaction between local hydrodynamics and algal community in epilithic biofilm. *Water Res* **47**: 2153–2163.

Gusnaniar, N., Sjollema, J., Nuryastuti, T., Peterson, B.W., van de Belt-Gritter, B., de Jong, E.D., *et al*. (2017) Structural changes in *S. epidermidis* biofilms after transmission between stainless steel surfaces. *Biofouling* **33**: 712–721.

Henriques, M., Silva, A., and Rocha, J. (2007) Extraction and quantification of pigments from a marine microalga : a simple and reproducible method. *Commun. Curr. Res. Educ. Top. Trends Appl. Microbiol*. **2**: 586–593.

Hirt, C.W., and Nichols, B.D. (1981) Volume of fluid (VOF) method for the dynamics of free boundaries. *J Comput Phys* **39**: 201–225.

King, R.K., Flick, G.J., Smith, S.A., Pierson, M.D., Boardman, G.D., and Coale, C.W. (2006) Comparison of bacterial presence in biofilms on different materials commonly found in recirculating aquaculture systems. *J Appl Aquaculture* **18**: 79–88.

Kotai, J. (1972) *Instructions for the Preparation of Modified Nutrient Solution Z8 for Algae*. Blindern, Oslo: Norwegian Institute for Water Research, p. 5.

Lawton, L., Marsalek, B., Padisak, J., and Chorus, I. (1999) Determination of cyanobacteria in the laboratory. In *Toxic Cyanobacteria in Water. A Guide to their Public Health Consequences, Monitoring and Management*, Chorus, I., and Bartram, J. (eds). London and New York: World Health Organization Report. E & FN Spon, pp. 347–367.

Martins, R., Pereira, P., Welker, M., Fastner, J., and Vasconcelos, V.M. (2005) Toxicity of culturable cyanobacteria strains isolated from the Portuguese coast. *Toxicon* **46**: 454–464.

Meireles, A., Fulgêncio, R., Machado, I., Mergulhão, F., Melo, L., and Simões, M. (2017) Characterization of the heterotrophic bacteria from a minimally processed vegetables plant. *LWT-Food Sci Technol* **85**: 293–300.

Mieszkin, S., Callow, M.E., and Callow, J.A. (2013) Interactions between microbial biofilms and marine fouling algae: a mini review. *Biofouling* **29**: 1097–1113.

Minchin, D., and Gollasch, S. (2003) Fouling and ships' hulls: how changing circumstances and spawning events may result in the spread of exotic species. *Biofouling* **19**: 111–122.

Moreira, J., Araújo, J.D.P., Miranda, J.M., Simões, M., Melo, L.F., and Mergulhão, F.J. (2014) The effects of surface properties on *Escherichia coli* adhesion are modulated by shear stress. *Colloids Surf B Biointerfaces* **123**: 1–7.

14622920, 2019, 11, Downloaded from https://ami-journals.onlinelibrary.wiley.com/doi/10.1111/1462-2920.14807 by Cochrane Portugal, Wiley Online Library on [20/01/2023]. See the Terms and Conditions (https://onlinelibrary.wiley.com/terms-and-conditions) on Wiley Online Library for rules of use; OA articles are governed by the applicable Creative Commons License

Moreira, J.M.R., Gomes, L.C., Simões, M., Melo, L.F., and Mergulhão, F.J. (2015a) The impact of material properties, nutrient load and shear stress on biofouling in food industries. *Food Bioprod Process* **95**: 228–236.

Moreira, J.M.R., Ponmozhi, J., Campos, J.B.L.M., Miranda, J.M., and Mergulhão, F.J. (2015b) Micro- and macro-flow systems to study *Escherichia coli* adhesion to biomedical materials. *Chem Eng Sci* **126**: 440–445.

Otsu, N. (1979) A threshold selection method from gray-level histograms. *IEEE Trans Syst Man Cybern* **9**: 62–66.

Porra, R., Thompson, W., and Kriedemann, P. (1989) Determination of accurate extinction coefficients and simultaneous equations for assaying chlorophylls *a* and *b* extracted with four different solvents: verification of the concentration of chlorophyll standards by atomic absorption spectroscopy. *Biochim Biophys Acta* **975**: 384–394.

Qian, P.Y., Rittschof, D., Sreedhar, B., and Chia, F.S. (1999) Macrofouling in unidirectional flow: miniature pipes as experimental models for studying the effects of hydrodynamics on invertebrate larval settlement. *Mar Ecol Prog Ser* **191**: 141–151.

Qian, P.Y., Rittschof, D., and Sreedhar, B. (2000) Macrofouling in unidirectional flow: miniature pipes as experimental models for studying the interaction of flow and surface characteristics on the attachment of barnacle, bryozoan and polychaete larvae. *Mar Ecol Prog Ser* **207**: 109–121.

Ramos, V., Morais, J., Castelo-Branco, R., Pinheiro, Â., Martins, J., Regueiras, A., *et al*. (2018) Cyanobacterial diversity held in microbial biological resource centers as a biotechnological asset: the case study of the newly established LEGE culture collection. *J Appl Phycol* **30**: 1437–1451.

Regueiras, A., Pereira, S., Costa, M.S., and Vasconcelos, V. (2018) Differential toxicity of cyanobacteria isolated from marine sponges towards echinoderms and crustaceans. *Toxins* **10**: 1–12.

Rossi, F., and De Philippis, R. (2015) Role of cyanobacterial exopolysaccharides in phototrophic biofilms and in complex microbial mats. *Life* **5**: 1218–1238.

Roy, G.J. (1983) *Notes on Instrumentation and Control*. Oxford, UK and Boston, MA: Newnes.

Salta, M., Wharton, J.A., Blache, Y., Stokes, K.R., and Briand, J.F. (2013) Marine biofilms on artificial surfaces: structure and dynamics. *Environ Microbiol* **15**: 2879–2893.

Sedlmeier, F., Janecek, J., Sendner, C., Bocquet, L., Netz, R.R., and Horinek, D. (2008) Water at polar and nonpolar solid walls (review). *Biointerphases* **3**: FC23–FC39.

Sener, G., Ozgur, E., Rad, A.Y., Uzun, L., Say, R., and Denizli, A. (2013) Rapid real-time detection of procalcitonin using a microcontact imprinted surface plasmon resonance biosensor. *Analyst* **138**: 6422–6428.

Taylor, D.A. (1996). Instrumentation and control. In *Introduction to Marine Engineering*, Taylor, D.A. (ed). Oxford, Boston: Butterworth-Heinemann, pp. 279–325.

Telegdi, J., Trif, L., and Románszki, L. (2016) Smart antibiofouling composite coatings for naval applications. In *Smart Composite Coatings and Membranes: Transport, Structural, Environmental and Energy Applications*, Montemor, M.F. (ed). Cambridge, UK: Woodhead Publishing, pp. 123–155.

Teodósio, J.S., Simões, M., Melo, L.F., and Mergulhão, F.J. (2011) Flow cell hydrodynamics and their effects on *E. coli* biofilm formation under different nutrient conditions and turbulent flow. *Biofouling* **27**: 1–11.

Thukkaram, M., Sitaram, S., Kannaiyan, S.K., and Subbiahdoss, G. (2014) Antibacterial efficacy of iron-oxide nanoparticles against biofilms on different biomaterial surfaces. *Int J Biomater* **2014**: 716080.

Wagner, M., and Horn, H. (2017) Optical coherence tomography in biofilm research: a comprehensive review. *Biotechnol Bioeng* **114**: 1386–1402.

Youngs, D. (1982) Time-dependent multi-material flow with large fluid distortion. In *Numerical Methods for Fluid Dynamics*, Morton, K., and Baibnes, M. (eds). New York: Academic Press, pp. 273–285.

Yuan, Y., and Lee, T.R. (2013) Contact angle and wetting properties. In *Surface science techniques. Springer Series, Surface Sciences*, Vol. **51**, Bracco, G., and Holst, B. (eds). Heidelberg: Springer-Verlag, pp. 3–34.

Supporting Information

Additional Supporting Information may be found in the online version of this article at the publisher's web-site:

Appendix S1. Supporting Information.

14622920, 2019, 11, Downloaded from https://ami-journals.onlinelibrary.wiley.com/doi/10.1111/1462-2920.14807 by Cochrane Portugal, Wiley Online Library on [20/01/2023]. See the Terms and Conditions (https://onlinelibrary.wiley.com/terms-and-conditions) on Wiley Online Library for rules of use; OA articles are governed by the applicable Creative Commons License

Supporting Information

S1 - Velocity profiles

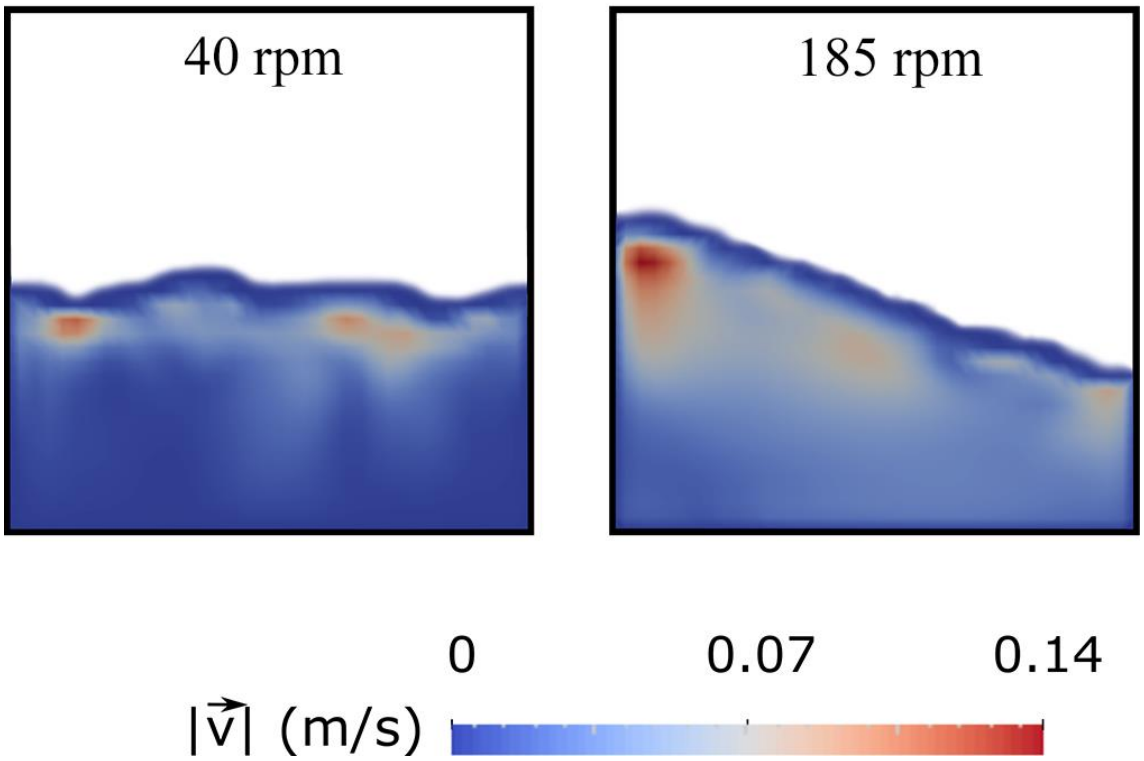

Figure S1. Velocity profiles obtained at both shaking frequencies: 40 rpm and 185 rpm.

S2 - Correlation between wet weight and chlorophyll a

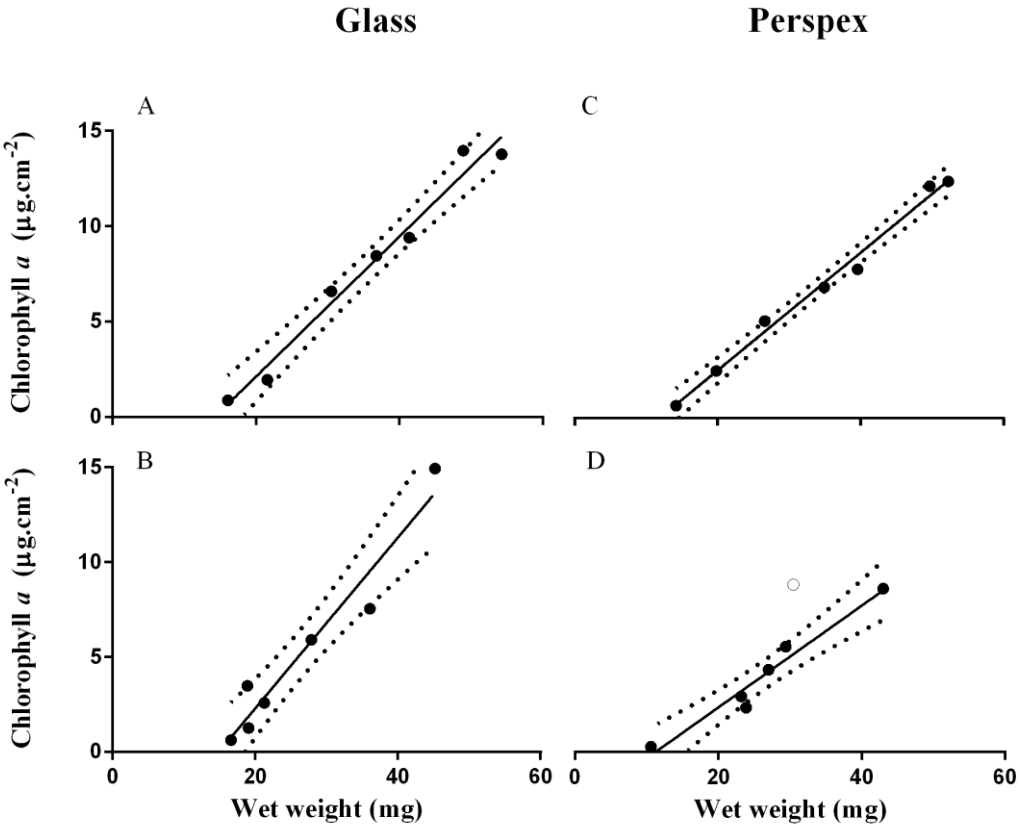

Figure S2.1 - Correlation between wet weight and chlorophyll *a* on *Nodosilinea* sp. LEGE 06020. Biofilm development in glass (A, B) and perspex (C, D), at two different shear rates, 4 s-1 (A, C) and 40 s-1 (B, D). Full line represents the linear regression whereas the dashed line represents the confidence limits (95%). Closed symbols refer to data points that were considered for the regression (all except one) and the single open symbol refers to a data point that was excluded from the regression.

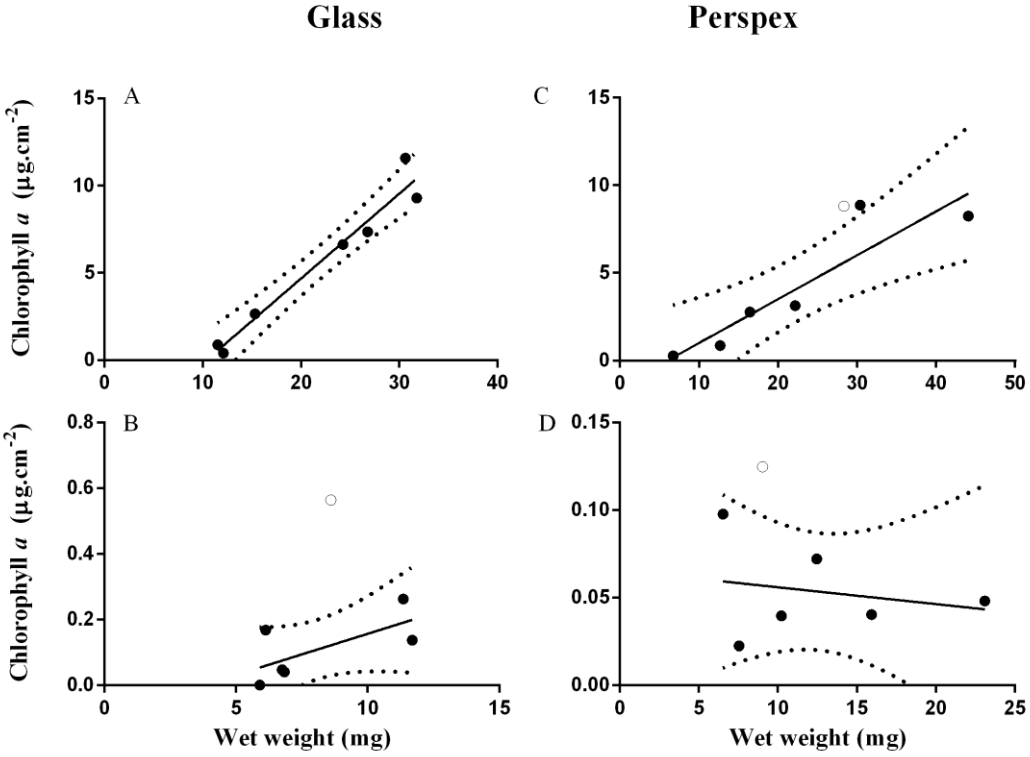

Figure S2.2 - Correlation between wet weight and chlorophyll *a* on unidentified filamentous Synechococcales LEGE 07185. Biofilm development in glass (A,B) and perspex (C,D), at two different shear rates, 4 s-1 (A,C) and 40 s-1 (B,D). Full line represents the linear regression whereas the dashed line represents the confidence limits (95%). Closed symbols refer to data points that were considered for the regression (all except three) and the open symbols refer to a data points that were excluded from the regression.

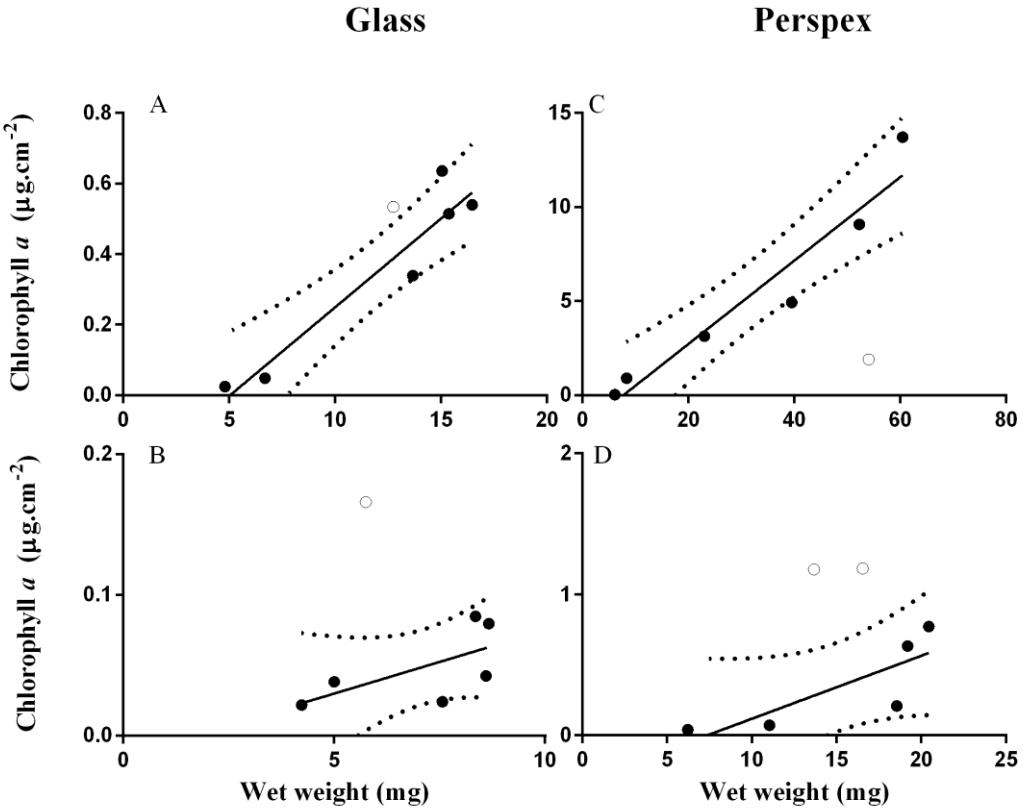

Figure S2.3 - Correlation between wet weight and chlorophyll *a* on *Nodosilinea* sp. LEGE 06022. Biofilm development in glass (A,B) and perspex (C,D), at two different shear rates, 4 s-1 (A,C) and 40 s-1 (B,D). Full line represents the linear regression whereas the dashed line represents the confidence limits (95%). Closed symbols refer to data points that were considered for the regression (all except five) and the open symbols refer to a data points that were excluded from the regression.

S3– Evaluation of cyanobacterial biofilm development under the same hydrodynamic condition on different surfaces

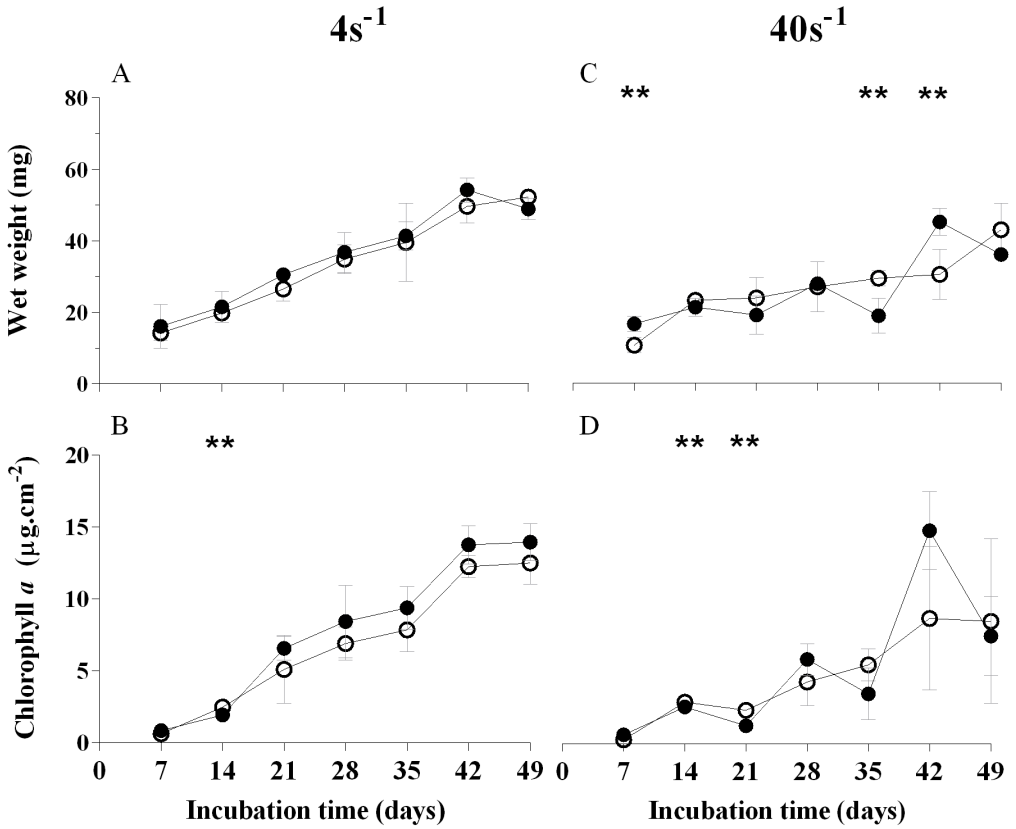

Figure S3.1 - Evaluation of *Nodosilinea* sp. LEGE 06020 biofilm development. The parameters analysed refer to wet weight (A,C), chlorophyll *a* (B,D). Biofilms were formed at 4 s^{-1} (A,B) or 40 s^{-1} (C,D), on two different surfaces, glass (closed circles) and perspex (open circles) during 49 days. Standard deviations from 3 replicates are represented. Symbols *; ** indicate statistically different values for $P < 0.1$ and $P < 0.05$ (respectively) at each incubation time.

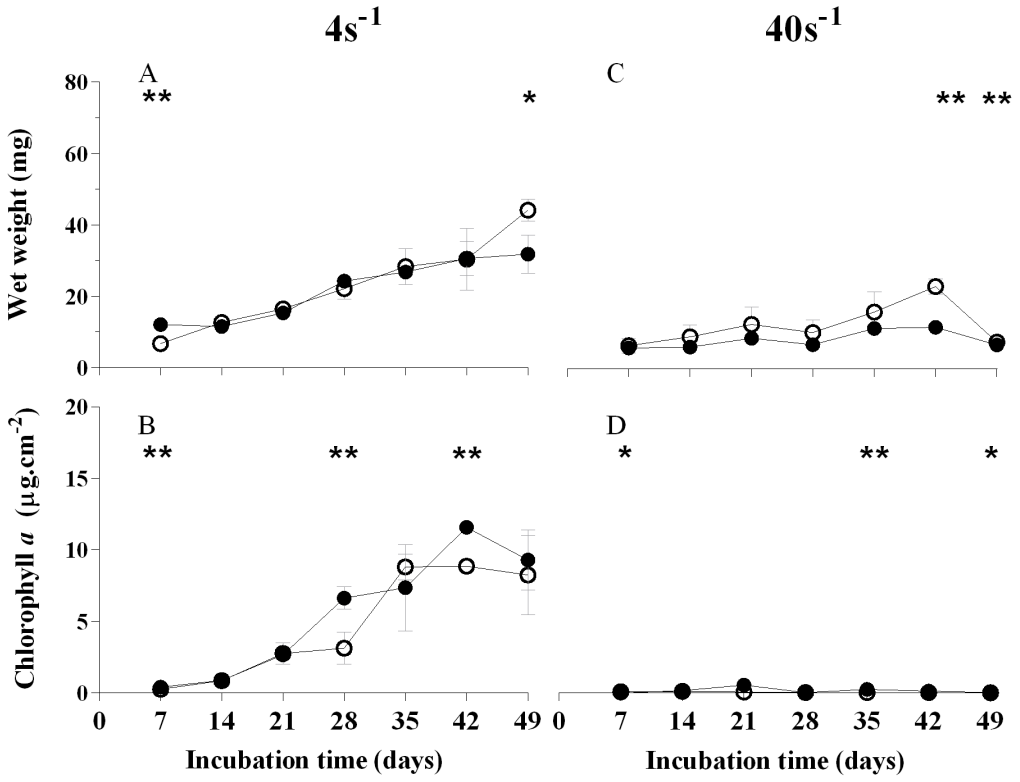

Figure S3.2 - Evaluation of unidentified filamentous Synechococcales LEGE 07185. biofilm development. The parameters analysed refer to wet weight (A,C), chlorophyll *a* (B,D). Biofilms were formed at 4 s^{-1} (A,B) or 40 s^{-1} (C,D), on two different surfaces, glass (closed circles) and perspex (open circles) during 49 days. Standard deviations from 3 replicates are represented. Symbols *; ** indicate statistically different values for $P < 0.1$ and $P < 0.05$ (respectively) at each incubation time.

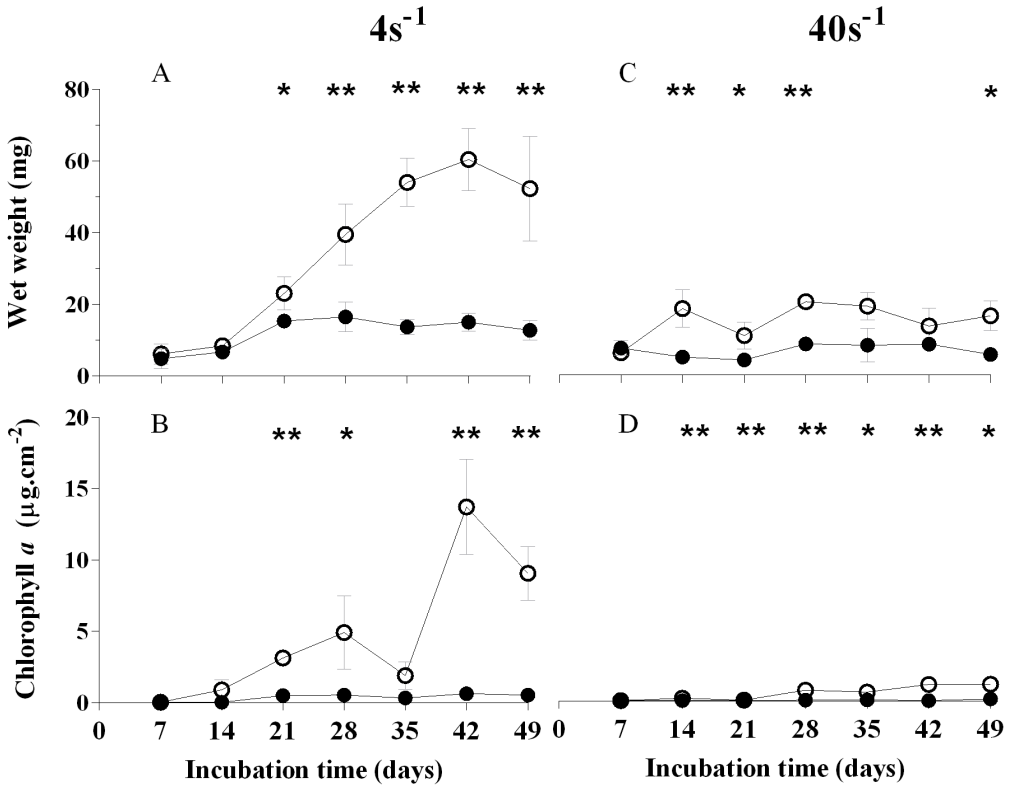

Figure S3.3 - Evaluation of *Nodosilinea* sp. LEGE 06022 biofilm development. The parameters analysed refer to wet weight (A,C), chlorophyll *a* (B,D). Biofilms were formed at 4 s^{-1} (A,B) or 40 s^{-1} (C,D), on two different surfaces, glass (closed circles) and perspex (open circles) during 49 days. Standard deviations from 3 replicates are represented. Symbols *; ** indicate statistically different values for $P < 0.1$ and $P < 0.05$ (respectively) at each incubation time.

Taylor & Francis
Taylor & Francis Group

Biofouling
The Journal of Bioadhesion and Biofilm Research

ISSN: (Print) (Online) Journal homepage: https://www.tandfonline.com/loi/gbif20

Characterization of planktonic and biofilm cells from two filamentous cyanobacteria using a shotgun proteomic approach

Maria João Leal Romeu, Dany Domínguez-Pérez, Daniela Almeida, João Morais, Alexandre Campos, Vítor Vasconcelos & Filipe J. M. Mergulhão

To cite this article: Maria João Leal Romeu, Dany Domínguez-Pérez, Daniela Almeida, João Morais, Alexandre Campos, Vítor Vasconcelos & Filipe J. M. Mergulhão (2020) Characterization of planktonic and biofilm cells from two filamentous cyanobacteria using a shotgun proteomic approach, Biofouling, 36:6, 631-645, DOI: 10.1080/08927014.2020.1795141

To link to this article: https://doi.org/10.1080/08927014.2020.1795141

View supplementary material

Published online: 26 Jul 2020.

Submit your article to this journal

Article views: 395

View related articles

View Crossmark data

Citing articles: 6 View citing articles

Full Terms & Conditions of access and use can be found at
https://www.tandfonline.com/action/journalInformation?journalCode=gbif20

BIOFOULING
2020, VOL. 36, NO. 6, 631–645
https://doi.org/10.1080/08927014.2020.1795141

Taylor & Francis
Taylor & Francis Group

Check for updates

Characterization of planktonic and biofilm cells from two filamentous cyanobacteria using a shotgun proteomic approach

Maria João Leal Romeu[a], Dany Domínguez-Pérez[b], Daniela Almeida[b], João Morais[b], Alexandre Campos[b], Vítor Vasconcelos[b,c] and Filipe J. M. Mergulhão[a]

[a]LEPABE - Laboratory for Process Engineering, Environment, Biotechnology and Energy, Faculty of Engineering, University of Porto, Rua Dr. Roberto Frias, Porto, Portugal; [b]CIIMAR - Interdisciplinary Centre of Marine and Environmental Research, University of Porto, Terminal de Cruzeiros do Porto de Leixões, Matosinhos, Portugal; [c]Department of Biology, Faculty of Sciences, University of Porto, Rua do Campo Alegre, Porto, Portugal

ABSTRACT

Cyanobacteria promote marine biofouling with significant impacts. A qualitative proteomic analysis, by LC-MS/MS, of planktonic and biofilm cells from two cyanobacteria was performed. Biofilms were formed on glass and perspex at two relevant hydrodynamic conditions for marine environments (average shear rates of $4\,s^{-1}$ and $40\,s^{-1}$). For both strains and surfaces, biofilm development was higher at $4\,s^{-1}$. Biofilm development of *Nodosilinea* sp. LEGE 06145 was substantially higher than *Nodosilinea* sp. LEGE 06119, but no significant differences were found between surfaces. Overall, 377 and 301 different proteins were identified for *Nodosilinea* sp. LEGE 06145 and *Nodosilinea* sp. LEGE 06119. Differences in protein composition were more noticeable in biofilms formed under different hydrodynamic conditions than in those formed on different surfaces. Ribosomal and photosynthetic proteins were identified in most conditions. The characterization performed gives new insights into how shear rate and surface affect the planktonic to biofilm transition, from a structural and proteomics perspective.

ARTICLE HISTORY
Received 13 May 2020
Accepted 6 July 2020
Published online 26 July 2020

KEYWORDS
Marine biofouling; cyanobacterial biofilms; shotgun proteomics; LC-MS/MS; hydrodynamic conditions; real-time imaging; optical coherence tomography

Introduction

Marine biofouling causes several ecological problems and severe economic impacts on aquatic environments and marine industries (Carvalho 2018). Biofilm formation on submerged equipment containing optical and electrochemical sensors (which are used for on-site monitoring with continuous measuring) can affect readings and lead to incorrect measurements (Delauney et al. 2010). Cyanobacteria and diatoms are responsible for the initiation of biofilm formation by the production of large amounts of extracellular polymeric substances (EPS), and they also represent the major components of marine biofilms (Bharti et al. 2017). Additionally, these microfouler organisms can promote the adhesion of macrofouler organisms such as invertebrate larvae, mussels, seaweeds and barnacles (Mieszkin et al. 2013).

Physico-chemical factors related to the surface being colonized (Crawford et al. 2012) and flow velocity and shear rate (Allen et al. 2018) are some of the most critical parameters that affect biofilm composition, structure and development. Moreover, these factors can also impact EPS production, energy metabolism and induce molecular changes in biofilms (Moreira et al. 2015). The development of novel antifouling strategies for marine applications is of paramount importance (Telegdi et al. 2016). Therefore, molecular studies capable of identifying the agents and pathways affecting the settlement of biofouling organisms are necessary to obtain new targets and develop more effective biofilm mitigation strategies.

Omics approaches such as genomics, transcriptomics, proteomics and metabolomics have been widely used to characterize bacterial virulence factors (Alexova et al. 2011; Babele et al. 2019) and provide new information about biofilm development and regulation (Leary et al. 2014; Parnasa et al. 2016). Specifically, proteomic studies have also been used to understand the molecular mechanisms involved in important cellular processes such as cell division, metabolism, transport, stress response and motility in these microbial communities (Parnasa et al. 2016;

CONTACT Filipe J. M. Mergulhão filipem@fe.up.pt
Supplemental data for this article can be accessed at https://doi.org/10.1080/08927014.2020.1795141.
© 2020 Informa UK Limited, trading as Taylor & Francis Group

Wang et al. 2020). Furthermore, proteomic analysis allows the study of interspecies interactions on biofilms (Herschend et al. 2017) and how biofilm development is affected by physiological and environmental factors (Chen et al. 2019). In a stressful condition, the long-term adaptation is governed by mechanisms of cellular regulation as the synthesis and/or modified expression of proteins. The identification of these proteins using high throughput proteomic tools has provided new insights into the cellular response to a defined stress condition and also regarding the cell signaling and stress response pathways that are activated under different conditions (Muthusamy et al. 2017; Battchikova et al. 2018). Since modifications in the proteome are associated with physiological and metabolic rearrangements at the genotype level during stress adaptation and tolerance, qualitative proteomic studies lead to the identification and characterization of these stress-responsive proteins (Babele et al. 2019). Therefore, qualitative proteomic experiments can provide a general picture of the physiological state of a given organism through the identification of proteins which are translated under different conditions.

The isolation and purification of stable and high-quality proteins is the most challenging task in cyanobacterial proteomic experiments (Pandhal et al. 2009), since cyanobacteria contain several proteases, oxidative enzymes, phycobiliproteins and other pigments which hinder the effective extraction, purification and recovery of less abundant proteins (Ow et al. 2011). In this context, novel extraction protocols have been developed and were a major step for today's high throughput proteomic workflows (Anderson et al. 2006). The development of high-resolution liquid chromatography (LC) and more advanced tandem mass spectrometry (MS/MS) enabled the development of shotgun proteomics (Babele et al. 2019). Since proteomes are directly digested and analyzed *in situ* by a combination of liquid chromatographic separation and analysis using high-speed tandem mass spectrometry, shotgun proteomics opened up opportunities to perform fast and reliable identification of cyanobacterial proteins (Anderson et al. 2006). Furthermore, LC–MS/MS data acquisition is nearly fully automated, which enables analysis in a high throughput mode leading to low variations, thus, improving the confidence of the results.

Although several studies investigated the proteome of planktonic and sessile forms, only a few address marine biofilms (Leary et al. 2014). The data available on cyanobacteria are sparse (Babele et al. 2019) and focus on well-studied model cyanobacteria, such as the unicellular cyanobacterium *Synechocystis* sp. PCC 6803 (Jahn et al. 2018). Moreover, the small number of proteomic studies performed on filamentous cyanobacteria is rather old and restricted to the cyanobacterial genera *Nostoc*, *Anabaena* and *Spirulina* (Anderson et al. 2006; Kurdrid et al. 2011).

The main aim of this study was to perform a qualitative proteomic analysis on filamentous cyanobacteria under planktonic and different conditions of biofilm development. To the best of the authors' knowledge, there are no proteomic studies evaluating the impact of different surfaces and different hydrodynamic conditions on cyanobacterial biofilm behavior. Since no proteomic analysis of the genus *Nodosilinea* is available, this represents the first work that investigated the proteome obtained from different conditions of biofilm development of this ubiquitous cyanobacterial genus. Cyanobacterial strains from the genus *Nodosilinea* are present in dissimilar geographies, including different continents (Europe, Antarctica, Asia and America), and specimens can also be found in different ecologies, such as brackish water, freshwater, marine and even terrestrial environments (Heidari et al. 2018; Ramos et al. 2018; Vázquez-Martínez et al. 2018; Radzi et al. 2019). This cosmopolitan distribution highlights the importance of studying biofilm formation by these organisms. Moreover, the relevance of studying these filamentous cyanobacterial strains is even more critical given the biofouling potential of these organisms. Indeed, some studies showed the high biofouling potential of the genus *Nodosilinea* on different surfaces. Additionally, cyanobacterial strains from this genus were recovered from biofilms on a house wall (Perkerson Iii et al. 2011), from a benthic mat in a thermal spring with very high natural radioactivity (Heidari et al. 2018) and even from mats collected in Antarctica (Radzi et al. 2019). *Nodosilinea* strains were also found on subaerial biofilms, which develop on mineral surfaces and on archaeological stone monuments experiencing extended periods of heat, insolation and dehydration (Vázquez-Martínez et al. 2018). These biofilms have been widely studied due to their impact on deterioration of cultural heritage.

Materials and methods

Organism and inocula preparation

Two cyanobacterial strains were used in this study, and both were obtained from the Blue Biotechnology and Ecotoxicology Culture Collection (LEGE-CC)

located at CIIMAR, Portugal (Ramos et al. 2018). *Nodosilinea* sp. LEGE 06145 was isolated from a sample scraped from a wave-exposed rock in a tide puddle collected at Moledo beach, Portugal (41.84963 N 8.866717 W). *Nodosilinea* sp. LEGE 06119 was isolated from a seawater sample collected in the surf zone at Burgau beach, Portugal (37.07156 N 8.774722 W) (Ramos et al. 2018). Cells from an initial 50 ml culture were grown for 30 days in 750 ml of Z8 medium (Kotai 1972) supplemented with 25 g l^{-1} of synthetic sea salts (Tropic Marin) and vitamin B_{12} (Sigma Aldrich, Merck, St Louis, MO, USA). Cultures were performed under 14 h light (10–30 µmol photons m^{-2} s^{-1})/10 h dark cycles, at 25 °C.

Biofilm formation

Biofilm formation was assessed on agitated 12-well microtiter plates (VWR International, Carnaxide, Portugal), since this platform was shown to mimic the hydrodynamic conditions found in marine environments (Romeu et al. 2019). In order to assess the effect of the surface on protein expression, biofilms were developed on glass (Vidraria Lousada, Lda, Portugal) and perspex (Neves & Neves, Lda, Portugal) coupons (1 cm^2). These represent commonly submerged artificial surfaces found on different equipment in aquatic and marine environments (Taylor 1996; King et al. 2006). Moreover, these surfaces present different hydrophobicity (perspex is relatively hydrophobic compared with glass) (Romeu et al. 2019). Surface preparation was performed as described in Romeu et al. (2019). All coupons were aseptically pre-weighed. Transparent double-sided adhesive tape was used to fix the coupons and once the tape was placed in the wells, all coupons and the plates were subjected to UV sterilization for 30 min, after which the sterile coupons were fixed. Since chlorophyll *a* concentration is commonly used as biomass indicator in aquatic environments, prior to inoculation each cyanobacterial suspension was adjusted to a chlorophyll *a* concentration of 1.5 µg ml^{-1}. Briefly, 2 ml of each suspension were incubated for 24 h at 4 °C in the dark for a maximal chlorophyll *a* extraction. The samples were then centrifuged at 3,202 *g*, for 5 min at room temperature, and the supernatant was transferred to a glass cuvette. The absorbance at 750 nm (turbidity), 665 nm (chlorophyll *a*) and 652 nm (chlorophyll *b*) was determined using a V-1200 spectrophotometer (VWR International China Co., Ltd, Shanghai, China). The chlorophyll *a* concentration (µg cm^{-2}) was calculated by the following Equation (1) (Porra et al. 1989):

$$\mathrm{Chl}a\left(\mu g\ ml^{-1}\right) = 16.29 \times A^{665} - 8.54 \times A^{652} \quad (1)$$

These measurements were performed in triplicate and the dilutions were performed using Z8 medium supplemented with 25 g l^{-1} of synthetic sea salts and vitamin B_{12}. After cyanobacterial suspension adjustment, planktonic samples for proteomic analysis were collected and kept at −80 °C.

A volume of 3 ml of adjusted cyanobacterial suspension in Z8 medium (prepared as described above) supplemented with nutritional factors, which support the growth and cyanobacteria maintenance (Kotai 1972), was inoculated in each well. In order to assess the hydrodynamic effect on protein expression, cyanobacterial biofilm formation at different shear rates was tested. In order to attain the shear rate values that can mimic aquatic environments, such as those found on a ship hull in a harbor and in partially submerged or even moored equipment and devices (as underwater cameras, flotation spheres, sensors and even transparent hulls of boats or their windows), microtiter plates were incubated at 25 °C in an orbital shaker with a 25 mm orbital radius (Agitorb 200ICP, Norconcessus, Portugal) at 185 rpm (achieving the average shear rate of 40 s^{-1}, Romeu et al. 2019). Moreover, since lower fluid velocities can promote marine biofouling (Flemming et al. 2009), biofilm development was also assessed at lower shear rate conditions (average shear rate of 4 s^{-1}, achieved at 40 rpm). Biofilm development was followed for seven weeks (49 days) since it is accepted that a two-month interval for maintenance is the minimum duration for economically viable underwater monitoring systems, as previously reported (Romeu et al. 2019). During this incubation time, the medium was replaced twice a week. In order to mimic real light exposure periods, a photoperiod of 14 h light (8–10 µmol photons m^{-2} s^{-1})/10 h dark cycles) was applied.

Biofilm analysis

Sampling was performed every seven days and at each sampling day, three coupons for each surface and hydrodynamic condition were analyzed for both cyanobacteria. The culture medium was carefully removed and the wells were filled with 3 ml of sterile sodium chloride solution (8.5 g l^{-1}) to evaluate the cyanobacterial biofilm structure and thickness by

optical coherence tomography (OCT). In order to complement the characterization of cyanobacterial biofilms, the determination of their wet weight and chlorophyll *a* content was performed.

Optical coherence tomography

Images from cyanobacterial biofilms developed on both surfaces and under the different hydrodynamic conditions were captured as reported in Romeu et al. (2019). Briefly, the captured volume was $\sim 4 \times 4 \times 3\,mm^3$ ($509 \times 313 \times 1{,}024$ pixels^3) and since biofilms are mainly composed (90%) of water (Bakke et al. 2001), the refractive index was set to 1.40. For each coupon, 2-D imaging was performed with a minimum of three fields of view, to ensure the accuracy and reliability of the results obtained. Image analysis was performed using a routine developed in the Image Processing Toolbox from MATLAB 8.0 and Statistics Toolbox 8.1 (The MathWorks, Inc., Natick, MA, USA). The processing steps include image denoising, detection of the surface layer/biofilm bottom and segmentation of the biofilm structure by the upper contour line of the biofilm. The acquired image is denoised using Haar wavelets (Mayer et al. 2012). The method used for the detection of the biofilm bottom consists of edge detection, using the Canny edge filter (Canny 1986) and straight-line detection, using the Hough line transform (Duda and Hart 1972). The highest peak in Hough space corresponds to the surface layer and biofilm bottom. For the segmentation of the biofilm structure, a Sobel operator is applied, and the result is thresholded. Then, the resulting binary image is dilated, using a vertical structuring element and a horizontal structuring element and the holes inside the biofilm are filled in. Finally, the contours of the resulting binary image are smoothed, by eroding the image with a diamond structuring element. In this way, a binary "mask" that covers the biofilm region is obtained. The biofilm is delimited by the upper boundary of this "mask" and by the surface layer/biofilm bottom. The mean of biofilm thickness was calculated based in the distance between the biofilm bottom and the upper contour line according the following Equation (2):

$$\overline{L}_F = \frac{1}{N} \sum_{i=1}^{N} L_{F,i} \tag{2}$$

where $L_{F,i}$ is a local biofilm thickness measurements at location i and N equals the number of thickness measurements and $\overline{L}_F$ is the mean biofilm thickness.

Wet weight determination and chlorophyll *a* quantification

The determination of the wet weight and chlorophyll *a* content of cyanobacterial biofilms was performed as reported in Romeu et al. (2019). Briefly, to determine the wet weight, coupons were detached from the wells and weighed. Biofilm wet weight was obtained as the difference from the initial coupon weight (determined prior to inoculation). Afterward, cyanobacterial cells were detached from the coupons by immersing each coupon in 2 ml of 8.5 g l^{-1} sodium chloride solution and vortexing, and the suspensions were incubated for 24 h at 4 °C in the dark for a maximal chlorophyll *a* extraction, as previously described through Equation 1.

Proteomics analysis

Protein extraction and sample preparation

Biomass of 40 biofilm samples comprising four replicates from each biofilm condition of *Nodosilinea* sp. LEGE 06145 and *Nodosilinea* sp. LEGE 06119 and four samples consisting of two replicates from planktonic samples of both the cyanobacterial strains were kept at −80 °C until protein extraction. Biomass for biofilm samples was obtained as previously described. Briefly, cyanobacterial biofilms were detached from the coupons by immersing each coupon in 2 ml of 8.5 g l^{-1} sodium chloride solution and vortexing. The total protein extraction was performed into sodium dithionite (SDT) buffer (2% SDS, 100 mM Tris/HCl pH 7.6, 0.1 M DTT) + protease inhibitors (PIs, Roche, 11697498001), as a variant of the method carried out by Campos et al. (2016). Briefly, the biomass from each replicate was weighed and a proper volume of SDT buffer was added to the samples (0.5 g ml^{-1} SDT), sonicated 5×4 s and 23 kHz − 105 µm (amplitude) and incubated at room temperature overnight. Afterward, samples were sonicated 5×4 s and 23 kHz − 105 µm (amplitude), heated for 3 min at 95 °C and subsequently centrifuged at 16,000 *g* for 20 min. Finally, the supernatant was collected, and total protein concentration was measured indirectly by optical density (OD) at 280 nm using a microplate reader (PowerWave; Biotek, VT, USA). Samples containing the extracted protein were stored for 24 h at −20 °C.

The extracted proteins were processed using the Filter Aided Sample Preparation (FASP) protocol described by Wiśniewski et al. (2009). In summary, this approach comprised the alkylation and digestion of 30 µg of the extracted proteins with trypsin (recombinant, proteomics grade, Roche, Basel,

Switzerland) at an enzyme to protein ratio of 1:100 (w/w) for 16 h at 37 °C using centrifugal filter units with a nominal molecular weight limit (NMWL) of 30 kDa (MRCPRT030, Millipore, Billerica, MA, USA). Through centrifugal filtration, peptides were recovered and acidified with trifluoracetic acid (TFA) (10% v v^{-1}). Samples were desalted and concentrated by reversed-phase extractions (C18 Tips, 100 µl, Thermo Scientific, Bremen, Germany, 87784) with acetonitrile (ACN) (50% v v^{-1}) and TFA (0.1% v v^{-1}) for peptide elution. Before LC-MS/MS analysis, samples were dried in the speed-vac and resuspended in formic acid (FA) (0.1% v v^{-1}) to a final concentration of 0.04–0.06 µg $µl^{-1}$.

LC-MS/MS analysis

FASP protein digests were processed using a nano LC-MS/MS, composed by an Ultimate 3000 liquid chromatography system coupled to a Q-Exactive Hybrid Quadrupole – Orbitrap mass spectrometer (Thermo Scientific). Samples were loaded onto a trapping cartridge (Acclaim PepMap C18 100A˚, 5 mm × 300 µm i.d., 160454, Thermo Scientific) in a mobile phase of 2% ACN, 0.1% FA at 10 µl min^{-1}. After 3 min loading, the trap column was switched in-line to a 15 cm by 75 µm inner diameter EASY-Spray column (ES800, PepMap RSLC, C18, 3 µm, Thermo Scientific) at 300 ml min^{-1}. Separation was generated by mixing A: 0.1% FA and B: 80% ACN, with the following gradient: 5 min (2.5% B to 10% B), 60 min (10% B to 35% B), 5 min (35% B to 99% B) and 5 min (hold 99% B). Subsequently, the column was equilibrated with 2.5% B for 12 min. Data acquisition was controlled by Xcalibur 4.0 and Tune 2.8 software (Thermo Scientific). The mass spectrometer was operated in data-dependent (dd) positive acquisition mode alternating between a full scan (m/z 380–1,580) and subsequent HCD MS/MS of the 10 most intense peaks from full scan (normalized collision energy of 27%). ESI spray voltage was 1.9 kV and capillary temperature was 275 °C. Global settings: use lock masses best (m/z 445.12003), lock mass injection Full MS, chrom. peak width (FWHM) 15 s. Full scan settings: 70k resolution (m/z 200), AGC target 3e6, maximum injection time 50 ms. dd settings: minimum AGC target 8e3, intensity threshold 7.3e4, charge exclusion: unassigned, 1, 8, >8, peptide match preferred, exclude isotopes on, dynamic exclusion 20 s. MS2 settings: microscans 1, resolution 35k (m/z 200), AGC target 2e5, maximum injection time 110 ms, isolation window 2.0 m/z, isolation offset 0.0 m/z, spectrum data type profile.

Protein identification

The raw data were analyzed and processed using the Proteome Discoverer 2.2.0.388 software (Thermo Scientific) and searched against the UniProt database for Bacteria taxonomic selection (2018_07 release). The Sequest HT search engine was used for protein identification. The ion mass tolerance was 10 ppm for precursor ions and 0.02 Da for-fragment ions. The maximum allowed missing cleavage sites was set to 2. Cysteine carbamidomethylation was defined as a constant modification. Methionine oxidation and protein N-terminus acetylation were defined as variable modifications. Peptide confidence was set to high. The processing node Percolator was enabled with the following settings: maximum delta Cn 0.05; decoy database search target FDR 1%, validation was based on q-value.

Protein distribution among different conditions of biofilm development

The distribution of protein identified among replicates and among the different conditions was analyzed by Venn diagram using an online free tool, available at the webserver of the Bioinformatics and Evolutionary Genomics Center (BEG/Van de Peer Lab site), Ghent University, Belgium, http://bioinformatics.psb.ugent.be/webtools/Venn/. For comparison purposes, the identified proteins from all replicates of each treatment were merged into a single file and duplicates removed. Finally, the corresponding distribution of unique and shared proteins among different conditions were reported.

Statistical analysis

All experiments were performed in triplicate. Data analysis was performed using the statistical program GraphPad Prism® for Windows, version 6.01 (GraphPad Software, Inc., San Diego, CA, USA) and results were compared using unpaired *t*-tests with a confidence level of 95% (**; $p < 0.05$) and 90% (*; $p < 0.1$).

Results and discussion

Biofilm development analysis

Monitoring of cyanobacterial biofilm development was done for 49 days (progress of wet weight,

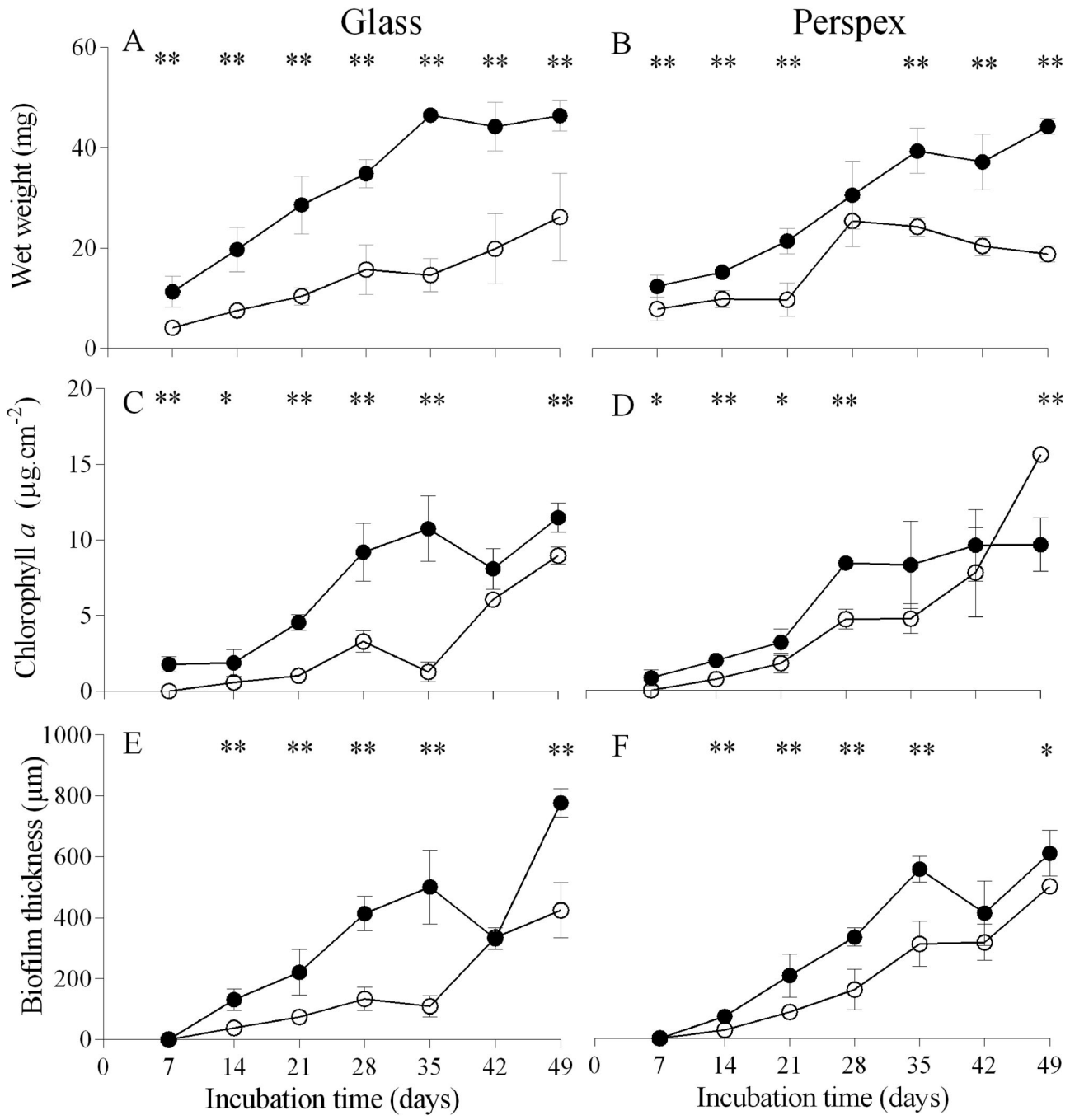

Figure 1. Evaluation of *Nodosilinea* sp. LEGE 06145 biofilm development. The parameters analyzed refer to wet weight (A, B), chlorophyll *a* (C, D) and biofilm thickness (E, F). Biofilms were formed in glass (A, C, E) or perspex (B, D, F), at two average shear rates, 4 s^{-1} (closed circles) and 40 s^{-1} (open circles) for 49 days. SDs from two biological assays with three replicates each are represented. Symbols * and ** indicate statistically different values for $p < 0.1$ and $p < 0.05$ (respectively) at each incubation time.

chlorophyll *a* and biofilm thickness), as shown in Figures 1 and 2. For both cyanobacterial strains and both surfaces, biofilm development was higher at the lowest shear rate. Compared with the values obtained at higher shear rate (40 s^{-1}), the biofilm mass obtained on a glass surface under lower shear conditions (4 s^{-1}) was on average 63.9% and 48% higher for *Nodosilinea* sp. LEGE 06145 (Figure 1a) and *Nodosilinea* sp. LEGE 06119 (Figure 2a), respectively. Likewise, on perspex, the biofilm wet weight was on average 40.6% higher for *Nodosilinea* sp. LEGE 06145 (Figure 1b) and 29.6% for *Nodosilinea* sp. LEGE 06119 (Figure 2b). The chlorophyll *a* content at 4 s^{-1} and on glass was, on average 64.6% and 98.8% higher for *Nodosilinea* sp. LEGE 06145 (Figure 1c) and *Nodosilinea* sp. LEGE 06119 (Figure 2c), respectively, whereas on perspex it was, on average, 35.7% higher for *Nodosilinea* sp. LEGE 06145 (Figure 1d) and

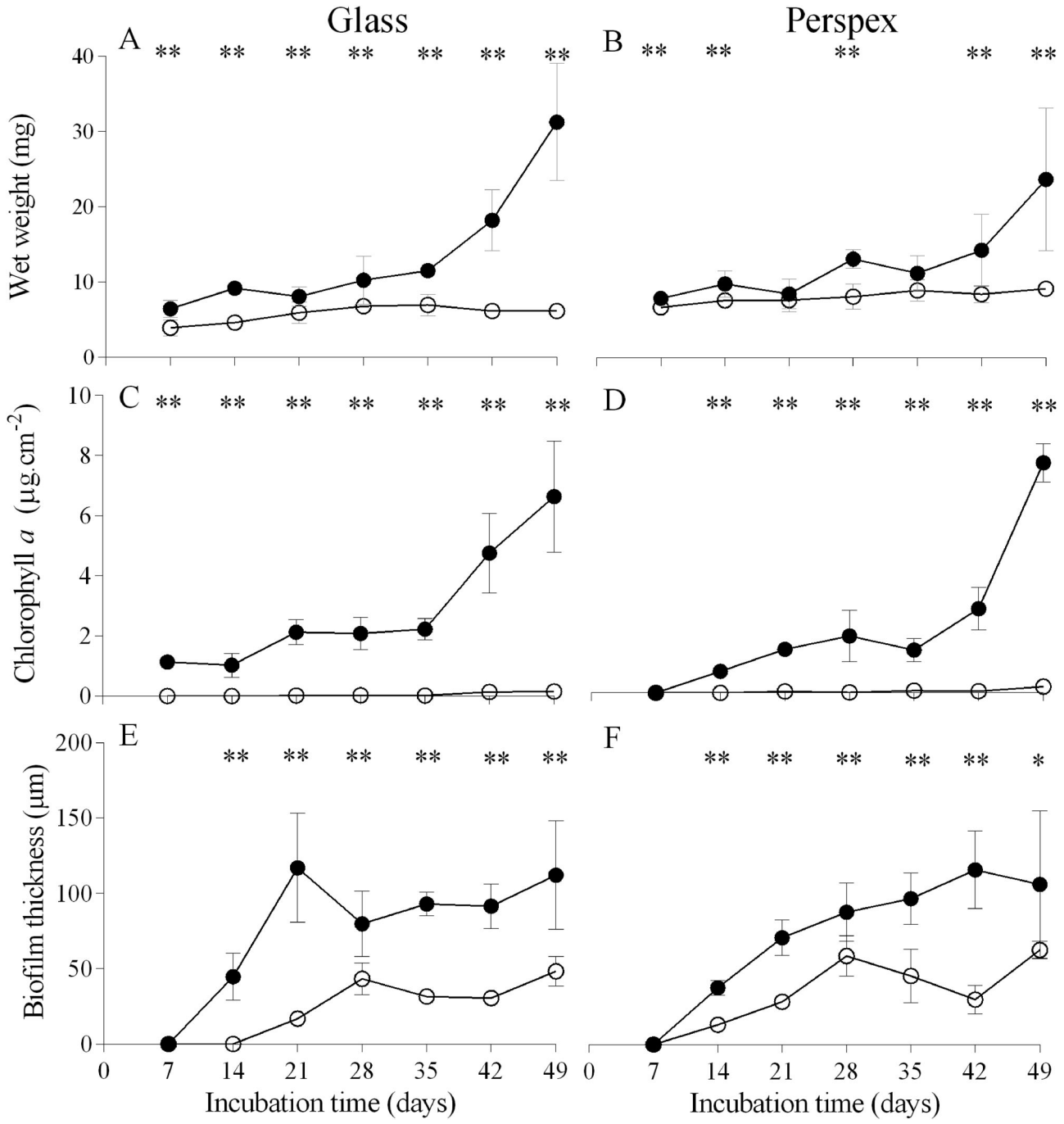

Figure 2. Evaluation of *Nodosilinea* sp. LEGE 06119 biofilm development. The parameters analyzed refer to wet weight (A, B), chlorophyll *a* (C, D) and biofilm thickness (E, F). Biofilms were formed in glass (A, C, E) or perspex (B, D, F), at two average shear rates, 4 s^{-1} (closed circles) and 40 s^{-1} (open circles) for 49 days. SDs from two biological assays with three replicates each are represented. Symbols * and ** indicate statistically different values for $p < 0.1$ and $p < 0.05$ (respectively) at each incubation time.

97.4% for *Nodosilinea* sp. LEGE 06119 (Figure 2d) compared with higher shear conditions. Since a correlation between chlorophyll *a* production and biofilm wet weight was observed (Supplementary material, SM1), chlorophyll *a* content monitorization was demonstrated to be a useful tool to follow cyanobacterial biofilm growth, as previously reported (Romeu et al. 2019).

Although some differences in biofilm development at different shear conditions were noticed in the early stages, major differences were found in the maturation phase of biofilm development (on general from day 28 and mainly in wet weight quantification), which corroborates previous results obtained with different cyanobacterial strains (Romeu et al. 2019). The increased shear rate during biofilm development may

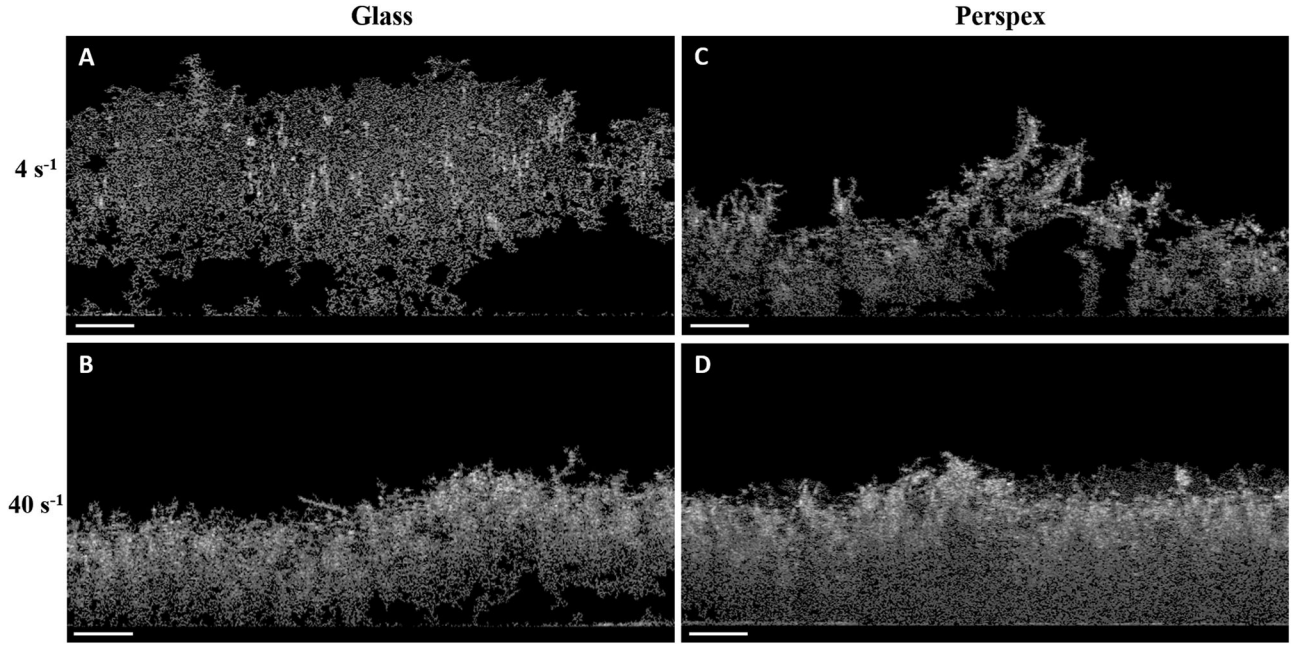

Figure 3. 2-D cross-sectional OCT images of *Nodosilinea* sp. LEGE 06145 biofilms formed after 49 days on glass and perspex at two different shear rates, 4 s^{-1} (A, C) and 40 s^{-1} (B, D). Scale bar = 200 µm.

promote sloughing events and erosion, affecting biofilm cohesion. Moreover, this difference in biofilm development between the two hydrodynamic conditions was more noticeable for *Nodosilinea* sp. LEGE 06119 (Figure 2a–d).

The biofilm thickness obtained on the glass surface under lower shear conditions was on average 54.5% and 64.2% higher for *Nodosilinea* sp. LEGE 06145 (Figure 1e) and *Nodosilinea* sp. LEGE 06119 (Figure 2e), respectively, when compared with those obtained at 40 s^{-1}. On perspex, the biofilm thickness was, on average 42.9% higher for *Nodosilinea* sp. LEGE 06145 (Figure 1f) and 54.3% for *Nodosilinea* sp. LEGE 06119 (Figure 2f). The highest value of biofilm thickness was observed at 4 s^{-1} on glass for *Nodosilinea* sp. LEGE 06145 (∼ 800 µm; Figure 1e, 49 days). Values of biofilm thickness obtained for *Nodosilinea* sp. LEGE 06119 were significantly lower, achieving a maximum of 120 µm at 4 s^{-1} on glass (Figure 2e). Indeed, all parameters analyzed showed that biofilm development by *Nodosilinea* sp. LEGE 06145 was substantially higher than by *Nodosilinea* sp. LEGE 06119 (Supplementary material, SM2).

Despite the different properties of glass and perspex, the latter of which is the most hydrophobic surface (Romeu et al. 2019), similar values of wet weight, chlorophyll *a* content and biofilm thickness were obtained for the biofilms formed on different surfaces at the same hydrodynamic conditions (Supplementary material, SM3). These findings, which show that the effect of surface hydrophobicity was less important than the hydrodynamic effect on cyanobacterial biofilm development, had previously been shown for other cyanobacterial strains (Romeu et al. 2019; Faria et al. 2020).

Figures 3 and 4 show representative 2-D cross-sectional images of *Nodosilinea* sp. LEGE 06145 and *Nodosilinea* sp. LEGE 06119, respectively, obtained from OCT at the end of the experiment (49 days). From these OCT images, the difference in biofilm development between the cyanobacterial strains is clear. Again, the differences in biofilm structure between hydrodynamic conditions were also more noticeable than between the two surfaces. Despite the lower biofilm biomass obtained at a higher shear rate (40 s^{-1}) for *Nodosilinea* sp. LEGE 06119 (Figure 4b, d), it is possible to observe that cyanobacterial biofilms obtained at 4 s^{-1} were less homogeneous in their structure, presenting three-dimensional streamers on the biofilm surface. The appearance of these structures was previously reported for other cyanobacterial biofilm formed under different hydrodynamic conditions (Romeu et al. 2019). Instead, biofilms formed under the higher shear rate presented a more compact structure. While a compacted structure may be relevant in biofilms formed under higher shear conditions to increase the biofilm cohesion and avoid biofilm sloughing and erosion, a lower degree of compaction in biofilms formed under lower shear rates is an appropriate adaptation to improve the mass transfer to the inner layers of the biofilm (Teodósio et al. 2011).

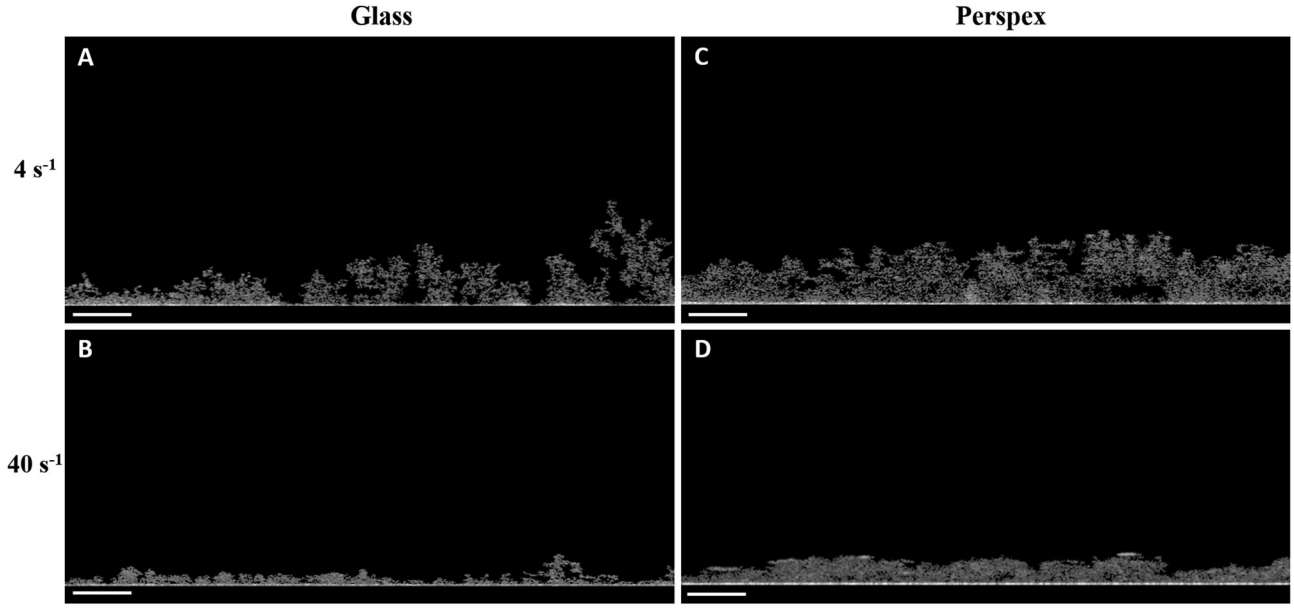

Figure 4. 2-D cross-sectional OCT images of *Nodosilinea* sp. LEGE 06119 biofilms formed after 49 days on glass and Perspex at two different shear rates, 4 s^{-1} (A, C) and 40 s^{-1} (B, D). Scale bar = 200 µm.

Proteomic analysis

A qualitative proteomic analysis by LC-MS/MS was performed, and the number and the distribution of proteins found for both cyanobacterial strains in different conditions is shown in Figure 5. The number of cyanobacterial proteins identified from all planktonic and biofilm samples is available in Supplementary material, SM4. A total of 377 and 301 different proteins were identified for *Nodosilinea* sp. LEGE 06145 and *Nodosilinea* sp. LEGE 06119, respectively, of which 108 were found in both cyanobacterial strains (Figure 5a). Among the 16 common proteins identified in the cyanobacterial planktonic samples (Figure 5b), none is exclusive to the planktonic form because they were identified in an additional biofilm condition. A previous quantitative proteomic study performed on the marine bacterium *Pseudoalteromonas lipolytica* TC8 also aimed at highlighting specific metabolic shifts between planktonic and biofilm cultures. This study showed that 90% of proteins were present in the proteomes of both planktonic and biofilm samples (Favre et al. 2018). Moreover, the percentage of proteins found in the four different biofilm conditions and which were identified in both cyanobacterial strains was similar and below 22%. Amongst the four possibilities tested for biofilm development, biofilms that were formed on perspex and at 40 s^{-1} showed a higher percentage of common proteins between the two cyanobacterial strains (21.1%, Figure 5f). Conversely, biofilms that were formed on perspex but at 4 s^{-1} showed a lower number of common proteins between the two cyanobacterial strains (7.8%, Figure 5d). A broad diversity in the protein expression profiles of each strain was observed. Similarly, substantial differences in protein expression among cyanobacterial strains at the same conditions were also observed in a study of *Microcystis aeruginosa* (Alexova et al. 2011) and only 29–43% of the identified proteins were found to be expressed in all six strains analyzed in this study. Moreover, a study performed with the marine cyanobacterium *Prochlorococcus* spp. showed that the elemental composition of their proteomes was strongly influenced by their site of isolation and the nutritional availability at that site (Lv et al. 2008). Since *Nodosilinea* sp. LEGE 06145 was isolated from a sample scraped from a wave-exposed rock in a tide puddle collected at Moledo beach and *Nodosilinea* sp. LEGE 06119 was isolated from a seawater sample collected in the surf zone collected at Burgau beach, the observed proteome diversity supports the view that strains should be considered as ecotypes adapted to survival in a particular environmental niche (Otsuka et al. 2001). For the same cyanobacterial strain, a higher number of proteins was identified on glass rather than on perspex, and comparing the two hydrodynamic conditions, a higher number of proteins was obtained at 4 s^{-1} for both cyanobacteria (Figure 5C–F). This lower shear condition corresponds to the scenario in which a higher amount of biofilm formation was observed (Figures 1–4). For both cyanobacterial strains, differences between the number of proteins identified from biofilms formed

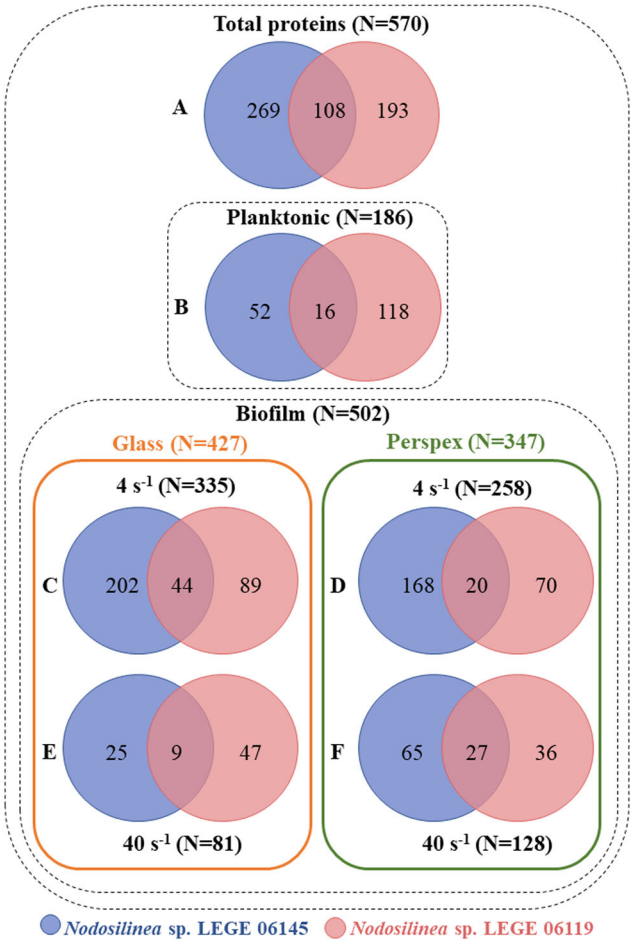

Figure 5. Venn diagrams obtained from the distribution of proteins identified among different conditions for the two cyanobacterial strains. The total of proteins for each condition is represented by (N=). The composite figure shows the unique and common proteins identified in both cyanobacterial strains at each condition represented from each Venn diagram: (A) total proteins identified on *Nodosilinea* sp. LEGE 06145 cells *vs* proteins identified on *Nodosilinea* sp. LEGE 06119 cells; (B) proteins identified on planktonic *Nodosilinea* sp. LEGE 06145 cells *vs* proteins identified on planktonic *Nodosilinea* sp. LEGE 06119 cells; (C) proteins identified on *Nodosilinea* sp. LEGE 06145 cells *vs* proteins identified on *Nodosilinea* sp. LEGE 06119 cells derived from biofilms formed on glass at $4\,s^{-1}$; (D) proteins identified on *Nodosilinea* sp. LEGE 06145 cells *vs* proteins identified on *Nodosilinea* sp. LEGE 06119 cells derived from biofilms formed on perspex at $4\,s^{-1}$; (E) proteins identified on *Nodosilinea* sp. LEGE 06145 cells *vs* proteins identified on *Nodosilinea* sp. LEGE 06119 cells derived from biofilms formed on glass at $40\,s^{-1}$; (F) proteins identified on *Nodosilinea* sp. LEGE 06145 cells *vs* proteins identified on *Nodosilinea* sp. LEGE 06119 cells derived from biofilms formed on perspex at $40\,s^{-1}$.

under different hydrodynamic conditions were more noticeable than those obtained for different surfaces (77.8% and 48.5% higher at $4\,s^{-1}$ than $40\,s^{-1}$ for *Nodosilinea* sp. LEGE 06145 and *Nodosilinea* sp. LEGE 06119, 28.1% and 33.4% higher on glass than perspex, for *Nodosilinea* sp. LEGE 06145 and *Nodosilinea* sp. LEGE 06119, respectively (Supplementary material, SM4). Except for the biofilms on glass at $40\,s^{-1}$ in which the number of proteins found in *Nodosilinea* sp. LEGE 06119 was 41.2% higher compared with *Nodosilinea* sp. LEGE 06145, in all biofilm samples, a higher number of proteins were identified in *Nodosilinea* sp. LEGE 06145. The complete list of identified proteins and their frequencies in different biofilm conditions is available in Supplementary material, SM5.

The identification and description of common proteins obtained from biofilm samples and for both cyanobacterial strains are presented in Table 1. While from biofilms formed on glass only one protein was identified in both cyanobacterial strains, 10 common proteins were identified from biofilms on the perspex surface. Additionally, 12 and 10 proteins for both cyanobacterial strains were identified in biofilm samples formed at $4\,s^{-1}$ and $40\,s^{-1}$, respectively. It should be noted that despite biofilm development being substantially lower in *Nodosilinea* sp. LEGE 06119 than *Nodosilinea* sp. LEGE 06145 (Supplementary material, SM2), these proteins were also found in this strain. The 50S ribosomal protein L7/L12 was identified in all biofilm conditions of the two cyanobacterial strains. This protein forms part of the ribosomal stalk, which helps the ribosome interact with guanosine triphosphate (GTP)-bound translation factors and it is responsible for accurate translation (Diaconu et al. 2005). This is an essential protein in the core metabolic functions and it was identified in all biofilm samples (Table 1 and Supplementary material, SM5). This result demonstrates the relevance and validity of the proteomic analysis performed in the present work. Additional cyanobacterial proteomic studies have revealed that 50% of proteins found could be assigned to core metabolic and transport functions (Anderson et al. 2006). However, a proteomic study performed with *Halorubrum lacusprofundi*, an extreme halophile archaeon, showed a decrease in the proteins involved in protein synthesis and folding in biofilms when compared with planktonic cells, including a large number of ribosomal proteins (Liao et al. 2016).

Proteins related to photosystems I and II and with allophycocyanin were found in three of the four biofilm condition groups (Table 1 in dark grey shading). The specific conditions in which these proteins were identified can be found in the Supplementary material, SM5. Photosystem I (PS I, plastocyaninferredoxin oxidoreductase) and photosystem II (PS II,

Table 1. Enumeration of proteins obtained from different biofilm samples in both cyanobacterial strains.

Biofilm development condition	Number of proteins found on both cyanobacterial strains	Accession number	Description
Glass	1	A0A1Z3HSI0	50S ribosomal protein L7/L12
Perspex	10	A0A077JIC2	Elongation factor Tu
		A0A0N7LBT2	Alkyl hydroperoxide reductase/thiol specific antioxidant/Mal allergen
		A0A1U7J348	Photosystem II CP43 reaction center protein
		A0A1U7J7J4	Allophycocyanin subunit beta
		A0A1U7JAP1	Allophycocyanin subunit beta
		A0A1U7JAR5	Photosystem I reaction center subunit X
		A0A1U7JAT3	Allophycocyanin
		A0A1Z3HSI0	50S ribosomal protein L7/L12
		A0A2P8ZU54	Photosystem I P700 chlorophyll a apoprotein A2
		I4HUB3	Carbon dioxide-concentrating mechanism protein CcmK
$4\,s^{-1}$	12	A0A073CH81	Photosystem I reaction center subunit XI
		A0A0N7LBT2	Alkyl hydroperoxide reductase/thiol specific antioxidant/Mal allergen
		A0A120MWU4	Transketolase
		A0A1U7J348	Photosystem II CP43 reaction center protein
		A0A1U7J7J4	Allophycocyanin subunit beta
		A0A1U7J8S7	Photosystem I reaction center subunit II
		A0A1Z3HSI0	50S ribosomal protein L7/L12
		A0A2P8VVE3	Allophycocyanin subunit beta
		A0A2P8W6V3	Amino acid ABC transporter substrate-binding protein
		A0A2P8ZWG1	HU family DNA-binding protein
		A0A2P8ZXU5	Phycobilisome rod-core linker polypeptide CpcG
		I4HUB3	Carbon dioxide-concentrating mechanism protein CcmK
$40\,s^{-1}$	7	A0A073CM30	PsaF
		A0A0U1Z975	Phycocyanin beta chain (Fragment)
		A0A1U7JAP1	Allophycocyanin subunit beta
		A0A1U7JAT3	Allophycocyanin
		A0A1Z3HSI0	50S ribosomal protein L7/L12
		A0A2P8ZU54	Photosystem I P700 chlorophyll a apoprotein A2
		K9F192	Phycobilisome protein

Note: For each protein, the frequency of appearance among the four biofilm conditions (glass, Perspex, $4\,s^{-1}$ and $40\,s^{-1}$) is indicated by different shaded colors (black – appearance in all four conditions; dark grey – appearance in three of four conditions; light grey – appearance in two of four conditions; without shading – appearance in only one of the four conditions).

waterplastoquinone oxidoreductase) are multisubunit protein complexes located in the thylakoid membranes of cyanobacteria, algae and higher plants (Nelson and Yocum 2006). Although in the present study the PsaF protein was only identified in biofilms of both the cyanobacterial strains formed at $40\,s^{-1}$ (Table 1), this protein is also related to photosystems (Photosystem I subunit III). A study performed by Huang et al. (2002) also identified proteins related to photosystems in the plasma membrane of *Synechocystis* PCC 6803. A proteomic study with different strains of *M. aeruginosa* showed that the majority of proteins shared among all strains were involved in photosynthesis and respiration (Alexova et al. 2011). Thus, the distribution of protein identification obtained in the present study is typical for cyanobacteria.

Allophycocyanin is a protein from the light-harvesting phycobiliprotein family, along with phycocyanin, phycoerythrin and phycoerythrocyanin, which may be found in the phycobilisome core complex (Sonani et al. 2015). Although proteins related to allophycocyanin were found in three of the four biofilm conditions, a protein fragment of phycocyanin beta chain and an additional non-specific phycobilisome protein were identified in both cyanobacterial strains for biofilms formed at $40\,s^{-1}$. Phycobilisomes are present in cyanobacteria and red algae and are formed by phycobiliproteins and also linker proteins (MacColl 1998). Allophycocyanin is considered an accessory pigment to chlorophyll and exhibits unique absorbance and fluorescence characteristics due to a lack of susceptibility to internal and external fluorescence quenching. Due to these features, allophycocyanin is ideal for highly sensitive studies such as flow cytometry and immunoassays (Manirafasha et al. 2016). Indeed, phycobiliproteins are regularly found in high abundance and they may constitute up to 50% of the total cellular protein of a cyanobacterium (Anderson et al. 2006). Previous proteomic studies with other cyanobacterial strains (*Synechocystis* PCC 6803) also identified proteins related to this phycobiliprotein family in their plasma membrane (Huang et al. 2002; Pisareva et al. 2007). In another study, which aimed to evaluate proteomic changes after heat

shock in *Synechocystis* PCC 6803, a decreased expression level for phycobilisome was observed (Slabas et al. 2006).

For both cyanobacterial strains, in biofilms formed on perspex and also at $4\,s^{-1}$ a protein from the peroxiredoxin superfamily was identified (alkyl hydroperoxide reductase/thiol specific antioxidant/Mal allergen). This protein protects cells against membrane oxidation through glutathione (GSH)-dependent reduction of phospholipid hydroperoxides to corresponding alcohols (Wood et al. 2003). A study performed with *Spirulina platensis*, which focused on comparative proteome analyses at low- and high-temperature stresses, indicated that low-temperature stress is tightly linked to oxidative stress as well as photosynthesis (Kurdrid et al. 2011). A quantitative proteomic study to define pathways and cellular processes involved in forming biofilms of *H. lacusprofundi* showed that these proteins associated with responses to oxidative stress are also related to biofilm forming ability (Liao et al. 2016). Although in the present study this protein was only found on perspex and also at $4\,s^{-1}$, this hydrodynamic condition resulted in greater biofilm development, which may have facilitated its detection.

Moreover, for both cyanobacterial strains, in biofilms formed on perspex and at $4\,s^{-1}$ a protein involved in the formation of the carboxysome (carbon dioxide-concentrating mechanism protein CcmK) was also found. Carboxysomes are polyhedral inclusion where the ribulose-1,5-bisphosphate carboxylase/oxygenase (Rubisco; the central enzyme in photosynthetic carbon assimilation) is sequestered. The CO_2 concentrating mechanism (CCM) is an adaptive and effective strategy evolved in cyanobacteria and also in eukaryotic microalgae for carbon acquisition, and it enables these organisms to survive when the CO_2 concentration limits photosynthesis (Wang et al. 2015). Baba et al. (2011) also studied this mechanism in the unicellular green alga *Chlamydomonas reinhardtii*. When the CO_2 concentration was elevated from the ambient air level to 3%, the algal growth rate increased 1.5-fold, and the amount and the composition of extracellular proteins clearly changed. However, significant changes were not found in intracellular proteins (Baba et al. 2011). In a study performed by Slabas et al. (2006), a decrease in Rubisco proteins was observed after heat shock in *Synechocystis* PCC 6803. Moreover, the CCM is a fundamental aspect of photosynthesis, metabolism, growth and biomass production in photosynthetic organisms and understanding this process provides guidance for potential molecular manipulation to improve biomass yield for commercial applications (Badger and Price 2003).

Despite the fact that in the present study, the elongation factor Tu and the amino acid ABC transporter substrate-binding protein were only identified for both cyanobacterial strains on biofilms formed on perspex and at $4\,s^{-1}$, respectively (Table 1), these proteins were found in other cyanobacterial studies, such as in the plasma membrane of *Synechocystis* PCC 6803 (Huang et al. 2002). Moreover, a higher abundance of elongation factors and ABC transporters in *Enterococcus faecalis* (Qayyum et al. 2016) and *H. lacusprofundi* (Liao et al. 2016) biofilms, respectively, was observed when compared with those obtained in planktonic cells.

Concluding remarks

In this study, standard methodologies for following cyanobacterial biofilm development were complemented with a qualitative proteomics approach. The results showed greater biofilm development at a lower shear rate ($4\,s^{-1}$) and it was also shown that hydrodynamic effects may be more important than surface properties in the formation of cyanobacterial biofilms. Moreover, the analysis of cyanobacterial biofilms by OCT is a useful methodology for understanding biofilm structure and dynamics under different conditions.

Cyanobacterial proteome analysis revealed that the strains under study had highly variable protein expression profiles, which may be a result of the adaptation of these organisms to the specific environmental niche that they occupy. Although this proteomic analysis was performed using a widely employed methodology and the proteome reported was biased on proteins expressed at higher levels, it is well known that there are limitations in the present technology for resolution and identification of proteins. Since none of the proteins identified in planktonic samples were exclusive to this form, that is, they were identified in an additional biofilm condition, the majority of the proteins were detected in both physiological states. The qualitative proteomic analysis investigated in this work was extremely relevant, given the few studies performed in this research field on filamentous cyanobacteria. Analyses of protein expression could provide an essential understanding of how cyanobacteria adapt to different environmental settings. However, in addition to studying which proteins were synthesized in the different conditions, it would be crucial to study the expression level of these

proteins, since biofilm development in these different conditions may be associated with quantitative differences in their proteome. Therefore, future work should focus on quantitative proteomic studies in order to allow the establishment of a relationship between the relative expression level of the identified proteins under different conditions. Moreover, due to their particular characteristics, cyanobacteria are promising organisms to be used in biotechnological processes. Vitamins, amino acids, fatty acids, lipopeptides and pigments belong to a broad spectrum of secondary metabolites and added-value compounds produced by cyanobacterial strains (Lau et al. 2015). For example, the allophycocyanin identified in two biofilm conditions of the present work is a valuable molecule to be applied in several biotechnological applications as fluorescent probes in flow cytometry and microarray assays, but also in the cosmetic, feed and food industries (Manirafasha et al. 2016). Moreover, as phycobiliproteins have been associated with antioxidant, anticancer and anti-inflammatory capacities, these compounds can also be used for medical purposes (Pagels et al. 2019). Improvements in cyanobacterial molecular biology are urgently required, since the omics tools available for these organisms are limited compared with heterotrophic model organisms (Sun et al. 2018).

Acknowledgements

This work was financially supported by: Base Funding - UIDB/00511/2020 of the Laboratory for Process Engineering, Environment, Biotechnology and Energy – LEPABE, funded by national funds through the FCT/MCTES (PIDDAC) and by the CVMAR+i – Industrial Innovation and Marine Biotechnology Valorisation, funded by INTERREG V A Espanha Portugal (POCTEP) [0302_CVMAR_I_1_P] and strategic funding UIDB/04423/2020 and UIDP/04423/2020 through national funds provided by FCT and European Regional Development Fund (ERDF), in the framework of the programme PT2020. M.J.R. acknowledges a PhD grant from FCT (SFRH/BD/140080/2018).

Disclosure statement

The authors declare that they have no conflict of interest.

ORCID

Maria João Leal Romeu http://orcid.org/0000-0002-1094-5425
Dany Domínguez-Pérez http://orcid.org/0000-0002-5211-972X
Daniela Almeida http://orcid.org/0000-0002-9874-933X
João Morais http://orcid.org/0000-0002-4190-0959
Alexandre Campos http://orcid.org/0000-0003-4621-885X
Vítor Vasconcelos http://orcid.org/0000-0003-3585-2417
Filipe J. M. Mergulhão http://orcid.org/0000-0001-5233-1037

References

Alexova R, Haynes PA, Ferrari BC, Neilan BA. 2011. Comparative protein expression in different strains of the bloom-forming cyanobacterium *Microcystis aeruginosa*. Mol Cell Proteom. 10:M110.003749. doi:10.1074/mcp.M110.003749

Allen AA, Habimana O, Casey E. 2018. The effects of extrinsic factors on the structural and mechanical properties of *Pseudomonas fluorescens* biofilms: a combined study of nutrient concentrations and shear conditions. Colloids Surf B Biointerf. 165:127–134. doi:10.1016/j.colsurfb.2018.02.035

Anderson DC, Campbell EL, Meeks JC. 2006. A soluble 3D LC/MS/MS proteome of the filamentous cyanobacterium *Nostoc punctiforme*. J Proteome Res. 5:3096–3104. doi:10.1021/pr060272m

Baba M, Suzuki I, Shiraiwa Y. 2011. Proteomic analysis of high-CO(2)-inducible extracellular proteins in the unicellular green alga, *Chlamydomonas reinhardtii*. Plant Cell Physiol. 52:1302–1314. doi:10.1093/pcp/pcr078

Babele PK, Kumar J, Chaturvedi V. 2019. Proteomic deregulation in cyanobacteria in response to abiotic stresses. Front Microbiol. 10:1–22. doi:10.3389/fmicb.2019.01315

Badger MR, Price GD. 2003. CO_2 concentrating mechanisms in cyanobacteria: molecular components, their diversity and evolution. J Exp Bot. 54:609–622. doi:10.1093/jxb/erg076

Bakke R, Kommedal R, Kalvenes S. 2001. Quantification of biofilm accumulation by an optical approach. J Microbiol Methods. 44:13–26. doi:10.1016/S0167-7012(00)00236-0

Battchikova N, Muth-Pawlak D, Aro EM. 2018. Proteomics of cyanobacteria: current horizons. Curr Opin Biotechnol. 54:65–71. doi:10.1016/j.copbio.2018.02.012

Bharti A, Velmourougane K, Prasanna R. 2017. Phototrophic biofilms: diversity, ecology and applications. J Appl Phycol. 29:2729–2744. doi:10.1007/s10811-017-1172-9

Campos A, Danielsson G, Farinha AP, Kuruvilla J, Warholm P, Cristobal S. 2016. Shotgun proteomics to unravel marine mussel (*Mytilus edulis*) response to long-term exposure to low salinity and propranolol in a Baltic Sea microcosm. J Proteomics. 137:97–106. doi:10.1016/j.jprot.2016.01.010

Canny J. 1986. A computational approach to edge detection. IEEE Trans Pattern Anal Mach Intell. 8:679–698. doi: 10.1109/TPAMI.1986.4767851.

Carvalho C. 2018. Marine biofilms: a successful microbial strategy with economic implications. Front Mar Sci. 5:1–11. doi:10.3389/fmars.2018.00126

Chen M, Hernandez-Prieto MA, Loughlin PC, Li Y, Willows RD. 2019. Genome and proteome of the chlorophyll f-producing cyanobacterium *Halomicronema hongdechloris*: adaptative proteomic shifts under different

light conditions. BMC Genomics. 20:1–15. doi:10.1186/s12864-019-5587-3

Crawford RJ, Webb HK, Truong VK, Hasan J, Ivanova EP. 2012. Surface topographical factors influencing bacterial attachment. Adv Colloid Interface Sci. 179–182:142–149. doi:10.1016/j.cis.2012.06.015

Delauney L, Compère C, Lehaitre M. 2010. Biofouling protection for marine environmental sensors. Ocean Sci. 6: 503–511. doi:10.5194/os-6-503-2010

Diaconu M, Kothe U, Schlünzen F, Fischer N, Harms JM, Tonevitsky AG, Stark H, Rodnina MV, Wahl MC. 2005. Structural basis for the function of the ribosomal L7/12 stalk in factor binding and GTpase activation. Cell. 121: 991–1004. doi:10.1016/j.cell.2005.04.015

Duda RO, Hart PE. 1972. Use of the Hough transformation to detect lines and curves in pictures. Commun Acm. 15: 11–15. doi:10.1145/361237

Faria SI, Teixeira-Santos R, Romeu MJ, Morais J, Vasconcelos V, Mergulhão FJ. 2020. The relative importance of shear forces and surface hydrophobicity on biofilm formation by coccoid cyanobacteria. Polymers (Basel). 12:653. doi:10.3390/polym12030653

Favre L, Ortalo-Magné A, Pichereaux C, Gargaros A, Burlet-Schiltz O, Cotelle V, Culioli G. 2018. Metabolome and proteome changes between biofilm and planktonic phenotypes of the marine bacterium *Pseudoalteromonas lipolytica* TC8. Biofouling. 34:132–148. doi:10.1080/08927014.2017.1413551

Flemming H-C, Murthy PS, Venkatesan R, Cooksey K. 2009. Marine and industrial biofouling. Costerton JW, editor. Los Angeles: Springer Berlin Heidelberg.

Heidari F, Hauer T, Zima J, Riahi H. 2018. New simple trichal cyanobacterial taxa isolated from radioactive thermal springs. Fottea. 18:137–149. doi:10.5507/fot.2017.024

Herschend J, Damholt ZBV, Marquard AM, Svensson B, Sørensen SJ, Hägglund P, Burmølle M. 2017. A metaproteomics approach to study the interspecies interactions affecting microbial biofilm development in a model community. Sci Rep. 7:1–13. doi:10.1038/s41598-017-16633-6

Huang F, Parmryd I, Nilsson F, Persson AL, Pakrasi HB, Andersson B, Norling B. 2002. Proteomics of *Synechocystis* sp. strain PCC 6803: identification of plasma membrane proteins. Mol Cell Proteom. 1: 956–966. doi:10.1074/mcp.m200043-mcp200

Jahn M, Vialas V, Karlsen J, Maddalo G, Edfors F, Forsström B, Uhlén M, Käll L, Hudson EP. 2018. Growth of cyanobacteria is constrained by the abundance of light and carbon assimilation proteins. Cell Rep. 25: 478–486.e8. doi:10.1016/j.celrep.2018.09.040

King RK, Flick GJ, Smith SA, Pierson MD, Boardman GD, Coale CW. 2006. Comparison of bacterial presence in biofilms on different materials commonly found in recirculating aquaculture systems. J Appl Aquac. 18:79–88. doi:10.1300/J028v18n01_05

Kotai J. 1972. Instructions for the preparation of modified nutrient solution Z8 for algae. Blindern, Oslo: Norwegian Institute for Water Research; vol. 11, p. 5.

Kurdrid P, Senachak J, Sirijuntarut M, Yutthanasirikul R, Phuengcharoen P, Jeamton W, Roytrakul S, Cheevadhanarak S, Hongsthong A. 2011. Comparative analysis of the *Spirulina platensis* subcellular proteome in response to low- and high-temperature stresses: uncovering cross-talk of signaling components. Proteome Sci. 9: 39. doi:10.1186/1477-5956-9-39

Lau NS, Matsui M, Abdullah AA. 2015. Cyanobacteria: photoautotrophic microbial factories for the sustainable synthesis of industrial products. Biomed Res Int. 2015: 754934. doi:10.1155/2015/754934

Leary DH, Li RW, Hamdan LJ, Hervey WJ, Lebedev N, Wang Z, Deschamps JR, Kusterbeck AW, Vora GJ. 2014. Integrated metagenomic and metaproteomic analyses of marine biofilm communities. Biofouling. 30:1211–1223. doi:10.1080/08927014.2014.977267

Liao Y, Williams TJ, Ye J, Charlesworth J, Burns BP, Poljak A, Raftery MJ, Cavicchioli R. 2016. Morphological and proteomic analysis of biofilms from the Antarctic archaeon. Sci Rep. 6:37454. doi:10.1038/srep3745

Lv J, Li N, Niu DK. 2008. Association between the availability of environmental resources and the atomic composition of organismal proteomes: evidence from *Prochlorococcus* strains living at different depths. Biochem Biophys Res Commun. 375:241–246. doi:10.1016/j.bbrc.2008.08.011

MacColl R. 1998. Cyanobacterial phycobilisomes. J Struct Biol. 124:311–334. doi:10.1006/jsbi.1998.4062

Manirafasha E, Ndikubwimana T, Zeng X, Lu Y, Jing K. 2016. Phycobiliprotein: potential microalgae derived pharmaceutical and biological reagent. Biochem Eng J. 109:282–296. doi:10.1016/j.bej.2016.01.025

Mayer MA, Borsdorf A, Wagner M, Hornegger J, Mardin CY, Tornow RP. 2012. Wavelet denoising of multiframe optical coherence tomography data. Biomed Opt Express. 3:572–589. doi:10.1364/BOE.3.000572

Mieszkin S, Callow ME, Callow JA. 2013. Interactions between microbial biofilms and marine fouling algae: a mini review. Biofouling. 29:1097–1113. doi:10.1080/08927014.2013.828712

Moreira JMR, Gomes LC, Simões M, Melo LF, Mergulhão FJ. 2015. The impact of material properties, nutrient load and shear stress on biofouling in food industries. Food Bioprod Process. 95:228–236. doi:10.1016/j.fbp.2015.05.011

Muthusamy S, Lundin D, Mamede Branca RM, Baltar F, González JM, Lehtiö J, Pinhassi J. 2017. Comparative proteomics reveals signature metabolisms of exponentially growing and stationary phase marine bacteria. Environ Microbiol. 19:2301–2319. doi:10.1111/1462-2920.13725

Nelson N, Yocum CF. 2006. Structure and function of photosystems I and II. Annu Rev Plant Biol. 57:521–565. doi:10.1146/annurev.arplant.57.032905.105350

Otsuka S, Suda S, Shibata S, Oyaizu H, Matsumoto S, Watanabe MM. 2001. A proposal for the unification of five species of the cyanobacterial genus *Microcystis* Kützing ex Lemmermann 1907 under the rules of the Bacteriological Code. Int J Syst Evol Microbiol. 51: 873–879. doi:10.1099/00207713-51-3-873

Ow SY, Salim M, Noirel J, Evans C, Wright PC. 2011. Minimising iTRAQ ratio compression through understanding LC-MS elution dependence and high-resolution HILIC fractionation. Proteomics. 11:2341–2346. doi:10.1002/pmic.201000752

Pagels F, Guedes AC, Amaro HM, Kijjoa A, Vasconcelos V. 2019. Phycobiliproteins from cyanobacteria: chemistry and biotechnological applications. Biotechnol Adv. 37: 422–443. doi:10.1016/j.biotechadv.2019.02.010

Pandhal J, Ow SY, Wright PC, Biggs CA. 2009. Comparative proteomics study of salt tolerance between a nonsequenced extremely halotolerant cyanobacterium and its mildly halotolerant relative using in vivo metabolic labeling and in vitro isobaric labeling. J Proteome Res. 8:818–828. doi:10.1021/pr800283q

Parnasa R, Nagar E, Sendersky E, Reich Z, Simkovsky R, Golden S, Schwarz R. 2016. Small secreted proteins enable biofilm development in the cyanobacterium *Synechococcus elongatus*. Sci Rep. 6:32209. doi:10.1038/srep32209

Perkerson Iii RB, Johansen JR, Kováčik L, Brand J, Kaštovský J, Casamatta DA. 2011. A unique pseudanabaenalean (Cyanobacteria) genus *Nodosilinea* gen. nov. based on morphological and molecular DATA(1). J Phycol. 47:1397–1412. doi:10.1111/j.1529-8817.2011.01077.x

Pisareva T, Shumskaya M, Maddalo G, Ilag L, Norling B. 2007. Proteomics of *Synechocystis* sp. PCC 6803. Identification of novel integral plasma membrane proteins. Febs J. 274:791–804. doi:10.1111/j.1742-4658.2006.05624.x

Porra R, Thompson W, Kriedemann P. 1989. Determination of accurate extinction coefficients and simultaneous equations for assaying chlorophylls *a* and *b* extracted with four different solvents: verification of the concentration of chlorophyll standards by atomic absorption spectroscopy. Biochim Biophys Acta. 975:384–394. doi:10.1016/S0005-2728(89)80347-0

Qayyum S, Sharma D, Bisht D, Khan AU. 2016. Protein translation machinery holds a key for transition of planktonic cells to biofilm state in *Enterococcus faecalis*: a proteomic approach. Biochem Biophys Res Commun. 474:652–659. doi:10.1016/j.bbrc.2016.04.145

Radzi R, Muangmai N, Broady P, Wan Omar WM, Lavoue S, Convey P, Merican F. 2019. *Nodosilinea signiensis* sp. nov. (Leptolyngbyaceae, Synechococcales), a new terrestrial cyanobacterium isolated from mats collected on Signy Island, South Orkney Islands, Antarctica. PLoS One. 14:e0224395. doi:10.1371/journal.pone.0224395

Ramos V, Morais J, Castelo-Branco R, Pinheiro Â, Martins J, Regueiras A, Pereira AL, Lopes VR, Frazão B, Gomes D, et al. 2018. Cyanobacterial diversity held in microbial biological resource centers as a biotechnological asset: the case study of the newly established LEGE culture collection. J Appl Phycol. 30:1437–1451. doi:10.1007/s10811-017-1369-y

Romeu MJ, Alves P, Morais J, Miranda JM, de Jong ED, Sjollema J, Ramos V, Vasconcelos V, Mergulhão F. 2019. Biofilm formation behaviour of marine filamentous cyanobacterial strains in controlled hydrodynamic conditions. Environ Microbiol. 21:4411–4424. doi:10.1111/1462-2920.14807

Slabas AR, Suzuki I, Murata N, Simon WJ, Hall JJ. 2006. Proteomic analysis of the heat shock response in *Synechocystis* PCC6803 and a thermally tolerant knockout strain lacking the histidine kinase 34 gene. Proteomics. 6:845–864. doi:10.1002/pmic.200500196

Sonani RR, Gupta GD, Madamwar D, Kumar V. 2015. Crystal structure of allophycocyanin from marine cyanobacterium *Phormidium* sp. Plos One. 10:e0124580. doi:10.1371/journal.pone.0124580

Sun T, Li S, Song X, Diao J, Chen L, Zhang W. 2018. Toolboxes for cyanobacteria: recent advances and future direction. Biotechnol Adv. 36:1293–1307. doi:10.1016/j.biotechadv.2018.04.007

Taylor DA. 1996. Introduction to marine engineering. Burlington, MA: Butterworth-Heinemann.

Telegdi J, Trif L, Románszki L. 2016. Smart anti-biofouling composite coatings for naval applications. In: Montemor MF, editor. Smart composite coatings and membranes transport, structural, environmental and energy applications. Cambridge, UK: Woodhead Publishing; p. 123–155.

Teodósio JS, Simões M, Melo LF, Mergulhão FJ. 2011. Flow cell hydrodynamics and their effects on *E. coli* biofilm formation under different nutrient conditions and turbulent flow. Biofouling. 27:1–11. doi:10.1080/08927014.2010.535206

Vázquez-Martínez J, Gutierrez-Villagomez JM, Fonseca-García C, Ramírez-Chávez E, Mondragón-Sánchez ML, Partida-Martínez L, Johansen JR, Molina-Torres J. 2018. *Nodosilinea chupicuarensis* sp. nov. (Leptolyngbyaceae, Synechococcales) a subaerial cyanobacterium isolated from a stone monument in central Mexico. Phytotaxa. 334:167. doi:10.11646/phytotaxa.334.2.6

Wang N, Sadiq FA, Li S, He G, Yuan L. 2020. Tandem mass tag-based quantitative proteomics reveals the regulators in biofilm formation and biofilm control of *Bacillus licheniformis*. Food Control. 110:107029. doi:10.1016/j.foodcont.2019.107029

Wang Y, Stessman DJ, Spalding MH. 2015. The CO_2 concentrating mechanism and photosynthetic carbon assimilation in limiting CO2: how Chlamydomonas works against the gradient. Plant J. 82:429–448. doi:10.1111/tpj.12829

Wiśniewski JR, Zougman A, Nagaraj N, Mann M. 2009. Universal sample preparation method for proteome analysis. Nat Methods. 6:359–362. doi:10.1038/nmeth.1322

Wood ZA, Schröder E, Harris JR, Poole LB. 2003. Structure, mechanism and regulation of peroxiredoxins. Trends Biochem Sci. 28:32–40. doi:10.1016/S0968-0004(02)00003-8

SUPPLEMENTARY MATERIAL

SM 1. Correlation between wet weight and chlorophyll *a* content

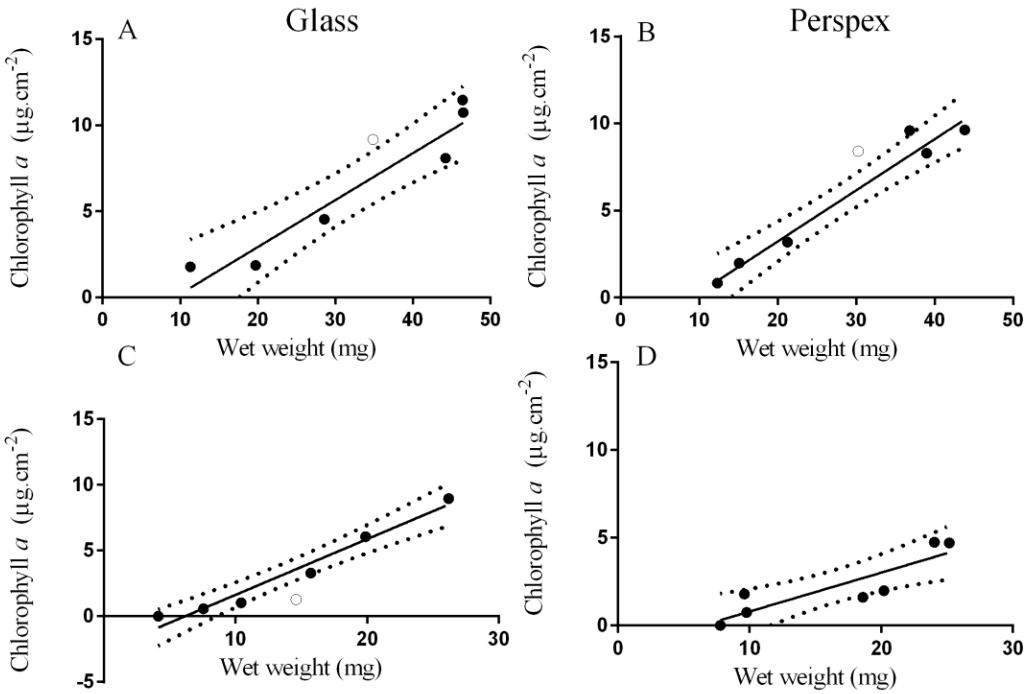

Figure SM 1.1. Correlation between wet weight and chlorophyll *a* on *Nodosilinea* sp. LEGE 06145. Biofilm development in glass (A, C) and perspex (B, D) at two different shear rates, 4 s^{-1} (A, B) and 40 s^{-1} (C, D). Full line represents the linear regression and the dashed line represents the confidence limits (95%). Closed symbols refer to data points that were considered for the regression (all except one) and the single open symbol refers to a data point that was excluded from the regression.

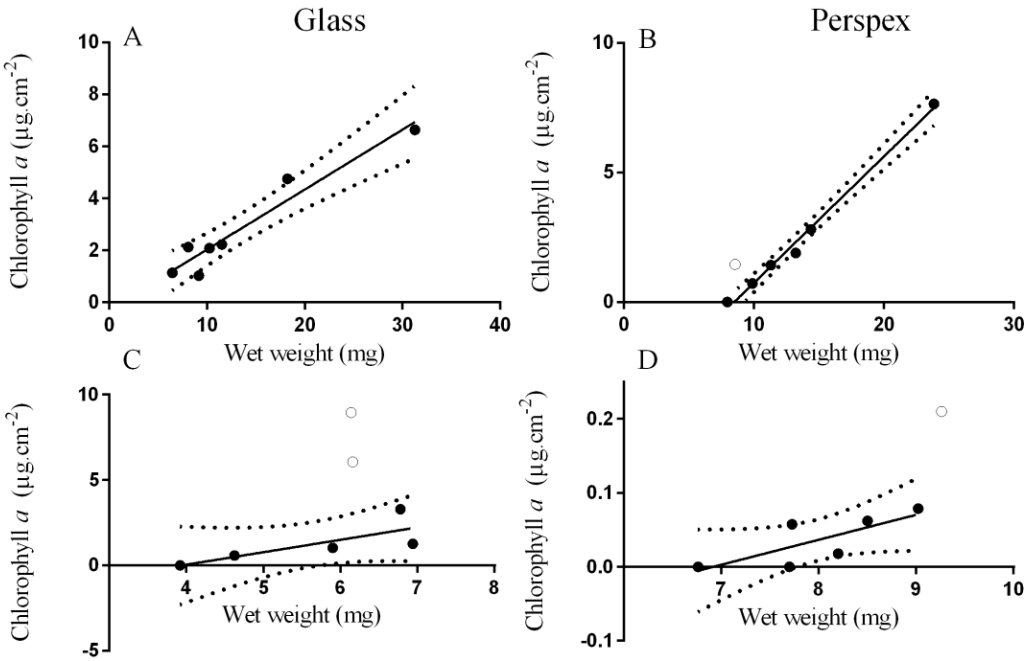

Figure SM 1.2. Correlation between wet weight and chlorophyll *a* on *Nodosilinea* sp. LEGE 06119. Biofilm development in glass (A, C) and perspex (B, D) at two different shear rates, 4 s^{-1} (A, B) and 40 s^{-1} (C, D). Full line represents the linear regression and the dashed line represents the confidence limits (95%). Closed symbols refer to data points that were considered for the regression (all except one) and open symbols refer to a data points that were excluded from the regression.

SM 2. Evaluation of biofilm development for different cyanobacterial strains, under the same hydrodynamic condition and the same surface

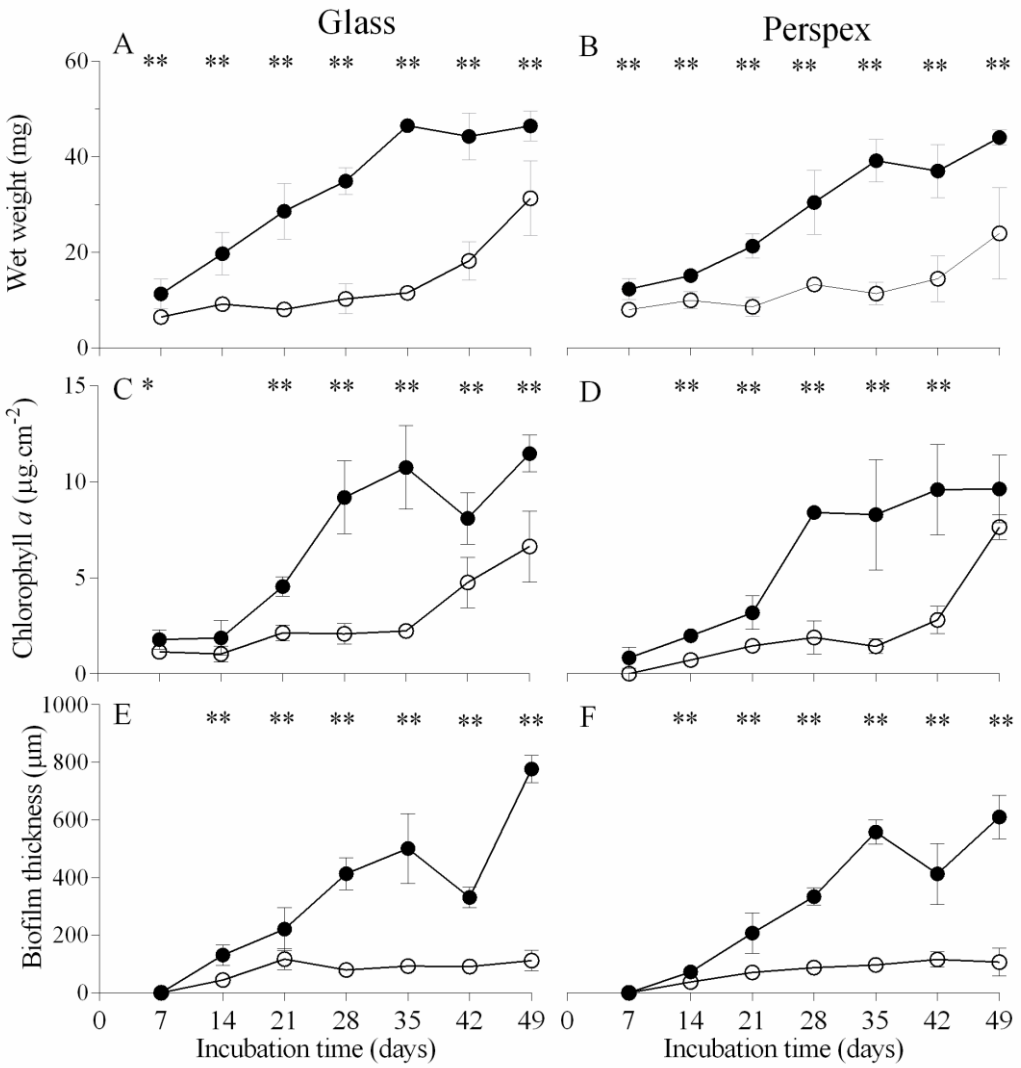

Figure SM 2.1. Evaluation of biofilm development under 4 s^{-1}. The parameters analysed refer to wet weight (A,B), chlorophyll *a* (C,D) and biofilm thickness (E,F). Biofilms were formed on two different surfaces, glass (A,C,E) and perspex (B,D,F) for 49 days. Closed and open circles refer to *Nodosilinea* sp. LEGE 06145 and *Nodosilinea* sp. LEGE 06119 biofilm development, respectively. Standard deviations from two biological assays with three replicates each, are represented. Symbols *; ** indicate statistically different values for $P < 0.1$ and $P < 0.05$ (respectively) at each incubation time.

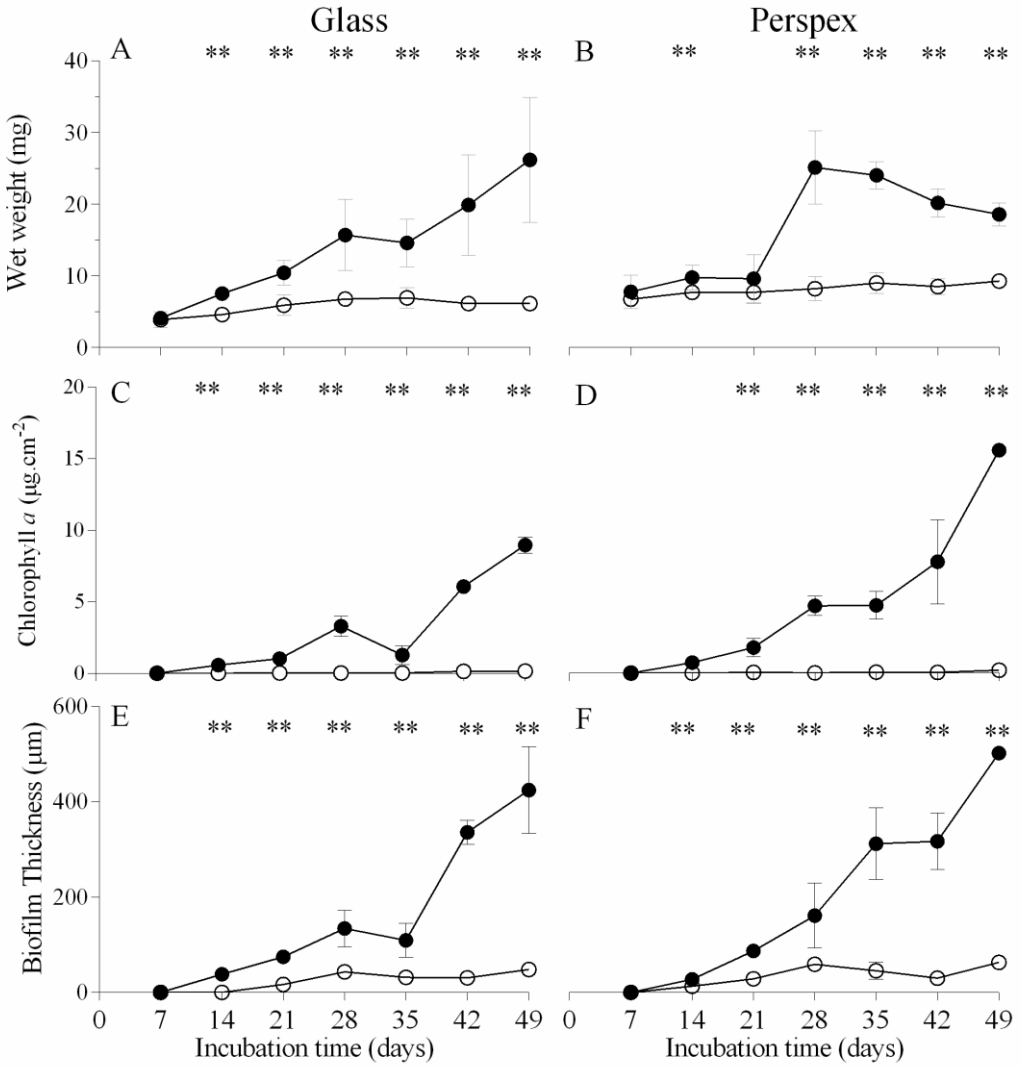

Figure SM 2.2. Evaluation of biofilm development under 40 s^{-1}. The parameters analysed refer to wet weight (A,B), chlorophyll *a* (C,D) and biofilm thickness (E,F). Biofilms were formed on two different surfaces, glass (A,C,E) and perspex (B,D,F) for 49 days. Closed and open circles refer to *Nodosilinea* sp. LEGE 06145 and *Nodosilinea* sp. LEGE 06119 biofilm development, respectively. Standard deviations from two biological assays with three replicates each, are represented. Symbols *; ** indicate statistically different values for $P < 0.1$ and $P < 0.05$ (respectively) at each incubation time.

SM 3. Evaluation of cyanobacterial biofilm development under the same hydrodynamic condition on different surfaces

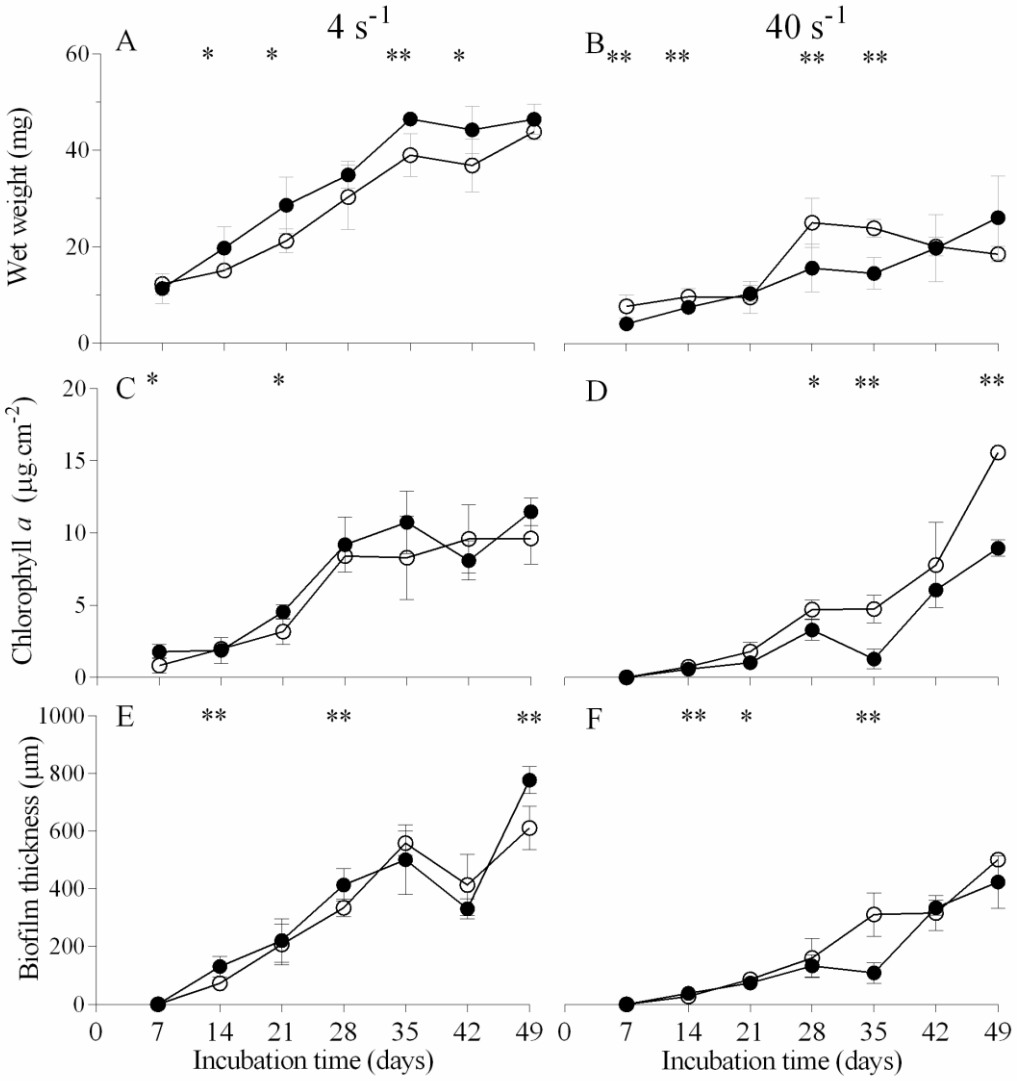

Figure SM 3.1. Evaluation of N*odosilinea* sp. LEGE 06145 biofilm development. The parameters analysed refer to wet weight (A,B), chlorophyll a (C,D) and biofilm thickness (E,F). Biofilms were formed at 4 s^{-1} (A,C,E) or 40 s^{-1} (B,D,F), on two different surfaces, glass (closed circles) and perspex (open circles) for 49 days. Standard deviations from two biological assays with three replicates each, are represented. Symbols *; ** indicate statistically different values for $P < 0.1$ and $P < 0.05$ (respectively) at each incubation time.

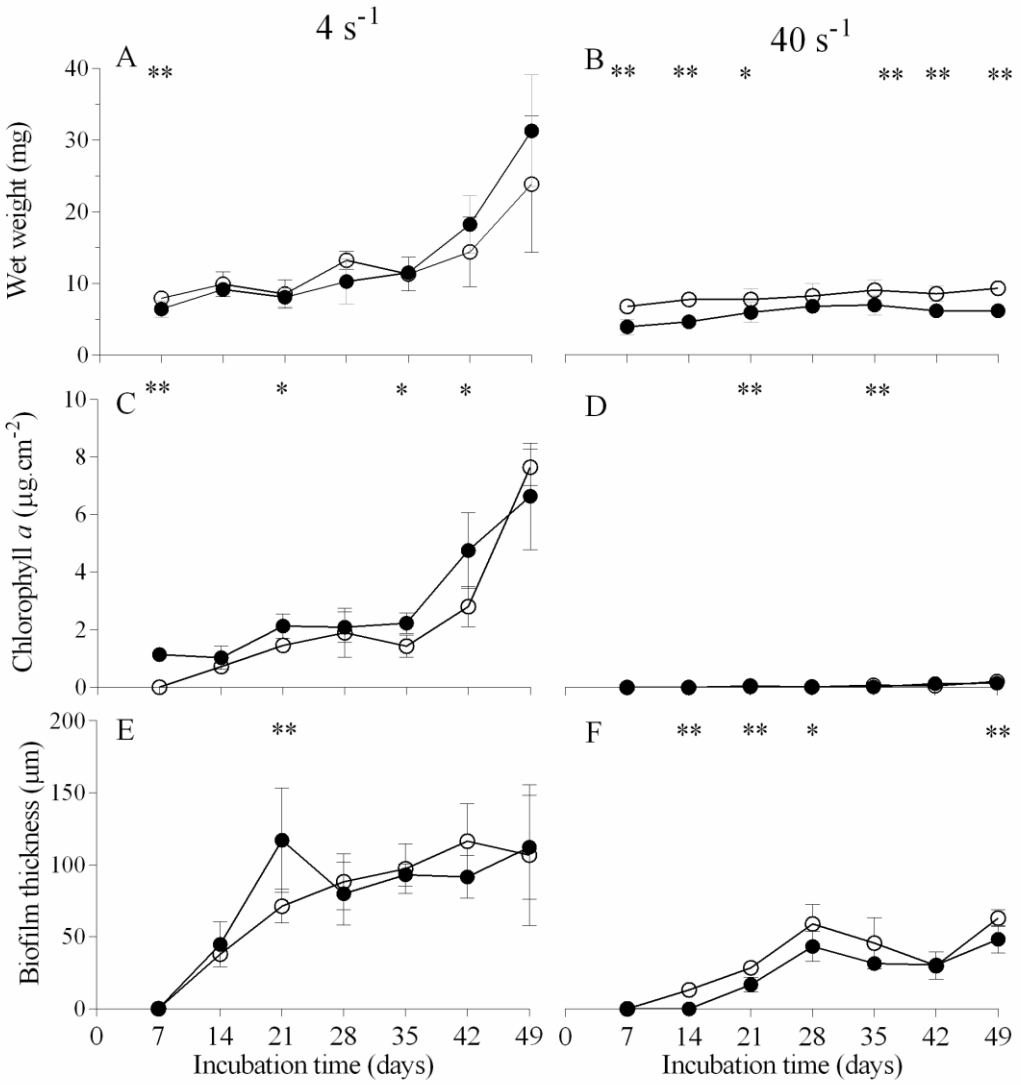

Figure SM 3.2. Evaluation of *Nodosilinea* sp. LEGE 06119 biofilm development. The parameters analysed refer to wet weight (A,B), chlorophyll *a* (C,D) and biofilm thickness (E,F). Biofilms were formed at 4 s^{-1} (A,C,E) or 40 s^{-1} (B,D,F), on two different surfaces, glass (closed circles) and perspex (open circles) for 49 days. Standard deviations from two biological assays with three replicates each, are represented. Symbols *; ** indicate statistically different values for $P < 0.1$ and $P < 0.05$ (respectively) at each incubation time.

SM 4. Proteomic analysis on cyanobacterial samples

Table SM 4.1 Number of proteins identified from planktonic and different biofilm samples.

		Cyanobacterial strains	
		***Nodosilinea* sp. LEGE 06145**	***Nodosilinea* sp. LEGE 06119**
Total protein identified		377	301
Planktonic samples		68	134
Biofilm samples		357	229
	Glass	261	167
	Perspex	232	125
	4 s^{-1}	311	192
	40 s^{-1}	100	99
	Glass 4 s^{-1}	246	133
	Perspex 4 s^{-1}	188	90
	Glass 40 s^{-1}	34	56
	Perspex 40 s^{-1}	92	63

SM 5. Proteomic analysis on cyanobacterial biofilm samples

Table SM 5.1 Number and identification of common proteins found under the different biofilm conditions. This table lists the proteins that were detected in more than 1 of the 8 experimental conditions. The frequency of appearance (from 2 to 8) is indicated in bold on the left column. For each subgroup (proteins that appear in 7 of the 8 conditions and so forth) the condition with the highest frequency of appearance is shaded (only frequencies of appearance higher than 55% were shaded.

Number of common proteins under the different biofilm conditions / Protein identification		*Nodosilinea* sp. LEGE 06119				*Nodosilinea* sp. LEGE 06145			
		4 s $^{-1}$		40 s $^{-1}$		4 s $^{-1}$		40 s $^{-1}$	
		glass	perspex	glass	perspex	glass	perspex	glass	perspex
8	A0A1Z3HSI0	x	x	x	x	x	x	x	x
7	A0A1U7J348	x	x	x	x	x	x		x
	A0A1U7J7J4	x	x	x	x	x	x		x
	A0A1U7JAP1		x	x	x	x	x	x	x
	A0A1U7JAT3		x	x	x	x	x	x	x
	A0A2P8ZU54		x	x	x	x	x	x	x
	I4HUB3	x	x	x	x	x	x		x
6*	A0A0N7LBT2	**x**	x		x	x	x		x
	A0A0U1Z975			x	x	x	x	x	x
	A0A162C5Y8	**x**			x	x	x	x	x
	A0A1U7J8S7	**x**	x	x		x	x		x
	A0A261KIT4		x	x		x	x	x	x
	A0A2P9A1R4	**x**			x	x	x	x	x
	A0A2P9A1T2	x			x	x	x	x	x
	F5UHJ9	x	x		x	x		x	x
5	A0A073CH81	x	x		x	x	x		
	A0A073CM30		x	x	x			x	x
	A0A077JIC2		x	x	x		x		x
	A0A1U7J0Z8	x			x	x	x	x	
	A0A1U7J9U5	x			x	x	x		x
	A0A1U7JAR5		x		x	x	x		x
	A0A2P8VVE3	x	x			x	x		x
	A0A2P8W059	x			x	x	x		x
	A0A2P8W6V3	x	x		x	x	x		
	A0A2P8ZWG1	x	x			x	x		x
	A0A2P8ZXU5	x	x			x	x		x
	A0A2P9A6M6	x			x	x	x		x
4	A0A0M2PWT4	x			x	x	x		
	A0A120MWU4	x	x			x	x		
	A0A165B204					x	x	x	x
	A0A1D8TY51	x	x	x	x				
	A0A1E5QVW6	x				x	x		x
	A0A1L9QY46	x	x	x	x				
	A0A1U7HVH4		x	x				x	x
	A0A1U7J679					x	x	x	x
	A0A1U7JB89	x	x		x				x
	A0A1U7JBA1	x	x	x	x				
	A0A1U7JBE0	x	x	x	x				
	A0A1Z4PQ70	x	x	x	x				
	A0A251ZAG5	x	x		x				x
	A0A2L2NU31				x		x	x	x
	A0A2P8W0E5				x	x	x		x
	A0A2P8W8A0	x				x	x		x
	A0A2P8ZU31					x	x	x	x
	A0A2P9A1V4					x	x	x	x
	A0A2P9A6M4	x			x	x	x		
	B0B2A7					x	x	x	x

		B4WMS8	x	x		x	x			
		B4WS90					x	x	x	x
	4	K9F192			x	x			x	x
		K9X5E3	x	x		x		x		
		A0A073CCC2					x	x		x
		A0A0C1UTD1	x				x	x		
		A0A0C1V458			x			x		x
		A0A0C1WHE0	x				x	x		
		A0A0P8C657					x	x		x
		A0A0P8CDR3					x	x		x
		A0A0T7BR98		x					x	x
		A0A1J0ABC8	x				x	x		
		A0A1J0PBA6		x	x	x				
		A0A1Q1EWS3	x	x	x					
		A0A1U7J0C2	x				x	x		
		A0A1U7J0I0					x	x		x
		A0A1U7J341	x					x		x
		A0A1U7J6Z9					x	x		x
		A0A1U7JBJ8	x		x	x				
		A0A1U7JBL0					x	x		x
		A0A1V8NDW1	x	x				x		
		A0A1Z3HRF8	x				x	x		
		A0A254VXE7					x		x	x
		A0A2E2G8H3				x	x	x		
		A0A2G4EW90					x	x		x
	3	A0A2P8VV58	x	x			x			
		A0A2P8VWZ0	x				x	x		
		A0A2P8W0U6	x		x	x				
		A0A2P8W6L9	x				x	x		
		A0A2P8W9Q5	x				x	x		
		A0A2P8WAN6					x	x		x
		A0A2P8WJE4	x	x	x					
		A0A2P8ZZK3	x				x	x		
		A0A2P9A1T6					x	x		x
		A0A2P9A5K6					x	x		x
		A0A2P9A6P1	x				x	x		
		A8ZQJ6	x		x	x				
		B2J5T3	x	x		x				
		B4VID1			x		x			x
		H9LIQ2					x	x		x
		I1YDD3	x				x	x		
		K9EH21					x		x	x
		K9VBM2		x		x	x			
		L8LZA3	x				x	x		
		Q7NL78		x					x	x
		Q7NMS0			x			x		x
		A0A0A1VZG0				x				x
		A0A0C1T9B4		x			x			
	2	A0A0C1WGB5					x	x		
		A0A0C1XWD0	x	x						
		A0A0D6AJ93					x	x		

	A0A0D6KIM4	x		x					
	A0A0D8ZR23	x				x			
	A0A0M1JQN5					x	x		
	A0A0N8KMT9	x			x				
	A0A0N8KPW9	x							x
	A0A0P4UWU7	x		x					
	A0A0P7ZJ21					x	x		
	A0A0P8A1K4				x				x
	A0A0S3TRY9							x	x
	A0A0V7ZNE4					x	x		
	A0A0X8WZ15					x	x		
	A0A120MWD1					x	x		
	A0A168V9D7		x						x
	A0A182ANB3					x	x		
	A0A1E5QRX1					x	x		
	A0A1J0AB12		x		x				
	A0A1J1JI14				x	x			
	A0A1J1KAB3					x	x		
	A0A1J1KU37					x	x		
	A0A1L9QVX3	x	x						
	A0A1Q4R6N6	x				x			
	A0A1Q6DDY3	x		x					
	A0A1Q8ZE73		x	x					
	A0A1Q8ZG15				x			x	
	A0A1U7HUT8	x		x					
	A0A1U7IYB9						x		x
	A0A1U7J140		x						x
2	A0A1U7J1A8					x	x		
	A0A1U7J2Q3					x	x		
	A0A1U7J2S0					x	x		
	A0A1U7J2T9					x	x		
	A0A1U7J2U2					x	x		
	A0A1U7J304					x	x		
	A0A1U7J3G7					x	x		
	A0A1U7J3I5					x	x		
	A0A1U7J481	x				x			
	A0A1U7J4J2	x				x			
	A0A1U7J4J9					x	x		
	A0A1U7J5R6					x	x		
	A0A1U7J6L3					x	x		
	A0A1U7J7B7					x	x		
	A0A1U7J8E3					x	x		
	A0A1U7J9P1					x	x		
	A0A1U7J9U4					x	x		
	A0A1U7JA40					x	x		
	A0A1U7JAE4					x	x		
	A0A1U7JAG3					x	x		
	A0A1U7JAN0					x	x		
	A0A1U7JB19					x	x		
	A0A1U7JB82						x		x
	A0A1Z3HIM7				x				x

A0A1Z3HIN6					x	x		
A0A1Z3HPV6	x			x				
A0A1Z3HSH6					x	x		
A0A1Z4GXM5					x	x		
A0A1Z4NKK4					x	x		
A0A1Z4QPV0		x	x					
A0A1Z4UGX5	x			x				
A0A1Z8NBM9	x			x				
A0A218N0M0					x	x		
A0A218QHQ5	x					x		
A0A251WGJ8	x					x		
A0A254WT29		x	x					
A0A2E1IMA9	x					x		
A0A2K2ZSH6	x		x					
A0A2N5JPX1					x	x		
A0A2N6L6G2		x						x
A0A2N6MRK8		x	x					
A0A2P8VR06					x	x		
A0A2P8VRH1					x	x		
A0A2P8VRR4	x				x			
A0A2P8VTT8					x	x		
A0A2P8VU31					x			x
A0A2P8W6J2					x	x		
A0A2P8W8E1					x	x		
A0A2P8W8P0					x	x		
A0A2P8W8U3					x	x		
A0A2P8W8Y6					x	x		
A0A2P8W907					x	x		
A0A2P8WDG7	x		x					
A0A2P8WID7					x	x		
A0A2P8ZR41					x	x		
A0A2P8ZSC4					x	x		
A0A2P8ZTP8					x	x		
A0A2P8ZWB0					x	x		
A0A2P8ZXT6					x	x		
A0A2P8ZZL1					x	x		
A0A2P9A1S7					x	x		
A0A2P9A525					x	x		
A0A2P9A675					x	x		
A0A2P9A6S9					x	x		
B4W482			x					x
B4WFP8	x			x				
D5A4Y5		x						x
K0J955					x	x		
K9FMV2					x	x		
K9PC88		x	x					
K9PUV5					x	x		
K9PW98	x		x					
K9SVF4	x					x		
K9UQL4					x	x		
K9XAV9					x	x		

L0L519							x	x
Q7NFT5	x	x						
T2IZZ1					x	x		
U9VTX8	x				x			
U9VXF7	x	x						
U9VXT1		x		x				

** As the distribution of these seven proteins among the 4 conditions (4 s^{-1}, 40 s^{-1}, glass and perspex) was similar (52%, 48%, 48% and 52%, respectively), there was not experimental condition in which the frequency of appearance was highlighted.*

Environmental Research 201 (2021) 111566

Contents lists available at ScienceDirect

Environmental Research

journal homepage: www.elsevier.com/locate/envres

Quantitative proteomic analysis of marine biofilms formed by filamentous cyanobacterium

M.J. Romeu [a,1], D. Domínguez-Pérez [b,1], D. Almeida [b], J. Morais [b], M.J. Araújo [b], H. Osório [c,d,e], A. Campos [b], V. Vasconcelos [b,f], F.J. Mergulhão [a,*]

[a] LEPABE, Laboratory for Process Engineering, Environment, Biotechnology and Energy, Faculty of Engineering, University of Porto, Rua Dr. Roberto Frias, 4200-465 Porto, Portugal
[b] CIIMAR, Interdisciplinary Centre of Marine and Environmental Research, University of Porto, Terminal de Cruzeiros do Porto de Leixões, Av. General Norton de Matos s/n, 4450-208, Matosinhos, Portugal
[c] i3S –Instituto de Investigação e Inovação em Saúde, Universidade do Porto, 4200-135, Porto, Portugal
[d] Institute of Molecular Pathology and Immunology of the University of Porto, IPATIMUP, Rua Júlio Amaral de Carvalho 45, 4200-135, Porto, Portugal
[e] Faculty of Medicine, University of Porto, Al. Prof. Hernâni Monteiro, 4200-319, Porto, Portugal
[f] Department of Biology, Faculty of Sciences, University of Porto, Rua do Campo Alegre, 4169-007, Porto, Portugal

ARTICLE INFO

Keywords:
Marine biofouling
Cyanobacterial biofilms
Shotgun proteomic
LC-MS/MS
Hydrodynamics
Fouling surfaces

ABSTRACT

Cyanobacterial molecular biology can identify pathways that affect the adhesion and settlement of biofouling organisms and, consequently, obtain novel antifouling strategies for marine applications. Proteomic analyses can provide an essential understanding of how cyanobacteria adapt to different environmental settings. However, only a few qualitative studies have been performed in some cyanobacterial strains. Considering the limited knowledge about protein expression in cyanobacteria in different growing conditions, a quantitative proteomic analysis by LC-MS/MS of biofilm cells from a filamentous strain was performed. Biofilms were also analysed through standard methodologies for following cyanobacterial biofilm development. Biofilms were formed on glass and perspex at two relevant hydrodynamic conditions for marine environments (average shear rates of 4 s^{-1} and 40 s^{-1}). Biofilm development was higher at 4 s^{-1} and no significant differences were found between surfaces. Proteomic analysis identified 546 proteins and 41 were differentially expressed. Differences in protein expression were more noticeable between biofilms formed on glass and perspex at 4 s^{-1}. When comparing biofilms formed on different surfaces, results suggest that biofilm development may be related to the expression of several proteins like a beta-propeller domain-containing protein, chaperone DnaK, SLH domain-containing proteins, an OMF family outer membrane protein, and/or additional uncharacterized proteins. Regarding the hydrodynamic effect, biofilm development can be related to SOD enzyme expression, to proteins related to photosynthetic processes and to a set of uncharacterized proteins with calcium binding domains, disordered proteins, and others involved in electron transfer activity. Studies that combine distinct approaches are essential for finding new targets for antibiofilm agents. The characterisation performed in this work provides new insights into how shear rate and surface affect cyanobacterial biofilm development and how cyanobacteria adapt to these different environmental settings from a macroscopic standpoint to a proteomics context.

1. Introduction

Marine biofouling has several economic, environmental, and ecological impacts (Bharti et al., 2017; Carvalho, 2018). Biofilms are a particular concern in aquaculture, heat exchangers, maritime transport, water desalination and the oil and gas industry. In biofilms, organisms cooperate and improve their chances of survival when subjected to harsh environmental conditions. Indeed, in marine environments, several parameters can affect the development of these biofilms, such as salt, nutrient and organic matter concentration, light access, pH,

* Corresponding author. LEPABE, Laboratory for Process Engineering, Environment, Biotechnology and Energy, Faculty of Engineering, University of Porto, Rua Dr. Roberto Frias, 4200-465, Porto, Portugal.
E-mail address: filipem@fe.up.pt (F.J. Mergulhão).
[1] These authors contributed equally to this work.

https://doi.org/10.1016/j.envres.2021.111566
Received 2 March 2021; Received in revised form 14 June 2021; Accepted 18 June 2021
Available online 25 June 2021
0013-9351/© 2021 Elsevier Inc. All rights reserved.

temperature, hydrodynamic conditions, as well as the abiotic or biotic surface in which biofilm formation occurs (Carvalho, 2018). Cyanobacteria dominate marine and phototrophic biofilms and they have cosmopolitan distribution due to their inherent capacity to withstand various biotic and abiotic stresses. These microfouler organisms can also promote the adhesion of macrofouler organisms such barnacles, mussels, algae and seaweeds in aquatic environments (Mieszkin et al., 2013). Integration among several disciplines, such as genetics, biology, and chemistry, is essential for progress in marine biofilm research. Therefore, cyanobacterial molecular biology is an emerging field for further developments and improvements (Santos-Merino et al., 2019; Sun et al., 2018). Analyses of protein expression can provide an essential understanding of how cyanobacteria adapt to different environmental settings. It is crucial to study the protein expression level in different conditions, particularly in biofilms, since biofilm development under altered conditions may be associated with quantitative differences in their proteome. Therefore, quantitative proteomics studies allow establishing a relationship between the relative expression level of the identified proteins under different conditions. However, few proteomics studies address marine biofilms (Leary et al., 2014), and cyanobacteria data is scarce (Babele et al., 2019). Moreover, the small number of quantitative proteomic studies performed with filamentous cyanobacterium is restricted to *Anabaena, Nostoc,* and *Spirulina* cyanobacterial genus. These studies only analysed the impact of limited and specific parameters on protein expression, such as temperature (Kurdrid et al., 2011), salt (Wang et al., 2013) and arsenic stress (Pandey et al., 2012), ultraviolet-B light exposure (Babele et al., 2015), uranium tolerance (Panda et al., 2017) or N_2-fixing and non-N_2-fixing conditions (Ow et al., 2008). Different factors have been reported on cyanobacterial biofilm development, such as the involvement of the signaling molecule cyclic dimeric GMP (Agostoni et al., 2016; Enomoto et al., 2014), extracellular proteins (Oliveira et al., 2015; Parnasa et al., 2016; Zilliges et al., 2008) or type IV pili (Allen et al., 2019).

Identifying proteins expressed in a defined condition is a useful tool to understand the cellular response and to identify pathways that are activated or down-regulated under different circumstances to which cells were subjected (Battchikova et al., 2018; Muthusamy et al., 2017). Knowledge about protein expression under different biofilm development conditions is essential to clarify their role on biofilm phenotypes. These studies can help to identify pathways affecting adhesion and settlement of biofouling organisms and can lead to new targets for the development of novel antifouling strategies for marine applications.

The Blue Biotechnology and Ecotoxicology Culture Collection (LEGE-CC) is a biological resource center that comprises more than 1000 different cyanobacterial and microalgae strains (Ramos et al., 2018). The unidentified filamentous cyanobacterium LEGE 06007 strain was used in this study, given the relevance of cyanobacteria on marine biofouling. This strain has also shown good biofilm formation behavior during pre-screening of the collection. Although several biological and physico-chemical parameters have been identified as modulators of biofilm development, the fouling surface properties and flow velocity/shear rate have a critical impact on marine biofilms (Faria et al., 2020a, 2020b, 2021). Hence, the first goal of this study was to perform a biofouling potential evaluation of this marine cyanobacterium, which has recently been restructured on taxonomic level (Ramos et al., 2018). Previously included on *Phormidium* genus, after a revaluation of taxonomic assignments based on approaches that combine morphological and phylogenetic data, evaluation of its characteristics did not allow an unequivocal identification at the genus or order level. The second aim of this study was to perform a quantitative proteomics analysis of this cyanobacterium under different biofilm development conditions to establish a relationship between the relative expression level of the identified proteins under different settings (different hydrodynamic conditions and surfaces) and biofilm development. For this purpose, we performed a shotgun proteomic analysis of the digested peptides obtained from two distinct sample preparation methods – the Filter Aided Sample Preparation (FASP) (Wiśniewski et al., 2009), and the single-pot solid-phase-enhanced sample-preparation (SP3) protocol (Hughes et al., 2019). To the best of our knowledge, there are no quantitative proteomics studies evaluating the impact of different surfaces and different hydrodynamic conditions on cyanobacterial biofilm behavior. Therefore, this is the first work investigating the biofouling potential of this cyanobacterial strain and its proteome profile obtained from different biofilm development conditions by applying standard methodologies for biofilm development and a quantitative proteomics approach. Since the information on the molecular basis of these processes in cyanobacteria is scarce, the quantitative proteomic analysis carried out in this work is extremely relevant. Moreover, few studies have been performed in this research field addressing filamentous cyanobacterial biofilms.

2. Materials and methods

2.1. Organism and inocula preparation

Unidentified filamentous cyanobacterium LEGE 06007 was isolated from a wave-exposed rock in the intertidal zone at São Martinho do Porto beach, Portugal (39.50694 N 9.136311 W), and it was obtained from the LEGE-CC located at CIIMAR, Matosinhos, Portugal (Ramos et al., 2018). Cells were grown in 750 mL culture in Z8 medium (Kotai, 1972) supplemented with 25 g l^{-1} of synthetic sea salts (Tropic Marin) and B_{12} vitamin (Sigma Aldrich, Merck, Saint Louis, MO, USA), which supports the growth and cyanobacteria maintenance. The culture was performed under 14 h light (10–30 μmol photons m^{-2} s^{-1})/10 h dark cycles, at 25 °C.

2.2. Biofilm formation

Biofilm development was evaluated on agitated 12-well microtiter plates (VWR International, Carnaxide, Portugal), since this platform was shown to mimic the hydrodynamic conditions found in marine environments (Romeu et al., 2019). To assess the surface effect on protein expression, biofilms were developed on glass (Vidraria Lousada, Lda, Portugal) and perspex (Neves & Neves, Lda, Portugal) coupons (1 cm^2). These substrates have different hydrophobicity (Romeu et al., 2019) and they also represent commonly submerged artificial surfaces found on different equipment in aquatic and marine environments such as underwater windows of boats, aquaculture equipment, flotation spheres, moored buoys, underwater cameras, measuring devices or sensors (Taylor, 1996; Blain et al., 2004; King et al., 2006). Surface preparation and sterilisation was performed as previously described (Romeu et al., 2019). Before inoculation, the cyanobacterial suspension was adjusted to a chlorophyll *a* concentration of 1.5 μg ml^{-1}, since chlorophyll *a* concentration is commonly used as biomass indicator in aquatic environments. After 2 ml of cyanobacterial suspension were incubated for 24 h at 4 °C in the dark for a maximal chlorophyll *a* extraction, the samples were centrifuged at 3202 g, for 5 min at room temperature and the supernatant was transferred to a glass cuvette. The absorbance at 750 nm (turbidity), 665 nm (chlorophyll *a*) and 652 nm (chlorophyll *b*) was determined using a V-1200 spectrophotometer (VWR International China Co., Ltd, Shanghai, China). The chlorophyll *a* concentration was calculated through the following equation (Porra et al., 1989):

$$\text{Chl } a\ (\mu g.ml^{-1}) = 16.29 \times A^{665} - 8.54 \times A^{652} \quad (1)$$

These measurements were assessed in triplicate and dilutions were performed using Z8 medium supplemented with 25 g l^{-1} of synthetic sea salts and vitamin B_{12}. Thus, a volume of 3 ml of adjusted cyanobacterial suspension was inoculated in each well, in which coupons of each surface were previously fixed with transparent double-sided adhesive tape. To assess the effect of hydrodynamics on protein expression, cyanobacterial biofilm formation at different shear rates was tested. Although a shear rate of 50 s^{-1} has been reported for a ship in a harbour

(Bakker et al., 2003), equipment and devices which are in similar environments such as partially submerged or even moored equipment, as underwater cameras, flotation spheres, sensors, and even transparent hulls of boats or their windows are likely to be subjected to similar shear values (Romeu et al., 2019). Microtiter plates were incubated at 25 °C in an orbital shaker with a 25 mm orbital radius (Agitorb 200ICP, Norconcessus, Portugal) at 185 rpm, yielding average and maximum shear rates of 40 and 120 s^{-1}, respectively (Romeu et al., 2019). Moreover, it has been reported that lower fluid velocities (0.2 m s^{-1}) promote the growth of filamentous green algae and cyanobacteria (Flemming et al., 2009; Minchin and Gollasch, 2003) and that marine biofouling can be favoured at low shear rates (Faria et al., 2020a). Therefore, biofilm development was also assessed at lower shear rate conditions (average shear rate of 4 s^{-1}, reaching a maximum value of 11 s^{-1}, which are obtained in the same incubator at a shaking frequency of 40 rpm). Overall, these values of shear rate include different ranges that can be found in marine environments and which are important for marine biofouling. Biofilm development was followed for seven weeks (49 days) since it is accepted that a two-month interval for maintenance is the minimum duration for economically viable underwater monitoring systems, as previously reported (Blain et al., 2004; Romeu et al., 2019). During this incubation time, the medium was replaced twice a week. In order to mimic real light exposure periods, a photoperiod of 14 h light (8–10 μmol photons m^{-2} s^{-1})/10 h dark cycles) was applied (Romeu et al., 2019). This methodology, which has been used to assess the antifouling performance of different surfaces, was further validated by field tests as previously described (Silva et al., 2021).

2.3. Biofilm analysis

Although the initial stages of biofilm formation could be assessed by counting the number of adhered cells if a coccoid cyanobacterium was used (Faria et al., 2021), this study uses a filamentous cyanobacterial strain which precludes reliable determination of adhered cell numbers. Since preliminary studies have shown that seven days was the minimum time to obtain reliable and quantifiable results through the methods used in this work, biofilm analysis was performed every seven days, at which three coupons for each surface and hydrodynamic condition were analysed. To eliminate loosely attached cyanobacteria, the culture medium was carefully removed, and the wells were filled with 3 ml of sterile sodium chloride solution (8.5 g l^{-1}) (Romeu et al., 2019) to evaluate the cyanobacterial biofilms structure by Optical Coherence Tomography (OCT). In order to complement the characterization of cyanobacterial biofilms, the determination of their wet weight and chlorophyll *a* content was performed. Additionally, the crystal violet assay was performed for total biomass quantification.

2.3.1. Optical Coherence Tomography

Images from cyanobacterial biofilms developed on both surfaces and under the different hydrodynamic conditions were captured as reported in Romeu et al. (2019). For each coupon, 2-D imaging was performed with a minimum of three fields of view, to ensure the accuracy and reliability of the results obtained. Image analysis was performed using a routine developed in the Image Processing Toolbox from MATLAB 8.0 and Statistics Toolbox 8.1 (The MathWorks, Inc., Natick, Massachusetts, USA) as reported in Romeu et al. (2020). The mean biofilm thickness was calculated according to the following equation (2):

$$\overline{L}_F = \frac{1}{N} \sum_{i=1}^{N} L_{F,i} \quad (2)$$

where $L_{F,i}$ is a local biofilm thickness measurement at location *i*, *N* equals the number of thickness measurements and $\overline{L}_F$ is the mean biofilm thickness.

Biofilm roughness was analysed by determining the roughness coefficient because this parameter allows comparing the structure of different biofilms, across different studies and across scales once this value is normalized to the mean biofilm thickness (Romeu et al., 2019). The relative roughness coefficient (R_a^*) was calculated using the following equation, according to Wagner and Horn (2017):

$$R_a^* = \frac{1}{N} \sum_{i=1}^{N} \frac{|L_{F,i} - \overline{L}_F|}{\overline{L}_F} \quad (3)$$

2.3.2. Wet weight determination and chlorophyll a quantification

The determination of cyanobacterial biofilms wet weight and chlorophyll *a* content was performed as reported in Romeu et al. (2019). In order to determine the wet weight, coupons were detached from the wells and weighed. Biofilm wet weight was obtained as the difference from the initial coupon weight (determined prior to inoculation). Afterwards, cyanobacterial cells were detached from the coupons by immersing each coupon in 2 ml of 8.5 g l^{-1} sodium chloride solution and vortexing. The suspensions were incubated for 24 h at 4 °C in the dark and chlorophyll *a* determination was performed as previously described through Eq. (1).

2.3.3. Crystal violet assay

Additional coupons, representative of all conditions, were transferred to sterile 24-well plates at each sampling day. Crystal violet assay was adapted from a previously described protocol (Moreira et al., 2017). Briefly, to fix the cyanobacterial biofilms, 1 ml of 100% (v/v) ethanol was added to each well for 15 min. Afterwards, culture plates were allowed to air dry at room temperature. The fixed biofilms were stained with 1 ml of 1% (v/v) crystal violet solution (Merck KGaA, Germany) for 5 min and to solubilize the crystal violet (CV), 1 ml of 33% (v/v) acetic acid (VWR, Portugal) was added to each well. Then, 200 μL of this solution was transferred to sterile 96-well plates, and the optical density was measured at 570 nm in a plate reader (SpectroStar Nano, BMG LABTECH).

2.3.4. Statistical analysis of biofilm development

A total of six replicates (two biological assays with three technical replicates each) were analysed. Data analysis was performed using the statistical program GraphPad Prism® for Windows, version 6.01 (GraphPad Software, Inc., San Diego, CA, USA) and results were compared using unpaired t-tests with a confidence level of 95% (**; $P < 0.05$) and 90% (*; $P < 0.1$).

2.4. Proteomics analysis

2.4.1. Protein extraction and sample preparation

At the last sampling time (49 days), biofilm samples of unidentified filamentous cyanobacterium LEGE 06007 strain from each condition were recovered for proteomic analysis and processed as previously described (Romeu et al., 2020) with some modifications. Briefly, cyanobacterial biofilms were detached from the surface by immersing each coupon in 2 ml of 8.5 g l^{-1} sodium chloride solution and vortexing. To maximise the biomass yield, suspensions obtained from four coupons of the same condition were pooled. The samples were centrifuged at 3202 g for 10 min at room temperature and the pellets of biomass originating from 24 biofilm samples comprising six independent-replicates from four different growing conditions were kept at −20 °C for further processing. Following previously described protocols (Campos et al., 2016), the amount of sample was calculated, and an appropriate volume of SDT buffer (0.5 g FW/ml SDT) + Protease inhibitors (PIs, Roche, 11697498001, Basel, Switzerland) was added to the samples. These were sonicated 10 × 3 s and 23 kHz–105 μm (amplitude) and incubated for 4 h at room temperature. Then, samples were heated for 3 min at 95 °C and subsequently centrifuged at 16,000 g for 20 min. Finally, the supernatant was collected, and total protein concentration was measured indirectly

by optical density (OD) at 280 nm using a DeNovix DS-11 Spectrophotometer (DeNovix Technologies, Wilmington, Delaware, USA). Samples containing the extracted protein were stored for 24 h at −20 °C.

The extracted proteins were processed using two distinct protocols based on FASP protocol described by Wiśniewski et al. (2009) and the SP3 (Hughes et al., 2019) technology.

2.4.1.1. FASP. Similar to previous works, the samples containing the extracted proteins stored at −20 °C were defrosted in ice for further processing using the FASP protocol as previously described (Almeida et al., 2020; Martins et al., 2020; Matos et al., 2020; Romeu et al., 2020). This approach comprised the alkylation with iodoacetamide and digestion of 40 μg of the extracted proteins with trypsin (recombinant, proteomics grade, Roche, Basel, Switzerland) at an enzyme to protein ratio of 1:100 (w/w) for 16 h at 37 °C using centrifugal filter units with nominal molecular weight limit (NMWL) of 30 kDa (MRCPRT030, Millipore, Billerica, MA, USA). Through centrifugal filtration, peptides were recovered and acidified with Trifluoracetic acid (TFA: 10% v/v). Samples were desalted and concentrated by reversed-phase extractions (C18 Tips, 100 μL, Thermo Scientific, Thermo Fisher Scientific, Wilmington, DE, USA) with acetonitrile (CAN: 50% v/v) and TFA (0.1% v/v) for peptide elution. Before LC-MS/MS analysis, samples were dried in a Concentrator Plus vacuum rotator (Eppendorf, Hamburg, Germany) and resuspended in 25 μL formic acid (FA: 0.1% v/v). The final concentration was determined with 2 μL of digested peptides, measured indirectly by optical density (OD) at 280 nm using a DeNovix DS-11 Spectrophotometer (DeNovix Technologies, Wilmington, Delaware, USA).

2.4.1.2. SP3. Prior to digestion, 100 μg of extracted proteins in approximately 5 μL were reduced in 45 μL SDT in new 1.5 mL Eppendorf tubes. Then, alkylation of samples was performed with 10 μL of 0.1 M iodoacetamide (AppliChem) in 8 M Urea, 0.1 M Tris/HCl pH 8.5 for 30 min in the dark at room temperature.

Digestion followed Hughes et al. (2019) SP3 for proteomics experiments with some modifications. New magnetized beads (Sera Mag SP3 beads, CAT#45152105050250 and CAT#65152105050250, GE Healthcare) were initially washed and reconstituted in water (HPLC grade, VWR) at a final concentration of 10 μg/μL (from an initial stock concentration of 50 mg/mL), using a magnetic rack (MagnaRack, Invitrogen) for 1 min, and the protein digestion was conducted according to specifications of the manufacturer. Then, after removing the supernatant, 100 μL ammonium bicarbonate (Fluka) 0.05 M was added to the tubes and incubated for 5 min at 1000 rpm. After bead spin and magnetizing, the supernatant containing the tryptic peptides was transferred to clean 1.5 mL Eppendorf tubes. The peptide concentration was estimated using the DeNovix (A280 application). Acidification was performed by adding 20 μL of formic acid 5% v/v (Optima LC/MS grade, Fisher Chemical) to the samples. Afterwards, tryptic peptides were dried in a Concentrator Plus vacuum rotator (Eppendorf, Hamburg, Germany) and resuspended in 25 μL formic acid (FA: 0.1% v/v). The final concentration was determined with 2 μL of digested peptides, measured indirectly by optical density (OD) at 280 nm using a DeNovix DS-11 Spectrophotometer (DeNovix Technologies, Wilmington, Delaware, USA). A detailed description of the SP3 protocol can be found in Appendix A.

2.4.2. LC-MS/MS analysis

Considering that both sample preparation methods are complementary, tryptic peptides from both methods were mixed in the same tube to a final concentration of 0.1 μg and 0.5 μg from FASP and SP3, respectively. Then, protein digests from both protocols were analysed in the same run with a nano LC-MS/MS, composed by an Ultimate 3000 liquid chromatography system coupled to a Q-Exactive Hybrid Quadrupole – Orbitrap mass spectrometer (Thermo Scientific, Bremen, Germany), as previously described (Osório et al., 2021). Separation was performed in a 15 cm by 75 μm inner diameter EASY-Spray column (ES800, PepMap RSLC, C18, 3 μm, Thermo Scientific, Bremen, Germany) at 300 nL/min using a gradient generated by mixing A: 0.1% FA and B: 80% ACN, in the following quantities: 5 min (2.5% B to 10% B), 60 min (10% B to 35% B), 5 min (35% B to 99% B) and 5 min (hold 99% B). Subsequently, the column was equilibrated with 2.5% B for 12 min. Data acquisition was controlled by Xcalibur 4.0 and Tune 2.8 software (Thermo Scientific, Bremen, Germany). The specific LC-MS parameters were full scan settings: 70 k resolution (m/z 200), AGC target 3e6, maximum injection time 50 ms dd settings: minimum AGC target 8e3, intensity threshold 7.3e4, charge exclusion: unassigned, 1, 8, >8, peptide match preferred, exclude isotopes on, dynamic exclusion 20s. MS2 settings: microscans 1, resolution 35 k (m/z 200), AGC target 2e5, maximum injection time 110 ms, isolation window 2.0 m/z, isolation offset 0.0 m/z, spectrum data type profile.

2.4.3. Protein identification

The raw data was analysed and processed using the Proteome Discoverer 2.2.0.388 software (Thermo Scientific) and searched against the UniProt database for Cyanobacteria taxonomic selection (2018_07 release). The Sequest HT search engine was used for protein identification. The ion mass tolerance was 10 ppm for precursor ions and 0.02 Da for-fragment ions. Maximum allowed missing cleavage sites was set to 2. Cysteine carbamidomethylation was defined as a constant modification. Methionine oxidation and protein N-terminus acetylation were defined as variable modifications. Peptide confidence was set to high. The processing node Percolator was enabled with the following settings: maximum delta Cn 0.05; decoy database search target false discovery rates (FDR) 1%, validation was based on q-value. Protein label-free quantitation was performed with the Minora feature detector node at the processing step. Precursor ion quantification was performed at the processing step with the following parameters: unique plus razor peptides were considered for quantification and precursor abundance was based on intensity.

2.4.4. Differential protein expression and enrichment

Statistical analyses applied to the proteomic data were performed using R software version 4.0.0. (Dessau and Pipper, 2008). The Differentially Expressed Proteins (DEPs) and/or gene enrichment were assessed using the "DEP" R package (Zhang et al., 2018), based on the *limma* algorithm (Ritchie et al., 2015). Missing values were filtered according to the fraction of protein found in each paired comparison with a cut-off of 0.33%, considering the possibility of having a minimum of 4 out of 6 replicates of at least one condition. Imputation of missing values was performed considering a non-random distribution (MNAR) using "MinProb" as an imputation function. Significant differences between conditions for each condition were paired tested by protein-wise linear models and empirical Bayes statistics. Finally, adjusted P-value (alpha = 0.05), and the $\log_2$ fold change (lfc = $\log_2(1.5)$, $\log_2$ fold change >0.6) were used as a filter threshold to classify them as DEPs or enriched genes. For comparison purposes, the distribution of DEPs among conditions was analysed by Venn diagrams using an online free tool, available at the webserver of the Bioinformatics and Evolutionary Genomics Center (BEG/Van de Peer Lab site), Ghent University, Belgium, http://bioinformatics.psb.ugent.be/webtools/Venn/.

2.4.5. Functional annotation

Functional classification (gene ontology) was carried out using the OmicsBox software version 1.4.11 (https://www.biobam.com/omicsbox/). Protein signatures were also obtained from the InterPro member databases (*e.g.* Pfam, PROSITE, PRINTS, ProDom, SMART, TIGRFAMs, PIRSF, SUPERFAMILY, Gene3D, and PANTHER) using the InterProScan software (Mitchell et al., 2019) integrated into the OmicsBox tool. All annotation and the corresponding gene ontology (GO) terms were then

transferred to the sequences and eventually merged with existing GO terms resulting from blast search. Additional functional analyses to determine over/underexpressed pathways were performed to the categorical GO terms corresponding to DEPs, using the hypergeometric distribution significance test (Fisher's exact test, $P < 0.05$).

3. Results and discussion

3.1. Biofilm development analysis

Cyanobacterial biofilm development was assessed for 49 days, and the wet weight, chlorophyll *a* content, total biomass and thickness evolution is shown in Fig. 1. Biofilm biomass was higher at the lowest shear rate for both surfaces, as it is particularly noticeable in the biofilm thickness obtained on glass (Fig. 1G). Previous studies performed with different filamentous cyanobacterial strains have shown that despite the tenfold difference in average shear rate, cyanobacterial biofilm behavior was similar in both hydrodynamic conditions for the first weeks of biofilm development (Romeu et al., 2019, 2020). In the present study, differences in biofilm development at different shear conditions were noticed in the early stages, but major differences were also found in the maturation phase of biofilm development. It is possible that sloughing and erosion events related to the shear rate also assume particular significance at later stages of biofilm development. Similar results were also obtained with coccoid cyanobacteria, *Synechocystis salina* and *Cyanobium* sp. strains, when glass and a polymeric epoxy coating were used (Faria et al., 2020a). The major differences between the two hydrodynamic conditions were observed from data obtained from thickness quantification (Fig. 1G and H) but also from biofilm wet weight (Fig. 1A and B). Biofilm mass obtained on glass under lower shear conditions (4 s^{-1}) was on average 71.5% higher when compared to the values obtained at a higher shear rate (40 s^{-1}; Fig. 1A). On perspex, biofilm wet weight at 4 s^{-1} was on average 53.9% higher (Fig. 1B). Whereas chlorophyll *a* content at 4 s^{-1} on glass and perspex was on

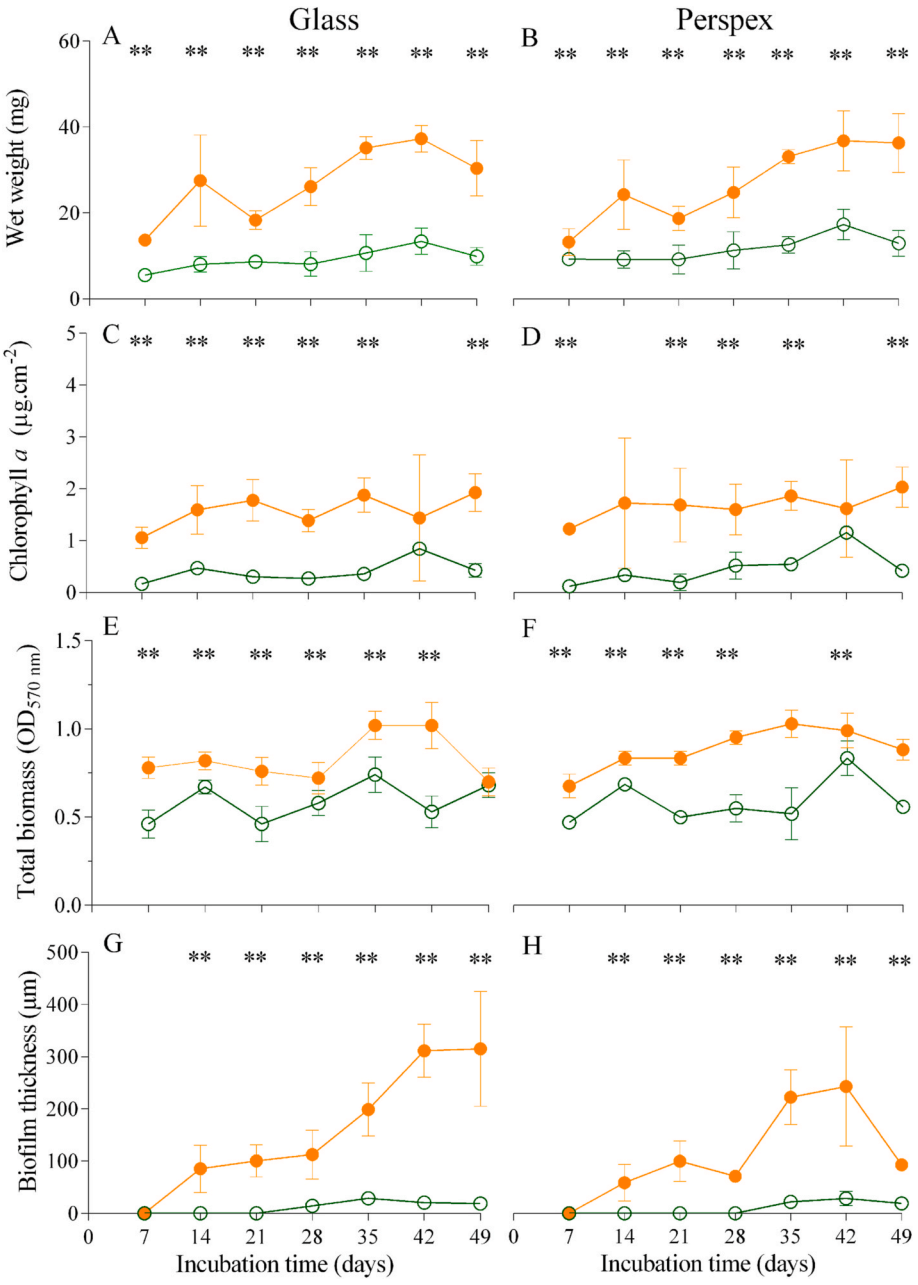

Fig. 1. Evaluation of unidentified filamentous cyanobacterium LEGE 06007 biofilm development. The parameters analysed refer to wet weight (A, B), chlorophyll *a* quantification (C, D), total biomass quantification by CV assay (E, F) and biofilm thickness (G, H). Biofilms were formed in glass (A, C, E, G) or perspex (B, D, F, H), at two average shear rates, 4 s^{-1} (closed circles, orange) and 40 s^{-1} (open circles, green) for 49 days. Standard deviations from two biological assays with three replicates each are represented. Symbol ** indicate statistically different values for $P < 0.05$ at each incubation time. (For interpretation of the references to colour in this figure legend, the reader is referred to the Web version of this article.)

average 75% higher (Fig. 1C and D) than at higher shear conditions. As previously reported (Chorus and Cavalieri, 2000; Romeu et al., 2019, 2020), chlorophyll *a* content monitorisation demonstrated to be a useful tool to follow cyanobacterial biofilm growth since a correlation between chlorophyll *a* production and biofilm wet weight was observed (Appendix B). Due to the complexity of filamentous cyanobacteria, there is a need to develop novel methodologies to study these organisms. To evaluate if the crystal violet assay (CV) can be a suitable approach for cyanobacterial biofilms analysis, quantification of total biomass was performed by CV. On glass, the total biomass quantified by this method was on average 28.1% higher at lower shear when compared to the values obtained at a higher shear rate (40 s^{-1}; Fig. 1E), whereas on perspex the average value obtained was about 33.2% higher at 4 s^{-1} (Fig. 1F). Data obtained from this parameter corroborates observations from additional parameters, since higher biofilm biomass was obtained at the lowest shear rate for both surfaces. A correlation between data obtained from total biomass quantification by CV and biofilm thickness and from wet weight was observed (Appendix C and D, respectively). Therefore, based on the results obtained for this strain, the quantification of total biomass from CV demonstrated to be useful tool to follow cyanobacterial biofilm growth.

Similar values of wet weight, chlorophyll *a* content, total biomass quantification and biofilm thickness were obtained for biofilms developed on different surfaces at the same hydrodynamic conditions (Appendix E), showing that the effect of surface properties was less important than the hydrodynamic effect on cyanobacterial biofilm development in a macroscopic biofilm evaluation. Despite the different hydrophobicity of glass and perspex (Romeu et al., 2019), these findings had already been shown for other coccoid (Faria et al., 2020a) and filamentous cyanobacterial strains (Romeu et al., 2019, 2020).

OCT analysis was used to analyse biofilm roughness and structure at different conditions. Biofilm roughness was only evaluated in the maturation phase of biofilm development, in which differences in biofilm thickness were more evident (from day 35). The analysis revealed that biofilms formed under the lower shear rate showed lower roughness coefficient values than those formed at higher shear on both surfaces (Appendix F). Once again, the values obtained from biofilms developed under the same hydrodynamic condition at different surfaces were very similar. Fig. 2 shows representative 2D cross-sectional images obtained from OCT at the end of the experiment (49 days). These figures highlight the importance of the hydrodynamic effect when compared to the surface effect. Previous studies showed that cyanobacterial biofilms developed under higher shear rates present a more compact structure (Romeu et al., 2019, 2020), which probably increases biofilm cohesion (Teodósio et al., 2011). In this study, the low biofilm biomass obtained under a higher shear rate (40 s^{-1}) on both surfaces (Fig. 2 B, D) did not enable a comprehensive interpretation of biofilm structure and compaction.

Excessive shear stress can cause increased cell mortality, decreased growth rate and cell viability, or even cell lysis. Different organisms have different tolerances for the damage caused by hydrodynamic forces (Sobczuk et al., 2006). Among photosynthetic organisms, green algae have the greatest tolerance to shear stress, followed by cyanobacteria, red algae and diatoms, with dinoflagellates comprising the most shear-sensitive species (Wang and Lan, 2018). In these organisms, the shear-sensitivity is determined primarily by cell wall strength, cell morphology and the presence of flagella. Cyanobacterial cell walls are mainly composed by peptidoglycan, they comprise three to four layers and range from 10 to 20 nm in thickness and an envelope may also surround the cell to form a sheath (Stanier and Cohen-Bazire, 1977). On biofilms, as cells are embedded in a matrix mainly composed by extracellular polymeric substances (EPS), the interaction between EPS components promotes biofilm cohesion, with stronger EPS interactions preventing biofilm mechanical failure (Cense et al., 2006). Moreover, it has been recognized that biofilms are viscoelastic materials (Gloag et al., 2020). Viscoelasticity allows biofilm survival, promoting the formation of stronger biofilms when exposed to higher shear forces. Therefore, viscoelasticity emerged as a general survival adaptation for biofilms in the surrounding environment, such as shear stresses. Several studies showed that viscoelasticity is an emergent behavior of bacteria when they form biofilms, and that these properties are largely governed by EPS (Peterson et al., 2013). In our study, if some cells rupture, the impact of organic matter release from the cells may not have a significant impact on biofilm development since the surrounding environment is constantly renewed.

3.2. Proteomic analysis

This work revealed for the first time the differential proteome expression of cyanobacterial biofilm cells developed in different conditions. Overall, 546 proteins were identified through the shotgun proteomics analysis from 24 biofilm samples of four different conditions (Appendix G). Herein, the total number of protein identified was relatively higher than a previous qualitative proteomic study performed on two different cyanobacterial strains at the same biofilm conditions (Romeu et al., 2020). Similar to the aforementioned study, most of the proteins identified in this work corresponded to intracellular proteins since the surrounding environment, supernatant and exudate were not analysed. However, excreted proteins may have also been identified since they may have been retained in the biofilm matrix.

3.2.1. Enrichment and distribution of DEPs among conditions

The quantitative proteomic analysis was performed with the "DEP" R package (Zhang et al., 2018), revealing a total of 41 DEPs (Fig. 3, Table 1). Some of these DEPs were also previously identified in the qualitative approach from different cyanobacterial strains (Romeu et al., 2020). Among these proteins, ribosomal proteins were found, and others involved in photosynthesis and respiration, which are essential in primary metabolic functions, as well as proteins associated with phycobilisomes and elongation factors. Although a macroscopic evaluation of biofilm revealed a greater difference between the two hydrodynamic conditions, the proteomic analysis showed a higher difference in protein expression between the biofilms formed on glass and perspex at 4 s^{-1}, followed by the biofilms formed on glass at 4 s^{-1} and 40 s^{-1}, which demonstrated the importance of studies addressing different approaches. Indeed, among the four comparisons performed, most of the proteomic variations corresponded to the paired-comparison between samples from glass *vs* perspex at 4 s^{-1} (Fig. 3A). In this comparison, 34

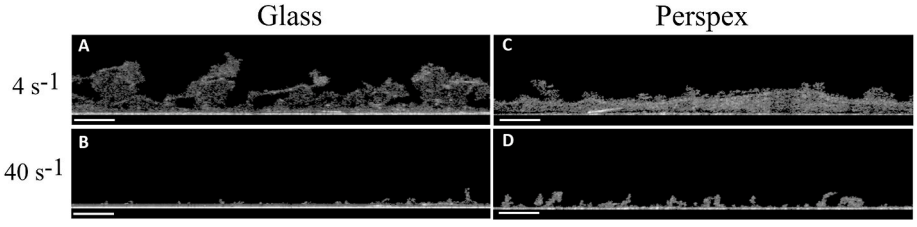

Fig. 2. 2D cross-sectional OCT images of unidentified filamentous cyanobacterium LEGE 06007 biofilms formed after 49 days on glass and perspex at two different shear rates, 4 s^{-1} (A, C) and 40 s^{-1} (B, D). Scale bar = 200 μm.

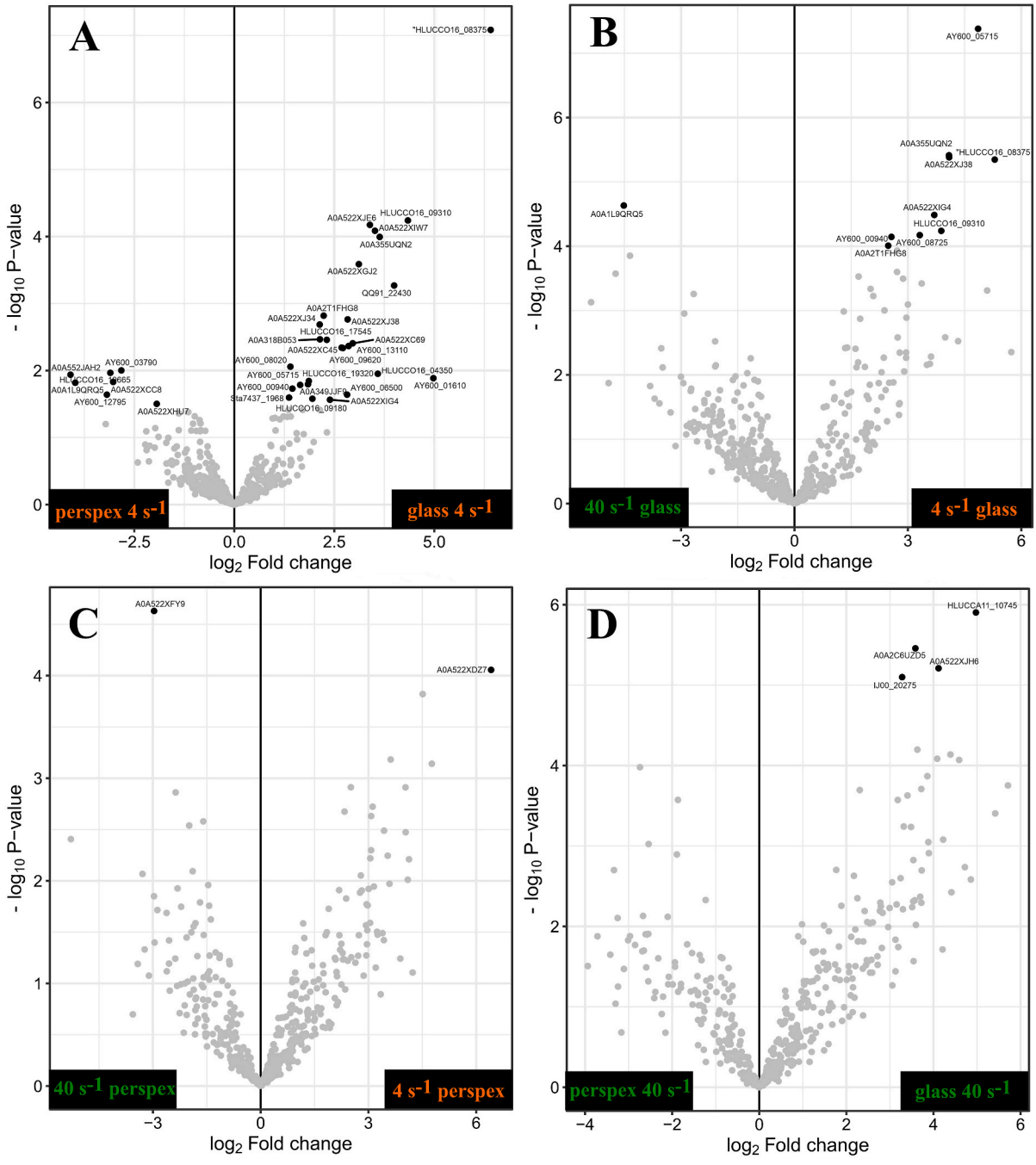

Fig. 3. Volcano plot of the differentially expressed proteins (DEPs) among the 4 biofilm conditions studied. Black points represent the DEPs showing the corresponding gene symbol, or the protein accession number when lacking the corresponding gene annotation. The axis depicts the *P* values ($-\log_{10}$) plotted against the fold changes ($\log_2$) between each paired-comparison. A) glass *vs* perspex at 4 s^{-1} (down and up-regulated proteins on glass at 4 s^{-1} when compared with perspex at 4 s^{-1}); B) 4 s^{-1} *vs* 40 s^{-1} on glass (down and up-regulated proteins at 4 s^{-1} on glass when compared with 40 s^{-1} on glass); C) 4 s^{-1} *vs* 40 s^{-1} on perspex (down and up-regulated proteins at 4 s^{-1} on perspex when compared with 40 s^{-1} on perspex); D) glass *vs* perspex at 40 s^{-1} (down and up-regulated proteins on glass at 40 s^{-1} when compared with perspex at 40 s^{-1}).

DEPs were found, where 27 DEPs were up-regulated and seven down-regulated in the glass surface relatively to perspex (Fig. 3A). 10 DEPs were identified in the comparison between at 4 s^{-1} *vs* 40 s^{-1} on glass (Fig. 3B), whereas two DEPs were found between samples from biofilms developed at 4 s^{-1} *vs* 40 s^{-1} on perspex (Fig. 3C). Finally, four up-regulated DEPs were revealed in the glass surface relatively to perspex in comparing between biofilms developed on glass vs perspex at 40 s^{-1}, (Fig. 3D).

3.2.2. Linking DEPs to the functional categories involved

Around 39.6% of the DEPs were related to metabolic processes and 11% with transport (Appendix H). Additionally, 4.9% and 3.3% were associated with the regulation of biological processes and response to a stimulus, respectively. Among the 34 DEPs identified on the glass surface relatively to perspex (Fig. 3A), nine of them overlapped with results from biofilm cells formed on glass at 4 s^{-1} vs 40 s^{-1} (Figs. 3B and 4). It is noteworthy that among these nine DEPs, a protein related to allophycocyanin was down-regulated in both comparisons, which suggests that

Table 1
List of the 41 DEPs and their corresponding accession number (Protein IDs), gene names, description and the log_2 fold-changes obtained from each comparison.

UniProt accession number	Gene Names	Description	glass *vs* perspex at 4 s^{-1}	4 s^{-1} *vs* 40 s^{-1} on glass	4 s^{-1} *vs* 40 s^{-1} on perspex	glass *vs* perspex at 40 s^{-1}
A0A0P8BXS9	HLUCCO16_08375	Uncharacterized protein (Fragment)	6.41	5.30		
A0A1L9QRQ5		Allophycocyanin	−3.98	−4.51		
A0A2T1FHG8		Elongation factor Tu	2.23	2.48		
A0A318B053		Aldehyde dehydrogenase	2.14			
A0A349JJF9		SLH domain-containing protein (Fragment)	1.84			
A0A355UQN2		50 S ribosomal protein L5	3.64	4.09		
A0A522XC45		Photosystem II CP43 reaction center protein	2.68			
A0A522XC69		Alpha/beta hydrolase	2.96			
A0A522XCC8		Isoleucine–tRNA ligase (Fragment)	−3.03			
A0A522XGJ2		SLH domain-containing protein	3.11			
A0A522XHU7		60 kDa chaperonin	−1.94			
A0A522XIG4		30 S ribosomal protein S8	2.39	3.70		
A0A522XIW7		O-acetylhomoserine aminocarboxypropyltransferase/cysteine synthase	3.52			
A0A522XJ34		50 S ribosomal protein L1	2.13			
A0A522XJ38		Phycobilisome rod-core linker polypeptide CpcG	2.83	4.09		
A0A522XJE6		Gfo/Idh/MocA family oxidoreductase	3.39			
A0A552JAH2		Chaperone protein DnaK	−4.10			
A0A168VPC8	AY600_00940	Uncharacterized protein	1.45	2.56		
A0A168UQZ4	AY600_01610	Cytochrome *c*-550	4.98			
A0A168SDR0	AY600_03790	Ferredoxin–NADP reductase	−2.83			
A0A168SSA6	AY600_05715	Cytochrome *c*6	1.65	4.86		
A0A168VLH9	AY600_06500	Uncharacterized protein	2.82			
A0A168WPD9	AY600_08020	Uncharacterized protein	1.40			
A0A168VRY4	AY600_09620	Beta-propeller domain-containing protein, methanol dehydrogenase	2.71			
A0A168UP82	AY600_12795	Elongation factor P	−3.19			
A0A168VMU3	AY600_13110	Ferredoxin	2.86			
A0A0P7Z9L3	HLUCCO16_04350	Photosystem I reaction center subunit XI	3.59			
A0A0P8DQC9	HLUCCO16_09180	Uncharacterized protein	1.95			
A0A0N8KPF0	HLUCCO16_09310	ATP synthase subunit delta	4.34	3.88		
A0A0P7ZV78	HLUCCO16_17545	OMF family outer membrane protein	2.31			
A0A0P8BGT0	HLUCCO16_19320	Phosphomannomutase	1.86			
A0A0P8BV27	HLUCCO16_19665	Uncharacterized protein	−3.10			
A0A0C1UQ05	QQ91_22430	Aconitate hydratase	4,00			
K9XV32	Sta7437_1968	Polyribonucleotide nucleotidyltransferase	1.37			
A0A168SH97	AY600_08725	Uncharacterized protein		3.31		
A0A522XDZ7		Superoxide dismutase			6.42	
A0A522XFY9		Uncharacterized protein			−2.97	
A0A2C6UZD5		Aldehyde dehydrogenase (Fragment)				3.59
A0A522XJH6		DUF2862 domain-containing protein				4.12
A0A0P8BNN3	HLUCCA11_10745	Phycocyanin, beta subunit				4.98
A0A0T7BVN2	IJ00_20275	Elongation factor Tu				3.28

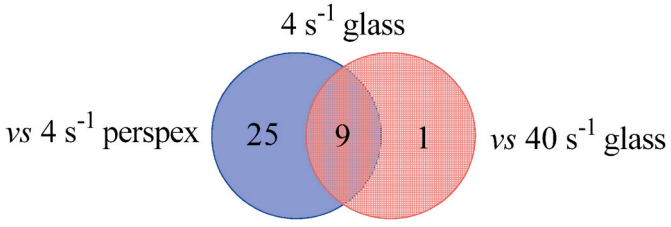

Fig. 4. Venn diagram displaying the unique and shared DEPs found between 4 s^{-1} glass *vs* 4 s^{-1} perpex and 4 s^{-1} glass *vs* 40 s^{-1} glass.

compared to perspex at 40 s^{-1}, the expression of this phycobiliprotein was decreased on glass (Fig. 3A) and at 4 s^{-1}, respectively (Fig. 3B, Table 1).

The same 8 up-regulated proteins were identified when comparing biofilms formed on glass and perspex at 4 s^{-1} (Fig. 3A) and when comparing biofilms formed on glass at both shear rates (Fig. 3B, Table 1). These proteins are mainly involved in metabolic process, photosynthetic activity, binding and transport, similarly to the unique 19 up-regulated sequences found in the biofilms developed on glass at 4 s^{-1} in comparison to perspex (Fig. 5). Among the eight shared proteins, a protein related to elongation factor Tu was identified (A0A2T1FHG8, Fig. 3A and B, Table 1). Indeed, elongation factors have already been described as virulence factors and associated with filament formation (López-Ochoa et al., 2017) and biofilm formation (Qayyum et al., 2016) in different organisms (Harvey et al., 2019). However, from the data obtained in the present study, it is possible to consider that this may not be the major factor for increased biofilm development. In fact, the up-regulation of an additional elongation factor Tu was also observed on biofilm cells developed at 40 s^{-1} in glass compared to perspex (A0A0T7BVN2; Table 1), and no considerable biofilm increase was observed in that case (Appendix E, Figure E.1 B, D, F, H). Moreover, an elongation factor P (AY600_12795) was down-regulated on glass when compared to biofilms formed on perspex at 4 s^{-1} (Fig. 3A, Table 1). Therefore, additional pathways and/or factors must have contributed to cyanobacterial biofilm development in these conditions. Additional up-regulated proteins shared between biofilms formed on glass and perspex at 4 s^{-1} (Fig. 3A) and biofilms developed at 4 s^{-1} and 40 s^{-1} on glass (Fig. 3B) include ribosomal proteins, proteins related to phycobilisome rod-core linker polypeptide CpcG, cytochrome *c*6, ATP synthase and two uncharacterized proteins (Table 1). It is noteworthy that both ribosomal proteins and those related to photosynthesis, as well as phycobilisome rod-core linker polypeptide CpcG have already been found in a previous qualitative proteomic study performed on biofilm cells from two different cyanobacterial species (Romeu et al., 2020). Since the same surfaces and hydrodynamic conditions were used in both studies, this suggests the relevance of this set of proteins in the cyanobacterial

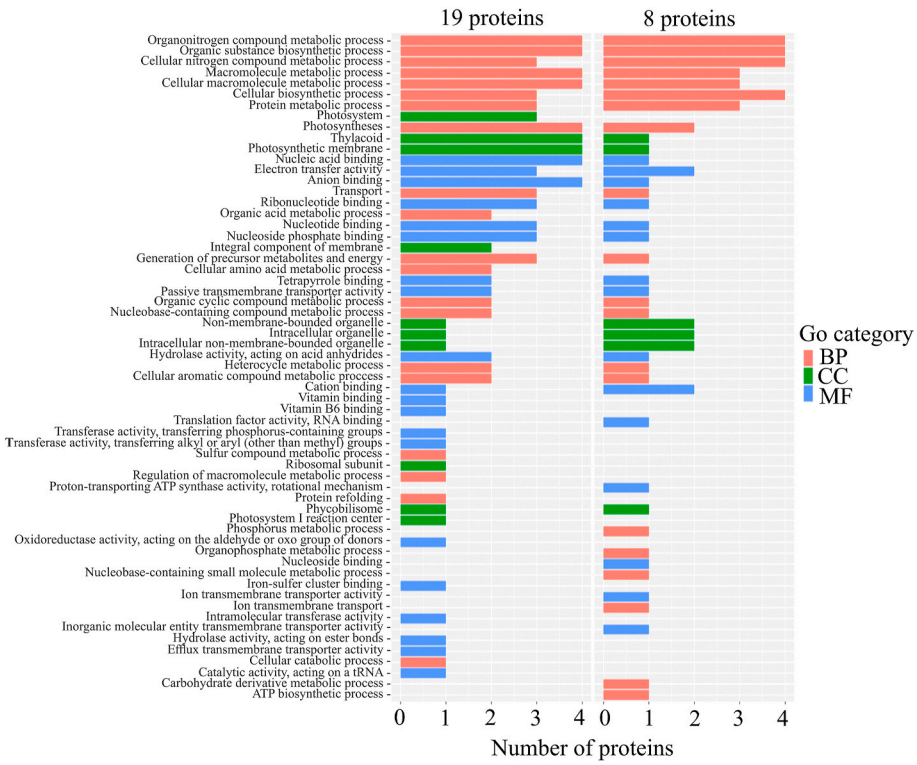

Fig. 5. Functional annotation of the three major GO Categories: Biological Process (BP), Molecular Function (MF) and Cellular Components (CC) according to the GO Distribution by Level (4). The figure shows the number of sequences (number of proteins) in a descendent manner matching GO-terms of the unique up-regulated DEPs (19 proteins) and the eight shared DEPs (8 proteins), overlapped between the comparison glass *vs* perspex at 4 s^{-1} and 4 s^{-1} *vs* 40 s^{-1} on glass. More details about GO annotation can be found in the Appendix I.

biofilm development in these conditions.

Among the two uncharacterized proteins shared between these two paired-comparison, proteins involved in the electron transport pathway of photosynthesis activity (A0A0P8BXS9) and related with calcium ion binding (A0A168VPC8) were identified. In addition, the unique protein not shared between glass *vs* perspex at 4 s^{-1} and 4 s^{-1} *vs* 40 s^{-1} on glass conditions was also an uncharacterized protein related to calcium ion binding (A0A168SH97, Fig. 4, Table 1), suggesting that calcium may play an important role in these cyanobacterial biofilms. Moreover, these two uncharacterized proteins related to calcium ion binding are disordered proteins. Although disordered proteins do not have unique structures, they possess biological functions. It is expected that disordered proteins possess some advantages over ordered proteins due their exceptional spatio-temporal heterogeneity and high conformational flexibility (Uversky, 2019). Indeed, they are more likely to maintain stability under extreme conditions due to the lack of structural conservation (Liu and Huang, 2014). In a real scenario, these proteins can perform their functions in complex environments, which can be affected by various factors such as hydrodynamic conditions or surface properties. Several proteins with disordered domains were identified in the cement-multicomplex adhesive-system from goose barnacles, applying a similar proteogenomic approach (Domínguez-Pérez et al., 2020, 2021). Moreover, additional studies described surface-coupling proteins as structurally disordered, which confers them elasticity (Cheng et al., 2010; Wang et al., 2018a).

Between the unique 19 up-regulated sequences found in the biofilms developed on glass at 4 s^{-1} when compared to perspex (Figs. 3A and 5, Table 1), uncharacterized proteins were also differentially expressed including one disordered protein (A0A168VLH9). In addition, proteins like a beta-propeller domain-containing protein, a methanol dehydrogenase (AY600_09620), the chaperone protein DnaK (A0A552JAH2), SLH domain-containing proteins (A0A349JJF9 and A0A522XGJ2) and OMF family outer membrane protein (HLUCCO16_17545) were also identified as DEPs. Although secreted beta-propeller proteins are largely unexplored in bacteria and even more in cyanobacteria, some studies suggest that they may be involved in the maintenance of the cell envelope, secretion, adhesion, and host immune responses (Fu et al., 2018; Kim et al., 2018). A study on *Vibrio cholerae* biofilms showed that the beta-propeller domains might form interactions with proteins or other substrates (including polysaccharides) within the biofilm matrix (Kaus et al., 2019). In a study on *Acinetobacter baumannii* cells it was observed that the expression of a chaperone-usher secretion system is required for pili formation and the concomitant attachment to plastic surfaces and biofilm formation (Tomaras et al., 2003). DnaJ2 and DnaK2 together behave as an RNA chaperone shielding the psbAII transcript from RNaseE-intervened degradation, in this way helping to prevent the inhibition of photosynthesis under conditions of stress (Ehrnsperger et al., 1997). Although cyanobacteria have many dnaK genes in their genome (Haslbeck et al., 2005), there is no knowledge regarding their relation to biofilm development. S-layer homology (SLH) domains are cell wall-targeting modules employed by various Gram-positive and -negative bacteria to display extracellular proteins such as enzymes and outer membrane proteins on the bacterial cell surface (Engelhardt and Peters, 1998). A study performed by Janesch et al. 2013), demonstrated the involvement of the SLH domain-containing protein SlhA in swarming and biofilm formation of *Paenibacillus alvei* (Janesch et al., 2013). Outer membrane proteins and outer membrane vesicles (OMV) have been relevant in biofilm studies. It was demonstrated that *Helicobacter pylori* TK1402 exhibited a strong ability for biofilm formation, and its OMVs play an important role in the formation of their extracellular matrix (Yonezawa et al., 2011). A proteomic study of *Burkholderia multivorans* C1576 revealed that OMVs production is the most important source of proteins for the biofilm matrix (Terán et al., 2020). OMVs are highly enriched in outer membrane proteins and siderophores. Of note, some of the identified proteins were proteins involved in reactive oxygen species (ROS) scavenging. Therefore, proteins responsible for detoxification of ROS are also a relevant fraction of both matrix- and OMVs-associated proteins. Accordingly, the data obtained in this study showed the possible role of a beta-propeller domain-containing protein, chaperone DnaK, SLH domain-containing proteins and an OMF family outer membrane protein on biofilm developed on glass at 4 s^{-1} in comparison to perspex for this cyanobacterial strain (Figs. 3A and 5,

Table 1).

Additionally, biofilm development on perspex at 4 s^{-1} was higher than at 40 s^{-1} (Fig. 1B, D, F). The proteomic analysis only revealed the underexpression of an uncharacterized protein (A0A522XFY9) and overexpression of an enzyme, superoxide dismutase (SOD) at 4 s^{-1} (A0A522XDZ7, Fig. 3C, Table 1) when compared with biofilm formed at 40 s^{-1}. Similar to previous uncharacterized proteins, the down-regulated protein identified in this paired comparison presented a disordered domain. SOD are ubiquitous enzymes that scavenge superoxide radicals to peroxide and molecular oxygen through alternate oxidation and reduction of their metal ions. Since cyanobacteria produce ROS that can damage cellular components leading to cell death, the co-evolution of an antioxidant system was necessary for their survival and SOD is the initial enzyme evolved to alleviate this toxic effect (Priya et al., 2007). Several SOD genes were found on cyanobacteria strains (Kaneko et al., 1996; Shirkey et al., 2000; Zhao et al., 2007), even on filamentous strains (Campbell and Laudenbach, 1995; Priya et al., 2007). Besides their role in oxidative stress and resistance, the relevance of SOD has already been reported in several studies from other bacteria than cyanobacteria on adhesion, biofilm formation and invasion of epithelial cells (Bink et al., 2011; Najmuldeen et al., 2019; Suo et al., 2012; Trémoulet et al., 2002; Wang et al., 2018b). Therefore, the higher biofilm development observed on perspex at 4 s^{-1} can also be related to the up-regulation of this enzyme in this filamentous cyanobacterial strain.

Moreover, with a higher biofilm development at 4 s^{-1}, the production of ROS may have increased along with respiration and photosynthesis, which may have prompted an increased activity of this enzyme to prevent damage caused by oxidative stress. A study on *Klebsiella pneumoniae* also shows the role of SOD in biofilm architecture and cell morphology (Najmuldeen et al., 2019). Although the detailed mechanisms of alterations in biofilm architecture are unclear, it could be speculated that *Klebsiella pneumoniae* biofilm architecture is significantly influenced by oxygen and by the activity of SOD. Therefore, alteration in biofilm architecture might occur in response to redox balance, which is essential for cellular function and survival. In the present study, a different structure was also observed for biofilms developed on perspex at 4 s^{-1} and 40 s^{-1} (Fig. 3C and D). Once again, SOD can present an active role in the biofilm architecture of this cyanobacterial strain between biofilms developed on perspex at 4 s^{-1} and 40 s^{-1}. The proteomic changes of SOD on all replicates from each condition throughout the experiment can be found in Appendix J.

Finally, the total of 27 up-regulated DEPs found on biofilm cells from glass at 4 s^{-1} compared to perspex, shows a different enrichment pattern than the seven down-regulated DEPs at the same condition when compared to the ones encoded in the whole proteome (Fig. 6). In the 27 up-regulated DEPs, the GO terms "electron transfer activity" and "electron transport chain", processes related to electron chain and actively involved in photosynthesis, were found as enriched categories (Fig. 6, Appendix I). On the other hand, in the seven down-regulated DEPs, GO terms related to enzyme binding and activity were found as an enriched category when compared with the total of proteins identified (Fig. 6, Appendix I). These findings confirm that cyanobacterial biofilm development is closely associated with the up-regulation of the photosynthesis process.

The analysis of 41 DEPs found in this study is extremely important. Indeed, combining macroscopic evaluation of biofilm development with information about DEPs from proteomic analysis may provide new clues for mitigating marine biofouling. Since this study identified which proteins were down and up-regulated under different biofilms conditions, novel antifouling strategies which target these proteins can potentially be developed.

4. Conclusions

The present study, which presented several analyses, from the molecular to the macroscopic level, revealed the importance of combining different approaches to evaluate a complex phenomenon like biofilm formation. Based on macroscopic evaluation (biofilm biomass, thickness and chlorophyll *a* quantification), the results showed that hydrodynamic effects might be more important than surface properties in the development of cyanobacterial biofilms. However, on the proteomic approach, a large differential protein expression was found between biofilms formed on glass and perspex at 4 s^{-1}. New quantitative clues were provided to understand the diversity and function of proteins in cyanobacterial biofilm development. Combining all approaches applied in this study, the higher biofilm development at 4 s^{-1} may be related to up-regulation of SOD and differential expression of some uncharacterized proteins and proteins related to the photosynthetic process. On the other hand, the differential biofilm development observed on different surfaces is probably associated with different expression of a beta-propeller domain-containing protein, chaperone DnaK, SLH domain-containg proteins and/or an OMF family outer membrane protein and also the differential expression of some uncharacterized proteins on this cyanobacterial strain. Indeed, the fact that 50% of uncharacterized proteins found as DEPs in this study presented a disordered domain was a significant finding for cyanobacterial biofilm studies as these proteins represent complex systems that are specifically regulated by various means. Some of those uncharacterized proteins could be considered as a new relevant group of biofilm adaptation proteins since structural disorder can be beneficial for their resistance to environmental perturbations.

Advances in "omics" technologies are constantly evolving and their application to marine biofilm studies is an emerging approach that can lead to new improvements in antifouling strategies. Future studies should focus on different cyanobacterial strains, as well as evaluation of EPS secretion on these different biofilm conditions. Proteomic analysis should also be performed at different biofilm stages to evaluate differences in proteomic profile along biofilm formation and maturation. Moreover, different omics approaches, such as metabolomic studies, may be useful to identify additional pathways that can be involved in these biofilm development conditions. These further studies should also focus on cyanobacterial gene modifications or deletions, which encode relevant proteins reported in the present study as crucial for biofilm development to clarify their role on biofilm phenotypes.

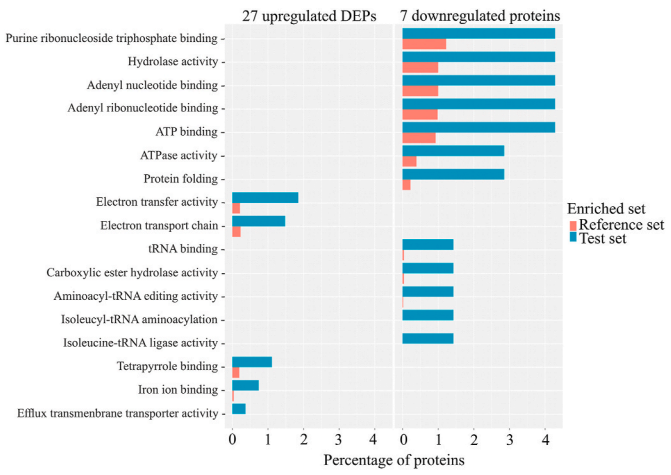

Fig. 6. Enrichment of DEPs revealed by the hypergeometric distribution significance test. The enriched GO terms (Fisher's exact test, $P < 0.05$) are represented by a stacked bar (in green) as the percentage of the GO terms found in the References Set (in red, represent all 546 identified). Each panel displays the set of 27 up-regulated and seven down-regulated DEPs found in the comparison glass *vs* perspex at 4 s^{-1}. More details about GO annotation can be found in the Appendix I. (For interpretation of the references to colour in this figure legend, the reader is referred to the Web version of this article.)

Declaration of competing interest

The authors declare that they have no known competing financial interests or personal relationships that could have appeared to influence the work reported in this paper.

Acknowledgements

This work was financially supported by: Base Funding - UIDB/00511/2020 of the Laboratory for Process Engineering, Environment, Biotechnology and Energy – LEPABE - funded by national funds through the FCT/MCTES (PIDDAC), project HealthyWaters (NORTE-01-0145-FEDER-000069), supported by Norte Portugal Regional Operational Programme (NORTE 2020), under the PORTUGAL 2020 Partnership Agreement, through the European Regional Development Fund (ERDF) and strategic funding UIDB/04423/2020 and UIDP/04423/2020 through national funds provided by FCT and ERDF, in the framework of the programme PT2020. This work was also supported by the FCT project MOREBIVALVES (PTDC/ASP-PES/31762/2017) and it had support from the Portuguese Mass Spectrometry Network, integrated in the National Roadmap of Research Infrastructures of Strategic Relevance (ROTEIRO/0028/2013; LISBOA-01-0145-FEDER-022125). M.J. R. acknowledges a PhD grant from FCT (SFRH/BD/140080/2018).

Appendix A-J. Supplementary data

Supplementary data to this article can be found online at https://doi.org/10.1016/j.envres.2021.111566.

References

Agostoni, M., Waters, C.M., Montgomery, B.L., 2016. Regulation of biofilm formation and cellular buoyancy through modulating intracellular cyclic di-GMP levels in engineered cyanobacteria. Biotechnol. Bioeng. 113, 311–319. https://doi.org/10.1002/bit.25712.

Allen, R., Rittmann, B.E., Curtiss, R., 2019. Axenic biofilm formation and aggregation by *Synechocystis* PCC 6803 is induced by changes in nutrient concentration, and requires cell surface structures. Appl. Environ. Microbiol. 85, 1–33. https://doi.org/10.1101/414151.

Almeida, D., Domínguez-Pérez, D., Matos, A., Agüero-Chapin, G., Osório, H., Vasconcelos, V., Campos, A., Antunes, A., 2020. Putative antimicrobial peptides of the posterior salivary glands from the cephalopod *Octopus vulgaris* revealed by exploring a composite protein database. Antibiotics 9, 1–20. https://doi.org/10.3390/antibiotics9110757.

Babele, P.K., Kumar, J., Chaturvedi, V., 2019. Proteomic De-regulation in cyanobacteria in response to abiotic stresses. Front. Microbiol. 10, 1–22. https://doi.org/10.3389/fmicb.2019.01315.

Babele, P.K., Singh, G., Kumar, A., Tyagi, M.B., 2015. Induction and differential expression of certain novel proteins in *Anabaena* L31 under UV-B radiation stress. Front. Microbiol. 6, 1–14. https://doi.org/10.3389/fmicb.2015.00133.

Bakker, D.P., Van Der Plaats, A., Verkerke, G.J., Busscher, H.J., Van Der Mei, H.C., 2003. Comparison of velocity profiles for different flow chamber designs used in studies of microbial adhesion to surfaces. Appl. Environ. Microbiol. 69, 6280–6287. https://doi.org/10.1128/aem.69.10.6280-6287.2003.

Battchikova, N., Muth-Pawlak, D., Aro, E.M., 2018. Proteomics of cyanobacteria: current horizons. Curr. Opin. Biotechnol. 54, 65–71. https://doi.org/10.1016/j.copbio.2018.02.012.

Bharti, A., Velmourougane, K., Prasanna, R., 2017. Phototrophic biofilms: diversity, ecology and applications. J. Appl. Phycol. 29, 2729–2744. https://doi.org/10.1007/s10811-017-1172-9.

Bink, A., Vandenbosch, D., Coenye, T., Nelis, H., Cammue, B.P.A., Thevissen, K., 2011. Superoxide dismutases are involved in *Candida albicans* biofilm persistence against miconazole. Antimicrob. Agents Chemother. 55, 4033–4037. https://doi.org/10.1128/AAC.00280-11.

Blain, S., Guillou, J., Tréguer, P.J., Woerther, P., Delauney, L., Follenfant, E., Gontier, O., Hamon, M., Leilde, B., Mer, D., Cnrs, U.M.R., Nicolas, P., Mer, D., Cnrs, F.R., Copernic, P.N., 2004. High frequency monitoring of the coastal marine environment using the MAREL buoy. J. Environ. Monit. 6, 569–575. https://doi.org/10.1016/S0005-2728(89)80347-0.

Campbell, W.S., Laudenbach, D.E., 1995. Characterization of four superoxide dismutase genes from a filamentous cyanobacterium. J. Bacteriol. 177, 964–972. https://doi.org/10.1128/jb.177.4.964-972.1995.

Campos, A., Danielsson, G., Farinha, A.P., Kuruvilla, J., Warholm, P., Cristobal, S., 2016. Shotgun proteomics to unravel marine mussel (*Mytilus edulis*) response to long-term exposure to low salinity and propranolol in a Baltic Sea microcosm. J. Proteomics 137, 97–106. https://doi.org/10.1016/j.jprot.2016.01.010.

Carvalho, C.C.C.R., 2018. Marine biofilms: a successful microbial strategy with economic implications. Front. Mar. Sci. 5, 1–11. https://doi.org/10.3389/fmars.2018.00126.

Cense, A.W., Peeters, E.A., Gottenbos, B., Baaijens, F.P., Nuijs, A.M., van Dongen, M.E., 2006. Mechanical properties and failure of *Streptococcus mutans* biofilms, studied using amicroindentation device. J. Microbiol. Methods 67, 463–472. https://doi.org/10.1016/j.mimet.2006.04.02.

Cheng, S., Cetinkaya, M., Gräter, F., 2010. How sequence determines elasticity of disordered proteins. Biophys. J. 99, 3863–3869. https://doi.org/10.1016/j.bpj.2010.10.011.

Chorus, I., Cavalieri, M., 2000. Cyanobacteria and algae. In: Bartram, J., Rees, G. (Eds.), Monitoring Bathing Waters: A Practical Guide to the Design and Implementation of Assessments and Monitoring Programmes. World Health Organization Report. E & FN Spon, London and New York, pp. 219–271.

Dessau, R.B., Pipper, C.B., 2008. ["R"–project for statistical computing]. Ugeskr. Laeger 170, 328–330.

Domínguez -Pérez, D., Almeida, D., Wissing, J., Machado, A.M., Jänsch, L., Castro, L.F., Antunes, A., Castro, L.F., Vasconcelos, V., Campos, A., Cunha, I., 2021. Proteogenomic characterization of the cement and adhesive gland of the pelagic gooseneck barnacle *Lepas anatifera*. Int. J. Mol. Sci. 22, 3370. https://doi.org/10.3390/ijms22073370.

Domínguez -Pérez, D., Almeida, D., Wissing, J., Machado, A.M., Jänsch, L., Castro, L.F., Antunes, A., Vasconcelos, V., Campos, A., Cunha, I., 2020. The quantitative proteome of the cement and adhesive gland of the Pedunculate Barnacle, *Pollicipes pollicipes*. Int. J. Mol. Sci. 21, 2524. https://doi.org/10.3390/ijms21072524.

Ehrnsperger, M., Gräber, S., Gaestel, M., Buchner, J., 1997. Binding of non-native protein to Hsp25 during heat shock creates a reservoir of folding intermediates for reactivation. EMBO J. 16, 221–229. https://doi.org/10.1093/emboj/16.2.221.

Engelhardt, H., Peters, J., 1998. Structural research on surface layers: a focus on stability, surface layer homology domains, and surface layer-cell wall interactions. J. Struct. Biol. 124, 276–302. https://doi.org/10.1006/jsbi.1998.4070.

Enomoto, G., Nomura, R., Shimada, T., Win, N.N., Narikawa, R., Ikeuchi, M., 2014. Cyanobacteriochrome SesA is a diguanylate cyclase that induces cell aggregation in *Thermosynechococcus*. J. Biol. Chem. 289, 24801–24809. https://doi.org/10.1074/jbc.M114.583674.

Faria, S.I., Teixeira-Santos, R., Gomes, L.C., Silva, E.R., Morais, J., Vasconcelos, V., Mergulhão, F.J.M., 2020b. Experimental assessment of the performance of two marine coatings to curb biofilm formation of microfoulers. Coatings 10, 893. https://doi.org/10.3390/coatings10090893.

Faria, S.I., Teixeira-Santos, R., Morais, J., Vasconcelos, V., Mergulhão, F.J.M., 2021. The association between initial adhesion and cyanobacterial biofilm development. FEMS Microbiol. Ecol. 97 https://doi.org/10.1093/femsec/fiab052 fiab052.

Faria, S.I., Teixeira-Santos, R., Romeu, M.J., Morais, J., Vasconcelos, V., Mergulhão, F.J.M., 2020a. The relative importance of shear forces and surface hydrophobicity on biofilm formation by coccoid cyanobacteria. Polymers 12, 653. https://doi.org/10.3390/polym12030653.

Flemming, H.-C., Murthy, P.S., Venkatesan, R., Cooksey, K., 2009. Marine and Industrial Biofouling, Biofouling. Springer Berlin Heidelberg, Los Angeles, USA. https://doi.org/10.1007/978-3-540-69796-1.

Fu, J., Zong, G., Zhang, P., Gu, Y., Cao, G., 2018. Deletion of the β-Propeller protein gene Rv1057 reduces ESAT-6 secretion and intracellular growth of *Mycobacterium tuberculosis*. Curr. Microbiol. 75, 401–409. https://doi.org/10.1007/s00284-017-1394-8.

Gloag, E.S., Fabbri, S., Wozniak, D.J., Stoodley, P., 2020. Biofilm mechanics: implications in infection and survival. Biofilms 2. https://doi.org/10.1016/j.bioflm.2019.100017, 100017.

Harvey, K.L., Jarocki, V.M., Charles, I.G., Djordjevic, S.P., 2019. The diverse functional roles of elongation factor tu (Ef-tu) in microbial pathogenesis. Front. Microbiol. 10, 1–19. https://doi.org/10.3389/fmicb.2019.02351.

Haslbeck, M., Franzmann, T., Weinfurtner, D., Buchner, J., 2005. Some like it hot: the structure and function of small heat-shock proteins. Nat. Struct. Mol. Biol. 12, 842–846. https://doi.org/10.1038/nsmb993.

Hughes, C.S., Moggridge, S., Müller, T., Sorensen, P.H., Morin, G.B., Krijgsveld, J., 2019. Single-pot, solid-phase-enhanced sample preparation for proteomics experiments. Nat. Protoc. 14, 68–85. https://doi.org/10.1038/s41596-018-0082-x.

Janesch, B., Koerdt, A., Messner, P., Schäffer, C., 2013. The S-Layer Homology Domain-containing protein SlhA from *Paenibacillus alvei* CCM 2051T is important for swarming and biofilm formation. PLoS One 8, 1–17. https://doi.org/10.1371/journal.pone.0076566.

Kaneko, T., Sato, S., Kotani, H., Tanaka, A., Asamizu, E., Nakamura, Y., Miyajima, N., Hirosawa, M., Sugiura, M., Sasamoto, S., Kimura, T., Hosouchi, T., Matsuno, A., Muraki, A., Nakazaki, N., Naruo, K., Okumura, S., Shimpo, S., Takeuchi, C., Wada, T., Watanabe, A., Yamada, M., Yasuda, M., Tabata, S., 1996. Sequence analysis of the genome of the unicellular cyanobacterium *Synechocystis* sp. strain PCC6803. II. Sequence determination of the entire genome and assignment of potential protein-coding regions (supplement). DNA Res. 3, 185–209. https://doi.org/10.1093/dnares/3.3.185.

Kaus, K., Biester, A., Chupp, E., Lu, J., Visudharomn, C., Olson, R., 2019. The 1.9 Acrystal structure of the extracellular matrix protein Bap1 from *Vibrio cholerae* provides insights into bacterial biofilm adhesion. J. Biol. Chem. 294, 14499–14511. https://doi.org/10.1074/jbc.RA119.008335.

Kim, Y.H., Choi, Y., Oh, Y.Y., Ha, N.C., Song, J., 2018. Plant growth-promoting activity of beta-propeller protein YxaL secreted from *Bacillus velezensis* strain GH1-13. bioRxiv 1–29. https://doi.org/10.1101/471185.

King, R.K., Flick, G.J., Smith, S.A., Pierson, M.D., Boardman, G.D., Coale, C.W., 2006. Comparison of bacterial presence in biofilms on different materials commonly found

in recirculating aquaculture systems. J. Appl. Aquacult. 18, 79–88. https://doi.org/10.1300/J028v18n01.
Kotai, J., 1972. Instructions for the preparation of modified nutrient solution Z8 for algae. Blindern, Oslo Nor. Instit. Water Res. 11, 5.
Kurdrid, P., Senachak, J., Sirijuntarut, M., Yutthanasirikul, R., Phuengcharoen, P., Jeamton, W., Roytrakul, S., Cheevadhanarak, S., Hongsthong, A., 2011. Comparative analysis of the *Spirulina platensis* subcellular proteome in response to low- and high-temperature stresses: uncovering cross-talk of signaling components. Proteome Sci. 9, 39. https://doi.org/10.1186/1477-5956-9-39.
Leary, D.H., Li, R.W., Hamdan, L.J., Hervey, W.J., Lebedev, N., Wang, Z., Deschamps, J. R., Kusterbeck, A.W., Vora, G.J., 2014. Integrated metagenomic and metaproteomic analyses of marine biofilm communities. Biofouling 30, 1211–1223. https://doi.org/10.1080/08927014.2014.977267.
Liu, Z., Huang, Y., 2014. Advantages of proteins being disordered. Protein Sci. 3, 539–550. https://doi.org/10.1002/pro.2443.
López-Ochoa, J., Montes-García, J.F., Vázquez, C., Sánchez-Alonso, P., Pérez-Márquez, V. M., Blackall, P.J., Vaca, S., Negrete-Abascal, E., 2017. *Gallibacterium* elongation factor-Tu possesses amyloid-like protein characteristics, participates in cell adhesion, and is present in biofilms. J. Microbiol. 55, 745–752. https://doi.org/10.1007/s12275-017-7077-0.
Martins, J.C., Domínguez-Pérez, D., Azevedo, C., Braga, A.C., Costa, P.R., Osório, H., Vasconcelos, V., Campos, A., 2020. Molecular responses of mussel *Mytilus galloprovincialis* associated to accumulation and depuration of marine biotoxins okadaic acid and dinophysistoxin-1 revealed by shotgun proteomics. Front. Mar. Sci. 7, 1–15. https://doi.org/10.3389/fmars.2020.589822.
Matos, A., Domínguez-Pérez, D., Almeida, D., Aguëro-Chapin, G., Campos, A., Osório, H., Vasconcelos, V., Antunes, A., 2020. Shotgun proteomics of Ascidians Tunic gives new insights on host-microbe interactions by revealing diverse antimicrobial peptides. Mar. Drugs 18. https://doi.org/10.3390/md18070362.
Mieszkin, S., Callow, M.E., Callow, J.A., 2013. Interactions between microbial biofilms and marine fouling algae: a mini review. Biofouling 29, 1097–1113. https://doi.org/10.1080/08927014.2013.828712.
Minchin, D., Gollasch, S., 2003. Fouling and Ships' Hulls : How Changing Circumstances and Spawning Events May Result in the Spread of Exotic Species, vol. 19, pp. 111–122. https://doi.org/10.1080/0892701021000057891.
Mitchell, A.L., Attwood, T.K., Babbitt, P.C., Blum, M., Bork, P., Bridge, A., Brown, S.D., Chang, H.Y., El-Gebali, S., Fraser, M.I., Gough, J., Haft, D.R., Huang, H., Letunic, I., Lopez, R., Luciani, A., Madeira, F., Marchler-Bauer, A., Mi, H., Natale, D.A., Necci, M., Nuka, G., Orengo, C., Pandurangan, A.P., Paysan-Lafosse, T., Pesseat, S., Potter, S.C., Qureshi, M.A., Rawlings, N.D., Redaschi, N., Richardson, L.J., Rivoire, C., Salazar, G.A., Sangrador-Vegas, A., Sigrist, C.J.A., Sillitoe, I., Sutton, G. G., Thanki, N., Thomas, P.D., Tosatto, S.C.E., Yong, S.Y., Finn, R.D., 2019. InterPro in 2019: improving coverage, classification and access to protein sequence annotations. Nucleic Acids Res. 47, D351–D360. https://doi.org/10.1093/nar/gky1100.
Moreira, J.M.R., Gomes, L.C., Whitehead, K.A., Lynch, S., Tetlow, L.A., Mergulhão, F.J., 2017. Effect of surface conditioning with cellular extracts on *Escherichia coli* adhesion and initial biofilm formation. Food Bioprod. Process. 104, 1–12. https://doi.org/10.1016/j.fbp.2017.03.008.
Muthusamy, S., Lundin, D., Mamede Branca, R.M., Baltar, F., González, J.M., Lehtiö, J., Pinhassi, J., 2017. Comparative proteomics reveals signature metabolisms of exponentially growing and stationary phase marine bacteria. Environ. Microbiol. 19, 2301–2319. https://doi.org/10.1111/1462-2920.13725.
Najmuldeen, H., Alghamdi, R., Alghofaili, F., Yesilkaya, H., 2019. Functional assessment of microbial superoxide dismutase isozymes suggests a differential role for each isozyme. Free Radic. Biol. Med. 134, 215–228. https://doi.org/10.1016/j.freeradbiomed.2019.01.018.
Oliveira, P., Pinto, F., Pacheco, C.C., Mota, R., Tamagnini, P., 2015. HesF, an exoprotein required for filament adhesion and aggregation in *Anabaena* sp. PCC 7120. Environ. Microbiol. 17, 1631–1648. https://doi.org/10.1111/1462-2920.12600.
Osório, H., Silva, C., Ferreira, M., Gullo, I., Máximo, V., Barros, R., Mendonça, F., Oliveira, C., Carneiro, F., 2021. Proteomics analysis of gastric cancer patients with diabetes mellitus. J. Clin. Med. 10, 407. https://doi.org/10.3390/jcm10030407.
Ow, S.Y., Cardona, T., Taton, A., Magnuson, A., Lindblad, P., Stensjö, K., Wright, P.C., 2008. Quantitative shotgun proteomics of enriched heterocysts from *Nostoc* sp. PCC 7120 using 8-plex isobaric peptide tags. J. Proteome Res. 7, 1615–1628. https://doi.org/10.1021/pr700604v.
Panda, B., Basu, B., Acharya, C., Rajaram, H., Apte, S.K., 2017. Proteomic analysis reveals contrasting stress response to uranium in two nitrogen-fixing *Anabaena* strains, differentially tolerant to uranium. Aquat. Toxicol. 182, 205–213. https://doi.org/10.1016/j.aquatox.2016.12.002.
Pandey, S., Rai, R., Rai, L.C., 2012. Proteomics combines morphological, physiological and biochemical attributes to unravel the survival strategy of *Anabaena* sp. PCC7120 under arsenic stress. J. Proteomics 75, 921–937. https://doi.org/10.1016/j.jprot.2011.10.011.
Parnasa, R., Nagar, E., Sendersky, E., Reich, Z., Simkovsky, R., Golden, S., Schwarz, R., 2016. Small secreted proteins enable biofilm development in the cyanobacterium *Synechococcus elongatus*. Sci. Rep. 6, 1–10. https://doi.org/10.1038/srep32209.
Peterson, B.W., van der Mei, H.C., Sjollema, J., Busscher, H.J., Sharma, P.K., 2013. A distinguishable role of eDNA in the viscoelastic relaxation of biofilms. mBio 4. https://doi.org/10.1128/mBio.00497-13.
Porra, R., Thompson, W., Kriedemann, P., 1989. Determination of accurate extinction coefficients and simultaneous equations for assaying chlorophylls *a* and *b* extracted with four different solvents: verification of the concentration of chlorophyll standards by atomic absorption spectroscopy. Biochim. Biophys. Acta 975, 384–394. https://doi.org/10.1016/S0005-2728(89)80347-0.
Priya, B., Premanandh, J., Dhanalakshmi, R.T., Seethalakshmi, T., Uma, L., Prabaharan, D., Subramanian, G., 2007. Comparative analysis of cyanobacterial superoxide dismutases to discriminate canonical forms. BMC Genom. 8, 1–10. https://doi.org/10.1186/1471-2164-8-435.
Qayyum, S., Sharma, D., Bisht, D., Khan, A.U., 2016. Protein translation machinery holds a key for transition of planktonic cells to biofilm state in *Enterococcus faecalis*: a proteomic approach. Biochem. Biophys. Res. Commun. 474, 652–659. https://doi.org/10.1016/j.bbrc.2016.04.145.
Ramos, V., Morais, J., Castelo-Branco, R., Pinheiro, Â., Martins, J., Regueiras, A., Pereira, A.L., Lopes, V.R., Frazão, B., Gomes, D., Moreira, C., Costa, M.S., Brûle, S., Faustino, S., Martins, R., Saker, M., Osswald, J., Leão, P.N., Vasconcelos, V.M., 2018. Cyanobacterial diversity held in microbial biological resource centers as a biotechnological asset: the case study of the newly established LEGE culture collection. J. Appl. Phycol. 30, 1437–1451. https://doi.org/10.1007/s10811-017-1369-y.
Ritchie, M.E., Phipson, B., Wu, D., Hu, Y., Law, C.W., Shi, W., Smyth, G.K., 2015. Limma powers differential expression analyses for RNA-sequencing and microarray studies. Nucleic Acids Res. 43, e47. https://doi.org/10.1093/nar/gkv007.
Romeu, M.J., Alves, P., Morais, J., Miranda, J.M., de Jong, E.D., Sjollema, J., Ramos, V., Vasconcelos, V., Mergulhão, F.J.M., 2019. Biofilm formation behaviour of marine filamentous cyanobacterial strains in controlled hydrodynamic conditions. Environ. Microbiol. 21, 4411–4424. https://doi.org/10.1111/1462-2920.14807.
Romeu, M.J.L., Domínguez-Pérez, D., Almeida, D., Morais, J., Campos, A., Vasconcelos, V., Mergulhão, F.J.M., 2020. Characterization of planktonic and biofilm cells from two filamentous cyanobacteria using a shotgun proteomic approach. Biofouling 36, 631–645. https://doi.org/10.1080/08927014.2020.1795141.
Santos-Merino, M., Singh, A.K., Ducat, D.C., 2019. New applications of synthetic biology tools for cyanobacterial metabolic engineering. Front. Bioeng. Biotechnol. 7, 1–24. https://doi.org/10.3389/fbioe.2019.00033.
Shirkey, B., Kovarcik, D.P., Wright, D.J., Wilmoth, G., Prickett, T.F., Helm, R.F., Gregory, E.M., Potts, M., 2000. Active Fe-containing superoxide dismutase and abundant sodF mRNA in *Nostoc commune* (cyanobacteria) after years of desiccation. J. Bacteriol. 182, 189–197. https://doi.org/10.1128/JB.182.1.189-197.2000.
Silva, E.R., Tulcidas, A.V., Ferreira, O., Bayón, R., Igartua, A., Mendoza, G., Mergulhão, F.J.M., Faria, S.I., Gomes, L.C., Carvalho, S., Bordado, J.C.M., 2021. Assessment of the environmental compatibility and antifouling performance of an innovative biocidal and foul-release multifunctional marine coating. Environ. Res. 198, 111219. https://doi.org/10.1016/j.envres.2021.111219.
Sobczuk, T.M., Camacho, F.G., Grima, E.M., Chisti, Y., 2006. Effects of agitation on the microalgae *Phaeodactylum tricornutum* and *Porphyridium cruentum*. Bioproc. Biosyst. Eng. 28, 243–250. https://doi.org/10.1007/s00449-005-0030-3.
Stanier, R.Y., Cohen-Bazire, G., 1977. Phototrophic prokaryotes: the cyanobacteria. Annu. Rev. Microbiol. 31, 225–274. https://doi.org/10.1146/annurev.mi.31.100177.001301.
Sun, T., Li, S., Song, X., Diao, J., Chen, L., Zhang, W., 2018. Toolboxes for cyanobacteria: recent advances and future direction. Biotechnol. Adv. 36, 1293–1307. https://doi.org/10.1016/j.biotechadv.2018.04.007.
Suo, Y., Huang, Y., Liu, Y., Shi, C., Shi, X., 2012. The expression of superoxide dismutase (SOD) and a putative ABC transporter permease is inversely correlated during biofilm formation in *Listeria monocytogenes* 4b G. PLoS One 7, 1–9. https://doi.org/10.1371/journal.pone.0048467.
Taylor, D.A., 1996. Introduction to Marine Engineering. Butterworth-Heinemann. https://doi.org/10.1007/s11103-011-9767-z.Plastid.
Teodósio, J.S., Simões, M., Melo, L.F., Mergulhão, F.J.M., 2011. Flow cell hydrodynamics and their effects on *E. coli* biofilm formation under different nutrient conditions and turbulent flow. Biofouling 27, 1–11. https://doi.org/10.1080/08927014.2010.535206.
Terán, L.C., Distefano, M., Bellich, B., Petrosino, S., Bertoncin, P., Cescutti, P., Sblattero, D., 2020. Proteomic studies of the biofilm matrix including outer membrane vesicles of *Burkholderia multivorans* c1576, a strain of clinical importance for cystic fibrosis. Microorganisms 8, 1–18. https://doi.org/10.3390/microorganisms8111826.
Tomaras, A.P., Dorsey, C.W., Edelmann, R.E., Actis, L.A., 2003. Attachment to and biofilm formation on abiotic surfaces by *Acinetobacter baumannii*: involvement of a novel chaperone-usher pili assembly system. Microbiology 149, 3473–3484. https://doi.org/10.1099/mic.0.26541-0.
Trémoulet, F., Duché, O., Namane, A., Martinie, B., Labadie, J.C., 2002. Comparison of protein patterns of *Listeria monocytogenes* grown in biofilm or in planktonic mode by proteomic analysis. FEMS Microbiol. Lett. 210, 25–31. https://doi.org/10.1016/S0378-1097(02)00571-2.
Uversky, V.N., 2019. Intrinsically disordered proteins and their "Mysterious" (meta) physics. Front. Phys. 7 https://doi.org/10.3389/fphy.2019.00010.
Wagner, M., Horn, H., 2017. Optical coherence tomography in biofilm research: a comprehensive review. Biotechnol. Bioeng. 114, 1386–1402. https://doi.org/10.1002/bit.26283.
Wang, C., Lan, C.Q., 2018. Effects of shear stress on microalgae: a review. Biotechnol. Adv. 36, 986–1002. https://doi.org/10.1016/j.biotechadv.2018.03.001.
Wang, H., Yang, Y., Chen, W., Ding, L., Li, P., Zhao, X., Wang, X., Li, A., Bao, Q., 2013. Identification of differentially expressed proteins of *Arthrospira (Spirulina) plantensis*-YZ under salt-stress conditions by proteomics and qRT-PCR analysis. Proteome Sci. 11, 1. https://doi.org/10.1186/1477-5956-11-6.
Wang, X., Wang, C., Xu, B., Wei, J., Xiao, Y., Huang, F., 2018a. Adsorption of intrinsically disordered barnacle adhesive proteins on silica surface. Appl. Surf. Sci. 427, 942–949. https://doi.org/10.1016/j.apsusc.2017.08.108.

Wang, Y., Yi, L., Zhang, J., Sun, L., Wen, W., Zhang, C., Wang, S., 2018b. Functional analysis of superoxide dismutase of *Salmonella* typhimurium in serum resistance and biofilm formation. J. Appl. Microbiol. 125, 1526–1533. https://doi.org/10.1111/jam.14044.

Wiśniewski, J.R., Zougman, A., Nagaraj, N., Mann, M., 2009. Universal sample preparation method for proteome analysis. Nat. Methods 6, 359–362. https://doi.org/10.1038/nmeth.1322.

Yonezawa, H., Osaki, T., Woo, T., Kurata, S., Zaman, C., Hojo, F., Hanawa, T., Kato, S., Kamiya, S., 2011. Analysis of outer membrane vesicle protein involved in biofilm formation of *Helicobacter pylori*. Anaerobe 17, 388–390. https://doi.org/10.1016/j.anaerobe.2011.03.020.

Zhang, X., Smits, A.H., Van Tilburg, G.B.A., Ovaa, H., Huber, W., Vermeulen, M., 2018. Proteome-wide identification of ubiquitin interactions using UbIA-MS. Nat. Protoc. 13, 530–550. https://doi.org/10.1038/nprot.2017.147.

Zhao, W., Guo, Q., Zhao, J., 2007. A membrane-associated Mn-superoxide dismutase protects the photosynthetic apparatus and nitrogenase from oxidative damage in the cyanobacterium *Anabaena* sp. PCC 7120. Plant Cell Physiol. 48, 563–572. https://doi.org/10.1093/pcp/pcm025.

Zilliges, Y., Kehr, J.C., Mikkat, S., Bouchier, C., De Marsac, N.T., Börner, T., Dittmann, E., 2008. An extracellular glycoprotein is implicated in cell-cell contacts in the toxic cyanobacterium *Microcystis aeruginosa* PCC 7806. J. Bacteriol. 190, 2871–2879. https://doi.org/10.1128/JB.01867-07.

APPENDIX A. Detailed description of the single-pot solid-phase-enhanced sample-preparation (SP3) protocol adapted from (Hughes et al., 2019)

Prior to the digestion, 100 µg of extracted proteins in approximately 5 µL were reduced in 45 µL SDT in new 1.5 mL Eppendorf tubes. Then, alkylation of samples was performed with 10 µL of 0.1 M iodoacetamide (AppliChem) in 8 M Urea, 0.1 M Tris/HCl pH 8.5 for 30 min. in the dark at room temperature.

Digestion followed Hughes *et al.*, 2019 SP3 for proteomics experiments with some modifications. New magnetized beads (Sera Mag SP3 beads, CAT#45152105050250 and CAT#65152105050250, GE Healthcare) were initially washed and reconstituted in water (HPLC grade, VWR) at a final concentration of 10 µg/µL (from an initial stock concentration of 50 mg/mL), using a magnetic rack (MagnaRack, Invitrogen) for 1 min. A 10:1 ratio (beads:proteins) was reached by adding 100 µL of beads to each tube followed by pipette mixing. Then, 160 µL of absolute ethanol (molecular biology grade, Fisher) was added to achieve 50% v/v, also followed by pipette mixing. Incubation was performed in an Eppendorf Thermomixer with shaking (1000 rpm) for 10 min at room temperature. Then, tubes with samples were placed in the magnetic rack and the supernatant was removed. Beads were gently reconstituted in 180 µL of 80% ethanol. Tubes were placed again in a magnetic rack and the supernatant was discarded. This cleaning step was performed three times. Extraction was then performed gently by adding 100 µL of ammonium bicarbonate (0.1 M pH 8) containing 0.04 µg/µL Trypsin/rLysC Mix (MS grade, Promega) to each tube at a 1:50 ratio (enzyme:protein) followed by an incubation period of 14 h at 37 ºC with mixing at 1000 rpm. Then, 1.300 mL of 100 % acetonitrile (HPLC grade, Chem-Lab NV) was added and incubated for 18 min at 1000 rpm. Beads were spun down, and tubes placed in the magnetic rack. The supernatant was discarded, and beads were washed twice with 180 µL acetonitrile 100 %. After removing the supernatant, 100 µL ammonium bicarbonate (Fluka) 0.05 M was added to the tubes and incubated for 5 min at 1000 rpm. After bead spin and magnetising, the supernatant containing the tryptic peptides was transferred to clean 1.5 mL Eppendorf tubes. The peptide concentration was estimated using the DeNovix (A280 application). Acidification was performed by adding 20 µL of formic acid 5% v/v (Optima LC/MS grade, Fisher Chemical) to the samples. Afterwards, tryptic peptides were dried in a Concentrator Plus vacuum rotator (Eppendorf, Hamburg, Germany) and resuspended in 25 µL formic acid (FA: 0.1% v/v). The final concentration was determined with 2 µL of digested peptides, measured indirectly by optical density (OD) at 280 nm using a DeNovix DS-11 Spectrophotometer (DeNovix Technologies, Wilmington, Delaware, USA).

Reference

- Hughes, C.S., Moggridge, S., Müller, T., Sorensen, P.H., Morin, G.B., Krijgsveld, J., 2019. Single-pot, solid-phase-enhanced sample preparation for proteomics experiments. Nat. Protoc. 14, 68–85. https://doi.org/10.1038/s41596-018-0082-x

APPENDIX B. Correlation between wet weight and chlorophyll *a* content

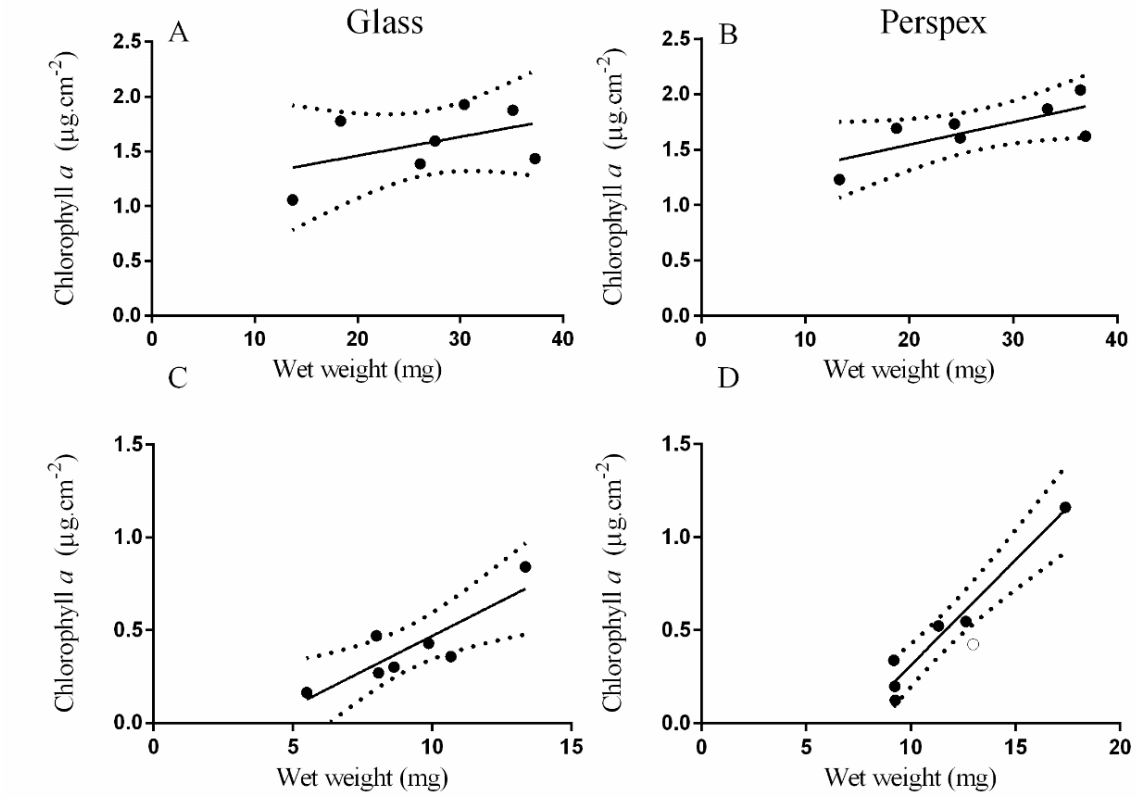

Figure B.1 Correlation between wet weight and chlorophyll *a* on biofilm development from unidentified filamentous cyanobacterium LEGE 06007. Biofilm development in glass (A, C) and perspex (B, D) at two different shear rates, 4 s^{-1} (A, B) and 40 s^{-1} (C, D). Full line represents the linear regression, and the dashed line represents the confidence limits (95%). Closed symbols refer to data points that were considered for the regression (all except one) and open symbols refer to data points that were excluded from the regression.

APPENDIX C. Correlation between crystal violet and biofilm thickness

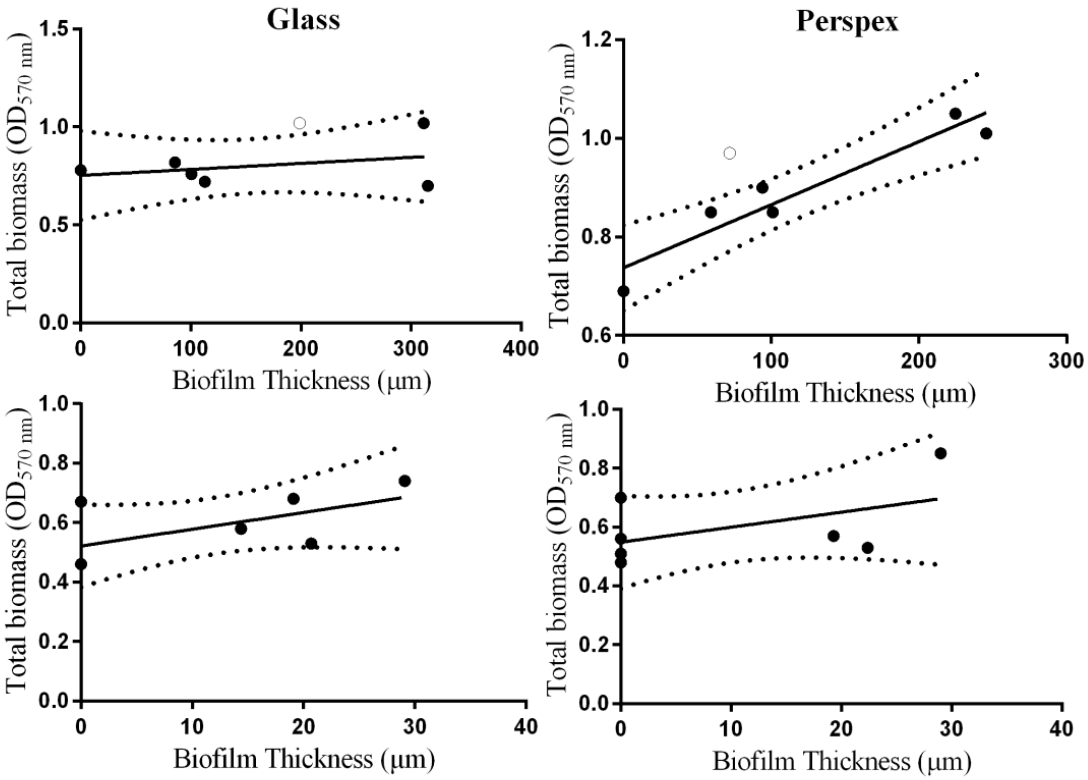

Figure C.1 Correlation between crystal violet and biofilm thickness on biofilm development from unidentified filamentous cyanobacterium LEGE 06007. Biofilm development in glass (A, C) and perspex (B, D) at two different shear rates, 4 s^{-1} (A, B) and 40 s^{-1} (C, D). Full line represents the linear regression, and the dashed line represents the confidence limits (95%). Closed symbols refer to data points that were considered for the regression (all except two) and open symbols refer to data points that were excluded from the regression.

APPENDIX D. Correlation between crystal violet and wet weight

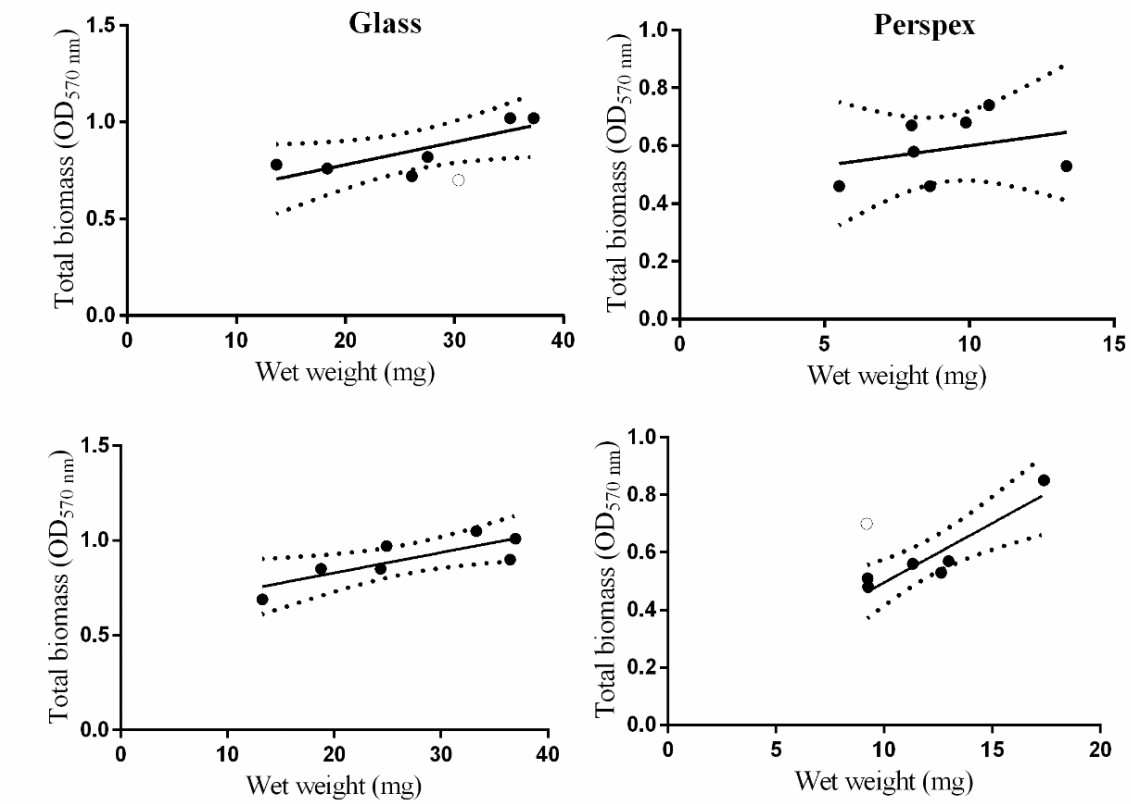

Figure D.1 Correlation between crystal violet and wet weight on biofilm development from unidentified filamentous cyanobacterium LEGE 06007. Biofilm development in glass (A, C) and perspex (B, D) at two different shear rates, 4 s^{-1} (A, B) and 40 s^{-1} (C, D). Full line represents the linear regression, and the dashed line represents the confidence limits (95%). Closed symbols refer to data points that were considered for the regression (all except two) and open symbols refer to data points that were excluded from the regression.

APPENDIX E. Evaluation of cyanobacterial biofilm development under the same hydrodynamic condition on different surfaces

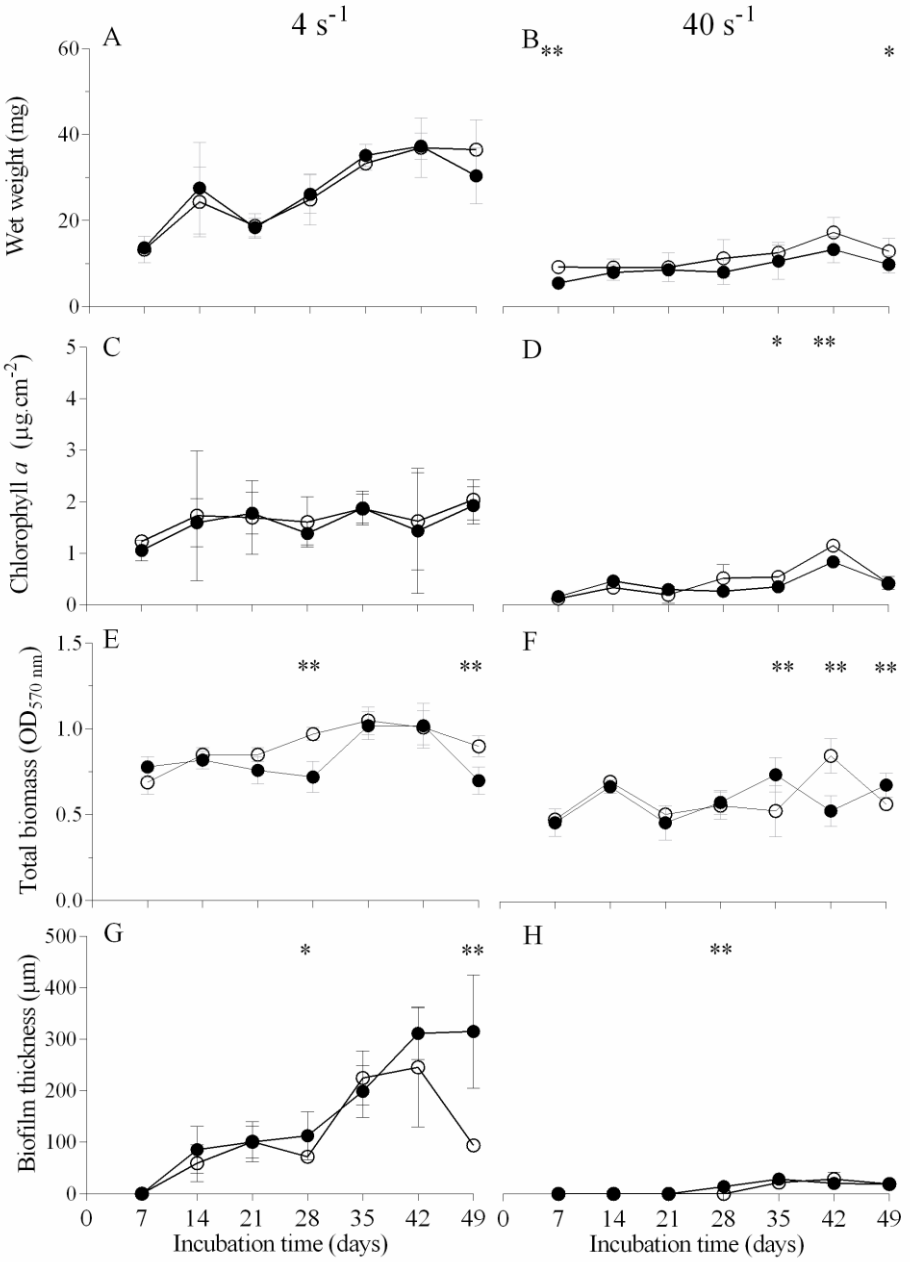

Figure E.1 Evaluation of unidentified filamentous cyanobacterium LEGE 06007 biofilm development. The parameters analysed refer to wet weight (A, B), chlorophyll *a* quantification (C, D), total biomass quantification by CV assay (E, F) and biofilm thickness (G, H). Biofilms were formed at 4 s^{-1} (A,C,E,G) or 40 s^{-1} (B,D,F,H) on two different surfaces, glass (closed circles) and perspex (open circles) for 49 days. Standard deviations from two biological assays with three replicates each, are represented. Symbols *; ** indicate statistically different values for $P < 0.1$ and $P < 0.05$ (respectively) at each incubation time.

APPENDIX F. Evaluation of roughness coefficient

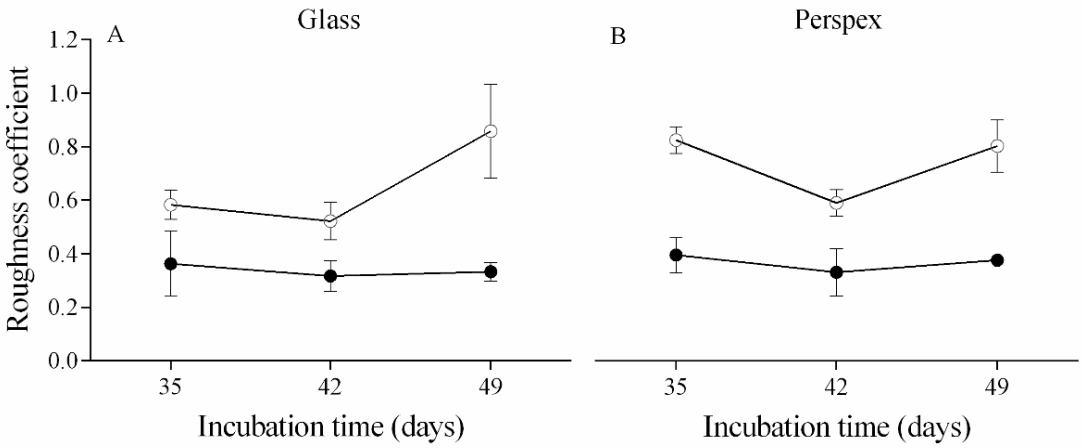

Figure F.1 Evaluation of roughness coefficient of unidentified filamentous cyanobacterium LEGE 06007 biofilm development on glass (A) and perspex (B) at 4 s^{-1} (closed circles) and 40 s^{-1} (open circles) between day 35 and day 49.

APPENDIX G. Summary of proteomic analysis.
Available at https://doi.org/10.1016/j.envres.2021.111566

APPENDIX H. Distribution of total proteins identified according to biological process.

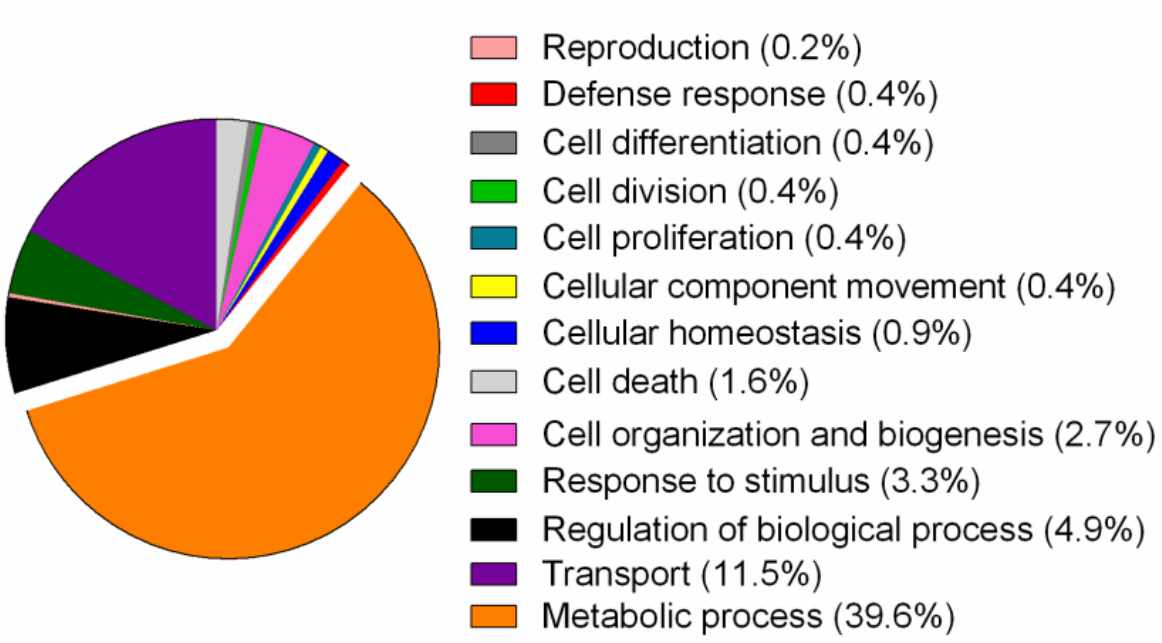

Figure H.1 Distribution of total proteins identified according to biological process (54% of proteins identified without associated biological process are not shown in this graph).

APPENDIX I. DEPs description and GO annotation.
Available at https://doi.org/10.1016/j.envres.2021.111566

APPENDIX J. SOD content throughout the experiment.

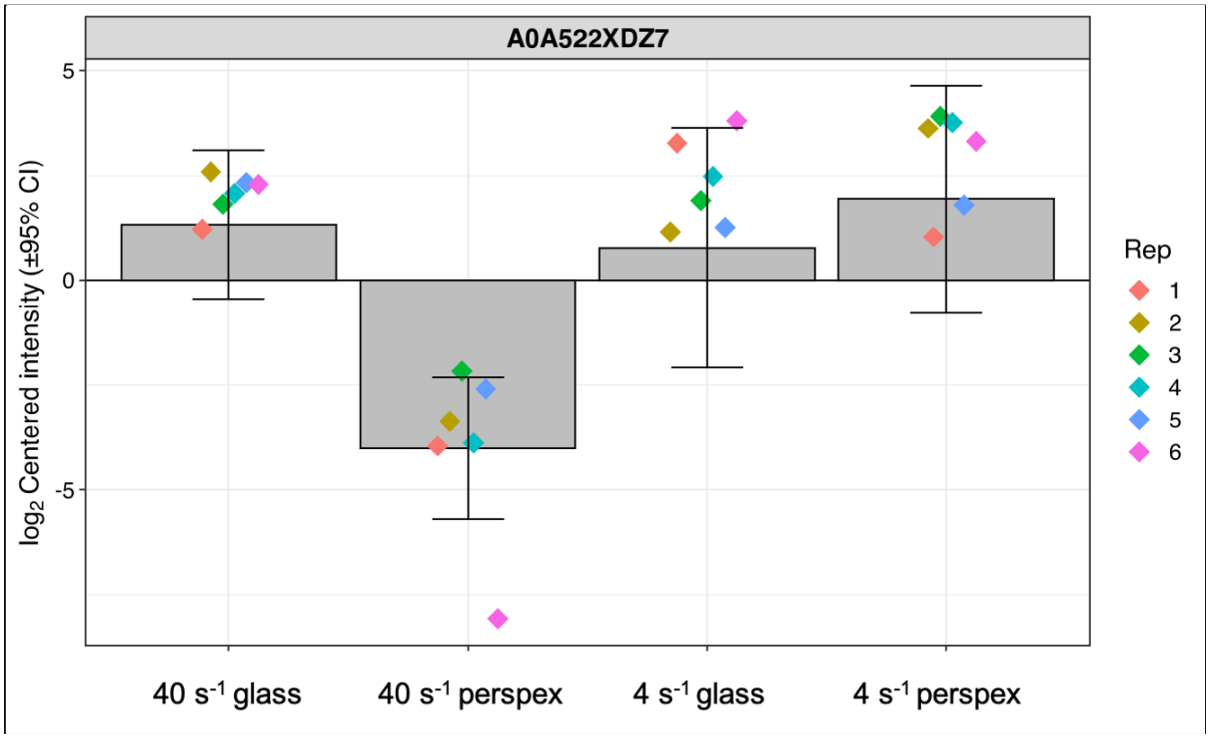

Figure J.1 - Bar plots depicting the content of the superoxide dismutase (SOD) throughout the experiment. The fold changes of SOD content of all replicates from each condition studied (40 s^{-1} glass, 40 s^{-1} perspex, 4 s^{-1} glass and 4 s^{-1} perspex) are depicted as centered log_2 intensities. Error bars represent the 95% confidence intervals.

npj biofilms and microbiomes

www.nature.com/npjbiofilms

ARTICLE OPEN

Check for updates

Hydrodynamic conditions affect the proteomic profile of marine biofilms formed by filamentous cyanobacterium

Maria J. Romeu[1,2,9], Dany Domínguez-Pérez[3,9], Daniela Almeida[3,4], João Morais[3], Mário J. Araújo[3], Hugo Osório[5,6,7], Alexandre Campos[3], Vítor Vasconcelos[3,8] and Filipe J. Mergulhão[1,2]✉

Proteomic studies on cyanobacterial biofilms can be an effective approach to unravel metabolic pathways involved in biofilm formation and, consequently, obtain more efficient biofouling control strategies. Biofilm development by the filamentous cyanobacterium *Toxifilum* sp. LEGE 06021 was evaluated on different surfaces, glass and perspex, and at two significant shear rates for marine environments (4 s^{-1} and 40 s^{-1}). Higher biofilm development was observed at 4 s^{-1}. Overall, about 1877 proteins were identified, and differences in proteome were more noticeable between hydrodynamic conditions than those found between surfaces. Twenty Differentially Expressed Proteins (DEPs) were found between 4 s^{-1} vs. 40 s^{-1}. On glass, some of these DEPs include phage tail proteins, a carotenoid protein, cyanophynase glutathione-dependent formaldehyde dehydrogenase, and the MoaD/ThiS family protein, while on perspex, DEPs include transketolase, dihydroxy-acid dehydratase, iron ABC transporter substrate-binding protein and protein NusG. This study contributes to developing a standardized protocol for proteomic analysis of filamentous cyanobacterial biofilms. This kind of proteomic analysis can also be useful for different research fields, given the broad spectrum of promising secondary metabolites and added-value compounds produced by cyanobacteria, as well as for the development of new antibiofilm strategies.

npj Biofilms and Microbiomes (2022)8:80 ; https://doi.org/10.1038/s41522-022-00340-w

INTRODUCTION

Over the past years, eutrophication and climate changes have been promoting cyanobacterial blooms in aquatic environments[1]. In addition to threatening the ecosystem, this phenomenon also degrades water quality for fisheries and public health[2]. Cyanobacteria can also affect animal and human health through their ability to produce cyanotoxins[3–6]. These toxins can also have detrimental effects through ingestion of contaminated food or even by drinking water during recreational activities[7]. Moreover, cyanobacteria blooms from benthic mat proliferations have increased worldwide[1]. Indeed, cyanobacteria are the major constituents of marine biofilms, and they respond quickly to environmental pattern changes, which allows them to have a diverse distribution. Besides the contamination of aquaculture facilities[8], marine biofilms cause problems related to the corrosion of different facilities and submerged equipment[9]. Marine biofouling can also lead to increased fuel consumption in ships and associated pollution[10,11], as well as the spread of invasive non-indigenous species on marine vessels between different ecosystems[12]. Overall, marine biofouling challenges include environmental, as well as economic and health concerns[13].

Several cues have been identified regarding cyanobacterial adhesion and biofilm formation, particularly for *Synechocystis*[14–17], *Thermosynechococcus elongatus*[18], *Microcystis aeruginosa*[19], *Anabaena* sp. PCC 7120[20], *Synechococcus elongatus* PCC 7942[21] and *Nostoc punctiforme*[15].

Advancements in omics technologies are continuously progressing. Although cyanobacteria proteomics has dealt with many technical challenges[22], cyanobacteria molecular biology is a promising field for further advancements[23,24]. The fouling surface properties and shear rate are two parameters that have a critical impact on marine biofilms[25,26]. In a previous qualitative proteomic study, the proteomic profile of biofilm cells from two cyanobacterial strains developed on glass and perspex, and at different shear forces was analysed[27]. The results revealed that variances in protein composition were more noticeable in biofilms formed under different hydrodynamic conditions than in those formed on different surfaces[27]. However, to identify pathways that are triggered under different circumstances to which cells were subjected, quantitative proteomic analyses are the most relevant tool[28,29]. A recent quantitative study performed with the unidentified filamentous cyanobacterium LEGE 06007 revealed 41 Differentially Expressed Proteins (DEPs)[30]. The proteomic profile can help in the characterization of virulence factors and cellular processes involved in biofilm regulation. Besides improving the fundamental understanding of biofilm development and behavior, the identification of these proteins using high throughput proteomic tools provides new insights into the response to stress conditions, including cell signaling and stress response pathways that are activated under different conditions. Therefore, as more proteins and their roles in biofilm development are explored, novel potential targets for biofilm control may be discovered. Moreover, by knowing which proteins are produced under stress

[1]LEPABE – Department of Chemical Engineering, Faculty of Engineering, University of Porto, Rua Dr. Roberto Frias s/n, 4200-465 Porto, Portugal. [2]ALiCE - Associate Laboratory in Chemical Engineering, Faculty of Engineering, University of Porto, Rua Dr. Roberto Frias s/n, 4200-465 Porto, Portugal. [3]CIIMAR – Interdisciplinary Centre of Marine and Environmental Research, University of Porto, Terminal de Cruzeiros do Porto de Leixões, Av. General Norton de Matos s/n, 4450-208 Matosinhos, Portugal. [4]Department of Biological Sciences, Clemson University, 055A Life Science Facility, 190 Collings Street, Clemson, SC 29634, US. [5]i3S – Instituto de Investigação e Inovação em Saúde, Universidade do Porto, 4200-135 Porto, Portugal. [6]Institute of Molecular Pathology and Immunology of the University of Porto, IPATIMUP, Rua Júlio Amaral de Carvalho 45, 4200-135 Porto, Portugal. [7]Faculty of Medicine, University of Porto, Al. Prof. Hernâni Monteiro, 4200-319 Porto, Portugal. [8]Department of Biology, Faculty of Sciences, University of Porto, Rua do Campo Alegre, 4169-007 Porto, Portugal. [9]These authors contributed equally: Maria J. Romeu, Dany Domínguez-Pérez. ✉email: filipem@fe.up.pt

conditions and which metabolic pathways are activated, it may be possible that new metabolites can be identified with antibiofilm properties. Cyanobacteria are known to produce nearly 800 bioactive secondary metabolites, and it is known that cyanobacteria are able to interfere with other organisms in their communities through the release of compounds into the surrounding medium[31]. The isolation of these metabolites led to the discovery of a strong inhibitory activity against other marine organisms and is currently being explored for the production of antifouling coatings[32]. However, data available on cyanobacterial proteomic are still scarce[33] and most of the studies focus on well-studied model cyanobacteria, such as the unicellular cyanobacterium *Synechocystis* sp. PCC 6803[34]. Different cyanobacterial strains should be considered, and this is of particular importance for filamentous cyanobacterial strains, in which the stress and predation resistance, as well as the improved resource acquisition, may be beneficial[35]. However, the standardization of the proteomic protocol in these organisms is a hard task, and the knowledge needs to be increased incrementally. This work mainly focuses on the improvement of proteomic methodology as well as on the significance of the results obtained and the raw data availability. Due to the high production of cellulose-rich pigments by cyanobacteria, all sample preparation, protein extraction and accurate quantification is a difficult endeavor and hinder the standardization of the proteomic protocol for these organisms. This study contributes to the development of a standardized protocol for proteomic analysis of filamentous cyanobacterial biofilms, enabling other groups to advance their research in this field and facilitating inter-lab comparisons. Moreover, this kind of proteomic analyses can also be useful for different research fields given the broad spectrum of promising secondary metabolites and added-value compounds produced by cyanobacteria[36] that can be used in biotechnological applications, cosmetic, feed and food industries[37] and medical purposes[38]. Synechococcales order includes both filamentous and single-celled types and involves several cyanobacteria genera, among which the ubiquitous *Nodosilinea, Synechococcus, Cyanobium* and *Leptolyngbya* genus. Unidentified Synechococcales include about 32 different strains, and some of them are able to produce common cyanotoxins such as β-methylamino-L-alanine[39,40]. These strains can be found in different ecosystems like brackish water, freshwater, marine, and even hypersaline environments. Moreover, cyanobacterial strains from Synechococcales are present in distinct geographies around the world, including Portugal, Chile, Mexico, and Morocco[39]. The Blue Biotechnology and Ecotoxicology Culture Collection (LEGE-CC) is a biological resource center, which among several additional organisms, maintains different cyanobacterial strains[39,40]. The unidentified filamentous Synechococcales LEGE 06021 strain was used in this study, given the relevance of cyanobacteria on marine biofouling. To complete the current study, a genus identification of this cyanobacterial strain was performed. This study addresses biofilm development of this filamentous cyanobacterial strain, as well as its proteomic profile when subjected to different conditions of shear and surfaces. Therefore, this study aims to characterise the biofouling potential of this filamentous cyanobacteria, on a long-term assay, under two different hydrodynamic conditions and with two surfaces, as well as to explore the quantitative proteomic profile under these different biofilm development conditions.

RESULTS

Phylogenetic analysis

Phylogenetic relationships of unidentified filamentous Synechococcales LEGE 06021 and other relatives were investigated by using a maximum likelihood phylogenetic tree constructed from their partial 16S rRNA gene sequences (Fig. 1). Our phylogenetic results confirmed that this strain belongs to the *Toxifilum* genus (related to the type species *Toxifilum mysidocida)*[41].

Biofilm development analysis

Wet weight, chlorophyll *a* content and biofilm thickness evolution from cyanobacterial biofilm under different conditions were assessed for 49 days (Fig. 2). Biofilm biomass was higher at the lowest shear rate on both surfaces. However, this tendency was more evident for biofilm thickness values obtained from perspex (Fig. 2f). Biofilm mass obtained on the glass surface under lower shear conditions ($4\,s^{-1}$) was on average 70.5% higher (Fig. 2a) when compared to the values obtained at a higher shear rate ($40\,s^{-1}$), whereas on perspex, biofilm wet weight was on average 57.3% higher (Fig. 2b). The chlorophyll *a* content at $4\,s^{-1}$ on glass was on average 87.5% higher (Fig. 2c) than at $40\,s^{-1}$, on perspex, it was, on average 83.9% higher (Fig. 2d). Regarding biofilm thickness, values obtained on glass under lower shear conditions were on average 87.0% higher (Fig. 2e), whereas on perspex, they were on average 93.3% higher (Fig. 2f). Moreover, the highest value of biofilm thickness was observed at $4\,s^{-1}$ on perspex (around 955.9 µm; Fig. 2f, 49 days). When biofilms developed under different surfaces at the same hydrodynamic conditions were compared, similar values from these four parameters were obtained (Supplementary Fig. 1). Figure 3 shows representative 2D cross-sectional images obtained by Optical Coherence Tomography (OCT) at 28 days and at the end of the experiment (49 days). This period corresponds to a maturation phase of biofilm development and the time at which major differences between the two hydrodynamics conditions were observed (Fig. 2).

Proteomic analysis

At the last sampling time, biofilm samples of *Toxifilum* LEGE 06021 were recovered for proteomic analysis. Altogether, 1877 proteins were identified from 24 biofilm samples of four different biofilm conditions using a shotgun proteomics approach (Supplementary Table 1). Among these proteins, 54.2% are related to metabolic processes, and 23.5% to proteomic metabolism (Supplementary Fig. 2).

The Principal Component Analysis (PCA) plot revealed a similar pattern among replicates of the same conditions, whereas some differences were visualized between the different shear rates for the same surface used (Fig. 4). As revealed by the macroscopic evaluation of cyanobacterial biofilm, the proteomic analysis also showed a higher difference in protein expression between the two hydrodynamic conditions than those found between the two surfaces. Indeed, these differences between different hydrodynamic conditions were quantitatively significant, resulting in 20 DEPs, of which 15 DEPs were found between the comparison at $4\,s^{-1}$ *vs.* $40\,s^{-1}$ on glass (Figs. 5a and 6a), whereas five DEPs were found between samples from biofilms developed at $4\,s^{-1}$ *vs.* $40\,s^{-1}$ on perspex (Figs. 5b and 6b). Most of these DEPs (around 50%) were found as up-regulated at $4\,s^{-1}$ *vs.* $40\,s^{-1}$ on glass (Fig. 6a). Like the GOs Categories of the two up-regulated DEPs found in $4\,s^{-1}$ *vs.* $40\,s^{-1}$ on perspex, these 11 up-regulated DEPs found in $4\,s^{-1}$ *vs.* $40\,s^{-1}$ on glass are related to cellular components (intracellular organelle, plastid, thylakoid, membrane-bounded organelle), cation binding and oxidoreductase activity (Fig. 7).

From all of DEPs found on glass, a fragment of condensation protein, uncharacterized proteins, PRC domain-containing proteins, one orange carotenoid protein, and enzymes like cyanophynase and glutathione-dependent formaldehyde dehydrogenase were identified as up-regulated at $4\,s^{-1}$ (Table 1). Among these uncharacterized proteins, two disordered proteins (A0A2T2W171 and A0A522XHL7), which are more likely to perform their function under extreme conditions[42], were also identified. Glutathione-dependent formaldehyde dehydrogenase seems to have a strong impact on biofilm development at this condition since this subset of 11 DEPs

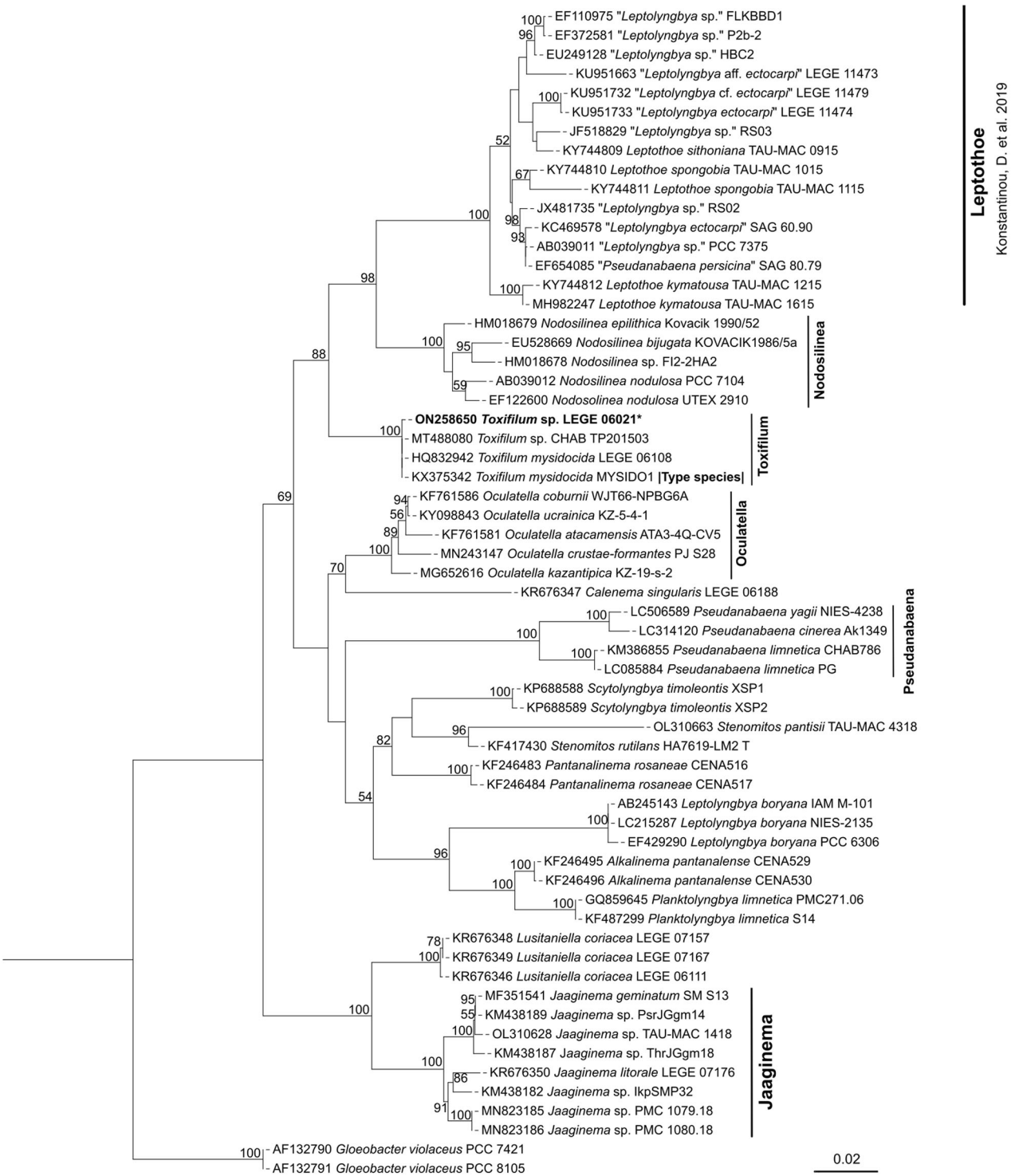

Fig. 1 Maximum likelihood (ML) phylogenetic tree based on 61 partial 16S rRNA gene sequences of cyanobacteria strains belonging to the orders Pseudanabaenales and Synechococcales. *Gloeobacter violaceus* PCC 7421 and *Gloeobacter violaceus* PCC 8105 were used as outgroup. Phylogenetic position of *Toxifilum* sp. LEGE 06021 is indicated in bold. Bootstrap values over 50% are indicated at the nodes. Black stars represent the strains whose sequences were obtained in this work. Strains labeled with quotes indicate that names correspond to Genbank labels.

contained three enriched GO terms related to S-(hydroxymethyl) glutathione dehydrogenase NAD/NADP activity (Fig. 7). Overall, all these up-regulated proteins found at 4 s^{-1} on glass are related to the photosynthetic process (Fig. 6). On the other hand, two phage tail proteins, a MoaD/ThiS family protein and an uncharacterized protein with a disordered domain, were found as down-regulated proteins on glass at 4 s^{-1} when compared with biofilm cells from 40 s^{-1} (Table 1).

On perspex, DEPs include iron ABC transporter substrate-binding protein and transketolase, as up-regulated proteins, and transcription termination/antitermination protein NusG, dihydroxy-acid dehydratase, and 30S ribosomal protein S16 as

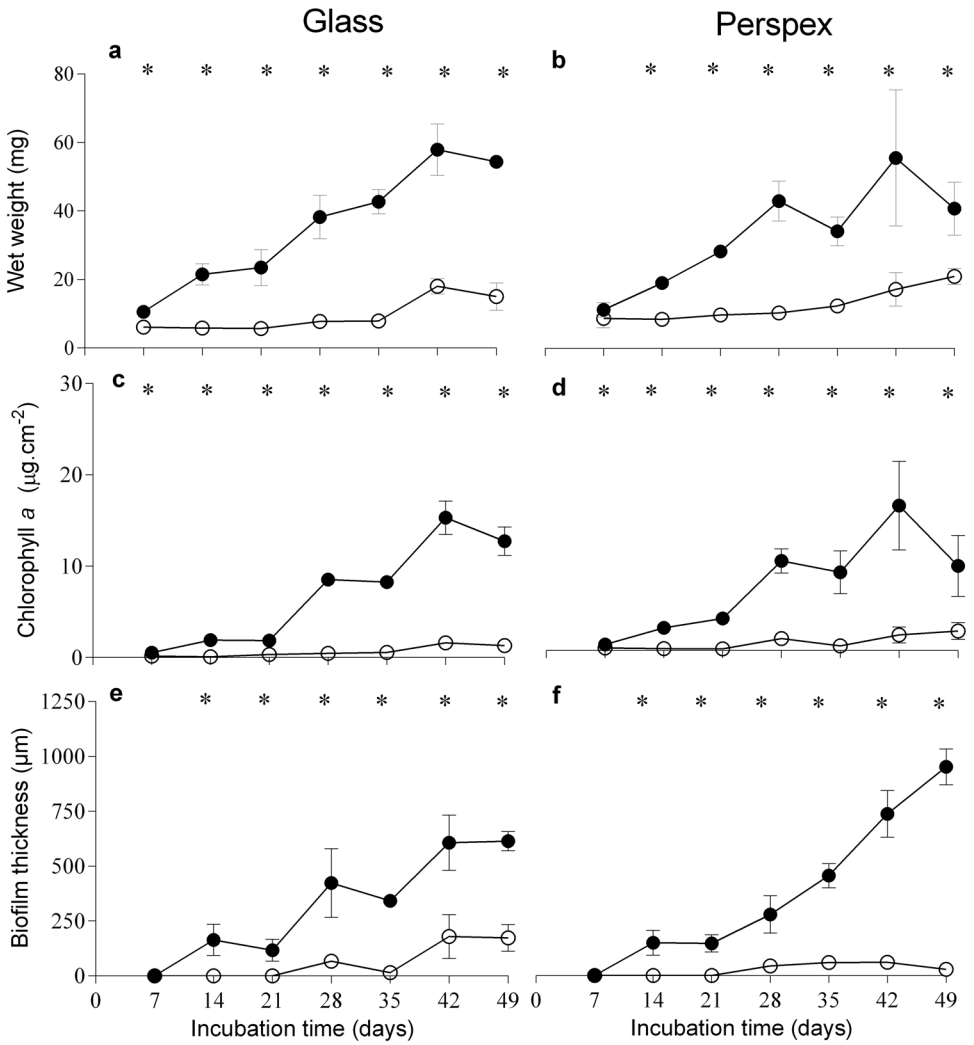

Fig. 2 Evaluation of *Toxifilum* sp. LEGE 06021 biofilm development. The parameters analysed refer to wet weight (**a**, **b**), chlorophyll *a* quantification (**c**, **d**) and biofilm thickness (**e**, **f**). Biofilms were formed in glass (**a**, **c**, **e**) or perspex (**b**, **d**, **f**), at two average shear rates, 4 s^{-1} (closed circles) and 40 s^{-1} (open circles) for 49 days. Standard deviations from two biological assays with three replicates each are represented. Symbol * indicate statistically different values for $P < 0.05$ (unpaired *t*-tests) at each incubation time.

down-regulated proteins at 4 s^{-1} (Table 1). More details about DEPs description and their GO annotation can be found in Supplementary Table 2.

DISCUSSION

Chlorophyll *a* content monitorization proved to be a useful tool for following cyanobacterial biofilm growth since a correlation between chlorophyll *a* production and biofilm wet weight was observed (Supplementary Fig. 3), as already reported for different filamentous cyanobacterial strains[27,30,43]. In the present study, differences in biofilm development at different shear conditions were noticed in the early stages of biofilm development, but major differences were found in the maturation phase of biofilm development, as previously observed for filamentous[27,30,43] and coccoid cyanobacteria[25]. Probably, the increased shear rate has a weaker impact during adhesion and initial biofilm formation, but later on, it may promote sloughing and erosion events, affecting biofilm cohesion and structure. At lower fluid velocities, external mass transfer of nutrients to the top layers of the biofilm is reduced and this may reduce diffusion to the inner layers of the biofilm[44]. It is therefore possible that the biofilm adapts its architecture to facilitate this nutrient transfer as previously shown for other bacterial biofilms produced under flow conditions[45]. Moreover, the lower biofilm biomass obtained under a higher shear rate (Fig. 3e–h) does not allow a detailed analysis of the biofilm structure. However, given the results obtained from biofilm thickness (Fig. 2e, f), in which the effect of fluid velocity was more noticeable during biofilm maturation rather than during cell adhesion, it seems that the increased shear stress was a significant obstacle to biofilm development at 40 s^{-1} most likely due to erosion/sloughing effects. Despite the different properties of glass and perspex, which is the most hydrophobic surface[43], the finding that the effect of surface hydrophobicity was less important than the hydrodynamic effect on cyanobacteria biofilm development had already been shown for other cyanobacterial strains[25,27,43].

Similar to a previous quantitative study, the majority of identified proteins were related to metabolic processes[30]. Due to optimizations performed in the experimental protocol, the total number of proteins identified in the present study was much higher (1877 vs 546), a 3.5-fold increase compared with our last publication using the FASP + SP3 protocol[30]. These results highly improved the quality of data (e.g., more peptides identified, fewer gaps in the proteomic profile comprising six replicates per condition tested). We were now able to identify several ribosomal proteins and others involved in photosynthesis and respiration,

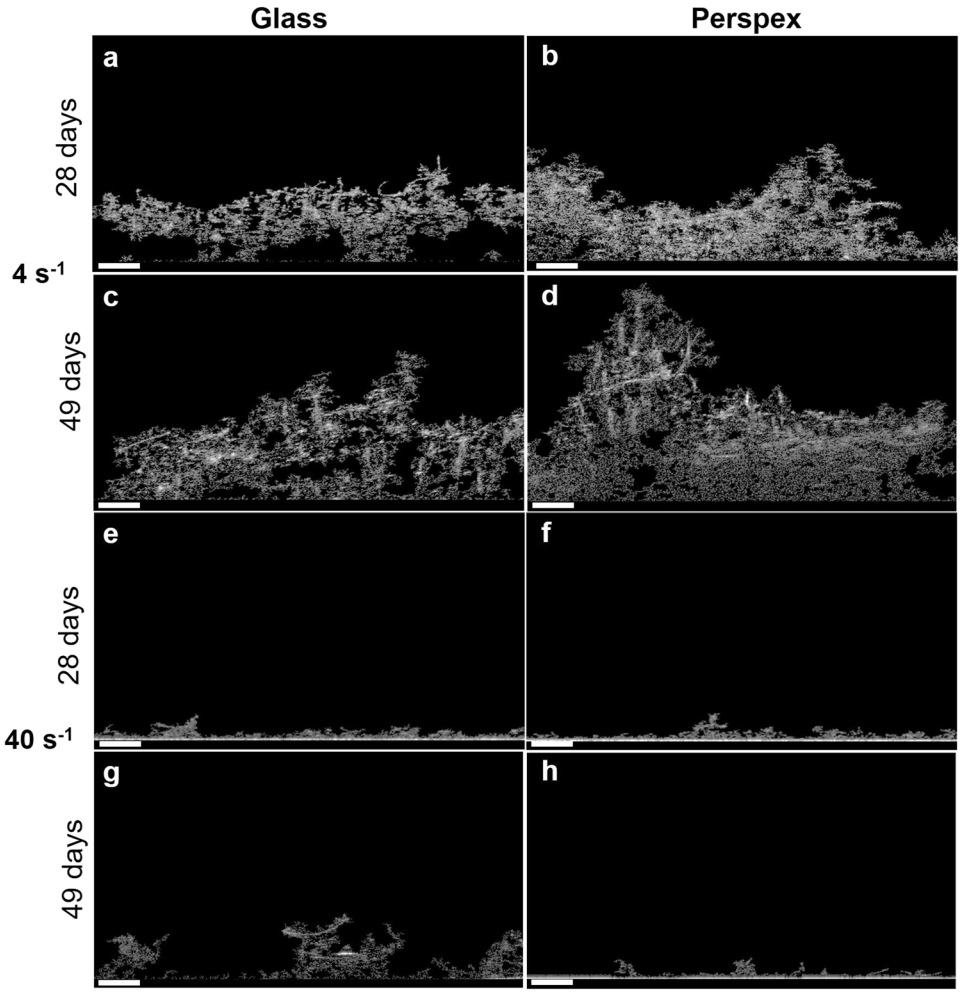

Fig. 3 2D cross-sectional OCT images of *Toxifilum* sp. LEGE 06021 biofilms. The representative images show biofilms formed on glass and perspex at two different shear rates, 4 s^{-1} (**a**–**d**) and 40 s^{-1} (**e**, **f**), and the biofilm structure evolution from days 28 to 49. Scale bar = 200 μm.

which are essential in primary metabolic functions, as well as proteins associated with phycobilisomes, elongation factors, and transporter proteins.

Previous studies performed on the proteome analysis of the adhesion and biofilm formation of other species also identified the presence of several proteins with disordered domains as DEPs[30,46]. Moreover, one of them is related to protein secretion (A0A522XHL7). PRC domain-containing proteins are involved in photosynthesis activity mainly by transferring electrons within the cyclic electron transport pathway. Produced by all photosynthetic organisms, carotenoids act as light-harvesting pigments and as protectors against oxidative stress[47]. Indeed, the photoactivation of the soluble orange carotenoid protein is the initial step for photoprotective mechanisms, which decrease the excitation energy that arrives at the photochemical centers by increasing thermal dissipation[48]. Cyanophycin is a water-insoluble peptide and a valuable exogenous substrate, which enables cyanobacteria to store nitrogen in environments subjected to fluctuating nitrogen supply[49]. A previous proteomic study performed on *Microcoleus* cyanobacteria also showed cyanophycinase expression throughout biofilm growth, suggesting active utilization of cyanophycin granules to cope with fluctuations in nutrient supply[50]. Glutathione-dependent formaldehyde dehydrogenase is one of the three pathways for the detoxification of formaldehyde widely distributed in biological processes[51]. Formaldehyde can be generated endogenously during redox processes, including during the enzymatic demethylation of methylated nucleic acids and proteins, leading to cellular dysfunction[52]. A study on *Acinetobacter baumannii 8399* showed the induction of *adhC1* gene, which encodes for a glutathione-dependent formaldehyde dehydrogenase, under iron limitation and its repression when the cells are cultured in the presence of free inorganic iron[53]. Moreover, in *Paracoccus denitrificans*, the expression of the gene encoding this enzyme is increased when either formaldehyde or metabolic sources of this compound, such as methanol, are present[54]. Likewise, in *Saccharomyces cerevisiae* the glutathione-dependent formaldehyde dehydrogenase expression level is increased by the presence of methylated compounds like methyl methanesulphonate or formaldehyde[55]. An additional study[56] demonstrated that a glutathione-dependent detoxification system was required for formaldehyde resistance and optimal survival of *Neisseria meningitidis* in biofilms, suggesting the role of this enzyme in this complex lifestyle.

Cyanobacterial development on glass at 40 s^{-1} promoted the up-regulation of two phage tail proteins, a MoaD/ThiS family protein and an uncharacterized protein with a disordered domain, when compared to 4 s^{-1}. Bacteriophage tail core is important for phage adsorption to the bacterial cell wall and host infection[57]. Although cyanophages have been barely investigated, they play an important role in regulating the dynamics of cyanobacterial communities in aquatic environments[58]. Cyanophages may introduce genes involved in photosynthesis, carbon metabolism, and nutrient acquisition into host cells during lysogeny, thereby modifying the metabolism of cyanobacteria and providing a

vehicle for horizontal transfer of genetic material and evolution and diversity of marine cyanobacteria[59,60]. Moreover, they also impact globally in the marine biogeochemical cycles[59,61].

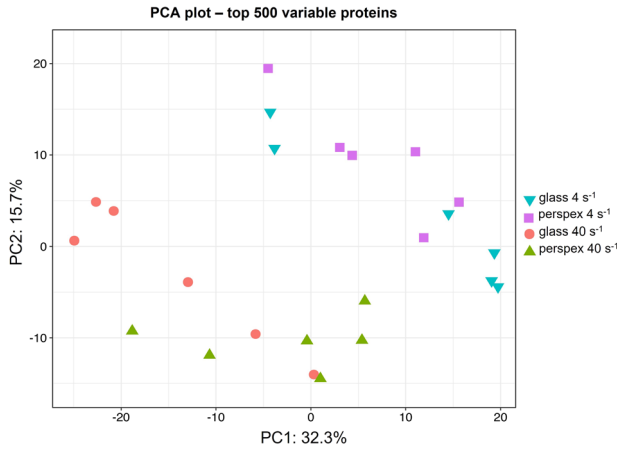

Fig. 4 Principal Component Analysis (PCA) of the proteins identified from marine biofilms formed by filamentous cyanobacteria under four different biofilm growing conditions. The PCA plot displays a grouping pattern among the six replicates studied from each biofilm condition formed on glass and perspex, but some differences were observed between the two hydrodynamic conditions studied (4 s^{-1} and 40 s^{-1}). The two principal components extracted (PC1 and PC2) can explain 48% of the total variability revealed among the proteins analysed. PCA was performed with the respective function provided within the "DEP" R package[101], used for the downstream proteomic analyses.

Cyanophages can play an essential role in the control of cyanobacterial blooms[61,62]. For example, phage lysis of *Nodularia* leads to the release of nitrogen and stimulates the growth of *Synechococcus*[61]. Therefore, it is noteworthy the identification of two phage tail proteins in this biofilm development condition due to their critical role in marine environments. Receptor-binding proteins could be used in genetic engineering to alter host ranges of cyanophages for biocontrol or to develop bacteriophage-based genetic tools for cyanobacteria[58]. Furthermore, cyanophages could potentially be used to control biofilms, opening up new developments in antifouling solutions. A recent study showed that phage protein reduces biofilm and improves antibiotic action[57]. MoaD and ThiS are sulfur carrier proteins required for the synthesis of cofactors of molybdenum and thiamin. Additionally, sulfur is one of the essential elements which is incorporated in proteins as thiol groups of cysteine residues[63]. Unlike in the previous works[27,30], the hydrodynamic effect was clearly revealed through PCA analyses, allowing us to consolidate that hydrodynamics may have a more significant effect than surface properties on biofilm formation (Fig. 4). The differential biofilm development observed on glass at 4 s^{-1} and 40 s^{-1} (Fig. 2) can be related to the differential expression of these proteins in this filamentous cyanobacterial strain. Indeed, GO distribution and GO enrichment of DEPs analysis (Fig. 7) revealed two enriched GO terms related to cysteine (cysteine metabolic process and cysteine biosynthetic process) and two additional GO terms related to sulfur metabolic pathways (sulfur compound metabolic process and sulfur amino acid biosynthetic process).

Iron ABC transporter substrate-binding protein, transketolase, transcription termination/antitermination protein NusG, dihydroxy-acid dehydratase, and 30 S ribosomal protein S16 were identified as DEPs on biofilm cells developed on perspex. ABC

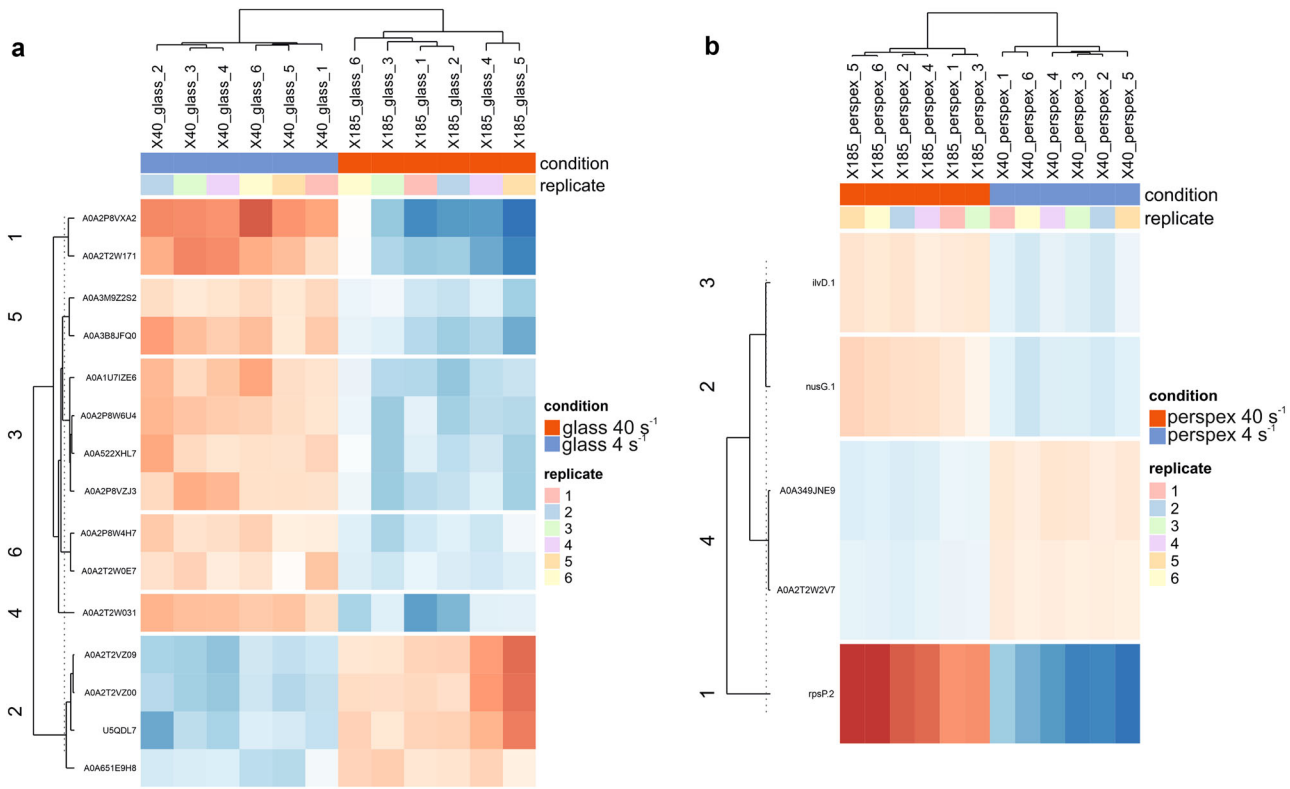

Fig. 5 Heatmaps of the Differentially Expressed Proteins (DEPs) identified between comparisons of the same surface studied at different hydrodynamics conditions. The figures display the DEPs resulting from the comparisons between the conditions (**a**) 4 s^{-1} *vs.* 40 s^{-1} on glass clustered in six groups by k-means clustering, and (**b**) 4 s^{-1} *vs.* 40 s^{-1} on perspex clustered in four groups. The rows show the corresponding UniProt accession of DEPs with their corresponding expression in the columns as the log_2 fold-change (red: enriched; blue: depleted) of the intensity from each replicate.

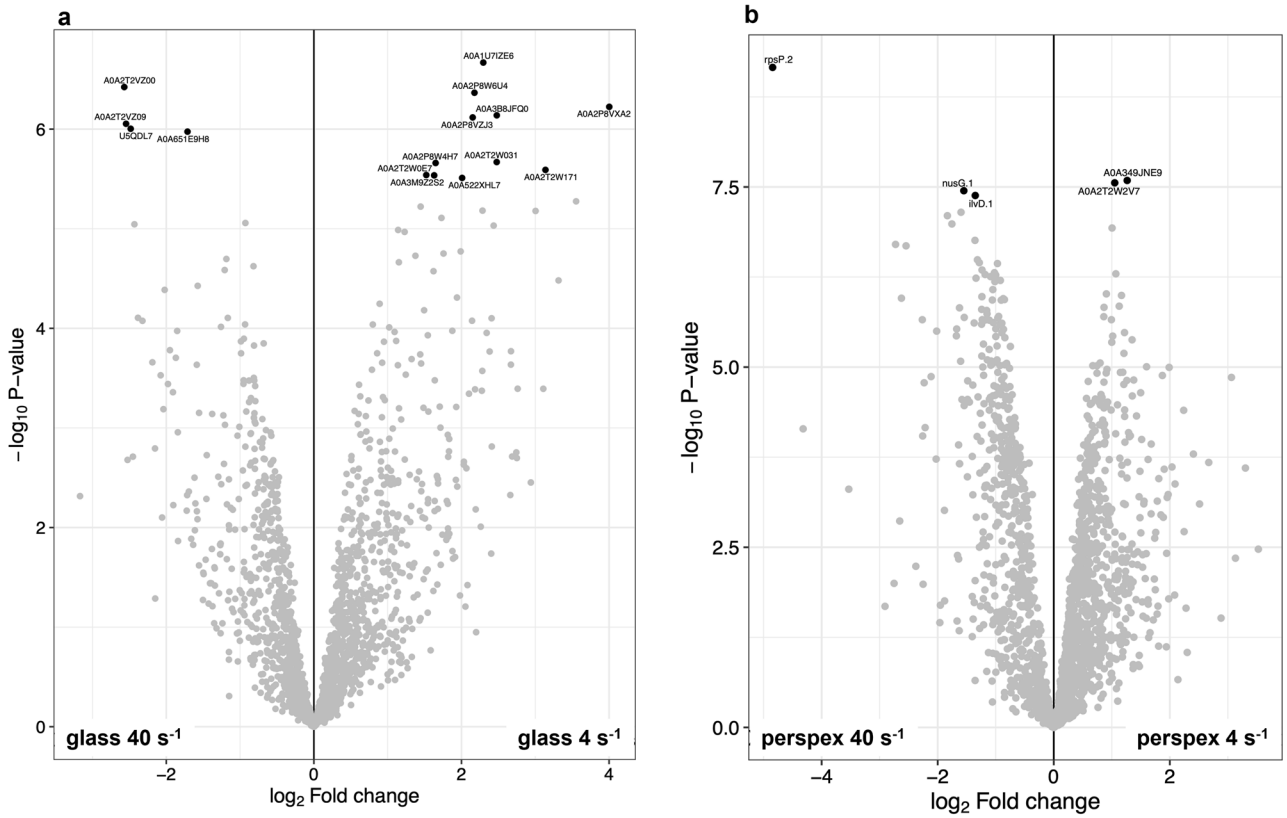

Fig. 6 Volcano plot of the differentially expressed proteins (DEPs) identified between comparisons of the same surface studied at different hydrodynamics conditions. The figure displays the DEPs (black dots) and their corresponding accession/gene names, as the resulting *P* values ($-\log_{10}$) in the y-axis, plotted against the fold changes ($\log_2$) in the x-axis, obtained between the comparisons 4 s^{-1} *vs.* 40 s^{-1} on glass (**a**) and on perspex (**b**).

transporters are vital in the transport of essential substrates across the cytoplasmic membrane[64]. In the case of iron, which is not always readily available from the environment, this metal is a relevant component of key molecules such as cytochromes, and its deficiency can impact ATP production, nucleotide synthesis, and the activity of numerous critical enzymes. Some studies emphasize the role of iron ABC transporters in stress response and virulence[65,66]. In fact, since at 4 s^{-1} the mass transfer of oxygen and nutrients to the inner layers of the biofilm may be reduced, the up-regulation of this protein can be considered as a virulence factor in biofilms. Moreover, a study performed in the anaerobic hyperthermophilic bacterium *Thermotoga maritima* also revealed the up-regulation of an iron ABC transporter on biofilm when compared with planktonic cells[67]. Therefore, they can also be considered as promising targets for antimicrobial strategies. Transketolase is one of the Calvin cycle enzymes involved in biosynthesis, metal ion binding, carbon metabolism, providing a link between glycolysis and the pentose-phosphate pathway[68]. Differential regulation of transketolase has been reported on adhesion, biofilm, and persistence studies. Indeed, a study on *Shewanella oneidensis* showed that transketolase was slightly up-regulated in *luxS* mutant, which developed an undifferentiated, loosely connected biofilm that covered the glass surface more homogenously than the wild type[69]. A proteomic analysis of the biofilm extracellular matrix of *Haemophilus influenzae* biofilms was compared with proteomic analysis of total proteins taken from planktonic bacteria, revealing that transketolase was associated only with the 96 h biofilms[70]. A study performed on *S. aureus* showed that inactivation of a gene that encodes a transketolase leads to a significant decrease in intracellular bacteria proliferation and survival in endothelial cells, associated with a non-persister-like phenotype, suggesting that transketolase is required for bacterial persistence[71].

All down-regulated proteins found at 4 s^{-1}, or up-regulated at 40 s^{-1}, on perspex are relevant to critical cyanobacterial processes. Indeed, NusG is an important transcription factor that modulates the initiation, elongation, and termination steps of bacterial transcription by RNA polymerase. Dihydroxy-acid dehydratase is related to amino acid synthesis and acquisition, whereas the ribosomal protein S16 is one of the 21 proteins which belong to the 30 S small subunit of the bacterial ribosome involved in translation and protein synthesis. A study that evaluated the whole-transcriptome shotgun sequencing to compare the *S. pneumoniae* transcriptome in biofilms and dispersed conditions showed down-regulation of dihydroxy-acid dehydratases and 30 S ribosomal protein S16 and up-regulation of ABC transporter proteins under actively dispersed cells[72]. This finding suggests that the behavior of these proteins is susceptible not only to different hydrodynamic conditions of biofilm development but also to different lifestyles (planktonic and biofilm). Interestingly, cyanobacterial dihydroxy-acid dehydratases have also been considered a promising growth inhibition target[73]. GO distribution and enrichment analysis (Fig. 7) also confirmed the involvement of these proteins in essential processes since GO terms as "protein-containing complex subunit organization, macromolecule biosynthetic process, cellular macromolecule biosynthetic process, cellular component organization or biogenesis, cellular component organization, cellular biosynthetic process, biosynthetic process" were identified for this biofilm condition.

Proteomic analyses performed on filamentous cyanobacteria demonstrated different mechanisms for biofilm regulation, which are strongly dependent on cyanobacterial species, as well as on

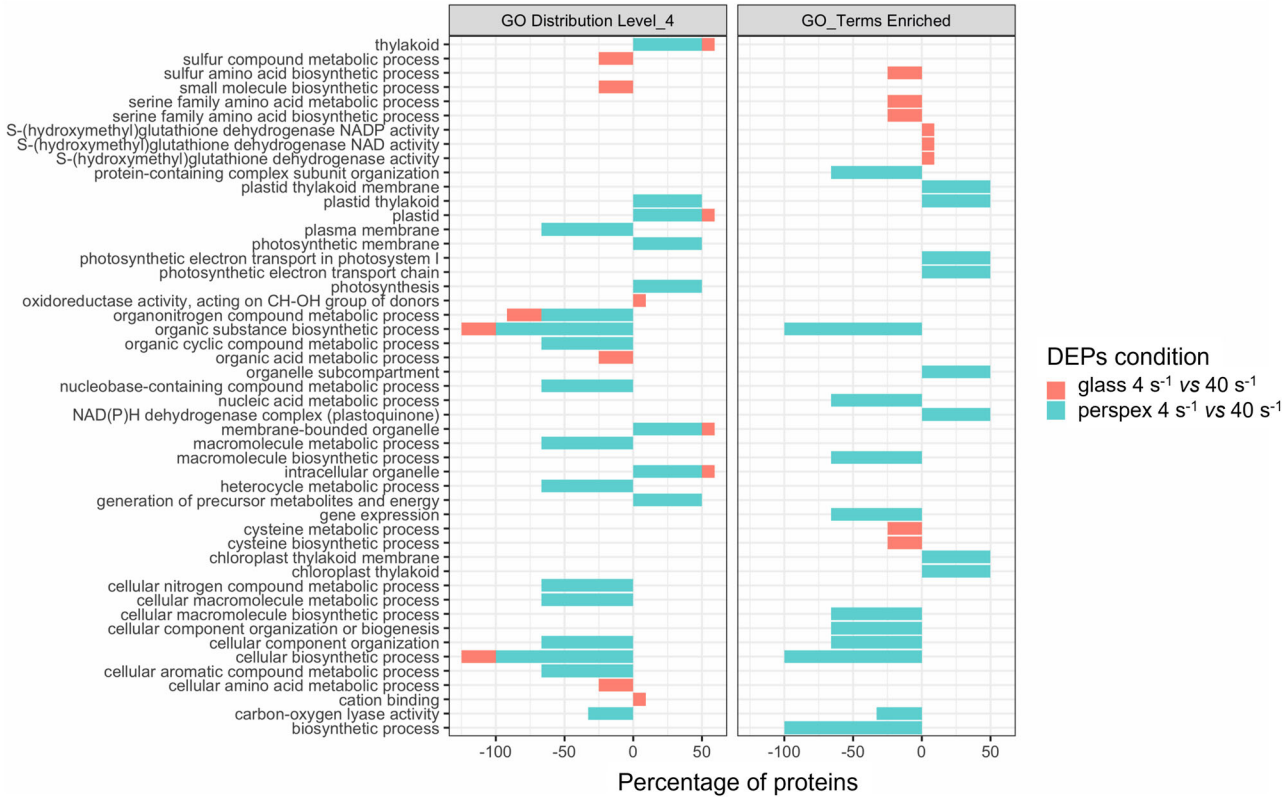

Fig. 7 Gene Ontology (GO) distribution and GO enrichment of Differentially Expressed Proteins (DEPs). In the left panel is shown the GO distribution by level 4 of the DEPs, whereas the right panel displays the corresponding enriched GO terms. The divergent stacked bars (negative and positive) represent the percentage of DEPs (x-axis) matching each GO Category (y-axis), relative to the number of DEPs found at both sides (up/down) of the tested conditions (DEPs Conditions). The total number of DEPs obtained from each comparison were 11-up/4-down (from glass 4 s^{-1} vs. 40 s^{-1}) and 2-up/3-down (from perspex 4 s^{-1} vs. 40 s^{-1}). The GO annotation was performed with the OmicsBox software version 1.4.11, as well as the enrichment analyses (Fisher's exact test, $P < 0.05$).

their isolation sites[27,30]. Although ribosomal proteins, proteins involved in photosynthesis and respiration, as well as proteins associated with phycobilisomes, elongation factors, and proteins with transporter activity were found in all these studies, a broad diversity in the DEP's profile of each strain was observed. Therefore, future studies should focus on different cyanobacterial strains to determine a proteomic profile according to the isolation site and/or the cyanobacterial genus.

The effective management of cyanobacterial growth is vital to restore ecosystem function, as well as to mitigate the biofouling effects. This work demonstrates how hydrodynamic conditions and surface properties affect biofilm development and the protein expression on biofilms cells. Macroscopic biofilm analysis revealed a higher biofilm development at the lowest shear rate, while surface effects were less pronounced. The quantitative proteomic analysis also revealed higher variations between biofilm formed at different shear rates when compared with protein profiles obtained from distinct surfaces. Among all DEPs found between 4 s^{-1} and 40 s^{-1}, up-regulated proteins associated with the photosynthesis process and related pathways were identified on both surfaces. However, it is important to highlight the influence of the glutathione-dependent formaldehyde dehydrogenase found on glass. While down-regulated proteins related to essential processes such as transcription and translation were found at 4 s^{-1} on perspex, on glass, these down-regulated proteins were linked to metabolic processes. Interestingly, phage tail proteins, which presented a significant effect on cyanobacteria blooms and aquatic environments, were also identified on glass.

The possible proteomic functions reported in this study were verified by their quantitative and relative expression in all biofilm conditions and supported by statistical analysis. Considering the lack of biomarkers identified in previous works using a similar approach, the role of the different DEPs can only be discussed by their biological signatures, such as protein domains, annotations, and their relationship in enriched pathways.

Further studies should include gene silencing or knockout strains to establish a stronger link between differential expression levels of a given protein and the impact on biofilm development and behavior. However, the methodologies required for performing this work in this type of organisms are still under development. Nevertheless, and even considering the low availability of data, this study demonstrates with statistical significance that some proteins are differentially expressed under the different conditions and these experimental variations induce changes in biofilm development. Although this is a limitation of our work, to the best of our knowledge, it reflects the state of the art of the research in this field. Additionally, two relevant and clear conclusions were achieved. Regarding the proteomic protocol improvement, the sample preparation, including ultrasounds treatment of the biomass in SDT buffer for cell rupture and protein extraction, followed by a combination of FASP and SP3 protocol, notably improves the peptide and protein identification by shotgun proteomics. Moreover, related to the SP3, in this study we demonstrated its suitability to capture and retain a higher number of peptides originating from complex samples. Regarding the effect of surface properties and hydrodynamic conditions on cyanobacterial biofilm development, it was shown that hydrodynamics had a stronger effect causing the up-regulation of 13 proteins and the downregulation of 7 proteins when biofilms

Table 1. List of the DEPs found between comparisons of the same surface studied at different hydrodynamics conditions.

UniProt accession	Description	Glass 4 s^{-1} *vs.* 40 s^{-1} (LFC)	Glass 4 s^{-1} *vs.* 40 s^{-1} (p.adj)	Perspex 4 s^{-1} *vs.* 40 s^{-1} (LFC)	Perspex 4 s^{-1} *vs.* 40 s^{-1} (p.adj)
A0A1U7IZE6	Orange carotenoid protein	2.3	0.01		
A0A2P8VXA2	Glutathione-dependent formaldehyde dehydrogenase	4	0.01		
A0A2P8VZJ3	Uncharacterized protein	2.15	0.01		
A0A2P8W4H7	Uncharacterized protein	1.65	0.03		
A0A2P8W6U4	PRC domain-containing protein	2.18	0.01		
A0A2T2VZ00	Phage tail protein	−2.57	0.01		
A0A2T2VZ09	Phage tail protein	−2.55	0.01		
A0A2T2W031	PRC domain-containing protein	2.48	0.03		
A0A2T2W0E7	Uncharacterized protein	1.52	0.04		
A0A2T2W171	Uncharacterized protein	3.14	0.03		
A0A3B8JFQ0	Condensation protein (Fragment)	2.48	0.01		
A0A3M9Z2S2	Cyanophycinase	1.63	0.04		
A0A522XHL7	Uncharacterized protein	2.01	0.04		
A0A651E9H8	MoaD/ThiS family protein	−1.71	0.01		
U5QDL7	Uncharacterized protein	−2.48	0.01		
A0A2T2W2V7	Transketolase			1.05	0.04
A0A349JNE9	Iron ABC transporter substrate-binding protein			1.27	0.04
A0A6G3Z7U9[a]	Dihydroxy-acid dehydratase			−1.35	0.05
A0A651DR21[b]	Transcription termination/ antitermination protein NusG			−1.55	0.05
A0A651DTD2[c]	30 S ribosomal protein S16			−4.84	0

The corresponding UniProt accession of DEPs is provided with their corresponding gene and a brief description, as well as the log 2-fold-changes (LFC) and the resulting and adjusted *P*-values (p.adj) for each comparison (4 s^{-1} *vs.* 40 s^{-1} on glass, and 4 s^{-1} *vs.* 40 s^{-1} on perspex).
Gene names: [a]ilvD; [b]nusG; [c]rpsP.

developed at a shear rate value of 4 s^{-1} with 40 s^{-1} are compared (Fig. 6).

Moreover, the isolation of marine organisms (namely marine bacteria) from fouled submerged surfaces (for instance ship hulls and pontoons) and the determination of their proteomic profile can provide information about the metabolic pathways that are activated during biofilm formation under these conditions. Since it is known that cyanobacteria interfere with other organisms in their communities through the release of compounds into the surrounding medium[31], the identification and in vitro production of these compounds can be exploited towards the development of marine antifouling strategies where the growth of different fouling organisms can be inhibited[32,74–76]. This concept has been applied in the use of nostocarboline, a carboline alkaloid from *Nostoc* 78-12 A, as an environmentally friendly candidate for antifouling coating against both prokaryotic and eukaryotic photosynthetic organisms[77,78]. Additionally, other metabolites derived from cyanobacteria have been explored as new candidates for antifouling coatings, such as the diterpenoid comnostin B, isolated from *Nostoc commune*, which shown a molluscicidal effect[79], or the *epi*-hapalindole E from *Fischerella* sp., which exhibited antibacterial, antifungal, antialgal and activities against mammalian cells[80]. Previous studies with portoamides, cyclic dodecapeptides isolated from the cyanobacterium *Phormidium* sp. LEGE 05292, also reveal a broad-spectrum bioactivity towards diverse biofouling species, given their allelopathic effect on the microalga *Chlorella vulgaris*[31] and the high effectiveness in the prevention of the attachment of mussel larvae[32], showing potential to be incorporated as an active ingredient in antifouling coatings.

This study is particularly important given the reduced number of studies addressing filamentous cyanobacterial biofilm development in conditions that mimic the natural environment and that are able to integrate macroscopic biofilm techniques and proteomic approaches. The relatively high number of uncharacterized proteins that were identified in this study is further proof that this area requires further interdisciplinary work so that new insights on biofilm formation and mitigation in marine environments can be obtained.

METHODS

DNA extraction, Amplification (PCR) and sequencing

A 50 ml culture of a cyanobacterium previously classified as unidentified filamentous Synechococcales LEGE 06021[39] was grown and cells were harvested after 2 - 3 weeks. Total genomic DNA was extracted using the commercial PureLink Genomic DNA Mini Kit (Invitrogen, USA), according to the manufacturer's instructions provided for Gram-negative bacteria. To obtain the sequence of 16 S rRNA gene, PCR amplification was performed using the 27F[81], CYA359F, CYA781R[82] and 1494R[81] oligonucleotide primers. PCR reactions were performed in a final volume of 20 µl containing 1x Green GoTaq Flexi Buffer, 2.5 mM of $MgCl_2$, 125.0 mM of each deoxynucleotide triphosphate, 1.0 µM of each primer, 0.5 U of GoTaq Flexi DNA Polymerase (Promega, Madison, WI, USA), 10 $mg.ml^{-1}$ of bovine serum albumin (BSA), and 10–30 ng of template DNA, on a Veriti™ 96-Well Thermal Cycler. The PCR conditions were as follows: initial denaturation at 95 °C for 2 min, followed by 35 cycles of denaturation at 95 °C for 1 min, annealing at 50 °C for 45 s, and extension at 72 °C for 1 min, with a final extension step at 72 °C for 5 min. The PCR reactions were

performed in duplicate. PCR products were separated by 1.5% agarose gel stained with SYBR® safe (Invitrogen, Waltham, MA, USA) and DNA fragments with the expected size were excised and purified using NZYGelpure (NzyTech, Genes and Enzymes, Lisbon, Portugal) according to the manufacturer's instructions. Sequencing was performed at GATC Biotech (Ebersberg, Germany) and the nucleotide sequence obtained was manually inspected for quality and assembled using the Geneious 11.1.5 software (Biomatters Ltd., Auckland, New Zealand). Possible chimera formation during the sequences was checked using the software DECIPHER[83]. The sequence obtained was inserted in the BLASTn (Basic Local Alignment and Search Tool for Nucleotides) database and the results were analysed. The sequence associated with this study was deposited in the GenBank database under the accession number ON258650.

Phylogenetic analysis

A total of 61 sequences were used in the final analysis, including 2 strains of *Gloeobacter violaceus* as outgroup, 58 sequences of cyanobacteria, including type, reference and related strains belonging to the orders Pseudanabaenales and Synechococcales were retrieved from GenBank (National Center for Biotechnology Information, NCBI, Bethesda, MD, USA), and 1 sequence of unidentified filamentous Synechococcales LEGE 06021 obtained in this work. Multiple sequence alignment was carried out using ClustalW in MEGA7[84,85], and sequences were manually proofread and edited. The best fit model was assessed using jModelTest 2.1.10[86] according to the Bayesian information criterion (BIC) and Akaike information criterion (AIC) scores. Maximum likelihood (ML) analysis was carried out using substitution model GTR + G + I with 1000 bootstrap resampling replicates using the MEGA7 software[85]. The final phylogenetic tree was visualized and edited on iTOL (Interactive Tree of Life)[87].

Organism and inoculum preparation

The cyanobacterium previously identified as unidentified filamentous Synechococcales LEGE 06021 was obtained from the Blue Biotechnology and Ecotoxicology Culture Collection (LEGE-CC) located at CIIMAR, Portugal[39]. This cyanobacterial strain was firstly isolated from a sample scraped from a wave-exposed rock in the intertidal zone at Coxos beach, Santo Isidoro, Portugal (39.00455 N 9.425842 W). Cells were grown in 750 ml culture in Z8 medium[88] supplemented with 25 $g.l^{-1}$ of synthetic sea salts (Tropic Marin) and B_{12} vitamin (Sigma Aldrich, Merck, Saint Louis, MO, USA). Cultures were performed under 14 h light (10–30 µmol photons m^{-2} s^{-1})/10 h dark cycles, at 25 °C.

Biofilm formation

In order to assess the biofouling potential on different surfaces, as well as to evaluate their protein expression profiles, biofilms were developed on glass (Vidraria Lousada, Lda, Portugal) and perspex (Neves & Neves, Lda, Portugal) coupons (1 cm^2). These represent typically submerged artificial surfaces found on different apparatus in aquatic environments such as aquaculture equipment, measuring devices and sensors, flotation spheres, moored buoys, underwater cameras, or even in underwater windows of boats[8,89,90] that can be affected by biofouling. Moreover, a previous study shows that these surfaces present different properties since perspex is relatively hydrophobic compared to glass[43]. Surface sterilization and preparation were performed as follows. Glass and perspex coupons were immersed in a solution of 2% (vol/vol) TEGO 2000® industrial detergent (Johnson Diversey, Northampton, United Kingdom)[91] and sterile distilled water for 20 min under agitation (150 rpm). In order to remove any remaining disinfectant, coupons were rinsed in sterile distilled water and air-dried. Additionally, glass coupons were autoclaved (121 °C, 15 min)[92]. After drying, all coupons were aseptically preweighted. Biofilm formation was evaluated on agitated 12-well microtiter plates (VWR International, Carnaxide, Portugal), since this platform was shown to mimic the hydrodynamic conditions found in marine environments[43]. Transparent double-sided adhesive tape was used to fix the coupons, and once the tape was placed in the wells, all coupons plates were subjected to UV sterilization for 30 min after which the sterile coupons were fixed. Moreover, to assess the hydrodynamic effect on protein expression, cyanobacterial biofilm formation at different shear rates was also tested. Briefly, to attain the shear rate values that can mimic aquatic environments, such as those found in a ship hull in a harbor and in partially submerged or even moored equipment and devices, microtiter plates were incubated at 25 °C in an orbital shaker with a 25 mm orbital diameter (Agitorb 200ICP, Norconcessus, Portugal) at 185 rpm (achieving the average shear rate of 40 s^{-1})[43]. Biofilm development was also assessed at lower shear rate conditions (average shear rate of 4 s^{-1}, achieved at 40 rpm) since lower fluid velocities can promote marine biofouling[93,94]. As chlorophyll *a* concentration is commonly used as biomass indicator in aquatic environments, the cyanobacterial suspension was adjusted to a chlorophyll *a* concentration of 1.5 µg.ml^{-1} to inoculation. Briefly, 2 ml of cyanobacterial suspension were incubated at 4 °C in the dark for a maximal chlorophyll *a* extraction. After 24 h, the samples were centrifuged at 3202 g for 5 min at room temperature, and the supernatant was transferred to a glass cuvette. The absorbance at 750 nm (turbidity), 665 nm (chlorophyll *a*), and 652 nm (chlorophyll *b*) was determined using a V-1200 spectrophotometer (VWR International China Co., Ltd, Shanghai, China). The chlorophyll *a* concentration was calculated through the following equation[95]:

$$\text{Chl } a\left(\mu g.ml^{-1}\right) = 16.29 \times A^{665} - 8.54 \times A^{652} \quad (1)$$

These measurements were assessed in triplicate, and dilutions were performed using Z8 medium supplemented with 25 $g.l^{-1}$ of synthetic sea salts and vitamin B_{12}. Thus, a volume of 3 ml of adjusted cyanobacterial suspension was inoculated in each well, in which coupons of each surface were previously fixed with transparent double-sided adhesive tape. Biofilm development was followed for 49 days (seven weeks) since it is accepted that a two-month interval for maintenance is the minimum duration for economically viable underwater monitoring systems[43,90]. During this incubation time, the medium was replaced twice a week. Moreover, to mimic real light exposure periods, a photoperiod of 14 h light (8–10 µmol photons m^{-2} s^{-1})/10 h dark cycles) was applied.

Biofilm analysis

Every seven days, biofilm analysis was performed and three coupons for each surface and hydrodynamic condition were analysed. The culture medium was carefully removed, and the wells were filled with 3 ml of sterile sodium chloride solution (8.5 $g.l^{-1}$)[43]. The solution was carefully removed to eliminate loosely attached cyanobacteria and subsequently, the wells were filled again with 3 ml of sterile sodium chloride solution to evaluate the cyanobacterial biofilms thickness and structure by OCT. In order to complement the characterization of cyanobacterial biofilms, the determination of their wet weight and chlorophyll *a* content was also performed.

Optical coherence tomography. Images from cyanobacterial biofilms developed on both surfaces and under the different hydrodynamic conditions were captured. For each coupon, 2D imaging was performed with a minimum of 3 fields of view to ensure the accuracy and reliability of the results obtained[43]. Image analysis was performed using a routine developed in the Image Processing Toolbox from MATLAB 8.0 and Statistics Toolbox 8.1

(The MathWorks, Inc., Natick, Massachusetts, USA)[27]. The mean of biofilm thickness was calculated based on the distance between the biofilm bottom and the upper contour line according to the following Eq. (2):

$$\bar{L}_F = \frac{1}{N}\sum_{i=1}^{N} L_{F,i} \quad (2)$$

where $L_{F,i}$ is a local biofilm thickness measurement at location *i*, *N* equals the number of thickness measurements, and $\bar{L}_F$ is the mean biofilm thickness.

Wet weight determination and chlorophyll a quantification. To determine the wet weight, coupons were detached from the wells, weighed, and the biofilm wet weight was obtained as the difference from the initial coupon weight (determined prior to inoculation)[30]. Subsequently, cyanobacterial cells were detached from the coupons by immersing each coupon in 2 ml of 8.5 $g.l^{-1}$ sodium chloride solution and vortexing. The suspensions were incubated for 24 h at 4 °C in the dark, and chlorophyll *a* determination was performed as previously described through Eq. 1.

Statistical analysis of biofilm development. A total of six replicates (two biological assays with three technical replicates each) were analysed. Data analysis was performed using the statistical program GraphPad Prism® for Windows, version 6.01 (GraphPad Software, Inc., San Diego, CA, USA), and results were compared using unpaired t-tests with a confidence level of 95% (*; $P < 0.05$).

Proteomics analysis

Protein extraction and sample preparation for proteomic analysis. At the last sampling time (49 days), biofilm samples of unidentified filamentous Synechococcales LEGE 06021 were recovered for proteomic analysis[30]. Cyanobacterial biofilms were detached from the coupons by immersing each coupon in 2 ml of 8.5 $g.l^{-1}$ sodium chloride solution and vortexing. The pooled samples from four coupons of the same condition were centrifuged at 3202 g for 10 min at room temperature, and the pellet of biomass from 24 biofilm samples comprising six independent replicates from four different growing conditions were kept at −80 °C for further processing. The amount of sample was calculated, and an appropriate volume of SDT buffer (0.5 g FW/ml SDT) + Protease inhibitors (PIs, Roche, 11697498001, Basel, Switzerland) was added to the samples, sonicated 10 × 3 s and 23 kHz – 105 µm (amplitude) and incubated for 4 h at room temperature. Afterward, samples were heated for 3 min at 95 °C and subsequently centrifuged at 16,000 g for 20 min. Finally, the supernatant was collected, and total protein concentration was measured indirectly by optical density (OD) at 280 nm using a DeNovix DS-11 Spectrophotometer (DeNovix Technologies, Wilmington, Delaware, USA). Samples containing the extracted protein were stored for 24 h at −20 °C.

The extracted proteins were processed according to Romeu et al.[30], which used a modified version of two distinct protocols based on FASP protocol described by[96] and the SP3 technology[97]. Herein, the samples containing 40 µg of the extracted proteins were processed by the FASP using centrifugal filter units with nominal molecular weight limit (NMWL) of 30 kDa (MRCPRT030, Millipore, Billerica, MA, USA), whereas 200 µg of the extracted proteins were reduced prior the digestion with trypsin in the SP3 protocol[30].

LC-MS/MS analysis. Considering both sample preparation methods are complementary, tryptic peptides from both methods were mixture in the same tube to a final concentration of 0.1 µg and 0.5 µg from FASP and SP3, respectively. Then, protein digests from both protocols were analysed in the same run with a nano LC-MS/MS, composed by an Ultimate 3000 liquid chromatography system coupled to a Q-Exactive Hybrid Quadrupole – Orbitrap mass spectrometer (Thermo Scientific, Bremen, Germany)[98]. Separation was performed in a 15 cm by 75 µm inner diameter EASY-Spray column (ES800, PepMap RSLC, C18, 3 µm, Thermo Scientific, Bremen, Germany) at 300 nl min^{-1} by generated by mixing A: 0.1% FA and B: 80% ACN, with the following gradient: 5 min (2.5% B to 10% B), 60 min (10% B to 35% B), 5 min (35% B to 99% B) and 5 min (hold 99% B). Subsequently, the column was equilibrated with 2.5% B for 12 min. Data acquisition was controlled by Xcalibur 4.0 and Tune 2.8 software (Thermo Scientific, Bremen, Germany). The specific LC-MS parameters were full scan settings: 70k resolution (m/z 200), AGC target 3e6, maximum injection time 50 ms. dd settings: minimum AGC target 8e3, intensity threshold 7.3e4, charge exclusion: unassigned, 1, 8, >8, peptide match preferred, exclude isotopes on, dynamic exclusion 20 s. MS2 settings: microscans 1, resolution 35k (m/z 200), AGC target 2e5, maximum injection time 110 ms, isolation window 2.0 m/z, isolation offset 0.0 m/z, spectrum data type profile.

The mass spectrometry proteomics data have been deposited to the ProteomeXchange Consortium via the PRIDE[99] partner repository with the data set identifier PXD029048.

Protein identification. The raw data were analysed and processed using the Proteome Discoverer 2.2.0.388 software (Thermo Scientific) and searched against the UniProt database for Cyanobacteria taxonomic selection (2018_07 release). The Sequest HT search engine was used for protein identification. The ion mass tolerance was 10 ppm for precursor ions and 0.02 Da for-fragment ions. Maximum allowed missing cleavage sites was set to 2. Cysteine carbamidomethylation was defined as a constant modification. Methionine oxidation and protein N-terminus acetylation were defined as variable modifications. Peptide confidence was set to high. The processing node Percolator was enabled with the following settings: maximum delta Cn 0.05; decoy database search target false discovery rates (FDR) 1%, validation was based on q-value. Protein label-free quantitation was performed with the Minora feature detector node at the processing step. Precursor ions quantification was performed at the processing step with the following parameters: unique plus razor peptides were considered for quantification, and precursor abundance was based on intensity.

Differential protein expression and enrichment. Statistical analyses applied to the proteomic data were performed using R software version 4.0.0.[100]. The Differentially Expressed Proteins (DEPs) and/or gene enrichment was assessed using the "DEP" R package[101], based on the *limma* algorithm[102]. Similar to previous work[30], the missing values were filtered according to the fraction of protein found in each paired comparison with a cut-off of 0.33%, considering the possibility to have a minimum of 4 out of 6 replicates at least one condition. Imputation of missing values was performed considering a non-random distribution (MNAR) using "MinProb" as an imputation function. Significant differences between conditions for each condition were paired tested by protein-wise linear models and empirical Bayes statistics. Finally, adjusted *P* value (alpha = 0.05) and the log2 fold change (lfc = log2(1.5), log2 fold change >0.6) were used as a filter threshold to classify them as DEPs or enriched genes.

Functional classification (gene ontology) was carried out using the OmicsBox software version 1.4.11 (https://www.biobam.com/omicsbox/). Additional functional analyses to determine over/under-expressed pathways were performed to the categorical GO terms corresponding to DEPs, using the hypergeometric distribution significance test (Fisher's exact test, $P < 0.05$).

DATA AVAILABILITY

The sequence associated with the cyanobacterial strain used in this study was deposited in the GenBank database under the accession number ON258650. The

mass spectrometry proteomics data have been deposited to the ProteomeXchange Consortium via the PRIDE partner repository with the data set identifier PXD029048. All other data that support the findings of this study are available from the corresponding author upon reasonable request.

Received: 9 November 2021; Accepted: 23 September 2022;
Published online: 17 October 2022

REFERENCES

1. Gaget, V., Humpage, A. R., Huang, Q., Monis, P. & Brookes, J. D. Benthic cyanobacteria: A source of cylindrospermopsin and microcystin in Australian drinking water reservoirs. *Water Res* **124**, 454–464 (2017).
2. Huisman, J. et al. Cyanobacterial blooms. *Nat. Rev. Microbiol.* **16**, 471–483 (2018).
3. Regueiras, A., Pereira, S., Costa, M. S. & Vasconcelos, V. Differential toxicity of cyanobacteria isolated from marine sponges towards echinoderms and crustaceans. *Toxins (Basel)* **10**, 1–12 (2018).
4. Breinlinger, S. et al. Hunting the eagle killer: A cyanobacterial neurotoxin causes vacuolar myelinopathy. *Science (80-.)* **371**, eaax9050 (2021).
5. Gibble, C. M., Peacock, M. B. & Kudela, R. M. Evidence of freshwater algal toxins in marine shellfish: Implications for human and aquatic health. *Harmful Algae* **59**, 59–66 (2016).
6. Miller, M. A. et al. Evidence for a novel marine harmful algal bloom: Cyanotoxin (microcystin) transfer from land to sea otters. *PLoS One* **5**, 1–11 (2010).
7. Buratti, F. M. et al. Cyanotoxins: producing organisms, occurrence, toxicity, mechanism of action and human health toxicological risk evaluation. *Arch. Toxicol.* **91**, 1049–1130 (2017).
8. King, R. K. et al. Comparison of bacterial presence in biofilms on different materials commonly found in recirculating aquaculture systems. *J. Appl. Aquac.* **18**, 79–88 (2006).
9. Delauney, L., Compare, C. & Lehaitre, M. Biofouling protection for marine environmental sensors. *Ocean Sci.* **6**, 503–511 (2010).
10. Schultz, M. P., Bendick, J. A., Holm, E. R. & Hertel, W. M. Economic impact of biofouling on a naval surface ship. *Biofouling* **27**, 87–98 (2011).
11. Davidson, I. et al. Mini-review: Assessing the drivers of ship biofouling management – aligning industry and biosecurity goals. *Biofouling* **32**, 411–428 (2016).
12. Mineur, F., Johnson, M. P., Maggs, C. A. & Stegenga, H. Hull fouling on commercial ships as a vector of macroalgal introduction. *Mar. Biol.* **151**, 1299–1307 (2007).
13. Caruso, G. Microbial colonization in marine environments: Overview of current knowledge and emerging research topics. *J. Mar. Sci. Eng.* **8**, 1–22 (2020).
14. Agostoni, M., Waters, C. M. & Montgomery, B. L. Regulation of biofilm formation and cellular buoyancy through modulating intracellular cyclic di-GMP levels in engineered cyanobacteria. *Biotechnol. Bioeng.* **113**, 311–319 (2016).
15. Duggan, P. S., Gottardello, P. & Adams, D. G. Molecular analysis of genes in Nostoc punctiforme involved in pilus biogenesis and plant infection. *J. Bacteriol.* **189**, 4547–4551 (2007).
16. Schatz, D. et al. Self-suppression of biofilm formation in the cyanobacterium Synechococcus elongatus. *Environ. Microbiol.* **15**, 1786–1794 (2013).
17. Allen, R., Rittmann, B. E. & Curtiss, R. Axenic biofilm formation and aggregation by synechocystis PCC 6803 is induced by changes in nutrient concentration, and requires cell surface structures. *bioRxiv* 1–33 (2018). https://doi.org/10.1101/414151.
18. Enomoto, G. et al. Cyanobacteriochrome SesA is a diguanylate cyclase that induces cell aggregation in Thermosynechococcus. *J. Biol. Chem.* **289**, 24801–24809 (2014).
19. Zilliges, Y. et al. An extracellular glycoprotein is implicated in cell-cell contacts in the toxic cyanobacterium Microcystis aeruginosa PCC 7806. *J. Bacteriol.* **190**, 2871–2879 (2008).
20. Oliveira, P., Pinto, F., Pacheco, C. C., Mota, R. & Tamagnini, P. HesF, an exoprotein required for filament adhesion and aggregation in Anabaena sp. PCC 7120. *Environ. Microbiol.* **17**, 1631–1648 (2015).
21. Parnasa, R. et al. Small secreted proteins enable biofilm development in the cyanobacterium Synechococcus elongatus. *Sci. Rep.* **6**, 1–10 (2016).
22. Pandhal, J., Ow, S. Y., Wright, P. C. & Biggs, C. A. Comparative proteomics study of salt tolerance between a nonsequenced extremely halotolerant cyanobacterium and its mildly halotolerant relative using in vivo metabolic labeling and in vitro isobaric labeling. *J. Proteome Res.* **8**, 818–828 (2009).
23. Santos-Merino, M., Singh, A. K. & Ducat, D. C. New applications of synthetic biology tools for cyanobacterial metabolic engineering. *Front. Bioeng. Biotechnol.* **7**, 1–24 (2019).
24. Sun, T. et al. Toolboxes for cyanobacteria: Recent advances and future direction. *Biotechnol. Adv.* **36**, 1293–1307 (2018).
25. Faria, S. I. et al. The Relative Importance of Shear Forces and Surface Hydrophobicity on Biofilm Formation by Coccoid Cyanobacteria. *Polym. (Basel)* **12**, 653 (2020).
26. Faria, S. et al. Unveiling the antifouling performance of different marine surfaces and their effect on the development and structure of cyanobacterial biofilms. *Microorganisms* **9**, 1102 (2021).
27. Romeu, M. J. et al. Characterization of planktonic and biofilm cells from two filamentous cyanobacteria using a shotgun proteomic approach. *Biofouling* **36**, 631–645 (2020).
28. Battchikova, N., Angeleri, M. & Aro, E. M. Proteomic approaches in research of cyanobacterial photosynthesis. *Photosynth. Res.* **126**, 47–70 (2015).
29. Muthusamy, S. et al. Comparative proteomics reveals signature metabolisms of exponentially growing and stationary phase marine bacteria. *Environ. Microbiol.* **19**, 2301–2319 (2017).
30. Romeu, M. J. et al. Quantitative proteomic analysis of marine biofilms formed by filamentous cyanobacterium. *Environ. Res.* **201**, 111566 (2021).
31. Leão, P. N. et al. Synergistic allelochemicals from a freshwater cyanobacterium. *Proc. Natl Acad. Sci. USA.* **107**, 11183–11188 (2010).
32. Antunes, J. et al. A multi-bioassay integrated approach to assess the antifouling potential of the cyanobacterial metabolites portoamides. *Mar. Drugs* **17**, 1–19 (2019).
33. Babele, P. K., Kumar, J. & Chaturvedi, V. Proteomic De-regulation in cyanobacteria in response to abiotic stresses. *Front. Microbiol.* **10**, 1–22 (2019).
34. Jahn, M. et al. Growth of Cyanobacteria Is Constrained by the Abundance of Light and Carbon Assimilation Proteins. *Cell Rep.* **25**, 478–486.e8 (2018).
35. Claessen, D., Rozen, D. E., Kuipers, O. P., Søgaard-Andersen, L. & van Wezel, G. P. Bacterial solutions to multicellularity: a tale of biofilms, filaments and fruiting bodies. *Nat. Rev. Microbiol.* **12**, 115–124 (2014).
36. Lau, N. S., Matsui, M. & Abdullah, A. A. A. Cyanobacteria: Photoautotrophic Microbial Factories for the Sustainable Synthesis of Industrial Products. *Biomed Res. Int.* **2015**, 754934 (2015).
37. Manirafasha, E., Ndikubwimana, T., Zeng, X., Lu, Y. & Jing, K. Phycobiliprotein: Potential microalgae derived pharmaceutical and biological reagent. *Biochem. Eng. J.* **109**, 282–296 (2016).
38. Pagels, F., Guedes, A. C., Amaro, H. M., Kijjoa, A. & Vasconcelos, V. Phycobiliproteins from cyanobacteria: Chemistry and biotechnological applications. *Biotechnol. Adv.* **37**, 422–443 (2019).
39. Ramos, V. et al. Cyanobacterial diversity held in microbial biological resource centers as a biotechnological asset: the case study of the newly established LEGE culture collection. *J. Appl. Phycol.* **30**, 1437–1451 (2018).
40. Mai, T., Johansen, J. R., Pietrasiak, N., Bohunicka, M. & Martin, M. P. Revision of the Synechococcales (Cyanobacteria) through recognition of four families including Oculatellaceae fam. nov. and Trichocoleaceae fam. nov. and six new genera containing 14 species. *Phytotaxa* **365**, 1–59 (2018).
41. Zimba, P. V., Huang, I.-S., Foley, J. E. & Linton, E. W. Identification of a new-to-science cyanobacterium, Toxifilum mysidocida gen. nov. & sp. nov. (Cyanobacteria, Cyanophyceae). *J. Phycol.* **53**, 188–197 (2017).
42. Liu, Z. & Huang, Y. Advantages of proteins being disordered. *Protein Sci.* **23**, 539–550 (2014).
43. Romeu, M. J. et al. Biofilm formation behaviour of marine filamentous cyanobacterial strains in controlled hydrodynamic conditions. *Environ. Microbiol.* **21**, 4411–4424 (2019).
44. Moreira, J. et al. Influence of flow rate variation on the development of Escherichia coli biofilms. *Bioprocess Biosyst. Eng.* **36**, 1787–1796 (2013).
45. Teodósio, J. S., Simões, M., Melo, L. F. & Mergulhão, F. J. Flow cell hydrodynamics and their effects on E. coli biofilm formation under different nutrient conditions and turbulent flow. *Biofouling* **27**, 1–11 (2011).
46. Domínguez-Pérez, D. et al. The Quantitative Proteome of the Cement and Adhesive Gland of the Pedunculate Barnacle, Pollicipes pollicipes. *Int. J. Mol. Sci.* **21**, 2524 (2020).
47. Melnicki, M. R. et al. Structure, Diversity, and Evolution of a New Family of Soluble Carotenoid-Binding Proteins in Cyanobacteria. *Mol. Plant* **9**, 1379–1394 (2016).
48. Lu, Y. et al. Native mass spectrometry analysis of oligomerization states of fluorescence recovery protein and orange carotenoid protein: Two proteins involved in the cyanobacterial photoprotection cycle. *Biochemistry* **56**, 160–166 (2017).
49. Watzer, B. & Forchhammer, K. Cyanophycin Synthesis Optimizes Nitrogen Utilization in the Unicellular Cyanobacterium Synechocystis sp. Strain PCC 6803. *Appl. Environ. Microbiol.* **84**, e01298–18 (2018).
50. Tee, H. S. et al. Tools for successful proliferation: diverse strategies of nutrient acquisition by a benthic cyanobacterium. *ISME J.* **14**, 2164–2178 (2020).

51. Chen, N. H., Djoko, K. Y., Veyrier, F. J. & McEwan, A. G. Formaldehyde Stress Responses in Bacterial Pathogens. *Front. Microbiol.* **7**, 257 (2016).
52. Denby, K. J. et al. The mechanism of a formaldehyde-sensing transcriptional regulator. *Sci. Rep.* **6**, 38879 (2016).
53. Echenique, J. R. et al. Acinetobacter baumannii has two genes encoding glutathione-dependent formaldehyde dehydrogenase: Evidence for differential regulation in response to iron. *Microbiology* **147**, 2805–2815 (2001).
54. Harms, N., Reijnders, W. N. M., Koning, S. & van Spanning, R. J. M. Two-Component System That Regulates Methanol and Formaldehyde Oxidation in Paracoccus denitrificans. *J. Bacteriol.* **183**, 664–670 (2001).
55. Weimer, E. P., Rao, E. & Brendel, M. Molecular structure and genetic regulation of SFA, a gene responsible for resistance to formaldehyde in Saccharomyces cerevisiae, and characterization of its protein product. *Mol. Gen. Genet. MGG* **237**, 351–358 (1993).
56. Chen, N. H. et al. A glutathione-dependent detoxification system is required for formaldehyde resistance and optimal survival of neisseria meningitidis in biofilms. *Antioxid. Redox Signal* **18**, 743–755 (2013).
57. Brzozowska, E., Pyra, A., Pawlik, K. & Gamian, A. The antibiofilm activity of dual-function tail tubular protein B from KP32 phage Abstract: *Preprints* **Preprints**, (2018).
58. Xiong, Z., Wang, Y., Dong, Y., Zhang, Q. & Xua, X. Cyanophage A-1(L) Adsorbs to Lipopolysaccharides of Anabaena sp. Strain PCC 7120 via the Tail Protein Lipopolysaccharide-Interacting Protein (ORF36). *J. Bacteriol.* **201**, 1–11 (2019).
59. Williamson, S. J. et al. The sorcerer II global ocean sampling expedition: Metagenomic characterization of viruses within aquatic microbial samples. *PLoS One* **3**, (2008).
60. Zborowsky, S. & Lindell, D. Resistance in marine cyanobacteria differs against specialist and generalist cyanophages. *Proc. Natl Acad. Sci. USA.* **116**, 16899–16908 (2019).
61. Bischoff, V., Zucker, F. & Moraru, C. Marine Bacteriophages. *Encycl. Virol.* **2021**, 322–341 (2021).
62. Mühling, M. et al. Genetic diversity of marine Synechococcus and co-occurring cyanophage communities: Evidence for viral control of phytoplankton. *Environ. Microbiol.* **7**, 499–508 (2005).
63. Kotera, M. et al. Sulfur is one of the essential elements, incorporated in proteins as thiol groups of cysteine residues as the result of anabolic reduction of sulfate. Sulfur also plays important roles in some cofactors such as molybdenum cofactor (Moco) and in modifi. *Genome Inform.* **24**, 104–115 (2010).
64. Delepelaire, P. Bacterial ABC transporters of iron containing compounds. *Res. Microbiol.* **170**, 345–357 (2019).
65. Nagayama, K. et al. Role of ABC transporter proteins in stress responses of Streptococcus mutans. *Oral. Health Dent. Manag* **13**, 359–365 (2014).
66. Tanaka, K. J., Song, S., Mason, K. & Pinkett, H. W. Selective substrate uptake: The role of ATP-binding cassette (ABC) importers in pathogenesis. *Biochim. Biophys. Acta - Biomembr.* **1860**, 868–877 (2018).
67. Pysz, M. A. et al. Transcriptional analysis of biofilm formation processes in the anaerobic, hyperthermophilic bacterium Thermotoga maritima. *Appl. Environ. Microbiol.* **70**, 6098–6112 (2004).
68. Liang, F. & Lindblad, P. Effects of overexpressing photosynthetic carbon flux control enzymes in the cyanobacterium Synechocystis PCC 6803. *Metab. Eng.* **38**, 56–64 (2016).
69. Bodor, A. M., Jänsch, L., Wissing, J. & Wagner-Döbler, I. The luxS mutation causes loosely-bound biofilms in Shewanella oneidensis. *BMC Res. Notes* **4**, 1–11 (2011).
70. Wu, S. et al. Biofilm-specific extracellular matrix proteins of nontypeable Haemophilus influenzae. *Pathog. Dis.* **72**, 143–160 (2014).
71. Tan, X. et al. Transketolase is involved in the control of Sigma B during chronic infection by Staphylococcus aureus. *bioRxiv* 538900 (2019).
72. Pettigrew, M. M. et al. Dynamic changes in the Streptococcus pneumoniae transcriptome during transition from biofilm formation to invasive disease upon influenza A virus infection. *Infect. Immun.* **82**, 4607–4619 (2014).
73. Zhang, P. et al. Cyanobacterial Dihydroxyacid Dehydratases Are a Promising Growth Inhibition Target. *ACS Chem. Biol.* **15**, 2281–2288 (2020).
74. Tan, K. et al. A review of allelopathy on microalgae. *Microbiol. (U. Kingd.)* **165**, 587–592 (2019).
75. Ma, H. et al. Growth inhibitory effect of Microcystis on Aphanizomenon flos-aquae isolated from cyanobacteria bloom in Lake Dianchi, China. *Harmful Algae* **42**, 43–51 (2015).
76. Gademann, K. Cyanobacterial natural products for the inhibition of biofilm formation and biofouling. *Chim. (Aarau)* **61**, 373–377 (2007).
77. Becher, P. G., Beuchat, J., Gademann, K. & Jüttner, F. Nostocarboline: isolation and synthesis of a new cholinesterase inhibitor from Nostoc 78-12A. *J. Nat. Prod.* **68**, 1793–1795 (2005).
78. Blom, J. F. et al. Potent Algicides Based on the Cyanobacterial Alkaloid Nostocarboline. *Org. Lett.* **8**, 737–740 (2006).
79. Jaki, B. et al. Novel extracellular diterpenoids with biological activity from the cyanobacterium Nostoc commune. *J. Nat. Prod.* **63**, 339–343 (2000).
80. Thanh Doan, N., Rickards, R. W., Rothschild, J. M. & Smith, G. D. Allelopathic actions of the alkaloid 12-epi-hapalindole E isonitrile and calothrixin A from cyanobacteria of the genera Fischerella and Calothrix. *J. Appl. Phycol.* **12**, 409–416 (2000).
81. Lane, D. J. 16S/23S rRNA sequencing. in *Nucleic Acid Techniques in Bacterial Systematics* 115–175 (John Wiley and Sons, 1991).
82. Nübel, U., Garcia-Pichel, F. & Muyzer, G. PCR primers to amplify 16S rRNA genes from cyanobacteria. *Appl. Environ. Microbiol.* **63**, 3327–3332 (1997).
83. Wright, E. S., Yilmaz, L. S. & Noguera, D. R. DECIPHER, a search-based approach to chimera identification for 16S rRNA sequences. *Appl. Environ. Microbiol.* **78**, 717–725 (2012).
84. Thompson, J. D., Higgins, D. G. & Gibson, T. J. CLUSTAL W: improving the sensitivity of progressive multiple sequence alignment through sequence weighting, position-specific gap penalties and weight matrix choice. *Nucleic Acids Res* **22**, 4673–4680 (1994).
85. Kumar, S., Stecher, G. & Tamura, K. MEGA7: Molecular Evolutionary Genetics Analysis version 7.0 for bigger datasets. *Mol. Biol. Evol.* **33**, msw054 (2016).
86. Darriba, D., Taboada, G. L., Doallo, R. & Posada, D. jModelTest 2: more models, new heuristics and parallel computing. *Nat. methods* **9**, 772 (2012).
87. Letunic, I. & Bork, P. Interactive Tree Of Life (iTOL) v5: an online tool for phylogenetic tree display and annotation. *Nucleic Acids Res* **49**, W293–W296 (2021).
88. Kotai, J. Instructions for the Preparation of Modified Nutrient Solution Z8 for Algae. *Norwegian Institute for Water Research, Oslo*, **5**, 11 (1972).
89. Taylor, D. A. *Introduction to Marine Engineering*. (Butterworth-Heinemann, 1996). https://doi.org/10.1016/B978-0-7506-2530-2.X5000-4.
90. Blain, S. et al. High frequency monitoring of the coastal marine environment using the MAREL buoy. *J. Environ. Monit.* **6**, 569–575 (2004).
91. Meireles, A. et al. Characterization of the heterotrophic bacteria from a minimally processed vegetables plant. *LWT - Food Sci. Technol.* https://doi.org/10.1016/j.lwt.2017.01.038 (2017).
92. Azevedo, N. F., Pacheco, A. P., Keevil, C. W. & Vieira, M. J. Adhesion of water stressed Helicobacter pylori to abiotic surfaces. *J. Appl. Microbiol.* **101**, 718–724 (2006).
93. Minchin, D. & Gollasch, S. Fouling and ships' hulls: How changing circumstances and spawning events may result in the spread of exotic species. *Biofouling*. **19**, 111–122 (2003).
94. Flemming, H.-C., Murthy, P. S., Venkatesan, R. & Cooksey, K. *Marine and Industrial Biofouling*. *Biofouling* vol. 4 (Springer Berlin Heidelberg, 2009).
95. Porra, R., Thompson, W. & Kriedemann, P. Determination of accurate extinction coefficients and simultaneous equations for assaying chlorophylls a and b extracted with four different solvents: verification of the concentration of chlorophyll standards by atomic absorption spectroscopy. *Biochim. Biophys. Acta* **975**, 384–394 (1989).
96. Wiśniewski, J. R., Zougman, A., Nagaraj, N. & Mann, M. Universal sample preparation method for proteome analysis. *Nat. Methods* **6**, 359–362 (2009).
97. Hughes, C. S. et al. Single-pot, solid-phase-enhanced sample preparation for proteomics experiments. *Nat. Protoc.* **14**, 68–85 (2019).
98. Osório, H. et al. Proteomics Analysis of Gastric Cancer Patients with Diabetes Mellitus. *J. Clin. Med.* **10**, 407 (2021).
99. Vizcaíno, J. A. et al. 2016 update of the PRIDE database and its related tools. *Nucleic Acids Res* **44**, D447–D456 (2016).
100. Dessau, R. B. & Pipper, C. B. ["R"-project for statistical computing]. *Ugeskr. Laeger*. **170**, 328–330 (2008).
101. Zhang, X. et al. Proteome-wide identification of ubiquitin interactions using UbIA-MS. *Nat. Protoc.* **13**, 530–550 (2018).
102. Ritchie, M. E. et al. Limma powers differential expression analyses for RNA-sequencing and microarray studies. *Nucleic Acids Res* **43**, e47 (2015).

ACKNOWLEDGEMENTS

This work was financially supported by: LA/P/0045/2020 (ALiCE), UIDB/00511/2020 and UIDP/00511/2020 (LEPABE), funded by national funds through FCT/MCTES (PIDDAC); project HealthyWaters (NORTE-01-0145-FEDER-000069), supported by Norte Portugal Regional Operational Programme (NORTE 2020), under the PORTUGAL 2020 Partnership Agreement, through the European Regional Development Fund (ERDF), and strategic funding UIDB/04423/2020 and UIDP/04423/2020 through national funds provided by FCT and ERDF, in the framework of the programme PT2020. This work was also supported by the FCT project MOREBIVALVES (PTDC/ASP-PES/31762/2017) and it had support from the Portuguese Mass Spectrometry Network, integrated in the National Roadmap of Research Infrastructures of Strategic

Relevance (ROTEIRO/0028/2013; LISBOA-01-0145-FEDER-022125). M.J.R. acknowledges a PhD grant from FCT (SFRH/BD/140080/2018).

AUTHOR CONTRIBUTIONS

Conceptualization, M.J.R., D.D-P., A.C., and F.J.M.; methodology, M.J.R., D.D-P. and J.M.; formal analysis, M.J.R., D.D-P., D.A., J.M., M.J.A., H.O., A.C.; resources, J.M., A.C., V.V. and F.J.M.; writing— M.J.R. and D.D-P.; writing—review and editing, D.A., J.M., M.J.A., H.O., A.C., V.V. and F.J.M.; supervision, F.J.M. All authors have read and agreed to the published version of the manuscript. M.J.R. and D.D.P. contributed equally to this work.

COMPETING INTERESTS

The authors declare no competing interests.

ADDITIONAL INFORMATION

Supplementary information The online version contains supplementary material available at https://doi.org/10.1038/s41522-022-00340-w.

Correspondence and requests for materials should be addressed to Filipe J. Mergulhão.

Reprints and permission information is available at http://www.nature.com/reprints

Publisher's note Springer Nature remains neutral with regard to jurisdictional claims in published maps and institutional affiliations.

Open Access This article is licensed under a Creative Commons Attribution 4.0 International License, which permits use, sharing, adaptation, distribution and reproduction in any medium or format, as long as you give appropriate credit to the original author(s) and the source, provide a link to the Creative Commons license, and indicate if changes were made. The images or other third party material in this article are included in the article's Creative Commons license, unless indicated otherwise in a credit line to the material. If material is not included in the article's Creative Commons license and your intended use is not permitted by statutory regulation or exceeds the permitted use, you will need to obtain permission directly from the copyright holder. To view a copy of this license, visit http://creativecommons.org/licenses/by/4.0/.

© The Author(s) 2022

ADDITIONAL INFORMATION

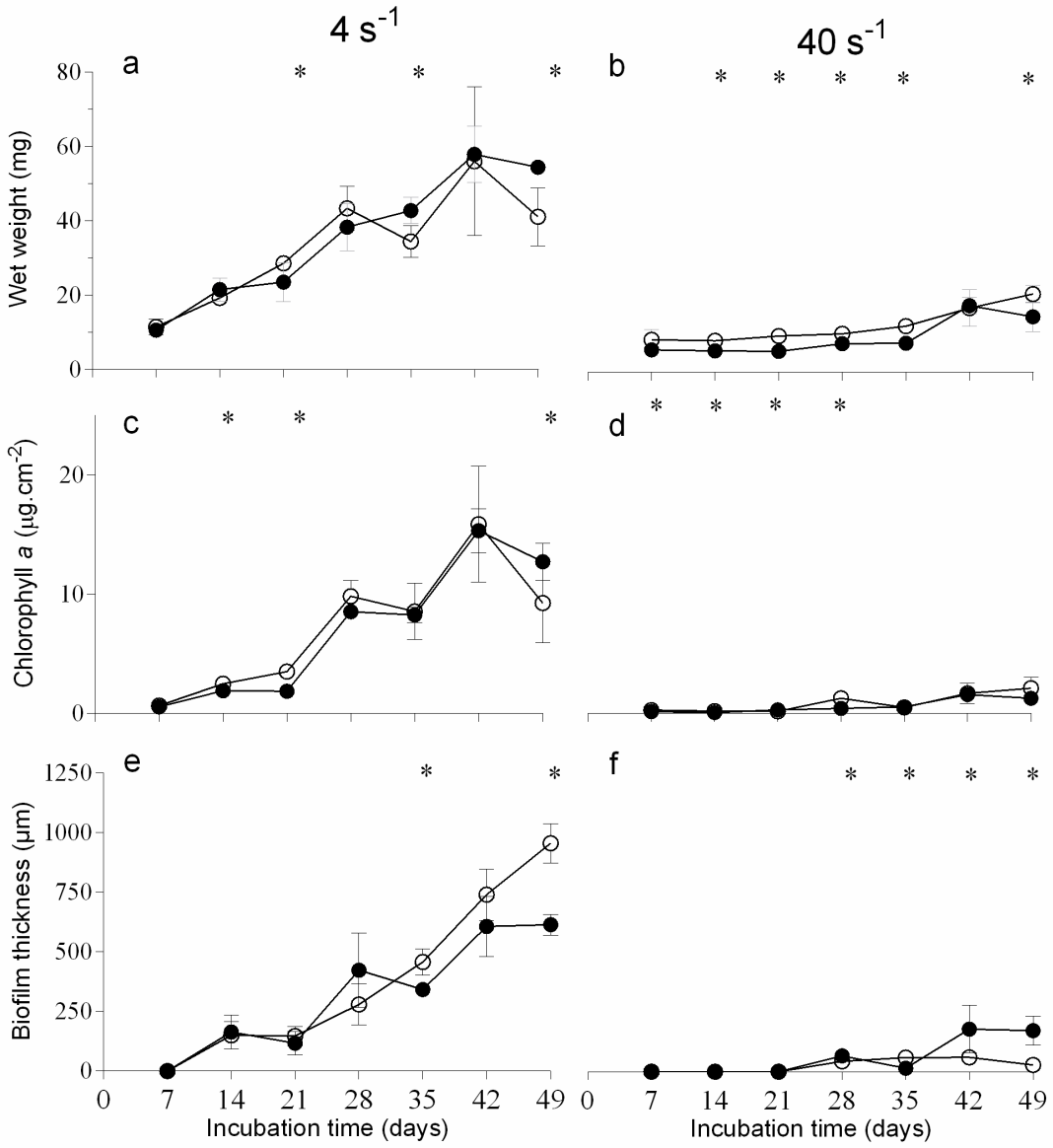

Supplementary Figure 1. Evaluation of unidentified filamentous Synechococcales LEGE 06021 biofilm development under the same hydrodynamic condition on different surfaces. The parameters analysed refer to wet weight (a, b), chlorophyll *a* quantification (c, d) and biofilm thickness (e, f). Biofilms were formed at 4 s^{-1} (a, c, e) or 40 s^{-1} (b, d, f) on two different surfaces, glass (closed circles) and perspex (open circles) for 49 days. Standard deviations from two biological assays with three replicates each are represented. Symbol * indicates statistically different values for $P < 0.05$ (unpaired t-tests) at each incubation time.

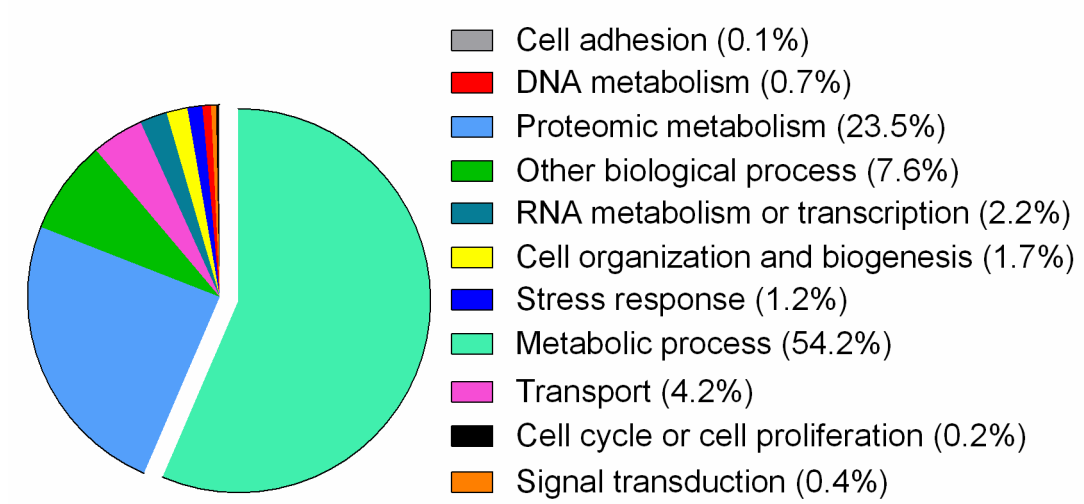

Supplementary Figure 2. Distribution of total proteins identified according to the biological process (34.8 % of proteins identified without an associated biological process are not shown in this graph).

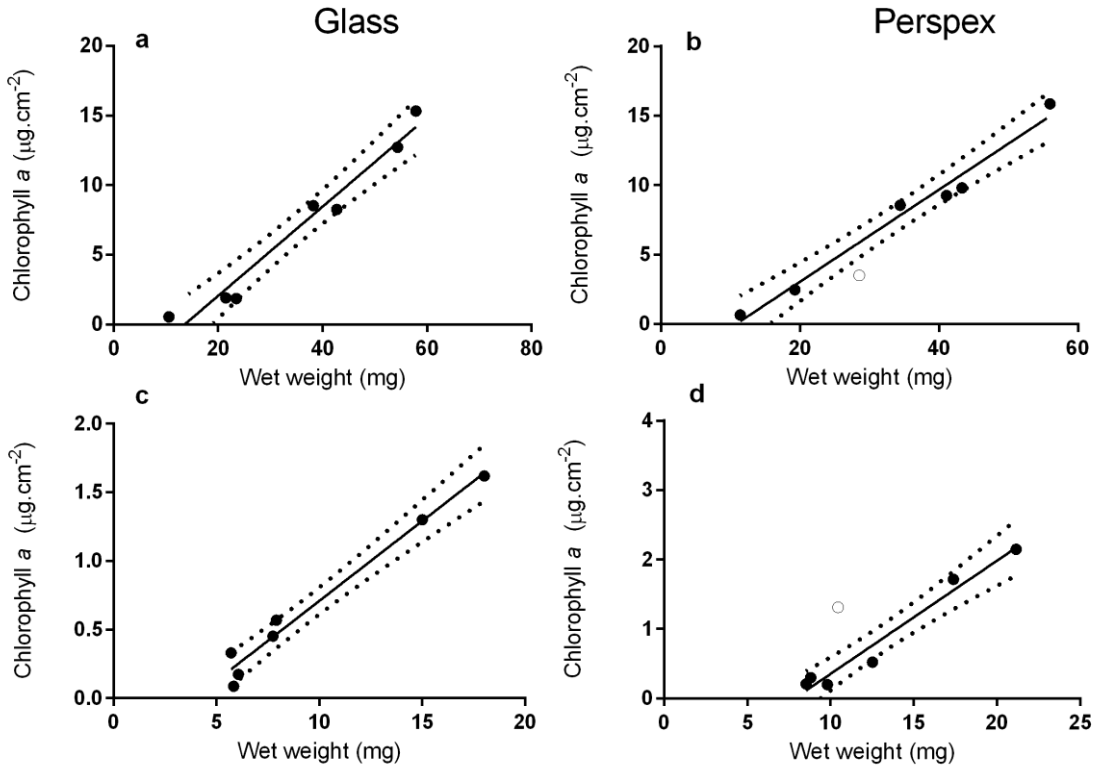

Supplementary Figure 3. Correlation between wet weight and chlorophyll *a* content on biofilm development from unidentified filamentous Synechococcales LEGE 06021. Biofilm development in glass (a, c) and perspex (b, d) at two different shear rates, 4 s^{-1} (a, b) and 40 s^{-1} (c, d). The full line represents the linear regression, and the dashed line represents the confidence limits (95 %). Closed symbols refer to data points that were considered for the regression (all except two), and open symbols refer to data points that were excluded from the regression.

Supplementary Table 1. Summary of proteomic analysis.

Available at https://www.nature.com/articles/s41522-022-00340-w

Supplementary Table 2. DEPs description and GO annotation.

Available at https://www.nature.com/articles/s41522-022-00340-w

FEMS Microbiology Ecology, 2023, **99**, 1–12
DOI: 10.1093/femsec/fiad004
Advance access publication date: 12 January 2023
Research Article

Characterization and biofouling potential analysis of two cyanobacterial strains isolated from Cape Verde and Morocco

Maria J. Romeu [1,2,†], João Morais[3,†], Luciana C. Gomes[1,2], Raquel Silva[3], Vítor Vasconcelos[3,4,*], Filipe J. M. Mergulhão[1,2,*]

[1]LEPABE - Laboratory for Process Engineering, Environment, Biotechnology and Energy, Faculty of Engineering, University of Porto, Rua Dr. Roberto Frias, 4200-465 Porto, Portugal
[2]ALiCE - Associate Laboratory in Chemical Engineering, Faculty of Engineering, University of Porto, Rua Dr. Roberto Frias, 4200-465 Porto, Portugal
[3]CIIMAR – Interdisciplinary Centre of Marine and Environmental Research, University of Porto, Terminal de Cruzeiros do Porto de Leixões, Av. General Norton de Matos s/n, 4450-208 Matosinhos, Portugal
[4]Department of Biology, Faculty of Sciences, University of Porto, Rua do Campo Alegre, 4169-007, Porto, Portugal
*Corresponding author. Chemical Engineering Department, Faculty of Engineering, University of Porto, Rua Dr. Roberto Frias 4200-465, Porto, Portugal; E-mail: filipem@fe.up.pt; Department of Biology, Faculty of Sciences, University of Porto, Rua do Campo Alegre, 4169-007, Porto, Portugal; E-mail: vmvascon@fc.up.pt.
†These authors contributed equally to this work.
Editor: [Martin W. Hahn]

Abstract

Cyanobacteria are new sources of value-added compounds but also ubiquitous and harmful microfoulers on marine biofouling. In this work, the isolation and identification of two cyanobacterial strains isolated from Cape Verde and Morocco, as well as their biofilm-forming ability on glass and Perspex under controlled hydrodynamic conditions, were performed. Phylogenetic analysis revealed that cyanobacterial strains isolated belong to *Leptothoe* and *Jaaginema* genera (*Leptothoe* sp. LEGE 181153 and *Jaaginema* sp. LEGE 191154). From quantitative and qualitative data of wet weight, chlorophyll *a* content and biofilm thickness obtained by optical coherence tomography, no significant differences were found in biofilms developed by the same cyanobacterial strain on different surfaces (glass and Perspex). However, the biofilm-forming potential of *Leptothoe* sp. LEGE 181153 proved to be higher compared with *Jaaginema* sp. LEGE 191154, particularly at the maturation stage of biofilm development. Three-dimensional biofilm images obtained from confocal laser scanning microscopy showed different patterns between both cyanobacterial strains and also among the two surfaces. Because standard methodologies to evaluate cyanobacterial biofilm formation, as well as two different optical imaging techniques, were used, this work also highlights the possibility of integrating different techniques to evaluate a complex phenomenon like cyanobacterial biofilm development.

Keywords: cyanobacteria characterization, cyanobacteria isolation, cyanobacterial biofilms, filamentous cyanobacteria, marine biofouling, surface effect

Introduction

Cyanobacteria are a widespread and significant group of photosynthetic prokaryotes responsible for the accumulation of oxygen in the Earth's environment (Lyons et al. 2014) and the evolution of eukaryotic organisms, according to the widely accepted endosymbiotic theory (Ku et al. 2015). They contribute to the nitrogen and carbon biogeochemical cycles, and can persist in harsh conditions due to their high adaptability (Berg and Sutula 2015, Anderson 2016). The metabolic flexibility between oxygen photosynthesis and respiration (Vermaas 2001, Mullineaux 2014) allows them to thrive in diverse environments. While some cyanobacteria can be associated with heterotrophic organisms in the desert to facilitate the productivity of soil crust (Pointing and Belnap 2012), some of them are the primary colonizers of ice sheets (Vincent 2000). Therefore, these particular bacteria are common in many habitats such as lakes, ponds, springs, wetlands, streams, rivers, soil crust, microbial mats, sands and rocks (Ramos et al. 2018). Cyanobacteria strains present considerable morphological diversity, comprising distinct degrees of complexity (Schirrmeister et al. 2011). When compared with unicellular coccoid morphology, the filamentous phenotype can be beneficial because it has a higher resistance to stress and predation, as well as improved resource acquisition (Claessen et al. 2014).

Cyanobacteria have been considered promising organisms for biotechnological processes due to the broad spectrum of secondary metabolites produced by some strains (Lau et al. 2015, Manirafasha et al. 2016). These added-value compounds can be applied to enhance the sustainable production of food and green energy sources (Singh et al. 2017), and they can also be used for medical purposes due to their antioxidant, anticancer and anti-inflammatory properties (Pagels et al. 2019). However, cyanobacteria can also have a detrimental impact on human purposes due to their ability to produce toxins (Breinlinger et al. 2021), promote cyanobacterial blooms (Huisman et al. 2018) and participate in the biofouling processes (Carvalho 2018). Marine biofouling consequences include environmental, economic, ecological and health concerns (Caruso 2020). The corrosion of different facilities and fouling in equipment may lead to incorrect measurements of submerged sensors and measuring devices, and high costs related to cleaning and/or repainting (Delauney et al. 2010),

Received: July 21, 2022. **Revised:** November 3, 2022. **Accepted:** January 5, 2023
© The Author(s) 2023. Published by Oxford University Press on behalf of FEMS. All rights reserved. For permissions, please e-mail: journals.permissions@oup.com

Downloaded from https://academic.oup.com/femsec/article/99/3/fiad004/6986251 by Universidade do Porto user on 14 March 2023

contributing to the industrial and economic consequences associated with biofouling. Moreover, the introduction and spread of invasive non-indigenous pathogens on marine vessels between different ecosystems (Davidson et al. 2009, Georgiades et al. 2021) and the contamination of aquaculture facilities (Bannister et al. 2019) may impact the ecology and global health. In the environmental field, marine biofouling can lead to increased fuel consumption by ships and, consequently, enhanced air pollution and greenhouse gas emissions (Hunsucker et al. 2018).

Marine biofouling is a complex process and it has been suggested that the adhesion and biofilm development by microfouler organisms may affect the continuous biofouling process, particularly for larval recruitment and settlement of macrofouler organisms (Antunes et al. 2019, Dobretsov and Rittschof 2020). Although their prevalence depends on the surface, geographical area and environmental settings, cyanobacteria are microfoulers and the major constituents of marine biofilms together with diatoms (Bharti et al. 2017, Antunes et al. 2020, Papadatou et al. 2021). These organisms produce extracellular polymeric substances (EPS), which are essential compounds of biofilm communities for maintaining their cohesion, structure and stability (Limoli et al. 2015, Rossi and De Philippis 2015, Anderson 2016).

Marine biofilms are affected by several factors, including physical, chemical and biological drivers (Caruso 2020, Faria et al. 2020b, 2021b). After the formation of the conditioning film comprising the adsorption of molecules (proteins, carbohydrates, etc.) from the surrounding environment, the second step in the biofouling process involves cell adhesion. Surface binding is considered a critical survival mechanism for enhancing organism interactions and accessing nutritional resources (Dang and Lovell 2016). Different materials are used in marine submerged man-made equipment, like aquaculture facilities (King et al. 2006, Cai and Arias 2017), underwater windows, sensors and measuring devices (Roy 1994, Taylor 1996, Davies and Rajapakse 2013), protective equipment, swim platforms, ship and boat structures and anchors (Taylor 1996, Mansour and Liu 2008, Molland 2008, Davies and Rajapakse 2013), which are susceptible to biofouling. Therefore, studies focused on the effects of substrate properties and organisms' variability in the growth stages of biofilms, and their composition, structure and behavior, are of great importance (Faria et al. 2020a, 2021a, c). Indeed, previous studies showed a broad diversity in the protein expression profiles of cyanobacterial biofilms isolated from different sites (Romeu et al. 2020), which may be a result of the adaptation of these organisms to the specific environmental niche that they occupy, such as their site of isolation and the nutritional availability at that site (Bragg et al. 2006, Lv et al. 2008). Through the simultaneous analysis of physiological characteristics, the distribution in the environment and the genome and/or proteomic profiles, it is possible to identify the environmental factors that are most important to drive evolution and shape populations. For instance, greater depths are associated with lower light intensity and temperature, but also with higher content of phosphorus (Coleman and Chisholm 2007). For instance, to the cyanobacterium *Prochlorococcus*, phosphorus availability is a key ecological factor and potential driver of evolution (Lv et al. 2008). Different *Prochlorococcus* strains possess distinct physiological adaptations for dealing with the low phosphorus availability, including the replacement of phospholipids with sulfolipids (Van Mooy et al. 2006), growth in a more limited range of phosphorus sources (Moore et al. 2005) and the upregulation of known phosphorus-assimilation genes and novel genes, which may enable them to tolerate phosphorus starvation periods (Martiny et al. 2006). Moreover, recent metagenomic studies showed that the abundance of phosphate transport genes is also correlated with phosphorus availability (Rusch et al. 2007). In the low-phosphorus waters of the Caribbean, the gene encoding a phosphate-binding protein is more abundant compared with the higher-phosphorus waters of the Pacific.

The main novelty of this study is the isolation, identification (morphological characterization) and assessment of the biofilm-formation potential of cyanobacterial strains isolated from under-explored marine environments and locations along the coast of Cape Verde and Morocco. These are locations with unknown biodiversity that will provide new knowledge and tools to help understand the impact of global changes in temperate areas. Cyanobacterial strains from these genera seem to be quite frequent, at least in the Atlantic Ocean, North Aegean Sea and Mediterranean Sea (Foster et al. 2009, Konstantinou et al. 2018, 2019, Ramos et al. 2018). As they are distributed around dissimilar geographies, including different continents and port areas, this cosmopolitan distribution highlights the importance of studying biofilm formation by these organisms, which, in turn, present a significant concern to public health, environment and aquatic ecology . Given the relevance of cyanobacteria to marine biofouling, their biofilm-forming ability was assessed for the first time in a long-term assay under controlled hydrodynamic conditions that mimics marine environments (Romeu et al. 2019), and using two different surfaces as the substratum for biofilm formation (glass and Perspex). These materials represent submerged artificial surfaces typically found on different aquatic apparatus such as sensors, flotation spheres, moored buoys, underwater cameras, aquaculture equipment, measuring devices, or even in underwater windows of boats (Taylor 1996, Blain et al. 2004, King et al. 2006) that can be affected by biofouling. Additionally, given the broad spectrum of promising secondary metabolites and value-added compounds produced by cyanobacteria (Lau et al. 2015) that can be used in biotechnological applications, cosmetics, feed and food industries (Manirafasha et al. 2016) and for medical purposes (Pagels et al. 2019), this kind of study can also be useful in different research fields.

Materials and methods

Sampling and isolation

Environmental samples were collected on 11 July 2019, near Mrizika Beach, Morroco (32°57'31.3'N 8°46'34.1'W), from a dried soil crust, and on 24 April 2019, at Calhau, Cape Verde (São Vicente Island–16°51'07.6'N 24°51'58.8'W), scraping from a port boat ramp with the help of a previously cleaned knife (Fig. 1). Samples were transferred to 15-ml tubes with Z8 medium (Kotai 1972) supplemented with 25 $g.l^{-1}$ of synthetic sea salts (Tropic Marin) and B_{12} vitamin (Sigma Aldrich, Merck, Saint Louis, MO, USA) (Croft et al. 2006, Helliwell et al. 2016) until further analysis. Isolation of cyanobacterial isolates was performed using the streak plate method (Rippka 1988). Briefly, using a sterile plastic Pasteur pipette, a homogeneous drop from each environmental sample was inoculated in different agar plates with Z8 medium, and with a loop, each sample was spread, making successive smears in the different quadrants of the plate. After approximately 1 month of growth under 14-h light (10–30 μmol photons m^{-2} s^{-1})/10-h dark cycles, at 25°C, isolated cells or filaments were picked up using a sterile surgical blade and transferred to 50-ml culture flasks with a liquid medium, growing in the previously described conditions. After 2–3 weeks of growth, isolation was confirmed by checking samples under the microscope.

Downloaded from https://academic.oup.com/femsec/article/99/3/fiad004/6986251 by Universidade do Porto user on 14 March 2023

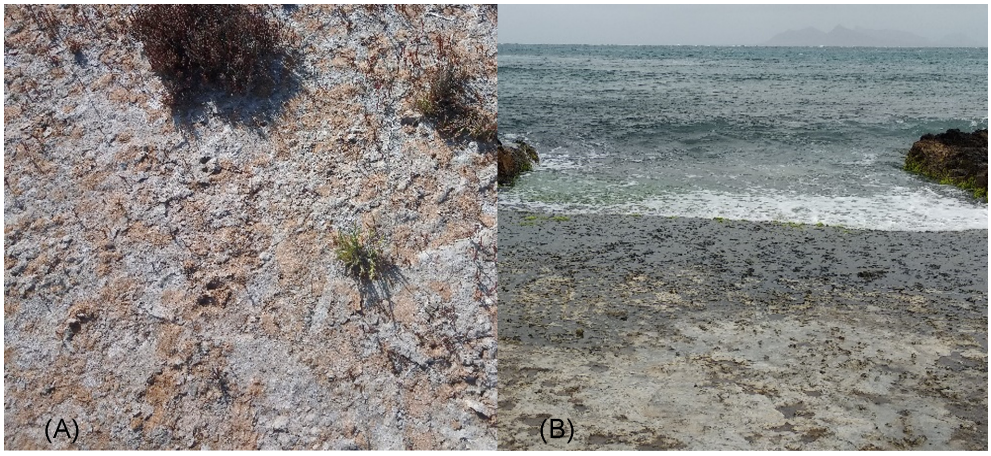

Figure 1. Sampling locations: (**A**) dried soil crust near Mrizika Beach, Morocco; (**B**) green mat on ramp port for boats at Calhau, São Vicente Island, Cape Verde.

DNA extraction, 16S rRNA gene amplification (PCR) and sequencing

The two filamentous cyanobacterial isolates obtained in this work were grown in 50-ml flasks in the conditions previously described and harvested by centrifugation (5000 *g* for 5 min at 4°C) after 2–3 weeks. Total genomic DNA was extracted using the commercial PureLink Genomic DNA Mini Kit (Invitrogen, USA), according to the manufacturer's instructions provided for Gram-negative bacteria. To obtain the 16S rRNA gene sequence, PCR amplification was performed using the oligonucleotide primers set 27F and 23S30R (Table 1). PCR reactions were performed in a final volume of 20 μl containing 1× Green GoTaq Flexi Buffer, 2.5 mM of $MgCl_2$, 125.0 mM of each deoxynucleotide triphosphate, 1.0 μM of each primer, 0.5 U of GoTaq Flexi DNA Polymerase (Promega, Madison, WI, USA), 10 mg.ml^{-1} of bovine serum albumin and 10–30 ng of template DNA, on a Veriti™ 96-Well Thermal Cycler (Applied Biosystems™, USA). The PCR conditions were as follows: initial denaturation at 94°C for 5 min, followed by 10 cycles of denaturation at 94°C for 45 s, annealing at 57°C for 45 s and extension at 72°C for 2 min, followed by 25 cycles of denaturation at 92°C for 45 s, annealing at 54°C for 45 s and extension at 72°C for 2 min with a final elongation step at 72°C for 7 min. The PCR reactions were performed in duplicate. PCR products were separated by 1.5% agarose gel stained with SYBR® safe (Invitrogen, Waltham, MA, USA), and DNA fragments with the expected size were excised and purified using NZYGelpure (NzyTech, Genes and Enzymes, Lisbon, Portugal) according to the manufacturer's instructions. Because the sequences were obtained by direct sequencing of purified amplicons, CYA359F, CYA781R and 1494R internal primers (Table 1) were used to improve the quality of the sequences. Sequencing was performed at GATC Biotech (Ebersberg, Germany) and the nucleotide sequences obtained were manually inspected for quality and assembled using the Geneious 11.1.5 software (Biomatters Ltd., Auckland, New Zealand). Possible chimera formation during the sequences was checked using the software DECIPHER (Wright et al. 2012). The sequences obtained were inserted in the BLASTn (Basic Local Alignment and Search Tool for Nucleotides) database and the results were analyzed. The sequences associated with this study were deposited in the GenBank database under the accession numbers ON311284 and ON311285.

Phylogenetic analysis

A total of 58 sequences were used in the final analysis, including two strains of *Gloeobacter violaceus* as an outgroup, 56 sequences of cyanobacteria, including type, reference and related strains belonging to the orders Pseudanabaenales and Synechococcales, were retrieved from GenBank (National Center for Biotechnology Information, NCBI, Bethesda, MD, USA), and two sequences of isolates obtained in this work. Multiple sequence alignment was carried out using ClustalW in MEGA7 (Thompson et al. 1994, Kumar et al. 2016), and sequences were manually proofread and edited. The best fit model was assessed using jModelTest 2.1.10 (Darriba et al. 2012) according to the Bayesian information criterion and Akaike information criterion scores. Maximum likelihood analysis was carried out using substitution model GTR+G+I with 1000 bootstrap resampling replicates using the MEGA7 software (Kumar et al. 2016). The final phylogenetic tree was visualized and edited on Interactive Tree of Life (Letunic and Bork 2021).

Light microscopy and morphological characterization

Morphological features (e.g. cell dimensions, shape, color, sheath, constriction at cross walls, specialized cells or shape of apical cells) of cyanobacterial strains isolated in this work were examined and imaged using a Leica DMLB light microscope coupled to a Leica ICC50 HD digital camera (Leica Microsystems, Germany). For each strain, microphotographs were taken using 400x and 1000x magnifications. Morphometric measurements were then performed using the image analysis software Leica Application Suite version 4.2.0 (Leica Microsystems). Cell dimensions were determined by measuring at least 20–30 cells for each strain along different positions of the slide preparation.

Biofilm formation assay

Cyanobacterial isolates were grown in 750 ml of Z8 medium (Kotai 1972) supplemented with 25 g.l^{-1} of synthetic sea salts (Tropic Marin) and B_{12} vitamin (Sigma Aldrich, Merck, Saint Louis, MO, USA), under 14-h light (10–30 μmol photons m^{-2} s^{-1})/10-h dark cycles at 25°C. To assess the biofilm-forming ability of both strains on different surfaces, biofilms were developed on

Downloaded from https://academic.oup.com/femsec/article/99/3/fiad004/6986251 by Universidade do Porto user on 14 March 2023

Table 1. Oligonucleotide primers used for 16S rRNA amplification.

Primer	Sequence 5′-3’	Reference
27F	AGAGTTTGATCCTGGCTCAG	(Lane, 1991)
359F	GGGGAATYTTCCGCAATGGG	(Nübel et al., 1997)
781R	GACTACWGGGGTATCTAATCCCWTT	(Nübel et al., 1997)
1494R	TACGGCTACCTTGTTACGAC	(Lane, 1991)
23S30R	CTTCGCCTCTGTGTGCCTAGGT	(Lepère et al., 2000)

commercial Perspex (Poly(methyl methacrylate)) surfaces (Neves & Neves, Lda, Portugal) and glass (Vidraria Lousada, Lda, Portugal) coupons (1 cm^2). Surface sterilization and preparation were performed as previously described (Romeu et al. 2019). Biofilms were formed on agitated 12-well microtiter plates (VWR International, Carnaxide, Portugal) because this platform was shown to mimic the hydrodynamic conditions found in marine environments (Romeu et al. 2019). To attain the shear rate values of aquatic environments, such as those found in a ship hull in a harbor (Bakker et al. 2003) and in partially submerged or even moored equipment and devices (average shear rate of 40 s^{-1}), microtiter plates were incubated at 25°C in an orbital shaker with a 25-mm orbital diameter (Agitorb 200ICP, Norconcessus, Portugal) at 185 rpm (Romeu et al. 2019). Biofilm formation in this system was shown to predict the biofouling behavior observed upon immersion in the sea for prolonged periods (Silva et al. 2021). Prior to inoculation, the cyanobacterial suspensions were adjusted to a chlorophyll *a* concentration of 1.5 $\mu g.ml^{-1}$ because chlorophyll *a* is commonly used as a biomass indicator in aquatic environments (Romeu et al. 2019, 2021). Briefly, 2 ml of cyanobacterial suspension were incubated at 4°C in the dark for maximal chlorophyll *a* extraction. After 24 h, the samples were centrifuged at 3202 *g* (Eppendorf Centrifuge 5810R, Hamburg, Germany) for 5 min at room temperature, and the supernatant was transferred to a glass cuvette. The absorbance at 750 nm (turbidity), 665 nm (chlorophyll *a*) and 652 nm (chlorophyll *b*) was determined using a V-1200 spectrophotometer (VWR International China Co., Ltd, Shanghai, China). The chlorophyll *a* concentration was calculated through the following equation (Porra et al. 1989):

$$\text{Chl } a\ (\mu g.\text{ml}^{-1}) = 16.29 \times A^{665} - 8.54 \times A^{652} \quad (1)$$

These measurements were assessed in triplicate, and dilutions were performed using Z8 medium supplemented with 25 $g.l^{-1}$ of synthetic sea salts and vitamin B_{12} (Sigma Aldrich). Then a volume of 3 ml of each cyanobacterial suspension (previously adjusted to chlorophyll *a* concentration of 1.5 $\mu g.ml^{-1}$) was inoculated in each well, in which coupons of each surface were previously fixed with transparent double-sided adhesive tape. Biofilm development was followed for 49 days (7 weeks) because it is accepted that a 2-month interval is the minimum duration for economically viable underwater monitoring systems (Blain et al. 2004, Romeu et al. 2019). During this incubation time, the medium was replaced twice a week. Moreover, to mimic real light exposure periods, a photoperiod of 14-h light (8–10 μmol photons m^{-2} s^{-1})/10-h dark cycles was applied.

Biofilm analysis

Biofilm analysis was performed every 7 days, in which two coupons of each surface were analyzed. The culture medium was carefully removed by gentle pipetting, and the wells were filled with 3 ml of sterile sodium chloride solution (8.5 $g.l^{-1}$) (Romeu et al. 2019). The solution was carefully removed to eliminate loosely attached cyanobacteria and, subsequently, the wells were filled again with 3 ml of sterile sodium chloride solution to evaluate the thickness and structure of the cyanobacterial biofilms by optical coherence tomography (OCT). To complement the characterization of cyanobacterial biofilms, the determination of their wet weight and chlorophyll *a* content was also performed over the 7 weeks. At the last sampling point (49 days), cyanobacterial biofilms of both strains formed on both surfaces were also analyzed by confocal laser scanning microscopy (CLSM).

Optical coherence tomography

Images from cyanobacterial biofilms developed on both surfaces were captured as reported in Romeu et al. (2019). For each coupon, two-dimensional (2D) imaging was performed with a minimum of three fields of view to ensure the reliability and accuracy of the results obtained. Image analysis was performed using a routine developed in the Image Processing Toolbox from MATLAB 8.0 and Statistics Toolbox 8.1 (MathWorks, Natick, MA, USA) as described in Romeu et al. (2020). The mean of biofilm thickness was calculated based on the distance between the biofilm bottom and the upper contour line according to the following equation (2):

$$\bar{L}_F = \frac{1}{N}\sum_{i=1}^{N} L_{F,i} \quad (2)$$

where $L_{F,i}$ is a local biofilm thickness measurement at location *i*, *N* equals the number of thickness measurements and $\bar{L}_F$ is the mean biofilm thickness.

Wet weight determination and chlorophyll a quantification

After OCT analysis, the determination of the biofilm wet weight and chlorophyll *a* content was performed as previously reported (Romeu et al. 2021). To determine the wet weight, sterile sodium chloride solution (8.5 $g.l^{-1}$) was carefully removed from the wells, and coupons were detached and weighed. The biofilm wet weight was obtained as the difference from the initial coupon weight, which was determined prior to inoculation. Subsequently, cyanobacterial cells were detached from the coupons by immersing each coupon in 2 ml of 8.5 $g.l^{-1}$ sodium chloride solution and vortexing (Romeu et al. 2019). The suspensions were incubated for 24 h at 4°C in the dark, and chlorophyll *a* determination was performed through Equation 1.

Confocal laser scanning microscopy

At the last sampling point (day 49), additional coupons were removed from the microplates, washed with saline solution and the biofilms were stained for 10 min with 6-μM cell-permeant nucleic acid markers: biofilms formed by the cyanobacterial strain isolated from Morocco (*Jaaginema* sp. LEGE 191154) were stained with SYTO®9 (a green fluorescent stain; Thermo Fisher Scientific, Waltham, MA, USA), whereas biofilms formed by the cyanobacterial strain isolated from Cape Verde (*Leptothoe* sp. LEGE 181153)

Downloaded from https://academic.oup.com/femsec/article/99/3/fiad004/6986251 by Universidade do Porto user on 14 March 2023

were marked with SYTO®61 (a red fluorescent stain; Thermo Fisher Scientific). Both stains were chosen to match the colors of cyanobacteria pigments visible by optical microscopy, as well as to have minimal interference. Each stained biofilm was mounted on a microscopic slide and image acquisition was performed using a Leica TCS SP5 II confocal laser scanning microscope (Leica Microsystems, Wetzlar, Germany). All biofilms were scanned using a 40× water objective lens (LEICA HCX PL APO CS 40.0x/1.10WATER UV) using a protocol previously described (Faria et al. 2020a, 2021a) with some modifications. Given the used stains, *Jaaginema* sp. LEGE 191154 biofilms were observed with a 488-nm argon laser, whereas *Leptothoe* sp. LEGE 181153 biofilms were imaged with a 633-nm helium-neon laser. A minimum of five stacks of horizontal-plane images (512×512 pixels, corresponding to 387.5 μm x 387.5 μm) with a z-step of 1 μm were acquired per sample.

Three-dimensional (3D) projections of the biofilms were constructed from the CLSM acquisitions using the 'Easy 3D' function of the IMARIS 9.1 software (Bitplane, Zurich, Switzerland). Biovolume ($\mu m^3.\mu m^{-2}$) was extracted from confocal image series with the plug-in COMSTAT2 (Heydorn et al. 2000) run in ImageJ 1.48v software (National Institutes of Health, Bethesda, MD, USA).

Statistical analysis

A total of four replicates (two biological assays with two technical replicates each) were analyzed. Data analysis was performed using the statistical program GraphPad Prism® for Windows, version 6.01 (GraphPad Software, Inc., San Diego, CA, USA). The D'Agostino-Pearson and Shapiro-Wilk normality tests were performed to check if the data distribution presented a normal distribution. Differences between biofilm wet weight, chlorophyll *a* quantification, biofilm thickness obtained by OCT and biovolume obtained by CLSM were evaluated using the unpaired, non-parametric Mann-Whitney test because the variables were not normally distributed. The error bars shown in the graphs correspond to the standard deviation of the mean. Statistically significant differences were considered for P values < 0.05 (corresponding to a confidence level greater than 95%; and asterisks * and ** denote significance where $P < 0.1$ and $P < 0.05$, respectively).

Results and Discussion

Phylogenetic analysis

The phylogenetic analysis of the 16S rRNA gene (Fig. 2) showed that the sequence from the cyanobacterium isolated from Cape Verde (*Leptothoe* sp. LEGE 181153) belongs to the *Leptothoe* clade, a recent genus described by Konstantinou et al. (2019), a clade with previous *Leptolyngbya* members but not related to the true (sensu stricto) *Leptolyngbya* clade. Sequence from the cyanobacterium isolated from Morocco (*Jaaginema* sp. LEGE 191154) fits in the *Jaaginema* clade, which consists of *Jaaginema litorale* LEGE 07176, a strain isolated from a wave-exposed rock on the Portuguese Coast (Ramos et al. 2018), *Jaaginema geminatum* SM S13 isolated from a hot spring in Iran (Heidari et al. 2018), *Jaaginema* sp. PsrJGgm14, from Psoroneria, a hot spring in Greece, *Jaaginema* sp. PMC 1079.18 and *Jaaginema* sp. PMC 1080.18, isolated from a dense periphytic biofilm covering the immersed branch fragment, Guadeloupe (Duperron et al. 2019), *Jaaginema* sp. TAU-MAC 1418 (Panou and Gkelis 2022), *Jaaginema* sp. ThrJGgm18 from Thermopyles Thermal Springs in Greece and *Jaaginema* sp. IkpSMP32, isolated from Apolon hot spring, also in Greece. The two cyanobacterial isolates obtained in this work were deposited at the Blue Biotechnology and Ecotoxicology Culture Collection (LEGE-CC) located at CIIMAR, Portugal (Ramos et al. 2018), under the names of *Leptothoe* sp. LEGE 181153 (cyanobacterial strain isolated from Cape Verde) and *Jaaginema* sp. LEGE 191154 (cyanobacterial strain isolated from Morocco).

Morphological description

Leptothoe sp. LEGE 181153 filaments present a single trichome per sheath, unbranched, straight to curved, occasionally wavy, densely and irregularly entangled. Sheaths are colorless, thin and slightly distinct. Trichomes are cylindrical, slightly constricted at the cross walls and pinkish. Cells are typically barrel-shaped, isodiametric to longer than wide, 2.0 ± 0.3 μm in length and 1.5 ± 0–2 μm in width. Cell content is homogeneous. Apical cells are rounded (Fig. 3A and C).

Jaaginema sp. LEGE 191154 presents blue-green filaments, unbranched, straight to curved and entangled in clusters, and without sheaths (sometimes with a fine mucilaginous layer around the trichomes). Trichomes can vary from not constricted to slightly constricted at the cross walls. Cells are cylindrical, longer than wide, 4.6 ± 1.1 μm in length and 2.7 ± 0.3 μm in width. Cell content is homogeneous. Apical cells are narrowed or rounded, without calyptra (Fig. 3B and D).

Biofilm development

The biofilm-forming capacity of the *Jaaginema* sp. LEGE 191154 and *Leptothoe* sp. LEGE 181153 strains on two different surfaces (glass and Perspex) was assessed. Results obtained for wet weight, chlorophyll *a* content and biofilm thickness for both cyanobacterial strains over 49 days are presented in Fig. 4. The values regarding the biofilm thickness (Fig. 4E and F) are indicated from day 21 because the biofilm thickness was below the OCT range on the first two sampling days. Biofilm development was similar for both cyanobacteria, regardless of the surface material, and the major differences between the strains were observed for the biofilm thickness parameter (Fig. 4E and F). This tendency was more evident in biofilm thickness values obtained for glass (Fig. 4E) from 35 to 49 days, which corresponds to a maturation stage of biofilm development. Interestingly, previous studies performed with filamentous (Romeu et al. 2019, 2020, 2021) and coccoid cyanobacteria (Faria et al. 2020b) also showed major differences in biofilm development in their maturation phase. The effects of different conditions may be less noticeable in the initial steps of biofilm formation, while the maturation stage promotes significant variances in biofilm composition and structure.

Also noteworthy is the behavior of both cyanobacterial biofilms developed on glass (Fig. 4A, C and E). While for wet weight and biofilm thickness, the values were similar up to 28 days and increased on *Leptothoe* sp. LEGE 181153 biofilms from 35 to 49 days, for chlorophyll *a* quantification, a different trend between cyanobacterial strains was observed over the 49 days. Indeed, biofilm mass and thickness obtained from 35 to 49 days for *Jaaginema* sp. LEGE 191154 were on average 29% and 54% lower, respectively, compared with the values obtained for *Leptothoe* sp. LEGE 181153 strain over the same period (Fig. 4A and E). In turn, chlorophyll *a* quantification obtained from 7 to 28 days for *Leptothoe* sp. LEGE 181153 was on average 77% lower compared with the values obtained for *Jaaginema* sp. LEGE 191154 (Fig. 4B), but from 35 to 49 days, the chlorophyll *a* amount of *Jaaginema* sp. LEGE 191154 biofilms was on average 58% lower compared with the values obtained for *Leptothoe* sp. LEGE 181153 (Fig. 4B), which supports the results obtained for wet weight and biofilm thickness on the

Downloaded from https://academic.oup.com/femsec/article/99/3/fiad004/6986251 by Universidade do Porto user on 14 March 2023

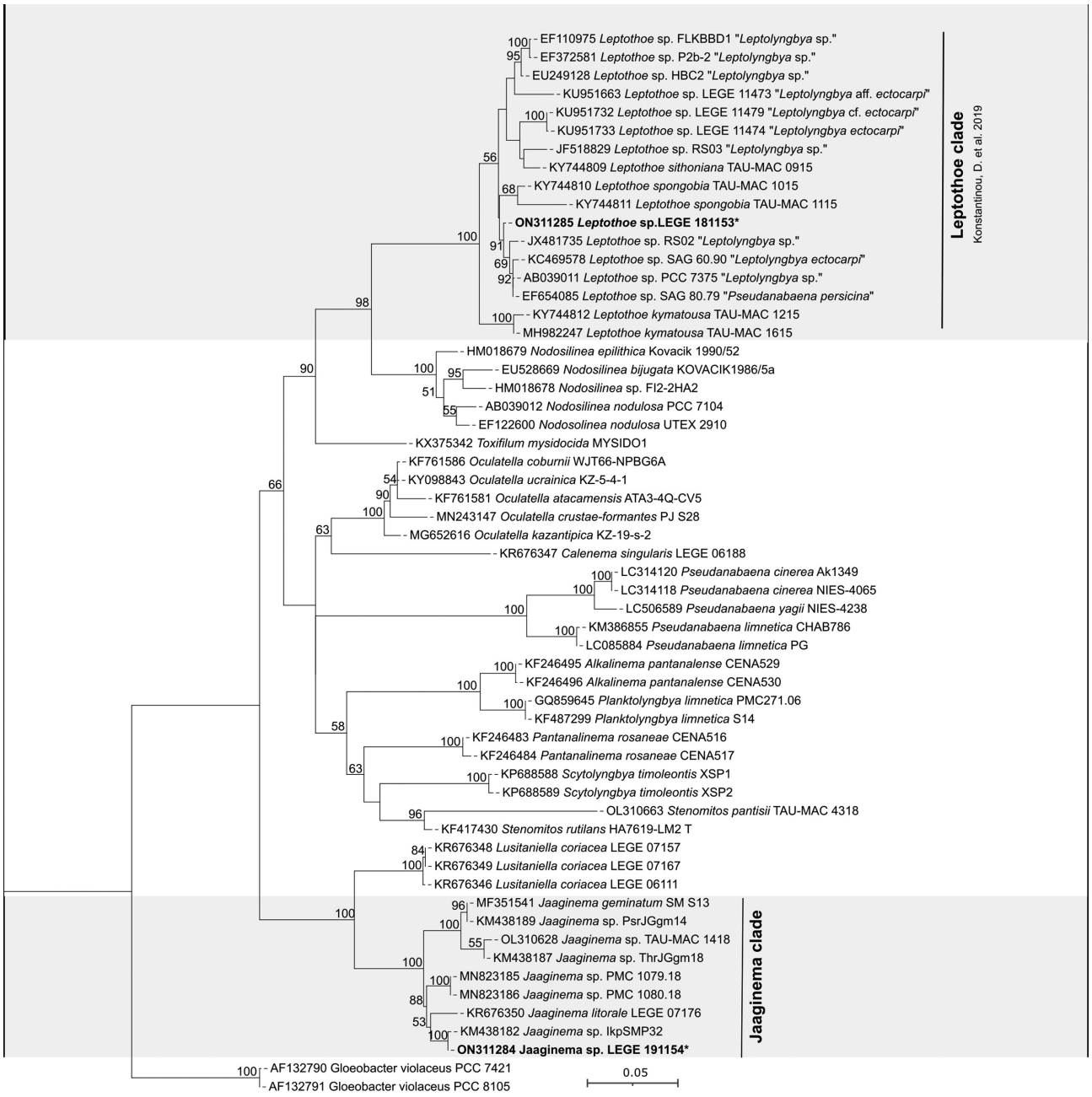

Figure 2. Maximum likelihood (ML) phylogenetic tree based on 58 partial 16S rRNA gene sequences of cyanobacterial strains belonging to the orders Pseudanabaenales and Synechococcales. *Gloeobacter violaceus* PCC 7421 and *Gloeobacter violaceus* PCC 8105 were used as outgroups. Phylogenetic positions of *Leptothoe* sp. LEGE 181153 and *Jaaginema* sp. LEGE 191154 are indicated in bold and with a black star. Bootstrap values over 50% are indicated at the nodes. Strains labeled with quotes indicate that names correspond to Genbank labels.

same days (Fig. 4A and E) . Chlorophyll *a* monitorization has been used to follow cyanobacterial biofilm growth (Romeu et al. 2019, 2020, 2021). Considering the similarity of values obtained for wet weight and biofilm thickness up to 28 days, and the opposite trend of chlorophyll *a* quantification during this period, two hypotheses arise. First, *Leptothoe* sp. LEGE 181153 biofilms developed from 7 to 28 days may contain a higher percentage of EPS and/or of void spaces/porous structure filled with water, which can contribute to the higher values of biofilm biomass and thickness, having no impact on chlorophyll *a* level. In turn, cyanobacterial cells in these initial stages of biofilm development may be metabolically less active, contributing to the low chlorophyll *a* amount detected. Additional analysis of empty spaces from 2D cross-sectional OCT images obtained for *Leptothoe* sp. LEGE 181153 biofilms formed on glass (Supplementary Data, Fig. 1. Evaluation of biofilm empty spaces) revealed that the percentage of empty spaces in biofilms developed in the initial stage (21 and 28 days) was similar to the values obtained for the later stages of biofilm development (35 and 42 days), and even lower than those obtained for the last day (49 days). Hence, a porous architecture was not detected in the early biofilm growth stage. Moreover, previous studies on filamentous (Romeu et al. 2019, 2020, 2022) and coccoid (Faria et al. 2020b) cyanobacterial biofilms also showed that in the initial stages of biofilm development, the chlorophyll *a* amount is lower than that

Downloaded from https://academic.oup.com/femsec/article/99/3/fiad004/6986251 by Universidade do Porto user on 14 March 2023

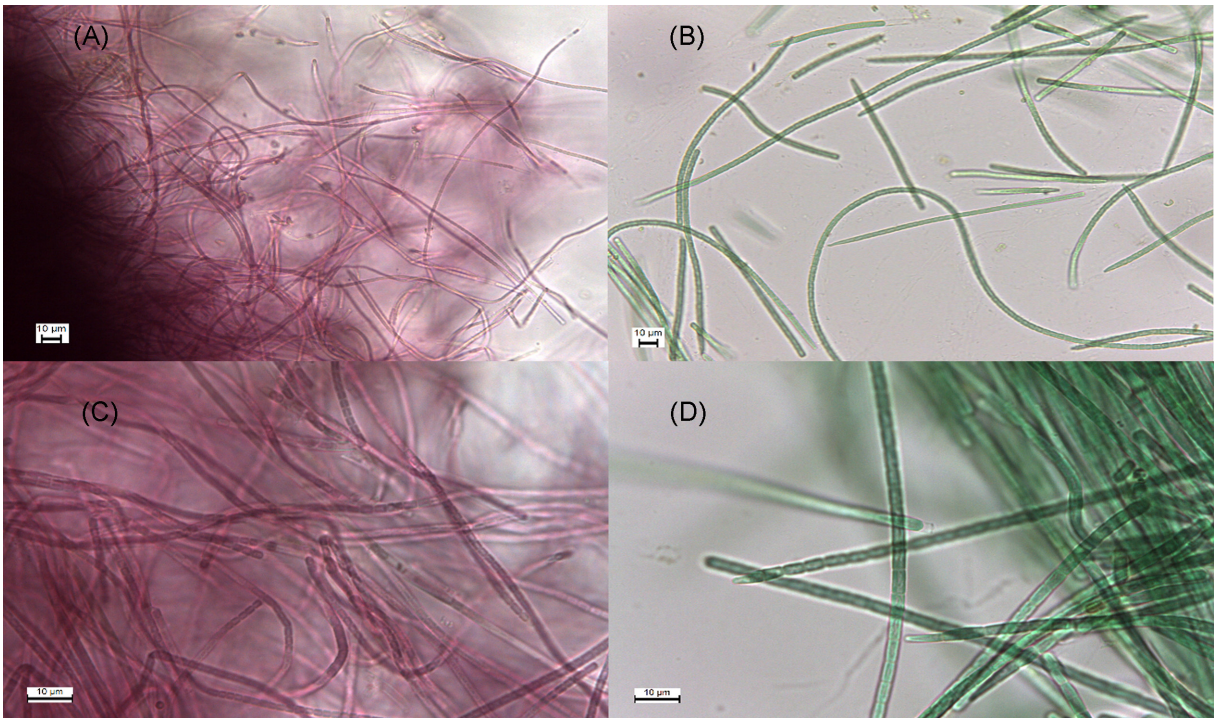

Figure 3. Light microscopy of (**A**) *Leptothoe* sp. LEGE 181153 (400x); (**B**) *Jaaginema* sp. LEGE 191154 (400x); (**C**) *Leptothoe* sp. LEGE 181153 (1000x); (**D**) *Jaaginema* sp. LEGE 191154 (1000x). Scale bars = 10 μm.

detected in the later stages of biofilm development. Therefore, it is more reasonable that *Leptothoe* sp. LEGE 181153 biofilms developed from 7 to 28 days presented metabolically less active cells and consequently low chlorophyll *a* production.

For both cyanobacterial strains, the biofouling potential on the two surfaces (glass and Perspex) was similar (Supplementary Data, Fig. 2. Evaluation of biofilm development on different surfaces). The major difference was observed for biofilm thickness obtained for the *Leptothoe* sp. LEGE 181153 strain at day 42 (Supplementary Data, Fig. 2E). On this day, a 69% decrease in biofilm thickness was achieved on Perspex in comparison with biofilms developed on glass. Although Perspex is relatively more hydrophobic than glass (Romeu et al. 2019), previous studies which comprise different genera of cyanobacteria and cyanobacteria isolated from different locations also showed that surface hydrophobicity on its own may not have a significant impact on cyanobacterial biofilm development (Romeu et al. 2019, 2020, Faria et al. 2020b).

Comparing the behavior of the cyanobacterial strains used in this study with strains isolated from the Portuguese coast (through laboratory experiments performed under the same conditions), it was possible to observe that the present cyanobacterial strains revealed higher biofilm development potential (Romeu et al. 2019, 2020, 2021). Indeed, based on the results obtained for wet weight, chlorophyll *a* quantification and biofilm thickness, among the six filamentous cyanobacterial strains isolated from the Portuguese coast, only two, *Nodosilinea* sp. LEGE 06020 (Romeu et al. 2019) and *Nodosilinea* sp. LEGE 06145 (Romeu et al. 2020), showed enhanced biofilm development ability. While both cyanobacterial strains used in this study presented biofilm wet weight, chlorophyll *a* content and biofilm thickness values between 5–40 mg, 0–6 μg.cm^{-2} and up to 150 μm, respectively, over the 49 days, the values achieved by *Nodosilinea* sp. LEGE 06020 (Romeu et al. 2019) and *Nodosilinea* sp. LEGE 06145 (Romeu et al. 2020) were between 5–50 mg, 0–15 μg.cm^{-2} and up to 600 μm.

Fig. 5 shows representative 2D cross-sectional images obtained by OCT at 35 and 49 days. This period corresponds to a maturation phase of biofilm development and the time at which major differences in biofilm thickness between the two cyanobacterial strains were observed (Fig. 4E and F). The representative 2D cross-sectional images obtained by OCT confirmed the quantitative results obtained from wet weight, chlorophyll *a* quantification and biofilm thickness over these days (Fig. 4). Indeed, thicker biofilms were formed by *Leptothoe* sp. LEGE 181153 and the major difference between both cyanobacterial strains was observed for the last day of the experiment (49 days). Alterations in biofilm structure along this maturation stage can also be noted through a qualitative analysis. For instance, biofilms at 35 days appear to be denser than biofilms developed after 49 days, in which some void spaces are visible (Fig. 5). Moreover, this finding is more evident for *Leptothoe* sp. LEGE 181153 biofilms, in which a denser structure can be noted at the biofilm bottom and streamers structures are shown at the biofilm top. An adjustment of biofilm structure may be required over time because, with the gradual biofilm growth, the inner layers of biofilms can have limited access to nutrients, oxygen and light (Teodósio et al. 2011, Najmuldeen et al. 2019, Gloag et al. 2020, Peterson et al. 2021). Therefore, this can be a vital adaptation strategy to ensure continuous cyanobacterial biofilm development.

At the end of the experiment, the structural differences between the two cyanobacterial biofilms developed on glass and Perspex were also evaluated using CLSM. Examples of 3D biofilm images are presented in Fig. 6 and biovolume values, which provide an estimate of the biomass in the biofilm (μm^3.μm^{-2}), are shown in Fig. 7. Once again, it is possible to observe that denser and thicker biofilms were formed by *Leptothoe* sp. LEGE 181153, regardless of the surface used. Indeed, biovolume obtained for *Jaaginema* sp. LEGE 191154 was on average 71% and 58% lower, respectively, compared with the values obtained for the *Leptothoe* sp.

Downloaded from https://academic.oup.com/femsec/article/99/3/fiad004/6986251 by Universidade do Porto user on 14 March 2023

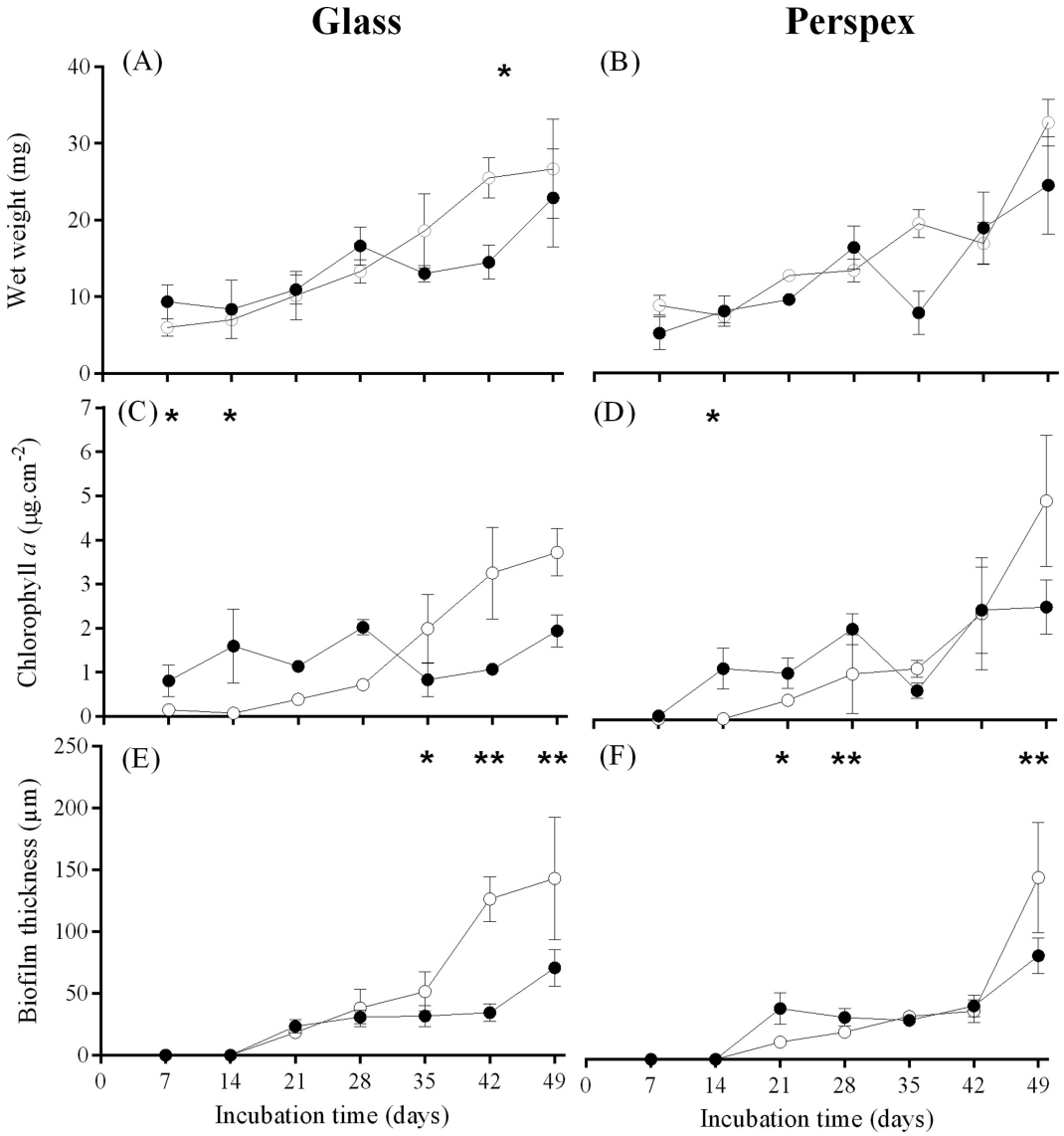

Figure 4. Evaluation of cyanobacterial biofilm development. The parameters analyzed refer to wet weight (**A**, **B**), chlorophyll *a* (**C**, **D**) and biofilm thickness (**E**, **F**). Biofilms of *Jaaginema* sp. LEGE 191154 (closed circles) and *Leptothoe* sp. LEGE 181153 (open circles) were formed on glass or Perspex at an average shear rate of 40 s^{-1} for 49 days. Symbols * and ** indicate statistically different values for $P < 0.1$ and $P < 0.05$ on each incubation time, respectively.

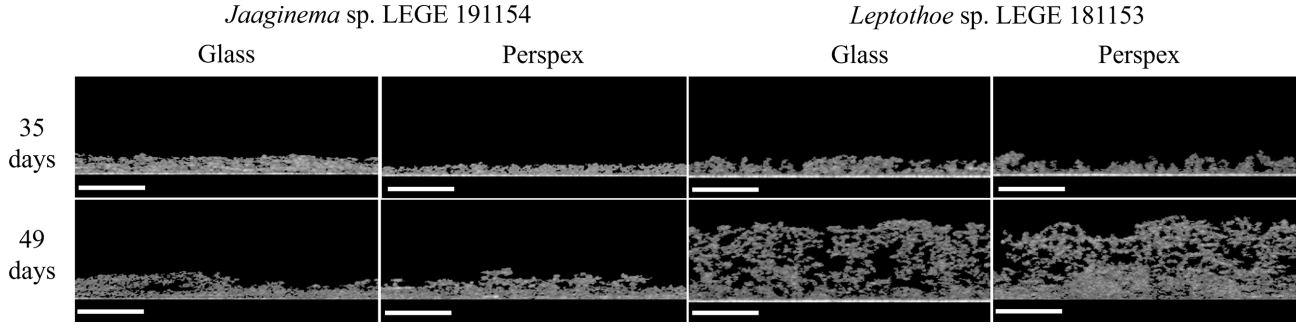

Figure 5. 2D cross-sectional OCT images of cyanobacterial biofilms formed at 35 and 49 days on glass and Perspex. Scale bars = 200 μm.

Downloaded from https://academic.oup.com/femsec/article/99/3/fiad004/6986251 by Universidade do Porto user on 14 March 2023

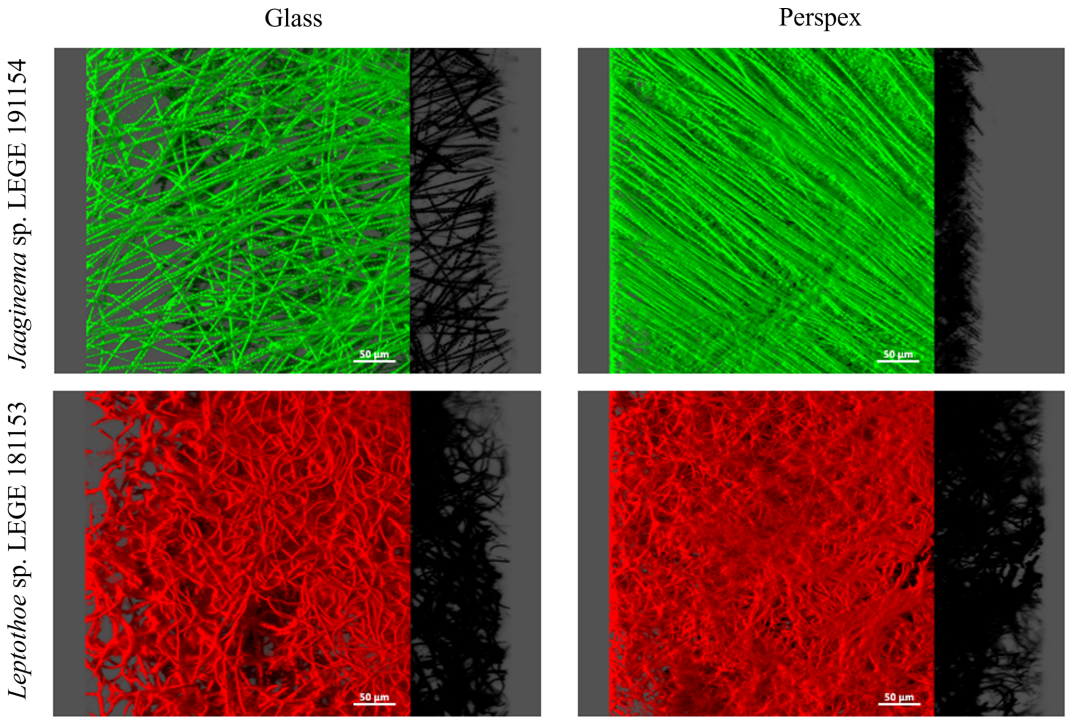

Figure 6. CLSM images of cyanobacterial biofilms formed after 49 days on glass and Perspex. Scale bars = 50 μm.

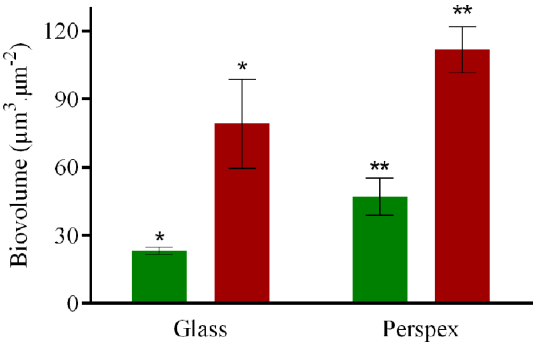

Figure 7. Biovolume obtained from CLSM z-stacks of *Jaaginema* sp. LEGE 191154 (green bars) and *Leptothoe* sp. LEGE 181153 (red bars) biofilms formed after 49 days on glass and Perspex. Symbols * and ** indicate statistically different values for $P < 0.1$ and $P < 0.05$ between both cyanobacterial strains on the same surface, respectively.

LEGE 181153 strain on glass and Perspex, respectively. These results corroborate the quantitative values obtained from biofilm wet weight, chlorophyll *a* concentration and biofilm thickness (Fig. 4), as well as the qualitative 2D images obtained from OCT on day 49 (Fig. 5). Moreover, 3D biofilm images obtained from CLSM showed different patterns between cyanobacterial strains but also among the two surfaces. While on biofilms formed by *Jaaginema* sp. LEGE 191154 extended and oriented filaments were detected, tangled and contracted filaments were formed by *Leptothoe* sp. LEGE 181153 (Fig. 6). In turn, filaments of biofilms formed on glass appeared individualized and distanced from each other, while on Perspex the filaments have a cohesive architecture (Fig. 6). Moreover, biovolume values obtained on glass range from 23 to 80 $\mu m^3.\mu m^{-2}$, and on Perspex from 47 to 112 $\mu m^3.\mu m^{-2}$ (Fig. 7). Unlike the porous structure of the biofilms developed on glass, the biofilms of both strains formed on the Perspex seem to have some organic matter such as EPS filling the voids (Fig. 7). Previous studies showed that the EPS abundance is more dependent on the environmental conditions (Mota et al. 2015) or the intrinsic characteristics of the organisms rather than on the physical and chemical features of the substratum (Del Mondo et al. 2018). However, a recent paper revealed that the amount of EPS can also be related to biofilm production on different surfaces (Maruthanayagam et al. 2020). Indeed, Maruthanayagam and his coworkers showed that cyanobacteria produced higher amounts of EPS on hydrophobic polymethyl methacrylate than on the hydrophilic glass surface.

The isolation and characterization of cyanobacterial strains are an important endeavor, due to their potential as new sources of added-value compounds, as well as their adverse and harmful impact on marine biofouling. In this work, two different cyanobacterial strains from underexplored locations in Morocco and Cape Verde were isolated and identified. Both strains showed the capacity to form biofilms, but *Leptothoe* sp. LEGE 181153 proved to be a better biofilm former than *Jaaginema* sp. LEGE 191154 under the hydrodynamic and nutritional conditions tested. Although no significant differences were found in biofilms developed by the same cyanobacterial strain on different surfaces, images obtained by CLSM denoted that biofilms formed on Perspex were denser. Thus, the biofilms of *Leptothoe* sp. LEGE 181153 may be more harmful in marine environments where this surface material is present. Additional assays may evaluate the expression of virulence, adhesion and biofilm development factors by the use of omics approaches to complement the present study (Babele et al. 2019, Romeu et al. 2022). Additionally, to consider the biofilm-forming potential of these cyanobacterial strains in real marine environments, it would be interesting to immerse these surfaces in the sea water for prolonged periods, as already performed by the group for other promising coatings against marine biofouling (Silva et al. 2021).

Downloaded from https://academic.oup.com/femsec/article/99/3/fiad004/6986251 by Universidade do Porto user on 14 March 2023

Supplementary data

Supplementary data are available at FEMSEC online.

Acknowledgements

J.M., R.S. and V.V. would like to thank Prof. Brahim Sabour from Faculty of Sciences El Jadida, University Chouaib Doukkali for all the help sampling in Morocco.

Conflicts of interest. None declared.

Funding

This work was financially supported by: LA/P/0045/2020 (ALiCE), UIDB/00511/2020 and UIDP/00511/2020 (LEPABE), funded by national funds through FCT/MCTES (PIDDAC); project HealthyWaters (NORTE-01-0145-FEDER-000069), supported by Norte Portugal Regional Operational Programme (NORTE 2020), under the PORTUGAL 2020 Partnership Agreement, through the European Regional Development Fund (ERDF); project EMERTOX (grant 734748), funded by H2020-MSCA-RISE 2016; Strategic Funding UIDB/04423/2020 and UIDP/04423/2020 through national funds provided by the Foundation for Science and Technology (FCT) and the European Regional Development Fund (ERDF) in the framework of the program PT2020. M.J.R and L.C.G. thank the Portuguese Foundation for Science and Technology (FCT) for the financial support of her PhD grant (SFRH/BD/140080/2018), and a work contract through the Scientific Employment Stimulus—Individual Call—[CEECIND/01700/2017], respectively.

References

Anderson O. Marine and estuarine natural microbial biofilms: ecological and biogeochemical dimensions. *AIMS Microbiol* 2016;**2**:304–31.

Antunes J, Leão P, Vasconcelos V. Marine biofilms: diversity of communities and of chemical cues. *Environ Microbiol Rep* 2019;**11**:287–305.

Antunes JT, Sousa AGG, Azevedo J *et al.* Distinct temporal succession of bacterial communities in early marine biofilms in a Portuguese Atlantic Port. *Front Microbiol* 2020;**11**:1–17.

Babele PK, Kumar J, Chaturvedi V. Proteomic de-regulation in cyanobacteria in response to abiotic stresses. *Front Microbiol* 2019;**10**:1–22.

Bakker DP, Plaats A Van Der, Verkerke GJ *et al.* Comparison of velocity profiles for different flow chamber designs used in studies of microbial adhesion to surfaces. *Appl Environ Microbiol* 2003;**69**:6280–7.

Bannister J, Sievers M, Bush F *et al.* Biofouling in marine aquaculture: a review of recent research and developments. *Biofouling* 2019;**35**:631–48.

Berg M, Sutula M. *Factors Affecting the Growth of Cyanobacteria with Special Emphasis on the Sacramento-San Joaquin Delta*. Costa Mesa (CA): Southern California Coastal Water Research Project. Technical Report 869, 2015.

Bharti A, Velmourougane K, Prasanna R. Phototrophic biofilms: diversity, ecology and applications. *J Appl Phycol* 2017;**29**:2729–44.

Blain S, Guillou J, Tréguer PJ *et al.* High frequency monitoring of the coastal marine environment using the MAREL buoy. *J Environ Monit* 2004;**6**:569–75.

Bragg JG, Thomas D, Baudouin-Cornu P. Variation among species in proteomic sulphur content is related to environmental conditions. *Proceedings Biol Sci* 2006;**273**:1293–300.

Breinlinger S, Phillips TJ, Haram BN *et al.* Hunting the eagle killer: a cyanobacterial neurotoxin causes vacuolar myelinopathy. *Science (80-)* 2021;**371**:eaax9050. https://doi.org/10.1126/science.aax9050

Cai W, Arias CR. Biofilm formation on aquaculture substrates by selected bacterial fish pathogens. *J Aquat Anim Heal* 2017;**29**:95–104.

Caruso G. Microbial colonization in marine environments: overview of current knowledge and emerging research topics. *J Mar Sci Eng* 2020;**8**:1–22.

Carvalho CCCR. Marine biofilms: a successful microbial strategy with economic implications. *Front Mar Sci* 2018;**5**:1–11.

Claessen D, Rozen DE, Kuipers OP *et al.* Bacterial solutions to multicellularity: a tale of biofilms, filaments and fruiting bodies. *Nat Rev Microbiol* 2014;**12**:115–24.

Coleman ML, Chisholm SW. Code and context: prochlorococcus as a model for cross-scale biology. *Trends Microbiol* 2007;**15**:398–407.

Croft MT, Warren MJ, Smith AG. Algae need their vitamins. *Eukaryot Cell* 2006;**5**:1175–83.

Dang H, Lovell CR. Microbial surface colonization and biofilm development in marine environments. *Microbiol Mol Biol Rev* 2016;**80**:91–138.

Darriba D, Taboada GL, Doallo R *et al.* jModelTest 2: more models, new heuristics and parallel computing. *Nat Methods* 2012;**9**:772.

Davidson IC, Brown CW, Sytsma MD *et al.* The role of containerships as transfer mechanisms of marine biofouling species. *Biofouling J Bioadhesion Biofilm Res* 2009;**25**:645–55.

Davies P, Rajapakse YDS. *Durability of Composites in a Marine Environment*. Netherlands: Springer, 2013.

Del Mondo A, Pinto G, Carbone DA *et al.* Biofilm architecture on different substrates of an Oculatella subterranea (Cyanobacteria) strain isolated from Pompeii archaeological site (Italy). *Environ Sci Pollut Res* 2018;**25**:26079–89.

Delauney L, Compare C, Lehaitre M. Biofouling protection for marine environmental sensors. *Ocean Sci* 2010;**6**:503–11.

Dobretsov S, Rittschof D. Love at first taste: induction of larval settlement by marine microbes. *Int J Mol Sci* 2020;**21**:731. https://doi.org/10.3390/ijms21030731

Duperron S, Beniddir MA, Durand S *et al.* New benthic cyanobacteria from Guadeloupe mangroves as producers of antimicrobials. *Mar Drugs* 2019;**18**:16. https://doi.org/10.3390/md18010016

Faria S, Gomes LC, Teixeira-Santos R *et al.* Developing new marine antifouling surfaces: learning from single-strain laboratory tests. *Coatings* 2021a;**11**:1–11.

Faria S, Teixeira-Santos R, Morais J *et al.* The association between initial adhesion and cyanobacterial biofilm development. *FEMS Microbiol Ecol* 2021b;**97**:fiab052.

Faria S, Teixeira-Santos R, Romeu MJ *et al.* Unveiling the antifouling performance of different marine surfaces and their effect on the development and structure of cyanobacterial biofilms. *Microorganisms* 2021c;**9**:1102.

Faria SI, Teixeira-Santos R, Gomes LC *et al.* Experimental assessment of the performance of two marine coatings to curb biofilm formation of microfoulers. *Coatings* 2020a;**10**:893. https://doi.org/10.3390/COATINGS10090893

Faria SI, Teixeira-Santos R, Romeu MJ *et al.* The relative importance of shear forces and surface hydrophobicity on biofilm formation by coccoid cyanobacteria. *Polymers* 2020b;**12**:653.

Foster JS, Green SJ, Ahrendt SR *et al.* Molecular and morphological characterization of cyanobacterial diversity in the stromatolites of highborne cay, bahamas. *ISME J* 2009;**3**:573–87.

Georgiades E, Scianni C, Davidson I *et al.* The role of vessel biofouling in the translocation of marine pathogens: management considerations and challenges. *Front Mar Sci* 2021;**8**:1–20.

Downloaded from https://academic.oup.com/femsec/article/99/3/fiad004/6986251 by Universidade do Porto user on 14 March 2023

Gloag ES, Fabbri S, Wozniak DJ *et al.* Biofilm mechanics: implications in infection and survival. *Biofilm* 2020;**2**:100017.

Heidari F, Zima J, Riahi H *et al.* New simple trichal cyanobacterial taxa isolated from radioactive thermal springs. *Fottea* 2018;**18**:137–49.

Helliwell KE, Lawrence AD, Holzer A *et al.* Cyanobacteria and eukaryotic algae use different chemical variants of vitamin B12. *Curr Biol* 2016;**26**:999–1008.

Heydorn A, Nielsen AT, Hentzer M *et al.* Quantification of biofilm structures by the novel computer program COMSTAT. *Microbiology* 2000;**146**:2395–407.

Huisman J, Codd GA, Paerl HW *et al.* Cyanobacterial blooms. *Nat Rev Microbiol* 2018;**16**:471–83.

Hunsucker KZ, Vora GJ, Hunsucker JT *et al.* Biofilm community structure and the associated drag penalties of a groomed fouling release ship hull coating. *Biofouling* 2018;**34**:162–72.

King RK, Flick GJ, Smith SA *et al.* Comparison of bacterial presence in biofilms on different materials commonly found in recirculating aquaculture systems. *J Appl Aquac* 2006;**18**:79–88.

Konstantinou D, Gerovasileiou V, Voultsiadou E *et al.* Sponges-cyanobacteria associations: global diversity overview and new data from the Eastern Mediterranean. *PLoS One* 2018;**13**:1–22.

Konstantinou D, Voultsiadou E, Panteris E *et al.* Leptothoe, a new genus of marine cyanobacteria (Synechococcales) and three new species associated with sponges from the Aegean Sea. *J Phycol* 2019;**55**:882–97.

Kotai J. Instructions for the preparation of modified nutrient Solution Z8 for algae. Blindern, Oslo: Norwegian Institute for Water Research, 1972, 5.

Ku C, Nelson-Sathi S, Roettger M *et al.* Endosymbiotic origin and differential loss of eukaryotic genes. *Nature* 2015;**524**:427–32.

Kumar S, Stecher G, Tamura K. MEGA7: molecular Evolutionary Genetics Analysis version 7.0 for bigger datasets. *Mol Biol Evol* 2016:msw054.

Lane DJ. 16S/23S rRNA sequencing. *Nucleic Acid Techniques in Bacterial Systematics*. Chichester, UK: JohnWiley and Sons, 1991, 115–75.

Lau NS, Matsui M, Abdullah AAA. Cyanobacteria: photoautotrophic microbial factories for the sustainable synthesis of industrial products. *Biomed Res Int* 2015;**2015**:754934. https://doi.org/10.1155/2015/754934

Lepère C, Wilmotte A, Meyer B. Molecular Diversity of Microcystis Strains (Cyanophyceae, Chroococcales) Based on 16S rDNA Sequences. *Syst Geogr Plants* 2000;**70**:275–83.

Letunic I, Bork P. Interactive Tree of Life (iTOL) v5: an online tool for phylogenetic tree display and annotation. *Nucleic Acids Res* 2021;**49**:W293–6.

Limoli DH, Jones CJ, Wozniak DJ. Bacterial extracellular polysaccharides in biofilm formation and function. *Microbiol Spectr* 2015;**3**:223–47. https://doi.org/10.1128/microbiolspec.MB-0011-2014

Lv J, Li N, Niu DK. Association between the availability of environmental resources and the atomic composition of organismal proteomes: evidence from prochlorococcus strains living at different depths. *Biochem Biophys Res Commun* 2008;**375**:241–6.

Lyons TW, Reinhard CT, Planavsky NJ. The rise of oxygen in Earth's early ocean and atmosphere. *Nature* 2014;**506**:307–15.

Manirafasha E, Ndikubwimana T, Zeng X *et al.* Phycobiliprotein: potential microalgae derived pharmaceutical and biological reagent. *Biochem Eng J* 2016;**109**:282–96.

Mansour A, Liu D. *The Principles of Naval Architecture Series: Strength of Ships and Ocean Structures*. Paulling JR (ed.), Jersey City, NJ: The Society of Naval Architects and Marine Engineers, 2008.

Martiny AC, Coleman ML, Chisholm SW. Phosphate acquisition genes in prochlorococcus ecotypes: evidence for genome-wide adaptation. *Proc Natl Acad Sci U S A* 2006;**103**:12552–7.

Maruthanayagam V, Basu S, Bhattacharya D *et al.* Effects of surface material on growth pattern and bioactive exopolymers production of intertidal cyanobacteria phormidium sp. *Indian J Geo-Marine Sci* 2020;**49**:1669–77.

Molland AF. Ship design, construction and operation. In *The Maritime Engineering Reference Book: A Guide to Ship Design, Construction and Operation*. United Kingdom: Butterworth-Heinemann, 2008.

Moore LR, Ostrowski M, Scanlan DJ *et al.* Ecotypic variation in phosphorus-acquisition mechanisms within marine picocyanobacteria. *Aquat Microb Ecol* 2005;**39**:257–69.

Mota R, Pereira SB, Meazzini M *et al.* Effects of heavy metals on cyanothece sp. CCY 0110 growth, extracellular polymeric substances (EPS) production, ultrastructure and protein profiles. *J Proteomics* 2015;**120**:75–94.

Mullineaux CW. Co-existence of photosynthetic and respiratory activities in cyanobacterial thylakoid membranes. *Biochim Biophys Acta* 2014;**1837**:503–11.

Najmuldeen H, Alghamdi R, Alghofaili F *et al.* Functional assessment of microbial superoxide dismutase isozymes suggests a differential role for each isozyme. *Free Radic Biol Med* 2019;**134**:215–28.

Nübel U, Garcia-Pichel F, Muyzer G. PCR primers to amplify 16S rRNA genes from cyanobacteria. *Appl Environ Microbiol* 1997;**63**:3327–32.

Pagels F, Guedes AC, Amaro HM *et al.* Phycobiliproteins from cyanobacteria: chemistry and biotechnological applications. *Biotechnol Adv* 2019;**37**:422–43.

Panou M, Gkelis S. Unravelling unknown cyanobacteria diversity linked with HCN production. *Mol Phylogenet Evol* 2022;**166**:107322.

Papadatou M, Robson SC, Dobretsov S *et al.* Marine biofilms on different fouling control coating types reveal differences in microbial community composition and abundance. *Microbiologyopen* 2021;**10**:1–17.

Peterson BW, van der Mei HC, Sjollema J *et al.* A distinguishable role of eDNA in the viscoelastic relaxation of biofilms. *MBio* 2021;**4**:e00497–13.

Pointing SB, Belnap J. Microbial colonization and controls in dryland systems. *Nat Rev Microbiol* 2012;**10**:551–62.

Porra R, Thompson W, Kriedemann P. Determination of accurate extinction coefficients and simultaneous equations for assaying chlorophylls a and b extracted with four different solvents: verification of the concentration of chlorophyll standards by atomic absorption spectroscopy. *Biochim Biophys Acta* 1989;**975**:384–94.

Ramos V, Morais J, Castelo-Branco R *et al.* Cyanobacterial diversity held in microbial biological resource centers as a biotechnological asset: the case study of the newly established LEGE culture collection. *J Appl Phycol* 2018;**30**:1437–51.

Rippka R. Isolation and purification of cyanobacteria. *Methods Enzymol* 1988;**167**:3–27.

Romeu MJ, Alves P, Morais J *et al.* Biofilm formation behaviour of marine filamentous cyanobacterial strains in controlled hydrodynamic conditions. *Environ Microbiol* 2019;**21**:4411–24.

Romeu MJ, Domínguez-Pérez D, Almeida D *et al.* Characterization of planktonic and biofilm cells from two filamentous cyanobacteria using a shotgun proteomic approach. *Biofouling* 2020;**36**:631–45.

Romeu MJ, Domínguez-pérez D, Almeida D *et al.* Hydrodynamic conditions affect the proteomic profile of marine biofilms formed by filamentous cyanobacterium. *Npj Biofilms Microbiomes* 2022;**8**:80.

Romeu MJ, Domínguez-Pérez D, Almeida D *et al.* Quantitative proteomic analysis of marine biofilms formed by filamentous cyanobacterium. *Environ Res* 2021:111566.

Downloaded from https://academic.oup.com/femsec/article/99/3/fiad004/6986251 by Universidade do Porto user on 14 March 2023

Rossi F, De Philippis R. Role of cyanobacterial exopolysaccharides in phototrophic biofilms and in complex microbial mats. *Life* 2015;**5**:1218–38.

Roy GJ. *Notes on Instrumentation and Control (Marine Engineering)*. Oxford, Boston: Newnes, 1994.

Rusch DB, Halpern AL, Sutton G *et al.* The Sorcerer II Global Ocean sampling expedition: northwest Atlantic through eastern tropical Pacific. *PLoS Biol* 2007;**5**:0398–431.

Schirrmeister BE, Antonelli A, Bagheri HC. The origin of multicellularity in cyanobacteria. *BMC Evol Biol* 2011;**11**:45.

Silva ER, Tulcidas A V, Ferreira O *et al.* Assessment of the environmental compatibility and antifouling performance of an innovative biocidal and foul-release multifunctional marine coating. *Environ Res* 2021;**198**:111219.

Singh R, Parihar P, Singh M *et al.* Uncovering potential applications of cyanobacteria and algal metabolites in biology, agriculture and medicine: current status and future prospects. *Front Microbiol* 2017;**8**:1–37.

Taylor DA. *Introduction to Marine Engineering*. United Kingdom: Butterworth-Heinemann, 1996.

Teodósio JS, Simões M, Melo LF *et al.* Flow cell hydrodynamics and their effects on E. Coli biofilm formation under different nutrient conditions and turbulent flow. *Biofouling* 2011;**27**:1–11.

Thompson JD, Higgins DG, Gibson TJ. CLUSTAL W: improving the sensitivity of progressive multiple sequence alignment through sequence weighting, position-specific gap penalties and weight matrix choice. *Nucleic Acids Res* 1994;**22**:4673–80.

Van Mooy BAS, Rocap G, Fredricks HF *et al.* Sulfolipids dramatically decrease phosphorus demand by picocyanobacteria in oligotrophic marine environments. *Proc Natl Acad Sci U S A* 2006;**103**:8607–12.

Vermaas WFJ. *Photosynthesis and Respiration in Cyanobacteria*, New York: Macmillan Publishers Ltd, Nature Publishing Group, 2001.

Vincent WF. Cyanobacterial dominance in the polar regions. In: Whitton BA, Potts M (eds.), *The Ecology of Cyanobacteria*. Dordrecht, the Netherlands: Springer Netherlands, 2000, 321–40.

Wright ES, Yilmaz LS, Noguera DR. DECIPHER, a search-based approach to chimera identification for 16S rRNA sequences. *Appl Environ Microbiol* 2012;**78**:717–25.

Downloaded from https://academic.oup.com/femsec/article/99/3/fiad004/6986251 by Universidade do Porto user on 14 March 2023

Supplementary Data

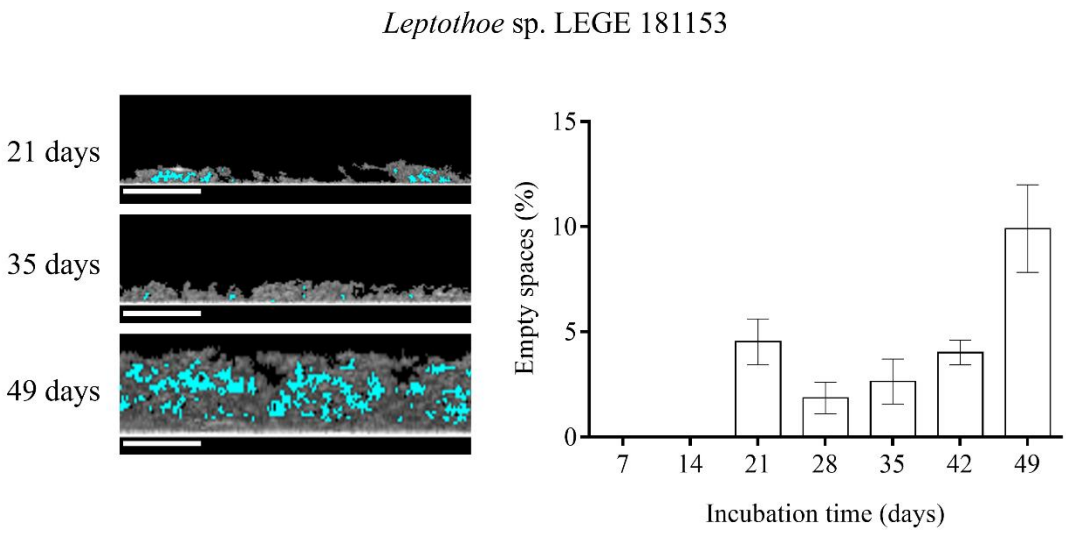

Figure 1. Evaluation of biofilm empty spaces. The parameter analysed refers to the percentage of empty spaces on *Leptothoe* sp. LEGE 181153 biofilms formed on glass for 49 days. The empty spaces on cyanobacterial biofilm structures were determined as described in Faria *et al.* 2021 and represented in blue **(**scale bar = 200 μm). The values regarding the percentage of empty spaces are indicated from day 21 since the biofilm thickness was below the OCT range on the first two sampling days.

Reference:
Faria S, Teixeira-Santos R, Romeu MJ *et al.* Unveiling the antifouling performance of different marine surfaces and their effect on the development and structure of cyanobacterial biofilms. *Microorganisms* 2021;**9**:1102.

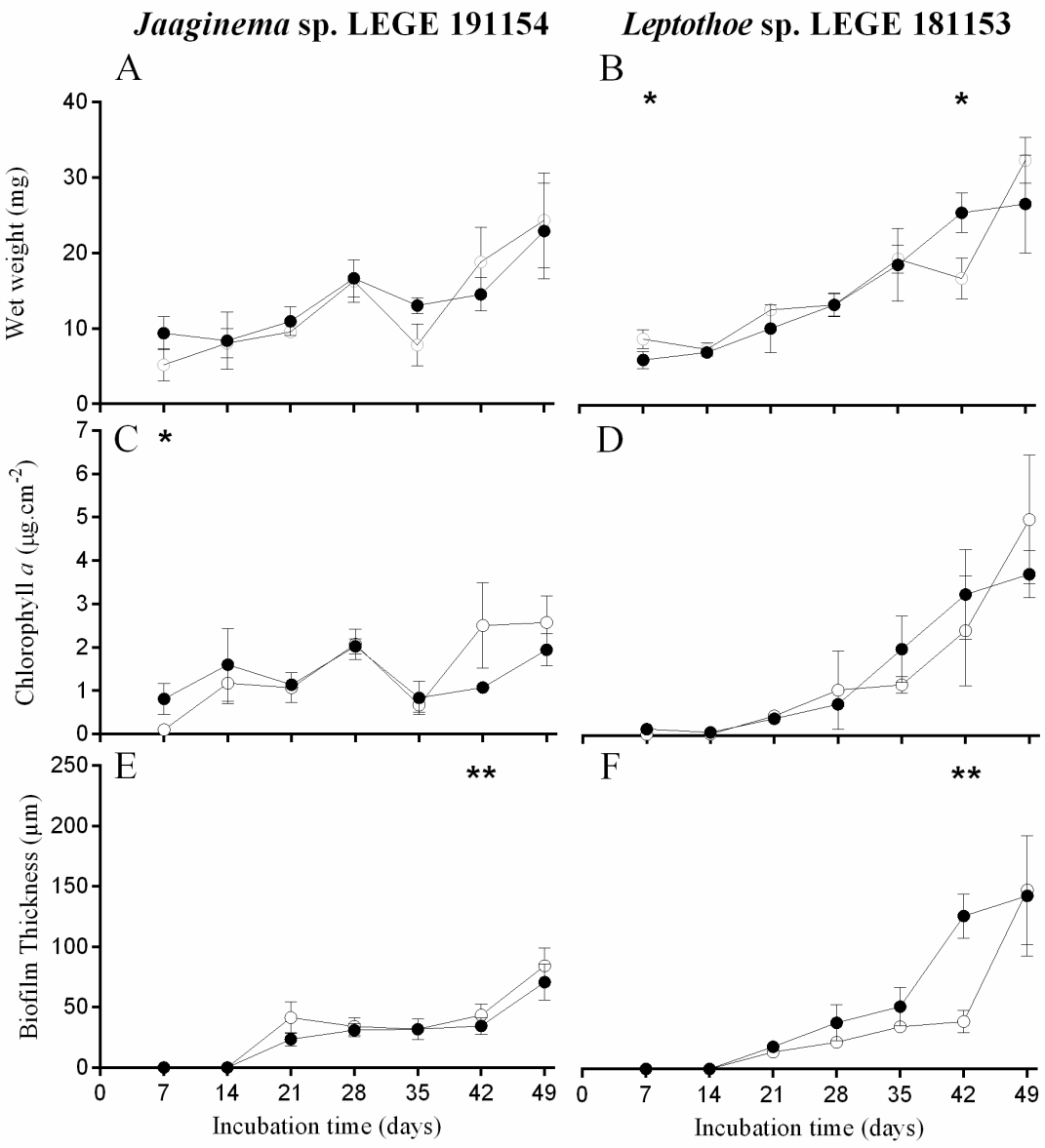

Figure 2. Evaluation of biofilm development on different surfaces. The parameters analysed refer to wet weight, chlorophyll *a* quantification, and biofilm thickness. Biofilms of *Jaaginema* sp. LEGE 191154 and *Leptothoe* sp. LEGE 181153 were formed on glass (closed circles) or perspex (open circles) at an average shear rate of 40 s^{-1} for 49 days. Symbols * and ** indicate statistically different values for $p < 0.1$ and $p < 0.05$ on each incubation time, respectively.

polymers

MDPI

Article

The Use of 3D Optical Coherence Tomography to Analyze the Architecture of Cyanobacterial Biofilms Formed on a Carbon Nanotube Composite

Maria J. Romeu [1,2], Marta Lima [1,2], Luciana C. Gomes [1,2], Ed. D. de Jong [3], João Morais [4], Vítor Vasconcelos [4,5], Manuel F. R. Pereira [2,6], Olívia S. G. P. Soares [2,6], Jelmer Sjollema [3] and Filipe J. Mergulhão [1,2,*]

1 LEPABE—Laboratory for Process Engineering, Environment, Biotechnology and Energy, Faculty of Engineering, University of Porto, Rua Dr. Roberto Frias, 4200-465 Porto, Portugal
2 ALiCE—Associate Laboratory in Chemical Engineering, Faculty of Engineering, University of Porto, Rua Dr. Roberto Frias, 4200-465 Porto, Portugal
3 Department of Biomedical Engineering, University of Groningen, University Medical Centre Groningen, Antonius Deusinglaan 1, 9713 AV Groningen, The Netherlands
4 CIIMAR—Interdisciplinary Centre of Marine and Environmental Research, University of Porto, Terminal de Cruzeiros do Porto de Leixões, Av. General Norton de Matos s/n, 4450-208 Matosinhos, Portugal
5 Department of Biology, Faculty of Sciences, University of Porto, Rua do Campo Alegre, 4169-007 Porto, Portugal
6 LSRE–LCM—Laboratory of Separation and Reaction Engineering–Laboratory of Catalysis and Materials, Faculty of Engineering, University of Porto, Rua Dr. Roberto Frias, 4200-465 Porto, Portugal
* Correspondence: filipem@fe.up.pt; Tel.: +351-225081668

check for updates

Citation: Romeu, M.J.; Lima, M.; Gomes, L.C.; Jong, E.D.d.; Morais, J.; Vasconcelos, V.; Pereira, M.F.R.; Soares, O.S.G.P.; Sjollema, J.; Mergulhão, F.J. The Use of 3D Optical Coherence Tomography to Analyze the Architecture of Cyanobacterial Biofilms Formed on a Carbon Nanotube Composite. *Polymers* **2022**, *14*, 4410. https://doi.org/10.3390/polym14204410

Academic Editors: Irena Maliszewska and Tomasz Czapka

Received: 14 September 2022
Accepted: 14 October 2022
Published: 19 October 2022

Publisher's Note: MDPI stays neutral with regard to jurisdictional claims in published maps and institutional affiliations.

Copyright: © 2022 by the authors. Licensee MDPI, Basel, Switzerland. This article is an open access article distributed under the terms and conditions of the Creative Commons Attribution (CC BY) license (https://creativecommons.org/licenses/by/4.0/).

Abstract: The development of environmentally friendly antifouling strategies for marine applications is of paramount importance, and the fabrication of innovative nanocomposite coatings is a promising approach. Moreover, since Optical Coherence Tomography (OCT) is a powerful imaging technique in biofilm science, the improvement of its analytical power is required to better evaluate the biofilm structure under different scenarios. In this study, the effect of carbon nanotube (CNT)-modified surfaces in cyanobacterial biofilm development was assessed over a long-term assay under controlled hydrodynamic conditions. Their impact on the cyanobacterial biofilm architecture was evaluated by novel parameters obtained from three-dimensional (3D) OCT analysis, such as the contour coefficient, total biofilm volume, biovolume, volume of non-connected pores, and the average size of non-connected pores. The results showed that CNTs incorporated into a commercially used epoxy resin (CNT composite) had a higher antifouling effect at the biofilm maturation stage compared to pristine epoxy resin. Along with a delay in biofilm development, a decrease in biofilm wet weight, thickness, and biovolume was also achieved with the CNT composite compared to epoxy resin and glass (control surfaces). Additionally, biofilms developed on the CNT composite were smoother and presented a lower porosity and a strictly packed structure when compared with those formed on the control surfaces. The novel biofilm parameters obtained from 3D OCT imaging are extremely important when evaluating the biofilm architecture and behavior under different scenarios beyond marine applications.

Keywords: marine biofouling; cyanobacterial biofilms; antifouling surfaces; carbon nanotubes; Optical Coherence Tomography

1. Introduction

Marine biofouling causes severe economic and energetic losses, along with critical environmental and ecological consequences. Carbon nanomaterials, including carbon nanotubes (CNTs), graphene, fullerenes, and diamond-like carbon, have been recognized for their antimicrobial and anti-adhesive properties [1]. Due to their remarkable mechanical

strength, high thermal conductivity, and structural stability, CNTs are promising nanomaterials for several applications, namely in the industrial, environmental, and medical fields [2,3]. CNTs have already been tested in antifouling formulations to prevent biofouling, mainly to protect ship hulls, as well as in composite materials that come into contact with seawater. Likewise, CNTs have been reported to impact the composition of marine biofilms, as well as the settlement of macrofouling organisms [4,5]. CNTs can be represented as a single rolled-up graphene sheet (single-walled carbon nanotubes, SWCNTs) or a series of concentric graphene sheets (multi-walled carbon nanotubes, MWCNTs) [6]. These carbon nanomaterials exhibit a concentric cylindrical structure with a diameter in the order of nanometers, varying according to the number of walls, and a length of several microns that is extendable by up to a few millimeters (around 4 mm). CNTs are generally incorporated into a polymeric matrix for application in protective coatings, such as polydimethylsiloxane (PDMS) [7], to improve their mechanical strength [8]. The main antibacterial and antifouling mechanisms of CNTs include the disruption of membrane integrity by electrostatic forces between the microbial outer surface and CNTs, leading to membrane oxidation. Moreover, reactive oxygen species generation may directly harm biological molecules of bacteria and/or indirectly prompt DNA destruction [1,9,10]. Although the mechanism behind the antifouling properties of CNTs is still not clear, their length, diameter, surface area, concentration, and treatment time play a significant role in their antifouling and antimicrobial activity [9–11]. Regarding CNT concentration, a loss of cell viability was shown to be correlated with increasing SWCNT loading. Remarkably, 5% SWCNTs may reduce biofilm development from *Bacillus anthracis* spores by 81%, while SWCNT concentrations $\geq$ 20% can inhibit biofilm formation [12]. Likewise, 0.1 wt% SWCNTs can decrease *Escherichia coli* biofilms by 18%, while, with 1 wt% SWCNTs, the biofilm reduction may reach 76% [13]. On the other hand, a study in which different CNT concentrations (0.1, 1, 2, 3, 4, and 5 wt%) were tested to inhibit *E. coli* biofilm development reported an increase in *E. coli* culturability for surfaces with CNT concentrations between 0.1 and 2 wt% compared to bare surfaces, while a decrease was observed for the remaining CNT concentrations [11]. Among these higher CNT concentrations, 3 wt% was the most promising surface for the inhibition of *E. coli* biofilms. Since CNTs' antimicrobial activity also depends on their dispersion state [14], a lower dispersion may occur at higher loadings (4 and 5 wt%), leading to a lower antimicrobial effect on CNT-based surfaces [11]. Moreover, it has also been reported that introducing small quantities of CNTs into a polymer network can result in a considerable increase in the antibacterial performance of that polymeric matrix [13]. In fact, polyvinyl-N-carbazole (97 wt%) with 3% of SWCNTs demonstrated similar or stronger bactericidal performance than the surfaces consisting of 100% SWCNTs [15].

The attachment by macrofoulers, such as calcareous hard-fouling organisms (barnacles, mussels, and tubeworms) and soft-fouling organisms (non-calcareous algae, sponges, anemones, tunicates, and hydroids), is responsible for the main consequences of marine biofouling. However, the prevention of adhesion and biofilm development by microfoulers such as bacteria, cyanobacteria, and diatoms reduces the progression of biofouling to the next stages. A deeper knowledge of biofilm behavior and how it interplays with the surrounding environment will enable the development of efficient methodologies to control biofouling and mitigate its negative impacts. New imaging technologies, biochemical methods, and molecular biology tools have contributed to the technological development of biofilm science. Optical Coherence Tomography (OCT) is an exciting modality that overcomes the time-consuming and destructive methodologies of biofilm analysis, such as some microscopic techniques. In addition to the tedious sample preparation, most of the relevant microscopic techniques applied to the study of biofilms require the staining of the sample or the use of fluorochromes, which are expensive and can interfere with the local properties of the biofilm [16]. Moreover, some of them provide low-resolution images only covering a small field of view (FOV). OCT presents several advantages over the common microscopic methods since it is a simple and inexpensive technique, does not require sample preparation and/or staining procedures, and allows for the reconstruction of 3D images

by *in situ*, non-invasive, and real-time imaging without affecting the biofilm structure [17]. Moreover, OCT can provide images at the mesoscale relatively quickly, and it allows for a great penetration depth, revealing several details of the biofilm structure [18]. Despite all of the advantages of this optical technique, only a limited set of image processing scripts have been specifically developed for processing OCT biofilm images. Furthermore, the analysis of structural parameters obtained from OCT is not advanced when compared, for instance, to microscopy techniques such as Confocal Laser Scanning Microscopy (CLSM). Indeed, there are several software tools and libraries for biofilm image processing from microscopy, including Image Structure Analyzer (ISA) [19], COMSTAT [20], PHobia Laser scanning microscopy Imaging Processor (PHLIP) [21], *bio*Image_L [22], and DAIME [23].

Studies focused on assessing the marine biofouling mitigation effect of CNT coatings can greatly contribute to improving the knowledge regarding the antifouling properties of these promising materials. Moreover, most marine studies focus on unicellular bacteria, and it is pertinent to address additional microfouler organisms such as filamentous cyanobacteria due to their improved stress and predation resistance [24]. Therefore, the main goal of this study was to analyze the potential of CNT-modified surfaces to delay cyanobacterial biofilms, as well as to evaluate their impact on biofilm architecture using an in-depth OCT analysis. CNTs were incorporated in a commercially available polymer, epoxy resin, since it is commonly used to coat the hulls of small recreational vessels [25,26] due to its unique physical, chemical, and mechanical properties, no safety issues, and low cost [27]. Additionally, epoxy composites have demonstrated high durability and resistance to fatigue and UV irradiation [28]. CNT loading (3 wt%) was chosen according to results obtained in previous studies, in which these carbon-based surfaces were tested to inhibit *E. coli* biofilm development in the medical field [11]. Additionally, textural modifications of CNTs were performed by ball milling (BM) treatment over 4 h to enhance its antimicrobial performance [29] by adjusting the CNT length and opening their closed ends to increase the specific surface area [30]. The textural modifications induced by ball-milling treatment proved to be effective in the inhibition of biofilm formation, reducing the amount of biofilm per surface area, biofilm thickness and surface coverage by 31, 47 and 27%, respectively, when compared to surfaces where CNTs were not ball-milled [11].

The specific aim of this study comprises the development of novel analysis parameters obtained from 3D OCT imaging to evaluate the biofilm structure. Since OCT is an *in situ*, non-destructive technique that can be applied to different fields (e.g., marine, medical, and industrial), and the knowledge of biofilm architecture is important to understand all phenomena related to this complex lifestyle, the analysis carried out in this work is extremely relevant. To the best of our knowledge, this is the first study evaluating the impact of CNT-modified surfaces on cyanobacterial biofilm behavior using an in vitro platform that mimics the hydrodynamic conditions prevailing in real marine environments.

2. Materials and Methods

2.1. Surface Preparation

To assess the surface antifouling performance on cyanobacterial biofilm development, two control surfaces (glass, a commonly submerged artificial surface found on different equipment in aquatic and marine environments, and epoxy resin, a commercially available coating) and a CNT composite were used. The epoxy resin-coated glass was prepared following the protocol described by Faria et al. [31]. Briefly, the epoxy resin was produced by HB Química (Matosinhos, Porto, Portugal) and consisted of a mixture of HB Eposurf 2 resin and HB Eposurf hardener in a ratio of 10:3 (v/v). To produce the epoxy resin-coated surfaces, 70 µL of epoxy resin was deposited on the top of glass coupons using spin coating (Spin150 PolosTM, Paralab, Porto, Portugal) at 6000 rpm, with increments of 1000 rpm, for 40 s. The surfaces were dried for over 12 h at room temperature and then for 3 h at 60 °C, according to the instructions of the manufacturer.

The methodology for the preparation of the CNT composite surface was adapted from Gomes et al. [11], in which the PDMS matrix was replaced by epoxy resin. Briefly,

commercially available pristine MWCNTs (NanocylTM NC3100, Sambreville, Belgium), produced by catalytic chemical vapor deposition with an average length and diameter of 1.5 μm and 9.5 nm, respectively, were used. CNTs were physically modified by BM treatment (Retsch MM200, Haan, Germany) at 15 vibrations s^{-1} for 4 h. After mixing the two epoxy resin portions, 3 wt% of CNTs was incorporated into the epoxy resin mixture since it was shown to be the most effective CNT load to reduce bacterial biofilm formation in previous studies [11]. After that, 70 μL of the composite (3 wt% CNT-BM/epoxy resin) was deposited on the top of the glass coupons using spin coating, as reported above. In previous work [11], our research group showed that bare PDMS surfaces and CNT composites had a similar film thickness (about 30 μm).

2.2. Surface Characterization

2.2.1. Water Contact Angle Measurements

The wettability of glass, epoxy resin, and CNT composite surfaces was assessed by measuring the contact angles with water (θ_w). This determination was performed using the sessile drop method on an SL200C optical contact angle meter (Solon Information Technology Co., Ltd., Shanghai, China) at room temperature (25 °C), as previously described [32]. At least 25 determinations for each material were made.

2.2.2. Atomic Force Microscopy (AFM)

AFM studies were performed using a Bruker Catalyst microscope in contact mode by a DNP-D cantilever with a spring constant of 0.06 N/m (Bruker, Billerica, MA, USA). The surface roughness was determined from random areas (75 × 75 or 100 × 100 μm^2) on two coupons of each material at room temperature. Surface roughness calculations and 2D images were made using the NanoScope Analysis software from Bruker. The roughness height parameter determined was the average roughness (R_a), which gives the average absolute deviation of the roughness irregularities from the mean line over one sampling length [33].

2.2.3. Scanning Electron Microscopy (SEM)

The surface morphology at nanometer resolution was assessed by SEM. All tested surfaces were fixed to SEM stubs using carbon pads (Agar Scientific, UK) and sputter-coated with gold in an SEM coating system (Polaron CVT Ltd., Milton Keynes, UK). The sputter coating conditions were: 5 mA (plasma current), pressure < 0.1 mbar, 800 V, and argon gas for 30 s. The secondary electron detector of a Supra 40VP scanning electron microscope (Carl Zeiss Ltd., Cambridge, UK) was used to obtain the images at an accelerating voltage of 2 kV under different magnifications. Three regions of three different coupons of each material were analyzed.

2.3. Organism and Inoculum Preparation

A filamentous cyanobacterial strain, *Nodosilinea* cf. *nodulosa* LEGE 10377, was obtained from the Blue Biotechnology and Ecotoxicology Culture Collection (LEGE-CC) located at the Interdisciplinary Centre of Marine and Environmental Research (CIIMAR), Matosinhos, Portugal [34]. This cyanobacterial strain was previously isolated from a marine sponge at an intertidal zone of Aguda Beach, Arcozelo, Portugal (41.04954 N 8.655339 W). Cyanobacterial cells were grown in 750 mL of Z8 medium [35], supplemented with 25 g/L of synthetic sea salts (Tropic Marin) and vitamin B_{12} (Sigma Aldrich, Merck, Saint Louis, MO, USA). Cultures were grown under 14 h light (10–30 μmol photons m^{-2} s^{-1}, λ = 380–700 nm)/10 h dark cycles at 25 °C.

2.4. Biofilm Formation

To mimic the hydrodynamic conditions found in marine environments, biofilm formation was evaluated on agitated 12-well microtiter plates (VWR International, Carnaxide, Portugal) under previously optimized conditions for cyanobacterial biofilm devel-

opment [36]. Firstly, transparent double-sided adhesive tape was placed in the wells to fix the coupons. All coupons and plates were then subjected to UV sterilization, after which the sterile coupons were fixed as previously described [11,36].

Prior to inoculation, the cyanobacterial suspensions were adjusted to a chlorophyll *a* concentration of 0.77 ± 0.03 µg/mL, since chlorophyll *a* quantification is a common method to estimate the biomass in marine environments, and this pigment is unique and predominant in all groups of cyanobacteria [36,37]. Briefly, cells were harvested by centrifugation (3202× *g*, for 5 min at room temperature), the supernatant was discarded and a volume of 2 mL of 99.8% methanol (Methanol ACS Basic, Scharlau Basic, Barcelona, Spain) was added. Then, the cyanobacterial suspension was incubated for 24 h at 4 °C in the dark for maximal chlorophyll *a* extraction, the samples were centrifuged at 3202× *g* for 5 min at room temperature and the supernatant was transferred to a glass cuvette. Absorbance measurements were performed at 750 nm (turbidity), 665 nm (chlorophyll *a*), and 652 nm (chlorophyll *b*) using a V-1200 spectrophotometer (VWR International China Co., Ltd., Shanghai, China). The values obtained were used to calculate the chlorophyll *a* concentration (µg/mL) through Equation (1) [38]:

$$Chl\ a\ (\mu g/mL) = 16.29 \times A^{665} - 8.54 \times A^{652} \quad (1)$$

These measurements were assessed in triplicate and dilutions were performed using Z8 medium supplemented with 25 g/L of synthetic sea salts and vitamin B_{12}. A volume of 3 mL of the respective adjusted cyanobacterial suspension was inoculated in each well. Microtiter plates were then incubated at 25 °C in an orbital shaker with a 25 mm orbital diameter (Agitorb 200ICP, Norconcessus, Ermesinde, Portugal) at 185 rpm, resulting in an average and maximum shear rate of 40 and 120 s^{-1}, respectively [36]. Biofilm formation in this system includes the shear rate estimated for a ship in a harbor, 50 s^{-1} [39], and it was shown to predict the biofouling behavior observed upon immersion in the sea for prolonged periods [40]. In order to mimic real light exposure periods, microtiter plates were kept under 14 h light (8–10 µmol photons m^{-2} s^{-1})/10 h dark cycles [36]. Biofilm development was followed for seven weeks (49 days) since a two-month interval for maintenance is the minimum duration for economically viable underwater monitoring systems [36]. During this incubation time, the medium was replaced twice a week.

2.5. Biofilm Analysis

Biofilm analysis was performed every seven days, in which two coupons of each surface were analyzed. The culture medium was carefully removed, and the wells were filled with 3 mL of sterile sodium chloride solution (8.5 g/L) [36]. The solution was carefully removed to eliminate loosely attached cyanobacteria. Subsequently, the wells were filled again with 3 mL of sterile sodium chloride solution to evaluate the structure of the cyanobacterial biofilms by OCT. To complement the characterization of cyanobacterial biofilms, the determination of their wet weight was also performed over the seven weeks, and at the end of the experiment, the morphology of cyanobacterial biofilms was evaluated by SEM.

2.5.1. Optical Coherence Tomography (OCT)

Images from cyanobacterial biofilms were captured and analyzed as previously described [36,41]. For each coupon, two-dimensional (2D) and 3D imaging were performed with a minimum of two FOVs to ensure the accuracy and reliability of the obtained results. The 2D and 3D coordinate systems used in this work are shown in Figure 1. For image analysis, the bottom of the biofilm was determined as the best-fitting parabole and hyperboloid, in 2D and 3D images, respectively, that connected the white pixels resulting from light reflection on the substratum surface. A gray-value threshold that separates the biofilm from the background was calculated based on the gray-value histogram of the entire ROI (region of interest) selected [42]. The upper contour line of the biofilm was defined as the pixels with the highest distance to the bottom that had a gray value higher than the gray-value

threshold and which were connected to the bottom of the biofilm. Objects not connected to the bottom were rejected from the biofilm structure, and the average biofilm thickness ($\overline{L}_F$) was calculated as a function of the number of pixels (or voxels) between the bottom of the biofilm and the upper contour line for each vertical line in the image ($\overline{L}_F$ is the mean of $L_{F,\,i}$ along the area described as $A_{x,z}$, where $L_{F,\,i}$ is the local biofilm thickness (μm) connected to the bottom at location i for each vertical x,z column (line of voxels)). In addition to biofilm thickness, novel parameters were analyzed from 3D analysis obtained by OCT, such as the contour coefficient, total biofilm volume, biovolume, volume of non-connected pores and the average size of non-connected pores. For this analysis, the voxel volume of a non-connected pore was defined as about 117 μm^3, and the standard minimum non-connected pore size in the analysis was 1000 μm^3. The values of the total biofilm volume, biovolume, and volume of non-connected pores were used as cumulative values along the $L_{F,\,i}$ to the maximum biofilm thickness obtained for each FOV. Consequently, the final values from these parameters were represented as the values achieved at the maximum biofilm thickness. A summary of all variables used in this section is presented in Table 1.

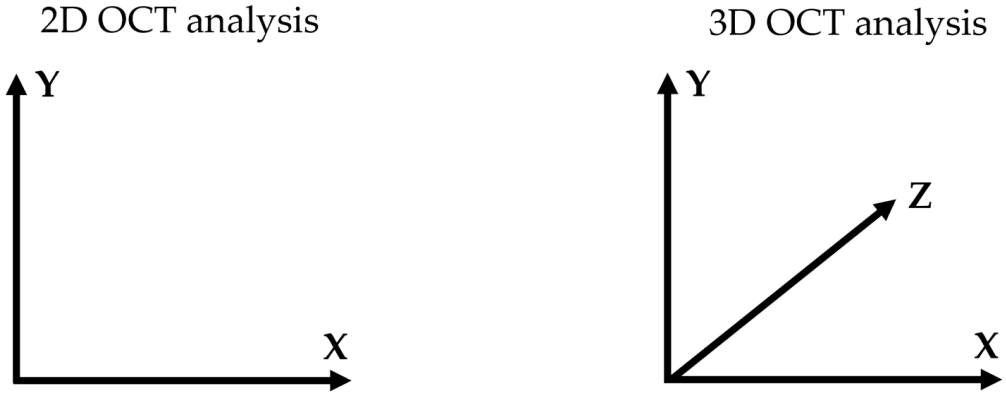

Figure 1. Two-dimensional and 3D coordinate systems for 2D and 3D OCT analyses, respectively. X represents the width, Y is the height, and Z refers to the depth.

Table 1. Variable definition.

Symbol	Description
x	Pixel position on the horizontal axis (width)
y	Pixel position on the vertical axis (height)
z	Pixel position on the perpendicular axis (depth)
i	Index of x,z position in the horizontal plane
N	Number of voxels in the horizontal plane of the region of interest (ROI)
V_{vox}	Volume of a voxel (μm^3)
$L_{F,\,i}$	Biofilm thickness at a given position i (μm)
$\overline{L}_F$	Average biofilm thickness (μm)
A_{ROI}	Total area of the ROI (mm^2)
$Acon_{x,z}$	Number of connected voxels identified as belonging to biofilm matrix/bacteria in the biofilm (biovolume) in a horizontal plane at position y
$Ancp_{x,z}$	Number of non-biofilm-connected voxels without an open connection to the environment (biofilm holes) in a horizontal plane at position y
$C_{F,i}$	Number of voxels identified as belonging to biofilm matrix/bacteria in the biofilm (biovolume) in column i (vertical line of voxels at position i) and connected to the environment (including corner voxels)

Contour Coefficient

The biofilm structure was analyzed by a novel structural parameter—the *contour coefficient*—defined as the number of voxels connected to the background divided by the number of voxels of a horizontal plane, $A_{x,z}$, according to Equation (2):

$$Contour\ coefficient = \frac{1}{N}\sum_{i=1}^{N}\frac{C_{F,i}}{A_{x,z}} \quad (2)$$

This parameter enables the analysis of the fraction of the biofilm that is exposed to the surrounding medium. Therefore, values close to 1 reflect a homogeneous and flat biofilm, while in biofilms with heterogeneous structures (e.g., biofilms with streamers), the values are higher than 1.

Total Biofilm Volume

The *total biofilm volume* is defined as the number of all connected voxels and non-connected voxels in all images of a horizontal plane multiplied by the voxel size, and it provides an estimate of the total volume of the biofilm (μm^3) per area of the ROI. The *total biofilm volume* is determined according to Equation (3):

$$Total\ biofilm\ volume\ \left(\mu m^3/mm^2\right) = \frac{\sum_{all\ planes}[(Acon_{x,z} + Ancp_{x,z}) \times V_{vox}]}{A_{ROI}} \quad (3)$$

Biovolume

The *biovolume* is defined by the number of all connected voxels in all images of a horizontal plane multiplied by the voxel size, and it provides an estimate of the biomass in the biofilm (μm^3) per area of the ROI. Biovolume is determined according to Equation (4):

$$Biovolume\ \left(\mu m^3/mm^2\right) = \frac{\sum_{all\ planes}[(Acon_{x,z}) \times V_{vox}]}{A_{ROI}} \quad (4)$$

Porosity

The percentage of biofilm *porosity* was quantified from data obtained from the *volume of non-connected pores* and the *total biofilm volume*, according to Equation (5):

$$Porosity\ (\%) = \frac{Volume\ of\ non-connected\ pores}{Total\ biofilm\ volume} \times 100 \quad (5)$$

The *volume of non-connected pores* (μm^3) per area of the ROI is defined as the number of non-connected voxels in all images of a stack multiplied by the voxel size and normalized by area, and it is determined according to Equation (6):

$$Volume\ of\ non-connected\ pores_{x,z}\left(\mu m^3/mm^2\right) = \frac{\sum_{all\ planes}[Ancp_{x,z} \times V_{vox}]}{A_{ROI}} \quad (6)$$

Average Size of Non-Connected Pores

The determination of the average size of *non-connected pores* inside the biofilm structure was quantified, assuming a minimum size of *non-connected pores* equal to 1000 μm^3 and defining a voxel size of 1 as corresponding to 117 μm^3, as reported above.

2.5.2. Wet Weight Determination

The determination of the biofilm wet weight was performed as previously reported [43]. Briefly, a sterile sodium chloride solution (8.5 g/L) was carefully removed from the wells, coupons were detached, weighed, and the biofilm wet weight was obtained as the difference from the initial coupon weight determined prior to inoculation.

2.5.3. Scanning Electron Microscopy (SEM)

After 49 days of incubation, the morphology of cyanobacterial biofilms formed on the three surface materials was analyzed by SEM. Coupons were removed from the microtiter plates, dehydrated in aqueous solutions of increasing ethanol concentrations (10, 25, 40, 50,

70, 80, 90, and 100% (*v*/*v*)) and left in a desiccator until SEM analysis [44]. The samples were then sputter-coated using the equipment and conditions described in Section 2.2.3 and observed in a Supra 40 VP scanning electron microscope (Carl Zeiss Ltd., Cambridge, UK) at a 2 kV accelerating voltage and a magnification of 1000×.

2.6. Statistical Analysis

A total of four replicates (two biological assays with two technical replicates each) were analyzed. Data analysis was performed using the statistical program GraphPad Prism® for Windows, version 6.01 (GraphPad Software, Inc., San Diego, CA, USA). Differences between biofilm wet weight, biofilm thickness, total biofilm volume, biovolume, porosity, and the average size of non-connected pores from data obtained by OCT were evaluated using one-way ANOVA with Tukey's multiple comparisons test. The error bars shown in the graphs correspond to the standard deviation (SD) of the mean. Statistically significant differences between the different surfaces for the same sampling day were considered for p-values < 0.05 (corresponding to a confidence level greater than 95%).

3. Results and Discussion

3.1. Surface Characterization

It is recognized that surface properties such as topography and physicochemistry affect their antiadhesive and/or antimicrobial behavior [45,46]. Thus, all tested surfaces were first investigated regarding (i) wettability by water contact angle measurements, (ii) topography and roughness by Atomic Force Microscopy (AFM), and (iii) morphology and structure by Scanning Electron Microscopy (SEM). The results obtained from the water contact angle measurements and roughness analysis are shown in Table 2. Given that substrates with a water contact angle (θ_w) of <90° are considered to be hydrophilic [47], glass is the most hydrophilic surface (θ_w = 40.9° ± 7.4°), followed by the CNT composite (θ_w = 68.9° ± 4.9°), and the epoxy resin-coated glass (θ_w = 76.3° ± 2.5°), which is significantly more hydrophobic (p < 0.05) than the resin composite. Lower hydrophobic properties caused by the incorporation of 3 wt% ball-milled CNTs were also observed in previous work in another polymeric matrix (PDMS) [11]. Regarding the average roughness (R_a) value determined by AFM (Table 2), glass and epoxy resin appeared to be smoother surfaces (R_a of 6.3 and 13 nm, respectively) than the CNT composite, which registered a R_a value of about 70 times higher than the remaining surfaces.

Table 2. Water contact angle measurements (θ_w) and roughness (R_a) determined for the tested surfaces.

Surface	Water Contact Angle	Roughness
	θ_w(°)	R_a(nm)
Glass	40.9 ± 7.4	6.3
Epoxy resin	76.3 ± 2.5	13.1
CNT composite	68.9 ± 4.9	644

Figure 2 reveals the topography and morphology of the tested surfaces obtained from AFM and SEM imaging, respectively. Glass and epoxy resin-coated glass were the most homogeneous and smooth materials (Figure 2a,b,d,e). In opposition, the CNT composite (Figure 2c,f) was the roughest surface, presenting CNT agglomerates that form small elevations on the material (Figure 2f).

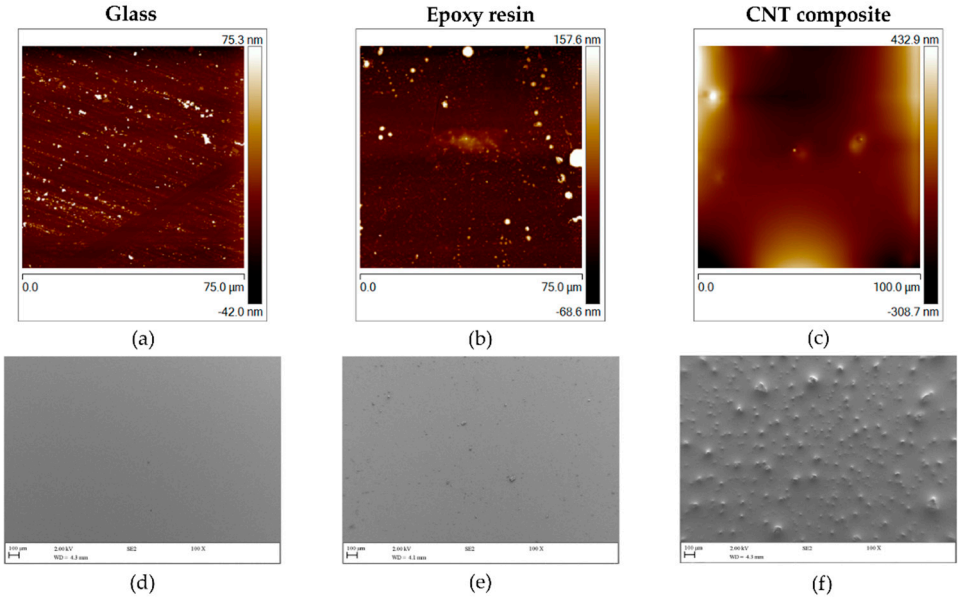

Figure 2. Two-dimensional AFM (**a**–**c**) and SEM (**d**–**f**) images of glass, epoxy resin, and CNT composite. The vertical color bars in the AFM images correspond to the *z*-range (surface height range) of the respective image. The SEM images have a magnification of 100× and the scale bar is equivalent to 100 µm.

3.2. Biofilm Formation

The structure of biofilms can be numerically quantified with imaging tools to investigate and monitor the effect of different compounds, surfaces and/or environmental factors on biofilm architecture. In the present work, cyanobacterial biofilm development on different surfaces was monitored over 7 weeks and the quantitative results obtained from 3D OCT analysis are shown in Figure 3. The values indicated in Figure 3b–f are only presented from day 14 since, for the first sampling day (day 7), the biofilm thickness was below the OCT range. In general, a gradual temporal increase in biofilm wet weight (Figure 3a), thickness (Figure 3b), and biovolume (Figure 3d) were observed, showing that this filamentous cyanobacterium is a good biofilm former. However, growth was more evident on glass and epoxy resin than on the CNT composite. In fact, for biofilm wet weight (Figure 3a), from day 7 to day 49, increases of 71%, 64%, and 49% were observed for glass, epoxy resin, and the CNT composite, respectively, and for biofilm thickness (Figure 3b), increases of 87%, 82%, and 72% were registered over time for the same surfaces. Regarding biovolume, increases of 77%, 64%, and 64% were observed for glass, epoxy resin and the CNT composite, which indicates that these CNT-modified surfaces can delay biofilm development when compared to pristine epoxy resin and glass. Moreover, on days 42 and 49, a reduction in cyanobacterial biofilm development was observed on the CNT composite surface. Regarding the biofilm thickness, on day 42, the values obtained on glass and epoxy surfaces were 58% and 47% higher than those obtained on the CNT composite surface, respectively, while on day 49, the biofilm thickness was 58% and 23% higher than those attained on the composite (Figure 3b). Additionally, the biovolume obtained on the glass and epoxy surface was 45% and 43% higher when compared to the values obtained on the CNT composite surface, respectively. Moreover, on day 49, these values were 46% and 6% higher as compared to the modified epoxy resin (Figure 3b). Since, in the early stages of biofilm formation (days 7, 14, and 21), all parameters were similar between the surfaces, the results suggest that the CNT composite surface may have a greater antifouling effect on the maturation stage of these cyanobacterial biofilms as compared to the other two types of substrates.

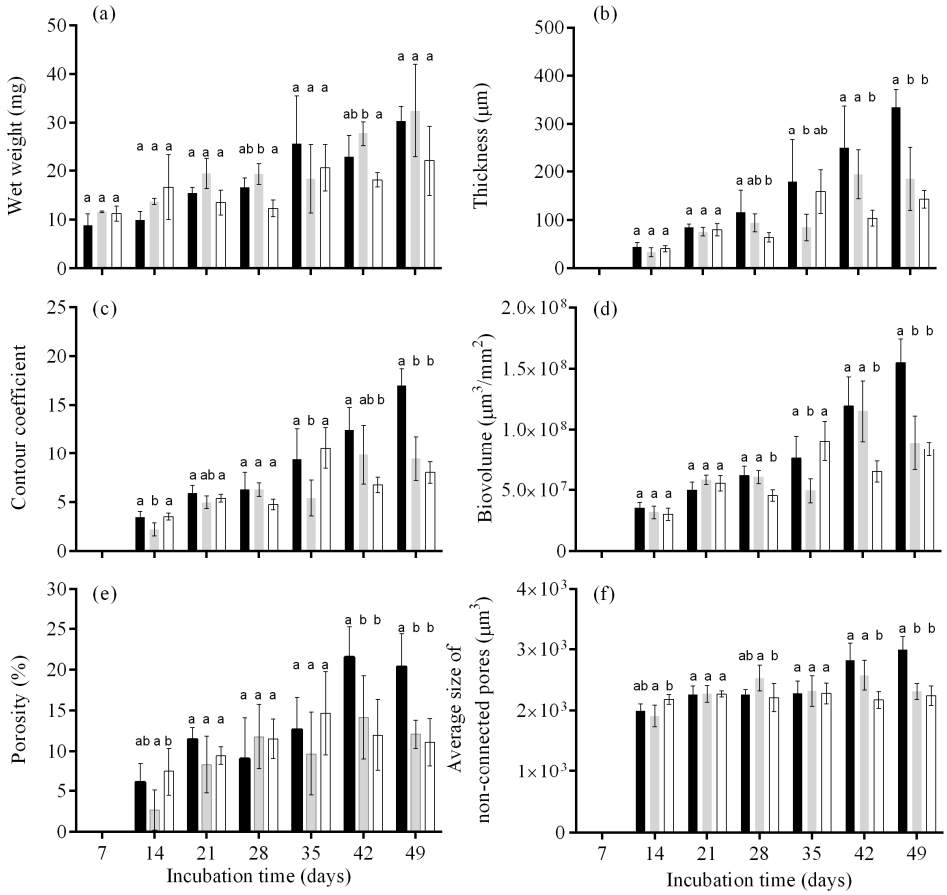

Figure 3. *Nodosilinea* cf. *nodulosa* LEGE 10377 biofilm development on different surfaces (glass—black, epoxy resin—grey, CNT composite—white). The parameters analyzed refer to biofilm wet weight (**a**), thickness (**b**), contour coefficient (**c**), biovolume (**d**), porosity (**e**), and average size of non-connected pores (**f**). Mean values and SD from two biological assays with two technical replicates each are represented. For each sampling day, different lowercase letters indicate significant differences between surfaces ($p \leq 0.05$; one-way ANOVA with Tukey's multiple comparisons test).

Surface topography plays a considerable role in the way in which marine fouling organisms adhere to surfaces, settle on them, and interact with them [48]. In the nanoregime, the topography can have a robust impact on the wettability of the surface, as well as a direct effect on the contact area available for fouler adhesion. Once more surface contact area is available, more settlement may take place and, consequently, the organisms may be more difficult to remove [49]. Moreover, the surface roughness may also promote an increase in the settlement and adhesion strength of biomolecules, including the proteinaceous adhesives used by many marine organisms [50]. Therefore, rough surfaces present an opportunity for fouling organisms to settle within and between the topographic features, protecting them from hydrodynamic forces [51]. Highly textured surfaces also provide greater surface area for adhesive cements to adhere [52]. Even though topography does not act as a unique mechanism, it is still a key feature that must be considered in the design of new materials. Since, in the early stages of biofilm formation, the values attained were similar between the surfaces (Figure 3), it appears that differences in surface properties, namely in average roughness (Table 2, Figure 2), may have been responsible for the differences registered in the later stages of biofilm development. Therefore, an antimicrobial effect rather than an anti-adhesive effect may explain the impact of CNT-modified surfaces in long-term cyanobacterial biofilm development. CNT composites may lead to unstable and weak biofilm development due to the piercing effect in the cell's membrane of the first biofilm layers [11]. However, this viability effect may be reflected only in the subsequent

biofilm layers, as cell-to-cell adhesion will be hampered if cells in the initial layers are damaged [53]. Moreover, biological processes such as cell reproduction and extracellular polymeric substance (EPS) production by these first-adhered impaired cells may affect biofilm development.

Biofilms formed on the CNT composite were also more homogenous on days 42 and 49 than those developed on glass and epoxy resin (Figure 3c), since the values of the contour coefficients were closer to 1, which reflects a homogeneous and flatter biofilm. Indeed, on day 42, the contour coefficient was around 46% and 32% lower for the CNT composite surface when compared to glass and epoxy resin, respectively. On the other hand, on day 49, these differences reached 53% and 15% when compared to the values obtained on glass and epoxy resin. Since the top of the biofilm grown on the carbon-based surface became flattened, without heterogeneous top structures (such as streamer structures), the superficial area in contact with the surrounding environment decreased, as well as the ability of nutrients and oxygen to penetrate within the biofilm. Likewise, in the maturation stage of biofilm development, a lower percentage of porosity (Figure 3e) and a smaller average size of non-connected pores (Figure 3f) were determined for biofilms formed on the CNT composite surface when compared with control surfaces.

The lower porosity and average size of non-connected pores may contribute to the lower viability of the cells located on the deepest biofilm layers since the internal mass transfer of nutrients to the inner layers of the biofilm may be hindered, contributing to the antimicrobial effect of these surfaces.

Figures 4–6 show representative 2D cross-sectional and 3D OCT images of *Nodosilinea* cf. *nodulosa* LEGE 10377 biofilms on glass, epoxy resin, and CNT composite after 49 days. Both 2D and 3D OCT images illustrate quantitative data on biofilm biomass and porosity (Figure 3). In fact, on the last day of the experiment, a higher percentage of biofilm biomass and porosity was observed on the glass surface when compared with the epoxy resin and the CNT composite surface. The biofilm top structure can also be observed as flatter for biofilms formed on the CNT composite than biofilms developed on glass and epoxy resin (Figures 4 and 5), as it was also indicated by quantitative data (Figure 3c). Moreover, in the biofilm formed on the glass, it was possible to observe long streamers, which can reach around 500 μm (Figure 4). On the other hand, according to representative 3D OCT images, biofilms developed on the CNT composite only present structures that reach around 250 μm. Through representative images of the size of non-connected pores, it was also possible to observe that these values can reach around 98,000 μm^3 in biofilms developed on glass, while values around 35,000 μm^3 and 19,000 μm^3 were achieved on epoxy resin and the CNT composite, respectively.

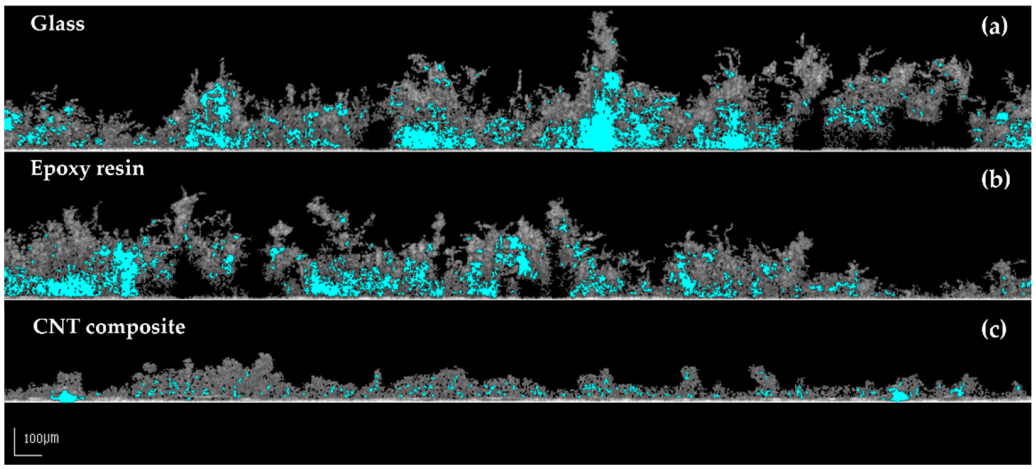

Figure 4. Representative 2D cross-sectional OCT images of *Nodosilinea* cf. *nodulosa* LEGE 10377 biofilms developed on glass (**a**), epoxy resin (**b**), and CNT composite (**c**) after 49 days. The empty spaces in the biofilm structure are filled in blue (scale bar = 100 μm).

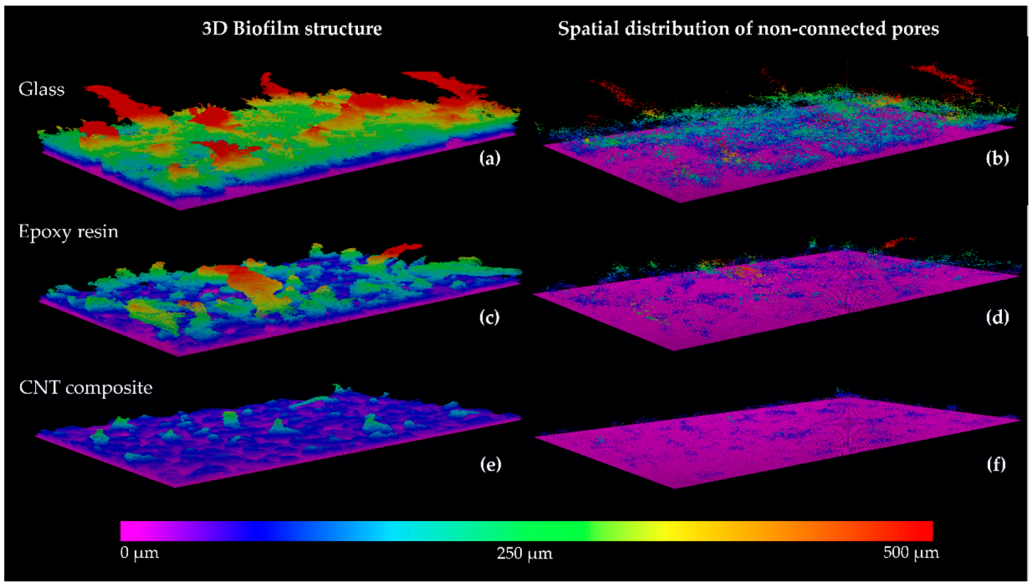

Figure 5. Representative 3D OCT images of *Nodosilinea* cf. *nodulosa* LEGE 10377 biofilms formed on glass (**a**), epoxy resin (**c**), and CNT composite (**e**) after 49 days. The spatial distribution of non-connected pores on the biofilm is also shown (**b**,**d**,**f**). The color scale shows the distance from the substrate surface.

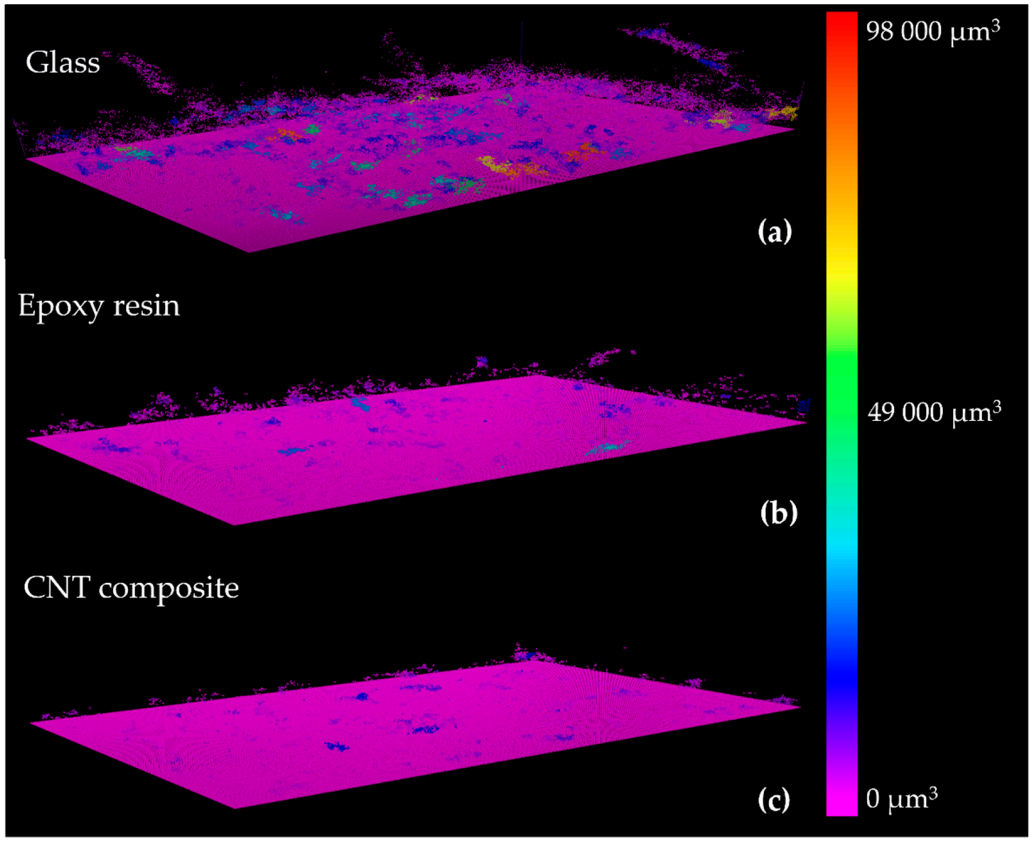

Figure 6. Representative 3D OCT images of the distribution of non-connected pores by size from *Nodosilinea* cf. *nodulosa* LEGE 10377 biofilms formed on glass (**a**), epoxy resin (**b**) and CNT composite (**c**) after 49 days. The color scale shows the range of the size of non-connected pores.

Mature biofilms consist of multidimensional heterogeneous structures with interstitial pores, which ensure the water and nutrient flow and that influence their resistance to

mechanical or chemical challenges [54–57]. Biofilm biomass, thickness, and structure have a strong effect on the performance of underwater marine devices [58]. Consequently, the knowledge of these biofouling parameters is essential for the design and maintenance of submerged marine equipment. In this work, CNT composite surfaces were tested for the prevention of cyanobacterial biofilms. Biofilms formed on this carbon-modified surface were more homogeneous, flatter, less porous, and had a tightly packed structure compared with the control surfaces, as it can be proved by the quantitative (Figure 3c,e,f) and qualitative (Figures 4–6) data. Although biofilm growth is reduced on these surfaces, which may be beneficial for the performance of nautical equipment, it may have an impact on the efficacy of methods to eradicate the biofilms formed on this surface material. Firstly, due to their lower porosity and a smaller average size of non-connected pores (Figure 3e,f), the internal mass transfer may be hampered, and chemical compounds used for biofouling control may not reach the inner layers of the biofilm [59]. Moreover, a homogeneous structure (Figure 3c) can be associated with greater cohesion across the whole biofilm structure. In this scenario, the detachment of biofilm components either by increasing hydrodynamic forces or by applying mechanical cleaning methods would be facilitated if a heterogeneous structure was present (such as the presence of some streamers). As a flatter biofilm was present, the detachment or removal phenomena may be hindered. Although there are several biofilm structural parameters described in the literature [60,61], there has been a tendency to use only a limited number of them [62–64]. This evidence makes cross-comparisons difficult and can be justified by the fact that only some of these parameters computed from biofilm images can be intuitively associated with identifiable biological processes. The analysis of biofilms based on biofilm weight, thickness, and biovolume alone, which are typically used for the description of biofilm structure, does not provide complete information on biofilm development. Only the combination of all evaluated structural parameters leads to a complete overview of biofilm behavior on the different surfaces. Moreover, the contour coefficient reported in this work may be a relevant parameter to replace or complement the analysis of biofilm roughness since more reliable structural biofilm information is provided by this novel parameter.

Analysis by SEM was also performed to assess the morphological differences shown by the cyanobacterial biofilms grown on the distinct surfaces (Figure 7). As observed by OCT (Figures 3–5), the SEM analysis reveals differences in the cyanobacterial biofilm growth patterns on different surfaces. The highest and lowest cyanobacterial biofilm amounts were observed on glass and the CNT composite surfaces, respectively. Indeed, SEM observations showed that while the biofilm formed on the control surfaces (glass and epoxy resin) looks like a dense filamentous network that covers practically the entire surface area, the biofilm grown on the composite surface presented lower-density cell aggregates.

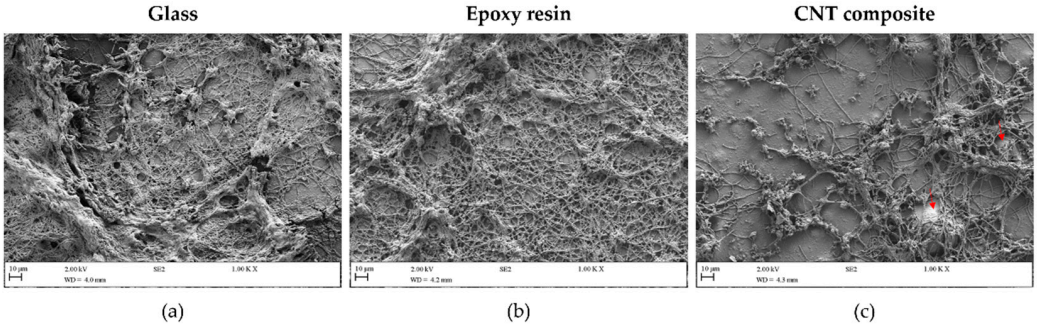

Figure 7. SEM images of *Nodosilinea* cf. *nodulosa* LEGE 10377 biofilms formed on glass (**a**), epoxy resin (**b**), and CNT composite (**c**) after 49 days of incubation. The red arrows in (**c**) indicate clusters of CNTs. Magnification = 1000×; scale bar = 10 µm.

OCT is a relevant tool for assessing the spatial organization and heterogeneity of biofilm since 2D and 3D datasets contain a representative description of the overall biofilm

structure at the mesoscale with µm-resolution [17]. Moreover, by OCT analysis, the laborious nature, as well as the costs entailed with microscopic techniques, can be reduced.

Few studies focus on longer assays for the assessment of CNTs on marine biofilm formation [65]. In fact, some *in vitro* studies have been performed between 6 [66] and 10 days [4], but only a study performed by Xie et al. [67] achieved the 20 days necessary to evaluate the antifouling effect of CNT-based antifouling coatings. Moreover, these studies focus on other marine bacteria, diatoms, algae, and macrofoulers [4,66,67]. For instance, an *in situ* study performed by Sun et al. [68] with pioneer biofilm bacteria over 24 days showed that all CNT/PDMS composites decreased Proteobacteria biofilm formation but increased cyanobacterial biofilm development. Other studies showed a promising reduction in biofilms formed by different microfoulers at different times on distinct CNT-based antifouling coatings [5,45,67,69–72].

In this study, biofilm was evaluated as a whole structure, including cells, water, and the compounds excreted by the cyanobacterial cells. Considering that a greater number of active cells in a biofilm can lead to greater surface colonization and biofilm development potential, future studies should include complementary techniques to assess the viability and/or the metabolic state of biofilm cyanobacterial cells [73,74]. Since the mechanisms behind the antifouling properties of CNTs are still not clear [2], it is relevant to conduct further assays in marine conditions with CNT-/epoxy resin surfaces, incorporating different CNT concentrations, lengths, diameters, and surface areas, as well as functionalized CNTs, with different polymeric matrices and different fouling organisms [2,9–11]. The generation of oxidative stress and mechanical damage through the direct perforation of the microorganisms' outer membranes and the release of intracellular content are some of the mechanisms that may be involved in CNT action [10]. Indeed, the representative SEM images of the morphology and structure of CNTs in the composite reveal the presence of CNT agglomerates (Figure 2f; Figure S1 in Supplementary Material), which can interact with the membrane of cyanobacterial cells by the known piercing phenomenon and be one of the strategies associated with the antifouling properties of these surfaces. *In situ* assays are also particularly recommended to assess the impact of these surfaces on the adhesion and biofilm formation of multiple microfouling organisms, as well as on the subsequent attachment of macrofoulers. Moreover, additional concerns with these nanostructured surfaces may be related to the fact that they may be damaged in harsh marine environments, leading to a reduction in their antifouling ability and lifespan. Hence, the development of robust and mechanically stabilized surfaces is critical [75].

Different biofilm techniques provide valuable and complementary information about different aspects of the complex biofilm structure. Therefore, a multidisciplinary approach that integrates different methodologies is recommended to obtain a more realistic biofilm representation and to better understand the complex phenomenon of marine biofilm development.

4. Conclusions

A set of novel structural parameters obtained from OCT imaging was developed to quantify the marine biofilm structure over time and on three different surface materials, one of them with recognized antifouling activity. CNT-modified surfaces delayed cyanobacterial biofilm development in the maturation stage of the biofilm. Biofilms developed on the composite had reduced wet weight, thickness, and biovolume and were smoother and less porous than those formed on epoxy resin and glass (control surfaces). Analysis of novel parameters obtained by OCT imaging enables a deeper understanding of the biofilm development process in different settings, including the marine environment.

Supplementary Materials: The following supporting information can be downloaded at: https://www.mdpi.com/article/10.3390/polym14204410/s1, Figure S1: Representative SEM image of an agglomerate of CNTs on the CNT composite surface. Magnification = 10,000×; scale bar = 1 µm.

Author Contributions: Conceptualization, M.J.R. and F.J.M.; methodology, M.J.R., M.L. and L.C.G.; software, E.D.d.J.; formal analysis, M.J.R. and L.C.G.; investigation, M.J.R., M.L. and L.C.G.; resources, M.F.R.P., V.V., J.S. and F.J.M.; data curation, M.J.R., M.L., L.C.G. and E.D.d.J.; writing—original draft preparation, M.J.R. and L.C.G.; writing—review and editing, E.D.d.J., J.M., M.F.R.P., O.S.G.P.S., J.S. and F.J.M.; supervision, V.V. and F.J.M.; funding acquisition, M.F.R.P., V.V., J.S. and F.J.M. All authors have read and agreed to the published version of the manuscript.

Funding: This research was funded by: LA/P/0045/2020 (ALiCE), UIDB/00511/2020 and UIDP/00511/2020 (LEPABE) and project PTDC/CTM-COM/4844/2020, funded by national funds through FCT/MCTES (PIDDAC); project HealthyWaters (NORTE-01-0145-FEDER-000069), supported by Norte Portugal Regional Operational Programme (NORTE 2020), under the PORTUGAL 2020 Partnership Agreement, through the European Regional Development Fund (ERDF); project EMERTOX (grant 734748), funded by H2020-MSCA-RISE 2016; Strategic Funding UIDB/04423/2020 and UIDP/04423/2020 through national funds provided by the Foundation for Science and Technology (FCT) and the European Regional Development Fund (ERDF) in the framework of the program PT2020; and project SurfSAFE supported by the European Union's Horizon 2020 Research and Innovation Programme under grant agreement no. 952471. M.J.R., L.C.G. and O.S.G.P.S. thank FCT for the financial support of a Ph.D. grant (SFRH/BD/140080/2018), and work contracts through the Scientific Employment Stimulus—Individual Call—[CEECIND/01700/2017] and the Scientific Employment Stimulus—Institutional Call—CEECINST/00049/2018, respectively. Support from the EURO-MIC COST Action (CA20130) is acknowledged.

Institutional Review Board Statement: Not applicable.

Informed Consent Statement: Not applicable.

Data Availability Statement: The data presented in this study are available from the corresponding author upon request.

Acknowledgments: Kathryn Whitehead from Manchester Metropolitan University is acknowledged for providing the scanning electron microscope used for surface and biofilm characterization.

Conflicts of Interest: The authors declare no conflict of interest.

References

1. Al-Jumaili, A.; Alancherry, S.; Bazaka, K.; Jacob, M.V. Review on the Antimicrobial Properties of Carbon Nanostructures. *Materials* **2017**, *10*, 1066. [CrossRef]
2. Teixeira-Santos, R.; Gomes, M.; Gomes, L.C.; Mergulhão, F.J. Antimicrobial and Anti-Adhesive Properties of Carbon Nanotube-Based Surfaces for Medical Applications: A Systematic Review. *iScience* **2021**, *24*, 102001. [CrossRef]
3. Venkataraman, A.; Amadi, E.V.; Chen, Y.; Papadopoulos, C. Carbon Nanotube Assembly and Integration for Applications. *Nanoscale Res. Lett.* **2019**, *14*, 220. [CrossRef]
4. Ba, M.; Zhang, Z.; Qi, Y. The Influence of MWCNTs-OH on the Properties of the Fouling Release Coatings Based on Polydimethylsiloxane with the Incorporation of Phenylmethylsilicone Oil. *Prog. Org. Coat.* **2019**, *130*, 132–143. [CrossRef]
5. Ji, Y.; Sun, Y.; Lang, Y.; Wang, L.; Liu, B.; Zhang, Z. Effect of CNT/PDMS Nanocomposites on the Dynamics of Pioneer Bacterial Communities in the Natural Biofilms of Seawater. *Materials* **2018**, *11*, 902. [CrossRef] [PubMed]
6. Lukowiak, A.; Kedziora, A.; Strek, W. Antimicrobial Graphene Family Materials: Progress, Advances, Hopes and Fears. *Adv. Colloid Interface Sci.* **2016**, *236*, 101–112. [CrossRef]
7. Lejars, M.; Margaillan, A.; Bressy, C. Fouling Release Coatings: A Nontoxic Alternative to Biocidal Antifouling Coatings. *Chem. Rev.* **2012**, *112*, 4347–4390. [CrossRef] [PubMed]
8. Dustebek, J.; Kandemir-Cavas, C.; Nitodas, S.F.; Cavas, L. Effects of Carbon Nanotubes on the Mechanical Strength of Self-Polishing Antifouling Paints. *Prog. Org. Coat.* **2016**, *98*, 18–27. [CrossRef]
9. Smith, A.M.; Callow, J.A. *Biological Adhesives*; Springer: Berlin/Heidelberg, Germany, 2006; Volume 23, ISBN 978-354-031-048-8.
10. Kang, S.; Herzberg, M.; Rodrigues, D.F.; Elimelech, M. Antibacterial Effects of Carbon Nanotubes: Size Does Matter! *Langmuir* **2008**, *24*, 6409–6413. [CrossRef]
11. Gomes, M.; Gomes, L.C.; Teixeira-Santos, R.; Pereira, M.F.R.; Soares, O.S.G.P.; Mergulhão, F.J. Optimizing Cnt Loading in Antimicrobial Composites for Urinary Tract Application. *Appl. Sci.* **2021**, *11*, 4038. [CrossRef]
12. Dong, X.; Yang, L. Inhibitory effects of single-walled carbon nanotubes on biofilm formation from *Bacillus anthracis* spores. *Biofouling* **2014**, *30*, 1165–1174. [CrossRef] [PubMed]
13. Schiffman, J.D.; Elimelech, M. Antibacterial activity of electrospun polymer mats with incorporated narrow diameter single-walled carbon nanotubes. *ACS Appl. Mater. Interfaces* **2011**, *3*, 462–468. [CrossRef] [PubMed]

14. Saleemi, M.A.; Fouladi, M.H.; Yong, P.V.C.; Wong, E.H. Elucidation of Antimicrobial Activity of Non-Covalently Dispersed Carbon Nanotubes. *Materials* **2020**, *13*, 1676. [CrossRef] [PubMed]
15. Ahmed, F.; Santos, C.M.; Vergara, R.A.M.V.; Tria, M.C.R.; Advincula, R.; Rodrigues, D.F. Antimicrobial applications of electroactive PVK-SWNT nanocomposites. *Environ. Sci. Technol.* **2012**, *46*, 1804–1810. [CrossRef]
16. Azeredo, J.; Azevedo, N.F.; Briandet, R.; Cerca, N.; Coenye, T.; Costa, A.R.; Desvaux, M.; Di Bonaventura, G.; Hébraud, M.; Jaglic, Z.; et al. Critical Review on Biofilm Methods. *Crit. Rev. Microbiol.* **2017**, *43*, 313–351. [CrossRef]
17. Wagner, M.; Horn, H. Optical Coherence Tomography in Biofilm Research: A Comprehensive Review. *Biotechnol. Bioeng.* **2017**, *114*, 1386–1402. [CrossRef]
18. Hou, J.; Wang, C.; Rozenbaum, R.T.; Gusnaniar, N.; de Jong, E.D.; Woudstra, W.; Geertsema-Doornbusch, G.I.; Atema-Smit, J.; Sjollema, J.; Ren, Y.; et al. Bacterial Density and Biofilm Structure Determined by Optical Coherence Tomography. *Sci. Rep.* **2019**, *9*, 9794. [CrossRef]
19. Yang, X.; Beyenal, H.; Harkin, G.; Lewandowski, Z. Quantifying Biofilm Structure Using Image Analysis. *J. Microbiol. Methods* **2000**, *39*, 109–119. [CrossRef]
20. Heydorn, A.; Nielsen, A.T.; Hentzer, M.; Sternberg, C.; Givskov, M.; Ersbøll, B.K.; Molin, S. Quantification of Biofilm Structures by the Novel Computer Program COMSTAT. *Microbiology* **2000**, *146 Pt 10*, 2395–2407. [CrossRef]
21. Mueller, L.N.; de Brouwer, J.F.C.; Almeida, J.S.; Stal, L.J.; Xavier, J.B. Analysis of a Marine Phototrophic Biofilm by Confocal Laser Scanning Microscopy Using the New Image Quantification Software PHLIP. *BMC Ecol.* **2006**, *6*, 1. [CrossRef]
22. Chávez de Paz, L.E. Image Analysis Software Based on Color Segmentation for Characterization of Viability and Physiological Activity of Biofilms. *Appl. Environ. Microbiol.* **2009**, *75*, 1734–1739. [CrossRef] [PubMed]
23. Daims, H.; Lücker, S.; Wagner, M. Daime, a Novel Image Analysis Program for Microbial Ecology and Biofilm Research. *Environ. Microbiol.* **2006**, *8*, 200–213. [CrossRef] [PubMed]
24. Claessen, D.; Rozen, D.E.; Kuipers, O.P.; Søgaard-Andersen, L.; van Wezel, G.P. Bacterial Solutions to Multicellularity: A Tale of Biofilms, Filaments and Fruiting Bodies. *Nat. Rev. Microbiol.* **2014**, *12*, 115–124. [CrossRef] [PubMed]
25. Chambers, L.D.; Stokes, K.R.; Walsh, F.C.; Wood, R.J.K. Modern Approaches to Marine Antifouling Coatings. *Surf. Coat. Technol.* **2006**, *201*, 3642–3652. [CrossRef]
26. Palmer, J.; Flint, S.; Brooks, J. Bacterial Cell Attachment, the Beginning of a Biofilm. *J. Ind. Microbiol. Biotechnol.* **2007**, *34*, 577–588. [CrossRef] [PubMed]
27. Mostafaei, A.; Nasirpouri, F. Preparation and Characterization of a Novel Conducting Nanocomposite Blended with Epoxy Coating for Antifouling and Antibacterial Applications. *J. Coat. Technol. Res.* **2013**, *10*, 679–694. [CrossRef]
28. Hoge, J.; Leach, C. Epoxy Resin Infused Boat Hulls. *Reinf. Plast.* **2016**, *60*, 221–223. [CrossRef]
29. Vagos, M.R.; Gomes, M.; Moreira, J.M.R.; Soares, O.S.G.P.; Pereira, M.F.R.; Mergulhão, F.J. Carbon Nanotube/Poly(Dimethylsiloxane) Composite Materials to Reduce Bacterial Adhesion. *Antibiotics* **2020**, *9*, 434. [CrossRef]
30. Soares, O.; Gonçalves, A.G.; Delgado, J.J.; Órfão, J.J.M.; Pereira, M.F.R. Modification of Carbon Nanotubes by Ball-Milling to Be Used as Ozonation Catalysts. *Catal. Today* **2015**, *249*, 199–203. [CrossRef]
31. Faria, S.I.; Teixeira-Santos, R.; Gomes, L.C.; Silva, E.R.; Morais, J.; Vasconcelos, V.; Mergulhão, F.J.M. Experimental Assessment of the Performance of Two Marine Coatings to Curb Biofilm Formation of Microfoulers. *Coatings* **2020**, *10*, 893. [CrossRef]
32. Luan, Y.; Van Der Mei, H.C.; Dijk, M.; Geertsema-Doornbusch, G.I.; Atema-Smit, J.; Ren, Y.; Chen, H.; Busscher, H.J. Polarization of Macrophages, Cellular Adhesion, and Spreading on Bacterially Contaminated Gold Nanoparticle-Coatings In Vitro. *ACS Biomater. Sci. Eng.* **2020**, *6*, 933–945. [CrossRef]
33. Alves, P.; Gomes, L.C.; Vorobii, M.; Rodriguez-Emmenegger, C.; Mergulhão, F.J. The Potential Advantages of Using a Poly(HPMA) Brush in Urinary Catheters: Effects on Biofilm Cells and Architecture. *Colloids Surf. B Biointerfaces* **2020**, *191*, 110976. [CrossRef] [PubMed]
34. Ramos, V.; Morais, J.; Castelo-Branco, R.; Pinheiro, Â.; Martins, J.; Regueiras, A.; Pereira, A.L.; Lopes, V.R.; Frazão, B.; Gomes, D.; et al. Cyanobacterial Diversity Held in Microbial Biological Resource Centers as a Biotechnological Asset: The Case Study of the Newly Established LEGE Culture Collection. *J. Appl. Phycol.* **2018**, *30*, 1437–1451. [CrossRef] [PubMed]
35. Kotai, J. *Instructions for the Preparation of Modified Nutrient Solution Z8 for Algae*; Norwegian Institute for Water Research: Blindern, Norway, 1972; p. 5.
36. Romeu, M.J.; Alves, P.; Morais, J.; Miranda, J.M.; de Jong, E.D.; Sjollema, J.; Ramos, V.; Vasconcelos, V.; Mergulhão, F.J.M. Biofilm Formation Behaviour of Marine Filamentous Cyanobacterial Strains in Controlled Hydrodynamic Conditions. *Environ. Microbiol.* **2019**, *21*, 4411–4424. [CrossRef] [PubMed]
37. Boyer, J.N.; Kelble, C.R.; Ortner, P.B.; Rudnick, D.T. Phytoplankton Bloom Status: Chlorophyll *a* Biomass as an Indicator of Water Quality Condition in the Southern Estuaries of Florida, USA. *Ecol. Indic.* **2009**, *9*, 56–67. [CrossRef]
38. Porra, R.; Thompson, W.; Kriedemann, P. Determination of Accurate Extinction Coefficients and Simultaneous Equations for Assaying Chlorophylls *a* and *b* Extracted with Four Different Solvents: Verification of the Concentration of Chlorophyll Standards by Atomic Absorption Spectroscopy. *Biochim. Biophys. Acta* **1989**, *975*, 384–394. [CrossRef]
39. Bakker, D.P.; Van Der Plaats, A.; Verkerke, G.J.; Busscher, H.J.; Mei, H.C. Van Der Comparison of Velocity Profiles for Different Flow Chamber Designs Used in Studies of Microbial Adhesion to Surfaces. *Appl. Environ. Microbiol.* **2003**, *69*, 6280–6287. [CrossRef]

40. Silva, E.R.; Tulcidas, A.V.; Ferreira, O.; Bayón, R.; Igartua, A.; Mendoza, G.; Mergulhão, F.J.M.; Faria, S.I.; Gomes, L.C.; Carvalho, S.; et al. Assessment of the Environmental Compatibility and Antifouling Performance of an Innovative Biocidal and Foul-Release Multifunctional Marine Coating. *Environ. Res.* **2021**, *198*, 111219. [CrossRef]
41. Faria, S.; Teixeira-Santos, R.; Romeu, M.J.; Morais, J.; de Jong, E.; Sjollema, J.; Vasconcelos, V.; Mergulhão, F.J. Unveiling the Antifouling Performance of Different Marine Surfaces and Their Effect on the Development and Structure of Cyanobacterial Biofilms. *Microorganisms* **2021**, *9*, 1102. [CrossRef]
42. Otsu, N. A Threshold Selection Method from Gray-Level Histograms. *IEEE Trans. Syst. Man. Cybern.* **1979**, *9*, 62–66. [CrossRef]
43. Romeu, M.J.; Domínguez-Pérez, D.; Almeida, D.; Morais, J.; Araújo, M.J.; Osório, H.; Campos, A.; Vasconcelos, V.; Mergulhão, F.J. Quantitative Proteomic Analysis of Marine Biofilms Formed by Filamentous Cyanobacterium. *Environ. Res.* **2021**, 111566. [CrossRef]
44. Alves, P.; Gomes, L.C.; Rodríguez-Emmenegger, C.; Mergulhão, F.J. Efficacy of A Poly(MeOEGMA) Brush on the Prevention of *Escherichia Coli* Biofilm Formation and Susceptibility. *Antibiotics* **2020**, *9*, 216. [CrossRef]
45. Fan, F.X.; Zheng, Y.M.; Ba, M.; Wang, Y.F.; Kong, J.J.; Liu, J.H.; Wu, Q. Long Time Super-Hydrophobic Fouling Release Coating with the Incorporation of Lubricant. *Prog. Org. Coat.* **2021**, *152*, 106136. [CrossRef]
46. Selim, M.S.; El-Safty, S.A.; Fatthallah, N.A.; Shenashen, M.A. Silicone/Graphene Oxide Sheet-Alumina Nanorod Ternary Composite for Superhydrophobic Antifouling Coating. *Prog. Org. Coat.* **2018**, *121*, 160–172. [CrossRef]
47. Mahltig, B. Smart Hydrophobic and Soil-Repellent Protective Composite Coatings for Textiles and Leather. In *Smart Composite Coatings and Membranes*; Montemor, M.F., Ed.; Woodhead Publishing: Sawston, UK, 2016; pp. 261–292. ISBN 978-178-242-283-9.
48. Leonardi, A.K.; Ober, C.K. Polymer-Based Marine Antifouling and Fouling Release Surfaces: Strategies for Synthesis and Modification. *Annu. Rev. Chem. Biomol. Eng.* **2019**, *10*, 241–264. [CrossRef] [PubMed]
49. Schumacher, J.F.; Aldred, N.; Callow, M.E.; Finlay, J.A.; Callow, J.A.; Clare, A.S.; Brennan, A.B. Species-Specific Engineered Antifouling Topographies: Correlations between the Settlement of Algal Zoospores and Barnacle Cyprids. *Biofouling* **2007**, *23*, 307–317. [CrossRef] [PubMed]
50. Yandi, W.; Mieszkin, S.; Martin-Tanchereau, P.; Callow, M.E.; Callow, J.A.; Tyson, L.; Liedberg, B.; Ederth, T. Hydration and Chain Entanglement Determines the Optimum Thickness of Poly(HEMA-Co-PEG10MA) Brushes for Effective Resistance to Settlement and Adhesion of Marine Fouling Organisms. *ACS Appl. Mater. Interfaces* **2014**, *6*, 11448–11458. [CrossRef] [PubMed]
51. Scardino, A.J.; Guenther, J.; de Nys, R. Attachment Point Theory Revisited: The Fouling Response to a Microtextured Matrix. *Biofouling* **2008**, *24*, 45–53. [CrossRef]
52. Brady, R.F.; Singer, I.L. Mechanical Factors Favoring Release from Fouling Release Coatings. *Biofouling* **2000**, *15*, 73–81. [CrossRef]
53. Moreira, J.M.R.; Gomes, L.C.; Whitehead, K.A.; Lynch, S.; Tetlow, L.A.; Mergulhão, F.J. Effect of Surface Conditioning with Cellular Extracts on *Escherichia Coli* Adhesion and Initial Biofilm Formation. *Food Bioprod. Process.* **2017**, *104*, 1–12. [CrossRef]
54. Bas, S.; Kramer, M.; Stopar, D. Biofilm Surface Density Determines Biocide Effectiveness. *Front. Microbiol.* **2017**, *8*, 2443. [CrossRef] [PubMed]
55. Laspidou, C.S.; Aravas, N. Variation in the Mechanical Properties of a Porous Multi-Phase Biofilm under Compression Due to Void Closure. *Water Sci. Technol.* **2007**, *55*, 447–453. [CrossRef] [PubMed]
56. Peterson, B.W.; van der Mei, H.C.; Sjollema, J.; Busscher, H.J.; Sharma, P.K.; Chapman, M.; Hultgren, S.J. A Distinguishable Role of EDNA in the Viscoelastic Relaxation of Biofilms. *MBio* **2021**, *4*, e00497-13. [CrossRef]
57. Peterson, B.W.; He, Y.; Ren, Y.; Zerdoum, A.; Libera, M.R.; Sharma, P.K.; van Winkelhoff, A.J.; Neut, D.; Stoodley, P.; van der Mei, H.C.; et al. Viscoelasticity of Biofilms and Their Recalcitrance to Mechanical and Chemical Challenges. *FEMS Microbiol. Rev.* **2015**, *39*, 234–245. [CrossRef]
58. Delauney, L.; Compare, C.; Lehaitre, M. Biofouling Protection for Marine Environmental Sensors. *Ocean Sci.* **2010**, *6*, 503–511. [CrossRef]
59. Sjollema, J.; Rustema-Abbing, M.; van der Mei, H.C.; Busscher, H.J. Generalized Relationship between Numbers of Bacteria and Their Viability in Biofilms. *Appl. Environ. Microbiol.* **2011**, *77*, 5027–5029. [CrossRef]
60. Milferstedt, K.; Pons, M.-N.; Morgenroth, E. Analyzing Characteristic Length Scales in Biofilm Structures. *Biotechnol. Bioeng.* **2009**, *102*, 368–379. [CrossRef]
61. Pons, M.-N.; Milferstedt, K.; Morgenroth, E. Biofilm Monitoring on Rotating Discs by Image Analysis. *Biotechnol. Bioeng.* **2009**, *103*, 105–116. [CrossRef]
62. de Carvalho, C.C.C.R.; da Fonseca, M.M.R. Assessment of Three-Dimensional Biofilm Structure Using an Optical Microscope. *Biotechniques* **2007**, *42*, 618–620. [CrossRef]
63. Luef, B.; Neu, T.R.; Zweimüller, I.; Peduzzi, P. Structure and Composition of Aggregates in Two Large European Rivers, Based on Confocal Laser Scanning Microscopy and Image and Statistical Analyses. *Appl. Environ. Microbiol.* **2009**, *75*, 5952–5962. [CrossRef]
64. Rodríguez, S.J.; Bishop, P.L. Three-Dimensional Quantification of Soil Biofilms Using Image Analysis. *Environ. Eng. Sci.* **2006**, *24*, 96–103. [CrossRef]
65. Sousa-Cardoso, F.; Teixeira-Santos, R.; Mergulhão, F.J.M. Antifouling Performance of Carbon-Based Coatings for Marine Applications: A Systematic Review. *Antibiotics* **2022**, *11*, 1102. [CrossRef] [PubMed]
66. Martinelli, E.; Suffredini, M.; Galli, G.; Glisenti, A.; Pettitt, M.E.; Callow, M.E.; Callow, J.A.; Williams, D.; Lyall, G. Amphiphilic Block Copolymer/Poly(Dimethylsiloxane) (PDMS) Blends and Nanocomposites for Improved Fouling-Release. *Biofouling* **2011**, *27*, 529–541. [CrossRef]

67. Xie, M.; Zhao, W.; Wu, Y. Preventing Algae Biofilm Formation via Designing Long-Term Oil Storage Surfaces for Excellent Antifouling Performance. *Appl. Surf. Sci.* **2021**, *554*, 149612. [CrossRef]
68. Sun, Y.; Lang, Y.; Yan, Z.; Wang, L.; Zhang, Z. High-Throughput Sequencing Analysis of Marine Pioneer Surface-Biofilm Bacteria Communities on Different PDMS-Based Coatings. *Colloids Surf. B Biointerfaces* **2020**, *185*, 110538. [CrossRef]
69. Sun, Y.; Lang, Y.; Sun, T.; Liu, Q.; Pan, Y.; Qi, Z.; Ling, N.; Feng, Y.; Yu, M.; Ji, Y.; et al. Antifouling Potential of Multi-Walled Carbon Nanotubes-Modified Chlorinated Rubber-Based Composites on the Colonization Dynamics of Pioneer Biofilm-Forming Eukaryotic Microbes. *Int. Biodeterior. Biodegrad.* **2020**, *149*, 104921. [CrossRef]
70. Sun, Y.; Zhang, Z. New Anti-Biofouling Carbon Nanotubes-Filled Polydimethylsiloxane Composites against Colonization by Pioneer Eukaryotic Microbes. *Int. Biodeterior. Biodegrad.* **2016**, *110*, 147–154. [CrossRef]
71. Yang, J.L.; Li, Y.F.; Guo, X.P.; Liang, X.; Xu, Y.F.; Ding, D.W.; Bao, W.Y.; Dobretsov, S. The Effect of Carbon Nanotubes and Titanium Dioxide Incorporated in PDMS on Biofilm Community Composition and Subsequent Mussel Plantigrade Settlement. *Biofouling* **2016**, *32*, 763–777. [CrossRef]
72. Zhang, D.; Liu, Z.; Wu, G.; Yang, Z.; Cui, Y.; Li, H.; Zhang, Y. Fluorinated Carbon Nanotube Superamphiphobic Coating for High-Efficiency and Long-Lasting Underwater Antibiofouling Surfaces. *ACS Appl. Bio Mater.* **2021**, *4*, 6351–6360. [CrossRef]
73. Mountcastle, S.E.; Vyas, N.; Villapun, V.M.; Cox, S.C.; Jabbari, S.; Sammons, R.L.; Shelton, R.M.; Walmsley, A.D.; Kuehne, S.A. Biofilm Viability Checker: An Open-Source Tool for Automated Biofilm Viability Analysis from Confocal Microscopy Images. *NPJ Biofilms Microbiomes* **2021**, *7*, 44. [CrossRef]
74. Van den Driessche, F.; Rigole, P.; Brackman, G.; Coenye, T. Optimization of Resazurin-Based Viability Staining for Quantification of Microbial Biofilms. *J. Microbiol. Methods* **2014**, *98*, 31–34. [CrossRef] [PubMed]
75. Jin, H.; Tian, L.; Bing, W.; Zhao, J.; Ren, L. Bioinspired Marine Antifouling Coatings: Status, Prospects, and Future. *Prog. Mater. Sci.* **2022**, *124*, 100889. [CrossRef]

Supplementary Material

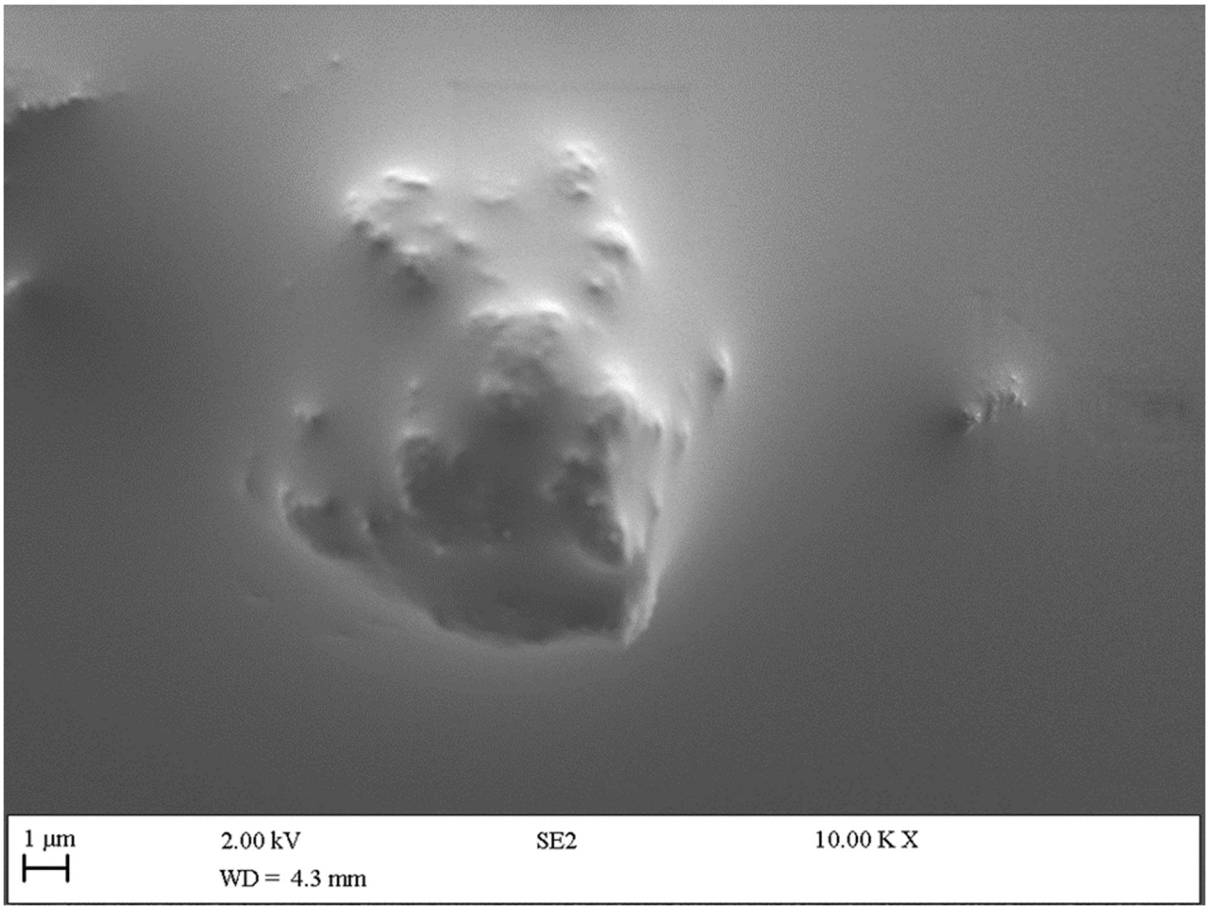

Figure S1. Representative SEM image of an agglomerate of CNTs on the CNT composite surface. Magnification = 10,000×; scale bar = 1 µm.

coatings

MDPI

Article

How do Graphene Composite Surfaces Affect the Development and Structure of Marine Cyanobacterial Biofilms?

Maria J. Romeu [1,2], Luciana C. Gomes [1,2], Francisca Sousa-Cardoso [1,2], João Morais [3], Vítor Vasconcelos [3,4], Kathryn A. Whitehead [5], Manuel F. R. Pereira [2,6], Olívia S. G. P. Soares [2,6] and Filipe J. Mergulhão [1,2,*]

1 LEPABE—Laboratory for Process Engineering, Environment, Biotechnology and Energy, Faculty of Engineering, University of Porto, Rua Dr. Roberto Frias, 4200-465 Porto, Portugal
2 ALiCE—Associate Laboratory in Chemical Engineering, Faculty of Engineering, University of Porto, Rua Dr. Roberto Frias, 4200-465 Porto, Portugal
3 CIIMAR—Interdisciplinary Centre of Marine and Environmental Research, University of Porto, Terminal de Cruzeiros do Porto de Leixões, Av. General Norton de Matos s/n, 4450-208 Matosinhos, Portugal
4 Department of Biology, Faculty of Sciences, University of Porto, Rua do Campo Alegre, 4169-007 Porto, Portugal
5 Microbiology at Interfaces, Manchester Metropolitan University, Chester Street, Manchester M1 5GD, UK
6 LSRE–LCM—Laboratory of Separation and Reaction Engineering–Laboratory of Catalysis and Materials, Faculty of Engineering, University of Porto, Rua Dr. Roberto Frias, 4200-465 Porto, Portugal
* Correspondence: filipem@fe.up.pt; Tel.: +351-225-081-668

Abstract: The progress of nanotechnology has prompted the development of novel marine antifouling coatings. In this study, the influence of a pristine graphene nanoplatelet (GNP)-modified surface in cyanobacterial biofilm formation was evaluated over a long-term assay using an in vitro platform which mimics the hydrodynamic conditions that prevail in real marine environments. Surface characterization by Optical Profilometry and Scanning Electron Microscopy has shown that the main difference between GNP incorporated into a commercially used epoxy resin (GNP composite) and both control surfaces (glass and epoxy resin) was related to roughness and topography, where the GNP composite had a roughness value about 1000 times higher than control surfaces. The results showed that, after 7 weeks, the GNP composite reduced the biofilm wet weight (by 44%), biofilm thickness (by 54%), biovolume (by 82%), and surface coverage (by 64%) of cyanobacterial biofilms compared to the epoxy resin. Likewise, the GNP-modified surface delayed cyanobacterial biofilm development, modulated biofilm structure to a less porous arrangement over time, and showed a higher antifouling effect at the biofilm maturation stage. Overall, this nanocomposite seems to have the potential to be used as a long-term antifouling material in marine applications. Moreover, this multifactorial study was crucial to understanding the interactions between surface properties and cyanobacterial biofilm development and architecture over time.

Keywords: antifouling surface; biofilm architecture; cyanobacterial biofilm; graphene; marine biofouling

check for updates

Citation: Romeu, M.J.; Gomes, L.C.; Sousa-Cardoso, F.; Morais, J.; Vasconcelos, V.; Whitehead, K.A.; Pereira, M.F.R.; Soares, O.S.G.P.; Mergulhão, F.J. How do Graphene Composite Surfaces Affect the Development and Structure of Marine Cyanobacterial Biofilms? *Coatings* **2022**, *12*, 1775. https://doi.org/10.3390/coatings12111775

Academic Editor: Mohor Mihelčič

Received: 20 October 2022
Accepted: 17 November 2022
Published: 20 November 2022

Publisher's Note: MDPI stays neutral with regard to jurisdictional claims in published maps and institutional affiliations.

Copyright: © 2022 by the authors. Licensee MDPI, Basel, Switzerland. This article is an open access article distributed under the terms and conditions of the Creative Commons Attribution (CC BY) license (https://creativecommons.org/licenses/by/4.0/).

1. Introduction

The oil, gas, and maritime industry are significantly impacted by biofouling, either through the costs related to the increased fuel consumption, hull cleaning, material deterioration, repainting, and corrosion [1], or even by the management intervention time and incorrect measurements in the submerged and moored sensors [2]. Ecologically, fouling events in marine environments promote species invasion and the establishment of exotic biofouling species in ports [3]. Moreover, biofouling can be a major concern in health-related problems since contamination of aquaculture facilities, such as fish cages, can occur by toxin accumulation, and air pollution may be increased through greenhouse gas emissions [4].

The non-toxic marine antifouling approaches available in the market are often expensive and not as effective as conventional biocides, which can accumulate in the marine environment and affect non-target aquatic organisms. Inorganic ingredient-based coatings have been used for biofouling prevention, including silver nanoparticles [5], carbon nanotubes (CNTs) [6], graphene [7], and metal oxides semiconductors such as zinc oxide (ZnO) [8] and titanium dioxide (TiO_2) [9]. Overall, antifouling marine paints containing nanomaterials have been reported to offer superhydrophobicity, microbial resistance, high durability, water repellency, anti-sticking, and anti-corrosive properties [10], being novel solutions for the sustainable development of the maritime industry. Advancements in materials technology have introduced carbon nanomaterials such as CNTs and graphene as a powerful approach for various applications in the marine and shipping industries [11]. Graphene consists of a single layer of carbon atoms arranged in a sp^2-bonded hexagonal pattern. It is considered one of the strongest and thinnest materials available, which shows high specific surface area, electrical conductivity, and thermal stability, making it appealing for different applications [12,13]. Moreover, due to its high strength level [14], this material is a breakthrough alternative in the naval industry. All these features make the application of graphene in technical processes of maritime industries attractive, such as in water management systems, desalination, removing toxic pollutants and filtering gasses, and as a coating material [15–17]. As a coating on marine structures, besides the anti-corrosive properties, graphene can also be used in de-icing surfaces for ship operations in extremely low-temperature regions, such as the Arctic and Antarctica, due to its electrical conductivity [15].

Nanotechnology-based technologies can be of great interest in creating novel low-toxic antifouling coatings [18]. However, analysis of the literature indicates that there is little information about the use of pristine graphene. Indeed, most in situ studies on graphene-based surfaces were performed with functionalized graphene and graphene oxide (GO) coatings [19–23]. Diatom adhesion was completely inhibited after 10 days by surfaces containing 0.36 wt% GO [24]. In turn, GO-silver nanoparticle coatings improved antibacterial and anti-algal properties [25], and showed more than 80% *Halomonas pacifica* biofilm inhibition [26]. Since the current trend is to study the potential of modified and functionalized graphene, the antibiofilm performance of graphene alone is poorly understood. Moreover, most in vitro studies are usually performed for short periods and under hydrodynamic conditions that do not mimic the real marine environment [27]. In fact, some of the in vitro studies have been performed until 24 h [6,23,25,28,29], most of them between days and weeks [7,19,20,24,30–33], but only a study performed by Fazli-Shokouhi et al. [34] extended the assay period for 3 months to evaluate the antifouling potential of graphene-based coatings. Moreover, these studies focus on organisms other than cyanobacteria, namely diatoms, algae, and macrofoulers. Therefore, the main goal of this work was to evaluate the potential of a graphene composite surface to prevent and control the development of biofilms by marine microfoulers over a long-term assay and using an in vitro platform that mimics the hydrodynamic conditions found in real marine scenarios. Cyanobacterial biofilm architecture was evaluated by three different imaging techniques: Optical Coherence Tomography (OCT), Confocal Laser Scanning Microscopy (CLSM), and Scanning Electron Microscopy (SEM). Since the epoxy resin is a commercially available coating generally used to coat the hulls of small recreational vessels [35,36] due to its exceptional physical, chemical, and mechanical properties, no safety issues, and low cost [37], pristine graphene nanoplatelets (GNP) were incorporated into this polymer matrix. Furthermore, epoxy composites exhibited high durability and resistance to fatigue and UV irradiation [38]. Surface characterization was also performed by water contact angle measurements, Optical Profilometry, and SEM.

2. Materials and Methods

Figure 1 presents the flowchart of the experimental work fully described in the upcoming sections.

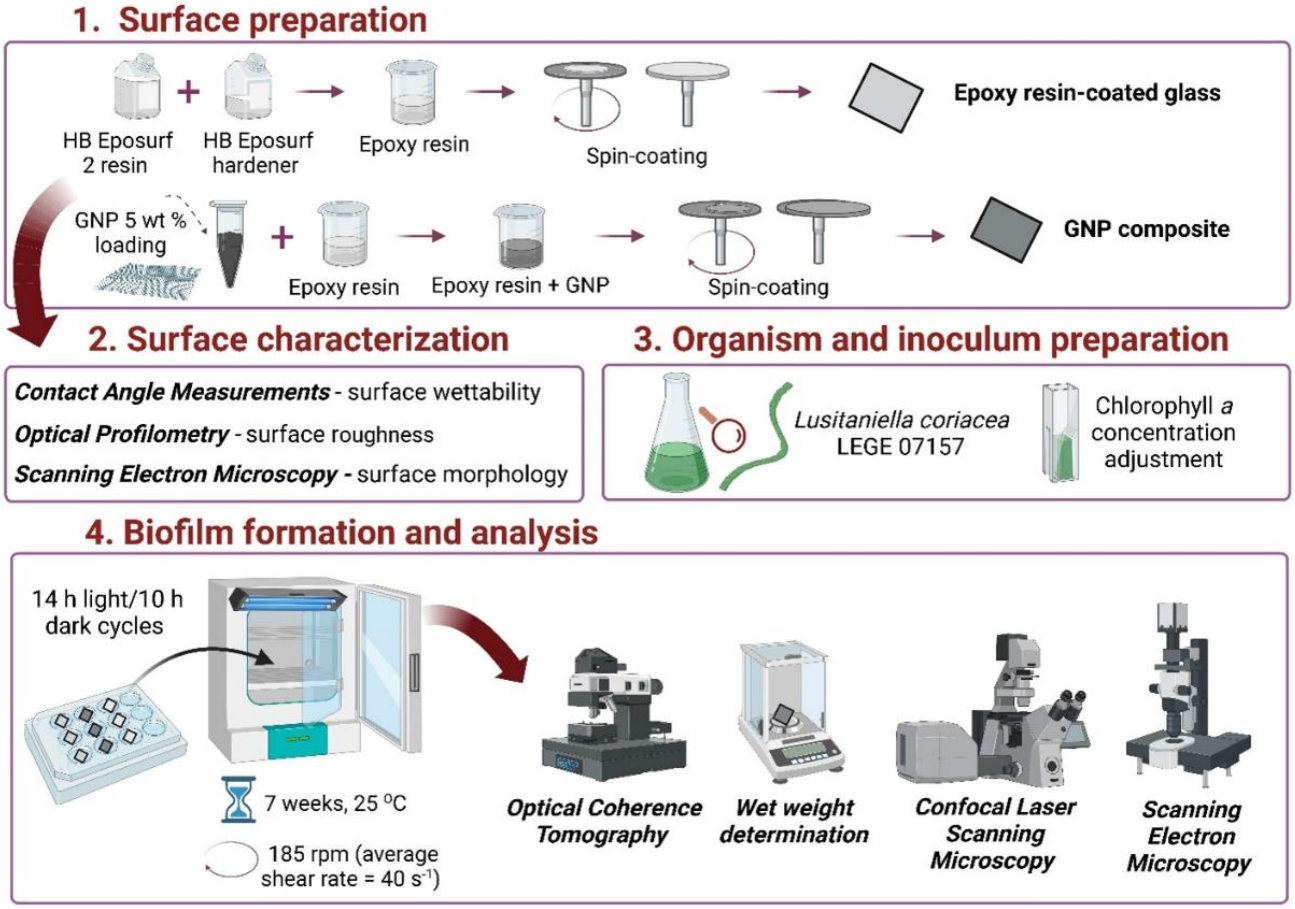

Figure 1. Scheme of the experimental steps of the present work.

2.1. Surface Preparation

Two control surfaces (glass, a commonly submerged artificial surface found on diverse equipment in aquatic environments, and epoxy resin, a commercially available marine coating) and a GNP composite were tested to determine their performance against cyanobacterial biofilm development. The epoxy resin-coated glass was prepared following the protocol described by Faria et al. [39]. Briefly, HB Eposurf 2 resin and HB Eposurf hardener, both from HB Química (Matosinhos, Portugal), were mixed in a ratio of 10:3 (*v*/*v*). To produce the epoxy resin-coated surfaces, 70 µL of the above mixture was placed on top of 1 cm × 1 cm glass coupons (Vidraria Lousada, Lda, Lousada, Portugal) using a spin coater (Spin150 PolosTM, Paralab, Porto, Portugal) at 6000 rpm for 40 s. After 12 h at room temperature, the surfaces were dried for 3 h at 60 °C.

The methodology for the preparation of the GNP composite was adapted from Oliveira et al. [40], in which the polydimethylsiloxane (PDMS) matrix was replaced by the epoxy resin. Briefly, after mixing the two epoxy resin components, 5 wt% of GNPs aggregates (Alfa Aesar, Thermo Fisher Scientific, Erlenbachweg, Germany) were incorporated into the epoxy resin mixture. The specific surface area (S_{BET}), external surface area (S_{meso}), micropore volume (V_{micro}), and total pore volume (V_p) of these GNPs are 464 $m^2\ g^{-1}$, 363 $m^2\ g^{-1}$, 0.045 $cm^3\ g^{-1}$, and 0.535 $cm^3\ g^{-1}$, respectively [40]. In the same study [40], 5 wt% was demonstrated to be an effective load in reducing single- and mixed-species biofilms of *Pseudomonas aeruginosa* and *Staphylococcus aureus* formation after 24 h. After the incorporation step, 70 µL of the composite (5 wt% GNP/epoxy resin) was deposited on glass squares by spin coating.

2.2. Surface Characterization

2.2.1. Wettability

The measurement of water contact angles (θ_w) was performed through the sessile drop method using an SL200C optical contact angle meter (Solon Information Technology Co., Ltd., Shanghai, China) as previously described [41,42]. At least 25 determinations for each material at room temperature were performed.

2.2.2. Optical Profilometry

Optical profilometry was used to determine the average roughness (S_a) of the glass, epoxy resin, and GNP composite surfaces, as previously performed by Whitehead et al. [43,44]. A MicroXAM surface mapping microscope (ADE Corporation, XYZ model 4400 mL system, Tucson, AZ, USA), with an objective of 50× and connected to an AD phase shift controller (Omniscan, Wrexham, UK), was used to image five areas (167 µm × 167 µm) of at least four different coupons. The MapView AE 2.17 software (Omniscan, Wrexham, UK) was chosen to determine the (S_a) values through extended range vertical scanning interferometry, and the 3D images were extracted by SPIP™ 6.7.9 software (Image Metrology A/S, Hørsholm, Denmark).

2.2.3. Scanning Electron Microscopy (SEM)

The surface morphology of the three surfaces used in this study was investigated using SEM. The surfaces were placed on SEM stubs (Agar Scientific, Stansted, UK) and sputter-coated with gold for 30 s in an SEM coating system (Polaron, London, UK). The secondary electron detector of a Supra 40VP scanning electron microscope (Carl Zeiss Ltd., Cambridge, UK) was used to obtain images of at least three coupons for each surface at an accelerating voltage of 2 kV.

2.3. Organism and Inoculum Preparation

A filamentous cyanobacterial strain *Lusitaniella coriacea* LEGE 07157 was obtained from the Interdisciplinary Centre of Marine and Environmental Research (CIIMAR), Matosinhos, Portugal [45]. *Lusitaniella coriacea* LEGE 07157 was isolated by rock surface scraping from a zone tide pool at Lavadores beach, Porto, Portugal (41.12919 N 8.668578 W). It was grown in Z8 medium [46] enhanced with 25 g L^{-1} of synthetic sea salts (Tropic Marin) and vitamin B_{12} (Sigma Aldrich, Merck, Saint Louis, MO, USA), and at 25 °C under 14 h light (10–30 µmol photons m^{-2} s^{-1}, λ = 380–700 nm)/10 h dark cycles, as recommended by Ramos et al. [45].

2.4. Biofilm Formation

Cyanobacterial suspensions were adjusted to a chlorophyll *a* concentration of 1.22 ± 0.09 µg mL^{-1} since this pigment is unique and predominant in all groups of cyanobacteria and its quantification is a standard methodology to estimate the biomass in marine environments [47,48]. Briefly, cyanobacterial cells were collected by centrifugation (3202× *g* for 5 min) and a volume of 2 mL of 99.8% methanol (Methanol ACS Basic, Scharlau Basic, Barcelona, Spain) was added. After 24 h of dark incubation at 4 °C, cyanobacterial suspensions were centrifuged and absorbance measurements of the supernatant were performed at 750 nm (turbidity), 665 nm (chlorophyll *a*), and 652 nm (chlorophyll *b*) (V-1200 spectrophotometer, VWR International China Co., Ltd., Shanghai, China). The values obtained were used to calculate chlorophyll *a* concentration (µg·mL^{-1}) through Equation (1) [49]:

$$Chl\ a\ \left(\mu g \cdot mL^{-1}\right) = 16.29 \times A^{665} - 8.54 \times A^{652} \quad (1)$$

Biofilm formation was tested on agitated 12-well plates (VWR International, Carnaxide, Portugal) under previously optimized conditions for cyanobacterial biofilm development [47]. All coupons and plates were subjected to UV sterilization, after which

the coupons were fixed on double-sided adhesive tape [40,47]. A volume of 3 mL of the adjusted cyanobacterial suspension was added to each well. To mimic the hydrodynamic conditions found in marine environments, microplates were then incubated at 25 °C in a shaker with a 25 mm orbital diameter (Agitorb 200ICP, Norconcessus, Ermesinde, Portugal) at 185 rpm, resulting in an average shear rate of 40 s^{-1} [47]. Biofilm formation in this platform includes the shear rate valued for a ship in a harbor, 50 s^{-1} [50], and it was shown to predict the biofouling behavior observed upon immersion in the sea for prolonged periods [51]. Moreover, to simulate marine biofilm formation on submerged surfaces, microtiter plates were kept under 14 h light (8–10 µmol photons m^{-2} s^{-1})/10 h dark cycles [47,52,53]. The light intensity was decreased from 10–30 µmol photons m^{-2} s^{-1} to 8–10 µmol photons m^{-2} s^{-1} because biofouling organisms have reduced access to light when in immersion (either by the effect of the marine equipment/device/ship to which they are attached, or by the influence of the biofilm structure in which the accumulation of different organisms occurs, and some of them are located in the inners layers of biofilm). Since a 2-month interval for maintenance is the minimum time for economically viable underwater monitoring systems [47], biofilm development was followed for 7 weeks (49 days), and during this incubation time, the medium was changed twice a week in the sample and control wells.

2.5. Biofilm Analysis

Two coupons of each surface were analyzed every 7 days. For that, the culture medium was removed and the wells were filled with 3 mL of sodium chloride solution (8.5 g L^{-1}) [47]. The solution was carefully removed and the wells were filled again with 3 mL of sodium chloride to assess the cyanobacterial biofilm structure through Optical Coherence Tomography (OCT). The determination of biofilm wet weight was also performed over 7 weeks, and at the end of the experiment (49 days), cyanobacterial biofilm architecture and morphology were analyzed by Confocal Laser Scanning Microscopy (CLSM) and SEM, respectively.

2.5.1. Optical Coherence Tomography (OCT)

Images from cyanobacterial biofilms were captured as reported by Romeu et al. [47] through OCT (Thorlabs Ganymede Spectral Domain Optical Coherence Tomography system with a central wavelength of 930 nm, Thorlabs GmbH, Dachau, Germany). Briefly, for each coupon, 2D imaging was performed (with a minimum of 2 fields of view) and evaluated through a routine developed in the Image Processing Toolbox from MATLAB 8.0 and Statistics Toolbox 8.1 (The MathWorks, Inc., Natick, MA, USA) [54]. The mean of biofilm thickness was calculated according to Equation (2):

$$\overline{L}_F = \frac{1}{N}\sum_{i=1}^{N} L_{F,i} \quad (2)$$

where $L_{F,i}$ is a local biofilm thickness measurement at location i, N equals the number of thickness measurements, and $\overline{L}_F$ is the mean biofilm thickness. The percentage of empty spaces in the biofilm structure, as well as their average size, was also assessed [55].

2.5.2. Wet Weight Determination

The determination of the biofilm wet weight was performed as previously reported [56] and considered as the difference from the initial coupon weight determined before inoculation.

2.5.3. Confocal Laser Scanning Microscopy (CLSM)

Biofilms with 49 days were stained with 6 µM SYTO®61 (Thermo Fisher Scientific, Waltham, MA, USA), mounted on a microscopic slide, and observed in a Leica TCS SP5 II Confocal Laser Scanning Microscope (Leica Microsystems, Wetzlar, Germany) with a 40× water objective lens (Leica HCX PL APO CS 40.0x/1.10WATER UV) and 633-nm helium-neon laser. Image stacking was acquired with a z-step of 1 µm for each sample at a

minimum of five random fields of 387.5 μm × 387.5 μm (equivalent to 512 pixels × 512 pixels. The "Easy 3D" tool of the IMARIS 9.1 software (Bitplane, Zurich, Switzerland) was used to create 3D projections of the biofilms. Additionally, biofilm architectural parameters such as biovolume (μm^3 μm^{-2}) and surface coverage (%) were determined using the COMSTAT image-analysis software [57].

2.5.4. SEM

After 49 days of incubation, *Lusitaniella coriacea* LEGE 07157 biofilms grown on the three tested surfaces were observed by SEM. Samples were taken from the microplates, dehydrated with increasing ethanol concentrations (10, 25, 40, 50, 70, 80, 90, and 100% (*v*/*v*)), and left in a desiccator until microscopic analysis [58]. Then, they were sputter-coated using the equipment and conditions described before and imaged in the Supra 40VP scanning electron microscope.

2.6. Statistical Analysis

Two biological experiments with two technical replicates each were analyzed. Quantitative parameters obtained from biofilm wet weight, OCT, and CLSM were compared using one-way ANOVA with Tukey's multiple comparisons test (GraphPad Prism® version 6.01, GraphPad Software, Inc., San Diego, CA, USA). Statistically significant differences between the different surfaces for the same sampling day were considered for p values < 0.05 (corresponding to a confidence level greater than 95%). The error bars represent the standard deviation (SD) of the mean.

3. Results and Discussion

3.1. Surface Analysis

It is known that surface properties, including wettability, roughness, and morphology, are important factors governing initial bacterial adhesion to surfaces and consequently affect the development of mature biofilms [59]. Therefore, the three tested surfaces (glass, epoxy resin, and GNP composite) were evaluated regarding (i) wettability by water contact angle measurements, (ii) topography and roughness by Optical Profilometry, and (iii) morphology by SEM.

Results obtained from water contact angle measurements are shown in Figure 2a. Contact angle determination provides information about the wettability of the surface, i.e., the tendency of the fluid to spread on a surface, and the hydrophobicity of the surface, which describes the tendency of non-polar molecular aggregation and, consequently, water molecule repulsion [60]. Surfaces can be classified as superhydrophilic, hydrophilic, hydrophobic, or superhydrophobic, if the contact angle of water with the surfaces is lower than 10°, between 10° and 90°, between 90° and 150°, or over 150°, respectively [61]. While glass is considered hydrophilic (θ_w = 40.9° ± 7.4°), the GNP composite (θ_w = 68.6° ± 2.4°) and epoxy-coated surfaces (θ_w = 76.3° ± 2.5°) are slightly more hydrophobic than glass. The wettability of the epoxy resin was weakly affected by the incorporation of graphene on the coating; the GNP composite is slightly more hydrophilic than the resin. Similar results were observed in previous studies [40,62]. In fact, in a study performed by Rafiee et al. [62], the water contact angle of a copper substrate coated with graphene was up to 90.6°, while that of the pure copper substrate was about 85.9°. Oliveira and her coworkers [40] also verified that 5 wt% GNP/PDMS and PDMS surfaces presented similar water contact angles, 121.8° and 110.2°, respectively. Since the wetting properties at the water–graphene interface had little effect on the water–substrate interaction, this peculiar wettability of graphene has been described by the term "wetting transparency of graphene" [62]. In the present study, as dispersed GNPs were used instead of graphene layers, it is conceivable to assume that the wettability of the substrate may be even less affected by the presence of graphene.

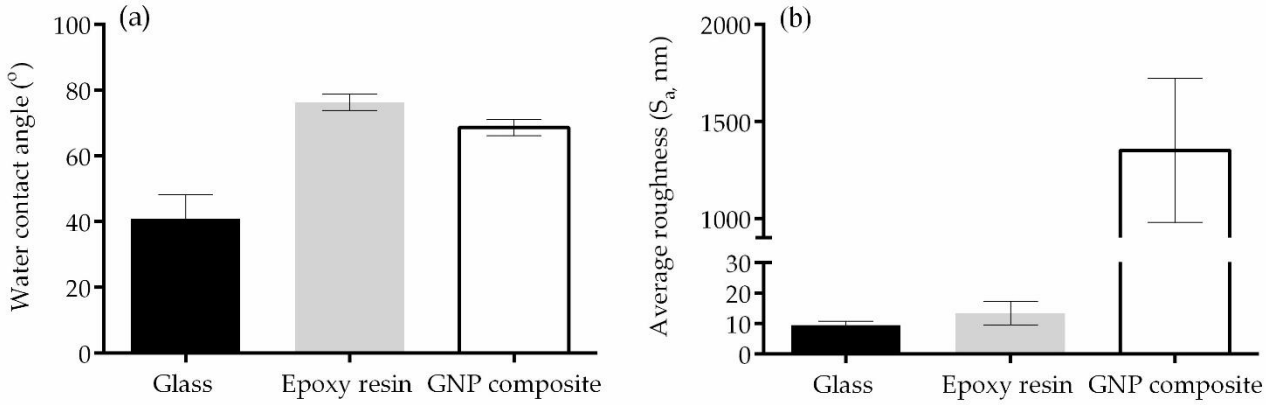

Figure 2. Water contact angles (**a**) and average roughness (S_a) (**b**) of the tested surfaces. The means ± SD are shown.

Results obtained from roughness analysis are shown in Figures 2b and 3. The GNP composite was the roughest surface (S_a = 1351 nm), followed by the epoxy resin (S_a = 13 nm) and glass (S_a = 10 nm). Therefore, the average roughness values of both control surfaces are on the nanometric scale, being about 1000 times lower than the roughness value determined for the GNP composite (Figure 2b). The difference in roughness and topography between the graphene composite and both control surfaces (glass and epoxy resin) is particularly evident in the 3D images of the surfaces given by profilometry (Figure 3). While glass and resin without incorporated carbon material were homogeneous and smooth surfaces (Figure 3a,b, respectively), the nanocomposite presented some irregularities distributed along the analyzed surface area (Figure 3c). Looking at the SEM images (Figure 4c,d), it was possible to confirm that these surface elevations correspond to agglomerated graphene nanoplatelets in the polymer matrix. Some of the larger agglomerates had sizes ranging from 7–30 µm.

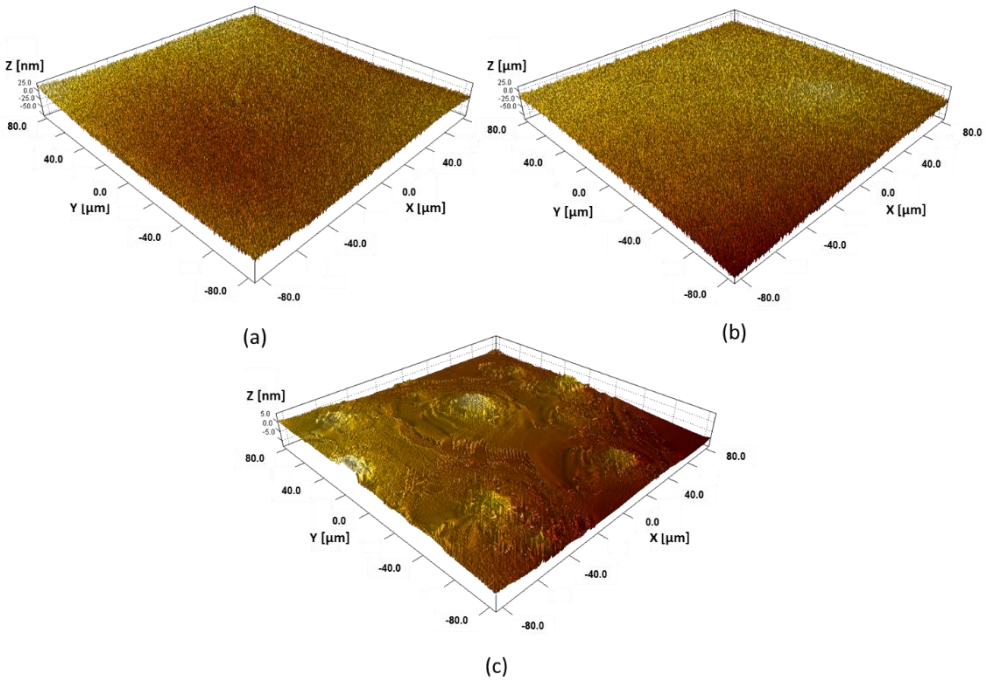

Figure 3. 3D profilometer images of glass (**a**), epoxy resin (**b**), and GNP composite (**c**).

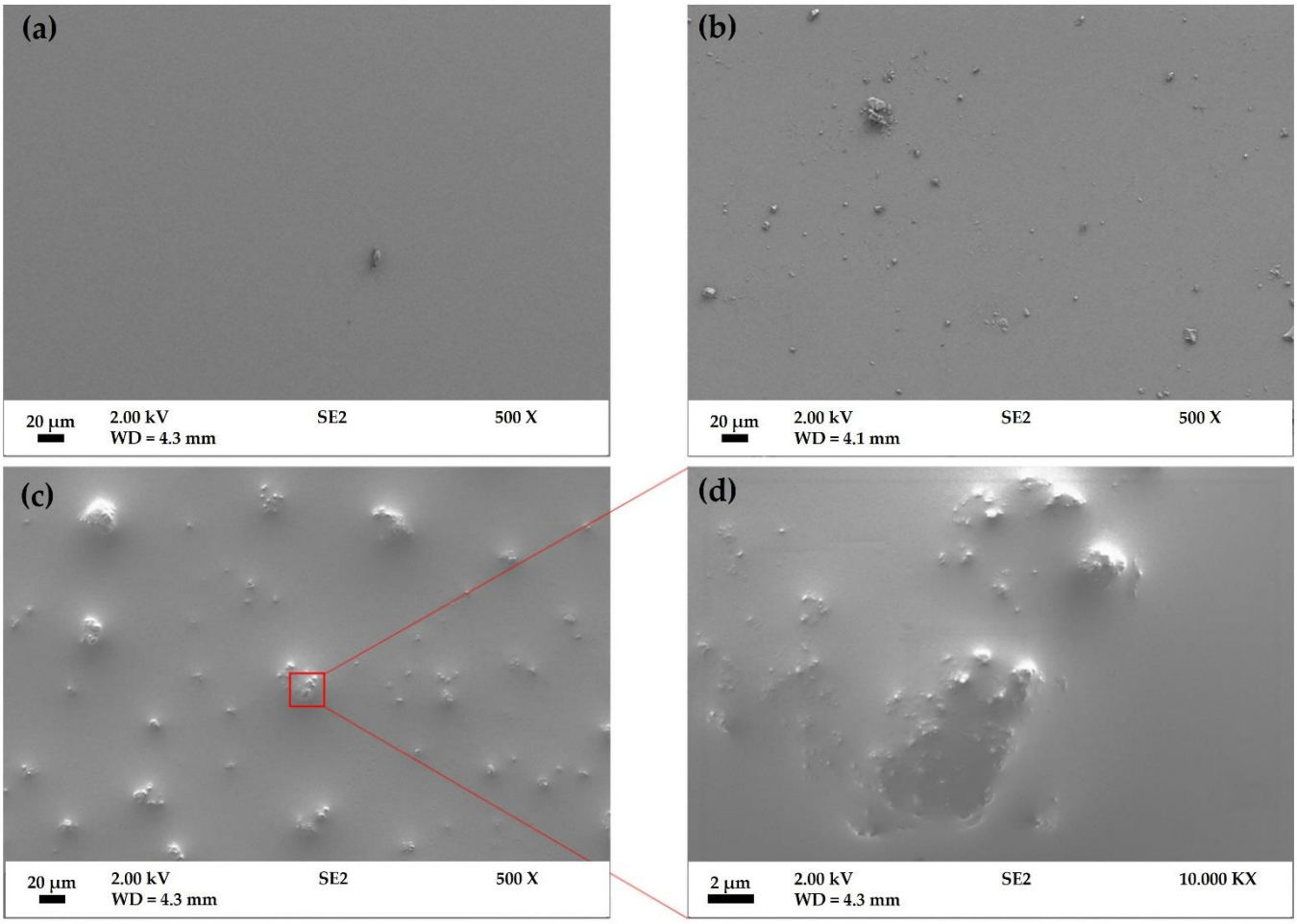

Figure 4. SEM images of glass (**a**), epoxy resin (**b**), GNP composite (**c**), and magnified GNP composite (**d**). The micrographs have a magnification of 500×, except for (**d**), which corresponds to a higher magnification image (10,000×) of the surface area marked in red in (**c**).

It is a challenge to disperse GNPs, especially compared to other carbon materials such as CNTs, due to the van der Waals forces and a strong π–π interaction between the individual GNP sheets, which are responsible for their layer-stacked compact structure [40,63]. Their incorporation in the polymeric resin may facilitate graphene dispersion, thus reducing the tendency to aggregate [64]. In the higher magnification image of the GNP composite (Figure 4d), it was interesting to detect some areas on top of the embedded GNP clusters where this carbon material was more exposed. It is described that one of the factors directing the antimicrobial activity of graphene is the agglomeration tendency, which causes a reduced surface area and shape alteration [65,66]. However, the presence of more exposed GNPs in the epoxy resin may facilitate their interaction with the microorganisms that come in contact with the surface, triggering the predominant antimicrobial mechanisms of this carbon nanomaterial—oxidative stress, mechanical damage of cell membrane/wall by nanoknives, and wrapping/trapping [66,67].

In vitro assays showed that no detectable leaching occured under the conditions used in this work as assessed by UV-Vis spectroscopy (data not shown).

3.2. Biofilm Development

As there are several mechanisms affecting the microbial response and the disruption of biofilm architecture, the long-term antifouling properties of a given surface for marine applications should be extensively studied. Although the Minimal Inhibitory Concentration (MIC) of the studied GNPs could not be determined for *Lusitaniella coriacea* LEGE 07167 (it is

a filamentous cyanobacterium and therefore cell numbers cannot be accurately determined), it was found to be higher than 5% (*w*/*v*, in a VNSS suspension assay) for a model marine bacterium (*Cobetia marina*). Cyanobacterial biofilm development was monitored over 7 weeks (49 days) and the quantitative results obtained from wet weight determination and 2D OCT analysis are shown in Figure 5. The values regarding the biofilm thickness, the percentage of empty spaces, and the average size of empty spaces on biofilm structure (Figure 5b–d) are indicated from day 14 since the biofilm thickness was below the OCT range on the first sampling day. Although a progressive increase in biofilm development was observed from the results of wet weight (Figure 5a) and biofilm thickness (Figure 5b), this evolution over the 7 weeks was more noticeable on glass and epoxy resin than on the GNP composite. Indeed, for biofilm wet weight (Figure 5a), from day 7 to day 49, an increase of 84 %, 77 %, and 67 % was observed for glass, epoxy resin, and GNP composite, respectively, while for biofilm thickness (Figure 5b), from day 14 to day 49, an increase of 85 %, 86 %, and 58 % was observed for the same surfaces. This behavior was also seen regarding biofilm architecture (Figure 5c) given that an increase of 92 %, 98 %, and just 28 % for the percentage of empty spaces was observed on glass, epoxy resin, and GNP composite. This suggests that graphene-modified surfaces may delay biofilm development (Figure 5a,b) and change its structure to a less porous arrangement (Figure 5c). Additionally, on days 35, 42, and 49, a reduction of biofilm wet weight and thickness was observed on the GNP composite surface when compared to the epoxy resin itself. In fact, on days 35, 42 and 49, the wet weight values obtained for the GNP composite were 46 %, 47 %, and 44 % lower than those obtained on the epoxy resin surface, respectively (Figure 5a). For biofilm thickness on the same days, the values obtained on the GNP composite were 46 %, 42 %, and 54 % lower than those obtained on the epoxy resin surface, respectively (Figure 5b). The delay effect caused by this carbon nanomaterial on cyanobacterial biofilm development, as well as the greater antifouling effect on the maturation stage of biofilm development, was also observed in previous work where CNT-modified surfaces were used as potential antifouling surfaces [42]. In addition, in the maturation stage of biofilm development (days 42 and 49), a lower percentage of empty spaces (Figure 5c) and an average size of empty spaces on biofilm structure (Figure 5d) were detected for biofilms formed on the GNP composite when compared with control surfaces (glass and epoxy resin).

Figure 6 shows representative 2D cross-sectional images of *Lusitaniella coriacea* LEGE 07157 biofilm development on glass, epoxy resin, and GNP composite after 49 days. These images corroborate the quantitative data obtained from biofilm biomass (Figure 5a,b) and empty spaces on biofilm architecture (Figure 5c,d) since a lower amount of biofilm mass and percentage of empty spaces and its average size were observed on the GNP composite compared to the control epoxy resin. Although the reduced biofilm development on the GNP-based coating may be beneficial for the performance of marine devices and/or equipment, the efficacy of chemical methods to eradicate biofilms formed on this surface material may be hampered. Given the lower percentage of empty spaces and their smaller average size shown in biofilms formed on the GNP composite, the diffusion of chemical compounds typically used for biofouling control through the inner layers of the biofilm may be hindered [68]. The biofilm structure could also be compared between the three surfaces. While a flatter and homogeneous biofilm was observed on glass (Figure 6a), biofilms formed on the epoxy resin (Figure 6b) and GNP composite (Figure 6c) had heterogeneous shapes. Additionally, more streamers could be observed on top of the biofilm developed on the epoxy resin surface (Figure 6b), which probably contributed to the higher thickness of biofilms developed on this surface compared to the GNP composite (Figure 5b). Opposing results were obtained in a previous study focused on CNT-based surfaces [42], in which a flatter and homogeneous cyanobacterial biofilm was observed on the CNT composite. However, this divergent finding may be related to the use of a different cyanobacterial strain and carbon-based surface.

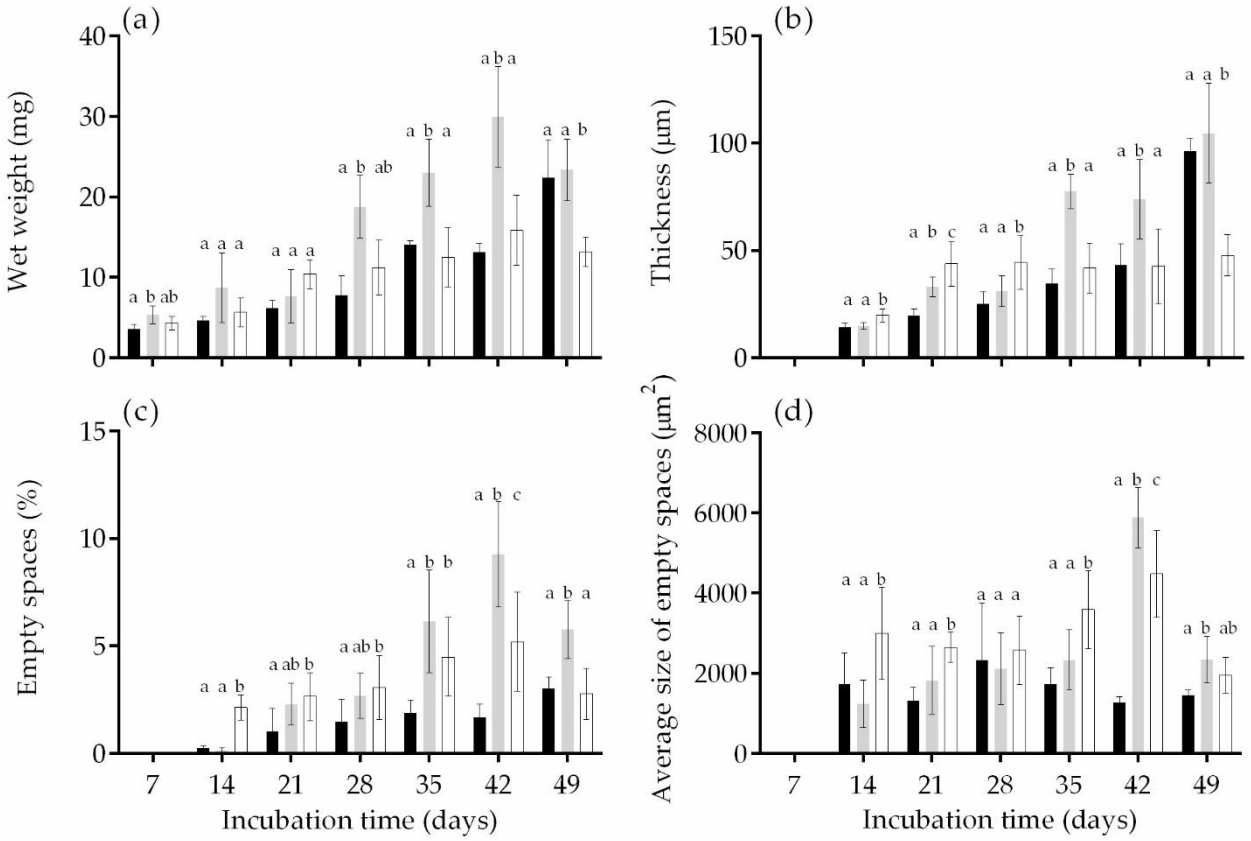

Figure 5. *Lusitaniella coriacea* LEGE 07157 biofilm development on different surfaces: glass (black), epoxy resin (grey), GNP composite (white). The parameters analyzed refer to biofilm wet weight (**a**), biofilm thickness (**b**), average percentage of empty spaces (**c**), and their respective average size (**d**) on biofilm structure. Mean values and SD from two biological assays with two technical replicates each are represented. For each sampling day, different lowercase letters (a, b, and c) indicate significant differences between surfaces ($p < 0.05$).

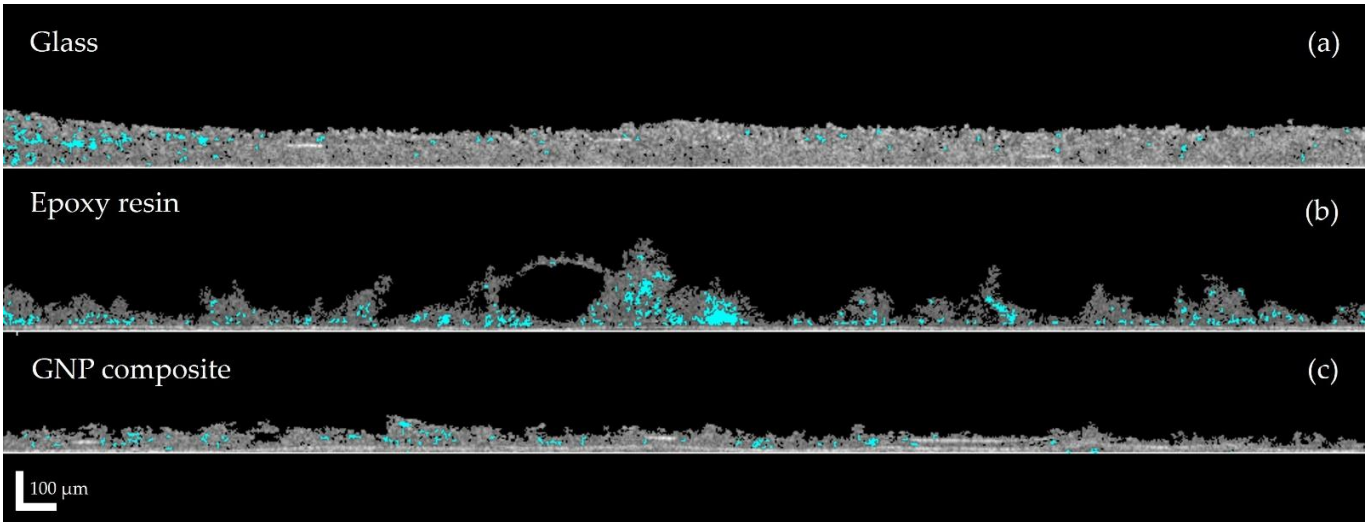

Figure 6. Representative 2D cross-sectional OCT images obtained for *Lusitaniella coriacea* LEGE 07157 biofilms on glass (**a**), epoxy resin (**b**), and GNP composite (**c**) after 49 days. The empty spaces on the biofilm structure are indicated in blue (scale bar = 100 µm).

Comparing the biofilm structure over the 49 days (Figure 5b,c), it was possible to observe different patterns between biofilms formed on the epoxy resin without and with

embedded GNPs. In the early stages of biofilm formation (days 14 to 28), biofilms formed on the GNP composite were thicker and presented a higher percentage of empty spaces when compared to the epoxy resin surface, while in the maturation phase (days 35 to 49) these parameters became lower. These findings suggest that the higher roughness of the GNP composite may initially promote the development of a porous and thicker biofilm, and at the maturation stage, a biofilm structural arrangement may occur. In fact, 2D cross-sectional OCT images obtained for *Lusitaniella coriacea* LEGE 07157 biofilms after 28 days (Figure S1 in Supplementary Material) revealed that biofilms formed on the GNP composite presented a higher number of streamers than the older biofilm (Figure 6c). Initially, to avoid the direct contact with GNP present on epoxy resin, cyanobacterial cells may have adapted their adhesion for vertical biofilm growth rather than a homogeneous development along the surface, contributing to the higher values of thickness between days 14 and 28. Although some previous studies revealed that the first dead cells could prevent the direct contact of live cells with graphene oxide (GO) surfaces, serving as a nutrient for live cells and consequently enhancing biofilm formation [69], the differences in architectural adaptation observed over time may provide an additional explanation for the antibiofilm mechanisms of the GNP composite. Indeed, values obtained from the biofilm roughness coefficient (Figure S2 in Supplementary Material) showed that all biofilms formed on day 28 presented a higher roughness compared with biofilms developed on day 49 ($p < 0.05$), including biofilms formed on the GNP composite.

Moreover, it was also hypothesized that the inability of *Lusitaniella coriacea* LEGE 07157 to form a dense and robust biofilm on the GNP composite was related to the damaging effect of graphene in the first cells adhered to the surface. These bacterial cells could be affected by the higher roughness of the graphene-based nanocomposite since the surface peaks corresponding to GNP clusters may directly affect bacterial viability by increasing the surface contact area and, consequently, the piercing action of exposed graphene particles. These initial adhered cells would become more fragile, probably leading to the improper adherence of the following layers of cells and hindering long-term biofilm formation. In previous work, Oliveira et al. [70] showed that 5 wt% GNP/PDMS surfaces reduced the number of total (57%), viable (69%), culturable (55%), and VBNC cells (85%) of 24-h *S. aureus* biofilms compared to PDMS [40]. Besides cell death, the increased permeability of cell membranes caused by nanoparticles may affect extracellular polymeric substances (EPS) production, resulting in a disrupted 3D structure of biofilm.

The CLSM analysis was performed to analyze structural differences between the biofilms formed on the three tested surface materials (glass, epoxy resin, and GNP composite; Figure 7). While the 49-day-old biofilm developed on glass was dense, preventing the observation of individual filaments on the cyanobacterial cells in the top view (Figure 7a), the biofilms formed on epoxy resin surfaces without and with GNPs (Figure 7b,c, respectively) displayed randomly distributed filaments. Furthermore, a drastic reduction in total biofilm amount was observed on the GNP composite when compared to both glass and epoxy resin surfaces. This was corroborated by the quantitative data extracted from the confocal stacks (Figure 7d,e), in which a decrease in biovolume (on average 86%, $p < 0.05$; Figure 7d) and surface coverage (on average 65%, $p < 0.05$; Figure 7e) was observed on the graphene-based surface compared to control surfaces.

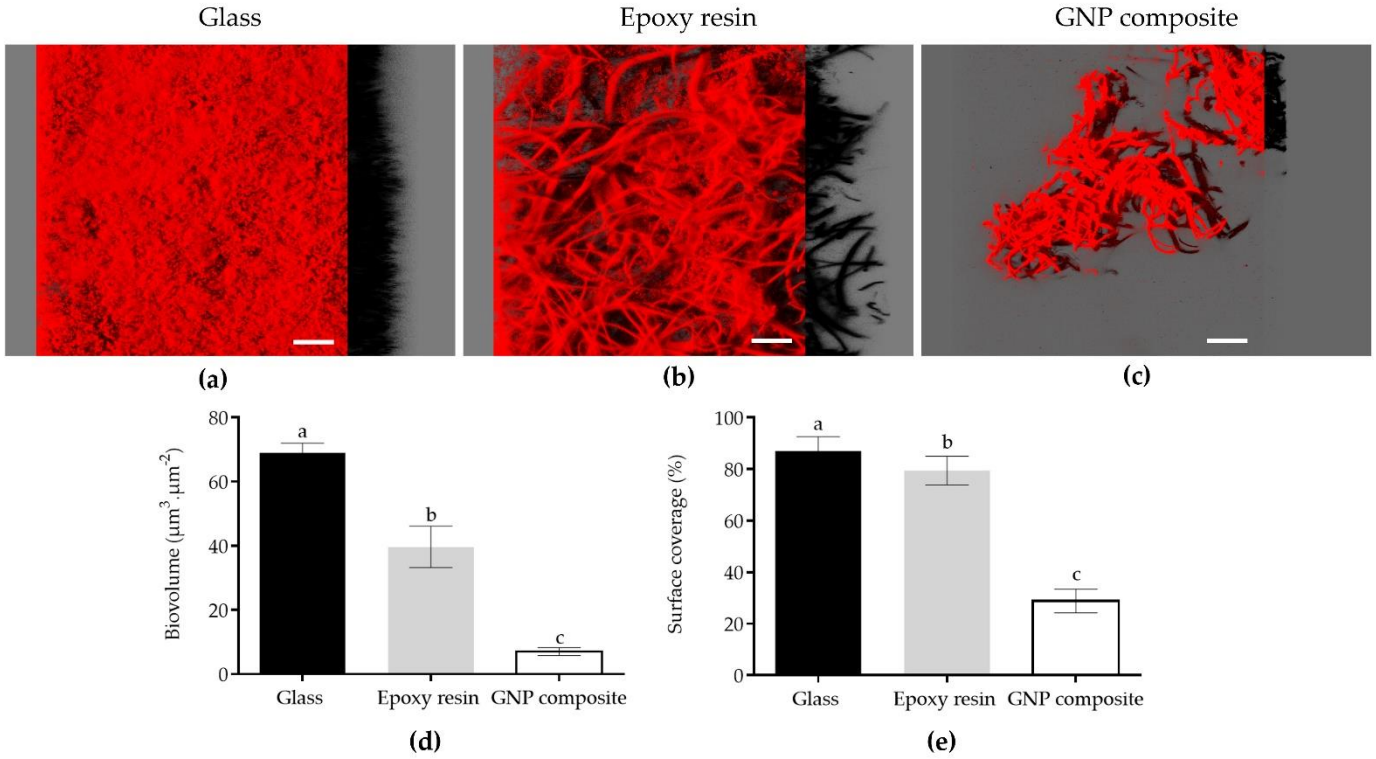

Figure 7. Three-dimensional confocal reconstructions of *Lusitaniella coriacea* LEGE 07157 biofilms grown on (**a**) glass, (**b**) epoxy resin, and (**c**) GNP composite after 49 days of incubation (white scale bars = 50 µm). These images show the biofilm aerial view, with the virtual shadow projection on the right (representative of biofilm thickness). Biovolume (**d**) and surface coverage (**e**) values of cyanobacterial biofilms were extracted from confocal files with the COMSTAT program. The means ± SD are presented. Different letters in the graphs (a, b, and c) indicate a significant difference among surfaces ($p < 0.05$).

The morphology of 49-day-old *Lusitaniella coriacea* LEGE 07157 biofilms on glass, epoxy resin, and GNP composite surfaces was also studied by SEM (Figure 8). The appearance of the biofilm developed on each surface was different, particularly when comparing the biofilm formed on glass (Figure 8a) with that formed on the epoxy resin without and with GNPs (Figure 8b,c, respectively). Indeed, the biofilm formed on the glass surface was very dense, and filamentous cyanobacteria were completely embedded in a complex matrix, which is a crucial feature of biofilm formation, making it impossible to distinguish the morphology of the individual *Lusitaniella coriacea* cells. Contrariwise, the electron micrograph of the epoxy resin surface (Figure 8b) displayed mesh-like structures around the *Lusitaniella* cells (possibly resulting from exopolysaccharide secretion), and filaments made of chains of cells that covered the entire surface and which were arranged in random directions. The cyanobacterial filaments were even more visible in the biofilm formed on the GNP composite, where the amount of extracellular material seemed to be lower and where uncovered areas of surface areas could be seen (Figure 8c). Therefore, SEM observations corroborated the results of the biofilm wet weight (Figure 5a), and those obtained by OCT (Figure 6) and CLSM (Figure 7), indicating that the graphene composite surface had a lower biofilm amount than the control surfaces after 49 days. Likewise, SEM micrographs also supported the finding that GNP-modified surfaces may decrease EPS production, resulting in a disrupted 3D structure of biofilm at the maturation stage. Similar results were obtained on CNT-based surfaces compared to the control surfaces (glass and epoxy resin) since SEM images of cyanobacterial biofilm grown on the CNT composite presented lower-density cell aggregates [42].

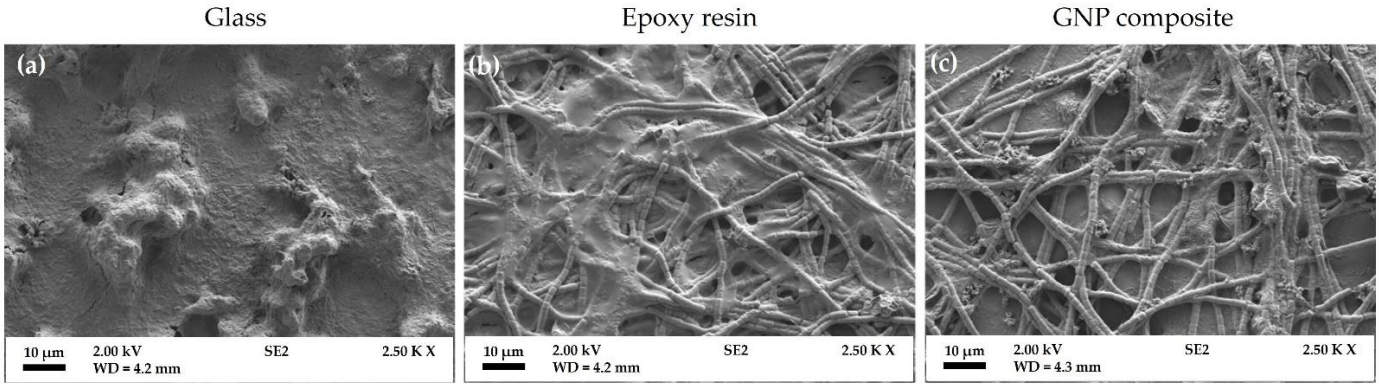

Figure 8. SEM micrographs of *Lusitaniella coriacea* LEGE 07157 biofilms grown on glass (**a**), epoxy resin (**b**), and GNP composite (**c**) after 49 days of incubation. Magnification = 2500×; scale bar = 10 µm.

This work may be limited by the use of cyanobacterial monocultures, the lack of field tests, and the absence of surface tribological characterization for long periods of immersion. Taking into account that the most studied forms of graphene within the marine context are GO and GO functionalized with metal nanoparticles [27], further experimental assays with other graphene-based surfaces for the marine environment should be performed. These assays can comprise different physical and chemical properties (e.g., dimension, number of layers, and functionalization), but also focus on factors related to the production of the surface (e.g., graphene loading, nanoparticle dispersion, and aggregation) [71–73]. Future in situ studies should also include other foulers, as well as being performed for a longer period since, in the present study, a distinct effect was observed over time. In fact, few studies on graphene-based surfaces were performed over one [19,20] or more months [34]. Although different optical techniques have been used in this study, further work should assess the metabolic state and the viability of biofilm cyanobacterial cells [74,75]. Omics approaches such as transcriptomic analysis to consider the expression of virulence factors and adhesion genes related to biofilm development [30], and proteomic analysis to elucidate cyanobacterial defense mechanisms to graphene toxicity, should also be considered [52,54,56]. Moreover, computational simulation approaches have been widely used for the characterization of novel materials [76]. Strong coupling between experimental data and numerical simulation is required for predicting macroscopic behavior with a fine description of local fields. By combining modeling approaches and corresponding experiments, the studies take advantage of the simplicity, efficiency, and mechanistic insight gained from the models, and the physicality, meaningful reproducibility, and reality check provided by the experiments [77]. Thus, future studies should include computational simulations to evaluate the potential use of GNP composites as a marine coatings.

4. Conclusions

Biofilms developed on the GNP composite had reduced wet weight, thickness, biovolume, and surface coverage in the maturation stage when compared to the control surfaces (glass and epoxy resin). Moreover, the GNP composite delayed cyanobacterial biofilm development and promoted the development of a less porous biofilm. As the graphene coating should serve as a long-term antifouling material for marine applications, the analysis of cyanobacterial biofilm behavior over time performed in this study is particularly relevant. The analysis of these GNP-based surfaces in vitro to assess their performance against mixed-species biofilms, and in situ to assess their effect on biofilm formation by additional microfoulers or to evaluate the potentially damaging effect of harsh marine environments on these nanostructured surfaces, will be performed in future studies. Therefore, upcoming tests should focus on tribological parameters such as the friction coefficient,

wear, temperature, and durability related to the application, and surface characterization for long-term assays.

Supplementary Materials: The following supporting information can be downloaded at: https://www.mdpi.com/article/10.3390/coatings12111775/s1, Figure S1: Representative 2D cross-sectional OCT images obtained for *Lusitaniella coriacea* LEGE 07157 biofilms on glass (a), epoxy resin (b), and GNP composite (c) after 28 days. The empty spaces on the biofilm structure are indicated in blue (scale bar = 100 μm).; Figure S2: Roughness coefficient[1] values of *Lusitaniella coriacea* LEGE 07157 biofilms on different surfaces: glass (black), epoxy resin (grey), and GNP composite (white). Mean values and SD from two biological assays with two technical replicates each are represented. For each surface, different lowercase letters indicate significant differences between the sampling day (day 28 vs. day 49; $p < 0.05$; unpaired t-test). The p value obtained for glass and epoxy resin was < 0.0001, and for GNP composite was 0.0104.

Author Contributions: Conceptualization, M.J.R. and F.J.M.; methodology, M.J.R., L.C.G. and F.S.-C.; formal analysis, M.J.R. and L.C.G.; investigation, M.J.R. and L.C.G.; resources, M.F.R.P., V.V., K.A.W. and F.J.M.; funding acquisition, M.F.R.P., V.V. and F.J.M.; data curation, M.J.R. and L.C.G.; writing—original draft preparation, M.J.R. and L.C.G.; writing—review and editing, J.M., M.F.R.P., O.S.G.P.S., K.A.W. and F.J.M.; supervision, V.V. and F.J.M. All authors have read and agreed to the published version of the manuscript.

Funding: This research was funded by: LA/P/0045/2020 (ALiCE), UIDB/00511/2020 and UIDP/00511/2020 (LEPABE) and project PTDC/CTM-COM/4844/2020, funded by national funds through FCT/MCTES (PIDDAC); project HealthyWaters (NORTE-01-0145-FEDER-000069), supported by Norte Portugal Regional Operational Programme (NORTE 2020), under the PORTUGAL 2020 Partnership Agreement, through the European Regional Development Fund (ERDF); Strategic Funding UIDB/04423/2020 and UIDP/04423/2020 through national funds provided by the Foundation for Science and Technology (FCT); ATLANTIDA (NORTE-01-0145-FEDER-000040), financed by the FEDER through the NORTE 2020 Program and the European Regional Development Fund (ERDF) in the framework of the program PT2020; project SurfSAFE supported by the European Union's Horizon 2020 Research and Innovation Programme under grant agreement no. 952471. M.J.R, L.C.G., and O.S.G.P.S. thank FCT for the financial support of a Ph.D. grant (SFRH/BD/140080/2018), and work contracts through the Scientific Employment Stimulus—Individual Call—[CEECIND/01700/2017] and the Scientific Employment Stimulus—Institutional Call—CEECINST/00049/2018, respectively. Support from the EURO-MIC COST Action (CA20130) is also acknowledged.

Institutional Review Board Statement: Not applicable.

Informed Consent Statement: Not applicable.

Data Availability Statement: The data presented in this study are available from the corresponding author upon request.

Conflicts of Interest: The authors declare no conflict of interest.

References

1. Schultz, M.P.; Bendick, J.A.; Holm, E.R.; Hertel, W.M. Economic impact of biofouling on a naval surface ship. *Biofouling* **2011**, *27*, 87–98. [CrossRef]
2. Delauney, L.; Compère, C.; Lehaitre, M. Biofouling protection for marine environmental sensors. *Ocean Sci.* **2010**, *6*, 503–511. [CrossRef]
3. Giakoumi, S.; Katsanevakis, S.; Albano, P.G.; Azzurro, E.; Cardoso, A.C.; Cebrian, E.; Deidun, A.; Edelist, D.; Francour, P.; Jimenez, C.; et al. Management priorities for marine invasive species. *Sci. Total Environ.* **2019**, *688*, 976–982. [CrossRef] [PubMed]
4. Bannister, J.; Sievers, M.; Bush, F.; Bloecher, N. Biofouling in marine aquaculture: A review of recent research and developments. *Biofouling* **2019**, *35*, 631–648. [CrossRef] [PubMed]
5. Kumar, S.; Bhattacharya, W.; Singh, M.; Halder, D.; Mitra, A. Plant latex capped colloidal silver nanoparticles: A potent anti-biofilm and fungicidal formulation. *J. Mol. Liq.* **2017**, *230*, 705–713. [CrossRef]
6. Zhang, D.; Liu, Z.; Wu, G.; Yang, Z.; Cui, Y.; Li, H.; Zhang, Y. Fluorinated carbon nanotube superamphiphobic coating for high-efficiency and long-lasting underwater antibiofouling surfaces. *ACS Appl. Bio Mater.* **2021**, *4*, 6351–6360. [CrossRef] [PubMed]
7. Jin, H.; Zhang, T.; Bing, W.; Dong, S.; Tian, L. Antifouling performance and mechanism of elastic graphene-silicone rubber composite membranes. *J. Mater. Chem. B* **2018**, *7*, 488–497. [CrossRef]

8. Kumar, S.; Boro, J.C.; Ray, D.; Mukherjee, A.; Dutta, J. Bionanocomposite films of agar incorporated with ZnO nanoparticles as an active packaging material for shelf life extension of green grape. *Heliyon* **2019**, *5*, e01867. [CrossRef]
9. Kim, J.; Baek, Y.; Hong, S.P.; Yoon, H.; Kim, S.; Kim, C.; Kim, J.; Yoon, J. Evaluation of thin-film nanocomposite RO membranes using TiO_2 nanotubes and TiO_2 nanoparticles: A comparative study. *Desalin. Water Treat.* **2016**, *57*, 24674–24681. [CrossRef]
10. Callow, J.A.; Callow, M.E. Trends in the development of environmentally friendly fouling-resistant marine coatings. *Nat. Commun.* **2011**, *2*, 244. [CrossRef]
11. Al-Jumaili, A.; Alancherry, S.; Bazaka, K.; Jacob, M.V. Review on the antimicrobial properties of carbon nanostructures. *Materials* **2017**, *10*, 1066. [CrossRef]
12. Xu, H.; Ma, L.; Jin, Z. Nitrogen-doped graphene: Synthesis, characterizations and energy applications. *J. Energy Chem.* **2018**, *27*, 146–160. [CrossRef]
13. Parra, C.; Montero-Silva, F.; Henríquez, R.; Flores, M.; Garín, C.; Ramírez, C.; Moreno, M.; Correa, J.; Seeger, M.; Häberle, P. Suppressing bacterial interaction with copper surfaces through graphene and hexagonal-boron nitride coatings. *ACS Appl. Mater. Interfaces* **2015**, *7*, 6430–6437. [CrossRef]
14. Naddaf, A.; Heris, S.Z.; Pouladi, B. An experimental study on heat transfer performance and pressure drop of nanofluids using graphene and multi-walled carbon nanotubes based on diesel oil. *Powder Technol.* **2019**, *352*, 369–380. [CrossRef]
15. Smaradhana, D.F.; Prabowo, A.R.; Ganda, A.N.F. Exploring the potential of graphene materials in marine and shipping industries—A technical review for prospective application on ship operation and material-structure aspects. *J. Ocean Eng. Sci.* **2021**, *6*, 299–316. [CrossRef]
16. Pan, L.; Liu, S.; Oderinde, O.; Li, K.; Yao, F.; Fu, G. Facile fabrication of graphene-based aerogel with rare earth metal oxide for water purification. *Appl. Surf. Sci.* **2018**, *427*, 779–786. [CrossRef]
17. Hu, M.; Cui, Z.; Li, J.; Zhang, L.; Mo, Y.; Dlamini, D.S.; Wang, H.; He, B.; Li, J.; Matsuyama, H. Ultra-low graphene oxide loading for water permeability, antifouling and antibacterial improvement of polyethersulfone/sulfonated polysulfone ultrafiltration membranes. *J. Colloid Interface Sci.* **2019**, *552*, 319–331. [CrossRef] [PubMed]
18. Balaure, P.C. Special Issue: Advances in engineered nanostructured antibacterial surfaces and coatings. *Coatings* **2022**, *12*, 1041. [CrossRef]
19. Selim, M.S.; El-Safty, S.A.; Fatthallah, N.A.; Shenashen, M.A. Silicone/graphene oxide sheet-alumina nanorod ternary composite for superhydrophobic antifouling coating. *Prog. Org. Coatings* **2018**, *121*, 160–172. [CrossRef]
20. Selim, M.S.; Fatthallah, N.A.; Higazy, S.A.; Hao, Z.; Mo, P.J. A comparative study between two novel silicone/graphene-based nanostructured surfaces for maritime antifouling. *J. Colloid Interface Sci.* **2022**, *606*, 367–383. [CrossRef]
21. Gu, J.; Li, L.; Huang, D.; Jiang, L.; Liu, L.; Li, F.; Pang, A.; Guo, X.; Tao, B. In situ synthesis of graphene@cuprous oxide nanocomposite incorporated marine antifouling coating with elevated antifouling performance. *Open J. Org. Polym. Mater.* **2019**, *9*, 47–62. [CrossRef]
22. Li, Y.; Huang, Y.; Wang, F.; Liang, W.; Yang, H.; Wu, D. Fabrication of acrylic acid modified graphene oxide (AGO)/acrylate composites and their synergistic mechanisms of anticorrosion and antifouling properties. *Prog. Org. Coatings* **2022**, *168*, 106910. [CrossRef]
23. Zhang, Z.; Chen, R.; Song, D.; Yu, J.; Sun, G.; Liu, Q.; Han, S.; Liu, J.; Zhang, H.; Wang, J. Guanidine-functionalized graphene to improve the antifouling performance of boron acrylate polymer. *Prog. Org. Coatings* **2021**, *159*, 106396. [CrossRef]
24. Jin, H.; Bing, W.; Tian, L.; Wang, P.; Zhao, J. Combined effects of color and elastic modulus on antifouling performance: A study of graphene oxide/silicone rubber composite membranes. *Materials* **2019**, *12*, 2608. [CrossRef] [PubMed]
25. Liu, Z.; Tian, S.; Li, Q.; Wang, J.; Pu, J.; Wang, G.; Zhao, W.; Feng, F.; Qin, J.; Ren, L. Integrated dual-functional ormosil coatings with AgNPs@rGO nanocomposite for corrosion resistance and antifouling applications. *ACS Sustain. Chem. Eng.* **2020**, *8*, 6786–6797. [CrossRef]
26. Zhang, X.; Mikkelsen, Ø. Graphene oxide/silver nanocomposites as antifouling coating on sensor housing materials. *J. Clust. Sci.* **2021**, *33*, 627–635. [CrossRef]
27. Sousa-Cardoso, F.; Teixeira-Santos, R.; Mergulhão, F.J.M. Antifouling performance of carbon-based coatings for marine applications: A systematic review. *Antibiotics* **2022**, *11*, 1102. [CrossRef]
28. Yee, M.S.-L.; Khiew, P.-S.; Chiu, W.S.; Tan, Y.F.; Kok, Y.-Y.; Leong, C.-O. Green synthesis of graphene-silver nanocomposites and its application as a potent marine antifouling agent. *Colloids Surf. B Biointerfaces* **2016**, *148*, 392–401. [CrossRef]
29. Jiang, T.; Qi, L.; Qin, W. Improving the environmental compatibility of marine sensors by surface functionalization with graphene oxide. *Anal. Chem.* **2019**, *91*, 13268–13274. [CrossRef] [PubMed]
30. Parra, C.; Dorta, F.; Jimenez, E.; Henríquez, R.; Ramírez, C.; Rojas, R.; Villalobos, P. A nanomolecular approach to decrease adhesion of biofouling-producing bacteria to graphene-coated material. *J. Nanobiotechnol.* **2015**, *13*, 82. [CrossRef]
31. Krishnamoorthy, K.; Jeyasubramanian, K.; Premanathan, M.; Subbiah, G.; Shin, H.S.; Kim, S.-J. Graphene oxide nanopaint. *Carbon N. Y.* **2014**, *72*, 328–337. [CrossRef]
32. Balakrishnan, A.; Jena, G.; George, R.P.; Philip, J. Polydimethylsiloxane-graphene oxide nanocomposite coatings with improved anti-corrosion and anti-biofouling properties. *Environ. Sci. Pollut. Res.* **2020**, *28*, 7404–7422. [CrossRef]
33. Manderfeld, E.; Kleinberg, M.N.; Thamaraiselvan, C.; Koschitzki, F.; Gnutt, P.; Plumere, N.; Arnusch, C.J.; Rosenhahn, A. Electrochemically activated laser-induced graphene coatings against marine biofouling. *Appl. Surf. Sci.* **2021**, *569*, 150853. [CrossRef]

34. Fazli-Shokouhi, S.; Nasirpouri, F.; Khatamian, M. Epoxy-matrix polyaniline/*p*-phenylenediamine-functionalised graphene oxide coatings with dual anti-corrosion and anti-fouling performance. *RSC Adv.* **2021**, *11*, 11627–11641. [CrossRef] [PubMed]
35. Chambers, L.D.; Stokes, K.R.; Walsh, F.C.; Wood, R.J.K. Modern approaches to marine antifouling coatings. *Surf. Coat. Technol.* **2006**, *201*, 3642–3652. [CrossRef]
36. Palmer, J.; Flint, S.; Brooks, J. Bacterial cell attachment, the beginning of a biofilm. *J. Ind. Microbiol. Biotechnol.* **2007**, *34*, 577–588. [CrossRef]
37. Mostafaei, A.; Nasirpouri, F. Preparation and characterization of a novel conducting nanocomposite blended with epoxy coating for antifouling and antibacterial applications. *J. Coatings Technol. Res.* **2013**, *10*, 679–694. [CrossRef]
38. Hoge, J.; Leach, C. Epoxy resin infused boat hulls. *Reinf. Plast.* **2016**, *60*, 221–223. [CrossRef]
39. Faria, S.I.; Teixeira-Santos, R.; Gomes, L.C.; Silva, E.R.; Morais, J.; Vasconcelos, V.; Mergulhão, F.J.M. Experimental assessment of the performance of two marine coatings to curb biofilm formation of microfoulers. *Coatings* **2020**, *10*, 893. [CrossRef]
40. Oliveira, I.M.; Gomes, M.; Gomes, L.C.; Pereira, M.F.R.; Soares, O.S.G.P.; Mergulhão, F.J. Performance of graphene/polydimethylsiloxane surfaces against *S. aureus* and *P. aeruginosa* single- and dual-species biofilms. *Nanomaterials* **2022**, *12*, 355. [CrossRef]
41. Faria, S.I.; Teixeira-Santos, R.; Romeu, M.J.; Morais, J.; Vasconcelos, V.; Mergulhão, F.J. The relative importance of shear forces and surface hydrophobicity on biofilm formation by coccoid cyanobacteria. *Polymers* **2020**, *12*, 653. [CrossRef] [PubMed]
42. Romeu, M.J.; Lima, M.; Gomes, L.C.; de Jong, E.D.; Vasconcelos, V.; Pereira, M.F.R.; Soares, O.S.G.P.; Sjollema, J.; Mergulhão, F.J. The use of 3D optical coherence tomography to analyze the architecture of cyanobacterial biofilms formed on a carbon nanotube composite. *Polymers* **2022**, *14*, 4410. [CrossRef] [PubMed]
43. Whitehead, K.; Kelly, P.; Li, H.; Verran, J. Surface topography and physicochemistry of silver containing titanium nitride nanocomposite coatings. *J. Vac. Sci. Technol. B Nanotechnol. Microelectron. Mater. Process. Meas. Phenom.* **2010**, *28*, 180. [CrossRef]
44. Skovager, A.; Whitehead, K.; Siegumfeldt, H.; Ingmer, H.; Verran, J.; Arneborg, N. Influence of flow direction and flow rate on the initial adhesion of seven *Listeria monocytogenes* strains to fine polished stainless steel. *Int. J. Food Microbiol.* **2012**, *157*, 174–181. [CrossRef] [PubMed]
45. Ramos, V.; Morais, J.; Castelo-Branco, R.; Pinheiro, Â.; Martins, J.; Regueiras, A.; Pereira, A.L.; Lopes, V.R.; Frazão, B.; Gomes, D.; et al. Cyanobacterial diversity held in microbial biological resource centers as a biotechnological asset: The case study of the newly established LEGE culture collection. *J. Appl. Phycol.* **2018**, *30*, 1437–1451. [CrossRef]
46. Kotai, J. Instructions for the Preparation of Modified Nutrient Solution Z8 for Algae. *Nor. Inst. Water Res.* **1972**, *11*, 5.
47. Romeu, M.J.; Alves, P.; Morais, J.; Miranda, J.M.; de Jong, E.D.; Sjollema, J.; Ramos, V.; Vasconcelos, V.; Mergulhão, F.J.M. Biofilm formation behaviour of marine filamentous cyanobacterial strains in controlled hydrodynamic conditions. *Environ. Microbiol.* **2019**, *21*, 4411–4424. [CrossRef]
48. Boyer, J.N.; Kelble, C.R.; Ortner, P.B.; Rudnick, D.T. Phytoplankton bloom status: Chlorophyll a biomass as an indicator of water quality condition in the southern estuaries of Florida, USA. *Ecol. Indic.* **2009**, *9*, S56–S67. [CrossRef]
49. Porra, R.J.; Thompson, W.A.; Kriedemann, P.E. Determination of accurate extinction coefficients and simultaneous equations for assaying chlorophylls a and b extracted with four different solvents: Verification of the concentration of chlorophyll standards by atomic absorption spectroscopy. *Biochim. Biophys. Acta BBA Bioenerg.* **1989**, *975*, 384–394. [CrossRef]
50. Bakker, D.P.; Van der Plaats, A.; Verkerke, G.J.; Busscher, H.J.; Mei, H.C. Van der comparison of velocity profiles for different flow chamber designs used in studies of microbial adhesion to surfaces. *Appl. Environ. Microbiol.* **2003**, *69*, 6280–6287. [CrossRef]
51. Silva, E.R.; Tulcidas, A.V.; Ferreira, O.; Bayón, R.; Igartua, A.; Mendoza, G.; Mergulhão, F.J.; Faria, S.I.; Gomes, L.C.; Carvalho, S.; et al. Assessment of the environmental compatibility and antifouling performance of an innovative biocidal and foul-release multifunctional marine coating. *Environ. Res.* **2021**, *198*, 111219. [CrossRef] [PubMed]
52. Romeu, M.J.; Domínguez-Pérez, D.; Almeida, D.; Morais, J.; Araújo, M.J.; Osório, H.; Campos, A.; Vasconcelos, V.; Mergulhão, F.J. Hydrodynamic conditions affect the proteomic profile of marine biofilms formed by filamentous cyanobacterium. *NPJ Biofilms Microbiomes* **2022**, *8*, 80. [CrossRef] [PubMed]
53. Faria, S.; Gomes, L.C.; Teixeira-Santos, R.; Morais, J.; Vasconcelos, V.; Mergulhão, F. Developing new marine antifouling surfaces: Learning from single-strain laboratory tests. *Coatings* **2021**, *11*, 90. [CrossRef]
54. Romeu, M.J.L.; Domínguez-Pérez, D.; Almeida, D.; Morais, J.; Campos, A.; Vasconcelos, V.; Mergulhão, F.J.M. Characterization of planktonic and biofilm cells from two filamentous cyanobacteria using a shotgun proteomic approach. *Biofouling* **2020**, *36*, 631–645. [CrossRef]
55. Faria, S.; Teixeira-Santos, R.; Romeu, M.J.; Morais, J.; Jong, E.; Sjollema, J.; Vasconcelos, V.; Mergulhão, F.J. Unveiling the antifouling performance of different marine surfaces and their effect on the development and structure of cyanobacterial biofilms. *Microorganisms* **2021**, *9*, 1102. [CrossRef] [PubMed]
56. Romeu, M.J.; Domínguez-Pérez, D.; Almeida, D.; Morais, J.; Araújo, M.J.; Osório, H.; Campos, A.; Vasconcelos, V.; Mergulhão, F. Quantitative proteomic analysis of marine biofilms formed by filamentous cyanobacterium. *Environ. Res.* **2021**, *201*, 111566. [CrossRef] [PubMed]
57. Heydorn, A.; Nielsen, A.T.; Hentzer, M.; Sternberg, C.; Givskov, M.; Ersbøll, B.K.; Molin, S. Quantification of biofilm structures by the novel computer program COMSTAT. *Microbiology* **2000**, *146*, 2395–2407. [CrossRef]
58. Alves, P.; Gomes, L.C.; Rodríguez-Emmenegger, C.; Mergulhão, F.J. Efficacy of a poly (MeOEGMA) brush on the prevention of *Escherichia coli* biofilm formation and susceptibility. *Antibiotics* **2020**, *9*, 216. [CrossRef]

59. Zheng, S.; Bawazir, M.; Dhall, A.; Kim, H.-E.; He, L.; Heo, J.; Hwang, G. Implication of surface properties, bacterial motility, and hydrodynamic conditions on bacterial surface sensing and their initial adhesion. *Front. Bioeng. Biotechnol.* **2021**, *9*, 643722. [CrossRef]
60. Yuan, Y.; Lee, T.R. Contact angle and wetting properties. In *Surface Science Techniques*; Springer Series in surface sciences 51; Bracco, G., Holst, B., Eds.; Springer: Berlin/Heidelberg, Germany, 2013; Volume 51, pp. 3–34. ISBN 978-3-642-34242-4.
61. Doshi, B.; Sillanpää, M.; Kalliola, S. A review of bio-based materials for oil spill treatment. *Water Res.* **2018**, *135*, 262–277. [CrossRef]
62. Rafiee, J.; Mi, X.; Gullapalli, H.; Thomas, A.V.; Yavari, F.; Shi, Y.; Ajayan, P.M.; Koratkar, N.A. Wetting transparency of graphene. *Nat. Mater.* **2012**, *11*, 217–222. [CrossRef]
63. Chatterjee, S.; Nüesch, F.A.; Chu, B.T.T. Comparing carbon nanotubes and graphene nanoplatelets as reinforcements in polyamide 12 composites. *Nanotechnology* **2011**, *22*, 275714. [CrossRef]
64. Santos, C.M.; Mangadlao, J.; Ahmed, F.; Leon, A.; Advincula, R.C.; Rodrigues, D. Graphene nanocomposite for biomedical applications: Fabrication, antimicrobial and cytotoxic investigations. *Nanotechnology* **2012**, *23*, 395101. [CrossRef]
65. Zou, X.; Zhang, L.; Wang, Z.; Luo, Y. Mechanisms of the antimicrobial activities of graphene materials. *J. Am. Chem. Soc.* **2016**, *138*, 2064–2077. [CrossRef]
66. Mohammed, H.; Kumar, A.; Bekyarova, E.; Al-Hadeethi, Y.; Zhang, X.; Chen, M.; Ansari, M.S.; Cochis, A.; Rimondini, L. Antimicrobial mechanisms and effectiveness of graphene and graphene-functionalized biomaterials. A scope review. *Front. Bioeng. Biotechnol.* **2020**, *8*, 465. [CrossRef] [PubMed]
67. Staneva, A.D.; Dimitrov, D.K.; Gospodinova, D.N.; Vladkova, T.G. Antibiofouling activity of graphene materials and graphene-based antimicrobial coatings. *Microorganisms* **2021**, *9*, 1839. [CrossRef] [PubMed]
68. Sjollema, J.; Rustema-Abbing, M.; van der Mei, H.C.; Busscher, H.J. Generalized relationship between numbers of bacteria and their viability in biofilms. *Appl. Environ. Microbiol.* **2011**, *77*, 5027–5029. [CrossRef]
69. Song, C.; Yang, C.-M.; Sun, X.-F.; Xia, P.-F.; Qin, J.; Guo, B.-B.; Wang, S.-G. Influences of graphene oxide on biofilm formation of gram-negative and gram-positive bacteria. *Environ. Sci. Pollut. Res.* **2017**, *25*, 2853–2860. [CrossRef] [PubMed]
70. Ahmed, B.; Ameen, F.; Rizvi, A.; Ali, K.; Sonbol, H.; Zaidi, A.; Khan, M.S.; Musarrat, J. Destruction of cell topography, morphology, membrane, inhibition of respiration, biofilm formation, and bioactive molecule production by nanoparticles of Ag, ZnO, CuO, TiO_2, and Al_2O_3 toward beneficial soil bacteria. *ACS Omega* **2020**, *5*, 7861–7876. [CrossRef]
71. Fatima, N.; Qazi, U.Y.; Mansha, A.; Bhatti, I.A.; Javaid, R.; Abbas, Q.; Nadeem, N.; Rehan, Z.A.; Noreen, S.; Zahid, M. Recent developments for antimicrobial applications of graphene-based polymeric composites: A review. *J. Ind. Eng. Chem.* **2021**, *100*, 40–58. [CrossRef]
72. Radhi, A.; Mohamad, D.; Rahman, F.S.A.; Abdullah, A.M.; Hasan, H. Mechanism and factors influence of graphene-based nanomaterials antimicrobial activities and application in dentistry. *J. Mater. Res. Technol.* **2021**, *11*, 1290–1307. [CrossRef]
73. Azizi-Lalabadi, M.; Hashemi, H.; Feng, J.; Jafari, S.M. Carbon nanomaterials against pathogens; the antimicrobial activity of carbon nanotubes, graphene/graphene oxide, fullerenes, and their nanocomposites. *Adv. Colloid Interface Sci.* **2020**, *284*, 102250. [CrossRef]
74. Mountcastle, S.E.; Vyas, N.; Villapun, V.M.; Cox, S.C.; Jabbari, S.; Sammons, R.L.; Shelton, R.M.; Walmsley, A.D.; Kuehne, S.A. Biofilm viability checker: An open-source tool for automated biofilm viability analysis from confocal microscopy images. *NPJ Biofilms Microbiomes* **2021**, *7*, 44. [CrossRef] [PubMed]
75. Van den Driessche, F.; Rigole, P.; Brackman, G.; Coenye, T. Optimization of resazurin-based viability staining for quantification of microbial biofilms. *J. Microbiol. Methods* **2014**, *98*, 31–34. [CrossRef]
76. Ammarullah, M.I.; Santoso, G.; Sugiharto, S.; Supriyono, T.; Wibowo, D.B.; Kurdi, O.; Tauviqirrahman, M.; Jamari, J. Minimizing risk of failure from ceramic-on-ceramic total hip prosthesis by selecting ceramic materials based on tresca stress. *Sustainability* **2022**, *14*, 13413. [CrossRef]
77. Dingreville, R.; Karnesky, R.A.; Puel, G.; Schmitt, J.-H. Synergies between computational modeling and experimental characterization of materials across length scales. *J. Mater. Sci.* **2015**, *51*, 1176–1177. [CrossRef]

Supplementary Material

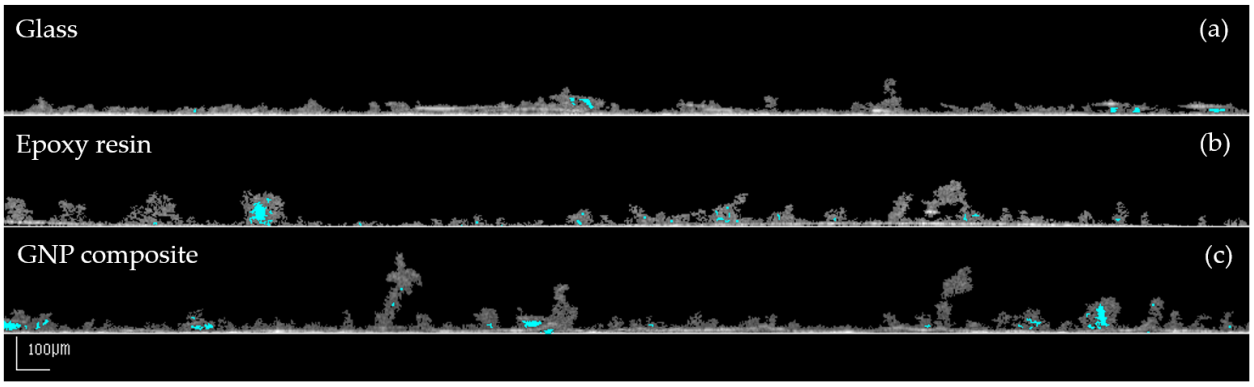

Figure S1. Representative 2D cross-sectional OCT images obtained for *Lusitaniella coriacea* LEGE 07157 biofilms on glass (a), epoxy resin (b), and GNP composite (c) after 28 days. The empty spaces on the biofilm structure are indicated in blue (scale bar = 100 µm).

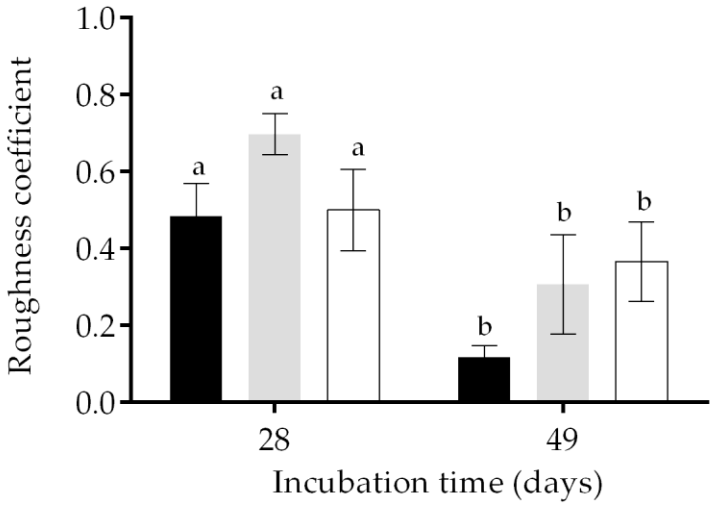

Figure S2. Roughness coefficient[1] values of *Lusitaniella coriacea* LEGE 07157 biofilms on different surfaces: glass (black), epoxy resin (grey), and GNP composite (white). Mean values and SD from two biological assays with two technical replicates each are represented. For each surface, different lowercase letters indicate significant differences between the sampling day (day 28 *vs* day 49; $P < 0.05$; unpaired t-test). The *p* value obtained for glass and epoxy resin was < 0.0001, and for GNP composite was 0.0104.

[1]The relative roughness coefficient ($R_{\propto}^{*}$) was calculated as previously reported (Romeu et al., 2019) using the following equation:

$$R_{\propto}^{*} = \frac{1}{N}\sum_{i=1}^{N}\frac{\left|L_{F,i} - \bar{L}_{F}\right|}{\bar{L}_{F}}$$

where $L_{F,i}$ is a local biofilm thickness measurement at location *i*, *N* equals the number of thickness measurements and $\bar{L}_F$ is the mean biofilm thickness.

References

Romeu, M.J.; Alves, P.; Morais, J.; Miranda, J.M.; de Jong, E.D.; Sjollema, J.; Ramos, V.; Vasconcelos, V.; Mergulhão, F.J.M. Biofilm Formation Behaviour of Marine Filamentous Cyanobacterial Strains in Controlled Hydrodynamic Conditions. *Environ. Microbiol.* **2019**, *21*, 4411–4424.